frontiers | Research Topics

Fibrosis: Etiology, pathophysiology, measurements, and therapy

Edited by
Yuxia Zhao, Panpan Hao, Peizhe Wang, Fujian Lu and Yanping Liu

Published in
Frontiers in Pharmacology



FRONTIERS EBOOK COPYRIGHT STATEMENT

The copyright in the text of individual articles in this ebook is the property of their respective authors or their respective institutions or funders. The copyright in graphics and images within each article may be subject to copyright of other parties. In both cases this is subject to a license granted to Frontiers.

The compilation of articles constituting this ebook is the property of Frontiers.

Each article within this ebook, and the ebook itself, are published under the most recent version of the Creative Commons CC-BY licence. The version current at the date of publication of this ebook is CC-BY 4.0. If the CC-BY licence is updated, the licence granted by Frontiers is automatically updated to the new version.

When exercising any right under the CC-BY licence, Frontiers must be attributed as the original publisher of the article or ebook, as applicable.

Authors have the responsibility of ensuring that any graphics or other materials which are the property of others may be included in the CC-BY licence, but this should be checked before relying on the CC-BY licence to reproduce those materials. Any copyright notices relating to those materials must be complied with.

Copyright and source acknowledgement notices may not be removed and must be displayed in any copy, derivative work or partial copy which includes the elements in question.

All copyright, and all rights therein, are protected by national and international copyright laws. The above represents a summary only. For further information please read Frontiers' Conditions for Website Use and Copyright Statement, and the applicable CC-BY licence.

ISSN 1664-8714
ISBN 978-2-8325-2559-3
DOI 10.3389/978-2-8325-2559-3

About Frontiers

Frontiers is more than just an open access publisher of scholarly articles: it is a pioneering approach to the world of academia, radically improving the way scholarly research is managed. The grand vision of Frontiers is a world where all people have an equal opportunity to seek, share and generate knowledge. Frontiers provides immediate and permanent online open access to all its publications, but this alone is not enough to realize our grand goals.

Frontiers journal series

The Frontiers journal series is a multi-tier and interdisciplinary set of open-access, online journals, promising a paradigm shift from the current review, selection and dissemination processes in academic publishing. All Frontiers journals are driven by researchers for researchers; therefore, they constitute a service to the scholarly community. At the same time, the *Frontiers journal series* operates on a revolutionary invention, the tiered publishing system, initially addressing specific communities of scholars, and gradually climbing up to broader public understanding, thus serving the interests of the lay society, too.

Dedication to quality

Each Frontiers article is a landmark of the highest quality, thanks to genuinely collaborative interactions between authors and review editors, who include some of the world's best academicians. Research must be certified by peers before entering a stream of knowledge that may eventually reach the public - and shape society; therefore, Frontiers only applies the most rigorous and unbiased reviews. Frontiers revolutionizes research publishing by freely delivering the most outstanding research, evaluated with no bias from both the academic and social point of view. By applying the most advanced information technologies, Frontiers is catapulting scholarly publishing into a new generation.

What are Frontiers Research Topics?

Frontiers Research Topics are very popular trademarks of the *Frontiers journals series*: they are collections of at least ten articles, all centered on a particular subject. With their unique mix of varied contributions from Original Research to Review Articles, Frontiers Research Topics unify the most influential researchers, the latest key findings and historical advances in a hot research area.

Find out more on how to host your own Frontiers Research Topic or contribute to one as an author by contacting the Frontiers editorial office: frontiersin.org/about/contact

Fibrosis: Etiology, pathophysiology, measurements, and therapy

Topic editors

Yuxia Zhao — Shandong University, China
Panpan Hao — Shandong University, China
Peizhe Wang — Department of Cardiology, Boston Children's Hospital, Harvard Medical School, United States
Fujian Lu — Boston Children's Hospital, Harvard Medical School, United States
Yanping Liu — Qilu Hospital, Shandong University, China

Citation

Zhao, Y., Hao, P., Wang, P., Lu, F., Liu, Y., eds. (2023). *Fibrosis: Etiology, pathophysiology, measurements, and therapy*. Lausanne: Frontiers Media SA. doi: 10.3389/978-2-8325-2559-3

Table of contents

05 Editorial: Fibrosis: etiology, pathophysiology, measurements, and therapy
Yanping Liu, Jiupan Xu, Yuxia Zhao and Panpan Hao

08 Bidirectional regulatory effects of Cordyceps on arrhythmia: Clinical evaluations and network pharmacology
Lijuan Wang, Helin Sun, Meina Yang, Yulin Xu, Linlin Hou, Haomiao Yu, Xueyin Wang, Zhongwen Zhang and Jinxiang Han

23 Exosomes in pathogenesis, diagnosis, and treatment of pulmonary fibrosis
Yang Yang, Yufei Liu, Yilu Chai, Ke Liu, Wei Hu, Keni Zhao, Yi Zhu, Peiyang Gao, Qingsong Huang and Chuantao Zhang

39 Effectiveness and mechanism of metformin in animal models of pulmonary fibrosis: A preclinical systematic review and meta-analysis
Xuanyu Wu, Xiang Xiao, Xinyu Chen, Maoyi Yang, Zhipeng Hu, Sijia Shuai, Qinwei Fu, Han Yang and Quanyu Du

62 Heidihuangwan alleviates renal fibrosis in rats with 5/6 nephrectomy by inhibiting autophagy
Ying-Ying Li, Zeng-Hui Tian, Guang-Hui Pan, Ping Zhao, De-Jun Pan, Jun-Qing Zhang, Li-Ying Ye, Fa-Rong Zhang and Xiang-Dong Xu

81 Lactacystin-induced kidney fibrosis: Protection by melatonin and captopril
Kristina Repova, Peter Stanko, Tomas Baka, Kristina Krajcirovicova, Silvia Aziriova, Jaroslav Hrenak, Andrej Barta, Stefan Zorad, Russel J. Reiter, Michaela Adamcova and Fedor Simko

92 Salusin-β, a TOR2A gene product, promotes proliferation, migration, fibrosis, and calcification of smooth muscle cells and accelerates the imbalance of vasomotor function and vascular remodeling in monocrotaline-induced pulmonary hypertensive rats
Xingxing Wang, Aidong Chen, Ruihua Hu, Feng Zhang, Shuxin Liang, Changlei Bao, Xuanxuan Liu, Haiyang Tang and Ying Han

110 Predictive value of myocardial strain on myocardial infarction size by cardiac magnetic resonance imaging in ST-segment elevation myocardial infarction with preserved left ventricular ejection fraction
Qiang Wang, Jian Wang, Yingjie Ma, Peng Wang, Yang Li, Jing Tian, Xiuzheng Yue, Guohai Su and Bin Li

121 ADAM17 knockdown mitigates while ADAM17 overexpression aggravates cardiac fibrosis and dysfunction *via* regulating ACE2 shedding and myofibroblast transformation
Jing Cheng, Fei Xue, Cheng Cheng, Wenhai Sui, Meng Zhang, Lei Qiao, Jing Ma, Xiaoping Ji, Wenqiang Chen, Xiao Yu, Bo Xi, Feng Xu, Guohai Su, Yuxia Zhao, Panpan Hao, Yun Zhang and Cheng Zhang

135 Therapeutic potential of topical administration of acriflavine against hypoxia-inducible factors for corneal fibrosis
Shuyan Zhu, Huimin Shan, Jianqiao Li, Lijie Pan, Shudan Wang, Jing Zhu, Hui Guo, Fenghua Mi, Xinyi Wu, Jia Yin and Kunpeng Pang

146 Corrigendum: Therapeutic potential of topical administration of acriflavine against hypoxia-inducible factors for corneal fibrosis
Shuyan Zhu, Huimin Shan, Jianqiao Li, Lijie Pan, Shudan Wang, Jing Zhu, Hui Guo, Fenghua Mi, Xinyi Wu, Jia Yin and Kunpeng Pang

148 Bariatric surgery for diabetic comorbidities: A focus on hepatic, cardiac and renal fibrosis
Huanxin Ding, Yun Zhang, Xiaomin Ma, Zhongwen Zhang, Qian Xu, Chuxuan Liu, Bingjun Li, Shuohui Dong, Linchuan Li, Jiankang Zhu, Mingwei Zhong and Guangyong Zhang

159 The role of p53 in liver fibrosis
Siyu Yu, Guang Ji and Li Zhang

166 Reappraisal of fibrosis-4 index and non-alcoholic fatty liver disease fibrosis score for advanced fibrosis in average-risk population
Huiyul Park, Eileen L. Yoon, Mimi Kim, Jonghyun Lee, Seon Cho, Dae Won Jun and Eun-Hee Nah

176 Metabolic reprogramming of pulmonary fibrosis
Jiaxin Li, Xiaoxuan Zhai, Xiao Sun, Shengchuan Cao, Qiuhuan Yuan and Jiali Wang

194 The effect of the cyclic GMP-AMP synthase-stimulator of interferon genes signaling pathway on organ inflammatory injury and fibrosis
Yuliang Liu, Yihui Li, Li Xue, Jie Xiao, Pengyong Li, Wanlin Xue, Chen Li, Haipeng Guo and Yuguo Chen

208 Molecular profiling of urinary extracellular vesicles in chronic kidney disease and renal fibrosis
Melanie Tepus, Elisa Tonoli and Elisabetta A. M. Verderio

230 Emodin ameliorates renal injury and fibrosis *via* regulating the miR-490-3p/HMGA2 axis
Liulin Wang, Xuerui Wang, Gang Li, Shanshan Zhou, Rui Wang, Qi Long, Min Wang, Liang Li, Hai Huang and Yuanming Ba

243 Post-myocardial infarction fibrosis: Pathophysiology, examination, and intervention
Xiaoying Yin, Xinxin Yin, Xin Pan, Jingyu Zhang, Xinhui Fan, Jiaxin Li, Xiaoxuan Zhai, Lijun Jiang, Panpan Hao, Jiali Wang and Yuguo Chen

frontiers | Frontiers in Pharmacology

TYPE Editorial
PUBLISHED 15 May 2023
DOI 10.3389/fphar.2023.1201830

Check for updates

OPEN ACCESS

EDITED BY
Filippo Drago,
University of Catania, Italy

REVIEWED BY
Carol M. Artlett,
Drexel University, United States
Ling Lin,
The Pennsylvania State University, United States

*CORRESPONDENCE
Panpan Hao,
panda.how@sdu.edu.cn
Yuxia Zhao,
yxzhao@sdu.edu.cn

RECEIVED 07 April 2023
ACCEPTED 09 May 2023
PUBLISHED 15 May 2023

CITATION
Liu Y, Xu J, Zhao Y and Hao P (2023), Editorial: Fibrosis: etiology, pathophysiology, measurements, and therapy.
Front. Pharmacol. 14:1201830.
doi: 10.3389/fphar.2023.1201830

COPYRIGHT
© 2023 Liu, Xu, Zhao and Hao. This is an open-access article distributed under the terms of the Creative Commons Attribution License (CC BY). The use, distribution or reproduction in other forums is permitted, provided the original author(s) and the copyright owner(s) are credited and that the original publication in this journal is cited, in accordance with accepted academic practice. No use, distribution or reproduction is permitted which does not comply with these terms.

Editorial: Fibrosis: etiology, pathophysiology, measurements, and therapy

Yanping Liu[1,2], Jiupan Xu[2], Yuxia Zhao[3]* and Panpan Hao[2]*

[1]Department of Radiology, Qilu Hospital of Shandong University, Jinan, Shandong, China, [2]National Key Laboratory for Innovation and Transformation of Luobing Theory, The Key Laboratory of Cardiovascular Remodeling and Function Research, Chinese Ministry of Education, Chinese National Health Commission and Chinese Academy of Medical Sciences, Department of Cardiology, Qilu Hospital of Shandong University, Jinan, Shandong, China, [3]Department of Traditional Chinese Medicine, Qilu Hospital of Shandong University, Jinan, Shandong, China

KEYWORDS

fibrosis, ADAM17, melatonin, emodin, salusin-β, hypoxia-inducible factor (HIF)

Editorial on the Research Topic
Fibrosis: etiology, pathophysiology, measurements, and therapy

Various stress injuries can cause organ fibrosis, depending on different pathogeneses and mechanisms. Excessive fibrosis aggravates pathological remodeling and functional deterioration of kidney, heart, lung, liver, etc. Progress has been made in the diagnosis and treatment of fibrosis; for example, the N-terminal propeptide of collagen type I and the amino-terminal peptide of procollagen type III have been shown to correlate with inflammation and fibrosis in the liver but not specifically with the liver (Lurie et al., 2015). In the absence of specific therapeutic targets, circulating biomarkers, and imaging techniques, fibrosis research is challenging.

For this Research Topic, we collected 7 review articles, 8 original research papers, and 2 meta-analyses in the field of organ fibrosis. One review (Yang et al.) focused on endogenous exosomes, as small extracellular vesicles, in the development, evaluation, and treatment of pulmonary fibrosis. Endogenous exosomes are involved in intercellular communication by delivering cellular cargoes to recipient cells, including nucleic acids, functional proteins, metabolites, etc., and in numerous biological processes, such as inflammation, extracellular matrix deposition, and epithelial-mesenchymal transition, showing promise for the evaluation and treatment of pulmonary fibrosis. Another review (Tepus et al.) examined the possibility of using extracellular vesicles to evaluate renal fibrosis. Molecular profiling data showed that extracellular vesicles have potential diagnostic and therapeutic value in chronic kidney disease. Techniques for the application of extracellular vesicles are not yet mature, as there are still obstacles in obtaining, preserving, and loading extracellular vesicles. Simplified and reproducible methods need to be explored for clinical application of extracellular vesicles, especially exosomes. Li et al. summarized novel mechanisms and therapeutic targets for metabolic reprogramming in myofibroblasts, endothelial cells, alveolar epithelial cells and macrophages during pulmonary fibrosis. How the tumor suppressor p53 is involved in the development and progression of liver fibrosis was discussed by Yu et al. Targeted regulation of p53 may be effective in the treatment of liver fibrosis. According to a review article (Liu et al.), cGAS/STING helps the body fight harmful factors, such as microorganisms and cancer, while many reports show the flip side that cGAS/STING enhances immunopathological responses and injury. cGAS/STING overactivation exacerbates immunopathological damage and fibrosis,

contributing to a new potential target for fibrosis assessment and intervention. Ding et al. reviewed the effects of bariatric surgery on cardiac, hepatic and renal comorbidities in patients with type 2 diabetes mellitus and the possible mechanisms. Clinical evidence shows that bariatric surgery is superior to drug therapy in terms of glycemic control and organ fibrosis, and that bariatric surgery has long-term benefits for cardiac, hepatic, renal, and other organ function by reversing fibrosis. Thus, bariatric surgery is recommended for the treatment of severely obese patients with type 2 diabetes. Yin et al. discussed the pathophysiology, evaluation, and intervention of postinfarction myocardial fibrosis. Regional fibrosis in infarcted zones and collagen deposition in noninfarcted zones promote pathological ventricular remodeling. Reperfusion in combination with new drugs such as angiotensin receptor neprilysin inhibitors and sodium/glucose cotransporter 2 inhibitors, as well as mineralocorticoid receptor antagonists and β-adrenoceptor antagonists, counteracts pathological ventricular remodeling and delays heart failure. Promising therapeutic options such as anti-inflammatory agents, bone marrow-derived cells, and microRNAs are being explored.

Six preclinical studies addressed the mechanisms and therapeutic strategies for organ fibrosis (Figure 1). Among them, three studies investigated therapeutic strategies for renal fibrosis (Li et al.; Repova et al.; Wang et al.). One herbal formulation, Heidihuangwan, was shown to improve renal fibrosis and functional deterioration in rats with 5/6 nephrectomy (Li et al.). Heidihuangwan inhibited autophagy through increasing insulin-like growth factor 1 level and its binding to its specific receptor and activating the PI3K/Akt signaling pathway, resulting in attenuation of renal fibrosis. Another study investigated whether lactacystin induces fibrotic renal remodeling and how melatonin and captopril affect these changes (Repova et al.). Lactacystin damaged rat kidneys, and treatment with melatonin or captopril increased glomerular density, decreased glomerular tuft area, and decreased hydroxyproline levels in kidneys. Melatonin or captopril therapy decreased intraglomerular and tubulointerstitial collagen I and III. Because melatonin did not lower blood pressure, the antifibrotic effect was probably achieved by its direct and pleiotropic actions. Considering the results on cardiac fibrosis from other studies and renal fibrosis from this experiment, the model of cardiorenal injury and fibrosis established using lactacystin is promising. In the third study (Wang et al.), investigators examined the role of emodin in renal fibrosis and the underlying mechanisms using a mouse model with unilateral ureteral obstruction and a rat renal tubule epithelial cell line stimulated with TGF-β1. Emodin increased miR-490-3p level, decreased high migration protein A2 level, and attenuated TGF-β1-dependent fibrosis.

With regard to cardiac fibrosis, Cheng et al. found that knockdown of ADAM17 attenuated left ventricular fibrosis and functional deterioration in diabetic mice, whereas overexpression of ADAM17 exacerbated it by shearing angiotensin-converting enzyme 2, downregulating angiotensin-(1–7) production and promoting myofibroblast transformation via the TGF-β1/Smad3 pathway. Targeted regulation of ADAM17/angiotensin-converting enzyme 2/angiotensin-(1–7) may be a promising approach to prevent and treat pathological ventricular remodeling.

A study by Wang et al. confirmed the detrimental effect of salusin-β on monocrotaline-induced pulmonary vascular remodeling. Increased salusin-β activity in pulmonary arteries of rats with pulmonary hypertension contributes to pulmonary artery smooth muscle cell proliferation and migration and vascular remodeling through upregulation of reactive oxygen species.

In a study by Zhu et al., a mouse model with mechanical corneal injury was used to investigate the effects of acriflavine, an inhibitor of hypoxia-inducible factor (HIF) dimerization, on corneal fibrosis and transparency. The results showed that inhibiting HIF alleviated corneal fibrosis and transparency in mechanically injured corneal stroma. Acriflavine inhibited corneal fibrosis by downregulating the TGF-β1 signaling pathway and myofibroblast transformation. In addition, inhibiting HIF also downregulated fibronectin level, which did not depend on the TGF-β1 pathway.

A preclinical meta-analysis (Wu et al.) evaluated the effects of metformin on pulmonary inflammation and fibrosis score in animal models of pulmonary fibrosis. The results showed that metformin can ameliorate pulmonary fibrosis in animals by activating AMPK, reducing TGF-β levels and phosphorylation of Smad2/3 and ERK1/

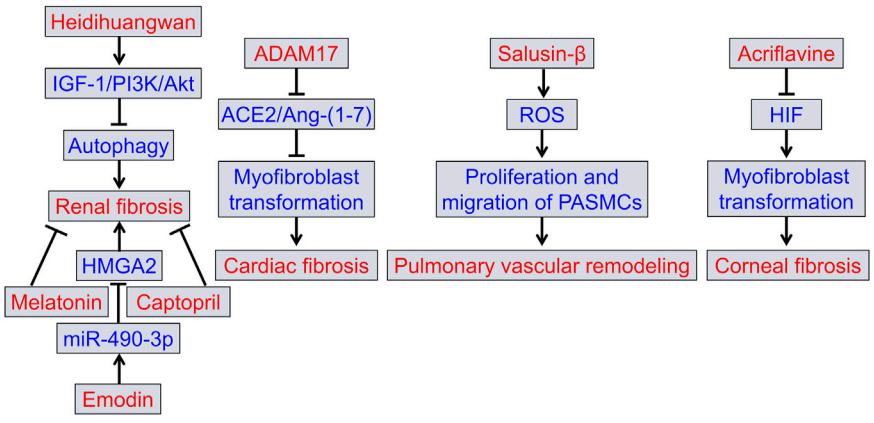


FIGURE 1
Summary of the preclinical studies in this Research Topic. ACE2, angiotensin-converting enzyme 2; ADAM17, a disintegrin and metalloprotease domain family protein 17; Ang-(1–7), angiotensin-(1–7); HIF, hypoxia-inducible factor; HMGA2, high mobility protein A2; IGF-1, insulin-like growth factor 1; PASMCs, pulmonary arterial smooth muscle cells; ROS, reactive oxygen species.

2, and inhibiting fibroblast proliferation and differentiation, epithelial-mesenchymal transition, and inflammation.

This Research Topic included two retrospective clinical studies, one of which examined the relationship between myocardial strain and infarct size in patients with preserved systolic function after myocardial infarction (Wang et al.). The global circumferential strain determined by cardiac magnetic resonance imaging had higher diagnostic accuracy than the global longitudinal strain in assessing infarct size. Park et al. analyzed magnetic resonance elastography of 6215 subjects at average risk for liver fibrosis. The diagnostic value of fibrosis-4 was confirmed to be better than the fibrosis score for nonalcoholic fatty liver disease in screening for liver fibrosis in such average-risk populations.

The efficacy of cordyceps in patients with cardiac arrhythmias and the identification of possible mechanisms have been studied using meta-analysis and network pharmacology (Wang et al.). Cordyceps improves sinus node and atrioventricular conduction by regulating PI3K/Akt and adrenergic signalling pathways in patients with cardiac arrhythmias, with no apparent side effects.

In conclusion, the broad coverage of this Research Topic opens numerous new perspectives on molecular mechanisms, evaluation, and therapeutic approaches in organ fibrosis.

Reference

Lurie, Y., Webb, M., Cytter-Kuint, R., Shteingart, S., and Lederkremer, G. Z. (2015). Non-invasive diagnosis of liver fibrosis and cirrhosis. *World J. Gastroenterol.* 21 (41), 11567–11583. doi:10.3748/wjg.v21.i41.11567

Author contributions

All authors listed have made a substantial, direct, and intellectual contribution to the work and approved it for publication.

Conflict of interest

The authors declare that the research was conducted in the absence of any commercial or financial relationships that could be construed as a potential conflict of interest.

Publisher's note

All claims expressed in this article are solely those of the authors and do not necessarily represent those of their affiliated organizations, or those of the publisher, the editors and the reviewers. Any product that may be evaluated in this article, or claim that may be made by its manufacturer, is not guaranteed or endorsed by the publisher.

frontiers | Frontiers in Pharmacology

TYPE Original Research
PUBLISHED 19 August 2022
DOI 10.3389/fphar.2022.948173

Check for updates

OPEN ACCESS

EDITED BY
Yanping Liu,
Shandong University, China

REVIEWED BY
Mingming Cao,
The First Affiliated Hospital of Harbin Medical University, China
Ming Lu,
Capital Medical University, China

*CORRESPONDENCE
Zhongwen Zhang,
zhangzhongwen@sdu.edu.cn
Jinxiang Han,
samshjx@sina.com

†These authors have contributed equally to this work and share the first authorship.

SPECIALTY SECTION
This article was submitted to Experimental Pharmacology and Drug Discovery, a section of the journal Frontiers in Pharmacology

RECEIVED 19 May 2022
ACCEPTED 18 July 2022
PUBLISHED 19 August 2022

CITATION
Wang L, Sun H, Yang M, Xu Y, Hou L, Yu H, Wang X, Zhang Z and Han J (2022), Bidirectional regulatory effects of Cordyceps on arrhythmia: Clinical evaluations and network pharmacology. *Front. Pharmacol.* 13:948173. doi: 10.3389/fphar.2022.948173

COPYRIGHT
© 2022 Wang, Sun, Yang, Xu, Hou, Yu, Wang, Zhang and Han. This is an open-access article distributed under the terms of the Creative Commons Attribution License (CC BY). The use, distribution or reproduction in other forums is permitted, provided the original author(s) and the copyright owner(s) are credited and that the original publication in this journal is cited, in accordance with accepted academic practice. No use, distribution or reproduction is permitted which does not comply with these terms.

Bidirectional regulatory effects of Cordyceps on arrhythmia: Clinical evaluations and network pharmacology

Lijuan Wang[1†], Helin Sun[1†], Meina Yang[2,3†], Yulin Xu[4], Linlin Hou[5], Haomiao Yu[2], Xueyin Wang[6], Zhongwen Zhang[2*] and Jinxiang Han[4*]

[1]Department of Endocrinology and Metabolism, Affiliated Hospital of Weifang Medical University Weifang China, Shandong Provincial Qianfoshan Hospital & The First Affiliated Hospital of Shandong First Medical University, Neck-Shoulder and Lumbocrural Pain Hospital of Shandong First Medical University, Jinan, China, [2]Department of Endocrinology and Metabolism, The First Affiliated Hospital of Shandong First Medical University, Jinan, China, [3]NHC Key Laboratory of Biotechnology Drugs(Shandong Academy of Medical Sciences), Biomedical Sciences College, Shandong First Medical University, Jinan, China, [4]Key Laboratory of Biotechnology Drug (Shandong Academy of Medical Sciences), Biomedical Sciences College and Shandong Medicinal Biotechnology Centre, Shandong First Medical University and Shandong Academy of Medical Sciences, Jinan, China, [5]Ambulatory Surgery Centers, Tai'an City Central Hospital, Tai'an, China, [6]Department of Endocrinology and Metabolism, Affiliated Hospital of Weifang Medical University, Weifang, China

Background: Cordyceps is a precious Chinese herbal medicine with rich bioactive ingredients and is used for regulating arrhythmia alongside routine treatments. However, the efficacy and potential mechanisms of Cordyceps on patients with arrhythmia remain unclear.

Methods: Randomized controlled trials of bradycardia treatment with Cordyceps were retrieved from diverse databases and available data. Dichotomous variables were expressed as a risk ratio (RR) with a 95% confidence interval (CI). Continuous variables were expressed as a standardized mean difference (SMD) with a 95% CI. Network pharmacology was used to identify potential targets of Cordyceps for arrhythmia. Metascape was used for gene ontology (GO) and genome (KEGG) pathway enrichment analysis.

Results: Nineteen trials included 1,805 patients with arrhythmia, of whom 918 were treated with Ningxinbao capsule plus routine drugs, and, as a control, 887 were treated with only routine drugs. Six trials reported on bradycardia and the other 13 on tachycardia. Treatment with Cordyceps significantly improved the total efficacy rate in both bradycardia (RR = 1.24; 95% CI, 1.15 to 1.35; P_z <0.00001) and tachycardia (RR = 1.27; 95% CI, 1.17 to 1.39; P_z <0.00001). Cordyceps also had beneficial secondary outcomes. No serious adverse events occurred in patients treated with Cordyceps. The results of KEGG pathway enrichment analysis were mainly connected to adrenergic signaling in cardiomyocytes and the PI3K-Akt signaling pathway. IL6, TNF, TP53, CASP3, CTNNB1, EGF, and NOS3 might be key targets for Cordyceps in the treatment of arrhythmia.

Conclusion: This study confirmed that Cordyceps has a certain positive effect on the treatment of arrhythmia and that its main mechanism may be through the regulation of adrenergic signaling in cardiomyocytes and the PI3K-Akt signaling pathway.

KEYWORDS

cordyceps, traditional Chinese medicine, arrhythmia, network pharmacology, meta-analysis

1 Introduction

Cardiovascular disease takes the lives of 17.7 million people every year, accounting for 31% of all global deaths, and this number will possibly rise to 23.6 million by 2030 (Borghi et al., 2018). Cardiac arrhythmias are mostly found in patients with organic cardiovascular diseases and are abnormalities or disturbances in the normal activation or beating of the heart muscles (Fu, 2015). Arrhythmias are a set of life-threatening cardiovascular diseases that can be divided into two types: bradyarrhythmias and tachyarrhythmias (Hategan et al., 2017; Black et al., 2019). Although the therapies for arrhythmias have attracted much attention, the efficacy and safety of modern medicines in the treatment of this disease are not satisfactory. Treatment with anti-arrhythmia drugs is not proven to reduce mortality, and the side effects of anti-arrhythmia drugs in patients' digestive and cardiovascular systems have been brought to the forefront (Hao et al., 2015).

In recent years, with the development of evidence-based studies, the effects of traditional Chinese medicine (TCM) have been further confirmed and valued. Chinese herbs and herbal formulas have been used for arrhythmia since the 1970s (Hao et al., 2015; Hao et al., 2017). Herbal formulas can improve symptoms and adjust the heart rate to a normal level in patients with arrhythmia (Liu et al., 2018). Cordyceps, under the trade name "Ningxinbao capsule"—a liquid submerged fermentation of dry mycelium powder (Hao et al., 2017; Hategan et al., 2017)—is a standardized traditional Chinese medication that is widely used in the arrhythmia treatment, including for atrioventricular block, refractory bradycardia, and conduction block (Zhang et al., 2017; Das et al., 2020). However, there is no credible scientific evidence supporting the use of Cordyceps in treating and preventing arrhythmia. Currently available randomized controlled trials (RCTs) are limited to small sample sizes with inconsistent outcomes. Drawing authoritative conclusions about the genuine benefits and possible side effects is thus difficult. Network pharmacology has become a new approach to drug mechanism research and drug development. In recent years, a variety of related databases and tools have provided crucial support for TCM network pharmacology (Zhang et al., 2019). We thus performed this meta-analysis to estimate the effectiveness and safety of Cordyceps compared to contemporary anti-arrhythmia drugs and placebos, by assessing total effectiveness rates, improvement in symptoms, changes in heart rates, and the incidence of drug-related adverse effects. Network pharmacology was also used to identify the potential mechanisms of Cordyceps for treating arrhythmia.

2 Materials and methods

2.1 Meta-analysis

2.1.1 RCT preparation

Literature was retrieved from the PubMed Database, the China National Knowledge Infrastructure (CNKI), the Wanfang Database, the China Scientific Journal Database (VIP), and the Chinese Biomedicine Literature Service System (SinoMed). Published review articles, editorials, and information from the internet (http://www.clinicaltrialresults.org, http://www.clinicaltrials.gov, and http://www.theheart.org), were also considered, covering the period from the earliest possible date up to December 30, 2021. Bradyarrhythmia, which is basically a heart rate below 60 beats per minute, can be due to sinus, atrial or junctional bradycardia, or problems with the conduction system, e.g., sinus bradycardia, sinoatrial block, atrioventricular block, and others (Kumar et al., 2012; Sidhu and Marine, 2020). Tachyarrhythmia, usually defined as a heart rate of more than 100 beats per minute, mainly involves premature beat, atrial flutter, atrial fibrillation, and so on (Boateng, 2013; Sagris et al., 2021). The search algorithms for PubMed were as follows: "Ningxinbao," "Cordyceps," AND ("arrhythmia" or "arrhythmia" or "bradyarrhythmia" or "bradycardia" or "sinoatrial block" or "sinus arrest" or "atrioventricular block" or "sick sinus syndrome" or "tachyarrhythmia" or "tachycardia" or "premature beat" or "premature ventricular contractions" or "tachycardia" or "flutter" or "fibrillation"), AND "randomized," AND "blind," with no restriction on subheadings. Similar but appropriate search terms were used for other literature databases or search engines. The reference lists of all included articles were searched for other relevant citations, and articles not included in the above electronic databases were checked manually. Whenever necessary, the authors of the included trials were contacted for additional information. Available citations were searched and selected by two authors (L. J. and H. L.) independently and in duplicate; two authors (L. J. and H. L.) abstracted data and assessed the methodological quality of the trials.

2.1.2 Inclusion and exclusion criteria of the studies

The inclusion criteria were as follows: 1) Study subjects were diagnosed as arrhythmic according to the corresponding guidelines. 2) All patients were randomized to receive treatment with Ningxinbao and contemporary medications, or contemporary medications only. 3) The sample size in each study group was ≥10 cases. 4) Follow-up in each study group was ≥2 weeks. 5) Quantitative measurements of surrogate endpoints and/or adverse cardiovascular events and/or adverse drug effects were available to facilitate outcome analysis.

Exclusion criteria were as follows: 1) Studies were non-randomized or non-blinded. 2) Patients enrolled had no definite diagnosis. 3) Different TCM medications were compared. 4) Studies reported only symptomatic changes in patients without objective laboratory measurements. 5) Methodological quality was poor with a Jadad score of <2.

2.1.3 Statistical analysis

RevMan 5.3.5 software (Cochrane Collaboration, London, United Kingdom) was used to synthesize the data. Continuous variables were expressed as mean difference (MD) with a 95% confidence interval (CI), and dichotomous variables as odds ratio (OR) with a 95% CI. Statistical significance was denoted by a two-tailed $p < 0.05$. Chi-square and I^2 tests were used to test the heterogeneity among trials. Moreover, the fail-safe number was used to estimate the extent of publication bias (Cheng et al., 2016).

2.2 Network pharmacology

2.2.1 Data collection

The ingredients of Cordyceps were collected from TCMSP (http://tcmspw.com/tcmsp.php), which is a system pharmacology platform designed for studying TCM comprehensively. Our condition was set with compounds OB ≥ 30%, DL ≥ 0.18, while some ingredients that did not meet the criteria, but had significant pharmacological activity were also selected for the next step. We retrieved the targets of tachyarrhythmia (atrial flutter, atrial fibrillation, premature ventricular beat, ventricular tachycardia, ventricular flutter, ventricular fibrillation, junctional escape and escape rhythm, nonparoxysmal junctional tachycardia, premature contraction of the atrioventricular junction, and sinus tachyarrhythmia), as well as the targets of bradyarrhythmia (sinus bradycardia, sinus arrest, sinoatrial block, atrioventricular block, intraventricular block, sick sinus syndrome) from GeneCards (https://www.genecards.org/), which are online servers for target identification. After gathering all the data, we took the intersections of Cordyceps and disease targets using the online drawing tool called Interactive Venn (http://www.interactivenn.net/).

2.2.2 Protein–protein interaction network construction

The PPI network of the genes was constructed using STRING (https://string-db.org/cgi/input.pl). The protein interaction network was downloaded from its "string_interactions.tsv" format file. For the list of names, we used common targets of Cordyceps with tachyarrhythmia and bradyarrhythmia. After finishing construction, we hid disconnected nodes in the network. Cytoscape 3.9 was used to build the protein-protein interaction network construction.

2.2.3 Functional and pathway enrichment analysis

For the biological and functional annotation of the genes within each herb-disease-target network and PPI, gene ontology (GO) analysis and Kyoto Encyclopedia of Genes and Genomes (KEGG) pathway enrichment analysis were performed using Metascape (http://www.metascape.org/). The function activities and the pathways were ranked by their nominal p values with a cut-off of 0.05.

2.3 Molecular docking

The 2D structural information was downloaded from the PubChem database (https://pubchem.ncbi.nlm.nih.gov/), and its mechanical structure was optimized by Chem3D software. The Uniprot database (https://www.uniprot.org/) was searched, and the 3D structures regulating the candidate target proteins in the PDB database were downloaded (http://www.rcsb.org/). Autodock tools 1.5.6 (http://autodock.Scripps.Edu/resources/tools) were used for water removal and hydrogenation, for calculating Gasteiger charge, and storing targets and bioactive components as a "pdbqt" format file. The binding conformations were visualized by PyMOL 2.4.0 and Discovery Studio 2019. A flowchart of the network pharmacology study is given in Figure 1.

3 Results

3.1 Pooled analysis

3.1.1 Study characteristics

In the end, 19 RCTs were included, all of which were published in Chinese. Six trials reported on bradyarrhythmia; the other 13 on tachyarrhythmia. The characteristics of the eligible 19 RCTs are listed in Table 1. The sample sizes ranged from 20 to 180 participants. The 19 RCTs enrolled 1,805 participants, of whom 918 were treated with Ningxinbao capsule plus routine drugs, and, as the control, 887 were treated with only routine drugs. The dosage of Ningxinbao capsule was 0.25 g thrice daily in one trial, and 0.5 g thrice daily in the others.

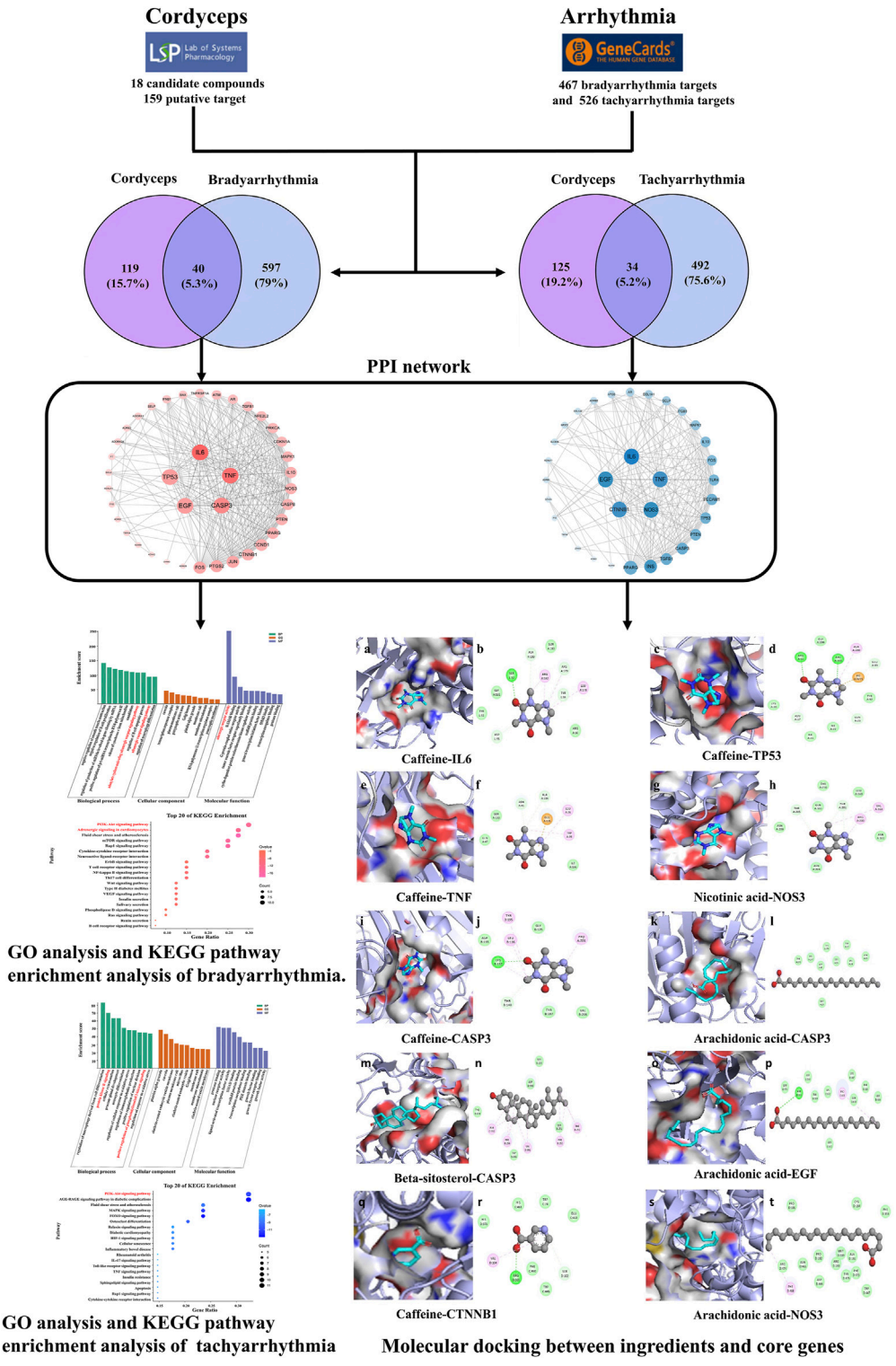


FIGURE 1
Flow chart investigating Cordyceps in the treatment of arrhythmia.

TABLE 1 Meta-analysis of arrhythmia patients' treatment with Cordyceps.

Category	*n*	Participants, n (cases/controls)	Heterogeneity	RR (95%CI)	Z-test
			P_h I^2 (%)		
Effective rate					
Bradyarrhythmia	5	236/225	0.18 37	1.24 (1.15–1.35)	z = 5.42; P_z <0.00001
Ventricular arrhythmia	5	259/257	0.08 51	1.27 (1.17–1.39)	z = 5.51; P_z <0.00001
Atrial arrhythmia	4	145/145	0.36 7	1.40 (1.20–1.63)	z = 4.24; P_z <0.0001
Multiple types of arrhythmias	4	182/176	<0.0001 88	1.34 (1.19–1.51)	z = 4.75; P_z <0.00001
Incidence of disease					
Ventricular premature beat	1	40/41	NA NA	0.34 (0.10–1.17)	z = 1.71; P_z = 0.09
Ventricular tachycardia	1	40/41	NA NA	1.02 (0.22–4.78)	z = 0.03; P_z = 0.97
Ventricular flutter	1	40/41	NA NA	0.51 (0.05–5.43)	z = 0.56; P_z = 0.58
Ventricular fibrillation	1	40/41	NA NA	0.13 (0.02–0.98)	z = 1.98; P_z = 0.05

P_z<0.05 shows a significant association. CI, confidence interval; NA, not available; RR, relative risk; Ph, *p*-values.

Treatment duration varied from 2 weeks to 1.5 years, and 16 trials used the efficacy rate as the primary outcome. Fourteen trials reported drug-related adverse reactions, including skin allergy, nausea, vomiting, abdominal discomfort, etc. All 19 trials were parallel group RCTs, the Jadad score was 4 in two trials, and 3 in the others.

3.1.2 Clinical endpoints

3.1.2.1 Bradyarrhythmia

A total of six trials (Zhang & Fan, 2009; Liu et al., 2014; Zeng, 2015; Zhong, 2016; Wang, 2017; Chen, 2018) reported on bradyarrhythmia, enrolling 641 participants, of whom 332 were treated with Ningxinbao capsule plus routine drugs, and, as the control, 309 were treated with only routine drugs. All the participants received routine treatments, including treating the primary disease, reducing blood pressure, decreasing myocardial oxygen consumption, improving myocardial blood supply, strengthening myocardial nutrition, and lipid regulation. The Jadad score was 4 in one trial (Zhong, 2016) and 3 in the others (Zhang & Fan, 2009; Liu et al., 2014; Zeng, 2015; Wang, 2017; Chen, 2018). Five trials used the effective rate as the primary outcome (Liu et al., 2014; Zeng, 2015; Zhong, 2016; Wang, 2017; Chen, 2018). Analyses from five eligible trials with 461 patients (236 in the Ningxinbao capsule groups and 225 in the control groups) exhibited a higher effectiveness rate in patients treated with Ningxinbao capsule plus routine therapy, compared with routine treatment alone (RR = 1.24; 95% CI, 1.15 to 1.35; z = 5.42; P_z < 0.00001; I^2 = 37%) (Table 1). Among the studies that provided a comparison, there was no significant difference in heart rate between the groups with and without Ningxinbao capsule after treatment. Pooled data from two trials (Zhang & Fan, 2009; Zeng, 2015) enrolling 272 patients (142 in Ningxinbao groups and 130 in control groups) indicated that the patients in the Ningxinbao groups had a significant increase in average heart rate (SMD = 1.10; 95% CI, 0.85 to 1.36; z = 8.44; P_z < 0.00001; I^2 = 0%) and minimal heart rate (SMD = 0.99; 95% CI, -0.49 to 2.46; z = 1.31; P_z = 0.19; I^2 = 97%), compared with the control groups (Table 2).

3.1.2.2 Tachyarrhythmia

A total of 13 trials (Xu & Zheng, 1992; Wang et al., 2002; Wang et al., 2009; Zhao, 2012; Wu, 2013; Tao et al., 2014; Li et al., 2016; Wang, 2016; Liu & Chen, 2018; Chen & Zhang, 2019; Cai et al., 2020; Wang, 2020; Cao et al., 2021) reported on tachyarrhythmia. enrolling 1,164 participants, of whom 586 were treated with Ningxinbao capsule plus routine drugs, and, as the control, 578 with only routine drugs. All the participants undertook routine treatment for both the primary disease and the relief of symptoms. Eleven trials (Xu & Zheng, 1992; Wang et al., 2002; Wang et al., 2009; Zhao, 2012; Wu, 2013; Li et al., 2016; Liu & Chen, 2018; Chen & Zhang, 2019; Cai et al., 2020; Wang, 2020; Cao et al., 2021) reported total effectiveness rate as an outcome measure, and our study demonstrates that the total effectiveness rate of the experimental group was higher than the control group, with the difference being statistically significant with obvious heterogeneity. Among the different types of tachyarrhythmia, including three subgroups, results were as follows: ventricular arrhythmia (RR = 1.27; 95% CI, 1.17 to 1.39; z = 5.51; P_z < 0.00001), atrial arrhythmia (RR = 1.40; 95% CI, 1.20 to 1.63; z = 4.24; P_z < 0.0001), and multiple types of arrhythmias (RR = 1.34; 95% CI, 1.19 to 1.51; z = 4.75; P_z < 0.00001) (Table 1).

Two trials (Wang et al., 2009; Cai et al., 2020) of 218 patients (110 in Ningxinbao groups and 108 in control groups), indicated that the patients in the Ningxinbao groups had a significant increase in average heart rate (SMD = −1.14; 95% CI, −2.83 to 0.56; z = 1.32; P_z = 0.19; I^2 = 0%) (Table 2).

TABLE 2 Meta-analysis of arrhythmia patients' treatment with Cordyceps.

Category	n	Participants, n (cases/controls)	Heterogeneity		SMD (95%CI)	Z-test
			P_h	I^2 (%)		
Average heart rate						
Bradyarrhythmia	2	142/130	0.92	0	1.10 (0.85–1.36)	z = 8.44; P_z<0.00001
Tachyarrhythmia	2	110/108	<0.00001	97	−1.14 (−2.83 to 0.56)	z = 1.32; P_z = 0.19
Minimal heart rate						
Bradyarrhythmia	2	142/130	<0.00001	97	0.99 (−0.49–2.46)	z = 1.31; P_z = 0.19
Inflammation index						
Hs-CRP	1	66/66	NA	NA	2.86 (2.37–3.35)	z = 11.46; P_z<0.00001
IL6	1	66/66	NA	NA	2.29 (1.84–2.73)	z = 10.15; P_z<0.00001
TNF	1	66/66	NA	NA	2.13 (1.70–2.56)	z = 9.72; P_z<0.00001

P_z<0.05 shows a significant association. CI, confidence interval; NA, not available; SMD, standardized mean difference; Ph, *p*-values.

One trial (Tao et al., 2014) reported the incidence of ventricular tachyarrhythmia, ventricular premature beat, ventricular flutter, and ventricular fibrillation during the Ningxinbao capsule treatment and follow-up. The result showed that the groups treated with Ningxinbao capsule had a greater reduction in the occurrence of ventricular premature beat (RR = 0.34; 95% CI, 0.10 to 1.17; z = 1.75; P_z = 0.09), ventricular tachyarrhythmia (RR = 1.02; 95% CI, 0.22 to 4.78; z = 0.03; P_z = 0.97), ventricular flutter (RR = 0.51; 95% CI, 0.05 to 5.43; z = 0.56; P_z = 0.58), and ventricular fibrillation (RR = 0.13; 95% CI, 0.02 to 0.98; z = 1.98; P_z = 0.05) (Table 1). One trial (Xu & Zheng, 1992) reported on the improvement of symptoms, and here the Ningxinbao capsule had a mild effect on relieving palpitation and chest distress caused by premature ventricular contraction (PVC). One trial (Cao et al., 2021) reported on a comparison of serum inflammatory factors between two groups that showed after 2 months of treatment that the levels of hs-CRP (SMD = 2.86; 2.37 to 3.35; z = 11.46; P_z < 0.00001), IL6 (SMD = 2.29; 1.84 to 2.73; z = 10.15; P_z< 0.00001), and TNF (SMD = 2.13; 1.70 to 2.56; z = 9.72; P_z <.00001) in the Ningxinbao capsule group were better than those in the control group (Table 2).

3.1.3 Adverse reactions

3.1.3.1 Bradyarrhythmia

Six trials on bradyarrhythmia (Zhang & Fan, 2009; Liu et al., 2014; Zeng, 2015; Zhong, 2016; Wang, 2017; Chen, 2018) reported drug-related adverse reactions. Three trials reported drug-related adverse events quantitatively (Zhong, 2016; Wang, 2017; Chen, 2018), and the results of these three trials showed that the incidence of adverse events in the Ningxinbao capsule group was 0%, 2.22%, and 0%, respectively, and the incidence of adverse events in the control group was 19.6%, 7.8%, and 17.9%, respectively. The incidence of adverse digestive system events in the Ningxinbao capsule group was significantly lower than in the control group.

3.1.3.2 Tachyarrhythmia

Eight trials reported drug-related adverse reactions quantitatively (Wang et al., 2002; Wu, 2013; Tao et al., 2014; Li et al., 2016; Wang, 2016; Chen & Zhang, 2019; Chen & Zhang, 2019; Cai et al., 2020; Cao et al., 2021), and a distinct difference was observed between the groups with and without the Ningxinbao capsule treatment in terms of adverse effect, which proved that the groups that included the Ningxinbao capsule had less adverse effects on patients' cardiovascular and digestive systems.

3.2 Network pharmacology

3.2.1 Data collection

Cordyceps, tachyarrhythmia, and bradyarrhythmia were selected for network pharmacology analysis. In total, 18 main ingredients from Cordyceps were described in the TCMSP database, and 159 related targets were collected. The main ingredients of Cordyceps are listed in Supplementary Table S2. We retrieved 526 and 467 genes from the GeneCards database for tachyarrhythmia and bradyarrhythmia, respectively. Cordyceps shared 34 common targets with bradyarrhythmia and 40 common targets with tachyarrhythmia. The intersections of Cordyceps and disease targets are displayed in Figure 2.

3.2.2 Protein–protein interaction network construction

In order to speculate on the role of targets in the disease, overlapping bradyarrhythmia and tachyarrhythmia targets were submitted to a string platform to establish the PPI network. Targets and interacting edges were sorted in descending order by degree, and arranged in a concentric circle according to a degree, as shown in Figure 3. After hiding disconnected nodes in the network, there were 40 targets with bradyarrhythmia and 33 with

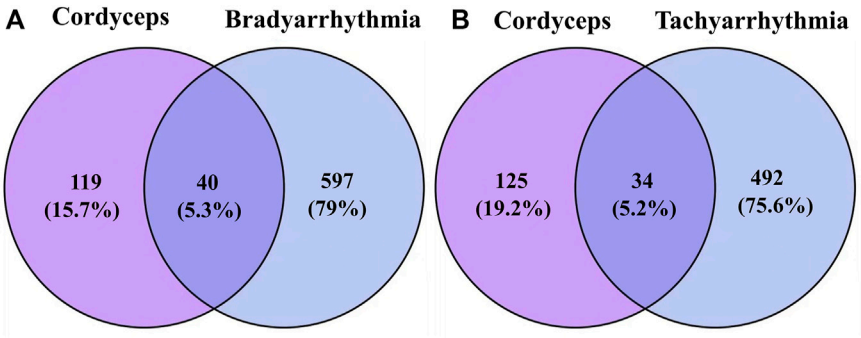


FIGURE 2
Venn diagram. **(A)** Purple stands for 159 targets of Cordyceps from TCMSP, blue stands for 526 targets of tachyarrhythmia, 40 in the central overlapping section are intersecting Cordyceps and bradyarrhythmia targets. **(B)** Purple stands for 159 targets of Cordyceps from TCMSP, blue stands for 647 targets of tachyarrhythmia, 34 in the central overlapping section are intersecting Cordyceps and tachyarrhythmia targets.

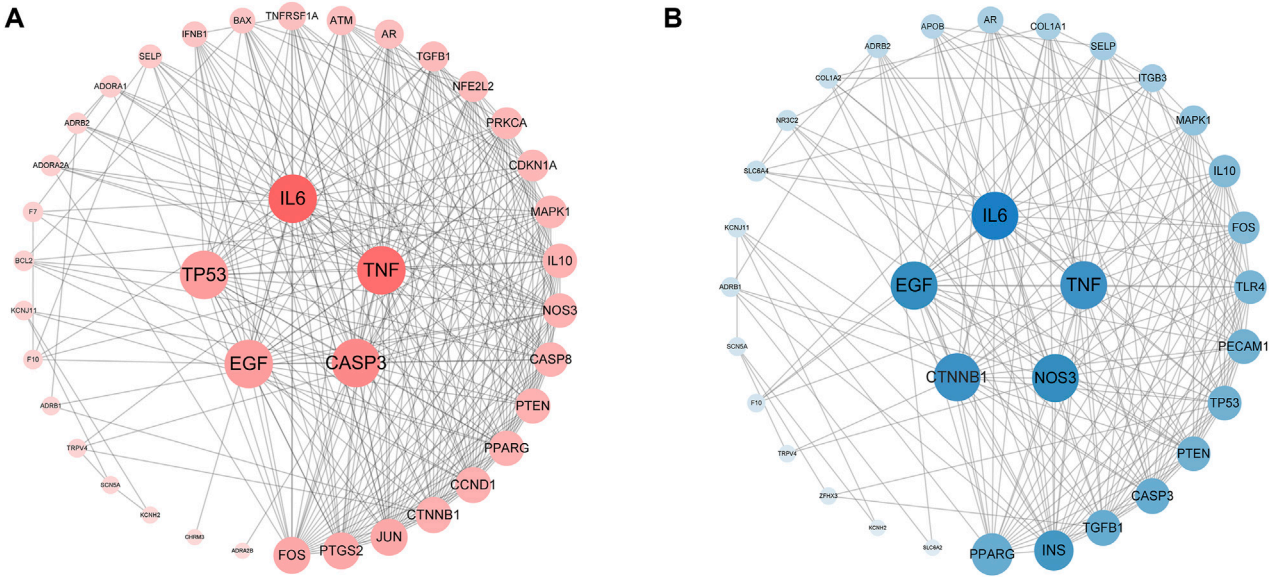


FIGURE 3
Protein–protein interaction network. **(A)** The pink nodes represent the targets of bradyarrhythmia; the PPI network structure of bradyarrhythmia has 40 nodes and 321 edges. **(B)** The blue nodes represent the targets of tachyarrhythmia; the PPI network structure of tachyarrhythmia has 33 nodes and 207 edges. The sizes of the nodes of the two images are illustrated from large to small in descending order of degree values.

tachyarrhythmia, with the targets in the innermost circle predicted to be important.

3.2.3 Functional and pathway enrichment analysis

GO functional analysis and KEGG pathway enrichment analysis were conducted to elucidate the biological effects on gene functions and signaling pathways of the related targets of Cordyceps in the treatment of arrhythmia. The top 10 GO items and top 20 KEGG pathways were selected based on the *p* values.

For bradyarrhythmia, the biological processes were mainly concentrated in negative regulation of smooth muscle contraction, negative regulation of B cell proliferation, regulation of production of miRNAs involved in gene silencing by miRNA, positive regulation of pri-miRNA transcription by RNA polymerase II, the release of cytochrome *c* from mitochondria, vasodilation, the adenylate cyclase-activating adrenergic receptor signaling pathway, regulation of the B cell apoptotic process, the adrenergic receptor signaling pathway, and regulation of macrophage

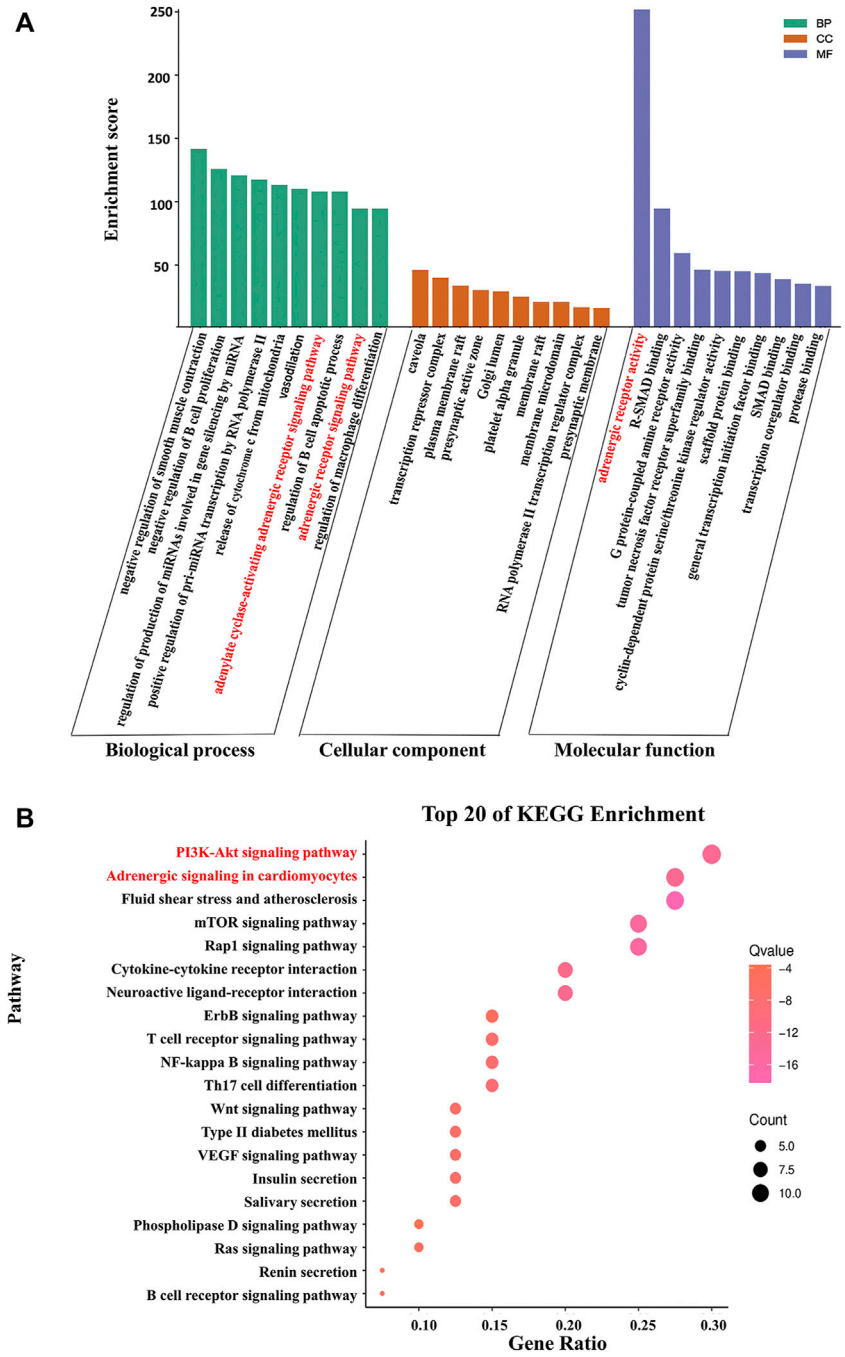


FIGURE 4
KEGG pathway enrichment analysis and GO functional enrichment analysis of Cordyceps in treating bradyarrhythmia. **(A)** GO functional analysis. The top 10 items of each part are shown. **(B)** KEGG pathway enrichment analysis. The sizes of the bubbles are illustrated from large to small in descending order of the number of potential targets involved in the pathway.

differentiation. The cellular components were mainly related to caveolae, the transcription repressor complex, the plasma membrane raft, and the presynaptic active zone. The molecular function was mainly enriched in adrenergic receptor activity, R-SMAD binding, and G protein-coupled amine receptor activity. KEGG pathway results showed that the top 20 pathways were mainly enriched in the PI3K-Akt signaling pathway, adrenergic signaling in cardiomyocytes, fluid shear stress and atherosclerosis, the mTOR signaling pathway, and the Rap1 signaling pathway (Figure 4).

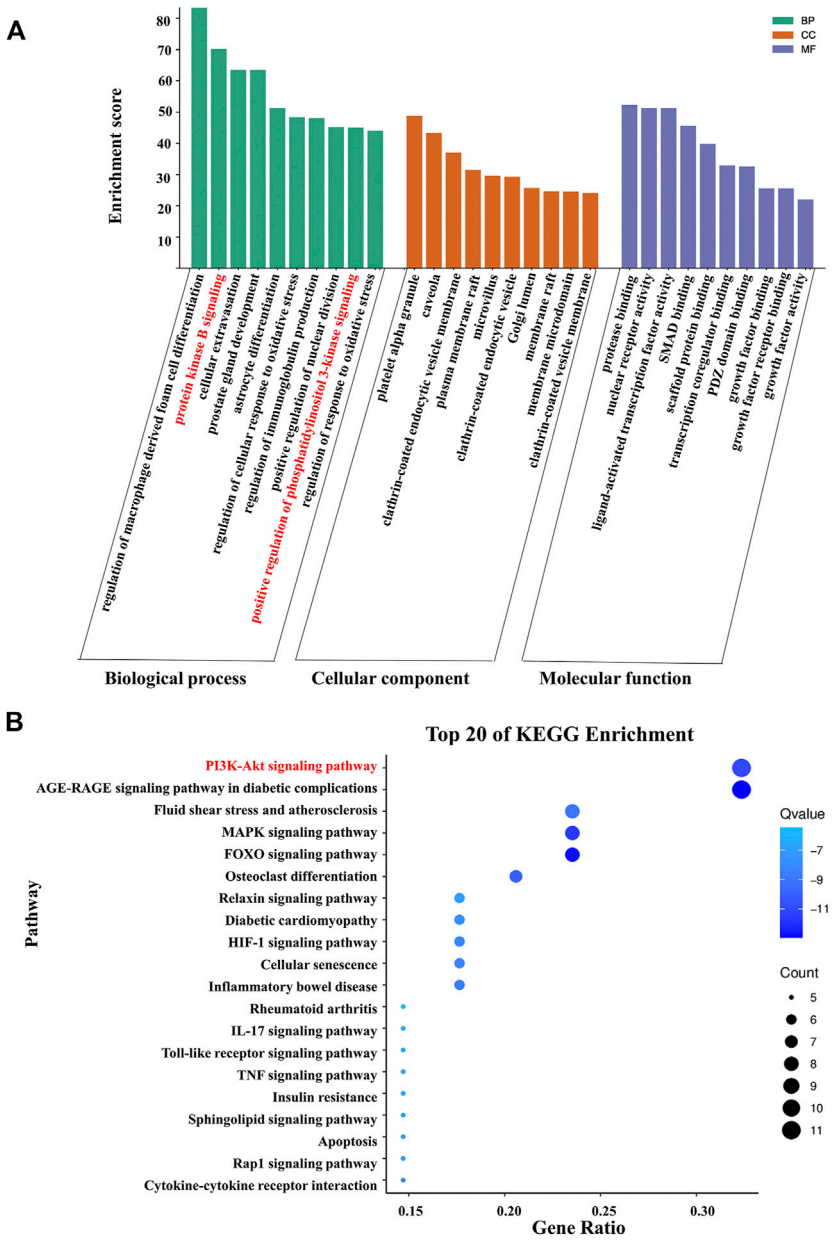


FIGURE 5
KEGG pathway enrichment analysis and GO functional enrichment analysis of Cordyceps in treating tachyarrhythmia. **(A)** GO functional analysis. The top 10 items of each part are shown. **(B)** KEGG pathway enrichment analysis. The sizes of the bubbles are illustrated from large to small in descending order of the number of potential targets involved in the pathway.

For tachyarrhythmia, the biological processes were mainly concentrated in the regulation of macrophage-derived foam cell differentiation, protein kinase B signaling, cellular extravasation, prostate gland development, astrocyte differentiation, regulation of cellular response to oxidative stress, regulation of immunoglobulin production, positive regulation of nuclear division, and positive regulation of phosphatidylinositol 3-kinase signaling. In terms of cellular components, the top 10 items were mainly related to platelet alpha granules, caveolae, the clathrin-coated endocytic vesicle membrane, and the plasma membrane raft. The molecular function was mainly enriched in protease binding, nuclear receptor activity, ligand-activated transcription factor activity, and SMAD binding. The KEGG

10.3389/fphar.2022.948173

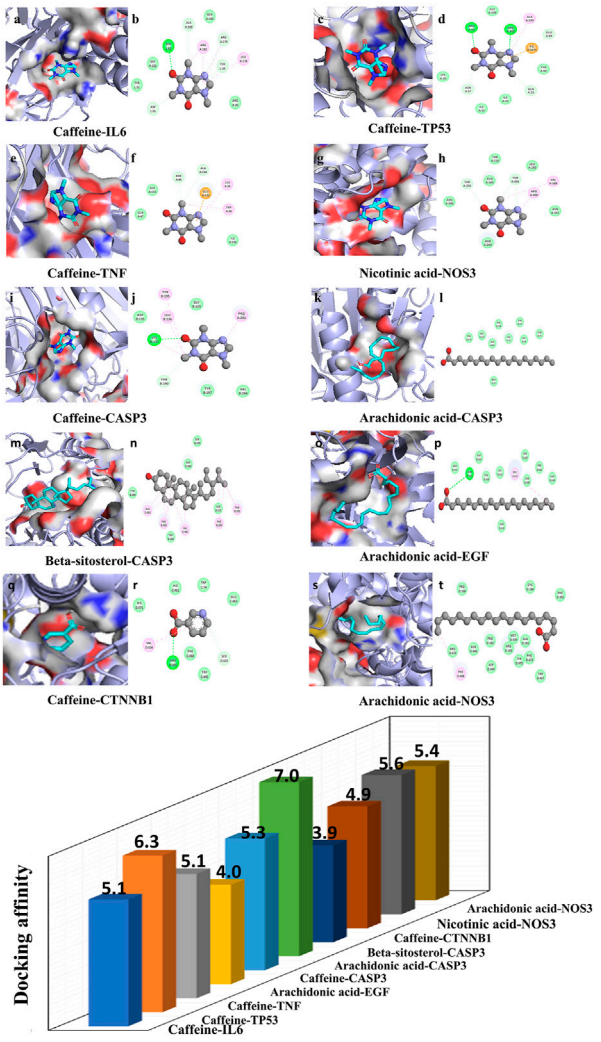


FIGURE 6
Molecular docking diagram. **(A)** Ten conformations of molecular docking simulation. Diagrams (3D) indicate that the molecular model of the compound is in the binding pocket of the protein. The compound is shown as a stick model with orange coloring. The amino acid residues surrounding are represented by surface style **(A,C,E,G,I,K,M,O,Q,S)**. Diagrams (2D) show the interactions between the compound and surrounding residues **(B,D,F,H,J,L,N,P,R,T)**. **(B)** The 3D column diagram shows the affinity of 10 conformations. *X*-axis: bioactive component, *Y*-axis: target names, *Z*-axis: docking affinity (absolute value of the binding energy). Taking the caffeine-IL6 docking, for example, the small molecule ligand caffeine potentially fits into the interface pocket formed by the interaction of amino acid residues in protein (Figure 6A). As shown in Figure 6 **(B)**, a hydrogen bond was formed with caffeine SER52 near the active site of IL6. The other essential residues (ASP55, TUR51, GLY101, ALA100, GLN183, ARG182, ARG179, TYR34, LEU178 and ARG30) through van der Waal's forces, carbon hydrogen bond, pi-donor hydrogen bond, pi–pi T-shaped, alkyl, and pi–alkyl. These forms of hydrogen bonds and interactions contribute to the stability of the binding of small molecules to the active sites of proteins.

pathway analysis revealed that common genes were mainly enriched in the PI3K-Akt signaling pathway, the AGE-RAGE signaling pathway in diabetic complications, fluid shear stress and atherosclerosis, the MAPK signaling pathway, and the FOXO signaling pathway (Figure 5).

3.3 Molecular docking

To confirm the valid bonding effects between ingredients of Cordyceps and key targets, molecular docking was performed by Autodock. The modes of 11 binding complexes are displayed in Figure 6, including caffeine-TNF docking (−5 kcal/mol), caffeine-IL6 docking (−5.1 kcal/mol), caffeine-TP53 docking (−6.3 kcal/mol), arachidonic acid-EGF docking (−4.0 kcal/mol), arachidonic acid-CASP3 docking (−3.9 kcal/mol), beta-sitosterol-CASP3 docking (−7.0 kcal/mol), caffeine-CASP3 docking (−5.3 kcal/mol), caffeine-CTNNB1(−4.9 kcal/mol), arachidonic acid-NOS3(−5.6 kcal/mol), and nicotinic acid-NOS3(−5.4 kcal/mol). The docking results are shown as molecular surface representations, which can effectively reflect the topical details of binding sites. The binding sites are shown in different colors on the protein surface, and hydrogen bonds are shown as dotted lines (Figure 6A). The absolute values of binding affinities (kcal/mol) of all docking patterns indicate a stable combination, and the details of the binding affinities are shown in Figure 6B.

4 Discussion

In this study, we investigated the efficacy, safety, and potential protective mechanism of Cordyceps in the treatment of arrhythmia. We found that Cordyceps could improve sinus node and atrioventricular conduction in patients with arrhythmia, without obvious adverse reactions. Its possible mechanism of protection is the modulation of adrenergic signaling in cardiomyocytes and the PI3K-Akt signaling pathway (Figure 7).

According to previous studies, the petroleum ether extract of Cordyceps improves the arrhythmia caused by aconitine, prolongs the induction time of arrhythmia, and reduces the duration and severity of arrhythmia in rats. The extract of Cordyceps also has an antagonistic effect on arrhythmia induced by barium chloride. The mechanism of its anti-arrhythmic action might involve the regulation of the transport of ion channels in the cell membrane (Mei et al., 1989). In our meta-analysis, Cordyceps exerts dual regulatory effects on arrhythmias. The underlying mechanisms of Cordyceps in the treatment of bradycardia are as follows: 1) Cordyceps not only increases the sinus heart rate but also improves the electrical activity of the sinus node and atrioventricular conduction. 2) Cordyceps could increase the blood flow of the heart and brain, improve microcirculation, and stabilize blood pressure. 3) Cordyceps might improve the activity of fibrinolytic enzymes, promote fibrinolysis, and reduce

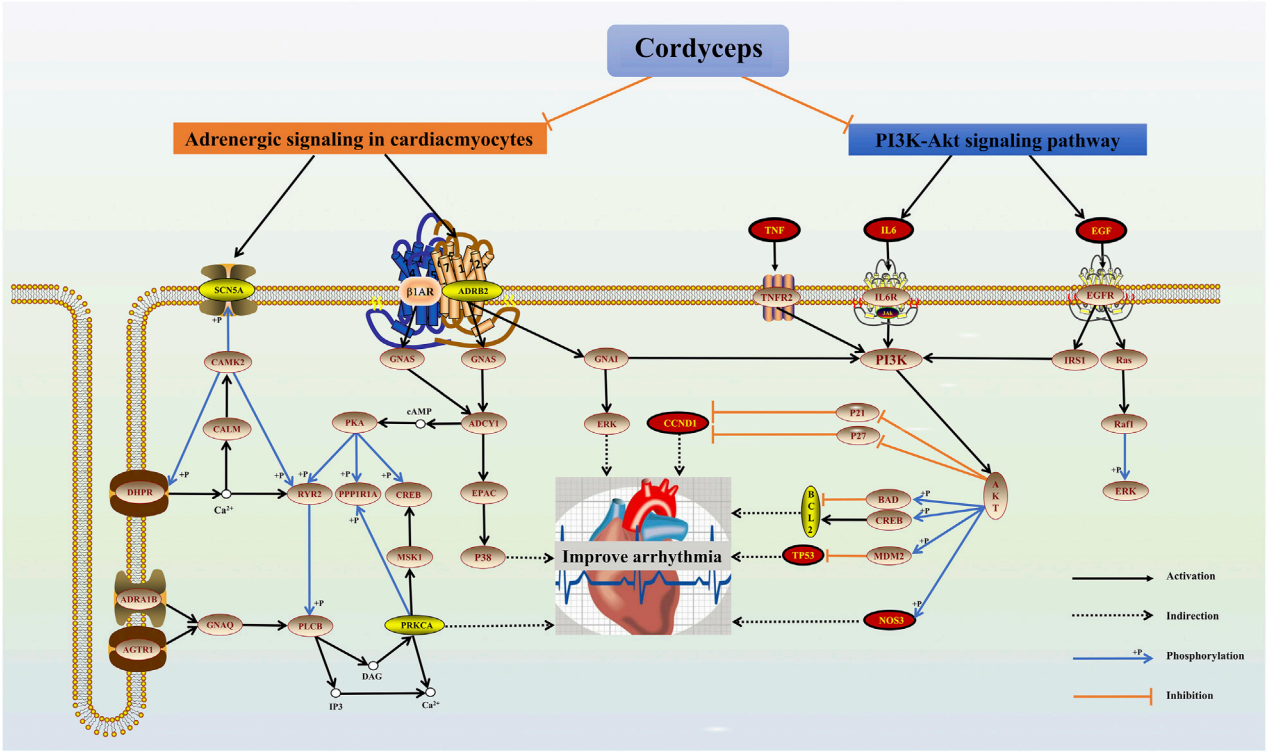


FIGURE 7
Mechanisms underlying the action of Cordyceps, a traditional Chinese medicine in cardiac function improvement. The red nodes represent the hub genes, the yellow nodes represent common genes, and the other nodes are the genes of the pathway.

blood viscosity. 4) Cordyceps might increase the activity of circulating superoxide dismutase and inhibit the production of lipid peroxides and free radicals (Zeng, 2015; Das et al., 2020).

Cordyceps contains a variety of chemical components, such as sterols amino acids, polysaccharides, organic acids, nucleosides, peptides, and trace elements. Caffeine plays an important role in preventing and treating arrhythmia. Previous studies have found that taking a certain amount of caffeine before aerobic exercise can delay the recovery of autonomic control of heart rate in young adults (Gonzaga et al., 2017). Low doses of caffeine can reduce heart rate during submaximal cycle ergometry (Flueck et al., 2016), while a high dose of caffeine (a dose of 150°mg) increases the heart rate of healthy people (Vukovich et al., 2005). The effect of caffeine on heart rate may be one of the reasons for the bidirectional regulation of heart rate by Cordyceps. It has been reported that beta-sitosterol can reduce blood lipids and prevent a variety of cardiovascular diseases. Beta-sitosterol can inhibit the arrhythmia induced by aconitine, ouabain, and myocardial ischemia (Zhang et al., 2013). Cinnamon is a plant with strong antioxidant activity. Due to its antioxidant properties, the ethanol extract of cinnamon bark protects the heart from ischemia-reperfusion injury (Sedighi et al., 2018). Arachidonic, linoleic, stearic, and oleic acids are the fatty acids in the human body that can reduce oxidative stress and hence help prevent cardiovascular disease (Sakai et al., 2017). Fatty acids and arachidonic acid prevent arrhythmias by modulating ion channel homeostasis, while intravenous application of arachidonic acid and linoleic acid-induced strong antiarrhythmic effects in three experimental arrhythmia models (Forster et al., 1976; Xiao et al., 2004). In order to better explore the mechanism of action of Cordyceps, we collected the common targets of Cordyceps, bradyarrhythmia, and tachyarrhythmia through network pharmacology constructed a PPI network, and performed enrichment analysis. Interestingly, two of the top 10 biological process items for bradyarrhythmia are associated with the adrenergic receptor and have molecular functional references to that receptor. According to KEGG results, which mainly enriched the PI3K-Akt signaling pathway and adrenergic signaling in cardiomyocytes, it is possible that the PI3K-Akt signaling pathway and adrenergic signaling in cardiomyocytes act together to regulate bradyarrhythmia. Two of the biological processes for tachyarrhythmia mentioned were positive regulation of protein kinase B signaling and phosphatidylinositol 3-kinase signaling. The results of the KEGG enrichment analysis suggest that Cordyceps may play a

role in the treatment of tachyarrhythmia through PI3K-Akt signaling. Subsequently, through molecular docking, the results showed that Cordyceps has good docking activity with the core gene hints of bradyarrhythmia and tachyarrhythmia targets.

According to the analysis of the PPI network, IL6, TNF, TP53, CASP3, CTNNB1, EGF, and NOS3 may be the key targets of Cordyceps in the treatment of arrhythmia. Previous studies have found that acute administration of IL6 to isolated rat hearts could recapitulate part of the Ca^{2+} handling phenotype. In addition, intraperitoneal injection of IL-6 in rats increased susceptibility to atrial fibrillation (Liao et al., 2021). TNF-α is a proinflammatory cytokine, which increases in several cardiac diseases. TNF-α rapidly increased spontaneous calcium release activity in mouse atrial cells via the mitochondrial reactive oxygen species pathway and promoted the possibility of arrhythmia-triggered activity (Zuo et al., 2019). There is growing evidence that IL-6 and TNF have significant inhibitory effects on myocardial metabolic processes in both ventricles, which can worsen the course of cardiovascular disease and increase the risk of tachyarrhythmia (Tverskaya et al., 2017). It has been experimentally confirmed that the mechanism of trimethyltin chloride induced bradyarrhythmia may indicate a close correlation between Na^+/K^+-ATPase activity and CASP3 protein expression (Liu et al., 2020). Cardiac tissue-specific plakoglobin and CTNNB1 are essential for the maintenance of cardiac conduction, while cardiac tissue-specific plakoglobin and rent series proteins are required to anchor the n-calcium mucoprotein/serial protein adhesion complex on the cytoskeleton. Loss of this connection leads to disruption of cardiac intercalated disc structure and the failure of the fatal cardiac arrhythmia (Swope et al., 2012). Previous studies have observed an increased incidence of arrhythmias in $NOS3^{-/-}$mice. NOS3 may prevent arrhythmias by modulating Ca^{2+} transient amplitude (Wang et al., 2008). TP53 is a transcription regulator and a significant tumor suppressor. Notably, TGF-β1 and TP53 in transplanted left ventricular tissue suggest a direct link between these genes and ventricular arrhythmias (Huizar et al., 2019; Haywood et al., 2020). Experimental results suggest that by interfering with beta-adrenergic receptor signaling, EGF protects the heart from the deleterious effects of adrenaline (Lorita et al., 2002).

The main mechanism of arrhythmia is a change in the physiological characteristics of the Na^+, K^+, and Ca^{2+} channels of the myocardial cell membrane, which leads to abnormal autonomic activity, triggering activity, and reentry excitement of the myocardium. Adrenergic receptors, as G protein-coupled receptors, play a key role in cardiac physiology in both health and disease. Previous investigations have indicated that cardiac adrenal receptors are directly involved in the control of intercellular electrical communication, which may be a key factor in maintaining normal intercellular conduction and the cardiac electrical network. This may in turn be related to the formation of arrhythmogenic substrates in some heart diseases (Salameh and Dhein, 2011). Adenine dinucleotide phosphate nicotinic acid is the most potent second messenger for Ca^{2+} release known to date. Stimulation of beta-adrenaline leading to Ca^{2+} release can induce arrhythmias (Nebel et al., 2013). The binding of sympathetic nervous system agonists to adrenergic receptors in cardiac myocytes can increase heart rate and myocardial contractility through cascade signaling pathways and protein kinase A (Papa et al., 2022). Enhanced α1-adrenoceptor stimulation affects intracellular Ca^{2+} signaling, thereby regulating heart rate (Luo et al., 2007). It has been shown in animal studies that α 1-adrenergic receptors can influence heart rate by inducing positive or negative inotropic responses by altering K^+ and Ca^{2+} currents, intracellular pH, and Ca^{2+} sensitivity of myofilaments (O'connell et al., 2014). Beta-adrenergic receptors induced an acute inhibitory K^+ response in the hearts of aging guinea pigs, and thus inhibited those receptors in reducing the occurrence of arrhythmias (Zou et al., 2021).

The movement of Ca^{2+} through the cell membrane generates various electrical currents to stimulate action potential, determining the cardiac cycle and cardiac function (Tosaki, 2020). Previous investigations have indicated that allicin may inhibit Ca^{2+} overload-induced apoptosis and the PI3K-mediated GRK2/PLC-γ/IP3R signaling pathway to protect against myocardial injury (Gao et al., 2021). In cardiomyocytes, PI3K-mediated regulation of Cav2.2α1/β2a transport is considered to be a general mechanism for regulating Ca^{2+} entry into excitatory cells (Viard et al., 2004). In addition, the fact that Akt regulates the C-terminal region of the Ca^{2+} channel function CaVβ2 through mediated phosphorylation of CaVβ2 in all excitable cells, including cardiomyocytes, highlights the biological relevance of this mechanism. More importantly, phosphorylation of CaVβ2 is thought to affect calcium influx and myocardial contractility, which is closely associated with the mechanism of arrhythmia (Ghigo et al., 2017). Previous research also indicates that elevated levels of angiotensin II may indirectly inhibit PI3Kα, and ultimately reduce the number of L-type Ca^{2+} channels in cardiac myocytes. These studies confirmed that PI3Kα is the main regulator of Ca^{2+} current regulation in cardiomyocytes (Liang et al., 2010). PI3K is believed to indirectly regulate ptdIns-3,4, 5-P3 in calcium signal transduction. The release of activated Ca^{2+}, in addition to ptdIns-3,4, 5-P3, has been identified as part of a signaling pathway used to regulate the cytoplasmic calcium concentration, suggesting that the functional link between the PI3K-Akt pathway and the calcium signaling pathway may be of broad importance (Blair & Marshall, 1997; Scharenberg & Kinet, 1998). The PI3K-Akt pathway is a key pathway for cardiac protection under stress conditions. Mice with reduced cardiac PI3K-Akt activity are very sensitive to atrial fibrillation, and clinical studies have found that surgical specimens from patients with atrial fibrillation showed significantly lower cardiac PI3K-Akt activity than patients with sinus rhythm (Pretorius et al.,

2009). The cardioprotective role of this pathway has been further highlighted by studies showing that increased PI3K-Akt activity improves the function of failing hearts in mouse models of heart failure (Mcmullen et al., 2014).

Our study presented a relatively strict illustration of the results. However, there were still some limitations. First, all trials included were published in Chinese and their sample sizes were small. Since all studies included were conducted in China, there might be a geographic bias, which limits generalization to the world. Second, all studies included reported positive results, which might reflect publication bias. Further, strictly designed multicenter RCTs are needed to assess the effectiveness and safety of TCM, especially long-term hard endpoints. Finally, in this study, the molecular mechanisms of Cordyceps were predicted only through network pharmacology, so further experiments are needed to confirm these mechanisms.

Taken together, based on meta-analysis, network pharmacology, and molecular docking technology, the results of our study suggest that Cordyceps is effective in stabilizing heart rates of patients with arrhythmia. It is hypothesized that Cordyceps may play a role in the treatment of cardiac arrhythmias by modulating adrenergic signaling in cardiomyocytes and the PI3K-Akt signaling pathway. However, the effect of Cordyceps on long-term outcomes in these patients remains unknown. It is hoped that our study will provide more references for the treatment of arrhythmia.

Data availability statement

The original contributions presented in the study are included in the article/Supplementary Material, and further inquiries can be directed to the corresponding authors.

Author contributions

HS, LW, MY, YX, LH, YHM, and XW analyzed data. HS participated in the design of the study and performed the statistical analysis. JH and ZZ conceived the study, participated in its design and coordination, and helped to draft the manuscript. All authors read and approved the final manuscript.

Funding

This work was supported by the Natural Science Foundation of China Nos. 82000788, 82004212, the Chinese Postdoctoral Science Foundation (2021M702040), Key Research & Development Plan of Shandong Province Nos. 2018GSF118176, 2019GSF108168, the Natural Science Foundation of Shandong Province (ZR2016HQ26), the Guangdong Basic and Applied Basic Research Foundation (2019A1515110023), and the Bethune-Merck's Diabetes Research Foundation Nos. B-0307-H-20200302, G2016014.

Conflict of interest

The authors declare that the research was conducted in the absence of any commercial or financial relationships that could be construed as a potential conflict of interest.

Publisher's note

All claims expressed in this article are solely those of the authors and do not necessarily represent those of their affiliated organizations, or those of the publisher, the editors, and the reviewers. Any product that may be evaluated in this article, or claim that may be made by its manufacturer, is not guaranteed or endorsed by the publisher.

Supplementary material

The Supplementary Material for this article can be found online at: https://www.frontiersin.org/articles/10.3389/fphar.2022.948173/full#supplementary-material

References

Black, N., D'souza, A., Wang, Y., Piggins, H., Dobrzynski, H., Morris, G., et al. (2019). Circadian rhythm of cardiac electrophysiology, arrhythmogenesis, and the underlying mechanisms. *Heart rhythm.* 16 (2), 298–307. doi:10.1016/j.hrthm.2018.08.026

Blair, L. A., and Marshall, J. (1997). IGF-1 modulates N and L calcium channels in a PI 3-kinase-dependent manner. *Neuron* 19 (2), 421–429. doi:10.1016/s0896-6273(00)80950-2

Boateng, S. (2013). Tachycardia. *Dis. Mon.* 9 (3), 74–82. doi:10.1016/j.disamonth.2012.12.003

Borghi, C., Rodriguez-Artalejo, F., De Backer, G., Dallongeville, J., Medina, J., Nuevo, J., et al. (2018). Serum uric acid levels are associated with cardiovascular risk score: A post hoc analysis of the eurika study. *Int. J. Cardiol.* 253, 167–173. doi:10.1016/j.ijcard.2017.10.045

Cai, J. R., Lin, W., Yang, G., Xing, H., Liu, D. L., and Tian, Y. J. (2020). Efficacy of Ningxinbao capsule combined with amiodarone hydrochloride tablets in the treatment of patients with paroxysmal atrial fibrillation [In Chinese]. *Mod. Diagnosis Ther.* 31 (16), 2557–2559.

Cao, D. P., Zhang, T., and Dou, Q. Y. (2021). Effect of Ningxinbao capsule combined with propafenone on the control of ventricular arrhythmias in patients [In Chinese]. *Chin. Health Eng.* 20 (05), 832–834. doi:10.19937/j.issn.1671-4199.2021.05.051

Chen, T., and Zhang, J. (2019). Clinical study of Ningxinbao capsule combined with propafenone for the treatment of ventricular arrhythmias [In Chinese]. *Mod. Drugs Clin.* 34 (03), 636–639. doi:10.7501/j.issn.1674-5515.2019.03.012

Chen, Y. (2018). Analysis of the effect of combination drug treatment of slow-onset arrhythmias in the elderly. *China Health Stand. Manag.* 9 (13), 132–134.

Cheng, J., Liu, Y., Li, G., Zhang, Z., Ma, L., Yang, X., et al. (2016). Noninvasive ventilation improves cardiac function in patients with chronic heart failure. *Oncotarget* 7 (31), 48918–48924. doi:10.18632/oncotarget.10441

Das, G., Shin, H. S., Leyva-Gómez, G., Prado-Audelo, M. L. D., Cortes, H., Singh, Y. D., et al. (2020). Cordyceps spp.: A review on its immune-stimulatory and other biological potentials. *Front. Pharmacol.* 11, 602364. doi:10.3389/fphar.2020.602364

Flueck, J. L., Schaufelberger, F., Lienert, M., Schäfer Olstad, D., Wilhelm, M., and Perret, C. (2016). Acute effects of caffeine on heart rate variability, blood pressure and tidal volume in paraplegic and tetraplegic compared to able-bodied individuals: A randomized, blinded trial. *PLoS One* 11 (10), e0165034. doi:10.1371/journal.pone.0165034

Forster, W., Mentz, P., Blass, K. E., and Mest, H. J. (1976). Antiarrhythmic effects of arachidonic, linoleic, linolenic, and oleic acid, and the influence of indomethacin and polyphloretinephosphate. *Adv. Prostaglandin Thromboxane Res.* 1, 433–438.

Fu, D. G. (2015). Cardiac arrhythmias: Diagnosis, symptoms, and treatments. *Cell. biochem. Biophys.* 73 (2), 291–296. doi:10.1007/s12013-015-0626-4

Gao, T., Yang, P., Fu, D., Liu, M., Deng, X., Shao, M., et al. (2021). The protective effect of allicin on myocardial ischemia-reperfusion by inhibition of $Ca^{(2+)}$ overload-induced cardiomyocyte apoptosis via the PI3K/GRK2/PLC-γ/IP3R signaling pathway. *Aging (Albany NY)* 13 (15), 19643–19656. doi:10.18632/aging.203375

Ghigo, A., Laffargue, M., Li, M., and Hirsch, E. (2017). PI3K and calcium signaling in cardiovascular disease. *Circ. Res.* 121 (3), 282–292. doi:10.1161/circresaha.117.310183

Gonzaga, L. A., Vanderlei, L. C. M., Gomes, R. L., and Valenti, V. E. (2017). Caffeine affects autonomic control of heart rate and blood pressure recovery after aerobic exercise in young adults: A crossover study. *Sci. Rep.* 7 (1), 14091. doi:10.1038/s41598-017-14540-4

Hao, P., Jiang, F., Cheng, J., Ma, L., Zhang, Y., and Zhao, Y. (2017). Traditional Chinese medicine for cardiovascular disease: Evidence and potential mechanisms. *J. Am. Coll. Cardiol.* 69 (24), 2952–2966. doi:10.1016/j.jacc.2017.04.041

Hao, P. P., Jiang, F., Chen, Y. G., Yang, J., Zhang, K., Zhang, M. X., et al. (2015). Traditional Chinese medication for cardiovascular disease. *Nat. Rev. Cardiol.* 12 (6), 318. doi:10.1038/nrcardio.2015.60

Hategan, L., Csányi, B., Ördög, B., Kákonyi, K., Tringer, A., Kiss, O., et al. (2017). A novel 'splice site' HCN4 Gene mutation, c.1737+1 G>T, causes familial bradycardia, reduced heart rate response, impaired chronotropic competence and increased short-term heart rate variability. *Int. J. Cardiol.* 241, 364–372. doi:10.1016/j.ijcard.2017.04.058

Haywood, M. E., Cocciolo, A., Porter, K. F., Dobrinskikh, E., Slavov, D., Graw, S. L., et al. (2020). Transcriptome signature of ventricular arrhythmia in dilated cardiomyopathy reveals increased fibrosis and activated TP53. *J. Mol. Cell. Cardiol.* 139, 124–134. doi:10.1016/j.yjmcc.2019.12.010

Huizar, J. F., Ellenbogen, K. A., Tan, A. Y., and Kaszala, K. (2019). Arrhythmia-induced cardiomyopathy: JACC state-of-the-art review. *Clin. Geriatr. Med.* 73 (18), 2328–2344. doi:10.1016/j.jacc.2019.02.045

Kumar, P., Kusumoto, F. M., and Goldschlager, N. (2012). Bradyarrhythmias in the elderly. *Clin. Geriatr. Med.* 28 (4), 703–715. doi:10.1016/j.cger.2012.08.004

Li, S. F., Chen, Y., Zhu, X., and Zhao, M. J. (2016). Efficacy observation of Ningxinbao capsule combined with verapamil in the treatment of premature ventricular contractions in coronary heart disease. [In Chinese. *Mod. Chin. Med.* 36 (01), 12–13+85. doi:10.13424/j.cnki.mtcm.2016.01.007

Liang, W., Oudit, G. Y., Patel, M. M., Shah, A. M., Woodgett, J. R., Tsushima, R. G., et al. (2010). Role of phosphoinositide 3-kinase A, protein kinase C, and L-type Ca^{2+} channels in mediating the complex actions of angiotensin II on mouse cardiac contractility. *Hypertension* 56 (3), 422–429. doi:10.1161/hypertensionaha.109.149344

Liao, J., Zhang, S., Yang, S., Lu, Y., Lu, K., Wu, Y., et al. (2021). Interleukin-6-Mediated-$Ca^{(2+)}$ handling abnormalities contributes to atrial fibrillation in sterile pericarditis rats. *Front. Immunol.* 12, 758157. doi:10.3389/fimmu.2021.758157

Liu, J. H., Chen, L. P., and Tao, Y. Z. (2014). Efficacy of Ningxinbao capsule combined with trimetazidine in the treatment of slow-onset arrhythmias in the elderly [In Chinese]. *J. Mod. Traditional Chin. West. Med.* 23 (02), 172–173. doi:10.3969/j.issn.1008-8849.2014.02.025

Liu, S., Tian, G., Chen, J., Zhang, X., Wu, A., Li, M., et al. (2018). Traditional Chinese medicine for bradyarrhythmia: Evidence and potential mechanisms. *Front. Pharmacol.* 9, 324. doi:10.3389/fphar.2018.00324

Liu, Y. H., and Chen, B. (2018). Clinical effects and post-combination safety of Ningxinbao capsule combined with Kordalong in the treatment of paroxysmal atrial fibrillation. [In Chinese. *World Abstr. latest Med. Inf.* 18 (45), 189+91. doi:10.19613/j.cnki.1671-3141.2018.45.095

Liu, Z., Tian, Z., Lv, J., Liu, W., Ma, Y., Hu, M., et al. (2020). Mechanism in bradycardia induced by Trimethyltin chloride: Inhibition activity and expression of $Na^{(+)}/K^{(+)}$-ATPase and apoptosis in myocardia. *J. Toxicol. Sci.* 45 (9), 549–558. doi:10.2131/jts.45.549

Lorita, J., Escalona, N., Faraudo, S., Soley, M., and Ramírez, I. (2002). Effects of epidermal growth factor on epinephrine-stimulated heart function in rodents. *Am. J. Physiol. Heart Circ. Physiol.* 283 (5), H1887–H1895. doi:10.1152/ajpheart.00217.2002

Luo, D. L., Gao, J., Fan, L. L., Tang, Y., Zhang, Y. Y., and Han, Q. D. (2007). Receptor subtype involved in alpha 1-adrenergic receptor-mediated Ca^{2+} signaling in cardiomyocytes. *Acta Pharmacol. Sin.* 28 (7), 968–974. doi:10.1111/j.1745-7254.2007.00605.x

Mcmullen, J. R., Boey, E. J., Ooi, J. Y., Seymour, J. F., Keating, M. J., and Tam, C. S. (2014). Ibrutinib increases the risk of atrial fibrillation, potentially through inhibition of cardiac PI3K-Akt signaling. *Blood* 124 (25), 3829–3830. doi:10.1182/blood-2014-10-604272

Mei, Q. B., Tao, J. Y., Gao, S. B., Xu, G. C., Chen, L. M., and Su, J. K. (1989). Antiarrhythmic effects of Cordyceps sinensis (berk.) sacc. *Zhongguo Zhong Yao Za Zhi* 14, 616–640.

Nebel, M., Schwoerer, A. P., Warszta, D., Siebrands, C. C., Limbrock, A. C., Swarbrick, J. M., et al. (2013). Nicotinic acid adenine dinucleotide phosphate (NAADP)-mediated calcium signaling and arrhythmias in the heart evoked by β-adrenergic stimulation. *J. Biol. Chem.* 288 (22), 16017–16030. doi:10.1074/jbc.M112.441246

O'connell, T. D., Jensen, B. C., Baker, A. J., and Simpson, P. C. (2014). Cardiac alpha1-adrenergic receptors: Novel aspects of expression, signaling mechanisms, physiologic function, and clinical importance. *Pharmacol. Rev.* 66 (1), 308–333. doi:10.1124/pr.112.007203

Papa, A., Kushner, J., and Marx, S. O. (2022). Adrenergic regulation of calcium channels in the heart. *Annu. Rev. Physiol.* 84, 285–306. doi:10.1146/annurev-physiol-060121-041653

Pretorius, L., Du, X. J., Woodcock, E. A., Kiriazis, H., Lin, R. C., Marasco, S., et al. (2009). Reduced phosphoinositide 3-kinase (p110alpha) activation increases the susceptibility to atrial fibrillation. *Am. J. Pathol.* 175 (3), 998–1009. doi:10.2353/ajpath.2009.090126

Sagris, M., Vardas, E. P., Theofilis, P., Antonopoulos, A. S., Oikonomou, E., and Tousoulis, D. (2021). Atrial fibrillation: Pathogenesis, predisposing factors, and genetics. *Int. J. Mol. Sci.* 23 (1), 6. doi:10.3390/ijms23010006

Sakai, C., Ishida, M., Ohba, H., Yamashita, H., Uchida, H., Yoshizumi, M., et al. (2017). Fish oil omega-3 polyunsaturated fatty acids attenuate oxidative stress-induced DNA damage in vascular endothelial cells. *PLoS One* 12 (11), e0187934. doi:10.1371/journal.pone.0187934

Salameh, A., and Dhein, S. (2011). Adrenergic control of cardiac gap junction function and expression. *Naunyn. Schmiedeb. Arch. Pharmacol.* 383 (4), 331–346. doi:10.1007/s00210-011-0603-4

Scharenberg, A. M., and Kinet, J. P. (1998). PtdIns-3, 4, 5-P3: A regulatory nexus between tyrosine kinases and sustained calcium signals. *Cell.* 94 (1), 5–8. doi:10.1016/s0092-8674(00)81214-3

Sedighi, M., Nazari, A., Faghihi, M., Rafieian-Kopaei, M., Karimi, A., Moghimian, M., et al. (2018). Protective effects of cinnamon bark extract against ischemia-reperfusion injury and arrhythmias in rat. *Phytother. Res.* 32 (10), 1983–1991. doi:10.1002/ptr.6127

Sidhu, S., and Marine, J. E. (2020). Evaluating and managing bradycardia. *Trends cardiovasc. Med.* 30 (5), 265–272. doi:10.1016/j.tcm.2019.07.001

Swope, D., Cheng, L., Gao, E., Li, J., and Radice, G. L. (2012). Loss of cadherin-binding proteins β-catenin and plakoglobin in the heart leads to gap junction remodeling and arrhythmogenesis. *Mol. Cell. Biol.* 32 (6), 1056–1067. doi:10.1128/mcb.06188-11

Tao, Y. Z., Zhao, X. Q., Liu, J. H., Ren, S. X., and Zhou, Wanxian. (2014). Clinical application of Ningxinbao capsule combined with amiodarone in unstable angina pectoris with ventricular arrhythmias [In Chinese]. *Hainan Med.* 25 (15), 2266–2268. doi:10.3969/j.issn.1003-6350.2014.15.0880

Tosaki, A. (2020). Arrhythmo geno pharmaco therapy. *Front. Pharmacol.* 11, 616. doi:10.3389/fphar.2020.00616

Tverskaya, M. S., Gankovskaya, L. V., Sukhoparova, V. V., and Virganskii, A. O. (2017). Effect of the natural cytokine complex on the structure and metabolism of contractile myocardium normally and under increased hemodynamic load. *Bull. Exp. Biol. Med.* 164 (2), 136–139. doi:10.1007/s10517-017-3942-4

Viard, P., Butcher, A. J., Halet, G., Davies, A., Nürnberg, B., Heblich, F., et al. (2004). PI3K promotes voltage-dependent calcium channel trafficking to the plasma membrane. *Nat. Neurosci.* 7 (9), 939–946. doi:10.1038/nn1300

Vukovich, M. D., Schoorman, R., Heilman, C., Jacob, P., 3rd, and Benowitz, N. L. (2005). Caffeine-herbal ephedra combination increases resting energy expenditure, heart rate and blood pressure. *Clin. Exp. Pharmacol. Physiol.* 32 (1-2), 47–53. doi:10.1111/j.1440-1681.2005.04152.x

Wang, H., Kohr, M. J., Wheeler, D. G., and Ziolo, M. T. (2008). Endothelial nitric oxide synthase decreases beta-adrenergic responsiveness via inhibition of the L-type Ca^{2+} current. *Am. J. Physiol. Heart Circ. Physiol.* 294 (3), H1473–H1480. doi:10.1152/ajpheart.01249.2007

Wang, L. D. (2016). Efficacy of Ningxinbao capsule combined with amiodarone in the treatment of paroxysmal atrial fibrillation [In Chinese]. *Inn. Mong. Tradit. Chin. Med.* 35 (01), 72–73. doi:10.16040/j.cnki.cn15-1101.2016.01.074

Wang, S. Y., Hu, X. M., and Zheng, Y. S. (2002). Efficacy of the combination of cardioplegia and ningxinbao in the treatment of 30 cases of premature ventricular contractions [In Chinese]. *Clin. Med.* 22 (04), 38–39. doi:10.3969/j.issn.1003-3548.2002.04.032

Wang, X. F. (2020). Analysis of the efficacy of Ningxinbao capsule combined with amiodarone hydrochloride tablets in the treatment of patients with paroxysmal atrial fibrillation [In Chinese]. *Med. Theory Pract.* 33 (18), 3004–3006. doi:10.19381/j.issn.1001-7585.2020.18.017

Wang, X., Lu, Q. X., Zhu, Y. A., and Wang, W. W. (2009). Efficacy of Ningxinbao combined with metoprolol tartrate in 63 cases of ventricular prophase contraction in viral myocarditis. *Clin. Pract. Med.* 18 (29), 709–710.

Wang, X. Y. (2017). Clinical value analysis of Ningxinbao capsule combined with trimetazidine in the treatment of slow-onset arrhythmias in the elderly in Chinese. *World Abstr. latest Med. Inf.* 17 (75), 94. . doi:10.19613/j.cnki.1671-3141.2017.75.074

Wu, Y. (2013). Efficacy of Ningxinbao combined with low-dose amiodarone in the treatment of cardiac arrhythmias in the elderly [In Chinese]. *J. Pract. Chin. Med.* 29 (07), 567–568. doi:10.3969/j.issn.1004-2814.2013.07.048

Xiao, Y. F., Ke, Q., Chen, Y., Morgan, J. P., and Leaf, A. (2004). Inhibitory effect of n-3 fish oil fatty acids on cardiac Na^{+}/Ca^{2+} exchange currents in HEK293t cells. *Biochem. Biophys. Res. Commun.* 321 (1), 116–123. doi:10.1016/j.bbrc.2004.06.114

Xu, J. M., and Zheng, H. J. (1992). Randomized double-blind controlled observation of 64 cases of arrhythmias treated with Ningxinbao capsules [In Chinese]. *Shanghai J. Traditional Chin. Med.* 2 (04), 4–5. doi:10.16305/j.1007-1334.1992.04.002

Zeng, J. H. (2015). Clinical study of trimetazidine combined with Ningxinbao in the treatment of acute inferior myocardial infarction causing bradyarrhythmias [In Chinese]. *Chin. Med. Sci.* 5 (08), 51–54.

Zhang, H., Li, Y., Mi, J., Zhang, M., Wang, Y., Jiang, Z., et al. (2017). GC-MS profiling of volatile components in different fermentation products of Cordyceps sinensis mycelia. *Molecules* 22 (10), 1800. doi:10.3390/molecules22101800

Zhang, H. N., Yang, Y. M., Wu, G. D., Zhang, H. C., and Gao, B. W. (2013). Isolation of effective components for the antiarrhythmic effect of monk medicine Guangzao [In Chinese]. *J. Baotou Med. Coll.* 29 (03), 1–4. doi:10.16833/j.cnki.jbmc.2013.03.001

Zhang, R., Zhu, X., Bai, H., and Ning, K. (2019). Network pharmacology databases for traditional Chinese medicine: Review and assessment. *Front. Pharmacol.* 10, 123. doi:10.3389/fphar.2019.00123

Zhang, X. Y., and Fan, J. S. (2009). Treatment of slow-onset arrhythmias with Ningxinbao capsules. [In Chinese. *China Mod. Distance Educ. Chin. Med.* 7 (12), 108. doi:10.3969/j.issn.1672-2779.2009.12.083

Zhao, N. H. (2012). Efficacy of amiodarone combined with Ningxinbao in the treatment of cardiac arrhythmias [In Chinese]. *Chin. Community Physicians Med. Spec.* 14 (03), 170. doi:10.3969/j.issn.1007-614x.2012.03.167

Zhong, W. Z. (2016). Clinical effect analysis of Ningxinbao capsule combined with trimetazidine in the treatment of slow-onset arrhythmias in the elderly [In Chinese]. *China Pharm. Guide* 14 (04), 182–183. doi:10.15912/j.cnki.gocm.2016.04.152

Zou, S., Qiu, S., Su, S., Zhang, J., Sun, J., Wang, Y., et al. (2021). Inhibitory G-protein-mediated modulation of slow delayed rectifier potassium channels contributes to increased susceptibility to arrhythmogenesis in aging heart. *Heart rhythm.* 18 (12), 2197–2209. doi:10.1016/j.hrthm.2021.09.014

Zuo, S., Li, L. L., Jiang, L., Liu, N., Dong, J. Z., and Ma, C. S. (2019). Acute modulation of intracellular calcium release by tumor necrosis factor alpha in mouse atrial cells. [In Chinese. *Chin. J. Cardiac Pacing Cardiac Electrophysiol.* 33 (03), 236–239. doi:10.13333/j.cnki.cjcpe.2019.03.008

frontiers | Frontiers in Pharmacology

TYPE Review
PUBLISHED 25 August 2022
DOI 10.3389/fphar.2022.927653

Check for updates

OPEN ACCESS

EDITED BY
Yanping Liu,
Shandong University, China

REVIEWED BY
Anshul S. Jadli,
University of Calgary, Canada
Jafar Rezaie,
Urmia University of Medical Sciences, Iran

*CORRESPONDENCE
Peiyang Gao,
gaopy930@126.com
Qingsong Huang,
huangqingsong5802@163.com
Chuantao Zhang,
zhangchuantao@cdutcm.edu.cn

†These authors have contributed equally to this work and share first authorship

SPECIALTY SECTION
This article was submitted to Experimental Pharmacology and Drug Discovery, a section of the journal Frontiers in Pharmacology

RECEIVED 24 April 2022
ACCEPTED 26 July 2022
PUBLISHED 25 August 2022

CITATION
Yang Y, Liu Y, Chai Y, Liu K, Hu W, Zhao K, Zhu Y, Gao P, Huang Q and Zhang C (2022), Exosomes in pathogenesis, diagnosis, and treatment of pulmonary fibrosis.
Front. Pharmacol. 13:927653.
doi: 10.3389/fphar.2022.927653

COPYRIGHT
© 2022 Yang, Liu, Chai, Liu, Hu, Zhao, Zhu, Gao, Huang and Zhang. This is an open-access article distributed under the terms of the Creative Commons Attribution License (CC BY). The use, distribution or reproduction in other forums is permitted, provided the original author(s) and the copyright owner(s) are credited and that the original publication in this journal is cited, in accordance with accepted academic practice. No use, distribution or reproduction is permitted which does not comply with these terms.

Exosomes in pathogenesis, diagnosis, and treatment of pulmonary fibrosis

Yang Yang[1†], Yufei Liu[1†], Yilu Chai[1†], Ke Liu[1], Wei Hu[1], Keni Zhao[1], Yi Zhu[1], Peiyang Gao[2]*, Qingsong Huang[1]* and Chuantao Zhang[1]*

[1]Department of Respiratory Medicine, Hospital of Chengdu University of Traditional Chinese Medicine, Chengdu, China, [2]Department of Critical Care Medicine, Hospital of Chengdu University of Traditional Chinese Medicine, Chengdu, China

Pulmonary fibrosis (PF) is a group of interstitial lung diseases that seriously endanger human life and health. Despite the current advances in research on the pathogenesis and treatment of PF, the overall quality of survival and survival rates of PF patients remain low, prompting the search for more effective therapeutic approaches. Exosomes are nanoscale vesicles with diameters ranging from approximately 30–150 nm, capable of transporting a variety of molecules in the body and mediating intercellular communication. There is an increasing number of studies focusing on the role of exosomes in PF. This review demonstrates the significance of exosomes in the pathogenesis, diagnosis, and treatment of PF. Exosomes are able to influence inflammatory, immune, and extracellular matrix deposition processes in PF and regulate the corresponding cytokines. Some exosomes detected in sputum, blood, and bronchoalveolar lavage fluid may be used as potential diagnostic and prognostic biomarkers for PF. Exosomes derived from several cells, such as mesenchymal stem cells, have demonstrated potential as PF therapeutic agents. Drug delivery systems using exosomes may also provide new insights into PF therapy.

KEYWORDS

exosomes, pulmonary fibrosis, pathogenesis, therapeutics, biomarkers

1 Introduction

Pulmonary fibrosis (PF) is an irreversible structural and functional change in the lung caused by excessive deposition of extra-alveolar matrix proteins resulting in fibrotic remodeling and alveolar destruction. PF is a severe risk to human life and health, with a median survival time of only 3–5 years after diagnosis of idiopathic pulmonary fibrosis (IPF). The pathogenesis of PF involves an inflammatory environment, oxidative stress, ageing, epigenetic and genetic and epithelial-mesenchymal transition (EMT) (Sundarakrishnan et al., 2018; Kinoshita and Goto, 2019; Yanagihara et al., 2020).

There are limited drugs available for the treatment of PF. Pirfenidone and nintedanib are commonly used in the treatment of PF. Although these two drugs can improve lung

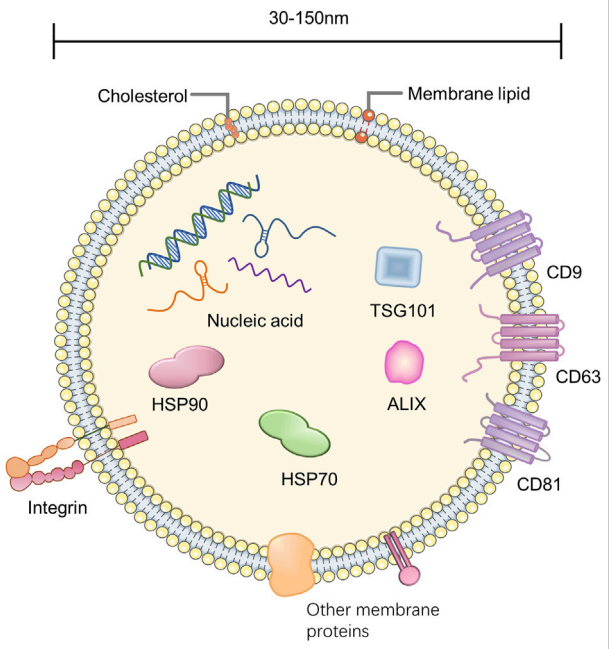


FIGURE 1
Composition of exosome.

function and reduce clinical symptoms to some extent, they do not have significant advantages in improving survival and stopping or even reversing disease progression. And there are also uncertainties in the use of these drugs in terms of treatment duration, initial selection, etc., (Sgalla et al., 2018; Sgalla et al., 2020).

As exosomes have been refined in recent years, more and more studies have uncovered the significance of exosomes in the development of disease, and exosomes are expected to be a safe emerging method for the diagnosis and treatment of PF (Guiot et al., 2019; Xie and Zeng, 2020).

2 Exosomes

Exosomes are nanoscale vesicles ranging from approximately 30–150 nm in diameter, produced and released by most cells, and are a subtype of extracellular vesicles (EVs) (Yang D. et al., 2020). Exosomes can be found in body fluids such as blood, saliva, amniotic fluid, urine, semen, bronchial fluid, and cerebrospinal fluid (Doyle and Wang, 2019). The discovery of exosomes dates back to the 1980s when exosomes were first identified in reticulocytes (Harding et al., 1983; Pan et al., 1985; Johnstone et al., 1987), and were initially thought of simply as a means of removing unwanted cellular components (Johnstone, 1992). With the intensive study of exosomes, they are now considered to be involved in the regulation of intercellular communication, playing specific roles in biological processes such as immune response (Anel et al., 2019), antigen presentation (Arima et al., 2019), cell differentiation (Lloret-Llinares et al., 2018) and tumour invasion (Zhang and Yu, 2019; Rezaie et al., 2022).

2.1 Composition of exosomes

The exosome is enclosed by a lipid bilayer and carries a variety of biologically active substances such as proteins, lipids, and nucleic acids (Wortzel et al., 2019) (Figure 1). The lipids of the exosome contain sphingolipids, phosphatidylserine, cholesterol, etc., (De Abreu et al., 2020). The nucleic acids carried by exosomes are divided into DNA and RNA, and RNA can include mRNA, microRNA (miRNA), tRNA, etc., (Keshtkar et al., 2021). Most exosomal proteins are associated with their formation and secretion, such as tetraspanins (e.g., CD9, CD63, CD81), heat shock proteins (e.g., HSP70, HSP90), TSG101, Alix, Rab GTPase, and Integrin. Furthermore, there are exosome-specific proteins secreted by specific cells, such as MHC-II from dendritic cells (Janockova et al., 2021; Liu et al., 2021).

2.2 Biogenesis, secretion and uptake of exosomes

Exosome production is associated with the endosomal system. Early-sorting endosome (ESE) formation is caused by invagination of the plasma membrane and endocytosis of the extracellular component cell surface proteins (Kalluri and LeBleu, 2020). The endoplasmic reticulum, Golgi complex, and mitochondria can participate in the maturation of the ESE (Hoyer et al., 2018; Shi et al., 2018; Amari and Germain, 2021). ESE can mature into late-sorting endosome (LSE) and eventually produce multivesicular bodies (MVBs, also known as MVEs) (Hessvik and Llorente, 2018). During this process, the endosomal membrane invaginates to produce intraluminal vesicles (ILVs), and MVBs contain a large number of ILVs (Abels and Breakefield, 2016). A portion of MVBs can be degraded by autophagosomal or lysosomal fusion, and a portion of MVBs fuse with the plasma membrane to release the contained ILVs as exosomes to be taken up and function extracellularly (Hassanpour et al., 2020) (Figure 2).

There are currently thought to be two pathways that regulate the formation of ILVs, one involving the endosomal sorting complex required for transport (ESCRT) and the other independent of ESCRT (Osaki and Okada, 2019). ESCRT is mainly composed of four complexes (ESCRT-0, ESCRT-I, ESCRT-II, and ESCRT-III) and associated proteins (e.g., VPS4, ALIX, TSG101) (Larios et al., 2020). ESCRT plays a role in ubiquitin-mediated and ubiquitin-independent cargo

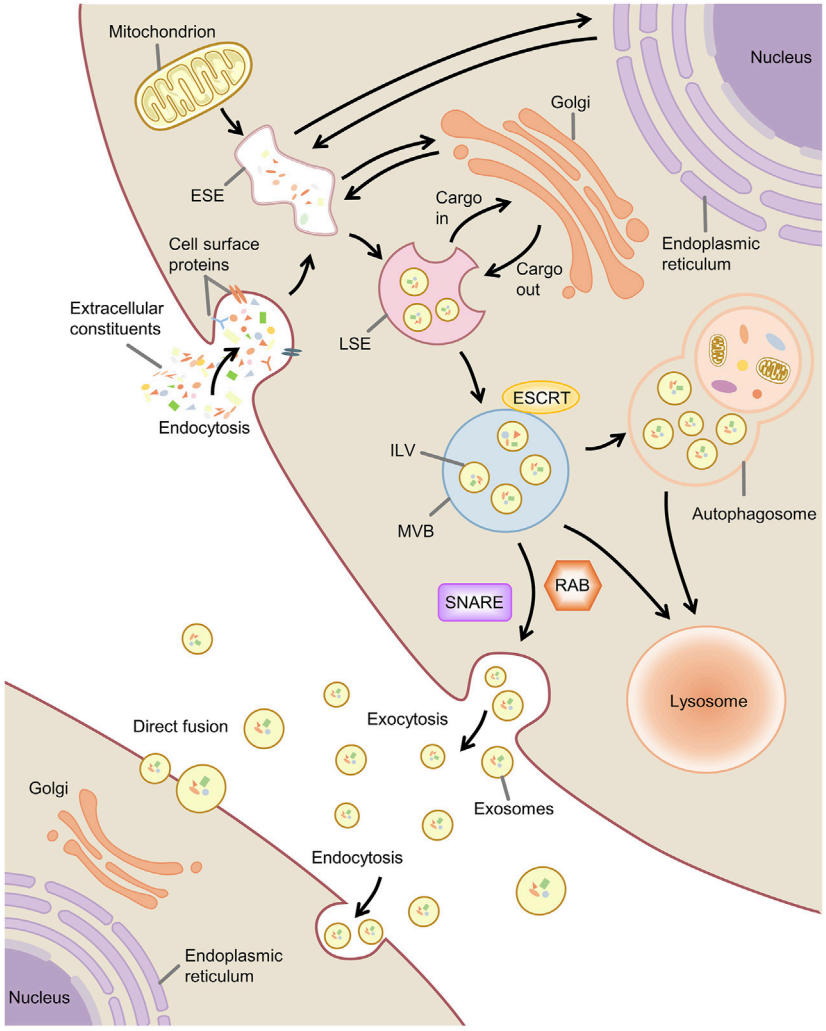


FIGURE 2
Biogenesis, secretion and uptake of exosome. Note: ESE, early-sorting endosome; LSE, late-sorting endosome; MVB, multivesicular body; ILV, intraluminal vesicle; ESCRT, endosomal sorting complex required for transport; SNARE, soluble N -ethylmaleimide-sensitive factor attachment protein receptor.

recognition and sorting and can induce membrane deformation, with substrates of the ESCRT pathway ultimately available in translocated to ILVs (Frankel and Audhya, 2018).

Another pathway regulating the formation of ILVs involves mainly ceramide and tetraspanins. The exosomes contain ceramides, cholesterol, sphingomyelin, and tetraspanins (Toh et al., 2018). Ceramide is essential for exosome formation and secretion, but the exact mechanism is unclear. Ceramide has been found that may promote the inward budding of MVBs to produce ILVs by affecting membrane curvature (Elsherbini and Bieberich, 2018). Ceramides, cholesterol, and sphingolipids are involved in forming lipid rafts (Wei et al., 2021). Lipid rafts play an essential function in membrane budding, may contribute to the assembly of proteins or other molecules into endosomes, and can regulate the formation of epidermal growth factor receptor-containing ILVs (Li et al., 2018; Wei et al., 2021). Tetraspanins have been shown to regulate the transport of selectively associated proteins and their function through membrane compartmentalization and play a role in membrane fusion and the production of ILVs (Böker et al., 2018; Ghossoub et al., 2020).

Exosomes contain unique contents of nucleic acids, proteins, and lipids, and the sorting mechanism of these exosomal cargoes is closely related to the ILVs formation pathway described above. Exosomal miRNAs play an essential role in intercellular communication. The type and amount of miRNAs loaded into exosomes depend on

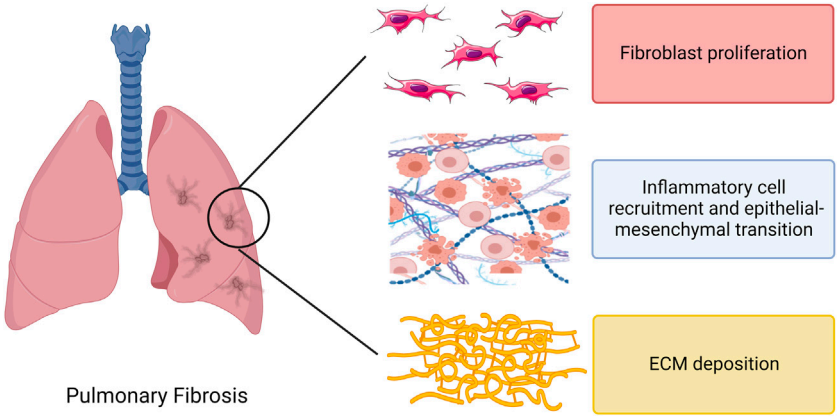


FIGURE 3
Direct effects of regulatory immune cells, fibroblasts and extracellular matrix in pulmonary fibrosis. Note: ECM, extracellular matrix.

the type of parental cells, cell-specific sorting mechanisms, and stimuli such as inflammation (Wozniak et al., 2020; Xie et al., 2022). According to current studies, the potential modes of miRNA sorting into exosomes can be summarized as the following: the neural sphingomyelinase 2-dependent pathway, the sumoylated heterogeneous nuclear ribonucleoproteins-dependent pathway, the 3′miRNA sequence-dependent pathway, and the miRNA-induced silencing complex-associated pathway. In addition, other membrane proteins (e.g., Vps4A), RNA-binding proteins (e.g., Argonaute 2, YB-1), and lipid rafts have also been associated with miRNA sorting (Wei H. et al., 2021; Xie et al., 2022).

The release of exosomes involves the translocation of MVBs to the plasma membrane and the fusion of MVBs with the plasma membrane. MVBs fuse with the plasma membrane and release the contained LIVs into the extracellular space as exosomes *via* exocytosis. The release of exosomes is currently thought to be associated with the cytoskeleton, Rab GTPase, and the soluble N-ethylmaleimide-sensitive factor attachment protein receptor (SNARE) (Hessvik and Llorente, 2018). The cytoskeleton regulates the translocation of MVBs to the plasma membrane, depending mainly on the interaction between actin and the microtubule cytoskeleton (Villarroya-Beltri et al., 2014; Gurunathan et al., 2021). Rab GTPases play a role in vesicle transport with the main functions of regulating vesicle budding, vesicle transport along with the cytoskeleton, and membrane fusion (Jin et al., 2021). For example, Rab11 facilitates the transportation of MVBs and the fusion of MVBs with the plasma membrane (Savina et al., 2005; Messenger et al., 2018), and Rab27 can regulate the docking of MVBs with the plasma membrane (Song et al., 2019), and Rab35 is a critical factor in regulating the transport of MVBs (Yang et al., 2019). SNARE is a central mechanism that mediates membrane fusion (Wang et al., 2017). It has been found to facilitate the docking of MVBs to the plasma membrane and thus contribute to exosome release (Yu et al., 2020).

After releasing outside the cell, exosomes are taken up and acted upon by the recipient cells mainly through membrane fusion and endocytosis (Gonda et al., 2019). The exosome uptake mechanism largely depends on the recipient cell (Horibe et al., 2018).

3 The function of exosomes in PF

In recent years, an increasing number of studies have focused on the role played by exosomes in PF. The initiation of PF is associated with lung injury and impaired repair, with multiple causes of lung epithelial cell injury followed by inflammatory cell recruitment and massive pro-inflammatory cytokine release, triggering an immune response. Monocytes and macrophages can drive fibrosis through an over-repair response to lung injury. The pro-fibrotic mediators act on lung fibroblasts, causing excessive proliferation and differentiation of fibroblasts, which in turn promotes the proliferation of myofibroblasts and the production of extracellular matrix (ECM), ultimately leading to PF pathological features such as excessive ECM deposition in lung tissue (Mei et al., 2021) (Figure 3). It has been reported in several publications that exosomes can influence inflammation and immunity, fibroblast proliferation and differentiation, ECM deposition, and other aspects of the PF disease process. The functions of exosomes reported so far in PF are highlighted in Figure 4 and discussed in more detail in subsequent sections.

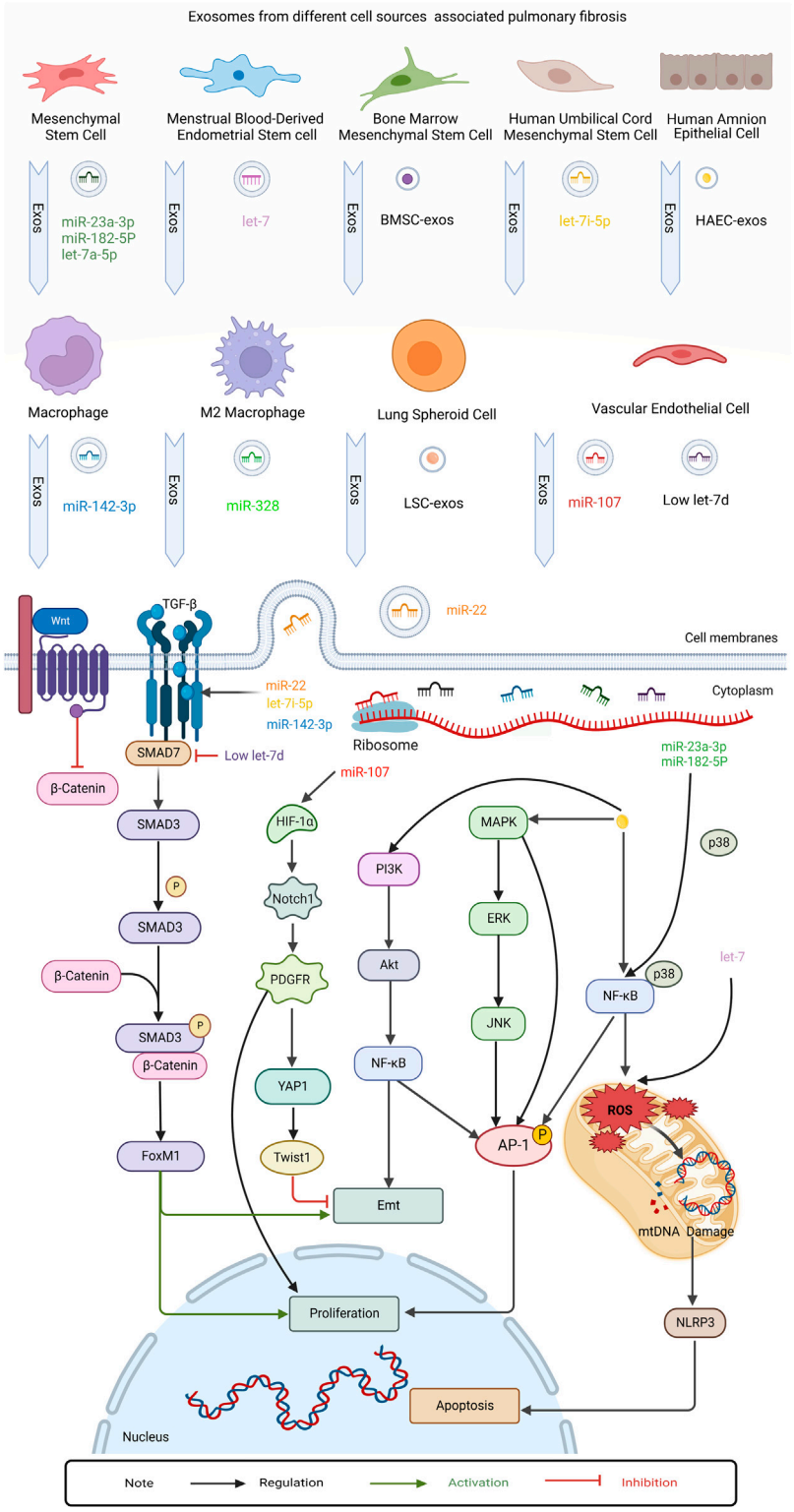


FIGURE 4
This figure summarizes the role of regulatory exosomes in PF. Mechanism investigation revealed that exosomes secreted by different kinds of cells, eg: human amnion epithelial cell (HAEC), Menstrual Blood-Derived Endometrial Stem Cell (MenSC), Mesenchymal stem cells (MSC), Human umbilical cord mesenchymal stem cell (HUCMSC), Bone marrow mesenchymal stem cell (BMSC), Pluripotent stem cell (iPSC), Lung spheroid cell(LSC), Vascular endothelial cell (EnC), Macrophage, M2 macrophages. The exosomes transmitted protein cargo and microRNAs regulated MAPK, NF-kb, PI3k/Akt, Wnt/β-catenin, TGFβRI/FoxM1/Smad/β-catenin, HIF-1α/Notch1/PDGFRβ/YAP1/ Twist1 signaling pathways. Finally these pathways assess their interaction with epithelial-mesenchymal transition, apoptosis and proliferation in contradicting findings.

3.1 Exosomes affect inflammation and immunity in PF

Fibrosis is the result of excessive trauma repair and tissue remodeling, which is considered to be chronic inflammation and eventual fibrosis caused by epithelial injury (Heukels et al., 2019). Inflammatory stimulation or persistence of the inflammatory state is an essential condition for the development of PF. Following injury, damaged epithelium and recruited inflammatory cells secrete a variety of mediators, including transforming growth factor-β (TGF-β) to regulate epithelial repair and promote fibroblast recruitment and myofibroblast activation (Hewlett et al., 2018).

Macrophages can polarize to M1 and M2 phenotypes after different environmental and cytokine stimuli. Under chronic inflammatory conditions, pro-inflammatory M1 macrophages slowly convert to the more anti-inflammatory M2 phenotype, secreting mediators that promote wound healing. M2-type macrophages regulate fibrosis by secreting various growth factors (including TGF-β) and other mechanisms (Heukels et al., 2019).

Oxidative stress and inflammation are closely linked and play a pro-fibrotic role in the fibrotic process. Under sustained stimulation, abnormally functioning mitochondria overproduce reactive oxygen species (ROS) (Lv et al., 2019). ROS can be involved in inflammation by affecting NF-κB signaling, TNF signaling, and so on (Blaser et al., 2016). In addition, abnormal production and accumulation of ROS can lead to cellular damage at the level of nucleic acids, proteins, lipids, and carbohydrates, thus participating in the pathogenesis of PF (Cameli et al., 2020).

Exosomes can down-regulate inflammatory cell infiltration during PF disease and participate in the regulation of PF disease through the mediation of some classical inflammatory pathways such as NF-κB, MAPK, and other pathways. In these studies, miRNAs contained in exosomes such as miR-23a-3p and miR-182-5p could play an important role in the regulation of PF (Tan et al., 2018; Royce et al., 2019; Xiao et al., 2020; Kaur et al., 2021). Exosomes can also regulate PF by affecting ROS. For example, exosomal let-7 exerts an anti-PF effect by regulating ROS and mitochondrial DNA damage (Sun et al., 2019).

Some studies have focused on the effect of exosomes on the differentiation and proliferation of immune cells. In these studies, exosomes could alleviate PF by modulating the phenotypic switch of monocytes and macrophages, enhancing macrophage phagocytosis, and inhibiting T cell proliferation (Tan et al., 2018; Mansouri et al., 2019; Zhou et al., 2021). For example, exosomes from induced pluripotent stem cells (iPSCs) attenuate PF by suppressing M2-type macrophages during PF through the miR-302a-3p/TET1 axis (Zhou et al., 2021).

Macrophages can participate in the progression of PF through their secreted exosomes. Macrophage-derived exosomes promote differentiation, proliferation, and migration of myofibroblasts after exposure to silica (Qin et al., 2021). In bleomycin-induced PF, one study found that macrophage-derived exosomes mediated intercellular communication between macrophages and fibroblasts by transferring angiotensin II type 1 receptors to lung fibroblasts (Sun N. N. et al., 2021). Another study showed that the M2 macrophage-derived exosome miRNA-328 enhances lung interstitial fibroblast proliferation and promotes PF by regulating FAM13A (Yao et al., 2019).

3.2 Exosomes affect ECM deposition in PF

Excessive ECM deposition is a characteristic feature of PF. The large number of cytokines produced after epithelial injury in PF stimulates fibroblasts to proliferate and differentiate into myofibroblasts, which leads to the production of high amounts of collagen, fibronectin, and other ECM proteins and their deposition in the interstitial lung, leading to reduced gas exchange and impaired lung function, and ultimately to respiratory failure (Chanda et al., 2019; Bueno et al., 2020; Mei et al., 2021).

A study showed that exosomes in bronchoalveolar lavage fluid (BALF) of PF rats, specifically exosome miR-204-5p, promote fibroblast proliferation and collagen deposition in lung tissue, indicating that exosomes may participate in the PF process by regulating ECM deposition (Zhu et al., 2021). Long noncoding RNA (lncRNA) HOTAIRM1 delivered by alveolar epithelial cell-derived exosomes was found to play a role in PF, and lncRNA HOTAIRM1 was able to promote lung fibroblast proliferation and differentiation and contribute to ECM remodeling by regulating the miR-30d-3p/HSF1/YY1 axis (Chen et al., 2022). Zhang et al. (2021) found that exosomes derived from bone marrow mesenchymal stem cells in a silicosis PF model reduced collagen accumulation in lung tissue and inhibited the expression of components of the Wnt/β-catenin pathway, which is closely related to EMT. Wnt5a was also found to be directly transported by EVs in PF and induced fibroblast proliferation, which incidentally consisted mainly of exosomes in that study (Martin-Medina et al., 2018). Phuong-Uyen C. Dinh et al. (2020) found that lung spheroid cell-derived exosomes (LSC-EXOs) reduced collagen deposition in PF induced by bleomycin or silica, in addition to inhibiting the proliferation of myofibroblasts. The above study illustrates the role of exosomes in regulating the proliferation of fibroblasts and myofibroblasts, which are the primary sources of ECM in PF, and this may be an entry point to investigate the mechanisms by which exosomes regulate ECM deposition (Tsukui et al., 2020).

TABLE 1 Biomarker potential of exosomes in PF.

Exosome—Cargos	Expression in PF (vs. Controls)	Source	Cohort selection	Clinical implication	References
let-7d	Downregulated	Serum	61 IPF patients and 15 controls	Promising diagnostic biomarkers for IPF	Lacedonia et al. (2021)
miR-16	Downregulated				
miR-142-3p	Upregulated	Sputum	16 IPF patients and 14 controls	Potential biomarkers for diagnosis and prediction of disease severity in IPF	Njock et al. (2019)
miR-33a-5p	Upregulated				
let-7d-5p	Downregulated				
miR-142-3p	Upregulated	Sputum	19 IPF patients and 23 controls	Promising diagnostic biomarkers for IPF	Guiot et al. (2020)
		Plasma	14 IPF patients and 14 controls		
miR-22-3p	Upregulated	BALF	8 IPF patients and 8 controls	Promising diagnostic biomarkers for IPF	Kaur et al. (2021)
miR-320a-3p	Upregulated				
miR-320b	Upregulated				
miR-24-3p	Upregulated				
miR-375-3p	Downregulated				
miR-200a-3p	Downregulated				
miR-200b-3p	Downregulated				
miR-141-3p	Downregulated				
miR-423-5p	Downregulated				
miR-125b	Upregulated	BALF	30 IPF patients and 16 controls	Promising diagnostic biomarkers for IPF	Liu et al. (2018)
miR-128	Upregulated				
miR-21	Upregulated				
miR-100	Upregulated				
miR-140-3p	Upregulated				
miR-374b	Upregulated				
let-7d	Downregulated				
miR-103	Downregulated				
miR-26	Downregulated				
miR-30a-5p	Downregulated				
miR-21-5p	Upregulated	Serum		Potential biomarkers for diagnosis and prognosis of IPF	Makiguchi et al. (2016)
CD19	Upregulated	Serum	90 IPF patients and 19 controls	Potential biomarkers for diagnosis of IPF; CD8 is a potential prognostic biomarker for IPF	D'Alessandro et al. (2021)
CD69	Upregulated				
CD8	Upregulated				
CD86	Upregulated				
CD209	Upregulated				
Cd133/1	Upregulated				
MCSP	Upregulated				
ROR1	Upregulated				
CD42a	Downregulated				

Note: PF, pulmonary fibrosis; IPF, idiopathic pulmonary fibrosis; BALF, bronchoalveolar lavage fluid.

3.3 Exosomes regulate PF-related cytokines

Cytokines can be involved in multiple aspects of inflammation and ECM deposition in PF (Luzina et al., 2015). TGF-β plays a vital role in the progression of PF, mediating fibroblast recruitment and differentiation, promoting ECM deposition, and inducing EMT. TGF-β can exert pro-fibrotic effects in cooperation with platelet-derived growth factor (PDGF), which itself can be involved in lung fibroblast proliferation and collagen synthesis (Chanda et al., 2019; Wang et al., 2020). Other cytokines such as connective tissue growth factor (CTGF), insulin-like growth factor, and CCL2 also modulate PF (Luzina et al., 2015).

Several studies have shown that exosomes can regulate PF through cytokines such as TGF-β. Activated TGF-β binds to its receptor and regulates the expression of target genes, including pro-fibrotic genes, through Smad proteins (Massagué, 2012). Smad7 is a negative regulator of TGF-β signaling that blocks the TGF-β1/Smads signaling pathway and inhibits fibroblast differentiation. A study elucidated that in cigarette smoke-induced PF, exosomes promote abnormal epithelial-fibroblast crosstalk by inhibiting Smad7 to activate the TGF-β1/Smad3 pathway (Bai et al., 2021). TGF-β1 and its receptor can regulate the transformation of lung pericytes into myofibroblasts. Han Xie et al. found that the lung vascular endothelium-derived exosome low let-7d targets transforming growth factor β receptor 1 (TGFβR1) to regulate the TGFβRI/FoxM1/Smad/β-catenin pathway, which drives lung pericytes fibrosis (Xie et al., 2020). In addition, exosomal miR-22 was found to significantly inhibit TGF-β1-induced α-smooth muscle actin (α-SMA) expression (Kuse et al., 2020). Guiot et al. (2020) found that the macrophage-derived exosome miR-142-3p was able to reduce TGFβR1 expression and inhibit TGF-β-induced fibrotic responses in alveolar epithelial cells and lung fibroblasts by targeting TGFβR1. The finding of another study demonstrated that human umbilical cord mesenchymal stem cell-derived exosome let-7i-5p could target TGFβR1 and inhibit lung fibroblast activation via the TGFβR1/Smad3 signaling pathway in a silica-induced PF model (Xu et al., 2022).

Platelet-derived growth factor receptor β (PDGFRβ) is expressed in pericytes, and a study demonstrated that the pulmonary vascular endothelial cell-derived exosome miR-107 could target HIF-1α to regulate PDGFRβ and mitigate pericyte-promoted PF progression by inhibiting the HIF-1α/Notch1/PDGFRβ/YAP1/Twist1 signaling pathway (Wang et al., 2021). Kuse et al. (2020) found in an *in vitro* PF model that exosomal miR-22 could attenuate the expression of CTGF, which is an important mediator of fibrosis and stimulates lung fibroblast differentiation, thereby inhibiting CTGF-induced α-SMA expression.

4 Exosomes as biomarkers of PF

The current diagnosis of PF is not straightforward and requires multidisciplinary collaboration between pulmonologists, pathologists, and radiologists, and there remains a recognized need for an accurate, early diagnosis of PF. Early diagnosis of PF is critical for prognosis with survival being poor in several fibrotic interstitial lung diseases, including IPF, and patients with PF may benefit more from early diagnosis and timely disease management (Spagnolo et al., 2012; Cottin et al., 2018). Biomarkers have objective detection and evaluation properties and can be used as indicators of physiological/pathological processes or pharmacological responses to therapeutic interventions, which are essential in PF (Guiot et al., 2017). To date, several studies have shown that exosomes detected in body fluids such as blood and sputum have the potential to be diagnostic, prognostic, and predictive biomarkers of PF (Table 1).

Hematological tests, sputum examination, and bronchoscopy are diagnostic tools for respiratory diseases, and exosomal miRNAs can be detected by these tests. Several studies have reported the potential of some exosomal miRNAs as biomarkers for the diagnosis of PF. Donato Lacedonia et al. (2021) analyzed the expression of exosomal miRNAs in the serum of IPF patients and found that let-7d and miR-16 were down-regulated compared to controls. Previous studies have shown that let-7d has a key regulatory role in the prevention of PF, while fewer works have been conducted on the association between miR-16 and PF, and further studies are necessary to determine their ability to act as biomarkers of IPF (Pandit et al., 2010; Huleihel et al., 2014; Liang et al., 2016; Min et al., 2016). Makon-Sébastien Njock and his colleagues worked on finding exosomal biomarkers of IPF in sputum. By analyzing sputum samples from IPF patients and healthy controls, they found that the significantly upregulated exosomes miR-142-3p, miR-33a-5p, and downregulated exosome let-7d-5p in sputum were promising diagnostic biomarkers, and notably, they demonstrated that exosomal miR-142-3p was negatively correlated with diffusing capacity/alveolar volume of carbon monoxide and exosomal let-7d-5p was positively correlated, which may help to evaluate the severity of IPF (Njock et al., 2019). When they further investigated the relationship between exosomal miR-142-3p and IPF, they found that in addition to its potential as a sputum biomarker for IPF, exosomal miR-142-3p was significantly upregulated in the plasma of IPF patients, making it more promising as a diagnostic modality for IPF (Guiot et al., 2020). Kaur et al. (2021) compared IPF patients with healthy nonsmokers and detected 55 differentially expressed exosomal miRNAs in IPF human lung tissue, also finding

TABLE 2 Potential therapeutic implication of exosomes in PF.

Source of exosomes	Extraction method	Experimental model	Exosome - cargos	Species	Delivery of exosomes	Potential therapeutic implication	References
BMSC	Differential Ultracentrifugation	Silca	Unknown	Rats	Intravenous injection	Alleviate PF, reduce collagen accumulation, inhibit TGF-β1 and decrease HYP content	Zhang et al. (2021)
BMSC	iodixanol (OptiPrep) cushion density flotation	Bleomycin	Unknown	Mice	Intravenous injection	Alleviate PF, reduce collagen accumulation and reduce the degree of apoptosis	Mansouri et al. (2019)
hucMSC	Ultracentrifugation + Exoquick exosome precipitation solution	Silca	Unknown	Mice	Intravenous injection	Alleviate PF, improve respiratory impairment and reduce collagen deposition in NIH-3T3 cells	Xu et al. (2020)
hucMSC	Ultracentrifugation + Exoquick exosome precipitation solution	Silca	let-7i-5p	Mice	Intravenous injection	Affect the expression of α-SMA, collagen type I, fibronectin, TGFβR1 and P-Smad3 in NIH-3T3 cells, and inhibit fibroblast activation	Xu et al. (2022)
hucMSC	Differential centrifugation	Bleomycin	Unknown	Mice	Intravenous injection	Reduced lung coefficient, improved lung histopathological changes and collagen deposition in mice with PF, reduced TGF-β1 expression, inhibited p-Smad2/3 and vimentin expression and increased E-cadherin expression	Yang et al. (2020b)
MSC	Ultracentrifugation	Lipopolysaccharide	miR-23a-3p miR-182-5p	Mice	Intravenous injection	Alleviate PF and injury, attenuate apoptosis and EMT progression	Xiao et al. (2020)
MSC	Ultracentrifugation	Monocrotaline	Unknown	Rats	Intravenous injection	Attenuate PF and pulmonary vascular remodelling, reduce right ventricular systolic pressure and right ventricular hypertrophy index	Zhang et al. (2020b)
MSC	Differential Centrifugation + Iodixanol (OptiPrep)	Hyperoxia	Unknown	Mice	Intravenous injection	Alleviate PF, reduce collagen accumulation, reduce pulmonary vascular remodelling and inflammation, improve lung function	Willis et al. (2018)
iPSC	Ultracentrifugation	Bleomycin	miR-302a-3p	Mice	Intravenous injection	Relieve PF, reduce collagen deposition, and inhibit the increase of M2 type macrophages	Zhou et al. (2021)
hESC	Ultracentrifugation	Radiation	Unknown	Mice	Intravenous injection	Alleviates PF and reduces collagen accumulation, macrophage infiltration and inflammation	Montay-Gruel et al. (2020)
MenSC	Differential centrifugation + exosome extraction kit (Wako Pure Chemicals Industry)	Bleomycin	let-7	Mice	Intravenous injection	Alleviate PF and alveolar epithelial cell damage, reduce collagen accumulation in lung tissue and adjust wet and dry specific gravity	Sun et al. (2019)
hAEC	Ultracentrifugation	Bleomycin	Unknown	Mice	Intranasal administration	Alleviate PF, reduce collagen accumulation and lung inflammation	Tan et al. (2018)
hAEC	Ultracentrifugation	Bleomycin	Unknown	Mice	Intranasal administration	Alleviate PF, reduce airway remodeling and inflammation, with the above effects being better when exosomes are combined with Serelaxin	Royce et al. (2019)

(Continued on following page)

TABLE 2 (*Continued*) Potential therapeutic implication of exosomes in PF.

Source of exosomes	Extraction method	Experimental model	Exosome - cargos	Species	Delivery of exosomes	Potential therapeutic implication	References
LSC	Ultrafiltration + Centrifugation	Bleomycin Silica	Unknown	Mice Rats	Nebulised inhalation	Alleviate PF, restore normal alveolar structure, reduce collagen accumulation and myofibroblast proliferation, and improve lung function	Dinh et al. (2020)
—	—	Bleomycin	miR-16	Mice	Intravenous injection	Relieve PF and reduce collagen accumulation	Inomata et al. (2021)
—	—	Bleomycin	miR-22	Mice	Intravenous injection	Alleviate PF, reduce PF scores and collagen accumulation	Kuse et al. (2020)

Note: BMSC, bone marrow mesenchymal stem/stromal cell; hucMSC, human umbilical cord mesenchymal stem cell; MSC, mesenchymal stem/stromal cell; iPSC, induced pluripotent stem cell; hESC, human embryonic stem cell; hAEC, human amnion epithelial cell; MenSC, menstrual blood-derived endometrial stem cell; LSC, lung spheroid cell; EnC, vascular endothelial cell; α-SMA, α-smooth muscle actin; TGF-β:transforming growth factor-β; TGFβR1, TGF-β receptor 1; P-Smad: phosphorylated smad; —, no relevant data.

significant downregulation of exosomes miR-375-3p, miR-200a-3p, miR-200b-3p, miR-141-3p, and miR-423-5p and upregulation of exosomes miR-22-3p, miR-320a-3p, miR-320b, and miR-24-3p in BALF-derived exosomes in IPF patients. Bronchoscopic lung cryobiopsy is a promising examination technique in the diagnosis of PF, allowing safer and more effective access to lung tissue with BALF, thus providing a source of feasibility for BALF exosomal miRNAs to become a diagnostic tool for PF (Tomassetti et al., 2016). Another study showed that exosomes miR-125b, miR-128, miR-21, miR-100, miR-140-3p, and miR-374b were upregulated in BALF from IPF patients, while let-7d, miR-103, miR-26, and miR-30a-5p were downregulated (Liu et al., 2018). These findings suggest the potential of BALF-derived exosomal miRNAs as PF biomarkers.

Furthermore, Makiguchi et al. (2016) found that serum EV miR-21-5p was upregulated throughout the progression of PF compared to controls in an animal model of bleomycin-induced PF, and they observed significantly higher EV miR-21-5p in the sera of IPF patients compared to healthy controls, suggesting that EV miR-21-5p is a candidate biomarker for IPF. Tomonori Makiguchi and his colleagues also confirmed the potential of serum EV miR-21-5p as a prognostic biomarker for IPF. According to their study, serum EV miR-21-5p correlated with the rate of lung volume loss in IPF patients, and Kaplan-Meier analysis indicated that patients with higher baseline serum EV miR-21-5p levels had significantly lower survival rates. Given that the investigators obtained serum EV miR-21-5p by Total Exosome Isolation reagent, serum exosome miR-21-5p may have the same biomarker potential. Kaur et al. (2020) suggested that downregulation of an exosomal lncRNA encoding a WT1 transcription factor in the plasma of smokers may represent a possibility for them to develop PF in the future . Miriana d'Alessandro et al. examined blood exosome surface epitopes in IPF patients and found many exosome surface epitopes CD19, CD69, CD8, CD86, CD209, Cd133/1, MCSP, and ROR1 were significantly higher in IPF patients and CD42a was lower than in controls. In addition, increased expression of CD8 was associated with poor prognosis in IPF in survival analysis. These results provide the basis for the use of blood exosome surface epitopes as candidate biomarkers for the diagnosis and prognosis of IPF (D'Alessandro et al., 2021).

5 Exosomes in PF treatment

5.1 Potential of exosomes as PF therapeutics

Lung transplantation is currently the most effective treatment for most PF. Still, only a small number of patients can benefit from it due to the limited availability of donor organs, rejection reactions, and the cost of treatment. The drug treatment options for PF are relatively limited, and taking IPF as an example, the main treatment options for IPF are nintedanib, pirfenidone, and a combination of both. Although they can slow down the disease progression of PF to some extent, these therapies have adverse drug reactions and do not have the ability to cure the disease. Many patients with PF have a low quality of life and a short survival time after diagnosis. Thus there is still an urgent need for a treatment that can stop or even reverse PF. An increasing number of studies are currently dedicated to the search for safe and effective new therapies for PF (Richeldi et al., 2017; Mei et al., 2021). As previously described, exosomes have the ability to regulate fibroblast proliferation and differentiation, ECM deposition, and EMT, and several studies have demonstrated the therapeutic potential of exosomes for PF in animal models, as shown in Table 2,

suggesting that exosomes may be a valuable clue to address this issue of developing new therapies for PF.

Mesenchymal stem/stromal cell-derived exosomes (MSC-EXOs) have been proposed as promising therapeutic tools for a variety of diseases (Ahmadi and Rezaie, 2021; Janockova et al., 2021) and have shown anti-fibrotic potential such as for liver, kidney, and cardiac fibrosis (Li et al., 2013; Eirin et al., 2017; Rong et al., 2019; Chen et al., 2020). MSCs are also a preferred source of exosomes for the study of PF treatment. Mansouri et al. (2019) found that bone marrow mesenchymal stem/stromal cell-derived exosomes (BMSC-EXOs) were effective in attenuating bleomycin-induced PF and modulating lung inflammation, and interestingly, the investigators observed that BMSC-EXOs significantly restored bleomycin-induced PF in mice after intravenous injection of BMSC-EXOs on day 7 post-modeling. The ability of BMSC-EXOs to reverse PF is of interest and needs to be studied in depth. In addition to this, they found that bone marrow-derived mononuclear cell transplantation pretreated by BMSC-EXOs could exert a preventive effect on PF. Another study demonstrated the ability of BMSC-EXOs to effectively alleviate silica-induced PF in a rat model of silicosis (Zhang et al., 2021). There are no effective therapies to slow down the progression of silicosis, especially its fibrosis, and exosomes offer a therapeutic idea for PF in silicosis. Xu et al. (2020) found that human umbilical cord MSC-derived exosomes (hucMSC-EXOs) exerted anti-PF effects in a mouse silicosis model, effectively reducing collagen deposition, attenuating pulmonary fibrosis-related indices, and improving impaired lung function in silicosis mice. Chunjie Xu and colleagues found through a more in-depth study that the exosome let-7i-5p in hucMSC-EXOs effectively attenuated collagen deposition in silicosis mice and improved silica-induced PF in mice by inhibiting fibroblasts (Xu et al., 2022). Another study elucidated that hucMSC-EXOs had the effect of alleviating bleomycin-induced PF and significantly attenuated the pathological changes, and reduced collagen deposition in the lung tissue of PF mice (Yang J. et al., 2020). Acute lung injury can lead to fibrosis in lung tissue. In studying the mechanisms by which MSC regulates the progression of acute lung injury, Xiao et al. (2020) found that MSC-EXOs have the potential to attenuate lipopolysaccharide-induced PF progression, and the investigators demonstrated that miR-23a-3p and miR-182-5p transported by MSC-EXOs have the ability to reverse the EMT process that is closely associated with PF. Zhang Z. et al. (2020b) found that MSC-EXOs also had the ability to attenuate PF in a rat model of monocrotaline-induced pulmonary arterial hypertension. Another study indicated that MSC-EXOs could also attenuate PF and improve lung function in a mouse model of hyperoxia-induced bronchopulmonary dysplasia (Willis et al., 2018).

Stem cell-derived exosomes other than MSCs have also demonstrated promising therapeutic effects on PF in several studies. In view of the potential therapeutic value of iPSCs and their derivatives in several diseases, Yan Zhou and colleagues, after observing the potential of iPSCs for the treatment of PF, further built on their findings that iPSC-derived exosomes (iPSC-EXOs) could alleviate bleomycin-induced PF in mice, and that miR-302a-3p carried by iPSC-EXOs was able to reduce collagen deposition and inhibit M2-type macrophage increase in mouse lungs (Zhou et al., 2016; Zhou et al., 2021). Pierre Montay-Gruel et al. administered human embryonic stem cell (hESC)-derived EVs intravenously to mice receiving chest radiation exposure, most of which were actually exosomes, and observed a significant reduction in radiation-induced PF. This study suggests that hESC-derived exosomes may have the potential to become a therapeutic pathway for radiation therapy-induced PF (Montay-Gruel et al., 2020). Menstrual blood-derived endometrial stem cells (MenSCs) have antifibrotic effects, and Lifang Sun et al. found that MenSC-derived exosomes (MenSC-EXOs) ameliorated bleomycin-induced PF and alveolar epithelial cell injury in mice, which may be closely related to exosomal let-7. The investigators observed that let-7 carried by MenSC-EXOs could inhibit the process of EMT in mice and attenuate lung histopathological changes and that MenSC-EXOs could also translocate let-7 into alveolar epithelial cells to attenuate cell damage (Sun et al., 2019).

In addition to the stem cell-derived exosomes described above, several other types of exosomes have the potential for the treatment of PF. Tan et al. (2018) endeavored to explore the feasibility of human amnion epithelial cell-derived exosomes (hAEC-EXOs) as a potential therapy for IPF. They performed early and late interventions in juvenile mice with bleomycin-induced PF via intranasal drip of hAEC-EXOs and found that hAEC-EXOs were able to exert anti-inflammatory and anti-fibrotic effects at different stages of PF, with the potential to prevent, mitigate and even reverse PF. They also showed that the aforementioned anti-PF effects of hAEC-EXOs in juvenile mice were reproduced in aged mice, which were used to simulate the clinical setting of elderly patients with IPF, demonstrating the therapeutic potential of hAEC-EXOs for various disease stages and ages of PF. Another study found that hAEC-EXOs, in combination with the anti-fibrotic drug serelaxin, exerted better anti-inflammatory, anti-fibrotic, and alleviating airway dysfunction in bleomycin-induced PF mice (Royce et al., 2019). Dinh et al. (2020) used a nebulizer to treat bleomycin-induced and silica-induced PF mice with nebulized inhaled lung spheroid cell exosomes (LSC-EXOs) and found that LSC-EXOs exerted anti-PF effects in both PF mouse models, reducing collagen accumulation and myofibroblast proliferation, and improving impaired lung function. In addition, their results suggest that LSC-EXOs may be superior to MSC-EXOs in attenuating PF. Exosomal miR-107 and let-7d produced by pulmonary vascular endothelial cells have been reported to inhibit the function of pericytes in PF, which provides a promising therapeutic target for PF (Xie et al., 2020; Wang et al., 2021). In addition, exosomal miR-22 and exosomal

miR-16 demonstrated experimentally their ability to ameliorate bleomycin-induced PF in mice through their mimics (Kuse et al., 2020; Inomata et al., 2021). In most of the above studies, an intravenous injection was chosen as the mode of exosome administration. Interestingly, in exploring the therapeutic potential of hAEC-EXOs and LSC-EXOs for PF, the investigators chose intranasal drip and nebulized inhalation administration, respectively, which enriches the effective routes of administration in anti-PF exosomes.

5.2 Potential of exosomes as PF drug delivery vehicles

With the development of nanomedicine, more and more literature has reported that nano-drug delivery systems can function as stable, safe, and effective drug delivery, and the progressive exploration of pulmonary drug delivery vehicles, including exosomes, has helped to advance the development of PF therapy (Skibba et al., 2020). Compared to nano-drug delivery systems such as *in vitro* synthesized liposomes, exosomes have unique drug delivery advantages. Exosomes are naturally secreted by organismal cells, can be widely and stably present in body fluids, and have better biocompatibility and lower immunogenicity. The lipid-rich composition of exosomes facilitates their loading of hydrophilic and lipophilic active pharmaceutical ingredients, which happens to be lipophilic for pirfenidone, a therapeutic drug for PF (Haak et al., 2017; Guiot et al., 2019). Exosomes are capable of mediating intercellular communication in the body, have the ability to target tissues and cells, and can cross biological barriers such as the blood-brain barrier (Zhang Y. et al., 2020; Saint-Pol et al., 2020). With these properties and abilities, exosomes have the potential to deliver PF therapeutic agents such as drugs and miRNAs.

There are already studies invested in the development of exosomes as drug delivery systems for anti-PF agents. Lingna Sun and coworkers designed a hybrid drug delivery system of fibroblast-derived exosomes and clodronate (CLD)-loaded liposomes (EL-CLD), which utilizes the affinity of fibroblast-derived exosomes for fibroblasts and CLD to reduce the uptake of drugs by the liver, proposing to solve the problem of poor selectivity and low delivery efficiency of PF therapeutic drugs to fibroblasts. In an animal model of PF, the investigators found that the anti-PF efficacy of Nintedanib was significantly increased when it was loaded with EL-CLD, thanks to the ability of EL-CLD to increase the delivery of nintedanib to the lung and its accumulation in fibrotic lung tissue, as well as to attenuate the macrophage-induced inflammatory response (Sun L. et al., 2021). Notably, the team has also developed another hybrid exosome-liposome drug delivery system that enhances the efficacy of nintedanib in the treatment of liver fibrosis (Ji et al., 2022). These findings highlight that the ability of exosomes to target delivery enables them to be advantageous in drug delivery, and furthermore, they demonstrate the feasibility and effectiveness of exosomes as delivery vehicles for anti-fibrotic, especially anti-PF drugs. However, the technology of exosome application for drug delivery is still immature. Problems such as how to extract exosomes efficiently and completely, how to improve the drug loading rate of exosomes, how to surface modify exosomes to improve their stability, and the types of drugs delivered are limiting the further development of this technology, and more research needs to be invested in tackling these challenges (Zhang Y. et al., 2020). Based on the barriers of exosomes as drug carriers, Yanzhen Yu and colleagues developed a functional ECM biomaterial capable of loading exosomes, which is able to capture and enrich exosomes without damaging the exosome membrane, increasing the stability of exosomes as carriers for delivery of anti-PF miR-29. The investigators observed that the application of this miR-29 exosome-enriched ECM material in bleomycin-induced PF mice resulted in good attenuation of lung tissue fibrosis in mice, which provided inspiration for optimizing the exosome delivery technology (Yu et al., 2021). Therefore, as the technology continues to improve, exosomes may hold a promising future as anti-PF agent delivery vehicles.

6 Conclusion

In recent years, research on exosomes has increased rapidly. In this context, many advances have been made in the study of the relationship between exosomes and a variety of respiratory diseases, including PF. Exosomes play an important role in communication between human cells, can participate in multiple physiopathological processes, and are closely associated with many therapeutic mechanisms (Guiot et al., 2019; Mashouri et al., 2019; Soraya et al., 2021; Yamada, 2021). According to several studies mentioned above, exosomes have the ability to participate in processes such as inflammation and immunity, ECM deposition, and EMT in PF, which is associated with the ability of exosomes to regulate inflammatory cell infiltration, immune cell proliferation, and fibroblast proliferation and differentiation in the lung, as well as to influence cytokines such as TGF-β1. Exosomes have great potential for the diagnosis and determination of prognosis in PF and show therapeutic promise for the prevention, mitigation, and even reversal of PF. In addition, the biocompatibility, low immunogenicity, and ability to target tissues of exosomes provide new insights into the development of anti-PF drug delivery systems.

However, there is still a long way to go to translate the potential of exosomes as biomarkers and therapeutics in PF into clinical applications that can benefit patients. The diagnostic and therapeutic mechanisms of exosomes in PF are currently unclear and need to be further investigated. The technical basis for the

clinical application of exosomes is immature due to obstacles such as exosome extraction, preservation, and drug loading. As highlighted at the 2021 annual meeting of the International Society for Extracellular Vesicles, clinical applications of EVs such as exosomes need to explore effective, rapid, simplified, reproducible, and scalable pathways. Clinical translation of current results and further achievements require continuous efforts of multidisciplinary teams (Picciolini et al., 2021). Despite these obstacles, the prospect of clinical application of exosomes in PF currently requires more efforts to be invested in the research of exosomes as a diagnostic method and new therapies for PF to benefit PF patients.

Author contributions

YY, WH, and KL searched the literature and wrote the first draft of the manuscript. YL and YC drew the figures. KZ and YZ processed the tables in the manuscript. PG, QH, and CZ contributed to the revision of the manuscript. All authors read and approved the submitted version.

Funding

Financial support was provided by Sichuan Science and technology program, Grant/Award Numbers: 2020JDRC0114, 2020YFH0164; Special subject of scientific research on traditional Chinese Medicine of Sichuan Administration of Traditional Chinese Medicine, Grant/Award Numbers: 2021MS093, 2021MS539; "100 Talent Plan" Project of Hospital of Chengdu University of Traditional Chinese Medicine, Grant/Award Number: Hospital office [2021] 42; The fifth batch of training objects of the National TCM Clinical Excellent Talents Training Program, Grant/Award Number: National TCM Renjiao Letter [2022] No. 1; Training objects of the National Traditional Chinese Medicine Innovation Backbone Talents Training Program, Grant/Award Number: National TCM Renjiao Letter [2019] No. 128.

Conflict of interest

The authors declare that the research was conducted in the absence of any commercial or financial relationships that could be construed as a potential conflict of interest.

Publisher's note

All claims expressed in this article are solely those of the authors and do not necessarily represent those of their affiliated organizations, or those of the publisher, the editors and the reviewers. Any product that may be evaluated in this article, or claim that may be made by its manufacturer, is not guaranteed or endorsed by the publisher.

References

Abels, E. R., and Breakefield, X. O. (2016). Introduction to extracellular vesicles: Biogenesis, RNA cargo selection, content, release, and uptake. *Cell. Mol. Neurobiol.* 36, 301–312. doi:10.1007/s10571-016-0366-z

Ahmadi, M., and Rezaie, J. (2021). Ageing and mesenchymal stem cells derived exosomes: Molecular insight and challenges. *Cell biochem. Funct.* 39, 60–66. doi:10.1002/cbf.3602

Amari, L., and Germain, M. (2021). Mitochondrial extracellular vesicles - origins and roles. *Front. Mol. Neurosci.* 14, 767219. doi:10.3389/fnmol.2021.767219

Anel, A., Gallego-Lleyda, A., De Miguel, D., Naval, J., and MARTíNEZ-Lostao, L. (2019). Role of exosomes in the regulation of T-cell mediated immune responses and in autoimmune disease. *Cell* 8, E154. doi:10.3390/cells8020154

Arima, Y., Liu, W., Takahashi, Y., Nishikawa, M., and Takakura, Y. (2019). Effects of localization of antigen proteins in antigen-loaded exosomes on efficiency of antigen presentation. *Mol. Pharm.* 16, 2309–2314. doi:10.1021/acs.molpharmaceut.8b01093

Bai, J., Deng, J., Han, Z., Cui, Y., He, R., Gu, Y., et al. (2021). CircRNA_0026344 via exosomal miR-21 regulation of Smad7 is involved in aberrant cross-talk of epithelium-fibroblasts during cigarette smoke-induced pulmonary fibrosis. *Toxicol. Lett.* 347, 58–66. doi:10.1016/j.toxlet.2021.04.017

Blaser, H., Dostert, C., Mak, T. W., and Brenner, D. (2016). TNF and ROS crosstalk in inflammation. *Trends Cell Biol.* 26, 249–261. doi:10.1016/j.tcb.2015.12.002

Böker, K., Lemus-Diaz, N., Rinaldi Ferreira, R., Schiller, L., Schneider, S., and Gruber, J. (2018). The impact of the CD9 tetraspanin on lentivirus infectivity and exosome secretion. *Mol. Ther.* 26, 634–647. doi:10.1016/j.ymthe.2017.11.008

Bueno, M., Calyeca, J., Rojas, M., and Mora, A. L. (2020). Mitochondria dysfunction and metabolic reprogramming as drivers of idiopathic pulmonary fibrosis. *Redox Biol.* 33, 101509. doi:10.1016/j.redox.2020.101509

Cameli, P., Carleo, A., Bergantini, L., Landi, C., Prasse, A., and Bargagli, E. (2020). Oxidant/antioxidant disequilibrium in idiopathic pulmonary fibrosis pathogenesis. *Inflammation* 43, 1–7. doi:10.1007/s10753-019-01059-1

Chanda, D., Otoupalova, E.Smith, S. R., Volckaert, T., De Langhe, S. P., and Thannickal, V. J. (2019). Developmental pathways in the pathogenesis of lung fibrosis. *Mol. Asp. Med.* 65, 56–69. doi:10.1016/j.mam.2018.08.004,

Chen, F., Li, X., Zhao, J., Geng, J., Xie, J., and Xu, B. (2020). Bone marrow mesenchymal stem cell-derived exosomes attenuate cardiac hypertrophy and fibrosis in pressure overload induced remodeling. *Vitro Cell. Dev. Biol. Anim.* 56, 567–576. doi:10.1007/s11626-020-00481-2

Chen, L., Yang, Y., Yue, R., Peng, X., Yu, H., and Huang, X. (2022). Exosomes derived from hypoxia-induced alveolar epithelial cells stimulate interstitial pulmonary fibrosis through a HOTAIRM1-dependent mechanism. *Lab. Invest.*. doi:10.1038/s41374-022-00782-y

Cottin, V., Hirani, N., Hotchkin, D., Nambiar, A., Ogura, T., Otaola, M., et al. (2018). Presentation, diagnosis and clinical course of the spectrum of progressive-fibrosing interstitial lung diseases. *Eur. Respir. Rev.* 27, 180076. doi:10.1183/16000617.0076-2018

D'alessandro, M., Soccio, P., Bergantini, L., Cameli, P., Scioscia, G., Foschino Barbaro, M. P., et al. (2021). Extracellular vesicle surface signatures in IPF patients: A multiplex bead-based flow cytometry approach. *Cell*, 10. 1045. doi:10.3390/cells10051045

De Abreu, R. C., Fernandes, H., Da Costa Martins, P. A., Sahoo, S., Emanueli, C., and Ferreira, L. (2020). Native and bioengineered extracellular vesicles for

cardiovascular therapeutics. *Nat. Rev. Cardiol.* 17, 685–697. doi:10.1038/s41569-020-0389-5

Dinh, P. C., Paudel, D., Brochu, H., Popowski, K. D., Gracieux, M. C., Cores, J., et al. (2020). Inhalation of lung spheroid cell secretome and exosomes promotes lung repair in pulmonary fibrosis. *Nat. Commun.* 11, 1064. doi:10.1038/s41467-020-14344-7

Doyle, L. M., and Wang, M. Z. (2019). Overview of extracellular vesicles, their origin, composition, purpose, and methods for exosome isolation and analysis. *Cells* 8, E727. doi:10.3390/cells8070727

Eirin, A., Zhu, X., Puranik, A., Tang, H., Mcgurren, K., van Wijnen, A., et al. (2017). Mesenchymal stem cell-derived extracellular vesicles attenuate kidney inflammation. *Kidney Int.* 92, 114–124. doi:10.1016/j.kint.2016.12.023

Elsherbini, A., and Bieberich, E. (2018). Ceramide and exosomes: A novel target in cancer biology and therapy. *Adv. Cancer Res.* 140, 121–154. doi:10.1016/bs.acr.2018.05.004

Frankel, E., and Audhya, A. (2018). ESCRT-dependent cargo sorting at multivesicular endosomes. *Semin. Cell Dev. Biol.* 74, 4–10. doi:10.1016/j.semcdb.2017.08.020

Ghossoub, R., CHéRY, M., Audebert, S., Leblanc, R., Egea-Jimenez, A., Lembo, F., et al. (2020). Tetraspanin-6 negatively regulates exosome production. *Proc. Natl. Acad. Sci. U. S. A.* 117, 5913–5922. doi:10.1073/pnas.1922447117

Gonda, A., Kabagwira, J., Senthil, G., and Wall, N. (2019). Internalization of exosomes through receptor-mediated endocytosis. *Mol. Cancer Res.* 17, 337–347. doi:10.1158/1541-7786.MCR-18-0891

Guiot, J., Cambier, M., Boeckx, A., Henket, M., Nivelles, O., Gester, F., et al. (2020). Macrophage-derived exosomes attenuate fibrosis in airway epithelial cells through delivery of antifibrotic miR-142-3p. *Thorax* 75, 870–881. doi:10.1136/thoraxjnl-2019-214077

Guiot, J., Moermans, C., Henket, M., Corhay, J., and Louis, R. (2017). Blood biomarkers in idiopathic pulmonary fibrosis. *Lung* 195, 273–280. doi:10.1007/s00408-017-9993-5

Guiot, J., Struman, I., Louis, E., Louis, R., Malaise, M., and Njock, M. S. (2019). Exosomal miRNAs in lung diseases: From biologic function to therapeutic targets. *J. Clin. Med.* 8, E1345. doi:10.3390/jcm8091345

Gurunathan, S., Kang, M., Qasim, M., Khan, K., and Kim, J. (2021). Biogenesis, membrane trafficking, functions, and next generation nanotherapeutics medicine of extracellular vesicles. *Int. J. Nanomedicine* 16, 3357–3383. doi:10.2147/IJN.S310357

Haak, A. J., Girtman, M. A., Ali, M. F., Carmona, E. M., Limper, A. H., and Tschumperlin, D. J. (2017). Phenylpyrrolidine structural mimics of pirfenidone lacking antifibrotic activity: A new tool for mechanism of action studies. *Eur. J. Pharmacol.* 811, 87–92. doi:10.1016/j.ejphar.2017.05.050

Harding, C., Heuser, J., and Stahl, P. (1983). Receptor-mediated endocytosis of transferrin and recycling of the transferrin receptor in rat reticulocytes. *J. Cell Biol.* 97, 329–339. doi:10.1083/jcb.97.2.329

Hassanpour, M., Rezabakhsh, A., Rezaie, J., Nouri, M., and Rahbarghazi, R. (2020). Exosomal cargos modulate autophagy in recipient cells via different signaling pathways. *Cell Biosci.* 10, 92. doi:10.1186/s13578-020-00455-7

Hessvik, N., and Llorente, A. (2018). Current knowledge on exosome biogenesis and release. *Cell. Mol. Life Sci.* 75, 193–208. doi:10.1007/s00018-017-2595-9

Heukels, P., Moor, C. C., von der THüSEN, J. H., Wijsenbeek, M. S., and Kool, M. (2019). Inflammation and immunity in IPF pathogenesis and treatment. *Respir. Med.* 147, 79–91. doi:10.1016/j.rmed.2018.12.015

Hewlett, J. C., Kropski, J. A., and Blackwell, T. S. (2018). Idiopathic pulmonary fibrosis: Epithelial-mesenchymal interactions and emerging therapeutic targets. *Matrix Biol.* 71-72, 112–127. doi:10.1016/j.matbio.2018.03.021

Horibe, S., Tanahashi, T., Kawauchi, S., Murakami, Y., and Rikitake, Y. (2018). Mechanism of recipient cell-dependent differences in exosome uptake. *BMC Cancer* 18, 47. doi:10.1186/s12885-017-3958-1

Hoyer, M. J., Chitwood, P. J., Ebmeier, C. C., Striepen, J. F., Qi, R. Z., Old, W. M., et al. (2018). A novel class of ER membrane proteins regulates ER-associated endosome fission. *Cell* 175, 254–265. e14. doi:10.1016/j.cell.2018.08.030

Huleihel, L., Ben-Yehudah, A., Milosevic, J., Yu, G., Pandit, K., Sakamoto, K., et al. (2014). Let-7d microRNA affects mesenchymal phenotypic properties of lung fibroblasts. *Am. J. Physiol. Lung Cell. Mol. Physiol.* 306, L534–L542. doi:10.1152/ajplung.00149.2013

Inomata, M., Kamio, K., Azuma, A., Matsuda, K., Usuki, J., Morinaga, A., et al. (2021). Rictor-targeting exosomal microRNA-16 ameliorates lung fibrosis by inhibiting the mTORC2-SPARC axis. *Exp. Cell Res.* 398, 112416. doi:10.1016/j.yexcr.2020.112416

Janockova, J., Slovinska, L., Harvanova, D., Spakova, T., and Rosocha, J. (2021). New therapeutic approaches of mesenchymal stem cells-derived exosomes. *J. Biomed. Sci.* 28, 39. doi:10.1186/s12929-021-00736-4

Ji, K., Fan, M., Huang, D., Sun, L., Li, B., Xu, R., et al. (2022). Clodronate-nintedanib-loaded exosome-liposome hybridization enhances the liver fibrosis therapy by inhibiting Kupffer cell activity. *Biomater. Sci.* 10, 702–713. doi:10.1039/d1bm01663f

Jin, H., Tang, Y., Yang, L., Peng, X., Li, B., Fan, Q., et al. (2021). Rab GTPases: Central coordinators of membrane trafficking in cancer. *Front. Cell Dev. Biol.* 9, 648384. doi:10.3389/fcell.2021.648384

Johnstone, R., Adam, M., Hammond, J., Orr, L., and Turbide, C. (1987). Vesicle formation during reticulocyte maturation. Association of plasma membrane activities with released vesicles (exosomes). *J. Biol. Chem.* 262, 9412–9420. doi:10.1016/s0021-9258(18)48095-7

Johnstone, R. (1992). The jeanne manery-Fisher memorial lecture 1991. Maturation of reticulocytes: formation of exosomes as a mechanism for shedding membrane proteins. *Biochem. Cell Biol.* 70, 179–190. doi:10.1139/o92-028

Kalluri, R., and Lebleu, V. (2020). The biology function and biomedical applications of exosomes. *Science* 367, eaau6977. doi:10.1126/science.aau6977

Kaur, G., Maremanda, K. P., Campos, M., Chand, H. S., Li, F., Hirani, N., et al. (2021). Distinct exosomal miRNA profiles from BALF and lung tissue of COPD and IPF patients. *Int. J. Mol. Sci.* 22, 11830. doi:10.3390/ijms222111830

Kaur, G., Singh, K., Maremanda, K. P., Li, D., Chand, H. S., and Rahman, I. (2020). Differential plasma exosomal long non-coding RNAs expression profiles and their emerging role in E-cigarette users, cigarette, waterpipe, and dual smokers. *PloS One* 15, e0243065. doi:10.1371/journal.pone.0243065

Keshtkar, S., Kaviani, M., Soleimanian, S., Azarpira, N., Asvar, Z., and Pakbaz, S. (2021). Stem cell-derived exosome as potential therapeutics for microbial diseases. *Front. Microbiol.* 12, 786111. doi:10.3389/fmicb.2021.786111

Kinoshita, T., and Goto, T. (2019). Molecular mechanisms of pulmonary fibrogenesis and its progression to lung cancer: A review. *Int. J. Mol. Sci.* 20, E1461. doi:10.3390/ijms20061461

Kuse, N., Kamio, K., Azuma, A., Matsuda, K., Inomata, M., Usuki, J., et al. (2020). Exosome-derived microRNA-22 ameliorates pulmonary fibrosis by regulating fibroblast-to-myofibroblast differentiation *in vitro* and *in vivo*. *J. Nippon. Med. Sch.* 87, 118–128. doi:10.1272/jnms.JNMS.2020_87-302

Lacedonia, D., Scioscia, G., Soccio, P., Conese, M., Catucci, L., Palladino, G. P., et al. (2021). Downregulation of exosomal let-7d and miR-16 in idiopathic pulmonary fibrosis. *BMC Pulm. Med.* 21, 188. doi:10.1186/s12890-021-01550-2

Larios, J., Mercier, V., Roux, A., and Gruenberg, J. (2020). ALIX- and ESCRT-III-dependent sorting of tetraspanins to exosomes. *J. Cell Biol.* 219. doi:10.1083/jcb.201904113

Li, S., Lin, Z., Jiang, X., and Yu, X. (2018). Exosomal cargo-loading and synthetic exosome-mimics as potential therapeutic tools. *Acta Pharmacol. Sin.* 39, 542–551. doi:10.1038/aps.2017.178

Li, T., Yan, Y., Wang, B., Qian, H., Zhang, X., Shen, L., et al. (2013). Exosomes derived from human umbilical cord mesenchymal stem cells alleviate liver fibrosis. *Stem Cells Dev.* 22, 845–854. doi:10.1089/scd.2012.0395

Liang, H., Liu, S., Chen, Y., Bai, X., Liu, L., Dong, Y., et al. (2016). miR-26a suppresses EMT by disrupting the Lin28B/let-7d axis: potential cross-talks among miRNAs in IPF. *J. Mol. Med.* 94, 655–665. doi:10.1007/s00109-016-1381-8

Liu, B., Jiang, T., Hu, X., Liu, Z., Zhao, L., Liu, H., et al. (2018). Downregulation of microRNA-30a in bronchoalveolar lavage fluid from idiopathic pulmonary fibrosis patients. *Mol. Med. Rep.* 18, 5799–5806. doi:10.3892/mmr.2018.9565

Liu, J., Ren, L., Li, S., Li, W., Zheng, X., Yang, Y., et al. (2021). The biology, function, and applications of exosomes in cancer. *Acta Pharm. Sin. B* 11, 2783–2797. doi:10.1016/j.apsb.2021.01.001

Lloret-Llinares, M., Karadoulama, E., Chen, Y., Wojenski, L., Villafano, G., Bornholdt, J., et al. (2018). The RNA exosome contributes to gene expression regulation during stem cell differentiation. *Nucleic Acids Res.* 46, 11502–11513. doi:10.1093/nar/gky817

Luzina, I. G., Todd, N. W., Sundararajan, S., and Atamas, S. P. (2015). The cytokines of pulmonary fibrosis: Much learned, much more to learn. *Cytokine* 74, 88–100. doi:10.1016/j.cyto.2014.11.008

Lv, M., Liu, Y., Ma, S., and Yu, Z. (2019). Current advances in idiopathic pulmonary fibrosis: the pathogenesis, therapeutic strategies and candidate molecules. *Future Med. Chem.* 11, 2595–2620. doi:10.4155/fmc-2019-0111

Makiguchi, T., Yamada, M., Yoshioka, Y., Sugiura, H., Koarai, A., Chiba, S., et al. (2016). Serum extracellular vesicular miR-21-5p is a predictor of the prognosis in idiopathic pulmonary fibrosis. *Respir. Res.* 17, 110. doi:10.1186/s12931-016-0427-3

Mansouri, N., Willis, G. R., Fernandez-Gonzalez, A., Reis, M., Nassiri, S., Mitsialis, S. A., et al. (2019). Mesenchymal stromal cell exosomes prevent and revert experimental pulmonary fibrosis through modulation of monocyte phenotypes. *JCI Insight* 4, 128060. doi:10.1172/jci.insight.128060

Martin-Medina, A., Lehmann, M., Burgy, O., Hermann, S., Baarsma, H. A., Wagner, D. E., et al. (2018). Increased extracellular vesicles mediate WNT5A signaling in idiopathic pulmonary fibrosis. *Am. J. Respir. Crit. Care Med.* 198, 1527–1538. doi:10.1164/rccm.201708-1580OC

Mashouri, L., Yousefi, H., Aref, A. R., Ahadi, A. M., Molaei, F., and Alahari, S. K. (2019). Exosomes: composition, biogenesis, and mechanisms in cancer metastasis and drug resistance. *Mol. Cancer* 18, 75. doi:10.1186/s12943-019-0991-5

Massagué, J. (2012). TGFβ signalling in context. *Nat. Rev. Mol. Cell Biol.* 13, 616–630. doi:10.1038/nrm3434

Mei, Q., Liu, Z., Zuo, H., Yang, Z., and Qu, J. (2021). Idiopathic pulmonary fibrosis: An update on pathogenesis. *Front. Pharmacol.* 12, 797292. doi:10.3389/fphar.2021.797292

Messenger, S., Woo, S., Sun, Z., and Martin, T. (2018). A Ca $^{2+}$-stimulated exosome release pathway in cancer cells is regulated by Munc13-4. *J. Cell Biol.* 217, 2877–2890. doi:10.1083/jcb.201710132

Min, H., Fan, S., Song, S., Zhuang, Y., Li, H., Wu, Y., et al. (2016). Plasma microRNAs are associated with acute exacerbation in idiopathic pulmonary fibrosis. *Diagn. Pathol.* 11, 135. doi:10.1186/s13000-016-0583-2

Montay-Gruel, P., Zhu, Y., Petit, B., Leavitt, R., Warn, M., Giedzinski, E., et al. (2020). Extracellular vesicles for the treatment of radiation-induced normal tissue toxicity in the lung. *Front. Oncol.* 10, 602763. doi:10.3389/fonc.2020.602763

Njock, M. S., Guiot, J., Henket, M. A., Nivelles, O., Thiry, M., Dequiedt, F., et al. (2019). Sputum exosomes: promising biomarkers for idiopathic pulmonary fibrosis. *Thorax* 74, 309–312. doi:10.1136/thoraxjnl-2018-211897

Osaki, M., and Okada, F. (2019). Exosomes and their role in cancer progression. *Yonago Acta Med.* 62, 182–190. doi:10.33160/yam.2019.06.002

Pan, B., Teng, K., Wu, C., Adam, M., and Johnstone, R. (1985). Electron microscopic evidence for externalization of the transferrin receptor in vesicular form in sheep reticulocytes. *J. Cell Biol.* 101, 942–948. doi:10.1083/jcb.101.3.942

Pandit, K., Corcoran, D., Yousef, H., Yarlagadda, M., Tzouvelekis, A., Gibson, K., et al. (2010). Inhibition and role of let-7d in idiopathic pulmonary fibrosis. *Am. J. Respir. Crit. Care Med.* 182, 220–229. doi:10.1164/rccm.200911-1698OC

Picciolini, S., RODà, F., Bedoni, M., and Gualerzi, A. (2021). Advances in the field of micro- and nanotechnologies applied to extracellular vesicle research: Take-home message from ISEV2021. *Micromachines* 12, 1563. doi:10.3390/mi12121563

Qin, X., Lin, X., Liu, L., Li, Y., Li, X., Deng, Z., et al. (2021). Macrophage-derived exosomes mediate silica-induced pulmonary fibrosis by activating fibroblast in an endoplasmic reticulum stress-dependent manner. *J. Cell. Mol. Med.* 25, 4466–4477. doi:10.1111/jcmm.16524

Rezaie, J., Ahmadi, M., Ravanbakhsh, R., Mojarad, B., Mahbubfam, S., Shaban, S. A., et al. (2022). Tumor-derived extracellular vesicles: The metastatic organotropism drivers. *Life Sci.* 289, 120216. doi:10.1016/j.lfs.2021.120216

Richeldi, L., Collard, H. R., and Jones, M. G. (2017). Idiopathic pulmonary fibrosis. *Lancet (London, Engl.* 389, 1941–1952. doi:10.1016/S0140-6736(17)30866-8

Rong, X., Liu, J., Yao, X., Jiang, T., Wang, Y., and Xie, F. (2019). Human bone marrow mesenchymal stem cells-derived exosomes alleviate liver fibrosis through the Wnt/β-catenin pathway. *Stem Cell Res. Ther.* 10, 98. doi:10.1186/s13287-019-1204-2

Royce, S. G., Patel, K. P., Mao, W., Zhu, D., Lim, R., and Samuel, C. S. (2019). Serelaxin enhances the therapeutic effects of human amnion epithelial cell-derived exosomes in experimental models of lung disease. *Br. J. Pharmacol.* 176, 2195–2208. doi:10.1111/bph.14666

Saint-Pol, J., Gosselet, F., Duban-Deweer, S., Pottiez, G., and Karamanos, Y. (2020). Targeting and crossing the blood-brain barrier with extracellular vesicles. *Cells* 9, E851. doi:10.3390/cells9040851

Savina, A., Fader, C., Damiani, M., and Colombo, M. (2005). Rab11 promotes docking and fusion of multivesicular bodies in a calcium-dependent manner. *Traffic* 6, 131–143. doi:10.1111/j.1600-0854.2004.00257.x

Sgalla, G., Franciosa, C., Simonetti, J., and Richeldi, L. (2020). Pamrevlumab for the treatment of idiopathic pulmonary fibrosis. *Expert Opin. Investig. Drugs* 29, 771–777. doi:10.1080/13543784.2020.1773790

Sgalla, G., Iovene, B., Calvello, M., Ori, M., Varone, F., and Richeldi, L. (2018). Idiopathic pulmonary fibrosis: pathogenesis and management. *Respir. Res.* 19, 32. doi:10.1186/s12931-018-0730-2

Shi, M., Chen, B., Mahajan, D., Boh, B. K., Zhou, Y., Dutta, B., et al. (2018). Amino acids stimulate the endosome-to-Golgi trafficking through Ragulator and small GTPase Arl5. *Nat. Commun.* 9, 4987. doi:10.1038/s41467-018-07444-y

Skibba, M., Drelich, A., Poellmann, M., Hong, S., and Brasier, A. R. (2020). Nanoapproaches to modifying epigenetics of epithelial mesenchymal transition for treatment of pulmonary fibrosis. *Front. Pharmacol.* 11, 607689. doi:10.3389/fphar.2020.607689

Song, L., Tang, S., Han, X., Jiang, Z., Dong, L., Liu, C., et al. (2019). KIBRA controls exosome secretion via inhibiting the proteasomal degradation of Rab27a. *Nat. Commun.* 10, 1639. doi:10.1038/s41467-019-09720-x

Soraya, H., Sani, N. A., Jabbari, N., and Rezaie, J. (2021). Metformin increases exosome biogenesis and secretion in U87 MG human glioblastoma cells: A possible mechanism of therapeutic resistance. *Arch. Med. Res.* 52, 151–162. doi:10.1016/j.arcmed.2020.10.007

Spagnolo, P., Tonelli, R., Cocconcelli, E., Stefani, A., and Richeldi, L. (2012). Idiopathic pulmonary fibrosis: diagnostic pitfalls and therapeutic challenges. *Multidiscip. Respir. Med.* 7, 42. doi:10.1186/2049-6958-7-42

Sun, L., Fan, M., Huang, D., Li, B., Xu, R., Gao, F., et al. (2021a). Clodronate-loaded liposomal and fibroblast-derived exosomal hybrid system for enhanced drug delivery to pulmonary fibrosis. *Biomaterials* 271, 120761. doi:10.1016/j.biomaterials.2021.120761

Sun, L., Zhu, M., Feng, W., Lin, Y., Yin, J., Jin, J., et al. (2019). Exosomal miRNA let-7 from menstrual blood-derived endometrial stem cells alleviates pulmonary fibrosis through regulating mitochondrial DNA damage. *Oxid. Med. Cell. Longev.* 2019, 4506303. doi:10.1155/2019/4506303

Sun, N. N., Zhang, Y., Huang, W. H., Zheng, B. J., Jin, S. Y., Li, X., et al. (2021b). Macrophage exosomes transfer angiotensin II type 1 receptor to lung fibroblasts mediating bleomycin-induced pulmonary fibrosis. *Chin. Med. J.* 134, 2175–2185. doi:10.1097/CM9.0000000000001605

Sundarakrishnan, A., Chen, Y., Black, L. D., Aldridge, B. B., and Kaplan, D. L. (2018). Engineered cell and tissue models of pulmonary fibrosis. *Adv. Drug Deliv. Rev.* 129, 78–94. doi:10.1016/j.addr.2017.12.013

Tan, J. L., Lau, S. N., Leaw, B., Nguyen, H. P. T., Salamonsen, L. A., Saad, M. I., et al. (2018). Amnion epithelial cell-derived exosomes restrict lung injury and enhance endogenous lung repair. *Stem Cells Transl. Med.* 7, 180–196. doi:10.1002/sctm.17-0185

Toh, W., Lai, R., Zhang, B., and Lim, S. (2018). MSC exosome works through a protein-based mechanism of action. *Biochem. Soc. Trans.* 46, 843–853. doi:10.1042/BST20180079

Tomassetti, S., Wells, A. U., Costabel, U., Cavazza, A., Colby, T. V., Rossi, G., et al. (2016). Bronchoscopic lung cryobiopsy increases diagnostic confidence in the multidisciplinary diagnosis of idiopathic pulmonary fibrosis. *Am. J. Respir. Crit. Care Med.* 193, 745–752. doi:10.1164/rccm.201504-0711OC

Tsukui, T., Sun, K.-H., Wetter, J. B., Wilson-Kanamori, J. R., Hazelwood, L. A., Henderson, N. C., et al. (2020). Collagen-producing lung cell atlas identifies multiple subsets with distinct localization and relevance to fibrosis. *Nat. Commun.* 11, 1920. doi:10.1038/s41467-020-15647-5

Villarroya-Beltri, C., Baixauli, F., GUTIéRREZ-VáZQUEZ, C., SáNCHEZ-Madrid, F., and Mittelbrunn, M. (2014). Sorting it out: regulation of exosome loading. *Semin. Cancer Biol.* 28, 3–13. doi:10.1016/j.semcancer.2014.04.009

Wang, F., Xia, H., and Yao, S. (2020). Regulatory T cells are a double-edged sword in pulmonary fibrosis. *Int. Immunopharmacol.* 84, 106443. doi:10.1016/j.intimp.2020.106443

Wang, T., Li, L., and Hong, W. (2017). SNARE proteins in membrane trafficking. *Traffic* 18, 767–775. doi:10.1111/tra.12524

Wang, Y. C., Xie, H., Zhang, Y. C., Meng, Q. H., Xiong, M. M., Jia, M. W., et al. (2021). Exosomal miR-107 antagonizes profibrotic phenotypes of pericytes by targeting a pathway involving HIF-1α/Notch1/PDGFRβ/YAP1/Twist1 axis *in vitro*. *Am. J. Physiol. Heart Circ. Physiol.* 320, H520–h534. doi:10.1152/ajpheart.00373.2020

Wei, D., Zhan, W., Gao, Y., Huang, L., Gong, R., Wang, W., et al. (2021). RAB31 marks and controls an ESCRT-independent exosome pathway. *Cell Res.* 31, 157–177. doi:10.1038/s41422-020-00409-1

Wei, H., Chen, Q., Lin, L., Sha, C., Li, T., Liu, Y., et al. (2021b). Regulation of exosome production and cargo sorting. *Int. J. Biol. Sci.* 17, 163–177. doi:10.7150/ijbs.53671

Willis, G. R., Fernandez-Gonzalez, A., Anastas, J., Vitali, S. H., Liu, X., Ericsson, M., et al. (2018). Mesenchymal stromal cell exosomes ameliorate experimental bronchopulmonary dysplasia and restore lung function through macrophage immunomodulation. *Am. J. Respir. Crit. Care Med.* 197, 104–116. doi:10.1164/rccm.201705-0925OC

Wortzel, I., Dror, S., Kenific, C. M., and Lyden, D. (2019). Exosome-mediated metastasis: Communication from a distance. *Dev. Cell* 49, 347–360. doi:10.1016/j.devcel.2019.04.011

Wozniak, A. L., Adams, A., King, K. E., Dunn, W., Christenson, L. K., Hung, W. T., et al. (2020). The RNA binding protein FMR1 controls selective exosomal miRNA cargo loading during inflammation. *J. Cell Biol.* 219, e201912074. doi:10.1083/jcb.201912074

Xiao, K., He, W., Guan, W., Hou, F., Yan, P., Xu, J., et al. (2020). Mesenchymal stem cells reverse EMT process through blocking the activation of NF-κB and Hedgehog pathways in LPS-induced acute lung injury. *Cell Death Dis.* 11, 863. doi:10.1038/s41419-020-03034-3

Xie, H., Gao, Y. M., Zhang, Y. C., Jia, M. W., Peng, F., Meng, Q. H., et al. (2020). Low let-7d exosomes from pulmonary vascular endothelial cells drive lung pericyte fibrosis through the TGFβRI/FoxM1/Smad/β-catenin pathway. *J. Cell. Mol. Med.* 24, 13913–13926. doi:10.1111/jcmm.15989

Xie, L., and Zeng, Y. (2020). Therapeutic potential of exosomes in pulmonary fibrosis. *Front. Pharmacol.* 11, 590972. doi:10.3389/fphar.2020.590972

Xie, S., Zhang, Q., and Jiang, L. (2022). Current Knowledge on exosome biogenesis, cargo-sorting mechanism and therapeutic implications. *Membranes* 12, 498. doi:10.3390/membranes12050498

Xu, C., Hou, L., Zhao, J., Wang, Y., Jiang, F., Jiang, Q., et al. (2022). Exosomal let-7i-5p from three-dimensional cultured human umbilical cord mesenchymal stem cells inhibits fibroblast activation in silicosis through targeting TGFBR1. *Ecotoxicol. Environ. Saf.* 233, 113302. doi:10.1016/j.ecoenv.2022.113302

Xu, C., Zhao, J., Li, Q., Hou, L., Wang, Y., Li, S., et al. (2020). Exosomes derived from three-dimensional cultured human umbilical cord mesenchymal stem cells ameliorate pulmonary fibrosis in a mouse silicosis model. *Stem Cell Res. Ther.* 11, 503. doi:10.1186/s13287-020-02023-9

Yamada, M. (2021). Extracellular vesicles: Their emerging roles in the pathogenesis of respiratory diseases. *Respir. Investig.* 59, 302–311. doi:10.1016/j.resinv.2021.02.006

Yanagihara, T., Chong, S. G., Vierhout, M., Hirota, J. A., Ask, K., and Kolb, M. (2020). Current models of pulmonary fibrosis for future drug discovery efforts. *Expert Opin. Drug Discov.* 15, 931–941. doi:10.1080/17460441.2020.1755252

Yang, D., Zhang, W., Zhang, H., Zhang, F., Chen, L., Ma, L., et al. (2020a). Progress, opportunity, and perspective on exosome isolation - efforts for efficient exosome-based theranostics. *Theranostics* 10, 3684–3707. doi:10.7150/thno.41580

Yang, J., Hu, H., Zhang, S., Jiang, L., Cheng, Y., Xie, H., et al. (2020b). Human umbilical cord mesenchymal stem cell-derived exosomes alleviate pulmonary fibrosis in mice by inhibiting epithelial-mesenchymal transition. *Nan Fang. Yi Ke Da Xue Xue Bao* 40, 988–994. doi:10.12122/j.issn.1673-4254.2020.07.11

Yang, L., Peng, X., Li, Y., Zhang, X., Ma, Y., Wu, C., et al. (2019). Long non-coding RNA HOTAIR promotes exosome secretion by regulating RAB35 and SNAP23 in hepatocellular carcinoma. *Mol. Cancer* 18, 78. doi:10.1186/s12943-019-0990-6

Yao, M. Y., Zhang, W. H., Ma, W. T., Liu, Q. H., Xing, L. H., and Zhao, G. F. (2019). microRNA-328 in exosomes derived from M2 macrophages exerts a promotive effect on the progression of pulmonary fibrosis via FAM13A in a rat model. *Exp. Mol. Med.* 51, 1–16. doi:10.1038/s12276-019-0255-x

Yu, Y., Liu, X., Zhao, Z., Xu, Z., Qiao, Y., Zhou, Y., et al. (2021). The extracellular matrix enriched with exosomes for the treatment on pulmonary fibrosis in mice. *Front. Pharmacol.* 12, 747223. doi:10.3389/fphar.2021.747223

Yu, Z., Shi, M., Stewart, T., Fernagut, P., Huang, Y., Tian, C., et al. (2020). Reduced oligodendrocyte exosome secretion in multiple system atrophy involves SNARE dysfunction. *Brain.* 143, 1780–1797. doi:10.1093/brain/awaa110

Zhang, E., Geng, X., Shan, S., Li, P., Li, S., Li, W., et al. (2021). Exosomes derived from bone marrow mesenchymal stem cells reverse epithelial-mesenchymal transition potentially via attenuating Wnt/β-catenin signaling to alleviate silica-induced pulmonary fibrosis. *Toxicol. Mech. Methods* 31, 655–666. doi:10.1080/15376516.2021.1950250

Zhang, L., and Yu, D. (2019). Exosomes in cancer development, metastasis, and immunity. *Biochim. Biophys. Acta. Rev. Cancer* 1871, 455–468. doi:10.1016/j.bbcan.2019.04.004

Zhang, Y., Bi, J., Huang, J., Tang, Y., du, S., and Li, P. (2020a). Exosome: A review of its classification, isolation techniques, storage, diagnostic and targeted therapy applications. *Int. J. Nanomedicine* 15, 6917–6934. doi:10.2147/IJN.S264498

Zhang, Z., Ge, L., Zhang, S., Wang, J., Jiang, W., Xin, Q., et al. (2020b). The protective effects of MSC-EXO against pulmonary hypertension through regulating Wnt5a/BMP signalling pathway. *J. Cell. Mol. Med.* 24, 13938–13948. doi:10.1111/jcmm.16002

Zhou, Y., Gao, Y., Zhang, W., Chen, Y., Jin, M., and Yang, Z. (2021). Exosomes derived from induced pluripotent stem cells suppresses M2-type macrophages during pulmonary fibrosis via miR-302a-3p/TET1 axis. *Int. Immunopharmacol.* 99, 108075. doi:10.1016/j.intimp.2021.108075

Zhou, Y., He, Z., Gao, Y., Zheng, R., Zhang, X., Zhao, L., et al. (2016). Induced pluripotent stem cells inhibit bleomycin-induced pulmonary fibrosis in mice through suppressing TGF-β1/smad-mediated epithelial to mesenchymal transition. *Front. Pharmacol.* 7, 430. doi:10.3389/fphar.2016.00430

Zhu, L., Chen, Y., Chen, M., and Wang, W. (2021). Mechanism of miR-204-5p in exosomes derived from bronchoalveolar lavage fluid on the progression of pulmonary fibrosis via AP1S2. *Ann. Transl. Med.* 9, 1068. doi:10.21037/atm-20-8033

frontiers | Frontiers in Pharmacology

TYPE Systematic Review
PUBLISHED 06 September 2022
DOI 10.3389/fphar.2022.948101

Check for updates

OPEN ACCESS

EDITED BY
Apostolos Zarros,
Pharmacological Research Observatory, United Kingdom

REVIEWED BY
Swarna Bale,
National Institute of Pharmaceutical Education and Research, India
Amit Khurana,
University Hospital RWTH Aachen, Germany

*CORRESPONDENCE
Han Yang,
15882458490@163.com
Quanyu Du,
quanydu@cdutcm.edu.cn

SPECIALTY SECTION
This article was submitted to Experimental Pharmacology and Drug Discovery, a section of the journal Frontiers in Pharmacology

RECEIVED 19 May 2022
ACCEPTED 11 August 2022
PUBLISHED 06 September 2022

CITATION
Wu X, Xiao X, Chen X, Yang M, Hu Z, Shuai S, Fu Q, Yang H and Du Q (2022), Effectiveness and mechanism of metformin in animal models of pulmonary fibrosis: A preclinical systematic review and meta-analysis. *Front. Pharmacol.* 13:948101. doi: 10.3389/fphar.2022.948101

COPYRIGHT
© 2022 Wu, Xiao, Chen, Yang, Hu, Shuai, Fu, Yang and Du. This is an open-access article distributed under the terms of the Creative Commons Attribution License (CC BY). The use, distribution or reproduction in other forums is permitted, provided the original author(s) and the copyright owner(s) are credited and that the original publication in this journal is cited, in accordance with accepted academic practice. No use, distribution or reproduction is permitted which does not comply with these terms.

Effectiveness and mechanism of metformin in animal models of pulmonary fibrosis: A preclinical systematic review and meta-analysis

Xuanyu Wu[1], Xiang Xiao[1], Xinyu Chen[1], Maoyi Yang[1], Zhipeng Hu[1], Sijia Shuai[1], Qinwei Fu[1], Han Yang[2]* and Quanyu Du[3]*

[1]Hospital of Chengdu University of Traditional Chinese Medicine, School of Clinical Medicine, Chengdu University of Traditional Chinese Medicine, Chengdu, China, [2]Department of Geriatrics, Hospital of Chengdu University of Traditional Chinese Medicine, Chengdu, China, [3]Department of Endocrinology, Hospital of Chengdu University of Traditional Chinese Medicine, Chengdu, China

Background: Pulmonary fibrosis (PF) is a lung disease with no curative drug, characterized by a progressive decrease in lung function. Metformin (MET) is a hypoglycemic agent with the advantages of high safety and low cost and has been used in several *in vivo* trials to treat fibrotic diseases.

Objective: This study aimed to explore the efficacy and safety of MET in treating PF and elaborate on its mechanism.

Methods: Eight databases were searched for *in vivo* animal trials of MET for PF from the time of database creation until 1 March 2022. The risk of bias quality assessment of the included studies was conducted using SYRCLE's risk of bias assessment. Pulmonary inflammation and fibrosis scores were the primary outcomes of this study. Hydroxyproline (HYP), type I collagen (collagen I), α-smooth muscle actin (α-SMA), transforming growth factor-β (TGF-β), Smad, AMP-activated protein kinase (AMPK), and extracellular signal–regulated kinase (ERK) protein expression in lung tissues and animal mortality were secondary outcomes. Effect magnitudes were combined and calculated using Revman 5.3 and Stata 16.0 to assess the efficacy and safety of MET in animal models of PF. Inter-study heterogeneity was examined using the I^2 or Q test, and publication bias was assessed using funnel plots and Egger's test.

Results: A total of 19 studies involving 368 animals were included, with a mean risk of bias of 5.9. The meta-analysis showed that MET significantly suppressed the level of inflammation and degree of PF in the lung tissue of the PF animal model. MET also reduced the content of HYP, collagen I, α-SMA, and TGF-β and phosphorylation levels of Smad2, Smad3, p-smad2/3/smad2/3, ERK1/2, and p-ERK1/2/ERK1/2 in lung tissues. MET also elevated AMPK/p-AMPK levels in lung tissues and significantly reduced animal mortality.

Conclusion: The results of this study suggest that MET has a protective effect on lung tissues in PF animal models and may be a potential therapeutic candidate for PF treatment.

Systematic Review Registration: https://www.crd.york.ac.uk/PROSPERO/display_record.php?RecordID=327285, identifier CRD42022327285.

KEYWORDS

pulmonary fibrosis, metformin, animal models, potential mechanisms, meta-analysis

1 Introduction

Pulmonary fibrosis (PF) is characterized by a progressive and irreversible decrease in lung function, eventually leading to respiratory failure and death. Chemical injury, drug toxicity, environmental factors, autoimmunity, and inflammatory infections are significant causes of PF pathogenesis (Thannickal et al., 2004). The most severe type of PF is idiopathic pulmonary fibrosis (IPF), which has no specific cause, with a median survival of 3–5 years after disease onset (Raghu et al., 2011; Thannickal, 2013; Travis et al., 2013). The global incidence of IPF has increased (Hutchinson et al., 2015), with a high incidence among older men, especially those with chronic diseases, such as hypertension and diabetes (King and Nathan, 2017).

In recent years, researchers have begun to link structural remodeling in the lungs to abnormalities in glucose metabolic pathways (Dos Santos et al., 2018). Diabetes mellitus (DM) is a systemic metabolic disease characterized by insulin deficiency or resistance, which causes a chronic hyperglycemic state. Inflammation, oxidative stress, and vascular damage caused by hyperglycemia often damage the cardiovascular system, kidneys, retina, and other organs (Kowluru and Chan, 2007; Kashihara et al., 2010; Folli et al., 2011; Fujita et al., 2013). The lungs possess a complex capillary network and are a target organ for diabetic microvascular injury. The correlation between DM and PF has attracted the attention of researchers in recent years. Patients with DM are at a higher risk of developing PF (Kopf et al., 2018). Hyperglycemia can thicken the alveolar septa, cause PF-related pathological structural changes in the lungs, and affect lung function, ultimately resulting in PF (Zou et al., 2017). Hyperglycemia causes inflammation and oxidative stress in the body, which are closely related to the core developmental mechanisms of PF, such as extracellular matrix (ECM) deposition, fibroblast/myofibroblast proliferation, and structural disruption of the lung tissue (Willis & Borok, 2007). Similarly, in a meta-analysis, a significant increase in the prevalence of DM was demonstrated in patients with IPF compared with that in controls, suggesting a potential positive association between DM and the development of IPF (Bai et al., 2021).

There is a lack of specific therapeutic drugs for the treatment of PF. Pirfenidone and nintedanib (Raghu et al., 2015; Teague et al., 2022), approved for the treatment of PF, have been shown to reduce the decline in forced vital capacity (FVC) and deterioration in the acute phase in patients with IPF (Richeldi et al., 2011; King et al., 2014). However, current studies show that these two drugs do not cure or reverse PF (Wollin et al., 2015); they can only prevent the development or further progression of PF. To date, no drug has been able to reverse already established PF (Dos Santos et al., 2018). Only a few patients can afford pirfenidone and nintedanib because they are expensive (Teague et al., 2022). Moreover, the diagnosis of IPF and the adverse effects of these drugs are uncertain (Maher et al., 2018; Maher and Strek, 2019). Lung transplantation is the best approach to prolong survival in patients with PF (Wynn, 2011). Therefore, it is essential to identify additional ways to treat PF. In 2018, Rangarajan et al. proposed that metformin (MET) could reverse bleomycin-induced PF in animal models. As an older drug, this new therapeutic effect of MET is appealing (Rangarajan et al., 2018). Additionally, MET is cheaper and more conducive to further research (Diabetes Prevention Program Research Group, 2012).

MET, a biguanide derivative that acts on the liver to reduce high blood glucose levels, is a commonly used first-line drug for the treatment of type 2 diabetes mellitus (T2DM) and has been used for more than 60 years (Bailey, 2017). The central mechanism of MET action is the inhibition of mitochondrial respiratory chain complex I (Batandier et al., 2006), which reduces adenosine triphosphate (ATP) production, as well as decreases adenosine monophosphate (AMP) deaminase activity and increases AMP content, thereby increasing the AMP/ATP ratio (Richeldi et al., 2011) and activating AMP-dependent protein kinase (AMPK). AMPK is a heterotrimeric protein with important roles in the metabolism and regulation of glucose, lipids, and energy (Lin & Hardie, 2018). AMPK activation enables cells to switch from an anabolic to a catabolic state (Viollet et al., 2012). It can reduce and improve DM (Foretz et al., 2019), obesity (Yerevanian & Soukas, 2019), effects of aging (Chaudhari et al., 2020), and cancer (Coyle et al., 2016).

Recent studies have shown that MET may inverse PF. MET may inhibit the transforming growth factor-beta (TGF-β)/Smad signaling pathway by activating AMPK signaling. Treatment of PF mouse models with MET resulted in significant improvement in several fibrosis marker indicators, including hydroxyproline (HYP), α-smooth muscle actin (α-SMA), TGF-β1, type I collagen (collagen I), and fibronectin. However, the anti-PF effect of MET

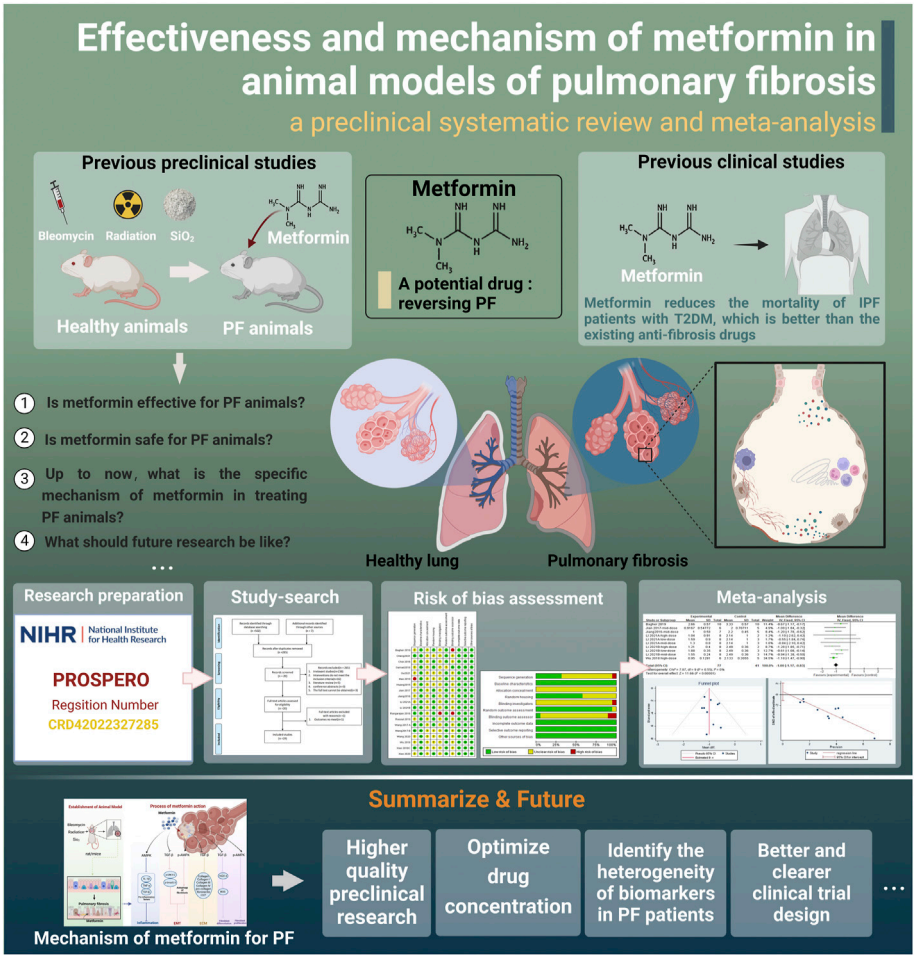


FIGURE 1
Research roadmap (created using BioRender.com).

disappeared when the same approach was used to treat AMPKa-deficient mice, suggesting that MET may act as an anti-PF agent by activating AMPK (Rangarajan et al., 2018). MET may inhibit the mammalian rapamycin (mTOR) signaling pathway *via* AMPK, upregulate Beclin1 and light chain 3 B (LC3B), downregulate p62 protein, and activate autophagy. It also inhibits the inflammatory cytokines TGF-β1, tumor necrosis factor-α (TNF-α), and interleukin-1β (IL-1β) and reduces alveolar inflammation. Elevated E-cadherin (E-Cad) levels decrease α-SMA and vimentin and inhibit the epithelial–mesenchymal transition (EMT) process (Li et al., 2021b). The anti-PF effect of MET involves the inhibition of reactive oxygen species (ROS) and lipid peroxidation product malondialdehyde (MDA), which catalyzes the expression of antioxidant proteins to inhibit intracellular oxidative stress and other pathways (Cheng et al., 2021).

We aimed to determine if MET could reverse PF. Our hypothesis was positive, and we believe that MET is a potential anti-fibrosis drug that needs to be developed and studied further. However, the efficacy and safety of MET to treat PF in animals is still uncertain and lacks sufficient evaluation; therefore, it is necessary to conduct a systematic evidence-based evaluation. Our goal was to systematically evaluate and meta-analyze the effectiveness and safety of MET in treating PF in animal models, determine the effect of MET on the related factors in the process of PF, and further explore its cellular and molecular mechanisms. A research roadmap is in Figure 1.

2 Materials and methods

This review was based on the Preferred Reporting Items for Systematic Reviews and Meta-analyses (PRISMA) statement checklist (Page et al., 2021). The protocol was registered in PROSPERO (registration number: CRD42022327285).

TABLE 1 Inclusion and exclusion criteria.

Principles	Inclusion criteria	Exclusion criteria
Animals	1. There is no restriction on the race, category, weeks of age, and sex of the included animals. Any animal previously used for pulmonary fibrosis (PF) modeling will be included	1. Not an animal model of PF. 2. Animals that have not been previously used to establish PF models
Interventions	2. Animal models of pulmonary fibrosis in the experimental and control groups are modeled using bleomycin, radiation, or silica	3. Not using bleomycin, radiation, or silica to establish PF animal models
	3. The experimental group received metformin/metformin hydrochloride. The control group was given saline or no measure of treatment	4. Treatment with metformin-based prescriptions or in combination with other drugs
	4. The route of administration is not restricted	5. Experimental design without a control group
Type	5. Randomized controlled animal experiments (*in vivo* studies) are required	6. Case reports, clinical trial studies, abstracts, editorials, reviews, conference abstracts, duplicate data, and incomplete text
Outcomes	6. (1) The primary outcome indicators are the histological effect of metformin on the degree of PF and pulmonary inflammation in animal models, using the pulmonary inflammation score to represent the degree of pulmonary inflammation and the pulmonary fibrosis score to represent the degree of PF.	7. No predetermined outcome indicators or available data
	(2) Secondary outcome indicators are the effects of metformin on fibrosis-related proteins *in vivo* in animal models of PF, including TGF-β, HYP, α-SMA, collagen I, AMPK, and extracellular signal–regulated kinase animal mortality	8. The literature does not use numerical quantification, and quantitative data are not available through the literature

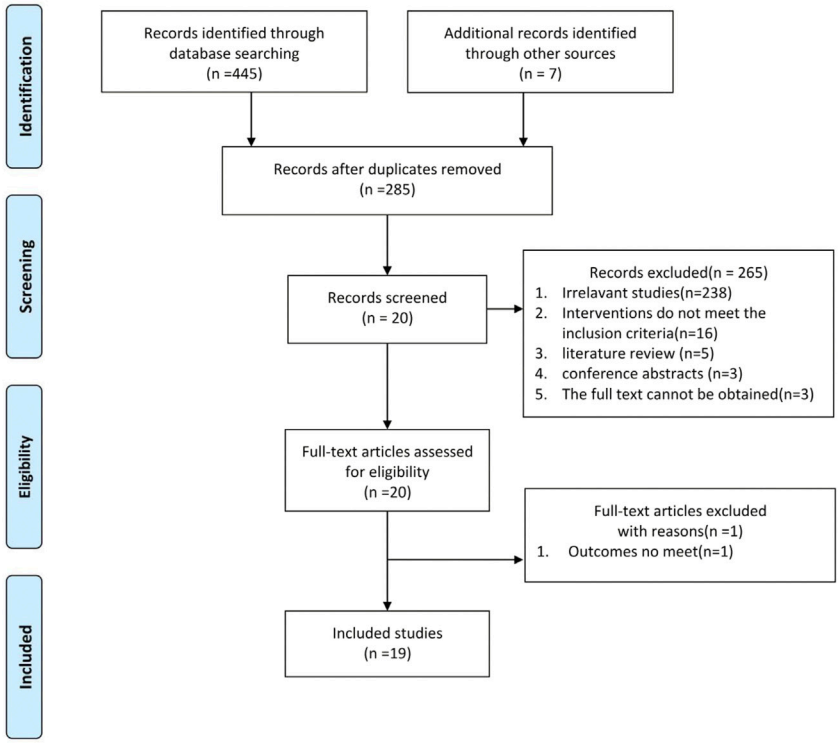


FIGURE 2
Flow diagram of the study-search process.

2.1 Data sources and search strategy

Eight databases were searched from the time of establishment to 1 March 2022: PubMed, EMBASE, Web of Science, Cochrane Library, China National Knowledge Infrastructure, Chinese Biomedical Database, VIP Database, and Wanfang Database. The abovementioned databases were searched with MET (e.g., metformin, dimethylguanylguanidine, and metformin HCl),

pulmonary fibrosis (e.g., pulmonary fibrosis, alveolitis, fibrosis, and idiopathic pulmonary fibrosis), and animal models (e.g., models, animal, animal model, and experimental) as the main keywords, and the references of the included studies were searched to obtain more available studies. The language used was limited to Chinese and English. A detailed search strategy for each database is provided in Supplementary Material S1.

2.2 Eligibility criteria and literature screening

The inclusion and exclusion criteria were predefined for the meta-analysis (Table 1) (Sun et al., 2021). Two investigators (XY-C and QW-F) independently screened the literature using EndNote X9 software. After eliminating duplicate literature, investigators excluded the literature that did not meet the inclusion criteria by reading the titles and abstracts and confirmed the final included literature by reading the full articles. In the event of disagreement, a third investigator (H-Y) arbitrated.

2.3 Data extraction

Two investigators (XX and SJ-S) independently extracted detailed data for the included studies using Excel 2019 software, including the first author, year of publication, modeling method and route, animal details, MET manufacturer batch, MET treatment regimen, narcotic drug use, ethical statement status, intervention site, primary/secondary outcomes, and between-group differences. Experimental data were uniformly recorded using the mean and standard deviation (SD), and if only standard error (SEM) was provided, the raw data were converted to standard deviation according to statistical principles. If the literature presented the experimental results graphically, Origin 2018 was used to extract data from the images, and multiple readings were obtained to reduce errors. If the literature lacked data or was reported unclearly, XY-W attempted to contact the corresponding author; if the original data were still unavailable, XY-W excluded the literature. After completing data extraction, the two investigators crosschecked the results. Disagreements were marked, summarized, discussed, and resolved in a meeting. The study was excluded if any essential results were not available.

2.4 Assessment of risk of bias

Two investigators (MY-Y and ZP-H) used SYRCLE's risk-of-bias quality assessment tool for animal experiments (Hooijmans et al., 2014). Risk of bias and methodological quality assessments of the included studies were performed. A score of 1 was assigned during the assessment process when the investigator judged an entry to be at low risk of bias, with a maximum score of 10 for one piece of literature. Disagreements were resolved by consensus or arbitration between the two authors (HY and QY-D).

2.5 Statistical analysis

For data processing of the included studies, one study contained multiple subgroups of MET doses, which were treated as independent experiments for this meta-analysis. The sample size of the control group for these independent studies was extracted by dividing the sample size of the control group by the number of experimental groups to avoid artificially increasing the sample size of the control group and further improving the accuracy of the study (Lin et al., 2020). In addition, the doses administered were pre-classified based on the inclusion of experiments to facilitate further subgroup analysis. The doses of administered MET were divided into three groups (0 < low-dose group <150 mg/kg, 150 mg/kg ≤ medium-dose group <300 mg/kg, and 300 mg/kg ≤ high-dose group ≤500 mg/kg) according to previous studies (Gamad et al., 2018; Wu, 2018; Hao et al., 2019; Li et al., 2021a; Li et al., 2021b; Cheng et al., 2021).

RevMan 5.3 and Stata 16.0 were used for data analysis in this meta-analysis. The lung tissue fibrosis score, inflammation score, and fibrosis-related proteins were analyzed as continuous variables. The mean difference (MD) and 95% confidence interval (CI) were used for the overall effect size comparison if the effect size units were the same or the assay was the same between studies. Moreover, the standardized mean difference (SMD) and 95% CI were used if the effect size units were different or if the assay differed between studies. Animal mortality was used as a dichotomous variable, and relative risk (RR) and 95% CI were used as the effect analysis statistics. Differences were considered statistically significant at $p < 0.05$.

Heterogeneity between studies was tested using the I^2 or Q-test. Heterogeneity was considered nonsignificant when $p > 0.1$ or $I^2 \leq 50$. When $p < 0.1$ or $I^2 > 50$, heterogeneity was considered significant, and sensitivity analysis was performed to determine the stability of the results. If any one piece of literature was found to have a more significant effect on inter-study heterogeneity, the effect sizes were combined after excluding that piece of literature. If there was excessive heterogeneity in important outcomes (i.e., inflammation score, fibrosis score, and TGF-β levels) and the cause could not be found after sensitivity analysis, subgroup analysis or meta-regression was used to further search for the source of heterogeneity. Dosage is the predetermined factor of subgroup analysis (Lin et al., 2020) because it may be an important factor affecting the effect (Garber et al., 1997). Each subgroup included at least two studies. For meta-regression, eight variables were analyzed: modeling method, route of administration, time of administration, animal sex, animal type, dosage, year of

publication, and manufacturer of MET. The effect of other possible factors on inter-study heterogeneity was explored in the analysis, and variables were considered sources of heterogeneity when $p < 0.05$. When heterogeneity was substantial and could not be eliminated, a random effects model was used instead of a fixed effects model. When more than ten studies were included, funnel plotting and observation were performed using Stata 16.0 with Egger's test (Sun et al., 2021). Publication bias was assessed by observing whether the funnel plot was symmetrical and the *p*-value of Egger's test. When the funnel plot was significantly asymmetrical and Egger's test $p < 0.05$, the difference was considered significant, i.e., having publication bias.

3 Results

3.1 Inclusion of study selection

Through a preliminary search of eight databases, 445 studies were identified. In addition, seven articles from our records met the requirements for this meta-analysis but did not appear in the search results, and we included those (Xavier et al., 2021). After removing duplicate studies, 285 articles remained, and we performed title and abstract readings to exclude 265 articles, including 238 irrelevant studies, 16 studies whose interventions did not meet inclusion requirements, five literature reviews, three conference abstracts, and three articles for which the full text was not available. The complete manuscripts of the 20 screened studies were then read, and one manuscript with an outcome that did not meet the requirements was excluded (Kheirollahi et al., 2019), resulting in 19 remaining studies (Huang, 2015; Choi et al., 2016; Jiang 2016; Jian 2017; Wang J. et al., 2017; Wang Y. et al., 2017; Gamad et al., 2018; Rangarajan et al., 2018; Wu 2018; Xiao et al., 2018; Farhood et al., 2019; Hao et al., 2019; Yahyapour et al., 2019; Wang et al., 2020; Xiao et al., 2020; Li et al., 2021a; Li et al., 2021b; Cheng et al., 2021; Gu et al., 2021). Six studies included multiple dose groups. Two independent trials were conducted with two levels of dosing (Choi et al., 2016; Hao et al., 2019), and four independent trials had three levels of dosing [Cheng et al., 2021; Gamad et al., 2018; Li et al., 2021a; Li et al., 2021b] out of the 29 independent studies. A flow chart of literature selection is shown in Figure 2.

3.2 Study characteristics

The characteristics of all the included studies are summarized in Supplementary Tables S2 and S3. Supplementary Table S2 shows the basic information of the included studies, and Supplementary Table S3 shows the modeling and drug treatment of the included studies. A total of 368 experimental and control animals were included in this meta-analysis. Eight of the 19 studies used mice, and the types of mice used included wild-type, C57BL/6, and NMRI. A total of 11 studies used rats; of these, eight used Sprague-Dawley rats, and three used Wistar rats. Of the studies that have elaborated on the sex of the animals, three used female, 15 used male, and one did not report sex. Only two studies have reported animals used as adults (Wang Y. et al., 2017; Gamad et al., 2018).

All included studies used three modalities, four used irradiation, three used silica particle tracheal injection, and 12 used bleomycin tracheal injection. Among the 12 studies using bleomycin, two did not report the companies of bleomycin manufacture, one was purchased from Fresenius Kabi Oncology Limited, India, one was from Hanhui Pharmaceuticals Co., Ltd., Zhejiang, China, four were from Zhejiang Hisun Pharmaceutical Co., Ltd., one was from Thermo Fisher Scientific, and three were from Nippon Kayaku, Takasaki, Japan. Modeling drugs may be an important factor affecting the results of this study. The conditions for subgroup analysis were not met, and a descriptive analysis was conducted for comparison. After modeling, the pathological manifestations of these 12 studies mentioned thickening of the alveolar septum, infiltration of inflammatory cells, and an increase in collagen fibers. Research on fibrosis and inflammation scores has also been reported. There were significant differences in fibrosis and inflammation scores between the two groups compared with that in the blank control group ($p < 0.05$). Therefore, it can be assumed that the bleomycin used in the literature included in this study were all positive in terms of their modeling effect.

All studies controlled the duration of MET treatment between 2 and 5 weeks, limiting the treatment duration to this range. MET used in the included studies was obtained from six different manufacturers, including Sino-American Shanghai Squibb Pharmaceuticals Ltd. (6), Sigma Aldrich Corporation, United States (5), Tehran Chemie Pharmaceutical Company (2), Beyotime Institute of Biotechnology, Shanghai Sine Pharmaceutical Laboratories Co., Ltd., and Cipla Pharmaceutical (1 each). Three studies did not specify the drug manufacturer used.

Drug dose is an important factor influencing the efficacy of MET (Garber et al., 1997). In the included studies, MET was administered at doses ranging from 65 to 500 mg/kg. The 29 independent studies included 11, nine, and nine studies in the low-, medium-, and high-dose groups, respectively. In the literature by Choi et al., 2016, two low-dose groups, 50 and 100 mg/kg, were present in the same study; both were considered low-dose groups, but the later combined effect sizes were distinguished by naming them Choi 2016 (50 mg/kg) and Choi 2016 (100 mg/kg).

Adverse reactions (i.e., animal deaths during the experiment) were reported in four of the 19 studies. Researchers who use animals in pursuit of academic goals must adhere to ethical principles. Among the included studies, 11 reported ethical considerations, whereas eight did not. A total of 13 studies

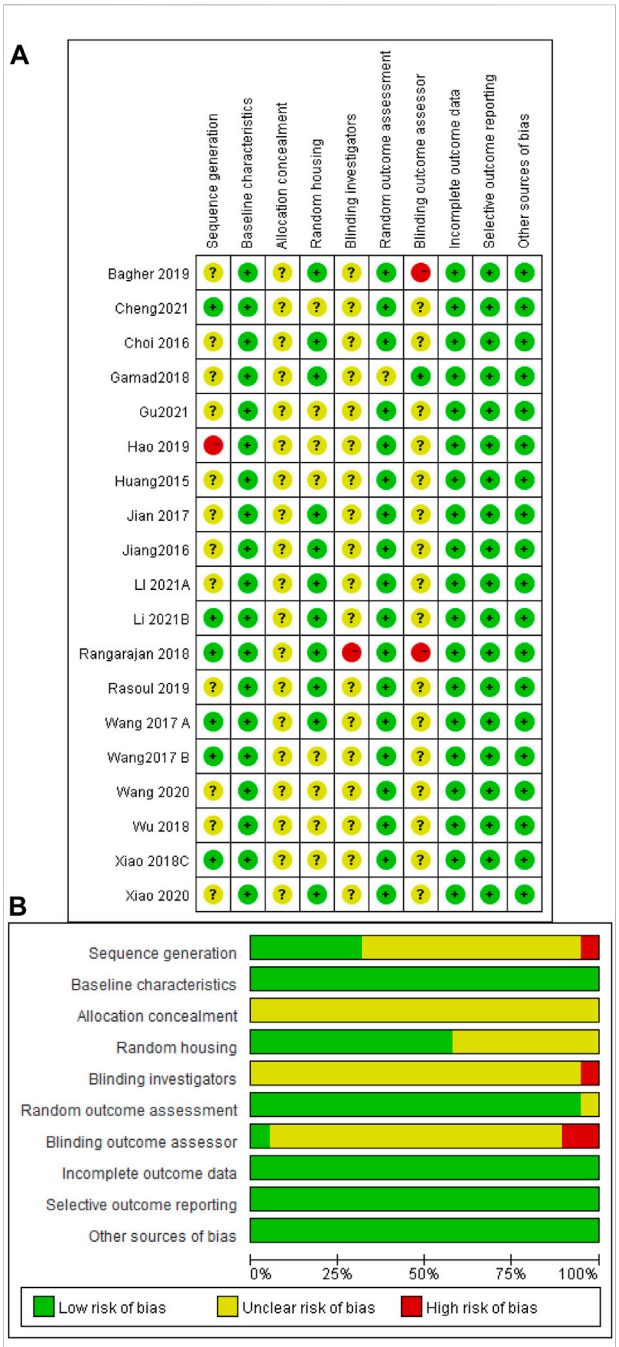


FIGURE 3
Risk of bias assessment table. Assessment of literature quality results obtained through the risk of bias by SYRCLE based on Cochrane tools. **(A)** Risk of bias summary diagram; review of authors' judgments for each risk of bias item for each included study. **(B)** Risk of bias diagram; overview of authors' judgments for each risk of bias item, expressed as a percentage of all included studies.

reported the use of anesthetics, of which six used pentobarbital sodium, four used chloral hydrate 10%, two used a combination of ketamine and xylazine, one study used isoflurane, and six did not report anesthesia. Of note, four studies reported ethical statements but did not report the use of anesthetics.

3.3 Risk of bias and quality of included studies

The risk of bias and quality of all studies were assessed and scored according to SYRCLE's risk of bias tool (Hooijmans et al., 2014) to obtain the included literature scores (Figure 3). The risk of bias scores of the included studies ranged between 5 and 7, with a mean of 5.9. Six studies were rated as low in terms of random sequence generation because they described the method of random sequence generation in detail. All studies were rated low for baseline characteristics because of the detailed description of animal characteristics and ensuring that animals were similar at baseline. When assessing allocation concealment, all studies showed unclear risk, and none described in detail whether animals were concealed at allocation. For the assessment of animal placement randomization, 11 studies were rated as low risk because they described in detail the consistency and randomization of the housing environment of the experimental animals. None of the included studies mentioned the animal keeper or the investigator performing blinding, and one study was rated as high risk because it did not describe the experimental procedure. One study was rated as having unclear risk in the evaluation of randomized outcomes because it did not state whether animals were randomly selected for outcome assessment. One study described the specific method of blinding the outcome assessor, while the remaining studies did not. Two of the remaining studies were judged to be at high risk because they explicitly did not blind the outcome assessors. None of the studies had incomplete data, selective outcome reporting, or other sources of bias.

3.4 Outcomes

3.4.1 Metformin reduced inflammation scores in lung tissues of pulmonary fibrosis animals

The effect sizes were combined for inflammation scores in the lung tissue of animals in ten independent experiments (Figure 4A). MET use significantly reduced lung inflammation scores in the treatment groups compared with that in controls [SMD = −1.00, 95% CI (−1.17, −0.83), $p < 0.00001$]. $I^2 = 0\%$, and there was no heterogeneity between studies. The funnel plot symmetry (Figure 4B) and Egger's test (Figure 4C) indicated no publication bias ($p > 0.05$).

3.4.2 Metformin reduced fibrosis scores in lung tissues of pulmonary fibrosis animals

A total of 23 independent studies reported fibrosis scores. The studies by Rasoul (2019) (Yahyapour et al., 2019) and Bagher

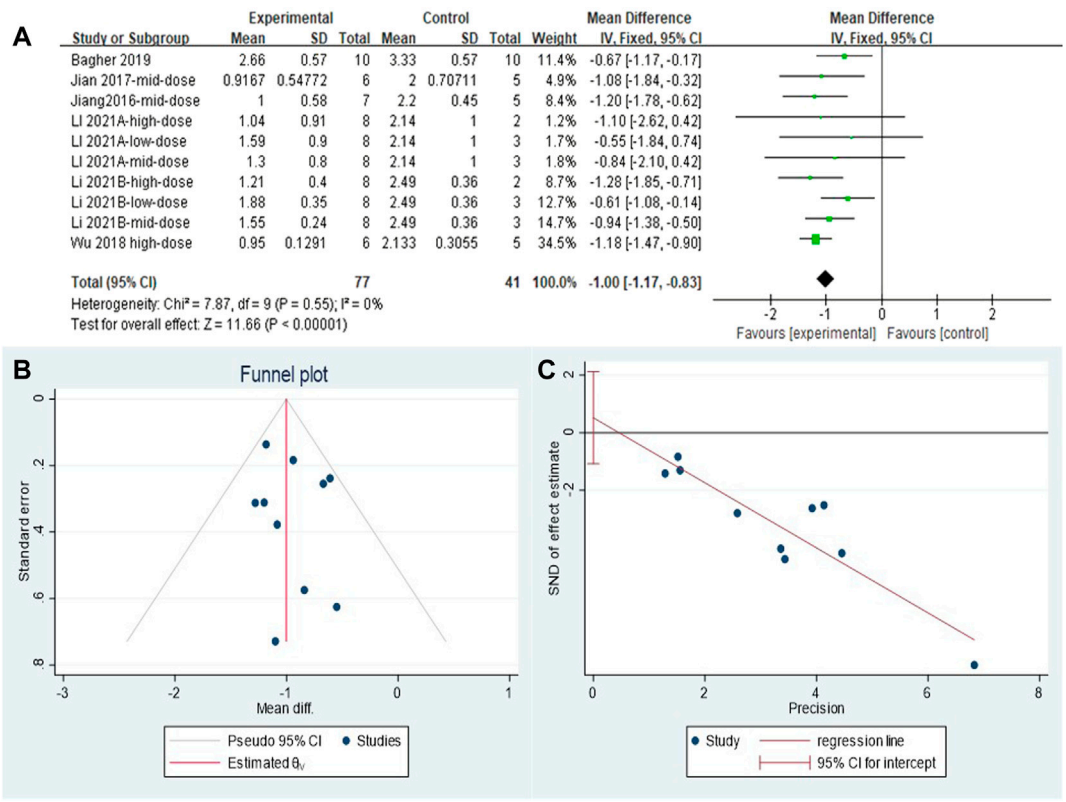


FIGURE 4
Effect of MET on inflammation scores of lung tissues in PF animals. **(A)** Forest plot of inflammation scores; **(B)** Funnel plot of inflammation scores; **(C)** Egger's test for inflammation scores.

(2019) (Farhood et al., 2019) were not included in the effect size analysis because their values did not meet the requirements for continuous variable effect size calculation. The effect sizes were combined for lung tissue fibrosis scores in animals from the 21 independent trials (Figure 5A), and the overall effect of MET was a significant reduction in lung fibrosis scores in the treatment groups compared with that in controls [SMD = −2.06, 95% CI (−2.73, −1.39), $p < 0.00001$] with high inter-study heterogeneity. Sensitivity analysis was subsequently performed (Figure 5B), excluding data from independent experiments; the heterogeneity did not decrease significantly, demonstrating the reliability of the results. We conducted subgroup analyses of the 21 trials and combined the effect sizes. The results showed a significant decrease in PF scores for all three dose levels of MET. However, subgroup analysis (Figure 5C) revealed a high degree of heterogeneity between high-dose, mid-dose, and low-dose subgroups, with I^2 values of 49, 80, and 69%, respectively. In addition, funnel plots (Figure 5D) and Egger's test (Figure 5E) indicated a publication bias ($p < 0.05$). To further explore the heterogeneity between studies, a meta-regression analysis of factors contributing to heterogeneity (modeling method, route of administration, time of administration, animal sex, animal type, dosage, year of publication, and manufacturer of MET) was performed (Table 2). However, the results showed that none of the abovementioned factors was a significant source of heterogeneity ($p > 0.05$).

3.4.3 Metformin reduced TGF-β in lung tissues of pulmonary fibrosis animals

The effect sizes for TGF-β were combined in 20 independent experiments (Figure 6A), and MET was effective in reducing TGF-β levels in the PF animal models [SMD = −2.54, 95% CI (−3.36, −1.72), $p < 0.00001$]. However, heterogeneity was observed between the studies, with $I^2 = 64\%$. Subgroup analysis was performed according to the different dose levels (Figure 6B). All three subgroups showed significant differences in TGF-β levels. In the high- and low-dose subgroups, heterogeneity disappeared. Heterogeneity was elevated in the mid-dose group and was mainly caused by the results from Wang Y. et al., (2017); heterogeneity was reduced after removing this literature (Figure 6C). Thus, we confirmed that the primary heterogeneity between the studies was due to the different doses of MET. The funnel plot (Figure 6D) and Egger's test (Figure 6E) indicated no publication bias ($p > 0.05$).

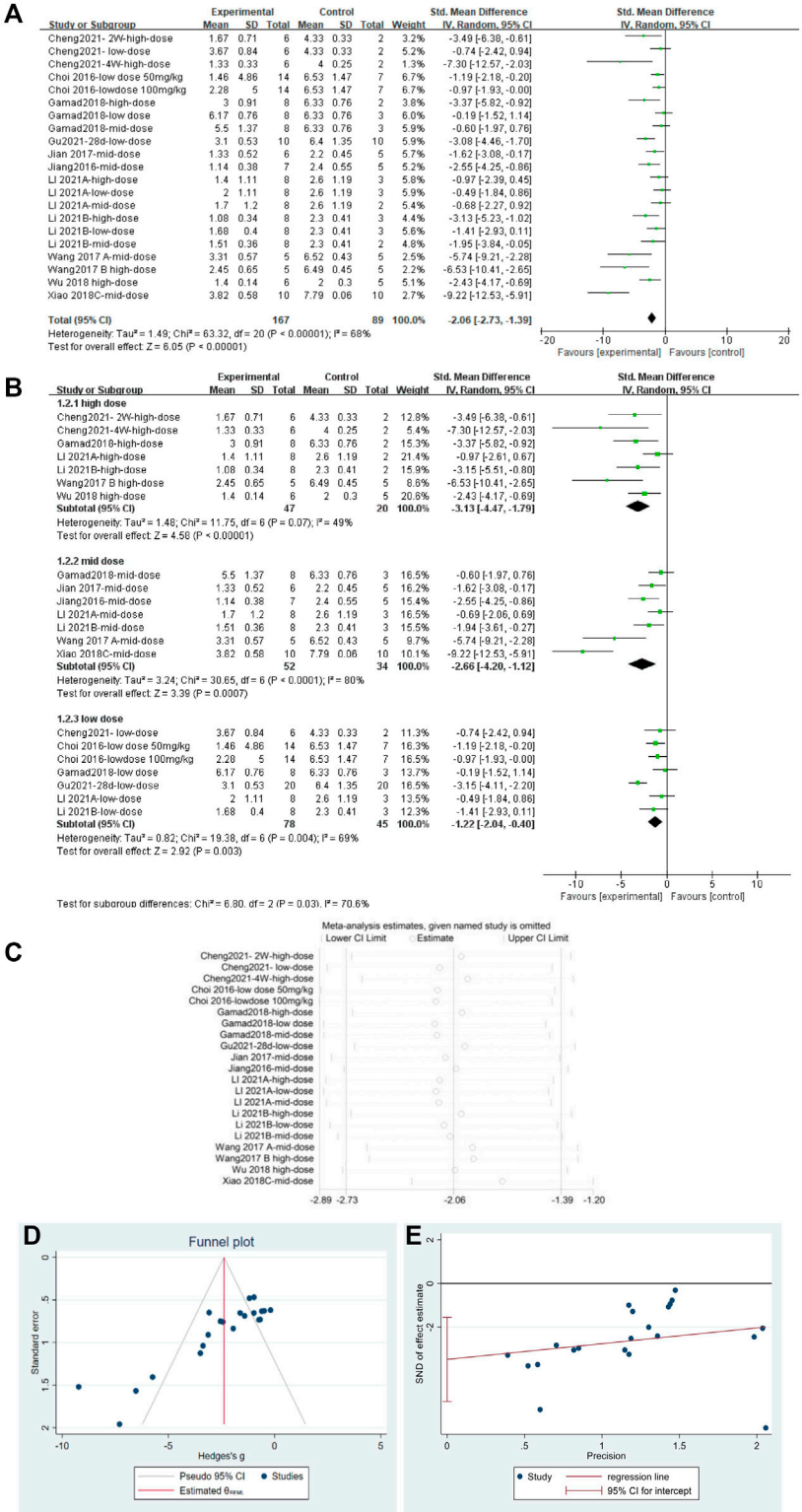


FIGURE 5
Effect of MET on fibrosis scores of lung tissues in PF animals. **(A)** Forest plot of fibrosis scores; **(B)** Forest plot of fibrosis scores (subgroups); **(C)** Sensitivity analysis of fibrosis scores; **(D)** Funnel plot of fibrosis scores; **(E)** Egger's test for fibrosis scores.

TABLE 2 Meta-regression analysis of the effect of MET on lung tissue fibrosis scores in PF animals.

Sources of heterogeneity	P>|t|	(95% Conf. Interval)	
Modeling Method	0.390	−1.573	3.696
Route of Administration	0.832	−1.863	2.266
Time of Administration	0.198	−0.499	2.118
Animal Sex	0.379	−3.520	8.474
Animal Type	0.315	−6.041	2.149
Dosage	0.306	−1.942	0.675
Year of Publication	0.336	−2.277	0.855
Manufacturers of MET	0.362	−0.652	1.631

3.4.4 Metformin reduced hydroxyproline content in lung tissues of pulmonary fibrosis animals

Effect sizes were combined for HYP content of animals from 18 independent experiments (Figure 7A), which showed that MET significantly reduced HYP content in the lung tissue of PF animals compared with that in controls [SMD = −3.80, 95% CI (−5.00,−2.61), $p < 0.00001$]. However, $I^2 = 77\%$ indicated an inter-study heterogeneity. Sensitivity analysis was performed (Figure 7B), thereby demonstrating the stability of these findings. Publication bias was indicated based on a funnel plot (Figure 7C) and Egger's test (Figure 7D) ($p < 0.05$).

3.4.5 Metformin reduced collagen I content in lung tissues of pulmonary fibrosis animals

The effect sizes of collagen I were combined from 15 independent experiments. The results (Figure 8A) indicated that MET was effective in reducing collagen I content in the lung tissue of animal models of PF compared with that in controls [SMD = −3.06, 95% CI (−3.98, −2.13), $p < 0.00001$]. $I^2 = 58\%$ indicated an inter-study heterogeneity, and sensitivity analysis (Figure 8B) confirmed the stability of the findings. Publication bias was judged based on a funnel plot (Figure 8C) and Egger's test (Figure 8D) ($p < 0.05$).

3.4.6 Metformin reduced α-SMA content in lung tissues of pulmonary fibrosis animals

The effect sizes for α-SMA were combined for 13 independent experiments (Figure 9A). MET significantly reduced α-SMA content in the lung tissue of PF animals compared with that in controls [SMD = −3.89, 95% CI (−5.24, −2.54), $p < 0.00001$]. The heterogeneity between studies was $I^2 = 68\%$. Sensitivity analysis (Figure 9B) confirmed the stability of the findings with some publication bias, identified using the funnel plot (Figure 9C) and Egger's test (Figure 9D) ($p < 0.05$).

3.4.7 Metformin reduced Smad2 and Smad3 phosphorylation levels in lung tissues of pulmonary fibrosis animals with p-Smad2/3/Smad2/3

Effect sizes were combined for p-Smad2, p-Smad3, Smad2/3, and p-Smad2/3/Smad2/3 in three, three, four, and two independent experiments, respectively. The Smad2/3 effect size was merged (Figures 10A and B). The use of MET significantly reduced the levels of p-Smad2 and p-Smad3 in the lung tissue of PF animals compared to those in controls (Figure 10A) [SMD = −10.14, 95% CI (−13.51, −6.78), $p < 0.00001$; SMD = −8.43, 95% CI (−11.15, −5.70), $p < 0.00001$; $I^2 = 46\%$ (low between-study heterogeneity; $I^2 = 0\%$ (no between-study heterogeneity)]. However, there was no significant difference in the change in Smad2/3 levels between the control and experimental groups [SMD = 0.34, 95% CI (−0.23, 0.92), $p > 0.05$; $I^2 = 0\%$ (no heterogeneity between studies)]. In the comparison of the control and experimental groups with p-Smad2/3/Smad2/3, (Figure 10B) MET significantly reduced this result [SMD = −0.19, 95% CI (−0.29, −0.08), $p < 0.05$], with heterogeneity between studies, $I^2 = 93\%$.

3.4.8 Metformin increased AMPK/p-AMPK content in lung tissues of pulmonary fibrosis animals

Five and three independent experiments were combined to determine the lung tissue AMPK and p-AMPK effect sizes, respectively. The results showed (Figures 11A and B) that the treatment of PF animals with MET significantly reduced AMPK and p-AMPK levels [SMD = 0.92, 95% CI (0.35, 1.48), $p < 0.001$; SMD = 0.81, 95% CI (0.78, 0.83), $p < 0.001$]. There was no heterogeneity in the effect sizes for AMPK; $p > 0.24$, $I^2 = 26\%$. The combined effect sizes of p-AMPK showed heterogeneity between studies and reduced after sensitivity analysis by removing the results from Wang Y. et al., (2017) (Figure 11C).

3.4.9 Metformin significantly reduced ERK1/2 phosphorylation levels in lung tissues of pulmonary fibrosis animals

The effect sizes of ERK1/2, p-ERK1/2, and p-ERK1/2/ERK1/2 (each metric contained two independent experiments) in the lung tissue of PF animals were combined for the included studies (Figures 12A–C). There was no significant difference in ERK1/2/β-actin levels after MET treatment compared to those in controls [SMD = 0.03, 95% CI (−0.02, 0.07), $p > 0.05$]. In the experimental group, the use of MET significantly reduced the phosphorylation levels of both p-ERK1/2/β-actin and p-ERK1/2/ERK1/2/β-actin overall [SMD = −6.03, 95% CI (−11.05, −1.01), $p < 0.05$; SMD = −3.67, 95% CI (−6.67, −0.67), $p < 0.05$] compared to those in the control group (Figures 12B and C). $I^2 = 0\%$ (with no heterogeneity between studies), $I^2 = 85\%$ (with high heterogeneity between studies), $I^2 = 24\%$ (with no heterogeneity between studies) are the results of sensitivity analyses for ERK1/2, p-ERK1/2, and p-ERK1/2/ERK1/2, respectively.

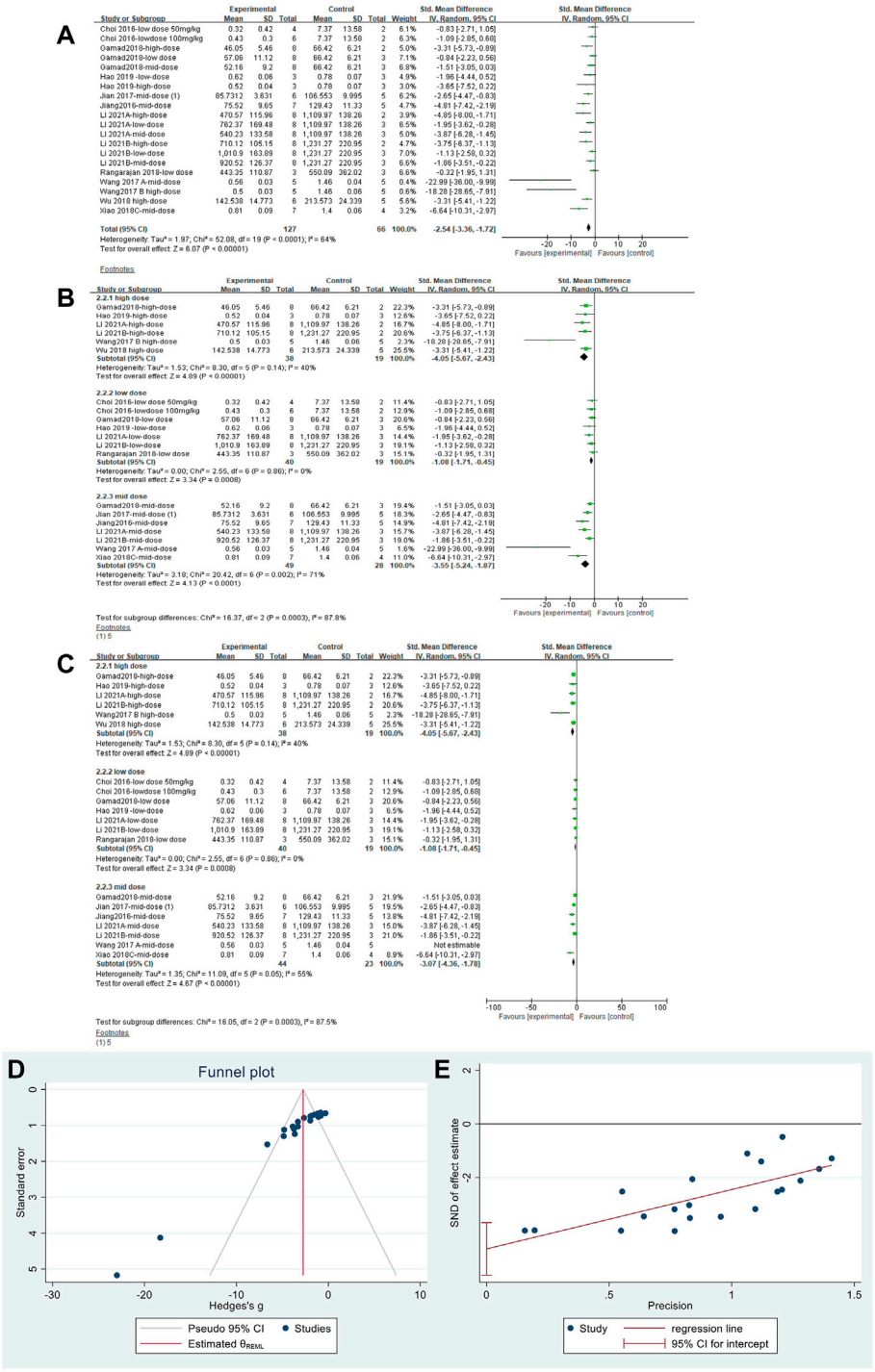


FIGURE 6
Effect of MET on TGF-β in lung tissues of PF animals. **(A)** Forest plot of TGF-β; **(B)** Forest plot of TGF-β (subgroups); **(C)** Forest plot of TGF-β [subgroups after removing Wang Y. et al., (2017)]; **(D)** Funnel plot of TGF-β; **(E)**. Egger's test for TGF-β.

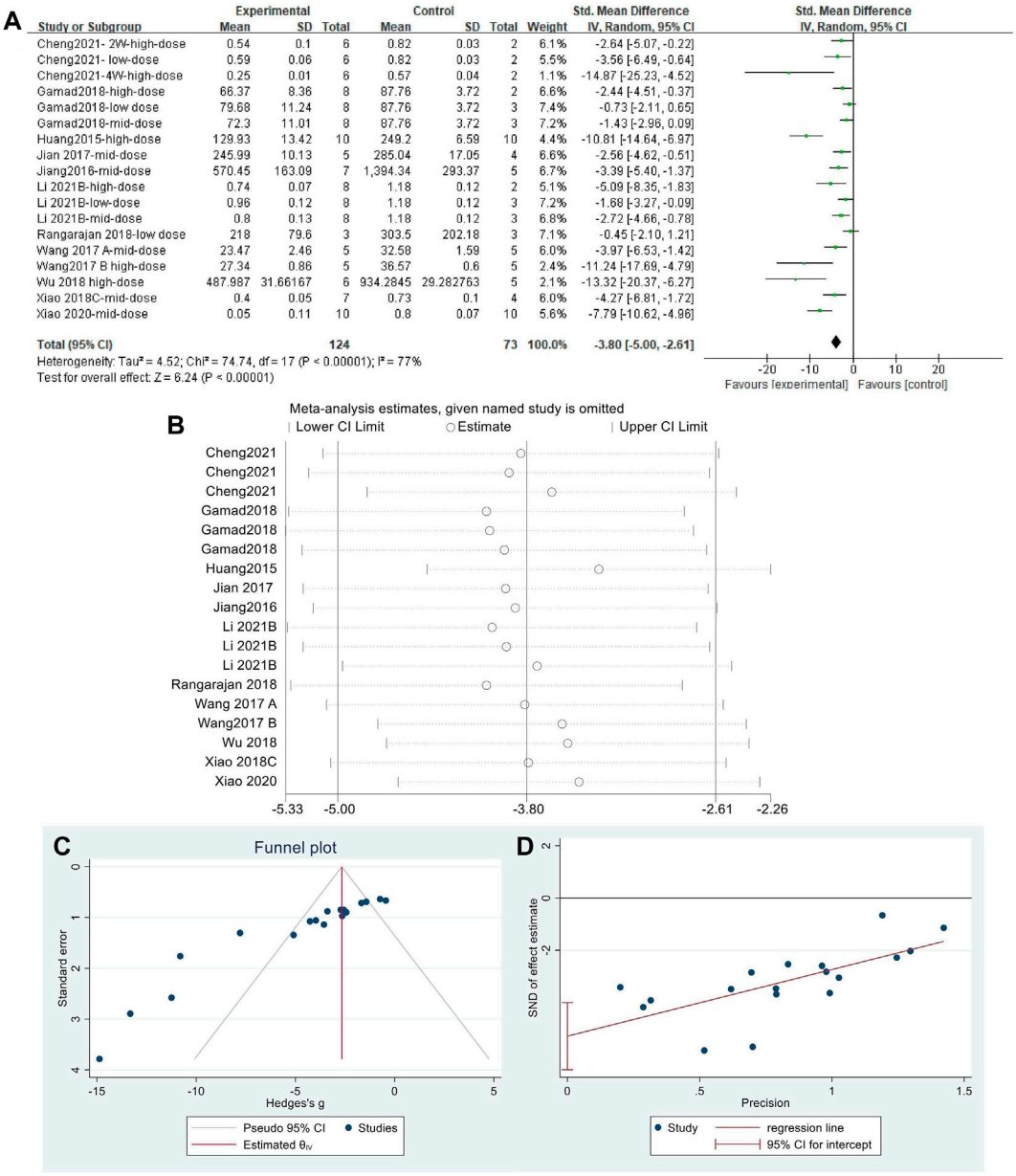


FIGURE 7
Effect of MET on HYP in lung tissues of PF animals. **(A)** Forest plot of HYP; **(B)** Sensitivity analysis of HYP; **(C)** Funnel plot of HYP; **(D)** Egger's test for HYP.

3.4.10 Metformin reduced mortality in pulmonary fibrosis animals

The effect sizes for mortality in PF animal models were combined for six independent experiments (Figure 13), and the protective effect of MET on mortality was significant compared to that of controls [RR = 0.54, 95% CI (0.30, 0.96), $p < 0.05$]. $I^2 = 0\%$, indicating no heterogeneity between studies.

4 Discussion

The non-standard use of a drug is a method to improve treatment and understanding of the disease. Compared to traditional drug development, exploring the treatment scope of existing drugs is more convenient, cheaper, and less risky (Jin and Wong, 2014; Tzouvelekis et al., 2018). A new function of the old drug MET, the anti-fibrotic effect, has been explored. Clinical

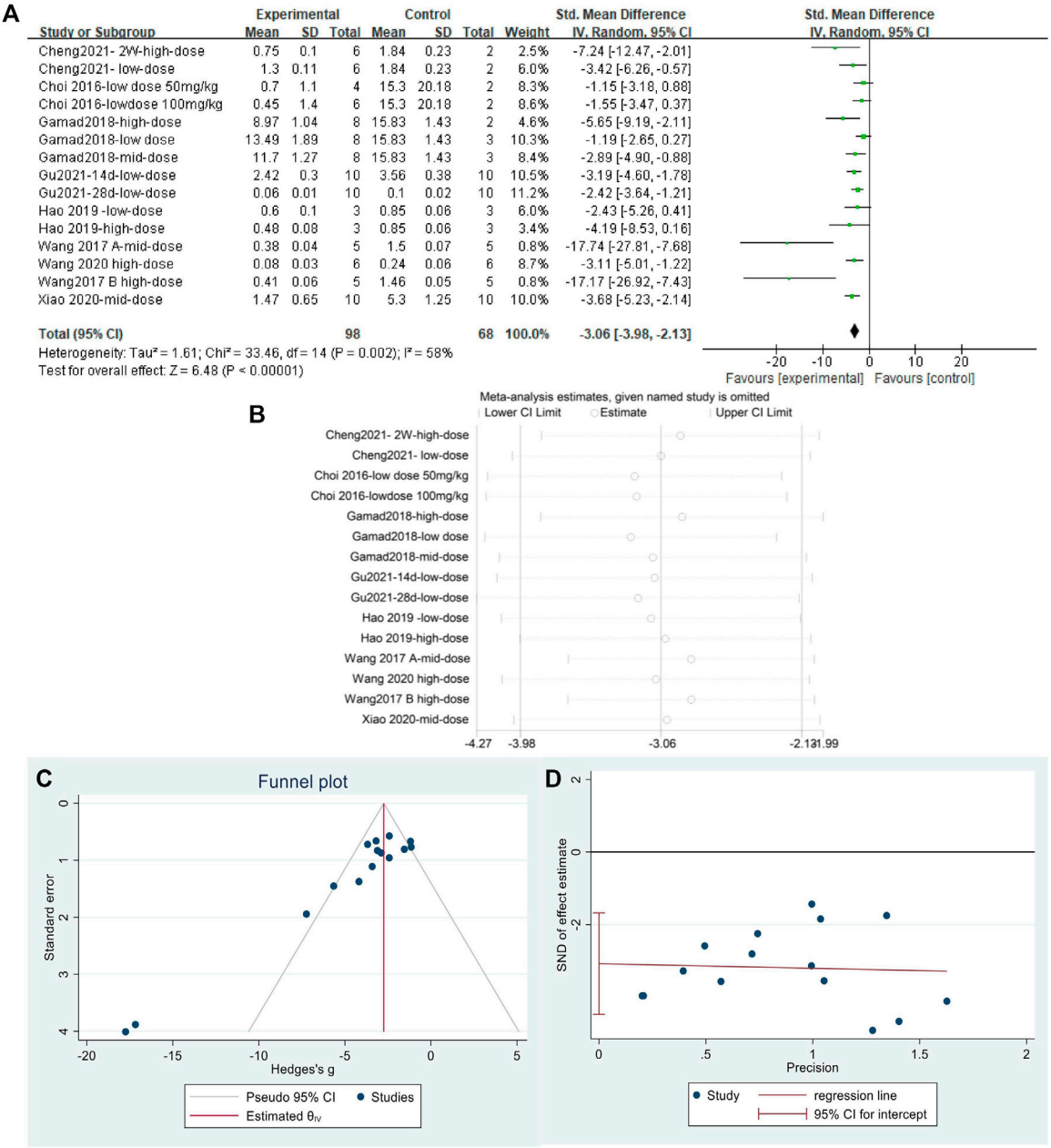


FIGURE 8
Effect of MET on collagen I in lung tissues of PF animals. **(A)** Forest plot of collagen I; **(B)** Sensitivity analysis of collagen I; **(C)** Funnel plot of collagen I; **(D)** Egger's test for collagen I.

studies using MET in treating patients with IPF are currently scarce, with two previous studies indicating no significant effect of MET on the clinical outcomes in patients with PF (Spagnolo et al., 2018; Lambert et al., 2021). However, both studies were limited by their small sample sizes (n = 28 and n = 71). In contrast, a recent retrospective cohort study that included 3,599 patients with IPF and T2DM showed a significant 54% reduction in all-cause mortality with MET treatment (Teague et al., 2022). This effect was substantially better than that of the current anti-fibrotic agents (23%) (Dempsey et al., 2019). This study confirms that our proposal for the use of MET for the treatment of PF is both scientific and innovative and provides strong practical evidence for our research. However, it is worth noting that this study observed the effect of MET in patients with PF and T2DM, and there is insufficient

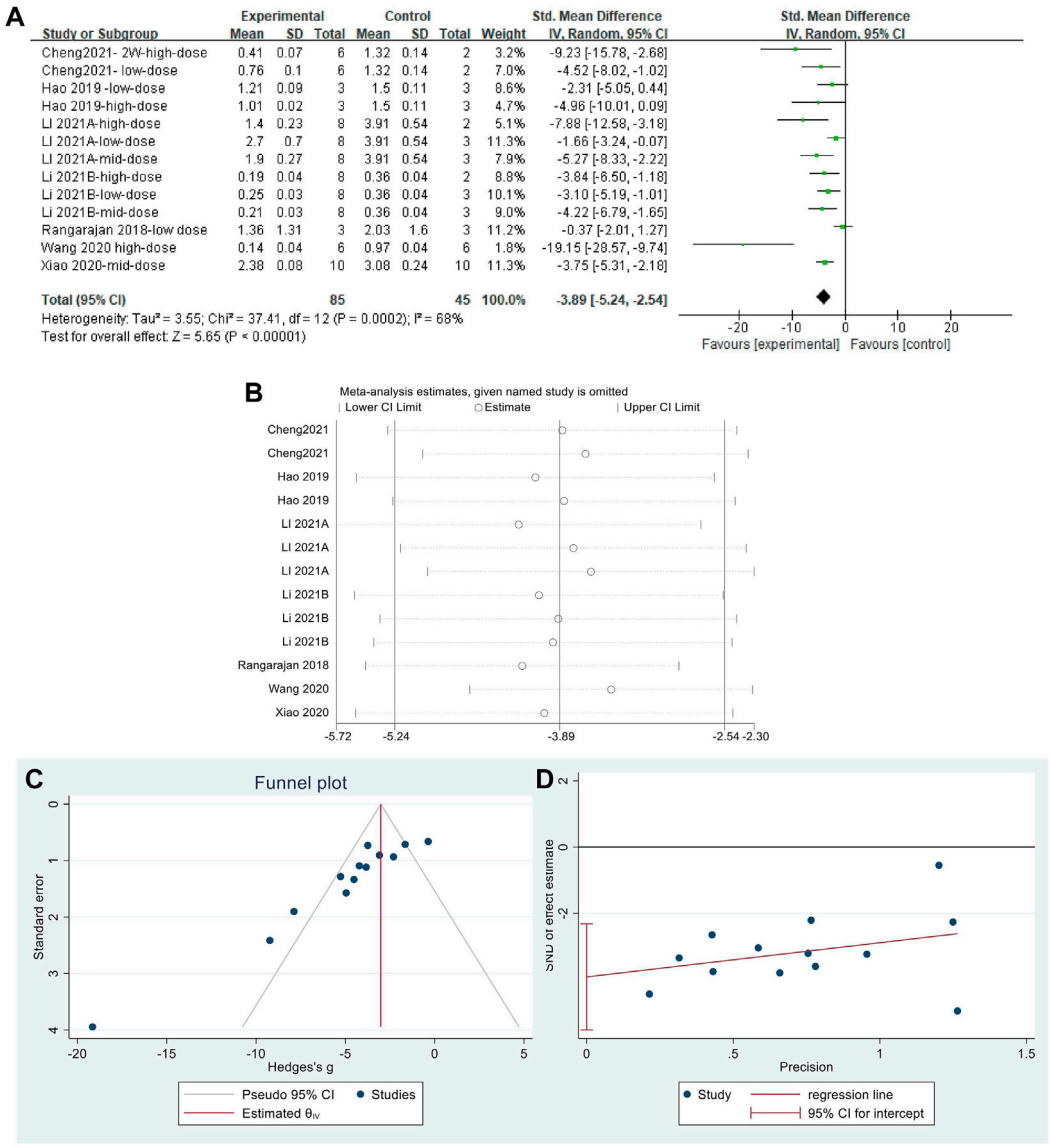


FIGURE 9
Effect of MET on α-SMA content in lung tissues of the PF animal models; **(A)** Forest plot of the α-SMA; **(B)** Sensitivity analysis of α-SMA; **(C)** Funnel plot of α-SMA; **(D)** Egger's test for α-SMA.

evidence of a direct causal relationship between MET and PF. In addition to its anti-fibrotic effect, MET also has cardioprotective and hypoglycemic effects (Holman et al., 2008; Roumie et al., 2012), which may be responsible for reducing mortality in patients with PF and T2DM (Teague et al., 2022). Therefore, further clinical trials are required. Preclinical studies often support the development of clinical trials. There are many preclinical studies on MET for PF animal models, but reviews summarizing these studies are scarce or incomplete. In addition, some of the published reviews on the mechanisms of MET for PF lack relatively complete experimental evidence or focus on specific aspects of the anti-PF mechanisms of MET. Systematic evaluation based on evidence is conducive to improving the quality of animal experiments and transforming from preclinical to clinical research.

4.1 Summary of current findings

To the best of our knowledge, this is the first systematic review and meta-analysis of the effects of MET in animal models of PF. During the literature screening process, we initially selected 20 articles but eventually included only 19 articles after careful reading. An article (Kheirollahi et al., 2019) was excluded from this study because it did not quantify the scoring

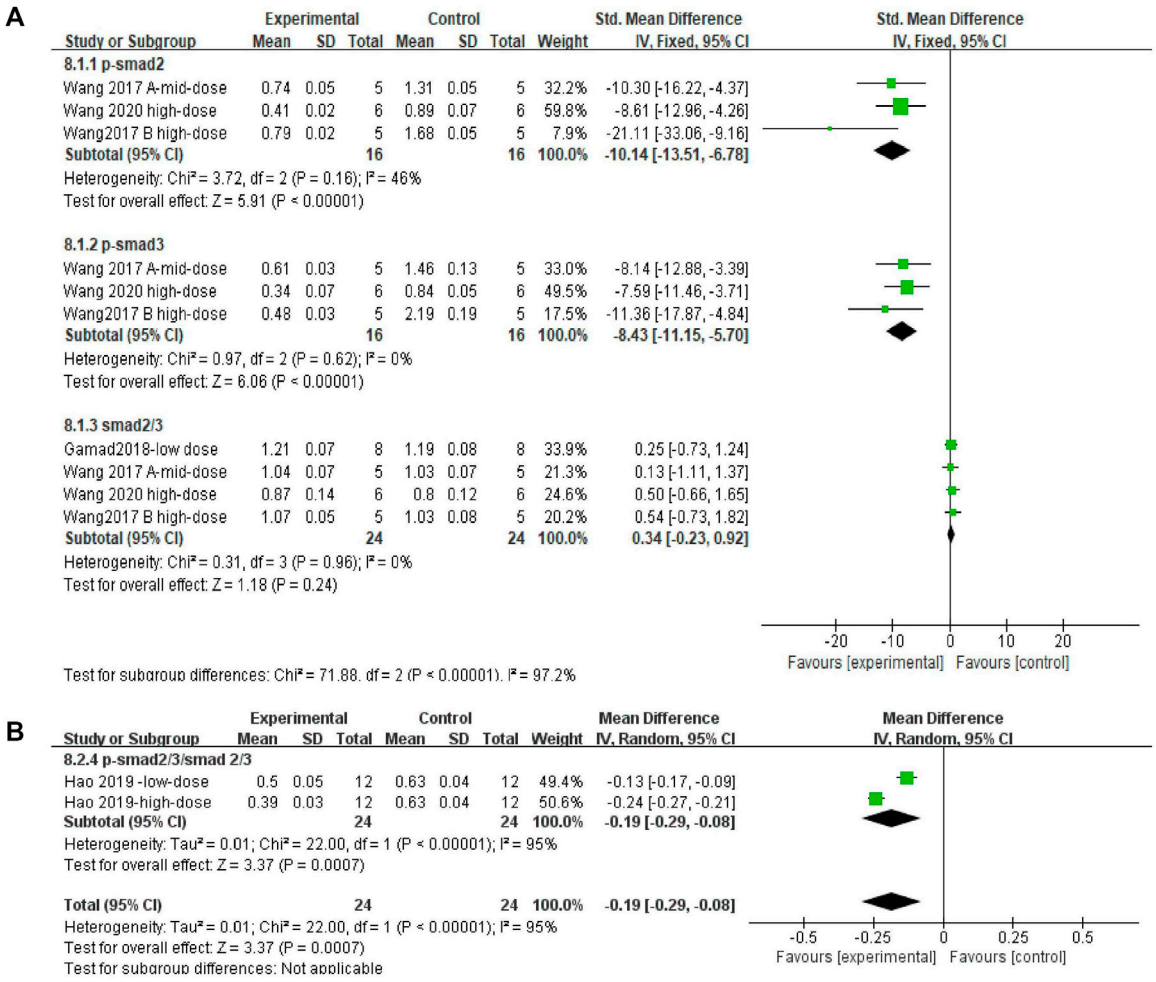


FIGURE 10
Effect of MET on Smad in lung tissues of PF animals. **(A)** Forest plot of p-Smad2, p-Smad3, and Smad2/3; **(B)** Forest plot of p-Smad2/3/Smad2/3.

of inflammation, degree of fibrosis, or collagen content in Masson-stained sections of animal lung tissue. Although the article used the degree of fibrosis (%) for evaluation, it was not the desired outcome indicator. A total of 19 studies that included 29 separate experiments involving 368 animals in both experimental and control groups were eventually used in this study. This meta-analysis showed that MET significantly reduced lung inflammation, fibrosis, and its associated markers in PF animal models. MET administration directly or indirectly improved almost all observed markers. The results of this study suggest that MET is a promising candidate for the treatment and suppression of PF.

4.2 Heterogeneity

Due to the different experimental designs included in the studies, there were multiple variables, such as modeling method, route of administration, time of administration, animal sex, animal type, dosage, year of publication, and manufacturer of MET, which may have contributed to the high heterogeneity of some of the outcomes (Bailoo et al., 2014; Chaudhari et al., 2020). We anticipated high heterogeneity before conducting the meta-analysis. Each independent experiment clearly stated the dose of MET and the dose fluctuation range in the included studies was 50–500 mg/kg. Therefore, the dose types in the included studies were classified according to the dose classification method mentioned in the Materials and Methods Section 2.5. Subgroups were introduced to calculate the fibrosis score and TGF-β level because their heterogeneity was too high (Lin et al., 2020). These two results demonstrated that different doses of MET could produce the same effect. Subgroup analysis combined with meta-regression results showed that dose did not affect the fibrosis score. There was no heterogeneity between the studies in the calculation of the inflammation score. Therefore, it cannot be determined whether the dose

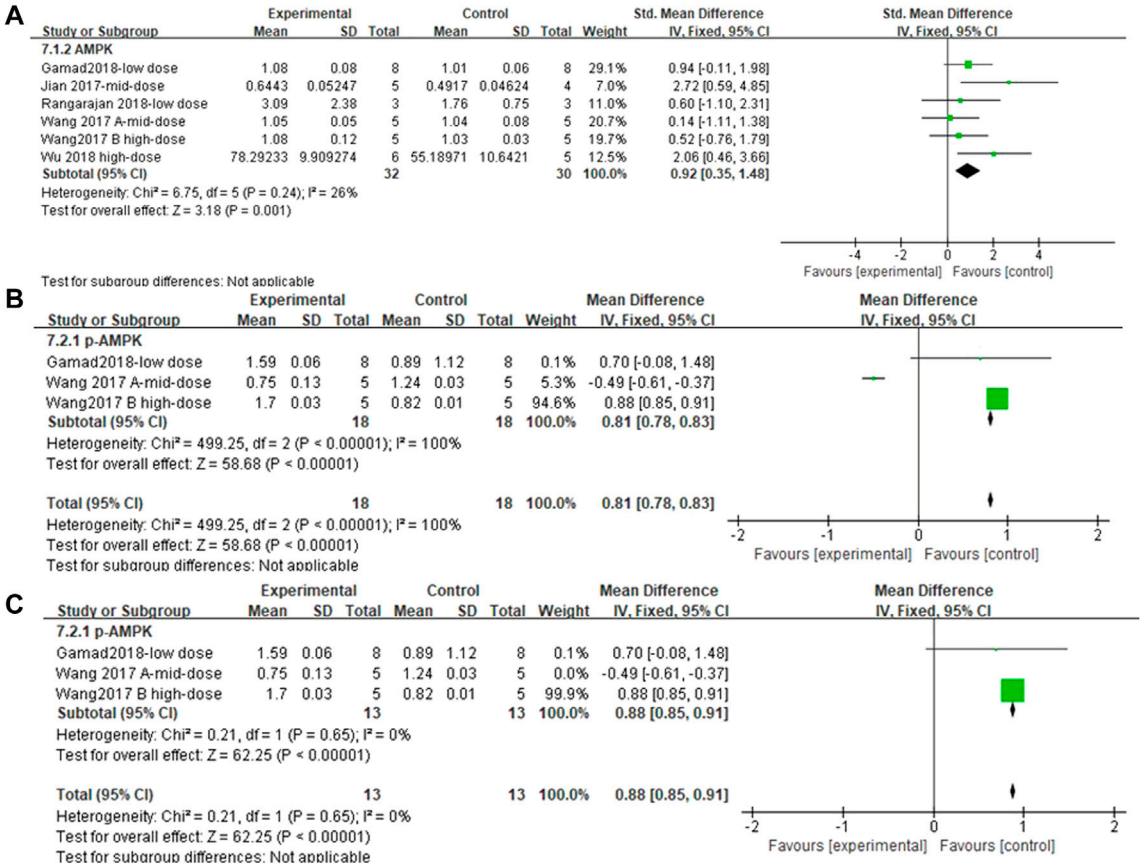


FIGURE 11
Effect of MET on AMPK/p-AMPK. **(A)** Forest plot of AMPK; **(B)** Forest plot of p-AMPK; **(C)** Forest plot of p-AMPK [after removing Wang Y. et al., (2017)].

significantly affected the heterogeneity of the inflammation score. Moreover, regarding TGF-β, it has been proven that the dose is the main factor affecting the level of heterogeneity because the heterogeneity reduced to varying degrees after subgroup analysis. Therefore, based on the existing evidence, there is no significant effect between dosage and the heterogeneity of fibrosis or inflammation score; however, the heterogeneity reduced in TGF-β analysis. In the fibrosis score analysis after subgroup analysis, dose and factors other than it were considered. The fibrosis score and the dose administered again proved to be unrelated in the regression analysis. We explored the influence of other possible factors on heterogeneity between studies. We conducted a meta-regression analysis of eight factors, including the mode of modeling, route of administration, time of administration, sex of animals, type of animals, the dosage of administration, year of publication, and MET manufacturer. However, these variables did not significantly affect heterogeneity. We believe that some other factors may contribute to high heterogeneity, such as subjective conditions, differences in scores given by different investigators, experimental conditions, and differences in testing equipment.

4.3 Interpretation and discussion of the study results

4.3.1 Selection of animal types

This study did not limit the types of experimental animals, as several animals have been used to construct animal models of PF (Tashiro et al., 2017). Different species of PF animal models are used to reflect patients with PF, a disease difficult to replicate fully. The animals used in the included studies were all male and female murine (mice and rats), which are commonly used for PF modeling. Redente et al. argued that male animals respond better to PF than females (Redente et al., 2011). However, in the present study, there was no significant effect of gender on the

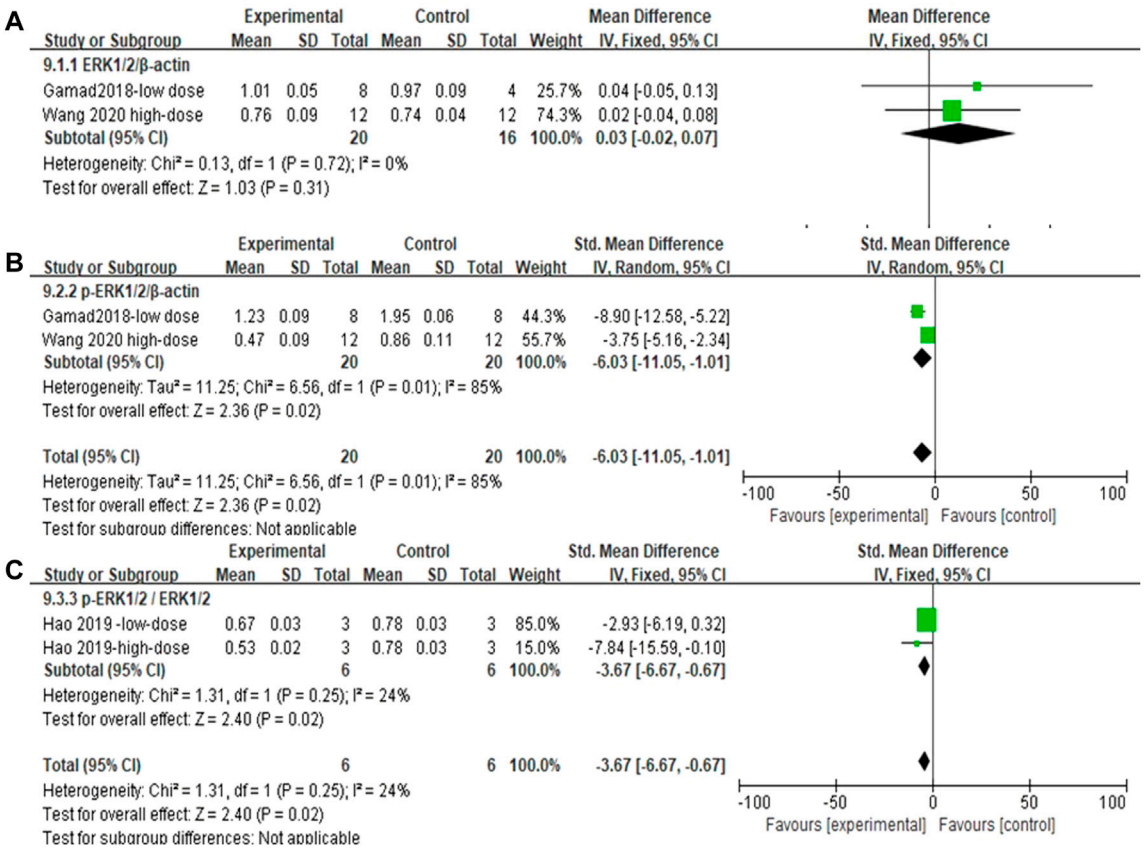


FIGURE 12
Effect of MET on ERK1/2 phosphorylation levels in lung tissues of PF animals. **(A)** Forest plot of ERK1/2; **(B)** Forest plot of ERK1/2p-ERK1/2; **(C)** Forest plot of ERK1/2p-ERK1/2/ERK1/2.

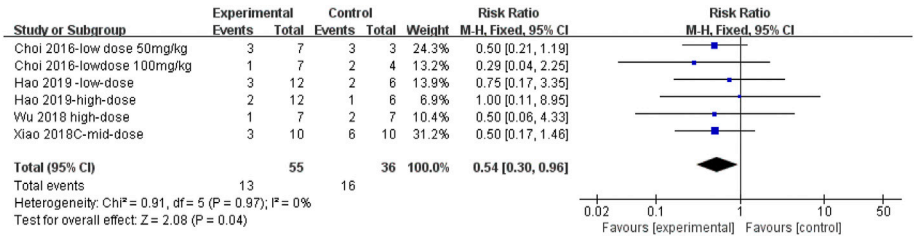


FIGURE 13
Effect of MET on mortality in animals.

findings based on the meta-regression of fibrosis scores ($p > 0.05$). It has been suggested that fibrosis occurring in young mice after receiving a single dose of bleomycin spontaneously regresses, but this was not observed in older mice (Degryse et al., 2010). Multiple modeling injections into young mice can better characterize human fibrosis (Degryse and Lawson, 2011; Wang et al., 2019). Of the included studies that used bleomycin interventions, only one mentioned modeling with multiple doses of bleomycin; the rest used a single dose for modeling. Of the included studies, only two mentioned the age of the animals. This suggests that in future relevant experiments, researchers should try to use older rats or administer multiple doses to younger rats to optimize the animal model and demonstrate the characteristics of human IPF (Degryse et al., 2010).

4.3.2 Modeling method

The current meta-analysis did not restrict the mode of modeling to better demonstrate the various states and etiologies of the PF development process. Bleomycin was used for modeling in 63% of the included studies (12), which aligns with the current consensus for studying animal models of PF (Jenkins et al., 2017). However, animal models of bleomycin are problematic, as previously described. Fibrosis in young mice may regress spontaneously (Jenkins et al., 2017) and is often bleomycin-induced. Bleomycin-induced PF is not fully representative of IPF because of the acute lung tissue damage that often leads to high mortality in animals (Tashiro et al., 2017). Another 16% 3) of the included studies used silica interventions, and 21% 4) used radiation interventions. Silica-induced PF demonstrated silicosis-induced PF (Davis et al., 1998), and the resulting PF lesions tended to be more persistent (Barbarin et al., 2004; Tashiro et al., 2017). Radiation-induced PF tends to be a slow process and is less dependent on TGF-β (Haston, 2012). The inclusion of these two modeling studies can, to some extent, compensate for the limitations of the bleomycin-induced PF model and provide a more comprehensive response to the therapeutic effect of MET on PF.

4.3.3 The effect and mechanism of metformin on animal models of pulmonary fibrosis

In this meta-analysis, the effect of MET on PF was divided into two aspects. MET administration reduced lung inflammation scores, and acute inflammation-dominated lung injury was the main feature of animal PF models in the early stages of PF development (1–10 days) (Moeller et al., 2008; Tashiro et al., 2017). Infiltration of inflammatory cells and damage to alveolar epithelial cells were the main manifestations during this period. This meta-analysis demonstrated that MET had a significant effect on the inflammatory state of the lungs at this stage. On the other hand, fibrosis in the lung generally starts with the deposition of the ECM. The progression of fibrosis on days 10–21, especially on day 14, was the peak of development (Tashiro et al., 2017). The present meta-analysis demonstrated the effect of MET on the fibrosis stage with regard to the fibrosis score of pathological lung tissue and the expression of fibrosis factors HYP, collagen I, and α-SMA. The use of MET significantly improves alveolar wall thickness and reduces collagen deposition in lung tissues, thereby reducing the extent of fibrosis in the lung tissue (Hao et al., 2019).

In addition, we explored the underlying mechanisms of MET in PF amelioration. The essence of PF is the excessive deposition of collagen and ECM proteins (Jones et al., 2018). The reasons behind considering collagen I, HYP, and α-SMA as factors to monitor the extent of fibrosis were: 1) Collagen I, the primary collagen involved in the ECM, is used as a targeting probe (Désogère et al., 2017) to determine the extent of fibrosis. HYP is a major component of collagen and is often used as an indicator of the total collagen content (Zhao et al., 2015). Investigators recommend HYP content reduction as the primary criterion for evaluating anti-fibrotic efficacy in preclinical animal models (Jenkins et al., 2017). α-SMA may reflect the levels of activated fibroblasts (Li et al., 2011). This study demonstrates the improvement in the degree of fibrosis (collagen I), anti-fibrotic effect (HYP), and level of collagen fibril activation (α-SMA) during MET treatment. Ultimately, MET reduced these three indicators, indicating that MET can influence fibroblast activation by modulating α-SMA, which improves the degree of fibrosis in the lung by reducing collagen I levels and exerting an anti-fibrotic effect. 2) Collagen I is a protein, and HYP is an amino acid (Xu et al., 2021). Taking these two markers as the research results is convenient for reactions at different functional levels. 3) In lung tissues, collagen I and III are the most important collagen proteins, and HYP reflects the overall collagen deposition. Selecting HYP and collagen I is also conducive to further exploring the mechanism and pathway of collagen deposition and determining whether MET improves PF by reducing the collagen I pathway. MET acts mainly through the regulation of AMPK (Rangarajan et al., 2018). It is believed that the activation of AMPK can inhibit the most crucial part of the PF process, the TGF-β signaling pathway (Wu et al., 2021). Therefore, this meta-analysis explored several indicators related to TGF-β, including TGF-β, AMPK, Smad, and ERK. The results showed that MET significantly affected AMPK and p-AMPK levels and significantly elevated TGF-β, Smad (p-Smad2, p-Smad3, and p-Smad2/3), and ERK (p-ERK1/2/β-actin and p-ERK1/2/ERK1/2) levels. This suggests the ability of MET to enhance anti-fibrotic and lung-protective effects by activating AMPK in animals post MET administration (Wynn and Ramalingam, 2012). This meta-analysis also demonstrated that MET inhibited the effect of EMT, as represented by α-SMA, which further inhibited the occurrence of PF. Notably, in the final merging of effect sizes for p-AMPK, we removed Wang Y. et al., (2017) because of the high heterogeneity of p-AMPK. MET did not result in elevated AMPK phosphorylation. This validates a previous view that MET may have non-AMPK–dependent pathways to prevent PF (Feng et al., 2017). In addition, not all indicators in this meta-analysis yielded satisfactory results. The effect of MET on Smad2/3 and ERK1/2/β-actin was $p > 0.05$, i.e., there was no significant difference between the control and experimental groups. However, the comparative results of the effect sizes associated with p-Smad2, p-Smad3, p-Smad2/3, p-ERK1/2/β-actin, and p-ERK1/2/ERK1/2 were $p < 0.05$, which was in accordance with our expectations. We speculated that the main reason for this discrepancy was that the number of included studies reporting the two outcomes of

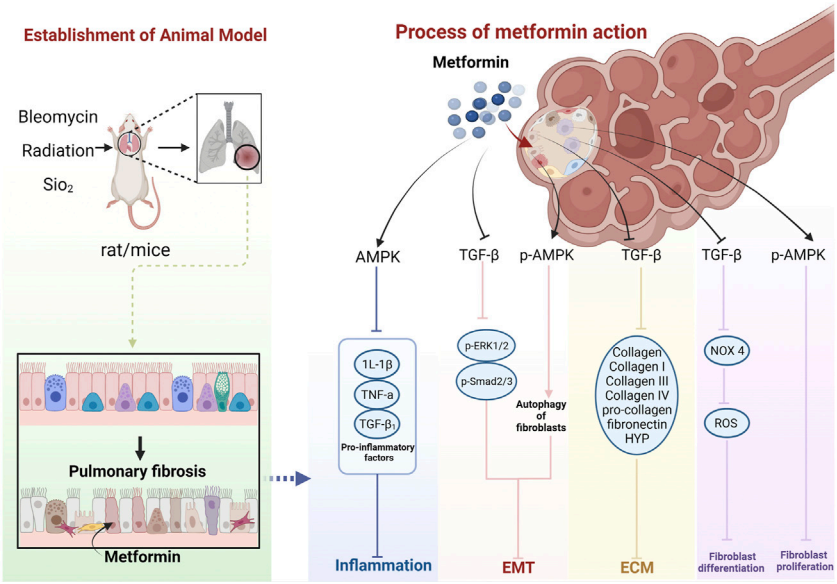


FIGURE 14
Schematic representation of the possible molecular mechanism of MET inhibition of PF. (Created using BioRender.com).

Smad2/3 and ERK1/2/β-actin was low, resulting in a combined effect size that does not reflect a broader and more realistic picture. However, it is possible that the time point selection of the assay resulted in a small difference between these two outcomes in the comparison of experimental and control groups and did not prove their significance when combining the effect sizes.

The cellular and molecular mechanisms underlying MET treatment in PF are unknown. The current focus is mainly on AMPK, suggesting that MET inhibits and ameliorates PF mainly through the AMPK pathway. However, there may also be non-AMPK pathway–dependent mechanisms (Wang Y. et al., 2017) (Figure 14)

4.3.3.1 Inhibitory effect of metformin on inflammatory response

MET further inhibits the inflammatory response by activating AMPK and inhibiting pro-inflammatory factors, such as IL-1β, TNF-α, and TGF-β1 (Jian, 2017; Li et al., 2021a; Li et al., 2021b).

4.3.3.2 Inhibition of EMT by metformin

MET inhibits the TGF-β pathway in lung fibroblasts, thereby diminishing the activity of its downstream molecules p-Smad2, p-Smad3, and p-ERK1/2 proteins (Wang et al., 2020), and inhibition of Smad2/3 phosphorylation can enhance E-Cad transcription (Huang, 2015), while leading to decreased expression of proteins, such as α-SMA (Li et al., 2021a; Li et al., 2021b), ultimately inhibiting EMT. MET can also inhibit EMT by upregulating p-AMPK and activating autophagy (Li et al., 2021a).

4.3.3.3 Inhibitory effect of metformin on fibroblast differentiation and proliferation

MET activates AMPK phosphorylation and inhibits fibroblast proliferation. AMPK can inhibit NADPH oxidase 4 (NOX4) expression downstream of TGF-β and reduce ROS production, thus, inhibiting Smad phosphorylation and myofibroblast differentiation (Sato et al., 2016).

4.3.3.4 Metformin reduces extracellular matrix deposition

MET downregulates TGF-β expression, which, in turn, inhibits COL, COL-I, COL III, COL-IV, pro-COL, and fibronectin production (Choi et al., 2016; Wang J. et al., 2017; Gamad et al., 2018; Hao et al., 2019), leading to a decrease in ECM deposition. HYP is a product of collagen catabolism, and an increase in its level implies an increased expression of collagen in tissues. This suggests that MET can reduce collagen in lung tissues by inhibiting HYP production, thus, reducing ECM deposition (Jian, 2017). MET also decreases TGF-β1, Smad2, and Smad3 phosphorylation levels, and the process of collagen I inhibition can be affected through a non-AMPK–dependent pathway (Wang Y. et al., 2017). In addition, MET may produce anti-fibrotic effects through other non-AMPK pathways (Gao et al., 2020). MET exerts an anti-fibrotic effect by inhibiting insulin-like growth factor 1 (IGF-1) (Xiao et al.,

2020). The MET hypoglycemic mechanism of MET also functions through IGF-1. Inhibition of IGF-1 prevents the activation of IGF-1 receptors and inhibits IGF-1-mediated downregulation of insulin sensitivity (Kang et al., 2016). MET can also exert anti-PF effects by inhibiting the regulation of NOX4 (Sato et al., 2016). Similarly, MET has been shown to prevent and treat T2DM and its complications, such as diabetic cataracts, by inhibiting NADPH oxidase and preventing ROS accumulation (Chen et al., 2022). MET may also induce lipid differentiation through activation of BMP2 release and the PPARγ phosphorylation pathway (Kheirollahi et al., 2019), a pathway that has also been reported to regulate glycemic effects (Schultze et al., 2012). It can also inhibit transglutaminase 2 (TG2) upstream of TGF-β1, which is involved in inhibiting the PI3K-Akt, TGF-β/Smad, and RTK/RAS/ERK pathways to exhibit an anti-fibrosis role (Hsu et al., 2017; Wang et al., 2020). Interestingly, the hypoglycemic effect of MET is also mediated by the PI3K-Akt pathway but with positive activation (Schultze et al., 2012).

In summary, the effects of MET on animal models of PF may proceed through four aspects: inhibition of the body's oxidative stress and inflammatory response by the AMPK pathway, EMT, fibroblast proliferation and differentiation, and ECM deposition; however, they can also function through non-AMPK–dependent pathways.

4.4 Limitations

Although this study's careful and detailed analysis was based on the Handbook for Systematic Evaluation of Animal Intervention Studies (de Vries et al., 2015), the studies included in this meta-analysis have some limitations. First, animal models cannot fully replicate the full range of human diseases (Perel et al., 2007). Furthermore, rodents recovered much faster than humans did. Therefore, we cannot confirm whether the results of the current meta-analysis can be applied to PF treatment in humans. Second, the age of the animals was poorly described by the investigators in the included studies, with only two studies mentioning the age and sex of the animals. Because rodent age and sex affect the effect of MET (Chaudhari et al., 2020), we cannot affirm whether the animal models in the current included studies are fully representative of the effect of MET on the primary onset population of PF. In addition, the included studies lacked many basic methods to reduce bias, such as concealment allocation and blinding of animal-keepers and investigators. Better quality animal models of PF can translate to human patients with PF and predict the effects of drugs in humans in a better way (Perel et al., 2007). Future research should focus on improving experimental methods, modeling approaches, and the quality of reporting of animal experiments to provide high-quality evidence.

4.5 Future of metformin for pulmonary fibrosis treatment

Research on the mechanism of MET in the treatment of PF requires further preclinical studies. In addition, the following issues may need to be addressed when transitioning from preclinical to clinical studies. 1) There may be a drug dose conversion problem with MET use in patients with PF. MET is a therapeutic agent for the treatment of systemic diseases, whereas PF is a restrictive disease. If the effect of MET on PF is to be studied, efficient drug delivery to the lungs must be considered to optimize the drug concentration in the lungs (Manning et al., 2019). To date, the preclinical studies used large doses of MET compared with regular doses to enable adequate efficacy in the lungs of animals. 2) Biomarkers in patients with IPF are often specific (Guiot et al., 2017), affecting patient mortality and drug response. Therefore, the clinical effectiveness of MET in patients with PF should be combined with ongoing studies on PF-specific biomarkers (Raghu et al., 2018). 3) PF may not be clinically isolated, often existing in combination with other diseases, and may be influenced by factors such as smoking, age, and sex of the patient, suggesting that confounding factors often influence these studies (Bai et al., 2021). This may be the reason for some bias in the studies and the impact of the results. Nevertheless, we hope that clinical studies on MET for PF will be conducted in the future. This is because there is more than adequate evidence from preclinical studies and positive evidence from retrospective cohort studies with larger sample sizes. However, given the respect and protection of life, future investigators must address the possible abovementioned shortcomings.

5 Conclusion

This study is the first systematic review and meta-analysis of the effects of MET in animal models of PF. The present meta-analysis showed that MET significantly improved PF in animal models. MET may reverse and attenuate PF by activating AMPK and inhibiting TGF-β, α-SMA, and other pathways, ultimately inhibiting the phenotypes of fibroblast proliferation and differentiation, EMT, collagen deposition, and inflammatory response in lung tissues. In conclusion, this study suggests that MET may be a potential candidate for the treatment of PF.

Data availability statement

The original contributions presented in the study are included in the article/Supplementary Materials; further inquiries can be directed to the corresponding authors.

Author contributions

QD designed the study. XW wrote the main body. XX, XC, QF, SS, MY, and ZH collected the data, performed data curation, and conducted the analyses. XW and XX prepared the pictures and tables. QD and HY revised and reviewed the manuscript. All authors contributed to manuscript revision and reading and approved the submitted version.

Funding

This work was supported by the China Postdoctoral Science Foundation (NO. 2020M683644XB), the National Natural Science Foundation of China (Nos. 82104829 and 82174347), and the Sichuan Provincial Administration of Traditional Chinese Medicine Science and Technology Research Project (NO. 2020JC0049).

Acknowledgments

We want to thank the Biorender for improving the quality of our pictures.

Conflict of interest

The authors declare that the research was conducted in the absence of any commercial or financial relationships that could be construed as a potential conflict of interest.

Publisher's note

All claims expressed in this article are solely those of the authors and do not necessarily represent those of their affiliated organizations, or those of the publisher, the editors, and the reviewers. Any product that may be evaluated in this article, or claim that may be made by its manufacturer, is not guaranteed or endorsed by the publisher.

Supplementary material

The Supplementary Material for this article can be found online at: https://www.frontiersin.org/articles/10.3389/fphar.2022.948101/full#supplementary-material

References

Bai, L., Zhang, L., Pan, T., Wang, W., Wang, D., Turner, C., et al. (2021). Idiopathic pulmonary fibrosis and diabetes mellitus: A meta-analysis and systematic review. *Respir. Res.* 22 (1), 175. PMID: 34103046; PMCID: PMC8188656. doi:10.1186/s12931-021-01760-6

Bailey, C. J. (2017). Metformin: Historical overview. *Diabetologia* 60 (9), 1566–1576. doi:10.1007/s00125-017-4318-z

Bailoo, J. D., Reichlin, T. S., and Wurbel, H. (2014). Refinement of experimental design and conduct in laboratory animal research. *ilar J.* 55 (3), 383–391. doi:10.1093/ilar/ilu037

Barbarin, V., Arras, M., Misson, P., Delos, M., McGarry, B., Phan, S. H., et al. (2004). Characterization of the effect of interleukin-10 on silica-induced lung fibrosis in mice. *Am. J. Respir. Cell. Mol. Biol.* 31 (1), 78–85. doi:10.1165/rcmb.2003-0299OC

Batandier, C., Guigas, B., Detaille, D., El-Mir, M. Y., Fontaine, E., Rigoulet, M., et al. (2006). The ROS production induced by a reverse-electron flux at respiratory-chain complex 1 is hampered by metformin. *J. Bioenerg. Biomembr.* 38 (1), 33–42. doi:10.1007/s10863-006-9003-8

Chaudhari, K., Reynolds, C. D., and Yang, S. H. (2020). Metformin and cognition from the perspectives of sex, age, and disease. *Geroscience* 42 (1), 97–116. doi:10.1007/s11357-019-00146-3

Chen, Y. Y., Wu, T. T., Ho, C. Y., Yeh, T. C., Sun, G. C., Tseng, C. J., et al. (2022). Blocking of SGLT2 to eliminate NADPH-induced oxidative stress in lenses of animals with fructose-induced diabetes mellitus. *Int. J. Mol. Sci.* 23 (13), 7142. PMID: 35806147; PMCID: PMC9266761. doi:10.3390/ijms23137142

Cheng, D., Xu, Q., Wang, Y., Li, G., Sun, W., Ma, D., et al. (2021). Metformin attenuates silica-induced pulmonary fibrosis via AMPK signaling. *J. Transl. Med.* 19 (1), 349. doi:10.1186/s12967-021-03036-5

Choi, S. M., Jang, A. H., Kim, H., Lee, K. H., and Kim, Y. W. (2016). Metformin reduces bleomycin-induced pulmonary fibrosis in mice. *J. Korean Med. Sci.* 31 (9), 1419–1425. doi:10.3346/jkms.2016.31.9.1419

Coyle, C., Cafferty, F. H., Vale, C., and Langley, R. E. (2016). Metformin as an adjuvant treatment for cancer: A systematic review and meta-analysis. *Ann. Oncol.* 27 (12), 2184–2195. doi:10.1093/annonc/mdw410

Davis, G. S., Leslie, K. O., and Hemenway, D. R. (1998). Silicosis in mice: Effects of dose, time, and genetic strain. *J. Environ. Pathol. Toxicol. Oncol.* 17 (2), 81–97.

de Vries, R. B. M., Hooijmans, C. R., Langendam, M. W., van Luijk, J., Leenaars, M., Ritskes-Hoitinga, M., et al. (2015). A protocol format for the preparation, registration and publication of systematic reviews of animal intervention studies. *Evidence-based Preclin. Med.* 2, e00007–9. doi:10.1002/ebm2.7

Degryse, A. L., and Lawson, W. E. (2011). Progress toward improving animal models for idiopathic pulmonary fibrosis. *Am. J. Med. Sci.* 341 (6), 444–449. (PMID: 21613932; PMCID: PMC3103078. doi:10.1097/MAJ.0b013e31821aa000

Degryse, A. L., Tanjore, H., Xu, X. C., Polosukhin, V. V., Jones, B. R., McMahon, F. B., et al. (2010). Repetitive intratracheal bleomycin models several features of idiopathic pulmonary fibrosis. *Am. J. Physiol. Lung Cell. Mol. Physiol.* 299 (4), L442–L452. doi:10.1152/ajplung.00026.2010

Dempsey, T. M., Sangaralingham, L. R., Yao, X., Sanghavi, D., Shah, N. D., and Limper, A. H. (2019). Clinical effectiveness of antifibrotic medications for idiopathic pulmonary fibrosis. *Am. J. Respir. Crit. Care Med.* 200 (2), 168–174. doi:10.1164/rccm.201902-0456OC

Désogère, P., Tapias, L. F., Hariri, L. P., Rotile, N. J., Rietz, T. A., Probst, C. K., et al. (2017). Type I collagen-targeted PET probe for pulmonary fibrosis detection and staging in preclinical models. *Sci. Transl. Med.* 9 (384), eaaf4696. PMID: 28381537; PMCID: PMC5568793. doi:10.1126/scitranslmed.aaf4696

Diabetes Prevention Program Research Group (2012). Long-term safety, tolerability, and weight loss associated with metformin in the Diabetes Prevention Program Outcomes Study. *Diabetes Care* 35 (4), 731–737. PMID: 22442396; PMCID: PMC3308305. doi:10.2337/dc11-1299

Dos Santos, C. C., Gopal, B., and Verma, S. (2018). Metformin: An old dog with a new trick? *Cell. Metab.* 28 (3), 334–336. PMID: 30184483. doi:10.1016/j.cmet.2018.08.018

Farhood, B., Aliasgharzadeh, A., Amini, P., Rezaeyan, A., Tavassoli, A., Motevaseli, E., et al. (2019). Mitigation of radiation-induced lung pneumonitis and fibrosis using metformin and melatonin: A histopathological study. *Med. Kaunas.* 55 (8), 417. doi:10.3390/medicina55080417

Feng, Y., Wang, S., Zhang, Y., and Xiao, H. (2017). Metformin attenuates renal fibrosis in both AMPKα2-dependent and independent manners. *Clin. Exp. Pharmacol. Physiol.* 44 (6), 648–655. doi:10.1111/1440-1681.12748

Folli, F., Corradi, D., Fanti, P., Davalli, A., Paez, A., Giaccari, A., et al. (2011). The role of oxidative stress in the pathogenesis of type 2 diabetes mellitus micro- and

macrovascular complications: Avenues for a mechanistic-based therapeutic approach. *Curr. Diabetes Rev.* 7 (5), 313–324. doi:10.2174/157339911797415585

Foretz, M., Guigas, B., and Viollet, B. (2019). Understanding the glucoregulatory mechanisms of metformin in type 2 diabetes mellitus. *Nat. Rev. Endocrinol.* 15 (10), 569–589. doi:10.1038/s41574-019-0242-2

Fujita, T., Hemmi, S., Kajiwara, M., Yabuki, M., Fuke, Y., Satomura, A., et al. (2013). Complement-mediated chronic inflammation is associated with diabetic microvascular complication. *Diabetes. Metab. Res. Rev.* 29 (3), 220–226. doi:10.1002/dmrr.2380

Gamad, N., Malik, S., Suchal, K., Vasisht, S., Tomar, A., Arava, S., et al. (2018). Metformin alleviates bleomycin-induced pulmonary fibrosis in rats: Pharmacological effects and molecular mechanisms. *Biomed. Pharmacother.* 97, 1544–1553. doi:10.1016/j.biopha.2017.11.101

Gao, J., Yuan, J., Wang, Q., Lei, T., Shen, X., Cui, B., et al. (2020). Metformin protects against PM2.5-induced lung injury and cardiac dysfunction independent of AMP-activated protein kinase α2. *Redox Biol.* 28, 101345. Epub 2019 Oct 19. PMID: 31669973; PMCID: PMC6838896. doi:10.1016/j.redox.2019.101345

Garber, A. J., Duncan, T. G., Goodman, A. M., Mills, D. J., and Rohlf, J. L. (1997). Efficacy of metformin in type II diabetes: Results of a double-blind, placebo-controlled, dose-response trial. *Am. J. Med.* 103 (6), 491–497. doi:10.1016/s0002-9343(97)00254-4

Gu, X., Han, Y. Y., Yang, C. Y., Ji, H. M., Lan, Y. J., Bi, Y. Q., et al. (2021). Activated AMPK by metformin protects against fibroblast proliferation during pulmonary fibrosis by suppressing FOXM1. *Pharmacol. Res.* 173, 105844. doi:10.1016/j.phrs.2021.105844

Guiot, J., Moermans, C., Henket, M., Corhay, J. L., and Louis, R. (2017). Blood biomarkers in idiopathic pulmonary fibrosis. *Lung* 195 (3), 273–280. Epub 2017 Mar 28. PMID: 28353114; PMCID: PMC5437192. doi:10.1007/s00408-017-9993-5

Hao, W., Zuo, D. Z., Zhang, J. X., Jiang, L. L., Xiong, Y., Li, X. W., et al. (2019). Inhibitory effect and mechanism of metformin on alveolar epithelial-mesenchymal transition in lung tissue of rats with pulmonary fibrosis. *Chin. J. Pathophysiol.* 35 (11), 2042–2049. doi:10.3969/j.issn.1000-4718.2019.11.018

Haston, C. K. (2012). Mouse genetic approaches applied to the normal tissue radiation response. *Front. Oncol.* 2, 94. doi:10.3389/fonc.2012.00094

Holman, R. R., Paul, S. K., Bethel, M. A., Matthews, D. R., and Neil, H. A. (2008). 10-year follow-up of intensive glucose control in type 2 diabetes. *N. Engl. J. Med.* 359 (15), 1577–1589. doi:10.1056/NEJMoa0806470

Hooijmans, C. R., Rovers, M. M., de Vries, R. B., Leenaars, M., Ritskes-Hoitinga, M., and Langendam, M. W. (2014). SYRCLE's risk of bias tool for animal studies. *BMC Med. Res. Methodol.* 14, 43. doi:10.1186/1471-2288-14-43

Hsu, H. S., Liu, C. C., Lin, J. H., Hsu, T. W., Hsu, J. W., Su, K., et al. (2017). Involvement of ER stress, PI3K/AKT activation, and lung fibroblast proliferation in bleomycin-induced pulmonary fibrosis. *Sci. Rep.* 7 (1), 14272. PMID: 29079731; PMCID: PMC5660192. doi:10.1038/s41598-017-14612-5

Huang, W. T. (2015). Study on the role and mechanism of metformin inhibition of EGFR-TKI-induced interstitial lung fibrosis. Master thesis. Chongqing (China): Third Military Medical University, 02, 01–58.

Hutchinson, J., Fogarty, A., Hubbard, R., and McKeever, T. (2015). Global incidence and mortality of idiopathic pulmonary fibrosis: A systematic review. *Eur. Respir. J.* 46 (3), 795–806. doi:10.1183/09031936.00185114

Jenkins, R. G., Moore, B. B., Chambers, R. C., Eickelberg, O., Königshoff, M., Kolb, M., et al. (2017). An official American thoracic society workshop report: Use of animal models for the preclinical assessment of potential therapies for pulmonary fibrosis. *Am. J. Respir. Cell. Mol. Biol.* 56 (5), 667–679. doi:10.1165/rcmb.2017-0096ST

Jian, Y. (2017). Effect of Metformin on AMPK/NF-κB signaling pathway on pulmonary fibrosis in rats. Master thesis. Zunyi (China): Zunyi Medical College 10, 01–53.

Jiang, H. Y. (2016). Intervention of metformin on bleomycin-induced pulmonary fibrosis in rats. Master thesis. Zunyi (China): Zunyi Medical College, 01–44.

Jin, G., and Wong, S. T. (2014). Toward better drug repositioning: Prioritizing and integrating existing methods into efficient pipelines. *Drug Discov. Today* 19, 637–644. doi:10.1016/j.drudis.2013.11.005

Jones, M. G., Andriotis, O. G., Roberts, J. J., Lunn, K., Tear, V. J., Cao, L., et al. (2018). Nanoscale dysregulation of collagen structure-function disrupts mechano-homeostasis and mediates pulmonary fibrosis. *Elife* 7, e36354. PMID: 29966587; PMCID: PMC6029847. doi:10.7554/eLife.36354

Kang, H. S., Cho, H. C., Lee, J. H., Oh, G. T., Koo, S. H., Park, B. H., et al. (2016). Metformin stimulates IGFBP-2 gene expression through PPARalpha in diabetic states. *Sci. Rep.* 6, 23665. PMID: 27009398; PMCID: PMC4806307. doi:10.1038/srep23665

Kashihara, N., Haruna, Y., Kondeti, V. K., and Kanwar, Y. S. (2010). Oxidative stress in diabetic nephropathy. *Curr. Med. Chem.* 17 (34), 4256–4269. doi:10.2174/092986710793348581

Kheirollahi, V., Wasnick, R. M., Biasin, V., Vazquez-Armendariz, A. I., Chu, X., Moiseenko, A., et al. (2019). Metformin induces lipogenic differentiation in myofibroblasts to reverse lung fibrosis. *Nat. Commun.* 10 (1), 2987. doi:10.1038/s41467-019-10839-0

King, C. S., and Nathan, S. D. (2017). Idiopathic pulmonary fibrosis: Effects and optimal management of comorbidities. *Lancet Respir. Med.* 5 (1), 72–84. doi:10.1016/S2213-2600(16)30222-3

King, T. E., Jr, Bradford, W. Z., Castro-Bernardini, S., Fagan, E. A., Glaspole, I., Glassberg, M. K., et al. (2014). A phase 3 trial of pirfenidone in patients with idiopathic pulmonary fibrosis. *N. Engl. J. Med.* 370, 2083–2092. doi:10.1056/NEJMoa1402582

Kopf, S., Groener, J. B., Kender, Z., Fleming, T., Brune, M., Riedinger, C., et al. (2018). Breathlessness and restrictive lung disease: An important diabetes-related feature in patients with type 2 diabetes. *Respiration.* 96 (1), 29–40. doi:10.1159/000488909

Kowluru, R. A., and Chan, P. S. (2007). Oxidative stress and diabetic retinopathy. *Exp. Diabetes Res.*, 43603. doi:10.1155/2007/43603

Lambert, E. M., Wuyts, W. A., Yserbyt, J., and De Sadeleer, L. J. (2021). Statins: Cause of fibrosis or the opposite? Effect of cardiovascular drugs in idiopathic pulmonary fibrosis. *Respir. Med.* 176, 106259. Epub 2020 Nov 26. PMID: 33276250. doi:10.1016/j.rmed.2020.106259

Li, M., Krishnaveni, M. S., Li, C., Zhou, B., Xing, Y., Banfalvi, A., et al. (2011). Epithelium-specific deletion of TGF-beta receptor type II protects mice from bleomycin-induced pulmonary fibrosis. *J. Clin. Invest.* 121, 277–287. doi:10.1172/JCI42090

Li, S. X., Li, C., Pang, X. R., Zhang, J., Yu, G. C., Yeo, A. J., et al. (2021a). Metformin attenuates silica-induced pulmonary fibrosis by activating autophagy via the AMPK-mTOR signaling pathway. *Front. Pharmacol.* 12, 719589. doi:10.3389/fphar.2021.719589

Li, S. X., Pang, X. R., Yan, H. Y., Zhang, J., Jia, Q., Li, C., et al. (2021b). Interventional effect of metformin on pulmonary inflammation and pulmonary fibrosis in silicotic rats. *Zhonghua Lao Dong Wei Sheng Zhi Ye Bing Za Zhi* 39 (10), 726–732. Chinese. doi:10.3760/cma.j.cn121094-20200930-00552

Lin, K., Chen, H., Chen, X., Qian, J., Huang, S., and Huang, W. (2020). Efficacy of curcumin on aortic atherosclerosis: A systematic review and meta-analysis in mouse studies and insights into possible mechanisms. *Oxid. Med. Cell. Longev.* 2020, 1520747. doi:10.1155/2020/1520747

Lin, S. C., and Hardie, D. G. (2018). Ampk: Sensing glucose as well as cellular energy status. *Cell. Metab.* 27 (2), 299–313. doi:10.1016/j.cmet.2017.10.009

Maher, T. M., and Strek, M. E. (2019). Antifibrotic therapy for idiopathic pulmonary fibrosis: Time to treat. *Respir. Res.* 20 (1), 205. PMID: 31492155; PMCID: PMC6731623. doi:10.1186/s12931-019-1161-4

Maher, T. M., Swigris, J. J., Kreuter, M., Wijsenbeek, M., Cassidy, N., Ireland, L., et al. (2018). Identifying barriers to idiopathic pulmonary fibrosis treatment: A survey of patient and physician views. *Respiration.* 96 (6), 514–524. Epub 2018 Aug 16. PMID: 30114692. doi:10.1159/000490667

Manning, E. P., Losier, A., Emeagwali, N., Ryu, C., and Honiden, S. (2019). New applications of old drugs as novel therapies in idiopathic pulmonary fibrosis. Metformin, hydroxychloroquine, and thyroid hormone. *Am. J. Respir. Crit. Care Med.* 199 (12), 1561–1563. PMID: 30822095; PMCID: PMC7051474. doi:10.1164/rccm.201809-1700RR

Moeller, A., Ask, K., Warburton, D., Gauldie, J., and Kolb, M. (2008). The bleomycin animal model: A useful tool to investigate treatment options for idiopathic pulmonary fibrosis? *Int. J. Biochem. Cell. Biol.* 40 (3), 362–382. Epub 2007 Aug 30. PMID: 17936056; PMCID: PMC2323681. doi:10.1016/j.biocel.2007.08.011

Page, M. J., McKenzie, J. E., Bossuyt, P. M., Boutron, I., Hoffmann, T. C., Mulrow, C. D., et al. (2021). The PRISMA 2020 statement: An updated guideline for reporting systematic reviews. *BMJ* 372, n71. doi:10.1136/bmj.n71

Perel, P., Roberts, I., Sena, E., Wheble, P., Briscoe, C., Sandercock, P., et al. (2007). Comparison of treatment effects between animal experiments and clinical trials: Systematic review. *BMJ* 334 (7586), 197. doi:10.1136/bmj.39048.407928.BE

Raghu, G., Collard, H. R., Egan, J. J., Martinez, F. J., Behr, J., Brown, K. K., et al. (2011). An official ATS/ERS/JRS/ALAT statement: Idiopathic pulmonary fibrosis: Evidence-based guidelines for diagnosis and management. *Am. J. Respir. Crit. Care Med.* 183 (6), 788–824. doi:10.1164/rccm.2009-040GL

Raghu, G., Rochwerg, B., Zhang, Y., Garcia, C. A., Azuma, A., Behr, J., et al. (2015). An official ATS/ERS/JRS/ALAT clinical practice guideline: Treatment of idiopathic pulmonary fibrosis. An update of the 2011 clinical practice guideline. *Am. J. Respir. Crit. Care Med.* 192 (2), e3–19. Erratum in: Am J Respir Crit Care

Med. 2015 Sep 1;192(5):644. Dosage error in article text. PMID: 26177183. doi:10.1164/rccm.201506-1063ST

Raghu, G., van den Blink, B., Hamblin, M. J., Brown, A. W., Golden, J. A., Ho, L. A., et al. (2018). Effect of recombinant human pentraxin 2 vs placebo on change in forced vital capacity in patients with idiopathic pulmonary fibrosis: A randomized clinical trial. *JAMA* 319, 2299–2307. doi:10.1001/jama.2018.6129

Rangarajan, S., Bone, N. B., Zmijewska, A. A., Jiang, S., Park, D. W., Bernard, K., et al. (2018). Metformin reverses established lung fibrosis in a bleomycin model. *Nat. Med.* 24 (8), 1121–1127. doi:10.1038/s41591-018-0087-6

Redente, E. F., Jacobsen, K. M., Solomon, J. J., Lara, A. R., Faubel, S., Keith, R. C., et al. (2011). Age and sex dimorphisms contribute to the severity of bleomycin-induced lung injury and fibrosis. *Am. J. Physiol. Lung Cell. Mol. Physiol.* 301 (4), L510–L518. Epub 2011 Jul 8. (PMID: 21743030; PMCID: PMC3191751. doi:10.1152/ajplung.00122.2011

Richeldi, L., Costabel, U., Selman, M., Kim, D. S., Hansell, D. M., Nicholson, A. G., et al. (2011). Efficacy of a tyrosine kinase inhibitor in idiopathic pulmonary fibrosis. *N. Engl. J. Med.* 365, 1079–1087. doi:10.1056/NEJMoa1103690

Roumie, C. L., Hung, A. M., Greevy, R. A., Grijalva, C. G., Liu, X., Murff, H. J., et al. (2012). Comparative effectiveness of sulfonylurea and metformin monotherapy on cardiovascular events in type 2 diabetes mellitus: A cohort study. *Ann. Intern. Med.* 157 (9), 601–610. doi:10.7326/0003-4819-157-9-201211060-00003

Sato, N., Takasaka, N., Yoshida, M., Tsubouchi, K., Minagawa, S., Araya, J., et al. (2016). Metformin attenuates lung fibrosis development via NOX4 suppression. *Respir. Res.* 17 (1), 107. doi:10.1186/s12931-016-0420-x

Schultze, S. M., Hemmings, B. A., Niessen, M., and Tschopp, O. (2012). PI3K/AKT, MAPK and AMPK signalling: Protein kinases in glucose homeostasis. *Expert Rev. Mol. Med.* 14, e1. PMID: 22233681. doi:10.1017/S1462399411002109

Spagnolo, P., Kreuter, M., Maher, T. M., Wuyts, W., Bonella, F., Corte, T. J., et al. (2018). Metformin does not affect clinically relevant outcomes in patients with idiopathic pulmonary fibrosis. *Respiration.* 96 (4), 314–322. Epub 2018 Jul 19. PMID: 30025392. doi:10.1159/000489668

Sun, T., Wang, P., Deng, T., Tao, X., Li, B., and Xu, Y. (2021). Effect of panax notoginseng saponins on focal cerebral ischemia-reperfusion in rat models: A meta-analysis. *Front. Pharmacol.* 11, 572304. doi:10.3389/fphar.2020.572304

Tashiro, J., Rubio, G. A., Limper, A. H., Williams, K., Elliot, S. J., Ninou, I., et al. (2017). Exploring animal models that resemble idiopathic pulmonary fibrosis. *Front. Med.* 4, 118. doi:10.3389/fmed.2017.00118

Teague, T. T., Payne, S. R., Kelly, B. T., Dempsey, T. M., McCoy, R. G., Sangaralingham, L. R., et al. (2022). Evaluation for clinical benefit of metformin in patients with idiopathic pulmonary fibrosis and type 2 diabetes mellitus: A national claims-based cohort analysis. *Respir. Res.* 23 (1), 91. PMID: 35410255; PMCID: PMC9004115. doi:10.1186/s12931-022-02001-0

Thannickal, V. J. (2013). Mechanistic links between aging and lung fibrosis. *Biogerontology* 14 (6), 609–615. doi:10.1007/s10522-013-9451-6

Thannickal, V. J., Toews, G. B., White, E. S., Lynch, J. P., 3rd, and Martinez, F. J. (2004). Mechanisms of pulmonary fibrosis. *Annu. Rev. Med.* 55, 395–417. doi:10.1146/annurev.med.55.091902.103810

Travis, W. D., Costabel, U., Hansell, D. M., King, T. E., Jr, Lynch, D. A., Nicholson, A. G., et al. (2013). An official American Thoracic Society/European Respiratory Society statement: Update of the international multidisciplinary classification of the idiopathic interstitial pneumonias. *Am. J. Respir. Crit. Care Med.* 188 (6), 733–748. doi:10.1164/rccm.201308-1483ST

Tzouvelekis, A., Tzilas, V., Dassiou, M., and Bouros, D. (2018). Metformin in idiopathic pulmonary fibrosis "seeking the holy-grail through drug-repositioning". *Respiration.* 96, 305–307. doi:10.1159/000490917

Viollet, B., Guigas, B., Sanz Garcia, N., Leclerc, J., Foretz, M., and Andreelli, F. (2012). Cellular and molecular mechanisms of metformin: An overview. *Clin. Sci.* 122 (6), 253–270. doi:10.1042/CS20110386

Wang, H., Zhang, G., Hou, H., Gao, Y., Gao, S., Ma, M., et al. (2019). Exploration of a model of pulmonary fibrosis in rats caused by different modes of bleomycin administration[J]. *Chin. J. Exp. Formulation* 25 (11), 73–79. doi:10.13422/j.cnki.syfjx.20191104

Wang, J., Wang, Y., Han, J., Mei, H., Yu, D., Ding, Q., et al. (2017). Metformin attenuates radiation-induced pulmonary fibrosis in a murine model. *Radiat. Res.* 188 (1), 105–113. doi:10.1667/RR14708.1

Wang, Y., Lin, C., Han, R., Lu, C., Li, L., Hu, C., et al. (2020). Metformin attenuates TGF-β1-induced pulmonary fibrosis through inhibition of transglutaminase 2 and subsequent TGF-β pathways. *3 Biotech.* 10 (6), 287. doi:10.1007/s13205-020-02278-2

Wang, Y., Xiong, Y. C., Xue, S. B., Wu, Z. H., and Peng, Z. J. (2017). Mechanism of effect of metformin on the prevention and treatment of radiographic pulmonary fibrosis in rats. *Chin. J. Radiat. Med. Prot.* 37 (10), 736–741. doi:10.3760/cma.j.issn.0254-5098.2017.10.003

Willis, B. C., and Borok, Z. (2007). TGF-beta-induced EMT: Mechanisms and implications for fibrotic lung disease. *Am. J. Physiol. Lung Cell. Mol. Physiol.* 293, L525–L534. doi:10.1152/ajplung.00163.2007

Wollin, L., Wex, E., Pautsch, A., Schnapp, G., Hostettler, K. E., Stowasser, S., et al. (2015). Mode of action of nintedanib in the treatment of idiopathic pulmonary fibrosis. *Eur. Respir. J.* 45 (5), 1434–1445. doi:10.1183/09031936.00174914

Wu, M., Xu, H., Liu, J., Tan, X., Wan, S., Guo, M., et al. (2021). Metformin and fibrosis: A review of existing evidence and mechanisms. *J. Diabetes Res.* 2021, 6673525. doi:10.1155/2021/6673525

Wu, Y. L. (2018). Effect of metformin on AMPK and LC3-II expression in lung tissue of rat pulmonary fibrosis model. Master thesis. Zunyi (China): Zunyi Medical College 01, 01–55.

Wynn, T. A. (2011). Integrating mechanisms of pulmonary fibrosis. *J. Exp. Med.* 208 (7), 1339–1350. doi:10.1084/jem.20110551

Wynn, T. A., and Ramalingam, T. R. (2012). Mechanisms of fibrosis: Therapeutic translation for fibrotic disease. *Nat. Med.* 18 (7), 1028–1040. doi:10.1038/nm.2807

Xavier, A., Toumi, H., and Lespessailles, E. (2021). Animal model for glucocorticoid induced osteoporosis: A systematic review from 2011 to 2021. *Int. J. Mol. Sci.* 23 (1), 377. doi:10.3390/ijms23010377

Xiao, H., Huang, X., Wang, S., Liu, Z., Dong, R., Song, D., et al. (2020). Metformin ameliorates bleomycin-induced pulmonary fibrosis in mice by suppressing IGF-1. *Am. J. Transl. Res.* 12 (3), 940–949. doi:10.1097/01.ccm.0000643508.83802.5f

Xiao, H. J., Huang, X. X., Liu, Z., Dong, R., Song, D. Y., Zhang, X., et al. (2018). Metformin protects against bleomycin-induced pulmonary fibrosis in mice. *Zhonghua Yi Xue Za Zhi* 98 (24), 1951–1955. doi:10.3760/cma.j.issn.0376-2491.2018.24.012

Xu, Y., Peng, W., Han, D., Feng, F., Wang, Z., Gu, C., et al. (2021). Maiwei Yangfei decoction prevents bleomycin-induced pulmonary fibrosis in mice. *Exp. Ther. Med.* 22 (5), 1306. Epub 2021 Sep 16. PMID: 34630661; PMCID: PMC8461617. doi:10.3892/etm.2021.10741

Yahyapour, R., Amini, P., Saffar, H., Motevaseli, E., Farhood, B., Pooladvand, V., et al. (2019). Protective effect of metformin, resveratrol and alpha-lipoic acid on radiation- induced pneumonitis and fibrosis: A histopathological study. *Curr. Drug Res. Rev.* 11 (2), 111–117. doi:10.2174/2589977511666191018180758

Yerevanian, A., and Soukas, A. A. (2019). Metformin: Mechanisms in human obesity and weight loss. *Curr. Obes. Rep.* 8 (2), 156–164. doi:10.1007/s13679-019-00335-3

Zhao, W., Ho, W. T., and Zhao, Z. J. (2015). Quantitative analyses of myelofibrosis by determining hydroxyproline. *Stem Cell. Investig.* 2, 2. PMID: 27358870; PMCID: PMC4923646. doi:10.3978/j.issn.2306-9759.2015.01.02

Zou, X. Z., Gong, Z. C., Liu, T., He, F., Zhu, T. T., Li, D., et al. (2017). Involvement of epithelial-mesenchymal transition afforded by activation of LOX-1/TGF-β1/KLF6 signaling pathway in diabetic pulmonary fibrosis. *Pulm. Pharmacol. Ther.* 44, 70–77. doi:10.1016/j.pupt.2017.03.012

frontiers | Frontiers in Pharmacology

TYPE Original Research
PUBLISHED 09 September 2022
DOI 10.3389/fphar.2022.977284

Check for updates

OPEN ACCESS

EDITED BY
Yuxia Zhao,
Shandong University, China

REVIEWED BY
Xin Wu,
Zhejiang Chinese Medical University, China
Weizu Li,
Anhui Medical University, China

*CORRESPONDENCE
Fa-Rong Zhang,
farongzhang@163.com
Xiang-Dong Xu,
zhengsanxiasd@126.com

†These authors have contributed equally to this work and share first authorship

SPECIALTY SECTION
This article was submitted to Experimental Pharmacology and Drug Discovery, a section of the journal Frontiers in Pharmacology

RECEIVED 24 June 2022
ACCEPTED 29 July 2022
PUBLISHED 09 September 2022

CITATION
Li Y-Y, Tian Z-H, Pan G-H, Zhao P, Pan D-J, Zhang J-Q, Ye L-Y, Zhang F-R and Xu X-D (2022), Heidihuangwan alleviates renal fibrosis in rats with 5/6 nephrectomy by inhibiting autophagy. *Front. Pharmacol.* 13:977284. doi: 10.3389/fphar.2022.977284

COPYRIGHT
© 2022 Li, Tian, Pan, Zhao, Pan, Zhang, Ye, Zhang and Xu. This is an open-access article distributed under the terms of the Creative Commons Attribution License (CC BY). The use, distribution or reproduction in other forums is permitted, provided the original author(s) and the copyright owner(s) are credited and that the original publication in this journal is cited, in accordance with accepted academic practice. No use, distribution or reproduction is permitted which does not comply with these terms.

Heidihuangwan alleviates renal fibrosis in rats with 5/6 nephrectomy by inhibiting autophagy

Ying-Ying Li[1†], Zeng-Hui Tian[1†], Guang-Hui Pan[2], Ping Zhao[3], De-Jun Pan[4], Jun-Qing Zhang[5], Li-Ying Ye[1], Fa-Rong Zhang[2*] and Xiang-Dong Xu[6*]

[1]College of First Clinical Medical, Shandong University of Traditional Chinese Medicine, Jinan, China, [2]Department of Nephrology, Affiliated Hospital of Shandong University of Traditional Chinese Medicine, Jinan, China, [3]Department of Nephrology, Tai'an City Hospital of Traditional Chinese Medicine, Tai'an, China, [4]Department of Clinical Laboratory, Affiliated Hospital of Shandong University of Traditional Chinese Medicine, Jinan, China, [5]College of Traditional Chinese Medicine, Shandong University of Traditional Chinese Medicine, Jinan, China, [6]Experimental Center, Affiliated Hospital of Shandong University of Traditional Chinese Medicine, Jinan, China

Renal fibrosis is a common pathway for the progression of various chronic kidney diseases (CKD), and the formation and deterioration will eventually lead to end-stage renal failure, which brings a heavy medical burden to the world. HeidihuangWan (HDHW) is a herbal formulation with stable and reliable clinical efficacy in the treatment of renal fibrosis. However, the mechanism of HDHW in treating renal fibrosis is not clear. In this study, we aimed to investigate the mechanism of HDHW to improve renal fibrosis. Wistar rats were randomly divided into the normal control group, 5/6 Nephrectomy group, astragaloside IV (AS-IV) group, HDHW group, and HDHW + IGF-1R inhibitor (JB1) group. Except for the normal control group, the rat renal fibrosis model was established by 5/6 nephrectomy and intervened with drugs for 8 weeks. Blood samples were collected to evaluate renal function. Hematoxylin-Eosin (HE), Periodic Acid-Schiff (PAS), Modified Masson's Trichrome (Masson) staining were used to evaluate the pathological renal injury, and immunohistochemistry and Western blotting were used to detect the protein expression of renal tissue. The results showed that HDHW was effective in improving renal function and reducing renal pathological damage. HDHW down-regulated the levels of fibrosis marker proteins, including α-smooth muscle actin (α-SMA), vimentin, and transforming growth factors−β(TGF-β), which in turn reduced renal fibrosis. Further studies showed

Abbreviations: CKD, Chronic kidney diseases; HDHW, HeidihuangWan; AS-IV, Astragaloside IV; Scr, Serum creatinine; BUN, blood urea nitrogen; HE, Hematoxylin-Eosin; PAS, Periodic Acid-Schiff; Masson, Modified Masson's Trichrome; α-SMA, α-smooth muscle actin; TGF-β, Transforming growth factors-β; PI3K, class I phosphatidylinositol-3 kinase; Akt, serine-threonine kinase; IGF-1, Insulin-like growth factor 1; IGF-1R, Insulin-like growth factor 1 receptor; ESRD, End-stage renal disease; CRF, Chronic renal failure; EMT, epithelial-mesenchymal transition; ECM, extracellular matrix; NF-κB, nuclear factor-kappaB; Wnt, wingless-type MMTV integration site; PKC, protein kinase C; ERK, extracellular regulated protein kinases; TCMs, Traditional Chinese medicines; RIF, Renal interstitial fibrosis; UHPLC-Q-Orbitrap-MS/MS, Ultra High Performance Liquid Chromatography-Quadrupole-Electrostatic Field Orbitrap Tandem Mass Spectrometry.

that HDHW down-regulated the expression of autophagy-related proteins Beclin1 and LC3II, indicating that HDHW inhibited autophagy. In addition, we examined the activity of the class I phosphatidylinositol-3 kinase (PI3K)/serine-threonine kinase (Akt)/mTOR pathway, an important signaling pathway regulating autophagy, and the level of insulin-like growth factor 1 (IGF-1), an upstream activator of PI3K/Akt/mTOR. HDHW upregulated the expression of IGF-1 and activated the PI3K/Akt/mTOR pathway, which may be a vital pathway for its inhibition of autophagy. Application of insulin-like growth factor 1 receptor (IGF-1R) inhibitor further confirmed that the regulation of autophagy and renal fibrosis by HDHW was associated with IGF-1-mediated activation of the PI3K/Akt/mTOR pathway. In conclusion, our study showed that HDHW inhibited autophagy by upregulating IGF-1 expression, promoting the binding of IGF-1 to IGF-1R, and activating the PI3K/Akt/mTOR signaling pathway, thereby reducing renal fibrosis and protecting renal function. This study provides support for the application and further study of HDHW.

KEYWORDS

heidihuangwan, renal fibrosis, autophagy, insulin-like growth factor 1, PI3K/Akt/mTOR

Introduction

Chronic kidney disease (CKD) is mainly characterized by irreversible impairment or loss of renal function, eventually leading to end-stage renal disease (ESRD) or chronic renal failure (CRF). It has become one of the serious global public health problems because of its high prevalence (GBD 2017 Disease and Injury Incidence and Prevalence Collaborators, 2018), high mortality (GBD 2017 Causes of Death Collaborators, 2018; GBD 2017 DALYs and HALE Collaborators, 2018), many complications (GBD Chronic Kidney Disease Collaboration, 2020), and lack of effective means of prevention and treatment (Zhang et al., 2022a). Renal fibrosis is the underlying pathological process of CKD independent of the underlying cause, and its formation and progression can lead to the destruction of normal kidney structure and loss of kidney function, eventually leading to end-stage renal failure (Liu et al., 2017). End-stage renal failure is difficult to reverse, and since most chronic kidney diseases lead to renal fibrosis, which in turn is an important pathological process leading to the continued progression of kidney damage. Therefore, there is a strong interest in identifying the underlying factors and pathogenesis of this process to reverse the progression of CKD (da Silva et al., 2015), and the development of new strategies for the treatment of this pathological process is considered to be extremely urgent for the prevention and treatment of CKD.

The pathogenesis of renal fibrosis is complex and has been outlined by some investigators as 4 pathological stages, mainly including Stage 1: Activation and injury stage. The renal disease leads to epithelial cell injury (E-calcine mucin shedding), fibroblast proliferation, and macrophage infiltration. Stage 2: Fibrogenic signaling stage. Inflammatory and fibrotic signaling pathways are activated. Stage 3: Fibrosis stage. Increased epithelial-mesenchymal transition (EMT) and extracellular matrix (ECM) deposition (EMT may also lead to ECM deposition). Stage 4: Destructive stage. Fibronectin, collagen, and α-SMA increase, eventually leading to renal failure (Zhuang et al., 2019). Multiple cellular targets and molecular pathways are involved in these stages, and the cellular targets mainly include the intrinsic renal cells such as podocytes (Xuan et al., 2021), tubular epithelial cells (Hu et al., 2022a), and thylakoid cells (Xiao et al., 2022), especially tubular epithelial cells, as interstitial myofibroblasts are the main effector cells in renal fibrosis, a large proportion of which are formed through the occurrence of EMT in tubular epithelial cells in the affected kidney (Hu et al., 2021). Molecular pathways mainly include nuclear factor-kappaB (NF-κB) (Wang et al., 2018a), TGF-β1/Smad (Loboda et al., 2016), Notch, wingless-type MMTV integration site (Wnt), Hedgehog (Edeling et al., 2016), protein kinase C (PKC)/extracellular regulated protein kinases (ERK), and PI3K/Akt (Liu et al., 2017), etc. Notably, related studies have shown that the PI3K/Akt signaling pathway can be used as an intervention target in renal fibrosis (Fan et al., 2022; Li et al., 2022), and also, the PI3K/Akt signaling pathway plays an important regulatory role in the process of cellular autophagy.

Autophagy is closely related to renal fibrosis, and a recent study found that sustained activation of autophagy is detrimental to the kidney after severe injury, leading to renal cell senescence and promoting renal fibrosis through the secretion of pro-fibrotic cytokines (Zheng et al., 2019). mTOR is one of the key regulators of autophagy in mammalian cells and can be activated by signal transducers including PI3K and Akt activation in response to insulin, IGF and other growth signals, which in turn inhibit

autophagy (Liang et al., 2022). And further studies have shown that IGF-1, as a PI3K/Akt activator, improves renal fibrosis indicators in UUO rats (Wu et al., 2016). Therefore, targeting the IGF-1/PI3K/Akt/mTOR pathway to inhibit the sustained activation of autophagy during renal fibrosis may be an appropriate approach for the treatment of renal fibrosis.

HDHW, which consisted of Shu Di Huang, Cang Zhu, Gan Jiang, and Da Zao, is a classical kidney tonic herbal compound, and a large number of previous studies by our group have shown that HDHW can reduce renal fibrosis and improve renal function (Changlei et al., 2013) by improving micro inflammatory status, lowering lipids, improving renal anemia, and regulating gastrointestinal hormone disorders (Sun et al., 2014a; Sun et al., 2014b; Yang et al., 2016; Zhao et al., 2017; Yang et al., 2019), with significant clinical efficacy (Zhang et al., 2009; Changlei et al., 2013). However, the mechanism of HDHW for the treatment of renal fibrosis is not well defined due to the complex composition and targets of the Chinese medicine compound, and it deserves further study. In the present study, we identified the main components of HDHW using high-performance liquid chromatography and further evaluated the effects of HDHW on renal function and renal fibrosis in 5/6 nephrectomized rats. We hypothesized that HDHW could modulate the activity of the IGF-1/PI3K/Akt/mTOR pathway, inhibits autophagy and ameliorate renal fibrosis.

Materials and methods

Drugs and reagents

The single herbal granules (batch number 19051981) used in this study to prepare the decoction of HDHW were purchased from the Affiliated Hospital of Shandong University of Traditional Chinese Medicine (Manufactured by Jiangyin Tianjiang Pharmaceutical Co., Ltd., Wuxi, Jiangsu, China). The formula granules of HDHW have been qualified by Jiangyin Tianjiang Pharmaceutical Co., Ltd., whose quality inspection center has been accredited by CNAS National Laboratory. The Chinese herbal formula granules are single herbal products that simulate the decoction of traditional Chinese medicine tonics and are refined from Chinese herbal tablets by extraction, concentration, and drying processes using modern science and technology. AS-IV and Carboxymethyl Cellulose (CMC)were purchased from Chuzhou Sinoda Biotechnology Co. IGF-1R inhibitor (JB1) (78617-10-4) was purchased from Topscience Co. Ltd., Shanghai, China, with a purity of ≥98% (HPLC). Antibodies against PI3K (4249), Akt (4691), p-Akt (4060) were purchased from Cell Signaling Technology (Danvers, MA, United States). Antibodies against p-mTOR (80596-1-RR), LC3I/II (14600-1-AP), α-SMA (14395-1-AP), IGF-1 (28530-1-AP) were from Proteintech (Wuhan, China). Antibodies against p-PI3K(AP0854), and Beclin1 (A17028) were from ABclonal (Shanghai, China). Antibodies against mTOR (ab134903) were from Abcam (Cambridge, United Kingdom). Horseradish enzyme-labeled goat anti-rabbit IgG (H+L) was purchased from Beijing Zhongsun Jinqiao Biotechnology Co.

Preparation of HeidihuangWan decoction

HDHW consists of Shu Di Huang, Cang Zhu, Gan Jiang, and Da Zao, and the herb information and composition ratio are shown in Table 1. The adult dosage of HDHW is 18.5g/60 kg. According to the equivalent dose ratio (6.3) converted from the body surface area of humans and rats, the dosage for rats is 1.94 g/kg. According to this ratio, the single herb granules were mixed and dissolved in ultrapure water. The decoction of HDHW was prepared. Some of the HDHW decoction was stored at −80°C and analyzed by UHPLC-Q-Orbitrap-MS/MS.

UHPLC-Q-orbitrap-MS/MS analysis

Add 1,000 μL of 80% methanol to 200 μL of the solution of HeidihuangWan Decoction, and vortex for 10 min. Centrifuge at 12,000 rpm for 10 min at 4°C. The supernatant was filtered and analyzed on the machine. Mass spectrometry conditions: ion source: electrospray ionization source (ESI); Scan mode: positive and negative ion switching scan; Detection mode: full mass/dd-MS2; Resolution: 70000 (full mass); 17500 (dd-MS2); Scan range: 100.0–1500.0 m/z; Electrospray voltage (Spary Voltage: 3.2 kV (Positive); Capillary Temperature: 300°C; Collision gas: high-purity argon (purity ≥99.999%); Collision energy (N)CE: 30; Sheath gas: nitrogen (purity ≥99.999%), 40 Arb; Auxiliary gas: nitrogen (purity ≥99.999%), 15 Arb, 350°C; Data acquisition time: 30.0 min. Chromatographic column: AQ-C18, 150 × 2.1 mm, 1.8 μm, Welch; Flow rate: 0.3 ml/min; Aqueous phase: 0.1% formic acid/water solution; Organic phase: methanol; Eluent: methanol; Column oven temperature: 35°C; Autosampler temperature: 10.0°C; Autosampler injection volume: 5.00 μL see Table 2 for the gradient elution procedure. The data for the high-resolution liquid mass acquisition was completed by CD2.1 (Thermo Fisher). Retention time correction, peak identification, peak extraction, peak integration, and peak alignment were performed. The data were then searched and compared through the mzCloud database.

Animal experiments

Animals

Seven-week-old male Wistar rats (200 ± 20 g) were used as research subjects. All animals were purchased from Beijing Viton

TABLE 1 | Composition of HeidihuangWan.

Chinses name	Scientific name	Plant part	Batch number	Adult daily dose of granules (g)	Corresponding	Composition (%)
		Used			Herb dose (g)	
Shu Di Huang	Rehmannia glutinosa (Gaetn.) Libosch. ex Fisch. et MeyPraeparata	Root	19051981	8	20	43.24
Cang Zhu	Atractylodes lancea (Thunb.)DC.	Rhizome	19070691	6	20	32.43
Gan Jiang	Zingiber oj-jicinale Rosc	Rhizome	19052411	0.5	3	16.22
Da Zao	Ziziphus jujuba Mill	Fruit	19060131	4	20	21.62

TABLE 2 Chromatographic gradient.

Time (min)	Water phase ratio (%)	Organic phase ratio (%)
1	98	2
5	80	20
10	50	50
15	20	80
20	5	95
27	5	95
28	98	2
30	98	2

Lihua Laboratory Animal Science and Technology Co. Ltd. (SCXK 2016-0006). All animal experiments were conducted in compliance with the National Institute of Health Guide for the Care and Use of Laboratory Animals and were approved by the Animal Ethics Committee of Shandong University of Traditional Chinese Medicine (SDUTCM20201019002).

Making animal models

According to the method of the literature (Ji and HE, 2019), after adaptive feeding of the rats for 1 week, the rats were anesthetized by intraperitoneal injection of sodium pentobarbital (35 mg/kg). Then the rats were fixed in a prone position, the skin was sterilized routinely, the right kidney was exposed, the perirenal membrane was stripped, the renal phylum was ligated, the right kidney was removed (the adrenal gland was preserved), and finally, the skin was sutured layer by layer. Ten days after the first operation, after anesthetizing the rat in the same manner, the renal parenchyma of the upper and lower poles of the left kidney was removed, followed by hemostasis using gelatin sponge compression. Finally, the abdominal cavity was closed. In addition, the normal control group did not remove the kidney, and only the perirenal membrane was stripped. Penicillin was injected intraperitoneally for 3 consecutive days after surgery to prevent infection (Figure 2A).

Grouping and drug administration

After 12 weeks of modeling, blood was collected through the tail vein of rats to detect serum creatinine (Scr) and blood urea nitrogen (BUN) levels, and the success of modeling was judged by the fact that the Scr and BUN in the operated rats were significantly higher than those in the normal group. The rats with successful modeling were randomly divided into the following groups: 5/6 Nephrectomy group, HDHW group, AS-IV group, HDHW + IGF-1R inhibitor (JB1) group, and another normal control group (n = 6). HDHW group was given HDHW decoction, AS-IV group was given AS-IV decoction (1.5 mg/kg) dissolved in 0.5% CMC (Zhu et al., 2014). The corresponding volume of saline was given to the 5/6 Nephrectomy group and normal control group. The HDHW + JB1 group was injected subcutaneously with JB1 at a concentration of 50 ng/uL for 7 consecutive days, with each injection dose of 18 ng/g, and given HDHW decoction. The oral administration time of each group was 10:00a.m. every day, and the injection time of JB1 was 9:00a.m. every day, while the corresponding volume of saline was injected at the same time in the remaining groups to ensure the accuracy of the experiment. After 8 weeks of continuous administration, the rats were anesthetized by intraperitoneal injection of sodium pentobarbital (35 mg/kg), blood was collected from the abdominal aorta, and the kidneys were immediately isolated and part of them was stored in the refrigerator at −80°C, and the other part was immersed in 4% paraformaldehyde for fixation.

Detection of serum biochemical indicators

After the end of the drug intervention, blood was collected through the abdominal aorta and the collected blood was left at room temperature for 2h, centrifuged at 3000 rpm for 20min,

collected supernatant, and detected Scr, BUN, aspartate aminotransferase (AST) and alanine aminotransferase (ALT) in rat serum according to the manufacturer's instructions.

Histological and immunohistochemical assays

The kidney tissue soaked in 4% paraformaldehyde-fixed for 48 h was cut into small pieces, dehydrated, embedded with paraffin wax, and cut into 4 μm slices. Perform hematoxylin-eosin (HE), Masson, periodic-acid Schiff (PAS), and immunohistochemistry (IHC) staining experiments according to the manufacturer's instructions. All sections were analyzed under an x200 advanced upright fluorescence microscope (Axio Imager. A2, ZEISS, Germany).

Hematoxylin-eosin staining

Dewax and hydrate to water. Stain nucleus with Hematoxylin Solution for 10 min.Rinse in running tap water. Differentiate with Differentiation Solution for 3 min, wash with tap water twice for 2 min each. Re-dyeing with Eosin Y Aqueous Solution for 1min. Quickly wash in deionized water. Dehydrated and transparent, then sealed with mounting medium. The nucleus is purple-blue, and the cytoplasm, basal membrane, and interstitial collagen are red to varying degrees.

Modified masson's trichrome staining

Dewax and hydrate to water. Incubate the section into Mordant Solution in a 60°C incubator for 1 h, and wash with running water. Drop Celestite Blue Solution onto the section and stain for 2 min. Slightly wash with distilled water twice, each for 20 s. Drop Mayer Hematoxylin Solution onto the section and stain for 2 min. Slightly wash with distilled water twice, each for 20 s. Differentiate by Acid Alcohol Differentiation Solution for several seconds. Rinse in running water for 10min. Drop Ponceau-Acid Fuchsin Solution onto the section and stain for 10min. Slightly wash with distilled water twice, each for 20 s. Treat with Phosphmolybic Acid Solution for 10 min. Discard the remaining dye solution and directly stain with Aniline Blue Solution for 5 min without washing with water. As the radio of 1:2, mix the Acetic Acid Solution and water to prepare the Acetic Acid working Solution, and rinse in the Acetic Acid working Solution for 2 min. Dehydrate quickly in 95% ethanol. Dehydrated and transparent, sealed with mounting medium. The nucleus is dark red, the collagen fibers are blue, and the muscle fibers, cytoplasm, and keratin are red.

Periodic acid-schiff staining

Dewax and hydrate to water. Rinse in tap water for 2 min, and wash with distilled water twice. Place in Oxidant for 6 min at room temperature. Wash with tap water once, and then wash with distilled water twice. Soak the section in Schiff Reagent in a dark place at room temperature, and stain for 15 min. Rinse in tap water for 10 min. Stain with Mayer Hematoxylin Solution for 1 min. Differentiate by Acidic Differentiation Solution for 3 s. Wash with tap water for 12 min to blue. Dehydrated and transparent, sealed with mounting medium. The nuclei are blue, and the basal membrane, collagen fibers, muscle fibers, and cytoplasm are red.

Immunohistochemical staining

Dewax and hydrate to water. Sections were submerged in citric acid antigen repair solution and heated in a microwave oven for antigen repair. Wash 3 times with PBS for 5 min each time. Sections were incubated in 3% H_2O_2 solution for 25 min at room temperature and protected from light. Wash 3 times with PBS for 5 min each time. The serum was closed for 30 min. Thereafter, the sections were incubated with anti-Beclin1 (1:100), anti-LC3 (1:500), anti-α-SMA (1:2000), anti-TGF-β (1:500), and anti-Vimentin (1:300), and incubated overnight at 4°C. The sections were washed 3 times with PBS for 5 min each time. Add secondary antibody (1:200) dropwise and incubate at room temperature for 50 min. Wash 3 times with PBS for 5 min each time. Add DAB working solution dropwise on the sections until a brownish-yellow positive signal is observed under the microscope. Rinse the sections with water to terminate the color development. The hematoxylin staining solution was used to re-stain the nuclei for 3 min, and the sections were rinsed with water. Fractionated with hematoxylin differentiation solution for 3s and rinsed with water. Hematoxylin blue-returning solution was used to return the blue color and rinsed with water. Conventional dehydration and transparency, sealed with mounting medium. Positive sites were brownish-yellow. Cumulative optical density was collected and calculated using Image-Pro Plus software (Media Cybernetics, United States).

Western blot analysis

Weigh the frozen kidney tissue and add 500 μL of tissue lysate (containing 5 μLPMSF, 5 μL phosphatase inhibitor) per 50 mg of kidney tissue and homogenize in a tissue homogenizer. The homogenized samples were continued to be lysed in ice water for 20 min and centrifuged at 12,000 rpm for 15 min at 4°C. The supernatant was collected and set aside at 4°C. Protein concentration was measured using the BCA Protein Quantitative Assay Kit. Mix SDS-PAGE protein loading buffer with protein samples at a ratio of 1:4, and adjust the protein sample concentration to 6 μg/μL by adding PBS. Heat at 100°C for 5 min to denature the protein sufficiently. 13 ul of the sample was uploaded to the gel for electrophoresis. The proteins in the gel were then transferred to PVDF membranes. 5% skim milk

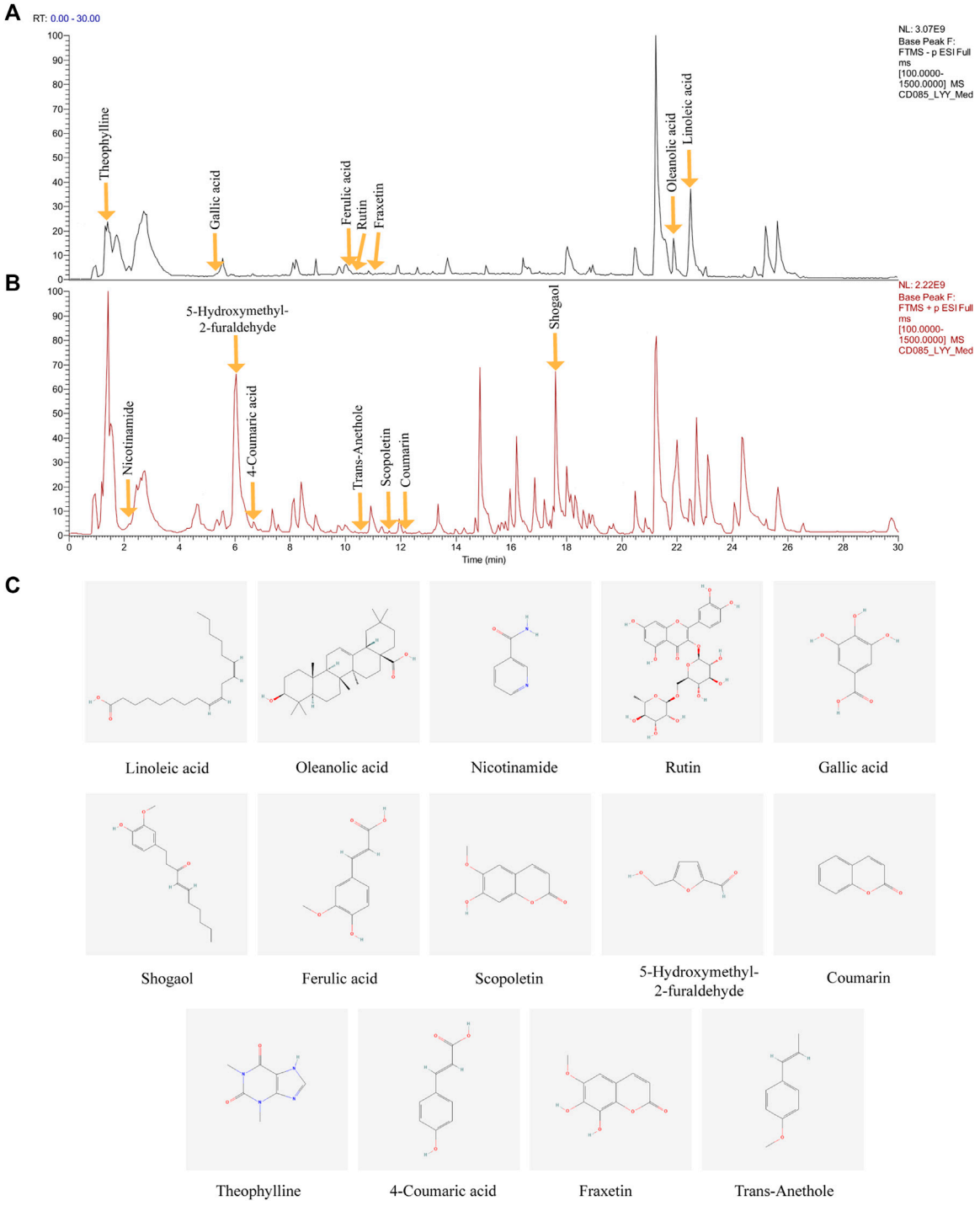


FIGURE 1
Identification of chemical components of HeidihuangWan decoction (HDHW). HDHW samples were examined by UHPLC-Q-Orbitrap-MS/MS. Total ion chromatography in negative **(A)** and positive **(B)** ion modes for HDHW samples are shown. **(C)** Molecular structure of constituents. UHPLC-Q-Orbitrap-MS/MS, Ultra High Performance Liquid Chromatography-Quadrupole-Electrostatic Field Orbitrap Tandem Mass Spectrometry.

was closed at room temperature for 2 h. The PVDF membranes were placed in primary antibody working solution (anti-PI3K 1:1000, anti-Akt 1:1000, anti-mTOR 1:10000, anti-p-Akt 1:2000, anti-p-PI3K 1:1000, anti-p-mTOR 1:10000, anti-LC3I/II 1:2000, anti-Beclin1 1:1500, anti-α-SMA 1:2000, anti-IGF-1 1:1000), incubated overnight at 4°C. Then, PVDF membranes were co-

TABLE 3 | Information on the fourteen chemical constituents of HDHW.

Name	Formula	Calc.MW	m/z	RT (min)	Compound peak area	Corresponding Chinese medicine
Linoleic acid	C18 H32 O2	280.24037	279.23309	22.216	318419116.3	Rehmannia Ginger
Oleanolic acid	C30 H48 O3	456.36027	455.35327	22.212	35474426.59	Jujube
Nicotinamide	C6 H6 N2 O	122.04828	123.05556	2.162	975771717.5	--
Rutin	C27 H30 O16	610.15316	609.14606	12.92	284463906.2	Jujube
Gallic acid	C7 H6 O5	170.02058	169.01329	5.251	288677199.2	Jujube
Shogaol	C17 H24 O3	276.17209	277.17935	17.609	7393025189	Ginger
Ferulic acid	C10 H10 O4	134.03601	193.04982	11.873	173170124.2	Rehmannia
Scopoletin	C10 H8 O4	192.04215	193.04959	11.504	263234163.8	--
5-Hydroxymethyl-2-furaldehyde	C6 H6 O3	126.03187	127.03912	6.036	25644994018	Rehmannia
Coumarin	C9 H6 O2	146.03671	147.04399	12.159	371288074.8	Jujube
trans-Anethole	C10 H12 O	148.08878	149.09605	10.624	100703628.5	--
Theophylline	C7 H8 N4 O2	180.06244	179.05499	1.337	5872606281	--
4-Coumaric acid	C9 H8 O3	164.04747	165.05476	6.63	210576680.5	Jujube
Fraxetin	C10 H8 O5	208.03659	207.02931	11.563	133322185.3	--

incubated with secondary antibodies (1:2500) at room temperature for 1 h. Finally, enhanced chemiluminescence reagents were added to the PVDF membranes and the target proteins were visualized by a chemiluminescence imaging system (GE Amersham Imager600, United States).

Data analysis

To ensure the accuracy of the experimental results, all experiments in this study were independently repeated 3 times. All statistical analyses were performed using SPSS 26.0 statistical software (IBM, United States). Statistical analysis among multiple groups was performed by one-way analysis of variance (ANOVA) followed by least significant difference (LSD) test or Dunnett's T3 test. Statistical analysis between the two groups was performed by independent samples *t*-test. All data were expressed as means ± standard deviations. When $p < 0.05$, the result was considered to be statistically significant. Graphs were constructed using GraphPad Prism 6.0.

Results

Composition analysis of HeidihuangWan decoction

The major compounds in the HDHW samples were identified by UHPLC-Q-Orbitrap-MS/MS analysis. The total negative (Figure 1A) and positive (Figure 1B) ion chromatograms of HDHW demonstrated the chemical composition of all compounds. Several components were found in HDHW. As shown in Figure 1C, fourteen compounds were distinguished: Linoleic acid, Oleanolic acid, Nicotinamide, Rutin, Gallic acid, Shogaol, Ferulic acid, Scopoletin, 5-Hydroxymethyl-2-furaldehyde, Coumarin, Theophylline, 4-Coumaric acid, Fraxetin, and Trans-Anethole. Then, we compared these components through the Traditional Chinese Medicine Systems Pharmacology Database and Analysis Platform (TCMSP) and found that Ferulic acid and 5-Hydroxymethyl-2-furaldehyde are the active components of Rehmannia glutinosa. Linoleic acid and Shogaol are the active ingredients of dried ginger. 4-Coumaric acid, Coumarin, Oleanolic acid, and Rutin are the active ingredients of jujube. We did not directly find the active ingredients of Atractylodes Rhizoma but found the ingredients often contained in aromatic medicines such as trans-Anethole, Oleanolic acid, and so on. In addition, the chemical structural formula, molecular weight, retention time, and peak area of these 14 components are shown in Table 3.

HeidihuangWan protects the renal function of 5/6 nephrectomy rats and reduces the pathological damage to the kidney

ALT and AST levels were detected in the normal control group and normal control+HDHW group to evaluate the safety of HDHW. The results showed that there was no significant difference in AST, ALT, and AST/ALT between the normal control group and the normal control+HDHW group ($p > 0.05$) (Figure 2F), which proved that HDHW had

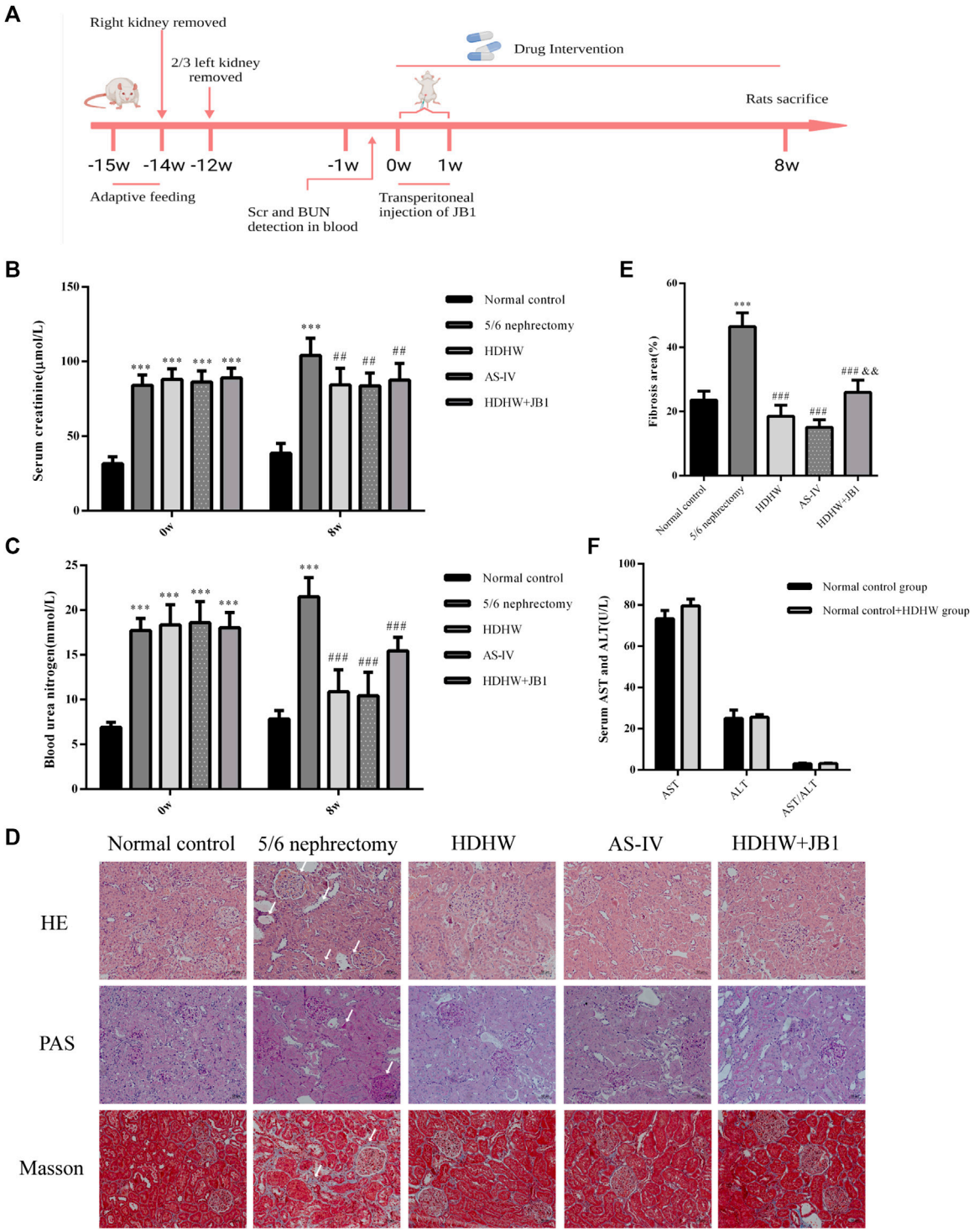


FIGURE 2
HeidihuangWan (HDHW) improves renal function and renal pathological damage in 5/6 nephrectomized rats. **(A)** Timeline of animal experiments. **(B)** Serum creatinine (Scr) and **(C)** blood urea nitrogen (BUN) levels before and after 8 weeks of drug intervention. **(D)** Hematoxylin-Eosin (HE), Periodic Acid-Schiff (PAS), Modified Masson's Trichrome (Masson) staining. Collagen fiber deposition was observed in the 5/6 nephrectomy group (arrows). **(E)** The degree of renal fibrosis was calculated using ImageJ software. **(F)** Serum aspartate aminotransferase (AST) and alanine aminotransferase (ALT) levels after drug intervention. Data are presented as mean ± SD, $n = 6$. The data are expressed as ***$p < 0.001$: compared with normal control group; ##$p < 0.01$, ###$p < 0.001$: compared with 5/6 nephrectomy group; &&$p < 0.01$: compared with HDHW group, respectively.

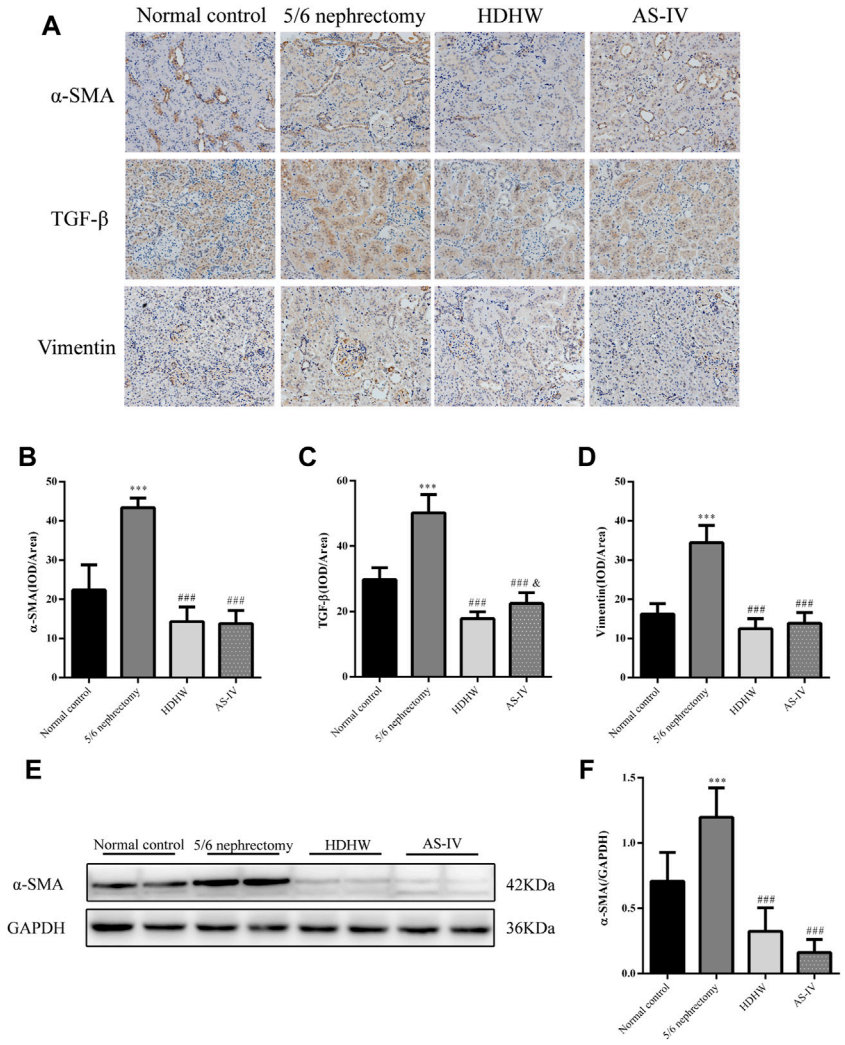


FIGURE 3
HeidihuangWan (HDHW) ameliorates renal fibrosis. **(A)** Immunohistochemical staining was used to analyze the expression of α-smooth muscle actin (α-SMA), transforming growth factor-β (TGF-β), and Vimentin. **(B,C,D)** Image-Pro Plus software was used to statistically analyze the immunohistochemical staining results of α-SMA, TGF-β, and Vimentin, respectively. **(E)** Western Blotting to detect the protein level of α-SMA. **(F)** Protein concentration analysis. Data are presented as mean ± SD, $n = 6$. The data are expressed as ***$p < 0.001$: compared with normal control group; ###$p < 0.001$: compared with 5/6 nephrectomy group; &$p < 0.05$: compared with HDHW group, respectively.

no hepatotoxicity. The levels of Scr and BUN were detected before administration of the rats to verify whether the 5/6 nephrectomy rat model was successfully constructed. Then, the levels of Scr, BUN, and renal pathological changes were detected after drug administration to verify the effect of HDHW on renal function in 5/6 nephrectomy rats. The results showed that after 12 weeks of modeling, the levels of Scr and BUN in the 5/6 nephrectomy group, HDHW group, AS-IV group, and HDHW+JB1 group were significantly increased ($p < 0.001$) (Figures 2B,C), compared with the normal control group. It indicated that the 5/6 nephrectomy rat model was successfully constructed in this study; After 8 weeks of drug intervention, the levels of Scr and BUN in the 5/6 nephrectomy group were significantly increased compared with the normal control group ($p < 0.001$); Compared with 5/6 nephrectomy group, Scr and BUN levels in HDHW group, AS-IV group were significantly decreased ($p < 0.01$) (Figures 2B,C). The renal pathological staining results (Figure 2D) showed that the size and shape of the glomeruli in the normal control group were normal, with clear borders; The internal brush border structure of the renal tubules was intact. In the 5/6 nephrectomy group, the glomeruli were irregular in shape, with balloon adhesion, interstitial widening, proximal tubular atrophy, distal tubular dilatation with enlarged lumen, and vacuolation of tubular epithelial cells,

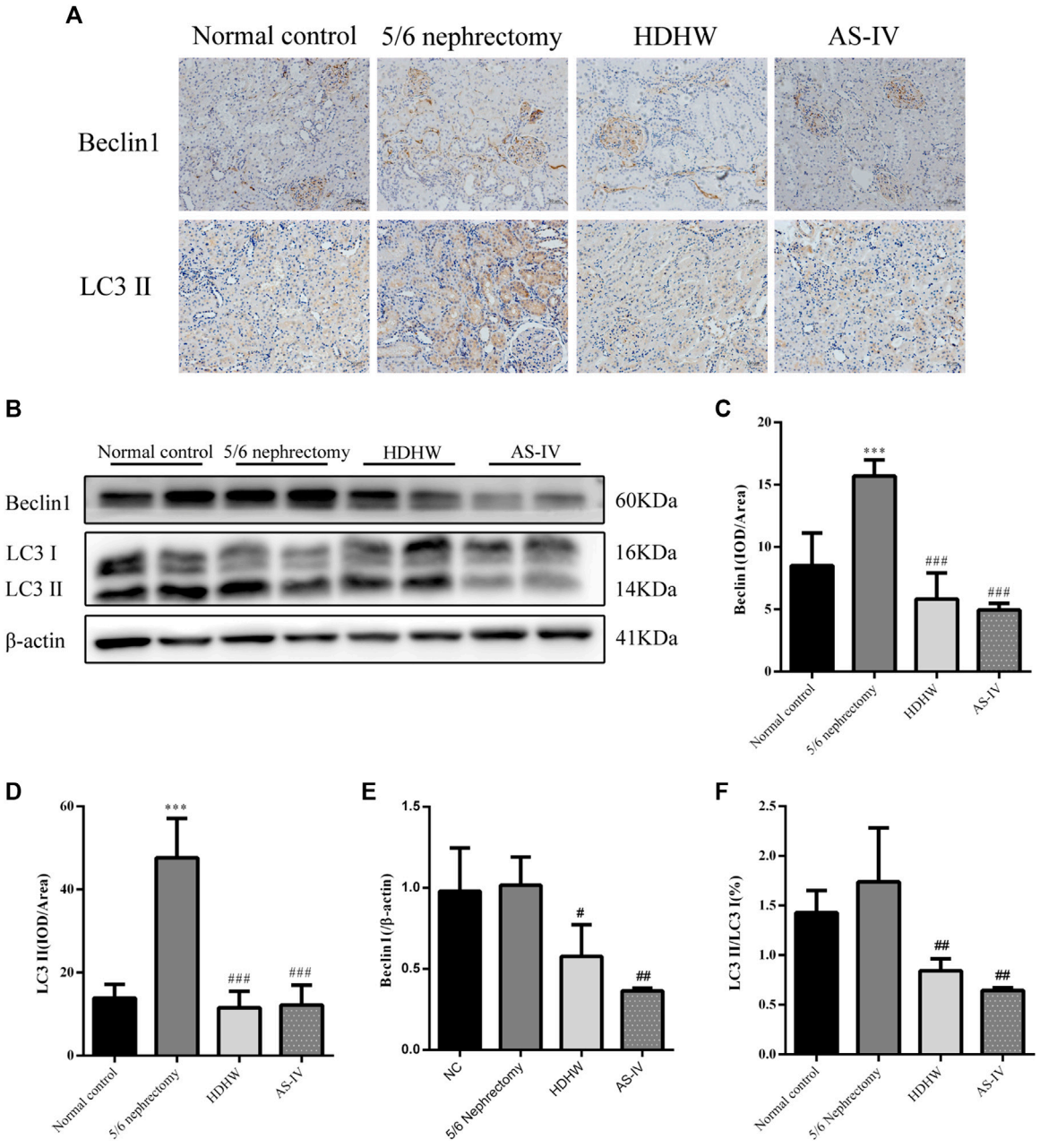


FIGURE 4
Effects of HeidihuangWan (HDHW) on autophagy. **(A)** Immunohistochemical staining analysis of Beclin1, LC3II expression. **(B)** Western Blotting to detect the protein levels of Beclin1, LC3II. **(C,D)** Image-Pro Plus software was used to statistically analyze the immunohistochemical staining results of Beclin1 and LC3II, respectively. **(E,F)** Protein concentration analysis. Data are presented as mean ± SD, $n = 6$. The data are expressed as ***$p < 0.001$: compared with normal control group; #$p < 0.05$, ##$p < 0.01$, ###$p < 0.001$: compared with 5/6 nephrectomy group, respectively.

accompanied by the infiltration of inflammatory cells in the renal interstitium and the proliferation of fibrous tissue was obvious. Compared with the 5/6 nephrectomy group, HDHW and AS-IV could alleviate these pathological lesions.

HeidihuangWan alleviates renal fibrosis

The pathological manifestations of renal fibrosis are dominated by increased collagenous components in the renal interstitium, tubular atrophy and dilated deformation,

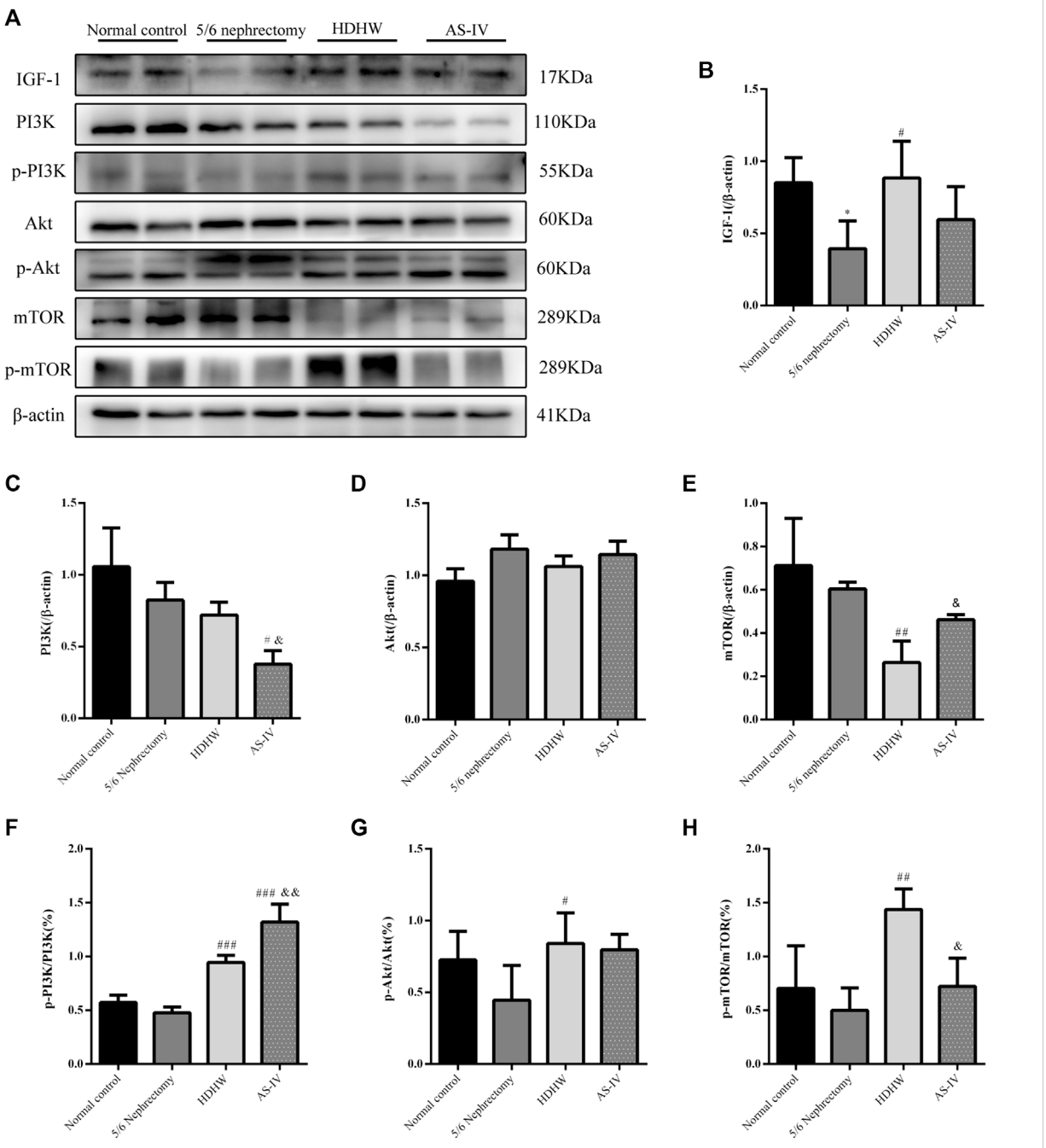


FIGURE 5
Effects of HeidihuangWan (HDHW) on IGF-1-mediated PI3K/Akt/mTOR pathway. **(A)** Western Blotting to detect the protein levels of IGF-1, PI3K, p-PI3K, Akt, p-Akt, mTOR, and p-mTOR. **(B,C,D,E,F,G,H)** Protein concentration analysis. Data are presented as mean ± SD, $n = 3$. The data are expressed as $*p < 0.05$: compared with normal control group; $\#p < 0.05$, $\#\#p < 0.01$, $\#\#p < 0.001$: compared with 5/6 nephrectomy group; $\&p < 0.05$, $\&\&p < 0.01$: compared with HDHW group, respectively.

myofibroblast proliferation, and excessive accumulation of extracellular matrix. α-SMA, TGF-β, and Vimentin are fibrosis marker proteins whose expression is positively correlated with the degree of renal fibrosis (Ma et al., 2019). Among them, α-SMA, a marker of fibroblasts, also showed a positive correlation with extracellular matrix expression (Wan et al., 2020), which is a reliable test to assess the degree of renal fibrosis. To assess the effect of HDHW on renal fibrosis, we performed Masson staining

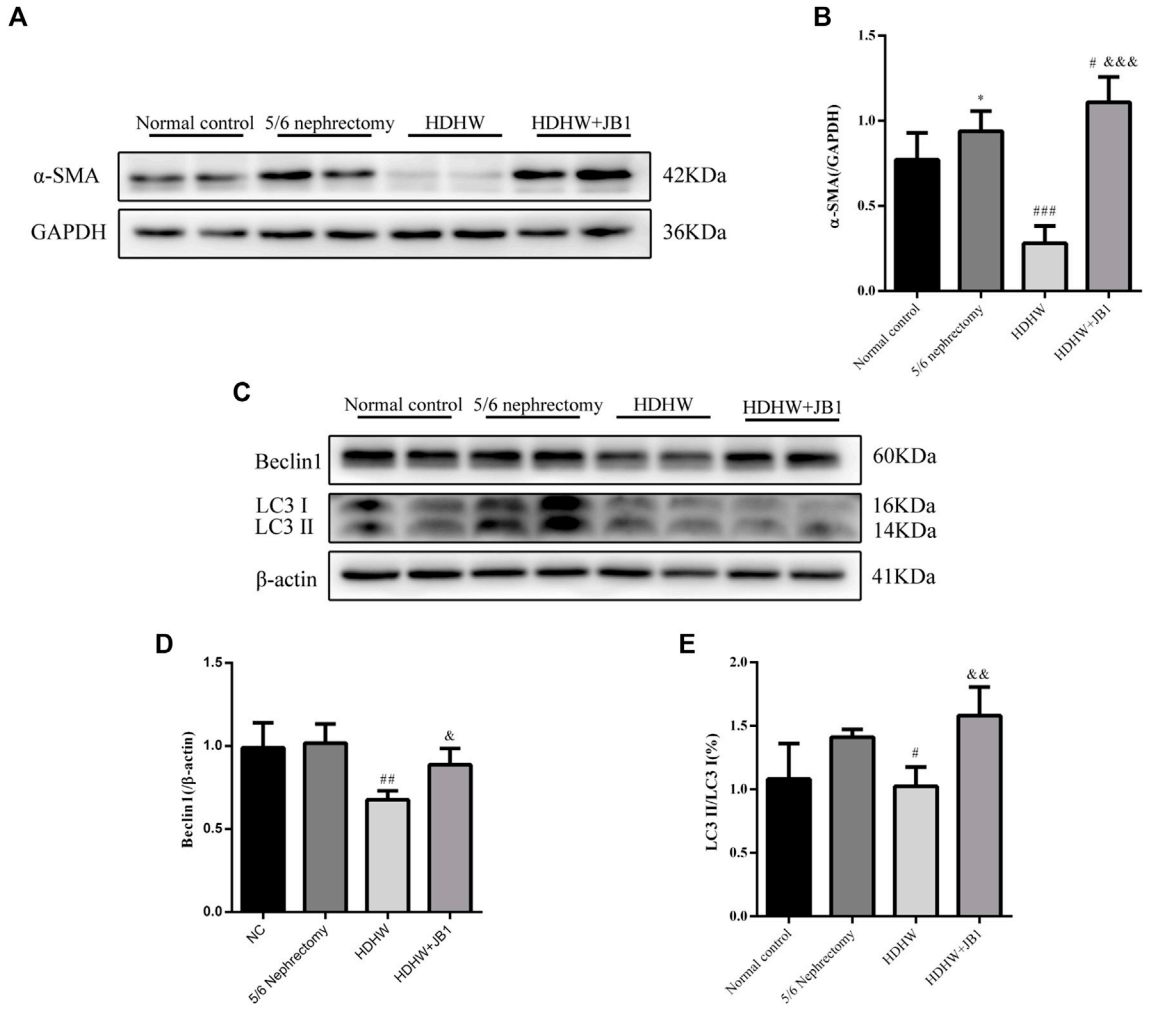


FIGURE 6
IGF-1R inhibitor (JB1) blocks the inhibitory effect of HeidihuangWan (HDHW) on renal fibrosis and autophagy. **(A,C)** Western Blotting for protein levels of α-SMA, Beclin1, LC3II. **(B,D,E)** Protein concentration analysis. Data are presented as mean ± SD, $n = 3$. The data are expressed as $^{*}p < 0.05$: compared with normal control group; $\#p < 0.05$, $\#\#p < 0.01$, $\#\#\#p < 0.001$: compared with 5/6 nephrectomy group; $\&p < 0.05$, $\&\&p < 0.01$, $\&\&\&p < 0.001$: compared with HDHW group, respectively.

and immunohistochemical staining for α-SMA, TGF-β, and Vimentin of rat kidney tissues, and further detected the level of α-SMA by Western blot. In Masson staining, red color indicates muscle fibers and blue color indicates collagen fibers. Compared with the normal control group, collagen fibers accumulated significantly in the renal tissue of the 5/6 nephrectomy group ($p < 0.001$); HDHW and AS-IV significantly reduced the number of collagen fibers compared with the 5/6 nephrectomy group ($p < 0.001$), which in turn improved renal fibrosis (Figures 2D,E). In addition, the expressions of α-SMA, TGF-β, and Vimentin in the kidney tissues of rats in the 5/6 nephrectomy group were significantly higher compared with the normal control group ($p < 0.001$); HDHW and AS-IV significantly down-regulated the expressions of α-SMA, TGF-β, and Vimentin compared with the 5/6 nephrectomy group ($p < 0.001$), and HDHW was more advantageous in downregulating TGF-β compared with the AS-IV group ($p < 0.05$) (Figure 3).

HeidihuangWan inhibits autophagy

Beclin1 (BECN1, Vps30 or Atg6) is a key component of the autophagy-stimulating complex. Beclin1 is involved in the initiation of autophagosome formation by forming a multiprotein complex. Microtubule-associated protein

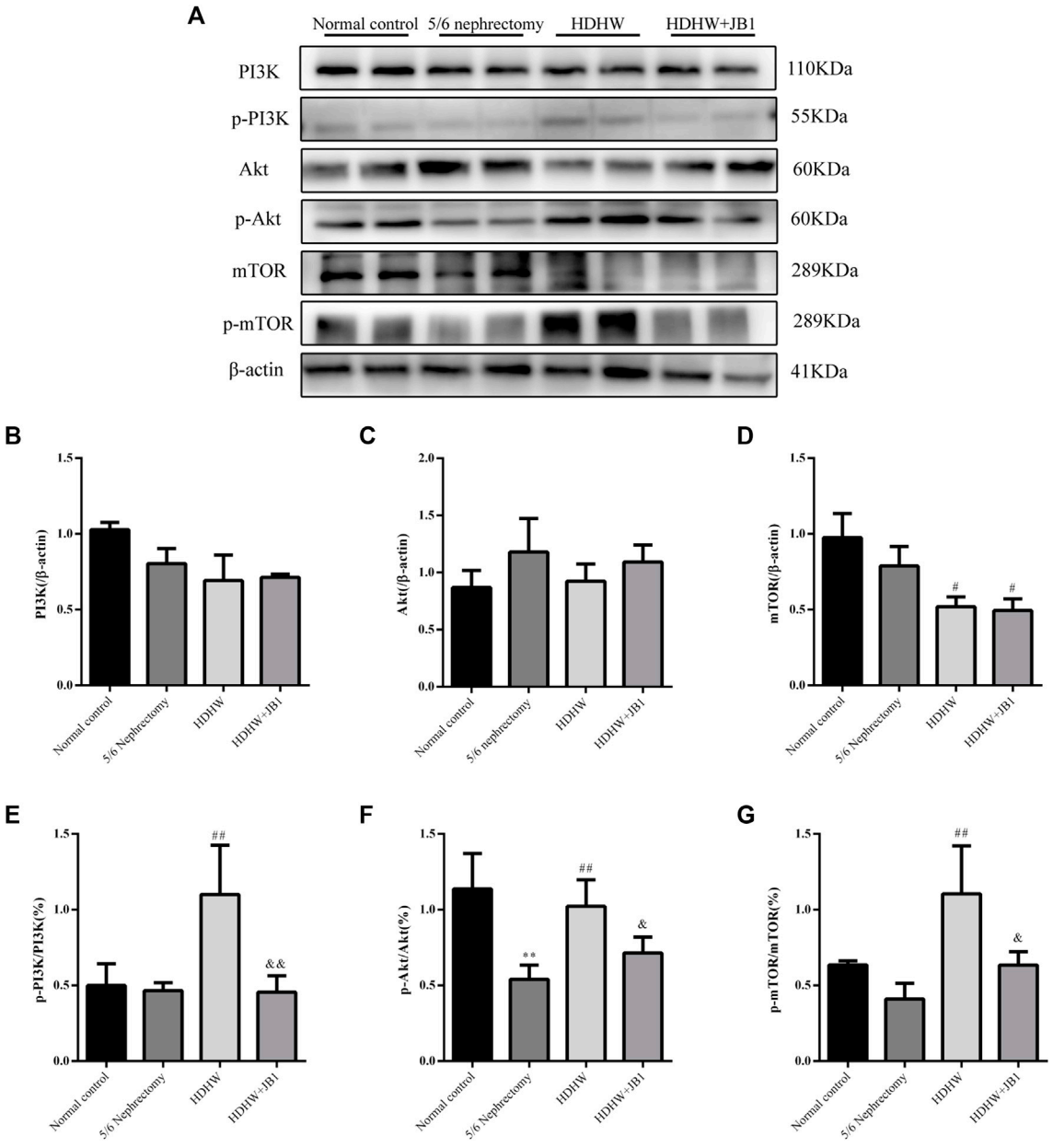


FIGURE 7
HeidihuangWan (HDHW) exerts nephroprotective effects by regulating the IGF-1-mediated PI3K/Akt/mTOR pathway. **(A)** Western Blotting for protein levels of PI3K, p-PI3K, Akt, p-Akt, mTOR, p-mTOR. **(B,C,D,E,F,G)** Protein concentration analysis. Data are presented as mean ± SD, $n = 3$. The data are expressed as $^{**}p < 0.01$: compared with normal control group; $\#p < 0.05$, $\#\#p < 0.01$: compared with 5/6 nephrectomy group; $\&p < 0.05$, $\&\&p < 0.01$: compared with HDHW group, respectively.

1 light chain 3 (LC3) is cleaved to LC3I immediately after synthesis. Cytoplasmic LC3I is then recruited to the membrane and converted to LC3II after coupling to phosphatidylethanolamine during autophagosome formation. Increased conversion of LC3I to LC3II provides evidence for autophagy in mammalian cells (Li et al., 2010). To assess the effect of HDHW on autophagy, we examined the levels of autophagy marker proteins Beclin1, LC3II/I in rat kidney tissue by Western blot and immunohistochemistry. Immunohistochemical analysis showed that the expression of Beclin1 and LC3II/I was significantly upregulated in the 5/6 nephrectomy group, compared with the normal control group ($p < 0.001$); Compared with the 5/6 nephrectomy group, HDHW and AS-IV significantly downregulated the

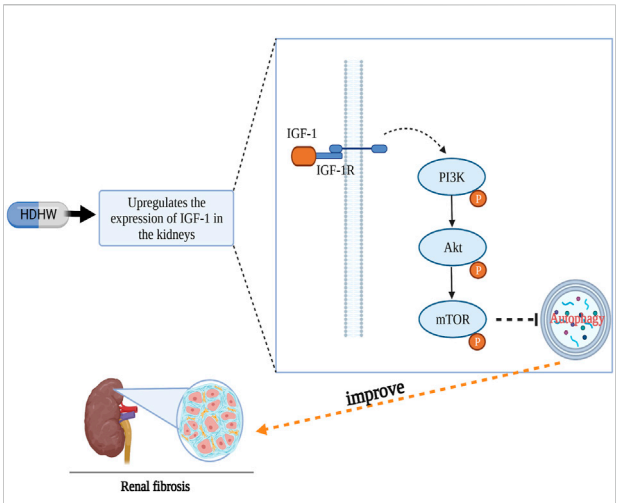


FIGURE 8
Diagram of the anti-renal fibrosis mechanism of HeidihuangWan.

expression of Beclin1 and LC3II/I ($p < 0.001$), and there was no difference between HDHW and AS-IV groups ($p > 0.05$) (Figures 4A,C,D). Western blot analysis also showed that HDHW and AS-IV could significantly down-regulate the expressions of Beclin1 and LC3II/I ($p < 0.05$) (Figures 4B,E,F).

HeidihuangWan affects the expression of IGF-1-mediated PI3K/Akt/mTOR signaling pathway

The PI3K/Akt/mTOR pathway is a key pathway that regulates autophagy, and activation of the PI3K/Akt/mTOR pathway can inhibit autophagy. IGF-1 is an upstream regulatory molecule of the PI3K/Akt/mTOR pathway. We examined the expression of IGF-1, PI3K, p-PI3K, Akt, p-Akt, mTOR, and p-mTOR in rat kidneys. The results showed that the expression of IGF-1 was down-regulated in the 5/6 nephrectomy group, compared with the normal control group ($p < 0.05$); HDHW up-regulated the expression of IGF-1, compared with the 5/6nephrectomy group ($p < 0.05$) (Figures 5A,B). Compared with the 5/6 nephrectomy group, the expression of PI3K and Akt in the HDHW group had no significant change ($p > 0.05$). However, the expression of mTOR was significantly down-regulated ($p < 0.01$), while the expressions of p-PI3K/PI3K, p-Akt/Akt, and p-mTOR/mTOR were significantly up-regulated ($p < 0.05$) (Figures 5A,C–H), indicating that HDHW activated IGF-1/PI3K/Akt/mTOR pathway. This may be the mechanism by which HDHW regulates autophagy and anti-nephrogenic fibrosis.

HeidihuangWan inhibits autophagy by regulating IGF-1-mediated PI3K/Akt/mTOR pathway and exerts anti-fibrosis effect

In order to further verify that the regulation of autophagy and the anti-fibrosis effect of HDHW is related to the IGF-1-mediated PI3K/Akt/mTOR pathway, we blocked the binding of IGF-1 to the IGF-1R receptor. Masson staining analyzed the amount of collagen fiber deposited; Western blot was used to detect the expression of fibrosis marker protein α-SMA, autophagy marker protein Beclin1, LC3II, and the expression of PI3K/Akt/mTOR signaling pathway proteins. The results showed that the deposition of collagen fibers in HDHW+JB1 group was significantly more than that in HDHW group ($p < 0.01$) (Figure 2E). Meanwhile, the expression of α-SMA was significantly up-regulated in the HDHW+JB1 group compared with the HDHW group ($p < 0.001$) (Figures 6A,B), indicating that the effect of HDHW in reducing renal fibrosis was related to the regulation of IGF-1 signaling. Compared with the HDHW group, the expressions of Beclin1 and LC3II/LC3I in the kidney tissue of the HDHW+JB1 group were significantly up-regulated ($p < 0.05$) (Figures 6C–E), indicating that the inhibitory effect of HDHW on autophagy was related to the regulation of IGF-1 signaling. Compared with HDHW group, PI3K, Akt and mTOR in kidney tissue of HDHW+JB1 group had no significant changes ($p > 0.05$) (Figures 7A–D), but the expression of p-PI3K/PI3K, p-Akt/Akt, and p-mTOR/mTOR were significantly down-regulated ($p < 0.05$) (Figures 7A,E–G), indicating that HDHW activates the PI3K/Akt/mTOR pathway by promoting the binding of IGF-1 to IGF-1R.

Discussion

It has been shown that single herbs (Liu et al., 2022; Qian et al., 2022), herbal extracts (Yu, 2020; Zheng et al., 2021; Cong et al., 2022; Ma et al., 2022), and Chinese medicine compounds (Chen et al., 2022a; Chen et al., 2022b; Wu et al., 2022; Zhao et al., 2022) have made great progress in the prevention and even treatment of renal fibrosis (Xu et al., 2021). They regulate multiple signaling pathways such as Wnt/β-catenin (Zhao et al., 2022), TGF-β1/Smad (Mao et al., 2019; Wu et al., 2022), Akt/mTOR (Lian et al., 2022), CX3CL1-RAF/MEK/ERK (Hu et al., 2022b), mTORC1/p70S6K (Chen et al., 2019), SIRT1-NF-κB (Wang et al., 2018b), and interfere with different cytokine or inflammatory factors expression to regulate the development and progression of renal fibrosis. The Chinese herbal extract AS-IV, which has been widely recognized to have significant anti-nephrogenic effects (Yu, 2020; Fu et al., 2022), is the main active component of Huangqi, a Chinese herbal medicine, and its mechanism has been richly studied and

repeatedly validated (Wang et al., 2018b; Chen et al., 2019; Mao et al., 2019; Hu et al., 2022b; Lian et al., 2022). Therefore, it was used as a positive control drug in this study. Traditional Chinese medicine (TCM) is a rich source of drug discovery with its multi-component, multi-target, and multi-pathway characteristics, which can enhance body functions and reduce drug toxicity through the synergistic effects of its main active ingredients. Studying the specific mechanism of TCM in the treatment of renal fibrosis can identify more potential targets for the treatment of renal fibrosis (Zhang et al., 2022b).

HDHW is a traditional Chinese medicine compound formula containing 4 herbs, including Shu Di Huang, Cang Zhu, Gan Jiang, and Da Zao. My supervisor has been working on the efficacy and mechanism of HDHW in the treatment of kidney diseases for more than 10 years. The good clinical efficacy and significant renal protection effect of HDHW prompted us to further study the mechanism of its renal protection. In this study, HDHW components were identified by UHPLC-Q-Orbitrap-MS/MS and 14 components were identified. Among these 14 ingredients, the anti-renal fibrosis effects of Linoleic acid (Zhan et al., 2015; Zhou et al., 2017), Oleanolic acid (Zhao and Luan, 2020), Nicotinamide (Kumakura et al., 2021), Rutin (Han et al., 2015; Wang et al., 2016), Gallic acid (Yousuf and Vellaichamy, 2015), Ferulic acid (Mir et al., 2018; Qi et al., 2020), Fraxetin (natural derivatives of coumarin) (Hsieh et al., 2021), and Theophylline (adenosine antagonist) (Tang et al., 2015) have been demonstrated. They exert antifibrotic effects mainly through autophagy regulation, apoptosis regulation, antioxidant, and anti-inflammatory. The identification of HDHW components provides additional evidence to support its anti-nephrogenic effects. In addition, we also detected the levels of Scr and BUN in rats and observed the renal pathological changes by HE, PAS, and Masson staining, and confirmed that HDHW significantly improved renal function in 5/6 nephrectomized rats, reduced atrophy of proximal tubules, infiltration of inflammatory cells, collagen deposition, and reduced fibrous tissue proliferation, which verified the renal protective effect of HDHW. Moreover, we also confirmed the inhibitory effect of HDHW on renal fibrosis from three indicators, α-SMA, Vimentin, and TGF-β, which we have never observed before. Interestingly, we found that HDHW also significantly reduced the expression of TGF-β in the kidneys of 5/6 nephrectomized rats and was more potent than the positive control drug AS-IV. TGF-β is an important molecule that accelerates renal fibrosis (Chen et al., 2022b). This suggests that TGF-β may also be a pathway for HDHW to improve renal fibrosis, but we did not continue to study the effect of HDHW on TGF-β-mediated pathways in this article.

Autophagy is closely associated with renal fibrosis (Tang et al., 2020). In the kidney, basal autophagy of renal cells is critical for maintaining renal homeostasis, structure, and function. In contrast, under stressful conditions, autophagy is altered as part of an adaptive response in kidney cells, a process that is tightly regulated by key regulators of autophagy, the mammalian target of rapamycin, AMP-activated protein kinases and deacetylases, and related signaling pathways. Activation of autophagy protects kidney cells under stress, while lack of autophagy increases kidney susceptibility to injury, leading to impaired renal function and accumulation of damaged mitochondria, which in turn leads to more severe renal fibrosis. However, other studies have found that persistent activation of autophagy is detrimental after severe renal injury, leading to renal cell senescence and promoting renal fibrosis by secreting pro-fibrotic cytokines (Liang et al., 2022). Therefore, maintaining the balance of autophagy is crucial for improving renal fibrosis.

Several researchers have pointed out that in certain diseases, the role of autophagy depends on the type of cells involved in the disease process and the stage of the disease (Tang et al., 2020). For example, under physiological conditions, podocytes have higher levels of basal autophagy (Bork et al., 2020) and renal tubular epithelial cells have lower levels of autophagy (Liu et al., 2012). In an ischemia-reperfusion-induced acute kidney injury mouse model, autophagy is enhanced in the proximal tubule after 1 day of reperfusion and is eliminated by fusion of autophagosomes with lysosomes on day 3 (Li et al., 2014; Cheng et al., 2015). These findings suggest that autophagy increases cell survival during the initial tubular injury but impedes normal renal repair during the recovery period. Some findings suggest a protective role for autophagy in renal fibrosis. For example, in a study of the anti-RIF mechanism of curcumin, the number of autophagosomes was reduced and LC3II and Beclin1 protein expression was decreased in the UUO rat model of renal interstitial fibrosis. At the same time, PI3K/Akt signaling pathway was activated and mTOR was upregulated. In contrast, curcumin reversed this process and attenuated RIF (Lu et al., 2021). The UUO mouse model exhibited mitochondrial damage, ROS production, TGF- β1/Smad pathway activation, epithelial-mesenchymal transition, and renal fibrosis, and these changes were ameliorated by the use of UMI-77 (mitochondrial autophagy activator) (Jin et al., 2022), suggesting that activation of autophagy protects the damaged kidney. In adult Sprague Dawley rats, the expression of autophagy marker proteins Beclin1, LC3II, PRR, ATG7, and ATG5 was significantly lower in glomeruli than in normal rats 8 weeks after undergoing 5/6 nephrectomy (Yildirim et al., 2021). In addition, a high phosphorus diet increased renal impairment and interstitial fibrosis in 5/6 nephrectomized Wistar rats, a process that was shown to be associated with inhibition of autophagy (Duayer et al., 2021). On the other hand, there is also evidence to support that autophagy activation promotes renal fibrosis. d. Zepeda-Orozco et al. (Li et al., 2010) first identified enhanced

autophagy in the obstructed kidney of the UUO mouse model, including accumulation of autophagosomes, increased expression of Beclin 1, and increased conversion of LC3I to II. Another study using UUO mice as a model of renal fibrosis came to similar conclusions, with increased Beclin 1 and LC3 expression and decreased P62 expression. At the same time, the levels of fibronectin, type I collagen, and α-SMA were significantly increased. However, injection of the autophagy inhibitor ODN significantly decreased the expression of Beclin1 and LC3 and reduced the expression of renal fibrosis marker proteins. This suggests that by inhibiting autophagy, renal fibrosis can be attenuated (Wu et al., 2021; Jung et al., 2022). In the UUO rat model, rats were executed on days 3, 7, and 14 after modeling, and time-dependent induction of autophagy was found in both the obstructed and contralateral unobstructed kidneys, and sustained activation of autophagy led to tubular apoptosis and renal fibrosis, whereas the autophagy inhibitor 3-methyladenine (3-MA) inhibited sustained autophagy-induced tubular apoptosis and renal fibrosis (Kim et al., 2012). Further *in vitro*, experimental studies confirmed that inhibition of mTOR in some proximal tubular cells resulted in sustained activation of autophagy and impaired proliferation of proximal tubular cells. Activation of mTOR inhibits autophagy and contributes to renal tubular repair (Li et al., 2014).

An interesting finding is that the role of autophagy in renal fibrosis differs in different models of renal fibrosis (Li et al., 2010; Lu et al., 2021; Yildirim et al., 2021); In the same model of renal fibrosis (Lu et al., 2021) (Kim et al., 2012), the role of autophagy in renal fibrosis differs even when the time points of intervention are essentially the same. The former may be related to the different pathological changes of renal injury induced by different modeling methods, such as the pathological changes in the 5/6 nephrectomy model: increased glomerular extramural matrix, a proliferation of thylakoid cells, capillary dilatation or occlusion, focal or total glomerular sclerosis, tubular atrophy or dilatation, massive protein tubular pattern, increased renal interstitium, and diffuse infiltration of inflammatory cells; The pathological changes in the UUO model are: renal interstitial collagen fiber hyperplasia, diffuse infiltration of inflammatory cells, tubular atrophy or dilation; glomerular basement membrane thickening, glomerular glassy changes (Ma et al., 2018). The latter requires more studies to reveal and justify. In conclusion, the relationship between autophagy and renal fibrosis needs more studies to reveal and prove. Unfortunately, our immunohistochemical results showed that the level of autophagy was elevated in the kidneys of 5/6 nephrectomized rats, supporting a pathological role of autophagy in renal injury. However, our Western Blot results showed that the autophagy level of 5/6 nephrectomy rats showed an upward trend compared with normal rats of the same age, but it was not statistically significant. Therefore, increasing the sample size of the study is necessary to further confirm the level of autophagy in the kidneys of 5/6 nephrectomized rats.

It has been shown that herbal medicines can exert antifibrotic effects by modulating autophagy (Ma et al., 2018). Cytoprotective effects of autophagy regulators have so far only been reported in animal models of kidney disease, and evidence that these findings can be applied to humans is currently lacking (Tang et al., 2020). The results of this study showed that HDHW could significantly down-regulate the expressions of Beclin1 and LC3II/I in the kidneys of 5/6 nephrectomized rats, suggesting that the anti-renal fibrosis of HDHW may be related to the inhibition of autophagy. Therefore, HDHW may be a promising regulator of autophagy. Further study revealed that HDHW can significantly up-regulate the expression of IGF-1 in the kidney of 5/6 nephrectomy rats, and at the same time significantly up-regulate the expressions of p-PI3K, p-Akt, and p-mTOR. This suggests that HDHW activates the IGF-1/PI3K/Akt/mTOR signaling pathway, a key pathway in regulating autophagy (Tang et al., 2020), which further supports the regulatory effect of HDHW on autophagy in renal fibrosis rats. To verify that the regulation of autophagy and the improvement of renal fibrosis by HDHW are related to the IGF-1-mediated PI3K/Akt/mTOR signaling pathway, this study blocked the binding of IGF-1 to IGF-1R by intraperitoneal injection of IGF-1R blocker JB1 and observed the expression of downstream signaling factors, including PI3K, Akt, mTOR, p-PI3K, p Akt, p-mTOR, as well as the expression of autophagy marker proteins including Beclin1, LC3II/I, and renal fibrosis marker proteins including α-SMA. The results of the study showed that the inhibitory effect of HDHW on autophagy and renal fibrosis was altered after blocking the binding of IGF-1 to IGF-1R, and the phosphorylation processes of PI3K, Akt, and mTOR were also blocked. This result confirms that HDHW can inhibit autophagy and attenuate renal fibrosis by upregulating IGF-1 expression, promoting the binding of IGF-1 to IGF-1R, and activating the autophagy-related pathway PI3K/Akt/mTOR. In addition, HDHW has been widely used in the clinical treatment of chronic kidney disease, especially chronic renal failure, with good therapeutic effects, and the autophagy-regulating effect of HDWH on renal fibrosis was found in this study, providing a reference for the lack of autophagy regulators for human use (Tang et al., 2020).

Conclusion

In conclusion, our results showed that HDHW improved renal function and renal pathological damage and attenuated renal fibrosis in 5/6 nephrectomized rats. The mechanism of HDHW ameliorating renal fibrosis may be that HDHW inhibits autophagy by upregulating IGF-1 expression, promoting the binding of IGF-1 to IGF-1R, and activating the autophagy-related pathway PI3K/Akt/mTOR, which in turn attenuate renal fibrosis (Figure 8).

Data availability statement

The original contributions presented in the study are included in the article/supplementary material, further inquiries can be directed to the corresponding authors.

Ethics statement

The animal study was reviewed and approved by the Ethics Committee of Shandong University of Traditional Chinese Medicine.

Author contributions

Y-YL was responsible for the overall experiment and article writing. Z-HT was in charge of literature search and data statistics. G-HP was responsible for the revision of the article. PZ was responsible for the experimental design and article revision. D-JP was responsible for blood biochemical testing. J-QZ, L-YY were responsible for the experimental operation. F-RZ, X-DX supervised and directed the conduct of the overall experiment and the writing of the article. All authors have reviewed and approved the final version of the manuscript.

Funding

This research was supported by the National Natural Science Foundation of China (no. 81774251).

Acknowledgments

We thank the National Natural Science Foundation of China (No. 81774251) for financial support. We thank Mr. Zi-Fa Li of the Experimental Center of Shandong University of Chinese Medicine for his guidance and support for animal experiments, and Ms. Yue-Hua Jiang of the Experimental Center of the Affiliated Hospital of Shandong University of Chinese Medicine for her guidance for the submission and experiments. We thank the Experimental Center, Shandong University of Traditional Chinese Medicine for technical support and assistance.

Conflict of interest

The authors declare that the research was conducted in the absence of any commercial or financial relationships that could be construed as a potential conflict of interest.

Publisher's note

All claims expressed in this article are solely those of the authors and do not necessarily represent those of their affiliated organizations, or those of the publisher, the editors and the reviewers. Any product that may be evaluated in this article, or claim that may be made by its manufacturer, is not guaranteed or endorsed by the publisher.

References

Bork, T., Liang, W., Yamahara, K., Lee, P., Tian, Z., Liu, S., et al. (2020). Podocytes maintain high basal levels of autophagy independent of mtor signaling. *Autophagy* 16 (11), 1932–1948. doi:10.1080/15548627.2019.1705007

Changlei, Z., Fang, W., Bin, D., Junyan, W., Junjun, J., and Farong, Z. (2013). Influence of heidihuang pill on renal index of patients with chronic renal failure. *J. Liaoning Univ. Traditional Chin. Med.* 15 (11). in chinese. doi:10.13194/j.issn.1673-842x.2013.11.052

Chen, R., Xu, L., Zhang, X., Sun, G., Zeng, W., and Sun, X. (2022). Protective effect and mechanism of Shenkang injection on adenine-induced chronic renal failure in rats. *Acta Cir. Bras.* 37 (3), e370304. doi:10.1590/acb370304

Chen, X., Yang, Y., Liu, C., Chen, Z., and Wang, D. (2019). Astragaloside IV ameliorates high glucose-induced renal tubular epithelial-mesenchymal transition by blocking mTORC1/p70S6K signaling in HK-2 cells. *Int. J. Mol. Med.* 43 (2), 709–716. doi:10.3892/ijmm.2018.3999

Chen, Z., Wu, S., Zeng, Y., Chen, Z., Li, X., Li, J., et al. (2022). FuZhengHuaYuJiangZhuTongLuoFang prescription modulates gut microbiota and gut-derived metabolites in UUO rats. *Front. Cell. Infect. Microbiol.* 12, 837205. doi:10.3389/fcimb.2022.837205

Cheng, H., Fan, X., Lawson, W. E., Paueksakon, P., and Harris, R. C. (2015). Telomerase deficiency delays renal recovery in mice after ischemia-reperfusion injury by impairing autophagy. *Kidney Int.* 88 (1), 85–94. doi:10.1038/ki.2015.69

Cong, C., Yuan, X., Hu, Y., Chen, W., Wang, Y., and Tao, L. (2022). Catalpol alleviates ang II-induced renal injury through NF-κB pathway and TGF-β1/smads pathway. *J. Cardiovasc. Pharmacol.* 79 (1), e116–e121. doi:10.1097/FJC.0000000000001148

da Silva, A. F., Silva, K., Reis, L. A., Teixeira, V. P., and Schor, N. (2015). Bone marrow-derived mesenchymal stem cells and their conditioned medium attenuate fibrosis in an irreversible model of unilateral ureteral obstruction. *Cell. Transpl.* 24 (12), 2657–2666. doi:10.3727/096368915X687534

Duayer, I. F., Duque, E. J., Fujihara, C. K., de Oliveira, I. B., Dos Reis, L. M., Machado, F. G., et al. (2021). The protein-independent role of phosphate in the progression of chronic kidney disease. *Toxins* 13 (7), 503. doi:10.3390/toxins13070503

Edeling, M., Ragi, G., Huang, S., Pavenstädt, H., and Susztak, K. (2016). Developmental signalling pathways in renal fibrosis: The roles of Notch, Wnt and Hedgehog. *Nat. Rev. Nephrol.* 12 (7), 426–439. doi:10.1038/nrneph.2016.54

Fan, Z., Chen, J., Yang, Q., and He, J. (2022). Network Pharmacology and experimental validation to reveal the pharmacological mechanisms of chongcaoyishen decoction against chronic kidney disease. *Front. Mol. Biosci.* 9, 847812. doi:10.3389/fmolb.2022.847812

Fu, Z., Iu, Z., and Zheng, Y. (2022). Research progress of astragaloside IV in the treatment of kidney disease. *Shanghai Pharm.* 43 (05). in chinese. doi:10.3969/j.issn.1006-1533.2022.05.011

GBD 2017 Causes of Death Collaborators (2018). Global, regional, and national age-sex-specific mortality for 282 causes of death in 195 countries and territories, 1980-2017: A systematic analysis for the global burden of disease study 2017. *Lancet (London, Engl.* 392 (10159), 1736–1788. doi:10.1016/S0140-6736(18)32203-7

GBD 2017 DALYs and HALE Collaborators (2018). Global, regional, and national disability-adjusted life-years (DALYs) for 359 diseases and injuries and

healthy life expectancy (HALE) for 195 countries and territories, 1990-2017: A systematic analysis for the global burden of disease study 2017. *Lancet (London, Engl.* 392 (10159), 1859–1922. doi:10.1016/S0140-6736(18)32335-3

GBD 2017 Disease and Injury Incidence and Prevalence Collaborators (2018). Global, regional, and national incidence, prevalence, and years lived with disability for 354 diseases and injuries for 195 countries and territories, 1990-2017: A systematic analysis for the global burden of disease study 2017. *Lancet (London, Engl.* 392 (10159), 1789–1858. doi:10.1016/S0140-6736(18)32279-7

GBD Chronic Kidney Disease Collaboration (2020). Global, regional, and national burden of chronic kidney disease, 1990-2017: A systematic analysis for the global burden of disease study 2017. *Lancet (London, Engl.* 395 (10225), 709–733. doi:10.1016/S0140-6736(20)30045-3

Han, Y., Lu, J. S., Xu, Y., Zhang, L., and Hong, B. F. (2015). Rutin ameliorates renal fibrosis and proteinuria in 5/6-nephrectomized rats by anti-oxidation and inhibiting activation of TGFβ1-smad signaling. *Int. J. Clin. Exp. Pathol.* 8 (5), 4725–4734.

Hsieh, Y. H., Hung, T. W., Chen, Y. S., Huang, Y. N., Chiou, H. L., Lee, C. C., et al. (2021). *In vitro* and *in vivo* antifibrotic effects of Fraxetin on renal interstitial fibrosis via the ERK signaling pathway. *Toxins* 13 (7), 474. doi:10.3390/toxins13070474

Hu, S., Hu, H., Wang, R., He, H., and Shui, H. (2021). microRNA-29b prevents renal fibrosis by attenuating renal tubular epithelial cell-mesenchymal transition through targeting the PI3K/AKT pathway. *Int. Urol. Nephrol.* 53 (9), 1941–1950. doi:10.1007/s11255-021-02836-4

Hu, T., Chen, F., Chen, D., and Liang, H. (2022). DNMT3a negatively regulates PTEN to activate the PI3K/AKT pathway to aggravate renal fibrosis. *Cell. Signal.* 96, 110352. doi:10.1016/j.cellsig.2022.110352

Hu, Y., Tang, W., Liu, W., Hu, Z., and Pan, C. (2022). Astragaloside IV alleviates renal tubular epithelial-mesenchymal transition via cx3cl1-RAF/MEK/ERK signaling pathway in diabetic kidney disease. *Drug Des. devel. Ther.* 16, 1605–1620. doi:10.2147/DDDT.S360346

Ji, J., and He, L-q. (2019). Effect of kangxianling decoction on renal fibrosis and ACE-ang?-at1r Axis in 5/6 nephrectomized rats. *Chin. J. Exp. Traditional Med. Formulae*, 57–62.

Jin, L., Yu, B., Liu, G., Nie, W., Wang, J., Chen, J., et al. (2022). Mitophagy induced by UMI-77 preserves mitochondrial fitness in renal tubular epithelial cells and alleviates renal fibrosis. *FASEB J. official Publ. Fed. Am. Soc. Exp. Biol.* 36 (6), e22342. doi:10.1096/fj.202200199RR

Jung, H. J., An, H. J., Gwon, M. G., Gu, H., Bae, S., Lee, S. J., et al. (2022). Anti-fibrotic effect of synthetic noncoding oligodeoxynucleotide for inhibiting mTOR and STAT3 via the regulation of autophagy in an animal model of renal injury. *Mol. (Basel, Switz.* 27 (3), 766. doi:10.3390/molecules27030766

Kim, W. Y., Nam, S. A., Song, H. C., Ko, J. S., Park, S. H., Kim, H. L., et al. (2012). The role of autophagy in unilateral ureteral obstruction rat model. *Nephrology* 17 (2), 148–159. doi:10.1111/j.1440-1797.2011.01541.x

Kumakura, S., Sato, E., Sekimoto, A., Hashizume, Y., Yamakage, S., Miyazaki, M., et al. (2021). Nicotinamide attenuates the progression of renal failure in a mouse model of adenine-induced chronic kidney disease. *Toxins* 13 (1), 50. doi:10.3390/toxins13010050

Li, D., Yu, K., Feng, F., Zhang, Y., Bai, F., Zhang, Y., et al. (2022). Hydroxychloroquine alleviates renal interstitial fibrosis by inhibiting the PI3K/Akt signaling pathway. *Biochem. Biophys. Res. Commun.* 610, 154–161. doi:10.1016/j.bbrc.2022.04.058

Li, L., Wang, Z. V., Hill, J. A., and Lin, F. (2014). New autophagy reporter mice reveal dynamics of proximal tubular autophagy. *J. Am. Soc. Nephrol.* 25 (2), 305–315. doi:10.1681/ASN.2013040374

Li, L., Zepeda-Orozco, D., Black, R., and Lin, F. (2010). Autophagy is a component of epithelial cell fate in obstructive uropathy. *Am. J. Pathol.* 176 (4), 1767–1778. doi:10.2353/ajpath.2010.090345

Lian, Y., Li, C., Li, J., Xie, Y., Liu, Q., Wu, M., et al. (2022). Astragaloside IV attenuated TGF-β1- induced epithelial-mesenchymal transition of renal tubular epithelial cells via connexin 43 and Akt/mTOR signaling pathway. *Tissue Cell.* 77, 101831. doi:10.1016/j.tice.2022.101831

Liang, S., Wu, Y. S., Li, D. Y., Tang, J. X., and Liu, H. F. (2022). Autophagy and renal fibrosis. *Aging Dis.* 13 (3), 712–731. doi:10.14336/AD.2021.1027

Liu, M., Ning, X., Li, R., Yang, Z., Yang, X., Sun, S., et al. (2017). Signalling pathways involved in hypoxia-induced renal fibrosis. *J. Cell. Mol. Med.* 21 (7), 1248–1259. doi:10.1111/jcmm.13060

Liu, S., Hartleben, B., Kretz, O., Wiech, T., Igarashi, P., Mizushima, N., et al. (2012). Autophagy plays a critical role in kidney tubule maintenance, aging and ischemia-reperfusion injury. *Autophagy* 8 (5), 826–837. doi:10.4161/auto.19419

Liu, X., Xu, H., Zang, Y., Liu, W., and Sun, X. (2022). Radix Rehmannia Glutinosa inhibits the development of renal fibrosis by regulating miR-122-5p/PKM axis. *Am. J. Transl. Res.* 14 (1), 103–119.

Loboda, A., Sobczak, M., Jozkowicz, A., and Dulak, J. (2016). TGF-β1/Smads and miR-21 in renal fibrosis and inflammation. *Mediat. Inflamm.* 2016, 8319283. doi:10.1155/2016/8319283

Lu, M., Li, H., Liu, W., Zhang, X., Li, L., and Zhou, H. (2021). Curcumin attenuates renal interstitial fibrosis by regulating autophagy and retaining mitochondrial function in unilateral ureteral obstruction rats. *Basic Clin. Pharmacol. Toxicol.* 128 (4), 594–604. doi:10.1111/bcpt.13550

Ma, Q., Li, R., Tie, X., Wang, Z., and Sun, W. (2019). Effects of Qufeng Tongluo Recipe on the expression of renal interstitial fibrosis-related protein α-SMA and vimentin in UUO rats. *Chin. Med. J.* 34 (08). in chinese. doi:10.16368/j.issn.1674-8999.2019.08.394

Ma, Y., Liu, C., and Tao, Y. (2018). Characteristics and research progress of animal models of renal fibrosis. *Chin. J. Laboratory Animals* 26 (03). in chinese.

Ma, Z., Zhu, L., Wang, S., Guo, X., Sun, B., Wang, Q., et al. (2022). Berberine protects diabetic nephropathy by suppressing epithelial-to-mesenchymal transition involving the inactivation of the NLRP3 inflammasome. *Ren. Fail.* 44 (1), 923–932. doi:10.1080/0886022X.2022.2079525

Mao, Q., Chen, C., Liang, H., Zhong, S., Cheng, X., and Li, L. (2019). Astragaloside IV inhibits excessive mesangial cell proliferation and renal fibrosis caused by diabetic nephropathy via modulation of the TGF-β1/Smad/miR-192 signaling pathway. *Exp. Ther. Med.* 18 (4), 3053–3061. doi:10.3892/etm.2019.7887

Mir, S. M., Ravuri, H. G., Pradhan, R. K., Narra, S., Kumar, J. M., Kuncha, M., et al. (2018). Ferulic acid protects lipopolysaccharide-induced acute kidney injury by suppressing inflammatory events and upregulating antioxidant defenses in Balb/c mice. *Biomed. Pharmacother. = Biomedecine Pharmacother.* 100, 304–315. doi:10.1016/j.biopha.2018.01.169

Qi, M. Y., Wang, X. T., Xu, H. L., Yang, Z. L., Cheng, Y., and Zhou, B. (2020). Protective effect of ferulic acid on STZ-induced diabetic nephropathy in rats. *Food Funct.* 11 (4), 3706–3718. doi:10.1039/c9fo02398d

Qian, X., Jiang, Y., Luo, Y., and Jiang, Y. (2022). The anti-hyperuricemia and anti-inflammatory effects of Atractylodes macrocephala in hyperuricemia and gouty arthritis rat models. *Comb. Chem. high throughput Screen.* doi:10.2174/1386207325666220603101540

Sun, X., Yu, N., and Zhang, F. (2014). Black Pill for 5/6 nephrectomy in renal failure rat model induced by blood rheology. *Jilin J. Traditional Chin. Med.* 34 (03). in chinese. doi:10.13463/j.cnki.jlzyy.2014.03.023

Sun, X., Yu, N., and Zhang, F. (2014). Heidi Huang Wan ameliorates the micro-inflammatory state in a 5/6 nephrectomy rat model of renal failure via an immunomodulatory mechanism. *Chin. J. Nephrol. Integr. Traditional Chin. West. Med.* 15 (05). in chinese.

Tang, C., Livingston, M. J., Liu, Z., and Dong, Z. (2020). Autophagy in kidney homeostasis and disease. *Nat. Rev. Nephrol.* 16 (9), 489–508. doi:10.1038/s41581-020-0309-2

Tang, J., Jiang, X., Zhou, Y., Xia, B., and Dai, Y. (2015). Increased adenosine levels contribute to ischemic kidney fibrosis in the unilateral ureteral obstruction model. *Exp. Ther. Med.* 9 (3), 737–743. doi:10.3892/etm.2015.2177

Wan, M., Luo, F., and Yan, Z. (2020). Effects of Shenshui Xiezhuo Decoction and its disassembled recipes on proteins related to pericyte-myofibroblast transdifferentiation. *J. Pract. Med.* 36 (09). in chinese. doi:10.3969/j.issn.1006-5725.2020.09.012

Wang, B., Liu, D., Zhu, Q. H., Li, M., Chen, H., Guo, Y., et al. (2016). Rutin ameliorates kidney interstitial fibrosis in rats with obstructive nephropathy. *Int. Immunopharmacol.* 35, 77–84. doi:10.1016/j.intimp.2016.03.029

Wang, W., Wang, X., Zhang, X. S., and Liang, C. Z. (2018). Cryptotanshinone attenuates oxidative stress and inflammation through the regulation of nrf-2 and NF-κB in mice with unilateral ureteral obstruction. *Basic Clin. Pharmacol. Toxicol.* 123 (6), 714–720. doi:10.1111/bcpt.13091

Wang, X., Gao, Y., Tian, N., Zhu, Z., Wang, T., Xu, J., et al. (2018). Astragaloside IV represses high glucose-induced mesangial cells activation by enhancing autophagy via SIRT1 deacetylation of NF-κB p65 subunit. *Drug Des. devel. Ther.* 12, 2971–2980. doi:10.2147/DDDT.S174058

Wu, S., Ji, L., Fan, X., Fang, S., Bao, J., Yuan, X., et al. (2022). Jieduquyuzishen prescription attenuates renal fibrosis in MRL/lpr mice via inhibiting EMT and TGF-β1/smad2/3 pathway. *Evid. Based. Complement. Altern. Med.* 2022, 4987323. doi:10.1155/2022/4987323

Wu, Y., Xun, Y., Zhang, J., Hu, H., Qin, B., Wang, T., et al. (2021). Resveratrol attenuates oxalate-induced renal oxidative injury and calcium oxalate crystal deposition by regulating TFEB-induced autophagy pathway. *Front. Cell. Dev. Biol.* 9, 638759. doi:10.3389/fcell.2021.638759

Wu, Z., Yu, Y., Niu, L., Fei, A., and Pan, S. (2016). IGF-1 protects tubular epithelial cells during injury via activation of ERK/MAPK signaling pathway. *Sci. Rep.* 6, 28066. doi:10.1038/srep28066

Xiao, L., Chen, A., Gao, Q., Xu, B., Guo, X., and Guan, T. (2022). Pentosan polysulfate ameliorates fibrosis and inflammation markers in SV40 MES13 cells by suppressing activation of PI3K/AKT pathway via miR-446a-3p. *BMC Nephrol.* 23 (1), 105. doi:10.1186/s12882-022-02732-8

Xu, H., Wu, T., and Huang, L. (2021). Therapeutic and delivery strategies of phytoconstituents for renal fibrosis. *Adv. Drug Deliv. Rev.* 177, 113911. doi:10.1016/j.addr.2021.113911

Xuan, C., Xi, Y. M., Zhang, Y. D., Tao, C. H., Zhang, L. Y., and Cao, W. F. (2021). Yiqi jiedu huayu decoction alleviates renal injury in rats with diabetic nephropathy by promoting autophagy. *Front. Pharmacol.* 12, 624404. doi:10.3389/fphar.2021.624404

Yang, K., Liu, J., and Zhang, F. (2019). Effects of black dihuang pill combined with ligustrazine on ET - 1, t - PA, PAI - 1 and expressions of matrix metalloproteinase MMP - 9 of aorta in rats with chronic renal failure. *Liaoning J. Traditional Chin. Med.* 46 (03). in chinese. doi:10.13192/j.issn.1000-1719.2019.03.056

Yang, K., Zhang, F., and Dong, B. (2016). Effects of Heidihuang Pill on spleen-stomach syndrome, nutritional status and gastrointestinal hormones in chronic renal failure. *Chin. J. Exp. Formulas* 22 (01). in chinese. doi:10.13422/j.cnki.syfjx.2016010176

Yildirim, D., Bender, O., Karagoz, Z. F., Helvacioglu, F., Bilgic, M. A., Akcay, A., et al. (2021). Role of autophagy and evaluation the effects of microRNAs 214, 132, 34c and prorenin receptor in a rat model of focal segmental glomerulosclerosis. *Life Sci.* 280, 119671. doi:10.1016/j.lfs.2021.119671

Yousuf, M. J., and Vellaichamy, E. (2015). Protective activity of gallic acid against glyoxal -induced renal fibrosis in experimental rats. *Toxicol. Rep.* 2, 1246–1254. doi:10.1016/j.toxrep.2015.07.007

Yu, Z. (2020). Effects of astragaloside IV combined with Bailing Capsules on inflammation and immune level in patients with renal failure maintained dialysis infection. *Contemp. Med.* 26 (01). in chinese. doi:10.3969/j.issn.1009-4393.2020.01.057

Zhan, Y., Shi, H., Caligiuri, S. P., Wu, Y., Declercq, V., Taylor, C. G., et al. (2015). Trans-10, cis-12-conjugated linoleic acid worsens renal pathology and alters cyclooxygenase derived oxylipins in obesity-associated nephropathy. *J. Nutr. Biochem.* 26 (2), 130–137. doi:10.1016/j.jnutbio.2014.09.011

Zhang, F., Wang, F., Fu, H., Zhou, X., Gao, W., and Zhang, F. (2009). Clinical observation of heidihuang pill in treating chronic renal failure. *Chin. J. Nephrol. Integr. Traditional Chin. West. Med.* 10 (02). in chinese. doi:10.3969/j.issn.1009-587X.2009.02.022

Zhang, S., Yin, C., Liu, X., and Ynag, K. (2022). Research progress of traditional Chinese medicine in the treatment of diabetic renal fibrosis. *Chin. J. Exp. Formulas* 28 (11). in chinese. doi:10.13422/j.cnki.syfjx.20220505

Zhang, Y., Mou, Y., Zhang, J., Suo, C., Zhou, H., Gu, M., et al. (2022). Therapeutic implications of ferroptosis in renal fibrosis. *Front. Mol. Biosci.* 9, 890766. doi:10.3389/fmolb.2022.890766

Zhao, D., and Luan, Z. (2020). Oleanolic acid attenuates renal fibrosis through TGF-β/smad pathway in a rat model of unilateral ureteral obstruction. *Evid. Based. Complement. Altern. Med.* 2020, 2085303. doi:10.1155/2020/2085303

Zhao, P., Liu, W., Zhang, L., and Zhang, F. (2017). Explore mechanism of hei dihuangwan in treating renal anemia based on autophagy and paracrine secretion. *Chin. J. Exp. Formulas* 23 (02). in chinese. doi:10.13422/j.cnki.syfjx.2017020146

Zhao, Y., Li, X., Wang, F., Huang, S., Du, H., Li, S., et al. (2022). Network Pharmacology and experimental verification strategies to illustrate the mechanism of jian-pi-yi-shen formula in suppressing epithelial-mesenchymal transition. *Front. Pharmacol.* 13, 873023. doi:10.3389/fphar.2022.873023

Zheng, C., Zhou, Y., Huang, Y., Chen, B., Wu, M., Xie, Y., et al. (2019). Effect of ATM on inflammatory response and autophagy in renal tubular epithelial cells in LPS-induced septic AKI. *Exp. Ther. Med.* 18 (6), 4707–4717. doi:10.3892/etm.2019.8115

Zheng, W., Huang, T., Tang, Q. Z., Li, S., Qin, J., and Chen, F. (2021). Astragalus polysaccharide reduces blood pressure, renal damage, and dysfunction through the TGF-β1-ILK pathway. *Front. Pharmacol.* 12, 706617. doi:10.3389/fphar.2021.706617

Zhou, Y., Cai, T., Xu, J., Jiang, L., Wu, J., Sun, Q., et al. (2017). UCP2 attenuates apoptosis of tubular epithelial cells in renal ischemia-reperfusion injury. *Am. J. Physiol. Ren. Physiol.* 313 (4), F926–f37. doi:10.1152/ajprenal.00118.2017

Zhu, Y., Tang, Y., and He, L. (2014). Antagonistic effect of astragaloside IV on renal interstitial fibrosis. *Liaoning J. Traditional Chin. Med.* 41 (12). in chinese. doi:10.13192/j.issn.1000-1719.2014.12.078

Zhuang, Q., Ma, R., Yin, Y., Lan, T., Yu, M., and Ming, Y. (2019). Mesenchymal stem cells in renal fibrosis: The flame of cytotherapy. *Stem Cells Int.* 2019, 8387350. doi:10.1155/2019/8387350

frontiers | Frontiers in Pharmacology

TYPE Brief Research Report
PUBLISHED 13 September 2022
DOI 10.3389/fphar.2022.978337

Check for updates

OPEN ACCESS

EDITED BY
Fujian Lu,
Boston Children's Hospital and Harvard Medical School, United States

REVIEWED BY
Walied Abdo,
Kafrelsheikh University, Egypt
Harlokesh Narayan Yadav,
All India Institute of Medical Sciences, India

*CORRESPONDENCE
Fedor Simko,
fedor.simko@fmed.uniba.sk

†These authors have contributed equally to this work and share first authorship

SPECIALTY SECTION
This article was submitted to Experimental Pharmacology and Drug Discovery, a section of the journal Frontiers in Pharmacology

RECEIVED 25 June 2022
ACCEPTED 25 August 2022
PUBLISHED 13 September 2022

CITATION
Repova K, Stanko P, Baka T, Krajcirovicova K, Aziriova S, Hrenak J, Barta A, Zorad S, Reiter RJ, Adamcova M and Simko F (2022), Lactacystin-induced kidney fibrosis: Protection by melatonin and captopril. *Front. Pharmacol.* 13:978337. doi: 10.3389/fphar.2022.978337

COPYRIGHT
© 2022 Repova, Stanko, Baka, Krajcirovicova, Aziriova, Hrenak, Barta, Zorad, Reiter, Adamcova and Simko. This is an open-access article distributed under the terms of the Creative Commons Attribution License (CC BY). The use, distribution or reproduction in other forums is permitted, provided the original author(s) and the copyright owner(s) are credited and that the original publication in this journal is cited, in accordance with accepted academic practice. No use, distribution or reproduction is permitted which does not comply with these terms.

Lactacystin-induced kidney fibrosis: Protection by melatonin and captopril

Kristina Repova[1†], Peter Stanko[1†], Tomas Baka[1†], Kristina Krajcirovicova[1], Silvia Aziriova[1], Jaroslav Hrenak[2], Andrej Barta[3], Stefan Zorad[4], Russel J. Reiter[5], Michaela Adamcova[6] and Fedor Simko[1,4,7]*

[1]Institute of Pathophysiology, Faculty of Medicine, Comenius University, Bratislava, Slovakia, [2]Medbase, Bern, Switzerland, [3]Institute of Normal and Pathological Physiology, Centre of Experimental Medicine, Slovak Academy of Sciences, Bratislava, Slovakia, [4]Institute of Experimental Endocrinology, Biomedical Research Center, Slovak Academy of Sciences, Bratislava, Slovakia, [5]Department of Cell Systems and Anatomy, UT Health San Antonio, Long School of Medicine, San Antonio, TX, United States, [6]Department of Physiology, Faculty of Medicine in Hradec Kralove, Charles University, Hradec Kralove, Czechia, [7]3rd Department of Internal Medicine, Faculty of Medicine, Comenius University, Bratislava, Slovakia

Lactacystin is a specific proteasome inhibitor that blocks the hydrolysis of intracellular proteins by ubiquitin/proteasome system inhibition. The administration of lactacystin to rats induced hypertension and remodeling of the left ventricle and aorta. This study tested whether lactacystin induces structural and fibrotic rebuilding of the kidneys and whether melatonin and captopril can prevent these potential changes. Six weeks of lactacystin administration to rats increased their average systolic blood pressure (SBP). In the kidneys, lactacystin reduced glomerular density, increased the glomerular tuft area, and enhanced hydroxyproline concentrations. It also elevated the intraglomerular proportion including the amounts of collagen (Col) I and Col III. Lactacystin also raised the tubulointerstitial amounts of Col I and the sum of Col I and Col III with no effect on vascular/perivascular collagen. Six weeks of captopril treatment reduced SBP, while melatonin had no effect. Both melatonin and captopril increased glomerular density, reduced the glomerular tuft area, and lowered the hydroxyproline concentration in the kidneys. Both drugs reduced the proportion and total amounts of intraglomerular and tubulointerstitial Col I and Col III. We conclude that chronic lactacystin treatment stimulated structural and fibrotic remodeling of the kidneys, and melatonin and captopril partly prevented these alterations. Considering the effect of lactacystin on both the heart and kidneys, chronic treatment with this drug may be a prospective model of cardiorenal damage suitable for testing pharmacological drugs as protective agents.

KEYWORDS

lactacystin, melatonin, captopril, kidney injury, fibrotic remodeling, cardiorenal damage

Introduction

Hypertension and diabetes are the leading causes of chronic kidney disease (CKD) (Hamrahian and Falkner, 2017). The pathogenesis of CKD in hypertension is multifactorial, involving genetic alterations, oxidative stress, endothelial dysfunction, and renin-angiotensin-aldosterone system (RAAS) disturbances (Mennuni et al., 2014). These factors promote inflammation, fibrosis, and both a reduced nephron count and a lower glomerular filtration rate (GFR) (Schlondorff, 2008). CKD is associated with a worsening cardiovascular prognosis and constitutes a serious health and social condition. Thus, there is a continuous search for new ways of protection in experimental models of hypertension.

Cardiovascular homeostasis is tightly bound to proper protein turnover, which is controlled by the ubiquitin-proteasome system (UPS). Proteasomes are multisubunit protease complexes that degrade damaged proteins in all parts of the cells (Pagan et al., 2013). The proteasomes specific to the heart involve a number of proteins with various biological impacts, such as atrogin (known as muscle atrophy F-box) participating in myocardial remodeling (Li et al., 2004); murine double minute 2 (MDM2), a ubiquitin ligase that mediates p53 participating on myocardial hypertrophy modulation (Chatterjee et al., 2011); the calcineurin-nuclear factor of the activated T cells (NFAT) pathway that mediates cardiac remodeling (Tang et al., 2010); sarcomere-associated protein MuRF1 associated with heart failure (Willis et al., 2009); or Nedd4 containing E3 ligase controlling the biological impact of multifunctional vascular endothelial growth factor (VEGF) (Murdaca et al., 2004). In the kidney, Nedd4L/Nedd4-2 seems to participate in distal nephron salt sensitivity (Ishigami et al., 2020), and ubiquitin-conjugating enzyme E2 contributes to HUWE1-mediated degradation of tubulointerstitial fibrosis (Wang et al., 2022). Pharmacological interference with proteasomes is emerging as a potential approach to influence various pathological processes.

Lactacystin is a proteasome inhibitor that blocks the hydrolysis and degradation of intracellular proteins by the UPS (Craiu et al., 1997). Chronic lactacystin administration induces a mild but significant rise in systolic blood pressure (BP) along with fibrotic remodeling of the left ventricle (LV) in Wistar rats (Simko et al., 2017), and hypertrophy of the aorta in L-NAME (L-NG-nitro arginine methyl ester)-induced hypertension (Vrankova et al., 2010). Several hypothetical mechanisms for hemodynamic alterations and heart and vessel damage by lactacystin have been proposed, such as enhanced oxidative stress (Vrankova et al., 2010; Huseby et al., 2016; Parajuli, 2019), decreased NO bioavailability (Simko et al., 2017; Sharma et al., 2020), sympathetic nervous system activation (Congo Carbajosa et al., 2015) and modification of various cytosolic, nuclear, and myofibrillar protein turnovers (Mearini et al., 2008). However, data on lactacystin's renal effects are not available.

The aim of this study was to test whether lactacystin induces structural and fibrotic rebuilding of the kidneys. Furthermore, we sought to determine whether melatonin prevents these potential alterations. Melatonin (N-acetyl-5-methoxytryptamine), the main product of the pineal gland, not only regulates biological circadian rhythms (Reiter et al., 2020), but exerts various pleiotropic protective effects on the heart, vasculature (Reiter et al., 2010; Simko et al., 2019, 2020; Domínguez-Rodríguez et al., 2021; Tobeiha et al., 2022) and kidneys (Russcher et al., 2012; Hrenák et al., 2013; Hrenak et al., 2015; Shi et al., 2019). The effects of melatonin were compared with captopril, a classical angiotensin-converting enzyme (ACE) inhibitor, which exerts a well-established antiremodeling action in several organs and various pathologies (Pfeffer et al., 1992; Pechánová et al., 1997; Simko et al., 2010, 2014; Repová-Bednárová et al., 2013) including lactacystin-induced LV remodeling (Simko et al., 2017).

Materials and methods

Animals and treatment

The experiments were conducted in conformance with the Guide for the Care and Use of Laboratory Animals published by the US National Institutes of Health (NIH Publication No. 85-23, revised 1996). The study protocol was approved by the ethics committee of the Institute of Pathological Physiology, Faculty of Medicine, at Comenius University in Bratislava, Slovakia.

Thirty-two adult (12-week-old) weight-matched male Wistar rats (obtained from the Department of Toxicology and Laboratory Animals Breeding, Slovak Academy of Sciences, Dobra Voda, Slovakia) were randomly divided into four groups (n = 8 per group) and treated for 6 weeks as follows: control (C; untreated), lactacystin (Lac; 5 μg/kg/day), lactacystin plus captopril (Lac + Cap; 5 μg/kg/day lactacystin + 100 mg/kg/day captopril), and lactacystin plus melatonin (Lac + Mel; 5 μg/kg/day lactacystin + 10 mg/kg/day melatonin). Lactacystin, captopril, and melatonin were dissolved in drinking water and their concentrations were adjusted to daily water consumption to ensure the correct dosage. The melatonin solutions were offered in non-transparent bottles to protect them from light.

Lactacystin and melatonin were purchased from Sigma-Aldrich Chemie, Munich, Germany, and captopril from Egis Pharmaceuticals, Budapest, Hungary.

The rats were housed in individual cages, maintained under standard laboratory conditions (12:12-h light-dark cycle at 22–24°C temperature and 45%–65% humidity), and fed a regular pelleted diet *ad libitum*. Systolic blood pressure (SBP) was measured once a week in each animal by non-invasive tail-

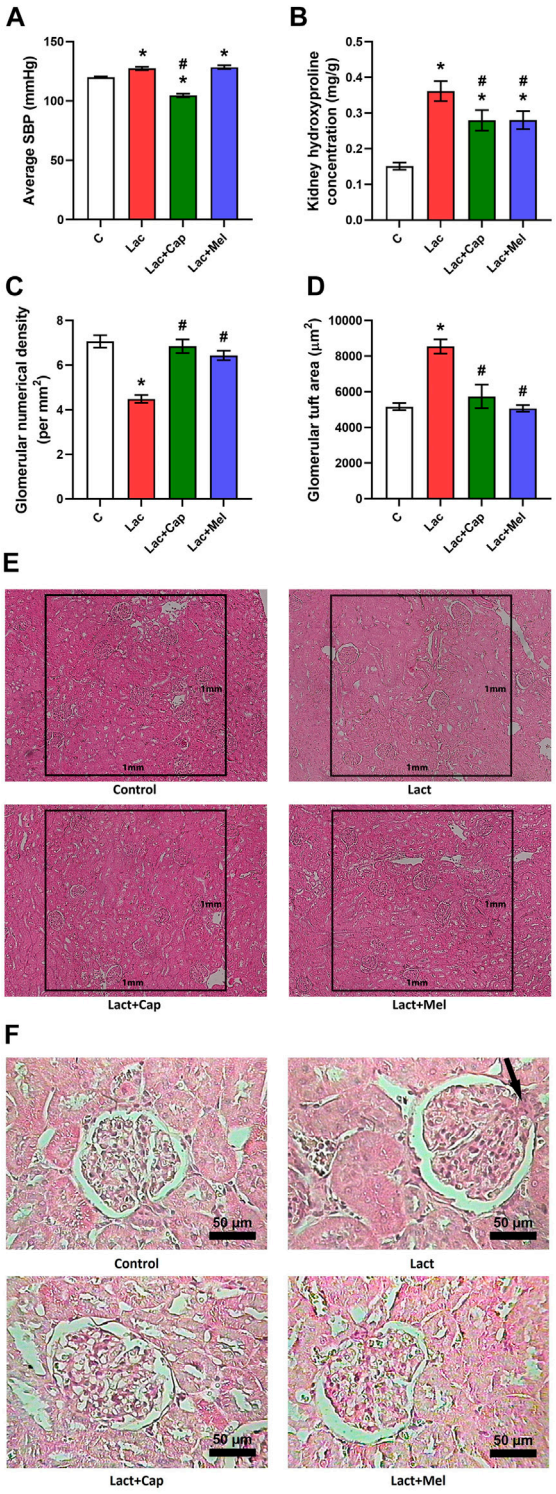


FIGURE 1
Effect of captopril (Lac + Cap) and melatonin (Lac + Mel) on average systolic blood pressure (SBP) **(A)**, renal hydroxyproline concentration **(B)**, and kidney morphology: glomerular numerical density per 1 mm^2 **(C)** and glomerular tuft area **(D)** of lactacystin-treated (Lac) rats; glomerular numerical density **(E)** and detailed images (*Continued*)

FIGURE 1
of the glomerular content **(F)** in lactacystin-treated rats: H-E-stained sections at ×10 **(E)** and ×100 **(F)** magnification using transmitted light microscopy; mesangial cell proliferation with extracellular matrix expansion (arrow). C, controls; *p < 0.05 vs. C; #p < 0.05 vs. Lac.

cuff plethysmography (Hugo-Sachs Elektronik, Freiburg, Germany). After 6 weeks of treatment, the rats were euthanized by isoflurane inhalation. Two halves of the left kidney were harvested for subsequent analyses: one half was fixed in 4% formaldehyde for histopathological analysis. The other was snap-frozen at −80°C for determination of hydroxyproline concentration.

Kidney histopathology

The kidney samples fixed in 4% formaldehyde were embedded in paraffin and cut into 5 μm-thick sections. Then, two sets of sections per sample were deparaffinized, rehydrated, and stained, one with hematoxylin-eosin (H-E) for glomerular morphometry, and the other with picrosirius red (PSR) for quantitative analysis of kidney fibrosis. Photomicrographs were taken using a NIKON Eclipse Ti C2+ microscope (NIKON, Tokyo, Japan) with transmitted or polarized light and subsequently analyzed with NIKON NIS-Elements Analysis software (NIKON, Tokyo, Japan) and ImageJ version 1.52p for Windows (National Institutes of Health, Bethesda, MD, United States).

The H-E-stained sections were analyzed using transmitted light microscopy at ×10 magnification and NIKON NIS-Elements Analysis software to assess glomerular morphometry, as previously described (Pechanova et al., 2006; Hrenák et al., 2013; Stanko et al., 2020). Glomerular density was determined by counting preserved glomeruli in a 1 mm^2 digital frame put over the kidney cortex at 10 microscopic fields per section; i.e., 80 digital frames were investigated per group. The glomerular tuft area was determined by measuring perpendicular maximum and minimum diameters (d_{max} and d_{min}, respectively) of 10 random glomerular tufts per section used for subsequent tuft area calculation as follows: glomerular tuft area = $\pi(d_{max}/2)(d_{min}/2)$; i.e., 80 glomerular tuft areas were calculated per group.

The PSR-stained sections were analyzed with polarized light microscopy, set at ×100 magnification, and ImageJ to allow for a quantitative assessment of kidney fibrosis, as previously described (Seccia et al., 2008; Stanko et al., 2020). Due to the birefringence shift by PSR, the thick type I collagen (Col I) was shown in red-orange shades, and the thin type III collagen (Col III) was visualized in green-yellow shades. Thus, the Col I and Col III volumes were determined as the percentage of red-orange and green-yellow shaded areas in a particular region of interest (ROI) by setting the

appropriate "hue" thresholds of the color spectrum in ImageJ. To assess glomerular fibrosis, 40 ROIs per section of 50 × 50 μm were placed in intraglomerular space; i.e., 320 intraglomerular ROIs were investigated per group. To assess tubulointerstitial fibrosis, 40 ROIs per section of 192 × 72 μm were placed at the interstitial cortex without glomeruli or vessels; i.e., 320 tubulointerstitial ROIs were investigated per group. To evaluate the amount of vascular/perivascular fibrosis, five ROIs per section were examined, tight-cropping a cross-section captured artery with a diameter between 50 and 100 μm; i.e., 40 vascular/perivascular ROIs were investigated per group.

The histopathological analysis was performed by an experienced investigator blinded to the group identity.

Determination of kidney hydroxyproline concentration

The kidney samples, snap-frozen and stored at −80°C, were dried at 100°C for 24 h and then hydrolyzed using a solution of 6 mol/L HCl. The hydroxyproline concentration was determined spectrophotometrically at 550 nm (Reddy and Enwemeka, 1996; Hrenák et al., 2013).

Statistical analysis

The results are presented as the mean ± SEM. The one-way, two-tailed analysis of variance (ANOVA), followed by a Holm-Sidak multiple comparisons test, was used for statistical analysis. p values below 0.05 were considered statistically significant. The statistical analysis was conducted using GraphPad Prism 8 for Windows (GraphPad Software, La Jolla, CA, United States).

Results

Systolic blood pressure

The SBP averaged over 6 weeks of treatment was 120.07 ± 0.58 mmHg in controls, and lactacystin raised the value by 6% ($p < 0.05$). In the lactacystin group, captopril lowered the average SBP by 18% ($p < 0.05$), while melatonin had no effect on average SBP (Figure 1A).

Glomerular morphometry

The glomerular numerical density was 7.06 ± 0.28 per mm^2 in controls; lactacystin decreased this value by 37% ($p < 0.05$). In the lactacystin group, both captopril and melatonin augmented the glomerular numerical density by 53% and 44% ($p < 0.05$ for both measures), respectively (Figures 1C,E).

The glomerular tuft area was 5.173 ± 198 μm^2 in controls, and lactacystin increased this value by 65% ($p < 0.05$). In the lactacystin group, both captopril and melatonin reduced the glomerular tuft area by 33% and 41% ($p < 0.05$ for both measures), respectively (Figures 1D,F).

Kidney hydroxyproline concentration

The kidney hydroxyproline concentration was 0.15 ± 0.05 mg/g in controls, and lactacystin raised ($p < 0.05$) it by 139%. In the lactacystin group, both captopril and melatonin lowered ($p < 0.05$) the kidney hydroxyproline concentration by 23% (Figure 1B).

Quantitative analysis of kidney fibrosis

For intraglomerular ROIs, the volume of Col I and Col III in controls was 0.90 ± 0.23 and 1.16 ± 0.30%, respectively. Lactacystin increased the proportion of both Col I and Col III by 101% and 103% ($p < 0.05$ for both measures), respectively. In the lactacystin group, captopril lowered the proportion of both Col I and Col III by 93% ($p < 0.05$ for both measures). Similarly, melatonin reduced the proportion of both Col I and Col III by 76% and 79% ($p < 0.05$ for both measures), respectively. The sum of Col I and Col III volume in intraglomerular ROIs was 2.06 ± 0.53% in controls, and lactacystin increased this value by 102% ($p < 0.05$). In the lactacystin group, both captopril and melatonin decreased the sum of Col I and Col III volume by 93% and 78% ($p < 0.05$ for both measures), respectively. The ratio of Col I to Col III (Col I/Col III) was 0.78 ± 0.09 in controls, and neither lactacystin, captopril, nor melatonin had any effect on the ratio (Figure 2).

For tubulointerstitial ROIs, the volume of Col I and Col III in controls were 2.57 ± 0.81 and 3.88 ± 1.34%, respectively. Lactacystin increased the proportion of Col I by 139% ($p < 0.05$) and enhanced the proportion of Col III by 131% (ns). In the lactacystin group, captopril reduced the proportion of both Col I and Col III by 94% and 96% ($p < 0.05$ for both measures), respectively. Similarly, melatonin decreased the proportion of both Col I and Col III by 83% and 84% ($p < 0.05$ for both measures), respectively. The sum of Col I and Col III volume in tubulointerstitial ROIs was 6.45 ± 2.13% in controls, and lactacystin increased this value by 134% ($p < 0.05$). In the lactacystin group, both captopril and melatonin reduced the sum of Col I and Col III volume by 95% and 84% ($p < 0.05$ for both measures), respectively. Col I/Col III was 0.78 ± 0.11 in controls, and lactacystin, captopril, or melatonin had no effect on the ratio (Figure 3).

In vascular/perivascular ROIs, Col I and Col III's volume in controls was 0.80 ± 0.12 and 0.64 ± 0.13%, respectively. Lactacystin had no significant effect on the volume of Col I and Col III. In the

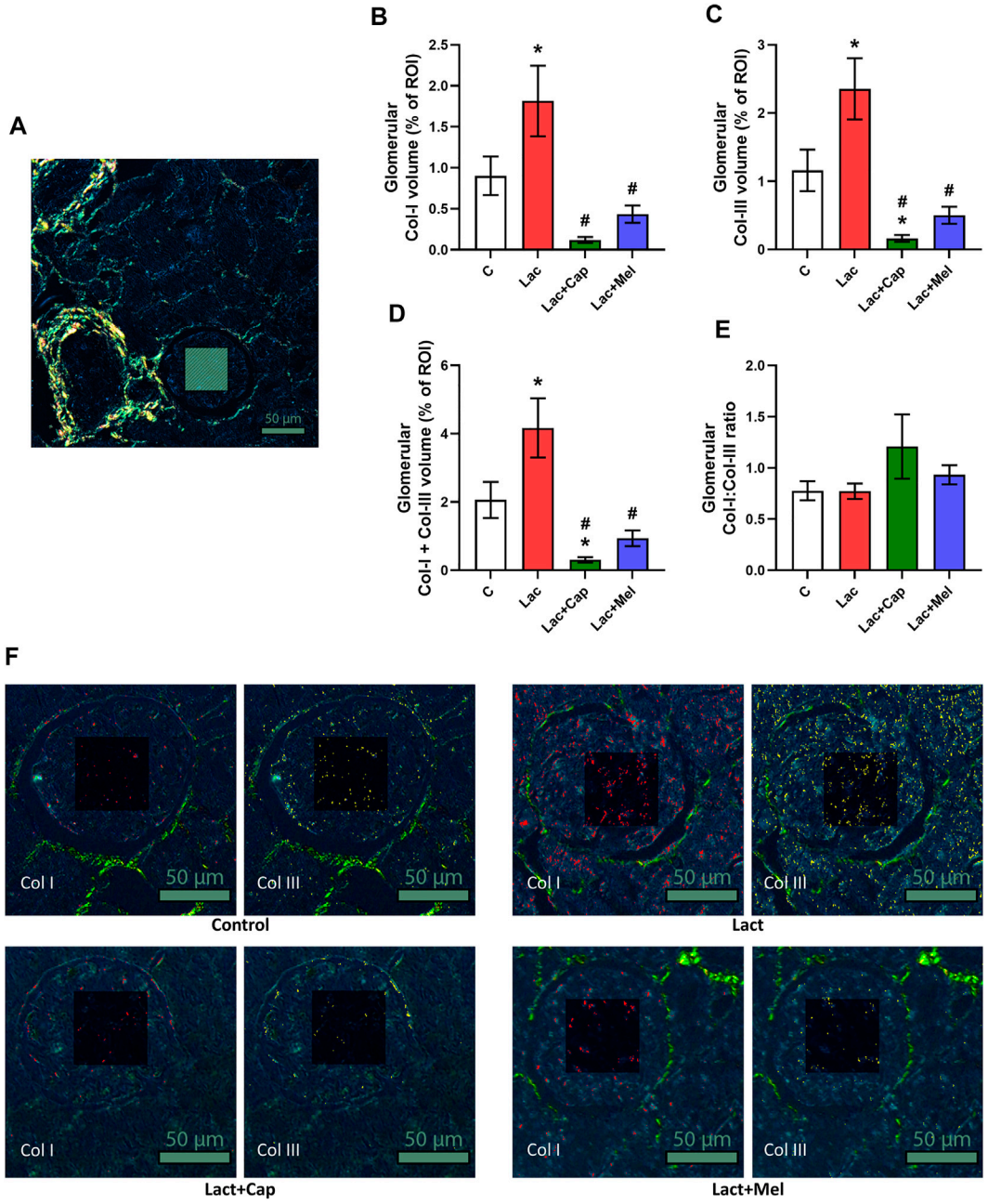


FIGURE 2
Effect of captopril (Lac + Cap) and melatonin (Lac + Mel) on glomerular fibrosis of lactacystin-treated (Lac) rats. PSR-stained section at ×100 magnification using polarized light microscopy **(A)**, the volume of collagen I (Col I) **(B)**, collagen III (Col III) **(C)**, the sum of collagen I + III **(D)**, the Col I/Col III ratio **(E)** and PSR-stained sections at ×200 magnification using polarized microscopy showing collagen I in red and collagen III in yellow **(F)**. C, controls; ROI, region of interest depicted as the shaded rectangle. Intraglomerular ROI dimensions: 50 µm × 50 µm. Scale bar: 50 µm. *$p < 0.05$ vs. C; #$p < 0.05$ vs. Lac.

lactacystin group, captopril reduced the proportion of both Col I and Col III by 76% and 90% ($p < 0.05$ for both measures), respectively, while melatonin had no effect. The sum of Col I and Col III volume in vascular/perivascular ROIs was 1.44 ± 0.24% in controls, and lactacystin did not significantly change this parameter. In the lactacystin group, captopril decreased the sum of Col I and Col III volume by 82% ($p < 0.05$), and melatonin had no effect. Col I/Col III was 1.45 ± 0.18 in controls, and lactacystin had no significant effect on the ratio. In the lactacystin group, captopril increased Col I/Col III ratio by 226% ($p < 0.05$), and melatonin had no effect (Figure 4).

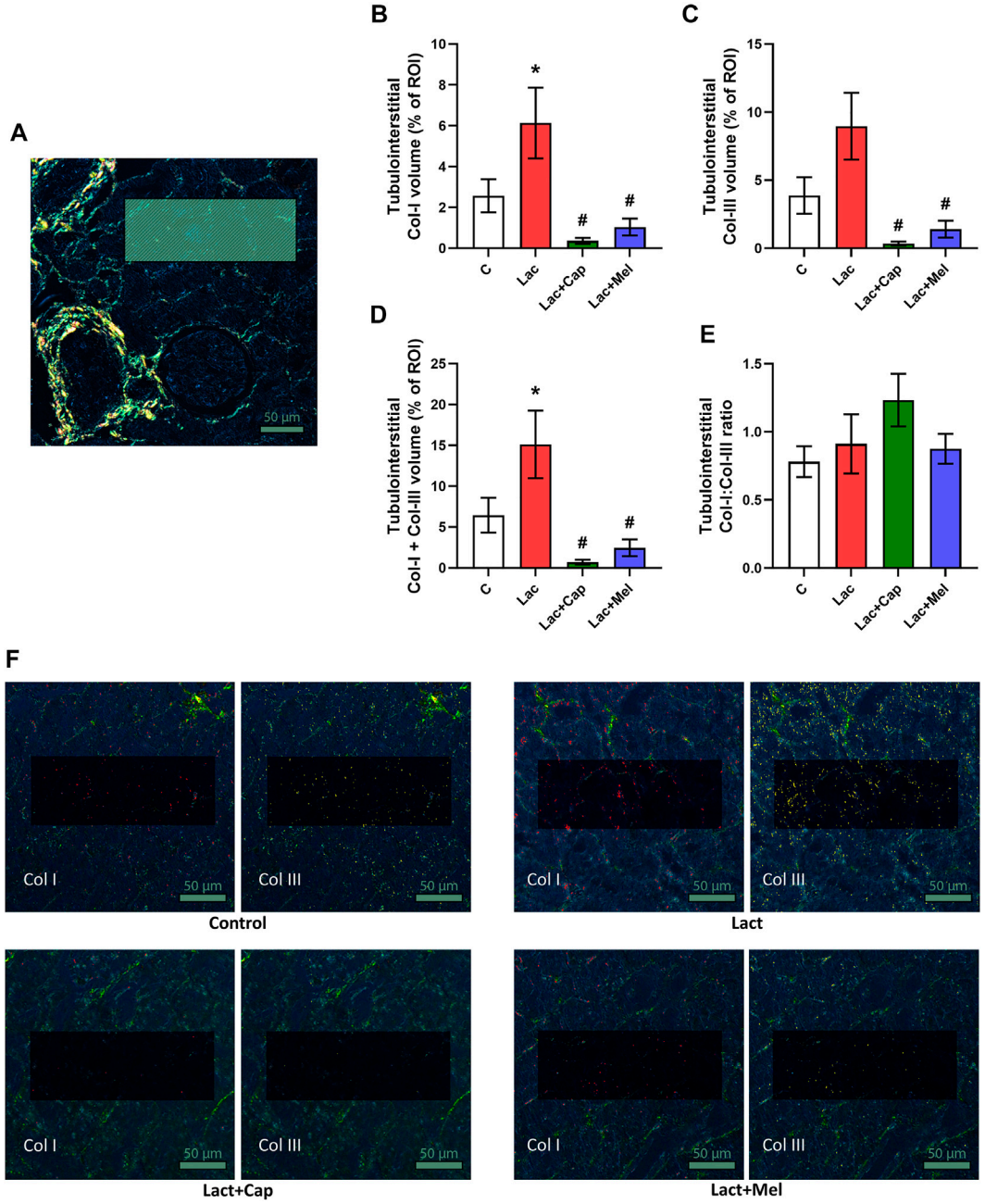


FIGURE 3
Effect of captopril (Lac + Cap) and melatonin (Lac + Mel) on tubulointerstitial fibrosis of lactacystin-treated (Lac) rats. PSR-stained section at ×100 magnification using polarized light microscopy **(A)**, the volume of collagen I (Col I) **(B)**, collagen III (Col III) **(C)**, the sum of collagen I + III **(D)**, the Col I/Col III ratio **(E)** and PSR-stained sections at ×100 magnification using polarized microscopy showing collagen I in red and collagen III in yellow **(F)**. C, controls; ROI, region of interest depicted as the shaded rectangle. Tubulointerstitial ROI dimensions: 72 µm × 192 µm. Scale bar: 50 µm. $^{*}p < 0.05$ vs. C; $^{\#}p < 0.05$ vs. Lac.

Discussion

Six weeks of lactacystin administration raised the average SBP. In kidneys, lactacystin reduced glomerular density, increased the glomerular tuft area, and enhanced the hydroxyproline concentration. Lactacystin likewise elevated the intraglomerular proportion and the sum of Col I and Col III, the tubulointerstitial proportion of Col I and the sum of Col I and Col III without an effect on vascular/perivascular collagen. Six weeks of captopril treatment reduced SBP, while melatonin had no effect. Both melatonin and

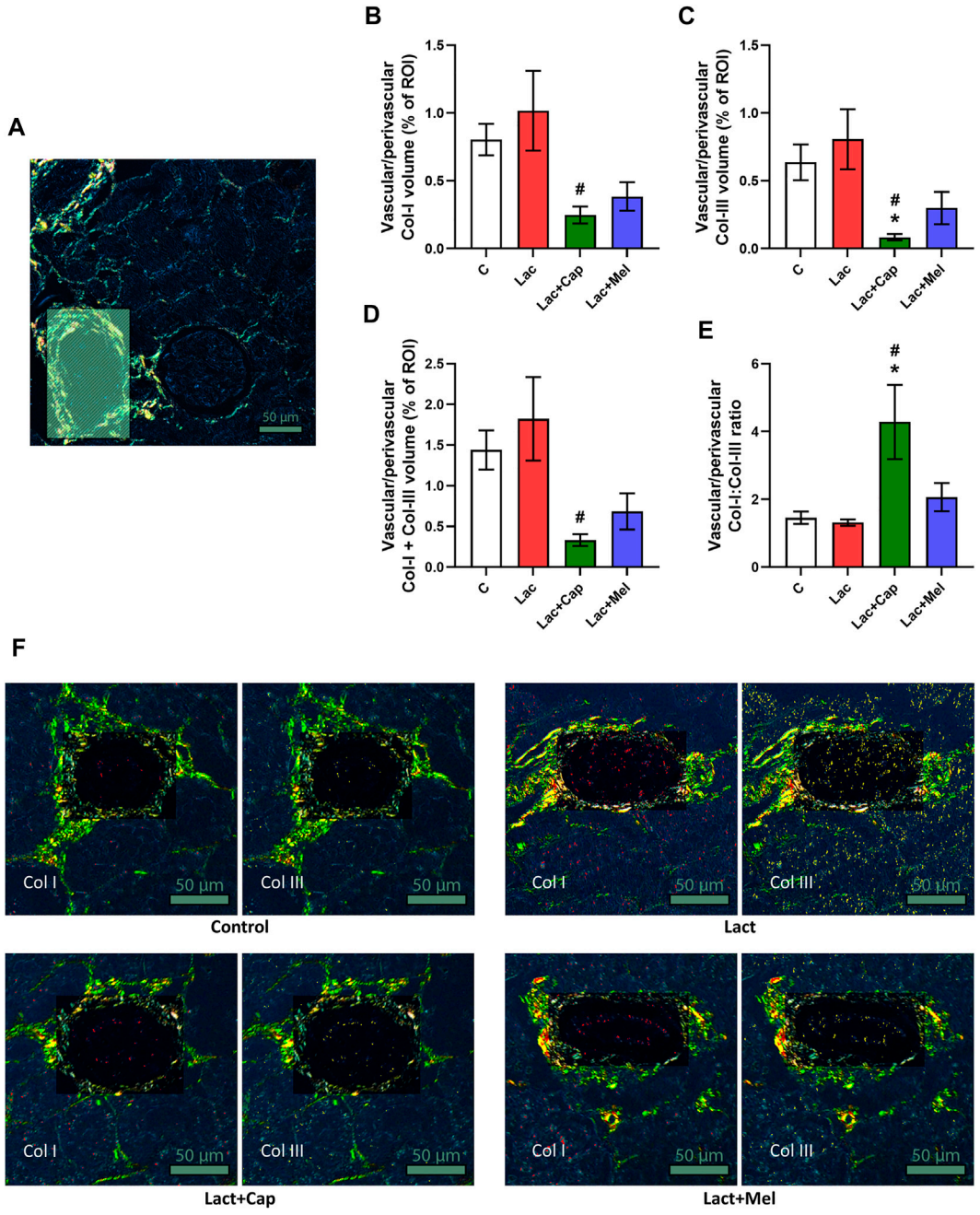


FIGURE 4
Effect of captopril (Lac + Cap) and melatonin (Lac + Mel) on vascular/perivascular fibrosis of lactacystin-treated (Lac) rats. PSR-stained section at ×100 magnification using polarized light microscopy **(A)**, the volume of collagen I (Col I) **(B)**, collagen III (Col III) **(C)**, the sum of collagen I + III **(D)**, the Col I/Col III ratio **(E)** and PSR-stained sections at ×100 magnification using polarized microscopy showing collagen I in red and collagen III in yellow **(F)**. C, controls; ROI, region of interest depicted as the shaded rectangle. Vascular/perivascular ROI dimensions: from 50 × 100 µm to 200 × 300 µm. Scale bar: 50 µm. $^{*}p < 0.05$ vs. C; $^{\#}p < 0.05$ vs. Lac.

captopril raised glomerular density, reduced the glomerular tuft area, and decreased hydroxyproline concentration in the kidneys. Both drugs reduced the proportion and sum of intraglomerular and tubulointerstitial Col I and Col III.

Since the UPS controls the protein turnover of both regulatory and structural proteins, it becomes an attractive target for pharmacological interventions. Lactacystin represents the classical, first discovered proteasome inhibitor, reported in 1991 (Ōmura and

Crump, 2019). Among other effects, lactacystin is considered to be an inhibitor of nuclear factor kappa B (NF-κB) transcription factor. Since NF-κB is assumed to be a checkpoint for hypertrophic growth mediated by humoral factors, inhibitors of NF-κB, such as lactacystin, are considered a possible way of protection. The net effect of lactacystin is challenging to estimate for two reasons: first, NF-κB is not only an essential factor for proliferation (Bellas et al., 1995); it may also interfere with nitric oxide synthesis, having the opposite effect (Vrankova et al., 2010; Simko et al., 2017). Moreover, lactacystin not only specifically blocks the degradation of the NF-κB inhibitor IκBα but can also modify other proteins involved in signaling processes (Vrankova et al., 2010).

In line with this, surprisingly, lactacystin did not reduce but increased blood pressure and fibrotic rebuilding in the left ventricle (Simko et al., 2017). Thus, lactacystin administration-induced BP elevation was recently characterized as a novel model of experimental hypertension (Vrankova et al., 2010; Simko et al., 2017; Sharma et al., 2020). Proteasome inhibition may cause hypertension either because of an increased endogenous protein inhibitor of neuronal nitric oxide synthase, leading to decreased NO bioavailability in the paraventricular nucleus (Sharma et al., 2020), or from tyrosine hydroxylase upregulation and activation in the hypothalamus and brainstem (Congo Carbajosa et al., 2015), both resulting in increased sympathetic outflow. Bearing in mind the remodeling of the heart (Simko et al., 2017) and aorta (Vrankova et al., 2010) in this model, it seems to be of importance to disclose whether lactacystin could act in a similar pro-proliferative way in hypertensive kidneys.

In this experiment, chronic lactacystin treatment was associated with the loss of glomeruli, indicated by decreased glomerular density and simultaneous glomerular hypertrophy, reflected in increased glomerular tuft area. Some authors consider the reduction of nephron density to be a risk factor for hypertension and CKD progression (Kanzaki et al., 2020). Furthermore, lactacystin treatment was associated with enhanced hydroxyproline concentration and site-specific fibrotic rebuilding of renal tissue. Published data suggest that chronic hypertension leads to the accumulation and dysregulation of extracellular matrix in the kidneys, resulting in renal fibrosis (Schlondorff, 2008). The fibrotic changes in the kidneys are common 1) in the glomerulus—glomerulosclerosis; 2) in the tubulointerstitium—interstitial fibrosis; and 3) in the vessels—arteriosclerosis and perivascular fibrosis (Bülow and Boor, 2019). The most abundant collagens expressed in the kidneys are types I and III. Col I forms long, thick, and stiff fibrils, decreasing tissue compliance (Sopakayang et al., 2012). In the early stages of renal fibrosis, Col I deposits in the glomerulus, tubulointerstitial space, and arterial wall (Alexakis et al., 2006). Col III is mainly found in softer tissues and is more distensible than Col I (Silver et al., 2001). In renal fibrosis, the expression of Col III increases in both interstitium and glomeruli (Alexakis et al., 2006). In the present study, an excessive deposition of Col I and Col III was observed in the glomerulus and tubulointerstitial space in lactacystin-treated hypertensive rats.

ACE inhibitor captopril reduces fibrosis associated with target organ damage. Indeed, captopril decreased the concentration of soluble collagen in the LV of rats with combined continuous light and L-NAME-induced hypertension (Simko et al., 2010), attenuated LV collagen deposition in SHR (Zhao et al., 2015), and reduced LV fibrosis in mice with transverse aortic constriction (Zhang et al., 2019) and Sprague-Dawley rats with L-NAME-induced hypertension (Sonoda et al., 2017). Similarly, in kidneys captopril reduced interstitial renal fibrosis in neonatal dogs with partial urethral obstruction (PUO) (Shirazi et al., 2007), ameliorated fibrosis in rats with PUO (Shirazi et al., 2014), and downregulated interstitial fibrosis in rats with unilateral ureteral obstruction (Hosseinian et al., 2019). In line with these data, our results show reduced intraglomerular, tubulointerstitial, and perivascular collagen accumulation and renal hydroxyproline concentration after 6 weeks of captopril administration in lactacystin-treated rats. In this experiment, captopril reduced the proportion and sum of intraglomerular and tubulointerstitial Col I and Col III, lowered the sum of vascular/perivascular Col I and Col III and increased the vascular/perivascular ratio of Col I to Col III, while reducing the kidney hydroxyproline concentration.

Melatonin exerts a vast number of pleiotropic protective effects on various tissues, including fibrosis amelioration. The antifibrotic effects of melatonin have been observed in the LV of lactacystin-treated rats (Simko et al., 2017), of SHRs (Simko et al., 2009), and in the LV and aorta of 24-h continuous light-exposed rats (Repová-Bednárová et al., 2013; Simko et al., 2014). In the kidneys, melatonin reduced renal fibrosis in mice with unilateral ureteral obstruction (Li et al., 2020), adenine-induced CKD mice (Yoon et al., 2020), diabetic mice (Li et al., 2019; Fan et al., 2020), prenatally diclofenac sodium injected rats (Khoshvakhti et al., 2015), and in human renal proximal tubule epithelial cells on a high glucose diet (Han et al., 2020). Accordingly, in this study, 6 weeks of melatonin treatment prevented intraglomerular and tubulointerstitial fibrosis development, alongside reduced renal hydroxyproline concentration in rats administered lactacystin. Although melatonin failed to reduce SBP in this experiment, its antifibrotic effects were likely a result of melatonin's direct, local actions, such as obvious antioxidant and radical scavenging actions (Simko et al., 2009; Reiter et al., 2018), modulation of the sympathetic and renin-angiotensin system (Simko and Paulis, 2013), and increasing NO bioavailability and antiproliferative action (Paulis and Simko, 2007; Simko and Paulis, 2007, 2013; Simko and Pechanova, 2009; Domínguez-Rodríguez et al., 2021).

The lactacystin administration induced fibrotic rebuilding of the kidneys. Both captopril and melatonin reduced the proportion and sum of intraglomerular and tubulointerstitial Col I and Col III and hydroxyproline concentration in the kidneys. Although captopril more prominently reduced Col I and Col III accumulation in the vascular/perivascular area compared to

melatonin, the Col I/Col III ratio rose. Considering the stiffness of Col I, the findings suggest that captopril might cause renal capillaries to become more rigid, altering renal perfusion. On the contrary, melatonin did not significantly change the renal vascular/perivascular fibrosis while maintaining a normal Col I/Col III ratio. Since it concurrently reduced glomerular fibrosis, melatonin may play a role in maintaining adequate glomerular perfusion and filtration. Thus, melatonin may be comparable or superior to ACE inhibition because of its distinct effect on renal collagen composition, potentially contributing to improved renal perfusion and filtration rate.

Conclusion

In a model of lactacystin-induced hypertension and organ damage, both melatonin and captopril raised glomerular density, reduced the glomerular tuft area, and lowered the kidney hydroxyproline concentration. Both drugs reduced the proportion and sum of intraglomerular and tubulointerstitial Col I and Col III. As melatonin failed to reduce SBP, its antifibrotic effects were supposedly delivered by melatonin's direct, local pleiotropic effects.

Considering the fibrotic remodeling of the left ventricle observed in previous works and the site-specific fibrotic rebuilding of the kidneys observed in this study, it seems reasonable to suggest that chronic treatment with lactacystin may be a perspective model of cardiorenal damage. Furthermore, we showed that melatonin, similar to captopril, is a promising means of protection against hypertensive kidney damage.

Limitations

It would be of interest to correlate the renal histopathologic findings with immunohistochemical analysis of growth factors, angiogenic factors, and markers of collagen turnover in the kidneys. Indeed, according to the literature, there is a correlation between the histopathological evidence of renal fibrosis and profibrotic renal tissue markers, such as transforming growth factor-β1 (TGF-β1), connective tissue growth factor (CTGF), and vascular endothelial growth factor A (VEGF-A) (Lopes et al., 2019). Moreover, the inhibition of matrix metalloproteinase (MMP)-9 (Wang et al., 2019) and decreased expression of MMP-1 (Nazneen et al., 2002) resulted in decreased histological evidence of renal fibrosis. However, these analyses were beyond the scope and possibilities of the present histopathological study.

Data availability statement

The raw data supporting the conclusion of this article will be made available by the authors, without undue reservation.

Ethics statement

The animal study was reviewed and approved by the Ethical Committee of the Institute of Pathophysiology, Faculty of Medicine, Comenius University, Bratislava, Slovakia.

Author contributions

KR, PS, TB, and FS conceived and designed the study and drafted the manuscript. KR, PS, TB, KK, SA, AB, and MA performed the experiments and acquired data. All authors participated in data analysis and interpretation, manuscript revision, and approved the submitted version.

Funding

This work was supported by the VEGA grants for scientific research Nos. 1/0035/19 and APVV-20-0421.

Conflict of interest

The authors declare that the research was conducted in the absence of any commercial or financial relationships that could be construed as a potential conflict of interest.

Publisher's note

All claims expressed in this article are solely those of the authors and do not necessarily represent those of their affiliated organizations, or those of the publisher, the editors and the reviewers. Any product that may be evaluated in this article, or claim that may be made by its manufacturer, is not guaranteed or endorsed by the publisher.

References

Alexakis, C., Maxwell, P., and Bou-Gharios, G. (2006). Organ-specific collagen expression: Implications for renal disease. *Nephron. Exp. Nephrol.* 102, e71–75. doi:10.1159/000089684

Bellas, R. E., Lee, J. S., and Sonenshein, G. E. (1995). Expression of a constitutive NF-kappa B-like activity is essential for proliferation of cultured bovine vascular smooth muscle cells. *J. Clin. Invest.* 96, 2521–2527. doi:10.1172/JCI118313

Bülow, R. D., and Boor, P. (2019). Extracellular matrix in kidney fibrosis: More than just a scaffold. *J. Histochem. Cytochem.* 67, 643–661. doi:10.1369/0022155419849388

Chatterjee, A., Mir, S. A., Dutta, D., Mitra, A., Pathak, K., and Sarkar, S. (2011). Analysis of p53 and NF-κB signaling in modulating the cardiomyocyte fate during hypertrophy. *J. Cell. Physiol.* 226, 2543–2554. doi:10.1002/jcp.22599

Congo Carbajosa, N. A., Carbajosa, N. A. L., Corradi, G., Verrilli, M. A. L., Guil, M. J., Vatta, M. S., et al. (2015). Tyrosine hydroxylase is short-term regulated by the ubiquitin-proteasome system in PC12 cells and hypothalamic and brainstem neurons from spontaneously hypertensive rats: Possible implications in hypertension. *PLoS One* 10, e0116597. doi:10.1371/journal.pone.0116597

Craiu, A., Gaczynska, M., Akopian, T., Gramm, C. F., Fenteany, G., Goldberg, A. L., et al. (1997). Lactacystin and clasto-lactacystin beta-lactone modify multiple proteasome beta-subunits and inhibit intracellular protein degradation and major histocompatibility complex class I antigen presentation. *J. Biol. Chem.* 272, 13437–13445. doi:10.1074/jbc.272.20.13437

Domínguez-Rodríguez, A., Abreu-González, P., Báez-Ferrer, N., Reiter, R. J., Avanzas, P., and Hernández-Vaquero, D. (2021). Melatonin and cardioprotection in humans: A systematic review and meta-analysis of randomized controlled trials. *Front. Cardiovasc. Med.* 8, 635083. doi:10.3389/fcvm.2021.635083

Fan, Z., Qi, X., Yang, W., Xia, L., and Wu, Y. (2020). Melatonin ameliorates renal fibrosis through the inhibition of NF-κB and TGF-β1/smad3 pathways in db/db diabetic mice. *Arch. Med. Res.* 51, 524–534. doi:10.1016/j.arcmed.2020.05.008

Hamrahian, S. M., and Falkner, B. (2017). Hypertension in chronic kidney disease. *Adv. Exp. Med. Biol.* 956, 307–325. doi:10.1007/5584_2016_84

Han, Y.-S., Yoon, Y. M., Go, G., Lee, J. H., and Lee, S. H. (2020). Melatonin protects human renal proximal tubule epithelial cells against high glucose-mediated fibrosis via the cellular prion protein-TGF-β-smad signaling Axis. *Int. J. Med. Sci.* 17, 1235–1245. doi:10.7150/ijms.42603

Hosseinian, S., Shahraki, S., Ebrahimzadeh Bideskan, A., Shafei, M. N., Sadeghnia, H. R., Soukhtanloo, M., et al. (2019). Thymoquinone alleviates renal interstitial fibrosis and kidney dysfunction in rats with unilateral ureteral obstruction. *Phytother. Res.* 33, 2023–2033. doi:10.1002/ptr.6376

Hrenák, J., Arendášová, K., Rajkovičová, R., Aziriová, S., Repová, K., Krajčírovičová, K., et al. (2013). Protective effect of captopril, olmesartan, melatonin and compound 21 on doxorubicin-induced nephrotoxicity in rats. *Physiol. Res.* 62, S181–S189. doi:10.33549/physiolres.932614

Hrenak, J., Paulis, L., Repova, K., Aziriova, S., Nagtegaal, E. J., Reiter, R. J., et al. (2015). Melatonin and renal protection: Novel perspectives from animal experiments and human studies (review). *Curr. Pharm. Des.* 21, 936–949. doi:10.2174/1381612820666140929092929

Huseby, N.-E., Ravuri, C., and Moens, U. (2016). The proteasome inhibitor lactacystin enhances GSH synthesis capacity by increased expression of antioxidant components in an Nrf2-independent, but p38 MAPK-dependent manner in rat colorectal carcinoma cells. *Free Radic. Res.* 50, 1–13. doi:10.3109/10715762.2015.1100730

Ishigami, T., Kino, T., Minegishi, S., Araki, N., Umemura, M., Ushio, H., et al. (2020). Regulators of epithelial sodium channels in aldosterone-sensitive distal nephrons (ASDN): Critical roles of Nedd4L/nedd4-2 and salt-sensitive hypertension. *Int. J. Mol. Sci.* 21, E3871. doi:10.3390/ijms21113871

Kanzaki, G., Tsuboi, N., Shimizu, A., and Yokoo, T. (2020). Human nephron number, hypertension, and renal pathology. *Anat. Rec.* 303, 2537–2543. doi:10.1002/ar.24302

Khoshvakhti, H., Yurt, K. K., Altunkaynak, B. Z., Türkmen, A. P., Elibol, E., Aydın, I., et al. (2015). Effects of melatonin on diclofenac sodium treated rat kidney: A stereological and histopathological study. *Ren. Fail.* 37, 1379–1383. doi:10.3109/0886022X.2015.1073556

Li, H.-H., Kedar, V., Zhang, C., McDonough, H., Arya, R., Wang, D.-Z., et al. (2004). Atrogin-1/muscle atrophy F-box inhibits calcineurin-dependent cardiac hypertrophy by participating in an SCF ubiquitin ligase complex. *J. Clin. Invest.* 114, 1058–1071. doi:10.1172/JCI22220

Li, J., Li, N., Yan, S., Lu, Y., Miao, X., Gu, Z., et al. (2019). Melatonin attenuates renal fibrosis in diabetic mice by activating the AMPK/PGC1α signaling pathway and rescuing mitochondrial function. *Mol. Med. Rep.* 19, 1318–1330. doi:10.3892/mmr.2018.9708

Li, N., Wang, Z., Gao, F., Lei, Y., and Li, Z. (2020). Melatonin ameliorates renal fibroblast-myofibroblast transdifferentiation and renal fibrosis through miR-21-5p regulation. *J. Cell. Mol. Med.* 24, 5615–5628. doi:10.1111/jcmm.15221

Lopes, T. G., de Souza, M. L., da Silva, V. D., Dos Santos, M., da Silva, W. I. C., Itaquy, T. P., et al. (2019). Markers of renal fibrosis: How do they correlate with podocyte damage in glomerular diseases? *PLoS One* 14, e0217585. doi:10.1371/journal.pone.0217585

Mearini, G., Schlossarek, S., Willis, M. S., and Carrier, L. (2008). The ubiquitin-proteasome system in cardiac dysfunction. *Biochim. Biophys. Acta* 1782, 749–763. doi:10.1016/j.bbadis.2008.06.009

Mennuni, S., Rubattu, S., Pierelli, G., Tocci, G., Fofi, C., and Volpe, M. (2014). Hypertension and kidneys: Unraveling complex molecular mechanisms underlying hypertensive renal damage. *J. Hum. Hypertens.* 28, 74–79. doi:10.1038/jhh.2013.55

Murdaca, J., Treins, C., Monthouël-Kartmann, M.-N., Pontier-Bres, R., Kumar, S., Van Obberghen, E., et al. (2004). Grb10 prevents Nedd4-mediated vascular endothelial growth factor receptor-2 degradation. *J. Biol. Chem.* 279, 26754–26761. doi:10.1074/jbc.M311802200

Nazneen, A., Razzaque, M. S., Liu, D., and Taguchi, T. (2002). Possible role of Ets-1 and MMP-1 in matrix remodeling in experimental cisplatin nephropathy. *Med. Electron Microsc.* 35, 242–247. doi:10.1007/s007950200028

Ōmura, S., and Crump, A. (2019). Lactacystin: First-in-class proteasome inhibitor still excelling and an exemplar for future antibiotic research. *J. Antibiot.* 72, 189–201. doi:10.1038/s41429-019-0141-8

Pagan, J., Seto, T., Pagano, M., and Cittadini, A. (2013). Role of the ubiquitin proteasome system in the heart. *Circ. Res.* 112, 1046–1058. doi:10.1161/CIRCRESAHA.112.300521

Parajuli, N. (2019). A cycle of altered proteasome and reactive oxygen species production in renal proximal tubular cells. *Toxicol. Forensic Med.* 4, 13–17. doi:10.17140/tfmoj-4-128

Paulis, L., and Simko, F. (2007). Blood pressure modulation and cardiovascular protection by melatonin: Potential mechanisms behind. *Physiol. Res.* 56, 671–684. doi:10.33549/physiolres.931236

Pechánová, O., Bernátová, I., Pelouch, V., and Simko, F. (1997). Protein remodelling of the heart in NO-deficient hypertension: The effect of captopril. *J. Mol. Cell. Cardiol.* 29, 3365–3374. doi:10.1006/jmcc.1997.0566

Pechanova, O., Matuskova, J., Capikova, D., Jendekova, L., Paulis, L., and Simko, F. (2006). Effect of spironolactone and captopril on nitric oxide and S-nitrosothiol formation in kidney of L-NAME-treated rats. *Kidney Int.* 70, 170–176. doi:10.1038/sj.ki.5001513

Pfeffer, M. A., Braunwald, E., Moyé, L. A., Basta, L., Brown, E. J., Cuddy, T. E., et al. (1992). Effect of captopril on mortality and morbidity in patients with left ventricular dysfunction after myocardial infarction. Results of the survival and ventricular enlargement trial. The SAVE Investigators. *N. Engl. J. Med.* 327, 669–677. doi:10.1056/NEJM199209033271001

Reddy, G. K., and Enwemeka, C. S. (1996). A simplified method for the analysis of hydroxyproline in biological tissues. *Clin. Biochem.* 29, 225–229. doi:10.1016/0009-9120(96)00003-6

Reiter, R. J., Manchester, L. C., Fuentes-Broto, L., and Tan, D.-X. (2010). Cardiac hypertrophy and remodelling: Pathophysiological consequences and protective effects of melatonin. *J. Hypertens.* 28 (1), S7–S12. doi:10.1097/01.hjh.0000388488.51083.2b

Reiter, R. J., Rosales-Corral, S., and Sharma, R. (2020). Circadian disruption, melatonin rhythm perturbations and their contributions to chaotic physiology. *Adv. Med. Sci.* 65, 394–402. doi:10.1016/j.advms.2020.07.001

Reiter, R. J., Tan, D. X., Rosales-Corral, S., Galano, A., Zhou, X. J., and Xu, B. (2018). Mitochondria: Central organelles for melatonin's antioxidant and anti-aging actions. *Molecules* 23, E509. doi:10.3390/molecules23020509

Repová-Bednárová, K., Aziriová, S., Hrenák, J., Krajčírovičová, K., Adamcová, M., Paulis, L., et al. (2013). Effect of captopril and melatonin on fibrotic rebuilding of the aorta in 24 hour light-induced hypertension. *Physiol. Res.* 62, S135–S141. doi:10.33549/physiolres.932592

Russcher, M., Koch, B., Nagtegaal, E., van der Putten, K., ter Wee, P., and Gaillard, C. (2012). The role of melatonin treatment in chronic kidney disease. *Front. Biosci.* 17, 2644–2656. doi:10.2741/4075

Schlondorff, D. O. (2008). Overview of factors contributing to the pathophysiology of progressive renal disease. *Kidney Int.* 74, 860–866. doi:10.1038/ki.2008.351

Seccia, T. M., Maniero, C., Belloni, A. S., Guidolin, D., Pothen, P., Pessina, A. C., et al. (2008). Role of angiotensin II, endothelin-1 and L-type calcium channel in the development of glomerular, tubulointerstitial and perivascular fibrosis. *J. Hypertens.* 26, 2022–2029. doi:10.1097/HJH.0b013e328309f00a

Sharma, N. M., Haibara, A. S., Katsurada, K., Liu, X., and Patel, K. P. (2020). Central angiotensin II-Protein inhibitor of neuronal nitric oxide synthase (PIN) axis contribute to neurogenic hypertension. *Nitric Oxide* 94, 54–62. doi:10.1016/j.niox.2019.10.007

Shi, S., Lei, S., Tang, C., Wang, K., and Xia, Z. (2019). Melatonin attenuates acute kidney ischemia/reperfusion injury in diabetic rats by activation of the SIRT1/Nrf2/HO-1 signaling pathway. *Biosci. Rep.* 39, BSR20181614. doi:10.1042/BSR20181614

Shirazi, M., Noorafshan, A., Bahri, M. A., and Tanideh, N. (2007). Captopril reduces interstitial renal fibrosis and preserves more normal renal tubules in neonatal dogs with partial urethral obstruction: A preliminary study. *Urol. Int.* 78, 173–177. doi:10.1159/000098078

Shirazi, M., Soltani, M.-R., Jahanabadi, Z., Abdollahifar, M.-A., Tanideh, N., and Noorafshan, A. (2014). Stereological comparison of the effects of pentoxifylline, captopril, simvastatin, and tamoxifen on kidney and bladder structure after partial urethral obstruction in rats. *Korean J. Urol.* 55, 756–763. doi:10.4111/kju.2014.55.11.756

Silver, F. H., Horvath, I., and Foran, D. J. (2001). Viscoelasticity of the vessel wall: The role of collagen and elastic fibers. *Crit. Rev. Biomed. Eng.* 29, 279–301. doi:10.1615/critrevbiomedeng.v29.i3.10

Simko, F., Hrenak, J., Dominguez-Rodriguez, A., and Reiter, R. J. (2020). Melatonin as a putative protection against myocardial injury in COVID-19 infection. *Expert Rev. Clin. Pharmacol.* 13, 921–924. doi:10.1080/17512433.2020.1814141

Simko, F., and Paulis, L. (2013). Antifibrotic effect of melatonin--perspective protection in hypertensive heart disease. *Int. J. Cardiol.* 168, 2876–2877. doi:10.1016/j.ijcard.2013.03.139

Simko, F., and Paulis, L. (2007). Melatonin as a potential antihypertensive treatment. *J. Pineal Res.* 42, 319–322. doi:10.1111/j.1600-079X.2007.00436.x

Simko, F., Pechanova, O., Pelouch, V., Krajcirovicova, K., Celec, P., Palffy, R., et al. (2010). Continuous light and L-NAME-induced left ventricular remodelling: Different protection with melatonin and captopril. *J. Hypertens.* 28 (1), S13–S18. doi:10.1097/01.hjh.0000388489.28213.08

Simko, F., Pechanova, O., Pelouch, V., Krajcirovicova, K., Mullerova, M., Bednarova, K., et al. (2009). Effect of melatonin, captopril, spironolactone and simvastatin on blood pressure and left ventricular remodelling in spontaneously hypertensive rats. *J. Hypertens. Suppl.* 27, S5–S10. doi:10.1097/01.hjh.0000358830.95439.e8

Simko, F., and Pechanova, O. (2009). Potential roles of melatonin and chronotherapy among the new trends in hypertension treatment. *J. Pineal Res.* 47, 127–133. doi:10.1111/j.1600-079X.2009.00697.x

Simko, F., Pechanova, O., Repova Bednarova, K., Krajcirovicova, K., Celec, P., Kamodyova, N., et al. (2014). Hypertension and cardiovascular remodelling in rats exposed to continuous light: Protection by ACE-inhibition and melatonin. *Mediat. Inflamm.* 2014, 703175. doi:10.1155/2014/703175

Simko, F., Pechanova, O., Repova, K., Aziriova, S., Krajcirovicova, K., Celec, P., et al. (2017). Lactacystin-induced model of hypertension in rats: Effects of melatonin and captopril. *Int. J. Mol. Sci.* 18, E1612. doi:10.3390/ijms18081612

Simko, F., Reiter, R. J., and Paulis, L. (2019). Melatonin as a rational alternative in the conservative treatment of resistant hypertension. *Hypertens. Res.* 42, 1828–1831. doi:10.1038/s41440-019-0318-3

Sonoda, K., Ohtake, K., Uchida, H., Ito, J., Uchida, M., Natsume, H., et al. (2017). Dietary nitrite supplementation attenuates cardiac remodeling in l-NAME-induced hypertensive rats. *Nitric Oxide* 67, 1–9. doi:10.1016/j.niox.2017.04.009

Sopakayang, R., De Vita, R., Kwansa, A., and Freeman, J. W. (2012). Elastic and viscoelastic properties of a type I collagen fiber. *J. Theor. Biol.* 293, 197–205. doi:10.1016/j.jtbi.2011.10.018

Stanko, P., Baka, T., Repova, K., Aziriova, S., Krajcirovicova, K., Barta, A., et al. (2020). Ivabradine ameliorates kidney fibrosis in L-NAME-induced hypertension. *Front. Med.* 7, 325. doi:10.3389/fmed.2020.00325

Tang, M., Li, J., Huang, W., Su, H., Liang, Q., Tian, Z., et al. (2010). Proteasome functional insufficiency activates the calcineurin-NFAT pathway in cardiomyocytes and promotes maladaptive remodelling of stressed mouse hearts. *Cardiovasc. Res.* 88, 424–433. doi:10.1093/cvr/cvq217

Tobeiha, M., Jafari, A., Fadaei, S., Mirazimi, S. M. A., Dashti, F., Amiri, A., et al. (2022). Evidence for the benefits of melatonin in cardiovascular disease. *Front. Cardiovasc. Med.* 9. doi:10.3389/fcvm.2022.888319

Vrankova, S., Parohova, J., Barta, A., Janega, P., Simko, F., and Pechanova, O. (2010). Effect of nuclear factor kappa B inhibition on L-NAME-induced hypertension and cardiovascular remodelling. *J. Hypertens.* 28 (1), S45–S49. doi:10.1097/01.hjh.0000388494.58707.0f

Wang, H., Gao, M., Li, J., Sun, J., Wu, R., Han, D., et al. (2019). MMP-9-positive neutrophils are essential for establishing profibrotic microenvironment in the obstructed kidney of UUO mice. *Acta Physiol.* 227, e13317. doi:10.1111/apha.13317

Wang, Z., Dong, H., Li, M., and Liang, X.-B. (2022). Ubiquitin-conjugating enzyme UBE2Q2 participates in HUWE1-mediated protection on renal tubulointerstitial fibrosis. *Sheng Li Xue Bao* 74, 117–124.

Willis, M. S., Schisler, J. C., Li, L., Rodríguez, J. E., Hilliard, E. G., Charles, P. C., et al. (2009). Cardiac muscle ring finger-1 increases susceptibility to heart failure *in vivo*. *Circ. Res.* 105, 80–88. doi:10.1161/CIRCRESAHA.109.194928

Yoon, Y. M., Go, G., Yun, C. W., Lim, J. H., Lee, J. H., and Lee, S. H. (2020). Melatonin suppresses renal cortical fibrosis by inhibiting cytoskeleton reorganization and mitochondrial dysfunction through regulation of miR-4516. *Int. J. Mol. Sci.* 21, E5323. doi:10.3390/ijms21155323

Zhang, Y., Zhang, L., Fan, X., Yang, W., Yu, B., Kou, J., et al. (2019). Captopril attenuates TAC-induced heart failure via inhibiting Wnt3a/β-catenin and Jak2/Stat3 pathways. *Biomed. Pharmacother.* 113, 108780. doi:10.1016/j.biopha.2019.108780

Zhao, M., Zheng, S., Yang, J., Wu, Y., Ren, Y., Kong, X., et al. (2015). Suppression of TGF-β1/Smad signaling pathway by sesamin contributes to the attenuation of myocardial fibrosis in spontaneously hypertensive rats. *PLoS One* 10, e0121312. doi:10.1371/journal.pone.0121312

frontiers | Frontiers in Pharmacology

TYPE Original Research
PUBLISHED 30 September 2022
DOI 10.3389/fphar.2022.928834

Check for updates

OPEN ACCESS

EDITED BY
Panpan Hao,
Shandong University, China

REVIEWED BY
Leigh M. Marsh,
Ludwig Boltzmann Institute for Lung Vascular Research, Austria
Roberto V. Reyes,
University of Chile, Chile

*CORRESPONDENCE
Haiyang Tang,
tanghy2008@yahoo.com
Ying Han,
yhancn@njmu.edu.cn

†These authors contributed equally to this work.

SPECIALTY SECTION
This article was submitted to Experimental Pharmacology and Drug Discovery, a section of the journal Frontiers in Pharmacology

RECEIVED 26 April 2022
ACCEPTED 17 August 2022
PUBLISHED 30 September 2022

CITATION
Wang X, Chen A, Hu R, Zhang F, Liang S, Bao C, Liu X, Tang H and Han Y (2022), Salusin-β, a TOR2A gene product, promotes proliferation, migration, fibrosis, and calcification of smooth muscle cells and accelerates the imbalance of vasomotor function and vascular remodeling in monocrotaline-induced pulmonary hypertensive rats. *Front. Pharmacol.* 13:928834. doi: 10.3389/fphar.2022.928834

COPYRIGHT
© 2022 Wang, Chen, Hu, Zhang, Liang, Bao, Liu, Tang and Han. This is an open-access article distributed under the terms of the Creative Commons Attribution License (CC BY). The use, distribution or reproduction in other forums is permitted, provided the original author(s) and the copyright owner(s) are credited and that the original publication in this journal is cited, in accordance with accepted academic practice. No use, distribution or reproduction is permitted which does not comply with these terms.

Salusin-β, a TOR2A gene product, promotes proliferation, migration, fibrosis, and calcification of smooth muscle cells and accelerates the imbalance of vasomotor function and vascular remodeling in monocrotaline-induced pulmonary hypertensive rats

Xingxing Wang[1†], Aidong Chen[1†], Ruihua Hu[1], Feng Zhang[1], Shuxin Liang[2], Changlei Bao[2,3], Xuanxuan Liu[4], Haiyang Tang[2*] and Ying Han[1*]

[1]Key Laboratory of Targeted Intervention of Cardiovascular Disease, Collaborative Innovation Center for Cardiovascular Disease Translational Medicine, and Department of Physiology, Nanjing Medical University, Nanjing, Jiangsu, China, [2]State Key Laboratory of Respiratory Disease, National Clinical Research Center for Respiratory Disease, Guangzhou Institute of Respiratory Health, The First Affiliated Hospital of Guangzhou Medical University, Guangzhou, Guangdong, China, [3]College of Veterinary Medicine, Northwest A&F University, Yangling, China, [4]Department of Physiology, Kangda College of Nanjing Medical University, Lianyungang, Jiangsu, China

Purpose: The hyper-proliferation, promoted migration, fibrosis, and calcification of pulmonary arterial smooth muscle cells (PASMCs) play critical roles in pulmonary artery (PA) continuous contraction and vascular remodeling, leading to elevated pulmonary arterial resistance and pulmonary hypertension (PH). In this study, we sought to ascertain the effects of a TOR2A gene product, salusin-β, on PASMCs' proliferation, migration, fibrosis, calcification, and the imbalance of vasomotor function as well as pulmonary vascular remodeling in monocrotaline (MCT)-induced PH rats and their underlying mechanisms.

Methods: Knockdown or overexpression of salusin-β in rats or PASMCs was performed through tail vein injection or cell transfection of virus. The right ventricular systolic pressure (RVSP) of the rat was measured by right ventricle catheterization. Sodium nitroprusside (SNP) or acetylcholine (ACh)-induced dose-dependent relaxation was used to evaluate the vasodilatation function. Primary PASMCs were isolated from the PAs of control and PH rats.

Results: The salusin-β protein expressions were significantly increased in PAs and PASMCs isolated from PH rats compared with control rats. Knockdown of salusin-β in rats decreased high K^+ solution-induced contraction, RVSP and RV hypertrophy index, improved SNP or ACh-induced vascular relaxation of PAs,

and relieved vascular remodeling and calcification of PAs from PH rats. Silencing salusin-β in PASMCs isolated from PH rats alleviated the proliferation, migration, fibrosis, and calcification, as well as the NAD(P)H oxidase activity and reactive oxygen species (ROS) level. Overexpression of salusin-β exerted the opposite effects on vasomotor function and vascular remodeling, and PASMCs proliferation, migration, fibrosis and calcification.

Conclusion: Increased salusin-β activity in PAs from PH rats contributes to PASMCs proliferation, migration, fibrosis, and calcification, leading to the imbalance of vascular contraction and relaxation and vascular remodeling through stimulating the production of NAD(P)H oxidase derived ROS.

KEYWORDS

pulmonary artrial smooth muscle cells, pulmonary hypertension, vasomotor function, reactive oxygen species, vascular remodeling

Introduction

Pulmonary hypertension (PH) is characterized by persistent increases in mean pulmonary arterial pressure (mPAP) and right ventricular systolic pressure (RVSP), which eventually lead to right heart failure with shortness of breath and syncope (Southgate et al., 2020). In the past decade, the death rate of PH has remained at a high level, increasing by 2.5% per year for women and 0.9% for men (Benza et al., 2012). Attenuated relaxation and continuous contraction of pulmonary arteries (PAs), sustained media hyperplasia and fibrosis, and increased wall stiffness lead to the decrease of lumen diameter and even occlusion of PAs, resulting in increases in pulmonary arterial resistance (PAR) and mPAP in PH (Pan et al., 2017; Zabini et al., 2018; Sommer et al., 2021). Pulmonary arterial smooth muscle cells (PASMCs) isolated from patients or animal models with PH exhibit a phenotypic switch from a differentiated state to a dedifferentiated/proliferative state. The structural and functional properties changes of PASMCs due to phenotypic switch are major causes for continuous contraction, increased media thickness (Murray et al., 1990; Brozovich et al., 2016), and migration, fibrosis, and calcification, which vitally decrease vessel elasticity and increase the stiffness of PAs in PH (Humbert et al., 2019; Sommer et al., 2021). However, at present, clinical therapy for PH mainly relies on vasodilators or anticoagulants. Established pharmacological therapies for PH rarely prevent or reverse pulmonary arterial wall thickening, stiffening, and hypercontractility (Gerthoffer, 2020). Therefore, it is important to determine the pathological mechanism of PH during continuous contraction and vascular remodeling for clinical therapy.

Through alternative splicing and RNA rearrangement, the torsin family two member A gene (TOR2A) productions include salusin-α and salusin-β, which both can be found in human plasma and urine (Suzuki et al., 2007). They are a class of vascular active peptides, and compared to salusin-α, salusin-β is more related with cardiovascular diseases and abundantly expressed in many organs and tissues including heart, brain, and kidneys, especially in the blood vessels (Suzuki et al., 2007). Recent studies have identified that salusin-β contributes to various diseases including atherosclerosis, hypertension, diabetes and metabolic syndrome (Watanabe et al., 2008). Salusin-β has also been reported to be involved in the regulation of proliferation, migration, fibrosis, and calcification of normal vascular smooth muscle cells (VSMCs) (Sun et al., 2015; Sun et al., 2019). Increased salusin-β expression contributed to vascular inflammation associated with pulmonary arterial hypertension in rats (Xu et al., 2016). However, whether salusin-β is associated with increased vascular tension and regulating the proliferation, migration, fibrosis, and calcification of PASMCs in PH, and its down-steam mechanisms remain unclear.

Therefore using monocrotaline (MCT)-induced PH rat model and derived PASMCs with salusin-β knockdown or overexpression, we evaluated the roles of salusin-β in regulating the proliferation, migration, fibrosis, and calcification of PASMCs, and the roles of it in regulating the imbalance of vasomotor function, vascular remodeling, and the development and progression of pulmonary hypertension, as well as its down-steam mechanisms.

Materials and methods

Animals

Male Sprague-Dawley rats were fed in the animal facility, which has controlled temperature and humidity in an automatic 12 h light/dark cycle. Rats were provided with standard chow and tap water *ad libitum*. Animal experiments were carried out according to the procedures approved by the Nanjing Medical University Experimental Animal Care committee and complied with the Guide for the Care and Use of Laboratory Animals published by the US National Institutes of Health (NIH publication, 8th edition, 2011).

Model of pulmonary hypertension

A single subcutaneous injection of MCT (60 mg/kg) was administered to male rats (200–250 g) to induce PH. Control rats were injected with vehicle (saline). Three weeks after MCT injection, animals were assessed for right ventricular pressure, vascular remodeling, and right ventricular hypertrophy (RVH).

Knockdown or overexpression of salusin-β in rats or pulmonary arterial smooth muscle cells

PH and control rats were injected with recombinant adeno-associated virus serotype 9 (AAV9) carrying the rat salusin-β short hairpin small–interfering RNA (shRNA, 3.69×10^{12} vg/ml, Shanghai Genechem Co., China) and scrambled *via* tail vein to knockdown salusin-β as previously reported (Ren et al., 2017). The AAV9 vectors encoding salusin-β (2.13×10^{12} vg/ml, constructed by Shanghai Genechem Co., China) were injected to overexpress the salusin-β gene in rats. The empty vectors were used as the negative control. To determine the validity of AAV9, after 2 weeks, expression level of salusin-β in the PAs of rats was measured using western blot. Knockdown or overexpression of salusin-β in PASMCs was performed by adenovirus infection (100MOI).

Hemodynamic measurements and evaluation of right ventricular hypertrophy

The rats were weighed and anaesthetized with an intraperitoneal injection of urethane (800 mg/kg). RVP was measured by a catheter connected with a pressure transducer and positioned in the right ventricle (RV) from the right jugular vein as previously described (Tang et al., 2016). The signal from the pressure transducer was recorded using a four-channel bridge amplifier (QUAD bridge, ADInstruments, Australia) and the PoweLab data analysis and processing system (8SP type, ADInstruments, Australia), and the right ventricular systolic pressure (RVSP) was calculated. After measuring the RVSP, the lung and heart of a rat were isolated, the RV, left ventricle (LV), and interventricular septum (S) were separated and weighted. Right ventricular hypertrophy (RVH) index was defined as the ratio of RV weight to the LV plus S weight [(RV/LV+S)].

Histopathology assessment

Lungs were isolated from rats, fixed in 4% paraformaldehyde, embedded in paraffin, sectioned at 4 μm thick and mounted onto slides. Every slide from different groups was made at same place of lung of rats. Subsequently, the slides were stained with hematoxylin and eosin (H&E), Masson, or von Kossa, and were observed under a light microscope form or photometric assay for PAs wall thickness, lumen diameter, vascular fibrosis, or vascular calcium deposition of PAs, respectively. The PAs wall thickness, lumen diameter, and collagen volume fraction (%) were measured by Image-Pro Plus 6.0 software. The statistics of collagen volume fraction (%), which is equal to the ratio of blue collagen deposition area/total cross-sectional area of blood vessels (%), were used to show the vascular fibrosis quantitatively. The statistics of the amount of calcificated distal PAs/the total amount of distal PAs (%) in one slide were used to show the ratio of calcificated PAs.

Isometric tension measurements

The tertiary-branch PAs rings (2 mm long) were isolated from rats and were superfused in Krebs-Henseleit solution [the composition was described in a previous report (Zhang et al., 2019)]. Then the PA ring was mounted to the jaw in a four-chambered myograph (620M, DMT, Denmark). In one rat, only one PA ring was used to test the tension response to one drug or one treatment factor. The resting tension was set at 0.1 g. After equilibration, arterial rings were stimulated with the high K^+ solution [the composition was described as previous reported (Zhang et al., 2019)] to evaluate contractile function. Sodium nitroprusside (SNP) is a nitric oxide (NO) donor which can cause the relaxation of vascular smooth muscle directly. SNP administration to PAs in a dose-dependent manner (10^{-9}~10^{-4} mol/L) after the prostaglandin F2α (PGF 2α) (1–5 μmol/L) induced pre-contraction was performed to evaluate PASMCs relaxing function. Acetylcholine (ACh) stimulates the release of NO in vascular endothelial cells, causing endothelium-dependent relaxation. ACh (10^{-9}~10^{-4} mol/L) administration in a dose-dependent manner after PGF 2α was also performed to evaluate vascular endothelium-dependent relaxation. The degree of relaxation is shown as a percentage of PGF 2α-induced contraction.

Culture of primary pulmonary arterial smooth muscle cells

PASMCs were isolated from the media of the PAs of control and PH rats, as previously reported (Sun et al., 2016b). After the perivascular adipose tissues and adventitia of the PAs were stripped off with forceps, the endothelium was carefully removed using a cotton swab. The tissues were minced and incubated with type I collagenase for digestion until the shape of the tissues disappeared and then centrifuged to isolate the cells. The isolated primary PASMCs were cultured in DMEM

containing 15% fetal bovine serum (FBS), penicillin (100 IU/ml), and streptomycin (10 mg/ml) (Gibco, Grand Island, NY, United States) at 37°C in an incubator with 5% CO_2 for 5 days. The PASMCs were identified by their substantial smooth muscle-specific α-actin (α-SMA) expression (a marker of VSMCs) without detectable vimentin (a marker of fibroblasts) and platelet endothelial cell adhesion molecule (PECAM)-1 (a marker of endothelial cells) expressions. The overall cell experiments were performed with the second to fifth passage of PASMCs. The same cell passage for each experiment was chosen individually.

CCK8 test

The proliferation of PASMCs was determined using the CCK8 test. First, PASMCs were seeded in the 96-well plate and the absorbance value was detected with a microplate reader at a wavelength of 450 nm. PASMCs were then subjected to virus infection for 24 h and 48 h. The absorbance values were again measured.

Wound-healing assay

Migration of PASMCs was assessed using a wound-healing assay as previously reported (Sun et al., 2016b). Briefly, PASMCs were plated into a 6-well plate and cultured to reach confluence. Then, cells were scratched to form a gap using a standard 200 μl pipette tip and were washed with PBS to remove the detached cells. Subsequently, the cells were incubated for 36 h with fresh medium and were observed at 0 and 36 h under an inverted microscope (Axio Vert. A1, Zeiss, Oberkochen, Germany).

Boyden chamber assay

PASMCs were seeded into FBS-free medium in the upper chamber of a 24-well transwell with an 8 μm pore size (Millipore, United States). The lower chamber was added with a complete medium containing 15% FBS. After being incubated for 24 h, cells on the upper surface of each filter were removed with a cotton swab and migrated cells on the lower surface were stained with crystal violet. Stained cells were counted in five random fields.

Western blot analysis

The salusin-β protein expression in PAs was detected by western blot as described in our previous reports (Wu et al., 2020). First, lysis buffer was used to extract protein samples and the BCA protein assay kit (BCA, Pierce, United States) was used to detect the protein concentration. Equal amounts of protein samples were added to an SDS-PAGE gel for electrophoresis and then transferred to a polyvinylidene fluoride (PVDF) membrane. The membranes were blocked in 5% skim milk at room temperature for 2 h and were incubated overnight at 4°C with anti-salusin-β IgG (1:1000, Clound-Clone Corp, United States), proliferating cell nuclear antigen (PCNA) antibody (1:2000, Abcam, United States), β-actin antibody (1:5000, Abways Technology Inc., Shanghai, China) or GAPDH antibody (1: 10000, Proteintech, China) followed by incubation with horseradish peroxidase-conjugated goat anti-rabbit IgG (1: 5000, Immunology Consultants Lab, Portland, OR, United States). Bands were detected with an enhanced chemiluminescence ECL system (Pierce Chemical, Rockford, IL, United States). The expression levels of salusin-β or PCNA proteins were normalized to those of GAPDH or β-actin protein, respectively.

TABLE 1 Primer pairs used in this study.

		Primer sequence (5′–3′)
Collagen I	Forward	TGGTGGTTATGACTTTGGTTACGAT
	Reverse	TGTGCGAGCTGGGTTCTTTCTA
Collagen III	Forward	CTCCTGCAGGCTAGAGAAGC
	Reverse	GATGCACTTTTTGCCCTTCTT
CTGF	Forward	CAGGGAGTAAGGGACACGA
	Reverse	ACAGCAGTTAGGAACCCAGAT
TGF-β1	Forward	GCTCCACGGAGAAGAACTGCT
	Reverse	CTGCTCCACCTTGGGCTTGC
GAPDH	Forward	GGAAAGCTGTGGCGTGAT
	Reverse	AAGGTGGAAGAATGGGAGTT

Measurement of Collagen I, Collagen III, connective tissue growth factor, and tansforming growth factor-β1 mRNA level

The levels of collagen I, collagen III, connective tissue growth factor (CTGF), and tansforming growth factor-β1 (TGF-β1) in PASMCs were used to evaluate the degree of fibrosis as previous report (Sun et al., 2015) and were measured using qPCR. Briefly, RNA was extracted with RNA-easy Isolation Reagent (Nuo Wei Zan, Biotechnology, China) according to the manufacturer's protocol. PrimeScript® RT reagent kits (Takara, Otsu, Shiga, Japan) and an ABI PRISM 7500 sequence detection PCR system (Applied Biosystems, Foster City, CA, United States) were used for quantitative RT-PCR. Fold-change of RNA was calculated using the $2^{-\Delta\Delta Ct}$, normalized to GAPDH expression. The primer sequences used are shown in Table 1.

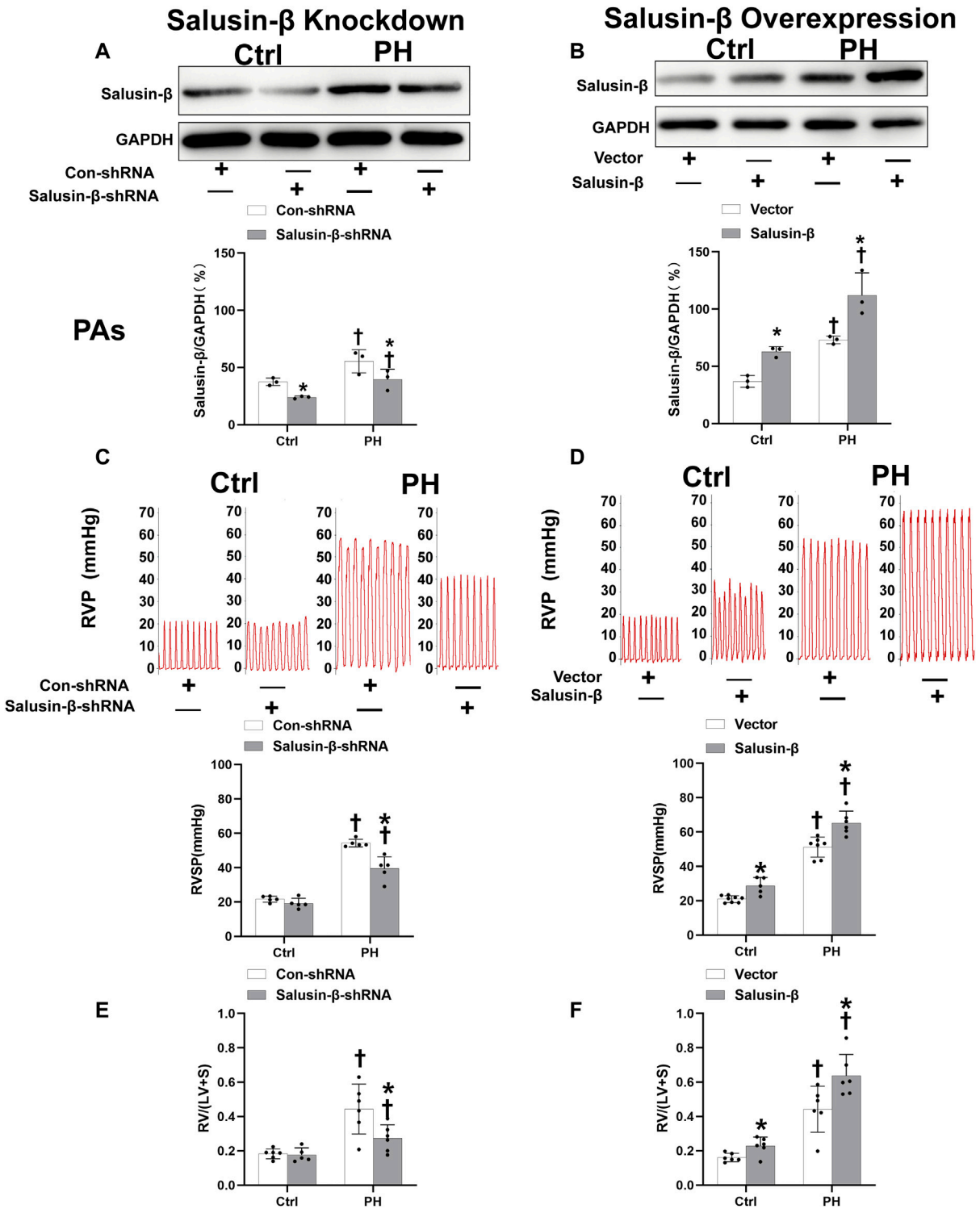


FIGURE 1
Effects of salusin-β knockdown on salusin-β protein expressions in PAs **(A)**, right ventricular pressure (RVP) and right ventricular systolic pressure (RVSP) **(C)**, and right ventricular hypertrophy index (RVHI) [RV/(LV + S)] **(E)**; as well as the effects of overexpression of salusin-β on its protein expressions in PAs **(B)**, RVP and RVSP **(D)**, and RVHI **(F)** in control and MCT-induced PH rats. Values are mean ± SE. *$p < 0.05$ compared with Con-shRNA or vector. †$p < 0.05$ compared with control (Ctrl) rats. n = 5–8 for each group.

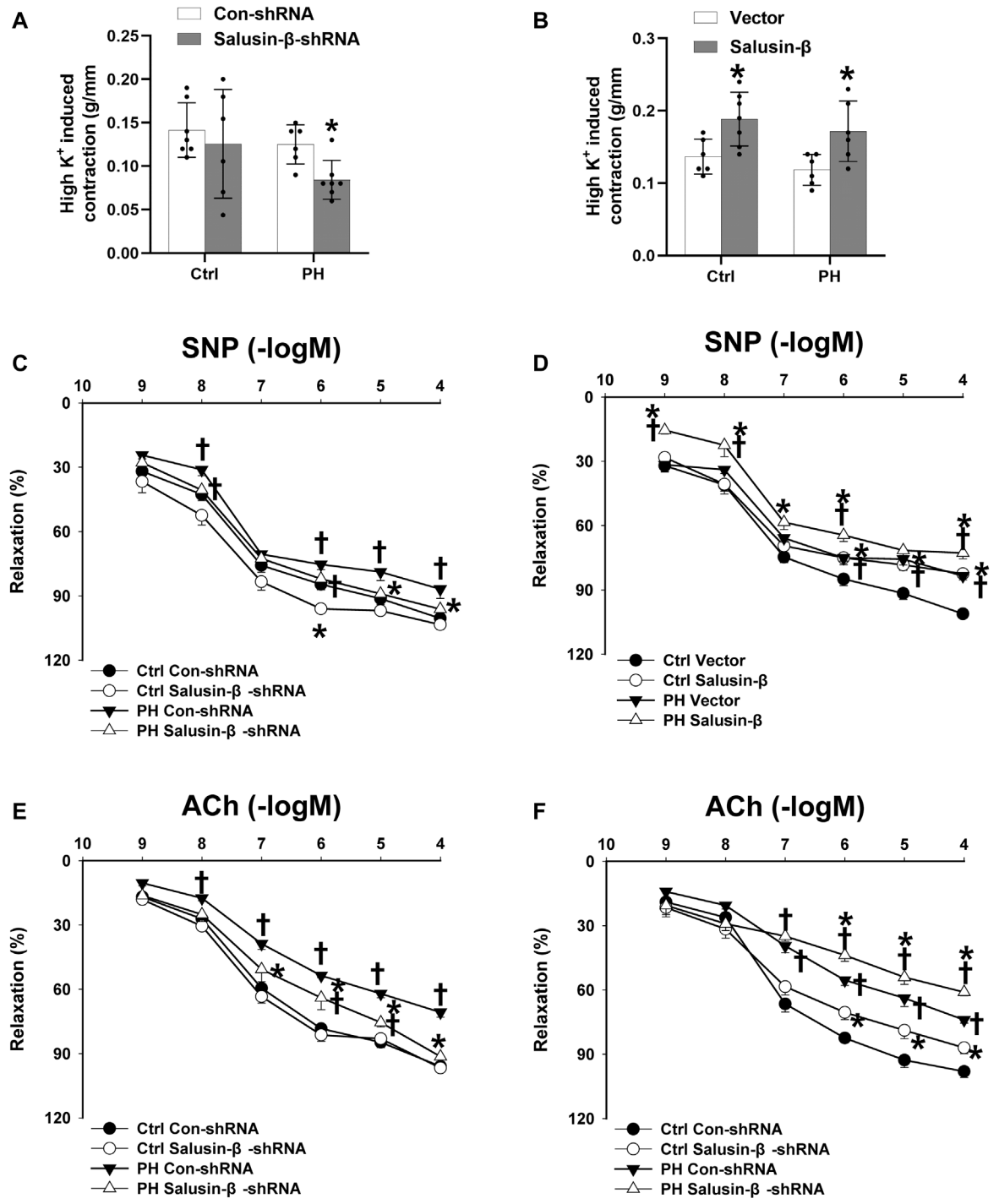


FIGURE 2
Effects of salusin-β knockdown on high K^+ solution-induced contraction **(A)**, sodium nitroprusside (SNP)-induced relaxation **(C)**, and acetylcholine (ACh)-induced relaxation of PAs **(E)**; as well as the effects of overexpression of salusin-β on high K+ solution-induced contraction **(B)**, SNP-induced relaxation **(D)**, and ACh-induced relaxation of PAs **(F)** in control and MCT-induced PH rats. Values are mean ± SE. *$p < 0.05$ compared with Con-shRNA or vector. †$p < 0.05$ compared with control (Ctrl) rats. n = 6–9 for each group.

Measurement of NAD(P)H oxidase activity and reactive oxygen species levels

To measure NAD(P)H oxidase activity and ROS levels, the enhanced lucigenin-derived chemiluminescence method was utilized, as we previously reported (Sun et al., 2016b; Lu et al., 2017). The dark-adapted lucigenin was added to PASMCs protein supernatants and reacted with the superoxide anions to induce the photon emission, which can be detected using a luminometer (Model 20/20n, Turner, CA, United States) for 1 time every 1 min until 10 times to represent the ROS level. To detect NAD(P)H oxidase activity, PASMCs protein supernatants were incubated with NAD(P)H (100 μM) to generate new superoxide anions before lucigenin application. The mean light unit (MLU) per minute per milligram of protein represents the values of ROS level and NAD(P)H oxidase activity.

Detection of alkaline phosphatase activity and calcium content

ALP activity was measured using an ALP assay kit (Nanjing Jiancheng Bioengineering Institute, Nanjing, China) according to the manufacturer's instructions as our previous reports (Zhou et al., 2013; Sun et al., 2019). The absorbance was determined at 520 nm, and the results were normalized to the protein content of each sample. Calcium content was measured using the o-cresolphthalein colorimetric method as previously described (Ma et al., 2016). The calcium levels in PASMCs samples were normalized to the protein content, as determined by the BCA method (Zhu et al., 2018).

Statistical analysis

Data are expressed as mean ± S.E. SPSS analysis software was used to perform statistical analysis. A comparison of means between two groups was performed using an unpaired Student's *t*-test. One-way or two-way ANOVA, followed by the Bonferroni test for post-hoc analysis, was performed when multiple comparisons were made. Statistical significance was set at $p < 0.05$.

Results

The salusin-β expressions in pulmonary arteries or pulmonary arterial smooth muscle cells in monocrotaline-induced PH and control rats

The protein expressions of salusin-β in both PAs (Figures 1A,B) and PASMCs (Figures 5A,B) of MCT-induced PH rats were higher than that in control rats. Knockdown of salusin-β gene in either rats or PASMCs decreased its expression, and overexpression of salusin-β significantly increased its expression, which confirmed the effectiveness of knockdown or overexpression of salusin-β in rats or PASMCs.

Effects of salusin-β knockdown or overexpression on RVSP, RVH index, high K^+ solution-induced contraction and SNP or ACh-induced relaxation of PAs

Compared to control rats, both the RVSP (Figures 1C,D) and RVH index (Figures 1E,F) of MCT-PH rats were significantly higher. There was no significant difference in high K^+ solution-induced PAs contraction between control and PH rats (Figures 2A,B), whereas both the SNP- and ACh-induced dose-dependent vasodilatation of PAs were significantly attenuated in PH rats (Figures 2C–F). Silencing of salusin-β gene in PH rats significantly decreased the RVSP (Figure 1C), RVH index (Figure 1E) and high K^+ solution-induced PAs contraction (Figure 2A), improved either SNP- (Figure 2C) or ACh-induced endothelium-independent vascular relaxation (Figure 2E), while overexpression of salusin-β worsened the above parameters in PH rats. It was worth noting that although knockdown of salusin-β had no significant roles in control rats, overexpression of salusin-β in control rats elevated the RVSP, RVH index, PAs contraction and attenuated SNP or ACh-induced PA relaxation (Figures 1D,F, 2B,D,F). The pEC50 and Rmax (%) data of SNP or ACh-induced dose-dependent vasodilatation of PAs in control and PH rats with different pretreatments were shown in Table 2, which suggested similar results.

Effects of salusin-β knockdown or overexpression on vascular remodeling of pulmonary arteries

From the representative H&E staining of lung tissues, we observed a significant increase in PA wall thickness and a decrease in lumen diameter, resulting in stenosis or even complete occlusion of PAs in MCT-PH rats compared to control rats (Figure 3A,B). The statistical graph also showed that the lumen diameter of PAs was decreased (Figure 3F), while media thickness (Figure 3E) and media thickness/lumen diameter of PAs (Figure 3G) in PH rats were significantly increased. Additionally, Masson staining of lung tissue images and statistical collagen volume fraction (%) showed severe vascular fibrosis of PAs in PH rats (Figures 3C,D,H). These results suggest the occurrence of vascular remodeling of PAs in PH rats. PAs from PH rats with salusin-β knockdown presented increased lumen diameter,

TABLE 2 pEC50 and Rmax (%) data of SNP or ACh-induced dose-dependent vasodilatation of PAs in Ctrl and PH rats with different pretreatments.

	Ctrl		PH	
	pEC50	Rmax	pEC50	Rmax
SNP				
Con-shRNA	7.59 ± 0.19	100.59 ± 2.22	7.43 ± 0.07	86.82 ± 4.33†
Salusin-β-shRNA	7.63 ± 0.12	103.60 ± 1.68	7.39 ± 0.12	96.17 ± 1.99*
Vector	7.36 ± 0.11	101.14 ± 0.60	7.31 ± 0.07	83.49 ± 1.84†
Salusin-β	7.43 ± 0.13	82.44 ± 2.13*	7.51 ± 0.19	73.63 ± 2.94*†
ACh				
Con-shRNA	7.17 ± 0.06	95.98 ± 1.49	6.98 ± 0.21	70.75 ± 2.26†
Salusin-β-shRNA	7.69 ± 0.15*	96.71 ± 1.21	6.84 ± 0.23†	91.38 ± 2.21*
Vector	7.17 ± 0.12	98.03 ± 2.89	6.79 ± 0.29	75.63 ± 0.73†
Salusin-β	7.61 ± 0.43	96.01 ± 0.96	6.27 ± 0.28†	63.34 ± 0.86*†

SNP, sodium nitroprusside; ACh, acetylcholine. Values are mean ± SE. *$p < 0.05$ vs. Con-shRNA or vector. $^{\dagger}p < 0.05$ vs. Ctrl. n = 6–9 for each group.

reduced media thickness, with a lower media thickness/lumen diameter ratio, and decreased vascular fibrosis, while salusin-β overexpression caused more severe vascular remodeling in PH rats (Figure 3).

Effects of salusin-β knockdown or overexpression on vascular calcification of pulmonary arteries

The representative Von Kossa staining of lung tissues and statistical data on the percentage of calcified PAs showed that PH rats had a certain degree of vascular calcification in the PAs (Figure 4). Knockdown of salusin-β decreased the degree of calcification and percentage of calcified PAs (Figures 4A,C), whereas the overexpression of salusin-β played the opposite role (Figures 4B,D) in MCT-PH rats. Furthermore, overexpression of salusin-β in control rats induced vascular calcification in the PAs (Figures 4B,D).

Effects of salusin-β knockdown or overexpression on pulmonary arterial smooth muscle cells proliferation

The results of CCK8 (Figures 5C,D) and elevated PCNA expression (Figures 5E,F) of PASMCs in PH rats showed that PASMC proliferation in PH rats was significantly increased compared to that in control rats. Salusin-β knockdown in PASMCs inhibited proliferation (Figures 5C,E), while overexpression of salusin-β further promoted the proliferation of PASMCs derived from PH rats (Figures 5D,F). In addition, the significant change was not found in silencing salusin-β in control rats, whereas enhanced PASMCs proliferation was observed in control rats with overexpression of salusin-β (Figure 5).

Effects of salusin-β knockdown or overexpression on pulmonary arterial smooth muscle cells migration

Boyden chamber assay (Figures 6A,B) and wound-healing assay results (Figures 6C,D) showed that PASMCs migration in PH rats was enhanced compared to that in control rats. Overexpression of salusin-β promoted the migration of PASMCs derived from both PH rats and control rats (Figures 6B,D), whereas knockdown of salusin-β only reduced the migration of PASMCs in PH rats (Figures 6A,C).

Effects of salusin-β knockdown or overexpression on pulmonary arterial smooth muscle cells fibrosis

The mRNA levels of collagen I (Figures 7A,B), collagen III (Figures 7C,D), CTGF (Figures 7E,F), and TGF-β1 (Figures 7G,H) in the PASMCs of control rats and MCT-PH rats were measured to evaluate the degree of fibrosis. The ΔCT values of each group were shown in Table 3.

We found that the mRNA levels of these fibrosis indices in PASMCs from MCT-PH rats were higher compared to those in control rats, which suggested that PASMC fibrosis was increased in PH. Knockdown of salusin-β attenuated, while the

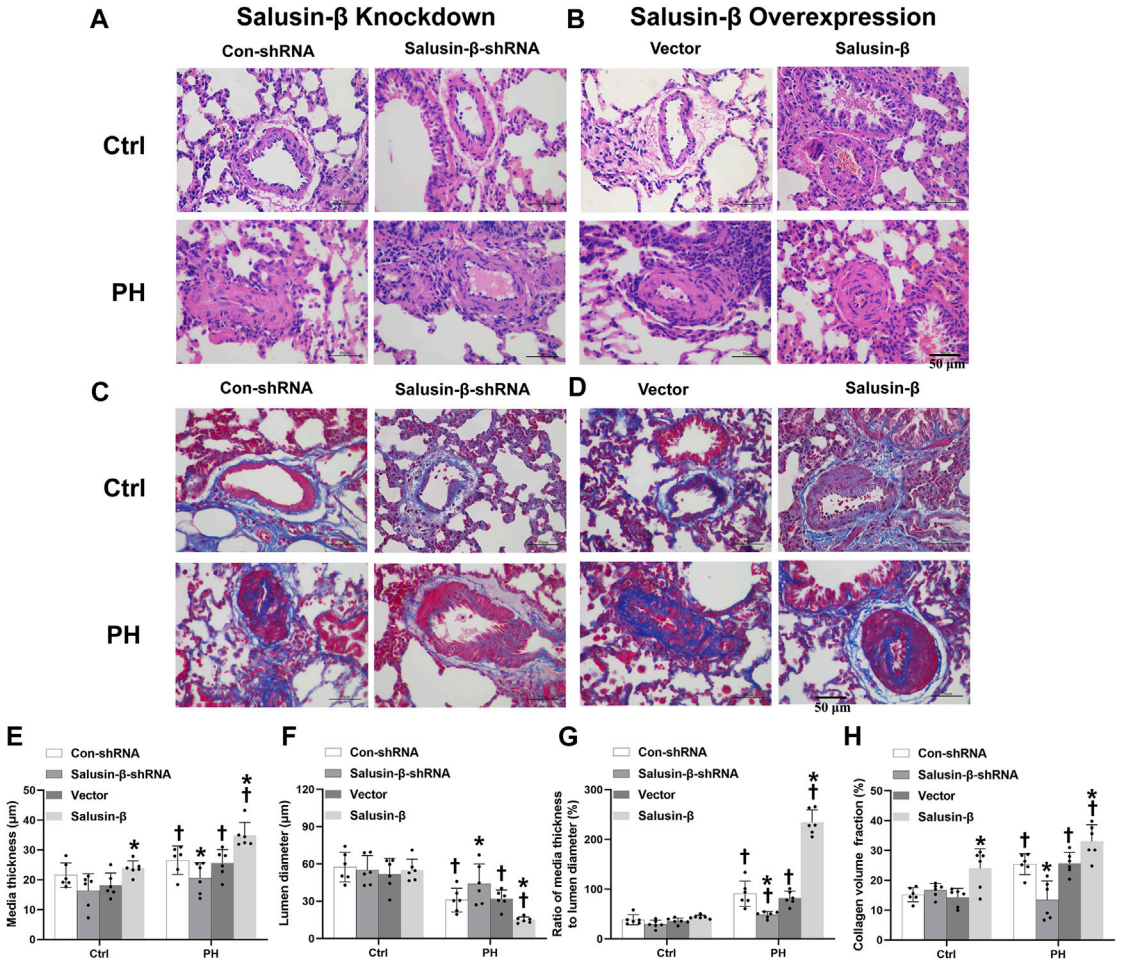


FIGURE 3
Representative images of lung tissue cross-sections with H and E staining **(A)** and Masson's staining (Blue indicates collagen deposition) **(C)** showing the effects of salusin-β knockdown on PAs vascular remodeling and fibrosis; lung tissue cross-sections with H and E staining **(B)** and Masson's staining **(D)** showing the effects of salusin-β overexpression on PAs vascular remodeling and fibrosis. The effects of salusin-β knockdown or overexpression on the media thickness **(E)**, lumen diameter **(F)**, media thickness/lumen diameter **(G)** and collagen volume fraction (%) **(H)** of PAs in control and MCT-induced PH rats. Values are mean ± SE. $^{*}p < 0.05$ compared with Con-shRNA or vector. $^{\dagger}p < 0.05$ compared with control (Ctrl) rats. $n = 6$ for each group.

overexpression of salusin-β enhanced the fibrosis of PASMCs from PH. Similarly, knockdown of salusin-β had no significant roles, while overexpression of salusin-β also elevated the PASMCs fibrosis index of control rats (Figure 7).

Effects of salusin-β knockdown or overexpression on pulmonary arterial smooth muscle cells calcification and oxidative stress

ALP activity is an indicator of calcification. Compared with PASMCs of control rats, both the ALP activity (Figures 8A,B) and calcium content (Figures 8C,D) in PASMCs of PH rats were higher, which indicated that the PH-PASMC calcification level was elevated. NAD(P)H oxidase activity (Figures 8E,F) and superoxide anions level (Figures 8G,H) in PASMCs of PH rats were also higher than those in PASMCs of control rats, suggesting the occurrence of oxidative stress. Silencing of salusin-β reversed the high ALP activity, calcium content, NAD(P)H oxidase activity, and superoxide anions level in PASMCs derived from PH rats, but had no significant effect on PASMCs from control rats. Overexpression of salusin-β increased the above indices of PASMCs derived from either PH rats or control rats (Figure 8).

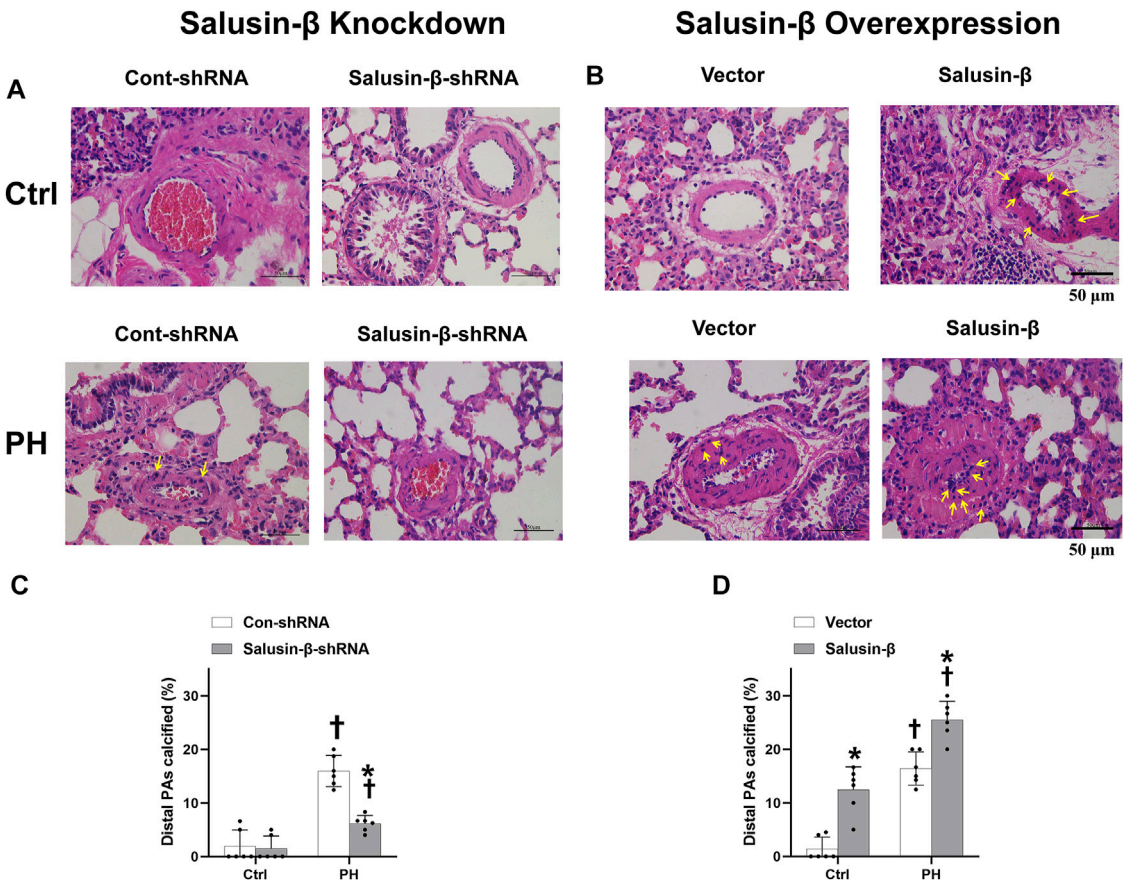


FIGURE 4
Representative images of lung tissue cross-sections with Von Kossa staining (The calcium deposits are black spots, with blue nuclei and a red background), in which the representative calcium deposits were indicated by yellow arrows **(A)** and statistical percentage of calcified PAs **(C)** showing the effects of salusin-β knockdown on vascular calcification in PAs; images of lung tissue cross-sections with Von Kossa staining **(B)** and percentage of calcified PAs **(D)** showing the effects of salusin-β overexpression on vascular calcification in PAs. Values are mean ± SE. *$p < 0.05$ compared with Con-shRNA or vector. †$p < 0.05$ compared with control (Ctrl) rats. $n = 6$ for each group.

Discussion

The proliferation, migration, fibrosis, and calcification of PASMCs are the major causes of vascular remodeling, which increases the media wall thickness and stiffness, narrows the blood vessel, and ultimately increases PAR and PAP in PH(Tang et al., 2015; Tang et al., 2016; Tanguay et al., 2019; Gerthoffer, 2020). Our previous studies reported that the TOR2A gene product, salusin-β, participates in the regulation of proliferation, migration, fibrosis, and calcification of normal VSMCs(Sun et al., 2015; Sun et al., 2019), as well as the regulation of vasoconstriction and vasodilatation function (Pan et al., 2021; Sun et al., 2021). Knockdown of salusin-β improves vascular relaxation, alleviates vascular remodeling, and decreases vasoconstriction in spontaneously hypertensive rats (Pan et al., 2021; Sun et al., 2021). However, whether salusin-β has similar effects in mediating morphology and function of PASMCs and vascular remodeling, as well as the vasoconstriction and vascular relaxation of PA in PH is still unclear. The present study found that the increased salusin-β activity of PAs in MCT-induced PH rats contributed to the proliferation, migration, fibrosis, and calcification of PASMCs, vascular remodeling, and the imbalance of vascular contraction and relaxation in MCT-induced PH through stimulating the production of NAD(P)H oxidase derived ROS. Reducing endogenous salusin-β levels by salusin-β gene knockdown decreased contractions of PAs, RVSP, and RV hypertrophy, improved the vascular relaxation and prevented the vascular remodeling in PH, while overexpression of salusin-β in rats or PASMCs deteriorates the symptom of PH, which provide a potential therapeutic target for PH.

The TOR2A gene product, salusin-β, is present in human plasma and urine and widely expressed in the lung (Suzuki et al., 2007), and is particularly abundant in vascular

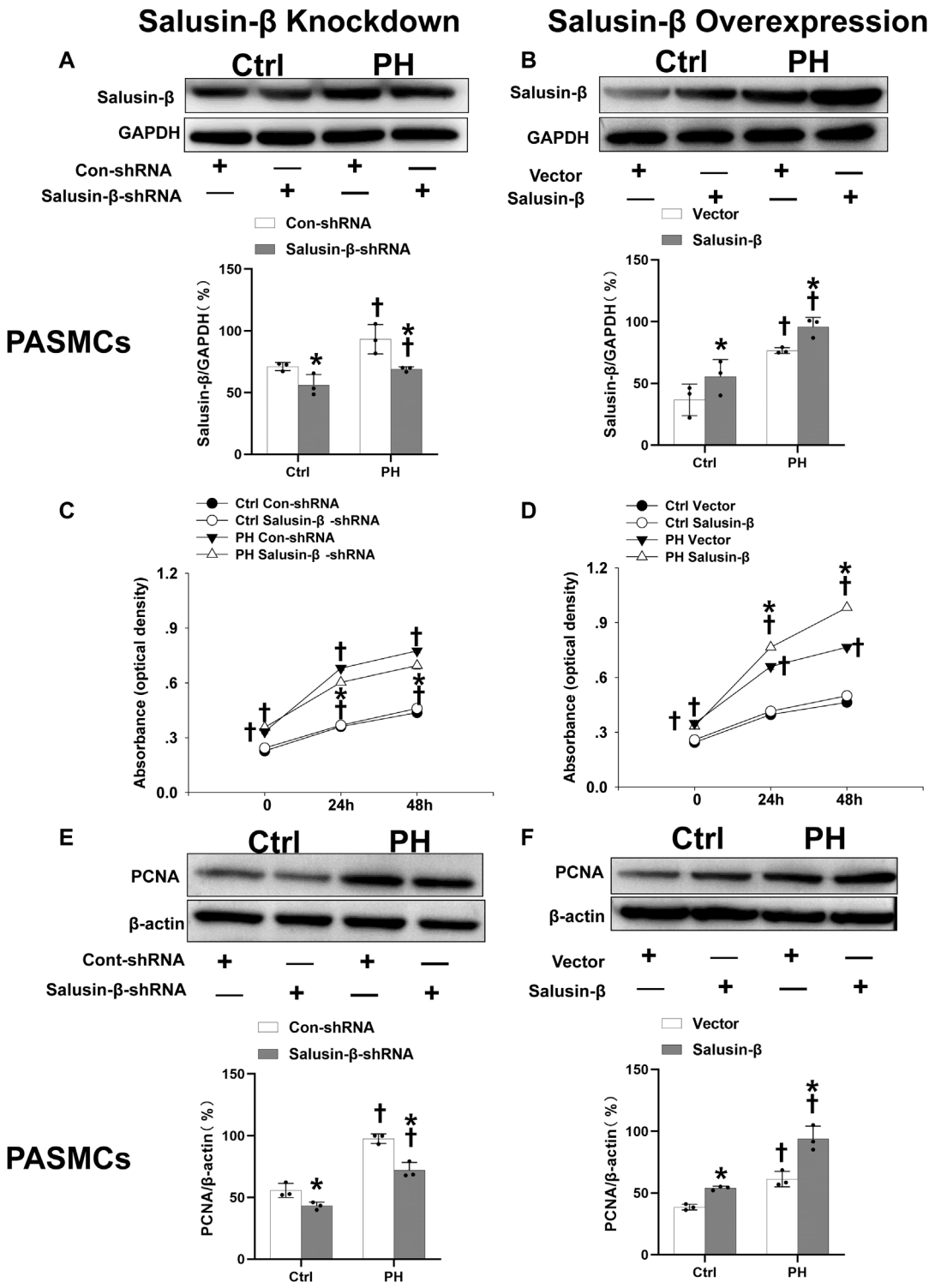


FIGURE 5
Effects of salusin-β knockdown on salusin-β protein expressions of PASMCs **(A)**, cell viability tested by CCK-8 assay **(C)** and protein expressions of proliferation marker proliferating cell nuclear antigen (PCNA) **(E)**; as well as the effects of overexpression of salusin-β on salusin-β protein expressions **(B)**, cell viability tested by CCK-8 assay **(D)** and proliferation marker PCNA protein expressions **(F)** in PASMCs isolated from control and MCT-induced PH rats. Values are mean ± SE. *$p < 0.05$ compared with Con-shRNA or vector. †$p < 0.05$ compared with control (Ctrl) rats. n = 3 for A, B, E, and F groups. n = 6 for C and D groups.

10.3389/fphar.2022.928834

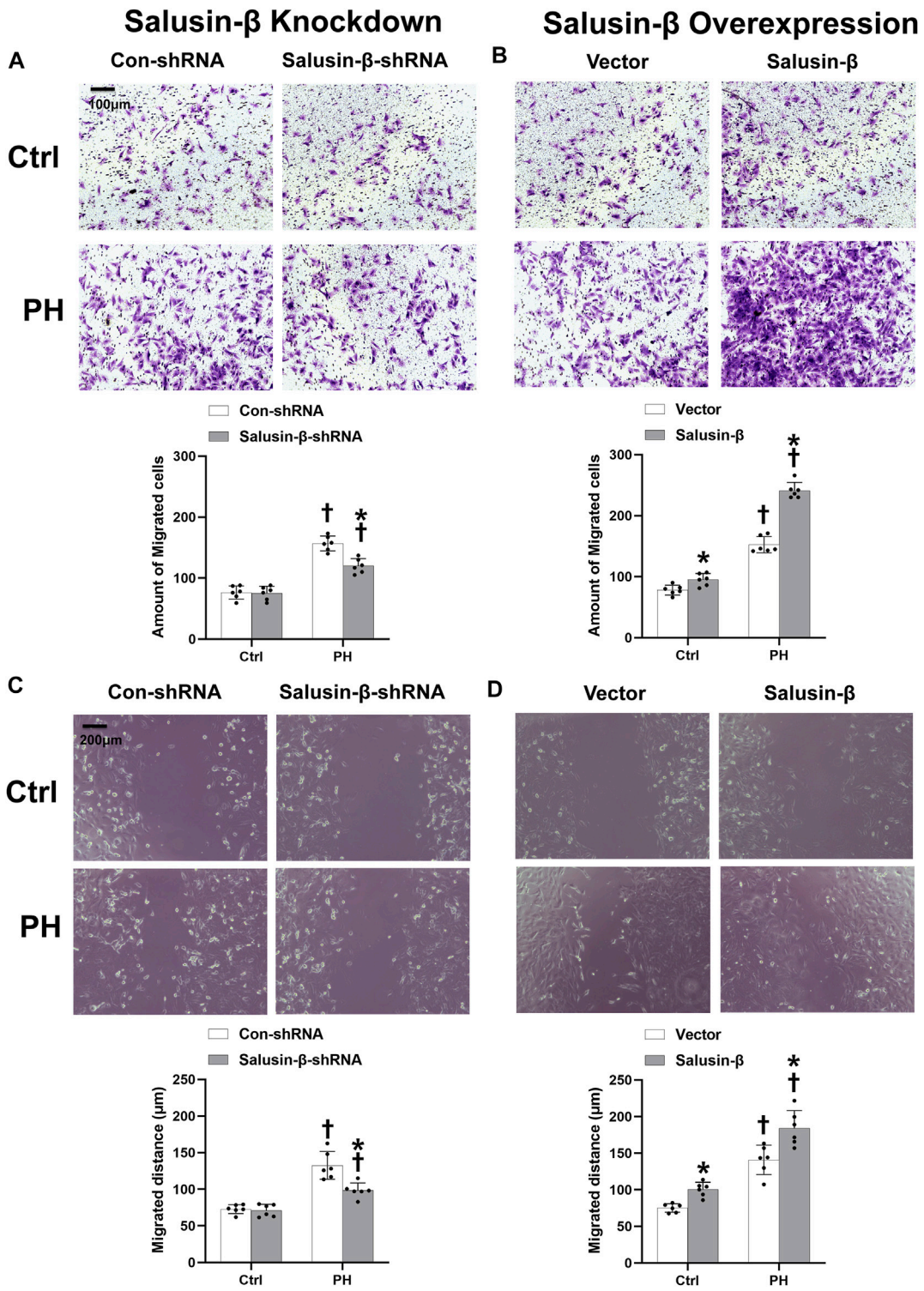


FIGURE 6
Effects of salusin-β knockdown on PASMCs migration evaluated by the boyden chamber assay **(A)** and a wound healing assay **(C)**; as well as the effects of overexpression of salusin-β on PASMCs migration evaluated by the boyden chamber assay **(B)** and a wound healing assay **(D)** in control and MCT-induced PH rats. Values are mean ± SE. *$p < 0.05$ compared with Con-shRNA or vector. †$p < 0.05$ compared with control (Ctrl) rats. $n = 6$ for each group.

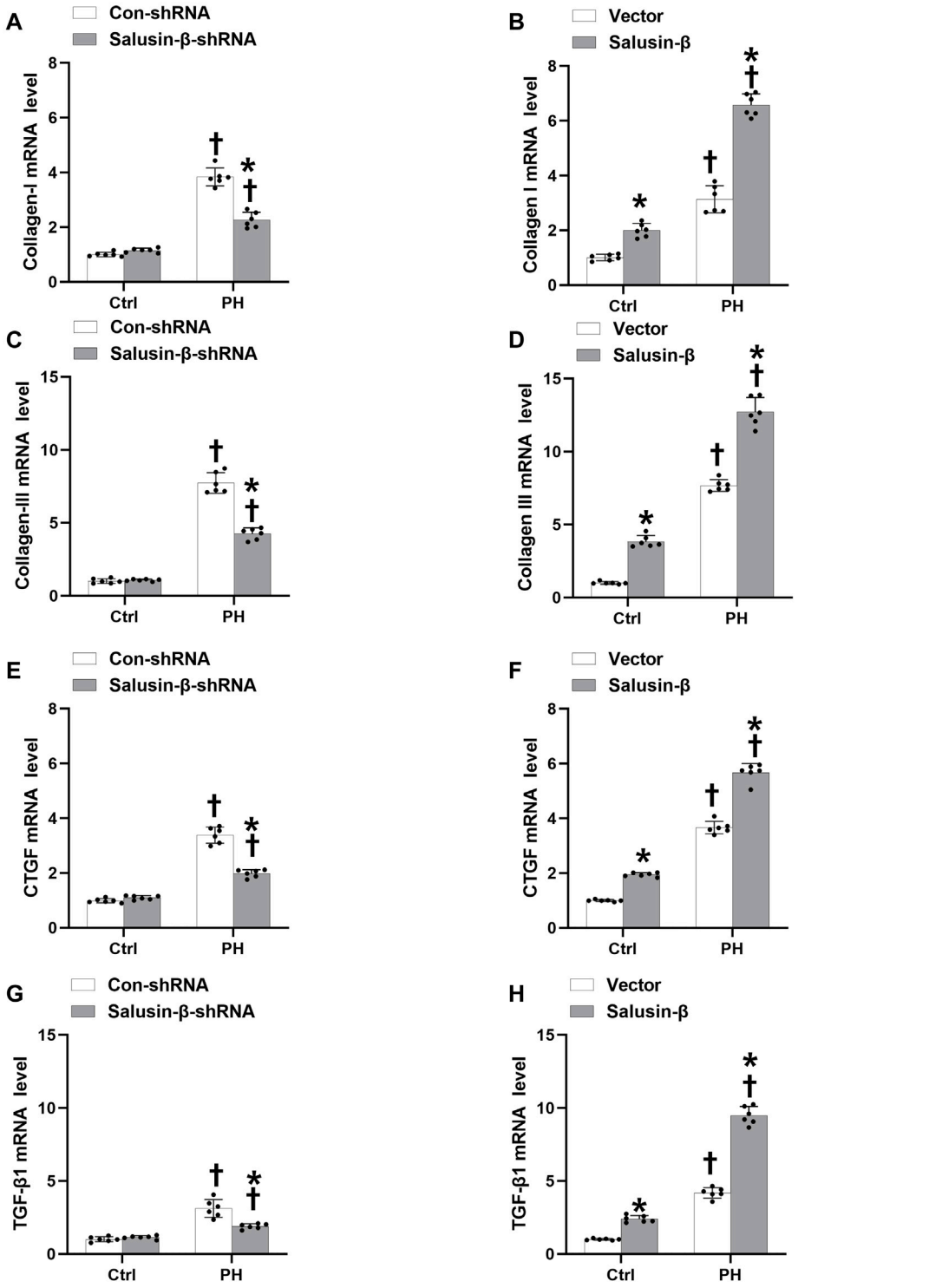


FIGURE 7
Effects of salusin-β knockdown on mRNA levels of fibrosis indexes of PASMCs: collagen I **(A)**, collagen III **(C)**, connective tissue growth factor (CTGF) **(E)** and transforming growth factor-β1 (TGF-β1) **(G)**; as well as the effects of overexpression of salusin-β on collagen I **(B)**, collagen III **(D)**, CTGF **(F)** and TGF-β1 **(H)** of PASMCs isolated from control and MCT-induced PH rats. Values are mean ± SE. *$p < 0.05$ compared with Con-shRNA or vector. †$p < 0.05$ compared with control (Ctrl) rats. $n = 6$ for each group.

TABLE 3 The ΔCT values for Collagen-I, Collagen-III, CTGF, and TGF-β1 during mRNA measurement using quantitative RT-PCR.

	Collagen-I		Collagen-III	
	Ctrl	PH	Ctrl	PH
Con-shRNA	5.53 ± 0.043	3.59 ± 0.05†	7.09 ± 0.09	4.14 ± 0.07†
Salusin-β-shRNA	5.33 ± 0.03	4.36 ± 0.06*†	6.99 ± 0.10	5.00 ± 0.09*†
Vector	5.52 ± 0.06	3.89 ± 0.05†	6.97 ± 0.05	4.03 ± 0.04†
Salusin-β	4.53 ± 0.08*	2.80 ± 0.04*†	5.03 ± 0.06	3.30 ± 0.07*†
	CTGF		**TGF-β1**	
	Ctrl	PH	Ctrl	PH
Con-shRNA	1.19 ± 0.04	−0.56 ± 0.06†	2.78 ± 0.09	1.17 ± 0.07†
Salusin-β-shRNA	1.05 ± 0.06	0.20 ± 0.02*†	2.59 ± 0.12	1.87 ± 0.09*†
Vector	1.09 ± 0.02	−0.78 ± 0.02†	2.50 ± 0.03	0.44 ± 0.04†
Salusin-β	1.03 ± 0.02*	−1.41 ± 0.04*†	1.24 ± 0.04*	−0.75 ± 0.03*†

Values are mean ± SE. *$p < 0.05$ vs. Con-shRNA or vector. $^{\dagger}p < 0.05$ vs. Ctrl. $n = 6$ for each group.

endothelial cells and VSMCs (Watanabe et al., 2008). We recently found that salusin-β participates in regulating the vascular constriction and relaxation function in spontaneously hypertensive rats (Pan et al., 2021; Sun et al., 2021). However, whether salusin-β also plays a regulating role in vasomotor function in pulmonary hypertension is still unknown.

The current study found that compared to control rats, the salusin-β protein expressions in both PAs and PASMCs were significantly increased in MCT-PH rats. The high K^+ solution-induced contraction is usually used to evaluate the contractile ability of vascular smooth muscle; and SNP, an NO donor, which acts on the VSMCs to directly induce vascular smooth muscle relaxation, can be used to evaluate the vasodilator ability of vascular smooth muscle. ACh stimulates endothelial cells to release NO, and NO then causes VSMCs to relax, which is called endothelium-dependent relaxation. We found that compared with control rats, both the SNP- and ACh-induced relaxation of PAs of MCT-PH rats were attenuated, indicating that both the endothelial function and the smooth muscle relaxing ability of PAs were impaired in PH. Tail vein injection of salusin-β shRNA improved either SNP-or ACh-induced vascular relaxation and decreased high K^+ solution-induced PAs contraction, while overexpression of salusin-β enhanced PAs contraction and worsened vascular relaxation in MCT-PH rats. In addition, although knockdown of salusin-β had no significant roles in control rats, overexpression of salusin-β in control rats similarly elevated PAs contraction and impaired SNP- or ACh-induced PAs relaxation. These results suggested that salusin-β has ability to enhance contraction, and impair endothelial function and PASMCs relaxation, and through that, it consequently increases PAR and PAP.

Furthermore, it is known that high K^+ solution-elicited contraction is mainly related either to smooth muscle mass or to the function of voltage-dependent calcium channels in pulmonary vascular smooth muscle (Karaki et al., 1986; Ishida et al., 2017). SNP-mediated vasodilatation is related to signaling dependent on soluble guanylate cyclase (GC)-cGMP-production-protein kinase G (PKG) signaling (Bilodeau-Goeseels, 2007). We speculated that salusin-β enhanced contraction might through increasing smooth muscle mass or enhancing the function of voltage-dependent calcium channels of PASMCs, and impaired PASMCs relaxation might through inhibiting GC-cGMP-PKG signaling, which would be studied in the future.

We further found that the RVSP and RVH index in MCT-PH rats were much higher than those of control rats, which were the subsequent results of the high PA pressure. Knockdown of salusin-β decreased RVSP and RVH index in PH rats, while overexpression of salusin-β not only increased RVSP and RVH index in MCT-PH rats, but also increased these parameters in control rats, which further suggested that salusin-β contributes to the pathogenesis and development of PH by influencing the vascular contraction and relaxation function of PAs.

Studies have reported that PASMCs undergo phenotypic changes under pathological conditions in PH, resulting in enhanced proliferation and migration and vascular remodeling (Tajsic and Morrell, 2011; Morris et al., 2019). Excessive hyperplasia and hypertrophy of PASMCs have become the most important pathological basis for pulmonary artery stenosis and increased PAR (You et al., 2018). Fibrosis and

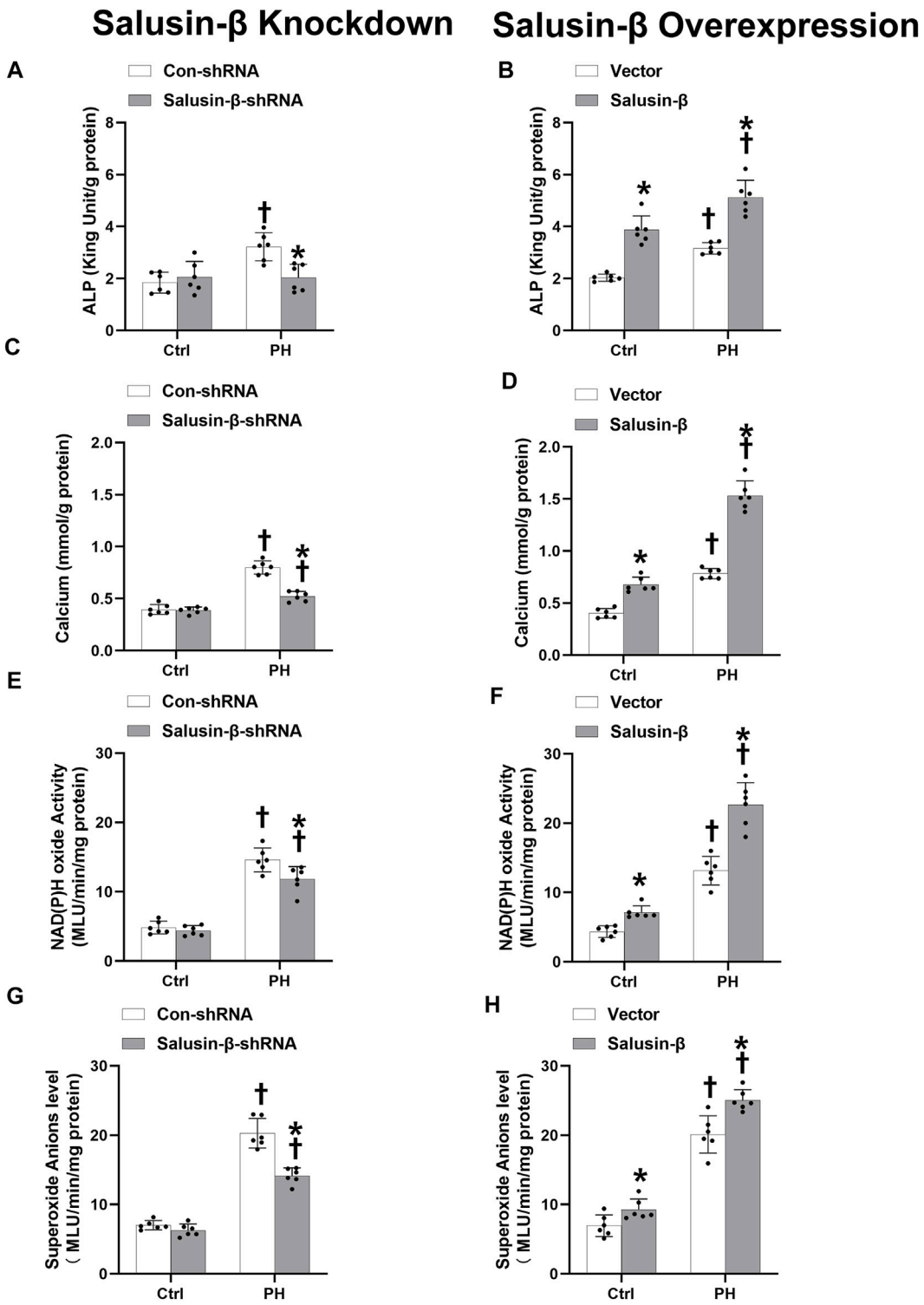


FIGURE 8
Effect of salusin-β knockdown on ALP activity **(A)**, calcium content **(C)**, NAD(P)H oxidase activity **(E)** and superoxide anions level **(G)**; as well as the effects of overexpression of salusin-β on ALP activity **(B)**, calcium content **(D)**, NAD(P)H oxidase activity **(F)** and superoxide anions level **(H)** of PASMCs isolated from control and MCT-induced PH rats. Values are mean ± SE. *$p < 0.05$ compared with Con-shRNA or vector. †$p < 0.05$ compared with control (Ctrl) rats. $n = 6$ for each group.

calcification of smooth muscles, which increases the stiffness of PAs, are also important causes for the vascular remodeling of pulmonary hypertension (Chan and Loscalzo, 2008; Ruffenach et al., 2016). Vascular fibrosis includes the deposition of extracellular matrix in the vascular wall, especially the accumulation of collagen and fibronectin. Excessive synthesis and deposition of collagen in the vascular wall increases vascular hardness (Lan et al., 2013; Thenappan et al., 2018). Since the 1960s, researchers have found that similar to other vascular lesions involving arterial thickening (e.g., atherosclerosis), vascular calcification is also ubiquitous and is associated with an increased risk of death in pulmonary hypertension (Ruffenach et al., 2016; Tanguay et al., 2019). Studies have suggested that salusin-β contributes to the progression of cardiovascular diseases such as atherosclerosis and hypertension, by regulating the proliferation, migration, fibrosis and calcification of VSMCs (Sun et al., 2015; Sun et al., 2019; Sommer et al., 2021) and vascular remodeling (Sun et al., 2015). Therefore we explored the effects of salusin-β on proliferation, migration, fibrosis, and calcification of PASMCs in PH *in vivo* and *in vitro*.

In the present study, we found that compared to control rats, there was a significant increase in PAs media wall thickness and a decrease in lumen diameter, resulting in stenosis or even complete occlusion of PAs in MCT-PH rats *in vivo*. Severe vascular fibrosis and proportional vascular calcification of small PAs of PH rats existed, which increased the stiffness of PAs and aggravated vascular remodeling in PH rats. Knockdown of salusin-β in PH rats increased lumen diameter, decreased media thickness and media thickness/lumen diameter, and relieved the vascular fibrosis and calcification of PAs, whereas salusin-β overexpression resulted in more severe vascular remodeling. *In vitro*, we also found that compared with PASMCs derived from control rats, the proliferation, migration, fibrosis, and calcification indices of PASMCs derived from MCT-PH rats were elevated. Overexpression of salusin-β not only further promoted them in PH-PASMCs but also elevated them in control-PASMCs. In contrast, knockdown of the salusin-β in PH-PASMCs decreased the proliferation and migration ability, as well as fibrosis and calcification index. These results indicated that salusin-β promotes the proliferation, migration, fibrosis, and calcification of PASMCs, and that endogenic salusin-β is involved in the mechanisms of these manifestations of vascular remodeling in PH.

Although the exact pathophysiology of PH is still unclear, there is increasing evidence that oxidative stress plays a vital role in the proliferation, migration, fibrosis, and remodeling of pulmonary arteries, leading to the development and progression of PH (Crosswhite and Sun, 2010; Xiao et al., 2020; Sekar, 2021). Furthermore, salusin-β has been reported to increase oxidative stress in VSMCs and induce the migration of VSMCs and intimal hyperplasia following vascular injury (Sun et al., 2015). Through stimulating the production of ROS, salusin-β promotes the foam cells formation and monocyte adhesion in atherosclerosis (Sun et al., 2016a). Our previous studies also have demonstrated that salusin-β regulates blood pressure and vascular function in spontaneously hypertensive rats through provoking the NAD(P)H oxidase derived ROS production in arteries (Pan et al., 2021; Sun et al., 2021). However, whether NAD(P)H oxidase-ROS also mediate the effects of salusin-β in pulmonary hypertension remains unclear. In the current study, compared with control, we found that both NAD(P)H oxidase activity and ROS level of PASMCs derived from MCT-PH rats were significantly increased, and overexpression of salusin-β further elevated them, while knockdown of salusin-β decreased them. In addition, overexpression of salusin-β also increased the NAD(P)H oxidase activity and ROS level in PASMCs derived from control rats. These results suggested that the elevated NAD(P)H oxidase activity-derived ROS production by endogenic salusin-β stimulation in PH might contribute to the proliferation, migration, fibrosis, and remodeling of the pulmonary arteries, which we will study in detail in the future.

In addition, we also found that there was the lack of effects of salusin-β knockdown in either the animals or cells experiments of control rats. We speculated that salusin-β might has not a prominent role under physiological conditions, but its overexpression resulting from other factors under pathological conditions contributed in turn to enhance PH characteristics, which we will study in detail in the future.

Conclusion

Increased salusin-β activity in PAs in PH rats contributes to proliferation, migration, fibrosis, and calcification of PASMCs, and eventually promotes vascular remodeling. Together with its capacity of promoting the imbalance of vascular contraction and relaxation of PAs, salusin-β plays an important role in elevating the pulmonary arterial resistance and pressure and promotes the pathogenesis and development of pulmonary hypertension. The roles of salusin-β is achieved might by stimulating the production of NAD(P)H oxidase-derived ROS. Reducing endogenous salusin-β may provide a new idea and strategy for the prevention and treatment of pulmonary hypertension in the future.

Data availability statement

The raw data supporting the conclusion of this article will be made available by the authors upon reasonable request.

Ethics statement

The animal study was reviewed and approved by the Nanjing Medical University Experimental Animal Care and complied with the Guide for the Care and Use of Laboratory Animals

published by the US National Institutes of Health (NIH publication, 8th edition, 2011).

Author contributions

YH and HT conceived and designed the experiments. XW, AC, and FZ performed the experiments. XW, RH, and CB analyzed the data. YH wrote the manuscript with input from HT and SL, and XL participated in the revision of the manuscript.

Funding

This work was sponsored by the National Key Research and Development Program of China (2019YFE0119400), the National Natural Science Foundation of China [81470538, 81970052, and 82170057], the Open Project of the State Key Laboratory of Respiratory Disease (SKLRD-OP-202114), and the Natural Science Foundation of the Jiangsu Higher Education Institutions of China (22KJD180003).

Conflict of interest

The authors declare that the research was conducted in the absence of any commercial or financial relationships that could be construed as a potential conflict of interest.

Publisher's note

All claims expressed in this article are solely those of the authors and do not necessarily represent those of their affiliated organizations, or those of the publisher, the editors, and the reviewers. Any product that may be evaluated in this article, or claim that may be made by its manufacturer, is not guaranteed or endorsed by the publisher.

References

Benza, R. L., Miller, D. P., Barst, R. J., Badesch, D. B., Frost, A. E., and McGoon, M. D. (2012). An evaluation of long-term survival from time of diagnosis in pulmonary arterial hypertension from the REVEAL Registry. *Chest* 142, 448–456. doi:10.1378/chest.11-1460

Bilodeau-Goeseels, S. (2007). Effects of manipulating the nitric oxide/cyclic GMP pathway on bovine oocyte meiotic resumption *in vitro*. *Theriogenology* 68, 693–701. doi:10.1016/j.theriogenology.2007.05.063

Brozovich, F. V., Nicholson, C. J., Degen, C. V., Gao, Y. Z., Aggarwal, M., and Morgan, K. G. (2016). Mechanisms of vascular smooth muscle contraction and the basis for pharmacologic treatment of smooth muscle disorders. *Pharmacol. Rev.* 68, 476–532. doi:10.1124/pr.115.010652

Chan, S. Y., and Loscalzo, J. (2008). Pathogenic mechanisms of pulmonary arterial hypertension. *J. Mol. Cell. Cardiol.* 44, 14–30. doi:10.1016/j.yjmcc.2007.09.006

Crosswhite, P., and Sun, Z. (2010). Nitric oxide, oxidative stress and inflammation in pulmonary arterial hypertension. *J. Hypertens.* 28, 201–212. doi:10.1097/HJH.0b013e328332bcdb

Gerthoffer, W. (2020). Epigenetic targets for oligonucleotide therapies of pulmonary arterial hypertension. *Int. J. Mol. Sci.* 21, E9222. doi:10.3390/ijms21239222

Humbert, M., Guignabert, C., Bonnet, S., Dorfmüller, P., Klinger, J. R., Nicolls, M. R., et al. (2019). Pathology and pathobiology of pulmonary hypertension: State of the art and research perspectives. *Eur. Respir. J.* 53, 1801887. doi:10.1183/13993003.01887-2018

Ishida, H., Saito, S. Y., Hishinuma, E., and Ishikawa, T. (2017). Differential contribution of nerve-derived noradrenaline to high K(+)-Induced contraction depending on type of artery. *Biol. Pharm. Bull.* 40, 56–60. doi:10.1248/bpb.b16-00590

Karaki, H., Kishimoto, T., Ozaki, H., Sakata, K., Umeno, H., and Urakawa, N. (1986). Inhibition of calcium channels by harmaline and other harmala alkaloids in vascular and intestinal smooth muscles. *Br. J. Pharmacol.* 89, 367–375. doi:10.1111/j.1476-5381.1986.tb10269.x

Lan, T.-H., Huang, X.-Q., and Tan, H.-M. (2013). Vascular fibrosis in atherosclerosis. *Cardiovasc. Pathol.* 22, 401–407. doi:10.1016/j.carpath.2013.01.003

Lu, Q.-B., Sun, J., Kang, Y., Sun, H.-J., Wang, H.-S., Wang, Y., et al. (2017). Superoxide anions and NO in the paraventricular nucleus modulate the cardiac sympathetic afferent reflex in obese rats. *Int. J. Mol. Sci.* 19, E59. doi:10.3390/ijms19010059

Ma, Y.-Y., Sun, L., Chen, X.-J., Wang, N., Yi, P.-F., Song, M., et al. (2016). Vinpocetine attenuates the osteoblastic differentiation of vascular smooth muscle cells. *PLoS One* 11, e0162295. doi:10.1371/journal.pone.0162295

Morris, H. E., Neves, K. B., Montezano, A. C., MacLean, M. R., and Touyz, R. M. (2019). *Notch3 signalling and vascular remodelling in pulmonary arterial hypertension*, 133. London, England: Clinical science, 2481

Murray, T. R., Marshall, B. E., and Macarak, E. J. (1990). Contraction of vascular smooth muscle in cell culture. *J. Cell. Physiol.* 143, 26–38. doi:10.1002/jcp.1041430105

Pan, M., Han, Y., Si, R., Guo, R., Desai, A., and Makino, A. (2017). Hypoxia-induced pulmonary hypertension in type 2 diabetic mice. *Pulm. Circ.* 7, 175–185. doi:10.1086/690206

Pan, Y., Sun, S., Wang, X., Chen, A., Fei, X., Wang, W., et al. (2021). Improvement of vascular function by knockdown of salusin-β in hypertensive rats via nitric oxide and reactive oxygen species signaling pathway. *Front. Physiol.* 12, 622954. doi:10.3389/fphys.2021.622954

Ren, X.-S., Ling, L., Zhou, B., Han, Y., Zhou, Y.-B., Chen, Q., et al. (2017). Silencing salusin-β attenuates cardiovascular remodeling and hypertension in spontaneously hypertensive rats. *Sci. Rep.* 7, 43259. doi:10.1038/srep43259

Ruffenach, G., Chabot, S., Tanguay, V. F., Courboulin, A., Boucherat, O., Potus, F., et al. (2016). Role for runt-related transcription factor 2 in proliferative and calcified vascular lesions in pulmonary arterial hypertension. *Am. J. Respir. Crit. Care Med.* 194, 1273–1285. doi:10.1164/rccm.201512-2380OC

Sekar, D. (2021). Extracellular vesicles are involved in oxidative stress and mitochondrial homeostasis in pulmonary arterial hypertension. *Hypertens. Res.* 44, 1028–1029. doi:10.1038/s41440-021-00672-8

Sommer, N., Ghofrani, H. A., Pak, O., Bonnet, S., Provencher, S., Sitbon, O., et al. (2021). Current and future treatments of pulmonary arterial hypertension. *Br. J. Pharmacol.* 178, 6–30. doi:10.1111/bph.15016

Southgate, L., Machado, R. D., Gräf, S., and Morrell, N. W. (2020). Molecular genetic framework underlying pulmonary arterial hypertension. *Nat. Rev. Cardiol.* 17, 85–95. doi:10.1038/s41569-019-0242-x

Sun, H.-J., Liu, T.-Y., Zhang, F., Xiong, X.-Q., Wang, J.-J., Chen, Q., et al. (2015). Salusin-β contributes to vascular remodeling associated with hypertension via promoting vascular smooth muscle cell proliferation and vascular fibrosis. *Biochim. Biophys. Acta* 1852, 1709–1718. doi:10.1016/j.bbadis.2015.05.008

Sun, H.-J., Zhao, M.-X., Liu, T.-Y., Ren, X.-S., Chen, Q., Li, Y.-H., et al. (2016a). Salusin-β induces foam cell formation and monocyte adhesion in human vascular smooth muscle cells via miR155/NOX2/NFκB pathway. *Sci. Rep.* 6, 23596. doi:10.1038/srep23596

Sun, H.-J., Zhao, M.-X., Ren, X.-S., Liu, T.-Y., Chen, Q., Li, Y.-H., et al. (2016b). Salusin-β promotes vascular smooth muscle cell migration and intimal hyperplasia

after vascular injury via ROS/NFκB/MMP-9 pathway. *Antioxid. Redox Signal.* 24, 1045–1057. doi:10.1089/ars.2015.6475

Sun, H., Zhang, F., Xu, Y., Sun, S., Wang, H., Du, Q., et al. (2019). Salusin-β promotes vascular calcification via nicotinamide adenine dinucleotide phosphate/reactive oxygen species-mediated klotho downregulation. *Antioxid. Redox Signal.* 31, 1352–1370. doi:10.1089/ars.2019.7723

Sun, S., Zhang, F., Pan, Y., Xu, Y., Chen, A., Wang, J., et al. (2021). A TOR2A gene product: Salusin-β contributes to attenuated vasodilatation of spontaneously hypertensive rats. *Cardiovasc. Drugs Ther.* 35, 125–139. doi:10.1007/s10557-020-06983-1

Suzuki, N., Shichiri, M., Akashi, T., Sato, K., Sakurada, M., Hirono, Y., et al. (2007). Systemic distribution of salusin expression in the rat. *Hypertens. Res.* 30, 1255–1262. doi:10.1291/hypres.30.1255

Tajsic, T., and Morrell, N. W. (2011). Smooth muscle cell hypertrophy, proliferation, migration and apoptosis in pulmonary hypertension. *Compr. Physiol.* 1, 295–317. doi:10.1002/cphy.c100026

Tang, H., Chen, J., Fraidenburg, D. R., Song, S., Sysol, J. R., Drennan, A. R., et al. (2015). Deficiency of Akt1, but not Akt2, attenuates the development of pulmonary hypertension. *Am. J. Physiol. Lung Cell. Mol. Physiol.* 308, L208–L220. doi:10.1152/ajplung.00242.2014

Tang, H., Yamamura, A., Yamamura, H., Song, S., Fraidenburg, D. R., Chen, J., et al. (2016). Pathogenic role of calcium-sensing receptors in the development and progression of pulmonary hypertension. *Am. J. Physiol. Lung Cell. Mol. Physiol.* 310, L846–L859. doi:10.1152/ajplung.00050.2016

Tanguay, V. F., Babin, C., Giardetti, G., Sohier-Poirier, C., Ménard-Cholette, V., Ranchoux, B., et al. (2019). Enhanced pulmonary artery radiodensity in pulmonary arterial hypertension: A sign of early calcification? *Am. J. Respir. Crit. Care Med.* 199, 799–802. doi:10.1164/rccm.201806-1027LE

Thenappan, T., Chan, S. Y., and Weir, E. K. (2018). Role of extracellular matrix in the pathogenesis of pulmonary arterial hypertension. *Am. J. Physiol. Heart Circ. Physiol.* 315, H1322-H1331–H1331. doi:10.1152/ajpheart.00136.2018

Watanabe, T., Nishio, K., Kanome, T., Matsuyama, T.-a., Koba, S., Sakai, T., et al. (2008). Impact of salusin-alpha and -beta on human macrophage foam cell formation and coronary atherosclerosis. *Circulation* 117, 638–648. doi:10.1161/CIRCULATIONAHA.107.712539

Wu, N., Ye, C., Zheng, F., Wan, G.-W., Wu, L.-L., Chen, Q., et al. (2020). MiR155-5p inhibits cell migration and oxidative stress in vascular smooth muscle cells of spontaneously hypertensive rats. *Antioxidants (Basel)* 9, E204. doi:10.3390/antiox9030204

Xiao, Y., Chen, P.-P., Zhou, R.-L., Zhang, Y., Tian, Z., and Zhang, S.-Y. (2020). Pathological mechanisms and potential therapeutic targets of pulmonary arterial hypertension: A review. *Aging Dis.* 11, 1623–1639. doi:10.14336/AD.2020.0111

Xu, T., Zhang, Z., Liu, T., Zhang, W., Liu, J., Wang, W., et al. (2016). Salusin-β contributes to vascular inflammation associated with pulmonary arterial hypertension in rats. *J. Thorac. Cardiovasc. Surg.* 152, 1177–1187. doi:10.1016/j.jtcvs.2016.05.056

You, B., Liu, Y., Chen, J., Huang, X., Peng, H., Liu, Z., et al. (2018). Vascular peroxidase 1 mediates hypoxia-induced pulmonary artery smooth muscle cell proliferation, apoptosis resistance and migration. *Cardiovasc. Res.* 114, 188–199. doi:10.1093/cvr/cvx234

Zabini, D., Granton, E., Hu, Y., Miranda, M. Z., Weichelt, U., Breuils Bonnet, S., et al. (2018). Loss of SMAD3 promotes vascular remodeling in pulmonary arterial hypertension via MRTF disinhibition. *Am. J. Respir. Crit. Care Med.* 197, 244–260. doi:10.1164/rccm.201702-0386OC

Zhang, F., Tang, H., Sun, S., Luo, Y., Ren, X., Chen, A., et al. (2019). Angiotensin-(1-7) induced vascular relaxation in spontaneously hypertensive rats. *Nitric Oxide* 88, 1–9. doi:10.1016/j.niox.2019.03.007

Zhou, Y. B., Gao, Q., Li, P., Han, Y., Zhang, F., Qi, Y. F., et al. (2013). Adrenomedullin attenuates vascular calcification in fructose-induced insulin resistance rats. *Acta Physiol.* 207, 437–446. doi:10.1111/apha.12033

Zhu, X., Zhou, Z., Zhang, Q., Cai, W., Zhou, Y., Sun, H., et al. (2018). Vaccarin administration ameliorates hypertension and cardiovascular remodeling in renovascular hypertensive rats. *J. Cell. Biochem.* 119, 926–937. doi:10.1002/jcb.26258

frontiers | Frontiers in Pharmacology

TYPE Original Research
PUBLISHED 14 October 2022
DOI 10.3389/fphar.2022.1015390

Check for updates

OPEN ACCESS

EDITED BY
Yanping Liu,
Shandong University, China

REVIEWED BY
Chen Cui,
Chinese Academy of Medical Sciences and Peking Union Medical College, China
Emanuele Gallinoro,
Cardiovascular Center, OLV Aalst, Belgium

*CORRESPONDENCE
Guohai Su,
gttstg@163.com
Bin Li,
qingquan0615@163.com

SPECIALTY SECTION
This article was submitted to Experimental Pharmacology and Drug Discovery, a section of the journal Frontiers in Pharmacology

RECEIVED 09 August 2022
ACCEPTED 03 October 2022
PUBLISHED 14 October 2022

CITATION
Wang Q, Wang J, Ma Y, Wang P, Li Y, Tian J, Yue X, Su G and Li B (2022), Predictive value of myocardial strain on myocardial infarction size by cardiac magnetic resonance imaging in ST-segment elevation myocardial infarction with preserved left ventricular ejection fraction.
Front. Pharmacol. 13:1015390.
doi: 10.3389/fphar.2022.1015390

COPYRIGHT
© 2022 Wang, Wang, Ma, Wang, Li, Tian, Yue, Su and Li. This is an open-access article distributed under the terms of the Creative Commons Attribution License (CC BY). The use, distribution or reproduction in other forums is permitted, provided the original author(s) and the copyright owner(s) are credited and that the original publication in this journal is cited, in accordance with accepted academic practice. No use, distribution or reproduction is permitted which does not comply with these terms.

Predictive value of myocardial strain on myocardial infarction size by cardiac magnetic resonance imaging in ST-segment elevation myocardial infarction with preserved left ventricular ejection fraction

Qiang Wang[1], Jian Wang[2], Yingjie Ma[1], Peng Wang[1], Yang Li[1], Jing Tian[1], Xiuzheng Yue[3], Guohai Su[1,4]* and Bin Li[1,4]*

[1]Department of Cardiology, Central Hospital Affiliated to Shandong First Medical University, Jinan, China, [2]Department of Radiology, Central Hospital Affiliated to Shandong First Medical University, Jinan, China, [3]Philips Healthcare, Beijing, China, [4]Research Center of Translational Medicine, Central Hospital Affiliated to Shandong First Medical University, Jinan, China

Background: The correlation between myocardial strain and infraction size by cardiac magnetic resonance imaging in ST-segment elevation myocardial infarction (STEMI) with preserved left ventricular ejection fraction (LVEF) is not clear.

Objective: To investigate the correlation between myocardial strain and myocardial infarction size in patients of acute STEMI with preserved LVEF.

Materials and Methods: A retrospective study was conducted to assess 31 patients with acute ST-segment elevation myocardial infarction (STEMI)after primary percutaneous coronary intervention (PCI) who received cardiac magnetic resonance (CMR) imaging during hospitalization at the Central Hospital of Shandong First Medical University from 2019 to 2022 and whose echocardiography indicated preserved LVEF (LVEF≥50%). The control group consisted of 21 healthy adults who underwent CMR during the same period. We compared the CMR characteristics, global and segmental strain between the two groups. Furthermore, the correlation between the global strain and the segmental strain of the left ventricle and late gadolinium enhancement (LGE) were evaluated.

Results: Compared with healthy controls, the left ventricular ejection fraction (LVEF) of STEMI patients with preserved LVEF was significantly decreased ($p < 0.05$). Moreover, the global radial strain (GRS) (24.09% [IQR:17.88–29.60%] vs. 39.56% [IQR:29.19–42.20%], $p < 0.05$), global circumferential strain (GCS) [–14.66% (IQR: 17.91–11.56%) vs. –19.26% (IQR: 21.03–17.73%), $p < 0.05$], and global longitudinal strains (GLS) (–8.88 ± 2.25% vs. –13.46 ± 2.63%, $p < 0.05$) were damaged in patients. Furthermore, GCS and GLS were associated

with LGE size (%left ventricle) (GCS: r = 0.58, $p < 0.05$; GLS: r = 0.37, $p < 0.05$). In the multivariate model, we found that LGE size was significantly associated with GCS (β coefficient = 2.110, $p = 0.016$) but was not associated with GLS (β coefficient = −0.102, $p = 0.900$) and LVEF (β coefficient = 0.227, $p = 0.354$). The receiver operating characteristic (ROC) results showed that GCS emerged as the strongest LGE size (LGE >25%) prognosticator among strain parameters (AUC: 0.836 [95% CI, 0.692—0.981], sensitivity: 91%, specificity: 80%) and was significantly better ($p = 0.001$) than GLS [AUC: 0.761 (95% CI, 0.583—0.939), sensitivity: 64%, specificity: 85%] and LVEF [AUC: 0.673 (95% CI, 0.469—0.877), sensitivity: 73%, specificity: 70%].

Conclusion: Among STEMI patients with preserved LVEF after PCI, CMR-FT-derived GCS had superior diagnostic accuracy than GLS and LVEF in predicting myocardial infarction size.

KEYWORDS

acute ST-segment elevation myocardial infarction, preserved left ventricle ejection fraction, magnetic resonance imaging, strain, late gadolinium enhancement (LGE)

Introduction

In the last decade, advances in reperfusion and preventive therapies have reduced ST-segment elevation myocardial infarction (STEMI)-related mortality in hospitalized patients (Szummer et al., 2017). Early revascularization is the key to saving ischemic myocardium and limiting the infarct size (Ibanez et al., 2017) and significantly reduces the incidence of adverse cardiovascular events and improves the prognosis of patients (Sugiyama et al., 2015). However, about 20% of patients experience recurrent cardiovascular events within a year following acute myocardial infarction (Pedersen et al., 2014). Thus, new assessment and diagnostic methods are necessary to develop judgments on cardiac function and infarct size and scope that are more accurate, which will assist cardiovascular physicians in making clinical decisions.

The left ventricular ejection fraction (LVEF) shown by echocardiography can reflect only global systolic function, whereas regional functional abnormalities or diastolic dysfunction cannot be accurately portrayed (Kim et al., 1999; Thiele et al., 2006). With LVEF, it is difficult to accurately determine the degree of cardiac damage and predict the infarct size (IS). Feature-tracking cardiac magnetic resonance (FT-CMR) has been developed as a more comprehensive method for measuring myocardial strain and establishing the functional status of the left ventricle, enabling the assessment of global and regional myocardial deformation (Smiseth et al., 2016). CMR examination is considered the *in vivo* reference standard for measuring infarct size in STEMI patients (Mahrholdt et al., 2005; Thiele et al., 2006). It is recommended that late gadolinium enhancement (LGE) be used for infraction size (IS) quantification (Mahrholdt et al., 2005; Thiele et al., 2006; Ibanez et al., 2019). However, data regarding the correlation between strain and LGE of FT-CMR in STEMI patients are scarce and sometimes controversial (Khan et al., 2015; Yu et al., 2021). The predictive value of strain by FT-CMR for the infarct size of STEMI patients with preserved LVEF remains unclear.

Therefore, we aimed to explore whether CMR myocardial strain could be more sensitive and accurate than LVEF in detecting the degree of cardiac dysfunction and predicting myocardial infarction size in STEMI patients with preserved LVEF. In addition, we aimed to find parameters related to the infarction size so we may better stratify patient risk in clinical practice and formulate treatment plans based on reference data.

Materials and methods

Study design and participants

The cases for this retrospective study originated from the Affiliated Central Hospital of Shandong First Medical University,

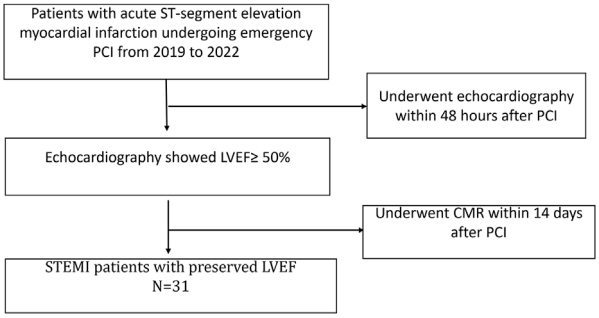


FIGURE 1
Flowchart of recruitment for patients. PCI, percutaneous coronary intervention; LVEF, left ventricular ejection fraction; CMR, Cardiac Magnetic Resonance.

which owns the first national chest pain emergency center in Jinan City. Our study selected patients who underwent emergency PCI and were hospitalized for acute ST-segment elevation myocardial infarction in the Central Hospital of Shandong First Medical University from 2019 to 2022. Thirty-one patients who underwent cardiac MRI over 14 days after PCI and whose echocardiography results showed LVEF ≥50% were selected for the study (Figure 1). Among the 31 STEMI patients with preserved left ventricular ejection fraction, 15 patients had single-vessel disease (48%), seven patients had double-vessel disease (23%), and nine patients had triple-vessel disease (29%). All these patients were admitted to our hospital with acute ST-segment elevation myocardial infarction, and we only performed revascularization of the culprit vessel during this hospitalization. Besides, all patients' culprit vessels recovered TIMI three blood flow after PCI. In addition, patients were treated with aspirin and platelet P2Y12 receptor antagonists such as clopidogrel or ticagrelor at discharge. Twenty-one healthy adults with no history of cardiovascular disease who had undergone CMR imaging during the screening period were selected as controls.

Based on the clinical baseline characteristics of the patients and the control group, the following information was obtained: age, gender, height, weight, body mass index (BMI), body surface area (BSA), smoking status, and history of hypertension, history of diabetes and of hyperlipidemia. The following are the diagnostic criteria for ST-segment elevation (measured at the J-point) in myocardial infarction: 1) Signs and symptoms consistent with myocardial ischemia (i.e., persistent chest pain lasting more than 30 min), 2) Electrocardiogram findings (ST-segment elevation measured at the J-point) suggestive of ongoing coronary artery acute occlusion, as in the following cases: at least two contiguous leads with ST-segment elevation of 2.5 mm in men <40 years, 2 mm in men 40 years, or 1.5 mm in women in leads V2—V3 or 1 mm in the other leads [in the absence of left ventricular (LV) hypertrophy or left bundle branch block (LBBB)] or new left bundle-branch block on the 18-lead electrocardiogram and elevated troponin I level (Ibanez et al., 2017). The exclusion criteria were as follows: aortic valve disease, infiltrative disease (cardiac amyloidosis, Anderson-Fabry disease, and Danon disease), or systemic disease. Patients with MRI contraindications, such as implanted pacemakers, metallic intracranial implants, claustrophobia, and renal function impairment, were also excluded. The local ethics committee approved this study, and all subjects gave written informed consent.

CMR imaging

Cardiac MRI was performed on 3.0 T MRI systems (Elition, Philips Healthcare, Best, the Netherlands) using a 32-channel phased-array abdomen coil. The protocol consisted of cine imaging and LGE imaging for analysis. First, standard cine images were acquired with end-expiratory breath hold steady-state free precession sequences (SSFP). Then, phase-sensitive inversion recovery (PSIR) was applied to late gadolinium enhancement (LGE) imaging. Infarct size was determined from the LGE images. The acquisitions of SSFP cine and PSIR were conducted in 2-chamber, 3-chamber, and 4-chamber long-axis planes, as well as a stack of contiguous short-axis slices, which encompassed the left ventricle from the atrioventricular ring to the apex.

Cine images were obtained using a steady-state free precession (SSFP) sequence with a breath-hold and ECG trigger for cardiac morphologic and functional analyses. The scanning parameters were as follows: repetition time (TR)/echo time (TE) = 2.8–3.0/1.4–1.5 ms, field of view (FOV) = 300 mm^2 × 300 mm^2, voxel = 2 mm × 2 mm × 6 mm, flip angle = 45°, and 6–8 mm slice thickness. LGE images were acquired 10–15 min after intravenous injection of 0.2 mmol/kg of gadolinium-based contrast agent (Jiangsu Hengrui Pharmaceutical Co., Ltd.) using a phase-sensitive inversion recovery (PSIR) sequence. The scanning parameters were as follows: TR/TE = 4.4/2.1 ms, FOV = 300 mm^2 × 300 mm^2, voxel = 1.5 mm × 1.5 mm × 10.0 mm, flip angle = 5°, and 10 mm slice thickness.

CMR analysis

All the analyses were conducted by two investigators with more than 5 years of experience each using the commercial software CVI42 (Circle Cardiovascular Imaging, Calgary, Canada). Endocardial and epicardial contours of the myocardium were applied, followed by subsequent software-driven automatic tracking (Figure 2). A quality adjustment was performed, and contours were amended manually, if necessary. Cardiac functional parameters were computed automatically. For quantification of contrast enhancement, the outline of the left ventricular myocardium was manually depicted, and LGE was detected by +5 SDs over the signal intensity of the normal myocardium. The LGE results were expressed as a percentage of the myocardial volume of the left ventricle (Global LGE size %). In addition, LV volumes, LV EF (LVEF), RV volumes, RV EF (RVEF), LA volumes, and LA EF (LAEF) were recorded. Feature-tracking was performed on standard long-axis cine (two, three, and four-chamber views) and short-axis cine to calculate the LV peak strain parameters, including global circumferential strain (GCS), global longitudinal strain (GLS), global radial strain (GRS), segmental peak circumferential strain, segmental peak longitudinal strain, and segmental peak radial strain (Figure 2).

Statistical analysis

Continuous variables were presented as mean ± standard deviation (SD) or median values with interquartile range (IQR),

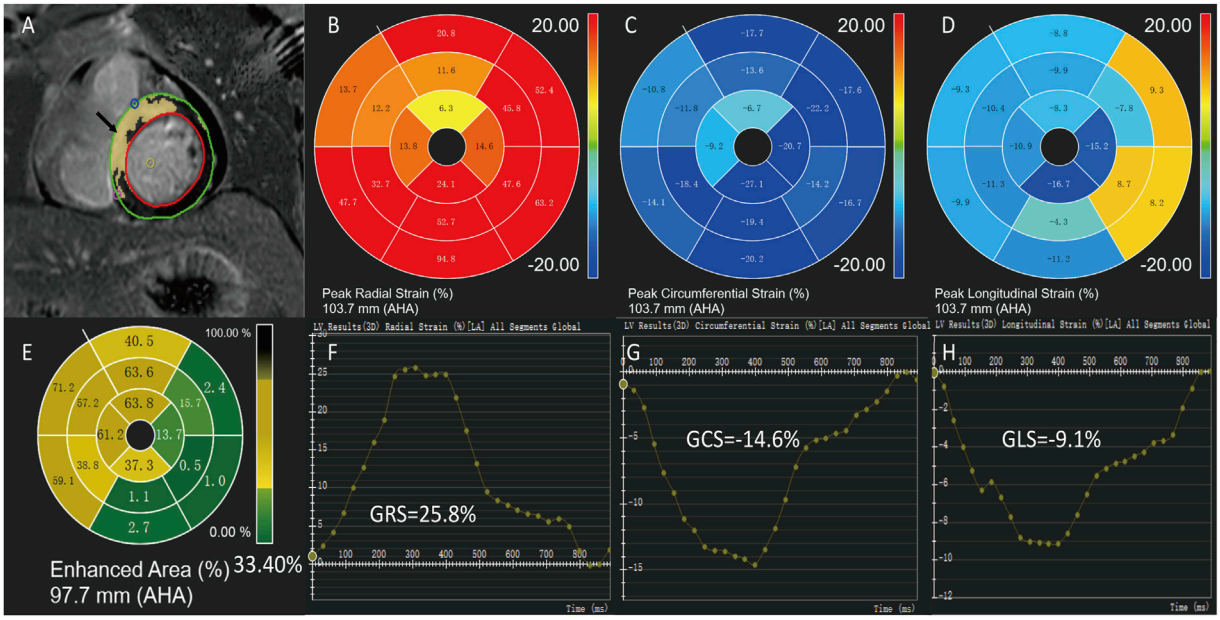


FIGURE 2
Measurement of cardiac magnetic resonance imaging. A 43-year-old male of ST-segment elevation myocardial infarction with preserved left ventricular ejection fraction. Epicardial (green) and endocardial (red) contours, LGE areas are marked in yellow **(A,E)**. Feature-tracking strain values of the same patient show global radial strain (GRS) = 25.8% **(B,F)**, global circumferential strain (GCS) = -14.6% **(C,G)** and global longitudinal strain (GLS) = -9.1% **(D,H)**.

TABLE 1 Baseline characteristics of the study population.

Variable	STEMI (n = 31)	Control (n = 21)	p-value
Age, years	51.90±12.32	54.90±12.81	0.405
Male, n (%)	25 (80.65)	13 (61.90)	0.239
Hight, m	1.73 [1.66–1.76]	1.70 [1.65–1.74]	0.304
Weight, kg	79.06±14.92	72.88±9.37	0.073
Body mass index, kg/m^2	26.12 [24.58–29.76]	24.91 [23.67–26.23]	0.119
Body surface area, m^2	1.93±0.21	1.83±0.15	0.057
Hypertension, n (%)	16 (51.61)	6 (28.57)	0.173
Hyperlipidemia, n (%)	10 (32.26)	2 (9.52)	0.093
Diabetes mellitus, n (%)	9 (29.03)	2 (9.52)	0.165
Smoke, n (%)	21 (67.74)	8 (38.10)	0.068
Culprit Vessel, n (%)			-
LAD	22 (70.97)	-	
RCA	9 (29.03)	-	

LAD, left anterior descending artery; RCA, right coronary artery.

depending on the normality variables. Student's t-test or Mann–Whitney U test was applied to compare the continuous variables. Categorical variables were presented as exact numbers with percentages, and the x^2 test or Fisher exact test was conducted for comparison. Correlation between variables was performed using Spearman's rank or Pearson correlation test. A multiple linear regression model was constructed to assess correlates of GCS, GLS, LVEF, and LGE size. The optimal cut-off values to identify the LGE size of STEMI patients, whether higher than 25% or not, were derived from receiver

TABLE 2 CMR parameters of the study population.

Variable	STEMI (n = 31)	Control (n = 21)	p-value
LVEF, %	49.48±9.50	62.88±6.96	<0.001
LV mass index, g/m^2	58.59 [51.88–66.70]	44.59 [42.11–52.23]	<0.001
LVEDV, mL	153.99 [134.30–175.72]	131.46 [118.83–152.88]	0.013
LVEDVi, mL/m^2	82.63 [70.51–90.83]	72.66 [66.47–77.94]	0.027
LVESV, mL	72.21 [57.20–85.53]	51.14 [37.93–58.40]	<0.001
LVESVi, mL/m^2	37.26 [30.09–49.22]	27.11 [23.52–31.67]	<0.001
LVSVi, mL/m^2	39.23 [33.24–44.77]	42.03 [39.62–51.18]	0.049
RVEF, %	54.66±7.88	54.31±7.07	0.866
RVEDV, mL	134.50±31.88	139.84±29.08	0.535
RVEDVi, mL/m^2	69.85±14.53	75.67±12.66	0.133
RVESVi, mL/m^2	31.74±8.79	34.79±8.45	0.216
RVSVi, mL/m^2	38.24±9.20	40.88±7.52	0.262
Global LGE size, %	18.23 [15.55–27.87]	-	-
GLS, %	−8.88±2.25	−13.46±2.63	<0.001
GRS, %	24.09 [17.88–29.60]	39.56 [29.19–42.20]	<0.001
GCS, %	−14.66 [−17.91–11.56]	−19.26 [−21.03–17.73]	<0.001
Basal LS%, %	41.01 [28.03–52.97]	62.58 [45.63–78.95]	<0.001
Basal RS, %	−14.15±3.68	−15.42±2.94	0.173
Basal CS, %	−7.39 [−8.77–5.12]	−9.89 [−11.92–7.62]	0.012
Mid LS, %	21.56±8.44	33.09±9.42	<0.001
Mid RS, %	−14.89±3.35	−19.43±2.31	<0.001
Mid CS, %	−8.91±3.11	−13.52±2.78	<0.001
Apical LS, %	18.26 [9.63–24.11]	27.34 [21.47–35.16]	0.003
Apical RS, %	−16.32±4.03	−22.15±2.64	<0.001
Apical CS, %	−11.77±2.78	−17.08±2.28	<0.001
LA size, mm	69.27±19.33	62.79±15.32	0.185
LAV $_{pre-a}$, mL	50.16 [39.49–60.29]	39.39 [33.68–48.14]	0.023
LAEF $_{total}$, %	53.42±9.31	58.93±5.78	0.011

LVEF, left ventricular ejection fraction; LV, left ventricular; LVEDVi, left ventricular end-diastolic volume index; LVESVi, left ventricular end-systolic volume index; LVSVi, left ventricular stroke volume index; RVEF, right ventricular ejection fraction; RVEDVi, right ventricular end-diastolic volume index; RVESVi, right ventricular end-systolic volume index; RVSVi, right ventricular stroke volume index; LGE, late gadolinium enhancement; GRS, global peak radial strain; GCS, global peak circumferential strain; GLS, global peak longitudinal strain; RS, radial strain; CS, circumferential strain; LS, longitudinal strain; LA, left atrium; LAV_{pre-a}, left atrial active pre-systolic volume; $LAEF_{total}$, left atrial total ejection fraction.

operating characteristics (ROC) analysis by the Youden Index. AUCs were compared using validated methods described by DeLong et al. (DeLong et al., 1988). All tests were two-sided, and $p < 0.05$ was considered statistically significant. All statistical analyses were conducted using R version 4.1.0 (The R Foundation, Austria).

Results

Baseline characteristics and CMR parameters

A total of 31 STEMI patients with preserved LVEF who met the selection criteria were retrospectively identified in this study (age 51.90 ± 12.32 years; 25 men); 21 healthy controls (age 54.90 ± 12.81 years; 13 men) were also included. No differences were observed between STEMI patients and healthy controls regarding age, gender, height, weight, body mass index (BMI), and body surface area (BSA) (Table 1). In addition, the patients had a high prevalence of hypertension (51.61%), hyperlipidemia (32.26%), and diabetes mellitus (29.03%) (Table 1).

CMR examinations were conducted between the STEMI patients with preserved LVEF and healthy subjects. An overview of assessed CMR parameters is presented in Table 2. We divided the left ventricle into apical, middle, and basal parts, according to the American Heart Association model (Cerqueira et al., 2002). LGE was distributed in each part of the left ventricle. Compared with the controls, all the CMR parameters of the left ventricle, including LVEF, were impaired in the STEMI group (all $p < 0.05$). However, we did

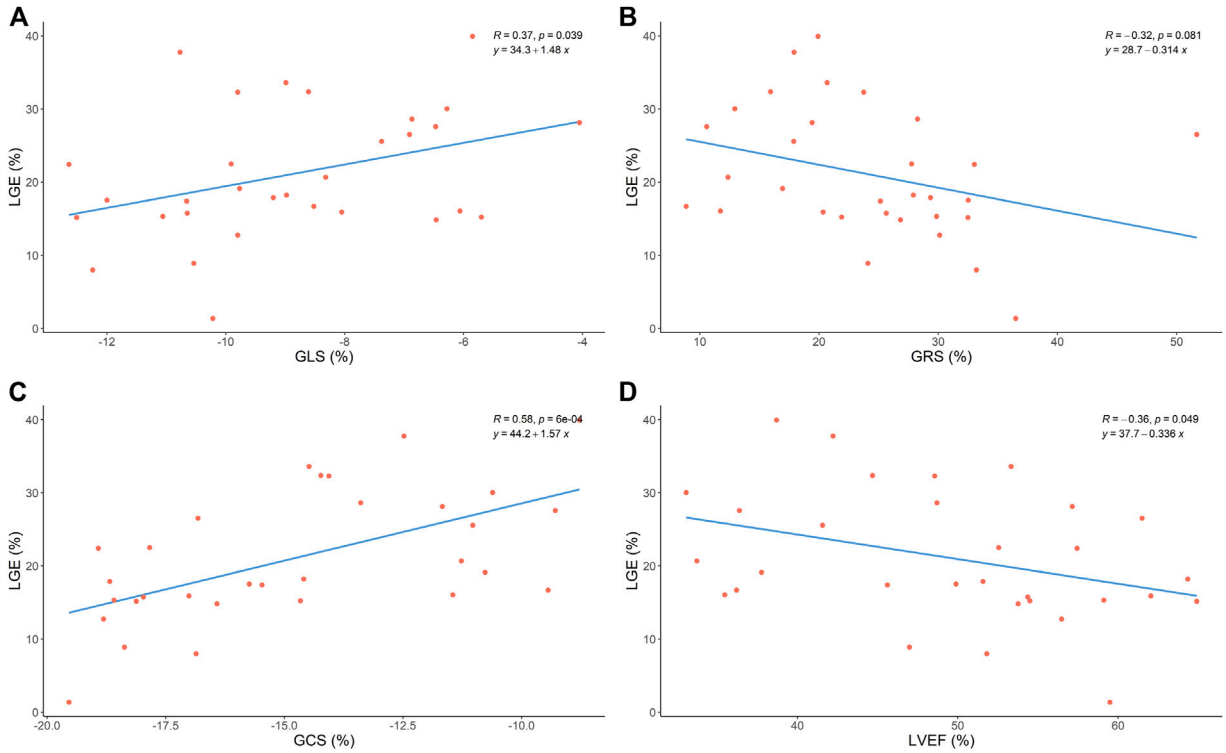


FIGURE 3
Correlation between global strain, LVEF and LGE size. GLS, global longitudinal strain; GRS, global radial strain; GCS, global circumferential strain; LVEF, left ventricular ejection fraction; LGE, late gadolinium enhancement.

not detect any impairments of the CMR parameters of the right ventricular in the STEMI group (all $p > 0.05$).

Global LGE size was 18.23% [IQR: 15.55–27.87] in the patients. GRS, GCS, and GLS were significantly lower in the STEMI patients than healthy controls (GRS: 24.09% [IQR: 17.88–29.60] vs 39.56% [IQR: 29.19–42.20], $p < 0.001$; GCS: 14.66% [IQR: 17.91–11.56] vs. −19.26% [IQR: 21.03–17.73], $p < 0.001$; GLS: 8.88 ± 2.25% vs. −13.46 ± 2.63%, $p < 0.001$). Furthermore, we divided the left ventricle into apical, middle, and basal parts, according to the American Heart Association model (Cerqueira et al., 2002). The segmental strain parameters (basal strain, mid strain, and apical strain) were impaired in patients with STEMI ($p < 0.05$) except basal radial strain ($p = 0.173$). In addition, the left atrial total ejection fraction of the STEMI patients was worse than in healthy controls ($p < 0.05$) (Table 2).

Association between LV strain, LVEF, and LGE

As Figure 3 shows, LV GCS and GLS were associated with LGE (GCS: r = 0.58, $p < 0.05$; GLS: r = 0.37, $p < 0.05$). However, we found that LV GRS was not associated with LGE (GRS: r = −0.32, $p > 0.05$). Also, an inverse correlation was found between LVEF and LGE (r = −0.36, $p < 0.05$).

TABLE 3 Multivariable linear regression analysis for LGE size.

Variable	Beta	95% CI	*p*-value
GCS	2.11	0.42 to 3.80	0.02
GLS	−0.10	−1.76 to 1.56	0.90
LVEF	0.23	−0.27 to 0.72	0.35

LGE, late gadolinium enhancement; GCS, global peak circumferential strain; GLS, global peak longitudinal strain; LVEF, left ventricular ejection fraction.

Multivariable regression analysis for LGE size

We constructed the multivariable linear models to assess the relationship of LGE with GCS, GLS, and LVEF. We found that LGE was significantly associated with GCS (β coefficient = 2.11, std error = 0.82, $p = 0.02$) but not associated with GLS (β coefficient = −0.102, std error = 0.80, $p = 0.90$) and LVEF (β coefficient = 0.23, std error = 0.24, $p = 0.35$) (Table 3).

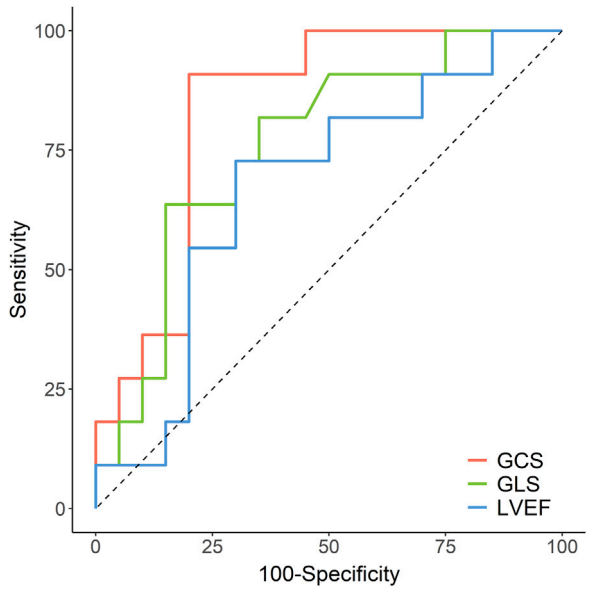


FIGURE 4
Receiver operating characteristic curves for accuracy of GCS, GLS and LVEF in the prediction of LGE>25%. GCS, global circumferential strain; GLS, global longitudinal strain; LVEF, left ventricular ejection fraction; LGE, late gadolinium enhancement.

Receiver operating characteristic analysis for prediction of LGE size

The area under the curve (AUC) for the ability of each cardiac function parameter to correctly identify the LGE size of the STEMI patients with preserved LVEF (whether higher than 25% or not) were as follows: GCS: 0.836 [95% CI, 0.692—0.981], $p = 0.001$; GLS: 0.761 [95% CI, 0.583–0.939], $p = 0.009$, and for LVEF: 0.673 [95% CI, 0.469—0.877], $p = 0.061$ (Figure 4). The cut-off values of GCS, GLS, and LVEF were −14.54% (sensitivity: 91%, specificity: 80%), −7.72% (sensitivity: 64%, specificity: 85%), and 49.30 (sensitivity: 73%, specificity: 70%), respectively. Furthermore, the comparison of the AUC values for the assessed cardiac function parameters showed that GCS had a significantly higher diagnostic accuracy than LVEF ($p < 0.05$) but no statistical significance with GLS ($p > 0.05$).

Discussion

In the present study, we investigated the characteristics of conventional CMR parameters and the correlation between the strain and LGE assessment by CMR-FT in STEMI patients with preserved LVEF. Our research has found that STEMI patients with preserved LVEF have impaired segmental strain, GLS, GCS, and GRS. Compared with healthy controls, STEMI patients had enlarged LVEDV, LVEDVi, LVESV, LVESVi, and $LAV_{pre\text{-}a}$. Additionally, LVSVi and total LA EF tended to decline in patients. However, we did not find any significant differences in RVEF, RVEDV, RVEDVi, RVESV, RVESVi, or RVSVi between the two groups. GCS, GLS, and LVEF were associated with LGE size. Furthermore, GCS had superior diagnostic accuracy to GLS and LVEF in identifying myocardial infarction size in the STEMI patients with preserved LVEF. This work demonstrates that it may be possible to detect infarction size when GCS is impaired.

Although an integrated myocardial infarction emergency system allows more patients to receive timely revascularization treatment and is more likely to minimize the size of the infarcted myocardium, it is essential to note that the adult heart does not possess any regenerative capacity. Therefore, a scar is formed when the infarcted myocardium heals. As part of the healing process, alarmins released by dying cells trigger a cascade of inflammatory reactions. When fibroblasts are activated by the renin-angiotensin-aldosterone system and released by transforming growth factor-β (Sun and Weber, 1996), they become myofibroblasts and produce an extracellular matrix (Moore-Morris et al., 2014). Generally, the procedure for healing an infarct is associated with a geometric remodeling of the chamber, characterized by dilation, hypertrophy, and progressive dysfunction of viable segments (Mukherjee et al., 2003).

Our study included STEMI patients with preserved LVEF, suggesting that left ventricular systolic function may be less affected by myocardial infarction, and infarct size may be smaller. However, compared with the control group, we found that the left ventricular volume CMR parameters LVEDV, LVEDVi, LVESV, and LVESVi were significantly increased ($p < 0.05$). Several different processes may cause expansion of the infarcted segment. First, this may reduce the number of layers across the ventricular wall due to the rearrangement of bundles of cardiomyocytes, accompanied by the elongation of these cardiomyocytes. Second, through activation of matrix metalloproteinases (MMPs), the interstitial matrix may be degradable, leading to increased dilation of the chambers (Radwan et al., 2021). Third, the organization, spatial polarization, and contraction of infarct myofibroblasts may result in perturbed scar maturation, stimulating the dilation of the chambers.

Compared with the control group, we did not find significant changes in right ventricular (RV) CMR parameters in patients ($p > 0.05$), perhaps due to the patient's left ventricular systolic function being preserved due to ventricular interdependence, resulting in little effect on the right ventricle. RV dysfunction is associated with worse in-hospital outcomes regardless of the localization of AMI and a lower 1-year survival rate (Mukherjee et al., 2003). Thus, we can infer that STEMI patients with preserved LVEF and normal right ventricular function are more likely to have better short-term outcomes.

In this study, left atrial (LA) parameters were also measured, and we found that LAEF was significantly decreased compared to the control group ($p < 0.05$). A more extensive analysis by Ledwoch and others, including 684 STEMI patients, measured LA function only by ejection fraction and found an independent association between LAEF and adverse clinical events. However, the prognostic value of LAEF was not incremental to LVEF (Ledwoch et al., 2018). Therefore, a reduction in LAEF is a predictor of adverse clinical events.

Different researchers have demonstrated that LVEF for predicting challenging clinical events post-STEMI is independent and incremental to established outcome factors such as echocardiography-based LVEF (Bodi et al., 2009; de Waha et al., 2010; de Waha et al., 2014). Additionally, LVEF is limited by reflecting only global systolic function while insufficiently conveying regional functional abnormalities (Smiseth et al., 2016; Amzulescu et al., 2019). Echocardiography showed that every subject in this study had a generally normal LVEF. Cardiologists have noted that the LVEF cannot predict the infarct size or estimate the degree of damage to its global or segmental functions. Hence, cardiologists cannot formulate treatment plans that are more appropriate and individualized, such as earlier and more appropriate use of angiotensin-converting enzyme inhibitor (ACEI), angiotensin receptor blockers (ARB), angiotensin receptor neprilysin inhibitor (ARNI), β-blockers, and sodium-dependent glucose transporters two inhibitors (SGLT-2i) (Paolisso et al., 2022). The results of our study suggest that LVEF measured by CMR in patients was significantly lower than in the control group (49.48 ± 9.5% vs. 62.88 ± 6.96%, $p < 0.05$). Nevertheless, LVEF is still critical, making it difficult for cardiologists to judge the infarction size accurately, predict outcomes, and give appropriate treatment guidance based on the parameter.

An analysis of myocardial strain evaluates deformations of the myocardium throughout the cardiac cycle, providing information on global and regional LV function (Smiseth et al., 2016; Amzulescu et al., 2019). Myocardial strain analysis is a powerful tool to quantify subtle and regional myocardial dysfunction over LVEF (Khan et al., 2016a; Mangion et al., 2017). CMR is currently considered the standard test for determining LV morphology, and the development of FT-CMR has enabled a highly accurate assessment of myocardial strain. Our analysis confirmed that several previous studies, including STEMI patients, demonstrated excellent intra- and inter-observer variability in FT-CMR (Eitel et al., 2018).

Several investigations have shown that cine-derived strain analyses can be performed with high accuracy and reproducibility after STEMI (Hor et al., 2010; Khan et al., 2015; Mangion et al., 2017). The global strain parameters derived from early CMR after STEMI have been prognostic. A study by Martin Reindl and others found that all three global strain measures (GLS, GRS, and GCS) are significantly correlated with major adverse cardiovascular events (MACE) (Reindl et al., 2019). Yu et al. reported that global strain was first impaired in anterior STEMI patients with normal LVEF (Yu et al., 2021). In our study, all global strain parameters (GLS, GCS, and GRS) and segmental strain parameters (apical, intermediate, and basal strains) except basal radial strain were significantly decreased in STEMI patients with preserved LVEF.

The results of this study are consistent with those of a previous study. Notably, our population did not define the site of myocardial infarction, indicating that global and segmental strain has decreased regardless of the location of the myocardial infarction in patients. However, the global strain had better reproducibility than the segmental strain in CMR feature-tracking (Dobrovie et al., 2019). Global strain is more accurate than segmental strain for assessing cardiac function and predicting the degree of cardiac damage. CMR is the gold standard for assessing of infarct size (IS) in STEMI patients. Accordingly, the quantification of acute IS by LGE should be performed 3—7 days after an MI (Lund et al., 2007). It has been demonstrated that acute IS quantified in this time frame is highly predictive of outcomes in STEMI patients (Larose et al., 2010). Microvascular obstruction (MVO) is recognized as a strong predictor of adverse clinical outcomes after STEMI. The index of microcirculatory resistance (IMR) provides assessment of coronary microvascular status early after primary PCI. IMR has been identified as a predictor of change in LVEF and IS after STEMI. De Maria GL et al. found a relation between IS assessed by CMR and microvascular dysfunction (De Maria et al., 2019). Therefore, IS measured in the acute phase after STEMI predicts LV remodeling and complex clinical outcomes (Lund et al., 2007; Eitel et al., 2013).

IS by LGE has been recommended as a primary CMR endpoint measure in experimental and clinical trials (Ibanez et al., 2019). For the relationship between LGE and global strain after myocardial infarction, there is only a moderate correlation between global strain and infarction size when assessed early post-STEMI. A study conducted by Khan et al. included 24 patients (8% with anterior myocardial infarctions) with STEMI who underwent CMR on average 2.2 days after PCI showed that there was a moderate correlation between the total IS and GLS, GCS, and GRS, which were significantly lower in segments with infarct than in segments without (Khan et al., 2015). A study by Yu et al. (Yu et al., 2021) included 129 acute anterior myocardial infarction patients who underwent CMR 1 month after surgery and showed a strong association between strain parameters and LGE (GRS: r = 0.65; GCS: r = 0.69; GLS: r = 0.61).

Unlike our study, previous ones did not delineate study populations based on LVEF, whereas we included patients with preserved LVEF. In addition, our patients underwent CMR up to 14 days after PCI, and the site of myocardial infarction included the anterior and inferior-posterior walls. Our results showed that there was a moderate correlation

between GCS and LGE (r = 0.58, $p < 0.05$) and a weak correlation between GLS and LGE (r = 0.37, $p < 0.05$), but we found no correlation between GRS and LGE ($p > 0.05$). In the multivariate model, we found that the LGE size was significantly associated with GCS (β coefficient = 2.110, $p = 0.016$) but was not associated with GLS (β coefficient = −0.102, $p = 0.900$) or LVEF (β coefficient = 0.227, $p = 0.354$).

Consistent with the above findings, GCS was correlated with the LGE size. Khan et al. also found a moderate correlation between GCS and IS but did not find a correlation between GLS and IS (Khan et al., 2015), possibly due to the small proportion of patients with anterior myocardial infarction that were included in their study as longitudinal myofibers are typically located in the mid-endocardium, and particularly in the anterior wall, which has a more significant impact on cardiac function. Yu et al. (Yu et al., 2021) found that GCS, GLS, and GRS were associated with LGE because they enrolled patients with anterior myocardial infarction regardless of LVEF. Larger infarcted myocardium in the anterior wall region may carry more substantial damage in both longitudinal myocardial fibers located in the mid-endocardium and circumferential myocardial fibers on the epicardial side. Therefore, GCS, GLS, and GRS are all correlated with LGE.

Based on the studies mentioned above, we believe there is a correlation between GCS and LGE in STEMI patients. A possible pathophysiological explanation is that the subendocardium is more susceptible to ischemic injury than the mid-myocardium and subepicardium. A "wavefront of necrosis" is, therefore, widely accepted as a mechanism of cardiomyocyte death that occurs during the progression of ischemic injury from the subendocardium to the subepicardium due to the increased duration of the insult (Reimer et al., 1977). In addition, circumferential myofibers are typically located on the epicardial aspect of the heart, so the infarct area spreads from the endocardium to the epicardium with prolonged ischemia time, and circumferential fibers suffer more damage as the infarct size expands (Bogaert et al., 2000).

Furthermore, the circumferential strain has a more excellent discriminative value for assessing the transmural extent of infarction in patients with recent MI (Koos et al., 2013). The circumferential strain rate has incremental prognostic use in predicting LV functional recovery in the longer term after an acute STEMI (Neizel et al., 2010). Moreover, our study found a weak correlation between GLS and LGE, perhaps because the selected patients had an approximately normal LVEF or only mild impairment. Longitudinal myofibers are typically located in the mid-endocardium, and the "wavefront phenomenon" describes ischemic myocardial injury starting at the subendocardial layers. Research has shown that GLS is a modest predictor of adverse remodeling of the LV and provides strong validity for the prediction of MACE post-STEMI. As a result, GLS may be slightly less affected than GCS in STEMI patients with preserved LVEF and only weakly correlated with LGE, suggesting that our study population may have a relatively good prognosis with a lower incidence of MACE than the general population with STEMI. GRS represents radially directed myocardial deformation toward the center of the LV cavity and indicates the LV thickening and thinning motion during the cardiac cycle. In contrast to the findings of Shiqin Yu, we found no significant correlation between GRS and LGE, possibly because about two-thirds of the patients in their study had decreased LVEF. It is possible that different infarct sizes and locations in patients can affect GRS differently.

A previous study reported that >25% of LGE extent was hard to recover and implied adverse outcomes despite successful revascularization (Kim et al., 2000). Our study showed that GCS discriminated well for LGE >25% (AUC: 0.836 [95% CI, 0.692—0.981]). However, GLS is less effective in predicting LGE >25% (AUC: 0.761 [95% CI, 0.583—0.939]). LVEF is not an ideal indicator of LGE >25% [AUC: 0.673 (95% CI, 0.469—0.877)]. Khan et al. found that accuracy in predicting segmental transmural LGE was greatest for FT-derived GCS (AUC: 0.772) (Khan et al., 2015). In patients with acute anterior myocardial infarction, Yu et al. found that segmental CS was more valuable in predicting segmental LGE >50% (AUC: 0.903) (Yu et al., 2021).

Therefore, we believe that GCS may effectively predict infarct size in STEMI patients with preserved LVEF. Although GLS is a better predictor of MACE, it is less accurate at predicting infarct size than GCS. Even though LVEF is one of the most commonly used clinical indicators to reflect cardiac function, it does not help predict infarct size. In a group of patients referred for CMR (11% with coronary artery disease) (Mordi et al., 2015), tagging-derived GCS was a multivariate predictor of MACE. Some patients develop renal impairment after acute MI, which makes them ineligible for gadolinium-contrast imaging. It is also possible to use strain imaging when gadolinium-contrast medium cannot be tolerated to assess infarct size. The strain provides more direct information on regional and global LV function in patients with acute MI than LVEF. Cardiologists can use CMR to measure GCS early after STEMI to estimate the infarct size and optimize drug therapy more efficiently. In addition, the myocardial strain has the potential to provide biomarkers that are predictive of LV recovery after STEMI. Patients with preserved LVEF may benefit from strain measurement in assessing treatment effectiveness predicated on improved precision and accuracy over LVEF. Using strain imaging in patient follow-up may facilitate the evaluation of infarct size, scarring, myocardial fibrosis, and MACE and allow cardiologists to adjust medications such as antiplatelet therapy (Khan et al., 2016b; Cimmino et al., 2020), angiotensin-converting enzyme inhibitor (ACEI), angiotensin receptor blockers (ARB), angiotensin receptor neprilysin inhibitor (ARNI), β-blockers and SGLT-2i (Paolisso et al., 2022) more precisely.

This study had several limitations. First, the sample size was relatively small. Second, this study was a single-center, retrospective study based on the preferred time point for assessing late gadolinium enhancement imaging. CMR scans were performed up to 14 days after MI, but it is not sure that this time point was optimal for the CMR measurements. Third, because the study focused on STEMI patients with preserved LVEF, extrapolating the findings to STEMI patients who had decreased LVEF or non-STEMI patients was limited. Moreover, we included patients with preserved LVEF based on echocardiographic findings, which were likely to be affected by equipment and operator factors. Furthermore, we could not perform predictive analysis on the relationship between strain, LGE, and prognosis due to a lack of follow-up for many patients. There may be a need for a more comprehensive prospective study with a more significant number of participants.

In conclusion, global and segmental strain were impaired in STEMI patients with preserved LVEF treated by contemporary primary percutaneous coronary intervention. GCS and LGE were correlated, and GCS, as determined by CMR, emerged as a strong and independent predictor of infarction size. Moreover, GCS had superior diagnostic accuracy to GLS and LVEF for predicting myocardial infarction size. Consequently, multiparametric CMR imaging (including the strain) has an emerging role in infarction size prediction in post-STEMI patients that warrants further research.

Data availability statement

The original contributions presented in the study are included in the article/Supplementary Material, further inquiries can be directed to the corresponding authors.

Ethics statement

The studies involving human participants were reviewed and approved by Jinan Central Hospital Medical Ethics Committee. Written informed consent for participation was not required for this study in accordance with the national legislation and the institutional requirements.

Written informed consent was obtained from the individual(s) for the publication of any potentially identifiable images or data included in this article.

Author contributions

QW conception and design of study, and drafted the article. JW analyzed images and acquired clinical data. XY critically revised the article. YM analyzed images. PW acquired clinical data. BL and GS conception and design of study and critically reviewed the article. JT performed statistical analysis and critically reviewed the article. YL acquired clinical data and critically reviewed the article. All authors read and approved the final article for publication.

Funding

The authors received subsequent financial support for the research, authorship, and/or publication of this article from the China Postdoctoral Science Foundation (No. 2020M682119), Natural Science Foundation of Shandong Province (No. ZR2020MH026), Postdoctoral Innovation Program of Shandong Province (No. 202102041), and Clinical Medicine Science and Technology Innovation Program of Jinan (No. 202019045).

Conflict of interest

Author XY was employed by the company Philips Healthcare.

The remaining authors declare that the research was conducted in the absence of any commercial or financial relationships that could be construed as a potential conflict of interest.

Publisher's note

All claims expressed in this article are solely those of the authors and do not necessarily represent those of their affiliated organizations, or those of the publisher, the editors and the reviewers. Any product that may be evaluated in this article, or claim that may be made by its manufacturer, is not guaranteed or endorsed by the publisher.

References

Amzulescu, M. S., De Craene, M., Langet, H., Pasquet, A., Vancraeynest, D., Pouleur, A. C., et al. (2019). Myocardial strain imaging: Review of general principles, validation, and sources of discrepancies. *Eur. Heart J. Cardiovasc. Imaging* 20 (6), 605–619. doi:10.1093/ehjci/jez041

Bodi, V., Sanchis, J., Nunez, J., Mainar, L., Lopez-Lereu, M. P., Monmeneu, J. V., et al. (2009). Prognostic value of a comprehensive cardiac magnetic resonance assessment soon after a first ST-segment elevation myocardial infarction. *JACC. Cardiovasc. Imaging* 2 (7), 835–842. doi:10.1016/j.jcmg.2009.03.011

Bogaert, J., Bosmans, H., Maes, A., Suetens, P., Marchal, G., and Rademakers, F. E. (2000). Remote myocardial dysfunction after acute anterior myocardial infarction: Impact of left ventricular shape on regional function: A magnetic resonance myocardial tagging study. *J. Am. Coll. Cardiol.* 35 (6), 1525–1534. doi:10.1016/s0735-1097(00)00601-x

Cerqueira, M. D., Weissman, N. J., Dilsizian, V., Jacobs, A. K., Kaul, S., Laskey, W. K., et al. (2002). Standardized myocardial segmentation and nomenclature for tomographic imaging of the heart. A statement for healthcare professionals from the Cardiac Imaging Committee of the Council on Clinical Cardiology of the

American Heart Association. *J. Nucl. Cardiol.* 9 (2), 240–245. doi:10.1067/mnc.2002.123122

Cimmino, G., Gallinoro, E., Di Serafino, L., De Luca, N., and Cirillo, P. (2020). Antiplatelet therapy in acute coronary syndromes. Lights and shadows of platelet function tests to guide the best therapeutic approach. *Curr. Vasc. Pharmacol.* 18 (3), 262–272. doi:10.2174/1570161117666190513105859

De Maria, G. L., Alkhalil, M., Wolfrum, M., Fahrni, G., Borlotti, A., Gaughran, L., et al. (2019). Index of microcirculatory resistance as a tool to characterize microvascular obstruction and to predict infarct size regression in patients with STEMI undergoing primary PCI. *JACC. Cardiovasc. Imaging* 12 (5), 837–848. doi:10.1016/j.jcmg.2018.02.018

de Waha, S., Desch, S., Eitel, I., Fuernau, G., Zachrau, J., Leuschner, A., et al. (2010). Impact of early vs. late microvascular obstruction assessed by magnetic resonance imaging on long-term outcome after ST-elevation myocardial infarction: A comparison with traditional prognostic markers. *Eur. Heart J.* 31 (21), 2660–2668. doi:10.1093/eurheartj/ehq247

de Waha, S., Eitel, I., Desch, S., Fuernau, G., Lurz, P., Stiermaier, T., et al. (2014). Prognosis after ST-elevation myocardial infarction: A study on cardiac magnetic resonance imaging versus clinical routine. *Trials* 15, 249. doi:10.1186/1745-6215-15-249

DeLong, E. R., DeLong, D. M., and Clarke-Pearson, D. L. (1988). Comparing the areas under two or more correlated receiver operating characteristic curves: A nonparametric approach. *Biometrics* 44 (3), 837–845. doi:10.2307/2531595

Dobrovie, M., Barreiro-Perez, M., Curione, D., Symons, R., Claus, P., Voigt, J. U., et al. (2019). Inter-vendor reproducibility and accuracy of segmental left ventricular strain measurements using CMR feature tracking. *Eur. Radiol.* 29 (12), 6846–6857. doi:10.1007/s00330-019-06315-4

Eitel, I., Stiermaier, T., Lange, T., Rommel, K. P., Koschalka, A., Kowallick, J. T., et al. (2018). Cardiac magnetic resonance myocardial feature tracking for optimized prediction of cardiovascular events following myocardial infarction. *JACC. Cardiovasc. Imaging* 11 (10), 1433–1444. doi:10.1016/j.jcmg.2017.11.034

Eitel, I., Wohrle, J., Suenkel, H., Meissner, J., Kerber, S., Lauer, B., et al. (2013). Intracoronary compared with intravenous bolus abciximab application during primary percutaneous coronary intervention in ST-segment elevation myocardial infarction: Cardiac magnetic resonance substudy of the AIDA STEMI trial. *J. Am. Coll. Cardiol.* 61 (13), 1447–1454. doi:10.1016/j.jacc.2013.01.048

Hor, K. N., Gottliebson, W. M., Carson, C., Wash, E., Cnota, J., Fleck, R., et al. (2010). Comparison of magnetic resonance feature tracking for strain calculation with harmonic phase imaging analysis. *JACC. Cardiovasc. Imaging* 3 (2), 144–151. doi:10.1016/j.jcmg.2009.11.006

Ibanez, B., Aletras, A. H., Arai, A. E., Arheden, H., Bax, J., Berry, C., et al. (2019). Cardiac MRI endpoints in myocardial infarction experimental and clinical trials: JACC scientific expert panel. *J. Am. Coll. Cardiol.* 74 (2), 238–256. doi:10.1016/j.jacc.2019.05.024

Ibanez, B., James, S., Agewall, S., Antunes, M. J., Bucciarelli-Ducci, C., Bueno, H., et al. (2017). 2017 ESC Guidelines for the management of acute myocardial infarction in patients presenting with ST-segment elevation: The Task Force for the management of acute myocardial infarction in patients presenting with ST-segment elevation of the European Society of Cardiology (ESC). *Eur. Heart J.* 39 (2), 119–177. doi:10.1093/eurheartj/ehx393

Khan, J. N., Greenwood, J. P., Nazir, S. A., Lai, F. Y., Dalby, M., Curzen, N., et al. (2016). Infarct size following treatment with second- versus third-generation P2Y12 antagonists in patients with multivessel coronary disease at ST-segment elevation myocardial infarction in the CvLPRIT study. *J. Am. Heart Assoc.* 5 (6), e003403. doi:10.1161/JAHA.116.003403

Khan, J. N., Nazir, S. A., Singh, A., Shetye, A., Lai, F. Y., Peebles, C., et al. (2016). Relationship of myocardial strain and markers of myocardial injury to predict segmental recovery after acute ST-segment-elevation myocardial infarction. *Circ. Cardiovasc. Imaging* 9 (6), e003457. doi:10.1161/CIRCIMAGING.115.003457

Khan, J. N., Singh, A., Nazir, S. A., Kanagala, P., Gershlick, A. H., and McCann, G. P. (2015). Comparison of cardiovascular magnetic resonance feature tracking and tagging for the assessment of left ventricular systolic strain in acute myocardial infarction. *Eur. J. Radiol.* 84 (5), 840–848. doi:10.1016/j.ejrad.2015.02.002

Kim, R. J., Fieno, D. S., Parrish, T. B., Harris, K., Chen, E. L., Simonetti, O., et al. (1999). Relationship of MRI delayed contrast enhancement to irreversible injury, infarct age, and contractile function. *Circulation* 100 (19), 1992–2002. doi:10.1161/01.cir.100.19.1992

Kim, R. J., Wu, E., Rafael, A., Chen, E. L., Parker, M. A., Simonetti, O., et al. (2000). The use of contrast-enhanced magnetic resonance imaging to identify reversible myocardial dysfunction. *N. Engl. J. Med.* 343 (20), 1445–1453. doi:10.1056/NEJM200011163432003

Koos, R., Altiok, E., Doetsch, J., Neizel, M., Krombach, G., Marx, N., et al. (2013). Layer-specific strain-encoded MRI for the evaluation of left ventricular function and infarct transmurality in patients with chronic coronary artery disease. *Int. J. Cardiol.* 166 (1), 85–89. doi:10.1016/j.ijcard.2011.10.004

Larose, E., Rodes-Cabau, J., Pibarot, P., Rinfret, S., Proulx, G., Nguyen, C. M., et al. (2010). Predicting late myocardial recovery and outcomes in the early hours of ST-segment elevation myocardial infarction traditional measures compared with microvascular obstruction, salvaged myocardium, and necrosis characteristics by cardiovascular magnetic resonance. *J. Am. Coll. Cardiol.* 55 (22), 2459–2469. doi:10.1016/j.jacc.2010.02.033

Ledwoch, J., Stiermaier, T., Fuernau, G., de Waha, S., Eitel, C., Poss, J., et al. (2018). Prognostic value and determinants of CMR-derived left atrial function assessed in STEMI. *JACC. Cardiovasc. Imaging* 11 (1), 148–150. doi:10.1016/j.jcmg.2017.02.010

Lund, G. K., Stork, A., Muellerleile, K., Barmeyer, A. A., Bansmann, M. P., Knefel, M., et al. (2007). Prediction of left ventricular remodeling and analysis of infarct resorption in patients with reperfused myocardial infarcts by using contrast-enhanced MR imaging. *Radiology* 245 (1), 95–102. doi:10.1148/radiol.2451061219

Mahrholdt, H., Wagner, A., Judd, R. M., Sechtem, U., and Kim, R. J. (2005). Delayed enhancement cardiovascular magnetic resonance assessment of non-ischaemic cardiomyopathies. *Eur. Heart J.* 26 (15), 1461–1474. doi:10.1093/eurheartj/ehi258

Mangion, K., McComb, C., Auger, D. A., Epstein, F. H., and Berry, C. (2017). Magnetic resonance imaging of myocardial strain after acute ST-segment-elevation myocardial infarction: A systematic review. *Circ. Cardiovasc. Imaging* 10 (8), e006498. doi:10.1161/CIRCIMAGING.117.006498

Moore-Morris, T., Guimaraes-Camboa, N., Banerjee, I., Zambon, A. C., Kisseleva, T., Velayoudon, A., et al. (2014). Resident fibroblast lineages mediate pressure overload-induced cardiac fibrosis. *J. Clin. Invest.* 124 (7), 2921–2934. doi:10.1172/JCI74783

Mordi, I., Bezerra, H., Carrick, D., and Tzemos, N. (2015). The combined incremental prognostic value of LVEF, late gadolinium enhancement, and global circumferential strain assessed by CMR. *JACC. Cardiovasc. Imaging* 8 (5), 540–549. doi:10.1016/j.jcmg.2015.02.005

Mukherjee, R., Brinsa, T. A., Dowdy, K. B., Scott, A. A., Baskin, J. M., Deschamps, A. M., et al. (2003). Myocardial infarct expansion and matrix metalloproteinase inhibition. *Circulation* 107 (4), 618–625. doi:10.1161/01.cir.0000046449.36178.00

Neizel, M., Korosoglou, G., Lossnitzer, D., Kuhl, H., Hoffmann, R., Ocklenburg, C., et al. (2010). Impact of systolic and diastolic deformation indexes assessed by strain-encoded imaging to predict persistent severe myocardial dysfunction in patients after acute myocardial infarction at follow-up. *J. Am. Coll. Cardiol.* 56 (13), 1056–1062. doi:10.1016/j.jacc.2010.02.070

Paolisso, P., Bergamaschi, L., Santulli, G., Gallinoro, E., Cesaro, A., Gragnano, F., et al. (2022). Infarct size, inflammatory burden, and admission hyperglycemia in diabetic patients with acute myocardial infarction treated with SGLT2-inhibitors: A multicenter international registry. *Cardiovasc. Diabetol.* 21 (1), 77. doi:10.1186/s12933-022-01506-8

Pedersen, F., Butrymovich, V., Kelbaek, H., Wachtell, K., Helqvist, S., Kastrup, J., et al. (2014). Short- and long-term cause of death in patients treated with primary PCI for STEMI. *J. Am. Coll. Cardiol.* 64 (20), 2101–2108. doi:10.1016/j.jacc.2014.08.037

Radwan, H., Hussein, E. M., and Refaat, H. (2021). Short- and long-term prognostic value of right ventricular function in patients with first acute ST elevation myocardial infarction treated by primary angioplasty. *Echocardiography* 38 (2), 249–260. doi:10.1111/echo.14974

Reimer, K. A., Lowe, J. E., Rasmussen, M. M., and Jennings, R. B. (1977). The wavefront phenomenon of ischemic cell death. 1. Myocardial infarct size vs duration of coronary occlusion in dogs. *Circulation* 56 (5), 786–794. doi:10.1161/01.cir.56.5.786

Reindl, M., Tiller, C., Holzknecht, M., Lechner, I., Beck, A., Plappert, D., et al. (2019). Prognostic implications of global longitudinal strain by feature-tracking cardiac magnetic resonance in ST-elevation myocardial infarction. *Circ. Cardiovasc. Imaging* 12 (11), e009404. doi:10.1161/CIRCIMAGING.119.009404

Smiseth, O. A., Torp, H., Opdahl, A., Haugaa, K. H., and Urheim, S. (2016). Myocardial strain imaging: How useful is it in clinical decision making? *Eur. Heart J.* 37 (15), 1196–1207. doi:10.1093/eurheartj/ehv529

Sugiyama, T., Hasegawa, K., Kobayashi, Y., Takahashi, O., Fukui, T., and Tsugawa, Y. (2015). Differential time trends of outcomes and costs of care for acute myocardial infarction hospitalizations by ST elevation and type of intervention in the United States, 2001-2011. *J. Am. Heart Assoc.* 4 (3), e001445. doi:10.1161/JAHA.114.001445

Sun, Y., and Weber, K. T. (1996). Angiotensin converting enzyme and myofibroblasts during tissue repair in the rat heart. *J. Mol. Cell. Cardiol.* 28 (5), 851–858. doi:10.1006/jmcc.1996.0080

Szummer, K., Wallentin, L., Lindhagen, L., Alfredsson, J., Erlinge, D., Held, C., et al. (2017). Improved outcomes in patients with ST-elevation myocardial infarction during the last 20 years are related to implementation of evidence-based treatments: Experiences from the SWEDEHEART registry 1995-2014. *Eur. Heart J.* 38 (41), 3056–3065. doi:10.1093/eurheartj/ehx515

Thiele, H., Kappl, M. J., Conradi, S., Niebauer, J., Hambrecht, R., and Schuler, G. (2006). Reproducibility of chronic and acute infarct size measurement by delayed enhancement-magnetic resonance imaging. *J. Am. Coll. Cardiol.* 47 (8), 1641–1645. doi:10.1016/j.jacc.2005.11.065

Yu, S., Zhou, J., Yang, K., Chen, X., Zheng, Y., Zhao, K., et al. (2021). Correlation of myocardial strain and late gadolinium enhancement by cardiac magnetic resonance after a first anterior ST-segment elevation myocardial infarction. *Front. Cardiovasc. Med.* 8, 705487. doi:10.3389/fcvm.2021.705487

frontiers | Frontiers in Pharmacology

TYPE Original Research
PUBLISHED 14 October 2022
DOI 10.3389/fphar.2022.997916

Check for updates

OPEN ACCESS

EDITED BY
Qiong Huang,
Central South University, China

REVIEWED BY
Kelong Ai,
Central South University, China
Hui Tao,
First Affiliated Hospital of Anhui Medical University, China

*CORRESPONDENCE
Panpan Hao,
panda.how@sdu.edu.cn
Yun Zhang,
zhangyun@sdu.edu.cn
Cheng Zhang,
zhangc@sdu.edu.cn

†These authors have contributed equally to this work

SPECIALTY SECTION
This article was submitted to Experimental Pharmacology and Drug Discovery, a section of the journal Frontiers in Pharmacology

RECEIVED 19 July 2022
ACCEPTED 03 October 2022
PUBLISHED 14 October 2022

CITATION
Cheng J, Xue F, Cheng C, Sui W, Zhang M, Qiao L, Ma J, Ji X, Chen W, Yu X, Xi B, Xu F, Su G, Zhao Y, Hao P, Zhang Y and Zhang C (2022), ADAM17 knockdown mitigates while ADAM17 overexpression aggravates cardiac fibrosis and dysfunction via regulating ACE2 shedding and myofibroblast transformation. *Front. Pharmacol.* 13:997916. doi: 10.3389/fphar.2022.997916

COPYRIGHT
© 2022 Cheng, Xue, Cheng, Sui, Zhang, Qiao, Ma, Ji, Chen, Yu, Xi, Xu, Su, Zhao, Hao, Zhang and Zhang. This is an open-access article distributed under the terms of the Creative Commons Attribution License (CC BY). The use, distribution or reproduction in other forums is permitted, provided the original author(s) and the copyright owner(s) are credited and that the original publication in this journal is cited, in accordance with accepted academic practice. No use, distribution or reproduction is permitted which does not comply with these terms.

ADAM17 knockdown mitigates while ADAM17 overexpression aggravates cardiac fibrosis and dysfunction *via* regulating ACE2 shedding and myofibroblast transformation

Jing Cheng[1,2†], Fei Xue[1†], Cheng Cheng[1], Wenhai Sui[1], Meng Zhang[1], Lei Qiao[1], Jing Ma[1], Xiaoping Ji[1], Wenqiang Chen[1], Xiao Yu[3], Bo Xi[4], Feng Xu[5], Guohai Su[6], Yuxia Zhao[1,7], Panpan Hao[1]*, Yun Zhang[1,6]* and Cheng Zhang[1,6]*

[1]The Key Laboratory of Cardiovascular Remodeling and Function Research, Chinese Ministry of Education, Chinese National Health Commission and Chinese Academy of Medical Sciences, The State and Shandong Province Joint Key Laboratory of Translational Cardiovascular Medicine, Department of Cardiology, Qilu Hospital, Cheeloo College of Medicine, Shandong University, Jinan, China, [2]Heart Center and Beijing Key Laboratory of Hypertension, Beijing Chaoyang Hospital, Capital Medical University, Beijing, China, [3]Key Laboratory Experimental Teratology of the Ministry of Education, Department of Physiology, School of Basic Medical Sciences, Cheeloo College of Medicine, Shandong University, Jinan, China, [4]Department of Epidemiology, School of Public Health, Cheeloo College of Medicine, Shandong University, Jinan, China, [5]Department of Emergency Medicine, Chest Pain Center, Shandong Provincial Clinical Research Center for Emergency and Critical Care Medicine, Qilu Hospital, Shandong University, Jinan, China, [6]Cardiovascular Disease Research Center of Shandong First Medical University, Central Hospital Affiliated to Shandong First Medical University, Jinan, China, [7]Department of Traditional Chinese Medicine, Qilu Hospital, Cheeloo College of Medicine, Shandong University, Jinan, China

A disintegrin and metalloprotease domain family protein 17 (ADAM17) is a new member of renin-angiotensin system (RAS) but its role in the pathogenesis of diabetic cardiomyopathy (DCM) is obscure. To test the hypothesis that ADAM17 knockdown mitigates while ADAM17 overexpression aggravates cardiac fibrosis *via* regulating ACE2 shedding and myofibroblast transformation in diabetic mice, ADAM17 gene was knocked down and overexpressed by means of adenovirus-mediated short-hairpin RNA (shRNA) and adenovirus vector carrying ADAM17 cDNA, respectively, in a mouse model of DCM. Two-dimensional and Doppler echocardiography, histopathology and immunohistochemistry were performed in all mice and *in vitro* experiments conducted in primary cardiofibroblasts. The results showed that ADAM17 knockdown ameliorated while ADAM17 overexpression worsened cardiac dysfunction and cardiac fibrosis in diabetic mice. In addition, ADAM17 knockdown increased ACE2 while reduced AT1R expression in diabetic hearts. Mechanistically, ADAM17 knockdown decreased while ADAM17 overexpression increased cardiac fibroblast-to-myofibroblast transformation through regulation of TGF-β1/Smad3 signaling pathway. In conclusion, ADAM17 knockdown attenuates while ADAM17 overexpression

aggravates cardiac fibrosis *via* regulating ACE2 shedding and myofibroblast transformation through TGF-β1/Smad3 signaling pathway in diabetic mice. Targeting ADAM17 may provide a promising approach to the prevention and treatment of cardiac fibrosis in DCM.

KEYWORDS

ADAM17, cardiac fibrosis, ACE2, myofibroblast transformation, TGF-β1/Smad3 signaling

Introduction

The incidence of diabetes has increased rapidly in recent years, and contributed tremendously to the burden of health cost worldwide (Williams et al., 2020). Cardiovascular complications, especially diabetic cardiomyopathy (DCM), are considered as the main cause of morbidity and mortality among diabetic patients (Cai and Kang, 2003). DCM is characterized by prominent cardiac fibrosis and left ventricular remodeling and systolic and diastolic dysfunction (Nakamura and Sadoshima, 2020). Although the pathogenesis of DCM is not completely understood, the vital role of overactivated renin-angiotensin system (RAS) in the development and progression of DCM has been widely recognized and administration of angiotensin converting enzyme inhibitors (ACEIs) and angiotensin receptor blockers (ARBs) have substantially improved the clinical outcomes of patients with DCM (McDonagh and Metra, 2021). However, these classical medications have inherent limitations which make them still insufficient to counteract overactivated RAS in a large number of patients with DCM and novel approaches to counterbalance overactivated RAS in these patients are highly warranted.

A disintegrin and metalloprotease domain family protein 17 (ADAM17), also known as tumor necrosis factor-α converting enzyme (TACE), is a metallopeptidase highly expressed in multiple tissues, such as heart, vessels and brain (Dreymueller et al., 2012). ADAM17 is an important biological regulator of cellular microenvironment by shedding more than 70 cytokines and their receptors (Lichtenthaler and Meinl, 2020) and thereby regulating inflammatory responses, oxidative stress, energy metabolism, and fatty acid metabolism (Zunke and Rose-John, 2017). Recently, it has been demonstrated that ADAM17 participates in the development of several cardiovascular diseases such as hypertensive cardiomyopathy, heart failure, and atherosclerotic heart disease (Iwata et al., 2009; Xu J. et al., 2016a; Chemaly et al., 2017). Angiotensin-converting enzyme 2 (ACE2) cleaves angiotensin II (Ang II) to produce angiotensin-(1–7) [Ang-(1–7)] and thus acts as a negative regulator of RAS (Simões and Teixeira, 2016). ACE2 overexpression and administration of exogenous Ang-(1–7) alleviated Ang II or diabetes-induced cardiac hypertrophy and fibrosis (Zhai et al., 2018; Dang et al., 2020). However, ADAM17 has been found to shed ACE2 on the cell membrane into the peripheral blood (Iwata et al., 2009), which reduces transmembrane ACE2 protein level and activity in the myocardium with a corresponding increase in soluble ACE2 level and activity in the serum. In addition, Ang II may activate ADAM17 leading to enhanced ACE2 shedding, which forms negative feedback of RAS (Patel et al., 2014a). Available evidence showed that ADAM17 expression was elevated in the myocardium of patients with dilated cardiomyopathy (Fedak et al., 2006) and ADAM17 gene silencing prevented Ang II-induced cardiac hypertrophy and fibrosis in mice (Wang et al., 2009). Our previous study found that dickkopf-3 (DKK3) overexpression adequately alleviated Ang II-induced myocardial fibrosis in mice through ADAM17/ACE2 pathway (Zhai et al., 2018). However, the role of ADAM17 in the prevention and treatment of cardiac fibrosis in DCM is still unclear.

Diabetes-induced myocardial fibrosis is characterized by interstitial and perivascular collagen deposition, which ultimately results in myocardial remodeling (Jia et al., 2018). Transformation of fibroblast to myofibroblast is a key step of cardiac fibrosis as myofibroblasts are the principal producer of extracellular matrix composition (ECM), and myofibroblasts are characterized and identified by the presence of α-smooth muscle actin (α-SMA) in these cells (He et al., 2018). Cardiac fibrosis results from collagen deposition and impaired degradation of extracellular matrix composition, and myofibroblast transformation is primarily regulated by TGF-β signaling in mice with myocardial infarction (Zhou et al., 2019). However, the mechanism underlying the role of ADAM17 in myofibroblast transformation has not been clarified. Thus, the present study was undertaken to test the hypothesis that ADAM17 knockdown mitigates while ADAM17 overexpression aggravates cardiac fibrosis *via* regulating ACE2 shedding and myofibroblast transformation through TGF-β1/Smad3 signaling pathway in diabetic mice.

Methods

Animal model

Fifty C57BL/6J male mice aged 8 weeks were randomly assigned to five groups: normal control (NC) group, diabetes mellitus (DM) group, DM + adenovirus vector (DM + Vector) group, DM + ADAM17-shRNA group, and DM + Ad-ADAM17 group. All mice except for NC group received intraperitoneal

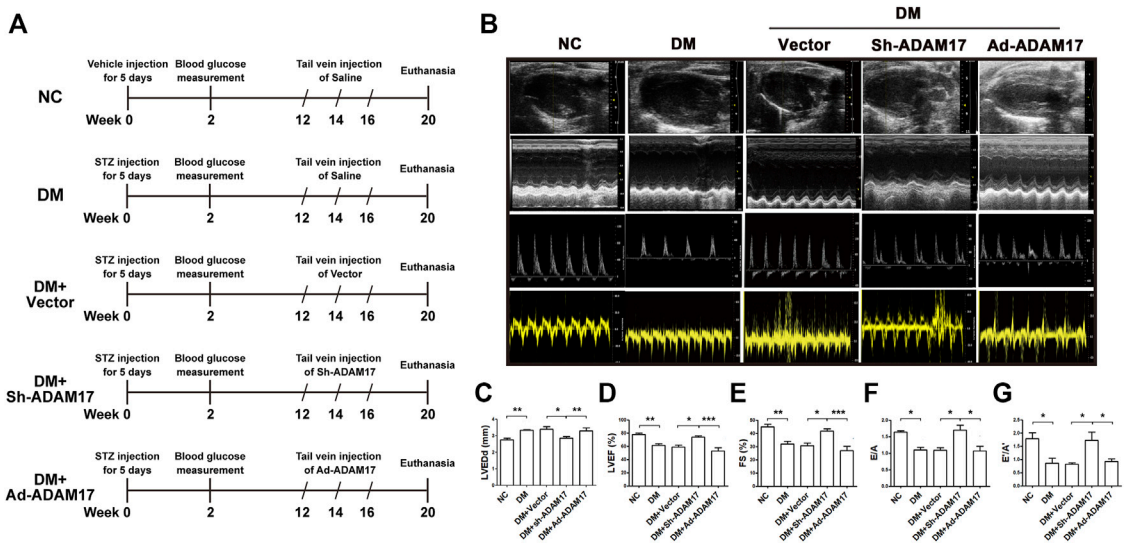


FIGURE 1
Time line of experimental studies and echocardiographic measurements in 5 groups of mice. **(A)** Animal grouping and time line of experimental studies in 5 groups of mice. **(B)** Representative two-dimensional echocardiograms (first row), M-mode echocardiograms (second row), pulse-wave Doppler spectra of mitral inflow (third row), and tissue Doppler spectra of mitral annulus (fourth row). **(C)** Measurements of left ventricular end-diastolic diameter (LVEDd) in 5 groups of mice. **(D)** Measurements of left ventricular ejection fraction (LVEF) in 5 groups of mice. **(E)** Measurements of fractional shortening (FS) in 5 groups of mice. **(F)** Measurements of ratio of early to late left ventricular filling velocity (E/A) in 5 groups of mice. **(G)** Measurements of ratio of early to late diastolic peak annular velocity (E′/A′) in 5 groups of mice. Data were expressed as the means ± SEM. *$p < 0.05$, **$p < 0.01$, ***$p < 0.001$. $n = 10$ per group.

injection of streptozotocin (STZ, Sigma-Aldrich, St Louis, MO) dissolved in 0.2 ml vehicle (0.1 M citrate buffer; pH 4.5) at a dosage of 55 mg/kg for five consecutive days to induce type 1 DM. Mice in the NC group received intraperitoneal injection of equivalent volume of saline. In all mice, fasting blood glucose levels were measured by a glucometer (ACCU-CHEK Advantage; Roche, Indianapolis, IN) 1 week after STZ injection. Only mice with blood glucose levels ≥16.7 mM were included in the four DM groups. Adenovirus-mediated shRNA against murine ADAM17 (ADAM17 shRNA) or adenovirus-mediated ADAM17 cDNA (Ad-ADAM17) was used to knockdown or increase ADAM17 expression, respectively (Figure 1A, Protocol). The sequence of ADAM17 shRNA was 5′-GGACCAAGGAGGAAAGTAT-3′. At 12, 14 and 16 weeks after diabetes induction, adenovirus vector carrying ADAM17 cDNA (SinoGenoMax, Beijing, China), 5×10^9 UT/200 uL adenovirus vector carrying ADAM17 shRNA (Genechem, Shanghai, China), and adenovirus vector of equivalent volume (Genechem, Shanghai, China) were injected *via* the tail vein in the DM + adenovirus vector group, DM + ADAM17-shRNA group and DM + Ad-ADAM17 group, respectively. All mice were fed with a normal diet throughout the experiment and body weight was measured before euthanasia. All animal experiments were in accordance with the Guide of the Care and Use of Laboratory Animals (NIH Publication No. 86–23, revised 1996) and approved by the Animal Care and Use Committee of Shandong University Qilu Hospital (Jinan, China).

Two-dimensional and Doppler echocardiography

Left ventricular systolic and diastolic function was assessed by transthoracic echocardiography using Vevo2100 imaging system (VisualSonics, Toronto, Canada) in all mice after anesthesia with isoflurane. Left ventricular end-diastolic diameter (LVEDd) and left ventricular ejection fraction (LVEF) and fractional shortening (FS) were measured by M-mode echocardiography in the left ventricular long axis view. The early (E) and late (A) diastolic mitral flow velocities were measure by pulsed Doppler in the four-chamber view and the ratio of E/A was calculated. The early (E′) and late (A′) diastolic mitral annular velocities were measure by tissue Doppler imaging in the four-chamber view and the ratio of E'/A' was derived.

Histopathology and immunohistochemistry

Mouse hearts were bisected transversely at the mid-ventricular level and then fixed in 4% paraformaldehyde for 12h. Paraffin-embedded specimens were sectioned (4 μm thick of slide) for subsequent experiments. Masson's trichrome staining was performed to detect myocardial fibrosis. Sections were

incubated with primary antibody of anti-ACE2 (dilution, 1:100; Abcam, Cambridge, MA) overnight at 4°C and subsequently incubated with goat anti-rabbit secondary antibody for 30 min at 37°C. Sections were stained with diaminobenzidine and counterstained with hematoxylin. Sections were analyzed using Image-Pro Plus 6.0.

Cell culture

Primary cardiofibroblasts were isolated from 1- to 3-day-old mouse as described previously (Kapadia et al., 2000). Briefly, hearts were excised from 1- to 3-day-old mouse, minced, and digested in 0.08% trypsin (GIBCO) in calcium-free Hanks' balanced salt solution (DHEPES) by serial digestion. Cardiofibroblasts were separated after 2-hr adhesion and cultured in Dulbecco's modified Eagle's medium containing 10% fetal bovine serum and 2 mM glutamine at 37°C under 5% CO_2 and 95% relative humidity condition. Cardiofibroblasts at 60% confluence were randomly divided into 6 groups who were disposed to different treatment: 1) 5.5 mM glucose (low glucose control, NC); 2) combination of 5.5 mM glucose and 27.8 mM mannitol (high osmotic pressure control, HO); 3) 33.3 mM glucose (high glucose, HG); 4) adenovirus-mediated scrambled shRNA prior to high glucose treatment (high glucose and scrambled vector (HG + Vector); 5) adenovirus-mediated ADAM17 shRNA prior to high glucose treatment (high glucose and ADAM17-ShRNA, HG + Sh-ADAM17) and 6) adenovirus-mediated ADAM17 plasmid prior to high glucose treatment (high glucose and ADAM17 plasmid, HG + Ad-ADAM17). To examine the effects of ADAM17 on fibroblast-myofibroblast transition, scrambled vector, adenovirus-mediated ADAM17 shRNA and ADAM17 plasmid were transfected 24 h prior to stimulation with different concentrations of glucose in cardiofibroblasts.

Quantitative real-time RT-PCR

Total RNA was extracted from primary cardiofibroblasts by using RNA Extraction Kit (CWBIO, Beijing, China). Applied Biosystems cDNA Reverse Transcription and CWBIO SYBR RT-PCR kits were used for quantitative real-time RT-PCR. The primer sequences for ADAM17, ACE2 and β-actin genes are listed in Supplementary Table S1. Quantitative values were obtained from the threshold cycle value (Ct value) and relative mRNA expression levels were analyzed by the $2^{-\triangle\triangle Ct}$ method.

ADAM17 activity assay

After treatment, cardiofibroblasts were lysed by activity assay buffer (pH 7.4; 50 mM Tris HCl, 25 mM NaCl, 4% glycerol and 10 mM $ZnCl_2$). ADAM17 activity was measured in triplicate for each sample by using the SensoLyte 520 TACE (α-Secretase) Activity Assay Kit (AnaSpec, Fremont, CA).

Enzyme-linked immunosorbent assay

Supernatant concentration of ACE2 was measured by ELISA kit (OmnimAbs, CA) following the manufacturer's instructions. All samples were detected in triplicate in a blinded manner.

Immunofluorescence staining

After treatment, cardiofibroblasts were washed with PBS and fixed with 4% paraformaldehyde for 15 min at room temperature. Then cells were blocked by 5% donkey serum (Sigma-Aldrich, St Louis, MO) for 1 h at room temperature after rinsing thoroughly. Cardiofibroblasts were incubated overnight at 4°C with anti-S100A4 (1:100; Proteintech, Wuhan, China) and anti-α-SMA (1:200; Abcam). Sections were then incubated with fluorescent secondary antibodies conjugated with Alexa Fluor 594-conjugated anti-rabbit (1:400; Abcam) and Alexa Fluor 488 anti-mouse (1:400; Abcam) for 1 h at room temperature. Nuclei were counterstained with 4',6 diamino-2-phenylindole (DAPI, Abcam). Images were captured though laser scanning confocal microscopy (ECLIPSE-Ni, Nikon, Japan).

Western blot analysis

Proteins from cardiofibroblasts and murine heart tissues were separated by 10% sodium dodecyl sulfate-polyacrylamide gel electrophoresis (SDS-PAGE). Then proteins were transferred to PVDF membrane from SDS-PAGE gel. Proteins in PVDF membrane were incubated with primary antibodies for collagen I (1:1,000; Abcam), collagen III (1:1,000; Abcam), TGF-β1 (1:1,000; Abcam), ADAM17 (1:1,000; Abcam), ACE2 (1:1,000; Abcam), Ang receptor type I (AT1R) (1:1,000; Abcam), Ang receptor type II (AT2R) (1:1,000; Abcam), MasR (1:1,000; OmnimAbs, CA), α-SMA (1:1,000; Abcam), p-p38 (1:1,000; Cell Signaling Technology, Danvers, MA), p38 (1:1,000; Cell Signaling Technology), p-Smad3 (1:1,000; Cell Signaling Technology), Smad3 (1:1,000; Cell Signaling Technology), and GAPDH (1:1,000; Abcam) overnight at 4°C. The membranes were then washed and incubated with horseradish peroxidase-conjugated secondary antibodies (1:5,000; Proteintech, Wuhan, China) for 1 h at room temperature. Protein levels of collagen I, collagen III, ADAM17, ACE2 and TGF-β1 were normalized to that of GAPDH, and levels of phospho-proteins were normalized to that of total proteins.

Data analysis

Continuous data were reported as the mean ± standard error of mean (SEM). Comparisons were analyzed by one-way analysis of variance (ANOVA) and Post hoc Bonferroni tests were performed in case of significant interactions of ANOVAs. p value <0.05 was considered statistically significant. GraphPad Prism version 7.0 (GraphPad Software Inc., San Diego, CA) was used for statistical analysis.

Results

ADAM17 knockdown ameliorated while ADAM17 overexpression worsened cardiac dysfunction in diabetic mice

At the end of the experiment, blood glucose level was significantly increased in all diabetic groups compared with the normal control group. However, blood glucose level did not differ between DM + adenovirus vector group and DM + ADAM17-shRNA group or DM + Ad-ADAM17 group (Supplementary Figure S1A).

Echocardiography was used to assess left ventricular systolic and diastolic function in all mice before euthanasia. As shown in Figure 1, LVEDd was increased whereas LVEF, FS, E/A and E'/A′ were decreased in DM and DM + Vector groups of mice in comparison with the NC group (Figures 1B–G). However, these measurements in cardiac size and function were substantially improved in the ADAM17-shRNA group relative to the DM + Vector group and basically returned to the NC group levels (Figures 1B–G). In contrast, LVEDd was again increased whereas LVEF, FS, E/A and E'/A' were decreased in DM + Ad-ADAM17 group in comparison with NC group and these differences were more significant for values of LVEF and FS. These results indicated that ADAM17 knockdown ameliorated while ADAM17 overexpression worsened cardiac dysfunction in diabetic mice.

ADAM17 knockdown prevented while ADAM17 overexpression promoted cardiac fibrosis in diabetic mice

HE staining showed that the heart size and the left ventricular cross-sectional area were larger in DM and DM + Vector groups than in the NC group, and normalized in the ADAM17-shRNA group, which were again increased in Ad-ADAM17 group (Figure 2A). Heart-to-body weight ratio was increased in DM and DM + Vector groups of mice *versus* the NC group, which was largely reversed in the DM + ADAM17-shRNA group but resumed in the DM + Ad-ADAM17 group (Figure 2B). Masson's trichrome staining showed that the left ventricular fibrotic area was dramatically increased in DM and DM + Vector groups of mice compared with that in the NC group, and such an increase was substantially abolished by ADAM17-shRNA treatment while reverted to a higher level by Ad-ADAM17 treatment relative to the DM + Vector group (Figures 2A,C). Furthermore, mice in the DM and DM + Vector groups exhibited a higher level of collagen I and collagen III expression compared with the NC group, which was offset by ADAM17-shRNA treatment but resumed by Ad-ADAM17 treatment (Figures 2D–F). These results suggested that ADAM17 inhibition prevented while ADAM17 overexpression promoted cardiac fibrosis in diabetic mice.

ADAM17 knockdown increased ACE2 while reduced AT1R expression in diabetic hearts

In comparison with the NC group, ADAM17 mRNA and protein expression in the myocardium was significantly increased in the DM group relative to the NC group, possibly due to an activated RAS in the setting of diabetes. However, ADAM17-shRNA treatment reduced cardiac ADAM17 mRNA and protein levels virtually to the levels of NC group which were again raised to high levels by Ad-ADAM17 treatment (Figures 3A–C). These results verified the successful knockdown and overexpression of ADAM17 in our DCM model, which were the premise of imaging, morphological, and molecular biological changes in these animals. By comparison, ACE2 expression did not differ between NC and DM or DM + Vector groups. However, ADAM17-shRNA treatment significantly increased the expression level of ACE2 protein in diabetic hearts as detected by both Western blot (Figures 3B,D) and immunohistochemistry (Figures 3E,F). In addition, AT1R protein expression was markedly higher in DM or DM + Vector groups than the NC group, possibly due to activated RAS and increased Ang II secretion in diabetic hearts ae revealed by our previous studies (Dong et al., 2012). ADAM17-shRNA treatment significantly reduced AT1R protein level as compared with DM + Vector group (Figures 3G,H), which was reverted by Ad-ADAM17 treatment. In contrast, no difference was observed in AT2R and MasR protein levels among five groups of mice.

ADAM17 knockdown decreased while ADAM17 overexpression increased myofibroblast transformation in diabetic hearts

As shown in Figure 4, the protein expression of α-SMA, a unique marker of cardio-myofibroblast, was remarkably increased in DM or DM + Vector groups relative to the NC group, which was blunted by ADAM17-shRNA treatment while

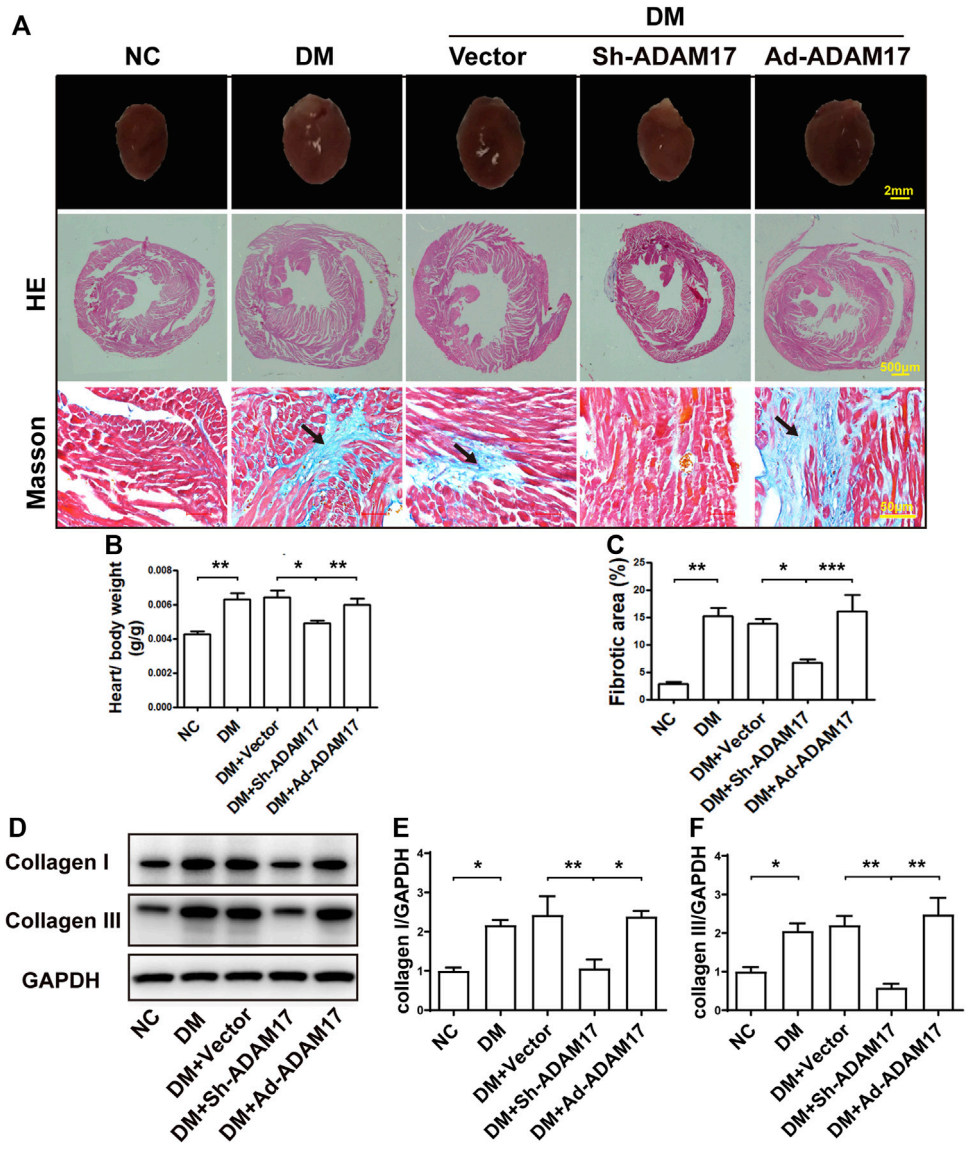


FIGURE 2
Comparison of heart size, cardiac fibrosis and myocardial collagen deposition in 5 groups of mice. **(A)** Representative images of cardiac cross sections (first row; scale bar: 2 mm), hematoxylin and eosin (HE) staining (second row, 40x, scale bar: 500 μm; third row, 400x, scale bar: 50 μm) and Masson's trichrome staining (fourth row; 400x, scale bar: 50 μm) in 5 groups of mice. **(B)** Measurements of heart/body weight ratio in 5 groups of mice. **(C)** Measurements of fibrotic area in cardiac cross sections in 5 groups of mice. **(D)** Representative Western blot images and quantification of collagen I **(E)** and III **(F)** expression in 5 groups of mice. Data were expressed as the means ± SEM. $*p < 0.05$, $**p < 0.01$, $***p < 0.001$. $n = 6$ per group.

raised again to a even higher level by Ad-ADAM17 treatment (Figures 4A,B). There was no significant difference in p38 phosphorylation level among 5 groups of mice (Figures 4A,C). Both TGF-β1 protein expression and Smad3 phosphorylation levels were significantly higher in DM or DM + Vector groups than the NC group, which were reduced to the NC group level in the ADAM17-shRNA group and resumed in the Ad-ADAM17 group (Figures 4A,D,E). Taken together, ADAM17 knockdown decreased while ADAM17 overexpression increased myofibroblast transformation in diabetic hearts.

Effects of high glucose treatment and ADAM17 gene manipulation on RAS *in vitro*

Primary cardiofibroblasts were divided into 6 groups depending to different treatments (NC, HO, HG, HG +

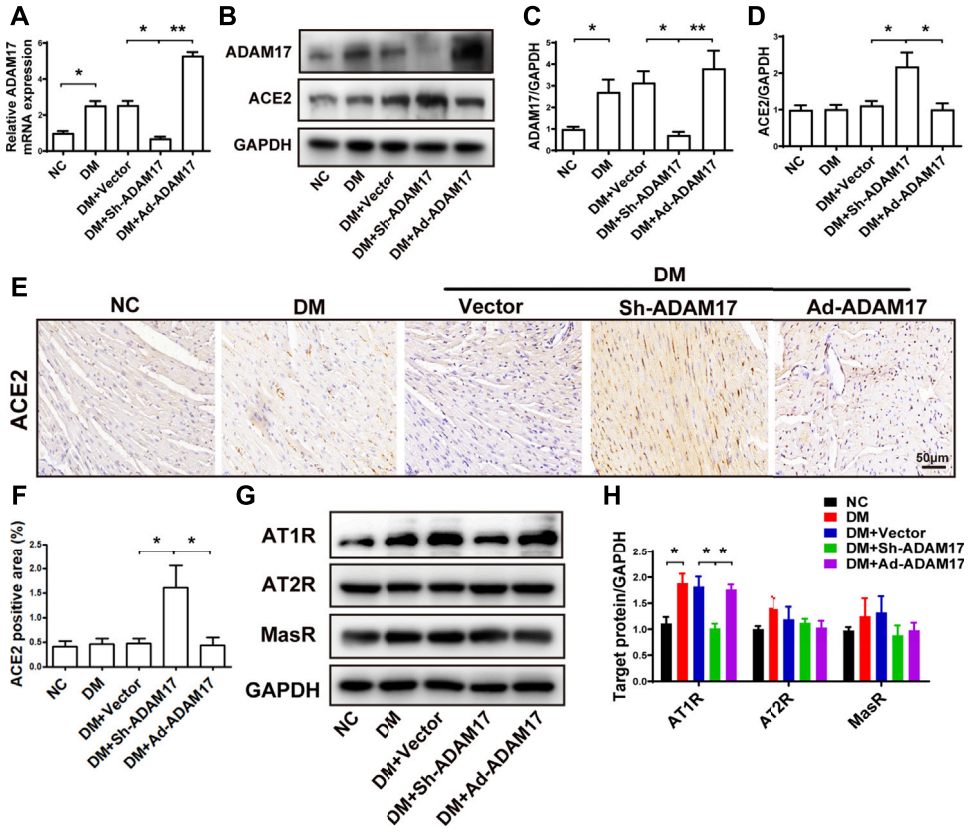


FIGURE 3
Comparison of ADAM17, ACE2, AT1R, AT2R and MasR expression in 5 groups of mice. **(A)** Quantification of mRNA level of ADAM17 in 5 groups of mice. **(B)** Representative Western blot images of ADAM17 and ACE2 in 5 groups of mice. **(C)** Quantification of protein expression of ADAM17 in 5 groups of mice. **(D)** Quantification of protein expression of ACE2 in 5 groups of mice. **(E)** Representative immunohistochemical staining of ACE2 (Scale: 50 μm) in 5 groups of mice. **(F)** Quantitative analysis of ACE2 expression in 5 groups of mice. **(G)** Representative Western blot images of AT1R, AT2R and MasR in 5 groups of mice. **(H)** Quantification of protein expression of AT1R, AT2R and MasR in 5 groups of mice. Data were expressed as the means ± SEM. $*p < 0.05$, $**p < 0.01$, $***p < 0.001$. $n = 6$ per group.

Vector, HG + Sh-ADAM17, and HG + Ad-ADAM17 groups). The HO group was used to assess the effect of a higher osmotic pressure on protein expression in the four HG groups *versus* the NC group. As no significant difference in the protein expression of ADAM17, ACE2, AT1R, AT2R and MasR was noted between the NC and HO groups, the possibility that a high osmotic pressure in cell culture solution may alter protein expression in the HG groups can be eliminated. (Figures 5A,B). ADAM17 mRNA and protein expression was significantly increased in the HG and HG + Vector groups relative to the NC groups, which returned to the baseline level in the HG + Sh-ADAM17 group while raised again in the HG + Ad-ADAM17 group (Figures 5A–D). ACE2 mRNA level was dramatically increased in cardiofibroblasts exposed to high glucose compared with the NC group, which was not altered by ADAM17 knockdown or overexpression (Figure 5E). No difference in ACE2 protein level was observed among cardiofibroblasts in the NC, HO, HG and HG + Vector, which was similar to our *in vivo* finding that ACE2 protein expression did not differ between NC and DM or DM + Vector groups of mice. In contrast, ADAM17 knockdown significantly increased ACE2 protein level in cardiofibroblasts stimulated with high glucose, which was abolished by ADAM17 overexpression (Figures 5A,B). By comparison, ACE2 protein level in the cell supernatant was significantly increased in HG group *versus* the NC and HO groups, and ADAM17 shRNA treatment significantly reduced ACE2 level in the supernatant (Figure 5F), indicating that ADAM17 may cleave ACE2 into supernatant under high glucose conditions. Furthermore, ADAM17 knockdown significantly reduced AT1R protein expression in cardiofibroblasts cultured in high glucose as compared with scramble vector treatment (Figures 5A,B). However, there was no significant difference in AT2R and MasR protein expressions in cardiofibroblasts among 6 groups of cardiofibroblasts (Figures 5A,B).

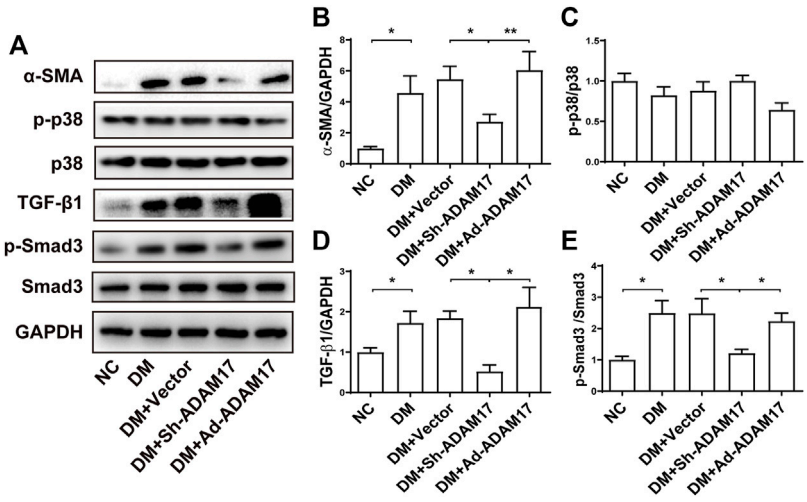


FIGURE 4
Comparison of α-SMA, p38, TGF-β1, and Smad3 expression in 5 groups of mice. **(A)** Representative Western blot images of α-SMA, p-p38, p38, TGF-β1, p-Smad3 and Smad3 in 5 groups of mice. **(B)** Quantification of α-SMA protein expression in 5 groups of mice. **(C)** Quantification of p38 phosphorylation in 5 groups of mice. **(D)** Quantification of TGF-β1 protein expression in 5 groups of mice. **(E)** Quantification of Smad3 phosphorylation in 5 groups of mice. Data were expressed as the means ± SEM. $*p < 0.05$, $**p < 0.01$, $***p < 0.001$. $n = 6$ per group.

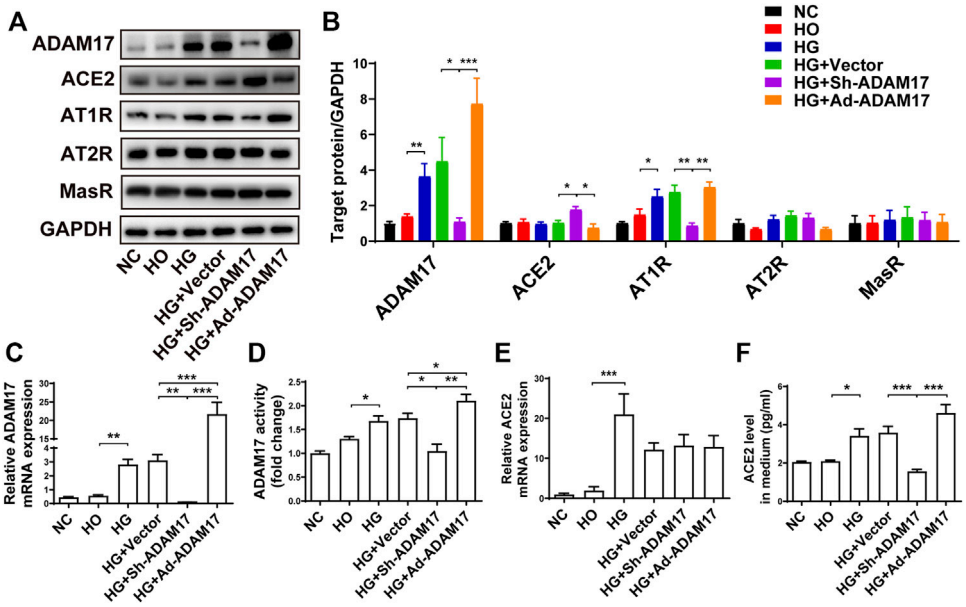


FIGURE 5
Comparison of ADAM17, ACE2, AT1R, AT2R and MasR expression in 6 groups of primary cardiofibroblasts. **(A)** Representative Western blot images of ADAM17, ACE2, AT1R, AT2R, and MasR in 6 groups of cardiofibroblasts. **(B)** Quantification of protein expression of ADAM17, ACE2, AT1R, AT2R, and MasR in 6 groups of cardiofibroblasts. **(C)** Quantification of mRNA level of ADAM17 in 6 groups of cardiofibroblasts. **(D)** Quantification of ADAM17 activity in 6 groups of cardiofibroblasts. **(E)** Quantification of mRNA level of ACE2 in 6 groups of cardiofibroblasts. **(F)** Quantification of ACE2 expression in the medium supernatant of 6 groups of cardiofibroblasts. Data were expressed as the means ± SEM. $*p < 0.05$, $**p < 0.01$, $***p < 0.001$. $n = 6$ per group.

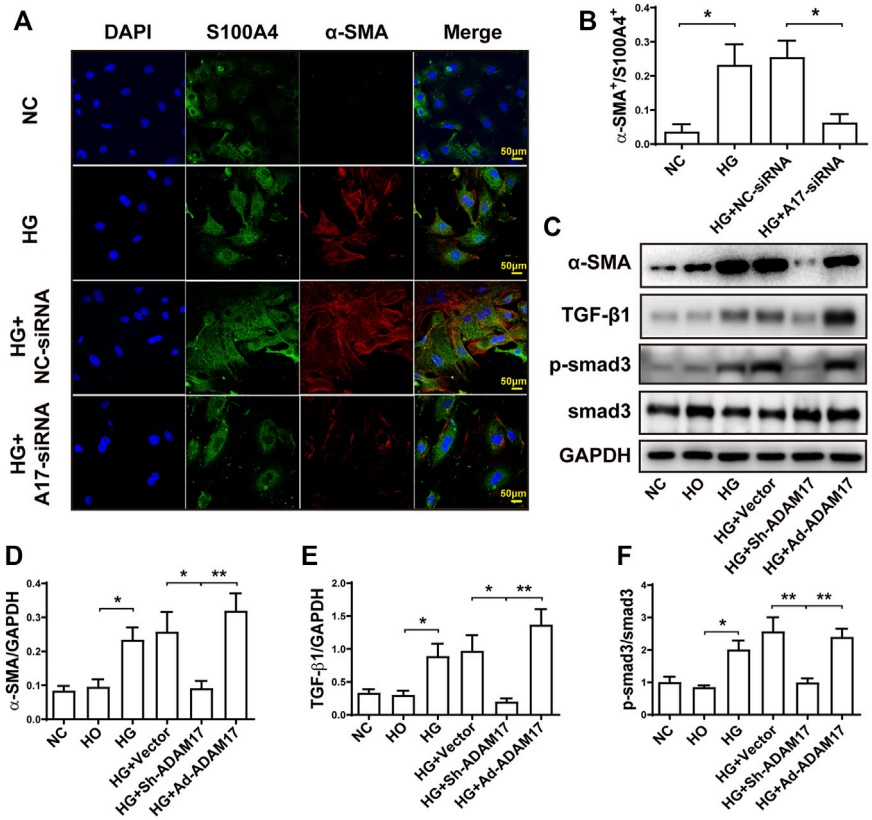


FIGURE 6
Comparison of α-SMA, S100A4, TGF-β1 and Smad3 in primary cardiofibroblasts. **(A)** Representative immunohistochemical staining of S100A4 and α-SMA (400x, scale bar: 50 μm) in 4 groups of cardiofibroblasts. **(B)** Quantification of α-SMA$^+$/S100A4$^+$ ratio in 4 groups of cardiofibroblasts. **(C)** Representative Western blot images of α-SMA, TGF-β1, Smad3 phosphorylation and Smad3 in 6 groups of cardiofibroblasts. **(D)** Quantification of α-SMA protein expression in 6 groups of cardiofibroblasts. **(E)** Quantification of TGF-β1 protein expression in 6 groups of cardiofibroblasts. **(F)** Quantification of Smad3 phosphorylation level in 6 groups of cardiofibroblasts. Data were expressed as the means ± SEM. *p < 0.05, **p < 0.01, ***p < 0.001. n = 6 per group.

ADAM17 knockdown and overexpression affected myofibroblast transformation through regulation of TGF-β1/Smad3 pathway *in vitro*

We further examined the effect of ADAM17 knockdown and overexpression on myofibroblast transformation and the underlying mechanism in primary cardiofibroblasts. As shown in Figure 6, the green and red staining represented S100A4-positive and α-SMA-positive cells, respectively, where S100A4 is a marker of cardiofibroblasts and α-SMA is a marker of myofibroblasts. High glucose stimulation significantly increased α-SMA$^+$/S100A4$^+$ ratio compared with NC group, while this ratio was normalized in the HG + ADAM17-siRNA group (Figures 6A,B). In addition, high glucose treatment significantly increased α-SMA and TGF-β1 protein expressions as well as Smad3 phosphorylation in cardiofibroblasts, relative to the NC group, which were reversed by ADAM17 knockdown but increased again by ADAM 17 overexpression (Figures 6C–F).

Discussion

There were several important findings in the present study. Frist, ADAM17 knockdown ameliorated while ADAM17 overexpression worsened cardiac dysfunction and cardiac fibrosis in diabetic mice. Second, ADAM17 knockdown increased ACE2 while reduced AT1R expression in diabetic hearts; Third, ADAM17 knockdown decreased while ADAM17 overexpression increased myofibroblast transformation through regulation of TGF-β1/Smad3 pathway. To the best of our knowledge, our study is the first to demonstrate the opposite effects of

ADAM17 knockdown and overexpression on cardiac fibrosis in diabetic hearts through regulating ACE2 shedding and myofibroblast transformation.

Ample evidence indicates that overactivation of RAS plays a key role in the pathogenesis of cardiac fibrosis in diabetic cardiomyopathy and attempts at diminishing RAS activity ameliorate cardiac pathology and function in this condition. ACE2, a homolog of ACE, is expressed widely in the heart which converts octapeptide angiotensin Ang II to heptapeptide Ang-(1–7), thus mitigating the deleterious effects of RAS (Nunes-Silva et al., 2017). Recent studies found that ACE2 ectodomain can be cleaved by ADAM17 and then released from the cell membrane into the extracellular milieu (Xu et al., 2017). In the present study, ACE2 mRNA level was increased in high glucose-treated cardiofibroblasts relative to the NC group, whereas ACE2 protein levels were not increased in HG-treated cardiofibroblasts or diabetic mice relative to the normal control group, which might be because an upregulated ACE2 mRNA level may increase ACE2 protein expression whereas upregulated ADAM17 expression may enhance ACE2 shedding in the diabetic condition, resulting in an unchanged ACE2 protein expression. However, ADAM17 knockdown significantly increased ACE2 protein levels in both diabetic hearts and HG-treated cardiofibroblasts. Similarly, protein levels of ADAM17 and AT1R were increased in diabetic hearts and HG-treated cardiofibroblasts, which were both reversed by ADAM17 knockdown. Patel et al. also found that Ang II infusion upregulated the expression of myocardial ADAM17, which was mediated by AT1R, and ADAM17 inhibition prevented ACE2 shedding (Patel et al., 2014a). Thus, our study provided evidence that ADAM17 knockdown diminished ACE2 shedding, thus preserving the ACE2 function to convert profibrotic Ang II to antifibrotic Ang-(1–7). As HG stimulation upregulated ADAM17 protein expression in cardiofibroblasts, ACE2 level in supernatant medium was increased secondary to enhanced ACE2 shedding. In contrast, ADAM17 knockdown significantly decreased ACE2 shedding, resulting in a declined ACE2 level in supernatant medium. Nonetheless, either knockdown or overexpression of ADAM17 exerted no effect on the mRNA level of ACE2.

DCM, as a serious diabetic complication, is characterized as abnormal cardiac structure and function. Cardiac fibrosis is a salient pathological feature of DCM manifested as accumulation of extracellular matrix proteins including collagen I and III, which may lead to an increased left and right ventricular stiffness and cardiac diastolic dysfunction (Hao P. P. et al., 2015b). Progressive cardiac fibrosis may ultimately induce cardiac systolic dysfunction and overt heart failure (Evangelista et al., 2019). Numerous studies have shown that TGF-β1 is an important mediator in fibrogenesis and DCM progression (Yue et al., 2017). In the current study, two-dimensional and Doppler echocardiography revealed left ventricular systolic and diastolic dysfunction in diabetic mice, which was significantly improved by ADAM17 shRNA treatment. In addition, ADAM17 knockdown decreased collagen deposition and downregulated collagen I, collagen III and TGF-β1 expression in diabetic hearts. On the contrary, ADAM17 overexpression enhanced collagen deposition and expression in the myocardium of diabetic mice. These results lend support to previous observations that ADAM17 systemic knockdown prevented cardiac hypertrophy and myocardial fibrosis in spontaneously hypertensive rodents (Wang et al., 2009), and ADAM17 antibody prevented cardiac hypertrophy and fibrosis induced by Ang II infusion (Takayanagi et al., 2016). Thus, ADAM17 inhibition reduced collagen I, collagen III and TGF-β1 expression, and ameliorated cardiac fibrosis in diabetic cardiomyopathy.

TGF-β, as a master regulator in tissue fibrosis, consists of three isoforms, TGF-β1, TGF-β2 and TGF-β3 (Zhao et al., 2020). TGF-β activation promoted myofibroblast differentiation and secretion of ECM components, such as collagen and fibronectin (Wang et al., 2021). TGF-β1 mediated fibrosis *via* its downstream Smad3 rather than Smad2 signaling (Meng et al., 2010). Loss of Smad3 reduced cardiac fibrosis and improved cardiac compliance (Biernacka et al., 2015). Besides, Smad3 binds to the promoter of α-SMA in mouse cardiofibroblasts and regulates its transcription (Li et al., 2011). Deletion of Smad3 protected against cardiac fibrosis under a number of conditions such as hypertension, myocardial infarction, and diabetes (Li et al., 2011). In addition, Smad3-deficient mice demonstrated reduction in both renal and cardiac fibrosis in STZ-induced type 1 diabetes and in obese diabetic mice (Wang et al., 2007; Biernacka et al., 2015). Taken together, accumulating evidence suggests that TGF-β/Smad3 signaling plays an important role in cardiovascular diseases, especially in the pathogenesis of DCM (Wang et al., 2021).

Upon myocardial injury, resting cardiac fibroblasts are transdifferentiated into contractile and secretory myofibroblasts, which produce and secret a large amount of TGF-β1, collagen I and collagen III to promote cardiac repairment. However, sustained activation of myofibroblasts may lead to excessive accumulation of extracellular matrix and cardiac fibrosis (Weber et al., 2013). As the quantity of cardiac fibroblasts are overwhelmingly beyond that of cardiomyocytes, an increased fibroblast-to-myofibroblast transformation have been recognized as an important biomarker of cardiac fibrosis (Frangogiannis, 2019). In this study, the expression α-SMA, a marker of myofibroblasts, was significantly increased in high glucose-treated cardiofibroblasts, indicating an enhanced fibroblast-to-myofibroblast transformation, which was reversed by ADAM17 knockdown, suggesting a normalized fibroblast-myofibroblast transformation. In addition, previous studies have shown that both canonical and non-canonical TGF-β signaling pathways play an important role in the development of cardiac fibrosis

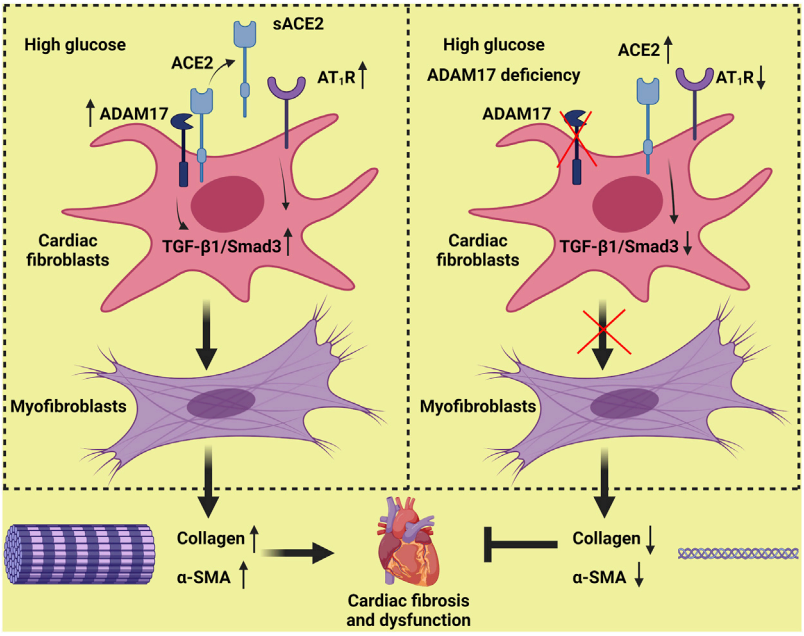


FIGURE 7
Proposed mechanisms underlying the roles of ADAM17 in cardiac fibrosis. High glucose increases ADAM17 activity, ACE2 shedding and AT1R expression, which activates TGF-β1/Smad3 signaling in cardiac fibroblasts, leading to an enhanced myofibroblast transformation and collagen deposition in the myocardium. ADAM17 deficiency attenuates ACE2 shedding and AT1R expression, which inactivates TGF-β1/Smad3 signaling in cardiac fibroblasts, leading to a reduced myofibroblast transformation and collagen deposition in the myocardium, thus ameliorating diabetes-induced left ventricular dysfunction and cardiac fibrosis.

(Finnson et al., 2020). In light of the interplay between ADAM17 and cardiac fibrosis, there may be a possible link between ADAM17 and TGF-β. In the present study, we found that ADAM17-shRNA treatment reversed the elevated levels of TGF-β1 protein expression and decreased the phosphorylation level of Smad3 in diabetic mice. This is consistent with a previous study where 25-O-methylalisol F (MAF), a novel RAS inhibitor, was found to attenuate tubulo-interstitial fibrosis and epithelial-mesenchymal transition *via* inhibiting Smad3 signaling without altering Smad2, PI3K, ERK1/2 and p38 phosphorylation in Ang II-stimulated fibroblasts (Chen et al., 2018). In addition, TGF-β was reported to promote fibroblast-to-myofibroblast transformation, and canonical TGF-β signaling upregulated Smad2/3 transcription factors thereby inducing cardiac fibrosis (Khalil et al., 2017). Thus, our results supported the notion that ADAM17 knockdown ameliorates cardiac fibrosis probably *via* TGF-β/Smad3 signaling in diabetes mice. Besides, a recent study showed that ADAM17 knockdown inhibited the expression of TGF-β in gastric carcinoma cells, with the downstream Smad2 and Smad3 also being attenuated (Xu M. et al., 2016b). Furthermore, Kawasaki disease and secondary coronary artery lesions are found to be associated with ADAM17 genetic variants through TGF-β/Smad3 signaling pathway (Peng et al., 2016). Thus, ADAM17 inhibition may play a protective role in cardiac fibrosis, which is likely mediated by TGF-β/Smad3 signaling pathway.

The majority of detrimental effects of Ang II is mediated *via* AT1R activation (Patel et al., 2014b). High glucose stimulation increases intracellular Ang II production in cardiomyocytes, resulting in an activation of the Ang II/AT1R pathway (Sukumaran et al., 2017). Previous studies demonstrated that administration of ACE2 activator increased ACE2 expression and activity while decreased AT1R expression in the myocardium of rats with DCM (Murça et al., 2012a; Murça et al., 2012b). In the present study, ADAM17 knockdown upregulated ACE2 expression and downregulated AT1R expression, but exerted no effect on AT2R and MasR expression. The study by Wang et al., who used ADAM17 knockdown to treat Ang II-induced cardiac hypertrophy and fibrosis in mice, did not explore the effect of ADAM17 knockdown on AT1R, AT2R and MasR expression (Wang et al., 2009). Other studies that used Ang-(1–7) or azilsartan to treat DCM in rats or mice found a significant reduction in AT1R expression in the myocardium but the effect on AT2R and MasR expression was variable (Hao P. et al., 2015a; Sukumaran et al., 2017). Thus, the major therapeutic benefit of ADAM17 knockdown in the current mouse model of DCM derived from AT1R inhibition.

There were a couple of limitations to the present study. First, adenovirus-mediated shRNA against murine ADAM17 was used to inhibit ADAM17 activity although cardiac fibroblast-specific knockout of ADAM17 may more effectively remove the function of ADAM17 in the pathogenesis of cardiac fibrosis. As there is no specific marker of cardiac fibroblast, we created a mouse model of fibroblast-specific knockout of ADAM17 and found severe sepsis and high mortality in these mice with unclear mechanism. To date, there has been no report in the literature of a successful mouse model of cardiac fibroblast-specific knockout of ADAM17. Second, although we found that ADAM17 knockdown ameliorated cardiac fibrosis probably *via* TGF-β/Smad3 signaling, we did not testify the causal relation between TGF-β/Smad3 signaling and cardiac fibrosis in our mouse model, and further studies are warranted in this regard. Finally, it has been shown that oxidative stress plays a major role in myocardial ischemia reperfusion injury (Chen et al., 2021; Zhao et al., 2022) and DCM (Ren et al., 2020), and it requires further investigation whether the therapeutic effects of ADAM17 knockdown on DCM involve suppression of oxidative stress.

In conclusion, ADAM17 knockdown ameliorated while ADAM17 overexpression worsened cardiac dysfunction and cardiac fibrosis in diabetic mice. The mechanism may involve reduced ACE2 shedding and myofibroblast transformation through inhibition of TGF-β1/Smad3 pathway by ADAM17 knockdown (Figure 7). Targeting ADAM17 may provide a promising approach to prevention and treatment of cardiac fibrosis in DCM.

Data availability statement

The original contributions presented in the study are included in the article/Supplementary Material, further inquiries can be directed to the corresponding authors.

Ethics statement

The animal study was reviewed and approved by Animal Care and Use Committee of Shandong University Qilu Hospital (Jinan, China).

Author contributions

JC, PH, FX, CC and LQ performed animal experiments. JC, JM, MZ and Wenhai Sui conducted cell culture and intervention. JC, PH and BX analyzed data and drafted the manuscript. XJ, WC, GS, YZ, XY, FX, PH, CZ and YZ reviewed and edited the manuscript. PH, YZ and CZ contributed to study design. All authors read and approved the final manuscript.

Funding

This work was supported by the International Collaboration and Exchange Program of China (81920108003), the Program of Introducing Talents of Discipline to Universities (BP0719033), the State Key Program of National Natural Science of China (82030051), the grants of the National Natural Science Foundation of China (82170267, 82000411), the Natural Science Foundation of Shandong Province (ZR2020QH023), Key Research and Development Plan of Shandong Province (2020ZLYS05, 2021SFGC0503, 2021ZDSYS05) and Taishan Scholar Project of Shandong Province of China (Zhang C).

Acknowledgments

We thank the BioRender, a web-based drawing tool, for providing some elements used in Figure 7.

Conflict of interest

The authors declare that the research was conducted in the absence of any commercial or financial relationships that could be construed as a potential conflict of interest.

Publisher's note

All claims expressed in this article are solely those of the authors and do not necessarily represent those of their affiliated organizations, or those of the publisher, the editors and the reviewers. Any product that may be evaluated in this article, or claim that may be made by its manufacturer, is not guaranteed or endorsed by the publisher.

Supplementary material

The Supplementary Material for this article can be found online at: https://www.frontiersin.org/articles/10.3389/fphar.2022.997916/full#supplementary-material

References

Biernacka, A., Cavalera, M., Wang, J., Russo, I., Shinde, A., Kong, P., et al. (2015). Smad3 signaling promotes fibrosis while preserving cardiac and aortic geometry in obese diabetic mice. *Circ. Heart Fail.* 8 (4), 788–798. doi:10.1161/circheartfailure.114.001963

Cai, L., and Kang, Y. J. (2003). Cell death and diabetic cardiomyopathy. *Cardiovasc. Toxicol.* 3 (3), 219–228. doi:10.1385/ct:3:3:219

Chemaly, M., McGilligan, V., Gibson, M., Clauss, M., Watterson, S., Alexander, H. D., et al. (2017). Role of tumour necrosis factor alpha converting enzyme (TACE/ADAM17) and associated proteins in coronary artery disease and cardiac events. *Arch. Cardiovasc. Dis.* 110 (12), 700–711. doi:10.1016/j.acvd.2017.08.002

Chen, H., Yang, T., Wang, M. C., Chen, D. Q., Yang, Y., and Zhao, Y. Y. (2018). Novel RAS inhibitor 25-O-methylalisol F attenuates epithelial-to-mesenchymal transition and tubulo-interstitial fibrosis by selectively inhibiting TGF-β-mediated Smad3 phosphorylation. *Phytomedicine* 42, 207–218. doi:10.1016/j.phymed.2018.03.034

Chen, L., Huang, Q., Zhao, T., Sui, L., Wang, S., Xiao, Z., et al. (2021). Nanotherapies for sepsis by regulating inflammatory signals and reactive oxygen and nitrogen species: New insight for treating COVID-19. *Redox Biol.* 45, 102046. doi:10.1016/j.redox.2021.102046

Dang, Z., Su, S., Jin, G., Nan, X., Ma, L., Li, Z., et al. (2020). Tsantan Sumtang attenuated chronic hypoxia-induced right ventricular structure remodeling and fibrosis by equilibrating local ACE-AngII-AT1R/ACE2-Ang1-7-Mas axis in rat. *J. Ethnopharmacol.* 250, 112470. doi:10.1016/j.jep.2019.112470

Dong, B., Yu, Q. T., Dai, H. Y., Gao, Y. Y., Zhou, Z. L., Zhang, L., et al. (2012). Angiotensin-converting enzyme-2 overexpression improves left ventricular remodeling and function in a rat model of diabetic cardiomyopathy. *J. Am. Coll. Cardiol.* 59 (8), 739–747. doi:10.1016/j.jacc.2011.09.071

Dreymueller, D., Pruessmeyer, J., Groth, E., and Ludwig, A. (2012). The role of ADAM-mediated shedding in vascular biology. *Eur. J. Cell. Biol.* 91 (6-7), 472–485. doi:10.1016/j.ejcb.2011.09.003

Evangelista, I., Nuti, R., Picchioni, T., Dotta, F., and Palazzuoli, A. (2019). Molecular dysfunction and phenotypic derangement in diabetic cardiomyopathy. *Int. J. Mol. Sci.* 20 (13), E3264. doi:10.3390/ijms20133264

Fedak, P. W., Moravec, C. S., McCarthy, P. M., Altamentova, S. M., Wong, A. P., Skrtic, M., et al. (2006). Altered expression of disintegrin metalloproteinases and their inhibitor in human dilated cardiomyopathy. *Circulation* 113 (2), 238–245. doi:10.1161/circulationaha.105.571414

Finnson, K. W., Almadani, Y., and Philip, A. (2020). Non-canonical (non-SMAD2/3) TGF-β signaling in fibrosis: Mechanisms and targets. *Semin. Cell. Dev. Biol.* 101, 115–122. doi:10.1016/j.semcdb.2019.11.013

Frangogiannis, N. G. (2019). Cardiac fibrosis: Cell biological mechanisms, molecular pathways and therapeutic opportunities. *Mol. Asp. Med.* 65, 70–99. doi:10.1016/j.mam.2018.07.001

Hao, P. P., Yang, J. M., Zhang, M. X., Zhang, K., Chen, Y. G., Zhang, C., et al. (2015b). Angiotensin-(1-7) treatment mitigates right ventricular fibrosis as a distinctive feature of diabetic cardiomyopathy. *Am. J. Physiol. Heart Circ. Physiol.* 308 (9), H1007–H1019. doi:10.1152/ajpheart.00563.2014

Hao, P., Yang, J., Liu, Y., Zhang, M., Zhang, K., Gao, F., et al. (2015a). Combination of angiotensin-(1-7) with perindopril is better than single therapy in ameliorating diabetic cardiomyopathy. *Sci. Rep.* 5, 8794. doi:10.1038/srep08794

He, Y., Ling, S., Sun, Y., Sheng, Z., Chen, Z., Pan, X., et al. (2018). DNA methylation regulates alpha-smooth muscle actin expression during cardiac fibroblast differentiation. *J. Cell. Physiol.* 234, 7174–7185. doi:10.1002/jcp.27471

Iwata, M., Silva Enciso, J. E., and Greenberg, B. H. (2009). Selective and specific regulation of ectodomain shedding of angiotensin-converting enzyme 2 by tumor necrosis factor alpha-converting enzyme. *Am. J. Physiol. Cell. Physiol.* 297 (5), C1318–C1329. doi:10.1152/ajpcell.00036.2009

Jia, G., Hill, M. A., and Sowers, J. R. (2018). Diabetic cardiomyopathy: An update of mechanisms contributing to this clinical entity. *Circ. Res.* 122 (4), 624–638. doi:10.1161/circresaha.117.311586

Kapadia, S. R., Yakoob, K., Nader, S., Thomas, J. D., Mann, D. L., and Griffin, B. P. (2000). Elevated circulating levels of serum tumor necrosis factor-alpha in patients with hemodynamically significant pressure and volume overload. *J. Am. Coll. Cardiol.* 36 (1), 208–212. doi:10.1016/s0735-1097(00)00721-x

Khalil, H., Kanisicak, O., Prasad, V., Correll, R. N., Fu, X., Schips, T., et al. (2017). Fibroblast-specific TGF-β-Smad2/3 signaling underlies cardiac fibrosis. *J. Clin. Invest.* 127 (10), 3770–3783. doi:10.1172/jci94753

Li, Z., Xie, W. B., Escano, C. S., Asico, L. D., Xie, Q., Jose, P. A., et al. (2011). Response gene to complement 32 is essential for fibroblast activation in renal fibrosis. *J. Biol. Chem.* 286 (48), 41323–41330. doi:10.1074/jbc.M111.259184

Lichtenthaler, S. F., and Meinl, E. (2020). To cut or not to cut: New rules for proteolytic shedding of membrane proteins. *J. Biol. Chem.* 295 (35), 12353–12354. doi:10.1074/jbc.H120.015304

Ma, T., Huang, X., Zheng, H., Huang, G., Li, W., Liu, X., et al. (2021). SFRP2 improves mitochondrial dynamics and mitochondrial biogenesis, oxidative stress, and apoptosis in diabetic cardiomyopathy. *Oxid. Med. Cell. Longev.* 2021, 9265016. doi:10.1155/2021/9265016

McDonagh, T. A., Metra, M., Adamo, M., Gardner, R. S., Baumbach, A., Bohm, M., et al. (2021). 2021 ESC Guidelines for the diagnosis and treatment of acute and chronic heart failure. *Eur. Heart J.* 42 (36), 3599–3726. doi:10.1093/eurheartj/ehab368

Meng, X. M., Huang, X. R., Chung, A. C., Qin, W., Shao, X., Igarashi, P., et al. (2010). Smad2 protects against TGF-beta/Smad3-mediated renal fibrosis. *J. Am. Soc. Nephrol.* 21 (9), 1477–1487. doi:10.1681/asn.2009121244

Murça, T. M., Almeida, T. C., Raizada, M. K., and Ferreira, A. J. (2012a). Chronic activation of endogenous angiotensin-converting enzyme 2 protects diabetic rats from cardiovascular autonomic dysfunction. *Exp. Physiol.* 97 (6), 699–709. doi:10.1113/expphysiol.2011.063461

Murça, T. M., Moraes, P. L., Capuruço, C. A., Santos, S. H., Melo, M. B., Santos, R. A., et al. (2012b). Oral administration of an angiotensin-converting enzyme 2 activator ameliorates diabetes-induced cardiac dysfunction. *Regul. Pept.* 177 (1-3), 107–115. doi:10.1016/j.regpep.2012.05.093

Nakamura, M., and Sadoshima, J. (2020). Cardiomyopathy in obesity, insulin resistance and diabetes. *J. Physiol.* 598 (14), 2977–2993. doi:10.1113/jp276747

Nunes-Silva, A., Rocha, G. C., Magalhaes, D. M., Vaz, L. N., Salviano de Faria, M. H., and Simoes, E. S. A. C. (2017). Physical exercise and ACE2-angiotensin-(1-7)-mas receptor Axis of the renin angiotensin system. *Protein Pept. Lett.* 24 (9), 809–816. doi:10.2174/0929866524666170728151401

Patel, V. B., Clarke, N., Wang, Z., Fan, D., Parajuli, N., Basu, R., et al. (2014a). Angiotensin II induced proteolytic cleavage of myocardial ACE2 is mediated by TACE/ADAM-17: A positive feedback mechanism in the RAS. *J. Mol. Cell. Cardiol.* 66, 167–176. doi:10.1016/j.yjmcc.2013.11.017

Patel, V. B., Parajuli, N., and Oudit, G. Y. (2014b). Role of angiotensin-converting enzyme 2 (ACE2) in diabetic cardiovascular complications. *Clin. Sci.* 126 (7), 471–482. doi:10.1042/cs20130344

Peng, Q., Deng, Y., Yang, X., Leng, X., Yang, Y., and Liu, H. (2016). Genetic variants of ADAM17 are implicated in the pathological process of Kawasaki disease and secondary coronary artery lesions via the TGF-β/SMAD3 signaling pathway. *Eur. J. Pediatr.* 175 (5), 705–713. doi:10.1007/s00431-016-2696-8

Ren, B-C., Zhang, Y-F., Liu, S-S., Cheng, X-J., Yang, X., Cui, X-G., et al. (2020). Curcumin alleviates oxidative stress and inhibits apoptosis in diabetic cardiomyopathy via Sirt1-Foxo1 and PI3K-Akt signalling pathways. *J. Cell. Mol. Med.* 24 (21), 12355–12367. doi:10.1111/jcmm.15725

Simões, E. S. A. C., and Teixeira, M. M. (2016). ACE inhibition, ACE2 and angiotensin-(1-7) axis in kidney and cardiac inflammation and fibrosis. *Pharmacol. Res.* 107, 154–162. doi:10.1016/j.phrs.2016.03.018

Sukumaran, V., Tsuchimochi, H., Tatsumi, E., Shirai, M., and Pearson, J. T. (2017). Azilsartan ameliorates diabetic cardiomyopathy in young db/db mice through the modulation of ACE-2/ANG 1-7/Mas receptor cascade. *Biochem. Pharmacol.* 144, 90–99. doi:10.1016/j.bcp.2017.07.022

Takayanagi, T., Forrester, S. J., Kawai, T., Obama, T., Tsuji, T., Elliott, K. J., et al. (2016). Vascular ADAM17 as a novel therapeutic target in mediating cardiovascular hypertrophy and perivascular fibrosis induced by angiotensin II. *Hypertension* 68 (4), 949–955. doi:10.1161/hypertensionaha.116.07620

Wang, A., Ziyadeh, F. N., Lee, E. Y., Pyagay, P. E., Sung, S. H., Sheardown, S. A., et al. (2007). Interference with TGF-beta signaling by Smad3-knockout in mice limits diabetic glomerulosclerosis without affecting albuminuria. *Am. J. Physiol. Ren. Physiol.* 293 (5), F1657–F1665. doi:10.1152/ajprenal.00274.2007

Wang, X., Oka, T., Chow, F. L., Cooper, S. B., Odenbach, J., Lopaschuk, G. D., et al. (2009). Tumor necrosis factor-alpha-converting enzyme is a key regulator of agonist-induced cardiac hypertrophy and fibrosis. *Hypertension* 54 (3), 575–582. doi:10.1161/hypertensionaha.108.127670

Wang, Y., Yu, K., Zhao, C., Zhou, L., Cheng, J., Wang, D. W., et al. (2021). Follistatin attenuates myocardial fibrosis in diabetic cardiomyopathy via the TGF-β-smad3 pathway. *Front. Pharmacol.* 12, 683335. doi:10.3389/fphar.2021.683335

Weber, K. T., Sun, Y., Bhattacharya, S. K., Ahokas, R. A., and Gerling, I. C. (2013). Myofibroblast-mediated mechanisms of pathological remodelling of the heart. *Nat. Rev. Cardiol.* 10 (1), 15–26. doi:10.1038/nrcardio.2012.158

Williams, R., Karuranga, S., Malanda, B., Saeedi, P., Basit, A., Besançon, S., et al. (2020). Global and regional estimates and projections of diabetes-related health

expenditure: Results from the International Diabetes Federation Diabetes Atlas, 9th edition. *Diabetes Res. Clin. Pract.* 162, 108072. doi:10.1016/j.diabres.2020.108072

Xu, J., Mukerjee, S., Silva-Alves, C. R., Carvalho-Galvão, A., Cruz, J. C., Balarini, C. M., et al. (2016a). A disintegrin and metalloprotease 17 in the cardiovascular and central nervous systems. *Front. Physiol.* 7, 469. doi:10.3389/fphys.2016.00469

Xu, J., Sriramula, S., Xia, H., Moreno-Walton, L., Culicchia, F., Domenig, O., et al. (2017). Clinical relevance and role of neuronal AT(1) receptors in ADAM17-mediated ACE2 shedding in neurogenic hypertension. *Circ. Res.* 121 (1), 43–55. doi:10.1161/circresaha.116.310509

Xu, M., Zhou, H., Zhang, C., He, J., Wei, H., Zhou, M., et al. (2016b). ADAM17 promotes epithelial-mesenchymal transition via TGF-β/Smad pathway in gastric carcinoma cells. *Int. J. Oncol.* 49 (6), 2520–2528. doi:10.3892/ijo.2016.3744

Yue, Y., Meng, K., Pu, Y., and Zhang, X. (2017). Transforming growth factor beta (TGF-β) mediates cardiac fibrosis and induces diabetic cardiomyopathy. *Diabetes Res. Clin. Pract.* 133, 124–130. doi:10.1016/j.diabres.2017.08.018

Zhai, C. G., Xu, Y. Y., Tie, Y. Y., Zhang, Y., Chen, W. Q., Ji, X. P., et al. (2018). DKK3 overexpression attenuates cardiac hypertrophy and fibrosis in an angiotensin-perfused animal model by regulating the ADAM17/ACE2 and GSK-3β/β-catenin pathways. *J. Mol. Cell. Cardiol.* 114, 243–252. doi:10.1016/j.yjmcc.2017.11.018

Zhao, T., Wu, W., Sui, L., Huang, Q., Nan, Y., Liu, J., et al. (2022). Reactive oxygen species-based nanomaterials for the treatment of myocardial ischemia reperfusion injuries. *Bioact. Mat.* 7, 47–72. doi:10.1016/j.bioactmat.2021.06.006

Zhao, Y., Sun, D., Chen, Y., Zhan, K., Meng, Q., Zhang, X., et al. (2020). Si-Miao-Yong-An Decoction attenuates isoprenaline-induced myocardial fibrosis in AMPK-driven Akt/mTOR and TGF-β/SMAD3 pathways. *Biomed. Pharmacother.* 130, 110522. doi:10.1016/j.biopha.2020.110522

Zhou, X. L., Fang, Y. H., Wan, L., Xu, Q. R., Huang, H., Zhu, R. R., et al. (2019). Notch signaling inhibits cardiac fibroblast to myofibroblast transformation by antagonizing TGF-β1/Smad3 signaling. *J. Cell. Physiol.* 234 (6), 8834–8845. doi:10.1002/jcp.27543

Zunke, F., and Rose-John, S. (2017). The shedding protease ADAM17: Physiology and pathophysiology. *Biochim. Biophys. Acta. Mol. Cell. Res.* 1864, 2059–2070. doi:10.1016/j.bbamcr.2017.07.001

frontiers | Frontiers in Pharmacology

TYPE Original Research
PUBLISHED 21 October 2022
DOI 10.3389/fphar.2022.996635

Check for updates

OPEN ACCESS

EDITED BY
Fujian Lu,
Boston Children's Hospital, Harvard Medical School Boston, United States

REVIEWED BY
Vivek Singh,
LV Prasad Eye Institute, India
Christian Stockmann,
University of Zurich, Switzerland

*CORRESPONDENCE
Jia Yin,
jia_yin@meei.harvard.edu
Kunpeng Pang,
k.pang@sdu.edu.cn

SPECIALTY SECTION
This article was submitted to Experimental Pharmacology and Drug Discovery, a section of the journal Frontiers in Pharmacology

RECEIVED 18 July 2022
ACCEPTED 12 October 2022
PUBLISHED 21 October 2022

CITATION
Zhu S, Shan H, Li J, Pan L, Wang S, Zhu J, Guo H, Mi F, Wu X, Yin J and Pang K (2022), Therapeutic potential of topical administration of acriflavine against hypoxia-inducible factors for corneal fibrosis.
Front. Pharmacol. 13:996635.
doi: 10.3389/fphar.2022.996635

COPYRIGHT
© 2022 Zhu, Shan, Li, Pan, Wang, Zhu, Guo, Mi, Wu, Yin and Pang. This is an open-access article distributed under the terms of the Creative Commons Attribution License (CC BY). The use, distribution or reproduction in other forums is permitted, provided the original author(s) and the copyright owner(s) are credited and that the original publication in this journal is cited, in accordance with accepted academic practice. No use, distribution or reproduction is permitted which does not comply with these terms.

Therapeutic potential of topical administration of acriflavine against hypoxia-inducible factors for corneal fibrosis

Shuyan Zhu[1], Huimin Shan[2], Jianqiao Li[2], Lijie Pan[2], Shudan Wang[3], Jing Zhu[2], Hui Guo[2], Fenghua Mi[2], Xinyi Wu[2], Jia Yin[3]* and Kunpeng Pang[2]*

[1]Xi'an People's Hospital (Xi'an Fourth Hospital), Shanxi Eye Hospital, Xi'an, Shanxi, China, [2]Department of Ophthalmology, Qilu Hospital of Shandong University, Jinan, Shandong, China, [3]Department of Ophthalmology, Harvard Medical School, Schepens Eye Research Institute of Massachusetts Eye and Ear, Boston, MA, United States

Transdifferentiation of keratocytes into fibroblasts or further into myofibroblasts, which produced denser and more disorganized extracellular matrix, is the major cause of corneal fibrosis and scarring, leading to corneal blindness. TGF-β1 is the critical cytokine for the myofibroblast's transdifferentiation and survival. Hypoxia Inducible Factor (HIF) was found to play an important role in promoting fibrosis in lung, kidney, and dermal tissues recently. Our preliminary study demonstrated that topical administration of the acriflavine (ACF), a drug inhibiting HIF dimerization, delayed corneal opacity and neovascularization after the alkali burn. To know whether ACF could prevent corneal fibrosis and improve corneal transparency, we created a mouse mechanical corneal injury model and found that topical administration of ACF significantly inhibited corneal fibrosis at day 14 post-injury. The reduction of myofibroblast marker α-SMA, and fibronectin, one of the disorganized extracellular matrix molecules, in the corneal stroma were confirmed by the examination of immunohistochemistry and real-time PCR. Furthermore, the ACF inhibited the expression of α-SMA and fibronectin in both TGF-β1 stimulated or unstimulated fibroblasts *in vitro*. This effect was based on the inhibition of HIF signal pathways since the levels of the HIF-1α downstream genes including Slc2a1, Bnip3 and VEGFA were downregulated. To our knowledge, this is the first time to implicate that HIFs might be a new treatment target for controlling corneal fibrosis in mechanical corneal injuries.

KEYWORDS

HIF, corneal fibrosis, corneal hypoxia, TGF-β1, extracellular matrix

Introduction

The cornea is an avascular and transparent tissue that covers the front of the eye and is responsible for appropriately 70% of the refractive power of the eye. The corneal fibrosis is the third most common cause of blindness, following cataracts and glaucoma (Ibrahim Al-Mashahedah et al., 2019). The risk factors for corneal fibrosis are highly complex and encompass a wide variety of factors such as physical trauma to the eye, chemical burns, infections, refractive surgery, etc. (Karamichos et al., 2010; Wilson et al., 2012; Ibrahim Al-Mashahedah et al., 2019). After the injury, the keratocytes that existed in the corneal stroma are stimulated to proliferate and differentiate into fibroblasts. In some wound sites, the fibroblasts are stimulated by inflammatory factors or cytokines such as transforming growth factor β (particularly TGF-β1 and TGF-β2) and further differentiate into the α -smooth muscle actin (α-SMA) expressed myofibroblasts, which produced denser and more disorganized extracellular matrix (e.g., fibronectin, etc.), resulting in corneal fibrosis and scarring (Gupta et al., 2011; Mittal et al., 2016). At present, treatment options are limited and consist primarily of corneal transplantation.

As an avascular tissue, the cornea is unique in consumption by acquiring oxygen from the atmosphere and is sensitive to the oxygen concentration change (Pang et al., 2021). Hypoxia caused by the contact lens wearing, inflammation, wounds and infections, results in the disruption of corneal epithelial barrier function, delay of the wound healing, alteration of the extracellular matrix, and leads to corneal neovascularization and opacity (Lee et al., 2020; Onochie et al., 2020; Bai et al., 2021). Moreover, the enhancement of hypoxia in the myofibroblast transdifferentiation has been found in many tissues, such as sclera (Wu et al., 2018), skin (Zhao et al., 2017), artery adventitia (Short et al., 2004), and nasal polyps (Moon et al., 2012). The widely known cellular response to oxygen changes is the hypoxia-inducible factors (HIFs). HIF is a heterodimeric complex comprising one of three major oxygen labile HIF-α subunits (HIF-1α, HIF-2α, or HIF-3α) dimerized with HIF-1β to form HIF-1, HIF-2, or HIF-3 transcriptional complexes, respectively (Koh and Powis, 2012). Under hypoxia or inflammatory conditions, HIF-α is stabilized and translocated to the nucleus, where it dimerizes with HIF-1β to transactivate a large number of target genes including those promoting angiogenesis (VEGFA), metabolism (GLUT1/3), cell proliferation and survival (Bnip3, TGF-α), etc. (Corcoran and O'Neil, 2016; Pullamsetti et al., 2020; Yang et al., 2020). Interestingly, multiple studies revealed that HIF played a critical role in promoting fibrosis (Basu et al., 2011; Brereton et al., 2022; Yuan et al., 2022). TGF-β has been reported to cause HIF stabilization (Basu et al., 2011). Noteworthily, the elevated mRNA level of HIFs has also been noted in injured (our preliminary study) or infected corneal tissues (Rao and Suvas, 2019). However, the effects and mechanisms of HIFs in the cornea are unknown and need to be further investigated.

In this study, we found that alkali burn led to hypoxia in the mice's anterior chamber and promoted the elevation of HIF-1α mRNA levels in the cornea. In order to know how HIFs affected the ocular outcomes after the burn, we treated the injured mice's eyes with the acriflavine (ACF), a drug inhibiting HIF dimerization by binding to the PAS-B subdomain of HIF-1α and HIF-2α, thereby leading to the inhibition of HIF DNA-binding and transcriptional activity (Lee et al., 2009). We found that ACF treatment delayed the corneal opacity and neovascularization after the injury. However, due to the complex mechanisms of corneal opacity resulting from the alkali-burn-induced limbal stem cell deficiency model, we created a mechanical corneal injury model as described previously to observe how it attenuated the corneal opacity (Mittal et al., 2016). We found that topical administration of ACF restored the corneal transparency during 28 days of follow-up, and inhibited the generation of fibrosis in the injured corneal stroma. Furthermore, ACF reduced the mRNA level of α-SMA and fibronectin in the corneal fibroblasts stimulated by TGF-β1, and downregulated the levels of HIF-1α downstream genes. To our knowledge, this was the first time to demonstrate that HIF signaling pathways played an important role in corneal fibrosis.

Materials and methods

Animals

Six- to eight-week-old male BALB/c and C57BL/6 wild-type mice were used in these experiments. All the protocols were approved by the Animal Care and Use Committee of Qilu Hospital, and all animals were treated according to the ARVO Statement for the Use of Animals in Ophthalmic and Vision Research.

Corneal injury and topical administration of acriflavine

Mice were anesthetized by intraperitoneal injection of Ketamine and Xylazine followed by one to two drops of topical 0.5% Proparacaine. Alkali burn induced corneal injury was generated in the right eye of each BALB/c mouse according to a previous report (Kethiri et al., 2019) with a minor modification. In brief, after the corneal and limbal epithelium was gently scraped by using a surgical scalpel No.15, topical application of 6 μl 0.1 M sodium hydroxide (NaOH) for 10 s was followed. The eye was rinsed immediately for 4 min with normal

saline after the burn, and followed by topical application of 0.05% and 0.01% ACF (w/w, dissolved in PBS) twice daily, respectively. PBS was used as a control. A scoring system was used to evaluate the corneal neovascularization and corneal opacity. Neovascularization was scored on a scale of 0–4 which was assigned to the five areas of each cornea (central, superior, inferior, nasal, and temporal) based on the occupied area of the new blood vessels: 0, no new blood vessels; 1, less than 30% area; 2, more than 30% area but less than 70%; 3, more than 70% area less than 100%; and 4, 100% area. A total score of each cornea was calculated (range 0–20). The corneal opacity was also scored on a scale of 0–4 where 0 = completely clear; 1 = slightly hazy, iris and pupils easily visible; 2 = slightly opaque, iris and pupils still detectable; 3 = opaque, pupils hardly detectable, and 4 = completely opaque with no view of the pupils (Yoeruek et al., 2008). The healing percentage of the corneal epithelium was calculated using the NIH ImageJ software. The anterior chamber oxygen was measured using the DP-PSt7-2 oxygen sensor (PreSens, Regensburg, Germany).

A modified protocol of mechanical corneal injury was performed in the right eye of each C57BL/6 mouse as previously described (Mittal et al., 2016). In brief, the surface of the central cornea was demarcated with a 2-mm trephine followed by gentle scraping of the central epithelium with a surgical scalpel No. 15. Next, the basement membrane and anterior portion were removed using a hand-held Algerbrush II (Alger Equipment). Two days after the injury, 0.01% ACF was topical administrated twice daily. PBS was used as a control. Digital corneal images were taken by using a slit-lamp microscope and the degree of opacity was calculated using the NIH ImageJ software. Anterior segment images were taken using anterior segment-optical coherence tomography (OCT) (Bioptigen Inc., Durham, NC). Central corneal thickness was measured using the OCT built-in software.

Immunofluorescent staining and histology

Cryosections of the whole eyeball were fixed in 4% paraformaldehyde for 20 min followed by incubating in 0.1% Triton X-100 and 2% BSA for 1 h at room temperature. The slides were incubated with anti-α-SMA (ab124964, Abcam), anti-fibronectin (15613-1-AP, ThermoFisher) and anti-CD45 (160302, Biolegend) antibodies at 4°C overnight, followed by immunostaining with Alexa Fluor 594 donkey anti-rabbit (A-21207, Invitrogen) or Alexa Fluor 488-donkey anti-rat (712-545-150, Jackson ImmunoResearch Europe Ltd.) secondary antibody for 1 h at room temperature. The slides were mounted with DAPI mounting medium (H-1200, Vector lab, Burlingame, CA) and photographed under a confocal laser scanning microscope (SP8, Leica, Wetzlar, Germany). For histological evaluation, corneal sections were stained with H&E and examined using bright-field microscopy (DMiL, Leica).

In vitro corneal fibroblasts stimulation

Corneas were harvested from C57BL/6 wide-type mice and the Descemet's-endothelium complex was stripped away with forceps. To loosen epithelial sheets, the remaining corneal stroma and epithelium were incubated in Dispase II (Roche) in Dulbecco's modified Eagle's medium (DMEM, Gibco) supplemented with 10% fetal bovine serum (FBS) and antibiotics (penicillin and streptomycin at 100 μg/ml) in 5% CO_2 at 37°C. After removal of the epithelium, the stroma was cut into small segments and digested in DMEM containing 3.3 mg/ml collagenase type II (Sigma-Aldrich) at 37°C with shaking for 90 min. The isolated keratocytes were grown in DMEM supplemented with 10% FBS at 37°C in a 5% CO_2 humidified atmosphere. One to three passage corneal fibroblasts were used for all experiments. The mouse corneal fibroblast was seeded at 1×10^5 cells in 24-well plates and starved in DMEM containing 1% FBS overnight. Then the cells were cultured in medium alone or stimulated with 100 ng/ml murine recombinant TGF-β1 (R&D Systems) in the presence or absence of 0.0001% acriflavine (Sigma-Aldrich) for 24 h. Cells were then used for the evaluation of α-SMA, fibronectin, and the HIF-1 downstream genes of Bnip3 and Slc2a1 by immunocytochemistry and real-time PCR.

Live/dead cells staining

The cell viability was evaluated using LIVE/DEAD™ Viability/Cytotoxicity Kit (L3224, Invitrogen) according to the product's procedure. In brief, corneal fibroblasts cells were incubated for 30 min at room temperature with a mixture of 2 μM calcein acetoxymethyl ester (Calcein AM) and 4 μM ethidium homodimer-1 (EthD-1). The live cells (green fluorescence) and dead cells (red fluorescence) were photographed using fluorescence microscope (DMi8, Leica).

RNA isolation and real-time PCR

Corneal tissues were harvested under dissecting microscope and placed in TRIzol solution (Invitrogen). Total RNA was isolated using the RNeasy Micro Kit (Qiagen) following the manufacturer's protocol and reverse-transcribed to cDNA with QuantiTect Rev. Transcription Kit (Qiagen). Real-time PCR was then performed using Taqman Universal PCR Mastermix (ThermoFisher) and pre-formulated Taqman primers for murine glyceraldehyde-3-phosphate dehydrogenase (GAPDH), *β*-Actin (Mm02619580_g1), HIF-1α (Mm00468869_m1), α-SMA (Mm00725412_m1), fibronectin (Mm01256744_m1), Bnip3 (Mm01275600_g1), Slc2a1 (Mm00441473_m1), and VEGFA (Mm00437306_m1) (ThermoFisher). The results were analyzed by the comparative

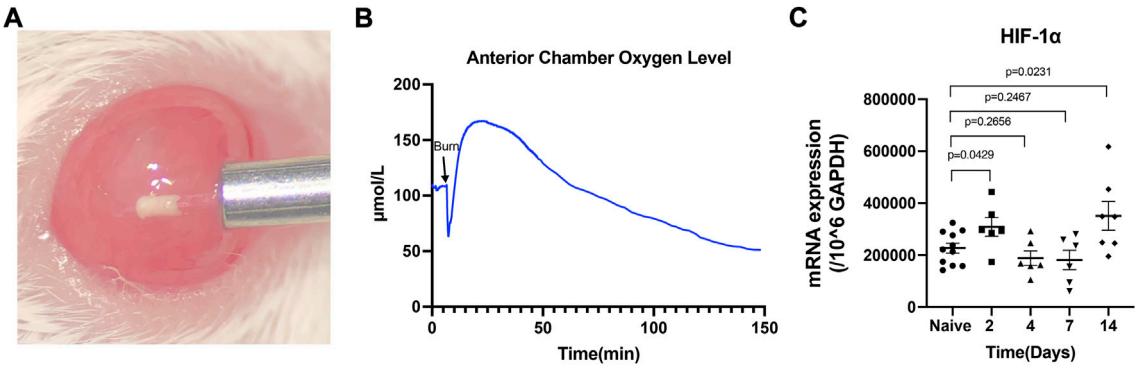


FIGURE 1
The alkali burn induced hypoxia in the mouse anterior chamber and elevated the HIF-1α mRNA level in the corneal tissue. Oxygen concentration in the anterior chamber **(B)** was recorded in real-time by inserting a micro-oxygen sensor **(A)**. The mRNA level of HIF-1α in naïve and day 2, 4, 7, 14 post-injured cornea was assayed by RT-PCR **(C)**. Data were presented as the mean ± SEM.

threshold cycle method and normalized to GAPDH or β-Actin as internal control.

Flow cytometry

A single-cell suspension of corneal cells was prepared by digesting the individual cornea with Liberase TL (2.5 mg/ml) (Sigma-Aldrich) as previously reported (Gaddipati et al., 2015). Cells were stained with fluorochrome-conjugated monoclonal antibodies against CD45 (103116, Biolegend), HIF-1α (IC1935G, R&D system) and their isotype controls (400623, 400132, Biolegend). The stained cells were analyzed using the LSRII flow cytometer (BD Biosciences, San Jose, CA) and FlowJo software.

Statistical analysis

The statistical analysis was conducted using GraphPad Prism software. Results are presented as means ± SEM. Comparisons between two groups were performed by an unpaired, two-tailed Student's *t*-test; and comparison among three groups was performed by One-way ANOVA test. The statistically significant was set at $p < 0.05$.

Results

The HIF-1α level was elevated in the alkali burn injured corneal tissue

In the alkali burn induced mouse corneal injury models, the oxygen level in the anterior chamber was downregulated immediately after the burn and then increased to a higher level of around 160 μmol/L in 10 min due to the corneal epithelium disruption. After that, the oxygen level decreased smoothly to a low level of around 60 μmol/L in 2 h (Figures 1A,B). We detected the HIF-1α mRNA level during the 14 days of follow-up and found that the mRNA levels of HIF-1α were significantly increased at 2 days and 14 days ($p = 0.0429$ and $p = 0.0231$, respectively) compared to the naïve cornea after the burn (Figure 1C). The protein level of HIF-1α in the injured cornea was much higher than in native corneal tissue after the injury as demonstrated by flow cytometry analysis (Supplementary Figure S1). However, the significant difference in HIF-1α mRNA level compared to the naïve corneal tissue was not observed at both 4 and 7 days of follow-up.

Acriflavine treatment delayed the corneal opacity and neovascularization after the burn

Besides limbal stem cell deficiency, neovascularization and corneal stromal fibrosis are both serious risk factors for blindness after alkali burn. Hence, we administered the drug ACF (0.01% and 0.05%, respectively) topically after the burn and determine how it worked in this model (Figure 2A). The scoring of corneal opacity and neovascularization were carried out in three groups at 7d post-injury. We found that both 0.01% and 0.05% ACF inhibited the corneal neovascularization ($p = 0.3337$ and $p = 0.0215$, respectively) and opacity ($p = 0.0250$ and $p = 0.0250$, respectively) compared to PBS treated group (Figures 2C,D). However, there were no significant differences in these three groups 10 days after alkali burn (data not shown). We also observed that ACF delayed epithelial healing in a dose-dependent manner by fluorescein staining (Figures 2B,E).

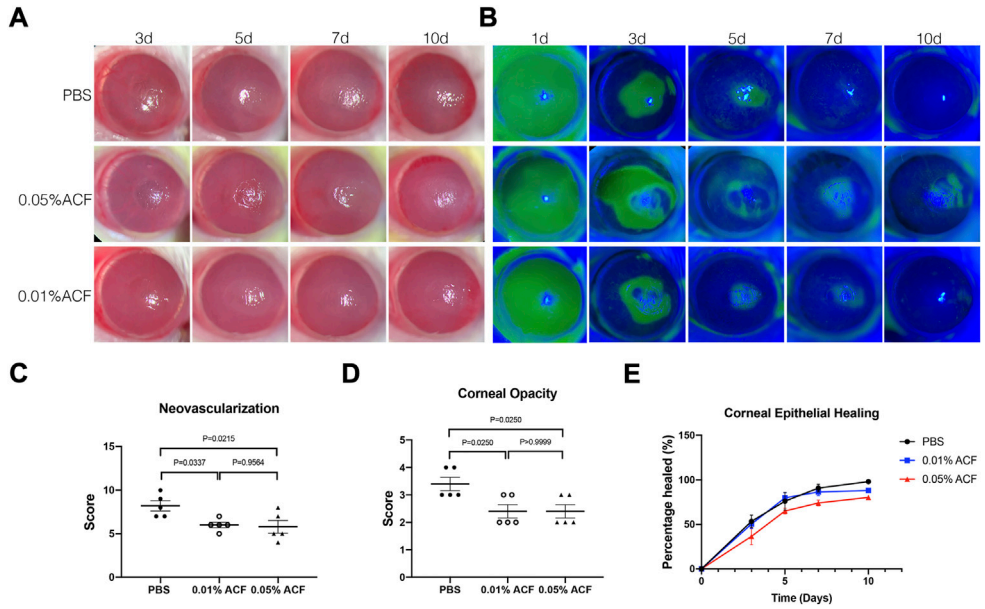


FIGURE 2
Topical administration of ACF delayed the corneal opacity and neovascularization after the alkali burn injury. **(A)** Slit-lamp photos of the alkali burn injury treated by 0.05% and 0.01% ACF. PBS treated group was as the control. A dose-dependent manner of delayed epithelium healing was observed in ACF treated group by fluorescein staining **(B,E)**. However, no significant difference was demonstrated among the three groups. On day 7 after the burn, both 0.05% and 0.01% ACF significantly reduced the neovascularization **(C)** and corneal opacity **(D)** compared to the control group. Data were presented as the mean ± SEM.

Although the ACF drugs inhibited the hemangiogenesis and corneal opacity at the early stage after the alkali burn, no significant difference was observed in a long-term follow-up. The reason might be the limbal stem cells deficiency and corneal conjunctivalization in the chronic-stage post-injury that the independent inhibition of HIF could not overcome these pathological processes.

Topical administration of acriflavine restored the corneal transparency in mechanical ocular injury

To determine whether topical ACF treatment has the potential to restore the corneal transparency following injury, we utilized a well-characterized sterile injury model of mouse cornea (Mittal et al., 2016) with a minor modification, as details were described in the Materials and methods. The injury was induced by the mechanical removal of the corneal epithelium and anterior stroma (Figure 3A); 2 days after the injury, topical 0.01% ACF was administrated twice daily (Figure 3B). Topical administration of PBS was used as the control group. Slit-lamp biomicroscopy was used to monitor the extent of corneal opacity and analyzed by ImageJ (NIH). The central corneal thickness was evaluated by OCT. On day 2 post-injury, both groups showed a significant development of corneal opacity. However, the corneas of mice administrated with topical 0.01% ACF showed a significant reduction in corneal opacity at days 14 and 28 post-injury compared to PBS treated group (p = 0.0237 at days 14; p = 0.0318 at days 28; Figures 3C,D). Moreover, the central corneal thickness was also significantly reduced at 28 days (101.3 ± 9.4 μm in ACF treated group and 112.7 ± 24.5 μm in the control group, p = 0.0376; Figures 3E,F).

Acriflavine treatment inhibited the generation of fibrosis in the injured corneal stroma

To confirm the efficacy of ACF in reducing corneal opacity formation and preserving transparency, the corneal tissues were harvested at days 2, 7, 14, and 28 post-injury to determine the expression of α-SMA and fibronectin at cellular and molecular levels in the corneal stroma. The confocal micrographs of immunofluorescent staining corneas showed a significant reduction in the expression of α-SMA and fibronectin in the ACF-treated corneas at 7, 14, 28 days post-injury compared with control corneas (Figures 4A,B; Supplementary Figures S2, S3B,C). These findings were also confirmed by real-time PCR in two groups 7 days after injury (p = 0.0075 and p = 0.0036, respectively; Figures 4E,F). H.E. staining of corneal cross-sections

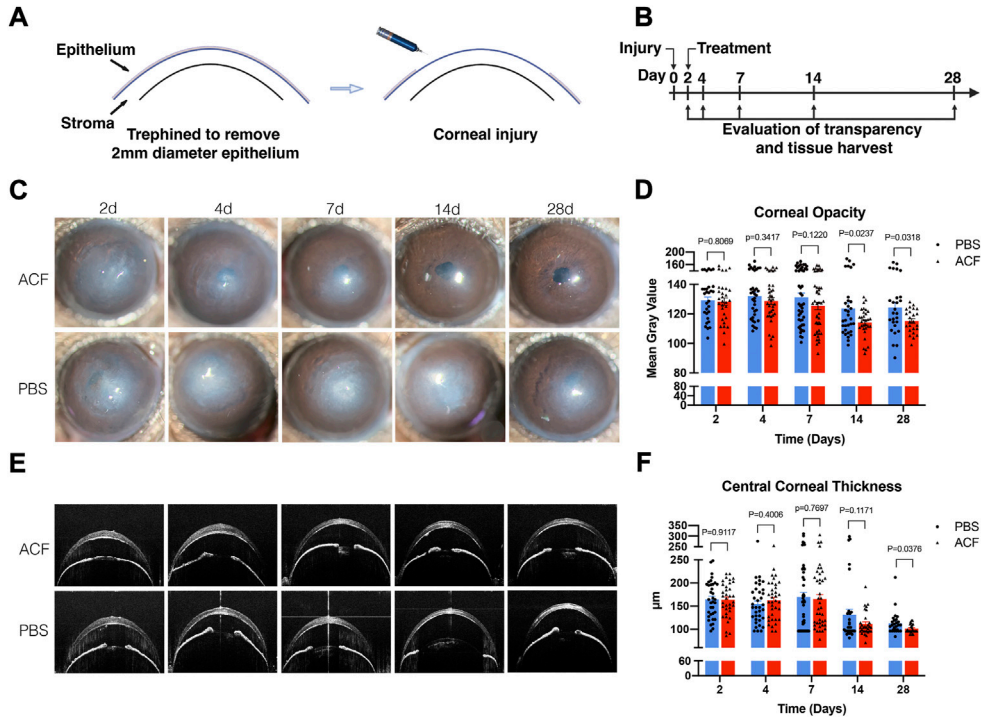


FIGURE 3
Topical administration of ACF restored the corneal transparency in mechanical ocular injury. The corneal injury was induced by the mechanical removal of the corneal epithelium and anterior stroma **(A)**. Two days after the injury, 0.01% ACF was topically administrated twice daily and followed for 28 days **(B)**. Slit-lamp photos demonstrated that ACF significantly reduced the corneal scarring and restored the corneal transparency at day 14 and 28 post-injury compared to PBS treated group **(C)**. The corneal opacity was analyzed by ImageJ **(D)**. The central corneal thickness was examined by OCT **(E)**, and showed a reduction 28 days after the injury **(E,F)**. Data were presented as the mean ± SEM.

revealed the increased stratification of the epithelial cell layer in the ACF-treated cornea (Supplementary Figure S4). We also examined the infiltration of leucocytes in the injured corneal stroma at two- and seven-days post-injury and did not find significant difference between the two groups (Figures 4C,D,G).

Inhibition of hypoxia-inducible factors reduced the expression of α-SMA and fibronectin in the corneal fibroblasts stimulated by TGF-β1

To determine whether ACF can directly inhibit the expression of α-SMA and fibronectin in the corneal fibroblasts, we stimulated the mouse corneal fibroblast with TGF-β1 in the absence or presence of ACF for 24 h. The unstimulated cultures served as a control group. Before this study, we analyzed the cell viability after the ACF treatment by using a Live/Dead Viability/Cytotoxicity Kit, and found that ACF did not affect the cell viability (Supplementary Figure S5). ACF suppressed the TGF-β1-induced α-SMA expression in corneal fibroblasts by the examination of the immunofluorescent staining and real-time PCR (Figures 5B,C). TGF-β1 stimulation could not promote the mRNA level of fibronectin in the corneal fibroblasts (p = 0.3877, Figure 5D). However, ACF treatment significantly reduced the baseline level of fibronectin as well as α-SMA in corneal fibroblasts (Figures 5A,C,D), suggesting that ACF could be effective in reversing pre-formed myofibroblasts into α-SMA negative fibroblasts and reducing the fibrosis. In addition, we found that the mRNA level of HIF-1α downstream gene Slc2a1, responsible for the production of glucose transporter protein-1 (GLUT-1), and the VEGFA, were both elevated by TGF-β1 stimulation. ACF down-regulated the Slc2a1 and VEGFA mRNA levels without the presence of TGF-β1 (Figures 5E,G). TGF-β1 had no effect on another HIF-1α downstream gene bnip3. However, it was significantly downregulated by the presence of ACF (Figure 5F).

Discussion

The fibrosis of the cornea can occur for many reasons including chemical burn, infections, trauma, inflammation,

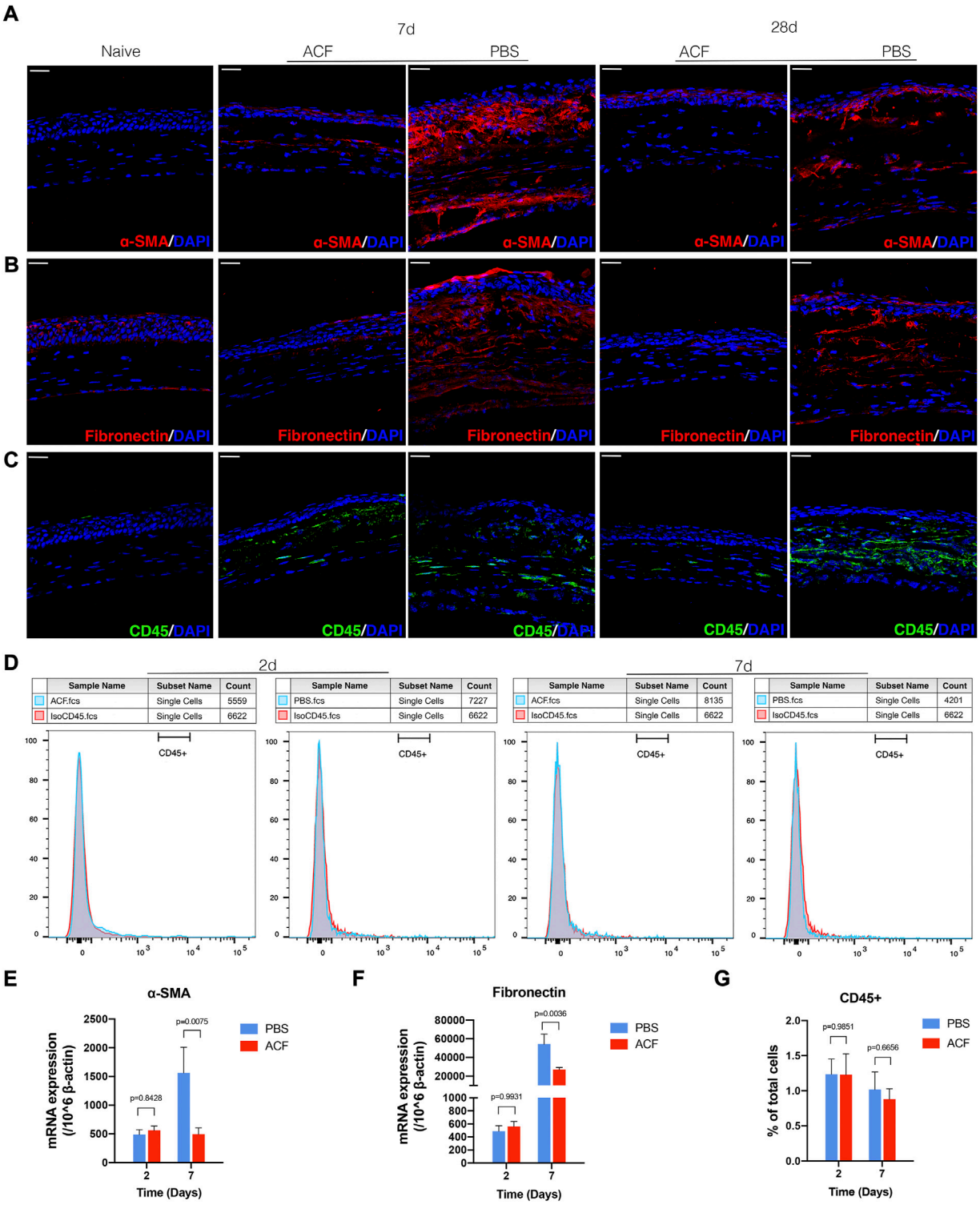


FIGURE 4
ACF inhibited the generation of fibrosis in the injured corneal stroma. Tissues were harvested at day 7 and 28 for immunohistochemistry evaluation. The immunofluorescent staining of α-SMA (red) and fibronectin (red) in corneal stroma were much higher in PBS treated control group **(A,B)**. The mRNA level of α-SMA and fibronectin at day 7 post-injury was consistent with the immunofluorescent staining result **(E,F)**. The infiltration of $CD45^+$ leucocytes in the corneal tissues was evaluated by immunofluorescent staining [**(C)**, green] and flow cytometry **(D,G)**, respectively. No significant difference was observed between the two groups at day 2 and 7 after the injury. Data were presented as the mean ± SEM. Scale bar: 10 μm.

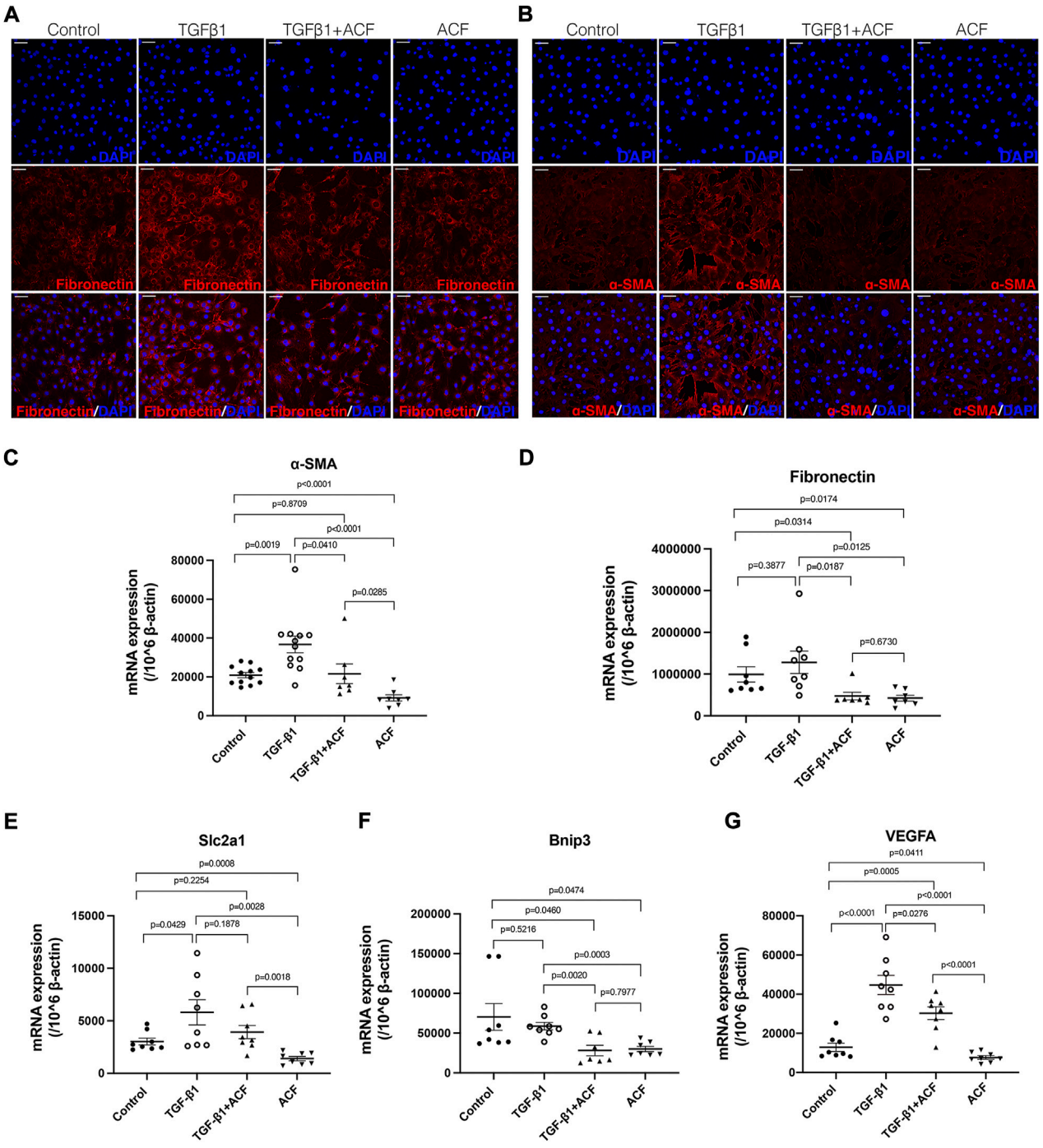


FIGURE 5
ACF inhibited the expression of α-SMA and fibronectin in the corneal fibroblasts. The corneal fibroblasts were cultured in medium alone or stimulated with 100 ng/ml murine recombinant TGF-β1 in the presence or absence of 0.0001% ACF for 24 h. **(A,B)** are the immunofluorescent staining of fibronectin (red) and α-SMA (red), respectively. The mRNA level of α-SMA was significantly reduced in the presence of ACF with or without TGF-β1 stimulation **(C)**. The mRNA level of fibronectin was not affected by TGF-β1 but reduced by the presence of ACF **(D)**. The mRNA level of HIF-1α downstream gene Slc2a1 was elevated by TGF-β1 stimulating **(E)**. ACF inhibited the Slc2a1 mRNA level without the presence of TGF-β1 **(E)**. The other HIF-1α downstream genes bnip3 **(F)** and VEGFA **(G)** were significantly downregulated by the presence of ACF. Data were presented as the mean ± SEM. Scale bar: 10 μm.

surgeries, or other corneal diseases, leading to corneal blindness (Wilson et al., 2012). TGF-β signaling pathway is the most well-known and robust inducer of fibrosis in the cornea (Bonnans et al., 2014). In the healthy cornea, the keratocytes in the stroma are quiescent and responsible for maintaining the balance of the stromal extracellular matrix (ECM) which is vital to corneal transparency (Pei et al., 2004). Upon injury, the keratocytes are driven by the TGF-β that enters the stroma mainly from the corneal epithelium and tears, and transdifferentiate into fibroblasts or myofibroblasts, thereby synthesizing a disorganized opaque matrix (such as fibronectin, type III collagen, tenascin C etc.) (de Oliveira et al., 2021). The α-SMA expressing myofibroblast is mainly responsible for corneal fibrosis, and sometimes is differentiated from other cells (e.g., bone marrow-derived fibrocytes) in the stroma (Kempuraj and Mohan, 2022; Wilson et al., 2022). Corneal hypoxia caused by contact lens wear or inflammation, usually results in corneal neovascularization (CNV), which often severely compromises vision by decreasing the transparency of corneal stroma (Safvati et al., 2009). The CNV-associated pericytes are α-SMA positive and have been found to have the capacity to transdifferentiate into myofibroblasts (Kostallari and Shah, 2019; Wilson et al., 2022). Therefore, under hypoxia conditions or serious corneal damage, multiple studies focused on the inhibition of CNV to prevent corneal opacity by blocking vascular endothelial growth factor (VEGF) receptors, attenuating inflammation or targeting the VEGF upstream regulator of HIF-1α (Peral et al., 2022).

HIF, a basic loop-helix-loop protein that forms a heterodimeric complex, is a crucial mediator of the hypoxic response, which transactivates a wide range of downstream genes including those promoting angiogenesis, anaerobic metabolism, resistance to apoptosis and potentially profibrotic (McNutt, 2013; Palazon et al., 2014). These genes include VEGF, erythropoietin (EPO), GLUT-1, Bnip3, connective tissue growth factor (CTGF), transforming growth factor-β1, platelet-derived growth factor (PDGF), etc. (Darby and Hewitson, 2016). Besides hypoxia, bacteria (Peyssonnaux et al., 2005), inflammatory cytokines (e.g., TNF-α, NF-κB, IL-6, IL-4) (Albina et al., 2001; Rius et al., 2008; Takeda et al., 2010; Dang et al., 2011) and reactive oxygen species (ROS) (Shatrov et al., 2003) were found to be responsible for HIF-1α or HIF-2α stabilization, which indicated that HIFs might play wide range roles in physiological function (Palazon et al., 2014). Noteworthily, normoxic TGF-β stimulation increased HIF-1α expression in human kidney epithelial cells (Basu et al., 2011). The increased production of matrix components such as fibronectin and collagen following the stabilization of HIF-1 in dermal fibroblasts has also been demonstrated (Darby and Hewitson, 2016). In most tissues, progressive fibrosis is observed if hypoxia persists (Ballermann and Obeidat, 2014). The fibrosis inhibition has also been noted in kidney and lung tissues by reducing or inhibiting the nuclear localization of HIF-1α or HIF-2α (Tanaka, 2016; Fu et al., 2021). As demonstrated previously, the blocking or reduction of HIF-1/2 signaling pathways in both renal and dermal cells has a negative effect on collagen synthesis and on the TGF- β stimulation of collagen synthesis (Darby and Hewitson, 2016). Hence the HIF pathways might be a potential target for inhibiting fibrosis.

The nuclear localization of HIF-1α and HIF-2α protein was observed in Herpes stromal keratitis (HSK)-developing corneas (Rao and Suvas, 2019). In this model, the stabilization of HIF-2α protein was detected in corneal epithelial cells, whereas HIF-1α protein stabilization was observed in infiltrating cells. Interestingly, in the alkali-burn-induced mouse limbal stem cell deficiency (LSCD) mouse model, we also observed that the burn induced the hypoxia in anterior chamber and significantly increased the mRNA levels of HIF-1α in the corneas at 2 and 14 days follow-up. As described before, HIF-1α was highly expressed in the inflammatory cells (Rao and Suvas, 2019). The elevation of HIF-1α 2 days after the burn might be due to the infiltration of leukocytes. After 14 days, the CNV fully covered the cornea and induced a second peak expression of HIF-1α. In order to determine how the HIFs worked in this model, we topically administrated acriflavine (ACF), a drug inhibiting HIF DNA-binding and transcriptional activity (Lee et al., 2009), and found that ACF delayed the CNV formation and corneal opacity during the follow-up. However, due to the combination of limbal stem cells dysfunction (LSCD) after the alkali burn, intervention on HIF signaling alone might not enough for the inhibition of CNV and improvement of corneal transparency in a long-term follow-up.

In order to reduce the effect of LSCD on the results and detect whether HIF signaling played a role in corneal fibrosis formation, we utilized a mechanical corneal injury mouse model according to a previous report (Mittal et al., 2016). Since ACF delayed the epithelium closure in a dose-dependent manner from LSCD models, we treated the mechanical corneal injury with a lower dose of ACF after the epithelium fully closed 2 days after the injury. Noteworthily, the topical administration of ACF significantly improved the corneal transparency beginning at days 14 post-injury. The inhibition of corneal fibrosis was confirmed by immunohistochemistry and real-time PCR that the expression of α-SMA and fibronectin were both reduced in the ACF-treated corneal stroma. To further confirm the effect of the ACF and HIF pathways on corneal fibrosis, we cultured the corneal fibroblasts *in vitro* followed by stimulating with TGF-β1 with or without ACF. Similar to the *in vivo* results, ACF reduced the expression of α-SMA and fibronectin in both TGF-β1 stimulated or unstimulated fibroblasts. The HIF-1α downstream genes of Slc2a1, Bnip3 and VEGFA were also downregulated, and indirectly confirmed that ACF inhibited corneal fibrosis by working on HIF pathways. These data were consistent with previous reports in other tissues (McNutt, 2013; Palazon et al., 2014; Tanaka, 2016; Fu et al., 2021). However, Rao and Suvas (2019) demonstrated a different result that the systemic administration of ACF increased the influx of neutrophils in progressing herpes stroma keratitis lesions, resulting in increased corneal opacity.

We also detected the infiltration of leukocytes in the mechanical injured corneal stroma and did not find any significant differences in ACF treated and PBS treated control group. Due to the different models and administration approaches between these two studies, HIF signals might play different roles in different etiologies of corneal stroma damage.

However, this study has drawbacks that need further investigation. As previously mentioned, the enhancement of hypoxia in the myofibroblast transdifferentiation has been found in many tissues, such as sclera, skin, etc. We detected that hypoxia and the elevated mRNA level of HIF-1α existed in the alkali burn injured corneal tissue, but we did not know exactly whether and how hypoxia directly affected the function and characteristics of keratocytes or fibroblasts in the injured corneal tissue or the formation of the corneal fibrosis. The *in vivo* or *in vitro* phenotypes and functions of keratocytes under hypoxia conditions are needed for further observation. In addition, although we observed that the inhibition of HIFs by using ACF improved the corneal transparency post-injury and reduced the transdifferentiation of myofibroblast, we did not know whether and how HIFs enhanced the fibrosis formation in the cornea stroma. For example, we should know if the elevation of HIFs in corneal tissue or keratocytes promoted corneal fibrosis or myofibroblast transdifferentiation *in vivo* and *in vitro*. Moreover, additional studies are needed to determine the precise mechanisms of the relationship between HIF and TGF-β1 pathways as well as the inhibition of fibronectin production by HIFs through which pathways.

In summary, we demonstrated that the inhibition of HIF signals reduced the corneal fibrosis in the mechanical damaged corneal stroma and improved corneal transparency. The ACF could be effective in reversing pre-formed myofibroblasts into α-SMA negative fibroblasts and reducing the corneal fibrosis. This mechanism involved the TGF-β1 pathways. Moreover, based on our study, inhibition of HIF signals also reduced the fibronectin expression in corneal fibroblast and deposition in corneal stroma, which was not TGF-β1 dependent. This is the first study to implicate that HIFs might be a new treatment target for controlling corneal fibrosis in mechanical corneal injuries.

Data availability statement

The original contributions presented in the study are included in the article/Supplementary Material, further inquiries can be directed to the corresponding author.

Ethics statement

The animal study was reviewed and approved by The Animal Care and Use Committee of Qilu Hospital.

Author contributions

JY and KP contributed to conception and design of the study. KP supervised the study. SZ, HS, SW, and KP conducted experiments and acquired data; HS and KP wrote the manuscript; LP analyzed data; FM assisted in conducting the experiments; JZ and HG assisted in analyzing data; JL and XW provided the reagents; KP designed research studies and revised the manuscript.

Funding

This study was funded by the National Natural Science Foundation of China (Nos 81400377 and 82070925).

Conflict of interest

The authors declare that the research was conducted in the absence of any commercial or financial relationships that could be construed as a potential conflict of interest.

Publisher's note

All claims expressed in this article are solely those of the authors and do not necessarily represent those of their affiliated organizations, or those of the publisher, the editors and the reviewers. Any product that may be evaluated in this article, or claim that may be made by its manufacturer, is not guaranteed or endorsed by the publisher.

Supplementary material

The Supplementary Material for this article can be found online at: https://www.frontiersin.org/articles/10.3389/fphar.2022.996635/full#supplementary-material

References

Albina, J. E., Mastrofrancesco, B., Vessella, J. A., Louis, C. A., Henry, W. L., and Reichner, J. S. (2001). HIF-1 expression in healing wounds: HIF-1alpha induction in primary inflammatory cells by TNF-alpha. *Am. J. Physiol. Cell Physiol.* 281, C1971–C1977. doi:10.1152/ajpcell.2001.281.6.c1971

Bai, Y., Hu, Y., Gao, Y., Wei, X., Li, J., Zhang, Y., et al. (2021). Oxygen self-supplying nanotherapeutic for mitigation of tissue hypoxia and enhanced photodynamic therapy of bacterial keratitis. *ACS Appl. Mat. Interfaces* 13, 33790–33801. doi:10.1021/acsami.1c04996

Ballermann, B. J., and Obeidat, M. (2014). Tipping the balance from angiogenesis to fibrosis in CKD. *Kidney Int. Suppl.* 4, 45–52. doi:10.1038/kisup.2014.9

Basu, R. K., Hubchak, S., Hayashida, T., Runyan, C. E., Schumacker, P. T., and Schnaper, H. W. (2011). Interdependence of HIF-1α and TGF-β/Smad3 signaling in

normoxic and hypoxic renal epithelial cell collagen expression. *Am. J. Physiol. Ren. Physiol.* 300, 898–905. doi:10.1152/ajprenal.00335.2010

Bonnans, C., Chou, J., and Werb, Z. (2014). Remodelling the extracellular matrix in development and disease. *Nat. Rev. Mol. Cell Biol.* 15, 786–801. doi:10.1038/nrm3904

Brereton, C. J., Yao, L., Davies, E. R., Zhou, Y., Vukmirovic, M., Bell, J. A., et al. (2022). Pseudohypoxic HIF pathway activation dysregulates collagen structure-function in human lung fibrosis. *Elife* 11, 69348. doi:10.7554/elife.69348

Corcoran, S., and O'Neill, L. (2016). HIF1α and metabolic reprogramming in inflammation. *J. Clin. Invest.* 126, 3699–3707. doi:10.1172/JCI84431

Dang, E. V., Barbi, J., Yang, H. Y., Jinasena, D., Yu, H., Zheng, Y., et al. (2011). Control of TH17/Treg balance by hypoxia-inducible factor 1. *Cell* 146, 772–784. doi:10.1016/j.cell.2011.07.033

Darby, I. A., and Hewitson, T. D. (2016). Hypoxia in tissue repair and fibrosis. *Cell Tissue Res.* 365, 553–562. doi:10.1007/s00441-016-2461-3

de Oliveira, R. C., Tye, G., Sampaio, L. P., Shiju, T. M., DeDreu, J. R., Menko, A. S., et al. (2021). TGFβ1 and TGFβ2 proteins in corneas with and without stromal fibrosis: delayed regeneration of apical epithelial growth factor barrier and the epithelial basement membrane in corneas with stromal fibrosis. *Exp. Eye Res.* 202, 108325. doi:10.1016/j.exer.2020.108325

Fu, Z., Xu, Y-S., and Cai, C-Q. (2021). Ginsenoside Rg3 inhibits pulmonary fibrosis by preventing HIF-1α nuclear localisation. *BMC Pulm. Med.* 21, 70. doi:10.1186/s12890-021-01426-5

Gaddipati, S., Estrada, K., Rao, P., Jerome, A. D., and Suvas, S. (2015). IL-2/Anti–IL-2 antibody complex treatment inhibits the development but not the progression of herpetic stromal keratitis. *J. Immunol.* 194, 273–282. doi:10.4049/jimmunol.1401285

Gupta, R., Yarnall, B. W., Giuliano, E. A., Kanwar, J. R., Buss, D. G., and Mohan, R. R. (2011). Mitomycin C: A promising agent for the treatment of canine corneal scarring. *Vet. Ophthalmol.* 14, 304–312. doi:10.1111/j.1463-5224.2011.00877.x

Ibrahim Al-Mashahedah, A. M., Kanwar, R. K., and Kanwar, J. R. (2019). Utility of nanomedicine targeting scar-forming myofibroblasts to attenuate corneal scarring and haze. *Nanomedicine* 14, 1049–1072. doi:10.2217/nnm-2017-0305

Karamichos, D., Guo, X. Q., Hutcheon, A. E. K., and Zieske, J. D. (2010). Human corneal fibrosis: An *in vitro* model. *Invest. Ophthalmol. Vis. Sci.* 51, 1382–1388. doi:10.1167/iovs.09-3860

Kempuraj, D., and Mohan, R. R. (2022). Autophagy in extracellular matrix and wound healing modulation in the cornea. *Biomedicines* 10, 339–420. doi:10.3390/biomedicines10020339

Kethiri, A. R., Raju, E., Bokara, K. K., Mishra, D. K., Basu, S., Rao, C. M., et al. (2019). Inflammation, vascularization and goblet cell differences in LSCD: Validating animal models of corneal alkali burns. *Exp. Eye Res.* 185, 107665. doi:10.1016/j.exer.2019.05.005

Koh, M. Y., and Powis, G. (2012). Passing the baton: The HIF switch. *Trends biochem. Sci.* 37, 364–372. doi:10.1016/j.tibs.2012.06.004

Kostallari, E., and Shah, V. H. (2019). Pericytes in the liver. *Adv. Exp. Med. Biol.* 1122, 153–167. doi:10.1007/978-3-030-11093-2_9

Lee, K. A., Zhang, H., Qian, D. Z., Rey, S., Liu, J. O., and Semenza, G. L. (2009). Acriflavine inhibits HIF-1 dimerization, tumor growth, and vascularization. *Proc. Natl. Acad. Sci. U. S. A.* 106, 17910–17915. doi:10.1073/pnas.0909353106

Lee, P., Chandel, N. S., and Simon, M. C. (2020). Cellular adaptation to hypoxia through hypoxia inducible factors and beyond. *Nat. Rev. Mol. Cell Biol.* 21, 268–283. doi:10.1038/s41580-020-0227-y

McNutt, M. (2013). Passing the baton. *Science* 340, 1141. doi:10.1126/science.1240779

Mittal, S. K., Omoto, M., Amouzegar, A., Sahu, A., Rezazadeh, A., Katikireddy, K. R., et al. (2016). Restoration of corneal transparency by mesenchymal stem cells. *Stem Cell Rep.* 7, 583–590. doi:10.1016/j.stemcr.2016.09.001

Moon, Y. M., Kang, H. J., Cho, J. S., Park, I. H., and Lee, H. M. (2012). Nox4 mediates hypoxia-stimulated myofibroblast differentiation in nasal polyp-derived fibroblasts. *Int. Arch. Allergy Immunol.* 159, 399–409. doi:10.1159/000337658

Onochie, O. E., Onyejose, A. J., Rich, C. B., and Trinkaus-Randall, V. (2020). The role of hypoxia in corneal extracellular matrix deposition and cell motility. *Anat. Rec.* 303, 1703–1716. doi:10.1002/ar.24110

Palazon, A., Goldrath, A. W., Nizet, V., and Johnson, R. S. (2014). HIF transcription factors, inflammation, and immunity. *Immunity* 41, 518–528. doi:10.1016/j.immuni.2014.09.008

Pang, K., Lennikov, A., and Yang, M. (2021). Hypoxia adaptation in the cornea: Current animal models and underlying mechanisms. *Anim. Model. Exp. Med.* 4, 300–310. doi:10.1002/ame2.12192

Pei, Y., Sherry, D. M., and McDermott, A. M. (2004). Thy-1 distinguishes human corneal fibroblasts and myofibroblasts from keratocytes. *Exp. Eye Res.* 79, 705–712. doi:10.1016/j.exer.2004.08.002

Peral, A., Mateo, J., Domínguez-Godínez, C. O., Carracedo, G., Gómez, J. A., Crooke, A., et al. (2022). Therapeutic potential of topical administration of siRNAs against HIF-1α for corneal neovascularization. *Exp. Eye Res.* 219, 109036. doi:10.1016/j.exer.2022.109036

Peyssonnaux, C., Datta, V., Cramer, T., Doedens, A., Theodorakis, E. A., Gallo, R. L., et al. (2005). HIF-1alpha expression regulates the bactericidal capacity of phagocytes. *J. Clin. Invest.* 115, 1806–1815. doi:10.1172/JCI23865

Pullamsetti, S. S., Mamazhakypov, A., Weissmann, N., Seeger, W., and Savai, R. (2020). Hypoxia-inducible factor signaling in pulmonary hypertension. *J. Clin. Invest.* 130, 5638–5651. doi:10.1172/JCI137558

Rao, P., and Suvas, S. (2019). Development of inflammatory hypoxia and prevalence of glycolytic metabolism in progressing herpes stromal keratitis lesions. *J. Immunol.* 202, 514–526. doi:10.4049/jimmunol.1800422

Rius, J., Guma, M., Schachtrup, C., Akassoglou, K., Zinkernagel, A. S., Nizet, V., et al. (2008). NF-kappaB links innate immunity to the hypoxic response through transcriptional regulation of HIF-1alpha. *Nature* 453, 807–811. doi:10.1038/nature06905

Safvati, A., Cole, N., Hume, E., and Willcox, M. (2009). Mediators of neovascularization and the hypoxic cornea. *Curr. Eye Res.* 34, 501–514. doi:10.1080/02713680902919557

Shatrov, V. A., Sumbayev, V. V., Zhou, J., and Brüne, B. (2003). Oxidized low-density lipoprotein (oxLDL) triggers hypoxia-inducible factor-1alpha (HIF-1alpha) accumulation via redox-dependent mechanisms. *Blood* 101, 4847–4849. doi:10.1182/blood-2002-09-2711

Short, M., Nemenoff, R. A., Zawada, W. M., Stenmark, K. R., and Das, M. (2004). Hypoxia induces differentiation of pulmonary artery adventitial fibroblasts into myofibroblasts. *Am. J. Physiol. Cell Physiol.* 286, 416–425. doi:10.1152/ajpcell.00169.2003

Takeda, N., O'Dea, E. L., Doedens, A., Kim, J. W., Weidemann, A., Stockmann, C., et al. (2010). Differential activation and antagonistic function of HIF-{alpha} isoforms in macrophages are essential for NO homeostasis. *Genes Dev.* 24, 491–501. doi:10.1101/gad.1881410

Tanaka, T. (2016). Expanding roles of the hypoxia-response network in chronic kidney disease. *Clin. Exp. Nephrol.* 20, 835–844. doi:10.1007/s10157-016-1241-4

Wilson, S. E., Sampaio, L. P., Shiju, T. M., Hilgert, G. S. L., and de Oliveira, R. C. (2022). Corneal opacity: Cell biological determinants of the transition from transparency to transient haze to scarring fibrosis, and resolution, after injury. *Invest. Ophthalmol. Vis. Sci.* 63, 22. doi:10.1167/iovs.63.1.22

Wilson, S. L., El Haj, A. J., and Yang, Y. (2012). Control of scar tissue formation in the cornea: Strategies in clinical and corneal tissue engineering. *J. Funct. Biomater.* 3, 642–687. doi:10.3390/jfb3030642

Wu, H., Chen, W., Zhao, F., Zhou, Q., Reinach, P. S., Deng, L., et al. (2018). Scleral hypoxia is a target for myopia control. *Proc. Natl. Acad. Sci. U. S. A.* 115, E7091–E7100. doi:10.1073/pnas.1721443115

Yang, G., Shi, R., and Zhang, Q. (2020). Hypoxia and oxygen-sensing signaling in gene regulation and cancer progression. *Int. J. Mol. Sci.* 21, 8162. doi:10.3390/ijms21218162

Yoeruek, E., Ziemssen, F., Henke-Fahle, S., Tatar, O., Tura, A., Grisanti, S., et al. (2008). Safety, penetration and efficacy of topically applied bevacizumab: Evaluation of eyedrops in corneal neovascularization after chemical burn. *Acta Ophthalmol.* 86, 322–328. doi:10.1111/j.1600-0420.2007.01049.x

Yuan, S., Wei, C., Liu, G., Zhang, L., Li, J., Li, L., et al. (2022). Sorafenib attenuates liver fibrosis by triggering hepatic stellate cell ferroptosis via HIF-1α/SLC7A11 pathway. *Cell Prolif.* 55, 13158. doi:10.1111/cpr.13158

Zhao, B., Guan, H., Liu, J. Q., Zheng, Z., Zhou, Q., Zhang, J., et al. (2017). Hypoxia drives the transition of human dermal fibroblasts to a myofibroblast-like phenotype via the TGF-β1/Smad3 pathway. *Int. J. Mol. Med.* 39, 153–159. doi:10.3892/ijmm.2016.2816

frontiers | Frontiers in Pharmacology

TYPE Correction
PUBLISHED 21 February 2023
DOI 10.3389/fphar.2023.1161682

Check for updates

OPEN ACCESS

APPROVED BY
Frontiers Editorial Office,
Frontiers Media SA, Switzerland

*CORRESPONDENCE
Jia Yin,
jia_yin@meei.harvard.edu
Kunpeng Pang,
k.pang@sdu.edu.cn

SPECIALTY SECTION
This article was submitted to Experimental Pharmacology and Drug Discovery, a section of the journal Frontiers in Pharmacology

RECEIVED 08 February 2023
ACCEPTED 09 February 2023
PUBLISHED 21 February 2023

CITATION
Zhu S, Shan H, Li J, Pan L, Wang S, Zhu J, Guo H, Mi F, Wu X, Yin J and Pang K (2023), Corrigendum: Therapeutic potential of topical administration of acriflavine against hypoxia-inducible factors for corneal fibrosis. *Front. Pharmacol.* 14:1161682. doi: 10.3389/fphar.2023.1161682

COPYRIGHT
© 2023 Zhu, Shan, Li, Pan, Wang, Zhu, Guo, Mi, Wu, Yin and Pang. This is an open-access article distributed under the terms of the Creative Commons Attribution License (CC BY). The use, distribution or reproduction in other forums is permitted, provided the original author(s) and the copyright owner(s) are credited and that the original publication in this journal is cited, in accordance with accepted academic practice. No use, distribution or reproduction is permitted which does not comply with these terms.

Corrigendum: Therapeutic potential of topical administration of acriflavine against hypoxia-inducible factors for corneal fibrosis

Shuyan Zhu[1], Huimin Shan[2], Jianqiao Li[2], Lijie Pan[2], Shudan Wang[3], Jing Zhu[2], Hui Guo[2], Fenghua Mi[2], Xinyi Wu[2], Jia Yin[3]* and Kunpeng Pang[2]*

[1]Xi'an People's Hospital (Xi'an Fourth Hospital), Shanxi Eye Hospital, Xi'an, China, [2]Department of Ophthalmology, Qilu Hospital of Shandong University, Jinan, Shandong, China, [3]Department of Ophthalmology, Harvard Medical School, Schepens Eye Research Institute of Massachusetts Eye and Ear, Boston, MA, United States

KEYWORDS

HIF, corneal fibrosis, corneal hypoxia, TGF-β1, extracellular matrix

A Corrigendum on
Therapeutic potential of topical administration of acriflavine against hypoxia-inducible factors for corneal fibrosis

by Zhu S, Shan H, Li J, Pan L, Wang S, Zhu J, Guo H, Mi F, Wu X and Pang K (2022). Front. Pharmacol. 13:996635. doi: 10.3389/fphar.2022.996635

In the published article, there was an error in the **Author** list, and author "Jia Yin" was erroneously excluded. The corrected **Author** list appears below.

"Shuyan Zhu[1], Huimin Shan[2], Jianqiao Li[2], Lijie Pan[2], Shudan Wang[3], Jing Zhu[2], Hui Guo[2], Fenghua Mi[2], Xinyi Wu[2], Jia Yin[3]*, Kunpeng Pang[2]*."

In the published article, Jia Yin's information was not included in the correspondence information. The corrected **Correspondence** information is "Jia Yin, jia_yin@meei.harvard.edu; Kunpeng Pang, k.pang@sdu.edu.cn."

In the published article, the **Author Contributions** statement did not mention Jia Yin's contributions. The correct statement is "JY and KP contributed to conception and design of the study. KP supervised the study. SZ, HS, SW, and KP conducted experiments and acquired data; HS and KP wrote the manuscript; LP analyzed data; FM assisted in conducting the experiments; JZ and HG assisted in analyzing data; JL and XW provided the reagents; KP designed research studies and revised the manuscript."

In the published article, the **Acknowledgements** statement was displayed as "We thank Dr. Jia Yin as an advisor for the hypoxia study." The correct statement is "None."

The authors apologize for this error and state that this does not change the scientific conclusions of the article in any way. The original article has been updated.

Publisher's note

All claims expressed in this article are solely those of the authors and do not necessarily represent those of their affiliated organizations, or those of the publisher, the editors and the reviewers. Any product that may be evaluated in this article, or claim that may be made by its manufacturer, is not guaranteed or endorsed by the publisher.

frontiers | Frontiers in Pharmacology

TYPE Review
PUBLISHED 21 October 2022
DOI 10.3389/fphar.2022.1016635

Check for updates

OPEN ACCESS

EDITED BY
Yanping Liu,
Qilu Hospital, Shandong University, China

REVIEWED BY
Reza Nemati,
Canterbury Health Laboratories, New Zealand
Bingxian Xie,
University of Pittsburgh, United States
Liyong Zhu,
Third Xiangya Hospital, Central South University, China
Cunchuan Wang,
First Affiliated Hospital of Jinan University, China

*CORRESPONDENCE
Guangyong Zhang,
guangyongzhang@hotmail.com

†These authors have contributed equally to this work

SPECIALTY SECTION
This article was submitted to Experimental Pharmacology and Drug Discovery, a section of the journal Frontiers in Pharmacology

RECEIVED 11 August 2022
ACCEPTED 06 October 2022
PUBLISHED 21 October 2022

CITATION
Ding H, Zhang Y, Ma X, Zhang Z, Xu Q, Liu C, Li B, Dong S, Li L, Zhu J, Zhong M and Zhang G (2022), Bariatric surgery for diabetic comorbidities: A focus on hepatic, cardiac and renal fibrosis. *Front. Pharmacol.* 13:1016635. doi: 10.3389/fphar.2022.1016635

COPYRIGHT
© 2022 Ding, Zhang, Ma, Zhang, Xu, Liu, Li, Dong, Li, Zhu, Zhong and Zhang. This is an open-access article distributed under the terms of the Creative Commons Attribution License (CC BY). The use, distribution or reproduction in other forums is permitted, provided the original author(s) and the copyright owner(s) are credited and that the original publication in this journal is cited, in accordance with accepted academic practice. No use, distribution or reproduction is permitted which does not comply with these terms.

Bariatric surgery for diabetic comorbidities: A focus on hepatic, cardiac and renal fibrosis

Huanxin Ding[1†], Yun Zhang[2†], Xiaomin Ma[2], Zhongwen Zhang[3], Qian Xu[2], Chuxuan Liu[1], Bingjun Li[2], Shuohui Dong[1], Linchuan Li[2], Jiankang Zhu[2], Mingwei Zhong[2] and Guangyong Zhang[1*]

[1]Department of General Surgery, Shandong Provincial Qianfoshan Hospital, Shandong University, Jinan, Shandong, China, [2]Department of General Surgery, The First Affiliated Hospital of Shandong First Medical University, Jinan, Shandong, China, [3]Department of Endocrinology, The First Affiliated Hospital of Shandong First Medical University, Jinan, Shandong, China

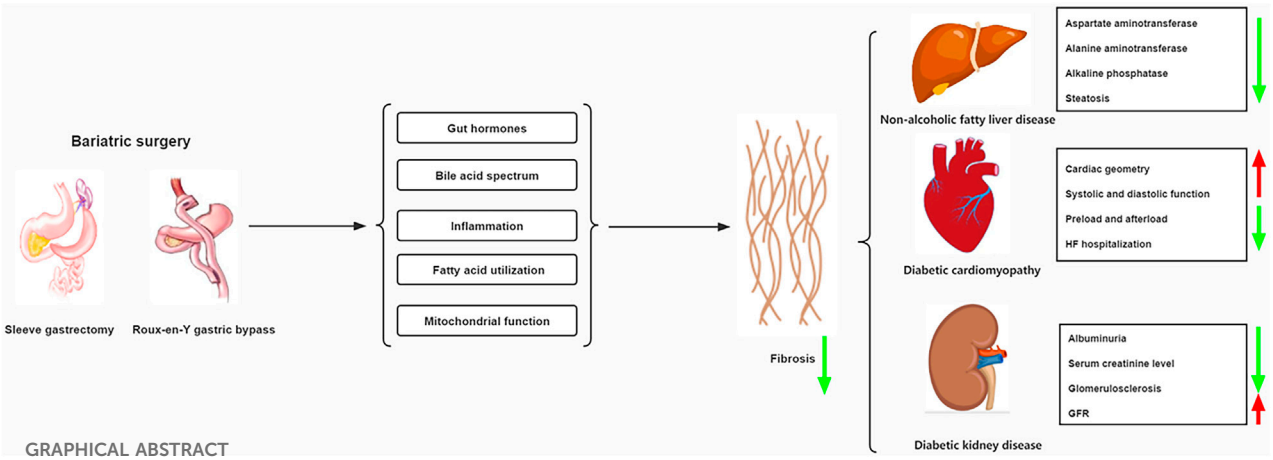
Continuously rising trends in diabetes render this disease spectrum an epidemic proportion worldwide. As the disease progresses, the pathological effects of diabetes may impair the normal function of several vital organs, eventually leading to increase the risk of other diabetic comorbidities with advanced fibrosis such as non-alcoholic fatty liver disease, diabetic cardiomyopathy, and diabetic kidney disease. Currently, lifestyle changes and drug therapies of hypoglycemic and lipid-lowering are effective in improving multi-organ function, but therapeutic efficacy is difficult to maintain due to poor compliance and drug reactions. Bariatric surgery, including sleeve gastrectomy and Roux-en-Y gastric bypass surgery, has shown better results in terms of prognosis for diabetes through long-term follow-up. Moreover, bariatric surgery has significant long-term benefits on the function of the heart, liver, kidneys, and other organs through mechanisms associated with reversal of tissue fibrosis. The aim of this review is to describe the impact of type 2 diabetes mellitus on hepatic, cardiac and renal fibrosis and to summarize the potential mechanisms by which bariatric surgery improves multiple organ function, particularly reversal of fibrosis.

KEYWORDS

bariatric surgery, Roux-en-Y gastric bypass, sleeve gastrectomy, diabetic cardiomyopathy, non-alcoholic fatty liver disease, diabetic kidney disease, fibrosis

1 Introduction

As a global prevalent metabolic disease, diabetes mellitus (DM) is characterized by a lack of insulin production or cellular uptake of insulin (2018). Insulin is essential for controlling glucose levels in the body (Tokarz et al., 2018). In type 2 diabetes mellitus (T2DM), insulin resistance (IR) affects the metabolism of carbohydrates, proteins and lipids, thereby promoting the development of hyperglycemia and hyperlipidemia (Taylor, 2013).



GRAPHICAL ABSTRACT
Pharmacological treatment and mechanisms of bariatric surgery for diabetic comorbidities.

The state of being chronically overweight combined with T2DM substantially increases the incidence of comorbidities such as non-alcoholic fatty liver disease (NAFLD), diabetic cardiomyopathy (DCM) and diabetic kidney disease (DKD) (Al-Sulaiti et al., 2019; La Sala and Pontiroli, 2020). As the degree of organ fibrosis increases, the functions of the liver, heart and kidney are gradually damaged and become more and more serious. The fibrotic process of these diseases has been slowed down to some extent by conservative medical management such as pharmacological interventions and lifestyle changes (Cox et al., 2013). However, low adherence makes it difficult to maintain positive treatment outcomes.

Over the past few decades, the role of bariatric surgery for long-term improvement in metabolic disease has received increasing attention (Hanipah and Schauer, 2020). There is substantial evidence that surgery is better at improving weight loss and T2DM outcomes than nonsurgical interventions, regardless of the type of surgery used. The 1991 National Institutes of Health guidelines recommend consideration of bariatric surgery in patients with a body mass index [BMI (calculated as weight in kilograms divided by height in meters squared)] of at least 40 kg or at least 35 kg with severe obesity-related comorbidities (1991). However, there is growing evidence that bariatric surgery should also be considered in people with T2DM with a BMI of 30–35 kg who are not adequately controlling hyperglycemia despite optimal T2DM medication Operation (Di Lorenzo et al., 2020). As the most commonly used bariatric surgery, Roux-en-Y gastric bypass (RYGB)and Sleeve gastrectomy (SG)not only have significant effect on weight loss and hypoglycemia, but also can improve or even reverse the complications of T2DM in the long term (Arterburn et al., 2020). Therefore, we summarize the effects of treating T2DM on fibrosis and the current status of bariatric surgery, with a focus on the underlying mechanisms by which bariatric surgery improves function and fibrosis of vital organs. This provides evidence that bariatric surgery may be a better treatment for these conditions.

2 Effects of type 2 diabetes mellitus on fibrosis of vital organs

Acute and chronic inflammation often triggers fibrosis in various vital organs (Mack, 2018; Henderson et al., 2020). Inflammation results in damage to resident epithelial cells and often endothelial cells, leading to increased release of inflammatory mediators including cytokines, chemokines, etc. This process contributes to the recruitment of numerous inflammatory cells, including lymphocytes, polymorphonuclear leukocytes, eosinophils, basophils, mast cells, and macrophages. These inflammatory cells trigger the activation of effector cells that drive the process of fibrosis (Wynn, 2004). Fibroblasts and myofibroblasts serve as key fibrotic effectors in several organs and are responsible for the synthesis of extracellular matrix (ECM) proteins (Hinz et al., 2007). The matrix proteins that make up fibrotic scars are mainly composed of interstitial collagens (types I and III), cellular fibronectin, and basement membrane proteins (Rockey et al., 1993). Molecular systems involved in fibrosis include platelet-derived growth factor (PDGF), connective tissue growth factor (CTGF), and the vasoactive peptide system, especially angiotensin II and endothelin-1 (Wynn, 2007).

Liver fibrosis is usually caused by an inflammatory process resulting in injuries to liver cells or bile duct cells.

Inflammation leads to the activation of effector cells, which contributes to the deposition of ECM (Bessone et al., 2019). Although multiple effectors synthesize ECM in the liver, hepatic stellate cells (HSCs) appear to be the major source of ECM. There is substantial evidence that hepatic stellate cells transform into myofibroblasts upon injury (Rockey et al., 1993). IR worsens with NAFLD disease progression and is considered a component of the pathogenesis of liver fibrosis (Friedman et al., 2018; Schwabe et al., 2020). One study showed that IR-related hyperinsulinemia directly stimulates HSCs proliferation and type I collagen secretion by activating PI3K and ERK-dependent pathways (Svegliati-Baroni et al., 1999). Inflammation can be caused by IR itself. Simultaneously, hepatocyte stress and death also promote inflammation, leading to macrophage recruitment and secretion of fibrotic-derived mediators, such as transforming growth factor beta (TGF-β), which is central to the liver fibrotic response (Koyama and Brenner, 2017; Tsuchida and Friedman, 2017).

Cardiomyocyte hypertrophy and excessive deposition of ECM are pivotal to the cardiac remodeling after injury (Porter and Turner, 2009). Cardiac fibrosis is generally divided into two types including reactive fibrosis and replacement fibrosis (Liu et al., 2021). Reactive fibrosis occurs in perivascular spaces. Replacement fibrosis occurs at the site of muscle cell loss. Fibrosis in the heart is attributed to fibroblasts, which are the most abundant cell type in the heart muscle. These cells are derived from cardiomyocyte-native fibroblasts, circulating fibroblasts, and fibroblasts resulting from the epithelial-mesenchymal transition (Zeisberg et al., 2007; Moore-Morris et al., 2014). The process by which all these cell types proliferate and differentiate into myofibroblasts after injury is driven by factors such as TGF-β, endothelin-1, and angiotensin II (Ang II). Type I and III interstitial collagen deposition was significantly increased in DCM patients compared with myocardial biopsies in non-diabetic patients, corroborating reports of cardiac interstitial and perivascular fibrosis found at earlier autopsy (van Hoeven and Factor, 1990; Shimizu et al., 1993). It has also been suggested that an important component of the increased cardiac fibrosis caused by T2DM may be replacement fibrosis. The above indicates that the two types of fibrosis are likely to coexist in DCM (Regan et al., 1977).

T2DM and hypertension are two major causes of renal fibrosis (Kaissling et al., 2013). Renal fibrosis is mediated by cellular components (e.g., inflammatory cells) and molecular components (e.g., cytokines, TGF-β, and endothelin-1) (Liu, 2011). The renin-angiotensin-aldosterone axis is particularly important in hypertension-induced fibrosis (Mezzano et al., 2001). The kidney has a unique cellular structure consisting of glomeruli, tubules, interstitium and capillaries. Damage to any of these sites triggers the deposition of ECM. Abnormal and excessive deposition of ECM proteins in the glomerular and interstitial regions are typical features of renal fibrosis (Sun et al., 2016). In DKD, T2DM and systemic hypertension exacerbate glomerular capillary pressure, leading to proteinuria, activation of cytokines and complement, and infiltration of immune cells, ultimately resulting in epithelial and interstitial fibrosis (Liu, 2011).

3 Non-alcoholic fatty liver disease

A large number of diabetic patients develop NAFLD and non-alcoholic steatohepatitis (NASH). NAFLD is the most common cause of chronic liver disease and includes a series of liver diseases ranging from simple steatosis to NASH, fibrosis and cirrhosis (Powell et al., 2021). The incidence of NAFLD is rising due to the diabetes pandemic, with a global prevalence of 24% in the general population (Younossi et al., 2018). NASH is an inflammatory subtype of NAFLD with evidence of steatosis and hepatocellular damage (ballooning) and inflammation, with or without fibrosis (Chalasani et al., 2018). Regardless of the underlying mechanism, significant weight loss is known to have beneficial effects on NASH, with sustained weight loss of 10% being associated with reduced liver fibrosis (Vilar-Gomez et al., 2015). An ideal treatment would effectively reverse liver damage and fibrosis without negatively affecting other metabolic parameters or cardiovascular complications.

3.1 Effects and underlying mechanisms of bariatric surgery in improving non-alcoholic fatty liver disease

Bariatric surgery can improve liver metabolism and reduce biochemical indicators of nonalcoholic fatty liver disease, including aspartate aminotransferase, alanine aminotransferase, and alkaline phosphatase, as well as histological parameters such as steatosis, fibrosis, Lobular inflammation and hepatocyte ballooning (Bower et al., 2015). Reduction in hepatic fat content and improvement in hepatic insulin resistance is one of the earliest beneficial effects of bariatric surgery and thus constitutes an attractive treatment option for NAFLD (Fakhry et al., 2019). General retrospective or cohort studies suggest that improvement in NAFLD after bariatric surgery is more likely than with other interventions; however, current data are insufficient to demonstrate a reduction in liver-specific mortality (Wolfe et al., 2016). Among patients with biopsy-proven NAFLD/NASH, the majority of SG and RYGB patients had essentially normal liver function in the 1-year follow-up, and the two procedures were equally effective in improving liver function (Cherla et al., 2020; de Brito et al., 2021). In addition, NAFLD patients underwent RYGB were more likely to experience

early transient deterioration of liver function than those underwent SG, possibly due to postoperative malabsorption or rapid weight loss (Kalinowski et al., 2017). However, RYGB seems to have more advantages in improving hepatic fibrosis (de Brito et al., 2021). Liver biopsies from 180 severely obese patients with biopsy-proven NASH after bariatric surgery showed that 84% of patients observed regression of NASH at 1 year after bariatric surgery, with no apparent recurrence within 1–5 years (p = 0.17). Fibrosis began to decrease 1 year after surgery and continued to decrease within 5 years (Lassailly et al., 2020).

3.1.1 Effects of altered gut hormone levels

GLP-1 is a peptide hormone and neurotransmitter with many metabolic and non-metabolic effects, secreted from the gut by L cells (Drucker, 2018). Increased GLP-1 levels improve beta cell function and insulin sensitivity (Lima et al., 2013). Elevated postprandial GLP-1 levels in patients after SG or RYGB (Jiménez et al., 2013; Jiménez et al., 2014). While most research on GLP-1 has focused on glucose metabolism, GLP-1 functions beyond glycemic control. GLP-1 promotes satiety, enhances insulin release, and inhibits glucagon release in response to nutrient intake (Jiménez et al., 2014). These findings point to possible mechanisms of relative glycemic control and weight loss found after surgery involving GLP-1, glucose homeostasis and T2DM remission. In NASH patients, GLP-1 reduces *de novo* lipogenesis, lipolysis-induced free fatty acid levels, and triglyceride-derived toxic metabolites (Armstrong et al., 2016b). In animal experiments comparing the therapeutic effects of liraglutide and bariatric surgery, bariatric surgery may enhance GLP-1 secretion by increasing serum bile acids and L cell proliferation in the ileum compared with liraglutide, thereby Ameliorates hepatic steatosis in obese rats (Kashihara et al., 2015). In addition, in a phase 2 trial on NAFLD, liraglutide resulted in some resolution of liver fibrosis (Armstrong et al., 2016a). On this basis, bariatric surgery appears to be more likely to alleviate the degree of liver fibrosis through a GLP-1-mediated mechanism.

In humans, hormone-like members of the FGF family include FGF-15/19 and FGF-21 (Itoh, 2010). The metabolism of FGF-19 and FGF-21 is involved in the regulation of bile acid biosynthesis, glucose metabolism and lipid metabolism in beta cells of pancreatic islets, liver and adipose tissue (Fisher et al., 2011). FGF-15 and FGF-21 have been shown to be protective against liver fibrosis in a mouse model (Zarei et al., 2018; Liu et al., 2020). Plasma FGF-19 and FGF-21 levels were analyzed in 28 patients who received RYGB (Harris et al., 2017). They found that RYGB surgery resulted in increased postprandial plasma FGF-19 concentrations. They also found that plasma FGF-21 exceeded baseline levels by approximately three times after RYGB surgery. Bariatric surgery induces FGF-15/19 expression in the distal small intestine *via* direct stimulation of FXR by bile acids (Huang et al., 2019; Eiken et al., 2020). Furthermore, FGF-15/19 acts in an endocrine-like manner to improve the metabolic function of insulin target tissues. DJB and SG surgery restores the FGF21 signaling pathway in the liver of high-fat diet/streptomycin-induced diabetic rats and increases FGF21 sensitivity (Liu et al., 2019).

PYY, also known as a short peptide of pancreatic polypeptide YY3-36, is released by L cells in the distal small intestine and colon (le Roux and Bloom, 2005). The main effects of PYY involve the central regulation of appetite as well as the regulation of blood glucose homeostasis (Batterham et al., 2003). In mouse models, PYY modulates weight loss after bypass surgery (Chandarana et al., 2011), while increased PYY has been observed in patients after bariatric surgery, both as a result of post-operative anatomical changes in the gastrointestinal tract (Magouliotis et al., 2017). Notably, several studies suggest that PYY3-36 levels are reduced in obesity and elevated after gastric bypass surgery, possibly contributing to increased satiety after this procedure (Price and Bloom, 2014; Guida et al., 2017). Overall, as PYY is strongly associated with weight loss and NAFLD after bariatric surgery, its role in metabolism warrants further investigation. Although more research is needed, elevated levels of PYY are associated with stabilization of blood glucose levels, metabolism, and body weight, which directly affect the incidence and complications of obesity and T2DM.

3.1.2 Changes in bile acid metabolism, transport and signal transduction

Both RYGB and SG have been shown to induce sustained increases in systemic bile acid (BA) concentrations and intestinal BA signaling, which are associated with improvements in insulin resistance and glycemic control (Belgaumkar et al., 2016; Risstad et al., 2017). Bile acids are signaling molecules and metabolic integrators, which involve in activating nuclear farnesoid X receptor (FXR) and membrane Takeda G-protein-coupled receptor 5 (TGR5) to regulate glucose, lipid and energy metabolism (Chiang and Ferrell, 2020). However, BA includes more than 20 components, each of which may have specific effects on metabolism (de Aguiar Vallim et al., 2013). Notably, 12α-hydroxylated bile acids promote liver fibrosis through TGR5-mediated p38MAPK and ERK1/2 signaling, but these bile acids were significantly reduced after SG (Wang et al., 2017; Xie et al., 2021). RYGB upregulates the expression of hepatic BA targets FXR and peroxisome proliferator-activated receptor-α (PPARα) in severely obese patients, and these changes are accompanied by regression of NASH and T2DM after 1 year (Francque et al., 2015; Mazzini et al., 2019). BA treatment of primary and immortalized human hepatocytes induces FXR and PPARα to downregulate glycolysis and restrict glucose entry into the Krebs cycle, thereby inhibiting fatty acid synthesis from excess glucose (Cai and Sewer, 2013). PPARα activation combined with PPARβ/δ agonists improves steatosis, inflammation and fibrosis in preclinical models of NAFLD, identifying new potential therapeutic areas (Pawlak et al., 2015). Activation of the gut FXR/FGF19 signaling pathway inhibits the key lipogenic enzyme, acetyl-CoA carboxylase, supporting the downregulation of *de novo* fatty acid production by hepatic FXR

and indirectly promoting fatty acid oxidation by downregulating the expression of carnitine palmitoyl transferase 1α (CPT1α) serving as a key mitochondrial fatty acid transporter. Recent studies have shown that CPT1α is elevated in HSCs from fibrotic patients and mouse models of fibrosis, and that CPT1α induces activation of these cells leading to fibrosis (Fondevila et al., 2022).

Although studies of the effects of SG on FXR and its downstream targets are lacking in humans, the observed increase in post-operative systemic FGF19 concentrations is consistent with enhanced gut FXR signaling following SG. Likewise, findings in FXR-deficient mouse models receiving SG suggest that FXR is essential to achieve the full metabolic benefits of surgery, including postoperative recovery of glucose tolerance and reduced energy intake (Ryan et al., 2014; Cavin et al., 2016). It is worth mentioning that FXR agonists have emerged as a potential therapy against liver fibrosis, despite the issue of side effects (Li et al., 2021). In addition to the direct effects of FXR signaling on hepatic BA, glucose, and fat metabolism, inhibition of intestinal FXR after RYGB is also associated with upregulation of TGR5 (Zhai et al., 2018), which may contribute to postprandial insulin hormone pancreatic elevation in enteroendocrine L cells after surgery Increased levels of GLP1 and PYY suggest a multifaceted antidiabetic effect (Trabelsi et al., 2015; Li et al., 2019).

3.1.3 Reversing inflammation

In a group of patients undergoing bariatric surgery, the expression of inflammatory genes in subcutaneous and visceral adipose tissue was proportional to the severity of NAFLD histology (Rosso et al., 2019). One year post-surgery, SG improved liver histology, especially the degree of fibrosis, in all NASH patients (Cabré et al., 2019). At the same time, there were significant differences in C-C chemokine receptor type 2 (CCR2) and Tumor necrosis factor-α (TNF-α) in preoperative plasma and liver between NASH patients and non-NASH patients, so it is considered that the improvement of liver fibrosis involves the regulation of oxidative stress and inflammation levels. TNF-α, a key cytokine upregulated in obesity, is mainly produced by macrophages (Kunz et al., 2021). Serum levels of various inflammatory markers correlate with liver inflammation, CD11c+ CD206+ and CCR2+ macrophage expansion in visceral adipose tissue of patients with NASH and/or fibrosis (Wentworth et al., 2010; du Plessis et al., 2015). Transplantation of visceral adipose tissue in obese mice increased hepatic macrophage accumulation and exacerbated steatohepatitis compared with a high cholesterol diet model (Bijnen et al., 2018).

Toll-like receptor 4 (TLR4) is considered to be one of the cutting-edge cross-communicators between gut bacteria and the host regulating inflammatory signaling and energy homeostasis (Sala et al., 2020). A pathway specific to liver fibrosis involves TLR4 and is associated with enhanced TGF-β signaling (Seki et al., 2007). TLR4 is activated on the surface of HSCs by gut bacterial lipopolysaccharides from the gut, triggering cell activation and fibrosis formation, thereby linking fibrosis to the microbiome (Sorribas et al., 2019). TLR4 expression in patients with NAFLD is associated with fibrosis (Vespasiani-Gentilucci et al., 2015). It has been shown that RYGB specifically reduces TLR4 expression in the small and large intestines of C57Blc/6J mice, and that TLR4 and myeloid differentiation factor 8 (MyD88, a key downstream signaling regulators) are required for RYGB-induced metabolic responses (Abu El Haija et al., 2021).

4 Diabetic cardiomyopathy

There is a broad link between T2DM and cardiovascular disease (CVD). T2DM causes cardiomyopathy and increases the risk of heart failure (HF) even independent of traditional HF risks, including hypertension (HTN), coronary heart disease (CHD), and valvular heart disease (VHD) (Dillmann, 2019). DCM is characterized by abnormal diastolic relaxation at an early stage (Jia et al., 2018). Numerous pathophysiological abnormalities collectively promote interstitial fibrosis, diastolic dysfunction, and later systolic dysfunction in cardiac tissue, resulting in clinical HF syndrome. A retrospective cohort study of 8,231 people with T2DM showed a 2.5-fold increased risk of HF in people with T2DM (Nichols et al., 2004). In addition, an observational study involving 25,958 men and 22,900 women showed that a 1% increase in HbA1c was associated with an 8% increased risk of HF regardless of blood pressure, obesity, age and the presence of coronary heart disease (Iribarren et al., 2001). Therefore, glycemic control in patients with T2DM is a key mechanism to prevent cardiac dysfunction and HF.

4.1 Effects and underlying mechanisms of bariatric surgery in improving diabetic cardiomyopathy

Bariatric surgery significantly improves cardiac geometry, function, providing a unique and effective treatment for patients with DCM and HF (Roth et al., 2020). Studies have shown that the remission rate of high blood pressure is 60%–70% within a year after bariatric surgery (Benaiges et al., 2019). In addition to controlling blood pressure, RYGB and SG are effective in reducing cardiovascular risk and the incidence of sudden macrovascular disease (Fisher et al., 2018; Blanco et al., 2019). In severely obese patients with T2DM, weight loss after bariatric surgery improves left ventricular end diastolic dimension (LVDD) (Elagizi et al., 2018). Notably, many patients with pre-existing cardiovascular disease can reduce or completely discontinue cardiovascular medications following bariatric surgery (English and Williams, 2018). Furthermore, according to a large retrospective analysis, bariatric surgery reduces in-

hospital mortality by nearly 50% and length of stay in hospitalized patients with HF (Aleassa et al., 2019).

4.1.1 Reducing heart load and cardiac fatty acid utilization

Preload and afterload, as well as systemic and local energy requirements, are decreased after bariatric surgery due to significant reductions in adipose tissue and mass (Lin et al., 2011). Concentrations of vasoconstrictors (e.g., enkephalinase, angiotensin II, renin, and endothelin-1) decreased significantly ($p < 0.05$) 6 months after RYGB by follow-up. These changes promote beneficial "reverse remodeling," improve fibrosis and the incidence of ventricular tachycardia (Massare et al., 2010) and reduce the incidence of sudden death (Spinale, 2007). Due to lipid metabolism disorder, excessive fat deposition in the heart can create a lipotoxic environment, and at the same time increase the uptake and utilization rate of fatty acids by the myocardium, thereby impairing cardiac function over time (Labbé et al., 2012; Shulman, 2014). By studying positron emission tomography scans of the hearts of 12 obese subjects with T2DM before and after bariatric surgery, Carreau et al. (2020) found that bariatric surgery reduces cardiac fatty acid utilization and enhances left ventricular function.

4.1.2 Improving mitochondrial function and regulating calcium homeostasis

Both cellular and tissue mitochondrial respiration were increased in patients receiving RYGB or SG compared to preoperatively (Nijhawan et al., 2013). Evidence suggests that in a rat model of DCM, SG restores mitochondrial dysfunction and fragmentation by activating 5′ adenosine monophosphate-activated protein kinase (AMPK) signaling (Li et al., 2022). Myocardial Ca^{2+} transients exhibit significantly higher amplitudes and faster decay after SG and DJB, suggesting that bariatric surgery can promote myocardial Ca^{2+} homeostasis in DCM rats (Huang et al., 2018). The above-mentioned postoperative repair of mitochondrial function and Ca^{2+} homeostasis can improve cardiac structure and cardiac function by reducing myocardial collagen deposition and fibrosis (Huang et al., 2018; Li et al., 2022). Despite this, there are currently few clinical studies on specific improvements in postoperative cardiac mitochondrial function and calcium homeostasis in patients undergoing bariatric surgery (Kindel and Strande, 2018).

4.1.3 Adjusting the enterocardiac axis and inhibiting inflammation

Other beneficial effects of bariatric surgery include altered gastrointestinal microbiota, changed bile acid profile, and increased postprandial GLP-1 in the days following surgery (Chambers et al., 2011; Ryan et al., 2014). Bariatric surgery may beneficially alter the enterocardiac axis through one or more of these mechanisms to further improve cardiac function beyond the effects of weight loss. Gut-secreted GLP-1 in cardiomyocytes is now known to lead to decreased apoptosis and increased glucose uptake, and to reverse myocardial fibrosis, independent of canonical insulin signaling (Bose et al., 2005; Helmstädter et al., 2020). Increased level of GLP-1 after bariatric surgery can reverse endothelial dysfunction and restore the endothelial protective properties of high-density lipoprotein (HDL) (Osto et al., 2015). In addition, GLP-1R agonists have been used to treat ischemia-reperfusion injury and HF.

Adiponectin (APN), the most abundant product of white adipose tissue (WAT), has been proposed as a potential prognostic biomarker and therapeutic target in patients with cardiometabolic disease, which is inversely associated with obesity (Messina et al., 2018). Adiponectin levels are associated with a reduction in total fat mass and atherosclerosis risk (Umeda et al., 2013) and are significantly elevated after bariatric surgery (Valenzano et al., 2020). Current studies have shown that APN reduces the degree of cardiac fibrosis by activating autophagy in macrophages and inhibiting Ang II-induced inflammatory responses (Qi et al., 2014). Serum Hsp60 (a kind of adipokine) was elevated in patients with DCM but decreased after bariatric surgery. As a predictor of cardiovascular disease, Hsp60 correlates with inflammatory markers and may be a molecular link between adipose tissue inflammation and the development of cardiovascular disease (Sell et al., 2017). TLR4 mediates HSP60-induced apoptosis in cardiac myocytes from WT mice, which appears to be involved in replacement fibrosis (Heiserman et al., 2015).

5 Diabetic kidney disease

Rising global prevalence of T2DM and chronic kidney disease (CKD) has prompted research into DKD (Anders et al., 2018). The leading cause of kidney failure worldwide is DKD (Reidy et al., 2014). More serious, All-cause mortality in DKD patients was 31% and 10-year mortality was 20% (Afkarian et al., 2013). Hyperglycemia is the main cause of the development of DKD. The earliest signs of DKD are microalbuminuria (>30 mg/day), which progresses to macroalbuminuria (>300 mg/day) and decreased glomerular filtration rate (GFR), culminating in end-stage renal disease (ESRD) (Rocco and Berns, 2009). Metabolic changes associated with T2DM can lead to glomerular hypertrophy, glomerulosclerosis, and tubulointerstitial inflammation and fibrosis (Tervaert et al., 2010). More than 40% of people with obesity and T2DM develop renal impairment as microvascular complications, and 30% go on to develop end-stage renal disease (Adler et al., 2003). Tight glycemic control significantly reduces the incidence of diabetic nephropathy, suggesting that hyperglycemia-induced metabolic changes, including changes in energy utilization and

mitochondrial dysfunction, play a key role in disease development (Reidy et al., 2014).

5.1 Effects and underlying mechanisms of bariatric surgery in improving diabetic kidney disease

A large retrospective observational cohort study of patients with T2DM showed that bariatric surgery significantly reduced the incidence of kidney disease relative to nonsurgical interventions (6.4% vs. 14%) (O'Brien et al., 2018). For patients with pre-existing kidney disease, almost 80% improvement in albuminuria in the short and long term after bariatric surgery including RYGB and SG (Young et al., 2019). Obvious renal histopathological lesions including glomerulosclerosis, mesangial matrix expansion, and podocyte hypertrophy are prevalent in T2DM and can be ameliorated by bariatric surgery (Navarro-Díaz et al., 2006). This is consistent with the anti-proteinuric effect of SG and RYGB in STZ-induced DKD rats (Canney et al., 2020; Xiong et al., 2020). Meanwhile, improvements in glomerular structure and ultrastructure were also observed in animal models. An observational retrospective cohort study demonstrated that bariatric surgery, particularly RYGB surgery, significantly improved Estimated glomerular filtration rate (eGFR) for up to 3 years. Bariatric surgery should be considered for patients with DKD who have failed lifestyle changes and medical therapy, which have potential benefits in slowing DKD progression (Friedman and Wolfe, 2016). As a means to improve outcomes in patients with renal disease, bariatric surgery has myriad potential roles that require more clinically relevant studies to explore (Martin et al., 2020).

Bariatric surgery reduces weight and improves hypertension and hyperglycemia, which may explain some of the positive effects on albuminuria (Navarro-Díaz et al., 2006; Getty et al., 2012). Important mechanisms of DKD pathogenesis are advanced glycation end products and oxidative stress (Giacco and Brownlee, 2010). However, the role of inflammation is increasingly recognized as key to the progression of kidney disease (Fenske et al., 2013).

Chronic low-grade inflammation is often associated with T2DM (Sabatino et al., 2017). C-reactive protein (CRP) is associated with the development of DKD (McDonald et al., 2004; Rao, 2012). CRP promotes renal fibrosis and inflammation in a TGF-β-dependent manner (You et al., 2021). Bariatric surgery may reduce CRP and repair the pro-inflammatory chemokine and cytokine milieu, while enhancing anti-inflammatory chemokine and cytokine production (Illán-Gómez et al., 2012). CC-chemokine ligand 2 (CCL2), a protein closely associated with obesity and diabetic nephropathy (Tesch, 2008). Bariatric surgery-induced reduction in CCL-2-related inflammation is associated with improved renal function and reduced renal fibrosis (Bueter et al., 2010; Monte et al., 2012; Fenske et al., 2013; Wu et al., 2014). Similar improvement in urinary CCL-2/creatinine ratio at 4 weeks after RYGB and SG, but additional effect of RYGB in reducing chemokine ligand 18 (CCL-18) (Bueter et al., 2010). The AMPK/TGF-β pathway has been identified as a key pathway regulating inflammation and profibrosis in diabetic nephropathy. In a rodent kidney model, RYGB partially reversed DKD fibrosis by reducing TGF-β signaling (Vangoitsenhoven et al., 2020). At the same time, renal fibrosis was reversed after surgery, which may be related to the blockade of the renin-angiotensin system (Lambers Heerspink et al., 2013; Berney et al., 2021). Furthermore, several recent observations suggest that elevated endogenous gut hormones, such as GLP-1, may be an intermediate mediator of the anti-inflammatory effects of RYGB (Navaneethan et al., 2010).

6 Summary and future perspective

In recent years, bariatric surgery has grown as an emerging treatment for T2DM and related comorbidities. Currently, there is a growing body of strong evidence for the efficacy and safety of bariatric surgery (Arterburn et al., 2020). Therefore, for severely obese patients with T2DM, it is necessary to add bariatric surgery to the treatment decision-making option.

High-quality evidence from randomized controlled trials suggests that bariatric surgery is superior to medical therapy for enhancing glycemic control and achieving T2DM remission. The continued global prevalence of NAFLD, DCM and DKD as comorbidities of T2DM means that this is an important priority for healthcare and research. Bariatric surgery to treat these major T2DM comorbidities has obvious advantages over medical treatment in terms of duration and improvement.

In T2DM, fibrosis in various organs is driven in part by inflammation caused by IR itself. TGF-β is a common mediator of organ fibrosis in T2DM (Rockey et al., 2015). Unfortunately, the role of TGF-β in bariatric surgery ameliorating myocardial fibrosis has not yet been elucidated. A liver-specific fibrotic pathway involving TLR4 has also been reported in studies of cardiomyocyte fibrosis. It can be seen from these that the molecular systems related to T2DM-induced fibrosis are very extensive and complex, and need to be further explored and clarified.

Future research should focus on identifying key transcriptional, proteomic, and metabolomic changes that occur in vital organs of the body such as the heart, liver, and kidneys after bariatric surgery, which will help differentiate between the benefits and harms of bariatric surgery in people with T2DM impact and can inform the design of novel medical treatments that replicate the beneficial effects of surgery, while providing ideas for addressing the adverse consequences of surgery, thereby maximizing its therapeutic benefits.

Author contributions

HD and YZ organize the article structure and write the full text. XM, ZZ, QX, and CL search literature. SD and BL make figure. JZ, LL, MZ, and GZ directed and revised the manuscript for this review.

Funding

This review was supported by the National Natural Science Foundation of China (Grant No. 81873647) and Major Basic Research Project of Natural Science Foundation of Shandong Province (Grant No. ZR2020ZD15).

Conflict of interest

The authors declare that the research was conducted in the absence of any commercial or financial relationships that could be construed as a potential conflict of interest.

Publisher's note

All claims expressed in this article are solely those of the authors and do not necessarily represent those of their affiliated organizations, or those of the publisher, the editors and the reviewers. Any product that may be evaluated in this article, or claim that may be made by its manufacturer, is not guaranteed or endorsed by the publisher.

References

Abu El Haija, M., Ye, Y., Chu, Y., Herz, H., Linden, B., Shahi, S. K., et al. (2021). Toll-like receptor 4 and myeloid differentiation factor 88 are required for gastric bypass-induced metabolic effects. *Surg. Obes. Relat. Dis.* 17 (12), 1996–2006. doi:10.1016/j.soard.2021.07.019

Adler, A. I., Stevens, R. J., Manley, S. E., Bilous, R. W., Cull, C. A., Holman, R. R., et al. (2003). Development and progression of nephropathy in type 2 diabetes: The United Kingdom prospective diabetes study (UKPDS 64). *Kidney Int.* 63 (1), 225–232. doi:10.1046/j.1523-1755.2003.00712.x

Afkarian, M., Sachs, M. C., Kestenbaum, B., Hirsch, I. B., Tuttle, K. R., Himmelfarb, J., et al. (2013). Kidney disease and increased mortality risk in type 2 diabetes. *J. Am. Soc. Nephrol.* 24 (2), 302–308. doi:10.1681/asn.2012070718

Al-Sulaiti, H., Diboun, I., Agha, M. V., Mohamed, F. F. S., Atkin, S., Dömling, A. S., et al. (2019). Metabolic signature of obesity-associated insulin resistance and type 2 diabetes. *J. Transl. Med.* 17 (1), 348. doi:10.1186/s12967-019-2096-8

Aleassa, E. M., Khorgami, Z., Kindel, T. L., Tu, C., Tang, W. H. W., Schauer, P. R., et al. (2019). Impact of bariatric surgery on heart failure mortality. *Surg. Obes. Relat. Dis.* 15 (7), 1189–1196. doi:10.1016/j.soard.2019.03.021

Anders, H. J., Huber, T. B., Isermann, B., and Schiffer, M. (2018). CKD in diabetes: Diabetic kidney disease versus nondiabetic kidney disease. *Nat. Rev. Nephrol.* 14 (6), 361–377. doi:10.1038/s41581-018-0001-y

Armstrong, M. J., Gaunt, P., Aithal, G. P., Barton, D., Hull, D., Parker, R., et al. (2016a). Liraglutide safety and efficacy in patients with non-alcoholic steatohepatitis (LEAN): A multicentre, double-blind, randomised, placebo-controlled phase 2 study. *Lancet* 387 (10019), 679–690. doi:10.1016/s0140-6736(15)00803-x

Armstrong, M. J., Hull, D., Guo, K., Barton, D., Hazlehurst, J. M., Gathercole, L. L., et al. (2016b). Glucagon-like peptide 1 decreases lipotoxicity in non-alcoholic steatohepatitis. *J. Hepatol.* 64 (2), 399–408. doi:10.1016/j.jhep.2015.08.038

Arterburn, D. E., Telem, D. A., Kushner, R. F., and Courcoulas, A. P. (2020). Benefits and risks of bariatric surgery in adults: A review. *Jama* 324 (9), 879–887. doi:10.1001/jama.2020.12567

American Diabetes Association (2018). 2. Classification and diagnosis of diabetes: Standards of medical care in diabetes-2018. *Diabetes Care* 41 (1), S13-S27–s27. doi:10.2337/dc18-S002

Batterham, R. L., Cohen, M. A., Ellis, S. M., Le Roux, C. W., Withers, D. J., Frost, G. S., et al. (2003). Inhibition of food intake in obese subjects by peptide YY3-36. *N. Engl. J. Med.* 349 (10), 941–948. doi:10.1056/NEJMoa030204

Belgaumkar, A. P., Vincent, R. P., Carswell, K. A., Hughes, R. D., Alaghband-Zadeh, J., Mitry, R. R., et al. (2016). Changes in bile acid profile After laparoscopic sleeve gastrectomy are associated with improvements in metabolic profile and fatty liver disease. *Obes. Surg.* 26 (6), 1195–1202. doi:10.1007/s11695-015-1878-1

Benaiges, D., Climent, E., Goday, A., Flores-Le Roux, J. A., and Pedro-Botet, J. (2019). Bariatric surgery and hypertension: Implications and perspectives after the GATEWAY randomized trial. *Cardiovasc. Diagn. Ther.* 9 (1), 100–103. doi:10.21037/cdt.2018.10.04

Berney, M., Vakilzadeh, N., Maillard, M., Faouzi, M., Grouzmann, E., Bonny, O., et al. (2021). Bariatric surgery induces a differential effect on plasma aldosterone in comparison to dietary advice alone. *Front. Endocrinol.* 12, 745045. doi:10.3389/fendo.2021.745045

Bessone, F., Razori, M. V., and Roma, M. G. (2019). Molecular pathways of nonalcoholic fatty liver disease development and progression. *Cell. Mol. Life Sci.* 76 (1), 99–128. doi:10.1007/s00018-018-2947-0

Bijnen, M., Josefs, T., Cuijpers, I., Maalsen, C. J., van de Gaar, J., Vroomen, M., et al. (2018). Adipose tissue macrophages induce hepatic neutrophil recruitment and macrophage accumulation in mice. *Gut* 67 (7), 1317–1327. doi:10.1136/gutjnl-2016-313654

Blanco, D. G., Funes, D. R., Giambartolomei, G., Lo Menzo, E., Szomstein, S., and Rosenthal, R. J. (2019). Laparoscopic sleeve gastrectomy versus roux-en-Y gastric bypass in cardiovascular risk reduction: A match control study. *Surg. Obes. Relat. Dis.* 15 (1), 14–20. doi:10.1016/j.soard.2018.09.488

Bose, A. K., Mocanu, M. M., Carr, R. D., Brand, C. L., and Yellon, D. M. (2005). Glucagon-like peptide 1 can directly protect the heart against ischemia/reperfusion injury. *Diabetes* 54 (1), 146–151. doi:10.2337/diabetes.54.1.146

Bower, G., Toma, T., Harling, L., Jiao, L. R., Efthimiou, E., Darzi, A., et al. (2015). Bariatric surgery and non-alcoholic fatty liver disease: A systematic review of liver biochemistry and histology. *Obes. Surg.* 25 (12), 2280–2289. doi:10.1007/s11695-015-1691-x

Bueter, M., Dubb, S. S., Gill, A., Joannou, L., Ahmed, A., Frankel, A. H., et al. (2010). Renal cytokines improve early after bariatric surgery. *Br. J. Surg.* 97 (12), 1838–1844. doi:10.1002/bjs.7264

Cabré, N., Luciano-Mateo, F., Fernández-Arroyo, S., Baiges-Gayà, G., Hernández-Aguilera, A., Fibla, M., et al. (2019). Laparoscopic sleeve gastrectomy reverses non-alcoholic fatty liver disease modulating oxidative stress and inflammation. *Metabolism.* 99, 81–89. doi:10.1016/j.metabol.2019.07.002

Cai, K., and Sewer, M. B. (2013). Diacylglycerol kinase θ couples farnesoid X receptor-dependent bile acid signalling to Akt activation and glucose homoeostasis in hepatocytes. *Biochem. J.* 454 (2), 267–274. doi:10.1042/bj20130609

Canney, A. L., Cohen, R. V., Elliott, J. A., C, M. A., Martin, W. P., Docherty, N. G., et al. (2020). Improvements in diabetic albuminuria and podocyte differentiation following Roux-en-Y gastric bypass surgery. *Diab. Vasc. Dis. Res.* 17 (1), 1479164119879039. doi:10.1177/1479164119879039

Carreau, A. M., Noll, C., Blondin, D. P., Frisch, F., Nadeau, M., Pelletier, M., et al. (2020). Bariatric surgery rapidly decreases cardiac dietary fatty acid partitioning and hepatic insulin resistance through increased intra-abdominal adipose tissue storage and reduced spillover in type 2 diabetes. *Diabetes* 69 (4), 567–577. doi:10.2337/db19-0773

Cavin, J. B., Couvelard, A., Lebtahi, R., Ducroc, R., Arapis, K., Voitellier, E., et al. (2016). Differences in alimentary glucose absorption and intestinal disposal of blood glucose after roux-en-Y gastric bypass vs sleeve gastrectomy. *Gastroenterology* 150 (2), 454–464. e459. doi:10.1053/j.gastro.2015.10.009

Chalasani, N., Younossi, Z., Lavine, J. E., Charlton, M., Cusi, K., Rinella, M., et al. (2018). The diagnosis and management of nonalcoholic fatty liver disease: Practice

guidance from the American Association for the Study of Liver Diseases. *Hepatology* 67 (1), 328–357. doi:10.1002/hep.29367

Chambers, A. P., Jessen, L., Ryan, K. K., Sisley, S., Wilson-Pérez, H. E., Stefater, M. A., et al. (2011). Weight-independent changes in blood glucose homeostasis after gastric bypass or vertical sleeve gastrectomy in rats. *Gastroenterology* 141 (3), 950–958. doi:10.1053/j.gastro.2011.05.050

Chandarana, K., Gelegen, C., Karra, E., Choudhury, A. I., Drew, M. E., Fauveau, V., et al. (2011). Diet and gastrointestinal bypass-induced weight loss: The roles of ghrelin and peptide YY. *Diabetes* 60 (3), 810–818. doi:10.2337/db10-0566

Cherla, D. V., Rodriguez, N. A., Vangoitsenhoven, R., Singh, T., Mehta, N., McCullough, A. J., et al. (2020). Impact of sleeve gastrectomy and Roux-en-Y gastric bypass on biopsy-proven non-alcoholic fatty liver disease. *Surg. Endosc.* 34 (5), 2266–2272. doi:10.1007/s00464-019-07017-0

Chiang, J. Y. L., and Ferrell, J. M. (2020). Bile acid receptors FXR and TGR5 signaling in fatty liver diseases and therapy. *Am. J. Physiol. Gastrointest. Liver Physiol.* 318 (3), G554-G573–g573. doi:10.1152/ajpgi.00223.2019

Cox, D. J., Gill Taylor, A., Dunning, E. S., Winston, M. C., Luk Van, I. L., McCall, A., et al. (2013). Impact of behavioral interventions in the management of adults with type 2 diabetes mellitus. *Curr. Diab. Rep.* 13 (6), 860–868. doi:10.1007/s11892-013-0423-7

de Aguiar Vallim, T. Q., Tarling, E. J., and Edwards, P. A. (2013). Pleiotropic roles of bile acids in metabolism. *Cell. Metab.* 17 (5), 657–669. doi:10.1016/j.cmet.2013.03.013

de Brito, E. S. M. B., Tustumi, F., de Miranda Neto, A. A., Dantas, A. C. B., Santo, M. A., and Cecconello, I. (2021). Gastric bypass compared with sleeve gastrectomy for nonalcoholic fatty liver disease: A systematic review and meta-analysis. *Obes. Surg.* 31 (6), 2762–2772. doi:10.1007/s11695-021-05412-y

Di Lorenzo, N., Antoniou, S. A., Batterham, R. L., Busetto, L., Godoroja, D., Iossa, A., et al. (2020). Clinical practice guidelines of the European association for endoscopic surgery (EAES) on bariatric surgery: Update 2020 endorsed by IFSO-ec, EASO and ESPCOP. *Surg. Endosc.* 34 (6), 2332–2358. doi:10.1007/s00464-020-07555-y

Dillmann, W. H. (2019). Diabetic cardiomyopathy. *Circ. Res.* 124 (8), 1160–1162. doi:10.1161/circresaha.118.314665

Drucker, D.J. (2018). Mechanisms of Action and Therapeutic Application of Glucagon-like Peptide-1. *Cell Metab.* 27 (4), 740–756. doi:10.1016/j.cmet.2018.03.001

du Plessis, J., van Pelt, J., Korf, H., Mathieu, C., van der Schueren, B., Lannoo, M., et al. (2015). Association of Adipose Tissue Inflammation With Histologic Severity of Nonalcoholic Fatty Liver Disease. *Gastroenterology* 149 (3), 635–648. doi:10.1053/j.gastro.2015.05.044

Eiken, A., Fuglsang, S., Eiken, M., Svane, M. S., Kuhre, R. E., Wewer Albrechtsen, N. J., et al. (2020). Bilio-enteric flow and plasma concentrations of bile acids after gastric bypass and sleeve gastrectomy. *Int. J. Obes.* 44 (9), 1872–1883. doi:10.1038/s41366-020-0578-7

Elagizi, A., Kachur, S., Lavie, C. J., Carbone, S., Pandey, A., Ortega, F. B., et al. (2018). An overview and update on obesity and the obesity paradox in cardiovascular diseases. *Prog. Cardiovasc. Dis.* 61 (2), 142–150. doi:10.1016/j.pcad.2018.07.003

English, W. J., and Williams, D. B. (2018). Metabolic and bariatric surgery: An effective treatment option for obesity and cardiovascular disease. *Prog. Cardiovasc. Dis.* 61 (2), 253–269. doi:10.1016/j.pcad.2018.06.003

Fakhry, T. K., Mhaskar, R., Schwitalla, T., Muradova, E., Gonzalvo, J. P., and Murr, M. M. (2019). Bariatric surgery improves nonalcoholic fatty liver disease: A contemporary systematic review and meta-analysis. *Surg. Obes. Relat. Dis.* 15 (3), 502–511. doi:10.1016/j.soard.2018.12.002

Fenske, W. K., Dubb, S., Bueter, M., Seyfried, F., Patel, K., Tam, F. W., et al. (2013). Effect of bariatric surgery-induced weight loss on renal and systemic inflammation and blood pressure: A 12-month prospective study. *Surg. Obes. Relat. Dis.* 9 (4), 559–568. doi:10.1016/j.soard.2012.03.009

Fisher, D. P., Johnson, E., Haneuse, S., Arterburn, D., Coleman, K. J., O'Connor, P. J., et al. (2018). Association between bariatric surgery and macrovascular disease outcomes in patients with type 2 diabetes and severe obesity. *Jama* 320 (15), 1570–1582. doi:10.1001/jama.2018.14619

Fisher, F. M., Estall, J. L., Adams, A. C., Antonellis, P. J., Bina, H. A., Flier, J. S., et al. (2011). Integrated regulation of hepatic metabolism by fibroblast growth factor 21 (FGF21) *in vivo*. *Endocrinology* 152 (8), 2996–3004. doi:10.1210/en.2011-0281

Fondevila, M. F., Fernandez, U., Heras, V., Parracho, T., Gonzalez-Rellan, M. J., Novoa, E., et al. (2022). Inhibition of carnitine palmitoyltransferase 1A in hepatic stellate cells protects against fibrosis. *J. Hepatol.* 77 (1), 15–28. doi:10.1016/j.jhep.2022.02.003

Francque, S., Verrijken, A., Caron, S., Prawitt, J., Paumelle, R., Derudas, B., et al. (2015). PPARα gene expression correlates with severity and histological treatment response in patients with non-alcoholic steatohepatitis. *J. Hepatol.* 63 (1), 164–173. doi:10.1016/j.jhep.2015.02.019

Friedman, A. N., and Wolfe, B. (2016). Is bariatric surgery an effective treatment for type II diabetic kidney disease? *Clin. J. Am. Soc. Nephrol.* 11 (3), 528–535. doi:10.2215/cjn.07670715

Friedman, S. L., Neuschwander-Tetri, B. A., Rinella, M., and Sanyal, A. J. (2018). Mechanisms of NAFLD development and therapeutic strategies. *Nat. Med.* 24 (7), 908–922. doi:10.1038/s41591-018-0104-9

Getty, J. L., Hamdallah, I. N., Shamseddeen, H. N., Wu, J., Low, R. K., Craig, J., et al. (2012). Changes in renal function following roux-en-Y gastric bypass: A prospective study. *Obes. Surg.* 22 (7), 1055–1059. doi:10.1007/s11695-012-0617-0

Giacco, F., and Brownlee, M. (2010). Oxidative stress and diabetic complications. *Circ. Res.* 107 (9), 1058–1070. doi:10.1161/circresaha.110.223545

Guida, C., Stephen, S., Guitton, R., and Ramracheya, R. D. (2017). The role of PYY in pancreatic islet physiology and surgical control of diabetes. *Trends Endocrinol. Metab.* 28 (8), 626–636. doi:10.1016/j.tem.2017.04.005

Hanipah, Z. N., and Schauer, P. R. (2020). Bariatric surgery as a long-term treatment for type 2 diabetes/metabolic syndrome. *Annu. Rev. Med.* 71, 1–15. doi:10.1146/annurev-med-053117-123246

Harris, L. I. S., Smith, G. I., Mittendorfer, B., Eagon, J. C., Okunade, A. L., Patterson, B. W., et al. (2017). Roux-en-Y gastric bypass surgery has unique effects on postprandial FGF21 but not FGF19 secretion. *J. Clin. Endocrinol. Metab.* 102 (10), 3858–3864. doi:10.1210/jc.2017-01295

Heiserman, J. P., Chen, L., Kim, B. S., Kim, S. C., Tran, A. L., Siebenborn, N., et al. (2015). TLR4 mutation and HSP60-induced cell death in adult mouse cardiac myocytes. *Cell. Stress Chaperones* 20 (3), 527–535. doi:10.1007/s12192-015-0577-0

Helmstädter, J., Frenis, K., Filippou, K., Grill, A., Dib, M., Kalinovic, S., et al. (2020). Endothelial GLP-1 (Glucagon-Like peptide-1) receptor mediates cardiovascular protection by liraglutide in mice with experimental arterial hypertension. *Arterioscler. Thromb. Vasc. Biol.* 40 (1), 145–158. doi:10.1161/atv.0000615456.97862.30

Henderson, N. C., Rieder, F., and Wynn, T. A. (2020). Fibrosis: From mechanisms to medicines. *Nature* 587 (7835), 555–566. doi:10.1038/s41586-020-2938-9

Hinz, B., Phan, S. H., Thannickal, V. J., Galli, A., Bochaton-Piallat, M. L., and Gabbiani, G. (2007). The myofibroblast: One function, multiple origins. *Am. J. Pathol.* 170 (6), 1807–1816. doi:10.2353/ajpath.2007.070112

Huang, H. H., Lee, W. J., Chen, S. C., Chen, T. F., Lee, S. D., and Chen, C. Y. (2019). Bile acid and fibroblast growth factor 19 regulation in obese diabetics, and non-alcoholic fatty liver disease after sleeve gastrectomy. *J. Clin. Med.* 8 (6), E815. doi:10.3390/jcm8060815

Huang, X., Liu, S., Wu, D., Cheng, Y., Han, H., Wang, K., et al. (2018). Facilitated Ca(2+) homeostasis and attenuated myocardial autophagy contribute to alleviation of diabetic cardiomyopathy after bariatric surgery. *Am. J. Physiol. Heart Circ. Physiol.* 315 (5), H1258-H1268–h1268. doi:10.1152/ajpheart.00274.2018

Hubbard, V. S., and Hall, W. H. (1991). Gastrointestinal surgery for severe obesity. *Obes. Surg.* 1 (3), 257–265. doi:10.1381/096089291765560962

Illán-Gómez, F., Gonzálvez-Ortega, M., Orea-Soler, I., Alcaraz-Tafalla, M. S., Aragón-Alonso, A., Pascual-Díaz, M., et al. (2012). Obesity and inflammation: Change in adiponectin, C-reactive protein, tumour necrosis factor-alpha and interleukin-6 after bariatric surgery. *Obes. Surg.* 22 (6), 950–955. doi:10.1007/s11695-012-0643-y

Iribarren, C., Karter, A. J., Go, A. S., Ferrara, A., Liu, J. Y., Sidney, S., et al. (2001). Glycemic control and heart failure among adult patients with diabetes. *Circulation* 103 (22), 2668–2673. doi:10.1161/01.cir.103.22.2668

Itoh, N. (2010). Hormone-like (endocrine) fgfs: Their evolutionary history and roles in development, metabolism, and disease. *Cell. Tissue Res.* 342 (1), 1–11. doi:10.1007/s00441-010-1024-2

Jia, G., Whaley-Connell, A., and Sowers, J. R. (2018). Diabetic cardiomyopathy: A hyperglycaemia- and insulin-resistance-induced heart disease. *Diabetologia* 61 (1), 21–28. doi:10.1007/s00125-017-4390-4

Jiménez, A., Casamitjana, R., Viaplana-Masclans, J., Lacy, A., and Vidal, J. (2013). GLP-1 action and glucose tolerance in subjects with remission of type 2 diabetes after gastric bypass surgery. *Diabetes Care* 36 (7), 2062–2069. doi:10.2337/dc12-1535

Jiménez, A., Mari, A., Casamitjana, R., Lacy, A., Ferrannini, E., and Vidal, J. (2014). GLP-1 and glucose tolerance after sleeve gastrectomy in morbidly obese subjects with type 2 diabetes. *Diabetes* 63 (10), 3372–3377. doi:10.2337/db14-0357

Kaissling, B., Lehir, M., and Kriz, W. (2013). Renal epithelial injury and fibrosis. *Biochim. Biophys. Acta* 1832 (7), 931–939. doi:10.1016/j.bbadis.2013.02.010

Kalinowski, P., Paluszkiewicz, R., Ziarkiewicz-Wróblewska, B., Wróblewski, T., Remiszewski, P., Grodzicki, M., et al. (2017). Liver

function in patients with nonalcoholic fatty liver disease randomized to roux-en-Y gastric bypass versus sleeve gastrectomy: A secondary analysis of a randomized clinical trial. *Ann. Surg.* 266 (5), 738–745. doi:10.1097/sla.0000000000002397

Kashihara, H., Shimada, M., Kurita, N., Sato, H., Yoshikawa, K., Higashijima, J., et al. (2015). Duodenal-jejunal bypass improves diabetes and liver steatosis via enhanced glucagon-like peptide-1 elicited by bile acids. *J. Gastroenterol. Hepatol.* 30 (2), 308–315. doi:10.1111/jgh.12690

Kindel, T. L., and Strande, J. L. (2018). Bariatric surgery as a treatment for heart failure: Review of the literature and potential mechanisms. *Surg. Obes. Relat. Dis.* 14 (1), 117–122. doi:10.1016/j.soard.2017.09.534

Koyama, Y., and Brenner, D. A. (2017). Liver inflammation and fibrosis. *J. Clin. Investig.* 127 (1), 55–64. doi:10.1172/jci88881

Kunz, H. E., Hart, C. R., Gries, K. J., Parvizi, M., Laurenti, M., Dalla Man, C., et al. (2021). Adipose tissue macrophage populations and inflammation are associated with systemic inflammation and insulin resistance in obesity. *Am. J. Physiol. Endocrinol. Metab.* 321 (1), E105–e121. doi:10.1152/ajpendo.00070.2021

La Sala, L., and Pontiroli, A. E. (2020). Prevention of diabetes and cardiovascular disease in obesity. *Int. J. Mol. Sci.* 21 (21), E8178. doi:10.3390/ijms21218178

Labbé, S. M., Grenier-Larouche, T., Noll, C., Phoenix, S., Guérin, B., Turcotte, E. E., et al. (2012). Increased myocardial uptake of dietary fatty acids linked to cardiac dysfunction in glucose-intolerant humans. *Diabetes* 61 (11), 2701–2710. doi:10.2337/db11-1805

Lambers Heerspink, H. J., de Borst, M. H., Bakker, S. J., and Navis, G. J. (2013). Improving the efficacy of RAAS blockade in patients with chronic kidney disease. *Nat. Rev. Nephrol.* 9 (2), 112–121. doi:10.1038/nrneph.2012.281

Lassailly, G., Caiazzo, R., Ntandja-Wandji, L.C., Gnemmi, V., Baud, G., Verkindt, H., et al. (2020). Bariatric Surgery Provides Long-term Resolution of Nonalcoholic Steatohepatitis and Regression of Fibrosis. *Gastroenterology* 159 (4), 1290–1301. doi:10.1053/j.gastro.2020.06.006

le Roux, C.W., and Bloom, S.R. (2005). Peptide YY, appetite and food intake. *Proc Nutr Soc* 64(2), 213-216. doi:10.1079/pns2005427

Li, J., Liu, C., Zhou, Z., Dou, B., Huang, J., Huang, L., et al. (2021). Isotschimgine alleviates nonalcoholic steatohepatitis and fibrosis via FXR agonism in mice. *Phytother. Res.* 35 (6), 3351–3364. doi:10.1002/ptr.7055

Li, P., Zhu, L., Yang, X., Li, W., Sun, X., Yi, B., et al. (2019). Farnesoid X receptor interacts with cAMP response element binding protein to modulate glucagon-like peptide-1 (7-36) amide secretion by intestinal L cell. *J. Cell. Physiol.* 234 (8), 12839–12846. doi:10.1002/jcp.27940

Li, S., Dong, S., Xu, Q., Shi, B., Li, L., Zhang, W., et al. (2022). Sleeve gastrectomy-induced AMPK activation attenuates diabetic cardiomyopathy by maintaining mitochondrial homeostasis via NR4A1 suppression in rats. *Front. Physiol.* 13, 837798. doi:10.3389/fphys.2022.837798

Lima, M. M., Pareja, J. C., Alegre, S. M., Geloneze, S. R., Kahn, S. E., Astiarraga, B. D., et al. (2013). Visceral fat resection in humans: Effect on insulin sensitivity, beta-cell function, adipokines, and inflammatory markers. *Obes. (Silver Spring)* 21 (3), E182–E189. doi:10.1002/oby.20030

Lin, C. H., Kurup, S., Herrero, P., Schechtman, K. B., Eagon, J. C., Klein, S., et al. (2011). Myocardial oxygen consumption change predicts left ventricular relaxation improvement in obese humans after weight loss. *Obes. (Silver Spring)* 19 (9), 1804–1812. doi:10.1038/oby.2011.186

Liu, M., López de Juan Abad, B., and Cheng, K. (2021). Cardiac fibrosis: Myofibroblast-mediated pathological regulation and drug delivery strategies. *Adv. Drug Deliv. Rev.* 173, 504–519. doi:10.1016/j.addr.2021.03.021

Liu, Q., Wang, S., Wei, M., Huang, X., Cheng, Y., Shao, Y., et al. (2019). Improved FGF21 sensitivity and restored FGF21 signaling pathway in high-fat diet/streptozotocin-induced diabetic rats after duodenal-jejunal bypass and sleeve gastrectomy. *Front. Endocrinol.* 10, 566. doi:10.3389/fendo.2019.00566

Liu, Y. (2011). Cellular and molecular mechanisms of renal fibrosis. *Nat. Rev. Nephrol.* 7 (12), 684–696. doi:10.1038/nrneph.2011.149

Liu, Y., Chen, K., Li, F., Gu, Z., Liu, Q., He, L., et al. (2020). Probiotic lactobacillus rhamnosus GG prevents liver fibrosis through inhibiting hepatic bile acid synthesis and enhancing bile acid excretion in mice. *Hepatology* 71 (6), 2050–2066. doi:10.1002/hep.30975

Mack, M. (2018). Inflammation and fibrosis. *Matrix Biol.* 68-69, 106–121. doi:10.1016/j.matbio.2017.11.010

Magouliotis, D. E., Tasiopoulou, V. S., Sioka, E., Chatedaki, C., and Zacharoulis, D. (2017). Impact of bariatric surgery on metabolic and gut microbiota profile: A systematic review and meta-analysis. *Obes. Surg.* 27 (5), 1345–1357. doi:10.1007/s11695-017-2595-8

Martin, W. P., White, J., López-Hernández, F. J., Docherty, N. G., and le Roux, C. W. (2020). Metabolic surgery to treat obesity in diabetic kidney disease, chronic kidney disease, and end-stage kidney disease; what are the unanswered questions? *Front. Endocrinol.* 11, 289. doi:10.3389/fendo.2020.00289

Massare, J., Berry, J. M., Luo, X., Rob, F., Johnstone, J. L., Shelton, J. M., et al. (2010). Diminished cardiac fibrosis in heart failure is associated with altered ventricular arrhythmia phenotype. *J. Cardiovasc. Electrophysiol.* 21 (9), 1031–1037. doi:10.1111/j.1540-8167.2010.01736.x

Mazzini, G. S., Khoraki, J., Dozmorov, M., Browning, M. G., Wijesinghe, D., Wolfe, L., et al. (2019). Concomitant PPARα and FXR activation as a putative mechanism of NASH improvement after gastric bypass surgery: A GEO datasets analysis. *J. Gastrointest. Surg.* 23 (1), 51–57. doi:10.1007/s11605-018-3938-z

McDonald, S., Maguire, G., Duarte, N., Wang, X. L., and Hoy, W. (2004). C-reactive protein, cardiovascular risk, and renal disease in a remote Australian Aboriginal community. *Clin. Sci.* 106 (2), 121–128. doi:10.1042/cs20030186

Messina, A., Monda, M., Valenzano, A., Messina, G., Villano, I., Moscatelli, F., et al. (2018). Functional changes induced by orexin A and adiponectin on the sympathetic/parasympathetic balance. *Front. Physiol.* 9, 259. doi:10.3389/fphys.2018.00259

Mezzano, S. A., Ruiz-Ortega, M., and Egido, J. (2001). Angiotensin II and renal fibrosis. *Hypertension* 38 (3), 635–638. doi:10.1161/hy09t1.094234

Monte, S. V., Caruana, J. A., Ghanim, H., Sia, C. L., Korzeniewski, K., Schentag, J. J., et al. (2012). Reduction in endotoxemia, oxidative and inflammatory stress, and insulin resistance after Roux-en-Y gastric bypass surgery in patients with morbid obesity and type 2 diabetes mellitus. *Surgery* 151 (4), 587–593. doi:10.1016/j.surg.2011.09.038

Moore-Morris, T., Guimarães-Camboa, N., Banerjee, I., Zambon, A. C., Kisseleva, T., Velayoudon, A., et al. (2014). Resident fibroblast lineages mediate pressure overload-induced cardiac fibrosis. *J. Clin. Investig.* 124 (7), 2921–2934. doi:10.1172/jci74783

Navaneethan, S. D., Kelly, K. R., Sabbagh, F., Schauer, P. R., Kirwan, J. P., and Kashyap, S. R. (2010). Urinary albumin excretion, HMW adiponectin, and insulin sensitivity in type 2 diabetic patients undergoing bariatric surgery. *Obes. Surg.* 20 (3), 308–315. doi:10.1007/s11695-009-0026-1

Navarro-Díaz, M., Serra, A., Romero, R., Bonet, J., Bayés, B., Homs, M., et al. (2006). Effect of drastic weight loss after bariatric surgery on renal parameters in extremely obese patients: Long-term follow-up. *J. Am. Soc. Nephrol.* 17 (12), S213–S217. doi:10.1681/asn.2006080917

Nichols, G. A., Gullion, C. M., Koro, C. E., Ephross, S. A., and Brown, J. B. (2004). The incidence of congestive heart failure in type 2 diabetes: An update. *Diabetes Care* 27 (8), 1879–1884. doi:10.2337/diacare.27.8.1879

Nijhawan, S., Richards, W., O'Hea, M. F., Audia, J. P., and Alvarez, D. F. (2013). Bariatric surgery rapidly improves mitochondrial respiration in morbidly obese patients. *Surg. Endosc.* 27 (12), 4569–4573. doi:10.1007/s00464-013-3125-y

O'Brien, R., Johnson, E., Haneuse, S., Coleman, K. J., O'Connor, P. J., Fisher, D. P., et al. (2018). Microvascular outcomes in patients with diabetes after bariatric surgery versus usual care: A matched cohort study. *Ann. Intern. Med.* 169 (5), 300–310. doi:10.7326/m17-2383

Osto, E., Doytcheva, P., Corteville, C., Bueter, M., Dörig, C., Stivala, S., et al. (2015). Rapid and body weight-independent improvement of endothelial and high-density lipoprotein function after roux-en-Y gastric bypass: Role of glucagon-like peptide-1. *Circulation* 131 (10), 871–881. doi:10.1161/circulationaha.114.011791

Pawlak, M., Lefebvre, P., and Staels, B. (2015). Molecular mechanism of PPARα action and its impact on lipid metabolism, inflammation and fibrosis in non-alcoholic fatty liver disease. *J. Hepatol.* 62 (3), 720–733. doi:10.1016/j.jhep.2014.10.039

Porter, K. E., and Turner, N. A. (2009). Cardiac fibroblasts: At the heart of myocardial remodeling. *Pharmacol. Ther.* 123 (2), 255–278. doi:10.1016/j.pharmthera.2009.05.002

Powell, E. E., Wong, V. W., and Rinella, M. (2021). Non-alcoholic fatty liver disease. *Lancet* 397 (10290), 2212–2224. doi:10.1016/s0140-6736(20)32511-3

Price, S. L., and Bloom, S. R. (2014). Protein PYY and its role in metabolism. *Front. Horm. Res.* 42, 147–154. doi:10.1159/000358343

Qi, G. M., Jia, L. X., Li, Y. L., Li, H. H., and Du, J. (2014). Adiponectin suppresses angiotensin II-induced inflammation and cardiac fibrosis through activation of macrophage autophagy. *Endocrinology* 155 (6), 2254–2265. doi:10.1210/en.2013-2011

Rao, S. R. (2012). Inflammatory markers and bariatric surgery: A meta-analysis. *Inflamm. Res.* 61 (8), 789–807. doi:10.1007/s00011-012-0473-3

Regan, T. J., Lyons, M. M., Ahmed, S. S., Levinson, G. E., Oldewurtel, H. A., Ahmad, M. R., et al. (1977). Evidence for cardiomyopathy in familial diabetes mellitus. *J. Clin. Investig.* 60 (4), 884–899. doi:10.1172/jci108843

Reidy, K., Kang, H. M., Hostetter, T., and Susztak, K. (2014). Molecular mechanisms of diabetic kidney disease. *J. Clin. Investig.* 124 (6), 2333–2340. doi:10.1172/jci72271

Risstad, H., Kristinsson, J. A., Fagerland, M. W., le Roux, C. W., Birkeland, K. I., Gulseth, H. L., et al. (2017). Bile acid profiles over 5 years after gastric bypass and duodenal switch: Results from a randomized clinical trial. *Surg. Obes. Relat. Dis.* 13 (9), 1544–1553. doi:10.1016/j.soard.2017.05.024

Rocco, M. V., and Berns, J. S. (2009). KDOQI in the era of global guidelines. *Am. J. Kidney Dis.* 54 (5), 781–787. doi:10.1053/j.ajkd.2009.08.001

Rockey, D. C., Bell, P. D., and Hill, J. A. (2015). Fibrosis--a common pathway to organ injury and failure. *N. Engl. J. Med.* 372 (12), 1138–1149. doi:10.1056/NEJMra1300575

Rockey, D. C., Housset, C. N., and Friedman, S. L. (1993). Activation-dependent contractility of rat hepatic lipocytes in culture and *in vivo*. *J. Clin. Investig.* 92 (4), 1795–1804. doi:10.1172/jci116769

Rosso, C., Kazankov, K., Younes, R., Esmaili, S., Marietti, M., Sacco, M., et al. (2019). Crosstalk between adipose tissue insulin resistance and liver macrophages in non-alcoholic fatty liver disease. *J. Hepatol.* 71 (5), 1012–1021. doi:10.1016/j.jhep.2019.06.031

Roth, A. E., Thornley, C. J., and Blackstone, R. P. (2020). Outcomes in bariatric and metabolic surgery: An updated 5-year review. *Curr. Obes. Rep.* 9 (3), 380–389. doi:10.1007/s13679-020-00389-8

Ryan, K. K., Tremaroli, V., Clemmensen, C., Kovatcheva-Datchary, P., Myronovych, A., Karns, R., et al. (2014). FXR is a molecular target for the effects of vertical sleeve gastrectomy. *Nature* 509 (7499), 183–188. doi:10.1038/nature13135

Sabatino, A., Regolisti, G., Cosola, C., Gesualdo, L., and Fiaccadori, E. (2017). Intestinal microbiota in type 2 diabetes and chronic kidney disease. *Curr. Diab. Rep.* 17 (3), 16. doi:10.1007/s11892-017-0841-z

Sala, P., Torrinhas, R., Fonseca, D. C., Machado, N. M., Singer, J., Singer, P., et al. (2020). Intestinal expression of toll-like receptor gene changes early after gastric bypass surgery and association with type 2 diabetes remission. *Nutrition* 79-80, 110885. doi:10.1016/j.nut.2020.110885

Schwabe, R. F., Tabas, I., and Pajvani, U. B. (2020). Mechanisms of fibrosis development in nonalcoholic steatohepatitis. *Gastroenterology* 158 (7), 1913–1928. doi:10.1053/j.gastro.2019.11.311

Seki, E., De Minicis, S., Osterreicher, C. H., Kluwe, J., Osawa, Y., Brenner, D. A., et al. (2007). TLR4 enhances TGF-beta signaling and hepatic fibrosis. *Nat. Med.* 13 (11), 1324–1332. doi:10.1038/nm1663

Sell, H., Poitou, C., Habich, C., Bouillot, J. L., Eckel, J., and Clément, K. (2017). Heat shock protein 60 in obesity: Effect of bariatric surgery and its relation to inflammation and cardiovascular risk. *Obes. (Silver Spring)* 25 (12), 2108–2114. doi:10.1002/oby.22014

Shimizu, M., Umeda, K., Sugihara, N., Yoshio, H., Ino, H., Takeda, R., et al. (1993). Collagen remodelling in myocardia of patients with diabetes. *J. Clin. Pathol.* 46 (1), 32–36. doi:10.1136/jcp.46.1.32

Shulman, G. I. (2014). Ectopic fat in insulin resistance, dyslipidemia, and cardiometabolic disease. *N. Engl. J. Med.* 371 (12), 1131–1141. doi:10.1056/NEJMra1011035

Sorribas, M., Jakob, M. O., Yilmaz, B., Li, H., Stutz, D., Noser, Y., et al. (2019). FXR modulates the gut-vascular barrier by regulating the entry sites for bacterial translocation in experimental cirrhosis. *J. Hepatol.* 71 (6), 1126–1140. doi:10.1016/j.jhep.2019.06.017

Spinale, F. G. (2007). Myocardial matrix remodeling and the matrix metalloproteinases: Influence on cardiac form and function. *Physiol. Rev.* 87 (4), 1285–1342. doi:10.1152/physrev.00012.2007

Sun, Y. B., Qu, X., Caruana, G., and Li, J. (2016). The origin of renal fibroblasts/myofibroblasts and the signals that trigger fibrosis. *Differentiation.* 92 (3), 102–107. doi:10.1016/j.diff.2016.05.008

Svegliati-Baroni, G., Ridolfi, F., Di Sario, A., Casini, A., Marucci, L., Gaggiotti, G., et al. (1999). Insulin and insulin-like growth factor-1 stimulate proliferation and type I collagen accumulation by human hepatic stellate cells: Differential effects on signal transduction pathways. *Hepatology* 29 (6), 1743–1751. doi:10.1002/hep.510290632

Taylor, R. (2013). Type 2 diabetes: Etiology and reversibility. *Diabetes Care* 36 (4), 1047–1055. doi:10.2337/dc12-1805

Tervaert, T. W., Mooyaart, A. L., Amann, K., Cohen, A. H., Cook, H. T., Drachenberg, C. B., et al. (2010). Pathologic classification of diabetic nephropathy. *J. Am. Soc. Nephrol.* 21 (4), 556–563. doi:10.1681/asn.2010010010

Tesch, G. H. (2008). MCP-1/CCL2: A new diagnostic marker and therapeutic target for progressive renal injury in diabetic nephropathy. *Am. J. Physiol. Ren. Physiol.* 294 (4), F697–F701. doi:10.1152/ajprenal.00016.2008

Tokarz, V. L., MacDonald, P. E., and Klip, A. (2018). The cell biology of systemic insulin function. *J. Cell. Biol.* 217 (7), 2273–2289. doi:10.1083/jcb.201802095

Trabelsi, M. S., Daoudi, M., Prawitt, J., Ducastel, S., Touche, V., Sayin, S. I., et al. (2015). Farnesoid X receptor inhibits glucagon-like peptide-1 production by enteroendocrine L cells. *Nat. Commun.* 6, 7629. doi:10.1038/ncomms8629

Tsuchida, T., and Friedman, S. L. (2017). Mechanisms of hepatic stellate cell activation. *Nat. Rev. Gastroenterol. Hepatol.* 14 (7), 397–411. doi:10.1038/nrgastro.2017.38

Umeda, L. M., Pereira, A. Z., Carneiro, G., Arasaki, C. H., and Zanella, M. T. (2013). Postprandial adiponectin levels are associated with improvements in postprandial triglycerides after Roux-en-Y gastric bypass in type 2 diabetic patients. *Metab. Syndr. Relat. Disord.* 11 (5), 343–348. doi:10.1089/met.2012.0042

Valenzano, A., Tartaglia, N., Ambrosi, A., Tafuri, D., Monda, M., Messina, A., et al. (2020). The metabolic rearrangements of bariatric surgery: Focus on orexin-A and the adiponectin system. *J. Clin. Med.* 9 (10), E3327. doi:10.3390/jcm9103327

van Hoeven, K. H., and Factor, S. M. (1990). A comparison of the pathological spectrum of hypertensive, diabetic, and hypertensive-diabetic heart disease. *Circulation* 82 (3), 848–855. doi:10.1161/01.cir.82.3.848

Vangoitsenhoven, R., Mulya, A., Mosinski, J. D., Brethauer, S. A., Schauer, P. R., Kirwan, J. P., et al. (2020). Effects of gastric bypass surgery on expression of glucose transporters and fibrotic biomarkers in kidney of diabetic fatty rats. *Surg. Obes. Relat. Dis.* 16 (9), 1242–1248. doi:10.1016/j.soard.2020.04.017

Vespasiani-Gentilucci, U., Carotti, S., Perrone, G., Mazzarelli, C., Galati, G., Onetti-Muda, A., et al. (2015). Hepatic toll-like receptor 4 expression is associated with portal inflammation and fibrosis in patients with NAFLD. *Liver Int.* 35 (2), 569–581. doi:10.1111/liv.12531

Vilar-Gomez, E., Martinez-Perez, Y., Calzadilla-Bertot, L., Torres-Gonzalez, A., Gra-Oramas, B., Gonzalez-Fabian, L., et al. (2015). Weight loss through lifestyle modification significantly reduces features of nonalcoholic steatohepatitis. *Gastroenterology* 149 (2), 367–378. e365; quiz e314-365. doi:10.1053/j.gastro.2015.04.005

Wang, M., Wu, Q., Xie, H., Shao, Y., Zhong, M., Zhang, X., et al. (2017). Effects of sleeve gastrectomy on serum 12α-hydroxylated bile acids in a diabetic rat model. *Obes. Surg.* 27 (11), 2912–2918. doi:10.1007/s11695-017-2714-6

Wentworth, J. M., Naselli, G., Brown, W. A., Doyle, L., Phipson, B., Smyth, G. K., et al. (2010). Pro-inflammatory CD11c+CD206+ adipose tissue macrophages are associated with insulin resistance in human obesity. *Diabetes* 59 (7), 1648–1656. doi:10.2337/db09-0287

Wolfe, B. M., Kvach, E., and Eckel, R. H. (2016). Treatment of obesity: Weight loss and bariatric surgery. *Circ. Res.* 118 (11), 1844–1855. doi:10.1161/circresaha.116.307591

Wu, H. J., Yiu, W. H., Li, R. X., Wong, D. W., Leung, J. C., Chan, L. Y., et al. (2014). Mesenchymal stem cells modulate albumin-induced renal tubular inflammation and fibrosis. *PLoS One* 9 (3), e90883. doi:10.1371/journal.pone.0090883

Wynn, T. A. (2007). Common and unique mechanisms regulate fibrosis in various fibroproliferative diseases. *J. Clin. Investig.* 117 (3), 524–529. doi:10.1172/jci31487

Wynn, T. A. (2004). Fibrotic disease and the T(H)1/T(H)2 paradigm. *Nat. Rev. Immunol.* 4 (8), 583–594. doi:10.1038/nri1412

Xie, G., Jiang, R., Wang, X., Liu, P., Zhao, A., Wu, Y., et al. (2021). Dysregulated bile acid signaling contributes to the neurological impairment in murine models of acute and chronic liver failure. *EBioMedicine* 66, 294–306. doi:10.1016/j.ebiom.2018.10.030

Xiong, Y., Zhu, W., Xu, Q., Ruze, R., Yan, Z., Li, J., et al. (2020). Sleeve gastrectomy attenuates diabetic nephropathy by upregulating nephrin expressions in diabetic obese rats. *Obes. Surg.* 30 (8), 2893–2904. doi:10.1007/s11695-020-04611-3

You, Y. K., Wu, W. F., Huang, X. R., Li, H. D., Ren, Y. P., Zeng, J. C., et al. (2021). Deletion of Smad3 protects against C-reactive protein-induced renal fibrosis and inflammation in obstructive nephropathy. *Int. J. Biol. Sci.* 17 (14), 3911–3922. doi:10.7150/ijbs.62929

Young, L., Nor Hanipah, Z., Brethauer, S. A., Schauer, P. R., and Aminian, A. (2019). Long-term impact of bariatric surgery in diabetic nephropathy. *Surg. Endosc.* 33 (5), 1654–1660. doi:10.1007/s00464-018-6458-8

Younossi, Z., Anstee, Q. M., Marietti, M., Hardy, T., Henry, L., Eslam, M., et al. (2018). Global burden of NAFLD and NASH: Trends, predictions, risk factors and prevention. *Nat. Rev. Gastroenterol. Hepatol.* 15 (1), 11–20. doi:10.1038/nrgastro.2017.109

Zarei, M., Barroso, E., Palomer, X., Dai, J., Rada, P., Quesada-López, T., et al. (2018). Hepatic regulation of VLDL receptor by PPARβ/δ and FGF21 modulates non-alcoholic fatty liver disease. *Mol. Metab.* 8, 117–131. doi:10.1016/j.molmet.2017.12.008

Zeisberg, E. M., Tarnavski, O., Zeisberg, M., Dorfman, A. L., McMullen, J. R., Gustafsson, E., et al. (2007). Endothelial-to-mesenchymal transition contributes to cardiac fibrosis. *Nat. Med.* 13 (8), 952–961. doi:10.1038/nm1613

Zhai, H., Li, Z., Peng, M., Huang, Z., Qin, T., Chen, L., et al. (2018). Takeda G protein-coupled receptor 5-mechanistic target of rapamycin complex 1 signaling contributes to the increment of glucagon-like peptide-1 production after roux-en-Y gastric bypass. *EBioMedicine* 32, 201–214. doi:10.1016/j.ebiom.2018.05.026

frontiers | Frontiers in Pharmacology

TYPE Mini Review
PUBLISHED 24 October 2022
DOI 10.3389/fphar.2022.1057829

Check for updates

OPEN ACCESS

EDITED BY
Yuxia Zhao,
Shandong University, China

REVIEWED BY
Panpan Hao,
Shandong University, China

*CORRESPONDENCE
Guang Ji,
jiliver@vip.sina.com,
jg@shutcm.edu.cn
Li Zhang,
zhangli.hl@163.com

SPECIALTY SECTION
This article was submitted to Experimental Pharmacology and Drug Discovery, a section of the journal Frontiers in Pharmacology

RECEIVED 30 September 2022
ACCEPTED 14 October 2022
PUBLISHED 24 October 2022

CITATION
Yu S, Ji G and Zhang L (2022), The role of p53 in liver fibrosis.
Front. Pharmacol. 13:1057829.
doi: 10.3389/fphar.2022.1057829

COPYRIGHT
© 2022 Yu, Ji and Zhang. This is an open-access article distributed under the terms of the Creative Commons Attribution License (CC BY). The use, distribution or reproduction in other forums is permitted, provided the original author(s) and the copyright owner(s) are credited and that the original publication in this journal is cited, in accordance with accepted academic practice. No use, distribution or reproduction is permitted which does not comply with these terms.

The role of p53 in liver fibrosis

Siyu Yu, Guang Ji* and Li Zhang*

Institute of Digestive Diseases, Longhua Hospital, Shanghai University of Traditional Chinese Medicine, Shanghai, China

The tumor suppressor p53 is the central hub of a molecular network, which controls cell proliferation and death, and also plays an important role in the occurrence and development of liver fibrosis. The abundant post-translational processing and modification endow the functional diversity of p53. Considering the relationship between p53 and liver fibrosis, drug intervention targeting p53 or management of p53 regulation might be effective strategies to treat liver fibrosis. Here, we systematically discuss the regulation of p53 in different liver cells (hepatocytes, immune cells, HSCs, *etc*) and the role of p53 in the development of liver fibrosis, and propose possible interventions to prevent the pathogenic processes of liver fibrosis.

KEYWORDS

liver fibrosis, p53, hepatic stellate cells, apoptosis, ferroptosis

Introduction

Liver fibrosis is a complex fibrogenic and inflammatory process, characterized by the accumulation of extracellular matrix (ECM), which distorts the hepatic architecture, and potentiates risks for cirrhosis and even hepatocellular carcinoma. Liver fibrosis generally results from chronic liver-damaging factors such as virus, alcohol, nonalcoholic steatohepatitis (NASH), cholestasis, autoimmune diseases (e.g., primary biliary cirrhosis, primary sclerosing cholangitis), drugs, parasitic infections, and genetic mutations (Acharya et al., 2021). All these hepatocellular injuries can activate the fibrogenic pathways and hepatic stellate cells (HSCs), and promote the differentiation of ECM-producing myofibroblasts (MFBs). HSCs are considered the main effector cells of liver fibrosis, quiescent HSCs reside in the Disse space and are the lipid storage cells, whereas the activation of HSCs involves a host of phenotypic changes, including loss of lipid droplets, trans-differentiation into MFBs, and expression of contractile fibers.

Physiologically, ECM is part of the boundary between blood flow and parenchyma, and fibrogenesis is a normal wound healing response. During the reparative process, ECM is made up of glycoproteins, proteoglycans, and non-fibrogenic type IV collagen, these components form a lattice-like matrix to support the proper arrangement and function of liver cells. However, upon various injuries, the synthesis of ECM is accelerated, and the non-fibrogenic type IV collagen is replaced by fibrogenic type I and II collagen, and the change of composition and density also alters the structure of the matrix and disrupt the normal structure of the liver (Bataller and Brenner, 2001). If the injury is acute or self-limiting, fibrogenic changes are transient and reversible. Once the primary disease is controlled or tissue damage is reduced, the activated HSCs can return to a quiescent state (Hernandez-Gea and Friedman, 2011; Seki and Brenner, 2015). Actually, spontaneous

regression of liver fibrosis can be observed on day 28 after carbon tetrachloride (CCl_4) intraperitoneally injections (Iredale et al., 1998). However, if the inflammatory response and the injury persist, the liver parenchyma is gradually replaced by scar tissues, which may further develop into cirrhosis and liver failure (Aydin and Akcali, 2018).

Currently, specific antifibrotic agents to treat liver fibrosis are still not available albeit several novel agents have entered the pre-clinical stage. Presently, clinical practice guidelines for liver fibrosis are only etiology-specific, to prevent progression and target the cause of liver injuries, such as antiviral drugs, alcohol withdrawal, treatment of metabolic disorders, and weight loss (Yamada et al., 2018; Damiris et al., 2020). The pathogenesis of liver fibrosis is rather complex, which involves cell-cell communication (e.g., hepatocytes and HSCs, liver macrophages and HSCs), activation and modulation of different signaling pathways, and immune system and tissue repair pathways among others. Therefore, understanding the mechanisms is fundamental for developing practicable drugs for liver fibrosis.

Since advanced liver fibrosis has the potential to progress into hepatocellular carcinoma, liver fibrosis is also considered a precancerous pathology. P53 is a well-known tumor suppressor gene, locates on human chromosome 17 with a relative molecular mass of about 53 kDa. Recent studies revealed that p53 also plays an important role in the development and progression of fibrosis. P53 interacts with fibrogenesis and fibrinolysis pathways, and mice with p53 deficiency spontaneously develop into liver fibrosis, suggesting that p53 is an important regulator of liver fibrosis.

P53 is required for the anti-fibrosis process

P53 gene (TP53) is crucial for maintaining genome integrity and intracellular homeostasis *via* initiating the survival process of cells such as cell cycle arrest, apoptosis, senescence, DNA damage and differentiation (Kanapathipillai, 2018; Lv et al., 2018). P53 protein locates on human chromosome 17 with a relative molecular mass of about 53 kDa. Physiologically, p53 protein is unstable and maintained at low levels under the action of negative regulatory factors in cells (Brooks and Gu, 2006; Blandino and Di Agostino, 2018) (Figure 1). However, TP53 is extremely susceptible to mutating all cancer types (Zhu et al., 2015; Sabapathy and Lane, 2019), it undergoes a variety of mutations such as point mutation, deletion, frameshift and rearrangement (Wu et al., 2020). When TP53 is mutated, the encoded P53 protein obtains a prolonged half-life and strong stability, which continuously accumulates in the nucleus and

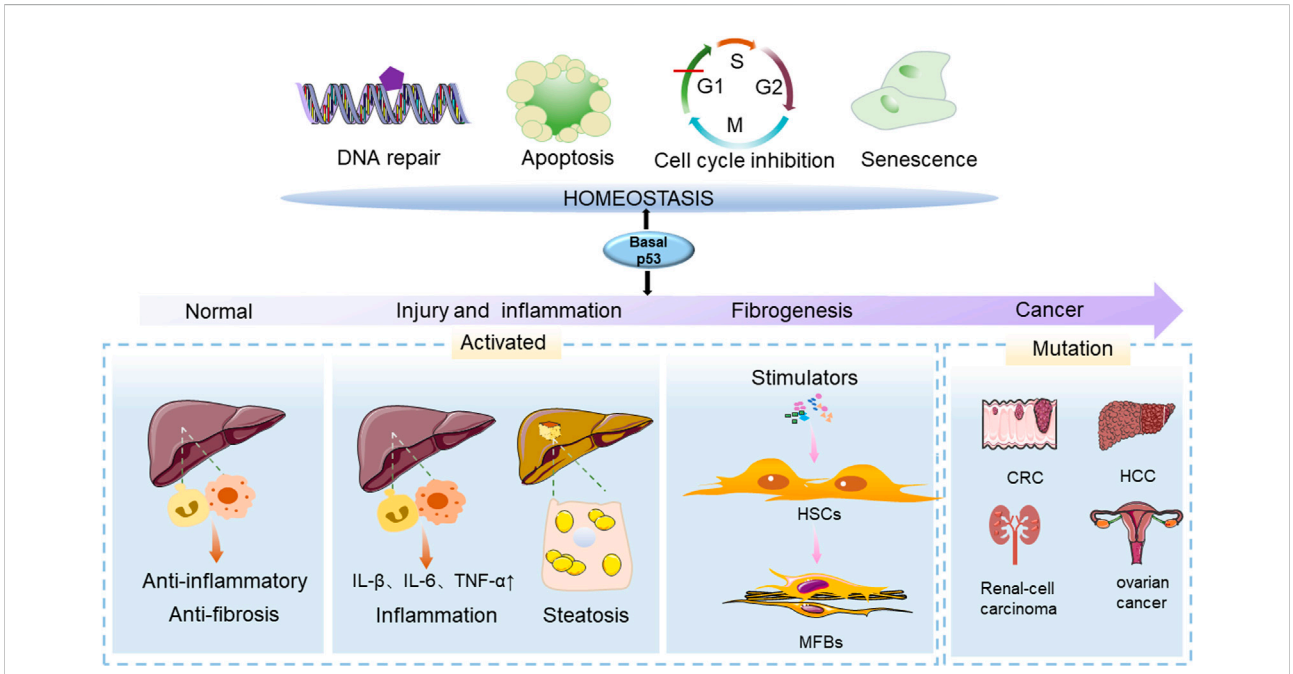


FIGURE 1
The function of p53 in physiological and pathological conditions of the liver. The p53 gene (TP53) is an important regulator in maintaining cellular homeostasis and can control cellular survival processes such as cell cycle arrest, apoptosis, senescence, DNA damage and differentiation. The effects of p53 on the liver are varied at different stages of liver injury. During the initial stage of p53 activation, it has anti-inflammatory and anti-fibrotic properties. In the presence of chronic liver injury, p53 activation and senescence in HSCs promote HSC accumulation, leading to the development of liver disease. Mutated p53 acquires carcinogenic properties, and contributes to the development of cancers.

loses its monitoring functions (Itahana and Itahana, 2018). Mutated p53 acquires carcinogenic properties, including cell proliferation, chemoresistance, disruption of tissue structures, promotion of migration, invasion and metastasis (Blandino and Di Agostino, 2018).

The transforming growth factor beta (TGF-β) pathway determines the synthesis and degradation of ECM during the process of fibrosis (Muthuramalingam et al., 2020). TGF-β binds to its receptors and recruits smooth muscle actin (Smad) and P53 to form transcriptionally-active multi-protein complexes. It is reported that increased $p53^{S15}$ phosphorylation accelerates renal damage and compromised organ function in experimental renal injury animals (Muthuramalingam et al., 2020). Tubular-specific p53 ablation or p53 inactivation in mice prevents epithelial G2/M arrest, reduces the secretion of fibrotic effectors, and attenuates the transition from acute to chronic kidney injury (Yang et al., 2010). In the presence of hypoxia, HIF-1α up-regulates p53 and activates TGF-β and CTGF-mediated signaling pathways, leading to ECM formation and renal fibrosis (Liu et al., 2019). Active TGF-β1 and p53 signaling pathways can be also observed during myocardial fibrosis in the heart tissue of dilated cardiomyopathy patients with ventricular tachycardia (Haywood et al., 2020). The use of Bleomycin can aggravate the process of pulmonary fibrosis by upregulating the expression of P53 and P21 in A549 human alveolar epithelial cells (Muthuramalingam et al., 2020). In response to silica, upregulation of p53 activates the RMRP/miR122 signaling pathway and promotes epithelial-mesenchymal transition (EMT), leading to the progression of pulmonary fibrosis in BALB/c mice (Li et al., 2021). Accordingly, the lung tissue damage and collagen deposition in p53 deficient mice are significantly reduced compared with wild-type mice, suggesting that inhibition of p53 expression could delay the progression of lung fibrosis (Wu et al., 2020).

The development of liver fibrosis attributes to HSC activation as well as the pathological change of hepatocytes and liver macrophages among others. Growing research suggests p53 accumulation in hepatocytes of several fibrotic liver diseases, such as NASH, viral hepatitis and primary biliary cirrhosis. The expression of the pro-apoptotic protein p53 is increased while anti-apoptotic protein Bcl-2 is inhibited with the enhancement of the inflammatory response in non-alcoholic fatty liver disease (NAFLD) patients (Panasiuk et al., 2006). Overexpression of p53 can be observed in 35% of samples in liver biopsies in patients with non-neoplastic liver disease, steatohepatitis and chronic hepatitis (Akyol et al., 1999). A study of p53 expression in the liver of patients with HCV infection showed that p53 was overexpressed in 7 of 40 patients (17.5%), indicating that overexpression of p53 may occur in the early stages of HCV-related liver disease (Rektorova et al., 2003). Liver macrophages includes the resident Kupffer cells and recruited liver macrophages. The crosstalk of hepatocytes, macrophages and HSCs can be triggered and facilitated by a range of chemical mediators, of which transforming growth factor beta (TGF-β) plays a prominent role (Poli, 2000).

Mutant $p53^{R172H}$ is associated with spontaneous liver inflammation and steatosis when combined with the loss of IL27 signaling (IL27RA), and mice develop microscopic and macroscopic steatosis, hepatocyte necrosis, immune cell infiltration and fibrosis with age (Dibra et al., 2016). P53 contributes to fibrotic disease progression by downregulating sirtuins in the liver, leading to telomere dysfunction. By inhibiting p53, mitochondrial function and liver fibrosis can be improved to some extent (Amano et al., 2019). IL-10 gene therapy can alleviate liver fibrosis in rats upon CCL_4 injection by restoring HSC senescence in the fibrotic liver, however, the effect is abrogated in p53 knockout rats, indicating p53 is required for the anti-fibrosis effect of IL-10 (Guo et al., 2021). Collectively, these studies suggested that the increase of p53 in response to various liver stimulation might a stress reaction to prevent disease progression, and p53 is involved and required in the anti-fibrosis process.

P53 interacts with fibrosis signaling

The stressed environment of the liver often leads to the activation of p53, resulting in changes in metabolic pathways and inducing apoptosis (Charni et al., 2014). Mdm2 is a protein that promotes p53 degradation, hepatocyte-specific Mdm2 knockout mice present endogenous p53 protein accumulation, which further upregulates connective tissue growth factor (CTGF) and formation of spontaneous liver fibrosis (Kodama et al., 2011). P14 $Cdk1Liv^{-/-}$ mice mimic the lack of division ability of hepatocytes in chronic hepatitis C (CHC) patients, and enhanced p53 signaling can be observed in the liver, accompanied by the progression to liver inflammation and fibrosis (Dewhurst et al., 2020). In methionine-and choline-deficient diet-fed mice, serum IGF-1 levels decreased with the progression of simple steatosis to NASH, and the expression of p53 and its downstream target gene p21 in the liver also increased, which might be involved in initiating cell apoptosis and enhance clearance of damaged hepatocytes (Farrell et al., 2009). P53 can directly regulate the expression of specific microRNAs, the most significant of which is the miR-34 site, including miR-34a, miR-34b, and miR-34c (Vousden and Prives, 2009). MiR-34a/SIRT1/p53 signaling pathway is activated in hepatocytes of CCL_4-induced fibrotic rats, leading to hepatocyte apoptosis, thereby activating hematopoietic stem cells and participating in the process of liver fibrosis (Tian et al., 2016). Levels of collagen markers in serum and the expression of p53 in liver tissue are positively correlated with serum miR-34a in CHC patients (Li et al., 2020). Triclosan induces liver injury in zebrafish by triggering the abnormal

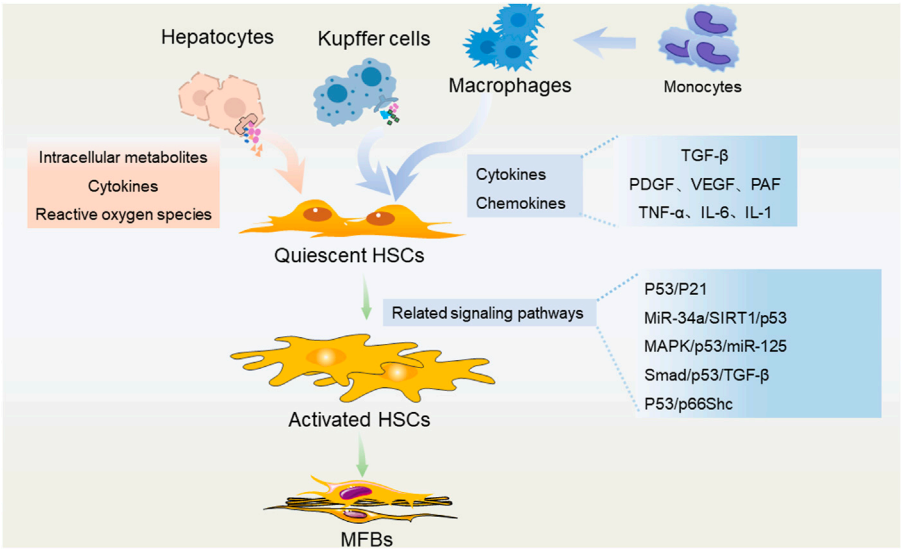


FIGURE 2
P53 in regulating different liver cells during the development of liver fibrosis. Hepatocytes, liver macrophages (Kupffer cells and recruited monocyte-derived macrophages) secrete a variety of intracellular metabolites, cytokines, chemokines, reactive oxygen species, etc., and activate HSCs through a variety of p53-related pathways. These pathological stimulations could promote the trans-differentiation of HSCs into MFBs, and subsequently lead to liver fibrosis.

expression of miR-125 that is mediated by the MAPK/p53 signaling pathway (Guo et al., 2021).

Monocytes and macrophages are known sources of TGF-β, and upon chronic liver injury, the secretion of TGF-β is significantly increased, which has a specific stimulatory effect on collagen formation. Experiments demonstrate that Kupffer cells isolated from alcoholic fibrosis rat liver express and release TGF-β, and Smad and p53 protein complexes synergistically activate TGF-β-induced transcription. P53 promotes the activation of multiple TGF-β target genes during embryonic development in *Xenopus*. In mammalian cells, TGF-β requires p53 for complete transcriptional activation of CDK inhibitor p21WAF1, and p53 deficient cells show impaired cellular inhibitory responses to TGF-β signaling (Cordenonsi et al., 2003). Loss of type II TGF-β receptor inactivated TGF-β signaling synergizes with inactivated p53 to promote hepatocellular carcinoma (Morris et al., 2012).

Hepatocyte apoptosis induced by p53 may lead to inflammatory cell infiltration, liver cirrhosis, and even liver cancer in the long term (Charni-Natan et al., 2019). In primary hepatocytes, TGF-β treatment increased the p53 and p66Shc signaling pathways, leading to excessive accumulation of reactive oxygen species (ROS) and apoptosis. The liver p53 and p66Shc signaling pathways are enhanced in a mouse model of NASH, and p53 deletion can inhibit the enhanced p66Shc signaling, reduce hepatic lipid peroxidation and the number of apoptotic hepatocytes, and improve the progression of nutritional steatohepatitis. The expression levels of p53, p21, and p66Shc are significantly elevated in liver specimens from NAFLD patients (Tomita et al., 2012). In primary rat hepatocytes, TGF-β1 trans-activates E2F-1, leads to Mdm-2 degradation and increases the expression of p53, and the levels of BAX protein and mRNA are significantly increased to induce hepatocyte apoptosis (Sola et al., 2003). Activation of p53 and TGF-β1/Smads signaling pathways leads to 10% fructose-induced epithelial-mesenchymal transition in rat hepatocytes, leading to liver fibrosis (Song et al., 2019).

P53 mediates the function of HSC

After an acute injury, activated HSCs can support hepatocyte proliferation and tissue repair, and as injury continues, activated HSCs migrate and accumulate at tissue repair sites, tans-differentiated into MFBs to secrete large quantities of ECM and initiate the liver fibrosis process (Bataller and Brenner, 2005; Passino et al., 2007). Therefore, inhibiting HSC activation and inducing the cell death of HSC are equally important in the anti-fibrosis process (Figure 2). Hepatocyte death and inflammation are reduced after neddylation inhibition, which may partially explain the reduction in HSC activation (Author Anonymous., 1989). As aforementioned, p53 is an active regulator of TGF-β1 secretion from hepatocytes and immune cells, and the quantity and stability of p53 in HSCs are necessary to block the development of fibrosis.

Promoting apoptosis is a promising strategy for fibrosis (Xue et al., 2022). As a well-known cancer suppressor, p53 is actively involved in cell apoptosis, ferroptosis, and senescence of cells. Activation of the p53/Bax/Bcl-2 signaling pathway promotes cell apoptosis, inhibits cell proliferation and migration, and reduces the production of ECM. In addition, increased p53 is associated with ROS production, which might further enhance cell apoptosis. P53 also ferroptosis to eliminate damaged cells (Wu and Prives, 2018; Stein et al., 2019). BRD7 directly binds to the N-terminal transactivation domain to promote mitochondrial translocation of p53, which in turn forms a complex with SLC25A28 to enhance the activity of SLC25A28, resulting in abnormal accumulation of redox-active iron and electron transfer chain hyperfunction, enhanced ferroptosis in HSCs and improved the degree of liver fibrosis in mice (Zhang et al., 2020). P53 is an upstream molecule that promotes artemether-induced ferroptosis in HSCs, and inhibits HSC activation accordingly. In CCL_4-induced liver fibrosis, artemether significantly downregulated many markers of HSC activation, including α-SMA, Col1a1, and fibronectin, and inhibited profibrotic receptors such as TGF-βR1, PDGF-βR and epidermal growth factor receptor (Wang et al., 2019).

Senescent cells also contribute to the generation of ECM and fibrotic scars during liver injury (Kim et al., 2013). In mice lacking key regulators of aging, HSCs obtain a sustaining proliferation and cause subsequent liver fibrosis. Transcriptomic analysis of senescent and apoptotic cells revealed that LY6D expression is enhanced in senescent cells in a p53-dependent pattern (Hu et al., 2022). P53 promotes senescence of activated HSCs during acute liver injury, simultaneously, decreased ECM and downregulated ECM-degrading enzymes can be observed. Natural killer (NK) cells are reported to preferentially clear senescent HSCs *in vitro* and *in vivo*, thereby protecting the liver from excessive fibrotic responses (Krizhanovsky et al., 2008). P53 can restrict malignant transformation by triggering cell-autonomous programs of cell-cycle arrest and cellular senescence. It is reported that ablation of a p53-dependent senescence program in HSCs increases liver fibrosis and cirrhosis, and enhances the progression to hepatocellular carcinoma (Lujambio et al., 2013).

Management of p53 is a promising strategy for liver fibrosis

Currently, eliminating irritation or ameliorating the cause of chronic liver diseases, such as the use of antiviral drugs, alcohol withdrawal, treatment of fatty liver disease and weight loss, are the common strategies for preventing liver fibrosis (Trautwein et al., 2015). However, in cases of advanced fibrosis, liver transplantation remains the only effective option (Taymouri and Taheri, 2016). As p53 is required for the anti-fibrosis process, management of p53 is a promising strategy.

Post-translational processing and modification determines the stability and transcriptional activity of p53 protein, and contribute to functional diversification. Phosphorylation is the most common post-translational modification of p53, which variously occurs at the N-terminus, DNA binding domain, C-terminus of p53, etc. Phosphorylation enhances the stabilization and transcriptional activity of p53 (Nguyen et al., 2014; Lv et al., 2018). Ubiquitination of p53 is mediated by E3 ubiquitin ligase (Cubillos-Rojas et al., 2017), ubiquitination and degradation of p53 disrupt p53-dependent transcription, and affect p53-promoted cell growth inhibition, G1 block and apoptosis (Sun et al., 2009; Sun et al., 2011). Multiple lysines at the carboxy terminus are major targets for the regulation of p53 acetylation (Gu and Roeder, 1997; Vaziri et al., 2001). Acetylation of p53 can increase the stability of p53 and play an important role in the activation of downstream target genes. Acetylated p53 (Ac-p53) improves the ability of p53 to bind to DNA, regulates the separation and distribution of p53 between the cytoplasm and nucleus, and promotes the recruitment of coactivators (Oda et al., 2000; Hofmann et al., 2002).

P53 can inhibit cell proliferation or induce apoptosis in tumor cells, as a key inhibitor of p53, Mdm2 has a high affinity to p53 protein. Overexpression of Mdm2 effectively inhibits the function of p53, and Mdm2 and its homolog Mdm4 are commonly overexpressed in human tumors (Grier et al., 2006). The use of potent and selective small molecule Mdm2 antagonists can disrupt the p53-Mdm2 interaction and activate the p53 pathway in cancer cells, resulting in cell cycle arrest, apoptosis, and inhibition of human tumor growth in nude mice (Vassilev et al., 2004). In addition to Mdm2, some ubiquitin ligases such as PIRH2 and COP1 can also promote the degradation of p53 (Collavin et al., 2010). Pifithrin -α, an inhibitor of p53, can reduce the level of nuclear p53 and reduce the activity of caspase3, thus alleviating apoptosis and necrosis (Schafer et al., 2003). Ursodeoxycholic acid (UDCA) specifically inhibits the E2F-1/p53 apoptosis pathway, reduces the stability of p53, decreases NF-κB degradation and downregulates Bcl-2, and alleviated TGF-β1-induced hepatocyte apoptosis in rats (Sola et al., 2003).

Conclusion and perspectives

Here we reviewed the pathogenesis of liver fibrosis and the research progress of tumor suppressor p53 in liver fibrosis. During fibrosis, the interaction between parenchymal cells and non-parenchymal cells, the activation of different immune cells and signaling pathways, and the release of various inflammatory mediators lead to the occurrence of inflammation, then activate HSCs, lead to the accumulation of ECM, and fibrosis scarring. P53 plays an inhibitory role in various tumor diseases, and mutated or modified p53 is endowed with different functions. In addition to its important role in the occurrence and

development of tumors, p53 is involved in fibrosis of different organs such as the liver, kidney, lung and heart, and management of p53 is found to be beneficial for all kinds of fibrosis.

Despite significant progress in basic research on liver fibrosis, the anti-fibrotic activity of many compounds has been demonstrated *in vitro* and in animal models (Trautwein et al., 2015), however, sensitive and specific biomarkers as non-invasive diagnostic tools and effective anti-fibrosis drugs have not yet been developed. The tumor suppressor 53 can regulate the fibrogenic process and potentiate a promising perspective for liver fibrosis. Each member of the P53 family has slightly different roles in tumors, so whether they also play different roles in the development of liver fibrosis is also worthy of further study. P53 regulates lipid metabolism, inflammation, and adipose tissue metabolism, indicating that metabolic-associated liver fibrosis might be more specific for p53 regulation. Therefore, a comprehensive understanding of the relationship between p53 and liver fibrosis is of great significance for the development of target drugs for the treatment of liver fibrosis.

Author contributions

LZ and GJ conceptualized the manuscript, SY retrieved the literature and drafted the manuscript, GJ and LZ revised the manuscript. All authors edited, revised, and approved the final version of this review.

Funding

This work was supported by grants from the National Natural Science Foundation of China (No. 82274448).

Conflict of interest

The authors declare that the research was conducted in the absence of any commercial or financial relationships that could be construed as a potential conflict of interest.

Publisher's note

All claims expressed in this article are solely those of the authors and do not necessarily represent those of their affiliated organizations, or those of the publisher, the editors and the reviewers. Any product that may be evaluated in this article, or claim that may be made by its manufacturer, is not guaranteed or endorsed by the publisher.

References

Acharya, P., Chouhan, K., Weiskirchen, S., and Weiskirchen, R. (2021). Cellular mechanisms of liver fibrosis. *Front. Pharmacol.* 12, 671640. doi:10.3389/fphar.2021.671640

Akyol, G., Dursun, A., Poyraz, A., Uluoglu, O., Ataoglu, O., Edaly, N., et al. (1999). P53 and proliferating cell nuclear antigen (PCNA) expression in non-tumoral liver diseases. *Pathol. Int.* 49 (3), 214–221. doi:10.1046/j.1440-1827.1999.00849.x

Amano, H., Chaudhury, A., Rodriguez-Aguayo, C., Lu, L., Akhanov, V., Catic, A., et al. (2019). Telomere dysfunction induces sirtuin repression that drives telomere-dependent disease. *Cell. Metab.* 29 (6), 1274–1290. doi:10.1016/j.cmet.2019.03.001

Author Anonymous (1989). Clinical experience with sulbactam/ampicillin in the treatment of obstetric and gynecologic infections. Rio de Janeiro, Brazil, October 25, 1988. Proceedings. *Suppl. Int. J. Gynecol. Obstet.* 2, 1–49.().

Aydin, M. M., and Akcali, K. C. (2018). Liver fibrosis. *Turk. J. Gastroenterol.* 29 (1), 14–21. doi:10.5152/tjg.2018.17330

Bataller, R., and Brenner, D. A. (2001). Hepatic stellate cells as a target for the treatment of liver fibrosis. *Semin. Liver Dis.* 21 (3), 437–451. doi:10.1055/s-2001-17558

Bataller, R., and Brenner, D. A. (2005). Liver fibrosis. *J. Clin. Invest.* 115 (2), 209–218. doi:10.1172/JCI24282

Blandino, G., and Di Agostino, S. (2018). New therapeutic strategies to treat human cancers expressing mutant p53 proteins. *J. Exp. Clin. Cancer Res.* 37 (1), 30. doi:10.1186/s13046-018-0705-7

Brooks, C. L., and Gu, W. (2006). p53 ubiquitination: Mdm2 and beyond. *Mol. Cell.* 21 (3), 307–315. doi:10.1016/j.molcel.2006.01.020

Charni, M., Rivlin, N., Molchadsky, A., Aloni-Grinstein, R., and Rotter, V. (2014). p53 in liver pathologies-taking the good with the bad. *J. Mol. Med.* 92 (12), 1229–1234. doi:10.1007/s00109-014-1223-5

Charni-Natan, M., Aloni-Grinstein, R., Osher, E., and Rotter, V. (2019). Liver and steroid hormones-can a touch of p53 make a difference? *Front. Endocrinol.* 10, 374. doi:10.3389/fendo.2019.00374

Collavin, L., Lunardi, A., and Del Sal, G. (2010). p53-family proteins and their regulators: hubs and spokes in tumor suppression. *Cell. Death Differ.* 17 (6), 901–911. doi:10.1038/cdd.2010.35

Cordenonsi, M., Dupont, S., Maretto, S., Insinga, A., Imbriano, C., and Piccolo, S. (2003). Links between tumor suppressors: p53 is required for TGF-beta gene responses by cooperating with smads. *Cell.* 113 (3), 301–314. doi:10.1016/s0092-8674(03)00308-8

Cubillos-Rojas, M., Schneider, T., Bartrons, R., Ventura, F., and Rosa, J. L. (2017). NEURL4 regulates the transcriptional activity of tumor suppressor protein p53 by modulating its oligomerization. *Oncotarget* 8 (37), 61824–61836. doi:10.18632/oncotarget.18699

Damiris, K., Tafesh, Z. H., and Pyrsopoulos, N. (2020). Efficacy and safety of anti-hepatic fibrosis drugs. *World J. Gastroenterol.* 26 (41), 6304–6321. doi:10.3748/wjg.v26.i41.6304

Dewhurst, M. R., Ow, J. R., Zafer, G., van Hul, N. K. M., Wollmann, H., Bisteau, X., et al. (2020). Loss of hepatocyte cell division leads to liver inflammation and fibrosis. *PLoS Genet.* 16 (11), e1009084. doi:10.1371/journal.pgen.1009084

Dibra, D., Xia, X., Mitra, A., Cutrera, J. J., Lozano, G., and Li, S. (2016). Mutant p53 in concert with an interleukin-27 receptor alpha deficiency causes spontaneous liver inflammation, fibrosis, and steatosis in mice. *Hepatology* 63 (3), 1000–1012. doi:10.1002/hep.28379

Farrell, G. C., Larter, C. Z., Hou, J. Y., Zhang, R. H., Yeh, M. M., Williams, J., et al. (2009). Apoptosis in experimental NASH is associated with p53 activation and TRAIL receptor expression. *J. Gastroenterol. Hepatol.* 24 (3), 443–452. doi:10.1111/j.1440-1746.2009.05785.x

Grier, J. D., Xiong, S., Elizondo-Fraire, A. C., Parant, J. M., and Lozano, G. (2006). Tissue-specific differences of p53 inhibition by Mdm2 and Mdm4. *Mol. Cell. Biol.* 26 (1), 192–198. doi:10.1128/MCB.26.1.192-198.2006

Gu, W., and Roeder, R. G. (1997). Activation of p53 sequence-specific DNA binding by acetylation of the p53 C-terminal domain. *Cell.* 90 (4), 595–606. doi:10.1016/s0092-8674(00)80521-8

Guo, Q., Chen, M., Chen, Q., Xiao, G., Chen, Z., Wang, X., et al. (2021). Silencing p53 inhibits interleukin 10-induced activated hepatic stellate cell senescence and fibrotic degradation *in vivo*. *Exp. Biol. Med.* 246 (4), 447–458. doi:10.1177/1535370220960391

Haywood, M. E., Cocciolo, A., Porter, K. F., Dobrinskikh, E., Slavov, D., Graw, S. L., et al. (2020). Transcriptome signature of ventricular arrhythmia in dilated

cardiomyopathy reveals increased fibrosis and activated TP53. *J. Mol. Cell. Cardiol.* 139, 124–134. doi:10.1016/j.yjmcc.2019.12.010

Hernandez-Gea, V., and Friedman, S. L. (2011). Pathogenesis of liver fibrosis. *Annu. Rev. Pathol.* 6, 425–456. doi:10.1146/annurev-pathol-011110-130246

Hofmann, T. G., Moller, A., Sirma, H., Zentgraf, H., Taya, Y., Droge, W., et al. (2002). Regulation of p53 activity by its interaction with homeodomain-interacting protein kinase-2. *Nat. Cell. Biol.* 4 (1), 1–10. doi:10.1038/ncb715

Hu, P. X., Sheng, M. Y., Liu, Y. P., and Zhang, C. Q. (2022). FOSL2 deficiency delays nonalcoholic steatohepatitis progression by regulating LY6D-mediated NLRP3 activation. *Hum. Cell.* 35 (6), 1752–1765. doi:10.1007/s13577-022-00760-y

Iredale, J. P., Benyon, R. C., Pickering, J., McCullen, M., Northrop, M., Pawley, S., et al. (1998). Mechanisms of spontaneous resolution of rat liver fibrosis. Hepatic stellate cell apoptosis and reduced hepatic expression of metalloproteinase inhibitors. *J. Clin. Invest.* 102 (3), 538–549. doi:10.1172/JCI1018

Itahana, Y., and Itahana, K. (2018). Emerging roles of p53 family members in glucose metabolism. *Int. J. Mol. Sci.* 19 (3), E776. doi:10.3390/ijms19030776

Kanapathipillai, M. (2018). Treating p53 mutant aggregation-associated cancer. *Cancers (Basel)* 10 (6), E154. doi:10.3390/cancers10060154

Kim, K. H., Chen, C. C., Monzon, R. I., and Lau, L. F. (2013). Matricellular protein CCN1 promotes regression of liver fibrosis through induction of cellular senescence in hepatic myofibroblasts. *Mol. Cell. Biol.* 33 (10), 2078–2090. doi:10.1128/MCB.00049-13

Kodama, T., Takehara, T., Hikita, H., Shimizu, S., Shigekawa, M., Tsunematsu, H., et al. (2011). Increases in p53 expression induce CTGF synthesis by mouse and human hepatocytes and result in liver fibrosis in mice. *J. Clin. Invest.* 121 (8), 3343–3356. doi:10.1172/JCI44957

Krizhanovsky, V., Yon, M., Dickins, R. A., Hearn, S., Simon, J., Miething, C., et al. (2008). Senescence of activated stellate cells limits liver fibrosis. *Cell.* 134 (4), 657–667. doi:10.1016/j.cell.2008.06.049

Li, M., Tang, J., Yang, H., Zhao, L., Liu, Y., Xu, H., et al. (2021). Short-term exposure to ambient particulate matter and outpatient visits for respiratory diseases among children: A time-series study in five Chinese cities. *Chemosphere* 263, 128214. doi:10.1016/j.chemosphere.2020.128214

Li, X., Zhang, W., Xu, K., and Lu, J. (2020). miR-34a promotes liver fibrosis in patients with chronic hepatitis via mediating Sirt1/p53 signaling pathway. *Pathol. Res. Pract.* 216 (5), 152876. doi:10.1016/j.prp.2020.152876

Liu, L., Zhang, P., Bai, M., He, L., Zhang, L., Liu, T., et al. (2019). p53 upregulated by HIF-1α promotes hypoxia-induced G2/M arrest and renal fibrosis *in vitro* and *in vivo*. *J. Mol. Cell. Biol.* 11 (5), 371–382. doi:10.1093/jmcb/mjy042

Lujambio, A., Akkari, L., Simon, J., Grace, D., Tschaharganeh, D. F., Bolden, J. E., et al. (2013). Non-cell-autonomous tumor suppression by p53. *Cell.* 153 (2), 449–460. doi:10.1016/j.cell.2013.03.020

Lv, W., Su, B., Li, Y., Geng, C., and Chen, N. (2018). KIAA0101 inhibition suppresses cell proliferation and cell cycle progression by promoting the interaction between p53 and Sp1 in breast cancer. *Biochem. Biophys. Res. Commun.* 503 (2), 600–606. doi:10.1016/j.bbrc.2018.06.046

Morris, S. M., Baek, J. Y., Koszarek, A., Kanngurn, S., Knoblaugh, S. E., and Grady, W. M. (2012). Transforming growth factor-beta signaling promotes hepatocarcinogenesis induced by p53 loss. *Hepatology* 55 (1), 121–131. doi:10.1002/hep.24653

Muthuramalingam, K., Cho, M., and Kim, Y. (2020). Cellular senescence and EMT crosstalk in bleomycin-induced pathogenesis of pulmonary fibrosis-an *in vitro* analysis. *Cell. Biol. Int.* 44 (2), 477–487. doi:10.1002/cbin.11248

Nguyen, T. A., Menendez, D., Resnick, M. A., and Anderson, C. W. (2014). Mutant TP53 posttranslational modifications: Challenges and opportunities. *Hum. Mutat.* 35 (6), 738–755. doi:10.1002/humu.22506

Oda, K., Arakawa, H., Tanaka, T., Matsuda, K., Tanikawa, C., Mori, T., et al. (2000). p53AIP1, a potential mediator of p53-dependent apoptosis, and its regulation by Ser-46-phosphorylated p53. *Cell.* 102 (6), 849–862. doi:10.1016/s0092-8674(00)00073-8

Panasiuk, A., Dzieciol, J., Panasiuk, B., and Prokopowicz, D. (2006). Expression of p53, Bax and Bcl-2 proteins in hepatocytes in non-alcoholic fatty liver disease. *World J. Gastroenterol.* 12 (38), 6198–6202. doi:10.3748/wjg.v12.i38.6198

Passino, M. A., Adams, R. A., Sikorski, S. L., and Akassoglou, K. (2007). Regulation of hepatic stellate cell differentiation by the neurotrophin receptor p75NTR. *Science* 315 (5820), 1853–1856. doi:10.1126/science.1137603

Poli, G. (2000). Pathogenesis of liver fibrosis: Role of oxidative stress. *Mol. Asp. Med.* 21 (3), 49–98. doi:10.1016/s0098-2997(00)00004-2

Rektorova, I., Rektor, I., Bares, M., Dostal, V., Ehler, E., Fanfrdlova, Z., et al. (2003). Pramipexole and pergolide in the treatment of depression in Parkinson's disease: A national multicentre prospective randomized study. *Eur. J. Neurol.* 10 (4), 399–406. doi:10.1046/j.1468-1331.2003.00612.x

Sabapathy, K., and Lane, D. P. (2019). Understanding p53 functions through p53 antibodies. *J. Mol. Cell. Biol.* 11 (4), 317–329. doi:10.1093/jmcb/mjz010

Schafer, T., Scheuer, C., Roemer, K., Menger, M. D., and Vollmar, B. (2003). Inhibition of p53 protects liver tissue against endotoxin-induced apoptotic and necrotic cell death. *FASEB J.* 17 (6), 660–667. doi:10.1096/fj.02-0774com

Seki, E., and Brenner, D. A. (2015). Recent advancement of molecular mechanisms of liver fibrosis. *J. Hepatobiliary. Pancreat. Sci.* 22 (7), 512–518. doi:10.1002/jhbp.245

Sola, S., Ma, X., Castro, R. E., Kren, B. T., Steer, C. J., and Rodrigues, C. M. (2003). Ursodeoxycholic acid modulates E2F-1 and p53 expression through a caspase-independent mechanism in transforming growth factor beta1-induced apoptosis of rat hepatocytes. *J. Biol. Chem.* 278 (49), 48831–48838. doi:10.1074/jbc.M300468200

Song, L., Chen, T. Y., Zhao, X. J., Xu, Q., Jiao, R. Q., Li, J. M., et al. (2019). Pterostilbene prevents hepatocyte epithelial-mesenchymal transition in fructose-induced liver fibrosis through suppressing miR-34a/Sirt1/p53 and TGF-β1/Smads signalling. *Br. J. Pharmacol.* 176 (11), 1619–1634. doi:10.1111/bph.14573

Stein, Y., Rotter, V., and Aloni-Grinstein, R. (2019). Gain-of-Function mutant p53: All the roads lead to tumorigenesis. *Int. J. Mol. Sci.* 20 (24), E6197. doi:10.3390/ijms20246197

Sun, L., Shi, L., Li, W., Yu, W., Liang, J., Zhang, H., et al. (2009). JFK, a Kelch domain-containing F-box protein, links the SCF complex to p53 regulation. *Proc. Natl. Acad. Sci. U. S. A.* 106 (25), 10195–10200. doi:10.1073/pnas.0901864106

Sun, L., Shi, L., Wang, F., Huangyang, P., Si, W., Yang, J., et al. (2011). Substrate phosphorylation and feedback regulation in JFK-promoted p53 destabilization. *J. Biol. Chem.* 286 (6), 4226–4235. doi:10.1074/jbc.M110.195115

Taymouri, S., and Taheri, A. (2016). Use of nanotechnology in diagnosis and treatment of hepatic fibrosis: A review. *Curr. Drug Deliv.* 13 (5), 662–672. doi:10.2174/1567201812666150907115404

Tian, X. F., Ji, F. J., Zang, H. L., and Cao, H. (2016). Activation of the miR-34a/SIRT1/p53 signaling pathway contributes to the progress of liver fibrosis via inducing apoptosis in hepatocytes but not in HSCs. *PLoS One* 11 (7), e0158657. doi:10.1371/journal.pone.0158657

Tomita, K., Teratani, T., Suzuki, T., Oshikawa, T., Yokoyama, H., Shimamura, K., et al. (2012). p53/p66Shc-mediated signaling contributes to the progression of non-alcoholic steatohepatitis in humans and mice. *J. Hepatol.* 57 (4), 837–843. doi:10.1016/j.jhep.2012.05.013

Trautwein, C., Friedman, S. L., Schuppan, D., and Pinzani, M. (2015). Hepatic fibrosis: Concept to treatment. *J. Hepatol.* 62, S15–S24. doi:10.1016/j.jhep.2015.02.039

Vassilev, L. T., Vu, B. T., Graves, B., Carvajal, D., Podlaski, F., Filipovic, Z., et al. (2004). *In vivo* activation of the p53 pathway by small-molecule antagonists of MDM2. *Science* 303 (5659), 844–848. doi:10.1126/science.1092472

Vaziri, H., Dessain, S. K., Ng Eaton, E., Imai, S. I., Frye, R. A., Pandita, T. K., et al. (2001). hSIR2(SIRT1) functions as an NAD-dependent p53 deacetylase. *Cell.* 107 (2), 149–159. doi:10.1016/s0092-8674(01)00527-x

Vousden, K. H., and Prives, C. (2009). Blinded by the light: The growing complexity of p53. *Cell.* 137 (3), 413–431. doi:10.1016/j.cell.2009.04.037

Wang, L., Zhang, Z., Li, M., Wang, F., Jia, Y., Zhang, F., et al. (2019). P53-dependent induction of ferroptosis is required for artemether to alleviate carbon tetrachloride-induced liver fibrosis and hepatic stellate cell activation. *IUBMB Life* 71 (1), 45–56. doi:10.1002/iub.1895

Wu, D., and Prives, C. (2018). Relevance of the p53-MDM2 axis to aging. *Cell. Death Differ.* 25 (1), 169–179. doi:10.1038/cdd.2017.187

Wu, Q., Zhang, K. J., Jiang, S. M., Fu, L., Shi, Y., Tan, R. B., et al. (2020). p53: A key protein that regulates pulmonary fibrosis. *Oxid. Med. Cell. Longev.* 2020, 6635794. doi:10.1155/2020/6635794

Xue, F., Cheng, J., Liu, Y., Cheng, C., Zhang, M., Sui, W., et al. (2022). Cardiomyocyte-specific knockout of ADAM17 ameliorates left ventricular remodeling and function in diabetic cardiomyopathy of mice. *Signal Transduct. Target. Ther.* 7 (1), 259. doi:10.1038/s41392-022-01054-3

Yamada, K., Mizukoshi, E., Seike, T., Horii, R., Kitahara, M., Sunagozaka, H., et al. (2018). Light alcohol consumption has the potential to suppress hepatocellular injury and liver fibrosis in non-alcoholic fatty liver disease. *PLoS One* 13 (1), e0191026. doi:10.1371/journal.pone.0191026

Yang, L., Besschetnova, T. Y., Brooks, C. R., Shah, J. V., and Bonventre, J. V. (2010). Epithelial cell cycle arrest in G2/M mediates kidney fibrosis after injury. *Nat. Med.* 16 (5), 535–543. doi:10.1038/nm.2144

Zhang, Z., Guo, M., Shen, M., Kong, D., Zhang, F., Shao, J., et al. (2020). The BRD7-P53-SLC25A28 axis regulates ferroptosis in hepatic stellate cells. *Redox Biol.* 36, 101619. doi:10.1016/j.redox.2020.101619

Zhu, J., Sammons, M. A., Donahue, G., Dou, Z., Vedadi, M., Getlik, M., et al. (2015). Gain-of-function p53 mutants co-opt chromatin pathways to drive cancer growth. *Nature* 525 (7568), 206–211. doi:10.1038/nature15251

frontiers | Frontiers in Medicine

TYPE Original Research
PUBLISHED 03 November 2022
DOI 10.3389/fmed.2022.1024836

Check for updates

OPEN ACCESS

EDITED BY
Yanping Liu,
Shandong University, China

REVIEWED BY
Kessarin Thanapirom,
Royal Free Hospital, United Kingdom
Panpan Hao,
Shandong University, China

*CORRESPONDENCE
Dae Won Jun
noshin@hanyang.ac.kr
Eun-Hee Nah
cellonah@hanmail.net;
cellonah@kahp.or.kr

†These authors have contributed equally to this work and share first authorship

‡These authors have contributed equally to this work

SPECIALTY SECTION
This article was submitted to Hepatology,
a section of the journal
Frontiers in Medicine

RECEIVED 22 August 2022
ACCEPTED 17 October 2022
PUBLISHED 03 November 2022

CITATION
Park H, Yoon EL, Kim M, Lee J, Cho S, Jun DW and Nah E-H (2022) Reappraisal of fibrosis-4 index and non-alcoholic fatty liver disease fibrosis score for advanced fibrosis in average-risk population.
Front. Med. 9:1024836.
doi: 10.3389/fmed.2022.1024836

COPYRIGHT
© 2022 Park, Yoon, Kim, Lee, Cho, Jun and Nah. This is an open-access article distributed under the terms of the Creative Commons Attribution License (CC BY). The use, distribution or reproduction in other forums is permitted, provided the original author(s) and the copyright owner(s) are credited and that the original publication in this journal is cited, in accordance with accepted academic practice. No use, distribution or reproduction is permitted which does not comply with these terms.

Reappraisal of fibrosis-4 index and non-alcoholic fatty liver disease fibrosis score for advanced fibrosis in average-risk population

Huiyul Park[1†], Eileen L. Yoon[2,3†], Mimi Kim[4], Jonghyun Lee[5], Seon Cho[6], Dae Won Jun[2,3,5*‡] and Eun-Hee Nah[6*‡]

[1]Department of Family Medicine, Myongji Hospital, Hanyang University College of Medicine, Seoul, South Korea, [2]Department of Internal Medicine, Hanyang University College of Medicine, Seoul, South Korea, [3]Hanyang Institute of Bioscience and Biotechnology, Hanyang University, Seoul, South Korea, [4]Department of Radiology, Hanyang University College of Medicine, Seoul, South Korea, [5]Department of Translational Medicine, Hanyang University Graduate School of Biomedical Science and Engineering, Seoul, South Korea, [6]Department of Laboratory Medicine, Health Promotion Research Institute, Seoul, South Korea

Background and aim: The current cut-offs for fibrosis-4 (FIB-4) and non-alcoholic fatty liver disease fibrosis score (NFS) are suboptimal for screening because of low accuracy and high false-negative rates in average-risk populations. This study aimed to reappraisal the performance of FIB-4 and NFS in such average-risk populations.

Methods: This is a cross-sectional study, which retrospectively reviewed the magnetic resonance elastography (MRE) data of 8,522 subjects. Individuals with history of significant alcohol consumption and those with positive viral serologic markers were excluded. Finally, 6,215 average-risk individuals were analyzed.

Results: The area under the receiver operating characteristic curves (AUROCs) of FIB-4 for the diagnosis of advanced hepatic fibrosis was higher than that in the NFS especially in the metabolically healthy. The AUROCs of FIB-4 for in the average-risk population was also higher than that in the NFS (0.840 in FIB-4 vs. 0.798, P = 0.036). However, the sensitivity of FIB-4 and NFS was low (69.6 and 61.4%, respectively) in applying the current cut-off of FIB-4 [1.3 (2.0)] and NFS [-1.455 (0.12)]. At cut-off of FIB-4 at 1.0, sensitivity (90.2%), and negative predictive value (99.7%) were improved.

Conclusion: The diagnostic performance of FIB-4 was better than that of NFS for screening hepatic fibrosis in average-risk populations. It is recommended to use FIB-4 rather than NFS, when screening for hepatic fibrosis in general population.

KEYWORDS

advanced hepatic fibrosis, fibrosis-4 index, non-alcoholic fatty liver disease fibrosis score, magnetic resonance elastography, average-risk population

Introduction

Socioeconomic burden of non-alcoholic fatty liver disease (NAFLD) has been increasing of late (1, 2). The most important risk factor for liver-related and overall mortality is the stage of hepatic fibrosis in patients with NAFLD (3, 4). Therefore, it is very important to screen and evaluate for the presence and severity of hepatic fibrosis in such patients (5–7). Prevalence of significant and advanced hepatic fibrosis in the general population is 5.1–9.5 and 1.3–2.6%, respectively (8, 9). Therefore, early detection of hepatic fibrosis in the general population is necessary to prevent liver-related events and to decrease medical costs. However, as no optimal screening algorithms and effective treatment for patients with NAFLD have yet been developed, screening for significant or advanced hepatic fibrosis is not recommended for general population.

Notably, health check-ups are extensively conducted for average-risk populations. Sonographic fatty liver and elevated liver enzyme levels are the most common reasons for referring patients from primary care centers to referral centers. However, the sensitivity of ultrasonography or biochemical tests for significant or advanced hepatic fibrosis is unsatisfactory. In recent times, the fibrosis-4 (FIB-4) index and non-alcoholic fatty liver disease fibrosis score (NFS) tests have become common as the first step to screen advanced hepatic fibrosis in individuals with known viral hepatitis and NAFLD (10). However, only one relevant large-scale study has been conducted for screening hepatic fibrosis in the general population (11). The study reported that FIB-4 and NFS were suboptimal for screening purposes because of the high risk of over-diagnosis in the general population (11). Therefore, special caution is needed when using the current low cut-off of FIB-4 or NFS as a single screening strategy in average-risk populations. New non-invasive methods or optimization of FIB-4 or NFS are needed for detecting fibrosis in low-prevalence fibrosis settings. However, the variables used in FIB-4 and NFS are generally already included in health check-up tests, and therefore, they do not require additional tests in primary care setting. Recent guidelines recommend to use FIB-4 and NFS over other non-invasive fibrosis markers as a first step screening tools, because they are mort well validated and have shown the best diagnostic accuracy among non-invasive fibrosis markers (10, 12). Moreover, considering that other tests (e.g., transient elastography) after FIB-4 and NFS are sequentially applied for the advanced hepatic fibrosis screening algorithm, FIB-4 and NFS tests as a first step are still attractive screening methods in primary care settings.

New cut-off or optimization of FIB-4 and NFS to reduce false-negatives and increase accuracy is needed for detecting fibrosis in low-prevalence fibrosis settings. This study is an attempt to conduct reappraisal the performance of FIB-4 or NFS and discuss the reasonable cut-off in average-risk populations.

Materials and methods

Study design

This was a retrospective, cross-sectional study. The subjects underwent magnetic resonance elastography (MRE) as part of their health check-up. The health check-up program was uniformly performed at 13 nationwide health-promotion centers. This study was approved by the institutional review board (IRB No. HY-2021-04-001-001) of Hanyang University Hospital, and the requirement for informed consent was waived.

Rationale for abdominal sonography and magnetic resonance elastography as health check-up

Abdominal sonography is one of the basic and most commonly performed health check-up examinations. It can be conducted either when the examinees prefer so or as part of an obligatory basic exam conducted every 1 or 2 years by companies under the Act of Employment in Korea. However, the MRE test is not included in the routine health check-up program. It is offered to patients as an additional option under their own expense. Patients with known chronic liver diseases are managed under a separate health check-up program run by the National Health Insurance Service in Korea. Therefore, they are less likely to be included in this study.

Inclusion and exclusion criteria

A total of 10,771 subjects who underwent MRE as part of their health check-up examination between January 1, 2017 and May 30, 2020 were included. Among them, 2,249 subjects were excluded owing to missing data on abdominal sonography and clinical information (e.g., metabolic risk abnormalities and variables used in FIB-4 and NFS). Individuals with history of significant alcohol consumption (≥210 g per week for men and ≥ 140 g per week for women) or chronic liver disease in the questionnaire and those with positive result in viral serologic markers (HBsAg and HCV Ab) were also excluded (n = 2,307) (**Figure 1**).

Clinical parameters of the subjects

Routine health check-up questionnaires were used to obtain the history of hypertension, diabetes mellitus (DM), or dyslipidemia and intake of the corresponding medications for these conditions, as well as the social history of alcohol intake. Anthropometric measurements included waist circumference, blood pressure, height, weight, total fat mass, and lean mass. Additionally, fasting serum glucose, total cholesterol, low-density lipoprotein cholesterol, high-density lipoprotein cholesterol, triglycerides, AST, ALT, and γ-glutamyl transferase levels were measured.

FIB-4 and NFS were calculated, and their low cutoff values of FIB-4 [1.3 (2.0)] and NFS [−1.455 (0.12)] were selected according to the method described by McPherson et al. (13). If age of subjects was 65 or more, the cutoff values of FIB-4 (2.0) and NFS (0.12) were used. If age of subjects was lower than 65, the cutoff values of FIB-4 (1.3) and NFS (−1.455) were used.

Definition of metabolically healthy and unhealthy groups

We defined the metabolic risk abnormalities as follows (14): (1) waist circumference ≥ 85 cm for women and ≥ 90 cm for men, (2) blood pressure ≥ 130/85 mmHg and/or taking hypertension medication, (3) serum triglyceride ≥ 150 mg/dL, (4) high-density lipoprotein cholesterol < 50 mg/dL for women and < 40 mg/dL for men, and (5) fasting glucose level ≥ 100 mg/dL with HbA1c ≥ 5.7% and/or taking diabetes medication. The metabolically unhealthy group was defined as having diabetes or two or more metabolic risk abnormalities as per our previous study (15). The metabolically healthy group was defined as those with no diabetes and only one or no metabolic risk abnormality.

Assessment of fatty liver and hepatic fibrosis severity

The presence of fatty liver was evaluated using ultrasonography. Severity was graded as normal, mild, moderate, or severe according to the degree of fat infiltration

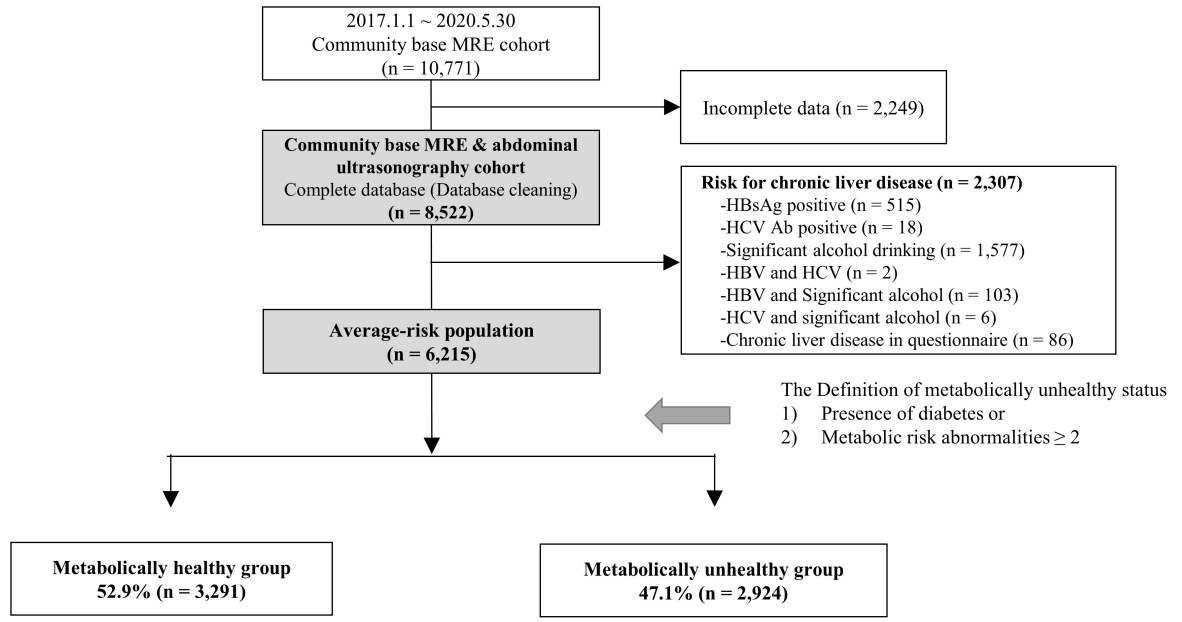


FIGURE 1
Study flow. MRE, magnetic resonance elastography.

(16). Liver echotexture, attenuation, and visualization of the intrahepatic vessel borders and/or the diaphragm were used as the indices. Liver stiffness was measured by MRE. All MRE examinations were performed on MRE hardware (GE Healthcare, Waukesha, Wisconsin, USA) with a 1.5-T imaging system using a two-dimensional MRE protocol (17). The acquired MRE images were automatically processed. Liver stiffness was assessed by a radiologist using regions of interest, excluding the vessels. The cut-off values for significant and advanced hepatic fibrosis were set at MRE values of $\geq$ 3.0 kPa (F2) and $\geq$ 3.6 kPa (F3), respectively (18). We used various cut-off values for advanced hepatic fibrosis for sensitivity analysis. The range of advanced fibrosis was defined as MRE values of 3.2–4.0 kPa for sensitivity analysis (19–23).

Statistical analyses

Continuous and categorical variables are presented as mean ± standard deviation and as numbers and percentages, respectively. Categorical variables were analyzed using either the χ^2-test or Fisher's exact test, whereas continuous variables were analyzed using Student's independent *t*-test. Statistical analyses were performed using SPSS version 26.0 for Windows (SPSS Inc., Chicago, IL, USA). The area under the receiver operating characteristic (AUROC) curves of FIB-4 and NFS were compared using DeLong's test in MedCalc version 20 (MedCalc Software Ltd., Ostend, Belgium). Statistical significance was set at $P < 0.05$.

Results

Baseline characteristics

A total of 6,215 average-risk subjects, who did not have chronic viral hepatitis and significant alcohol intake, were identified as the average-risk group for this study and were analyzed (**Figure 1**). These subjects had 26.4, 9.2, and 23.2% prevalence of hypertension, diabetes, and metabolic syndrome, respectively (**Table 1**). The prevalence of sonographic fatty liver in total, metabolic healthy, and unhealthy group was 47.7, 31.1, and 66.3%, respectively. The prevalence of significant and advanced hepatic fibrosis diagnosed according to MRE findings in this average-risk group was 6.6 and 1.6%, respectively. The proportion of metabolically healthy individuals in this average-risk group was 52.9%. The prevalence of significant and advanced hepatic fibrosis in the metabolically healthy group was 3.9 and 0.8%, respectively.

Comparison of diagnostic performance for advanced fibrosis between fibrosis-4 and NAFLD fibrosis score in the average-risk group

The AUROC of FIB-4 for the diagnosis of advanced hepatic fibrosis in the average-risk group was higher than that in

TABLE 1 Baseline characteristics of the average-risk population according to metabolic status.

	Total subjects (*n* = 6,215)	Metabolically healthy group (*n* = 3,291)	Metabolically unhealthy group (*n* = 2,924)	*P*-value
Age (years)†	47.5 ± 10.1	45.9 ± 10	49.3 ± 10	<0.001
Male	5,031 (80.9)	2,514 (76.4)	2,517 (86.1)	<0.001
Hypertension	1,642 (26.4)	279 (8.5)	1,363 (46.6)	<0.001
Diabetes	571 (9.2)	0 (0)	571 (19.5)	<0.001
Alcohol consumption (g/week)†	57.2 ± 0.7	38.1 ± 55.3	42.8 ± 59.3	0.001
Number of metabolic risks†	1.52 ± 1.29	0.49 ± 0.5	2.68 ± 0.87	<0.001
Metabolic syndrome	1,442 (23.2)	0 (0)	1,442 (23.2)	<0.001
BMI (kg/m^2)†	24.8 ± 3.2	23.4 ± 2.5	26.3 ± 3.1	<0.001
Waist circumference (cm)†	85.5 ± 9	81.2 ± 7.6	90.2 ± 8	<0.001
SBP (mmHg)†	116 ± 13	111 ± 11	121 ± 13	<0.001
DBP (mmHg)†	75 ± 9	71 ± 8	78 ± 9	<0.001
AST (IU/L)†	29 ± 17	26 ± 14	32 ± 19	<0.001
ALT (IU/L)†	31 ± 29	25 ± 25	38 ± 31	<0.001
GGT (U/L)†	55 ± 83	41 ± 70	71 ± 94	<0.001
Triglyceride (mg/dL)†	144 ± 111	100 ± 56	194 ± 135	<0.001
HDL (mg/dL)†	53 ± 13	57 ± 12	48 ± 11	<0.001
Glucose (mg/dL)†	99 ± 20	91 ± 8	108 ± 25	<0.001
FIB-4†	1.11 ± 0.6	1.07 ± 0.53	1.15 ± 0.68	<0.001
NFS†	-2.28 ± 1.2	-2.59 ± 1.09	-1.93 ± 1.21	<0.001
Liver stiffness (kPa)†	2.33 ± 0.58	2.27 ± 0.58	2.4 ± 0.57	<0.001
Sonographic fatty liver	2,963 (47.7)	1,024 (31.1)	1,939 (66.3)	<0.001
Significant hepatic fibrosis	411 (6.6)	129 (3.9)	282 (9.6)	<0.001
Advanced hepatic fibrosis	102 (1.6)	25 (0.8)	77 (2.6)	<0.001

Data are expressed as number (percent). †Data are shown as mean ± standard deviation. Metabolically healthy group was defined as having less than two metabolic risks and not having diabetes. AST, aspartate transaminase; ALT, alanine transaminase; BMI, body mass index; DBP, diastolic blood pressure; FIB-4, fibrosis-4 index; GGT, γ-glutamyl transferase; HDL, high-density lipoprotein; MRE, magnetic resonance elastography; NFS, non-alcoholic fatty liver disease fibrosis score; SBP, systolic blood pressure.

the NFS (0.840 in FIB-4 vs. 0.798, P = 0.036) (Figure 2A). A comparison of AUROCs of FIB-4 and NFS in the fatty-liver group (Figure 2C) and the metabolically unhealthy group (Figure 2E) did not show any difference in the diagnostic performance of FIB-4 and NFS. However, the AUROCs of FIB-4 in the non-fatty liver group (0.872 in FIB-4 vs. 0.777 in NFS, P = 0.010) and the metabolically healthy group (0.862 in FIB-4 vs. 0.702 in NFS, P = 0.001) were significantly higher than those of NFS (Figures 2B,D). FIB-4 was found to be better for diagnosing advanced hepatic fibrosis than NFS in the average-risk group, because a considerable number of metabolically healthy (52.9%) subjects were included in this category.

Sensitivity of fibrosis-4 and NAFLD fibrosis score to screen advanced fibrosis in the average-risk group

When we used the current cut-off of FIB-4 [1.3 (2.0)] and NFS [−1.455 (0.12)] for diagnosing advanced fibrosis (MRE value ≥ 3.6 kPa), the sensitivity and positive predictive value (PPV) were found to be low under most conditions (Figure 3 and Table 2). FIB-4 and NFS had low sensitivity (69.6 and 61.4%, respectively). In addition, the sensitivity of NFS further decreased in metabolically healthy (44.0%) and non-fatty liver (59.0%) groups when we applied the current low cut-off. The diagnostic performance of FIB-4 for advanced hepatic fibrosis was evaluated at different cut-off values (Table 3). As the cut-off value was increased from 0.9 to 1.3, the sensitivity decreased from 92.2 to 75.5% in the average-risk group. When the low cut-off of FIB-4, used as a first screening test for advanced hepatic fibrosis in the average-risk group, was lowered to 1.0, the sensitivity was 90.2% and the negative predictive value was 99.7%.

Sensitivity analysis for diagnostic performance of fibrosis-4 in patients with specific conditions

Sensitivity analysis of the AUROCs of FIB-4 and NFS using various cut-off values for MRE (3.2–4.0 kPa) was performed (Table 4 and Figure 4). The AUROC of FIB-4 for hepatic fibrosis using various cut-off values for MRE (3.2–4.0 kPa) in an average-risk population was 0.709–0.896 (Table 4). Notably, the AUROC of FIB-4 for diagnosing hepatic fibrosis in the

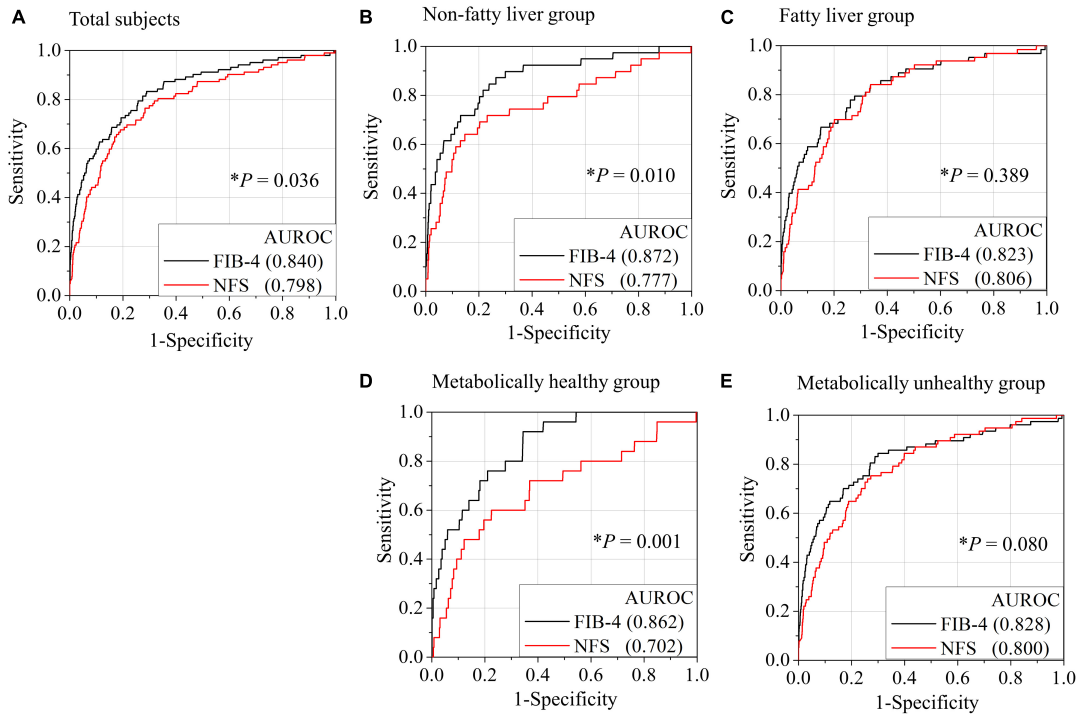


FIGURE 2
Comparison of AUROCs for advanced hepatic fibrosis (≥ 3.6 kPa) between FIB-4 and NFS based on the presence of fatty liver or metabolic status. Receiver operating characteristic (ROC) curves for the diagnosis of advanced fibrosis by FIB-4 or NFS in all subjects **(A)**, non-fatty liver group **(B)**, fatty liver group **(C)**, metabolically healthy group **(D)**, and metabolically unhealthy group **(E)**. A metabolically healthy state was defined as having less than two metabolic risks and not having diabetes. *P-value when the ROC curve by FIB-4 was compared with the ROC curve by NFS. NFS, NAFLD fibrosis score; FIB-4, fibrosis-4 index; AUROC, area under the receiver operating characteristic curve.

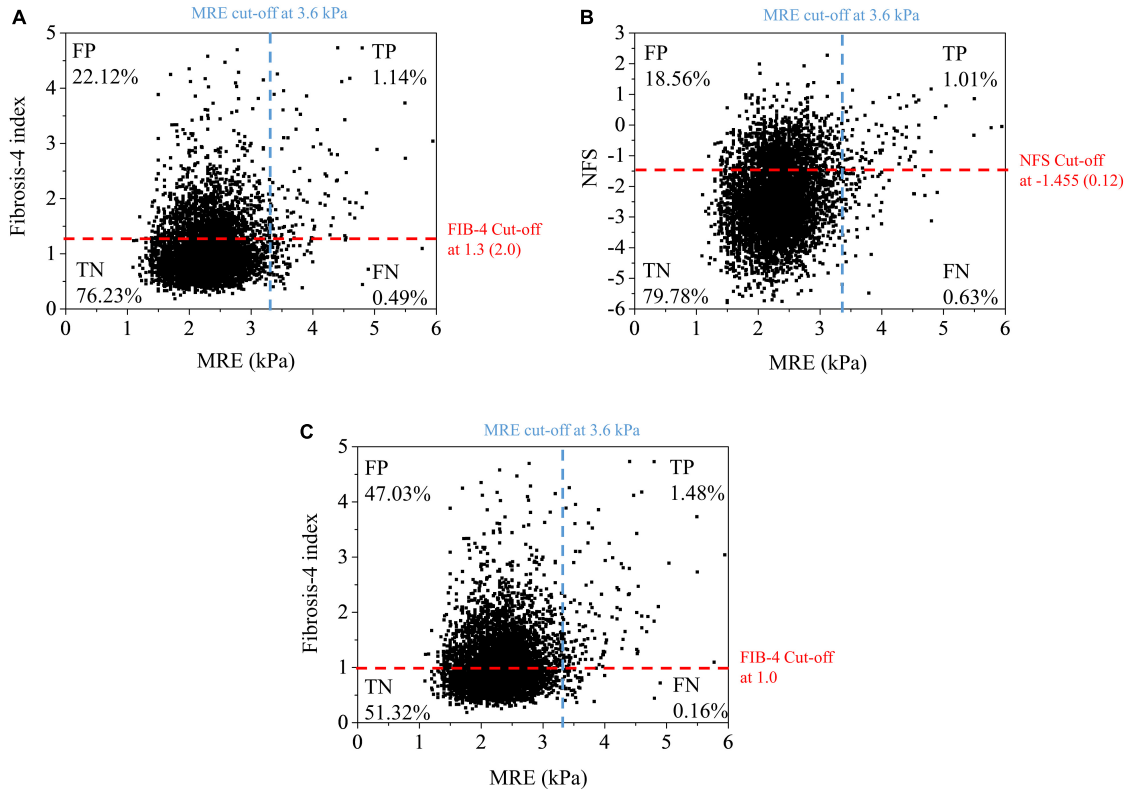


FIGURE 3
Scatter plot of liver stiffness measured by MRE vs. fibrosis-4 index **(A,C)** at different cut-off values and NFS **(B)**. Pearson correlation coefficient: MRE – FIB-4 (0.232), MRE – NFS (0.192). FN, false negative; FP, false positive; MRE, magnetic resonance elastography; NFS, NAFLD fibrosis score; FIB-4, fibrosis-4 index; TN, true negative; TP, true positive.

metabolically healthy group at different cut-off values for MRE was significantly higher than that of NFS, except for the cut-off value at 4.0 kPa (Figure 4). However, no difference in AUROCs was noted between FIB-4 and NFS in both the fatty liver and metabolically unhealthy groups at all cut-off values (Table 4).

Discussion

Hepatic fibrosis, which is important risk factor in the prognosis of NAFLD patients is related not only to traditional TGF-β pathway, but also FOSL2, ADAM17, and angiotensin pathway (24–26). It is very important to identify high-risk groups by assessing the stage of hepatic fibrosis in suspected NAFLD patients (27). Currently, most guidelines recommend use of FIB-4 or NFS as a test for screening advanced liver fibrosis patients. We evaluated the diagnostic performance of FIB-4 and NFS in the average-risk group. The diagnostic performance of both FIB-4 (AUROC: 0.840) and NFS (AUROC: 0.798) was good even in the average-risk group. The diagnostic performance of FIB-4 was better than that of NFS for screening hepatic fibrosis in the average-risk group, while it was comparable to that of NFS in the metabolically healthy group. However, the diagnostic performance of the NFS decreased in the metabolically healthy and non-fatty liver groups. Because the current FIB-4 low cut-off has low accuracy and leads to false-negative results, it cannot be used as a single screening strategy in the average-risk group. Although diagnostic performance of FIB-4 was good, our large cohort reconfirmed considerable proportion of false-negative subjects with FIB-4 and very low PPV in the average-risk population. Currently, routine screening for advanced hepatic fibrosis is not recommended in general and average-risk populations. However, given that a considerable proportion of the general and average-risk population undergo health check-ups, a screening for hepatic fibrosis must be performed for those individuals who have already undergone medical check-ups based on a reasonable referral algorithm. Although the accuracy and positive-predictive value of FIB-4 are still not satisfactory, physicians can calculate FIB-4 using the pre-existing health check-up test item at no additional cost. FIB-4 can be a very attractive first screening method in a medical check-up setting, because additional sequential test can back-up the low positive-predictive value. Therefore, if we can increase the sensitivity of FIB-4 by adjusting the low cut-off values, FIB-4 can become

TABLE 2 Comparison of FIB-4 and NFS for diagnostic performance of advanced hepatic fibrosis in various groups.

	Advanced fibrosis* *n* (%)	Sensitivity (%)	Specificity (%)	PPV (%)	NPV (%)
FIB-4 to use low cut-off; 1.3 (2.0)					
Total subjects	102 (2.6)	69.6	77.5	4.9	99.3
Non-fatty liver group	39 (1.2)	71.8	76.7	3.6	99.6
Metabolically healthy group	25 (0.8)	64.0	78.2	2.2	99.6
Fatty liver group	63 (2.1)	68.3	78.4	6.4	99.1
Metabolically unhealthy group	77 (2.6)	71.4	76.7	7.7	99.0
NFS to use low cut-off; −1.455 (0.12)					
Total subjects	102 (2.6)	61.4	81.1	5.2	99.2
Non-fatty liver group	39 (1.2)	59.0	82.6	4.0	99.4
Metabolically healthy group	25 (0.8)	44.0	89.0	3.0	99.5
Fatty liver group	63 (2.1)	62.9	79.5	6.2	99.0
Metabolically unhealthy group	77 (2.6)	67.1	72.1	6.1	98.8

*Prevalence of subjects with advanced hepatic fibrosis among total subjects (n = 6,215), and the non-fatty liver (n = 3,252), metabolically healthy (n = 3,291), fatty liver (n = 2,963), and metabolically unhealthy (n = 2,924) groups. FIB-4, fibrosis-4 index; MRE, magnetic resonance elastography; NFS, non-alcoholic fatty liver disease fibrosis score; NPV, negative predictive value; PPV, positive predictive value.

TABLE 3 Comparison of diagnostic performance for advanced hepatic fibrosis (MRE cut-off values ≥ 3.6) according to the various cut-off values of FIB-4.

	Sensitivity	Specificity	PPV	NPV	Accuracy
FIB-4 to use low cut-off; 1.3 (2.0)					
Total subjects	69.6	77.5	4.9	99.3	77.4
Metabolically healthy group	64.0	78.2	2.2	99.6	78.1
FIB-4 to use low cut-off; 0.9					
Total subjects	92.2	42.1	2.6	99.7	42.9
Metabolically healthy group	100.0	43.6	1.3	100	44.0
FIB-4 to use low cut-off; 1.0					
Total subjects	90.2	52.2	3.1	99.7	52.8
Metabolically healthy group	96.0	53.8	1.6	99.9	54.1
FIB-4 to use low cut-off; 1.1					
Total subjects	87.3	60.9	3.6	99.7	61.3
Metabolically healthy group	92.0	61.9	1.8	99.9	62.2
FIB-4 to use low cut-off; 1.2					
Total subjects	83.3	69.0	4.3	99.6	69.2
Metabolically healthy group	80.0	69.8	2.0	99.8	69.9
FIB-4 to use low cut-off; 1.3					
Total subjects	75.5	75.4	4.9	99.5	75.4
Metabolically healthy group	76.0	76.7	2.4	99.8	76.7

FIB-4, fibrosis-4 index; MRE, magnetic resonance elastography; NFS, non-alcoholic fatty liver disease fibrosis score; NPV, negative predictive value; PPV, positive predictive value.

the most cost-effective first-line screening test in average-risk populations.

FIB-4 and NFS have different variables because of different disease entities of the target population at the time of development. Clinical characteristics between two cohorts are very different only when their average BMIs (25 vs. 32) are compared (28, 29). Therefore, metabolic components such as BMI and the presence of impaired fasting glycemia or diabetes were included as variables only in the NFS formula. Consequently, the diagnostic performance of NFS is more easily affected by the metabolic status of the target population than that of FIB-4.

Interestingly, FIB-4 as an indicator of hepatic fibrosis worked well when applied to not only the fatty liver group (AUROC = 0.823) but also the non-fatty liver group (AUROC = 0.872) or metabolically healthy group (AUROC = 0.862). Conversely, the AUROCs of NFS in the non-fatty liver group (AUROC = 0.777) and metabolically healthy group (AUROC = 0.702) were lower or comparable to those in the fatty-liver group (AUROC = 0.800). Both FIB-4 and NFS have been validated well in patients with fatty liver or metabolic unhealthy. So, it makes sense that all of FIB-4 and NFS work well in subjects with fatty liver or metabolic unhealthy. However, the validation of FIB-4 and NFS especially in non-fatty liver or metabolic healthy has been very limited. Our results showed the AUROC of FIB-4 in metabolic healthy was even higher than that in metabolic unhealthy. The inverse tendency was also observed in NFS. Moreover, nearly 53% of total subjects were metabolically healthy. That is why the AUROC of FIB-4 was also significantly higher than that of NFS in all subjects (0.840 in FIB-4 vs. 0.798 in NFS, P = 0.036). Therefore, FIB-4 use should be recommended for screening subjects with hepatic fibrosis burden in average-risk groups.

Careful interpretation of the results obtained is required for several reasons. Most importantly, hepatic societies do not recommend routine screening for hepatic fibrosis in subjects without a risk of advanced hepatic fibrosis. We completely understand the concerns about unnecessary examinations. However, a non-negligible number of subjects with hepatic fibrosis (0.3–2.1%; MRE cut-off value = 3.2–4.0 kPa) were present in our cohort, although they were metabolically healthy and had no risk of viral and alcoholic hepatitis. The prevalence of hepatic fibrosis in all subjects was 0.9–3.9% (MRE cut-off value = 3.2–4.0 kPa). Moreover, the global hepatic fibrosis burden is gradually increasing owing to an increase in metabolic diseases. Therefore, preliminary studies for screening subjects with the hepatic fibrosis burden in the general and average-risk populations are needed. Our study is the first step in this regard.

TABLE 4 Comparison of AUROC for hepatic fibrosis between FIB-4 and NFS in various groups according to different MRE cut-off values.

	MRE cut-off	AUROC		*P*-value
		FIB-4	NFS	
Total	3.2	0.709	0.699	0.803
	3.4	0.751	0.745	0.761
	3.6	0.840	0.798	0.036
	3.8	0.867	0.843	0.174
	4.0	0.896	0.877	0.529
Non-fatty liver group	3.2	0.728	0.682	0.151
	3.4	0.759	0.706	0.129
	3.6	0.872	0.777	0.01
	3.8	0.925	0.867	0.122
	4.0	0.933	0.900	0.467
Metabolically healthy group	3.2	0.732	0.631	<0.001
	3.4	0.756	0.638	0.001
	3.6	0.862	0.702	0.001
	3.8	0.913	0.808	0.03
	4.0	0.956	0.880	0.105
Fatty liver group	3.2	0.704	0.704	0.706
	3.4	0.752	0.76	0.671
	3.6	0.823	0.806	0.389
	3.8	0.841	0.824	0.336
	4.0	0.876	0.860	0.622
Metabolically unhealthy group	3.2	0.695	0.688	0.984
	3.4	0.744	0.742	0.899
	3.6	0.828	0.800	0.08
	3.8	0.85	0.823	0.111
	4.0	0.878	0.852	0.346

Metabolically healthy group was defined as sharing less than two metabolic risks and not having diabetes. AUROC, area under the receiver operating characteristic curve; FIB-4, fibrosis-4 index; MRE, magnetic resonance elastography; NFS, non-alcoholic fatty liver disease fibrosis score.

Further study of the current cut-off values of FIB-4 for the average-risk group is needed. The current cut-off values proposed by McPherson et al. were originally optimized for screening subjects with advanced hepatic fibrosis among high-risk groups, such as those with fatty liver, viral hepatitis, and significant alcohol intake. A recent study reported that the FIB-4 and NFS have low accuracy for screening liver fibrosis in the general population (11). They pointed out the lower PPV for advanced fibrosis (LSM $\geq$ 12 kPa) by using a low cutoff value of FIB-4 (1.90% vs. 23.97%) and NFS (2.57% vs. 29.27%) in general population, compared to those in the high risk group. PPV and NPV are affected by the prevalence of disease. In the case of general population, whose disease prevalence is low, the low PPV is expected. In our study on average-risk subjects, similar PPV (4.9% in FIB-4, 5.9% in NFS) was observed when the current cut-off values were used. Non-negligible false-positive rates in FIB-4 (22.12%) and (18.56%) are observed (**Figure 3**). The accuracy of the current FIB-4 low cut-off was not satisfactory to be used as a single screening strategy in the average-risk group.

However, the screening strategy in the general population should focus on not missing patients with high hepatic fibrosis burden and finding subjects who can be managed through intensive lifestyle modification at the primary care center. If we consider this purpose, then we believe that the current low PPV and high false-positive rate can be tolerated, and even the lower cut-off values with relaxed standard are more appropriate for the general population. Shah et al. also suggested that a cut-off of 1.0 in FIB-4 can be appropriate for a primary care referral pathway (30). Our data also showed an increase in sensitivity (69.6–90.2% in total subjects; 64.0–96.0% in the metabolically healthy group) and comparable PPV and NPV when the cut-off value of 1.0 was used instead of using the previous optimal cut-off value [1.3 (2.0)], although more subjects without hepatic fibrosis were identified as positive (47.03% vs. 22.12%) (**Figure 3**). It is difficult to suggest what is the optimal cut-off value of FIB-4 for screening advanced hepatic fibrosis in general population based on our study alone. Another validation study for the new cut-off value and the socioeconomic assessment for application of FIB-4 for screening advanced hepatic fibrosis in general population should be needed in the future.

This study has some limitations as well. First, MRE, not liver biopsy, was performed to evaluate the degree of hepatic fibrosis. When comparing the diagnostic performance, the use of gold standard methods such as liver biopsy is necessary. However, it is impossible to routinely perform such methods in a health check-up setting. In this study, we evaluated MRE data because it is the most reliable non-invasive diagnostic method for estimating liver stiffness. Second, the proportion of men was higher than that of women in the study cohort. Moreover, there is a possibility that people concerned with liver health were more likely to be included in study, because MRE was offered as an additional option to be tested with their own expense. There is a possibility of selection bias. Large number of excluded subjects (n = 2,249) due to missing data can be another source of selection bias. Nevertheless, the overall prevalence of hypertension (26.4%), DM (9.2%), and metabolic syndrome (23.2%) was comparable to that in the general population. Third, there is no consensus on MRE cut-off values for advanced hepatic fibrosis. In this study, an MRE cut-off value of 3.6 kPa was used for advanced fibrosis. However, a similar result was obtained when the MRE cut-off value was set at either 3.2 or 4.0 kPa in the sensitivity analysis. Therefore, we believe that our results are reliable regardless of the cut-off values.

In conclusion, the AUROCs of FIB-4 and NFS for advanced fibrosis did not differ between the metabolically unhealthy and fatty liver groups. However, the AUROC of FIB-4 for advanced fibrosis was higher than that of NFS, particularly in the

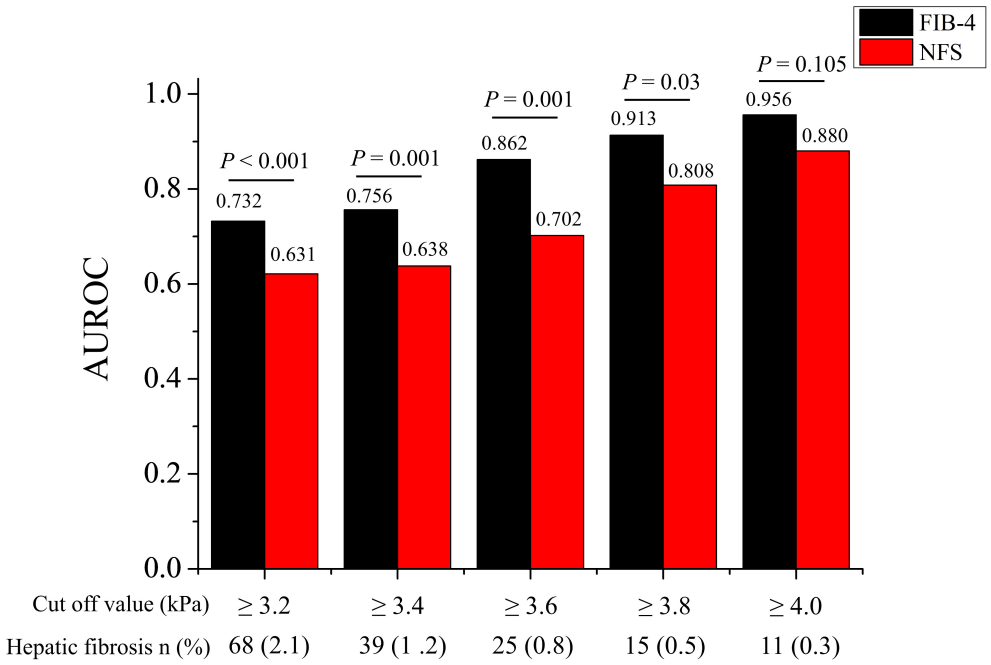


FIGURE 4
Comparison of AUROC for advanced hepatic fibrosis between FIB-4 and NFS in the metabolically healthy group at various MRE cut-off values (3.2–4.0 kPa). AUROC, area under the receiver operating characteristic curve; FIB-4, fibrosis-4 index; NFS, NAFLD fibrosis score.

metabolically healthy and non-fatty liver groups. As more than half the average-risk population were consisted of metabolically healthy individuals, FIB-4 showed better performance for diagnosing advanced fibrosis when applied to the whole group with average-risk. It is recommended to use FIB-4 rather than NFS, when screening for hepatic fibrosis in general population.

Data availability statement

The original contributions presented in this study are included in the article/supplementary material, further inquiries can be directed to the corresponding author/s.

Ethics statement

The studies involving human participants were reviewed and approved by the Institutional Review board (IRB No. HY-2021-04-001-001) of Hanyang University Hospital. The ethics committee waived the requirement of written informed consent for participation.

Author contributions

DJ: concept, design, and interpretation of data. EY, JL, MK, SC, and E-HN: data collection and management. HP: writing of the manuscript. DJ and E-HN: supervision. All authors read and approved the manuscript.

Funding

This work was supported by the Research Program funded by the Korea National Institute of Health (grant no. 2022-ER0906-00).

Conflict of interest

The authors declare that the research was conducted in the absence of any commercial or financial relationships that could be construed as a potential conflict of interest.

Publisher's note

All claims expressed in this article are solely those of the authors and do not necessarily represent those of their affiliated organizations, or those of the publisher, the editors and the reviewers. Any product that may be evaluated in this article, or claim that may be made by its manufacturer, is not guaranteed or endorsed by the publisher.

References

1. Paik JM, Kabbara K, Eberly KE, Younossi Y, Henry L, Younossi ZM. Global burden of NAFLD and chronic liver disease among adolescents and young adults. *Hepatology.* (2022) 75:1204–17. doi: 10.1002/hep.32228

2. Estes C, Chan HL, Chien RN, Chuang WL, Fung J, Goh GB-B, et al. Modelling NAFLD disease burden in four Asian regions—2019−2030. *Aliment Pharmacol Ther.* (2020) 51:801–11. doi: 10.1111/apt.15673

3. Dulai PS, Singh S, Patel J, Soni M, Prokop LJ, Younossi Z, et al. Increased risk of mortality by fibrosis stage in nonalcoholic fatty liver disease: systematic review and meta−analysis. *Hepatology.* (2017) 65:1557–65. doi: 10.1002/hep.29085

4. Vilar-Gomez E, Calzadilla-Bertot L, Wong VW-S, Castellanos M, Aller-de la Fuente R, Metwally M, et al. Fibrosis severity as a determinant of cause-specific mortality in patients with advanced nonalcoholic fatty liver disease: a multinational cohort study. *Gastroenterology.* (2018) 155:443–57.e17. doi: 10.1053/j.gastro.2018.04.034

5. European Association for the Study of the Liver [EASL], European Association for the Study of Diabetes [EASD], European Association for the Study of Obesity [EASO]. EASL-EASD-EASO Clinical Practice Guidelines for the management of non-alcoholic fatty liver disease. *Obesity Facts.* (2016) 9:65–90. doi: 10.1159/000443344

6. Chalasani N, Younossi Z, Lavine JE, Charlton M, Cusi K, Rinella M, et al. The diagnosis and management of nonalcoholic fatty liver disease: practice guidance from the American Association for the Study of Liver Diseases. *Hepatology.* (2018) 67:328–57. doi: 10.1002/hep.29367

7. Oh H, Jun DW, Saeed WK, Nguyen MH. Non-alcoholic fatty liver diseases: update on the challenge of diagnosis and treatment. *Clin Mol Hepatol.* (2016) 22:327. doi: 10.3350/cmh.2016.0049

8. Kang KA, Jun DW, Kim MS, Kwon HJ, Nguyen MH. Prevalence of significant hepatic fibrosis using magnetic resonance elastography in a health check−up clinic population. *Aliment Pharmacol Ther.* (2020) 51:388–96. doi: 10.1111/apt.15626

9. Nah E-H, Cho S, Kim S, Chu J, Kwon E, Cho H-I. Prevalence of liver fibrosis and associated risk factors in the Korean general population: a retrospective cross-sectional study. *BMJ Open.* (2021) 11:e046529. doi: 10.1136/bmjopen-2020-046529

10. Panel CPG, Berzigotti A, Tsochatzis E, Boursier J, Castera L, Cazzagon N, et al. EASL Clinical Practice Guidelines on non-invasive tests for evaluation of liver disease severity and prognosis–2021 update. *J Hepatol.* (2021) 75:659–89. doi: 10.1016/j.jhep.2021.05.025

11. Graupera I, Thiele M, Serra-Burriel M, Caballeria L, Roulot D, Wong GL-H, et al. Low accuracy of FIB-4 and NAFLD fibrosis scores for screening for liver fibrosis in the population. *Clin Gastroenterol Hepatol.* (2021) S1542-3565:1358–1356. doi: 10.1016/j.cgh.2021.12.034

12. Kanwal F, Shubrook JH, Adams LA. Clinical care pathway for the risk stratification and management of patients with nonalcoholic fatty liver disease. *Gastroenterology.* (2021) 161:1657–69. doi: 10.1053/j.gastro.2021.07.049

13. McPherson S, Hardy T, Dufour JF, Petta S, Romero-Gomez M, Allison M, et al. Age as a confounding factor for the accurate non-invasive diagnosis of advanced NAFLD Fibrosis. *Am J Gastroenterol.* (2017) 112:740–51. doi: 10.1038/ajg.2016.453

14. Alberti K, Eckel RH, Grundy SM, Zimmet PZ, Cleeman JI, Donato KA, et al. Harmonizing the metabolic syndrome: a joint interim statement of the international diabetes federation task force on epidemiology and prevention; national heart, lung, and blood institute; American heart association; world heart federation; international atherosclerosis society; and international association for the study of obesity. *Circulation.* (2009) 120:1640–5. doi: 10.1161/CIRCULATIONAHA.109.192644

15. Park H, Yoon EL, Kim M, Cho S, Kim J-H, Jun DW, et al. Selecting the target population for screening of hepatic fibrosis in primary care centers in Korea. *J Clin Med.* (2022) 11:1474. doi: 10.3390/jcm11061474

16. Mittelstaedt C. *General ultrasound*. New York: Churchill (1992).

17. Yin M, Talwalkar JA, Glaser KJ, Manduca A, Grimm RC, Rossman PJ, et al. Assessment of hepatic fibrosis with magnetic resonance elastography. *Clin Gastroenterol Hepatol.* (2007) 5:1207–13.e2. doi: 10.1016/j.cgh.2007.06.012

18. Hsu C, Caussy C, Imajo K, Chen J, Singh S, Kaulback K, et al. Magnetic resonance vs transient elastography analysis of patients with nonalcoholic fatty liver disease: a systematic review and pooled analysis of individual participants. *Clin Gastroenterol Hepatol.* (2019) 17:630–7.e8. doi: 10.1016/j.cgh.2018.05.059

19. Cui J, Heba E, Hernandez C, Haufe W, Hooker J, Andre MP, et al. MRE is superior to ARFI for the diagnosis of fibrosis in patients with biopsy-proven NAFLD: a prospective study. *Hepatology.* (2016) 63:453. doi: 10.1002/hep.28337

20. Furlan A, Tublin ME, Yu L, Chopra KB, Lippello A, Behari J. Comparison of 2D shear wave elastography, transient elastography, and MR elastography for the diagnosis of fibrosis in patients with nonalcoholic fatty liver disease. *Am J Roentgenol.* (2020) 214:W20–6. doi: 10.2214/AJR.19.21267

21. Lee Y-S, Yoo YJ, Jung YK, Kim JH, Seo YS, Yim HJ, et al. Multiparametric MR is a valuable modality for evaluating disease severity of nonalcoholic fatty liver disease. *Clin Trans Gastroenterol.* (2020) 11:4. doi: 10.14309/ctg.0000000000000157

22. Loomba R, Cui J, Wolfson T, Haufe W, Hooker J, Szeverenyi N, et al. Novel 3D magnetic resonance elastography for the noninvasive diagnosis of advanced fibrosis in NAFLD: a prospective study. *Am J Gastroenterol.* (2016) 111:986. doi: 10.1038/ajg.2016.65

23. Imajo K, Honda Y, Kobayashi T, Nagai K, Ozaki A, Iwaki M, et al. Direct comparison of US and MR elastography for staging liver fibrosis in patients with nonalcoholic fatty liver disease. *Clin Gastroenterol Hepatol.* (2020) 20:908–17.e11. doi: 10.1016/j.cgh.2020.12.016

24. Hu P-X, Sheng M-Y, Liu Y-P. FOSL2 deficiency delays nonalcoholic steatohepatitis progression by regulating LY6D-mediated NLRP3 activation. *Hum Cell.* (2022) 2022:1–14. doi: 10.1007/s13577-022-00760-y

25. Xue F, Cheng J, Liu Y. Cardiomyocyte-specific knockout of ADAM17 ameliorates left ventricular remodeling and function in diabetic cardiomyopathy of mice. *Signal Trans Target Ther.* (2022) 7:1–16. doi: 10.1038/s41392-022-01054-3

26. Zhang M, Sui W, Xing Y. Angiotensin IV attenuates diabetic cardiomyopathy via suppressing FoxO1-induced excessive autophagy, apoptosis and fibrosis. *Theranostics.* (2021) 11:8624. doi: 10.7150/thno.48561

27. Park H, Yoon EL, Kim M. Selecting the target population for screening of hepatic fibrosis in primary care centers in Korea. *J Clin Med.* (2022) 11:1474.

28. Sterling RK, Lissen E, Clumeck N, Sola R, Correa MC, Montaner J, et al. Development of a simple noninvasive index to predict significant fibrosis in patients with HIV/HCV coinfection. *Hepatology.* (2006) 43:1317–25. doi: 10.1002/hep.21178

29. Angulo P, Hui JM, Marchesini G, Bugianesi E, George J, Farrell GC, et al. The NAFLD fibrosis score: a noninvasive system that identifies liver fibrosis in patients with NAFLD. *Hepatology.* (2007) 45:846–54. doi: 10.1002/hep.21496

30. Shah S, Dhami-Shah H, Kamble S, Shukla A. FIB-4 cut-off of 1.3 may be inappropriate in a primary care referral pathway for patients with non-alcoholic fatty liver disease. *J Hepatol.* (2020) 73:216–7. doi: 10.1016/j.jhep.2019.12.025

frontiers | Frontiers in Pharmacology

TYPE Review
PUBLISHED 14 November 2022
DOI 10.3389/fphar.2022.1031890

Check for updates

OPEN ACCESS

EDITED BY
Robert Hamanaka,
The University of Chicago, United States

REVIEWED BY
Benoit Allard,
Université de La Réunion, France
Pavel Solopov,
Old Dominion University, United States

*CORRESPONDENCE
Jiali Wang,
wangjiali_2000@126.com
Qiuhuan Yuan,
xiaoqiu0707@aliyun.com
Shengchuan Cao,
caoshengchuan@126.com

SPECIALTY SECTION
This article was submitted to Experimental Pharmacology and Drug Discovery, a section of the journal Frontiers in Pharmacology

RECEIVED 30 August 2022
ACCEPTED 01 November 2022
PUBLISHED 14 November 2022

CITATION
Li J, Zhai X, Sun X, Cao S, Yuan Q and Wang J (2022), Metabolic reprogramming of pulmonary fibrosis. *Front. Pharmacol.* 13:1031890. doi: 10.3389/fphar.2022.1031890

COPYRIGHT
© 2022 Li, Zhai, Sun, Cao, Yuan and Wang. This is an open-access article distributed under the terms of the Creative Commons Attribution License (CC BY). The use, distribution or reproduction in other forums is permitted, provided the original author(s) and the copyright owner(s) are credited and that the original publication in this journal is cited, in accordance with accepted academic practice. No use, distribution or reproduction is permitted which does not comply with these terms.

Metabolic reprogramming of pulmonary fibrosis

Jiaxin Li[1,2,3,4], Xiaoxuan Zhai[1,2,3,4], Xiao Sun[1,2,3,4], Shengchuan Cao[1,2,3,4]*, Qiuhuan Yuan[1,2,3,4]* and Jiali Wang[1,2,3,4]*

[1]Department of Emergency Medicine, Qilu Hospital of Shandong University, Jinan, China, [2]Shandong Provincial Clinical Research Center for Emergency and Critical Care Medicine, Institute of Emergency and Critical Care Medicine of Shandong University, Chest Pain Center, Qilu Hospital of Shandong University, Jinan, China, [3]Key Laboratory of Emergency and Critical Care Medicine of Shandong Province, Key Laboratory of Cardiopulmonary-Cerebral Resuscitation Research of Shandong Province, Shandong Provincial Engineering Laboratory for Emergency and Critical Care Medicine, Qilu Hospital of Shandong University, Jinan, China, [4]The Key Laboratory of Cardiovascular Remodeling and Function Research, Chinese Ministry of Education, Chinese Ministry of Health and Chinese Academy of Medical Sciences, The State and Shandong Province Joint Key Laboratory of Translational Cardiovascular Medicine, Qilu Hospital of Shandong University, Jinan, China

Pulmonary fibrosis is a progressive and intractable lung disease with fibrotic features that affects alveoli elasticity, which leading to higher rates of hospitalization and mortality worldwide. Pulmonary fibrosis is initiated by repetitive localized micro-damages of the alveolar epithelium, which subsequently triggers aberrant epithelial-fibroblast communication and myofibroblasts production in the extracellular matrix, resulting in massive extracellular matrix accumulation and interstitial remodeling. The major cell types responsible for pulmonary fibrosis are myofibroblasts, alveolar epithelial cells, macrophages, and endothelial cells. Recent studies have demonstrated that metabolic reprogramming or dysregulation of these cells exerts their profibrotic role *via* affecting pathological mechanisms such as autophagy, apoptosis, aging, and inflammatory responses, which ultimately contributes to the development of pulmonary fibrosis. This review summarizes recent findings on metabolic reprogramming that occur in the aforementioned cells during pulmonary fibrosis, especially those associated with glucose, lipid, and amino acid metabolism, with the aim of identifying novel treatment targets for pulmonary fibrosis.

KEYWORDS

pulmonary fibrosis, metabolic reprogramming, glucose metabolism, lipid metabolism, amino acid metabolism, myofibroblasts

Introduction

Pulmonary fibrosis (PF), a progressive and intractable lung disease that affects alveoli elasticity, is characterized by exaggerated inflammatory and fibrotic responses that lead to pulmonary fibrotic remodeling and extracellular matrix deposition, which in turn perpetuates fibrosis formation in a vicious cycle of fibrosis formation (Distler et al., 2019). Idiopathic pulmonary fibrosis (IPF), the classic and most common type, which

TABLE 1 Overview of the connection of metabolites with pro-inflammatory and pro-fibrotic pathways in Pulmonary fibrosis.

Cell type	Metabolic type	Metabolites	Associated pathway	References
Myofibroblasts	Glucose metabolism	succinic acid	Myofibroblasts differentiation by stabilizing HIF-1α	Wang et al. (2021)
		lactate	TGF-β-induced myofibroblasts differentiation	Kottmann et al. (2012)
	Lipid metabolism	LPA	Fibroblasts recruitment and vascular leak	Tager et al. (2008)
		S1P	TGF-β- and S1P-induced myofibroblasts differentiation	Huang and Natarajan, (2015)
		GPX4	TGF-β-induced myofibroblasts differentiation	Tsubouchi et al. (2019)
		PGE2	Inhibits myofibroblasts apoptosis, proliferation, and differentiation	White et al. (2005); Wettlaufer et al. (2016); Suryadevara et al. (2020)
		Lipoxins A4	Myofibroblasts dedifferentiation	Roach et al. (2015)
	Amino acid metabolism	Glycine	Collagen production	Nigdelioglu et al. (2016); Hamanaka and Mutlu (2021)
		serine	Collagen production	O'Leary et al. (2020)
		proline	Collagen production	Hamanaka et al. (2019)
		Glutamine	Myofibroblasts differentiation and collagen production	Bernard et al. (2018)
Alveolar epithelial cells	Lipid metabolism	Elovl6	Inhibits alveolar epithelial cells apoptosis and TGF-β1 expression	Sunaga et al. (2013)
	Amino acid metabolism	Glutamine	Antioxidant defense	Shaghaghi et al. (2021)
		Dimethylarginine dimethylaminohydrolase	Inhibits NOS activity	Pullamsetti et al. (2011)
Macrophages	Glucose metabolism	Lactate	TGF-β-induced myofibroblasts differentiation	Cui et al. (2021)
	Amino acid metabolism	Arginine	Collagen production	Endo et al. (2003); Niese et al. (2010); Meziani et al. (2018)

accounts for 20% of Interstitial lung diseases, is a chronic progressive and irreversible lung disease that usually rapidly progresses to respiratory failure and death (median interval from diagnosis to death is 3 years (Lederer and Martinez, 2018). It has been estimated that the overall prevalence of PF in European countries is about 75 cases per 100,000 people (Wijsenbeek and Cottin, 2020). The high incidence and serious clinical outcomes of PF have prompted a deep exploration of PF's pathogenesis.

It has been well established that damage and/or dysfunction of alveolar epithelial (AE) cells occurs during the initial stage of the disease (Kasper and Haroske, 1996; Winters et al., 2019; Moss et al., 2022). Then the dysregulated AE cells interact with mesenchymal cells, immune cells, and endothelial cells through various molecular mechanisms, triggering the activation of fibroblasts and myofibroblasts (Moss et al., 2022), which eventually leads to inappropriate deposition of extracellular matrix (Kendall and Feghali-Bostwick, 2014).

Metabolic reprogramming or dysregulation of fibroblasts, epithelial cells, immune cells, and various other types of cells have been shown to be involved in the pathogenesis of pulmonary fibrosis (Ung et al., 2021). In PF, enhanced glucose metabolism affects cell differentiation, cell proliferation, autophagy, and inflammatory responses. Glucose metabolism in epithelial cells and macrophages can metabolize glucose into lactate even in the presence of oxygen, a phenomenon known as the "Warburg effect" (Liberti and Locasale, 2016; Janssen et al., 2020; Alysandratos et al., 2021). Additionally, metabolic pathways of nucleotide, lipid, or amino acid synthesis require a glycolytic intermediate (Para et al., 2019). Fatty acid oxidation is a catabolic process in which fatty acids are broken down to produce ATP (Hooff et al., 2010). It is currently considered that lipid metabolism may affect PF through several pathways, along with increased fatty acid synthesis and decreased fatty acid oxidation (Kendall and Feghali-Bostwick, 2014). Amino acids are involved in multiple metabolic pathways that are essential for cell survival, and are sources of energy, precursors to biosynthetic processes, and help maintain tissue homeostasis (Lieu et al., 2020). Most evidence suggests that alterations in amino acid metabolism during fibrosis are associated with non-essential amino acids, and increased amino acid metabolism promotes collagen synthesis and thus affects the progression of fibrosis (Gaugg et al., 2019).

This review mainly discusses recent progress in research on metabolic reprogramming of myofibroblasts, AE cells, macrophages, and endothelial cells in PF, most of which are

TABLE 2 Overview of therapeutic targets and related mechanisms in pulmonary fibrosis.

Cell type	Metabolic type	Therapeutic target	Mechanism	References
Myofibroblasts	Glucose metabolism	PFKFB3	Promoting aerobic glycolysis and lactate production	Xu et al. (2022)
		PDK	Promoting fibroblast differentiation induced by the HIF-1α/PDK1 axis	Goodwin et al. (2018)
		Subunit A of succinate dehydrogenase	Inhibiting TGF-β1-induced elevation of succinate dehydrogenase and succinate	Wang et al. (2021)
		LDH	Promoting TGF-β-induced myofibroblasts transformation	Kottmann et al. (2012)
				Judge et al. (2018)
		GLUT	Promoting α-SMA expression in lung fibroblasts	Cho et al. (2017)
				Li et al. (2022)
		Circular RNAs	CircHIPK3/miR-30a-3p/FOXK2 pathway can prevent fibroblast activation and proliferation	Chen et al. (2017)
		Caveolin-1	Inhibiting the increased expression of glycolysis and profibrotic marker proteins through p53/microRNA-34a signaling pathway	Gopu et al. (2020)
	Lipid metabolism	LPA	Promoting fibroblasts recruitment and vascular leak	Tager et al. (2008)
		S1P	Promoting TGF-β- and S1P-induced differentiation of fibroblasts to myofibroblasts	Huang and Natarajan, (2015)
		GPX4	Regulating the oxidative modification of phospholipids	Cole-Ezea et al. (2012)
		PGE2	Inhibiting a variety of myofibroblasts functions, including apoptosis, proliferation, and differentiation	Wettlaufer et al. (2016); Suryadevara et al. (2020); White et al. (2005); Penke et al. (2018); Molina-Molina et al. (2006)
				Ivanova et al. (2013)
		Lipoxins A4	Inhibiting TGF-β1-dependent of Smad2/3 nuclear translocation	Roach et al. (2015)
	Amino acid metabolism	phosphoglycerate dehydrogenase	Promoting the synthesis of collagen	Hamanaka and Mutlu, (2021)
		Phosphoserine transaminase 1	Promoting the synthesis of collagen	Jiang et al. (2020)
		PI3K	Promoting the activation of the PI3K-Akt-mTOR pathway	O'Leary et al. (2020)
		Δ1-pyrroline-5-carboxylic acid synthase	Promoting in synthesis of collagen production	Hamanaka et al. (2019)
		GLS1	Enhancing levels of glutaminolysis through SMAD3 and p38-MAPK-dependent signaling pathways	Bernard et al. (2018)
				Esguerra and Zhao, (2019)
			The activation of PPAR-γ can decrease GLS1 protein levels and enhance DEPTOR stability through the intervention of the 2-hydroxyglutarate-KDM4A axis	Miao et al. (2022)
		Nrf2	Depleting glutamate and inhibiting myofibroblast activation	An et al. (2019)
AE2 cells	Lipid metabolism	Mfsd2a	Stabilizing surfactant levels, as well as surfactant lipid composition	Wong et al. (2022)
		FASN	Promoting the expression of profibrotic genes and stabilize lung function	Jung et al. (2018)
		Elovl6	Promoting apoptosis, and reactive oxygen species, and impairing cellular uptake of long-chain FAs	Sunaga et al. (2013)
		ApoA-I	Reducing the inflammatory proteins	Kim et al. (2010)
		Mitofusin 1/2	Maintaining the stability of surfactant protein gene	Chung et al. (2019)
	Glucose metabolism	Enolase 1	Reducing glucose absorption and promoting AE2 differentiation into ciliated and secretory cells by inhibiting autophagy	Aboushousha et al. (2021)
		GLUT1	Promoting AE2 cell proliferation	Li et al. (2020)
		Glutamine		Shaghaghi et al. (2021)

(Continued on following page)

TABLE 2 (*Continued*) Overview of therapeutic targets and related mechanisms in pulmonary fibrosis.

Cell type	Metabolic type	Therapeutic target	Mechanism	References
	Amino acid metabolism		Supporting mitochondrial respiration and metaboliting production	
		Dimethylarginine dimethylaminohydrolase	Promoting NOS activity	Pullamsetti et al. (2011)
Macrophages	Glucose Metabolism	LDHA	Promoting silica exposure-induced high levels of iNOS, TNF-α, Arg-1, IL-10, and MCP1	Mao et al. (2021) Judge et al. (2017)
		VHL	Regulating the transcription of Spp1 *via* inhibiting HIF1α-mediated glycolytic metabolism	Zhang et al. (2018)
	Lipid metabolism	GM-CSF	Enhancing the clearance of oxidized lipids and preventing damage to anti-fibrotic molecules	Romero et al. (2015) Moore et al. (2000)
		Surfactant protein C	Enhancing the expression of cholesterol metabolism and transport genes	Ruwisch et al. (2020)
		FXR	Regulating intracellular lipids through targets include the B class oxidized phospholipid scavenger receptor, CD36, and the lipid chaperone, ApoE	Silverstein et al. (2010) Li et al. (2012)
		GPR84	Promoting phagocytosis and secreting pro-inflammatory factors	Chen et al. (2020) Marsango et al. (2022)
	Amino acid metabolism	Arginine	Promoting the synthesis of collagen	Niese et al. (2010)
ECs	Glucose metabolism	Ras homolog-related kinase subtype 2	Promoting intracellular pH and cell migration	Lee et al. (2020)
	Lipid metabolism	phospholipase D	Altering pulmonary vascular pathophysiology	Parinandi et al. (1999) Patel et al. (2011)

derived from studies about IPF, with the aim of providing a comprehensive foundation for the development of targeted therapies (Tables 1, 2).

Myofibroblasts

Key enzyme alterations in glucose, lipid, and amino acid metabolism lead to the activation and persistence of myofibroblasts in the lung tissue, which influences the progression of pulmonary fibrosis (Figure 1).

Glucose metabolism in myofibroblasts

Increased aerobic glycolysis in lung fibroblasts promotes its differentiation into myofibroblasts (Bernard et al., 2015; Hu et al., 2020). The irreversible rate-limiting enzymes involved in glycolysis, including hexokinase, phosphofructokinase, and pyruvate dehydrogenase kinase (PDK), are all significantly up-regulated in myofibroblasts during PF. An allosteric activator of phosphofructokinase-1, 6-phosphofructo-2-kinase/fructose-2,6-biphosphatase 3 (PFKFB3) is also upregulated in Transforming growth factor-β (TGF-β)-induced myofibroblasts, and the inhibition of PFKFB3 effectively decreases levels of myofibroblasts differentiation and pulmonary fibrosis (Xie et al., 2015). PFKFB3 expression can be increased by the secretion of TNF-α in lung fibroblasts, while PFKFB3 suppression effectively blocks TNF-α-induced aerobic glycolysis and lactate production in fibroblasts (Xu et al., 2022). The anti-fibrotic effect of Anlotinib is demonstrated to inhibit PFKFB3-dependent glycolysis, which can be post-transcriptionally regulated by the RNA-binding protein PCBP3 (Chen et al., 2021).

Hypoxia is one of the prominent features in fibrotic diseases (Higgins et al., 2008). Hypoxia-inducible factor-1 (HIF-1)-mediated anaerobic glycolysis provides the metabolic reprogramming necessary for the survival of hypoxic cells (Goodwin et al., 2018). PDK1, a direct target gene of HIF-1, can be induced by TGF-β and is responsible for cellular hypoxic adaptation by enhancing glycolysis and inhibiting mitochondrial respiration (Kim et al., 2006). Dichloroacetate, a PDK1 inhibitor, can efficiently inhibit fibroblast differentiation induced by the HIF-1α/PDK1 axis (Goodwin et al., 2018). In addition, succinic acid, the metabolic product of glycolysis, has been reported to promote the differentiation of lung myofibroblasts by stabilizing HIF-1α (Wang L. et al., 2021). These studies indicate that HIF-1α is an important regulator of pulmonary fibrosis. Dichloroacetate, a potent PDK inhibitor, effectively inhibits TGF-β-mediated myofibroblast differentiation *in vitro* and induces pulmonary

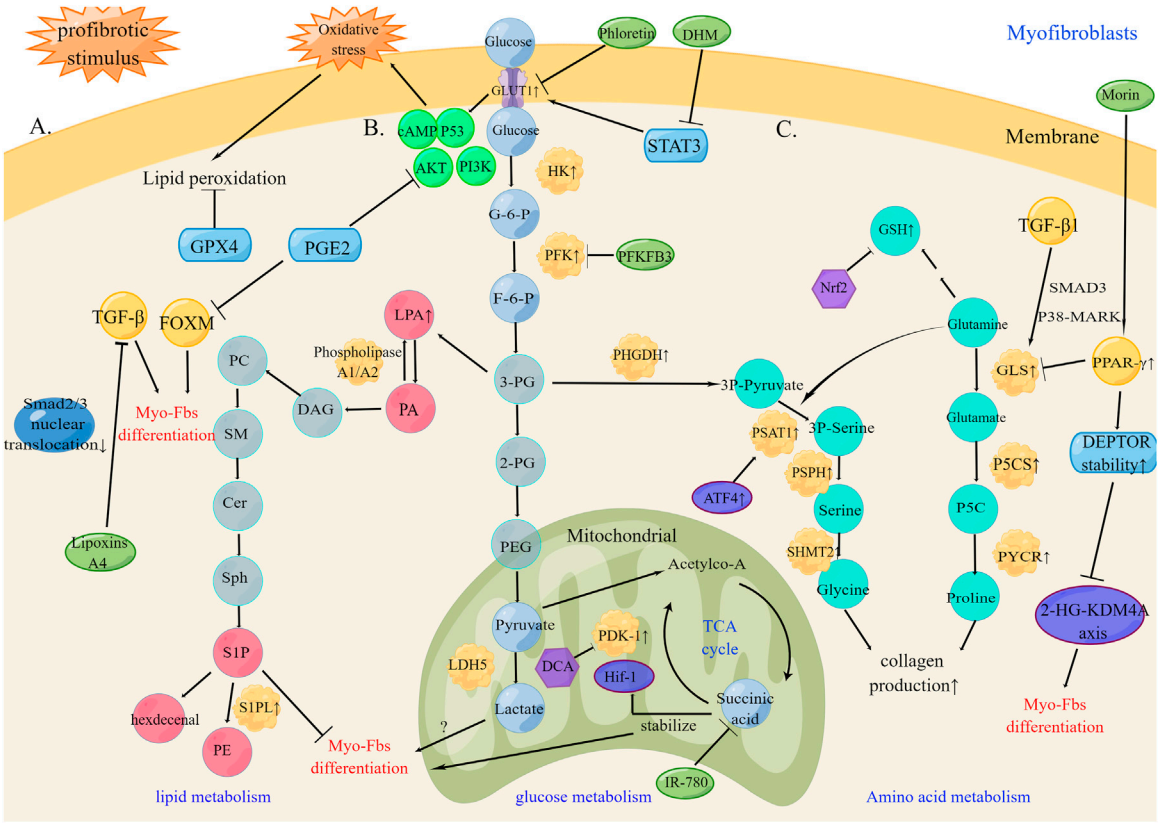


FIGURE 1
Metabolic reprogramming of myofibroblasts in pulmonary fibrosis **(A)**. Under profibrotic stimulus, lipid metabolism increases phospholipid synthesis and lipid peroxidation products. The therapeutic targets GPX4, PGE2, and TGF-β can inhibit myofibroblasts differentiation **(B)**. Under profibrotic stimulus, increased aerobic glycolysis up-regulates HK, PFK, and PDK and GLUT1 expression by changes in metabolic status and oxidative stress promote myofibroblasts differentiation into myofibroblasts by the HIF-1α/PDK1 axis. The therapeutic targets PFKB3, PDK1, and succinic acid can inhibit myofibroblasts differentiation **(C)**. Under profibrotic stimulus, amino acid metabolism promotes glutaminolysis and increases Glycine and GSH production leading to collagen production. The therapeutic targets PPAR-γ and DEPTOR stability can inhibit collagen production and myofibroblasts differentiation. PC, Polycarbonate; SM, sphingomyelin; Cer, ceramide; Sph, sphingosine; DAG, Diacylglycerol; HK, hexokinase; G-6-P, glucose-6-phosphate; PFK, phosphofructokinase; F-6-P, fructose-6-phosphate; 3-PG, 3-phosphoglycerate; 2-PG, 2- phosphoglycerate; PEG, phosphoenolpyruvate; DCA, Dichloroacetate; TCA cycle, tricarboxylic acid cycle; 3P-pyruvate, 3-phosphohydroxy-pyruvate; 3P Serine, 3-phosphohydroxy-serine; PHGDH, phosphoglycerate dehydrogenase; PSAT1, phosphorylated serine aminotransferase 1; PSPH, phosphorylated serine phosphatase; SHMT2, serine hydroxymethyltransferase 2; P5CS, Δ1-pyrroline-5-carboxylic acid synthase; PYCR, pyrroline-5-carboxylate reductase.

fibrosis *in vivo*, causing altered fibroblast metabolism (Goodwin et al., 2018). A near-infrared small molecule dye, IR-780, can target subunit A of succinate dehydrogenase in fibroblasts, and inhibit TGF-β1-induced elevation of succinate dehydrogenase and succinate, thereby preventing the formation of pulmonary fibrosis and respiratory dysfunction (Wang Z. et al., 2021).

The conversion of pyruvate to lactate is catalyzed by lactate dehydrogenases (LDHs). There is a total of five isoenzymes (Drent et al., 1996). It has been now well established from a variety of studies that lactate dehydrogenase 5 (LDH5) might play a role in TGF-β-induced myofibroblast differentiation (Kottmann et al., 2012). Gossypol, a natural non-selective LDH inhibitor, reduces TGF-β-induced myofibroblasts transformation in primary human lung fibroblasts and radiation-induced pulmonary fibrosis in mice (Judge et al., 2018). However, a recent study demonstrated that a potent small molecule inhibitor (compound 408) can inhibit LDH5 in human lung fibroblasts by reducing aerobic glycolysis and lactate production, rather than by affecting fibroblast-to-myofibroblasts differentiation (Schruf et al., 2019). Glucose transporter 1 (GLUT1) is the most conserved and widely distributed glucose transporter in mammalian cells (Thorens and Mueckler, 2010). Recent research found that GLUT1 expression is regulated by changes in metabolic status and oxidative stress, which involve signaling molecules such as cAMP, p53, phosphoinositide 3-kinase (PI3K), and AKT (Wieman et al., 2007; Zhang et al., 2013). Inhibition of GLUT1 decreases α-SMA expression in lung fibroblasts,

indicating a direct link between glycolytic activation and the pro-fibrotic transformation of myofibroblasts (Cho et al., 2017). Phloretin can activate AMP-activated protein kinase *via* inhibiting GLUT1-dependent glycolysis, modulate key metabolic pathways of fibroblast activation, and significantly inhibit bleomycin-induced pulmonary fibrosis in mice (Cho et al., 2017). Dihydromyricetin can alleviate lung fibrosis in mouse models through STAT3/pSTAT3/GLUT1 signaling pathway and inhibit fibroblast or myofibroblast differentiation, proliferation, and migration (Li et al., 2022). These *in vivo* experiments provide new directions for clinical translation.

Circular RNAs, which are post-transcriptional regulators of gene expression, have been found to be dysregulated in many fibrotic diseases, such as cardiac fibrosis, renal fibrosis, liver fibrosis, and pulmonary fibrosis (Wang et al., 2019; Li J. et al., 2020; Gu et al., 2020). TGF-β1 triggers the expression of circHIPK3 in fibroblasts, enhancing FOXK2 expression by sponging miR-30a-3p. The knockdown of FOXK2 abolished increased levels of glycolytic and fibrotic markers induced by TGF-β1, while knockdown of circHIPK3 prevented fibroblast activation and proliferation (Chen et al., 2017). Therefore, strategies that target the circHIPK3/miR-30a-3p/FOXK2 pathway may provide therapeutic benefits against pulmonary fibrosis.

Deletion of Caveolin-1 in tumor-associated fibroblasts is thought to reverse the Warburg effect (Guido et al., 2012). Previous studies have shown that restoration of Caveolin-1 expression or Caveolin-1 scaffolding domain peptide-or its 7-amino acid deletion fragment Caveolin-1 scaffolding domain peptide 7-inhibited the increased expression of glycolysis and profibrotic marker proteins in fibrotic lung fibroblasts, restoring the expression of baseline p53 and its downstream transcriptional target microRNA-34a (Gopu et al., 2020). Caveolin-1 scaffolding domain peptide 7 may be a promising future therapeutic drug that can be used to inhibit uncontrolled glycolysis in fibrotic lung fibroblasts.

Senescent fibroblasts in chronic obstructive pulmonary disease (COPD) exhibit decreased glycolysis and mitochondrial respiration, leading to a great deal of ROS production and mitochondria biogenesis (Lerner et al., 2016). Heme oxygenase-1 reduces cellular and mitochondrial ROS production in COPD fibroblasts, which in turn improves mitochondrial respiration, glycolysis and ATP recovery (Even et al., 2018).

Lipid metabolism in myofibroblasts

Lipid metabolism may affect PF *via* several pathways, including phospholipid synthesis, lipid peroxidation products, and lipid mediators. Sphingolipids emerge as potential regulators of tissue fibrosis because of their modulatory effect on cell migration, gene expression, and cell-cell interactions. In particular, lysophosphatidic acid (LPA) and sphingosine 1-phosphate (S1P) play important roles in the pathogenesis of PF (Shea and Tager, 2012; Pyne et al., 2013). LPA is a key metabolic molecule involved in the *de novo* biosynthesis of phospholipids, causes an increase in bronchoalveolar lavage (BAL) fluid levels in IPF patients compared with the controls (Tager et al., 2008; Natarajan et al., 2013). LPA is mainly generated from phosphatidic acid (PA) by phospholipase A1 or phospholipase A2 (Zhao and Natarajan, 2013). LPA1/LPA2 receptor-deficient mice are proven to be protected from bleomycin-induced pulmonary fibrosis by mediating fibroblasts recruitment and vascular leak (Tager et al., 2008). BMS-986020, a high-affinity small molecule antagonist of LPA1 and being tested in the Phase 2 Trial, improves biomarkers of fibrosis or inflammation (Palmer et al., 2018).

It is also found that sphingosine-1-phosphate (S1P), the final product of sphingolipid metabolism, is upregulated in BAL fluid of IPF patients. S1P can be irreversibly degraded by S1P lyase to hexadecenal and phosphoethanolamine (Nagahashi et al., 2014). S1P lyase over-expression attenuates TGF-β- and S1P-induced differentiation of fibroblasts to myofibroblasts, which was mediated by up-regulating autophagy in lung fibroblasts (Huang and Natarajan, 2015). Sphingosylphosphorylcholine (SPC) is a kind of sheath lipid metabolites, SPC stimulates collagen gel contraction through S1P2 receptor and Rho/Rho kinase pathway, induces the transformation of fibroblasts into myofibroblasts, and participates in airway remodeling, thus provides a new target for the intervention of COPD (Wang et al., 2014). Therefore, targeting sphingolipid metabolism provides a novel therapeutic method of ameliorating human pulmonary fibrosis.

25-hydroxycholesterol (25-HC), enzymatically produced by cholesterol 25-hydroxylase in macrophages, are increased in COPD lungs (Sugiura et al., 2012). The elevated 25-HC may contribute to fibroblasts-mediated lung tissue remodeling by promoting myofibroblasts differentiation and the excessive release of matrix metalloproteinases through the NF-kB-TGF-β-dependent pathway (Ichikawa et al., 2013).

A number of studies have demonstrated an increase in lipid peroxidation products in exhaled breath condensate and bronchoalveolar lavage fluid of patients with PF, suggesting the involvement of lipid peroxidation imbalance in the pathogenesis of PF (Montuschi et al., 1998; Kanoh et al., 2005). Glutathione peroxidases 4 (GPX4), which is commonly referred to as phospholipid hydroperoxide GPX, regulates the oxidative modification of phospholipids, including cholesteryl ester and cardiolipin (Cole-Ezea et al., 2012). Current evidence suggests that GPX4-regulated lipid peroxidation was involved in the TGF-β-induced differentiation of human lung fibroblasts (Tsubouchi et al., 2019). Reducing levels of lipid peroxidation using GPX4 may be a promising therapeutic method for PF.

Lipid mediators, also known as oxidized lipids (oxylipin), are a series of oxidative metabolites generated by the auto-oxidation

of polyunsaturated fatty acids or under the action of specific enzymes (cyclooxygenase, lipoxygenases, cytochromeP450). Prostaglandin E2 (PGE2), a cyclooxygenase-2-derived eicosanoid, is an endogenously produced lipid mediator that inhibits a variety of myofibroblasts functions, including apoptosis, proliferation, and differentiation. The anti-fibrotic cascade of lung myofibroblasts regulation between PGE2 receptors 1–4 and the TGF-β/TGF-β R1/TGF-β R2 signaling pathway, while PGE2 has been reported to directionally reverse most of the genes (708 of 1277) altered by TGF-β (Wettlaufer et al., 2016; Suryadevara et al., 2020). PGE2 can also inhibit myofibroblasts differentiation through AKT dephosphorylation and elimination of PI3K signaling (White et al., 2005). Moreover, inhibition of FOXM1 expression by PGE2 can achieve myofibroblasts dedifferentiation and anti-apoptosis by interfering with the binding of FOXM1 to the promoter elements of the target genes (Penke et al., 2018). Clinical translation of PGE2 may be a promising therapy for PF patients. Losartan enhances the synthesis of PGE2 in experimental pulmonary fibrosis and has been widely used as a new treatment for pulmonary fibrosis in clinical practice (Molina-Molina et al., 2006). Inhalation of PGE2 in the form of liposomes into the lung can effectively improve pulmonary fibrosis, which is expected to become a therapeutic option for inhaled treatment of pulmonary fibrosis (Ivanova et al., 2013).

Lipoxins are also produced from membrane arachidonic acid through biochemical synthesis that involves the enzymes, 5-lipoxygenases, and 15-lipoxygenases (Bannenberg and Serhan, 2010). Lipoxins A4 inhibits various TGF-β1-dependent profibrotic responses in IPF-derived human lung myofibroblasts due to the inhibition of Smad2/3 nuclear translocation, and promotes human lung myofibroblasts dedifferentiation in the resting state (Roach et al., 2015).

Amino acid metabolism in myofibroblasts

Numerous studies have demonstrated that collagen production by lung fibroblasts was independent of extracellular amino acids and mainly relied on the *de novo* production of amino acids (Nigdelioglu et al., 2016). Glycine is the main amino acid involved in the synthesis of collagen. During the *de novo* synthesis of glycine, the amino group provided by glutamate converts the glycolytic intermediate 3-phosphoglycerate into glycine, combined with the participation of phosphoglycerate dehydrogenase, phosphorylated serine aminotransferase 1, phosphorylated serine phosphatase and serine hydroxymethyltransferase 2 (Hamanaka and Mutlu, 2021). TGF-β induces the expression of the aforementioned enzymes, while the inhibition of *de novo* glycine synthesis caused by the phosphoglycerate dehydrogenase inhibitor, NCT503, decreases levels of bleomycin-induced lung failure in mice (Hamanaka et al., 2018).

Phosphoserine transaminase 1 is a key enzyme involved in serine synthesis (Jiang et al., 2020), and its loss is sufficient to inhibit collagen synthesis. It has been documented that TGF-β promotes the accumulation of activating transcription factor 4 (ATF4), which is required for the increased expression of serine-glycine synthesis enzymes in response to TGF-β. Furthermore, TGF-β activates the PI3K-Akt-mTOR pathway, while inhibition of PI3K prevents the activation of downstream signaling pathways and the induction of ATF4 (O'Leary et al., 2020), indicating that mTORC1 and ATF4 are important regulators of serine-glycine metabolic reprogramming in myofibroblasts.

De novo proline biosynthesis has also been found to be involved in pulmonary fibrosis. α-ketoglutarate, an intermediate of the citric acid cycle, is converted to glutamate by glutamate transaminase. Δ1-pyrroline-5-carboxylic acid synthase, which is encoded by the aldehyde dehydrogenase 18A1, is responsible for the conversion of glutamate to pyrrole acid, which is then converted to proline by pyrroline-5-carboxylate reductase. During the process of the *de novo* conversion of proline from glutamate, its knockout is sufficient to inhibit collagen production in lung fibroblasts (Hamanaka et al., 2019).

Glutaminolysis has been recently shown to be required for myofibroblast differentiation and collagen production (Bernard et al., 2018). Glutamine is first converted to glutamate by glutaminase (GLS) and then converted to α-ketoglutarate by glutamate dehydrogenase or aminotransferases. This process complements the Krebs cycle, which supports cellular energy production and biosynthetic reactions (Altman et al., 2016). TGF-β1-induced glutaminolysis underlies the persistent activation of HIF-1 by increasing succinate and fumarate levels, thereby supporting the glycolytic switch. TGF-β1 induces GLS1 expression *via* SMAD3 and p38-MAPK-dependent signaling pathways, which are accompanied by enhanced levels of glutaminolysis in myofibroblasts. The GLS1 inhibitor, CB-839, exerts a protective effect in mice exposed to bleomycin or adenovirus expressing active TGF-β1 (Bernard et al., 2018; Esguerra and Zhao, 2019). Additionally, PPAR-γ is a regulator of GLS1-mediated glutaminolysis (Genovese et al., 2005). Morin (3, 5, 7, 2, 4-pentahydroxyflavonoid) has recently been shown to inhibit the transformation of fibroblasts to myofibroblasts by activating PPAR-γ, decreasing GLS1 protein levels, and inhibiting glutaminolysis, thereby enhancing DEPTOR stability through the intervention of the 2-hydroxyglutarate-KDM4A axis (Miao et al., 2022). The glutamine metabolite, 2-hydroxyglutarate (Chowdhury et al., 2011; Carbonneau et al., 2016), is a specific inhibitor of Jumonji domain-containing histone demethylases activity. DEPTOR is extremely unstable, whereas catalytically active KDM4A, a Jumonji domain-containing histone demethylases, negatively regulates mTORC1 activation. Glutaminolysis-related mTOR activation in organ fibrosis not only regulates collagen expression but also

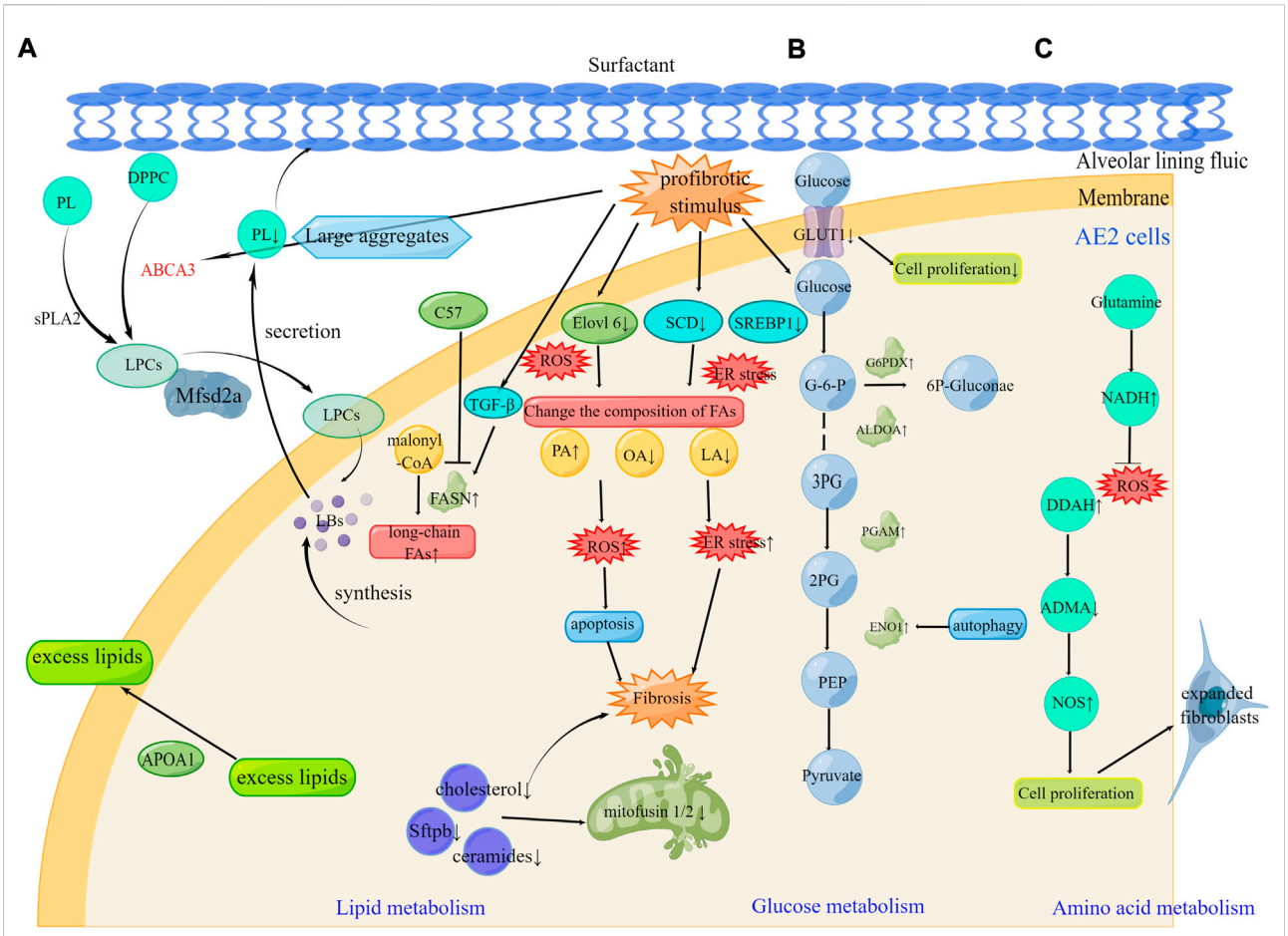


FIGURE 2
Metabolic reprogramming of AE2 cells in pulmonary fibrosis **(A)**. Alteration of FAs composition leading to ER stress and ROS, abnormal lipid uptake on the lung surface, and reduced lipid production caused by mitochondrial destruction all contribute to fibrosis progression. The therapeutic targets Mfsd2a, FASN, and ApoA1 can be effective in the development of pulmonary fibrosis **(B)**. Under profibrotic stimulus, increased PGAM, ENO1, ALDOA, and G6PDX affect glucose metabolism. The therapeutic targets GLUT1 and ENO1 can be effective in the development of pulmonary fibrosis **(C)**. Under profibrotic stimulus, increased DDAH activity inhibited the NOS inhibitor ADMA contributing to the pool of expanded fibroblasts. The therapeutic targets glutamine and DDAH can be effective in the development of pulmonary fibrosis. DPPC, Dipalmitoylphosphatidylcholine; sPLA2, secreted phospholipase 2; LPCs, lysophosphatidylcholines; LBs, Lamellar bodies; SCD, stearyl CoA desaturase; SREBP1, sterol regulatory element-binding protein 1; ER stress, endoplasmic reticulum stress; FA, Fatty acid; PA, Palmitic acid; OA, oleic acid; LA, linoleic acid; G6PDX, glucose-6-phosphate dehydrogenase; ALDOA, aldolase A fructose bisphosphate; PGAM, phosphoglycerate mutase; ENO1, enolase 1; DDAH, dimethylaminohydrolase; ADMA, asymmetric dimethylarginine.

controls autophagy and mitochondrial levels in myofibroblasts (Ge et al., 2018). Notably, the mTOR inhibitor, rapamycin, attenuates inflammatory cell infiltration and collagen deposition, thereby antagonizing PF (Gui et al., 2015). In addition to rapamycin, some studies have found that Morin, a natural flavonoid, affects mTOR1 to achieve anti-fibrosis.

Cytosolic glutamate is critical for maintaining redox balance and protecting cells from oxidative stress by producing glutathione (GSH) (Chen and Cui, 2015). Nuclear factor-erythroid 2-related factor 2 (Nrf2) binds to the antioxidant response elements and stimulates the transcription of antioxidant proteins, as well as proteins involved in GSH biosynthesis and regeneration. Increased GSH production by Nrf2 activation may inhibit myofibroblast activation by limiting glutamate availability for cell growth (Motohashi and Yamamoto, 2004). Tanshinone IIA, a Chinese herbal medicine derived from Salvia miltiorrhiza, inhibits fibrotic responses and TGF-β1-dependent epithelial-to-mesenchymal transition in pulmonary fibrosis. Tanshinone IIA activation of Nrf2 depletes glutamate involved in GSH synthesis, thereby inhibiting myofibroblast activation (An et al., 2019). An individual's ability to regulate antioxidant defense mechanisms, such as GSH levels in response to cigarette smoke, has also been linked to the development of COPD in smokers (Snider, 1989). Smoke inhibits fibroblasts repair, reflected in collagen gel contraction and fibronectin production, possibly regulated by intracellular GSH levels (Kim et al., 2002).

Alveolar epithelial cells

Alveolar epithelial (AE) cells include alveolar epithelial type I (AE1) and alveolar epithelial type II (AE2) cell types that integrate into the epithelium at extensive intercellular junctions (Ruaro et al., 2021). AE2 cells are the major driver of PF pathogenesis (Winters et al., 2019). Dysregulation of lipid, glucose, and amino acid metabolism in AE2 cells have been demonstrated during the development of PF (Figure 2).

Lipid metabolism in alveolar epithelial type II cells

De novo lipid synthesis, an important feature of AE2 cells, is required to generate lipid-rich surfactants, by which respiratory epithelial cells can be soaked in by reducing surface tension and resisting environmental challenges (Ingenito et al., 2000; Schmidt et al., 2001). The reprogramming of lipid metabolism in AE2 cells is one of the main mechanisms that lead to PF.

Dipalmitoylphosphatidylcholine, the main pulmonary surfactant phospholipid (PL) secreted by AE2 (Pérez-Gil, 2008), is synthesized by fatty acid acyl chain remodeling *via* the cyclic activity of Land on unsaturated fatty acids (FAs). Dipalmitoylphosphatidylcholine is then transported to lysosomes called lamellar bodies *via* the surfactant transporter ABCA3 like organelles. Lamellar bodies are secreted into large aggregated membrane bilayers and are rapidly absorbed into the PL monolayers to form lung surfactant films. Through the ventilation process, the surfactant film becomes disordered, and the surfactant PL has also been shown to be hydrolyzed by secreted phospholipase in the alveolar space to generate lysophosphatidylcholines (Bernhard et al., 2004; Ban et al., 2007). Previous studies have found that mutations in ABCA3, such as the most common missense mutation E292V, lead to the development of IPF. Mutations in ABCA3 result in chronic surfactant insufficiency and decrease PL in bronchoalveolar lavage (Beers et al., 2017). Inhibition of Mfsd2a in AE2 cells results in hypertrophy, a lack of steady-state surfactant levels, and alteration in surfactant lipid composition (Wong et al., 2022). Since Mfsd2a plays an important role in maintaining surfactant homeostasis, it remains to be determined whether it can play a role in pulmonary fibrosis.

Fatty acid synthase (FASN) is an essential anabolic enzyme for the *de novo* synthesis of FAs (Menendez and Lupu, 2007). FASN catalyzes the reduction of malonyl-CoA to synthesize long-chain fatty acids (Chung et al., 2019). TGF-β has been reported to increase FASN expression in mouse and human fibroblasts in a smad2/3-dependent, mTORC1-dependent manner. Most importantly, cyanin-derived FASN inhibitor C75, reduces the expression of profibrotic genes and stabilizes lung function (Jung et al., 2018). Recent studies performed mRNA sequencing of lung tissue obtained from surgical lung biopsies of patients with early IPF and IPF during transplantation, and have verified that FASN is downregulated in AE cells, ciliated cells, and alveolar macrophages in IPF lung tissue (Qian et al., 2021). Moreover, the loss of AE2 cell-specific FASN results in a reduction of lipid synthesis and aggravates pulmonary fibrosis induced by bleomycin (BLM). The role of FASN during lipid metabolism in pulmonary fibrosis needs to be explored further.

Elongation and desaturation of FAs from the core of lipid biosynthesis determines their function and metabolic fate. Enzymes that are involved in FA elongation and saturation, such as stearyl CoA desaturase, and related molecules, such as sterol regulatory element-binding protein 1, have been reported to be down-regulated during the development of PF, with endoplasmic reticulum stress playing an important role in the downregulation. The elongation of long-chain FAs family member 6 (Elovl6), an important rate-limiting enzyme of lipid biosynthesis, catalyzes the extension reaction of palmitate (C16:0) to stearate (C18:0). The loss of Elovl6 induces apoptosis and the production of reactive oxygen species, and most importantly, impairs cellular uptake of long-chain FAs (Sunaga et al., 2013). Elovl6-mediated FA metabolism in AE2 cells is perturbed in models of pulmonary fibrosis, which may have important implications for lung pathology and therapy.

Lipid synthesis is regulated not only by lipid synthases but also by other molecular mechanisms. Apolipoprotein A1, the most abundant protein in high density lipoprotein, has recently been found to be potentially increased in the lung tissue by alveolar epithelial cells and macrophages, to remove excess lipids from cells to prevent lipid overload. ApoA1 exerts a protective effect against lung injury and fibrosis (Kim et al., 2010; Eh et al., 2013; Gordon et al., 2016).

Emerging evidence suggests that mitochondrial disturbances and reduced levels of energy production lead to the disturbance of various metabolic processes (Shaghaghi et al., 2021). The mitochondrial damage-induced loss of mitofusin 1 and mitofusin 2, GTPase proteins that coordinates the fusion of the mitochondrial outer membrane, abolishes the lipogenic metabolic responses of the AE2 cells, which finally leads to pulmonary fibrosis (Chung et al., 2019). Dysregulated lipogenic metabolic responses include the reduced production of liposomes, such as cholesterol and ceramides, and the significant down-regulation of surfactant protein genes (Sftpb, Sftpc). Overall, AE2 lipid metabolism deficiency drives pulmonary fibrosis, providing an innovative mechanism and potential pharmacological target.

Glucose metabolism in alveolar epithelial type II

Aerobic glycolysis and pentose phosphate pathways are essential for AE2 cell activation, proliferation, and regeneration (Li et al., 2019). During the early stage of PF, the lactose levels are elevated in AE2 cells due to the "Warburg effect", which then induces an increase in TGF-β expression that

promotes fibrosis. However, during the middle and late stages, the levels of most glycolytic metabolites are decreased in AE2 cells (Roque and Romero, 2021). Recent studies have shown that the expression of key glycolytic enzymes, such as phosphoglycerate mutase, enolase 1, and aldolase A fructose bisphosphate are elevated in PF. The rate-limited enzyme glucose-6-phosphate dehydrogenase of the pentose phosphate pathway is also upregulated. Autophagy is responsible for alterations of enolase 1 levels during AE2 cell proliferation and the regulation of lung homeostasis in PF (Li X. et al., 2020). Inhibition of autophagy reduces glucose uptake, and glucose deprivation or blockade of glycolysis reduces the proliferative capacity of AE2 cells and promotes their differentiation into ciliated and secretory cells (Aboushousha et al., 2021). In addition to the above-mentioned metabolic enzymes that lead to enhanced glucose metabolism, GLUT1 also plays an important role. During bleomycin-induced injury, conditional deletion of GLUT1 reduces AE2 cell proliferation and impairs AE2 cell recovery *in vivo*. Under this injury condition, the glycolysis and pentose phosphate pathways are enhanced in AE2 cells (Li J. et al., 2020). Thus, the role of aerobic glycolysis and pentose phosphate pathways in AE2 cells in pulmonary fibrosis provides a basis for a better understanding of pulmonary homeostasis and injury repair.

Amino acid metabolism in alveolar epithelial type II

The demand for amino acids increases during various pathological conditions, including pulmonary fibrosis (Gaugg et al., 2019). Glutamine is involved in antioxidant defense through multiple mechanisms, including the production of NADPH to regulate the synthesis of various ROS detoxification enzymes and the core protein of cellular antioxidant defense glutathione. It has been demonstrated that a profound metabolic shift occurs during glucose metabolism, requiring cells to rely on other metabolic fuels, such as glutamine, to support mitochondrial respiration and metabolite production, thereby inhibiting the progression of pulmonary fibrosis (Shaghaghi et al., 2021). Mechanically, diminished mitochondrial respiratory function in pulmonary fibrosis can be restored by adding glutamine to the culture medium of AE2 cells. Except for directly increasing the amino acid content, enzymes that regulate amino acid metabolism are equally important for protection against pulmonary fibrosis. Dimethylarginine dimethylaminohydrolase metabolizes asymmetric dimethylarginine and monomethylarginine to l-citrulline and dimethylamine, both of which are endogenous inhibitors of NOS (Pullamsetti et al., 2011). Dimethylarginine dimethylaminohydrolase inhibitors increase intracellular asymmetric dimethylarginine concentrations to levels that are sufficiently to inhibit NOS activity, resulting in the inhibition of pulmonary fibrosis progression. Together, these studies underlie the important role of amino acid metabolism and may offer possible therapeutic avenues for the attenuation of pulmonary fibrosis.

Macrophages

Pulmonary macrophage populations are mainly composed of alveolar macrophages (AMs) and interstitial macrophages (IMs), which reside in the alveoli and parenchyma respectively (Guilliams et al., 2013). In addition, pulmonary macrophages can also change their phenotype through polarization into either classically activated macrophages (M1) or alternatively activated macrophages (M2), which play important roles in homeostasis and tissue remodeling in PF (Locati et al., 2013).

Glucose metabolism in macrophages

M1 macrophages mainly rely on glycolysis for energy and pro-inflammatory effects, while M2 macrophages preferentially utilize oxidative phosphorylation to promote repair of pulmonary tissue damage (Viola et al., 2019). Enhanced glycolysis in alveolar macrophages obtained from fibrotic lungs is caused by the increased expression of important glycolytic mediators or enzymes induced by the M1 activator, IFN-γ, and LPS, such as GLUT1, hexokinase 2, phosphofructokinase liver type and LDHB (Xie et al., 2017). However, these molecules are not induced by the M2 inducers, IL-4, IL-10, or TGF-1. Moreover, inhibition of glycolysis mitigates the increase in the expression of M2 phenotype markers in alveolar macrophages obtained from fibrotic lungs (Xie et al., 2017).

Except during the inflammatory response, macrophages also rely on glycolysis to produce high levels of lactate (Soto-Heredero et al., 2020), which sustain a low pH in the extracellular space and activate TGF-β1-induced fibrotic signaling (Kottmann et al., 2012). The silencing of LDHA, the enzyme that catalyzes lactate production, can suppress silica exposure-induced high levels of iNOS, TNF-α, Arg-1, IL-10, and MCP1 in NR8383 alveolar macrophages (Mao et al., 2021). Mechanically, lactate can increase histone lactylation at the profibrotic gene promoters of macrophages (Cui et al., 2021), providing a novel therapeutic target for PF. The regulation of lactate level can be accomplished by directly blocking lactate production in lung macrophages, or by depleting extracellular lactate, thereby reducing lactate entry into lung macrophages and other cell types. The LDHA inhibitor gossypol inhibits ionizing radiation- and bleomycin-induced pulmonary fibrosis (Judge et al., 2017). Oxalate, a competitive inhibitor of LDHA, has

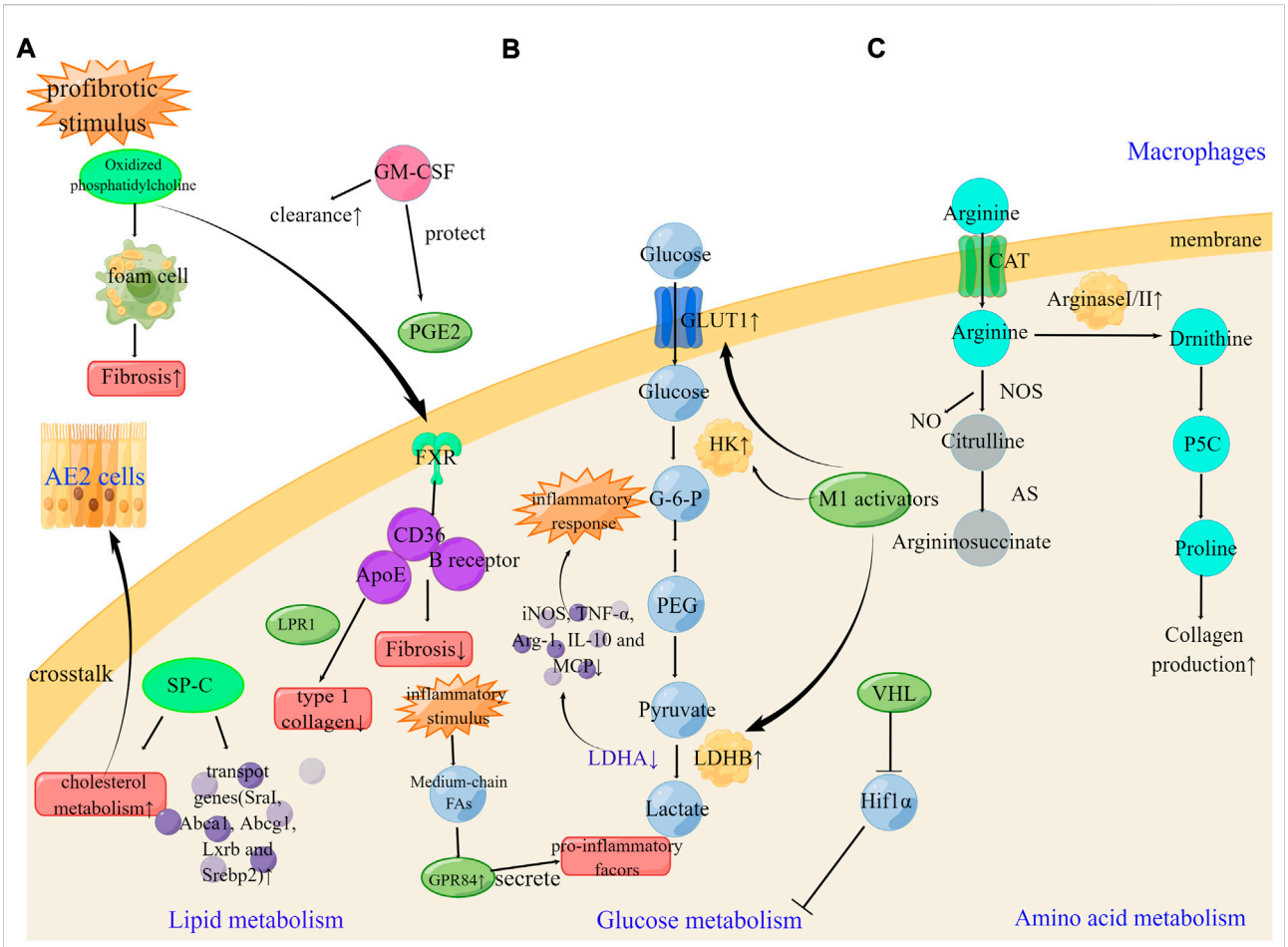


FIGURE 3
Metabolic reprogramming of macrophages cells in pulmonary fibrosis **(A)**. GM-CSF, SP-C, and FXR can enhance the clearance of oxidized lipids and regulate lipid metabolism. The therapeutic targets FXR, ApoE and GPR84 can be effective in the development of pulmonary fibrosis **(B)**. Under profibrotic stimulus, M1 activators increase GLUT1, hexokinase, and LDHB leading to enhance glucose metabolism. Silencing of LDHA can suppress high levels of iNOS, TNF-α, Arg-1, IL-10, and MCP1. The therapeutic targets LDHA and VHL can be effective in the development of pulmonary fibrosis **(C)**. Arginase metabolism is partially dependent on the transport of arginine through CAT2 in peritoneal macrophages. The therapeutic targets Arginase can be effective in the development of pulmonary fibrosis. SP-C, surfactant protein C; LPR1 lipoprotein receptor–related protein 1; B receptor; B class oxidized phospholipid scavenger receptor.

likewise been shown to maintain macrophage homeostasis by ameliorating the increase in glycolysis and endoplasmic reticulum stress induced by the exposure of macrophages to silica (Mao et al., 2022).

Under normoxia, HIF1α is kept at low levels due to the recognition and ubiquitination of E3 ligase von Hippel-Lindau (VHL) and the ensuing proteasomal degradation (Semenza, 2011). Loss of VHL results in an upshift in glycolysis, impairs mitochondrial respiration and alters gene expression characteristics in the AMs. VHL regulates the transcription of Spp1, a hypoxia-responsive gene in tumor cells, *via* inhibiting HIF1α-mediated glycolytic metabolism in AMs (Zhang et al., 2018), indicating that VHL is a key regulator of alveolar macrophages in PF (Figure 3).

Metabolic dysfunction is a key factor in the toxicity of cigarette smoke on alveolar macrophages. Cigarette smoke inhibits mitochondrial respiration in alveolar macrophages while inducing glycolysis and reactive oxygen species. These defects were alleviated by the free radical scavenger N-acetylcysteine, which also restored phagocytosis to baseline levels (Aridgides et al., 2019). CPUY192018, a nuclear factor erythrocyte-2-related factor 2 (Nrf2) activator, can inhibit glycolysis, enhance antioxidant stress, and produce satisfactory therapeutic effects on macrophages of COPD patients and cigarette smoke extract-induced COPD mice, which is expected to be a potential treatment for COPD (Wang L. et al., 2021). These studies provide a further fundamental mechanistic basis for the use of antioxidants in COPD.

Lipid metabolism in macrophages

Profibrotic injury-induced early and persistent metabolic changes in AE2 cells, which then lead to the inhibition of lipid synthesis and the release of stored lipids into the distal airspaces of the lung. Subsequently, the extracellular accumulation of oxidized lipids promoted the development of macrophage foam cells, which results in a fibrotic cascade (Ingenito et al., 2000; Schmidt et al., 2001; Forbes et al., 2007). Granulocyte-macrophage colony-stimulating factor (GM-CSF) is a 23-kDa glycoprotein member of the hematopoietic cytokine family that regulates the proliferation and differentiation of cells of the granulocyte-macrophage lineage (Baldwin, 1992). Recently, GM-CSF has been shown to improve pulmonary fibrosis *via* regulating lipid metabolism. Oxidized phosphatidylcholine is sufficient to induce foam cell formation and can promote fibrosis in mice, while GM-CSF treatment can enhance lipid clearance in macrophages (Romero et al., 2015). PGE2 exerts a protective effect on fibroblasts as previously mentioned, and GM-CSF deficiency leads to an enhanced level of fibrosis in bleomycin-induced pulmonary fibrosis, with a mechanism of action involved in this effect identified as the impaired production of potent anti-fibrotic PGE2 in macrophages (Moore et al., 2000). GM-CSF not only enhanced the clearance of oxidized lipids in macrophages but also prevented damage to anti-fibrotic molecules. PGD2, another COX metabolite, is produced in CD68-positive monocytes/macrophages, and may inhibit immune cell infiltration in an autocrine or paracrine manner by inhibiting inflammation in bleomycin-induced pulmonary fibrosis (Kida et al., 2016). Pharmacological approaches that enhance lipid efflux or prevent foam cell formation may be promising for preventing or treating pulmonary fibrosis.

A multitude of evidence has indicated the key role of surfactant protein C deficiency for the pathogenesis of IPF (Ruwisch et al., 2020; Sehlmeyer et al., 2020). Increased cholesterol levels in mouse lung tissue after bleomycin treatment have been attributed to paracrine lipid crosstalk between alveolar epithelial cells and alveolar macrophages. Preliminary observations suggest that this crosstalk may be impaired by the absence of surfactant protein C. The addition of surfactant protein C to cholesterol-containing lipid vesicles enhances the expression of cholesterol metabolism and transport genes (such as Pparg, SraI, Abca1, Abcg1, Lxrb and Srebp2) in alveolar macrophage cell lines (Ruwisch et al., 2020), which is a potential novel lipid-protein axis involved in lung remodeling in PF.

Apolipoprotein E (ApoE) is produced almost exclusively by monocyte-derived Alveolar macrophages. The expression of ApoE is significantly increased and enriched in dense fibrotic regions of IPF lungs. ApoE depends on lipoprotein receptor–related protein 1 to promote macrophage phagocytosis of type 1 collagen (Cui et al., 2020).

Several transcription factors and fatty acid receptors regulate lipid homeostasis in macrophages and have been implicated in the progression of pulmonary fibrosis. Nitrogen mustard, a known lung-targeting vesicular agent, can cause acute injury and fibrosis, and activated macrophages have been demonstrated to contribute to the pathological response to nitrogen mustard. Nitrogen mustard-induced changes sustained oxidative stress, and are mediated by Nrf2 and iNOS signaling pathways, which are associated with the accumulation of oxidized phospholipids in lung macrophages and epithelial cells (Venosa et al., 2019). The farnesoid-X receptor (FXR) has been hypothesized to regulate intracellular lipids. The number of FXR-positive macrophages in the lung is increased after nitrogen mustard administration and may represent a compensatory attempt to limit the fibrotic process. The FXR agonist, obeticholic acid, inhibited the development of bleomycin-induced fibrosis, potentially due to the attenuated production of key inflammatory mediators. At present, putative FXR targets include the B class oxidized phospholipid scavenger receptor, CD36, and the lipid chaperone, ApoE (Silverstein et al., 2010; Li et al., 2012).

G-protein-coupled receptor 84 (GPR84), the fifth most recognized fatty acid receptor, is involved in initiating Gi signaling, resulting in reduced cAMP production through the inhibition of adenylate cyclase. Medium-chain fatty acids with a chain lengths of C9-C14 are GPR84 agonists. After acute inflammatory stimulation, Medium-chain fatty acids activated GPR84 to promote phagocytosis and secrete pro-inflammatory factors (Chen et al., 2020; Marsango et al., 2022). Current research has demonstrated that GPR84 antagonists have great potential for the treatment of pulmonary fibrosis. However, further studies are needed to determine whether clinical translation can be achieved (Figure 3).

Amino acid metabolism in macrophages

Arginine is a precursor for proline and polyamine synthesis, and since proline is an important component of collagen, the supply of proline may be a key factor during the process of pulmonary fibrosis. Arginine metabolizing enzymes are involved in the production of proline or polyamines (Durante et al., 2001; Ignarro et al., 2001). Arginase exists as two subtypes, the hepatic (arginase I) subtype and the extrahepatic (arginase II) subtype. Previous studies have emphasized that both arginase I and II are induced during bleomycin-induced pulmonary fibrosis. Arginase I is induced in macrophages, whereas arginase II is induced in a variety of cells, including macrophages and myofibroblasts. Arginine is transported into the intracellular space by cationic amino acid transporters (CATs) and is a precursor for the synthesis of urea, polyamines,

phosphocreatine, nitric oxide, and proteins (Endo et al., 2003). More importantly, arginase activity is partially dependent on the transport of arginine through CAT2 in peritoneal macrophages. Therefore, arginase may play a role in CAT2-mediated pulmonary fibrosis (Niese et al., 2010), emphasizing the role of amino acid metabolism reprogramming in pulmonary fibrosis. At the steady state, IMs express 10-fold more arginase I than AMs, while Arg-140-fold upregulation has been detected in IMs isolated from radiation-induced lung fibrosis. The expression of colony-stimulating factor receptor-1 was mainly expressed on IMs, and the use of anti-CSF1R neutralizing antibody results in the specific depletion of pro-fibrotic IMs, without affecting the number of AMs, and can also reverse radiation-induced lung fibrosis (Meziani et al., 2018) (Figure 3).

Endothelial cells

Early observations of pulmonary fibrosis show that vascular abnormalities, including pulmonary system anastomosis and neovascularization around the fibrotic area (Hamada et al., 2007; Ley et al., 2011), along with the metabolic disturbance of ECs play an important role (Lee et al., 2020).

Glucose metabolism in endothelial cells

Pulmonary microvascular endothelial cells (PMVECs) are highly glycolytic due to their rapid growth rate (Parra-Bonilla et al., 2010). This active form of glycolysis induces extracellular acidosis, which inhibits PMVECs migration, while glycolysis acts as a negative feedback mechanism. KD025 (SLx-2119) is a relatively new inhibitor of Ras homolog-related kinase subtype 2. Studies have shown that KD025 shifts the PMVEC metabolic pathway from glycolysis to oxidative phosphorylation in a Ras homolog-related kinase subtype 2-independent manner, reduces intracellular pH and cell migration, and enhances the integrity of the lung endothelial barrier *in vivo* (Lee et al., 2020). Currently, KD025 is being tested in multiple Phase II clinical trials for use in the treatment of fibrotic lung disease, including idiopathic pulmonary fibrosis.

The role of HIF-1 in the reprogramming of glucose metabolism in pulmonary fibrosis has been previously mentioned, and identification of the switch from HIF-1 to HIF-2 in endothelial cells (EC) can ensure the continued activity of the hypoxia-adaptive pathway, thereby prolonging the hypoxia survival time. The conversion of HIF-1 to HIF-2 was disturbed by the stabilization of HIF1α and endothelial PAS domain protein 1 mRNAs in EC, which then induced the reprogramming of glucose metabolism. Exploiting the regulation of endothelial cell adaptation to hypoxia may be a potential therapeutic intervention against pulmonary fibrosis (Bartoszewski et al., 2019).

Lipid metabolism in endothelial cells

IL-6 is a pro-inflammatory cytokine produced by endothelial cells and is actively involved in local vascular inflammatory responses (Podor et al., 1989). Previous studies have investigated the intracellular fatty acid composition modulated the production of IL-6, which is elevated in bleomycin-induced lung endothelial cells in a time-dependent and dose-dependent manner. In other words, endothelial IL-6 production may be upregulated by 18:2 n-6 and/or its derived metabolites, although this process is not directly dependent on prostacyclin or other cyclooxygenase metabolites. It has been currently established that a diet lower than 18:2 n-6 can exert a protective effect against bleomycin-induced pulmonary fibrosis (Karmiol et al., 1993). However, the fatty acid effects exerted by lipoxygenase and/or cyclooxygenase metabolites require further studies to confirm whether they can be used as a novel method of treatment for PF.

Oxidative stress-induced activation of phospholipase D and related lipid signaling enzymes are key factors involved in ECs' dysfunction, leading to altered pulmonary vascular pathophysiology during oxidative exposure in pulmonary hypertension and pulmonary fibrosis (Parinandi et al., 1999). In addition, bleomycin-induced cytotoxicity of bovine lung microvascular ECs may be due to the signaling cascade involving PA and other PA-derived signaling mediators, such as LPA and diacylglycerol (Patel et al., 2011). Therefore, the phospholipase D pathway in vascular endothelial cells may be a potential therapeutic target for PF.

Perspectives

Previous studies have found that men have a 40% higher risk of transplant or death than women in pulmonary fibrosis (PF) (Zaman et al., 2020). Higher smoking rates in men may account for some of the differences in gender (Ley and Collard, 2013), while mutations in telomerase and surfactant proteins associated with PF fared better in women than in men (Pandit et al., 2020). Whether there is some metabolic difference related to gender in the development of pulmonary fibrosis needs further exploration. With the advent of novel and cost-effective metabolite profiling techniques, metabolic reprogramming has been found to occur during the pathogenic process of pulmonary fibrosis. In this review, we showed that glucose metabolism is enhanced in fibroblasts, macrophages, and vascular endothelial cells, but inhibited in epithelial cells, which results in the targeting of glycolysis during pulmonary fibrosis. The enzymes and related molecular pathways were found to be therapeutically advantageous. Lipid metabolism is mainly characterized by increased lipid synthesis and fatty acid oxidation in fibroblasts, macrophages, and vascular endothelial cells. In epithelial cells, lipid metabolism is inhibited at an early stage, resulting in the accumulation of lipid oxidation. Enzymes, key molecular pathways of fatty acid oxidation, and lipid mediators form the core of currently available treatment

methods. Amino acids, which are the main components of collagen, show increased levels of synthesis or decreased levels of decomposition in fibroblasts, macrophages, and epithelial cells. Therefore, the targeting of important enzymes in amino acid metabolism may be a main therapeutic strategy. Future research is required to promote the development and translation of drugs that target the metabolic disturbance in PF.

Author contributions

JL and XZ guided the scope and research background of the research and wrote the manuscript. XS and SC wrote the original version of this manuscript. QY and JW critically revised the manuscript.

Funding

This study was supported by the State Key Program of the National Natural Science Foundation of China (82030059), National Natural Science Foundation of China (82102292, 81900435, 82172178, 82072144, 81873950, 81873953, 81960420, 81901934), Natural Science Foundation of Shandong Province (ZR2021LSW003, ZR2021MH231), National Key R&D Program of China (2020YFC1512700, 2020YFC1512705, 2020YFC1512703), National S&T Fundamental Resources Investigation Project (2018FY100600, 2018FY100602), Taishan Pandeng Scholar Program of Shandong Province (tspd20181220), Taishan Young Scholar Program of Shandong Province (tsqn20161065, tsqn201812129), Youth Top-Talent Project of National Ten Thousand Talents Plan, and Qilu Young Scholar Program, High-level Talents Project of Natural Science Foundation of Hainan Province (2019RC222). All the figures were created by Figdraw (www.figdraw.com)

Conflict of interest

The authors declare that the research was conducted in the absence of any commercial or financial relationships that could be construed as a potential conflict of interest.

Publisher's note

All claims expressed in this article are solely those of the authors and do not necessarily represent those of their affiliated organizations, or those of the publisher, the editors and the reviewers. Any product that may be evaluated in this article, or claim that may be made by its manufacturer, is not guaranteed or endorsed by the publisher.

References

Aboushousha, R., Elko, E., Chia, S. B., Manuel, A. M., van de Wetering, C., van der Velden, J., et al. (2021). Glutathionylation chemistry promotes interleukin-1 beta-mediated glycolytic reprogramming and pro-inflammatory signaling in lung epithelial cells. *FASEB J.* 35, e21525. doi:10.1096/fj.202002687RR

Altman, B. J., Stine, Z. E., and Dang, C. V. (2016). From Krebs to clinic: Glutamine metabolism to cancer therapy. *Nat. Rev. Cancer* 16, 619–634. doi:10.1038/nrc.2016.71

Alysandratos, K. D., Russo, S. J., Petcherski, A., Taddeo, E. P., Acín-Pérez, R., Villacorta-Martin, C., et al. (2021). Patient-specific iPSCs carrying an SFTPC mutation reveal the intrinsic alveolar epithelial dysfunction at the inception of interstitial lung disease. *Cell Rep.* 36, 109636. doi:10.1016/j.celrep.2021.109636

An, L., Peng, L. Y., Sun, N. Y., Yang, Y. L., Zhang, X. W., Li, B., et al. (2019). Tanshinone IIA activates nuclear factor-erythroid 2-related factor 2 to restrain pulmonary fibrosis via regulation of redox homeostasis and glutaminolysis. *Antioxid. Redox Signal.* 30, 1831–1848. doi:10.1089/ars.2018.7569

Aridgides, D. S., Mellinger, D. L., Armstrong, D. A., Hazlett, H. F., Dessaint, J. A., Hampton, T. H., et al. (2019). Functional and metabolic impairment in cigarette smoke-exposed macrophages is tied to oxidative stress. *Sci. Rep.* 9, 9624. doi:10.1038/s41598-019-46045-7

Baldwin, G. C. (1992). The biology of granulocyte-macrophage colony-stimulating factor: Effects on hematopoietic and nonhematopoietic cells. *Dev. Biol.* 151, 352–367. doi:10.1016/0012-1606(92)90175-g

Ban, N., Matsumura, Y., Sakai, H., Takanezawa, Y., Sasaki, M., Arai, H., et al. (2007). ABCA3 as a lipid transporter in pulmonary surfactant biogenesis. *J. Biol. Chem.* 282, 9628–9634. doi:10.1074/jbc.M611767200

Bannenberg, G., and Serhan, C. N. (2010). Specialized pro-resolving lipid mediators in the inflammatory response: An update. *Biochim. Biophys. Acta* 1801, 1260–1273. doi:10.1016/j.bbalip.2010.08.002

Bartoszewski, R., Moszyńska, A., Serocki, M., Cabaj, A., Polten, A., Ochocka, R., et al. (2019). Primary endothelial cell-specific regulation of hypoxia-inducible factor (HIF)-1 and HIF-2 and their target gene expression profiles during hypoxia. *FASEB J.* 33, 7929–7941. doi:10.1096/fj.201802650RR

Beers, M. F., Knudsen, L., Tomer, Y., Maronn, J., Zhao, M., Ochs, M., et al. (2017). Aberrant lung remodeling in a mouse model of surfactant dysregulation induced by modulation of the Abca3 gene. *Ann. Anat.* 210, 135–146. doi:10.1016/j.aanat.2016.11.015

Bernard, K., Logsdon, N. J., Benavides, G. A., Sanders, Y., Zhang, J., Darley-Usmar, V. M., et al. (2018). Glutaminolysis is required for transforming growth factor-β1-induced myofibroblast differentiation and activation. *J. Biol. Chem.* 293, 1218–1228. doi:10.1074/jbc.RA117.000444

Bernard, K., Logsdon, N. J., Ravi, S., Xie, N., Persons, B. P., Rangarajan, S., et al. (2015). Metabolic reprogramming is required for myofibroblast contractility and differentiation. *J. Biol. Chem.* 290, 25427–25438. doi:10.1074/jbc.M115.646984

Bernhard, W., Pynn, C. J., Jaworski, A., Rau, G. A., Hohlfeld, J. M., Freihorst, J., et al. (2004). Mass spectrometric analysis of surfactant metabolism in human volunteers using deuteriated choline. *Am. J. Respir. Crit. Care Med.* 170, 54–58. doi:10.1164/rccm.200401-089OC

Carbonneau, M., M Gagné, L., Lalonde, M. E., Germain, M. A., Motorina, A., Guiot, M. C., et al. (2016). The oncometabolite 2-hydroxyglutarate activates the mTOR signalling pathway. *Nat. Commun.* 7, 12700. doi:10.1038/ncomms12700

Chen, L., and Cui, H. (2015). Targeting glutamine induces apoptosis: A cancer therapy approach. *Int. J. Mol. Sci.* 16, 22830–22855. doi:10.3390/ijms160922830

Chen, L. H., Zhang, Q., Xie, X., and Nan, F. J. (2020). Modulation of the G-protein-coupled receptor 84 (GPR84) by agonists and antagonists. *J. Med. Chem.* 63, 15399–15409. doi:10.1021/acs.jmedchem.0c01378

Chen, S., Jiang, S., Hu, F., Xu, Y., Wang, T., and Mei, Q. (2017). Foxk2 inhibits non-small cell lung cancer epithelial-mesenchymal transition and proliferation through the repression of different key target genes. *Oncol. Rep.* 37, 2335–2347. doi:10.3892/or.2017.5461

Chen, W., Zhang, J., Zhong, W., Liu, Y., Lu, Y., Zeng, Z., et al. (2021). Anlotinib inhibits PFKFB3-driven glycolysis in myofibroblasts to reverse pulmonary fibrosis. *Front. Pharmacol.* 12, 744826. doi:10.3389/fphar.2021.744826

Cho, S. J., Moon, J. S., Lee, C. M., Choi, A. M., and Stout-Delgado, H. W. (2017). Glucose transporter 1-dependent glycolysis is increased during aging-related lung fibrosis, and phloretin inhibits lung fibrosis. *Am. J. Respir. Cell Mol. Biol.* 56, 521–531. doi:10.1165/rcmb.2016-0225OC

Chowdhury, R., Yeoh, K. K., Tian, Y. M., Hillringhaus, L., Bagg, E. A., Rose, N. R., et al. (2011). The oncometabolite 2-hydroxyglutarate inhibits histone lysine demethylases. *EMBO Rep.* 12, 463–469. doi:10.1038/embor.2011.43

Chung, K. P., Hsu, C. L., Fan, L. C., Huang, Z., Bhatia, D., Chen, Y. J., et al. (2019). Mitofusins regulate lipid metabolism to mediate the development of lung fibrosis. *Nat. Commun.* 10, 3390. doi:10.1038/s41467-019-11327-1

Cole-Ezea, P., Swan, D., Shanley, D., and Hesketh, J. (2012). Glutathione peroxidase 4 has a major role in protecting mitochondria from oxidative damage and maintaining oxidative phosphorylation complexes in gut epithelial cells. *Free Radic. Biol. Med.* 53, 488–497. doi:10.1016/j.freeradbiomed.2012.05.029

Cui, H., Jiang, D., Banerjee, S., Xie, N., Kulkarni, T., Liu, R. M., et al. (2020). Monocyte-derived alveolar macrophage apolipoprotein E participates in pulmonary fibrosis resolution. *JCI Insight* 5, 134539. doi:10.1172/jci.insight.134539

Cui, H., Xie, N., Banerjee, S., Ge, J., Jiang, D., Dey, T., et al. (2021). Lung myofibroblasts promote macrophage profibrotic activity through lactate-induced histone lactylation. *Am. J. Respir. Cell Mol. Biol.* 64, 115–125. doi:10.1165/rcmb.2020-0360OC

Distler, J., Györfi, A. H., Ramanujam, M., Whitfield, M. L., Königshoff, M., and Lafyatis, R. (2019). Shared and distinct mechanisms of fibrosis. *Nat. Rev. Rheumatol.* 15, 705–730. doi:10.1038/s41584-019-0322-7

Drent, M., Cobben, N. A., Henderson, R. F., Wouters, E. F., and van Dieijen-Visser, M. (1996). Usefulness of lactate dehydrogenase and its isoenzymes as indicators of lung damage or inflammation. *Eur. Respir. J.* 9, 1736–1742. doi:10.1183/09031936.96.09081736

Durante, W., Liao, L., Reyna, S. V., Peyton, K. J., and Schafer, A. I. (2001). Transforming growth factor-beta(1) stimulates L-arginine transport and metabolism in vascular smooth muscle cells: Role in polyamine and collagen synthesis. *Circulation* 103, 1121–1127. doi:10.1161/01.cir.103.8.1121

Eh, L., Lee, E. J., Hj, K., As, J., Es, K., Uh, S. T., et al. (2013). Overexpression of apolipoprotein A1 in the lung abrogates fibrosis in experimental silicosis. *PLoS ONE* 8, e55827. doi:10.1371/journal.pone.0055827

Endo, M., Oyadomari, S., Terasaki, Y., Takeya, M., Suga, M., Mori, M., et al. (2003). Induction of arginase I and II in bleomycin-induced fibrosis of mouse lung. *Am. J. Physiol. Lung Cell. Mol. Physiol.* 285, L313–L321. doi:10.1152/ajplung.00434.2002

Esguerra, V., and Zhao, Y. (2019). Preventing glutaminolysis: A potential therapy for pulmonary fibrosis. *Am. J. Respir. Cell Mol. Biol.* 61, 408–409. doi:10.1165/rcmb.2019-0119ED

Even, B., Fayad-Kobeissi, S., Gagliolo, J. M., Motterlini, R., Boczkowski, J., Foresti, R., et al. (2018). Heme oxygenase-1 induction attenuates senescence in chronic obstructive pulmonary disease lung fibroblasts by protecting against mitochondria dysfunction. *Aging Cell* 17, e12837. doi:10.1111/acel.12837

Forbes, A., Pickell, M., Foroughian, M., Yao, L. J., Lewis, J., and Veldhuizen, R. (2007). Alveolar macrophage depletion is associated with increased surfactant pool sizes in adult rats. *J. Appl. Physiol.* 103, 637–645. doi:10.1152/japplphysiol.00995.2006

Gaugg, M. T., Engler, A., Bregy, L., Nussbaumer-Ochsner, Y., Eiffert, L., Bruderer, T., et al. (2019). Molecular breath analysis supports altered amino acid metabolism in idiopathic pulmonary fibrosis. *Respirology* 24, 437–444. doi:10.1111/resp.13465

Ge, J., Cui, H., Xie, N., Banerjee, S., Guo, S., Dubey, S., et al. (2018). Glutaminolysis promotes collagen translation and stability via α-Ketoglutarate-mediated mTOR activation and proline hydroxylation. *Am. J. Respir. Cell Mol. Biol.* 58, 378–390. doi:10.1165/rcmb.2017-0238OC

Genovese, T., Cuzzocrea, S., Di Paola, R., Mazzon, E., Mastruzzo, C., Catalano, P., et al. (2005). Effect of rosiglitazone and 15-deoxy-Delta12, 14-prostaglandin J2 on bleomycin-induced lung injury. *Eur. Respir. J.* 25, 225–234. doi:10.1183/09031936.05.00049704

Goodwin, J., Choi, H., Hsieh, M. H., Neugent, M. L., Ahn, J. M., Hayenga, H. N., et al. (2018). Targeting hypoxia-inducible factor-1α/pyruvate dehydrogenase kinase 1 Axis by dichloroacetate suppresses bleomycin-induced pulmonary fibrosis. *Am. J. Respir. Cell Mol. Biol.* 58, 216–231. doi:10.1165/rcmb.2016-0186OC

Gopu, V., Fan, L., Shetty, R. S., Nagaraja, M. R., and Shetty, S. (2020). Caveolin-1 scaffolding domain peptide regulates glucose metabolism in lung fibrosis. *JCI Insight* 5, 137969. doi:10.1172/jci.insight.137969

Gordon, E. M., Figueroa, D. M., Barochia, A. V., Yao, X., and Levine, S. J. (2016). High-density lipoproteins and apolipoprotein A-I: Potential new players in the prevention and treatment of lung disease. *Front. Pharmacol.* 7, 323. doi:10.3389/fphar.2016.00323

Gu, X., Jiang, Y. N., Wang, W. J., Zhang, J., Shang, D. S., Sun, C. B., et al. (2020). Comprehensive circRNA expression profile and construction of circRNA-related ceRNA network in cardiac fibrosis. *Biomed. Pharmacother. = Biomedecine Pharmacother.* 125, 109944. doi:10.1016/j.biopha.2020.109944

Gui, Y. S., Wang, L., Tian, X., Li, X., Ma, A., Zhou, W., et al. (2015). mTOR overactivation and compromised autophagy in the pathogenesis of pulmonary fibrosis. *PLoS ONE* 10, e0138625. doi:10.1371/journal.pone.0138625

Guido, C., Whitaker-Menezes, D., Capparelli, C., Balliet, R., Lin, Z., Pestell, R. G., et al. (2012). Metabolic reprogramming of cancer-associated fibroblasts by TGF-β drives tumor growth: Connecting TGF-β signaling with "Warburg-like" cancer metabolism and L-lactate production. *Cell Cycle* 11, 3019–3035. doi:10.4161/cc.21384

Guilliams, M., De Kleer, I., Henri, S., Post, S., Vanhoutte, L., De Prijck, S., et al. (2013). Alveolar macrophages develop from fetal monocytes that differentiate into long-lived cells in the first week of life via GM-CSF. *J. Exp. Med.* 210, 1977–1992. doi:10.1084/jem.20131199

Hamada, K., Nagai, S., Tanaka, S., Handa, T., Shigematsu, M., Nagao, T., et al. (2007). Significance of pulmonary arterial pressure and diffusion capacity of the lung as prognosticator in patients with idiopathic pulmonary fibrosis. *Chest* 131, 650–656. doi:10.1378/chest.06-1466

Hamanaka, R. B., and Mutlu, G. M. (2021). The role of metabolic reprogramming and de novo amino acid synthesis in collagen protein production by myofibroblasts: Implications for organ fibrosis and cancer. *Amino Acids* 53, 1851–1862. doi:10.1007/s00726-021-02996-8

Hamanaka, R. B., Nigdelioglu, R., Meliton, A. Y., Tian, Y., Witt, L. J., O'Leary, E., et al. (2018). Inhibition of phosphoglycerate dehydrogenase attenuates bleomycin-induced pulmonary fibrosis. *Am. J. Respir. Cell Mol. Biol.* 58, 585–593. doi:10.1165/rcmb.2017-0186OC

Hamanaka, R. B., O'Leary, E. M., Witt, L. J., Tian, Y., Gökalp, G. A., Meliton, A. Y., et al. (2019). Glutamine metabolism is required for collagen protein synthesis in lung fibroblasts. *Am. J. Respir. Cell Mol. Biol.* 61, 597–606. doi:10.1165/rcmb.2019-0008OC

Higgins, D. F., Kimura, K., Iwano, M., and Haase, V. H. (2008). Hypoxia-inducible factor signaling in the development of tissue fibrosis. *Cell Cycle* 7, 1128–1132. doi:10.4161/cc.7.9.5804

Hooff, G. P., Wood, W. G., Müller, W. E., and Eckert, G. P. (2010). Isoprenoids, small GTPases and Alzheimer's disease. *Biochim. Biophys. Acta* 1801, 896–905. doi:10.1016/j.bbalip.2010.03.014

Hu, X., Xu, Q., Wan, H., Hu, Y., Xing, S., Yang, H., et al. (2020). PI3K-Akt-mTOR/PFKFB3 pathway mediated lung fibroblast aerobic glycolysis and collagen synthesis in lipopolysaccharide-induced pulmonary fibrosis. *Lab. Invest.* 100, 801–811. doi:10.1038/s41374-020-0404-9

Huang, L. S., and Natarajan, V. (2015). Sphingolipids in pulmonary fibrosis. *Adv. Biol. Regul.* 57, 55–63. doi:10.1016/j.jbior.2014.09.008

Ichikawa, T., Sugiura, H., Koarai, A., Kikuchi, T., Hiramatsu, M., Kawabata, H., et al. (2013). 25-hydroxycholesterol promotes fibroblast-mediated tissue remodeling through NF-κB dependent pathway. *Exp. Cell Res.* 319, 1176–1186. doi:10.1016/j.yexcr.2013.02.014

Ignarro, L. J., Buga, G. M., Wei, L. H., Bauer, P. M., Wu, G., and del Soldato, P. (2001). Role of the arginine-nitric oxide pathway in the regulation of vascular smooth muscle cell proliferation. *Proc. Natl. Acad. Sci. U. S. A.* 98, 4202–4208. doi:10.1073/pnas.071054698

Ingenito, E. P., Mora, R., and Mark, L. (2000). Pivotal role of anionic phospholipids in determining dynamic behavior of lung surfactant. *Am. J. Respir. Crit. Care Med.* 161, 831–838. doi:10.1164/ajrccm.161.3.9903048

Ivanova, V., Garbuzenko, O. B., Reuhl, K. R., Reimer, D. C., Pozharov, V. P., and Minko, T. (2013). Inhalation treatment of pulmonary fibrosis by liposomal prostaglandin E2. *Eur. J. Pharm. Biopharm.* 84, 335–344. doi:10.1016/j.ejpb.2012.11.023

Janssen, W. J., Danhorn, T., Harris, C., Mould, K. J., Lee, F. F., Hedin, B. R., et al. (2020). Inflammation-induced alternative pre-mRNA splicing in mouse alveolar macrophages. *G3* 10, 555–567. doi:10.1534/g3.119.400935

Jiang, J., Zhang, L., Chen, H., Lei, Y., Zhang, T., Wang, Y., et al. (2020). Regorafenib induces lethal autophagy arrest by stabilizing PSAT1 in glioblastoma. *Autophagy* 16, 106–122. doi:10.1080/15548627.2019.1598752

Judge, J. L., Lacy, S. H., Ku, W. Y., Owens, K. M., Hernady, E., Thatcher, T. H., et al. (2017). The lactate dehydrogenase inhibitor gossypol inhibits radiation-induced pulmonary fibrosis. *Radiat. Res.* 188, 35–43. doi:10.1667/RR14620.1

Judge, J. L., Nagel, D. J., Owens, K. M., Rackow, A., Phipps, R. P., Sime, P. J., et al. (2018). Prevention and treatment of bleomycin-induced pulmonary fibrosis with the lactate dehydrogenase inhibitor gossypol. *PLoS ONE* 13, e0197936. doi:10.1371/journal.pone.0197936

Jung, M. Y., Kang, J. H., Hernandez, D. M., Yin, X., Andrianifahanana, M., Wang, Y., et al. (2018). Fatty acid synthase is required for profibrotic TGF-β signaling. *FASEB J.* 32, 3803–3815. doi:10.1096/fj.201701187R

Kanoh, S., Kobayashi, H., and Motoyoshi, K. (2005). Exhaled ethane: An *in vivo* biomarker of lipid peroxidation in interstitial lung diseases. *Chest* 128, 2387–2392. doi:10.1378/chest.128.4.2387

Karmiol, S., Remick, D. G., Kunkel, S. L., and Phan, S. H. (1993). Regulation of rat pulmonary endothelial cell interleukin-6 production by bleomycin: Effects of cellular fatty acid composition. *Am. J. Respir. Cell Mol. Biol.* 9, 628–636. doi:10.1165/ajrcmb/9.6.628

Kasper, M., and Haroske, G. (1996). Alterations in the alveolar epithelium after injury leading to pulmonary fibrosis. *Histol. Histopathol.* 11, 463–483.

Kendall, R. T., and Feghali-Bostwick, C. A. (2014). Fibroblasts in fibrosis: Novel roles and mediators. *Front. Pharmacol.* 5, 123. doi:10.3389/fphar.2014.00123

Kida, T., Ayabe, S., Omori, K., Nakamura, T., Maehara, T., Aritake, K., et al. (2016). Prostaglandin D2 attenuates bleomycin-induced lung inflammation and pulmonary fibrosis. *PLoS ONE* 11, e0167729. doi:10.1371/journal.pone.0167729

Kim, H. J., Liu, X., Wang, H., Kohyama, T., Kobayashi, T., Wen, F. Q., et al. (2002). Glutathione prevents inhibition of fibroblast-mediated collagen gel contraction by cigarette smoke. *Am. J. Physiol. Lung Cell. Mol. Physiol.* 283, L409–L417. doi:10.1152/ajplung.00059.2002

Kim, J. W., Tchernyshyov, I., Semenza, G. L., and Dang, C. V. (2006). HIF-1-mediated expression of pyruvate dehydrogenase kinase: A metabolic switch required for cellular adaptation to hypoxia. *Cell Metab.* 3, 177–185. doi:10.1016/j.cmet.2006.02.002

Kim, T. H., Lee, Y. H., Kim, K. H., Lee, S. H., Cha, J. Y., Shin, E. K., et al. (2010). Role of lung apolipoprotein A-I in idiopathic pulmonary fibrosis: Antiinflammatory and antifibrotic effect on experimental lung injury and fibrosis. *Am. J. Respir. Crit. Care Med.* 182, 633–642. doi:10.1164/rccm.200905-0659OC

Kottmann, R. M., Kulkarni, A. A., Smolnycki, K. A., Lyda, E., Dahanayake, T., Salibi, R., et al. (2012). Lactic acid is elevated in idiopathic pulmonary fibrosis and induces myofibroblast differentiation via pH-dependent activation of transforming growth factor-β. *Am. J. Respir. Crit. Care Med.* 186, 740–751. doi:10.1164/rccm.201201-0084OC

Lederer, D. J., and Martinez, F. J. (2018). Idiopathic pulmonary fibrosis. *N. Engl. J. Med.* 378, 1811–1823. doi:10.1056/NEJMra1705751

Lee, J. Y., Stevens, R. P., Kash, M., Zhou, C., Koloteva, A., Renema, P., et al. (2020). KD025 shifts pulmonary endothelial cell bioenergetics and decreases baseline lung permeability. *Am. J. Respir. Cell Mol. Biol.* 63, 519–530. doi:10.1165/rcmb.2019-0435OC

Lerner, C. A., Sundar, I. K., and Rahman, I. (2016). Mitochondrial redox system, dynamics, and dysfunction in lung inflammaging and COPD. *Int. J. Biochem. Cell Biol.* 81, 294–306. doi:10.1016/j.biocel.2016.07.026

Ley, B., and Collard, H. R. (2013). Epidemiology of idiopathic pulmonary fibrosis. *Clin. Epidemiol.* 5, 483–492. doi:10.2147/CLEP.S54815

Ley, B., Collard, H. R., and King, T. E., Jr. (2011). Clinical course and prediction of survival in idiopathic pulmonary fibrosis. *Am. J. Respir. Crit. Care Med.* 183, 431–440. doi:10.1164/rccm.201006-0894CI

Li, G., Thomas, A. M., Williams, J. A., Kong, B., Liu, J., Inaba, Y., et al. (2012). Farnesoid X receptor induces murine scavenger receptor Class B type I via intron binding. *PLoS ONE* 7, e35895. doi:10.1371/journal.pone.0035895

Li, J., Li, P., Zhang, G., Qin, P., Zhang, D., and Zhao, W. (2020). CircRNA TADA2A relieves idiopathic pulmonary fibrosis by inhibiting proliferation and activation of fibroblasts. *Cell Death Dis.* 11, 553. doi:10.1038/s41419-020-02747-9

Li, K., Li, M., Li, W., Yu, H., Sun, X., Zhang, Q., et al. (2019). Airway epithelial regeneration requires autophagy and glucose metabolism. *Cell Death Dis.* 10, 875. doi:10.1038/s41419-019-2111-2

Li, X., Wu, J., Sun, X., Wu, Q., Li, Y., Li, K., et al. (2020). Autophagy reprograms alveolar progenitor cell metabolism in response to lung injury. *Stem Cell Rep.* 14, 420–432. doi:10.1016/j.stemcr.2020.01.008

Li, Z., Geng, J., Xie, B., He, J., Wang, J., Peng, L., et al. (2022). Dihydromyricetin alleviates pulmonary fibrosis by regulating abnormal fibroblasts through the STAT3/p-STAT3/GLUT1 signaling pathway. *Front. Pharmacol.* 13, 834604. doi:10.3389/fphar.2022.834604

Liberti, M. V., and Locasale, J. W. (2016). The Warburg effect: How does it benefit cancer cells. *Trends biochem. Sci.* 41, 211–218. doi:10.1016/j.tibs.2015.12.001

Lieu, E. L., Nguyen, T., Rhyne, S., and Kim, J. (2020). Amino acids in cancer. *Exp. Mol. Med.* 52, 15–30. doi:10.1038/s12276-020-0375-3

Locati, M., Mantovani, A., and Sica, A. (2013). Macrophage activation and polarization as an adaptive component of innate immunity. *Adv. Immunol.* 120, 163–184. doi:10.1016/B978-0-12-417028-5.00006-5

Mao, N., Fan, Y., Liu, W., Yang, H., Yang, Y., Li, Y., et al. (2022). Oxamate attenuates glycolysis and ER stress in silicotic mice. *Int. J. Mol. Sci.* 23, 3013. doi:10.3390/ijms23063013

Mao, N., Yang, H., Yin, J., Li, Y., Jin, F., Li, T., et al. (2021). Glycolytic reprogramming in silica-induced lung macrophages and silicosis reversed by Ac-sdkp treatment. *Int. J. Mol. Sci.* 22, 10063. doi:10.3390/ijms221810063

Marsango, S., Barki, N., Jenkins, L., Tobin, A. B., and Milligan, G. (2022). Therapeutic validation of an orphan G protein-coupled receptor: The case of GPR84. *Br. J. Pharmacol.* 179, 3529–3541. doi:10.1111/bph.15248

Menendez, J. A., and Lupu, R. (2007). Fatty acid synthase and the lipogenic phenotype in cancer pathogenesis. *Nat. Rev. Cancer* 7, 763–777. doi:10.1038/nrc2222

Meziani, L., Mondini, M., Petit, B., Boissonnas, A., Thomas de Montpreville, V., Mercier, O., et al. (2018). CSF1R inhibition prevents radiation pulmonary fibrosis by depletion of interstitial macrophages. *Eur. Respir. J.* 51, 1702120. doi:10.1183/13993003.02120-2017

Miao, Y., Geng, Y., Yang, L., Zheng, Y., Dai, Y., and Wei, Z. (2022). Morin inhibits the transformation of fibroblasts towards myofibroblasts through regulating "PPAR-γ-glutaminolysis-DEPTOR" pathway in pulmonary fibrosis. *J. Nutr. Biochem.* 101, 108923. doi:10.1016/j.jnutbio.2021.108923

Molina-Molina, M., Serrano-Mollar, A., Bulbena, O., Fernandez-Zabalegui, L., Closa, D., Marin-Arguedas, A., et al. (2006). Losartan attenuates bleomycin induced lung fibrosis by increasing prostaglandin E2 synthesis. *Thorax* 61, 604–610. doi:10.1136/thx.2005.051946

Montuschi, P., Ciabattoni, G., Paredi, P., Pantelidis, P., du Bois, R. M., Kharitonov, S. A., et al. (1998). 8-Isoprostane as a biomarker of oxidative stress in interstitial lung diseases. *Am. J. Respir. Crit. Care Med.* 158, 1524–1527. doi:10.1164/ajrccm.158.5.9803102

Moore, B. B., Coffey, M. J., Christensen, P., Sitterding, S., Ngan, R., Wilke, C. A., et al. (2000). GM-CSF regulates bleomycin-induced pulmonary fibrosis via a prostaglandin-dependent mechanism. *J. Immunol.* 165, 4032–4039. doi:10.4049/jimmunol.165.7.4032

Moss, B. J., Ryter, S. W., and Rosas, I. O. (2022). Pathogenic mechanisms underlying idiopathic pulmonary fibrosis. *Annu. Rev. Pathol.* 17, 515–546. doi:10.1146/annurev-pathol-042320-030240

Motohashi, H., and Yamamoto, M. (2004). Nrf2-Keap1 defines a physiologically important stress response mechanism. *Trends Mol. Med.* 10, 549–557. doi:10.1016/j.molmed.2004.09.003

Nagahashi, M., Hait, N. C., Maceyka, M., Avni, D., Takabe, K., Milstien, S., et al. (2014). Sphingosine-1-phosphate in chronic intestinal inflammation and cancer. *Adv. Biol. Regul.* 54, 112–120. doi:10.1016/j.jbior.2013.10.001

Natarajan, V., Dudek, S. M., Jacobson, J. R., Moreno-Vinasco, L., Huang, L. S., Abassi, T., et al. (2013). Sphingosine-1-phosphate, FTY720, and sphingosine-1-phosphate receptors in the pathobiology of acute lung injury. *Am. J. Respir. Cell Mol. Biol.* 49, 6–17. doi:10.1165/rcmb.2012-0411TR

Niese, K. A., Chiaramonte, M. G., Ellies, L. G., Rothenberg, M. E., and Zimmermann, N. (2010). The cationic amino acid transporter 2 is induced in inflammatory lung models and regulates lung fibrosis. *Respir. Res.* 11, 87. doi:10.1186/1465-9921-11-87

Nigdelioglu, R., Hamanaka, R. B., Meliton, A. Y., O'Leary, E., Witt, L. J., Cho, T., et al. (2016). Transforming growth factor (TGF)-β promotes de Novo serine synthesis for collagen production. *J. Biol. Chem.* 291, 27239–27251. doi:10.1074/jbc.M116.756247

O'Leary, E. M., Tian, Y., Nigdelioglu, R., Witt, L. J., Cetin-Atalay, R., Meliton, A. Y., et al. (2020). TGF-B promotes metabolic reprogramming in lung fibroblasts via mTORC1-dependent ATF4 activation. *Am. J. Respir. Cell Mol. Biol.* 63, 601–612. doi:10.1165/rcmb.2020-0143OC

Palmer, S. M., Snyder, L., Todd, J. L., Soule, B., Christian, R., Anstrom, K., et al. (2018). Randomized, double-blind, placebo-controlled, Phase 2 trial of BMS-986020, a lysophosphatidic acid receptor antagonist for the treatment of idiopathic pulmonary fibrosis. *Chest* 154, 1061–1069. doi:10.1016/j.chest.2018.08.1058

Pandit, P., Perez, R. L., and Roman, J. (2020). Sex-based differences in interstitial lung disease. *Am. J. Med. Sci.* 360, 467–473. doi:10.1016/j.amjms.2020.04.023

Para, R., Romero, F., George, G., and Summer, R. (2019). Metabolic reprogramming as a driver of fibroblast activation in PulmonaryFibrosis. *Am. J. Med. Sci.* 357, 394–398. doi:10.1016/j.amjms.2019.02.003

Parinandi, N. L., Scribner, W. M., Vepa, S., Shi, S., and Natarajan, V. (1999). Phospholipase D activation in endothelial cells is redox sensitive. *Antioxid. Redox Signal.* 1, 193–210. doi:10.1089/ars.1999.1.2-193

Parra-Bonilla, G., Alvarez, D. F., Al-Mehdi, A. B., Alexeyev, M., and Stevens, T. (2010). Critical role for lactate dehydrogenase A in aerobic glycolysis that sustains

pulmonary microvascular endothelial cell proliferation. *Am. J. Physiol. Lung Cell. Mol. Physiol.* 299, L513–L522. doi:10.1152/ajplung.00274.2009

Patel, R. B., Kotha, S. R., Sherwani, S. I., Sliman, S. M., Gurney, T. O., Loar, B., et al. (2011). Pulmonary fibrosis inducer, bleomycin, causes redox-sensitive activation of phospholipase D and cytotoxicity through formation of bioactive lipid signal mediator, phosphatidic acid, in lung microvascular endothelial cells. *Int. J. Toxicol.* 30, 69–90. doi:10.1177/1091581810388850

Penke, L. R., Speth, J. M., Dommeti, V. L., White, E. S., Bergin, I. L., and Peters-Golden, M. (2018). FOXM1 is a critical driver of lung fibroblast activation and fibrogenesis. *J. Clin. Invest.* 128, 2389–2405. doi:10.1172/JCI87631

Pérez-Gil, J. (2008). Structure of pulmonary surfactant membranes and films: The role of proteins and lipid-protein interactions. *Biochim. Biophys. Acta* 1778, 1676–1695. doi:10.1016/j.bbamem.2008.05.003

Podor, T. J., Jirik, F. R., Loskutoff, D. J., Carson, D. A., and Lotz, M. (1989). Human endothelial cells produce IL-6. *Ann. N. Y. Acad. Sci.* 557, 374–387. discussion 386-387. doi:10.1111/j.1749-6632.1989.tb24030.x

Pullamsetti, S. S., Savai, R., Dumitrascu, R., Dahal, B. K., Wilhelm, J., Konigshoff, M., et al. (2011). The role of dimethylarginine dimethylaminohydrolase in idiopathic pulmonary fibrosis. *Sci. Transl. Med.* 3, 87ra53. doi:10.1126/scitranslmed.3001725

Pyne, N. J., Dubois, G., and Pyne, S. (2013). Role of sphingosine 1-phosphate and lysophosphatidic acid in fibrosis. *Biochim. Biophys. Acta* 1831, 228–238. doi:10.1016/j.bbalip.2012.07.003

Qian, W., Xia, S., Yang, X., Yu, J., Guo, B., Lin, Z., et al. (2021). Complex involvement of the extracellular matrix, immune effect, and lipid metabolism in the development of idiopathic pulmonary fibrosis. *Front. Mol. Biosci.* 8, 800747. doi:10.3389/fmolb.2021.800747

Roach, K. M., Feghali-Bostwick, C. A., Amrani, Y., and Bradding, P. (2015). Lipoxin A4 attenuates constitutive and TGF-β1-dependent profibrotic activity in human lung myofibroblasts. *J. Immunol.* 195, 2852–2860. doi:10.4049/jimmunol.1500936

Romero, F., Shah, D., Duong, M., Penn, R. B., Fessler, M. B., Madenspacher, J., et al. (2015). A pneumocyte-macrophage paracrine lipid axis drives the lung toward fibrosis. *Am. J. Respir. Cell Mol. Biol.* 53, 74–86. doi:10.1165/rcmb.2014-0343OC

Roque, W., and Romero, F. (2021). Cellular metabolomics of pulmonary fibrosis, from amino acids to lipids. *Am. J. Physiol. Cell Physiol.* 320, C689–C695. doi:10.1152/ajpcell.00586.2020

Ruaro, B., Salton, F., Braga, L., Wade, B., Confalonieri, P., Volpe, M. C., et al. (2021). The history and mystery of alveolar epithelial type II cells: Focus on their physiologic and pathologic role in lung. *Int. J. Mol. Sci.* 22, 2566. doi:10.3390/ijms22052566

Ruwisch, J., Sehlmeyer, K., Roldan, N., Garcia-Alvarez, B., Perez-Gil, J., Weaver, T. E., et al. (2020). Air space distension precedes spontaneous fibrotic remodeling and impaired cholesterol metabolism in the absence of surfactant protein C. *Am. J. Respir. Cell Mol. Biol.* 62, 466–478. doi:10.1165/rcmb.2019-0358OC

Schmidt, R., Meier, U., Yabut-Perez, M., Walmrath, D., Grimminger, F., Seeger, W., et al. (2001). Alteration of fatty acid profiles in different pulmonary surfactant phospholipids in acute respiratory distress syndrome and severe pneumonia. *Am. J. Respir. Crit. Care Med.* 163, 95–100. doi:10.1164/ajrccm.163.1.9903029

Schruf, E., Schroeder, V., Kuttruff, C. A., Weigle, S., Krell, M., Benz, M., et al. (2019). Human lung fibroblast-to-myofibroblast transformation is not driven by an LDH5-dependent metabolic shift towards aerobic glycolysis. *Respir. Res.* 20, 87. doi:10.1186/s12931-019-1058-2

Sehlmeyer, K., Ruwisch, J., Roldan, N., and Lopez-Rodriguez, E. (2020). Alveolar dynamics and beyond - the importance of surfactant protein C and cholesterol in lung homeostasis and fibrosis. *Front. Physiol.* 11, 386. doi:10.3389/fphys.2020.00386

Semenza, G. L. (2011). Oxygen sensing, homeostasis, and disease. *N. Engl. J. Med.* 365, 537–547. doi:10.1056/NEJMra1011165

Shaghaghi, H., Para, R., Tran, C., Roman, J., Ojeda-Lassalle, Y., Sun, J., et al. (2021). Glutamine restores mitochondrial respiration in bleomycin-injured epithelial cells. *Free Radic. Biol. Med.* 176, 335–344. doi:10.1016/j.freeradbiomed.2021.10.006

Shea, B. S., and Tager, A. M. (2012). Role of the lysophospholipid mediators lysophosphatidic acid and sphingosine 1-phosphate in lung fibrosis. *Proc. Am. Thorac. Soc.* 9, 102–110. doi:10.1513/pats.201201-005AW

Silverstein, R. L., Li, W., Park, Y. M., and Rahaman, S. O. (2010). Mechanisms of cell signaling by the scavenger receptor CD36: Implications in atherosclerosis and thrombosis. *Trans. Am. Clin. Climatol. Assoc.* 121, 206–220.

Snider, G. L. (1989). Chronic obstructive pulmonary disease: Risk factors, pathophysiology and pathogenesis. *Annu. Rev. Med.* 40, 411–429. doi:10.1146/annurev.me.40.020189.002211

Soto-Heredero, G., Gómez de Las Heras, M. M., Gabandé-Rodríguez, E., Oller, J., and Mittelbrunn, M. (2020). Glycolysis - a key player in the inflammatory response. *FEBS J.* 287, 3350–3369. doi:10.1111/febs.15327

Sugiura, H., Koarai, A., Ichikawa, T., Minakata, Y., Matsunaga, K., Hirano, T., et al. (2012). Increased 25-hydroxycholesterol concentrations in the lungs of patients with chronic obstructive pulmonary disease. *Respirology* 17, 533–540. doi:10.1111/j.1440-1843.2012.02136.x

Sunaga, H., Matsui, H., Ueno, M., Maeno, T., Iso, T., Syamsunarno, M. R., et al. (2013). Deranged fatty acid composition causes pulmonary fibrosis in Elovl6-deficient mice. *Nat. Commun.* 4, 2563. doi:10.1038/ncomms3563

Suryadevara, V., Ramchandran, R., Kamp, D. W., and Natarajan, V. (2020). Lipid mediators regulate pulmonary fibrosis: Potential mechanisms and signaling pathways. *Int. J. Mol. Sci.* 21, E4257. doi:10.3390/ijms21124257

Tager, A. M., LaCamera, P., Shea, B. S., Campanella, G. S., Selman, M., Zhao, Z., et al. (2008). The lysophosphatidic acid receptor LPA1 links pulmonary fibrosis to lung injury by mediating fibroblast recruitment and vascular leak. *Nat. Med.* 14, 45–54. doi:10.1038/nm1685

Thorens, B., and Mueckler, M. (2010). Glucose transporters in the 21st century. *Am. J. Physiol. Endocrinol. Metab.* 298, E141–E145. doi:10.1152/ajpendo.00712.2009

Tsubouchi, K., Araya, J., Yoshida, M., Sakamoto, T., Koumura, T., Minagawa, S., et al. (2019). Involvement of GPx4-regulated lipid peroxidation in idiopathic pulmonary fibrosis pathogenesis. *J. Immunol.* 203, 2076–2087. doi:10.4049/jimmunol.1801232

Ung, C. Y., Onoufriadis, A., Parsons, M., McGrath, J. A., and Shaw, T. J. (2021). Metabolic perturbations in fibrosis disease. *Int. J. Biochem. Cell Biol.* 139, 106073. doi:10.1016/j.biocel.2021.106073

Venosa, A., Smith, L. C., Murray, A., Banota, T., Gow, A. J., Laskin, J. D., et al. (2019). Regulation of macrophage foam cell formation during nitrogen mustard (NM)-Induced pulmonary fibrosis by lung lipids. *Toxicol. Sci.* 172, 344–358. doi:10.1093/toxsci/kfz187

Viola, A., Munari, F., Sánchez-Rodríguez, R., Scolaro, T., and Castegna, A. (2019). The metabolic signature of macrophage responses. *Front. Immunol.* 10, 1462. doi:10.3389/fimmu.2019.01462

Wang, L., Chen, X., Li, X., Liu, D., Wang, X., Chang, X., et al. (2021). Developing a novel strategy for COPD therapy by targeting Nrf2 and metabolism reprogramming simultaneously. *Free Radic. Biol. Med.* 169, 436–445. doi:10.1016/j.freeradbiomed.2021.03.039

Wang, W., Dong, R., Guo, Y., He, J., Shao, C., Yi, P., et al. (2019). CircMTO1 inhibits liver fibrosis via regulation of miR-17-5p and Smad7. *J. Cell. Mol. Med.* 23, 5486–5496. doi:10.1111/jcmm.14432

Wang, X. Q., Mao, L. J., Fang, Q. H., Kobayashi, T., Kim, H. J., Sugiura, H., et al. (2014). Sphingosylphosphorylcholine induces α-smooth muscle actin expression in human lung fibroblasts and fibroblast-mediated gel contraction via S1P2 receptor and Rho/Rho-kinase pathway. *Prostagl. Other Lipid Mediat.* 108, 23–30. doi:10.1016/j.prostaglandins.2014.02.002

Wang, Z., Chen, L., Huang, Y., Luo, M., Wang, H., Jiang, Z., et al. (2021). Pharmaceutical targeting of succinate dehydrogenase in fibroblasts controls bleomycin-induced lung fibrosis. *Redox Biol.* 46, 102082. doi:10.1016/j.redox.2021.102082

Wettlaufer, S. H., Scott, J. P., McEachin, R. C., Peters-Golden, M., and Huang, S. K. (2016). Reversal of the transcriptome by prostaglandin E2 during myofibroblast dedifferentiation. *Am. J. Respir. Cell Mol. Biol.* 54, 114–127. doi:10.1165/rcmb.2014-0468OC

White, E. S., Atrasz, R. G., Dickie, E. G., Aronoff, D. M., Stambolic, V., Mak, T. W., et al. (2005). Prostaglandin E(2) inhibits fibroblast migration by E-prostanoid 2 receptor-mediated increase in PTEN activity. *Am. J. Respir. Cell Mol. Biol.* 32, 135–141. doi:10.1165/rcmb.2004-0126OC

Wieman, H. L., Wofford, J. A., and Rathmell, J. C. (2007). Cytokine stimulation promotes glucose uptake via phosphatidylinositol-3 kinase/Akt regulation of Glut1 activity and trafficking. *Mol. Biol. Cell* 18, 1437–1446. doi:10.1091/mbc.e06-07-0593

Wijsenbeek, M., and Cottin, V. (2020). Spectrum of fibrotic lung diseases. *N. Engl. J. Med.* 383, 958–968. doi:10.1056/NEJMra2005230

Winters, N. I., Burman, A., Kropski, J. A., and Blackwell, T. S. (2019). Epithelial injury and dysfunction in the pathogenesis of idiopathic PulmonaryFibrosis. *Am. J. Med. Sci.* 357, 374–378. doi:10.1016/j.amjms.2019.01.010

Wong, B. H., Mei, D., Chua, G. L., Galam, D. L., Wenk, M. R., Torta, F., et al. (2022). The lipid transporter Mfsd2a maintains pulmonary surfactant homeostasis. *J. Biol. Chem.* 298, 101709. doi:10.1016/j.jbc.2022.101709

Xie, N., Cui, H., Ge, J., Banerjee, S., Guo, S., Dubey, S., et al. (2017). Metabolic characterization and RNA profiling reveal glycolytic dependence of profibrotic

phenotype of alveolar macrophages in lung fibrosis. *Am. J. Physiol. Lung Cell. Mol. Physiol.* 313, L834–L844. doi:10.1152/ajplung.00235.2017

Xie, N., Tan, Z., Banerjee, S., Cui, H., Ge, J., Liu, R. M., et al. (2015). Glycolytic reprogramming in myofibroblast differentiation and lung fibrosis. *Am. J. Respir. Crit. Care Med.* 192, 1462–1474. doi:10.1164/rccm.201504-0780OC

Xu, Q., Mei, S., Nie, F., Zhang, Z., Feng, J., Zhang, J., et al. (2022). The role of macrophage-fibroblast interaction in lipopolysaccharide-induced pulmonary fibrosis: An acceleration in lung fibroblast aerobic glycolysis. *Lab. Invest.* 102, 432–439. doi:10.1038/s41374-021-00701-7

Zaman, T., Moua, T., Vittinghoff, E., Ryu, J. H., Collard, H. R., and Lee, J. S. (2020). Differences in clinical characteristics and outcomes between men and women with idiopathic pulmonary fibrosis: A multicenter retrospective cohort study. *Chest* 158, 245–251. doi:10.1016/j.chest.2020.02.009

Zhang, C., Liu, J., Liang, Y., Wu, R., Zhao, Y., Hong, X., et al. (2013). Tumour-associated mutant p53 drives the Warburg effect. *Nat. Commun.* 4, 2935. doi:10.1038/ncomms3935

Zhang, W., Li, Q., Li, D., Li, J., Aki, D., and Liu, Y. C. (2018). The E3 ligase VHL controls alveolar macrophage function via metabolic-epigenetic regulation. *J. Exp. Med.* 215, 3180–3193. doi:10.1084/jem.20181211

Zhao, Y., and Natarajan, V. (2013). Lysophosphatidic acid (LPA) and its receptors: Role in airway inflammation and remodeling. *Biochim. Biophys. Acta* 1831, 86–92. doi:10.1016/j.bbalip.2012.06.014

frontiers | Frontiers in Pharmacology

TYPE Review
PUBLISHED 05 December 2022
DOI 10.3389/fphar.2022.1033982

Check for updates

OPEN ACCESS

EDITED BY
Fujian Lu,
Boston Children's Hospital, Harvard Medical School, United States

REVIEWED BY
Danilo Guerini,
Novartis Institutes for BioMedical Research, Switzerland
Daiju Fukuda,
Osaka Metropolitan University, Japan

*CORRESPONDENCE
Haipeng Guo,
Haipeng198334@163.com
Yuguo Chen,
chen919085@sdu.edu.cn

†These authors have contributed equally to this work

SPECIALTY SECTION
This article was submitted to Experimental Pharmacology and Drug Discovery, a section of the journal Frontiers in Pharmacology

RECEIVED 01 September 2022
ACCEPTED 21 November 2022
PUBLISHED 05 December 2022

CITATION
Liu Y, Li Y, Xue L, Xiao J, Li P, Xue W, Li C, Guo H and Chen Y (2022), The effect of the cyclic GMP-AMP synthase-stimulator of interferon genes signaling pathway on organ inflammatory injury and fibrosis.
Front. Pharmacol. 13:1033982.
doi: 10.3389/fphar.2022.1033982

COPYRIGHT
© 2022 Liu, Li, Xue, Xiao, Li, Xue, Li, Guo and Chen. This is an open-access article distributed under the terms of the Creative Commons Attribution License (CC BY). The use, distribution or reproduction in other forums is permitted, provided the original author(s) and the copyright owner(s) are credited and that the original publication in this journal is cited, in accordance with accepted academic practice. No use, distribution or reproduction is permitted which does not comply with these terms.

The effect of the cyclic GMP-AMP synthase-stimulator of interferon genes signaling pathway on organ inflammatory injury and fibrosis

Yuliang Liu[1,2,3†], Yihui Li[1,2,3†], Li Xue[2,3,4†], Jie Xiao[1,2,3], Pengyong Li[1,2,3], Wanlin Xue[1,2,3], Chen Li[1,2,3], Haipeng Guo[1,2,3*] and Yuguo Chen[2,3,4*]

[1]Department of Critical Care Medicine, Qilu Hospital, Cheeloo College of Medicine, Shandong University, Jinan, Shandong, China, [2]The Key Laboratory of Emergency and Critical Care Medicine of Shandong Province, Qilu Hospital, Cheeloo College of Medicine, Shandong University, Jinan, Shandong, China, [3]The Key Laboratory of Cardiovascular Remodeling and Function Research, Chinese Ministry of Education and Chinese Ministry of Health, Qilu Hospital, Cheeloo College of Medicine, Shandong University, Jinan, Shandong, China, [4]Department of Emergency Medicine and Chest Pain Center, Qilu Hospital, Cheeloo College of Medicine, Shandong University, Jinan, Shandong, China

The cyclic GMP-AMP synthase-stimulator of interferon genes signal transduction pathway is critical in innate immunity, infection, and inflammation. In response to pathogenic microbial infections and other conditions, cyclic GMP-AMP synthase (cGAS) recognizes abnormal DNA and initiates a downstream type I interferon response. This paper reviews the pathogenic mechanisms of stimulator of interferon genes (STING) in different organs, including changes in fibrosis-related biomarkers, intending to systematically investigate the effect of the cyclic GMP-AMP synthase-stimulator of interferon genes signal transduction in inflammation and fibrosis processes. The effects of stimulator of interferon genes in related auto-inflammatory and neurodegenerative diseases are described in this article, in addition to the application of stimulator of interferon genes-related drugs in treating fibrosis.

KEYWORDS

cyclic GMP-AMP synthase-stimulator of interferon genes signaling pathway, organ fibrosis, innate immunity, remodeling, inflammation

Introduction

Fibrosis is a normal byproduct of chronic tissue injury and is required to regenerate of injured tissues and organs. Although fibrosis is beneficial in the short term, the long-term progression of fibrosis may cause dysfunction or even failure of cells and organs (Rockey et al., 2015; Henderson et al., 2020). Excessive fibrosis leads to abnormal remodeling and progressive dysfunction of several organs, including the heart, kidneys, lungs, liver, and other organs (Zhang and Zhang, 2020). Stress reactions and injuries (autoimmunity,

sepsis, viruses, coronavirus disease 2019, inflammation, ischemia, metabolic abnormalities, toxins, *etc.*) can lead to organ fibrosis (Mack, 2018; Zhou et al., 2018; Horowitz and Thannickal, 2019; Sun Z. et al., 2020; McDonald, 2021; Ung et al., 2021). In addition, the pathophysiological process of fibrosis involves numerous signal transduction pathways, such as Ca2+, Janus kinase (JAK)/signal transducer and activator of transcription (STAT), phosphatidylinositol-3-kinase (PI3K)/protein kinase B (Akt), renin-angiotensin-aldosterone (RAAS), transforming growth factor beta (TGF-β)/Smad, wingless/integrated (Wnt)/β-catenin and many others (Mezzano et al., 2001; Goh et al., 2015; Hu et al., 2018; Feng et al., 2019; Hu H. H. et al., 2020; Montero et al., 2021; Qin et al., 2021). These signaling pathways interact to form a complex network of pathogenic mechanisms for fibrosis.

Ishikawa and Barber's team discovered STING in 2008 and demonstrated that STING could facilitate the expression of type I interferons (IFN-1) as a defense against viral infection (Ishikawa and Barber, 2008). Since then, STING, one of the key participants in innate immunity, has gradually entered our view. Its primary physiological role is to trigger responses such as innate immunity and inflammation after recognising abnormal DNA (both exogenous pathogenic and endogenous DNA) by the cGAS (Hopfner and Hornung, 2020). Recent studies have shown that STING signal transduction occurs in the remodeling and fibrosis of various organs. The above process involves the interaction of multiple mechanisms, such as TGF-β/Smad and JAK/STAT signal transduction pathways.

There are still no effective treatments for fibrosis. Therefore, more research is essential to understand how fibrosis works and to discover viable therapeutic strategies. This article mainly explores the effects of STING and related molecules in exacerbating inflammation and promoting fibrosis in different organ diseases, exploring possible new directions for therapeutic targets. Molecular mechanisms of STING and its interactions with other signaling pathways are also included, which are extremely valuable for further clarification of the pathological process of organ fibrosis. In addition, studies of STING-related drugs were reviewed to explore their mechanisms of action and research advances. Finally, we elucidate current issues and perspectives for further research in the future.

Summary of the cyclic GMP-AMP synthase-stimulator of interferon genes signal transduction process

The discovery of the cyclic GMP-AMP synthase-stimulator of interferon genes signal transduction pathway

STING (or called ERIS, MITA, MPYS, TMEM173) (Jin et al., 2008; Zhong et al., 2008; Ishikawa et al., 2009; Sun et al., 2009), which is located in the endoplasmic reticulum (ER), was first reported by Ishikawa and Barber's team in 2008. It contributes to activating interferon regulatory factor 3 (IRF3) and nuclear factor-kappa B (NF-κB) to increase IFN-1 production and thus resist virus attack (Ishikawa and Barber, 2008). Zhong et al. further demonstrated the vital effect of TANK binding kinase 1 (TBK1) in STING-induced IRF3 activation (Zhong et al., 2008). In 2013, Wu and Sun et al. discovered that cyclic guanosine monophosphate-adenosine monophosphate (cyclic GMP-AMP, or cGAMP) in mammalian cells could act as an endogenous second messenger to sense cytoplasmic DNA, thereby triggering STING and downstream interferon production (Wu et al., 2013). In the same year, they identified a new DNA sensor in the cytoplasm called cGAS, which identifies cytoplasmic DNA and promotes cGAMP production, thereby activating STING (Sun et al., 2013). At this point, the overall structure of the cGAS-STING signal transduction path was understood, and new studies related to its more specific perspectives have begun to emerge one after another.

Activation and physiological effects of the cyclic GMP-AMP synthase-stimulator of interferon genes signal transduction pathway

As mentioned above, the initiation of the STING signal transduction needs to be triggered by cytoplasmic DNA. Sources of cytoplasmic DNA include bacteria, viruses, tumor cells, micronuclei, damaged mitochondria, *etc.* cGAS senses DNA from the above sources and undergoes conformational changes, thereby catalyzing the synthesis of the second messenger cGAMP containing 2′-5′ and 3′-5′ phosphodiester bonds from ATP and GTP (Ablasser et al., 2013; Gao et al., 2013; Zhang et al., 2013). Notably, the way cGAS recognizes DNA is highly correlated with DNA length, which means that only DNA of a certain length can effectively activate cGAS and promote the production of IFN (Andreeva et al., 2017; Luecke et al., 2017). It was shown that STING located in the endoplasmic reticulum had bound a large amount of TBK1 before being activated, and these TBK1 were also in an equally inactive state (Zhang et al., 2019). The conformation of STING changed after binding to cGAMP. The structural site used to bind the ligand rotates 180° clockwise relative to the transmembrane part and releases the C-terminal tail. Eventually, multiple STING molecules in parallel undergo oligomerization and form disulfide bonds on cysteine residue 148 to stabilize the structure (Ergun et al., 2019; Shang et al., 2019). At the same time, STING, which binds cGAMP, exits the ER and translocates to the ER-Golgi intermediate compartment (ERGIC) and the Golgi. This is a coat protein complex II (COP II)-dependent process and is also regulated by ADP-ribosylation factor (ARF) GTPases (Dobbs et al., 2015; Gui et al., 2019). TBK1 bound to STING is approached by forming a STING

polymer and eventually activated by trans-autophosphorylation (Zhang et al., 2019; Zhao et al., 2019). Activated TBK1 catalyzes the phosphorylation of serine residues in the pLxIS motif on the C-terminal tail domain of STING, thereby allowing IRF3 to be recruited and bound to this motif (Liu et al., 2015). At this time, the neighboring TBK1 phosphorylates and dimerizes IRF3, which then regulates gene expression to generate IFN-1. Furthermore, inhibitor of kappa B kinase (IKK) is also recruited by STING to activate downstream NF-κB and facilitate the synthesis of pro-inflammatory cytokines such as interleukin-1 (IL-1), interleukin-6 (IL-6) and tumor necrosis factor-alpha (TNF-α). Notably, it remains undetermined whether this process requires the mediating role of TBK1 (Konno et al., 2013; Abe and Barber, 2014; Fang et al., 2017; de Oliveira Mann et al., 2019; Balka et al., 2020).

Based on previous research, the effective range of cGAS-STING has been extended to include all aspects of resistance to infection by pathogenic microorganisms (bacteria, viruses, parasites), anti-tumor, fibrosis, immunity, and inflammation. Inflammation is closely associated with fibrosis, and the former is often the initiating factor of the latter (Mack, 2018). Pro-inflammatory cytokines can be generated by the activated STING pathway and promote the onset and spread of inflammation. It can, for example, promote the conversion of endothelial cells, which are one of the vital participants in the formation and spread of inflammation (Zhao et al., 2021), into a pro-inflammatory phenotype (Pober and Sessa, 2007). In addition, activated endothelial cells can produce abundant chemokines and recruit mononuclear macrophages (Butcher, 1991) capable of producing inflammation-associated cytokines and TGF-β (Arabpour et al., 2021). Previous extensive conclusions have shown that TGF-β is conducive to the multiplication of fibroblasts and the aggregation of ECM, such as collagen (Fine and Goldstein, 1987; Clark et al., 1997). The above is only one aspect of STING-driven inflammation and fibrosis, and more specific molecular mechanisms remain to be added.

cyclic GMP-AMP synthase-stimulator of interferon genes is one of the interconnected and interacting pro-fibrotic signal pathways

TGF-β signal transmission contributes to fibrogenesis (Meng et al., 2016). TGF-beta receptor II (TGF-β RII) is activated by autophosphorylation after binding to TGF-β. TGF-β RII then recruits and phosphorylates TGF-beta receptor I (TGF-β RI), the next factor that activates Smad2/3. During this process, Smad4 forms a trimer with activated Smad2/3. It is transported to the nucleus, thereby enhancing the synthesis of a range of molecules associated with fibrosis, including fibronectin, alpha-smooth muscle actin (α-SMA), collagen, and so on (Heldin and Moustakas, 2016; Meng et al., 2016; Hu et al., 2018). In addition, the above processes facilitate the transformation of non-myofibroblasts into myofibroblasts and the activation of myofibroblasts, thus promoting the deposition of ECM (Mack and Yanagita, 2015; Meng et al., 2016). Activation of ER stress can be observed in mice receiving aortic banding or angiotensin II-induced cardiomyocytes, and in mice receiving CCl_4 (Iracheta-Vellve et al., 2016; Zhang et al., 2020). ER stress was shown to facilitate the stimulation of the cGAS-STING axis (Zhang et al., 2020), thereby promoting the generation of IFN-1 and NF-κB. Pro-inflammatory cytokines produced by NF-κB can promote the transcription and expression of TGF-β isoforms (Villiger et al., 1993). Notably, macrophages at the site of inflammation can continue to secrete inflammation-associated cytokines or TGF-β (Arabpour et al., 2021). In addition, angiotensin II can also promote the generation of TGF-β (Liu et al., 2017). As a result of the above interactions, the cGAS-STING signaling axis establishes an interconnection with the TGF-β/Smad signal transduction process, which is involved in fibrogenesis.

Numerous studies have confirmed that the JAK/STAT signal transduction is also closely relevant to the fibrotic process in many diseases, such as diabetic nephropathy (Zhang et al., 2021). The cGAS-STING signaling pathway produces interleukins and interferons that can function as ligands for the JAK/STAT signaling pathway. The receptor undergoes dimerization upon attachment to the ligand. JAK then couples to the receptor and undergoes phosphorylation activation, which then recruits and phosphorylates STAT, at which point the phosphorylated STAT forms a dimer and enters the nucleus, thereby regulating transcription and expression of the relevant genes (Morris et al., 2018; Bharadwaj et al., 2020; Montero et al., 2021; Zhang et al., 2021).

As a possible inducing factor of fibrosis, apoptosis is closely related to STING (Iracheta-Vellve et al., 2016). BCL-2-associated X protein (BAX) is an apoptosis-promoting protein involved in the mitochondrial apoptotic pathway, and its levels can be upregulated by STING (Li A. et al., 2019). On the one hand, BAX increases the permeability of the mitochondrial membrane to induce the leakage of cytochrome C and then initiates apoptosis through caspase-9 and downstream caspase-3/7 (Murthy et al., 2020; Xiong et al., 2021). On the other hand, mitochondrial DNA (mtDNA) released from mitochondria can activate cGAS. In addition, ER stress is also involved in promoting the interconnection between STING and BAX (Murthy et al., 2020). STING can also activate the MAPK pathway, but the exact mechanism remains to be investigated (Hopfner and Hornung, 2020). From the information available to date, the pro-fibrotic effects of STING are achieved, at least in part, through several of the classical fibrotic pathways described above. Activated STING mediates inflammatory tissue damage, thereby inducing the process of tissue repair and fibrosis. The TGF-β pathway is an essential player in the latter, actively

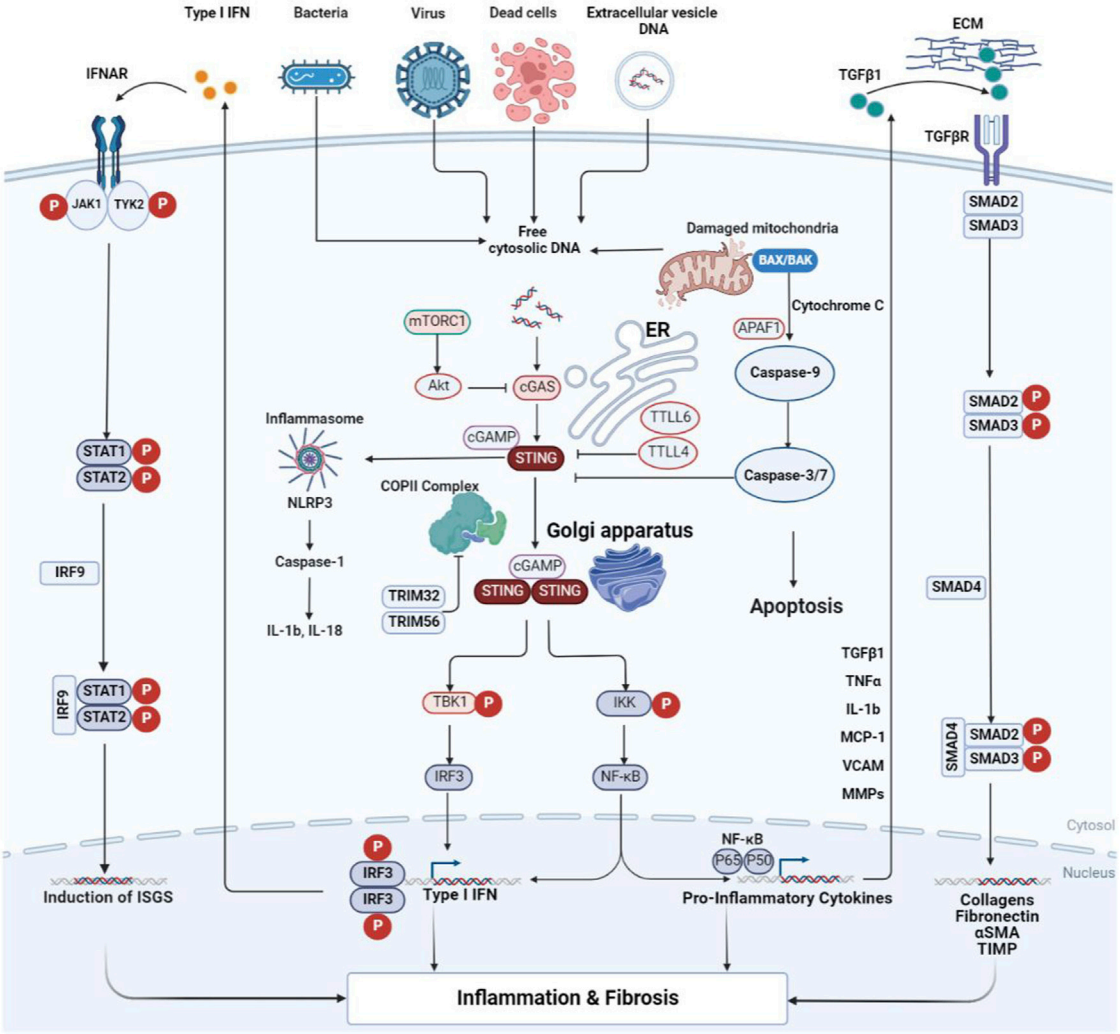


FIGURE 1
Crosstalk of the cGAS-STING signal transduction during inflammation and fibrosis. Cytoplasmic DNA from bacteria, viruses, dead cells, mitochondria, and extracellular vesicles is recognized by cGAS and thus activates STING. STING then exits the ER and transfers to the Golgi apparatus. During this process, STING completes the recruitment of TBK1 and IKK, as well as the activation of IRF3 and NF-κB. TGF-β activates TGF-β receptors, resulting in phosphorylation of Smad2/3. The activated Smad2/3 enters the nucleus to promote transcription of fibrosis-related genes. The pro-inflammatory cytokines produced by NF-κB can act on the signal transmission process of TGF-β/Smad. IFN from the STING pathway activates the IFN receptor, which is sequentially phosphorylated by the receptor-coupled JAK as well as downstream STAT, and the phosphorylated STAT dimer transfers to the nucleus to modulate gene transcription. cGAS is subject to negative regulatory effects induced by mTORC1 and Akt. It can also be inhibited in activity by TTLL4 and TTLL6, thus antagonizing the activation of STING. The apoptosis of the Bax pathway is initiated by caspase-9 and executed by caspase3/7, thus inhibiting the effect of cGAS initiation. α-SMA, alpha smooth muscle actin; Akt, protein kinase B; APAF1, apoptotic protease activating factor-1; BAX, BCL2-associated X protein; cGAMP, cyclic GMP-AMP; cGAS, cyclic GMP-AMP synthase; COP II, coat protein complex II; ECM, extracellular matrix; ER, endoplasmic reticulum; IFN, interferon; IFNAR, the interferon-α/β receptor; IKK, inhibitor of kappa B kinase; IL, interleukin; IRF, interferon regulatory factor; ISGs, interferon-stimulated genes; JAK1, janus kinase 1; MCP-1, monocyte chemoattractant protein-1; MMPs, matrix metalloproteinases; mTORC1, mechanistic target of rapamycin complex 1; NF-κB, nuclear factor-kappa B; NLRP3, NOD-like receptor thermal protein domain associated protein 3; STAT, signal transducer and activator of transcription; STING, stimulator of interferon genes; TBK1, TANK binding kinase 1; TGF-β, transforming growth factor beta; TGFβR, transforming growth factor beta receptor; TIMP, tissue inhibitor of metalloproteinase; TNF, tumor necrosis factor; TRIM, tripartite motif; TTLL, tubulin tyrosine ligase-like enzymes; TYK2, tyrosine kinase 2; VCAM, vascular cell adhesion molecule.

responding to the STING-induced inflammatory microenvironment. In addition, STING activates numerous downstream effector molecules (e.g., NF-κB, IL-6, NLRP3, *etc.*) that synergistically promote inflammatory responses, thereby exacerbating tissue damage (Li N. et al., 2019). To summarize, cGAS-STING forms an intricate network with numerous molecules and mechanisms involved in the fibrosis process (the above process is summarized in Figure 1).

The cyclic GMP-AMP synthase-stimulator of interferon genes signal path is a mediator of inflammatory and fibrotic processes in numerous diseases

The aberrantly activated cyclic GMP-AMP synthase-stimulator of interferon genes axis drives autoimmune and autoinflammatory diseases

STING-mediated physiological effects are critical for fighting pathogenic microorganisms such as viruses and bacteria and maintaining normal host immune function. However, excessive stimulation of cGAS and STING for various reasons can also lead to autoimmune and autoinflammatory diseases.

Aicardi-Goutières syndrome (AGS) can be caused by mutations in the human three-prime repair exonuclease 1 (*Trex1*) gene, which is essential for DNA degradation and preventing cytoplasmic DNA accumulation (Gall et al., 2012; Gao et al., 2015). Previous findings have suggested that intact *Trex1* negatively regulates STING-mediated effects. Fibromyositis of the heart occurs in *Trex1*-deficient mice, especially extensive fibrosis near the endocardium. In addition, fibromyositis also occurs in the skeletal muscles and tongue (Gall et al., 2012). In addition, mutations in *Trex1* have previously been shown to be highly relevant to familial chilblain lupus (FCL), retinal vasculopathy with cerebral leukodystrophy (RVCL), and systemic lupus erythematosus (SLE) (Lee-Kirsch et al., 2007; Rice et al., 2007; Rice et al., 2015). In recent years, elevated levels of cytoplasmic double-stranded DNA (dsDNA), IFN-1, and ISGs have been found in SLE patients, suggesting start-up of the cGAS-STING axis (Gkirtzimanaki et al., 2018; Kato et al., 2018; Wang et al., 2018). IFN-1 is an important link in the progression of SLE and is secreted mainly by dendritic cells and plasma cells (Murayama et al., 2020; Thim-Uam et al., 2020). Similarly, a dNTPase named sterile alpha motif and HD domain-containing protein 1 (SAMHD1) activates the exonuclease activity of MRE11 and thus participates in DNA replication, contributing to the degradation of part of the nascent DNA. In contrast, mutations in SAMHD1 cause chronic stimulation of STING, which is critical for AGS pathogenesis (Coquel et al., 2018). Mutations or deficiencies of the ribonuclease H2 (*RNASEH2*) gene will affect the integrity of DNA, which in turn leads to AGS (Mackenzie et al., 2016; Aditi et al., 2021). In addition, there are still many mutations in genes that are associated with AGS, all of which play a role in nucleic acid metabolism and are not described here.

Overactivation of the STING signal transduction and downstream overproduction of interferon are thought to contribute to autoinflammatory diseases. For example, functionally acquired mutations in STING are directly related to STING-associated vasculopathy with onset in infancy (SAVI). Its main manifestations include rashes, vasculitis, interstitial lung disease, and so on (Liu et al., 2014). These manifestations are similar to the clinical features of COPA syndrome (Volpi et al., 2018). COPA syndrome is an autoimmune disease caused by COPI coat complex subunit alpha (*COPA*) mutations with persistent release and accumulation of IFN-1 (Lepelley et al., 2020). COPA is indispensable for vesicular transport from the Golgi to the ER (Brandizzi and Barlowe, 2013), so mutations in *COPA* cause STING to stay in the Golgi and overstimulate IFN-1 production (Deng et al., 2020; Lepelley et al., 2020). The above results are sufficient to demonstrate that overstimulation of STING deviates from normal immune function and thus leads to adverse effects.

The role of stimulator of interferon genes in cardiac remodeling and fibrosis

Cardiac fibrosis is the terminal form of almost all types of heart disease (Czubryt and Hale, 2021), and STING is interspersed with fibrosis in various cardiac diseases. It has been shown that STING expression is increased in the hearts of dilated cardiomyopathy and hypertrophic cardiomyopathy patients, and in mice with myocardial remodeling caused by aortic banding. In addition, knockout of STING exhibited reduced levels of fibrosis biomarkers such as α-SMA, collagen type I (Col I), and collagen type III (Col III), and ER stress may be associated with this process (Zhang et al., 2020). Similarly, in cardiac failure mice induced by transverse aortic contraction, the above gene expression did not show an increase after cGAS knockout, revealing the effect of STING in pathological remodeling caused by cardiac pressure overload (Hu D. et al., 2020). It has also been demonstrated that the knockdown of STING reduces myocardial injury caused by STING-IRF3-activated NLRP3 (Li N. et al., 2019). The above studies revealed that the cGAS-STING path is an important participant in several heart diseases and tends to aggravate their damage, while inhibition of this signal axis may reduce the extent of fibrosis.

Stimulator of interferon genes in pulmonary inflammation and fibrosis

Pulmonary fibrosis exhibits a high morbidity and mortality rate in various diseases. It severely impairs lung function and dramatically affects patients' quality of life. However, few effective treatments are still available, so the search for new biomarkers and therapeutic strategies is essential. Current research suggests that the pro-fibrotic effects of STING are seen in a variety of lung diseases. Researchers used the induction of silica to create lung inflammatory injury and fibrosis in mice. They observed cleavage of caspase-3 and gasdermin D (GSDMD) and

phosphorylation of mixed-lineage kinase domain-like protein (MLKL). This demonstrates that silica-treated lung cells die by apoptosis, pyroptosis, and necroptosis. The dead cells consequently leak dsDNA, which triggers the action of STING and subsequent INF-1 (Benmerzoug et al., 2018). Similarly, the lungs of mice exposed to cigarette smoke are injured and release dsDNA that initiates the process of cGAS-STING signal transduction, which aggravates inflammatory injury and fibrosis in the lungs, providing a new possible therapeutic idea for COPD (Nascimento et al., 2019). Bleomycin (BLM), an anticancer drug, is often used to induce pulmonary fibrosis. According to some research, STING is how BLM causes pulmonary fibrosis to develop. After BLM treatment, the release of dsDNA was increased and activated the STING-mediated type 1 interferon response (Seo et al., 2021). This process involves the TGF-β/Smad path, as evidenced by elevated phosphorylated Smad2/3, α-SMA and Col-1 (Shi et al., 2022). Furthermore, STING expression was positively correlated with TGF-β-induced fibrosis (Sun S. C. et al., 2020), indicating a synergistic effect of STING and TGF-β in the fibrogenesis process. The application of some materials, such as graphitized multi-walled carbon nanotubes (GMWCNTs) in medicine can also induce inflammation and fibrosis of the lungs, showing thickening of the alveolar wall and upregulation of STING, TGF-β, and collagen levels in the diseased lungs (Han et al., 2021). The development of the coronavirus disease 2019 (COVID-19) has also been mentioned to involve the STING signaling-mediated type I interferon response (Neufeldt et al., 2022). Mitochondrial dysfunction, mtDNA release, cell fusion, and nucleus disruption induced by severe acute respiratory syndrome coronavirus two infection largely contribute to the activation of this pathway (Ren et al., 2021; Zhou et al., 2021; Liu X. et al., 2022; Domizio et al., 2022). While early INF-1 helps to fight viral infection, late-stage IFN-1 has been shown to exacerbate the severe COVID-19 inflammatory response and may be associated with poor prognosis (Wang N. et al., 2020; Lee et al., 2020; Lee and Shin, 2020; Galani et al., 2021). Both tissue damage and many inflammation-associated cytokines contribute to fibrosis after COVID-19. As well as the above traditional cGAS-STING-TBK1-IRF3 axis, Zhang et al. reported a non-classical STING-protein kinase RNA-like endoplasmic reticulum kinase (PERK)-eukaryotic initiation factor 2 alpha (eIF2α) signaling pathway, which is independent of each other and the direct activation of PERK by STING precedes that of TBK1-IRF3. The activation of PERK-eIF2α can be observed in mice with BLM-induced pulmonary fibrosis, and either knockout of STING or inhibition of eIF2α can reduce pulmonary fibrosis (Zhang et al., 2022). This provides a new possibility for a therapeutic approach targeting STING.

Stimulator of interferon genes and fibrosis in liver diseases

Fibrosis can be the common outcome of chronic liver disease, regardless of the cause (Iracheta-Vellve et al., 2016). Illness and fibrosis often characterise liver injury from various causes (such as nonalcoholic steatohepatitis and hepatitis virus) (Kisseleva and Brenner, 2021). Nonalcoholic steatohepatitis (NASH) can be considered as one of a series of types of nonalcoholic fatty liver disease (NAFLD), and its characteristics include liver inflammatory reaction, steatosis, damage to hepatocytes, and varying levels of fiber deposition (Friedman et al., 2018; Schuster et al., 2018; Pierantonelli and Svegliati-Baroni, 2019). In mice with these diseases, STING deficiency or disruption reduced hepatic steatosis, inflammatory damage and fibrous deposition (Luo et al., 2018), as indicated by the down-regulated Col1A1 and α-SMA contents (Yu et al., 2019). In addition, researchers analyzed liver samples from NASH patients and found that overall levels of STING and phosphorylated TBK1 were significantly elevated and consistent with the severity of fibrosis. At the same time, hepatic stellate cells (HSCs) were activated, and the overall levels of Col1A1, fibronectin, and TGF-β1 were significantly upregulated (Wang X. et al., 2020). Infection with schistosomiasis is also accompanied by liver fibrosis (He et al., 2020). Liang et al. used western blotting to detect fibrosis indicators in mice parasitized by Schistosoma japonicum and found that cGAS knockout mice showed less severe and a smaller proportion of fibrosis than control mice. Notably, STING knockout mice did not exhibit the above results, leading the researchers to conclude that neither STING nor IFN-β is involved in the fibrotic process in the liver following Schistosoma japonicum infection (Liang et al., 2022). Initiation of the STING signal transduction is attributed to the leakage of mtDNA to the outside of the mitochondria, followed by upregulation of pro-inflammatory cytokine expression by NF-κB, which ultimately promotes fibrosis (Yong et al., 2021; Shen et al., 2022). Additionally, liver damage and fibrosis caused by microbial DNA can also be mediated by STING signaling (Luo et al., 2022). The activation and conversion of HSCs to myofibroblasts has been shown in numerous studies to be crucial for the formation of fibrosis (Tsuchida and Friedman, 2017), revealing the role of STING activation of HSCs in fibrosis. In summary, STING may be one of the markers of liver fibrosis progression and a target for treatment.

Stimulator of interferon genes and kidney disease

Fibrosis of the kidney is the universal pathological manifestation of chronic renal disease (Romagnani et al., 2017). It can eventually destroy the kidney's normal function and seriously threaten patients' health. For mitochondrial DNA to remain intact, transcription factor A (*TFAM*) is essential. Enhanced cGAS-STING signaling was observed in kidney samples deficient in *TFAM*, accompanied by poor renal function, high levels of inflammation, and fibrosis, suggesting

that STING-mediated renal fibrosis can be induced by mtDNA (Allison, 2019; Chung et al., 2019). Hao et al. studied a folic acid-induced fibrosis model in mice with renal insufficiency and found that the overall levels of STING, TBK1, IRF3, and perforin were elevated in IL-2-treated NK cells. After treatment with STING inhibitors and high-dose Shenkang injection, the levels of these substances decreased significantly and were accompanied by an improvement in renal function. In addition, similar results from *in vitro* experiments verified the above findings. It is proven that Shenkang injection can exert its anti-fibrosis effect by inhibiting the STING pathway (Hao et al., 2022). The increased expression of STING, TBK1 and IRF3 could also be seen in the renal tubular epithelial cells of G2APOL1 (G2 coding variant of apolipoprotein L1) mice, while the collagen deposition decreased significantly after knockout of STING. Similarly, STING inhibitors showed protective effects on renal function, such as reducing the concentration of serum creatinine, blood urea nitrogen, proteinuria, and the degree of fibrosis (Wu et al., 2021). Furthermore, some studies have found that in rhabdomyolysis-induced acute kidney injury mice deficient in absent in melanoma 2 (*AIM2*), dsDNA released from injured muscle cells is turned to activate STING and increase the expression of IFN-1 and NF-κB, exacerbating inflammation and fibrosis due to the inability of *AIM2* deficiency to scavenge inflammatory macrophages in time (Baatarjav et al., 2022).

The relationship between stimulator of interferon genes and neurodegenerative diseases

In recent years, some new achievements have been made in researching the cGAS-STING axis in degenerative neurologic disorders. Alzheimer's disease (AD) is a prevalent neurologic degenerative condition, and its pathological manifestations are mainly characterized by amyloid beta-peptide (Aβ) plaques and tau neurofibrillary tangles (Jack et al., 2018; Scheltens et al., 2021). In addition, more and more studies suggest that neuroinflammation is a key driver of AD progression. Hou et al. conducted a study using an APP/PS1 mutant mouse model of AD and used the nicotinamide adenine dinucleotide (NAD) precursor nicotinamide riboside (NR) as a treatment and found significantly elevated levels of NLRP3 inflammasome in APP/PS1 mutant mice. And both DNA damage and the degree of inflammation were improved by using NR. Moreover, STING and cGAS expression was increased in microglia, and NR decreased cytoplasmic DNA levels in human AD fibroblasts, suggesting that neural inflammation may be induced by signaling associated with cGAS and STING (Hou et al., 2021).

Parkinson's disease (PD) is another common neurologic degenerative condition. Both in the intrastriatal αSyn preformed fibril (αSyn-PFF) mouse model of PD and in microglia cultured *in vitro*, αSyn-PFFs caused DNA damage, as evidenced by increased levels of γH2A.X, a marker of DNA damage. Furthermore, activation of TBK1 in mice and increased STING expression in human Parkinson's disease patients show that STING activation contributes to α-synuclein-induced neuroinflammation and degeneration (Hinkle et al., 2022).

In mice with amyotrophic lateral sclerosis (ALS), accumulated TAR DNA-binding protein 43 in the cytoplasm can lead to mtDNA leakage and thus activate cGAS, ultimately causing upregulation of NF-κB and IFN-1 levels. In contrast, in STING-deficient ALS mice, neuroinflammation and degeneration were ameliorated (Yu et al., 2020). In addition, the amplification of the GGGGCC sequence in the open reading frame 72 of chromosome 9p (*C9ORF72*) is directly related to the pathogenesis of most familial ALS (DeJesus-Hernandez et al., 2011; Renton et al., 2011), and deletion of *C9ORF72* can promote STING-mediated IFN-1 production (McCauley et al., 2020). Superoxide dismutase 1 (*SOD1*) mutations are another common cause of inherited ALS (Chen et al., 2013; Mejzini et al., 2019), resulting in misfolding of the SOD1 protein. In *SOD1* mutant ALS mice, cGAS senses mitochondrial destruction and activates STING (Tan et al., 2022). This evidence provides a new option for effective interventions in neurodegenerative diseases, that is, to suppress STING.

Stimulator of interferon genes and other diseases

In BLM-induced systemic sclerosis mice, an increase in cytoplasmic DNA was observed, which promoted the translocation of RNA polymerase III A (POLR3A) and activated the POLR3A/STING pathway. The result is the activation of fibroblasts, increased collagen, vascular endothelial injury, and fibrosis. Both knockout of STING and the use of H-151 (an inhibitor of STING) can reduce the fibrosis and vascular lesions of systemic sclerosis (Liu C. et al., 2022). Mouse colitis and human inflammatory bowel disease (IBD) have the characteristics of chronic inflammatory injury and fibrosis, and the high expression of STING can also be observed in their intestines (Shmuel-Galia et al., 2021). Notably, in addition to exacerbating colonic inflammation caused by intestinal microorganisms, STING promotes the expression of the cytokine IL-10, which has anti-inflammatory properties, to diminish the extent of colitis. In addition, it also reduces the production of intestinal polyps and may reduce the potential for conversion of colitis to cancer. This demonstrates the function of STING in maintaining immune homeostasis (Ahn et al., 2017). On the other hand, the mutated autophagy-related protein 16-like 1 (*Atg16l1*) gene triggers impaired autophagy, resulting in reduced STING and cytoplasmic DNA clearance, which is closely associated with IBD. Treatment with IL-22 can activate the cGAS-STING pathway by endoplasmic reticulum stress or by

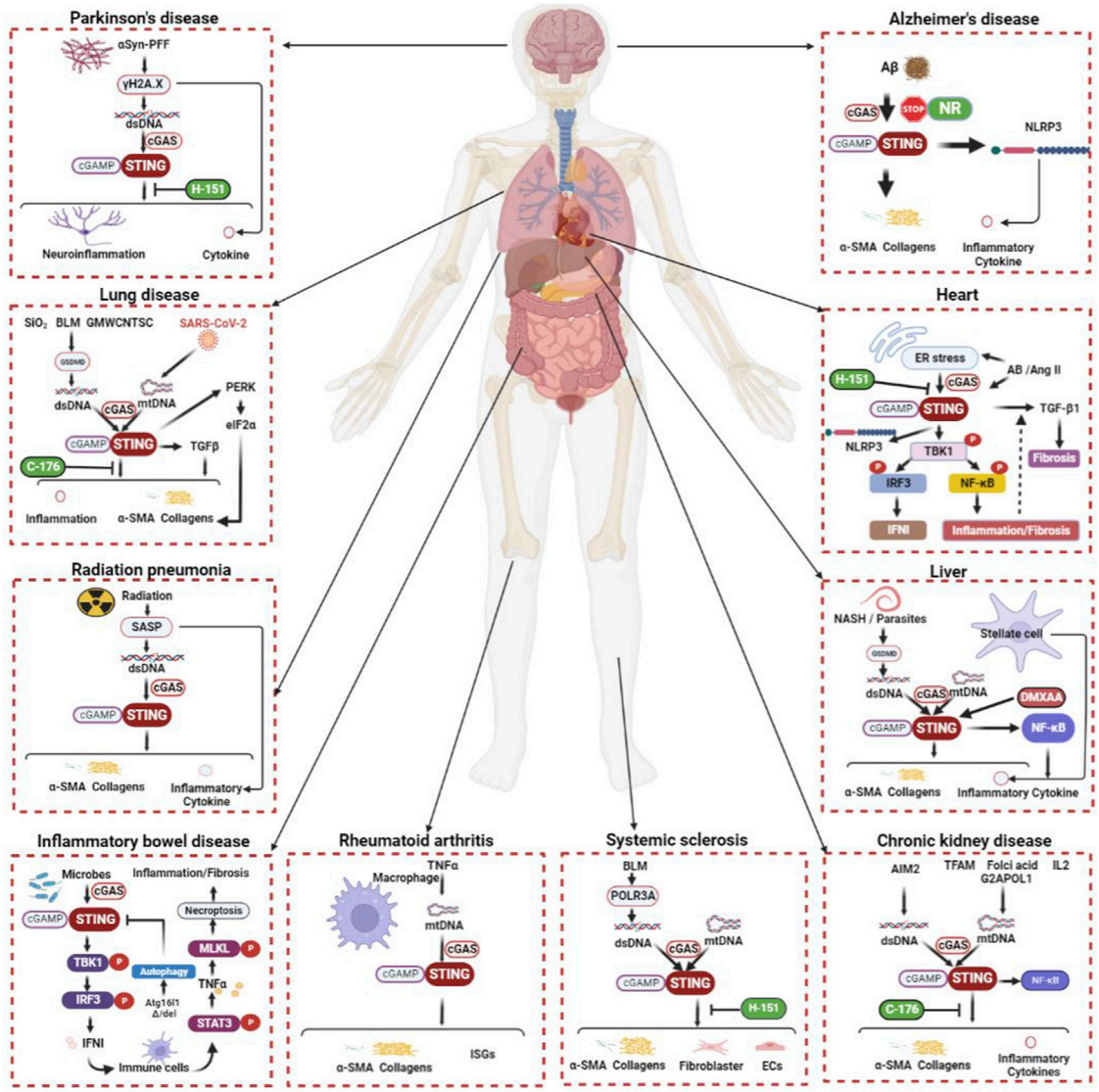


FIGURE 2
The cGAS-STING signaling pathway during organ inflammation and fibrosis. The cGAS-STING signal transduction process is inseparably linked to inflammation and fibrogenesis in multiple systems, including respiratory, circulatory, digestive, urinary, and neurological systems. The etiology of fibrosis includes inflammation, injury, toxins, radiation, foreign bodies, parasites, immunity, *etc.* STING works with TGF-β and many other molecular mechanisms to promote fibrosis in various organs. Although not all fibrosis etiologies and related mechanisms can be described exhaustively here, it is certain that the above pathways have a place in the fibrosis of different human systems. α-SMA, alpha smooth muscle actin; αSyn-PFF, αSyn preformed fibril; Aβ, amyloid beta-peptide; AB, aortic banding; AIM2, absent in melanoma 2; Ang-II, angiotensin II; Atg16l1, autophagy-related protein 16-like 1; BLM, bleomycin; cGAMP, cyclic GMP-AMP; DMXAA, 5,6-dimethylxanthenone-4-acetic acid; dsDNA, double-stranded DNA; ECs, epithelial cells; eIF2α, eukaryotic initiation factor 2 alpha; ER, endoplasmic reticulum; G2APOL1, G2 coding variant of apolipoprotein L1; GMWCNTs, graphitized multi-walled carbon nanotubes GSDMD, gasdermin D; IFN, interferon; IL, interleukin; IRF, interferon regulatory factor; ISGs, interferon-stimulated genes; MLKL, mixed-lineage kinase domain-like protein; mtDNA, mitochondrial DNA; NASH, nonalcoholic steatohepatitis; NF-κB, nuclear factor kappa-B; NLRP3, NOD-like receptor thermal protein domain associated protein 3; NR, nicotinamide riboside; PERK, protein kinase RNA-like endoplasmic reticulum kinase; POLR3A, RNA polymerase III A; SARS-CoV-2, severe acute respiratory syndrome coronavirus 2; SASP, senescence-associated secretory phenotype; STAT, signal transducer and activator of transcription; STING, stimulator of interferon genes; TBK1, TANK binding kinase 1; TFAM, mitochondrial transcription factor A; TGF-β, transforming growth factor beta; TNF, tumor necrotic factor.

increasing cytoplasmic DNA, and deletion or mutation of the *Atg16l1* gene has been shown to enhance the IFN-1 levels elevated by IL-22, thereby exacerbating intestinal inflammatory injury (Aden et al., 2018). The above results reveal the association of the *Atg16l1* gene, STING and IL-22 in IBD. In addition, recent results show that in mouse ovarian granulosa cells, mtDNA can activate the STING pathway through a similar mechanism, causing an increase in

cytokines such as TNF-α, thereby promoting the spread of inflammation and interstitial hyperplasia (Liu K. et al., 2022). Rheumatoid arthritis can be driven by TNF, which also relies on STING-IRF3-mediated interferon production. In THP-1 cells chronically treated with TNF, mtDNA was observed to be released into the cytoplasm and bound to cGAS to initiate a downstream inflammatory response, consistent with elevated ISGs in the joints of the mouse model (Willemsen et al., 2021).

Radiation therapy is an important cancer treatment, but the clinical complications it causes should not be ignored. Treating malignant tumors with radiation is often complicated by lung radiation damage, which can eventually cause pulmonary fibrosis. The activated STING signal axis exists in the macrophages of mice with radiation pneumonia (RP), suggesting a possible association with inflammation and fibrosis in RP (Yang et al., 2022a). In addition, radiation has been shown to accelerate cancer cell senescence and is associated with an elevated senescence-associated secretory phenotype (SASP). This process involves the recognition of radiation-induced dsDNA by cGAS and thus activates the subsequent effects of STING (Glück et al., 2017; Takahashi et al., 2018; Constanzo et al., 2021). Furthermore, SASP after radiation therapy is thought to promote fibrosis (Nguyen et al., 2018). This partially explains how STING contributes to fibrogenesis by radiation treatment for cancer. In Figure 2, the connection between STING and the illnesses of each of the organs mentioned above is depicted uniformly.

Application of stimulator of interferon genes agonists and antagonists

Theoretically, STING agonists can aggravate the fibrogenic effect of cGAS-STING signaling. Therefore, STING activators are not usually used to treat fibrosis. STING agonists, such as DMXAA, have been shown to aggravate liver inflammation and steatosis in mice, as well as increase TNF-α and IL-6 expression (Yu et al., 2019). In addition, wild-type mouse BMDMs were co-cultured with human liver stellate cells in conditions containing TGF-β. When the above cells were treated with DMXAA, the phosphorylation level of p38 and the content of molecules associated with fibrous deposition (e.g. α-SMA) were increased (Luo et al., 2018). Therefore, the application of STING activators in fibrosis treatment is limited except for experimental purposes. STING agonists utilize the principle of cGAS-STING-induced type I interferon response and are now commonly used in clinical practice as one of the anti-tumor treatments (Jiang et al., 2020; Wang Y. et al., 2020; Amouzegar et al., 2021). DMXAA and ADU-S100 (an agonist of STING) attenuated motor dysfunction in mice with bone tumors and reduced abnormal behavior in mice due to bone pain. X-rays showed that bone destruction due to tumors was also ameliorated by STING agonists (Wang et al., 2021). In the BRCA1-deficient mouse breast cancer model, DMXAA also promoted the polarization of macrophages to M1 in the tumor microenvironment, thus enhancing the anti-tumor activity of macrophages (Wang et al., 2022). In a clinical trial of melanoma, breast cancer, lymphoma, ovarian cancer, and many other tumor types, ADU-S100 showed good safety and tolerance, accompanied by immune activation such as increased levels of inflammation and active T cell proliferation (Meric-Bernstam et al., 2022). In addition, the melanoma model of B16-F10 mice was treated with c-di-GMP packaged with nanoparticles, and the result was that the drug resistance of the tumor to anti-PD-1 was reduced (Nakamura et al., 2021). In addition to these, many CDN analogues or synthetic agonists still play a role in a variety of solid tumor types (Jiang et al., 2020). The types, effects, safety, mechanisms, and modes of action of these agonists will be important future research directions in tumor immunity.

As STING inhibitors, C-178 and C-176 belong to nitrofuran derivatives. The nitro and furan rings are essential for maintaining activity, and the group at the 4-position of the phenyl ring also influences the magnitude of their effects. These two compounds were shown to inhibit palmitoylation of STING by covalent modification of cysteine 91 (Cys91) (Haag et al., 2018), whereas palmitoylation of Cys88/91 is essential for STING activation (Mukai et al., 2016). In mice, C-178 and C-176 partially reversed the activating effect of CMA (a STING agonist) on STING. In addition, using C-176 reduced some clinical manifestations of AGS syndrome in *Trex1* knockout mice. However, the above two inhibitors did not show inhibitory effects on human STING (hsSTING) (Haag et al., 2018). C-176 inhibits perinuclear translocation of STING and NF-κB translocation into the nucleus, thereby reducing upregulated inflammatory cytokines and ultimately reducing fibronectin expression to reduce liver fibrosis (Shen et al., 2022). In addition, C-176 attenuated kidney fibrosis and GMWCNTs-mediated inflammatory injury and fibrous deposition in the lung, thereby protecting organ function (Chung et al., 2019; Han et al., 2021). Intestinal reperfusion injury can involve the lungs and cause acute tissue damage. C-176 can significantly reduce apoptosis in this case, thereby improving lung injury and subsequent fibrosis. Notably, STING inhibition was accompanied by an increase in AMPK phosphorylation levels, which suggests an interaction between AMPK and STING from another perspective (Yang et al., 2022b). Indole urea (H-151) is derived from 3-acylamino indole, which is also a derivative of nitrofuran. It is a selective STING inhibitor with high efficiency and a strong inhibitory effect on both mouse STING and hsSTING (Haag et al., 2018). It improves heart function in mice after myocardial infarction (MI) by reducing STING-induced type 1 interferon response and inflammation. In addition, cardiac remodeling, apoptosis of cardiomyocytes, and the generation of fibrotic biomarkers, including α-SMA, collagen, *etc.*, were reduced (Hu et al., 2022; Rech et al., 2022). However, using H-151 did not seem beneficial in improving mortality in the early stages of MI (Rech et al., 2022).

Similarly, endogenous nitro fatty acids (NO2-FA) can also reduce IFN-1 production by inhibiting the palmitoylation of

STING (Hansen et al., 2018). It is a product of endogenous unsaturated fatty acids nitrated by nitrogen dioxide and has anti-inflammatory properties (Delmastro-Greenwood et al., 2015). The cyclic peptide Actin C is a chlorinated cyclopentapeptides extracted from the natural medicinal plant Aster Tataricus and belongs to one kind of Compositae cyclopeptide. It is composed of one protein amino acid and four non-protein amino acids. In addition, it also contains two chlorine atoms as functional groups. Astin C is a STING antagonist that acts at the site on STING that binds cyclic dinucleotide (CDN), and the recruitment of IRF3 by STING is thus blocked (Li et al., 2018). It is worth noting that NO2-FAs, Astin C, and tetradroisoquinolone acetic acid (compound 18, an inhibitor of STING) (Siu et al., 2019) were found to be less effective against human STING. In addition to the above, Hong et al. substituted phenoxy-methyl in a group of compounds containing benzene-1-sulfonamido-3-amide groups with phenol hydroxyl groups, resulting in the compound SN-011, a STING inhibitor with high affinity for the CDN-binding pocket, which improved systemic inflammation and clinical outcomes in *Trex1* knockout mice and was shown to be effective in both mice and humans, with lower toxicity and higher specificity than H-151 (Hong et al., 2021). ISD017 is a fusion peptide of the influenza hemagglutinin protein and is located in the N-terminal region of the HA2 peptide chain of hemagglutinin. It is another STING inhibitor effective in both mice and humans. It relies on the STING ER retention factor stromal interaction molecule 1 (STIM1) to prevent STING migration from the ER to the Golgi, thereby blocking the downstream activity (Prabakaran et al., 2021). Given that SN-011 and ISD017 are relatively new results, their detailed mechanisms and anti-fibrotic effects remain to be investigated. Details of the application of STING-related drugs can be found in the Supplementary Material.

From the currently available information, there is no doubt that STING inhibitors are effective in improving fibrosis, so more and more in-depth animal experiments and clinical trials are essential for the clinical translation of STING inhibitors.

Discussion and prospect

According to general belief, the cGAS-STING axis assists the body in combating potentially adverse factors such as bacteria, viruses, and tumors. However, a large number of new results on the cGAS-STING signal transduction pathway that exaggerate inflammatory damage and its pro-fibrotic effects show its bad side. It is now well established that activated cGAS-STING promotes inflammatory injury and subsequent fibrotic repair, which enriches the mechanistic system of fibrosis and contributes to the search for new therapeutic strategies against fibrosis. In addition, the effects of cGAS-STING pathway activation gave us many insights. As previously mentioned, auto-inflammatory diseases characterized by STING overactivation and IFN-1 overexpression (e.g., SAVI and AGS) have more promising therapeutic targets. STING inhibitors will fundamentally block the progression of this type of disease by preventing the continued transmission of STING signals, thereby reducing excessive inflammatory damage. Inflammation and fibrosis are often two juxtaposed processes in tissue injury, which means that numerous patients with congenital autoimmune diseases would benefit from STING inhibitors, as they often suffer irreversible organ remodeling. In addition, considering the source of DNA recognized by cGAS, we believe that the administration of membrane stabilizers or drugs that protect the integrity of the nuclear membrane for specific diseases such as radiological lung injury could help to block the conduction of this pathway from upstream of STING.

However, many unknown aspects still need to be answered by future research. For instance, how to discriminate between one's DNA and exogenous deleterious DNA, how to maintain appropriate inflammation, and how to circumvent the pathogenic effects of STING while making full use of its immune defenses are all important research directions. The signaling networks involved in fibrosis are intricate, and here we identify some of the mechanisms of STING based on existing studies. However, the specific detailed mechanisms of cGAS-STING to promote fibrosis remains to be refined, and this will be the focus of future studies. Many STING inhibitors reverse the inflammation and fibrosis of diseased organs in animal experiments. In addition, more and more STING antagonists sensitive to human STING have been screened out *in vitro*. The scope of application of STING inhibitors will expand gradually, and we believe that future clinical trials will further verify the potential of STING inhibitors.

Author contributions

YLL, HG, YC, and CL were responsible for the design of this study. YLL, YHL, and LX searched the literature and wrote this manuscript. YLL, YHL, LX, JX, and HG participated in the design and drawing of the figures. PL, WX, and CL worked together on the preparation and revision of the Supplementary Material. All authors participated in reading and revising this paper and approved the submitted version.

Funding

This work was supported by grants from the National Natural Science Foundation of China (82172165), the Taishan Young Scholar Program of Shandong Province (tsqn202103171), and the Clinical Research Foundation of Shandong Province Medical Association (YXH2020ZX024). The project is funded by the China Postdoctoral Science Foundation (2020T130072ZX)

and the Clinical Research Center of Shandong University (2020SDUCRCC007).

Acknowledgments

We wish to thank our colleagues from the Department of Critical Care Medicine, Qilu Hospital of Shandong University, for their valuable comments on the manuscript.

Conflict of interest

The authors declare that the research was conducted in the absence of any commercial or financial relationships that could be construed as a potential conflict of interest.

Publisher's note

All claims expressed in this article are solely those of the authors and do not necessarily represent those of their affiliated organizations, or those of the publisher, the editors and the reviewers. Any product that may be evaluated in this article, or claim that may be made by its manufacturer, is not guaranteed or endorsed by the publisher.

Supplementary material

The Supplementary Material for this article can be found online at: https://www.frontiersin.org/articles/10.3389/fphar.2022.1033982/full#supplementary-material

References

Abe, T., and Barber, G. N. (2014). Cytosolic-DNA-mediated, STING-dependent proinflammatory gene induction necessitates canonical NF-κB activation through TBK1. *J. Virol.* 88 (10), 5328–5341. doi:10.1128/jvi.00037-14

Ablasser, A., Goldeck, M., Cavlar, T., Deimling, T., Witte, G., Röhl, I., et al. (2013). cGAS produces a 2'-5'-linked cyclic dinucleotide second messenger that activates STING. *Nature* 498 (7454), 380–384. doi:10.1038/nature12306

Aden, K., Tran, F., Ito, G., Sheibani-Tezerji, R., Lipinski, S., Kuiper, J. W., et al. (2018). ATG16L1 orchestrates interleukin-22 signaling in the intestinal epithelium via cGAS-STING. *J. Exp. Med.* 215 (11), 2868–2886. doi:10.1084/jem.20171029

Aditi, Downing, S. M., Schreiner, P. A., Kwak, Y. D., Li, Y., Shaw, T. I., et al. (2021). Genome instability independent of type I interferon signaling drives neuropathology caused by impaired ribonucleotide excision repair. *Neuron* 109 (24), 3962–3979.e6. doi:10.1016/j.neuron.2021.09.040

Ahn, J., Son, S., Oliveira, S. C., and Barber, G. N. (2017). STING-dependent signaling underlies IL-10 controlled inflammatory colitis. *Cell Rep.* 21 (13), 3873–3884. doi:10.1016/j.celrep.2017.11.101

Allison, S. J. (2019). STING activation by cytoplasmic mtDNA triggers renal inflammation and fibrosis. *Nat. Rev. Nephrol.* 15 (11), 661. doi:10.1038/s41581-019-0211-y

Amouzegar, A., Chelvanambi, M., Filderman, J. N., Storkus, W. J., and Luke, J. J. (2021). STING agonists as cancer therapeutics. *Cancers (Basel)* 13 (11), 2695. doi:10.3390/cancers13112695

Andreeva, L., Hiller, B., Kostrewa, D., Lässig, C., de Oliveira Mann, C. C., Jan Drexler, D., et al. (2017). cGAS senses long and HMGB/TFAM-bound U-turn DNA by forming protein-DNA ladders. *Nature* 549 (7672), 394–398. doi:10.1038/nature23890

Arabpour, M., Saghazadeh, A., and Rezaei, N. (2021). Anti-inflammatory and M2 macrophage polarization-promoting effect of mesenchymal stem cell-derived exosomes. *Int. Immunopharmacol.* 97, 107823. doi:10.1016/j.intimp.2021.107823

Baatarjav, C., Komada, T., Karasawa, T., Yamada, N., Sampilvanjil, A., Matsumura, T., et al. (2022). dsDNA-induced AIM2 pyroptosis halts aberrant inflammation during rhabdomyolysis-induced acute kidney injury. *Cell Death Differ*. doi:10.1038/s41418-022-01033-9

Balka, K. R., Louis, C., Saunders, T. L., Smith, A. M., Calleja, D. J., D'Silva, D. B., et al. (2020). TBK1 and IKKε act redundantly to mediate STING-induced NF-κB responses in myeloid cells. *Cell Rep.* 31 (1), 107492. doi:10.1016/j.celrep.2020.03.056

Benmerzoug, S., Rose, S., Bounab, B., Gosset, D., Duneau, L., Chenuet, P., et al. (2018). STING-dependent sensing of self-DNA drives silica-induced lung inflammation. *Nat. Commun.* 9 (1), 5226. doi:10.1038/s41467-018-07425-1

Bharadwaj, U., Kasembeli, M. M., Robinson, P., and Tweardy, D. J. (2020). Targeting janus kinases and signal transducer and activator of transcription 3 to treat inflammation, fibrosis, and cancer: Rationale, progress, and caution. *Pharmacol. Rev.* 72 (2), 486–526. doi:10.1124/pr.119.018440

Brandizzi, F., and Barlowe, C. (2013). Organization of the ER-Golgi interface for membrane traffic control. *Nat. Rev. Mol. Cell Biol.* 14 (6), 382–392. doi:10.1038/nrm3588

Butcher, E. C. (1991). Leukocyte-endothelial cell recognition: three (or more) steps to specificity and diversity. *Cell* 67 (6), 1033–1036. doi:10.1016/0092-8674(91)90279-8

Chen, S., Sayana, P., Zhang, X., and Le, W. (2013). Genetics of amyotrophic lateral sclerosis: an update. *Mol. Neurodegener.* 8, 28. doi:10.1186/1750-1326-8-28

Chung, K. W., Dhillon, P., Huang, S., Sheng, X., Shrestha, R., Qiu, C., et al. (2019). Mitochondrial damage and activation of the STING pathway lead to renal inflammation and fibrosis. *Cell Metab.* 30 (4), 784–799.e5. doi:10.1016/j.cmet.2019.08.003

Clark, R. A., McCoy, G. A., Folkvord, J. M., and McPherson, J. M. (1997). TGF-beta 1 stimulates cultured human fibroblasts to proliferate and produce tissue-like fibroplasia: a fibronectin matrix-dependent event. *J. Cell. Physiol.* 170 (1), 69–80. doi:10.1002/(SICI)1097-4652(199701)170:1<69::AID-JCP8>3.0.CO;2-J

Constanzo, J., Faget, J., Ursino, C., Badie, C., and Pouget, J. P. (2021). Radiation-induced immunity and toxicities: The versatility of the cGAS-STING pathway. *Front. Immunol.* 12, 680503. doi:10.3389/fimmu.2021.680503

Coquel, F., Silva, M. J., Técher, H., Zadorozhny, K., Sharma, S., Nieminuszczy, J., et al. (2018). SAMHD1 acts at stalled replication forks to prevent interferon induction. *Nature* 557 (7703), 57–61. doi:10.1038/s41586-018-0050-1

Czubryt, M. P., and Hale, T. M. (2021). Cardiac fibrosis: Pathobiology and therapeutic targets. *Cell. Signal.* 85, 110066. doi:10.1016/j.cellsig.2021.110066

de Oliveira Mann, C. C., Orzalli, M. H., King, D. S., Kagan, J. C., Lee, A. S. Y., and Kranzusch, P. J. (2019). Modular architecture of the STING C-terminal tail allows interferon and NF-κB signaling adaptation. *Cell Rep.* 27 (4), 1165–1175.e5. doi:10.1016/j.celrep.2019.03.098

DeJesus-Hernandez, M., Mackenzie, I. R., Boeve, B. F., Boxer, A. L., Baker, M., Rutherford, N. J., et al. (2011). Expanded GGGGCC hexanucleotide repeat in noncoding region of C9ORF72 causes chromosome 9p-linked FTD and ALS. *Neuron* 72 (2), 245–256. doi:10.1016/j.neuron.2011.09.011

Delmastro-Greenwood, M., Hughan, K. S., Vitturi, D. A., Salvatore, S. R., Grimes, G., Potti, G., et al. (2015). Nitrite and nitrate-dependent generation of anti-inflammatory fatty acid nitroalkenes. *Free Radic. Biol. Med.* 89, 333–341. doi:10.1016/j.freeradbiomed.2015.07.149

Deng, Z., Chong, Z., Law, C. S., Mukai, K., Ho, F. O., Martinu, T., et al. (2020). A defect in COPI-mediated transport of STING causes immune dysregulation in COPA syndrome. *J. Exp. Med.* 217 (11), e20201045. doi:10.1084/jem.20201045

Dobbs, N., Burnaevskiy, N., Chen, D., Gonugunta, V. K., Alto, N. M., and Yan, N. (2015). STING activation by translocation from the ER is associated with infection and autoinflammatory disease. *Cell Host Microbe* 18 (2), 157–168. doi:10.1016/j.chom.2015.07.001

Domizio, J. D., Gulen, M. F., Saidoune, F., Thacker, V. V., Yatim, A., Sharma, K., et al. (2022). The cGAS-STING pathway drives type I IFN immunopathology in COVID-19. *Nature* 603 (7899), 145–151. doi:10.1038/s41586-022-04421-w

Ergun, S. L., Fernandez, D., Weiss, T. M., and Li, L. (2019). STING polymer structure reveals mechanisms for activation, hyperactivation, and inhibition. *Cell* 178 (2), 290–301. doi:10.1016/j.cell.2019.05.036

Fang, R., Wang, C., Jiang, Q., Lv, M., Gao, P., Yu, X., et al. (2017). NEMO-IKKβ are essential for IRF3 and NF-κB activation in the cGAS-STING pathway. *J. Immunol.* 199 (9), 3222–3233. doi:10.4049/jimmunol.1700699

Feng, J., Armillei, M. K., Yu, A. S., Liang, B. T., Runnels, L. W., and Yue, L. (2019). Ca(2+) signaling in cardiac fibroblasts and fibrosis-associated heart diseases. *J. Cardiovasc. Dev. Dis.* 6 (4), E34. doi:10.3390/jcdd6040034

Fine, A., and Goldstein, R. H. (1987). The effect of transforming growth factor-beta on cell proliferation and collagen formation by lung fibroblasts. *J. Biol. Chem.* 262 (8), 3897–3902. doi:10.1016/s0021-9258(18)61441-3

Friedman, S. L., Neuschwander-Tetri, B. A., Rinella, M., and Sanyal, A. J. (2018). Mechanisms of NAFLD development and therapeutic strategies. *Nat. Med.* 24 (7), 908–922. doi:10.1038/s41591-018-0104-9

Galani, I. E., Rovina, N., Lampropoulou, V., Triantafyllia, V., Manioudaki, M., Pavlos, E., et al. (2021). Untuned antiviral immunity in COVID-19 revealed by temporal type I/III interferon patterns and flu comparison. *Nat. Immunol.* 22 (1), 32–40. doi:10.1038/s41590-020-00840-x

Gall, A., Treuting, P., Elkon, K. B., Loo, Y. M., Gale, M., Jr., Barber, G. N., et al. (2012). Autoimmunity initiates in nonhematopoietic cells and progresses via lymphocytes in an interferon-dependent autoimmune disease. *Immunity* 36 (1), 120–131. doi:10.1016/j.immuni.2011.11.018

Gao, P., Ascano, M., Wu, Y., Barchet, W., Gaffney, B. L., Zillinger, T., et al. (2013). Cyclic [G(2', 5')pA(3', 5')p] is the metazoan second messenger produced by DNA-activated cyclic GMP-AMP synthase. *Cell* 153 (5), 1094–1107. doi:10.1016/j.cell.2013.04.046

Gao, D., Li, T., Li, X. D., Chen, X., Li, Q. Z., Wight-Carter, M., et al. (2015). Activation of cyclic GMP-AMP synthase by self-DNA causes autoimmune diseases. *Proc. Natl. Acad. Sci. U. S. A.* 112 (42), E5699–E5705. doi:10.1073/pnas.1516465112

Gkirtzimanaki, K., Kabrani, E., Nikoleri, D., Polyzos, A., Blanas, A., Sidiropoulos, P., et al. (2018). IFNα impairs autophagic degradation of mtDNA promoting autoreactivity of SLE monocytes in a STING-dependent fashion. *Cell Rep.* 25 (4), 921–933.e5. doi:10.1016/j.celrep.2018.09.001

Glück, S., Guey, B., Gulen, M. F., Wolter, K., Kang, T. W., Schmacke, N. A., et al. (2017). Innate immune sensing of cytosolic chromatin fragments through cGAS promotes senescence. *Nat. Cell Biol.* 19 (9), 1061–1070. doi:10.1038/ncb3586

Goh, G. B., Pagadala, M. R., Dasarathy, J., Unalp-Arida, A., Sargent, R., Hawkins, C., et al. (2015). Renin-angiotensin system and fibrosis in non-alcoholic fatty liver disease. *Liver Int.* 35 (3), 979–985. doi:10.1111/liv.12611

Gui, X., Yang, H., Li, T., Tan, X., Shi, P., Li, M., et al. (2019). Autophagy induction via STING trafficking is a primordial function of the cGAS pathway. *Nature* 567 (7747), 262–266. doi:10.1038/s41586-019-1006-9

Haag, S. M., Gulen, M. F., Reymond, L., Gibelin, A., Abrami, L., Decout, A., et al. (2018). Targeting STING with covalent small-molecule inhibitors. *Nature* 559 (7713), 269–273. doi:10.1038/s41586-018-0287-8

Han, B., Wang, X., Wu, P., Jiang, H., Yang, Q., Li, S., et al. (2021). Pulmonary inflammatory and fibrogenic response induced by graphitized multi-walled carbon nanotube involved in cGAS-STING signaling pathway. *J. Hazard. Mater.* 417, 125984. doi:10.1016/j.jhazmat.2021.125984

Hansen, A. L., Buchan, G. J., Rühl, M., Mukai, K., Salvatore, S. R., Ogawa, E., et al. (2018). Nitro-fatty acids are formed in response to virus infection and are potent inhibitors of STING palmitoylation and signaling. *Proc. Natl. Acad. Sci. U. S. A.* 115 (33), E7768–e7775. doi:10.1073/pnas.1806239115

Hao, J., Huang, X., Guan, J., Feng, J., Li, D., Cao, S., et al. (2022). Shenkang injection protects against renal fibrosis by reducing perforin expression through the STING/TBK1/IRF3 signaling pathways in natural killer cells. *Phytomedicine.* 104, 154206. doi:10.1016/j.phymed.2022.154206

He, X., Wang, Y., Fan, X., Lei, N., Tian, Y., Zhang, D., et al. (2020). A schistosome miRNA promotes host hepatic fibrosis by targeting transforming growth factor beta receptor III. *J. Hepatol.* 72 (3), 519–527. doi:10.1016/j.jhep.2019.10.029

Heldin, C. H., and Moustakas, A. (2016). Signaling receptors for TGF-β family members. *Cold Spring Harb. Perspect. Biol.* 8 (8), a022053. doi:10.1101/cshperspect.a022053

Henderson, N. C., Rieder, F., and Wynn, T. A. (2020). Fibrosis: from mechanisms to medicines. *Nature* 587 (7835), 555–566. doi:10.1038/s41586-020-2938-9

Hinkle, J. T., Patel, J., Panicker, N., Karuppagounder, S. S., Biswas, D., Belingon, B., et al. (2022). STING mediates neurodegeneration and neuroinflammation in nigrostriatal α-synucleinopathy. *Proc. Natl. Acad. Sci. U. S. A.* 119 (15), e2118819119. doi:10.1073/pnas.2118819119

Hong, Z., Mei, J., Li, C., Bai, G., Maimaiti, M., Hu, H., et al. (2021). STING inhibitors target the cyclic dinucleotide binding pocket. *Proc. Natl. Acad. Sci. U. S. A.* 118 (24), e2105465118. doi:10.1073/pnas.2105465118

Hopfner, K. P., and Hornung, V. (2020). Molecular mechanisms and cellular functions of cGAS-STING signalling. *Nat. Rev. Mol. Cell Biol.* 21 (9), 501–521. doi:10.1038/s41580-020-0244-x

Horowitz, J. C., and Thannickal, V. J. (2019). Mechanisms for the resolution of organ fibrosis. *Physiol. (Bethesda)* 34 (1), 43–55. doi:10.1152/physiol.00033.2018

Hou, Y., Wei, Y., Lautrup, S., Yang, B., Wang, Y., Cordonnier, S., et al. (2021). NAD(+) supplementation reduces neuroinflammation and cell senescence in a transgenic mouse model of Alzheimer's disease via cGAS-STING. *Proc. Natl. Acad. Sci. U. S. A.* 118 (37), E1876–E1885. doi:10.1073/pnas.1718819115

Hu, H. H., Chen, D. Q., Wang, Y. N., Feng, Y. L., Cao, G., Vaziri, N. D., et al. (2018). New insights into TGF-β/Smad signaling in tissue fibrosis. *Chem. Biol. Interact.* 292, 76–83. doi:10.1016/j.cbi.2018.07.008

Hu, D., Cui, Y. X., Wu, M. Y., Li, L., Su, L. N., Lian, Z., et al. (2020). Cytosolic DNA sensor cGAS plays an essential pathogenetic role in pressure overload-induced heart failure. *Am. J. Physiol. Heart Circ. Physiol.* 318 (6), H1525–H1537. doi:10.1152/ajpheart.00097.2020

Hu, H. H., Cao, G., Wu, X. Q., Vaziri, N. D., and Zhao, Y. Y. (2020). Wnt signaling pathway in aging-related tissue fibrosis and therapies. *Ageing Res. Rev.* 60, 101063. doi:10.1016/j.arr.2020.101063

Hu, S., Gao, Y., Gao, R., Wang, Y., Qu, Y., Yang, J., et al. (2022). The selective STING inhibitor H-151 preserves myocardial function and ameliorates cardiac fibrosis in murine myocardial infarction. *Int. Immunopharmacol.* 107, 108658. doi:10.1016/j.intimp.2022.108658

Iracheta-Vellve, A., Petrasek, J., Gyongyosi, B., Satishchandran, A., Lowe, P., Kodys, K., et al. (2016). Endoplasmic reticulum stress-induced hepatocellular death pathways mediate liver injury and fibrosis via stimulator of interferon genes. *J. Biol. Chem.* 291 (52), 26794–26805. doi:10.1074/jbc.M116.736991

Ishikawa, H., and Barber, G. N. (2008). STING is an endoplasmic reticulum adaptor that facilitates innate immune signalling. *Nature* 455 (7213), 674–678. doi:10.1038/nature07317

Ishikawa, H., Ma, Z., and Barber, G. N. (2009). STING regulates intracellular DNA-mediated, type I interferon-dependent innate immunity. *Nature* 461 (7265), 788–792. doi:10.1038/nature08476

Jack, C. R., Jr., Bennett, D. A., Blennow, K., Carrillo, M. C., Dunn, B., Haeberlein, S. B., et al. (2018). NIA-AA Research Framework: Toward a biological definition of Alzheimer's disease. *Alzheimers Dement.* 14 (4), 535–562. doi:10.1016/j.jalz.2018.02.018

Jiang, M., Chen, P., Wang, L., Li, W., Chen, B., Liu, Y., et al. (2020). cGAS-STING, an important pathway in cancer immunotherapy. *J. Hematol. Oncol.* 13 (1), 81. doi:10.1186/s13045-020-00916-z

Jin, L., Waterman, P. M., Jonscher, K. R., Short, C. M., Reisdorph, N. A., and Cambier, J. C. (2008). MPYS, a novel membrane tetraspanner, is associated with major histocompatibility complex class II and mediates transduction of apoptotic signals. *Mol. Cell. Biol.* 28 (16), 5014–5026. doi:10.1128/mcb.00640-08

Kato, Y., Park, J., Takamatsu, H., Konaka, H., Aoki, W., Aburaya, S., et al. (2018). Apoptosis-derived membrane vesicles drive the cGAS-STING pathway and enhance type I IFN production in systemic lupus erythematosus. *Ann. Rheum. Dis.* 77 (10), 1507–1515. doi:10.1136/annrheumdis-2018-212988

Kisseleva, T., and Brenner, D. (2021). Molecular and cellular mechanisms of liver fibrosis and its regression. *Nat. Rev. Gastroenterol. Hepatol.* 18 (3), 151–166. doi:10.1038/s41575-020-00372-7

Konno, H., Konno, K., and Barber, G. N. (2013). Cyclic dinucleotides trigger ULK1 (ATG1) phosphorylation of STING to prevent sustained innate immune signaling. *Cell* 155 (3), 688–698. doi:10.1016/j.cell.2013.09.049

Lee, J. S., and Shin, E. C. (2020). The type I interferon response in COVID-19: implications for treatment. *Nat. Rev. Immunol.* 20 (10), 585–586. doi:10.1038/s41577-020-00429-3

Lee, J. S., Park, S., Jeong, H. W., Ahn, J. Y., Choi, S. J., Lee, H., et al. (2020). Immunophenotyping of COVID-19 and influenza highlights the role of type I interferons in development of severe COVID-19. *Sci. Immunol.* 5 (49), eabd1554. doi:10.1126/sciimmunol.abd1554

Lee-Kirsch, M. A., Gong, M., Chowdhury, D., Senenko, L., Engel, K., Lee, Y. A., et al. (2007). Mutations in the gene encoding the 3'-5' DNA exonuclease TREX1 are associated with systemic lupus erythematosus. *Nat. Genet.* 39 (9), 1065–1067. doi:10.1038/ng2091

Lepelley, A., Martin-Niclós, M. J., Le Bihan, M., Marsh, J. A., Uggenti, C., Rice, G. I., et al. (2020). Mutations in COPA lead to abnormal trafficking of STING to the Golgi and interferon signaling. *J. Exp. Med.* 217 (11), e20200600. doi:10.1084/jem.20200600

Li, S., Hong, Z., Wang, Z., Li, F., Mei, J., Huang, L., et al. (2018). The cyclopeptide Astin C specifically inhibits the innate immune CDN sensor STING. *Cell Rep.* 25 (12), 3405–3421. doi:10.1016/j.celrep.2018.11.097

Li, A., Yi, M., Qin, S., Song, Y., Chu, Q., and Wu, K. (2019). Activating cGAS-STING pathway for the optimal effect of cancer immunotherapy. *J. Hematol. Oncol.* 12 (1), 35. doi:10.1186/s13045-019-0721-x

Li, N., Zhou, H., Wu, H., Wu, Q., Duan, M., Deng, W., et al. (2019). STING-IRF3 contributes to lipopolysaccharide-induced cardiac dysfunction, inflammation, apoptosis and pyroptosis by activating NLRP3. *Redox Biol.* 24, 101215. doi:10.1016/j.redox.2019.101215

Liang, L., Shen, Y., Hu, Y., Liu, H., and Cao, J. (2022). cGAS exacerbates Schistosoma japonicum infection in a STING-type I IFN-dependent and independent manner. *PLoS Pathog.* 18 (2), e1010233. doi:10.1371/journal.ppat.1010233

Liu, Y., Jesus, A. A., Marrero, B., Yang, D., Ramsey, S. E., Sanchez, G. A. M., et al. (2014). Activated STING in a vascular and pulmonary syndrome. *N. Engl. J. Med.* 371 (6), 507–518. doi:10.1056/NEJMoa1312625

Liu, S., Cai, X., Wu, J., Cong, Q., Chen, X., Li, T., et al. (2015). Phosphorylation of innate immune adaptor proteins MAVS, STING, and TRIF induces IRF3 activation. *Science* 347 (6227), aaa2630. doi:10.1126/science.aaa2630

Liu, Z., Huang, X. R., Chen, H. Y., Fung, E., Liu, J., and Lan, H. Y. (2017). Deletion of angiotensin-converting enzyme-2 promotes hypertensive nephropathy by targeting Smad7 for ubiquitin degradation. *Hypertension* 70 (4), 822–830. doi:10.1161/hypertensionaha.117.09600

Liu, C., Tang, J., Luo, W., Liu, S., Sun, X., Hong, W., et al. (2022). DNA from macrophages induces fibrosis and vasculopathy through POLR3A/STING/type I interferon axis in systemic sclerosis. *Rheumatol. Oxf.*, keac324. doi:10.1093/rheumatology/keac324

Liu, K., Zhao, X., Guo, M., Zhu, J., Li, D., Ding, J., et al. (2022). Microcystin-leucine arginine (MC-LR) induces mouse ovarian inflammation by promoting granulosa cells to produce inflammatory cytokine via activation of cGAS-STING signaling. *Toxicol. Lett.* 358, 6–16. doi:10.1016/j.toxlet.2022.01.003

Liu, X., Wei, L., Xu, F., Zhao, F., Huang, Y., Fan, Z., et al. (2022c). SARS-CoV-2 spike protein-induced cell fusion activates the cGAS-STING pathway and the interferon response. *Sci. Signal.* 15 (729), eabg8744. doi:10.1126/scisignal.abg8744

Luecke, S., Holleufer, A., Christensen, M. H., Jønsson, K. L., Boni, G. A., Sørensen, L. K., et al. (2017). cGAS is activated by DNA in a length-dependent manner. *EMBO Rep.* 18 (10), 1707–1715. doi:10.15252/embr.201744017

Luo, X., Li, H., Ma, L., Zhou, J., Guo, X., Woo, S. L., et al. (2018). Expression of STING is increased in liver tissues from patients with NAFLD and promotes macrophage-mediated hepatic inflammation and fibrosis in mice. *Gastroenterology* 155 (6), 1971–1984. doi:10.1053/j.gastro.2018.09.010

Luo, Z., Ji, Y., Zhang, D., Gao, H., Jin, Z., Yang, M., et al. (2022). Microbial DNA enrichment promotes liver steatosis and fibrosis in the course of non-alcoholic steatohepatitis. *Acta Physiol.* 235 (3), e13827. doi:10.1111/apha.13827

Mack, M., and Yanagita, M. (2015). Origin of myofibroblasts and cellular events triggering fibrosis. *Kidney Int.* 87 (2), 297–307. doi:10.1038/ki.2014.287

Mack, M. (2018). Inflammation and fibrosis. *Matrix Biol.* 68-69, 106–121. doi:10.1016/j.matbio.2017.11.010

Mackenzie, K. J., Carroll, P., Lettice, L., Tarnauskaitė, Ž., Reddy, K., Dix, F., et al. (2016). Ribonuclease H2 mutations induce a cGAS/STING-dependent innate immune response. *Embo J.* 35 (8), 831–844. doi:10.15252/embj.201593339

McCauley, M. E., O'Rourke, J. G., Yáñez, A., Markman, J. L., Ho, R., Wang, X., et al. (2020). C9orf72 in myeloid cells suppresses STING-induced inflammation. *Nature* 585 (7823), 96–101. doi:10.1038/s41586-020-2625-x

McDonald, L. T. (2021). Healing after COVID-19: are survivors at risk for pulmonary fibrosis? *Am. J. Physiol. Lung Cell. Mol. Physiol.* 320 (2), L257–l265. doi:10.1152/ajplung.00238.2020

Mejzini, R., Flynn, L. L., Pitout, I. L., Fletcher, S., Wilton, S. D., and Akkari, P. A. (2019). ALS genetics, mechanisms, and therapeutics: Where are we now? *Front. Neurosci.* 13, 1310. doi:10.3389/fnins.2019.01310

Meng, X. M., Nikolic-Paterson, D. J., and Lan, H. Y. (2016). TGF-β: the master regulator of fibrosis. *Nat. Rev. Nephrol.* 12 (6), 325–338. doi:10.1038/nrneph.2016.48

Meric-Bernstam, F., Sweis, R. F., Hodi, F. S., Messersmith, W. A., Andtbacka, R. H. I., Ingham, M., et al. (2022). Phase I dose-escalation trial of MIW815 (ADU-S100), an intratumoral STING agonist, in patients with advanced/metastatic solid tumors or lymphomas. *Clin. Cancer Res.* 28 (4), 677–688. doi:10.1158/1078-0432.Ccr-21-1963

Mezzano, S. A., Ruiz-Ortega, M., and Egido, J. (2001). Angiotensin II and renal fibrosis. *Hypertension* 38, 635–638. doi:10.1161/hy09t1.094234

Montero, P., Milara, J., Roger, I., and Cortijo, J. (2021). Role of JAK/STAT in interstitial lung diseases; molecular and cellular mechanisms. *Int. J. Mol. Sci.* 22 (12), 6211. doi:10.3390/ijms22126211

Morris, R., Kershaw, N. J., and Babon, J. J. (2018). The molecular details of cytokine signaling via the JAK/STAT pathway. *Protein Sci.* 27 (12), 1984–2009. doi:10.1002/pro.3519

Mukai, K., Konno, H., Akiba, T., Uemura, T., Waguri, S., Kobayashi, T., et al. (2016). Activation of STING requires palmitoylation at the Golgi. *Nat. Commun.* 7, 11932. doi:10.1038/ncomms11932

Murayama, G., Chiba, A., Kuga, T., Makiyama, A., Yamaji, K., Tamura, N., et al. (2020). Inhibition of mTOR suppresses IFNα production and the STING pathway in monocytes from systemic lupus erythematosus patients. *Rheumatol. Oxf.* 59 (10), 2992–3002. doi:10.1093/rheumatology/keaa060

Murthy, A. M. V., Robinson, N., and Kumar, S. (2020). Crosstalk between cGAS-STING signaling and cell death. *Cell Death Differ.* 27 (11), 2989–3003. doi:10.1038/s41418-020-00624-8

Nakamura, T., Sato, T., Endo, R., Sasaki, S., Takahashi, N., Sato, Y., et al. (2021). STING agonist loaded lipid nanoparticles overcome anti-PD-1 resistance in melanoma lung metastasis via NK cell activation. *J. Immunother. Cancer* 9 (7), e002852. doi:10.1136/jitc-2021-002852

Nascimento, M., Gombault, A., Lacerda-Queiroz, N., Panek, C., Savigny, F., Sbeity, M., et al. (2019). Self-DNA release and STING-dependent sensing drives inflammation to cigarette smoke in mice. *Sci. Rep.* 9 (1), 14848. doi:10.1038/s41598-019-51427-y

Neufeldt, C. J., Cerikan, B., Cortese, M., Frankish, J., Lee, J. Y., Plociennikowska, A., et al. (2022). SARS-CoV-2 infection induces a pro-inflammatory cytokine response through cGAS-STING and NF-κB. *Commun. Biol.* 5 (1), 45. doi:10.1038/s42003-021-02983-5

Nguyen, H. Q., To, N. H., Zadigue, P., Kerbrat, S., De La Taille, A., Le Gouvello, S., et al. (2018). Ionizing radiation-induced cellular senescence promotes tissue fibrosis after radiotherapy. A review. *Crit. Rev. Oncol. Hematol.* 129, 13–26. doi:10.1016/j.critrevonc.2018.06.012

Pierantonelli, I., and Svegliati-Baroni, G. (2019). Nonalcoholic fatty liver disease: Basic pathogenetic mechanisms in the progression from NAFLD to NASH. *Transplantation* 103 (1), e1–e13. doi:10.1097/tp.0000000000002480

Pober, J. S., and Sessa, W. C. (2007). Evolving functions of endothelial cells in inflammation. *Nat. Rev. Immunol.* 7 (10), 803–815. doi:10.1038/nri2171

Prabakaran, T., Troldborg, A., Kumpunya, S., Alee, I., Marinković, E., Windross, S. J., et al. (2021). A STING antagonist modulating the interaction with STIM1 blocks ER-to-Golgi trafficking and inhibits lupus pathology. *EBioMedicine* 66, 103314. doi:10.1016/j.ebiom.2021.103314

Qin, W., Cao, L., and Massey, I. Y. (2021). Role of PI3K/Akt signaling pathway in cardiac fibrosis. *Mol. Cell. Biochem.* 476 (11), 4045–4059. doi:10.1007/s11010-021-04219-w

Rech, L., Abdellatif, M., Pöttler, M., Stangl, V., Mabotuwana, N., Hardy, S., et al. (2022). Small molecule STING inhibition improves myocardial infarction remodeling. *Life Sci.* 291, 120263. doi:10.1016/j.lfs.2021.120263

Ren, H., Ma, C., Peng, H., Zhang, B., Zhou, L., Su, Y., et al. (2021). Micronucleus production, activation of DNA damage response and cGAS-STING signaling in syncytia induced by SARS-CoV-2 infection. *Biol. Direct* 16 (1), 20. doi:10.1186/s13062-021-00305-7

Renton, A. E., Majounie, E., Waite, A., Simón-Sánchez, J., Rollinson, S., Gibbs, J. R., et al. (2011). A hexanucleotide repeat expansion in C9ORF72 is the cause of chromosome 9p21-linked ALS-FTD. *Neuron* 72 (2), 257–268. doi:10.1016/j.neuron.2011.09.010

Rice, G., Newman, W. G., Dean, J., Patrick, T., Parmar, R., Flintoff, K., et al. (2007). Heterozygous mutations in TREX1 cause familial chilblain lupus and dominant Aicardi-Goutieres syndrome. *Am. J. Hum. Genet.* 80 (4), 811–815. doi:10.1086/513443

Rice, G. I., Rodero, M. P., and Crow, Y. J. (2015). Human disease phenotypes associated with mutations in TREX1. *J. Clin. Immunol.* 35 (3), 235–243. doi:10.1007/s10875-015-0147-3

Rockey, D. C., Bell, P. D., and Hill, J. A. (2015). Fibrosis--a common pathway to organ injury and failure. *N. Engl. J. Med.* 372 (12), 1138–1149. doi:10.1056/NEJMra1300575

Romagnani, P., Remuzzi, G., Glassock, R., Levin, A., Jager, K. J., Tonelli, M., et al. (2017). Chronic kidney disease. *Nat. Rev. Dis. Prim.* 3, 17088. doi:10.1038/nrdp.2017.88

Scheltens, P., De Strooper, B., Kivipelto, M., Holstege, H., Chételat, G., Teunissen, C. E., et al. (2021). Alzheimer's disease. *Lancet* 397 (10284), 1577–1590. doi:10.1016/s0140-6736(20)32205-4

Schuster, S., Cabrera, D., Arrese, M., and Feldstein, A. E. (2018). Triggering and resolution of inflammation in NASH. *Nat. Rev. Gastroenterol. Hepatol.* 15 (6), 349–364. doi:10.1038/s41575-018-0009-6

Seo, S. U., Jeong, J. H., Baek, B. S., Choi, J. M., Choi, Y. S., Ko, H. J., et al. (2021). Bleomycin-induced lung injury increases resistance to influenza virus infection in a type I interferon-dependent manner. *Front. Immunol.* 12, 697162. doi:10.3389/fimmu.2021.697162

Shang, G., Zhang, C., Chen, Z. J., Bai, X. C., and Zhang, X. (2019). Cryo-EM structures of STING reveal its mechanism of activation by cyclic GMP-AMP. *Nature* 567 (7748), 389–393. doi:10.1038/s41586-019-0998-5

Shen, R., Yang, K., Cheng, X., Guo, C., Xing, X., Sun, H., et al. (2022). Accumulation of polystyrene microplastics induces liver fibrosis by activating cGAS/STING pathway. *Environ. Pollut.* 300, 118986. doi:10.1016/j.envpol.2022.118986

Shi, W., Hao, J., Wu, Y., Liu, C., Shimizu, K., Li, R., et al. (2022). Protective effects of heterophyllin B against bleomycin-induced pulmonary fibrosis in mice via AMPK activation. *Eur. J. Pharmacol.* 921, 174825. doi:10.1016/j.ejphar.2022.174825

Shmuel-Galia, L., Humphries, F., Lei, X., Ceglia, S., Wilson, R., Jiang, Z., et al. (2021). Dysbiosis exacerbates colitis by promoting ubiquitination and accumulation of the innate immune adaptor STING in myeloid cells. *Immunity* 54 (6), 1137–1153.e8. doi:10.1016/j.immuni.2021.05.008

Siu, T., Altman, M. D., Baltus, G. A., Childers, M., Ellis, J. M., Gunaydin, H., et al. (2019). Discovery of a novel cGAMP competitive ligand of the inactive form of STING. *ACS Med. Chem. Lett.* 10 (1), 92–97. doi:10.1021/acsmedchemlett.8b00466

Sun, W., Li, Y., Chen, L., Chen, H., You, F., Zhou, X., et al. (2009). ERIS, an endoplasmic reticulum IFN stimulator, activates innate immune signaling through dimerization. *Proc. Natl. Acad. Sci. U. S. A.* 106 (21), 8653–8658. doi:10.1073/pnas.0900850106

Sun, L., Wu, J., Du, F., Chen, X., and Chen, Z. J. (2013). Cyclic GMP-AMP synthase is a cytosolic DNA sensor that activates the type I interferon pathway. *Science* 339 (6121), 786–791. doi:10.1126/science.1232458

Sun, S. C., Han, R., Hou, S. S., Yi, H. Q., Chi, S. J., and Zhang, A. H. (2020a). Juglanin alleviates bleomycin-induced lung injury by suppressing inflammation and fibrosis via targeting sting signaling. *Biomed. Pharmacother.* 127, 110119. doi:10.1016/j.biopha.2020.110119

Sun, Z., Yang, Z., Wang, M., Huang, C., Ren, Y., Zhang, W., et al. (2020b). Paraquat induces pulmonary fibrosis through Wnt/β-catenin signaling pathway and myofibroblast differentiation. *Toxicol. Lett.* 333, 170–183. doi:10.1016/j.toxlet.2020.08.004

Takahashi, A., Loo, T. M., Okada, R., Kamachi, F., Watanabe, Y., Wakita, M., et al. (2018). Downregulation of cytoplasmic DNases is implicated in cytoplasmic DNA accumulation and SASP in senescent cells. *Nat. Commun.* 9 (1), 1249. doi:10.1038/s41467-018-03555-8

Tan, H. Y., Yong, Y. K., Xue, Y. C., Liu, H., Furihata, T., Shankar, E. M., et al. (2022). cGAS and DDX41-STING mediated intrinsic immunity spreads intercellularly to promote neuroinflammation in SOD1 ALS model. *iScience* 25 (6), 104404. doi:10.1016/j.isci.2022.104404

Thim-Uam, A., Prabakaran, T., Tansakul, M., Makjaroen, J., Wongkongkathep, P., Chantaravisoot, N., et al. (2020). STING mediates lupus via the activation of conventional dendritic cell maturation and plasmacytoid dendritic cell differentiation. *iScience* 23 (9), 101530. doi:10.1016/j.isci.2020.101530

Tsuchida, T., and Friedman, S. L. (2017). Mechanisms of hepatic stellate cell activation. *Nat. Rev. Gastroenterol. Hepatol.* 14 (7), 397–411. doi:10.1038/nrgastro.2017.38

Ung, C. Y., Onoufriadis, A., Parsons, M., McGrath, J. A., and Shaw, T. J. (2021). Metabolic perturbations in fibrosis disease. *Int. J. Biochem. Cell Biol.* 139, 106073. doi:10.1016/j.biocel.2021.106073

Villiger, P. M., Kusari, A. B., ten Dijke, P., and Lotz, M. (1993). IL-1 beta and IL-6 selectively induce transforming growth factor-beta isoforms in human articular chondrocytes. *J. Immunol.* 151 (6), 3337–3344.

Volpi, S., Tsui, J., Mariani, M., Pastorino, C., Caorsi, R., Sacco, O., et al. (2018). Type I interferon pathway activation in COPA syndrome. *Clin. Immunol.* 187, 33–36. doi:10.1016/j.clim.2017.10.001

Wang, J., Dai, M., Cui, Y., Hou, G., Deng, J., Gao, X., et al. (2018). Association of abnormal elevations in IFIT3 with overactive cyclic GMP-AMP synthase/stimulator of interferon genes signaling in human systemic lupus erythematosus monocytes. *Arthritis Rheumatol.* 70 (12), 2036–2045. doi:10.1002/art.40576

Wang, N., Zhan, Y., Zhu, L., Hou, Z., Liu, F., Song, P., et al. (2020). Retrospective multicenter cohort study shows early interferon therapy is associated with favorable clinical responses in COVID-19 patients. *Cell Host Microbe* 28 (3), 455–464.e2. doi:10.1016/j.chom.2020.07.005

Wang, X., Rao, H., Zhao, J., Wee, A., Li, X., Fei, R., et al. (2020). STING expression in monocyte-derived macrophages is associated with the progression of liver inflammation and fibrosis in patients with nonalcoholic fatty liver disease. *Lab. Invest.* 100 (4), 542–552. doi:10.1038/s41374-019-0342-6

Wang, Y., Luo, J., Alu, A., Han, X., Wei, Y., and Wei, X. (2020). cGAS-STING pathway in cancer biotherapy. *Mol. Cancer* 19 (1), 136. doi:10.1186/s12943-020-01247-w

Wang, K., Donnelly, C. R., Jiang, C., Liao, Y., Luo, X., Tao, X., et al. (2021). STING suppresses bone cancer pain via immune and neuronal modulation. *Nat. Commun.* 12 (1), 4558. doi:10.1038/s41467-021-24867-2

Wang, Q., Bergholz, J. S., Ding, L., Lin, Z., Kabraji, S. K., Hughes, M. E., et al. (2022). STING agonism reprograms tumor-associated macrophages and overcomes resistance to PARP inhibition in BRCA1-deficient models of breast cancer. *Nat. Commun.* 13 (1), 3022. doi:10.1038/s41467-022-30568-1

Willemsen, J., Neuhoff, M. T., Hoyler, T., Noir, E., Tessier, C., Sarret, S., et al. (2021). TNF leads to mtDNA release and cGAS/STING-dependent interferon responses that support inflammatory arthritis. *Cell Rep.* 37 (6), 109977. doi:10.1016/j.celrep.2021.109977

Wu, J., Sun, L., Chen, X., Du, F., Shi, H., Chen, C., et al. (2013). Cyclic GMP-AMP is an endogenous second messenger in innate immune signaling by cytosolic DNA. *Science* 339 (6121), 826–830. doi:10.1126/science.1229963

Wu, J., Raman, A., Coffey, N. J., Sheng, X., Wahba, J., Seasock, M. J., et al. (2021). The key role of NLRP3 and STING in APOL1-associated podocytopathy. *J. Clin. Invest.* 131 (20), e136329. doi:10.1172/jci136329

Xiong, Y., Tang, Y. D., and Zheng, C. (2021). The crosstalk between the caspase family and the cGAS–STING signaling pathway. *J. Mol. Cell Biol.* 13 (10), 739–747. doi:10.1093/jmcb/mjab071

Yang, M., Fan, Q., Hei, T. K., Chen, G., Cao, W., Meng, G., et al. (2022a). Single-cell transcriptome analysis of radiation pneumonitis mice. *Antioxidants (Basel)* 11 (8), 1457. doi:10.3390/antiox11081457

Yang, M., Ma, Y. X., Zhi, Y., Wang, H. B., Zhao, L., Wang, P. S., et al. (2022b). Inhibitors of IFN gene stimulators (STING) improve intestinal ischemia-reperfusion-induced acute lung injury by activating AMPK signaling. *Eur. J. Med. Res.* 27 (1), 79. doi:10.1186/s40001-022-00703-1

Yong, H., Wang, S., and Song, F. (2021). Activation of cGAS/STING pathway upon TDP-43-mediated mitochondrial injury may be involved in the pathogenesis of liver fibrosis. *Liver Int.* 41 (8), 1969–1971. doi:10.1111/liv.14895

Yu, Y., Liu, Y., An, W., Song, J., Zhang, Y., and Zhao, X. (2019). STING-mediated inflammation in Kupffer cells contributes to progression of nonalcoholic steatohepatitis. *J. Clin. Invest.* 129 (2), 546–555. doi:10.1172/jci121842

Yu, C. H., Davidson, S., Harapas, C. R., Hilton, J. B., Mlodzianoski, M. J., Laohamonthonkul, P., et al. (2020). TDP-43 triggers mitochondrial DNA release via mPTP to activate cGAS/STING in ALS. *Cell* 183 (3), 636–649.e18. doi:10.1016/j.cell.2020.09.020

Zhang, M., and Zhang, S. (2020). T cells in fibrosis and fibrotic diseases. *Front. Immunol.* 11, 1142. doi:10.3389/fimmu.2020.01142

Zhang, X., Shi, H., Wu, J., Zhang, X., Sun, L., Chen, C., et al. (2013). Cyclic GMP-AMP containing mixed phosphodiester linkages is an endogenous high-affinity ligand for STING. *Mol. Cell* 51 (2), 226–235. doi:10.1016/j.molcel.2013.05.022

Zhang, C., Shang, G., Gui, X., Zhang, X., Bai, X. C., and Chen, Z. J. (2019). Structural basis of STING binding with and phosphorylation by TBK1. *Nature* 567 (7748), 394–398. doi:10.1038/s41586-019-1000-2

Zhang, Y., Chen, W., and Wang, Y. (2020). STING is an essential regulator of heart inflammation and fibrosis in mice with pathological cardiac hypertrophy via endoplasmic reticulum (ER) stress. *Biomed. Pharmacother.* 125, 110022. doi:10.1016/j.biopha.2020.110022

Zhang, Y., Jin, D., Kang, X., Zhou, R., Sun, Y., Lian, F., et al. (2021). Signaling pathways involved in diabetic renal fibrosis. *Front. Cell Dev. Biol.* 9, 696542. doi:10.3389/fcell.2021.696542

Zhang, D., Liu, Y., Zhu, Y., Zhang, Q., Guan, H., Liu, S., et al. (2022). A non-canonical cGAS-STING-PERK pathway facilitates the translational program critical for senescence and organ fibrosis. *Nat. Cell Biol.* 24 (5), 766–782. doi:10.1038/s41556-022-00894-z

Zhao, B., Du, F., Xu, P., Shu, C., Sankaran, B., Bell, S. L., et al. (2019). A conserved PLPLRT/SD motif of STING mediates the recruitment and activation of TBK1. *Nature* 569 (7758), 718–722. doi:10.1038/s41586-019-1228-x

Zhao, H., Wu, L., Yan, G., Chen, Y., Zhou, M., Wu, Y., et al. (2021). Inflammation and tumor progression: Signaling pathways and targeted intervention. *Signal Transduct. Target. Ther.* 6 (1), 263. doi:10.1038/s41392-021-00658-5

Zhong, B., Yang, Y., Li, S., Wang, Y. Y., Li, Y., Diao, F., et al. (2008). The adaptor protein MITA links virus-sensing receptors to IRF3 transcription factor activation. *Immunity* 29 (4), 538–550. doi:10.1016/j.immuni.2008.09.003

Zhou, J., Zhong, J., Huang, Z., Liao, M., Lin, S., Chen, J., et al. (2018). TAK1 mediates apoptosis via p38 involve in ischemia-induced renal fibrosis. *Artif. Cells Nanomed. Biotechnol.* 46, 1016–1025. doi:10.1080/21691401.2018.1442841

Zhou, Z., Zhang, X., Lei, X., Xiao, X., Jiao, T., Ma, R., et al. (2021). Sensing of cytoplasmic chromatin by cGAS activates innate immune response in SARS-CoV-2 infection. *Signal Transduct. Target. Ther.* 6 (1), 382. doi:10.1038/s41392-021-00800-3

frontiers | Frontiers in Pharmacology

TYPE Review
PUBLISHED 12 January 2023
DOI 10.3389/fphar.2022.1041327

Check for updates

OPEN ACCESS

EDITED BY
Yanping Liu,
Qilu Hospital, Shandong University, China

REVIEWED BY
Ankur Vijay Dnyanmote,
Izaak Walton Killam Children's Hospital, Canada
Yiqin Shi,
Fudan University, China
Panpan Hao,
Shandong University, China

*CORRESPONDENCE
Elisabetta A. M. Verderio,
elisabetta.verderio-edwards@ntu.ac.uk

SPECIALTY SECTION
This article was submitted to Experimental Pharmacology and Drug Discovery, a section of the journal Frontiers in Pharmacology

RECEIVED 10 September 2022
ACCEPTED 21 December 2022
PUBLISHED 12 January 2023

CITATION
Tepus M, Tonoli E and Verderio EAM (2023), Molecular profiling of urinary extracellular vesicles in chronic kidney disease and renal fibrosis.
Front. Pharmacol. 13:1041327.
doi: 10.3389/fphar.2022.1041327

COPYRIGHT
© 2023 Tepus, Tonoli and Verderio. This is an open-access article distributed under the terms of the Creative Commons Attribution License (CC BY). The use, distribution or reproduction in other forums is permitted, provided the original author(s) and the copyright owner(s) are credited and that the original publication in this journal is cited, in accordance with accepted academic practice. No use, distribution or reproduction is permitted which does not comply with these terms.

Molecular profiling of urinary extracellular vesicles in chronic kidney disease and renal fibrosis

Melanie Tepus[1], Elisa Tonoli[1] and Elisabetta A. M. Verderio[1,2]*

[1]Centre for Health, Ageing and the Understanding of Disease (CHAUD), School of Science and Technology, Nottingham Trent University, Nottingham, United Kingdom, [2]Department of Biological, Geological, and Environmental Sciences, Alma Mater Studiorum, University of Bologna, Bologna, Italy

Chronic kidney disease (CKD) is a long-term kidney damage caused by gradual loss of essential kidney functions. A global health issue, CKD affects up to 16% of the population worldwide. Symptoms are often not apparent in the early stages, and if left untreated, CKD can progress to end-stage kidney disease (ESKD), also known as kidney failure, when the only possible treatments are dialysis and kidney transplantation. The end point of nearly all forms of CKD is kidney fibrosis, a process of unsuccessful wound-healing of kidney tissue. Detection of kidney fibrosis, therefore, often means detection of CKD. Renal biopsy remains the best test for renal scarring, despite being intrinsically limited by its invasiveness and sampling bias. Urine is a desirable source of fibrosis biomarkers as it can be easily obtained in a non-invasive way and in large volumes. Besides, urine contains biomolecules filtered through the glomeruli, mirroring the pathological state. There is, however, a problem of highly abundant urinary proteins that can mask rare disease biomarkers. Urinary extracellular vesicles (uEVs), which originate from renal cells and carry proteins, nucleic acids, and lipids, are an attractive source of potential rare CKD biomarkers. Their cargo consists of low-abundant proteins but highly concentrated in a nanosize-volume, as well as molecules too large to be filtered from plasma. Combining molecular profiling data (protein and miRNAs) of uEVs, isolated from patients affected by various forms of CKD, this review considers the possible diagnostic and prognostic value of uEVs biomarkers and their potential application in the translation of new experimental antifibrotic therapeutics.

KEYWORDS

kidney, renal fibrosis, urinary extracellular vesicles (uEVs), biomarkers, chronic kidney disease (CKD), urine

1 Introduction

1.1 Extracellular vesicles

"For some years the small dancing bodies in the plasma of the blood have proved a veritable mare's nest to many workers. What are they? And where do they come from?" (Horder, 1899). Particles of the size and characteristics of extracellular vesicles (EVs) were first suggested as "blood dust" in 1899 (Horder, 1899). They were detected in blood initially (Johnstone et al., 1987) as "particulate material (platelet-dust)" that could be isolated by ultracentrifugation, high in phospholipid content and showing coagulant function (Wolf, 1967). In particular, the presence of "50-nm buds into the extracellular milieu" was reported during the *in vitro* maturation of sheep reticulocytes, recovered by centrifugation at 100,000xg. In these particles it was noted that the transferrin receptor faced the extracellular medium, according to the later consolidated notion that one membrane inversion occurs in the initial endocytosis and a second

inversion in the stage of intra-vesicular budding, in the biogenesis of these vesicles. Although EVs were initially proposed to contain discarded products into the medium or fluids, it is now well established that EVs are small membrane-bound carriers of proteins, nucleic acids, and lipids. There are several types of EVs that differ in their origin, size, and content, classified as large apoptotic bodies, microvesicles (also called ectosomes), exosomes (Van Niel et al., 2018), and smallest exomeres (Zhang H et al., 2018). Exosomes, which are 40–100 nm in size, are intraluminal vesicles that are formed within the endosomes, the multivesicular body (MVB), by the inward budding of endosomal membrane and are released after the fusion of endosome with the plasma membrane. The mechanisms of exosome biogenesis are complex processes that vary according to the cell type, stimuli received by the cells and the cargo. Sorting of the cargo into exosomes and exosome secretion involves subunits of endosomal sorting complex required for transport (ESCRT) machinery, consisting of four protein complexes (ESCRT-0, -1, -2, -3), as well as ESCRT-associated proteins such as apoptosis-linked gene-2-interacting protein X (ALIX) and tumor susceptibility gene 101 (TSG101). However, cargo clustering and membrane budding can occur in both ESCRT-dependent and ESCRT-independent manners (Bruno et al., 2016; Hessvik and Llorente, 2017). Ectosomes, on the other hand, are 100–1000 nm in size and their biogenesis is based on outward budding at the plasma membrane from where are released in the extracellular space (Heijnen et al., 1999). As both categories of EVs (exosomes and ectosomes) are recovered in the extracellular environment and there is no consensus on endosomal or ectosomal markers to track their origin, the International Society for extracellular vesicles has proposed to refer to them according to their size, as simply "small extracellular vesicles" and "large extracellular vesicles" (Théry et al., 2018).

1.2 Chronic kidney disease and renal fibrosis

In chronic kidney disease (CKD) the essential kidney functions progressively decrease, with irreversible alterations of the kidney structure. The leading causes of CKD are recognized as being diabetes and hypertension (Couser et al., 2011) but many kinds of kidney injuries and loss of functional nephrons can induce and accelerate the pathology.

CKD is a growing public health issue with an estimated prevalence of 8%–16% worldwide (Bikbov et al., 2020). It is reported to be the 12th largest global cause of death, either as a primary condition or due to secondary causes such as stroke or cardiovascular disease. The number of people with CKD reached 700 million in 2017. Many of these patients are often asymptomatic until they progress to an advanced stage. Adequate screening and early treatment of renal disorders prevent the onset of CKD and applied disease management strategies reduce the progression to end-stage kidney disease (ESKD). However, when CKD progresses to ESKD, dialysis and kidney transplantation are the only options left. Renal replacement techniques are lifesaving, but also very costly treatments, as a consequence, many low-income countries are in shortages of such services, resulting in premature deaths (Bikbov et al., 2020; Jha et al., 2013).

In 2002, the National Kidney Foundation guidelines classified CKD into five stages according to estimated glomerular filtration rate (eGFR) levels (mL/min/1.73 m^2). A decade later, the guidelines further detailed stage 3 into stages 3a and 3b (Table 1) recommending a classification of CKD based on both eGFR and albuminuria (Pavkov et al., 2018). Moreover, albuminuria levels, either albumin excretion rate (AER) or albumin-to-creatinine ratio (ACR), are distinguished into three stages (Table 2) (Inker et al., 2014).

TABLE 1 Classification of CKD based on estimated glomerular filtration rate (eGFR).

eGFR (ml/min/1.73 m^2)	
Stage 1	≥90
Stage 2	60–89
Stage 3a	45–59
Stage 3b	30–44
Stage 4	15–29
Stage 5	<15

A number of nephrotic syndromes and renal conditions can lead to the development of CKD and are associated with increased rate of mortality and morbidity (Kolb et al., 2021), from glomerulonephritis, to inherited conditions and auto-immune diseases. Diabetic nephropathy (DN) is the most common cause of ESKD, and autosomal dominant polycystic kidney disease (ADPKD) is one of the most common genetic kidney diseases. The topic of CKD types is discussed along urinary EVs (uEVs) biomarkers in Section 2. In addition to determined aetiologies, widespread environmental toxins, such as lead (Skerfving and Bergdahl, 2007), pose a risk for the development of CKD. Increased blood levels of lead are associated with decreased eGFR and increased odds of developing CKD, especially in patients aged ≥60 (Spector et al., 2011). Dietary factors such as phosphorus and protein can be detrimental to the development and progression of CKD. Phosphaturia induces tubular injury, inflammation, interstitial fibrosis and reduced renal Klotho, a coreceptor for the hormone fibroblast growth factor 23 (FGF23) necessary to reduce the renal phosphate reabsorption and thus maintain normal serum phosphate levels (Gutierrez et al., 2005; Urakawa et al., 2006; Santamaría et al., 2018). Several drugs have been associated with renal damage and increased CKD incidence, including for example, antiretroviral drugs used for HIV treatment such as tenofovir disoproxil fumarate, indinavir, and atazanavir (Kopp et al., 1997; Mocroft et al., 2010). Excessive intake of anabolic steroids can lead to hepatotoxicity and glomerulosclerosis, linked to the development of glomeruli hypertrophy and podocytes loss in response to body mass increase (Herlitz et al., 2010). Other examples are that of chemotherapy drugs (e.g., cisplatin and methotrexate) or non-steroidal anti-inflammatory drugs, which are known to induce acute kidney injury (reviewed by Izzedine and Perazella, 2017). Furthermore, nephrotoxicity might also be promoted by alterations in the mechanisms of renal excretion of certain drugs *via* specific transporters located on the basolateral and apical membranes of renal TECs, such as organic cation/anion transporters (OCT and OAT respectively) and efflux transporters (e.g., multidrug resistance proteins and P-glycoprotein) (Izzedine and Perazella, 2017).

Renal fibrosis has been recently linked to disorders of lipid metabolism, with abnormal accumulation of lipids in the kidney tissue and dysregulation of signaling pathways

TABLE 2 Classification of CKD based on albuminuria measured as albumin excretion rate (AER) or albumin-to-creatinine ratio (ACR).

	Albuminuria		
	AER (mg/24 h)	ACR (mg/g)	ACR (mg/mmol)
Stage A1	<30	<30	<3
Stage A2	30–300	30–300	3–30
Stage A3	>300	>300	>30

ACR is calculated by dividing albumin concentration in milligrams with creatinine concentration in grams. To express ACR in mg/mmol, mg/g values are multiplied by the conversion factor of .113, based on the molar mass of creatinine.

(reviewed in Yuan et al., 2022). Extensive accumulation of lipid droplets in TECs, podocytes, mesangial cells and fenestrated endothelial cells is observed in DN patients (Herman-Edelstein et al., 2014), accompanied by downregulation of acyl-CoA oxidase 1 (ACOX1), carnitine palmitoyltransferase 1 (CPT1), and peroxisome proliferator-activated receptors (PPAR-α and -β), and upregulation of LDL receptor and fatty acid transporter CD36 (Herman-Edelstein et al., 2014). Genome wide unbiased transcriptome analysis confirmed downregulation of critical fatty acid oxidation (FAO) enzymes and regulators in the fibrotic kidney (Kang et al., 2015).

Renal fibrosis is the common underlying cause of all progressive kidney diseases, and the final manifestation of CKD as it progresses to ESKD. Renal fibrosis may be defined as unsuccessful wound-healing of kidney tissues which have undergone chronic and sustained injury. A dynamic system, renal fibrosis involves extracellular matrix (ECM) components and renal and infiltrated cell types. This topic has been extensively reviewed in the past decade, for example by Webster et al., 2017; Boor et al., 2010. As schematically shown in Figure 1, renal fibrosis is characterized by excessive deposition of connective tissue in the kidney parenchyma, in concert with the process of epithelial to mesenchymal transition (EMT) of tubular epithelial cells (TEC) into myofibroblasts, the key mediators in the remodeling of fibrotic tissue. EMT is a highly orchestrated process involving loss of epithelial cell adhesion, *de novo* α-smooth muscle actin (α-SMA) expression, disruption of tubular basement membrane and increased cell migration and invasion (Yang and Liu, 2001).

Activation of myofibroblasts is a common manifestation of fibrosis in multiple organs, but their origin is different. In renal fibrosis, fibroblasts, together with pericytes acquire the phenotype of myofibroblasts. These scar-forming cells increasingly produce ECM components and express α-SMA (Kuppe et al., 2021). It has been reported that half of the accumulated myofibroblasts arise from the local proliferation of resident fibroblasts, while the other half originates from either the differentiation of bone marrow-derived mesenchymal stem cells or through cell transformations like EMT or endothelial-to-mesenchymal transition (EndMT) (LeBleu et al., 2013). In liver fibrosis, the predominant source of myofibroblasts are hepatic lipocytes that synthesize and secrete collagen and are therefore considered precursors of fibroblast-like cells in pathological fibrosis (Friedman et al., 1985). In cardiac fibrosis, in addition to α-SMA-expressing myofibroblasts, cartilage intermediate layer protein 1 (CILP-1)-fibroblasts and thrombospondin-4 (THBS4)-fibroblasts have emerged as predominant fibrogenic populations (McLellan et al., 2020). Pulmonary mesenchymal cells, on the other hand, are very heterogeneous with two main mesenchymal lineages identified, namely mesenchymal alveolar niche cells that support alveolar growth and regeneration and axin2+ myofibrogenic progenitor cells, which contribute to pathologically damaging myofibroblasts after injury (Zepp et al., 2017).

The cytokine transforming growth factor-beta (TGF-β) is the major modulator of EMT and a main inducer of profibrotic events in multiple organs *via* the SMAD pathway (Clouthier et al., 1997; Sime et al., 1997; Deten et al., 2001). By mediating the migration of mesenchymal fibroblasts to the adjacent interstitial parenchyma TGF-β enhances ECM production and accumulation, thus contributing to the deterioration of renal function (Sato et al., 2003). TGF-β signaling interacts with other cell signaling pathways such as the renin-angiotensin-aldosterone system (RAAS), a critical pathway leading to CKD, in which renin promotes production of angiotensin I (Ang I), which is converted to Ang II by angiotensin-converting enzyme (ACE) (AlQudah et al., 2020). Treatment of mesangial cells with Ang II, a pro-fibrotic effector of RAAS, induces the synthesis and secretion of TGF-β, increasing ECM components such as biglycan, fibronectin, and collagen I, in glomerulosclerosis (Kagami et al., 1994). Ang II was found to induce renal inflammatory injury and fibrosis through binding to its well-known receptor AT1R (Zhang et al., 2015) and to myeloid differentiation protein-2 (MD2) (Xu et al., 2017). Despite the classical RAAS pathway of fibrosis, there is an alternative RAAS pathway in which ACE2 is key to catalyze Ang II to Ang I-VII conversion, counteracting the pathological effects of the classical pathway (Liu et al., 2012). Furthermore, Ang IV attenuates diabetic fibrosis and myocyte apoptosis as observed in cardiac tissue (Zhang et al., 2021). Another key mediator of fibrosis development, platelet derived growth factor (PDGF), induces mitogen-activated protein kinase (MAPK) signaling *via* focal adhesion kinase (FAK) activation promoting vast fibroblasts and myofibroblasts proliferation and ECM synthesis (Li et al., 2000; Andrae et al., 2008). All of these pro-fibrotic cytokines and growth factors (such as TGF-β, PDGF) are produced by activated leukocytes and macrophages that accumulate in the glomerulus and interstitium of fibrotic tissue (Duffield, 2014).

A key enzyme that has a pathological role in renal scarring is transglutaminase 2 (TG2), a member of a large family of enzymes responsible for Ca^{2+} dependent transamidation, which is regarded as the most abundant member in kidney (Burhan et al., 2016). TG2 is a recognized marker of kidney fibrosis progression, by cross-linking and stabilizing the ECM, but also by activating TGF-β *via* a heparan sulfate/syndecan-4 interaction (Figure 1) (Scarpellini et al., 2014; Verderio et al., 2016; Burhan et al., 2016). TG2 is externalized in experimental models of CKD and found secreted in urine (Da Silva Lodge et al., 2022) and in urinary vesicles (Furini et al., 2018). Another

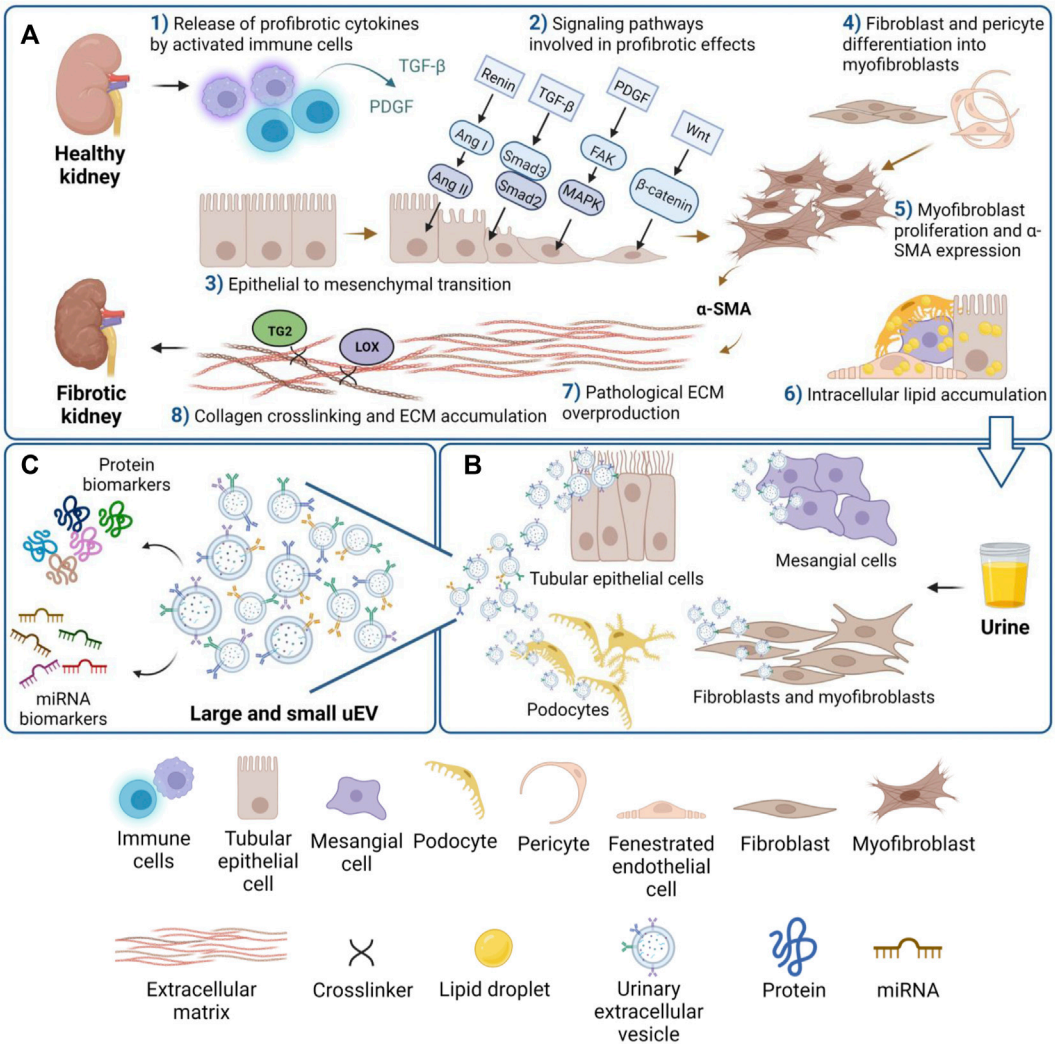


FIGURE 1
Overview of the main cell and tissue changes leading to kidney fibrosis. **(A)** Schematic view of eight of the main events involved in fibrosis: activation of cells and release of cytokines (1); activation of profibrotic signaling pathways (2); EMT (3); differentiation of mesenchymal cell types to activated myofibroblasts (4); α-SMA expression (5); accumulation of lipids drops in renal cells (6); ECM synthesis and overproduction (7); collagen crosslinking (8). **(B)** uEVs secreted from specific renal cell types can be collected in urine, and **(C)** the uEVs cargo of protein and miRNA likely mirrors the fibrotic state.

group of ECM cross-linking enzymes whose increased activity is associated with tissue fibrosis is the lysyl oxidase (LOX) family, which has been reported in hepatic (Siegel et al., 1978), pulmonary (Counts et al., 1981), and renal fibrosis (Goto et al., 2005). A recent study on human samples found increased serum LOX levels in patients with renal fibrosis, thus suggesting serum LOX as a diagnostic marker for renal fibrosis (Zhang et al., 2020; Zhang X et al., 2022).

Renal fibrosis correlates with loss of renal function, which is especially evident in the pathology of diabetic nephropathy (DN) (Qian et al., 2008). The outcome of CKD may vary among individuals and is linked to fibrosis progression. Three forms of CKD can be distinguished based on how it develops over the years: "stable CKD" when patients maintain stable eGFR levels, "reversal CKD" when eGFR levels improve and "progressive CKD" when eGFR levels irreversibly decrease over the years, a stage reached by majority of CKD patients (Zhong et al., 2017). In addition to eGFR and albuminuria, which are the most common tests used in clinical practice, additional screening tests such as measurements of proteinuria, serum creatinine and/or cystatin C and serum urea may be used. There is not a perfect test as each of these approaches have some limitations, since age, body size, gender, muscle mass, as well as different disease aetiologies can affect their sensitivity and specificity (Rysz et al., 2017). Kidney biopsy is the gold standard for diagnosing and determining the severity of CKD. It is the best test of fibrosis although intrinsically imperfect being an invasive and biased procedure, not always specific to a particular pathology (Corapi et al., 2012; Bleyer et al., 2017). Detection of renal fibrosis often means diagnosis of CKD and several markers of CKD and fibrosis have been proposed (Lopes et al., 2019). However, as these markers are hard to trace in biofluids, there is a raising interest in biomarkers which are cargo of urinary EVs, where biomarkers are concentrated and protected thus potentially more accessible to test the onset of fibrosis and CKD progression.

1.3 Urine as a source of biomarkers

Urine is an ideal source of biomarkers, since it contains cellular elements, biochemicals and proteins that are filtered through the glomeruli, but are also derived from renal tubule excretion and urogenital tract secretion, all of which can reflect potentially a physio-pathological state. Virtually all types of kidney cells are identifiable in urine (podocyte, proximal tubule, loop of Henle, and collecting duct), but also macrophages, lymphocytes, and bladder cells, as recently validated by single-cell transcriptomic of urine samples (Abedini et al., 2021).

Moreover, urine is easily accessible in large volumes, and it is collected in a non-invasive way (Harpole et al., 2016). A number of urinary proteins have been proposed as biomarkers of kidney damage in kidney disease progression, such as uromodulin (Prajczer et al., 2010), kidney injury marker 1 (KIM1) (van Timmeren et al., 2007), and neutrophil gelatinase-associated lipocalin (NGAL) (Viau et al., 2010). Furthermore, microRNAs (miRNAs), small ~22 nucleotide long RNA molecules that play a key role in posttranscriptional gene regulation, have also been reported to correlate with CKD, for example miR-126, miR-155, miR-29b (Beltrami et al., 2018), miR-1228-3p, and miR-27b-3p (Conserva et al., 2019), and miR-196a (Zhang C et al., 2018). The miRNA biogenesis is a multi-step process that starts in the nucleus from non-protein monocistronic or polycistronic coding genes (Bartel, 2004). Following transport of pre-miRNA to the cytoplasm, mature and functional miRNAs are generated and incorporated in the RNA-Induced Silencing Complex (RISC) to target messenger RNA (mRNA) to the 3' untranslated region (Bernstein et al., 2001). Target mRNAs are degraded by endonuclease Argonaute (RISC complex), or their expression repressed (Wilson and Doudna, 2013). Deregulation of miRNAs is linked with renal fibrosis and CKD (Li et al., 2013; Macconi et al., 2012; Lv et al., 2018).

Because urine allows testing of kidney health, it is of great interest to establish whether urinary molecules can be detected in a sensitive and specific way to assist in early diagnosis and prognosis of kidney disease. As the majority of urinary proteins such as albumin and IgG are filtered from the blood, they are qualitatively similar to the abundant plasma proteins (Spahr et al., 2001). Being highly concentrated in pathology, they greatly interfere with the detection of other urinary rare biomarkers (Filip et al., 2015), limiting dramatically the sensitivity of the approach. Instead, EVs which can be isolated from urine and mirror cell changes in pathology may offer an alternative sensitive platform for biomarkers discovery. Therefore, EVs molecules may better meet the definition of "good biomarker" (Bennet and Devarajan, 2017).

1.4 Urinary extracellular vesicles

In urine, "membrane-bound vesicles" with procoagulant activity were firstly reported in a 100,000xg precipitate and characterized as 100 nm to 1.1 micron particles by scanning electron microscopy (Wiggins et al., 1986). After initial observations in normal urine, analysis of urine specimens of patients with renal injury led to the discovery that the proximal tubule sheds enzymes from the brush border into urine early post-injury, and in particular patients with glomerulonephritis were found to excrete "blebs" of 100–300 nm. Glomerular podocytes were reported to release vesicles coated by complement receptor-1, which was proposed as a possible marker for podocyte injury (Pascual et al., 1994). An advanced first characterization of EVs in human urine (uEVs) was first reported in 2004 (Pisitkun et al., 2004). Here uEVs were isolated by an ultracentrifugation protocol and investigated by immunogold electron microscopy. Proteomic profiling of uEVs led to the characterization of the protein cargo, showing the presence of endosomal pathway proteins and providing an explanation of how certain proteins such as aquaporin-2 (AQP2) are released in urine. Therefore, the idea that uEVs could be a tool for disease biomarker discovery started to form. We know now that uEVs can be released by cells from kidney, bladder, and the urogenital tract in general (reviewed by Erdbrügger and Le, 2016), and although urine may contain some of circulating EVs from serum, the majority of uEVs are thought to originate from renal cells (as schematically illustrated in Figure 1B). The reason may be in the mechanical and charge barrier of the glomerulus, which would prevent serum EVs from easily passing through under physiological conditions (Pisitkun et al., 2004; Gildea et al., 2014).

Small and large uEVs are believed to have analogous functions to circulating EVs in mediating cell-to-cell communication and intercellular signal transmission, and their cargo is expected to reflect physiological and pathophysiological conditions of the renal cells (Gildea et al., 2014; Street et al., 2011). Recently new nanoparticles, denominated exomeres have been identified through asymmetric-flow field-flow fractionation, a separation technique based on hydrodynamic size, which has brought to their discovery (Zhang H et al., 2018). Their size is about 35 nm making exomeres the smallest type of extracellular particles compared to large and small EVs. Although there is evidence that exomeres carry functional cargo too and thus play a role in cellular communication (Zhang et al., 2019), there are no full reports yet of exomeres in the renal system.

Apart from carrying and delivering their cargo to target cells, EVs have the ability to change the phenotype of the target cells by transferring different populations of proteins and nucleic acids (Quesenberry et al., 2014). This makes them a powerful mechanism of disease spreading. For example, it has been demonstrated that TGF-β-containing EVs secreted from injured epithelial cells, after their uptake by target cells, can stimulate profibrotic effects such as promoting cell proliferation, type I collagen production and α-SMA and F-actin expression on the same cell type from which they are secreted (Borges et al., 2013). On the other hand, EVs released from different cell types such as mesenchymal stem cells have shown renal protective and pro-survival effects in acute kidney injury both *in vitro* and *in vivo* once uptaken by TECs (Bruno et al., 2012). Another example is provided by CD133, a glycoprotein also known as prominin-1 and marker of kidney progenitor cells involved in tissue repair. CD133-containing EVs released by this population of stem cells have been shown to favor renal regeneration after injury (Ranghino et al., 2015). Given these mounting discoveries, there is a great interest in the detection of proteins and nucleic acids isolated from uEVs for potential application as diagnostic, prognostic, and therapeutic biomarkers for CKD (Cocucci and Meldolesi, 2015; Zhang et al., 2016a), a condition which still relies on invasive tools to establish renal fibrosis.

1.5 Tracking the cell origin of urinary extracellular vesicles

Extracellular vesicles are not all the same and they can be classified based on differences in size, however, what ultimately gives them an

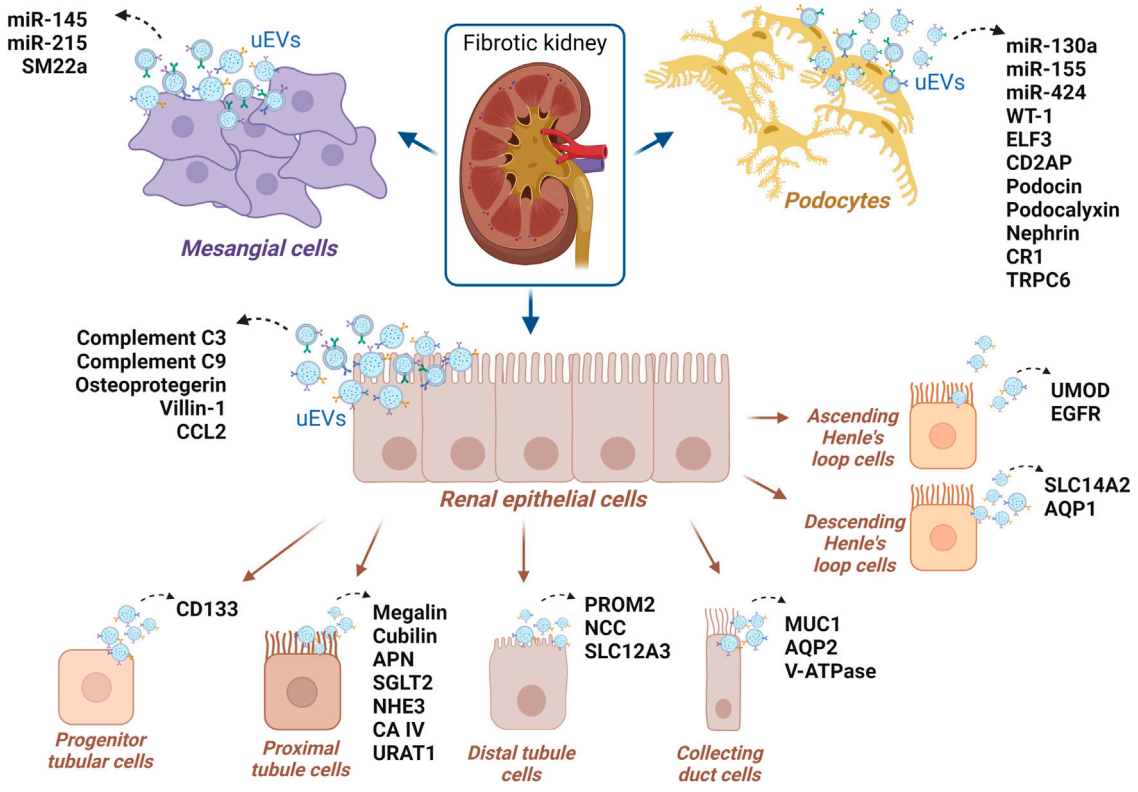


FIGURE 2
uEVs proteins and uEVs miRNAs suggested as potential markers of CKD, for which the renal cell origin has been reported in the literature.

identity is their cargo. The most well-established vesicular markers are tetraspanins (CD9, CD63, CD37, CD81, and CD82), the most abundant proteins in the membrane of small EVs, with roles in cell adhesion, motility, membrane fusion, protein transport and signaling (Andreu and Yáñez-Mó, 2014). TSG101, ALIX, and clathrin are EVs markers associated with MVB biogenesis while annexins and small GTPases retinoic acid-binding (Rab) proteins are implicated in membrane transport, docking and fusion with target cells. Other markers involved with exosomal biogenesis are heat shock proteins Hsp70 and Hsp90 (Reddy et al., 2018). Membrane receptor integrins and lipid raft flotillins are also prominent markers (Merchant et al., 2017; Cricrì et al., 2021). Apart from generic markers, EVs display a cargo specific to the cell type from which they originate (Figure 2), and it is this which should enable tracking the cell origin of isolated EVs and therefore the cell type undergoing the pathological change. The International Society of Extracellular Vesicles (ISEV) has recently summarized protein markers specific to diverse cell types and segments within the kidney, upon evaluations by flow cytometry and Western blotting (reviewed by Erdbrugger et al., 2021). TECs are a source of CD24-containing uEVs, also known as cluster of differentiation-24 or heat stable antigen CD24. The presence of uEVs from podocytes may be determined by podocin, podocalyxin (PCLP1), nephrin, Wilms' tumor-1 (WT 1), complement receptor-1 (CR1), and canonical transient receptor potential-6 (TRPC6). Urinary EVs from proximal tubular cells typically carry megalin, cubilin, aminopeptidase-N (APN), sodium/glucose cotransporter-2 (SGLT2), carbonic anhydrase (CAIV), Na^+/H^+ exchanger isoform-3 (NHE3) as well as urate transporter-1 (URAT1) (Turco et al., 2016). To identify uEVs from descending limb of Henle's, solute carrier family-14 member 2 (SLC14A2) and aquaporin-1 (AQP1) may be utilized, while uromodulin and epidermal growth factor receptor (EGFR) should mirror the ascending limb origin, type-2 Na^+-K^+-$2Cl^-$ cotransporter (NKCC2) the Henle's loop (Turco et al., 2016). Moreover, it was commented before that progenitor tubular cells secrete EVs displaying CD133 (Prominin-1) (Erdbrugger et al., 2021). Collecting duct cells uEVs are marked by the presence of mucin-1, a glycoprotein that activates protective pathways in TECs after hypoxia in acute kidney injury (Pastor-Soler et al., 2015), but also AQP2 and V-ATPase (Turco et al., 2016). Distal tubule-derived uEVs typically display prominin-2, thiazide-sensitive Na-Cl cotransporter (NCC), and solute carrier family 12 member 3 (SLC12A3) (Pomatto et al., 2017; Erdbrugger et al., 2021; Turco et al., 2016). Beta-1 adrenergic receptor (β-1 AR) was reported as an uEVs marker of juxtaglomerular cells, and transgelin (SM22 alpha) of mesangial cell origin, while claudin-1 and cytokeratin eight are uEVs markers of parietal cell origin (Bowman's capsule) and cytokeratin-19–20 of the transitional epithelium (renal pelvis) (Turco et al., 2016). Some uEVs markers are shared by more than one cell-type, especially ACE which was detected in uEVs from glomerulus and proximal tubules, AQP1 in uEVs from proximal tubules and Henle's loop, and AQP2 found in the uEVs from distal tubules and collecting duct (Erdbrugger et al., 2021). Although there are still no known specific EVs markers for fibroblasts, PDGFRβ and CD73 which are highly expressed in the plasma membrane of fibroblasts, are employed as markers for respectively interstitial and cortical fibroblasts, despite also recognizing pericytes or proximal tubular cells (Asada et al., 2011; Schiessl et al., 2018; Perry

et al., 2019; Arai et al., 2021). Recently, naked cuticle homolog 2 (NKD2) has been suggested as a marker of myofibroblasts and a potential therapeutic target, as its knockdown markedly reduces the expression of ECM components independently of TGF-β (Kuppe et al., 2021). NKD2 is a negative regulator of Wnt/β-catenin signaling, another pathway involved in fibrosis development, which is stimulated by TGF-β and plays a role in fibroblast activation and ECM synthesis (Akhmetshina et al., 2012).

2 Candidate markers of CKD types in urinary extracellular vesicles

2.1 Diabetic nephropathy

Diabetic nephropathy (DN), also termed diabetic kidney disease (DKD), is a type of glomerulonephritis usually characterized by the presence of persisting elevated albuminuria, diabetic renal lesions, and decreased eGFR in diabetic patients (Alsaad and Herzenberg, 2007). Multiple sections of the kidney undergo structural alterations such as thickening of the glomerular basement membrane (GBM), capillary and tubular basement membrane, as well as loss of endothelial fenestrations, mesangial matrix expansion, and drop in podocyte (Alicic et al., 2017). Podocytes can be functionally and structurally injured early in DN pathology, and a decrease in their number and density is associated with the development of proteinuria and DN progression (Su et al., 2010). Albuminuria is a strong predictor, however DN can also present low levels of albuminuria or albuminuria can regress (Kramer et al., 2003). Being driven by a rather heterogeneous array of pathways, from inflammation to tubular injury, the identification of patients progressing to ESKD is difficult and much effort has been placed to discover urine and plasma biomarkers of high-risk disease.

Apart from persistent albuminuria, DN is characterized by renal lesions, which are shown to be very heterogeneous in renal biopsies from type 2 diabetes (T2D) patients (Gambara et al., 1993). Moreover, DN in both insulin-dependent (Parving et al., 1988) and non-insulin-dependent (Parving et al., 1992) diabetic patients can be manifested by proliferative retinopathy and blindness, neuropathy, arterial hypertension, and is associated with increased morbidity and mortality. Monitoring DN through plasma or urine protein fingerprint has been exploited *via* a variety of proteomics approaches although hampered by the abnormal albumin level found in this condition (Van et al., 2017). Tubular injury marker kidney injury molecule-1 (KIM-1), traceable in blood and urine, has been proposed to lead to DN progression (Sabbisetti et al., 2014; Schrauben et al., 2021; Vaidya et al., 2011). Another tubular injury marker is N-acetyl-β-D-glucosaminidase (NAG) which has been linked with DN in patients with type-1 diabetes (T1D) (Vaidya et al., 2011), while haptoglobin emerged as a strong predictor of DN in patients with T2D (Bhensdadia et al., 2013). Meta-analysis of urinary liver-type fatty acid-binding protein (L-FABP) has shown potential of L-FABP to detect all stages of DN and predict disease severity and progression in patients with either T1D or T2D (Zhang L et al., 2022). A protein fingerprint of DN progression has been proposed by the Chronic Renal Insufficiency Cohort (CRIC) Study (Schrauben et al., 2021).

Growing attention has been paid to the relationships between uEVs cargo and DN detection and progression. The findings are summarized in Table 3 and include early and recent studies.

An initial investigation (Sun et al., 2012) was conducted on urine microvesicles obtained by capturing the microvesicles *via* a monoclonal antibody (AD-1) originally raised *versus* membrane-bound liver alkaline phosphatase from human liver cancer serum (Cheruvanky et al., 2007) and measuring dipeptidyl peptidase-IV (DPP IV or CD26) activity, an enzyme highly concentrated in the cortex. The rationale was that DPP IV is responsible for the degradation of active glucagon-like peptide-1 after meal intake, which in turn increases insulin secretion, thus it positively correlates with T2D. As expected, urinary microvesicle-DPP IV excretion was elevated in the T2D cohort compared with controls and positively correlated with ACR in diabetic patients with T2D, suggesting that urinary microvesicle-bound DPP IV could be linked with the severe DN.

Another early investigation on a larger cohort, this time based on uEVs isolated by a differential centrifugation method (Kalani et al., 2013) reported elevated levels of Wilm's Tumor-1 (WT1) in the uEVs of T1D with proteinuria compared with patients without proteinuria, whereas in the non-diabetic control group WT1 expression was absent. WT1 is a zinc-finger transcription factor that plays a role in podocyte maturation and is used as a molecular marker of podocytes to assess podocyte lesions (Zhou et al., 2008; Su et al., 2010). It is believed that increased WT1 levels in uEVs can represent a decline in renal function in diabetics, since higher levels of exosomal WT1 were strongly associated with increased urinary protein excretion and with elevated serum creatinine and lower eGFR. Since urinary exosomal WT1 can be detected earlier than proteinuria and glomerular damage, WT1 may be regarded as a biomarker of early renal injury in diabetics (Kalani et al., 2013).

Work by Zubiri et al. (2014) identified three possible markers of DN in uEVs but in a small group of T2D patients with kidney disease. These were α-microglobulin/bikunin precursor (AMBP), a membrane glycoprotein that is expressed in liver and kidney; histone-lysine N-methyltransferase (MLL3), a protein involved in the methylation of Lys-4 of histone H3, a tag for epigenetic transcriptional activation (Cho et al., 2007); voltage-dependent anion-selective channel protein 1 (VDAC1), a channel on the outer membrane of mitochondria and plasma membrane (Lawen et al., 2005), which was found downregulated in the DN urinary exosomes, however, its presence in most cell types makes it a non-selective marker of kidney disease in DN.

In the streptozotocin (STZ)-induced rat model of early DN, differential proteomic gel electrophoresis analysis of the renal tissue extract revealed downregulation of the regucalcin protein (or senescence marker protein-30 (SMP30)), a protein involved in cellular calcium homeostasis and control of oxidative stress in DN. In a pilot study investigating regucalcin in the uEVs, the same trend was confirmed in DN rats and in humans (Zubiri et al., 2015).

Comparative proteomics between whole urine samples and urinary exosomes in a large study on patients with DN revealed exosomal ceruloplasmin and gelatinase as early biomarkers of kidney disease (Gudehithlu et al., 2015). Gelatinases, also known as matrix metalloproteinases, are proteins involved in the breakdown of ECM components such as collagen, laminin,

TABLE 3 Proteins isolated from uEVs, proposed to be biomarkers of CKD.

CKD etiology	uEV protein	Expression	Sample size	Method of analysis	Source
DN	Dipeptidyl peptidase-4 (DPP IV)	DN ↑	Normoalbuminuria, *n* = 43; Microalbuminuria, *n* = 50; Macroalbuminuria, *n* = 34	ELISA	Sun et al. (2012), *Diab Vasc Dis Res*
DN	Wilms's tumor 1 transcription factor (WT1)	DN ↑	T1D, *n* = 48; Control, *n* = 25	Immunoblotting	Kalani et al. (2013), *PLoS ONE*
DN	α-microglobulin/bikunin precursor (AMBP)	DN ↑	DN, *n* = 5; Control, *n* = 5	LC-MS/MS + SRM	Zubiri et al. (2014), *Journal of Proteomics*
	Histone-lysine N-methyltransferase (MLL3)				
	Voltage-dependent anion-selective channel protein 1 (VDAC1)	DN ↓			
DN	Gelatinase	DN ↓	DN, *n* = 82	Fluorometric assay using FITC-gelatin as a substrate	Gudehithlu et al. (2015), *Am J Nephrol*
	*Ceruloplasmin			Sandwich ELISA	
DN	Regucalcin	DN ↓	DN, *n* = 4; Control, *n* = 3	Immunoblotting	Zubiri et al. (2015), *Transl Res.*
DN	Cathepsin A, C, D, L, X/Z/P	DN ↑	DN, *n* = 37; Control, *n* = 12	Proteome profiler human protease and inhibitor array kit	Musante et al. (2015), *J Diabetes Res*
	Kallikrein 13				
	Proteinase 3				
	Cystatin B				
DN	C-megalin	T2D ↑	T2D, *n* = 33; Control = 11	Immunoblotting	De et al. (2017), *Diabetes*
DN	Epithelium-specific transcription factor (ELF3)	DN ↑	DN, *n* = 25; MCD, *n* = 25; Control, *n* = 5	Immunoblotting	Sakurai et al. (2019), *PLoS ONE*
DN	CD73	DN ↑	DN, *n* = 10; Diabetics, *n* = 48; Control, *n* = 10	Immunoblotting	Cappelli et al. (2020), *Biochim Biophys Acta Mol Basis Dis*
DN ADPKD	Osteoprotegerin (OPG)	DN and ADPKD ↑	CKD, *n* = 14; Control, *n* = 4	LC-MS/MS + SRM QQQ-LC/MS	Benito-Martin et al. (2013), *PLoS ONE*
ADPKD	Periplakin	ADPKD ↑	ADPKD, *n* = 6; Control, *n* = 6	LC-MS/MS + Immunoblotting	Salih et al. (2016), *JASN*
	Envoplakin				
	Villin-1				
	Complement C3				
	Complement C9				
IgAN	*Ceruloplasmin	IgAN ↑	IgAN, *n* = 5; TBMN, *n* = 7; Control, *n* = 7	LC-MS/MS	Moon et al. (2011), *Proteomics*
	α-1-antitrypsin				
	Aminopeptidase N (APN)	IgAN ↓			
TBMN	Vasorin precursor	TBMN ↑			
IgAN	CCL2 mRNA	IgAN ↑	IgAN, *n* = 6; Control, *n* = 6	Real-time RT-PCR	Feng et al. (2018), *Am J Pathol*
IgAN MN FSGS LN	*Ceruloplasmin	MN, IgAN, FSGS, LN ↑	MN, *n* = 9; IgAN, *n* = 7; FSGS, *n* = 10; LN, *n* = 10; Control, *n* = 15	Sandwich ELISA	Gudehithlu et al. (2019), *Clin Exp Nephrol*
FSGS	Dipeptidase 1 (DPEP1)	FSGS ↓	CKD, *n* = 12; Control, *n* = 12	LC-MS/MS	Stokman et al. (2019), *Journal of Proteomics*

(Continued on following page)

TABLE 3 (*Continued*) Proteins isolated from uEVs, proposed to be biomarkers of CKD.

CKD etiology	uEV protein	Expression	Sample size	Method of analysis	Source
Nephronophthisis	Protocadherin Fat 4 (FAT4)	Nephronophthisis ↓			
CKD pool	Versican core protein (VCAN)	CKD ↑			
CKD pool	CD2AP mRNA	CKD ↓	CKD, *n* = 32; Control, *n* = 7	Real-time RT-PCR	Lv et al. (2014), *Clinica Chimica Acta*
CKD pool	CD133	CKD ↓	CKD, *n* = 12; Control, *n* = 7	Cytofluorimetric analysis	Dimuccio et al. (2020), *Am J Physiol Renal Physiol*

*recurrent in different studies; ↑ denotes increased and ↓ decreased expression compared to controls.

elastin, and fibronectin. Their dysregulation is associated with pathological processes of fibrotic diseases, inflammation, and tumor progression (Thrailkill et al., 2007). Ceruloplasmin is an acute-phase plasma protein with various physiological roles such as copper carrying, facilitating transferrin-mediated iron transfer and uptake, plasma ferroxidase activity and scavenging free radicals; therefore, it is protective against tissue damage under inflammatory conditions (Arnaud et al., 1988). The two proteins were previously reported to be altered in the diabetic state (Thrailkill et al., 2007; Del Prete et al., 1997; Narita et al., 2006) so it is not surprising they have been pinpointed as uEVs proteins in DN. The levels of exosomal gelatinase and ceruloplasmin correlated with their changes in renal tissue, but not when considering their levels in the full urine, showing a better role of uEVs in mirroring the cell pathological phenotype. Therefore, gelatinase and ceruloplasmin could potentially be utilized as biomarkers of DN according to Gudehithlu et al. (2015). However, uEVs ceruloplasmin was not uniquely linked to DN as it emerged as a potential early biomarker of membranous nephropathy (MN), IgA nephropathy (IgAN), lupus nephritis (LN), and focal segmental glomerulosclerosis (FSGS). In all of these conditions, exosomal ceruloplasmin was consistently higher in CKD compared to control subjects (Gudehithlu et al., 2019). This was also confirmed in a longitudinal study performed on a passive Heymann nephritis (PHN) rat animal model, which is a homologous condition to human MN, showing that the level of urine exosomal ceruloplasmin increased significantly 1 week before the onset of proteinuria (Gudehithlu et al., 2019).

More recently, a study by Sakurai et al. (2019) uncovered induction of the epithelium-specific transcription factor ELF3 in the exosomes of podocytes cultured in a diabetic condition. ELF3 induction was inhibited by neutralization of the bone morphogenetic protein 4 (BMP4), which in turn regulates TGF-β receptor II - SMAD3 signaling (i.e., entrance of SMAD3 protein in the nucleus and transcription of proliferation genes) (Sakurai et al., 2019). Hence, a link between EVs ELF3 with TGF-β signaling was established, moreover exosomal ELF3 was also found to be specific for DN as present in uEVs DN patients and not in the uEVs of other CKD patients. Because it also correlated with eGFR decline, it was proposed as an early marker for podocyte injuries in DN.

Numerous studies have also identified microRNAs (miRNAs) biomarker candidates of uEVs origin in DN (Table 4). Early research in T1D patients with microalbuminuria versus normoalbuminuria and non-diabetic controls suggested the possibility to stratify T1D patients with and without kidney disease through uEVs. In particular, miR-130a, expressed by human podocytes, and miR-145, a marker of glomerular mesangial cells, were found to be enriched in urinary exosomes of patients with T1D who developed symptoms of microalbuminuria. miR-145 upregulation was confirmed *in vivo* in murine experimental models (diabetic/non-diabetic model) and mesangial cells *in vitro* (Barutta et al., 2013). Furthermore, urinary exosomal miR-155 and miR-424 were downregulated in incipient DN (Barutta et al., 2013). We know that miR-155 could participate in the inflammatory response in endothelial cells by targeting human angiotensin II type I receptor (hAT1R) (Louafi et al., 2010) and that miR-424 can bind to vascular endothelial growth factor (VEGF), receptor 2 (VEGFR2) and fibroblast growth factor receptor 1 (FGFR1), with reduction of endothelial cell proliferation, migration and morphogenesis (Chamorro-Jorganes et al., 2011). As these miRNAs are expressed by podocytes, their significantly reduced expression in podocyte-derived exosomes may be a useful indicator of early-stage DN (Barutta et al., 2013).

In a similar uEVs DN study but with a duplicated sample size, miR-192, miR-194, and miR-215 were found to be significantly increased in the microalbuminuric group of T2D-linked DN patients when compared to the normoalbuminuric group and healthy controls, but were decreased in the macroalbuminuric group (Jia et al., 2016). Furthermore, miR-192 and miR-215 expression levels significantly correlated with those of TGF-β1 in uEVs. Therefore, also these miRNAs are potential biomarkers in the early stages of DN, with miR-192 as a stronger candidate, having a markedly higher expression levels than the other two (Jia et al., 2016). The involvement of miR-192 in the development of DN has been previously reported in both *in vitro* and *in vivo* studies showing that its inhibition can result in a significant increase of its target Zinc Finger E-Box Binding Homeobox 1/2 (ZEB1/2), which in turn reduced the expression of collagen, TGF-β and fibronectin, known mediators of renal fibrosis (Putta et al., 2012). On the other hand, miR-194 has been found to play a role in renal ischemia-reperfusion injury, which often causes acute kidney injury and renal fibrosis, leading to renal failure. An *in vitro* study, performed on the human kidney proximal TEC line HK-2, showed that miR-194 expression was reduced in ischemia-reperfusion injury resulting in inhibition of HK-2 cell survival (Shen et al., 2018). When miR-194 was overexpressed using miR-194 mimics, the secretion of oxidative stress markers and pro-inflammatory cytokines was suppressed and HK-2 cell survival was

TABLE 4 miRNAs isolated from uEVs proposed as biomarkers of CKD.

CKD etiology	uEVs miRNA	Expression	Sample size	Method of analysis	Source
DN	*miR-155	DN (T1D) ↓	Microalbuminuria, *n* = 12; Normoalbuminuria, *n* = 12; Control, *n* = 10	Human TaqMan miRNA array A	Barutta et al. (2013), *Plos One*
	miR-424				
	miR-130a	DN (T1D) ↑			
	miR-145				
Early-stage DN	miR-192	DN (T2D) ↑	Normoalbuminuria, *n* = 30; Microalbuminuria, *n* = 30; Macroalbuminuria, *n* = 30; Control, *n* = 10	RT-qPCR	Jia et al. (2016), *J Diabetes Res*
	*miR-194				
	miR-215				
DN	miR-15b	DN (T2D) ↑	T2D albuminuric, *n* = 90; Normo-albuminuric, *n* = 46; Control, *n* 44	SYBR green custom miScript miRNA PCR Array	Eissa et al. (2016), *J Diabetes Complicat*
	miR-34a				
	miR-636				
DN	miR-320c	DN ↑	DN, *n* = 8; T2D, *n* = 8; Control, *n* = 8	Agilent microarrays	Delić et al. (2016), *Plos One*
DN	miR-877-3p	DN ↑	DN, *n* = 5; T2D, *n* = 5	miRCURY LNA array	Xie et al. (2017), *J Diabetes Res*
FSGS MCD	miR-1225-5p	MCD ↑	FSGS, *n* = 16; MCD, *n* = 5; Control, *n* = 5	MiRNA microarrays and TaqMan qRT-PCR	Ramezani et al. (2015), *Eur J Clin Invest*
	miR-1915	FSGS ↓			
	miR-663				
	*miR-155	FSGS ↑			
SLE	miR-335*	SLE ↑	SLE = 28; Control = 12	RT-qPCR	Perez-Hernandez et al. (2015), *Plos One*
	miR-302d				
	miR-200c				
	miR-146a				
LN	miR-26a	LN ↑	LN, *n* = 13; Control, *n* = 8	RT-qPCR	Ichii et al. (2014), *Plos One*
LNIV	miR-3135b	LNIV ↑	Active LNIV, *n* = 5; Active LNIV-CC, *n* = 5; Inactive LNIV, *n* = 4; Control, *n* = 3	miRNA high-throughput sequencing	Li et al. (2018), *J Biol Res (Thessalon)*
LNIV-CC	miR-654-5p	LNIV-CC ↑			
Renal fibrosis in LN	miR-21, miR-150, miR-29c	LN ↑ (miR-21, miR-150), ↓ (miR-29c)	LN, *n* = 45; Control, *n* = 20	miRCURY LNA Universal RT microRNA PCR	Sole *et al.* 2019), *Cells*
Paediatric NS	*miR-194-5P	Paediatric NS ↑	NS, *n* = 5 (pool of 25); Control, *n* = 4 (pool of 20)	High-throughput Illumina sequencing	Chen et al. (2019), *EBioMedicine*
	miR-146b-5p				
	miR-378a-3p				
	miR-23b-3p				
	miR-30a-5p				
IgAN	*miR-150	IgAN ↑	IgAN, *n* = 22; Control, *n* = 6	NanoString nCounter miRNA Expression Assay	Szeto et al. (2019), *BMC Nephrology*
	miR-204	IgAN ↓			
	miR-555				
Renal fibrosis	*miR-29	Renal fibrosis ↓	CKD, *n* = 32; Control, *n* = 7	RT-qPCR	Lv et al. (2013), *Am J Physiol Renal Physiol*
	miR-200				
CKD pool	miR-181a	CKD ↓	CKD, *n* = 15; Control, *n* = 10	Total RNA NGS	Khurana et al. (2017), *RNA*

(Continued on following page)

TABLE 4 (*Continued*) miRNAs isolated from uEVs proposed as biomarkers of CKD.

CKD etiology	uEVs miRNA	Expression	Sample size	Method of analysis	Source
CKD pool	*miR-21	CKD ↑	CKD, n = 41; Control, n = 5	RT-qPCR	Lange et al. (2019), *J Cell Mol Med*
CKD pool	*miR-21-5p	CKD ↑	DN (T2D), n = 14; DN (T2D) normal renal function, n = 15	PCR panels and individual PCR	Zang et al. (2019), *Sientific Reports*
	miR-30b-5p	CKD ↓			
CKD pool	miR-451	CKD ↑	CKD, n = 48; Control, n = 23	RT-qPCR	Kumari et al. (2020), *Front Physiol*

*recurrent in different studies; ↑ denotes increased and ↓ decreased expression compared to controls.

improved through miR-194 binding and inhibition of its downstream target Ras homologue enriched in brain (RHEB) (Shen et al., 2018). miR-215 has been shown to be involved in mesangial cell phenotypic transition into myofibroblasts mediated by TGF-β. In particular, inhibition of miR-215 significantly reduced the mesangial cell phenotypic transition, whereas its overexpression enhanced it, by targeting catenin-beta interacting protein 1 (CTNNBIP1). CTNNBIP1 has a function in suppressing the Wnt/β-catenin signaling pathway that promotes the activation and upregulation of α-SMA and fibronectin, therefore, when miR-215 binds CTNNBIP1, the activated Wnt/β-catenin pathway freely contributes to the pathogenesis of DN (Mu et al., 2013).

Urinary exosomal miR-15b, miR-34a, and miR-636 belong to a unique genetic cluster and share functions related to renal diseases and diabetes mellitus, such as regulation of cell proliferation, apoptosis and cytokine release. An *in silico* analysis suggests that all three miRNAs share common target mRNAs involved in glucose homeostasis, angiogenesis and DN (Eissa et al., 2016). In a large T2D albuminuric study group, all three miRNAs were upregulated compared with normoalbuminuric patients and healthy control group (Eissa et al., 2016). However, in about 30% of normoalbuminuric patients, these miRNAs were also found increased. Their dysregulation correlated with age, BMI, hypertension, serum creatinine, glycosylated hemoglobin (HbA1C) and ACR, suggesting their potential application in diagnosing DN in T2D subjects (Eissa et al., 2016).

Further research (Delić et al., 2016) detected over 300 miRNAs in a small sample size of DN patients, healthy controls and non-CKD subjects, and singled out miR-320c and miR-6068 as the most upregulated miRNAs. In particular, miR-320c expression showed a significant positive correlation with urinary ACR, and a negative correlation with eGFR. Therefore, urinary exosomal miR-320c was suggested as a possible diagnostic biomarker for DN (Delić et al., 2016). Thrombospondin-1 and -4 (TSP-1; TSP-4) and bone morphogenetic-6 (BMP6), all involved in TGF-β signaling, were revealed as putative miR-320c targets using the miR-Walk database. In the HK2 cell line, BMP6 has been shown to suppress the profibrogenic effects of TGF-β by inhibition of EMT and deposition of matrix proteins and by preventing enhanced adhesion behavior (Yan et al., 2009). TSP-1 has been identified as an activator of TGF-β, found increased in the glomeruli of DN patients, co-expressed with p-SMAD2/3, and its inhibition has resulted in reduced renal impairment and proteinuria (Hohenstein et al., 2008). TSP-4 plays a role in regulating collagen mRNA levels and its deficiency significantly increases cardiac fibrosis (Frolova et al., 2012). Therefore, it could be inferred that miR-320c may be utilized to trace DN, because it regulates TGF-β function and fibrosis progression.

miR-877-3p was identified as a candidate biomarker for DN in two studies: a small-scale study showing it was significantly upregulated in DN compared to T2D (Xie et al., 2017) and a transcriptomic analysis where it was also found to be significantly increased in urinary exosomes from the CKD group compared to healthy controls (Khurana et al., 2017). Predicted targets of miR-877-3p revealed a possible link with cell death, epidermal growth factor receptor signaling, response to hypoxia and to Akt/FoxO signaling (Xie et al., 2018). Specifically, miR-887-3p might accelerate renal dysfunction *via* PI3K/Akt, which in turn leads to the inactivation of the transcription factor FoxO3a and the subsequent downregulation of its proapoptotic genes, consequently inducing TGF-β-mediated mesangial cell survival and oxidative stress in the early DN (Kato et al., 2006).

The differences in miRNAs detected in the various studies are noticeable and may reflect the diverse pathways underlying DN or a lack of reproducibility in uEVs data or different sensitivities of the technologies supporting miRNA evaluation (Table 4).

2.2 Autosomal dominant polycystic kidney disease

Autosomal dominant polycystic kidney disease (ADPKD) is an inherited kidney disease caused by mutations in genes PKD1 and PKD2 encoding for proteins polycystin-1 (PC-1) and polycystin-2 (PC-2). PC-1 has features of ion channel and G-protein coupled receptor (GPCR) and PC-2 is a calcium-permeable non-selective cation channel, which in healthy conditions form a complex in the primary cilia that is important for intracellular calcium regulation (Ta et al., 2020). When polycystin function is lost, this in turn leads to a decreased intracellular calcium and increased cyclic adenosine monophosphate (cAMP) levels/protein kinase A activation, activating downstream mTOR signaling responsible for impaired tubulogenesis, cell proliferation, increased fluid secretion and interstitial inflammation (Mise et al., 2018; Chebib et al., 2015). The formation of fluid-filled cysts disrupts the renal parenchyma and often progresses to ESKD (Ong et al., 2015), which in 5%–10% of cases is caused by ADPKD. Although the molecular basis of the disease is known, the complex mechanism of cyst growth and expansion is still little understood. In an initial small-scale clinical

study, profiling of a mixed cohort of DN and ADPKD patients led to the identification of osteoprotegerin (OPG) in uEVs and its increased expression in patients with CKD compared to healthy controls (Benito-Martin et al., 2013). OPG is a glycoprotein secreted from proximal TECs that belongs to the tumor necrosis factor (TNF) receptor superfamily involved in the regulation of the skeletal, vascular, and immune system. It is believed to act as a decoy receptor for the death ligand TNF-related apoptosis-inducing ligand (TRAIL) and in DN both OPG and TRAIL appear to be highly expressed (Lorz et al., 2008).

A specific investigation of uEVs proteomics in ADPKD revealed about 30 proteins of which periplakin, envoplakin, villin-1, and complements C3 and C9 were further validated (Salih et al., 2016). Villin-1 is an actin-modifying protein which in kidney is mostly expressed in the proximal tubules, likely to be functionally linked to polycystin-1 as both have a role in cell motility and actin reorganization (Tomar et al., 2006; Castelli et al., 2015). Plakins are transmembrane cytolinker proteins with multiple functions, including participation in the binding of adhesive junctions such as desmosomes (Huber, 2003). Although polycystin-1 is associated with desmosomal proteins, in ADPKD it is no longer colocalized with desmosomes resulting in mispolarization of desmosomal proteins, which may explain the abundant amounts of plakins in patients with ADPKD (Silberberg et al., 2005). The complement system C9 and C3 components are believed to be involved in the progression of ADPKD by mediating cyst-lining epithelial cell proliferation, infiltration of tubulointerstitial inflammatory cells and development of fibrosis. Complement C3 and C9 may be locally produced by cysts epithelial cells and packed in uEVs in patients with ADPKD (Salih et al., 2016). Moreover, inhibition of the complement system results in decreased cyst growth, further confirming its involvement in ADPKD pathogenesis (Wang et al.,2014).

2.3 Immunoglobulin A nephropathy and thin basement membrane nephropathy

Immunoglobulin A nephropathy (IgAN) and thin basement membrane nephropathy (TBMN) are characterized by hematuria as a visible or microscopic symptom. Although they are separate kidney conditions the initial clinical presentation may be similar. IgAN, the most common autoimmune type of glomerulonephritis, can manifest from asymptomatic hematuria to rapidly progressive kidney disease. IgAN is due to the presence of galactose-deficient IgAs which are regarded as abnormal by other circulating antibodies, leading to immune complexes which cause inflammation in the glomerulus. In particular, the underlying mechanism involves aberrant glycosylation of IgA1, synthesis of galactose-deficient IgA1 antibodies, formation of immune complexes by binding of the galactose-deficient IgA1 and anti-glycan/glycopeptide antibodies, and finally accumulation of the immune complexes in the glomerular mesangium (Rodrigues et al., 2017; Suzuki et al., 2011). Dysregulation of mucosal IgA production has been reported to cause an inflammatory response to the immune complexes resulting in proliferation of mesangial cells, expansion of ECM, release of cytokines and growth factors, damage to podocytes and tubular cells, all of which led to renal function deterioration (Radford et al., 1997; Lai et al., 2009). The affected patients are characterized by proteinuria and persistent hematuria. Another CKD type characterized by persistent microscopic hematuria but without significant proteinuria is TBMN, an autosomal dominant disorder associated with mutations in type IV collagen genes COL4A3 and COL4A4 leading to reduced thickness and stability of the glomerular basement membrane (GBM) (Badenas et al., 2002; Tryggvason and Patrakka, 2006; Haas, 2006). Although early clinical symptoms are similar for IgAN and TBMN, the outcome is different as IgAN is more severe leading to ESKD in many patients.

A small-scale study has tried to discriminate IgAN and TBMN based on differences in the uEVs proteome (Moon et al., 2011) (Table 3). Compared to healthy controls, over 30 uEVs proteins were found upregulated in IgAN and over 50 proteins upregulated in TBMN. Validation in additional sample cohorts (12 patients with IgAN, 12 patients with TBMN, six healthy volunteers) revealed uEVs vasorin precursor as linked with TBMN, while APN, α-1-antitrypsin and ceruloplasmin as associated with IgAN. Vasorin is a cell-membrane protein, predominantly expressed in vascular smooth muscle cells, that binds directly to TGF-β with its extracellular domain and reduces TGF-β downstream signaling, thereby preventing apoptosis and fibrosis (Ikeda et al., 2004). Interestingly, vasorin was found to be one of the significantly differentially expressed proteins also in a total urinary proteome study of IgAN, being downregulated compared to controls (Samavat et al., 2015). APN is an enzyme catalyzing the removal of basic and neutral amino acid residues from bioactive oligopeptides, which is expressed on the cell brush border membranes of the small intestine, glomerular epithelial and mesangial cells, and it is present in uEVs originating from renal proximal tubules (section 1.5). The involvement of APN in kidney pathologies, mostly *via* binding to its main substrate Ang II is well described (Look et al., 1989; Vlahović and Stefanović, 1998). α-1-antitrypsin, also called Serpin A1, is a member of a superfamily of serine protease inhibitors that targets neutrophil proteases, elastase, cathepsin G, and proteinase 3, but also has moderate affinity for plasmin and thrombin (Clemmensen et al., 2011; Law et al., 2006). α-1-antitrypsin peptides, along with β2-microglobulin fragments, were the most prominent peptides to show a negative correlation with baseline eGFR in CKD (Schanstra et al., 2015).

Exosomal chemokine (C-C motif) ligand 2 (CCL2) was also linked to IgA nephropathy in a study by (Feng et al., 2018). Although the initial group size was small, CCL2 mRNA could effectively distinguish IgAN cohorts from control groups in a validated experiment with a larger cohort of IgAN, MCD, MN and healthy controls, and CCL2 mRNA correlated with the severity of tubulointerstitial fibrosis and C3 deposition in IgAN, with the highest expression of uEVs CCL2 mRNA in patients with >50% biopsy area of tubular atrophy and fibrosis (Feng et al., 2018; Lv et al., 2018).

Among the proposed IgAN uEVs markers, also miRNAs have emerged (Szeto et al., 2019) (Table 4). Digital transcriptomics (NanoString nCounter) initially revealed an array of miRNAs with significantly different expression between IgAN and healthy which upon validation narrowed down to three miRNAs in particular. These were miR-150 which was significantly increased, while miR-204 and miR-555 were significantly decreased in IgAN. Especially, miR-204 displayed the best diagnostic accuracy. Looking at the biological processes involved, it is known that miR-204 antagonizes EMT by targeting specificity protein-1 transcription factor (SP1) in TEC after induction of acute kidney injury protecting renal tubules from chronic fibrotic changes (Chen et al., 2017), therefore it is reasonable to see its change in CKD pathology.

2.4 Focal segmental glomerulosclerosis and minimal change disease

Focal segmental glomerulosclerosis (FSGS) and minimal change disease (MCD) are forms of podocytopathies characterized by the appearance of primary lesions of podocytes or visceral epithelial cells. In particular, FSGS is a sclerotic glomerular disease frequently progressing to ESKD and recurrent in ~25% of kidney transplant patients. They are separate conditions that differ in prognosis and treatment despite the similarities (Cravedi et al., 2013). FSGS can be either primary, secondary (due to viral infection, medication) or genetic and presents tubulointerstitial scarring. The affected glomeruli show segmental solidification of the glomerular tuft. MCD, on the other hand, is characterized by extensive podocyte injury and the presence of normal-looking glomeruli and scar-free tubulointerstitium at the ultrastructural level (Rosenberg and Kopp, 2017).

A comparative study of differentially expressed miRNAs in FSGS and MCD in plasma and urinary EVs (Ramezani et al., 2015) revealed over 150 miRNAs. Among them specific miRNAs could discriminate between the two forms of CKD. miR-1225-5p was validated as upregulated in MCD compared to FSGS and healthy controls, while miR-155 as upregulated in FSGS compared to MCD and controls. miR-1915 and miR-663 were decreased in FSGS compared to MCD and controls, and in addition linked to proteinuria and eGFR changes (Table 4). Previous studies had shown that all these miRNAs are involved in the pathogenesis and progression of renal diseases. In particular, miR-1225-5p and miR-1915 regulate the expression of genes that are involved in maintaining adult renal stem/progenitor cells (ARPCs), for instance key markers of renal progenitors CD133 and PAX2 and genes involved in the repair mechanisms of ARPCs, such as Toll-like receptor 2 (TLR2). Moreover, they are thought to be specifically expressed in ARPCs, and therefore a decrease in their expression levels in the FSGS kidney may potentially reflect the loss of ARPCs (Sallustio et al., 2013). miR-663 has been reported to target renin (*REN*) and apolipoprotein E (*APOE*) mRNAs and a decrease in miR-663 has been associated with an increase in renin mRNA in patients with hypertension (Marques et al., 2011). miR-155 has been reported to target SMAD2 mRNA and repress SMAD2 protein expression, thereby affecting TGF-β-induced SMAD phosphorylation and signaling and altering downstream expression of various genes involved in fibrosis, inflammation and angiogenesis (Louafi et al., 2010).

2.5 Lupus nephritis

An autoimmune form of CKD, Lupus nephritis (LN) is a severe glomerulonephropathy that occurs as a frequent complication of systemic lupus erythematosus (SLE), a common type of Lupus. LN occurs as a consequence of the binding of antibodies to multiple intrarenal autoantigens. It can involve the formation of "tertiary lymph follicles" within the kidney including proinflammatory B cells, and the secretion of autoantibodies by plasma cells (Lech, 2013). A serious complication is the appearance of a cellular crescent, consisting of severe active vascular, glomerular and tubulointerstitial lesions, that manifest in up to 50% of patients with LN (Zhang et al., 2016b).

A small size study in LN patients' uEVs revealed elevation of miR-26a, the expression of which concurs to regulate podocyte homeostasis and positively correlates with urinary protein levels (Ichii et al., 2014) (Table 4).

In a parallel study, the presence of active LN versus SLE was associated with uEVs miR-146a (Perez-Hernandez et al., 2015), which also displayed a higher glomerular expression in patients with LN, correlating with disease severity (Lu et al., 2012). Furthermore, an increase in miR-335*, miR-302d, highly abundant in human urine (Weber et al., 2010), and miR-200c, was associated with SLE (Perez-Hernandez et al., 2015). miR-200c was previously reported to discriminate patients with acute kidney injury from healthy individuals in urine (Ramachandran et al., 2013).

In a further small-scale study, the urinary exosomal miRNA expression profiles in patients with type IV lupus nephritis (LNIV), patients with LNIV with cellular crescent (LNIV-CC), and healthy subjects were analyzed by high-throughput miRNA sequencing (Li et al., 2018). Validations revealed that miR-3135b was significantly enhanced in LNIV, while miR-654-5p was significantly enhanced in LNIV-CC. miR-146a-5p (found in LNIV by Perez-Hernandez et al., 2015) did not show a significant difference in expression between LNIV-CC and LNIV cohorts (Li et al., 2018). A link between miR-3135b or miR-654-5p with kidney disease was not previously reported, but miR-3135b had been associated with dilated cardiomyopathy (Wang et al., 2017), and miR-654-5p with prostate cancer cell proliferation (Östling et al., 2011).

Among all these uEVs studies in LN, a multi-marker urinary exosomal panel emerged as a stronger approach to the early detection of LN (Solé et al., 2019) and for identifying ESKD risk. Three miRNAs (miR-21, miR-150, and miR-29c) were found to correlate with the chronicity index in the renal biopsy, *via* inducing profibrotic changes such as formation of collagen (COL4A1) and potentially targeting the VEGFA and SP1 genes (Solé et al., 2019) leading to activation of pSMAD2/3 and the coactivator p300, and progression of glomerulonephritis (Kassimatis et al., 2010).

2.6 Pediatric nephrotic syndrome

Pediatric nephrotic syndrome (NS) is a chronic childhood glomerular disease associated with glomerular podocyte dysfunction due to primary T-cell disorder. It is usually preceded by MCD and FSGS but can also be caused by genetic disorders or be secondary to other diseases such as infections and neoplasia (Eddy and Symons, 2003).

Five potential miRNA biomarkers for pediatric NS were detected by high-throughput Illumina sequencing followed by RT-qPCR validation (Chen et al., 2019). The expressions of miR-194-5p, miR-146b-5p, miR-378a-3p, miR-23b-3p, and miR-30a-5p were significantly increased in pediatric NS compared to healthy control samples, and remarkably reduced during the period of clinical remission. Among them, uEVs miR-194-5p, and miR-23b-3p had the highest diagnostic accuracy and could

discriminate between high proteinuria and low proteinuria, hence predict the severity of pediatric NS (Chen et al., 2019). miR-194-5p was also reported in uEVs of patients with early DN (Jia et al., 2016) (Section 2.1). The miR-146 family was also involved in LNIV as commented in Section 2.5 (Perez-Hernandez et al., 2015), while miR-378a-3p targets glomerular matrix protein nephronectin (NPNT) decreasing its levels (Müller-Deile et al., 2017). Moreover, miR-23b-3p and miR-30a-5p are specific in exosomes and enriched in human urine (Cheng et al., 2014). Therefore, the individual miRNAs of this panel were not totally unexpected as they did recur in the literature as either present in uEVs or linked with kidney pathology.

2.7 All-purpose markers of CKD

UEVs proteomics and transcriptomics have also been utilized to identify generic markers of CKD. An early investigation, on biopsy-proven pools of CKD patients including DN, FSGS and IgAN, identified miR-29 and miR-200 families as downregulated in uEVs of patients with CKD (Lv et al., 2013). In terms of biological significance, *in vitro* and *in vivo* studies had shown downregulation of miR-29 in conditions of renal fibrosis and both miR-29 and miR-200 respectively targeted TGF-β1-induced production of collagens I and III (Qin et al., 2011), ZEB1/2 and fibronectin. Hence it is logical that their downregulation may be pro-fibrotic (Tang et al., 2013). A generic marker of CKD may be CD2-associated protein (CD2AP). CD2AP is expressed in the podocyte foot processes in the glomerulus, helping to keep the integrity of the slit diaphragm *via* interactions with other podocyte proteins (Kravets and Mallipattu, 2020). The transcript of CD2AP was found to be reduced in the uEVs of CKD patients with heavy proteinuria compared to moderate and mild proteinuria patients indicating a negative correlation of CD2AP with proteinuria severity (Lv et al., 2014).

Furthermore, in the attempt to relate non-coding RNAs to CKD stages, miR-181a emerged as 200-fold reduced in expression in all four stages of CKD compared to healthy controls (Khurana et al., 2017). As circulating miR-181a from human serum was significantly increased in samples of patients with nephrotic syndrome (Sui et al., 2014), a reduced level of miR-181a in uEVs (Khurana et al., 2017) appears a logical finding.

When miRNAs previously linked to CKD such as miR-21, miR-30a-5p and miR-92a (Baker et al., 2017; Zhang et al., 2014; Henique et al., 2017) were searched in the uEVs of patients with CKD arising from different aetiologies (Lange et al., 2019), only miR-21 resulted significantly different (upregulated) between CKD patients and healthy controls, showing a negative correlation with eGFR (Lange et al., 2019). A further study revealed that miR-21-5p was increased and miR-30b-5p downregulated in patients with diabetic and non-diabetic CKD compared to controls. Although they cannot be regarded as specific biomarkers of DN, their dysregulation in expression may be linked with renal impairment (Zang et al., 2019).

In more recent investigations, when a CKD cohort was divided into diabetic and non-diabetic subgroups, miR-451 emerged as significantly higher in the non-diabetic CKD subgroup and to negatively correlate with eGFR decrease (Kumari et al., 2020). In primary human proximal tubule cells miR-451 knockdown resulted in enhanced expression of downstream mRNA targets, including tyrosine 3-monooxygenase/tryptophan 5-monooxygenase activation protein zeta (YWHAZ) (Kumari et al., 2020), which in DN downregulates p38 MAPK signaling, with inhibition of glomerular mesangial cell proliferation. Therefore, it was proposed that miR-451 may play a protective role in early DN (Zhang et al., 2012).

2.8 uEVs protein and miRNA with proposed prognostic value in CKD

CKD stratification markers and early markers of disease progression are much needed as currently CKD is diagnosed by means of a kidney biopsy which can confirm fibrosis only at the point when it is already well established and advanced. At this stage the risk for the patient to progress to ESKD is high and part of the kidney function is lost. Only few studies have focused on CKD stratification markers, such as a study by (Musante et al., 2015) which has relied on uEVs protease and protease inhibitors to stratify DN patients. Several proteases were found differently expressed in the uEVs of the DN cohort, of which cathepsins of various classes, kallikrein-13, and proteinase-3 were the most significantly altered. Among the protease inhibitors, uEVs cystatin B was the most significantly changed in all DN groups compared to healthy subjects, but also linked to normoalbuminuria. While uEVs cathepsins were the most increased in the micro-macroalbuminuric groups, kallikrein 13 and proteinase-3 were most expressed in the norm-microalbuminuric groups with a decrease in the macroalbuminuric group (Musante et al., 2015). Hence this set of uEVs proteins potentially allow DN patient stratification based on the degree of albuminuria.

C-megalin (gp330), a large membrane glycoprotein of a low density lipoprotein receptor (LDLR) family (Saito et al., 1994) has also been shown to be associated with albuminuria progression when identified in uEVs from DN subjects. C-megalin correlates with ACR, and negatively correlates with eGFR (De et al., 2017). Advanced glycation end products and fatty acid-enriched proteins have been identified as toxic megalin ligands, which are filtered by glomeruli and once reabsorbed cause proximal TEC injury (Kuwahara et al., 2016).

Nephronophthisis-related ciliopathies (NPH-RC) are a group of autosomal recessive cystic kidney diseases associated with impairments in the structure and function of the primary cilia, a common genetic cause of ESKD (Choi et al., 2019). Stokman et al. (2019) studied uEVs proteins in patients with NPH-RC and found several proteins differently expressed at different stages of CKD and healthy controls. In particular, dipeptidase 1 (DPEP1), an enzyme located in the proximal convoluted tubules responsible for dipeptide hydrolysis (Nafar et al., 2014), and protocadherin Fat 4 (FAT4), present in cilia in kidney cells with a key role in the polarity of planar cells (Saburi et al., 2008), were downregulated in uEVs from the CKD cohorts. Versican core protein (VCAN), an extracellular matrix proteoglycan normally expressed in the kidneys at low levels (Rudnicki et al., 2012), was upregulated in uEVs of CKD cohorts. The expression of these discriminating proteins correlated with the severity of CKD so that they were most decreased (DPEP1 and FAT4) and increased (VCAN) in the advanced stage of CKD (Stokman et al., 2019).

It has been recently reported that AQP1 and AQP2, water channels also found in uEVs (Pisitkun et al., 2004), become reduced in uEVs during advanced CKD (Oshikawa-Hori et al., 2021). Comparison of different stages of CKD have shown that AQP1 and AQP2 are significantly reduced in stages 4 and 5 of CKD at a high level of diagnostic accuracy (Oshikawa-Hori et al., 2021), which increases when uEVs AQP and AQP2 are considered in combination as markers of advanced CKD.

All the markers discussed in this section have been combined and listed in Figure 3.

3 Urine handling and storage

Despite urine being a valuable source of biomarkers from the urogenital tract, lack of consensus for standardization of urine collection, processing, handling and storage, as well as uEVs isolation and downstream analysis, may be responsible for the high inter-individual sample variability, hampering the discovery of reliable biomarker candidates (Barreiro et al., 2021). Information on collection, storage, and timing of uEVs isolation for the reviewed studies is summarized in Table 5. Over 90% of the reviewed studies provide access to information on urine sample collection and processing protocols. Approximately 30% of the studies relied on first-morning or early-morning urine, 15% second-morning urine, and few others reported mid-day urine or overnight urine collection. In over 30% of the studies urine samples were treated with protease inhibitors. The effect of collection timing on uEVs and uEVs biomarkers has been reported by Zhou et al., 2006 showing that the total amount in uEVs protein was similar between first and second-morning urine, and that four tested exosomal proteins remained constant. This study suggests that both first and second morning urine collections can be used for uEVs isolation and protein analysis (Zhou et al., 2006). In most studies, urine samples were centrifuged to remove cells and cell debris, however a wide variation in centrifugal speeds and times was reported (Table 5), with the most frequent centrifugation set at 2,000xg. Regarding the timing of uEVs isolation, in about half of the studies uEVs were isolated immediately after urine collection, while in the other half of the studies urine was stored for later uEVs isolation and further analysis at a temperature ≤80°C. There are few reports linking uEVs quality to storage temperature, showing that freezing uEVs at −20°C results in greater loss in uEVs proteome, while freezing at −80°C preserved above 85% of specific uEVs proteins (Zhou et al., 2006). A more recent study reported that storing uEVs at −20°C reduces RNA and protein yield compared to −80°C, although uEVs morphology is not affected (Barreiro et al., 2021). Therefore, storing uEVs at −80°C appears to be critical for the successful uEVs conservation and subsequent analysis of the uEVs cargo. Details on uEVs storage length are hardly provided in the literature.

4 Conclusion and future perspectives

Urinary EVs are a precious source of proteins and miRNAs, which although scarcely present in soluble form in full urine, are concentrated in EVs and discoverable through uEVs proteomics and transcriptomics. Since 2012, several proteins and individual

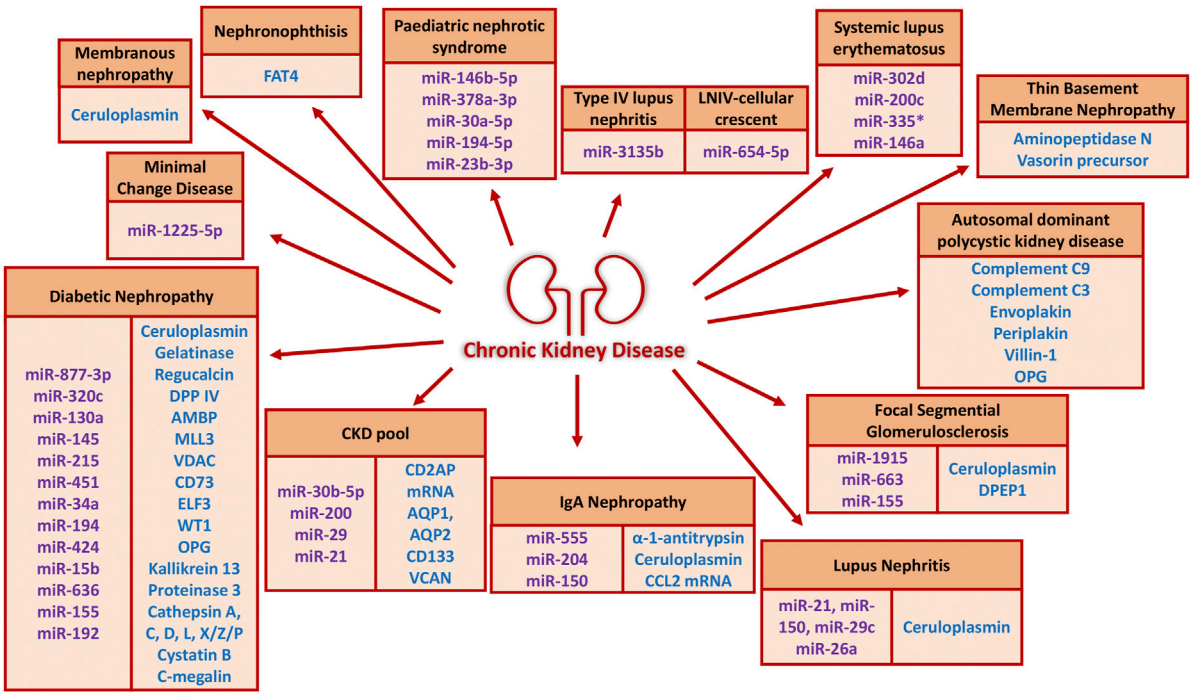


FIGURE 3
uEVs proteins and miRNAs of potential diagnostic and prognostic value in the literature (since 2012) grouped according to CKD etiologies. The protein cargo is shown in blue and the miRNA cargo in purple.

TABLE 5 Urine handling and storage conditions as reported in the studies included in this review.

Urine collection	Spot urine (Kalani et al., 2013; Zang et al., 2019; Kumari et al., 2020)	First/early-morning urine (Lv et al., 2013; Lv et al., 2014; Musante et al., 2015; Perez-Hernandez et al., 2015; Jia et al., 2016; Xie et al., 2017; Feng et al., 2018; Li et al., 2018; Szeto et al., 2019; Cappelli et al., 2020)	Second-morning urine (Benito-Martin et al., 2013; Zubiri et al., 2014; Salih et al., 2016; De et al., 2017)	Unspecified morning urine (Moon et al 2011; Chen et al., 2019; Lange et al., 2019; Dimuccio et al., 2020)	Not the first morning urine (Stokman et al., 2019)	Mid-day urine (Ramezani et al., 2015)	Voided urine (Eissa et al., 2016)	Overnight urine collection (Barutta et al., 2013)	Unspecified (Sun et al., 2012; Ichii et al., 2014; Gudehithlu et al., 2015; Zubiri et al., 2015; Delić et al., 2016; Khurana et al., 2017; Sakurai et al., 2019; Gudehithlu et al., 2019; Solé et al., 2019)
Timing of uEVs isolation	Right away (on sample collection) ~ 47% of studies	After thawing ~ 47% of studies	Unspecified (Ichii et al., 2014; Khurana et al., 2017)						
Centrifugation to remove cell debris	300 × g (10 min at RT or 15 min at 4°C) (Benito-Martin et al., 2013; Jia et al., 2016; Sakurai et al., 2019)	300 × g (10 min) then 17,000 × g (20 min) at 4°C (Barutta et al., 2013)	500 × g (10 min); then 2,000 × g (20 min) at 4°C (Stokman et al., 2019)	1,000 × g (15–20 min) at 4°C (Gudehithlu et al, 2015; Gudehithlu et al., 2019)	2,000 × g (10–15 min) (Ramezani et al., 2015; Delić et al., 2016; Xie et al., 2017; Zang et al., 2019)	2,000 × g (20–30 min) (Lv et al., 2013; Lv et al., 2014; Musante et al., 2015; Feng et al., 2018)	2,250 × g or 2,500 × g (30 min) (Perez-Hernandez et al., 2015; Li et al., 2018)	3,000 × g (10 min) at RT (Chen et al., 2019)	3,000 × g for 30 min; then 13,000 × g (5 min) at 4°C (Szeto et al., 2019)
Addition of protease inhibitors	Described ~ 35% of the studies	Unspecified ~ 62% of studies	Not used (Musante et al., 2015)						
Storage condition of urine/uEVs	~ −80°C Most studies (94%)	Unspecified (Ichii et al., 2014; De et al., 2017)							

miRNAs which are uEVs cargo have been proposed as promising CKD biomarkers. Our review has reported 33 different proteins and 37 different RNA in uEVs selected among the most relevant to CKD. The criteria was to select those molecules emerged from unbiased often "big data" screening but validated through a second targeted approach and ideally also confirmed in larger cohorts. The "hunt" for uEVs markers started approximately a decade ago and has taken place for most CKD types up to now. However, studies are far from uniform both in terms of CKD stage or eGFR and the way urine samples are collected, stored and processed to isolate EVs. Either because of the intrinsic variability of uEVs composition in the individual subjects, or depending on the urine collection timing and storage conditions, or because CKD classifications have also loose margins and overlap, a huge number of different molecules have emerged as potential disease markers. A selection of uEVs proteins such as gelatinase and ELF3 in DN, plakins (periplakin, envoplakin) and complements (C3 and C9) in ADPKD, and ribonucleic acids such as CCL2 mRNA in IgAN, miR-194-5p and miR-23b in pediatric NS have been linked to CKD severity and therefore they may have usefulness as stratification markers if not a potential prognostic value. There is a great variety of miRNA proposed. A bunch of miRNAs (miR-21, miR-150, and miR-29) have been reported to better mirror CKD in combination rather than individually, and together with miR-155, miR-194 are recurrent in different uEVs biomarkers discovery studies. Among the potential uEVs protein biomarkers, only ceruloplasmin was detected in more than one CKD study, associated with several kidney diseases, and as such uEVs ceruloplasmin may be regarded as a general marker of CKD pathology. Not many studies have compared the effectiveness of biomarkers detection from uEVs and full unfractionated urine, however uEVs ceruloplasmin has emerged as a better marker for early kidney disease.

A benefit of uEVs markers is that they generally better reflect early changes in the kidney than full urine and as such precede proteinuria. This is a key point that warrants future scrutiny, especially as new tools allowing direct uEVs marker quantifications in biofluids without necessity to isolate uEVs have emerged and are available to the scientific community (e.g. Exoview platform, Tonoli et al., 2022).

Attempts to relate the selected uEVs CKD markers to the molecular cell biology process underlying disease development have been reviewed or suggested in our evaluation. Future research in this direction may lead to better insights on the pathology and help reveal potentially new mechanisms as well as anti-fibrotic targets. The uEVs cell origin is particularly informative as it allows to track the molecular and cellular events underlying the CKD condition predicting the disease evolution. Although much effort has been made to identify specific cell markers in uEVs, this area is still not well consolidated and again uEVs markers quantifications directly in the biofluids should accelerate progress. Tracking the cell origin of uEVs by means of spatial transcriptomics is also a potential way to build the larger picture of CKD progression. Lastly, despite considerable effort by many groups globally, all the studies reviewed here included less than 1000 CKD patients when considered together,

of which half were DN. Larger size clinical studies should address these key points to reveal the full usefulness of the uEVs approach over full urine tests, and as such accelerate translation of uEVs biomarker discoveries into clinical practice to offer a real alternative to kidney biopsy.

Author contributions

EAMV contributed to the conception and design of the study; MT and ET acquired and analyzed the data; MT drafted the first manuscript; MT prepared figures and tables; EAMV revised the manuscript for important intellectual content; EAMV and MT wrote the second draft with the help of ET. All authors contributed to the article and approved the submitted version.

Funding

MT is supported by a NTU Vice Chancellor competitive PhD bursary and funds by UCB Biopharma (to EAMV).

Acknowledgments

We thank Prof Timothy Johnson (Mestag Therapeutics and University of Sheffield) for useful discussions and Dr Hernandez-Fuentes (UCB Biopharma) for general help.

Conflict of interest

The authors declare that the research was conducted in the absence of any commercial or financial relationships that could be construed as a potential conflict of interest.

Publisher's note

All claims expressed in this article are solely those of the authors and do not necessarily represent those of their affiliated organizations, or those of the publisher, the editors and the reviewers. Any product that may be evaluated in this article, or claim that may be made by its manufacturer, is not guaranteed or endorsed by the publisher.

References

Abedini, A., Zhu, Y. O., Chatterjee, S., Halasz, G., Devalaraja-Narashimha, K., Shrestha, R., et al. (2021). Urinary single-cell profiling captures the cellular diversity of the kidney. *J. Am. Soc. Nephrol.* 32 (3), 614–627. doi:10.1681/ASN.2020050757

Akhmetshina, A., Palumbo, K., Dees, C., Bergmann, C., Venalis, P., Zerr, P., et al. (2012). Activation of canonical Wnt signalling is required for TGF-β-mediated fibrosis. *Nat. Commun.* 3 (1), 735. doi:10.1038/ncomms1734

Alicic, R. Z., Rooney, M. T., and Tuttle, K. R. (2017). Diabetic kidney disease: Challenges, progress, and possibilities. *Clin. J. Am. Soc. Nephrol.* 12 (12), 2032–2045. doi:10.2215/CJN.11491116

AlQudah, M., Hale, T. M., and Czubryt, M. P. (2020). Targeting the renin-angiotensin-aldosterone system in fibrosis. *Matrix Biol.* 91-92, 92–108. doi:10.1016/j.matbio.2020.04.005

Alsaad, K. O., and Herzenberg, A. M. (2007). Distinguishing diabetic nephropathy from other causes of glomerulosclerosis: An update. *J. Clin. Pathology* 60 (1), 18–26. doi:10.1136/jcp.2005.035592

Andrae, J., Gallini, R., and Betsholtz, C. (2008). Role of platelet-derived growth factors in physiology and medicine. *Genes & Dev.* 22 (10), 1276–1312. doi:10.1101/gad.1653708

Andreu, Z., and Yáñez-Mó, M. (2014). Tetraspanins in extracellular vesicle formation and function. *Front. Immunol.* 5, 442. doi:10.3389/fimmu.2014.00442

Arai, H., Sato, Y., and Yanagita, M. (2021). Fibroblast heterogeneity and tertiary lymphoid tissues in the kidney. *Immunol. Rev.* 302 (1), 196–210. doi:10.1111/imr.12969

Arnaud, P., Gianazza, E., and Miribel, L. (1988). Ceruloplasmin. *Methods Enzym.* 163, 441–452. doi:10.1016/0076-6879(88)63042-4

Asada, N., Takase, M., Nakamura, J., Oguchi, A., Asada, M., Suzuki, N., et al. (2011). Dysfunction of fibroblasts of extrarenal origin underlies renal fibrosis and renal anemia in mice. *J. Clin. Investigation* 121 (10), 3981–3990. doi:10.1172/JCI57301

Badenas, C., Praga, M., Davila, S., Mila, M., Antignac, C., Darnell, A., et al. (2002). Mutations in the COL4A4 and COL4A3 genes cause familial benign hematuria. *J. Am. Soc. Nephrol.* 13 (5), 1248–1254. doi:10.1681/ASN.V1351248

Baker, M. A., Davis, S. J., Liu, P., Pan, X., Williams, A. M., Iczkowski, K. A., et al. (2017). Tissue-specific MicroRNA expression patterns in four types of kidney disease. *J. Am. Soc. Nephrol.* 28 (10), 2985–2992. doi:10.1681/ASN.2016121280

Barreiro, K., Dwivedi, O. P., Valkonen, S., Groop, P., Tuomi, T., Holthofer, H., et al. (2021). Urinary extracellular vesicles: Assessment of pre-analytical variables and development of a quality control with focus on transcriptomic biomarker research. *J. Extracell. Vesicles* 10 (12), e12158. doi:10.1002/jev2.12158

Bartel, D. P. (2004). MicroRNAs: Genomics, biogenesis, mechanism, and function. *Cell* 116 (2), 281–297. doi:10.1016/s0092-8674(04)00045-5

Barutta, F., Tricarico, M., Corbelli, A., Annaratone, L., Pinach, S., Grimaldi, S., et al. (2013). Urinary exosomal MicroRNAs in incipient diabetic nephropathy. *Plos One* 8 (11), e73798. doi:10.1371/journal.pone.0073798

Beltrami, C., Simpson, K., Jesky, M., Wonnacott, A., Carrington, C., Holmans, P., et al. (2018). Association of elevated urinary miR-126, miR-155, and miR-29b with diabetic kidney disease. *Am. J. Pathology* 188 (9), 1982–1992. doi:10.1016/j.ajpath.2018.06.006

Benito-Martin, A., Ucero, A. C., Zubiri, I., Posada-Ayala, M., Fernandez-Fernandez, B., Cannata-Ortiz, P., et al. (2013). Osteoprotegerin in exosome-like vesicles from human cultured tubular cells and urine. *PlosOne* 8 (8), e72387. doi:10.1371/journal.pone.0072387

Bennet, M. R., and Devarajan, P. (2017). "Chapter one - characteristics of an ideal biomarker of kidney disease," in *Biomarkers of kidney disease*. Editor C. L. Edelstein (Elsevier), 1–20.

Bernstein, E., Caudy, A. A., Hammond, S. M., and Hannon, G. J. (2001). Role for a bidentate ribonuclease in the initiation step of RNA interference. *Nature* 409 (6818), 363–366. doi:10.1038/35053110

Bhensdadia, N. M., Hunt, K. J., Lopes-Virella, M. F., Michael Tucker, J., Mataria, M. R., Alge, J. L., et al. (2013). Urine haptoglobin levels predict early renal functional decline in patients with type 2 diabetes. *Kidney Int.* 83 (6), 1136–1143. doi:10.1038/ki.2013.57

Bikbov, B., Purcell, C. A., Levey, A. S., Smith, M., Abdoli, A., Abebe, M., et al. (2020). Global, regional, and national burden of chronic kidney disease, 1990–2017: A systematic analysis for the global burden of disease study 2017. *Lancet* 395 (10225), 709–733. doi:10.1016/S0140-6736(20)30045-3

Bleyer, A. J., Kidd, K., Živná, M., and Kmoch, S. (2017). Autosomal dominant tubulointerstitial kidney disease. *Adv. Chronic Kidney Dis.* 24 (2), 86–93. doi:10.1053/j.ackd.2016.11.012

Boor, P., Ostendorf, T., and Floege, J. (2010). Renal fibrosis: Novel insights into mechanisms and therapeutic targets. *Nat. Reviews.Nephrology* 6 (11), 643–656. doi:10.1038/nrneph.2010.120

Borges, F. T., Melo, S. A., Özdemir, B. C., Kato, N., Revuelta, I., Miller, C. A., et al. (2013). TGF-β1-Containing exosomes from injured epithelial cells activate fibroblasts to initiate tissue regenerative responses and fibrosis. *J. Am. Soc. Nephrol.* 24 (3), 385–392. doi:10.1681/ASN.2012101031

Bruno, S., Grange, C., Collino, F., Deregibus, M. C., Cantaluppi, V., Biancone, L., et al. (2012). Microvesicles derived from mesenchymal stem cells enhance survival in a lethal model of acute kidney injury. *PLoS ONE* 7 (3), e33115. doi:10.1371/journal.pone.0033115

Bruno, S., Porta, S., and Bussolati, B. (2016). Extracellular vesicles in renal tissue damage and regeneration. *Eur. J. Pharmacol.* 790, 83–91. doi:10.1016/j.ejphar.2016.06.058

Burhan, I., Furini, G., Lortat-Jacob, H., Atobatele, A. G., Scarpellini, A., Schroeder, N., et al. (2016). Interplay between transglutaminases and heparan sulphate in progressive renal scarring. *Sci. Rep.* 6 (1), 31343. doi:10.1038/srep31343

Cappelli, C., Tellez, A., Jara, C., Alarcón, S., Torres, A., Mendoza, P., et al. (2020). The TGF-β profibrotic cascade targets ecto-5′-nucleotidase gene in proximal tubule epithelial cells and is a traceable marker of progressive diabetic kidney disease. *Biochimica Biophysica Acta Mol. Basis Dis.* 1866 (7), 165796. doi:10.1016/j.bbadis.2020.165796

Castelli, M., De Pascalis, C., Distefano, G., Ducano, N., Oldani, A., Lanzetti, L., et al. (2015). Regulation of the microtubular cytoskeleton by Polycystin-1 favors focal adhesions turnover to modulate cell adhesion and migration. *BMC Cell Biol.* 16 (1), 15. doi:10.1186/s12860-015-0059-3

Chamorro-Jorganes, A., Araldi, E., Penalva, L. O. F., Sandhu, D., Fernández-Hernando, C., and Suárez, Y. (2011). MicroRNA-16 and microRNA-424 regulate cell-autonomous angiogenic functions in endothelial cells via targeting vascular endothelial growth factor receptor-2 and fibroblast growth factor receptor-1. *Arterioscler. Thromb. Vasc. Biol.* 31 (11), 2595–2606. doi:10.1161/ATVBAHA.111.236521

Chebib, F. T., and Torres, V. (2015). Autosomal dominant polycystic kidney disease: Core curriculum 2016. *Am. J. Kidney Dis.* 67 (5), 792–810. doi:10.1053/j.ajkd.2015.07.037

Chen, S., Wu, P., Sun, L., Zhou, B., Niu, W., Liu, S., et al. (2017). miR-204 regulates epithelial-mesenchymal transition by targeting SP1 in the tubular epithelial cells after acute kidney injury induced by ischemia-reperfusion. *Oncol. Rep.* 37 (2), 1148–1158. doi:10.3892/or.2016.5294

Chen, T., Wang, C., Yu, H., Ding, M., Zhang, C., Lu, X., et al. (2019). Increased urinary exosomal microRNAs in children with idiopathic nephrotic syndrome. *EBioMedicine* 39, 552–561. doi:10.1016/j.ebiom.2018.11.018

Cheng, L., Sun, X., Scicluna, B. J., Coleman, B. M., and Hill, A. F. (2014). Characterization and deep sequencing analysis of exosomal and non-exosomal miRNA in human urine. *Kidney Int.* 86 (2), 433–444. doi:10.1038/ki.2013.502

Cheruvanky, A., Zhou, H., Pisitkun, T., Kopp, J. B., Knepper, M. A., Yuen, P. S. T., et al. (2007). Rapid isolation of urinary exosomal biomarkers using a nanomembrane ultrafiltration concentrator. *Am. J. Physiology - Ren. Physiology* 292 (5), 1657–1661. doi:10.1152/ajprenal.00434.2006

Cho, Y., Hong, T., Hong, S., Guo, H., Yu, H., Kim, D., et al. (2007). PTIP associates with MLL3-and MLL4-containing histone H3 lysine 4 methyltransferase complex. *J. Biol. Chem.* 282 (28), 20395–20406. doi:10.1074/jbc.M701574200

Choi, Y. J., Halbritter, J., Braun, D. A., Schueler, M., Schapiro, D., Rim, J. H., et al. (2019). Mutations of ADAMTS9 cause nephronophthisis-related ciliopathy. *Am. J. Hum. Genet.* 104 (1), 45–54. doi:10.1016/j.ajhg.2018.11.003

Clemmensen, S. N., Jacobsen, L. C., Rørvig, S., Askaa, B., Christenson, K., Iversen, M., et al. (2011). Alpha-1-antitrypsin is produced by human neutrophil granulocytes and their precursors and liberated during granule exocytosis. *Eur. J. Haematol.* 86 (6), 517–530. doi:10.1111/j.1600-0609.2011.01601.x

Clouthier, D. E., Comerford, S. A., and Hammer, R. E. (1997). Hepatic fibrosis, glomerulosclerosis, and a lipodystrophy-like syndrome in PEPCK-TGF-beta1 transgenic mice. *J. Clin. Investigation* 100 (11), 2697–2713. doi:10.1172/JCI119815

Cocucci, E., and Meldolesi, J. (2015). Ectosomes and exosomes: Shedding the confusion between extracellular vesicles. *Trends Cell Biol.* 25 (6), 364–372. doi:10.1016/j.tcb.2015.01.004

Conserva, F., Barozzino, M., Pesce, F., Divella, C., Oranger, A., Papale, M., et al. (2019). Urinary miRNA-27b-3p and miRNA-1228-3p correlate with the progression of kidney fibrosis in diabetic nephropathy. *Sci. Rep.* 9 (1), 11357. doi:10.1038/s41598-019-47778-1

Corapi, K. M., Chen, J. L. T., Balk, E. M., and Gordon, C. E. (2012). Bleeding complications of native kidney biopsy: A systematic review and meta-analysis. *Am. J. Kidney Dis. Official J. Natl. Kidney Found.* 60 (1), 62–73. doi:10.1053/j.ajkd.2012.02.330

Counts, D. F., Evans, J. N., Dipetrillo, T. A., Sterling, K. M., and Kelley, J. (1981). Collagen lysyl oxidase activity in the lung increases during bleomycin-induced lung fibrosis. *J. Pharmacol. Exp. Ther.* 219, 675–678.

Couser, W. G., Remuzzi, G., Mendis, S., and Tonelli, M. (2011). The contribution of chronic kidney disease to the global burden of major noncommunicable diseases. *Kidney Int.* 80 (12), 1258–1270. doi:10.1038/ki.2011.368

Cravedi, P., Kopp, J. B., and Remuzzi, G. (2013). Recent progress in the pathophysiology and treatment of FSGS recurrence. *Am. J. Transplant.* 13 (2), 266–274. doi:10.1111/ajt.12045

Cricrì, G., Bellucci, L., Montini, G., and Collino, F. (2021). Urinary extracellular vesicles: Uncovering the basis of the pathological processes in kidney-related diseases. *Int. J. Mol. Sci.* 22 (12), 6507. doi:10.3390/ijms22126507

Da Silva Lodge, M., Pullen, N., Pereira, M., and Johnson, T. S. (2022). Urinary levels of pro-fibrotic transglutaminase 2 (TG2) may help predict progression of chronic kidney disease. *PloS One* 17 (1), e0262104. doi:10.1371/journal.pone.0262104

De, S., Kuwahara, S., Hosojima, M., Ishikawa, T., Kaseda, R., Sarkar, P., et al. (2017). Exocytosis-mediated urinary full-length megalin excretion is linked with the pathogenesis of diabetic nephropathy. *Diabetes (New York, N.Y.)* 66 (5), 1391–1404. doi:10.2337/db16-1031

Del Prete, D., Anglani, F., Forino, M., Ceol, M., Fioretto, P., Nosadini, R., et al. (1997). Down-regulation of glomerular matrix metalloproteinase-2 gene in human NIDDM. *Diabetologia* 40 (12), 1449–1454. doi:10.1007/s001250050848

Delić, D., Eisele, C., Schmid, R., Baum, P., Wiech, F., Gerl, M., et al. (2016). Urinary exosomal miRNA signature in type II diabetic nephropathy patients. *PloS One* 11 (3), e0150154. doi:10.1371/journal.pone.0150154

Deten, A., Hölzl, A., Leicht, M., Barth, W., Zimmer, H., and Holzl, A. (2001). Changes in extracellular matrix and in transforming growth factor beta isoforms after coronary artery ligation in rats. *J. Mol. Cell. Cardiol.* 33 (6), 1191–1207. doi:10.1006/jmcc.2001.1383

Dimuccio, V., Peruzzi, L., Brizzi, M. F., Cocchi, E., Fop, F., Boido, A., et al. (2020). Acute and chronic glomerular damage is associated with reduced CD133 expression in urinary extracellular vesicles. *Ren. Physiol.* 318 (2), F486–F495. doi:10.1152/ajprenal.00404.2019

Duffield, J. S. (2014). Cellular and molecular mechanisms in kidney fibrosis. *J. Clin. Investigation* 124 (6), 2299–2306. doi:10.1172/JCI72267

Eddy, A. A., and Symons, J. M. (2003). Nephrotic syndrome in childhood. *Lancet (British Ed.* 362 (9384), 629–639. doi:10.1016/S0140-6736(03)14184-0

Eissa, S., Matboli, M., Aboushahba, R., Bekhet, M. M., and Soliman, Y. (2016). Urinary exosomal microRNA panel unravels novel biomarkers for diagnosis of type 2 diabetic kidney disease. *J. Diabetes its Complicat.* 30 (8), 1585–1592. doi:10.1016/j.jdiacomp.2016.07.012

Erdbrugger, U., Blijdorp, C. J., Bijnsdorp, I., V., Borras, F. E., Burger, D., Bussolati, B., et al. (2021). Urinary extracellular vesicles: A position paper by the urine task force of the international society for extracellular vesicles. *J. Extracell. Vesicles* 10 (7), e12093. doi:10.1002/jev2.12093

Erdbrügger, U., and Le, T. H. (2016). Extracellular vesicles in renal diseases: More than novel biomarkers? *J. Am. Soc. Nephrol.* 27 (1), 12–26. doi:10.1681/ASN.2015010074

Feng, Y., Lv, L. L., Wu, W. J., Li, Z. L., Chen, J., Ni, H. F., et al. (2018). Urinary exosomes and exosomal CCL2 mRNA as biomarkers of active histologic injury in IgA nephropathy. *Am. J. pathology* 188 (11), 2542–2552. doi:10.1016/j.ajpath.2018.07.017

Filip, S., Vougas, K., Zoidakis, J., Latosinska, A., Mullen, W., Spasovski, G., et al. (2015). Comparison of depletion strategies for the enrichment of low-abundance proteins in urine. *Plos One* 10 (7), e0133773. doi:10.1371/journal.pone.0133773

Friedman, S. L., Roll, F. J., Boyles, J., and Bissell, D. M. (1985). Hepatic lipocytes: The principal collagen-producing cells of normal rat liver. *Proc. Natl. Acad. Sci. - PNAS* 82 (24), 8681–8685. doi:10.1073/pnas.82.24.8681

Frolova, E. G., Sopko, N., Blech, L., Popović, Z. B., Li, J., Vasanji, A., et al. (2012). Thrombospondin-4 regulates fibrosis and remodeling of the myocardium in response to pressure overload. *FASEB J.* 26 (6), 2363–2373. doi:10.1096/fj.11-190728

Furini, G., Schroeder, N., Huang, L., Boocock, D., Scarpellini, A., Coveney, C., et al. (2018). Proteomic profiling reveals the transglutaminase-2 externalization pathway in kidneys after unilateral ureteric obstruction. *J. Am. Soc. Nephrol.* 29 (3), 880–905. doi:10.1681/ASN.2017050479

Gambara, V., Mecca, G., Remuzzi, G., and Bertani, T. (1993). Heterogeneous nature of renal lesions in type II diabetes. *J. Am. Soc. Nephrol.* 3 (8), 1458–1466. doi:10.1681/ASN.V381458

Gildea, J. J., Seaton, J. E., Victor, K. G., Reyes, C. M., Bigler Wang, D., Pettigrew, A. C., et al. (2014). Exosomal transfer from human renal proximal tubule cells to distal tubule and collecting duct cells. *Clin. Biochem.* 47 (15), 89–94. doi:10.1016/j.clinbiochem.2014.06.018

Goto, Y., Uchio-Yamada, K., Anan, S., Yamamoto, Y., Ogura, A., and Manabe, N. (2005). Transforming growth factor-beta1 mediated up-regulation of lysyl oxidase in the kidneys of hereditary nephrotic mouse with chronic renal fibrosis. *Virchows Archiv Int. J. Pathology* 447 (5), 859–868. doi:10.1007/s00428-005-0001-8

Gudehithlu, K., Hart, P., Joshi, A., Garcia-Gomez, I., Cimbaluk, D., Dunea, G., et al. (2019). Urine exosomal ceruloplasmin: A potential early biomarker of underlying kidney disease. *Clin. Exp. Nephrol.* 23 (8), 1013–1021. doi:10.1007/s10157-019-01734-5

Gudehithlu, K. P., Garcia-Gomez, I., Vernik, J., Brecklin, C., Kraus, M., Cimbaluk, D. J., et al. (2015). In diabetic kidney disease urinary exosomes better represent kidney specific protein alterations than whole urine. *Am. J. Nephrol.* 42 (6), 418–424. doi:10.1159/000443539

Gutierrez, O., Isakova, T., Rhee, E., Shah, A., Holmes, J., Collerone, G., et al. (2005). Fibroblast growth factor-23 mitigates hyperphosphatemia but accentuates calcitriol deficiency in chronic kidney disease. *J. Am. Soc. Nephrol.* 16 (7), 2205–2215. doi:10.1681/ASN.2005010052

Haas, M. (2006). Thin glomerular basement membrane nephropathy: Incidence in 3471 consecutive renal biopsies examined by electron microscopy. *Archives Pathology Laboratory Med.* 130 (5), 699–706. doi:10.1043/1543-2165(2006)130[699:TGBMNI]2.0.CO;2

Harpole, M., Davis, J., and Espina, V. (2016). Current state of the art for enhancing urine biomarker discovery. *Expert Rev. Proteomics* 13 (6), 609–626. doi:10.1080/14789450.2016.1190651

Heijnen, H. F. G., Schiel, A. E., Fijnheer, R., Geuze, H. J., and Sixma, J. J. (1999). Activated platelets release two types of membrane vesicles: Microvesicles by surface shedding and exosomes derived from exocytosis of multivesicular bodies and α-granules. *Blood* 94 (11), 3791–3799. doi:10.1182/blood.v94.11.3791

Henique, C., Bollée, G., Loyer, X., Grahammer, F., Dhaun, N., Camus, M., et al. (2017). Genetic and pharmacological inhibition of microRNA-92a maintains podocyte cell cycle quiescence and limits crescentic glomerulonephritis. *Nat. Commun.* 8 (1), 1829. doi:10.1038/s41467-017-01885-7

Herlitz, L. C., Markowitz, G. S., Farris, A. B., Schwimmer, J. A., Stokes, M. B., Kunis, C., et al. (2010). Development of focal segmental glomerulosclerosis after anabolic steroid abuse. *J. Am. Soc. Nephrol.* 21 (1), 163–172. doi:10.1681/ASN.2009040450

Herman-Edelstein, M., Scherzer, P., Tobar, A., Levi, M., and Gafter, U. (2014). Altered renal lipid metabolism and renal lipid accumulation in human diabetic nephropathy. *J. Lipid Res.* 55 (3), 561–572. doi:10.1194/jlr.P040501

Hessvik, N. P., and Llorente, A. (2017). Current knowledge on exosome biogenesis and release. *Cell. Mol. Life Sci. CMLS* 75 (2), 193–208. doi:10.1007/s00018-017-2595-9

Hohenstein, B., Daniel, C., Hausknecht, B., Boehmer, K., Riess, R., Amann, K. U., et al. (2008). Correlation of enhanced thrombospondin-1 expression, TGF-β signalling and proteinuria in human type-2 diabetic nephropathy. *Nephrol. Dial. Transplant.* 23 (12), 3880–3887. doi:10.1093/ndt/gfn399

Horder, E. G. (1899). Blood dust or blood granules: A new constituent of the blood? *Lancet* 154 (3972), 1015. doi:10.1016/s0140-6736(01)59201-6

Huber, O. (2003). Structure and function of desmosomal proteins and their role in development and disease. *Cell. Mol. Life Sci. CMLS* 60 (9), 1872–1890. doi:10.1007/s00018-003-3050-7

Ichii, O., Otsuka-Kanazawa, S., Horino, T., Kimura, J., Nakamura, T., Matsumoto, M., et al. (2014). Decreased miR-26a expression correlates with the progression of podocyte injury in autoimmune glomerulonephritis. *PloS One* 9 (10), e110383. doi:10.1371/journal.pone.0110383

Ikeda, Y., Imai, Y., Kumagai, H., Nosaka, T., Morikawa, Y., Hisaoka, T., et al. (2004). Vasorin, a transforming growth factor beta-binding protein expressed in vascular smooth muscle cells, modulates the arterial response to injury *in vivo*. *Proc. Natl. Acad. Sci. U. S. A.* 101 (29), 10732–10737. doi:10.1073/pnas.0404117101

Inker, L. A., Astor, B. C., Fox, C. H., Isakova, T., Lash, J. P., Peralta, C. A., et al. (2014). KDOQI US commentary on the 2012 KDIGO clinical practice guideline for the evaluation and management of CKD. *Am. J. Kidney Dis. Official J. Natl. Kidney Found.* 63 (5), 713–735. doi:10.1053/j.ajkd.2014.01.416

Izzedine, H., and Perazella, M. A. (2017). Anticancer drug-induced acute kidney injury. *Kidney Int. Rep.* 2 (4), 504–514. doi:10.1016/j.ekir.2017.02.008

Jha, V., Garcia-Garcia, G., Iseki, K., Li, Z., Naicker, S., Plattner, B., et al. (2013). Chronic kidney disease: Global dimension and perspectives. *Lancet* 382 (9888), 260–272. doi:10.1016/S0140-6736(13)60687-X

Jia, Y., Guan, M., Zheng, Z., Zhang, Q., Tang, C., Xu, W., et al. (2016). miRNAs in urine extracellular vesicles as predictors of early-stage diabetic nephropathy. *J. Diabetes Res.* 2016 (7932765), 7932765. doi:10.1155/2016/7932765

Johnstone, R. M., Adam, M., Hammond, J. R., Orr, L., and Turbide, C. (1987). Vesicle formation during reticulocyte maturation. Association of plasma membrane activities with released vesicles (exosomes). *J. Biol. Chem.* 262 (19), 9412–9420. doi:10.1016/s0021-9258(18)48095-7

Kagami, S., Border, W. A., Miller, D. E., and Noble, N. A. (1994). Angiotensin II stimulates extracellular matrix protein synthesis through induction of transforming growth factor-beta expression in rat glomerular mesangial cells. *J. Clin. Investigation* 93 (6), 2431–2437. doi:10.1172/JCI117251

Kalani, A., Mohan, A., Godbole, M. M., Bhatia, E., Gupta, A., Sharma, R. K., et al. (2013). Wilm's tumor-1 protein levels in urinary exosomes from diabetic patients with or without proteinuria. *PlosOne* 8 (3), e60177. doi:10.1371/journal.pone.0060177

Kang, H. M., Ahn, S. H., Choi, P., Ko, Y., Han, S. H., Chinga, F., et al. (2015). Defective fatty acid oxidation in renal tubular epithelial cells has a key role in kidney fibrosis development. *Nat. Med.* 21 (1), 37–46. doi:10.1038/nm.3762

Kassimatis, T. I., Nomikos, A., Giannopoulou, I., Lymperopoulos, A., Moutzouris, D., Varakis, I., et al. (2010). Transcription factor Sp1 expression is upregulated in human glomerulonephritis: Correlation with pSmad2 3 and p300 expression and renal injury. *Ren. Fail.* 32 (2), 243–253. doi:10.3109/08860220903411164

Kato, M., Yuan, H., Xu, Z., Lanting, L., Li, S., Wang, M., et al. (2006). Role of the akt/FoxO3a pathway in TGF-beta1-mediated mesangial cell dysfunction: A novel mechanism related to diabetic kidney disease. *J. Am. Soc. Nephrol.* 17 (12), 3325–3335. doi:10.1681/ASN.2006070754

Khurana, R., Ranches, G., Schafferer, S., Lukasser, M., Rudnicki, M., Mayer, G., et al. (2017). Identification of urinary exosomal noncoding RNAs as novel biomarkers in chronic kidney disease. *RNA Camb.* 23 (2), 142–152. doi:10.1261/rna.058834.116

Kolb, A., Gallacher, P. J., Campbell, J., O'Neill, M., Smith, J. R., Bell, S., et al. (2021). A national registry study of patient and renal survival in adult nephrotic syndrome. *Kidney Int. Rep.* 6 (2), 449–459. doi:10.1016/j.ekir.2020.10.033

Kopp, J. B., Miller, K. D., Mican, J. A. M., Feuerstein, I. M., Vaughan, E., Baker, C., et al. (1997). Crystalluria and urinary tract abnormalities associated with indinavir. *Ann. Intern. Med.* 127 (2), 119–125. doi:10.7326/0003-4819-127-2-199707150-00004

Kramer, H. J., Nguyen, Q. D., Curhan, G., and Hsu, C. (2003). Renal insufficiency in the absence of albuminuria and retinopathy among adults with type 2 diabetes mellitus. *JAMA J. Am. Med. Assoc.* 289 (24), 3273–3277. doi:10.1001/jama.289.24.3273

Kravets, I., and Mallipattu, S. K. (2020). The role of podocytes and podocyte-associated biomarkers in diagnosis and treatment of diabetic kidney disease. *J. Endocr. Soc.* 4 (4), bvaa029. doi:10.1210/jendso/bvaa029

Kumari, M., Mohan, A., Ecelbarger, C. M., Gupta, A., Prasad, N., and Tiwari, S. (2020). miR-451 loaded exosomes are released by the renal cells in response to injury and associated with reduced kidney function in human. *Front. Physiology* 11, 234. doi:10.3389/fphys.2020.00234

Kuppe, C., Ibrahim, M. M., Kranz, J., Zhang, X. T., Ziegler, S., Perales-Paton, J., et al. (2021). Decoding myofibroblast origins in human kidney fibrosis. *Nat. Lond.* 589 (7841), 281–286. doi:10.1038/s41586-020-2941-1

Kuwahara, S., Hosojima, M., Kaneko, R., Aoki, H., Nakano, D., Sasagawa, T., et al. (2016). Megalin-mediated tubuloglomerular alterations in high-fat diet–induced kidney disease. *J. Am. Soc. Nephrol.* 27 (7), 1996–2008. doi:10.1681/ASN.2015020190

Lai, K. N., Leung, J. C. K., Chan, L. Y. Y., Saleem, M. A., Mathieson, P. W., Tam, K. Y., et al. (2009). Podocyte injury induced by mesangial-derived cytokines in IgA nephropathy. *Nephrol. Dial. Transplant.* 24 (1), 62–72. doi:10.1093/ndt/gfn441

Lange, T., Artelt, N., Kindt, F., Stracke, S., Rettig, R., Lendeckel, U., et al. (2019). MiR-21 is up-regulated in urinary exosomes of chronic kidney disease patients and after glomerular injury. *J. Cell. Mol. Med.* 23 (7), 4839–4843. doi:10.1111/jcmm.14317

Law, R. H. P., Zhang, Q., McGowan, S., Buckle, A. M., Silverman, G. A., Wong, W., et al. (2006). An overview of the serpin superfamily. *Genome Biol.* 7 (5), 216. doi:10.1186/gb-2006-7-5-216

Lawen, A., Ly, J. D., Lane, D. J. R., Zarschler, K., Messina, A., and Pinto, V. D. (2005). Voltage-dependent anion-selective channel 1 (VDAC1)—A mitochondrial protein, rediscovered as a novel enzyme in the plasma membrane. *Int. J. Biochem. cell Biol.* 37 (2), 277–282. doi:10.1016/j.biocel.2004.05.013

LeBleu, V. S., Taduri, G., O'Connell, J., Teng, Y., Cooke, V. G., Woda, C., et al. (2013). Origin and function of myofibroblasts in kidney fibrosis. *Nat. Med.* 19 (8), 1047–1053. doi:10.1038/nm.3218

Lech, M., and Anders, H. J. (2013). The pathogenesis of lupus nephritis. *J. Am. Soc. Nephrol.* 24 (9), 1357–1366. doi:10.1681/ASN.2013010026

Li, R., Chung, A. C., Dong, Y., Yang, W., Zhong, X., and Lan, H. Y. (2013). The microRNA miR-433 promotes renal fibrosis by amplifying the TGF-β/Smad3-Azin1 pathway. *Kidney Int.* 84 (6), 1129–1144. doi:10.1038/ki.2013.272

Li, X., Ponten, A., Aase, K., Karlsson, L., Abramsson, A., Uutela, M., et al. (2000). PDGF-C is a new protease-activated ligand for the PDGF alpha-receptor. *Nat. Cell Biol.* 2 (5), 302–309. doi:10.1038/35010579

Li, Y., Xu, X., Tang, X., Bian, X., Shen, B., Zhao, H., et al. (2018). MicroRNA expression profile of urinary exosomes in Type IV lupus nephritis complicated by cellular crescent. *J. Biol. Res. Thessalon. Greece)* 25 (1), 16–13. doi:10.1186/s40709-018-0088-0

Liu, Z., Huang, X. R., Chen, H. Y., Penninger, J. M., and Lan, H. Y. (2012). Loss of angiotensin-converting enzyme 2 enhances TGF-β/Smad-mediated renal fibrosis and NF-κB-driven renal inflammation in a mouse model of obstructive nephropathy. *Lab Invest.* 92 (5), 650–661. doi:10.1038/labinvest.2012.2

Look, A. T., Ashmun, R. A., Shapiro, L. H., and Peiper, S. C. (1989). Human myeloid plasma membrane glycoprotein CD13 (gp150) is identical to aminopeptidase N. *J. Clin. Investigation* 83 (4), 1299–1307. doi:10.1172/JCI114015

Lopes, T. G., de Souza, M. L., da Silva, V. D., dos Santos, M., Itaquy, T. P., Garbin, H. I., et al. (2019). Markers of renal fibrosis: How do they correlate with podocyte damage in glomerular diseases? *PLoS ONE* 14 (6), e0217585. doi:10.1371/journal.pone.0217585

Lorz, C., Benito-Martin, A., Boucherot, A., Ucero, A. C., Rastaldi, M. P., Henger, A., et al. (2008). The death ligand TRAIL in diabetic nephropathy. *J. Am. Soc. Nephrol.* 19 (5), 904–914. doi:10.1681/ASN.2007050581

Louafi, F., Martinez-Nunez, R. T., and Sanchez-Elsner, T. (2010). Micro-RNA-155 targets SMAD2 and modulates the response of macrophages to transforming growth factor-β. *J. Biol. Chem.* 285 (53), 41328–41336. doi:10.1074/jbc.m110.146852

Lu, J., Kwan, B. C., Lai, K. M., Tam, L. S., Li, E. K., Chow, K. M., et al. (2012). Glomerular and tubulointerstitial miR-638, miR-198 and miR-146a expression in lupus nephritis. *Nephrology (Carlton)* 17 (4), 346–351. doi:10.1111/j.1440-1797.2012.01573.x

Lv, L., Feng, Y., Wen, Y., Wu, W., Ni, H., Li, Z., et al. (2018). Exosomal CCL2 from tubular epithelial cells is critical for albumin-induced tubulointerstitial inflammation. *J. Am. Soc. Nephrol.* 29 (3), 919–935. doi:10.1681/ASN.2017050523

Lv, L. L., Cao, Y. H., Ni, H. F., Xu, M., Liu, D., Liu, H., et al. (2013). MicroRNA-29c in urinary exosome/microvesicle as a biomarker of renal fibrosis. *Am. J. Physiology – Ren. Physiology* 305 (8), 1220–1227. doi:10.1152/ajprenal.00148.2013

Lv, L. L., Cao, Y. H., Pan, M. M., Liu, H., Tang, R. N., Ma, K. L., et al. (2014). CD2AP mRNA in urinary exosome as biomarker of kidney disease. *Clin. Chim. Acta* 428, 26–31. doi:10.1016/j.cca.2013.10.003

Macconi, D., Tomasoni, S., Romagnani, P., Trionfini, P., Sangalli, F., Mazzinghi, B., et al. (2012). MicroRNA-324-3p promotes renal fibrosis and is a target of ACE inhibition *J. Am. Soc. Nephrol.* 23 (9), 1496–1505. doi:10.1681/ASN.2011121144

Marques, F. Z., Campain, A. E., Tomaszewski, M., Zukowska-Szczechowska, E., Yang, Y. H. J., Charchar, F. J., et al. (2011). Gene expression profiling reveals renin mRNA overexpression in human hypertensive kidneys and a role for MicroRNAs. *Hypertension* 58 (6), 1093–1098. doi:10.1161/HYPERTENSIONAHA.111.180729

Martín-Fernández, B., Rubio-Navarro, A., Cortegano, I., Ballesteros, S., Alía, M., Cannata-Ortiz, P., et al. (2016). Aldosterone induces renal fibrosis and inflammatory M1-macrophage subtype via mineralocorticoid receptor in rats. *PloS One* 11 (1), e0145946. doi:10.1371/journal.pone.0145946

McLellan, M., Skelly, D., Dona, M., Squiers, G., Farrugia, G., Gaynor, T., et al. (2020). High-resolution transcriptomic profiling of the heart during chronic stress reveals cellular drivers of cardiac fibrosis and hypertrophy. *Circ. (New York, N.Y.)* 142 (15), 1448–1463. doi:10.1161/CIRCULATIONAHA.119.045115

Merchant, M. L., Rood, I. M., Deegens, J. K. J., and Klein, J. B. (2017). Isolation and characterization of urinary extracellular vesicles: Implications for biomarker discovery. *Nat. Reviews.Nephrology* 13 (12), 731–749. doi:10.1038/nrneph.2017.148

Mise, A. D., Tamma, G., Ranieri, M., Centrone, M., Mekahli, D., Levtchenko, E. N., et al. (2018). Activation of Calcium-Sensing Receptor increases intracellular calcium and decreases cAMP and mTOR in PKD1 deficient cells. *Sci. Rep.* 8 (1), 5704–5714. doi:10.1038/s41598-018-23732-5

Mocroft, A., Kirk, O., Reiss, P., de Wit, S., Sedlacek, D., Beniowski, M., et al. (2010). Estimated glomerular filtration rate, chronic kidney disease and antiretroviral drug use in HIV-positive patients. *AIDS Lond.* 24 (11), 1667–1678. doi:10.1097/QAD.0b013e328339fe53

Moon, P., Lee, J., You, S., Kim, T., Cho, J., Kim, I., et al. (2011). Proteomic analysis of urinary exosomes from patients of early IgA nephropathy and thin basement membrane nephropathy. *Proteomics* 11 (12), 2459–2475. doi:10.1002/pmic.201000443

Mu, J., Pang, Q., Guo, Y., Chen, J., Zeng, W., Huang, Y., et al. (2013). Functional implications of MicroRNA-215 in TGF-β1-induced phenotypic transition of mesangial cells by targeting CTNNBIP1. *PloS One* 8 (3), e58622. doi:10.1371/journal.pone.0058622

Müller-Deile, J., Dannenberg, J., Schroder, P., Lin, M., Miner, J. H., Chen, R., et al. (2017). Podocytes regulate the glomerular basement membrane protein nephronectin by means of miR-378a-3p in glomerular diseases. *Kidney Int.* 92 (4), 836–849. doi:10.1016/j.kint.2017.03.005

Musante, L., Tataruch, D., Gu, D., Liu, X., Forsblom, C., Groop, P., et al. (2015). Proteases and protease inhibitors of urinary extracellular vesicles in diabetic nephropathy. *J. Diabetes Res.* 2015, 289734. doi:10.1155/2015/289734

Nafar, M., Kalantari, S., Samavat, S., Rezaei-Tavirani, M., Rutishuser, D., and Zubarev, R. A. (2014). The novel diagnostic biomarkers for focal segmental glomerulosclerosis. *Int. J. Nephrol.* 2014, 574261. doi:10.1155/2014/574261

Narita, T., Hosoba, M., Kakei, M., and Ito, S. (2006). Increased urinary excretions of immunoglobulin g, ceruloplasmin, and transferrin predict development of microalbuminuria in patients with type 2 diabetes. *Diabetes Care* 29 (1), 142–144. doi:10.2337/diacare.29.1.142

National Kidney Foundation (2002). *K/DOQI clinical practice guidelines. For chronic kidney disease: Evaluation, classification and stratification*. Available at: https://www.kidney.org/sites/default/files/docs/ckd_evaluation_classification_stratification.pdf.

Ong, A. C. M., Devuyst, O., Knebelmann, B., and Walz, G. (2015). Autosomal dominant polycystic kidney disease: The changing face of clinical management. *Lancet* 385 (9981), 1993–2002. doi:10.1016/S0140-6736(15)60907-2

Oshikawa-Hori, S., Yokota-Ikeda, N., Sonoda, H., Sasaki, Y., and Ikeda, M. (2021). Reduced urinary release of AQP1- and AQP2-bearing extracellular vesicles in patients with advanced chronic kidney disease. *Physiol. Rep.* 9 (17), e15005. doi:10.14814/phy2.15005

Östling, P., Leivonen, S. K., Aakula, A., Kohonen, P., Mäkelä, R., Hagman, Z., et al. (2011). Systematic analysis of microRNAs targeting the androgen receptor in prostate cancer cells. *Cancer Res.* 71 (5), 1956–1967. doi:10.1158/0008-5472.CAN-10-2421

Parving, H., Gall, M., Skøtt, P., Jørgensen, H. E., Løkkegaard, H., Jørgensen, F., et al. (1992). Prevalence and causes of albuminuria in non-insulin-dependent diabetic patients. *Kidney Int.* 41 (4), 758–762. doi:10.1038/ki.1992.118

Parving, H., Hommel, E., Mathiesen, E., Skøtt, P., Edsberg, B., Bahnsen, M., et al. (1988). Prevalence of microalbuminuria, arterial hypertension, retinopathy, and neuropathy in patients with insulin dependent diabetes. *Bmj* 296 (6616), 156–160. doi:10.1136/bmj.296.6616.156

Pascual, M., Steiger, G., Sadallah, S., Paccaud, J. P., Carpentier, J. L., James, R., et al. (1994). Identification of membrane-bound CR1 (CD35) in human urine: evidence for its release by glomerular podocytes. *J. Exp. Med.* 179 (3), 889–899. doi:10.1084/jem.179.3.889

Pastor-Soler, N. M., Sutton, T. A., Mang, H. E., Kinlough, C. L., Gendler, S. J., Madsen, C. S., et al. (2015). Muc1 is protective during kidney ischemia-reperfusion injury. *Am. J. Physiology. Ren. Physiology* 308 (12), F1452–F1462. doi:10.1152/ajprenal.00066.2015

Pavkov, M. E., Collins, A. J., Coresh, J., and Nelson, R. G. (2018). "Kidney disease in diabetes," in *Diabetes in America*. 3rd Edn. Editors C. C. Cowie, S. S. Casagrande, A. Menke, et al. (Bethesda, MD: National Institute of Diabetes and Digestive and Kidney Diseases).

Perez-Hernandez, J., Forner, M. J., Pinto, C., Chaves, F. J., Cortes, R., and Redon, J. (2015). Increased urinary exosomal micrornas in patients with systemic lupus erythematosus. *PloS One* 10 (9), e0138618. doi:10.1371/journal.pone.0138618

Perry, H. M., Görldt, N., Sung, S. J., Huang, L., Rudnicka, K. P., Encarnacion, I. M., et al. (2019). Perivascular CD73 + cells attenuate inflammation and interstitial fibrosis in the kidney microenvironment. *Am. J. Physiology. Ren. Physiology* 317 (3), F658–F669. doi:10.1152/ajprenal.00243.2019

Pisitkun, T., Shen, R. F., and Knepper, M. (2004). Identification and proteomic profiling of exosomes in human urine. *Proc. Natl. Acad. Sci. - PNAS* 101 (36), 13368–13373. doi:10.1073/pnas.0403453101

Pomatto, M. A. C., Gai, C., Bussolati, B., and Camussi, G. (2017). Extracellular vesicles in renal pathophysiology. *Front. Mol. Biosci.* 4, 37. doi:10.3389/fmolb.2017.00037

Prajczer, S., Heidenreich, U., Pfaller, W., Kotanko, P., Lhotta, K., and Jennings, P. (2010). Evidence for a role of uromodulin in chronic kidney disease progression. *Nephrol. Dial. Transplant.* 25 (6), 1896–1903. doi:10.1093/ndt/gfp748

Putta, S., Lanting, L., Sun, G., Lawson, G., Kato, M., and Natarajan, R. (2012). Inhibiting MicroRNA-192 ameliorates renal fibrosis in diabetic nephropathy. *J. Am. Soc. Nephrol. JASN* 23 (3), 458–469. doi:10.1681/ASN.2011050485

Qian, Y., Feldman, E., Pennathur, S., Kretzler, M., and Brosius, F. C. (2008). From fibrosis to sclerosis: Mechanisms of glomerulosclerosis in diabetic nephropathy. *Diabetes (New York, N.Y.)* 57 (6), 1439–1445. doi:10.2337/db08-0061

Qin, W., Chung, A. C. K., Huang, X. R., Meng, X., Hui, D. S. C., Yu, C., et al. (2011). TGF-β/Smad3 signaling promotes renal fibrosis by inhibiting miR-29. *J. Am. Soc. Nephrol. JASN* 22 (8), 1462–1474. doi:10.1681/ASN.2010121308

Quesenberry, P. J., Goldberg, L. R., Aliotta, J. M., Dooner, M. S., Pereira, M. G., Wen, S., et al. (2014). Cellular phenotype and extracellular vesicles: Basic and clinical considerations. *Stem Cells Dev.* 23 (13), 1429–1436. doi:10.1089/scd.2013.0594

Radford, M. G., Donadio, J. V., Bergstralh, E. J., and Grande, J. P. (1997). Predicting renal outcome in IgA nephropathy. *J. Am. Soc. Nephrol.* 8 (2), 199–207. doi:10.1681/ASN.V82199

Ramachandran, K., Saikumar, J., Bijol, V., Koyner, J. L., Qian, J., Betensky, R. A., et al. (2013). Human miRNome profiling identifies microRNAs differentially present in the urine after kidney injury. *Clin. Chem. Baltim. Md* 59 (12), 1742–1752. doi:10.1373/clinchem.2013.210245

Ramezani, A., Devaney, J., Cohen, S., Wing, M. R., Scott, R., Knoblach, S., et al. (2015). Circulating and urinary microRNA profile in focal segmental glomerulosclerosis: A pilot study. *Eur. J. Clin. Investigation* 45 (4), 394–404. doi:10.1111/eci.12420

Ranghino, A., Dimuccio, V., Papadimitriou, E., and Bussolati, B. (2015). Extracellular vesicles in the urine: Markers and mediators of tissue damage and regeneration. *Clin. Kidney J.* 8 (1), 23–30. doi:10.1093/ckj/sfu136

Reddy, V. S., Madala, S. K., Trinath, J., and Reddy, G. B. (2018). Extracellular small heat shock proteins: Exosomal biogenesis and function. *Cell Stress & Chaperones* 23 (3), 441–454. doi:10.1007/s12192-017-0856-z

Rodrigues, J. C., Haas, M., and Reich, H. N. (2017). IgA nephropathy. *Clin. J. Am. Soc. Nephrol. CJASN* 12 (4), 677–686. doi:10.2215/CJN.07420716

Rosenberg, A. Z., and Kopp, J. B. (2017). Focal segmental glomerulosclerosis. *Clin. J. Am. Soc. Nephrol.* 12 (3), 502–517. doi:10.2215/CJN.05960616

Rudnicki, M., Perco, P., Neuwirt, H., Noppert, S. J., Leierer, J., Sunzenauer, J., et al. (2012). Increased renal versican expression is associated with progression of chronic kidney disease. *PlosOne* 7 (9), e44891. doi:10.1371/journal.pone.0044891

Rysz, J., Gluba-Brzozka, A., Franczyk, B., Jablonowski, Z., and Cialkowska-Rysz, A. (2017). Novel biomarkers in the diagnosis of chronic kidney disease and the prediction of its outcome. *Int. J. Mol. Sci.* 18 (8), 1702. doi:10.3390/ijms18081702

Sabbisetti, V. S., Waikar, S. S., Antoine, D. J., Smiles, A., Wang, C., Ravisankar, A., et al. (2014). Blood kidney injury molecule-1 is a biomarker of acute and chronic kidney injury and predicts progression to ESRD in type I diabetes. *J. Am. Soc. Nephrol.* 25 (10), 2177–2186. doi:10.1681/ASN.2013070758

Saburi, S., Hester, I., Fischer, E., Pontoglio, M., Eremina, V., Gessler, M., et al. (2008). Loss of Fat4 disrupts PCP signaling and oriented cell division and leads to cystic kidney disease. *Nat. Genet.* 40 (8), 1010–1015. doi:10.1038/ng.179

Saito, A., Pietromonaco, S., Loo, A. K.-., and Farquhar, M. G. (1994). Complete cloning and sequencing of rat gp330/"megalin, " a distinctive member of the low density lipoprotein receptor gene family. *Proc. Natl. Acad. Sci. - PNAS* 91 (21), 9725–9729. doi:10.1073/pnas.91.21.9725

Sakurai, A., Ono, H., Ochi, A., Matsuura, M., Yoshimoto, S., Kishi, S., et al. (2019). Involvement of Elf3 on Smad3 activation-dependent injuries in podocytes and excretion of urinary exosome in diabetic nephropathy. *PLoS ONE* 14 (5), e0216788. doi:10.1371/journal.pone.0216788

Salih, M., Demmers, J. A., Bezstarosti, K., Leonhard, W. N., Losekoot, M., van Kooten, C., et al. (2016). Proteomics of urinary vesicles links plakins and complement to polycystic kidney disease. *J. Am. Soc. Nephrol.* 27 (10), 3079–3092. doi:10.1681/ASN.2015090994

Sallustio, F., Serino, G., Costantino, V., Curci, C., Cox, S. N., De Palma, G., et al. (2013). miR-1915 and miR-1225-5p regulate the expression of CD133, PAX2 and TLR2 in adult renal progenitor cells. *Plos One* 8 (7), e68296. doi:10.1371/journal.pone.0068296

Samavat, S., Kalantari, S., Nafar, M., Rutishauser, D., Rezaei-Tavirani, M., Parvin, M., et al. (2015). Diagnostic urinary proteome profile for immunoglobulin a nephropathy. *Iran. J. Kidney Dis.* 9 (3), 239–248.

Santamaría, R., Díaz-Tocados, J. M., Pendón-Ruiz de Mier, M. V., Robles, A., Salmerón-Rodríguez, M. D., Ruiz, E., et al. (2018). Increased phosphaturia accelerates the decline in renal function: A search for mechanisms. *Sci. Rep.* 8 (1), 13701–13714. doi:10.1038/s41598-018-32065-2

Sato, M., Muragaki, Y., Saika, S., Roberts, A. B., and Ooshima, A. (2003). Targeted disruption of TGF-beta1/Smad3 signaling protects against renal tubulointerstitial fibrosis induced by unilateral ureteral obstruction. *J. Clin. Investigation* 112 (10), 1486–1494. doi:10.1172/JCI19270

Scarpellini, A., Linghong, H., Burhan, I., Schroeder, N., Funck, M., Johnson, T. S., et al. (2014). Syndecan-4 knockout leads to reduced extracellular transglutaminase-2 and

protects against tubulointerstitial fibrosis. *J. Am. Soc. Nephrol.* 25 (5), 1013–1027. doi:10.1681/ASN.2013050563

Schanstra, J. P., Zürbig, P., Alkhalaf, A., Argiles, A., Bakker, S. J. L., Beige, J., et al. (2015). Diagnosis and prediction of CKD progression by assessment of urinary peptides. *J. Am. Soc. Nephrol. JASN* 26 (8), 1999–2010. doi:10.1681/ASN.2014050423

Schiessl, I. M., Grill, A., Fremter, K., Steppan, D., Hellmuth, M., and Castrop, H. (2018). Renal interstitial platelet-derived growth factor receptor- β cells support proximal tubular regeneration. *J. Am. Soc. Nephrol.* 29 (5), 1383–1396. doi:10.1681/ASN.2017101069

Schrauben, S. J., Shou, H., Zhang, X., Anderson, A. H., Bonventre, J. V., Chen, J., et al. (2021). Association of multiple plasma biomarker concentrations with progression of prevalent diabetic kidney disease: Findings from the chronic renal insufficiency cohort (CRIC) study. *J. Am. Soc. Nephrol.* 32 (1), 115–126. doi:10.1681/ASN.2020040487

Shen, Y., Zhao, Y., Wang, L., Zhang, W., Liu, C., and Yin, A. (2018). MicroRNA-194 overexpression protects against hypoxia/reperfusion-induced HK-2 cell injury through direct targeting Rheb. *J. Cell. Biochem.* 120 (5), 8311–8318. doi:10.1002/jcb.28114

Siegel, R. C., Chen, K. H., Greenspan, J. S., and Aguiar, J. M. (1978). Biochemical and immunochemical study of lysyl oxidase in experimental hepatic fibrosis in the rat. *Proc. Natl. Acad. Sci. - PNAS* 75 (6), 2945–2949. doi:10.1073/pnas.75.6.2945

Silberberg, M., Charron, A. J., Bacallao, R., and Wandinger-Ness, A. (2005). Mispolarization of desmosomal proteins and altered intercellular adhesion in autosomal dominant polycystic kidney disease. *Am. J. physiology. Ren. physiology* 288 (6), 1153–1163. doi:10.1152/ajprenal.00008.2005

Sime, P. J., Xing, Z., Graham, F. L., Csaky, K. G., and Gauldie, J. (1997). Adenovector-mediated gene transfer of active transforming growth factor-beta1 induces prolonged severe fibrosis in rat lung. *J. Clin. Investigation* 100 (4), 768–776. doi:10.1172/JCI119590

Skerfving, S., and Bergdahl, I. A. (2007). "Lead," in *Handbook on toxicology of metals*. Editor G. F. Nordberg (Amsterdam, Netherlands: Elsevier), 599–643.

Solé, C., Moliné, T., Vidal, M., Ordi-Ros, J., and Cortés-Hernández, J. (2019). An exosomal urinary miRNA signature for early diagnosis of renal fibrosis in lupus nephritis. *Cells (Basel, Switz.* 8 (8), 773. doi:10.3390/cells8080773

Spahr, C. S., Davis, M. T., Mcginley, M. D., Robinson, J. H., Bures, E. J., Beierle, J., et al. (2001). Towards defining the urinary proteome using liquid chromatography-tandem mass spectrometry. I. Profiling an unfractionated tryptic digest. *Proteomics* 1 (1), 93–107. doi:10.1002/1615-9861(200101)1:1<93::AID-PROT93>3.0.CO;2-3

Spector, J. T., Navas-Acien, A., Fadrowski, J., Guallar, E., Jaar, B., and Weaver, V. M. (2011). Associations of blood lead with estimated glomerular filtration rate using MDRD, CKD-EPI and serum cystatin C-based equations. *Nephrol. Dial. Transplant. - Oxf. Acad.* 26 (9), 2786–2792. doi:10.1093/ndt/gfq773

Stokman, M. F., Bijnsdorp, I. V., Schelfhorst, T., Pham, T. V., Piersma, S. R., Knol, J. C., et al. (2019). Changes in the urinary extracellular vesicle proteome are associated with nephronophthisis-related ciliopathies. *J. Proteomics* 192, 27–36. doi:10.1016/j.jprot.2018.07.008

Street, J. M., Birkhoff, W., Menzies, R. I., Webb, D. J., Bailey, M. A., and Dear, J. W. (2011). Exosomal transmission of functional aquaporin 2 in kidney cortical collecting duct cells. *J. Physiology* 589 (24), 6119–6127. doi:10.1113/jphysiol.2011.220277

Su, J., Li, S. J., Chen, Z. H., Zeng, C. H., Zhou, H., Li, L. S., et al. (2010). Evaluation of podocyte lesion in patients with diabetic nephropathy: Wilms' tumor-1 protein used as a podocyte marker. *Diabetes Res. Clin. Pract.* 87 (2), 167–175. doi:10.1016/j.diabres.2009.10.022

Sui, W., Lin, H., Li, H., Yan, Q., Chen, J., and Dai, Y. (2014). Circulating microRNAs as potential biomarkers for nephrotic syndrome. *Iran. J. Kidney Dis.* 8 (5), 371–376.

Sun, A., Deng, J., Guan, G., Chen, S., Liu, Y., Cheng, J., et al. (2012). Dipeptidyl peptidase-IV is a potential molecular biomarker in diabetic kidney disease. *Diabetes & Vasc. Dis. Res.* 9 (4), 301–308. doi:10.1177/1479164111434318

Suzuki, H., Kiryluk, K., Novak, J., Moldoveanu, Z., Herr, A. B., Renfrow, M. B., et al. (2011). The pathophysiology of IgA nephropathy. *J. Am. Soc. Nephrol. JASN* 22 (10), 1795–1803. doi:10.1681/ASN.2011050464

Szeto, C., Wang, G., Ng, J. K., Kwan, B. C., Mac-Moune Lai, F., Chow, K., et al. (2019). Urinary miRNA profile for the diagnosis of IgA nephropathy. *BMC Nephrol.* 20 (1), 77. doi:10.1186/s12882-019-1267-4

Ta, C. M., Vien, T. N., Ng, L. C. T., and DeCaen, P. G. (2020). Structure and function of polycystin channels in primary cilia. *Cell. Signal.* 72, 109626. doi:10.1016/j.cellsig.2020.109626

Tang, O., Chen, X., Shen, S., Hahn, M., and Pollock, C. A. (2013). MiRNA-200b represses transforming growth factor-β1-induced EMT and fibronectin expression in kidney proximal tubular cells. *Am. J. Physiology Ren. Physiology* 304 (10), 1266–F1273. doi:10.1152/ajprenal.00302.2012

Théry, C., Witwer, K. W., Aikawa, E., Andriantsitohaina, R., Baharvand, H., Bauer, N. N., et al. (2018). Minimal information for studies of extracellular vesicles 2018 (MISEV2018): A position statement of the international society for extracellular vesicles and update of the MISEV2014 guidelines. *J. Extracell. Vesicles* 7 (1), 1535750. doi:10.1080/20013078.2018.1535750

Thrailkill, K. M., Bunn, R. C., Moreau, C. S., Cockrell, G. E., Simpson, P. M., Coleman, H. N., et al. (2007). Matrix metalloproteinase-2 dysregulation in type 1 diabetes. *Diabetes Care* 30 (9), 2321–2326. doi:10.2337/dc07-0162

Tomar, A., George, S., Kansal, P., Wang, Y., and Khurana, S. (2006). Interaction of phospholipase C-gamma1 with villin regulates epithelial cell migration. *J. Biol. Chem.* 281 (42), 31972–31986. doi:10.1074/jbc.M604323200

Tonoli, E., Verduci, I., Gabrielli, M., Prada, I., Forcaia, G., Coveney, C., et al. (2022). Extracellular transglutaminase-2, nude or associated with astrocytic extracellular vesicles, modulates neuronal calcium homeostasis. *Prog. Neurobiol.* 216, 102313. doi:10.1016/j.pneurobio.2022.102313

Tryggvason, K., and Patrakka, J. (2006). Thin basement membrane nephropathy. *J. Am. Soc. Nephrol.* 17 (3), 813–822. doi:10.1681/ASN.2005070737

Turco, A. E., Lam, W., Rule, A. D., Denic, A., Lieske, J. C., Miller, V. M., et al. (2016). Specific renal parenchymal-derived urinary extracellular vesicles identify age-associated structural changes in living donor kidneys. *J. Extracell. Vesicles* 5 (1), 29642. doi:10.3402/jev.v5.29642

Urakawa, I., Yamazaki, Y., Shimada, T., Iijima, K., Hasegawa, H., Okawa, K., et al. (2006). Klotho converts canonical FGF receptor into a specific receptor for FGF23. *Nature* 444 (7120), 770–774. doi:10.1038/nature05315

Vaidya, V., Niewczas, M., Ficociello, L., Johnson, A., Collings, F., Warram, J., et al. (2011). Regression of microalbuminuria in type 1 diabetes is associated with lower levels of urinary tubular injury biomarkers, kidney injury molecule-1, and N-acetyl-β-D-glucosaminidase. *Kidney Int.* 79 (4), 464–470. doi:10.1038/ki.2010.404

Van, J. A. D., Scholey, J. W., and Konvalinka, A. (2017). Insights into diabetic kidney disease using urinary proteomics and bioinformatics. *J. Am. Soc. Nephrol.* 28 (4), 1050–1061. doi:10.1681/ASN.2016091018

Van Niel, G., D'Angelo, G., and Raposo, G. (2018). Shedding light on the cell biology of extracellular vesicles. *Nat. Rev. Mol. Cell Biol.* 19 (4), 213–228. doi:10.1038/nrm.2017.125

van Timmeren, M. M., van den Heuvel, M. C., Bailly, V., Bakker, S., van Goor, H., and Stegeman, C. A. (2007). Tubular kidney injury molecule-1 (KIM-1) in human renal disease. *J. Pathology* 212 (2), 209–217. doi:10.1002/path.2175

Verderio, E. A. M., Furini, G., Burhan, I. W., and Johnson, T. S. (2016). "Transglutaminases: Expression in kidney and relation to kidney fibrosis," in *Transglutaminases: Multiple functional modifiers and targets for new drug discovery* (Springer), 229–263.

Viau, A., El Karoui, K., Laouari, D., Burtin, M., Nguyen, C., Mori, K., et al. (2010). Lipocalin 2 is essential for chronic kidney disease progression in mice and humans. *J. Clin. Investigation* 120 (11), 4065–4076. doi:10.1172/JCI42004

Vlahović, P., and Stefanović, V. (1998). Kidney ectopeptidases. Structure, functions and clinical significance. *Pathologie-Biologie* 46 (10), 779–786.

Wang, H., Chen, F., Tong, J., Li, Y., Cai, J., Wang, Y., et al. (2017). Circulating microRNAs as novel biomarkers for dilated cardiomyopathy. *Cardiol. J.* 24 (1), 65–73. doi:10.5603/CJ.a2016.0097

Wang, X., Gao, X., Liu, Y., Pan, C., Hu, H., Beyer, R. P., et al. (2014). Excessive activation of the alternative complement pathway in autosomal dominant polycystic kidney disease. *J. Intern. Med.* 276 (5), 470–485. doi:10.1111/joim.12214

Weber, J. A., Baxter, D. H., Zhang, S., Huang, D. Y., Huang, K. H., Lee, M. J., et al. (2010). The microRNA spectrum in 12 body fluids. *Clin. Chem. Baltim. Md* 56 (11), 1733–1741. doi:10.1373/clinchem.2010.147405

Webster, A. C., Nagler, E. V., Morton, R. L., and Masson, P. (2017). Chronic kidney disease. *Lancet* 389 (10075), 1238–1252. doi:10.1016/S0140-6736(16)32064-5

Wiggins, R. C., Glatfelter, A., Kshirsagar, B., and Brukman, J. (1986). Procoagulant activity in normal human urine associated with subcellular particles. *Kidney Int.* 29 (2), 591–597. doi:10.1038/ki.1986.39

Wilson, R. C., and Doudna, J. A. (2013). Molecular mechanisms of RNA interference. *Annu. Rev. Biophysics* 42 (1), 217–239. doi:10.1146/annurev-biophys-083012-130404

Wolf, P. (1967). The nature and significance of platelet products in human plasma. *Br. J. Haematol.* 13 (3), 269–288. doi:10.1111/j.1365-2141.1967.tb08741.x

Xie, T., Wang, Y., Deng, N., Huang, G., Taghavifar, F., Geng, Y., et al. (2018). Single-cell deconvolution of fibroblast heterogeneity in mouse pulmonary fibrosis. *Cell Rep.* 22 (13), 3625–3640. doi:10.1016/j.celrep.2018.03.010

Xie, Y., Jia, Y., Xie, C., Hu, F., Xue, M., and Xue, Y. (2017). Urinary exosomal MicroRNA profiling in incipient type 2 diabetic kidney disease. *J. Diabetes Res.* 2017, 6978984. doi:10.1155/2017/6978984

Xu, Z., Li, W., Han, J., Zou, C., Huang, W., Yu, W., et al. (2017). Angiotensin II induces kidney inflammatory injury and fibrosis through binding to myeloid differentiation protein-2 (MD2). *Sci. Rep.* 7 (1), 44911. doi:10.1038/srep44911

Yan, J., Yang, S., Zhang, J., and Zhu, T. (2009). BMP6 reverses TGF-beta1-induced changes in HK-2 cells: Implications for the treatment of renal fibrosis: Implications for the treatment of renal fibrosis. *Acta Pharmacol. Sin.* 30 (7), 994–1000. doi:10.1038/aps.2009.56

Yang, J., and Liu, Y. (2001). Dissection of key events in tubular epithelial to myofibroblast transition and its implications in renal interstitial fibrosis. *Am. J. Pathology* 159 (4), 1465–1475. doi:10.1016/S0002-9440(10)62533-3

Yuan, Q., Tang, B., and Zhang, C. (2022). Signaling pathways of chronic kidney diseases, implications for therapeutics. *Signal Transduct. Target. Ther.* 7 (1), 182. doi:10.1038/s41392-022-01036-5

Zang, J., Maxwell, A. P., Simpson, D. A., and McKay, G. J. (2019). Differential expression of urinary exosomal MicroRNAs miR-21-5p and miR-30b-5p in individuals with diabetic kidney disease. *Sci. Rep.* 9 (1), 10900–10910. doi:10.1038/s41598-019-47504-x

Zepp, J. A., Zacharias, W. J., Frank, D. B., Cavanaugh, C. A., Zhou, S., Morley, M. P., et al. (2017). Distinct mesenchymal lineages and niches promote epithelial self-renewal and myofibrogenesis in the lung. *Cell* 170 (6), 1134–1148. e10. doi:10.1016/j.cell.2017.07.034

Zhang, C., Liang, S., Cheng, S., Li, W., Wang, X., Zheng, C., et al. (2018). Urinary miR-196a predicts disease progression in patients with chronic kidney disease. *J. Transl. Med.* 16 (91), 91. doi:10.1186/s12967-018-1470-2

Zhang, H., Freitas, D., Kim, H. S., Fabijanic, K., Li, Z., Chen, H., et al. (2018). Identification of distinct nanoparticles and subsets of extracellular vesicles by asymmetric flow field-flow fractionation. *Nat. Cell Biol.* 20 (3), 332–343. doi:10.1038/s41556-018-0040-4

Zhang, H., Unal, H., Desnoyer, R., Han, G. W., Patel, N., Katritch, V., et al. (2015). Structural basis for ligand recognition and functional selectivity at angiotensin receptor. *J. Biol. Chem.* 290 (49), 29127–29139. doi:10.1074/jbc.M115.689000

Zhang L, L., Xue, S., Wu, M., and Dong, D. (2022). Performance of urinary liver-type fatty acid-binding protein in diabetic nephropathy: A meta-analysis. *Front. Med.* 9, 914587. doi:10.3389/fmed.2022.914587

Zhang, M., Sui, W., Xing, Y., Cheng, J., Cheng, C., Xue, F., et al. (2021). Angiotensin IV attenuates diabetic cardiomyopathy via suppressing FoxO1-induced excessive autophagy, apoptosis and fibrosis. *Theranostics* 11 (18), 8624–8639. doi:10.7150/thno.48561

Zhang, Q., Higginbotham, J. N., Jeppesen, D. K., Yang, Y., Li, W., McKinley, E. T., et al. (2019). Transfer of functional cargo in exomeres. *Cell Rep.* 27 (3), 940–954. e6. doi:10.1016/j.celrep.2019.01.009

Zhang, W., Yuan, M., Hong, L., Zhou, Q., Chen, W., Yang, S., et al. (2016a). Clinical outcomes of lupus nephritis patients with different proportions of crescents. *Lupus* 25 (14), 1532–1541. doi:10.1177/0961203316642312

Zhang, W., Zhang, C., Chen, H., Li, L., Tu, Y., Liu, C., et al. (2014). Evaluation of MicroRNAs miR-196a, miR-30a-5P, and miR-490 as biomarkers of disease activity among patients with FSGS. *Clin. J. Am. Soc. Nephrol.* 9 (9), 1545–1552. doi:10.2215/CJN.11561113

Zhang, W., Zhou, X., Zhang, H., Yao, Q., Liu, Y., and Dong, Z. (2016b). Extracellular vesicles in diagnosis and therapy of kidney diseases. *Am. J. Physiology-Renal Physiology* 311 (5), F844–F851. doi:10.1152/ajprenal.00429.2016

Zhang, X., Li, X., Zhou, W., Liu, X., Huang, J., Zhang, Y., et al. (2020). Serum lysyl oxidase is a potential diagnostic biomarker for kidney fibrosis. *Am. J. Nephrol.* 51 (11), 907–918. doi:10.1159/000509381

Zhang, X., Zhou, W., Niu, Y., Zhu, S., Zhang, Y., Li, X., et al. (2022). Lysyl oxidase promotes renal fibrosis via accelerating collagen cross-link driving by β-arrestin/ERK/STAT3 pathway. *FASEB J.* 36 (8), e22427. doi:10.1096/fj.202200573R

Zhang, Z., Luo, X., Ding, S., Chen, J., Chen, T., Chen, X., et al. (2012). MicroRNA-451 regulates p38 MAPK signaling by targeting of Ywhaz and suppresses the mesangial hypertrophy in early diabetic nephropathy. *FEBS Lett.* 586 (1), 20–26. doi:10.1016/j.febslet.2011.07.042

Zhong, J., Yang, H. C., and Fogo, A. B. (2017). A perspective on chronic kidney disease progression. *Am. J. Physiology. Ren. Physiology* 312 (3), F375–F384. doi:10.1152/ajprenal.00266.2016

Zhou, H., Cheruvanky, A., Hu, X., Matsumoto, T., Hiramatsu, N., Cho, M. E., et al. (2008). Urinary exosomal transcription factors, a new class of biomarkers for renal disease. *Kidney Int.* 74 (5), 613–621. doi:10.1038/ki.2008.206

Zhou, H., Yuen, P. S. T., Pisitkun, T., Gonzales, P. A., Yasuda, H., Dear, J. W., et al. (2006). Collection, storage, preservation, and normalization of human urinary exosomes for biomarker discovery. *Kidney Int.* 69 (8), 1471–1476. doi:10.1038/sj.ki.5000273

Zubiri, I., Posada-Ayala, M., Benito-Martin, A., Maroto, A. S., Martin-Lorenzo, M., Cannata-Ortiz, P., et al. (2015). Kidney tissue proteomics reveals regucalcin downregulation in response to diabetic nephropathy with reflection in urinary exosomes. *Transl. Res. J. Laboratory Clin. Med.* 166 (5), 474–484. e4. doi:10.1016/j.trsl.2015.05.007

Zubiri, I., Posada-Ayala, M., Sanz-Maroto, A., Calvo, E., Martin-Lorenzo, M., Gonzales-Calero, L., et al. (2014). Diabetic nephropathy induces changes in the proteome of human urinary exosomes as revealed by label-free comparative analysis. *J. proteomics* 96, 92–102. doi:10.1016/j.jprot.2013.10.037

frontiers | Frontiers in Pharmacology

TYPE Original Research
PUBLISHED 03 March 2023
DOI 10.3389/fphar.2023.1042093

Check for updates

OPEN ACCESS

EDITED BY
Yanping Liu,
Qilu Hospital, Shandong University, China

REVIEWED BY
Panpan Hao,
Shandong University, China
Honglei Guo,
Nanjing Medical University, China

*CORRESPONDENCE
Yuanming Ba,
bayuanming@126.com

†These authors have contributed equally to this work

SPECIALTY SECTION
This article was submitted to Experimental Pharmacology and Drug Discovery, a section of the journal Frontiers in Pharmacology

RECEIVED 12 September 2022
ACCEPTED 14 February 2023
PUBLISHED 03 March 2023

CITATION
Wang L, Wang X, Li G, Zhou S, Wang R, Long Q, Wang M, Li L, Huang H and Ba Y (2023), Emodin ameliorates renal injury and fibrosis *via* regulating the miR-490-3p/HMGA2 axis.
Front. Pharmacol. 14:1042093.
doi: 10.3389/fphar.2023.1042093

COPYRIGHT
© 2023 Wang, Wang, Li, Zhou, Wang, Long, Wang, Li, Huang and Ba. This is an open-access article distributed under the terms of the Creative Commons Attribution License (CC BY). The use, distribution or reproduction in other forums is permitted, provided the original author(s) and the copyright owner(s) are credited and that the original publication in this journal is cited, in accordance with accepted academic practice. No use, distribution or reproduction is permitted which does not comply with these terms.

Emodin ameliorates renal injury and fibrosis *via* regulating the miR-490-3p/HMGA2 axis

Liulin Wang[1,2,3†], Xuerui Wang[4,5,6†], Gang Li[1,2,3], Shanshan Zhou[1,2,3], Rui Wang[1,2,3], Qi Long[1,2,3], Min Wang[1,2,3], Liang Li[1,2,3], Hai Huang[1,2,3] and Yuanming Ba[1,2,3*]

[1]Hubei Provincial Hospital of Tranditional Chinese Medicine, Wuhan, China, [2]Affiliated Hospital of Hubei University of Traditional Chinese Medicine, Wuhan, China, [3]Hubei Provincial Academy of Traditional Chinese Medicine, Wuhan, China, [4]Beijing Hospital of Traditional Chinese Medicine, Capital Medical University, Beijing, China, [5]Beijing Key Laboratory of Basic Research With Traditional Chinese Medicine on Infectious Diseases, Beijing, China, [6]Beijing Institute of Chinese Medicine, Beijing, China

Renal fibrosis is a major pathological feature of chronic kidney disease (CKD). While emodin is reported to elicit anti-fibrotic effects on renal injury, little is known about its effects on microRNA (miRNA)-modulated mechanisms in renal fibrosis. In this study, we established a unilateral ureteral obstruction (UUO) model and a transforming growth factor (TGF)-β1-induced normal rat renal tubular epithelial cell line (NRK-52E) model to investigate the protective effects of emodin on renal fibrosis and its miRNA/target gene mechanisms. Dual-luciferase assay was performed to confirm the direct binding of miRNA and target genes in HEK293 cells. Results showed that oral administration of emodin significantly ameliorated the loss of body weight and the increase in physicochemical parameters, including serum uric acid, creatinine, and urea nitrogen in UUO mice. Inflammatory cytokines, including tumor necrosis factor-α, monocyte chemoattractant protein-1, and interleukin (IL)-1β, but not IL-6, were down-regulated by emodin administration. Emodin decreased the expression levels of TGF-β1 and fibrotic-related proteins, including alpha-smooth muscle actin, Collagen IV, and Fibronectin, and increased the expression of E-cadherin. Furthermore, miR-490-3p was decreased in UUO mice and negatively correlated with increased expression of high migration protein A2 (HMGA2). We further confirmed HMGA2 was the target of miR-490-3p. Transfection of miR-490-3p mimics decreased, while transfection of miR-490-3p inhibitors increased fibrotic-related proteins and HMGA2 expression levels in TGF-β1-induced NRK-52E cells. Furthermore, transfection of miR-490-3p mimics enhanced the anti-fibrotic effects of emodin, while transfection of miR-490-3p inhibitors abolished the protective effects of emodin. Thus, as a novel target of emodin that prevents renal fibrosis in the HMGA2-dependent signaling pathway, miR-490-3p has potential implications in CKD pathology.

KEYWORDS

emodin, renal fibrosis, microRNA, inflammatory factor, HMGA2

1 Introduction

Chronic kidney disease (CKD) involves sustained damage of the renal parenchyma and chronic deterioration of renal function (Akchurin, 2019). The global burden of CKD is a major public health problem, especially in high-income countries (Gaitonde et al., 2017), with approximately 10% of adults worldwide affected by some form of CKD, resulting in

12 million deaths each year (Xie et al., 2018; Collaboration, 2020). Although there are many known causes of CKD, including diabetes mellitus, glomerulonephritis, and cystic kidney disease, the etiology of CKD remains incompletely understood (Kalantar-Zadeh et al., 2021). At present, CKD treatment primarily involves slowing disease progression and preventing complications by managing modifiable risk factors, such as diabetes and blood pressure, and initiating nephroprotective drug regimens in the early stages of disease (Curtis and Komenda, 2020). Thus, the discovery of novel therapeutic agents that can prevent or delay the progression of disease will contribute to CKD treatment.

Increasing evidence suggests that renal fibrosis is a common final stage of CKD (Klinkhammer et al., 2017). Similar to wound healing, renal fibrosis is a dynamic process with early beneficial effects on injury, but can lead to persistent pathological fibrosis, glomerulosclerosis, tubular atrophy and dilatation, and tubulointerstitial fibrosis (Boor et al., 2010; Djudjaj and Boor, 2019). Over the past 2 decades, microRNAs (miRNAs) have been implicated in fibrosis of various organs, and their role in renal fibrosis has attracted widespread attention, with new therapeutic strategies targeting miRNAs showing considerable promise (Van der Hauwaert et al., 2015; Fan et al., 2020). Transforming growth factor (TGF)-β is a key driver of renal fibrosis and is involved in the dynamic pathophysiological processes leading to CKD and end-stage renal disease (ESRD) (Ma and Meng, 2019). Recent evidence indicates that multiple miRNAs are involved in renal fibrosis through the TGF-β pathway (Zhong et al., 2013; Sun et al., 2018; Sun et al., 2021). For example, MiR-490-3p is known to play a key regulatory role in silica-induced pulmonary fibrosis (Cheng et al., 2021). Studies have also found that miR-490 is decreased in unilateral ureteral obstruction (UUO) model mice (Chung et al., 2010; Qin et al., 2011), and elevated in the urine of active segmental glomerulonephritis patients (Zhang et al., 2014). However, while miR-490 appears to play a crucial role in the pathogenesis of CKD, little is known regarding its functional role.

Emodin is a naturally occurring anthraquinone derivative and active ingredient of rhubarb (Liu et al., 2016), with diverse biological and pharmacological properties, including anticancer, anti-inflammatory, antioxidant, antibacterial, antiviral, anti-diabetic, immunosuppressive, and renoprotective activities (Dong et al., 2016). Emodin is reported to suppress renal fibrosis *via* multiple mechanisms (Ma et al., 2018; Yang et al., 2020; Liu et al., 2021), and is involved in the regulation of miRNAs in several diseases (Xiang et al., 2017; Cao et al., 2019; Xie et al., 2019). We previously reported that a stewed rhubarb decoction mitigated chronic renal failure progression in mice (Wang et al., 2022). However, further experimental research is needed to explore the potential fibrotic effects of emodin on CKD. Here, we hypothesized that miR-490-3p may be involved in the pathological process of renal fibrosis in CKD and that emodin may exert anti-fibrotic effects on CKD *via* regulation of miR-490-3p.

2 Materials and methods

2.1 Animals

Male C57BL/6 mice (age 8–10 weeks, weight 20–24 g) were purchased from Beijing Huafukang Biotechnology Co., Ltd. (Beijing, China). The mice were maintained in an environmentally controlled rearing room (temperature: 22°C ± 2°C, humidity: 50% ± 5%, 12-h light/dark cycle) for 1 week of adaptive feeding, with distilled water and sterilized food freely available. The experimental protocols used in this study were approved by the Ethics Committee for Animal Experimentation of the Hubei Provincial Hospital of Traditional Chinese Medicine (NO. 2019008) and were conducted according to the Guidelines for Animal Experimentation of the Hubei Provincial Hospital of Traditional Chinese Medicine.

2.2 UUO model

The UUO mouse model was established as described previously (Zhou et al., 2020). Briefly, mice were anesthetized with pentobarbital sodium (40 mg/kg body weight) by an intraperitoneal injection. The left ureter was isolated through a median incision and ligated at two points with 5–0 silk. Mice in the sham-operated control group received the same operation, except the ureter was not ligated or cut.

2.3 Treatment protocols

Emodin (Shanghai Yuanye Bio-Technology Co., Ltd. China) was dissolved in pyrogen-free saline and sodium carboxymethyl cellulose (Beijing ITA Biotechnology Co., Ltd., China). Daily oral emodin treatment was started 2 h after UUO surgery for 14 continuous days, with 10 mg/kg, 20 mg/kg, and 40 mg/kg considered as low (EM-L), medium (EM-M), and high (EM-H) dosages. Losartan (LST, Merck Sharp and Dohme., Ltd., United States) was dissolved in pyrogen-free saline as a positive control. Daily oral LST treatment (10 mg/kg) was started 2 h after UUO surgery for 14 continuous days. All sham and UUO mice were treated with the same volume of saline and sodium carboxymethyl cellulose as the vehicle for treatment.

2.4 Cell culture and treatment

The normal rat renal tubular epithelial cell line NRK-52E was purchased from American Type Culture Collection (ATCC, Manassas, United States), and routinely cultured in Dulbecco's modified Eagle's medium (DMEM, Wisent, Nanjing, China) containing 10% fetal bovine serum (Gibco, Gaithersburg, MD, United States), 100 U/ml penicillin (Gibco, Carlsbad, CA, United States), and 100 μg/mL streptomycin (Gibco, Carlsbad, CA, United States) at 37°C with 5% CO_2. In the first experiment, NRK-52E cells were pretreated with serum-free medium for 24 h, then exposed to 40 μM or 80 μM emodin (Shanghai Yuanye Bio-Technology Co., Ltd., China) for 24 h. In the second experiment, NRK-52E cells were pretreated with serum-free medium for 24 h, then exposed to 10 ng/mL TGF-β1 (R&D Systems, MN, United States) with or without 40 μM or 80 μM emodin for 24 h. In the third experiment, HEK293 cells were transfected with miR-490-3p mimics, miR-490-3p inhibitors, and negative controls (NCs), then treated with or without 10 ng/mL TGF-β1 for 24 h. In the fouth

experiment, NRK-52E cells transfected with miR-490-3p mimics, miR-490-3p inhibitors, and NCs were treated with or without 80 μM emodin for 24 h, then exposed to 10 ng/mL TGF-β1 for 24 h. All control groups were treated with the same volume of vehicle.

2.5 Transfection of miRNA mimics and inhibitors

The miR-490-3p mimics (5'-CAACCUGGAGGACUCCAUGCUG-3'), inhibitors (5'-AUUCGUCCUCCUGACCAUGGUC-3'), and NCs were obtained from Biomics Biotech (Nantong, China). The NRK-52E cells were transfected with 50 nM miR-490-3p mimics or inhibitors, and corresponding NCs at the same concentration, using Liposome 2000 reagent (Invitrogen, United States) according to the manufacturer's instructions. Cells were collected 24 h after transfection for further experimental analysis.

2.6 Luciferase reporter assay

HEK293 cells were co-transfected with NCs or miR-490-3p mimics (50 nM), CMV-Renilla, HMGA2 promoter-luciferase using Lipofectamine 2000 reagent (Invitrogen, United States) following the manufacturer's protocols. The plasmids were constructed and provided by Hunan Fenghui Biotechnology Co., Ltd. (Cat. BR082). Luciferase activities were measured 48 h after transfection using dual-luciferase assay kits according to the manufacturer's protocols (Promega, United States).

2.7 Cell counting Kit-8 (CCK-8) assay

The cytotoxicity of emodin was determined by CCK-8 assay. Cells were seeded into 96-well plates. According to the instructions of the CCK-8 kit (Beyotime, Shanghai, China), each well was supplied with 10 μL of CCK-8 after treatment, then incubated at 37°C for 4 h. Absorbance was recorded at 450 nm, and experiments were performed in parallel and in triplicate.

2.8 Physiological and biochemical parameters

Body weights were recorded on day 14 after UUO surgery. Plasma creatinine, urea, and uric acid levels were detected using a creatinine colorimetric kit, urea colorimetric kit, and uric acid colorimetric kit (Bohu Biotechnology Co., Ltd. Shanghai, China), respectively, according to the manufacturer's instructions.

2.9 Histological examination

Renal tissues were fixed in 4% formaldehyde, dehydrated, embedded, and sectioned at 5 μm thickness. Renal sections were stained with hematoxylin and eosin (H&E) or Masson's trichrome staining (Solarbio Life Sciences, Beijing, China) according to the manufacturer's instructions. Sections were observed and scored in a blinded manner. Tubular injury scores based on morphological damage (epithelial necrosis, tubular necrotic debris, and tubular dilatation) were quantified in three or four sections and 10–12 regions per kidney, with a score range of 0–4 (0: 0%; 1: <25%; 2: 26%–50%; 3: 51%–75%; 4: ≥76% of renal tubular injury) (Liu N. et al., 2015; Ren et al., 2021). All positive signals from the histological images (at least three areas per sample) were quantified using ImageJ v1.8.0 software (National Institutes of Health, Bethesda, MD, United States).

2.10 Enzyme-linked immunosorbent assay (ELISA)

Mouse blood was collected from the abdominal aorta 14 days after UUO surgery and centrifuged at 3,000 r/min for 15 min. Serum was collected and stored in a −80°C refrigerator for testing. The levels of interleukin (IL)-1β, tumor necrosis factor-α (TNF-α), IL-6, and monocyte chemoattractant protein-1 (MCP-1) were detected using ELISA kits (ABclonal Biotechnology Co., Ltd. China) according to the manufacturer's protocols.

2.11 Western blot analysis

Total proteins were isolated from kidney tissues and cells using RIPA lysis and extraction buffer (Biyuntian, Shanghai, China). Protein content was determined using BCA protein assay reagent (Thermo, Rockford, IL, United States). The proteins were separated by sodium dodecyl sulfate polyacrylamide gel electrophoresis (SDS-PAGE) and transferred to polyvinylidene fluoride (PVDF) membranes. The membranes were blocked in 5% skim milk in phosphate-buffered saline-Tween at room temperature for 1 h and probed with specific antibodies overnight at 4°C. Primary antibodies included alpha-smooth muscle actin (α-SMA) (1:1,000, Abcam, United Kingdom), Collagen IV (1:1,000, Abcam, United Kingdom), Fibronectin (1:1,000, Abcam, United Kingdom), E-cadherin (1:1,000, Abcam, UK), TGF-β1 (1:1,000, Abcam, United Kingdom), HMGA2 (1:1,000, Invitrogen, United States), and β-actin (1:1,000, Boster, China). Horseradish peroxidase-conjugated secondary antibodies (Sigma, United States) were used for detection of specific proteins for an additional 60 min β-actin was used as the loading control. After a final wash with tris-buffer physiological saline (TBST), immunoreactive bands were detected using an Odyssey Imaging Analyzer (LAS-4000; Toyobo Engineering, Osaka, Japan). Signal intensity was measured using ImageJ and normalized to β-actin signal intensity.

2.12 RNA extraction and real-time polymerase chain reaction (Real-time PCR)

Total RNA from mouse renal tissues, HEK293 cells, and NRK-52E cells was extracted using Trizol Reagent (Invitrogen) according to the manufacturer's instructions. For miRNA, total RNA was reverse transcribed into cDNA using a microRNA First-Strand cDNA Synthesis Kit (Sangong Biotech, Shanghai, China). For mRNA, cDNA was obtained using the GoScript Reverse

TABLE 1 The sequences of the primers.

Name	Sequences
miR-490-3p	Forward: 5'-AACACGTGCAACCTGGAGGAC-3'
	Reverse: 5'-ATCCAGTGCAGGGTCCGAGG-3'
U6	Forward: 5′-GCTTCGGCAGCACATATACTAAAAT-3′
	Reverse: 5′-GCTTCGGCAGCACATATACTAAAAT-3′
mus-HMGA2	Forward: 5'-CCTAAGAGACCCAGAGGAAGA-3'
	Reverse: 5'- CGACTTGTTGTGGCCATTTC-3'
homo-HMGA2	Forward: 5'- GTCCCTCTAAAGCAGCTCAAA-3'
	Reverse: 5'- TGAGCAGGCTTCTTCTGAAC-3'
rattus-HMGA2	Forward: 5'- CTGGACGTCCGGTGTTGGT-3'
	Reverse: 5'-AACACCTTTCGGGAGACGGG-3'
mus-MCP-1	Forward: 5'-TTAAAAACCTGGATCGGAACCAA-3'
	Reverse: 5'-GCATTAGCTTCAGATTTACGGGT-3'
mus-TNFα	Forward: 5'-ACCCTCACACTCAGATCATCTTC-3'
	Reverse: 5'-TGGTGGTTTGCTACGACGT-3'
mus-IL-6	Forward: 5'-ACAAAGCCAGAGTCCTTCAGAGA-3'
	Reverse: 5'-CTGTTAGGAGAGCATTGGAAATTG-3'
mus-IL-1β	Forward: 5'-TGGCAACTGTTCCTG-3'
	Reverse: 5'-GGAAGCAGCCCTTCATCTTT -3'
mus-GAPDH	Forward: 5'- TGTGTCCGTCGTGGATCTGA-3'
	Reverse: 5'- CCTGCTTCACCACCTTCTTGAT-3'
homo-GAPDH	Forward: 5'- CTGCCAACGTGTCAGTGGTG-3'
	Reverse: 5'- GTCGCTGTTGAAGTCAGAGGAG-3'
rattus-GAPDH	Forward:5'-ACAGTCCATGCCATCACTGCC-3'
	Reverse:5'-GCCTGCTTCACCACCTTCTTG-3'

Transcription System Kit (Promega, Madison, WI, United States). GAPDH and small nuclear U6 were used as endogenous controls for mRNA and miRNA levels respectively. Gene expression levels were analyzed by Real-time PCR performed using 2 × SYBR master mix (Takara, Otsu, Shiga, Japan) and a BioRad iCycler iQ5 (BioRad, Hercules, CA, United States). GAPDH and U6 were used as the endogenous controls for measurement of mRNA expression level and miRNA expression analysis, relative mRNA expressions were compared with normalized Sham group. All samples were run in duplicate. Primer sequences are listed in Table 1.

2.13 Statistical analysis

All experimental data were analyzed using SPSS v20.0 and expressed as mean ± standard deviation (x ± s). One-way analysis of variance (ANOVA) was used for comparisons between multiple groups, and $p < 0.05$ was considered statistically significant. All data in the manuscript were analyzed by an investigator blind to the experimental groups.

3 Results

3.1 Emodin ameliorates the physiological, biochemical and pathological damage in UUO mice

As shown in Figure 1, after 14 days of treatment, significant differences in body weight and creatinine, urea nitrogen, and uric acid levels were observed between the UUO and Sham groups. Data showed that body weight in the UUO group was significantly lower compared to the Sham group, while body weight in the EM-H group was significantly higher compared to the UUO group (Figure 1A). In addition, EM-L, EM-M, and EM-H treatment reduced creatinine, urea nitrogen, and uric acid levels to varying degrees in the UUO mice (Figures 1B–D), with emodin at 40 mg/kg showing the strongest modulatory effect.

We used H&E and Masson's trichrome staining to evaluate renal damage and fibrosis. Glomeruli and tubules in the Sham group were structurally normal, with closely aligned tubules. However, kidneys in the UUO mice exhibited severe structural disorder, inflammatory cell infiltration, tubular atrophy, and necrosis (Figures 1E,F). Based on Masson's trichrome staining, banded interstitial fibrosis and collagen fiber hyperplasia were observed in the UUO mice (Figures 1G,H). In contrast, treatment with emodin and LST alleviated these pathological changes in the UUO mice (Figures 1E–H).

3.2 Emodin reduces inflammatory cytokines release in UUO mice

To further investigate the effects of emodin, we used Real-time PCR and ELISA to detect the inflammatory factors TNF-α, MCP-1, IL-6, and IL-1β in UUO mice. Compared with the Sham group, inflammatory factors in the UUO group increased significantly, after emodin intervention, TNF-α, MCP-1 and IL-1β decreased significantly in the UUO mice, while IL-6 showed a non-significant decrease (Figures 2A–F). These data indicated that emodin can reduce inflammation in UUO mice.

3.3 Emodin regulates fibrotic related protein expressions in UUO mice

We used western blot analysis to fibrotic related protein expressions. The protein expression levels of Fbronectin, α-SMA, Collagen IV, and TGF-β1 increased, while that of E-cadherin decreased significantly in the UUO mice. In contrast, emodin decreased Fbronectin, α-SMA, Collagen IV, and TGF-β1 expression and increased E-cadherin expression (Figures 3A,B), suggesting that emodin can reduce fibrosis in UUO mice.

10.3389/fphar.2023.1042093

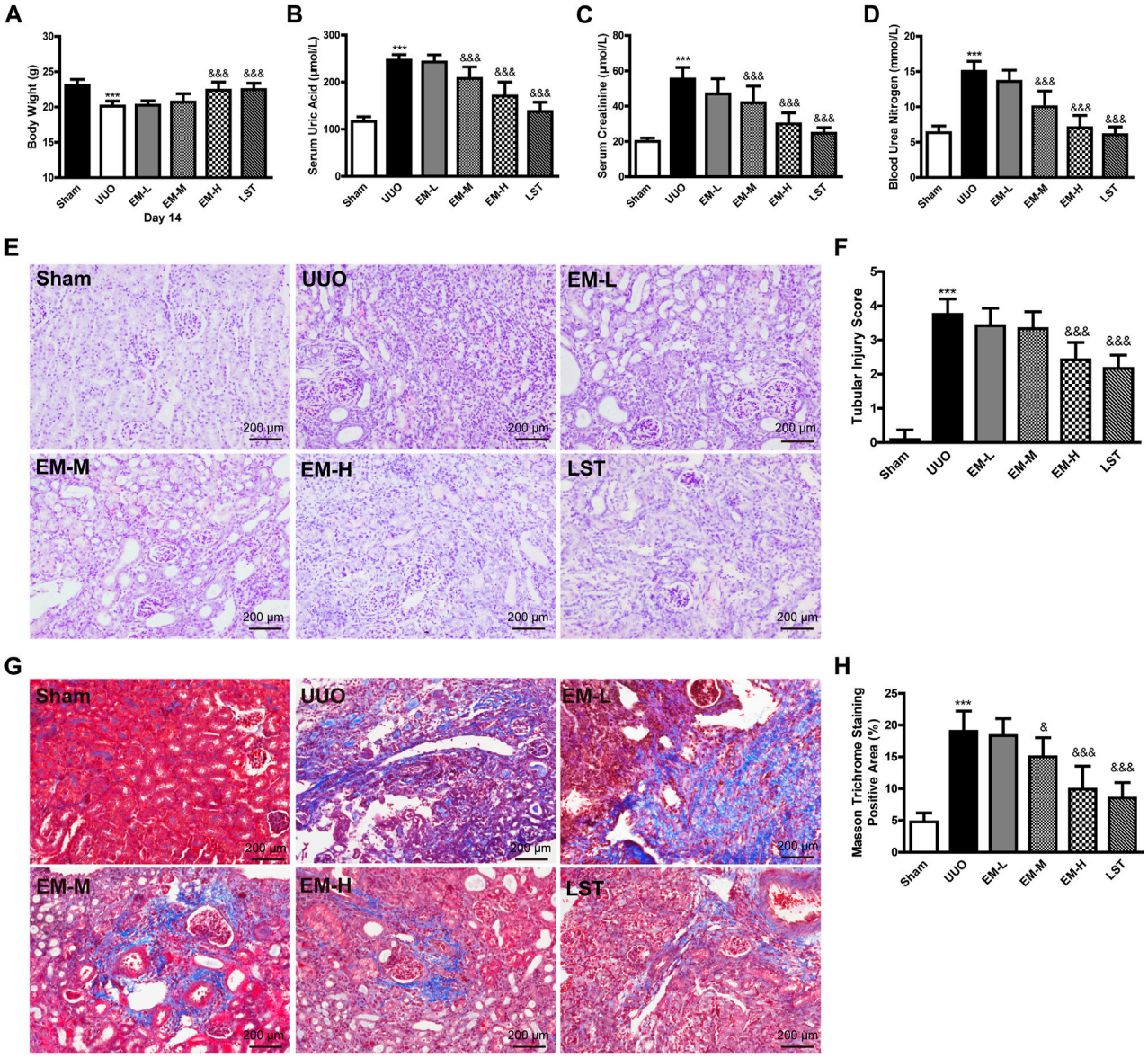


FIGURE 1
Emodin ameliorates the physiological, biochemical and pathological damage in UUO mice. Mice were randomly divided into Sham, UUO, EM-L, EM-M, EM-H, and LST groups. Mice were administrated with dosages of 10 mg/kg, 20 mg/kg, 40 mg/kg emodin, or 10 mg/kg Losartan started 2 h after UUO surgery, daily, orally, for 14 continuous days. **(A)** Body weight, **(B)** levels of uric acid, **(C)** levels of creatinine, and **(D)** levels of urea nitrogen were detected at day 14. Representative pictures of renal **(E)** H&E and **(G)** masson staining. Scale bar = 200 μm. **(F)** Tubule injury index score and **(H)** masson trichromatic positive area were calculated at day 14. Data were shown as mean ± SD (n = 10 per group). *compared with Sham, $^{\delta}$compared with UUO, *$p < 0.05$, **$p < 0.01$,***$p < 0.001$ of each symbol, respectively. $^{\delta}p < 0.05$, $^{\delta\delta}p < 0.01$, $^{\delta\delta\delta}p < 0.001$ of each symbol, respectively. UUO, unilateral ureteral obstruction; EM-L, emodin low dosage; EM-M, the emodin medium dosage, EM-H, emodin high dosage; LST, Losartan.

3.4 Decreased miR-490-3p expression and increased HMGA2 expression are negatively correlated in UUO mice

We compared the endogenous expression levels of miR-490-3p and HMGA2 in the kidney tissues of male C57BL/6 mice in the Sham and UUO groups by Real-time PCR. As shown in Figure 4A, miR-490-3p expression was significantly lower in the kidneys of the UUO group than the matched Sham group. However, HMGA2 mRNA expression was increased (Figure 4B), and miR-490-3p expression was negatively correlated with HMGA2 expression (Figure 4C), further suggesting that miR-490-3p and HMG2A may be associated with pathological injury in UUO mice.

3.5 Emodin reversed the fibrosis in TGF-β1-induced NRK-52E cells

To investigate the effects of emodin on NRK-52E cell fibrosis, we first investigated the effects of emodin on NRK-52E cell viability

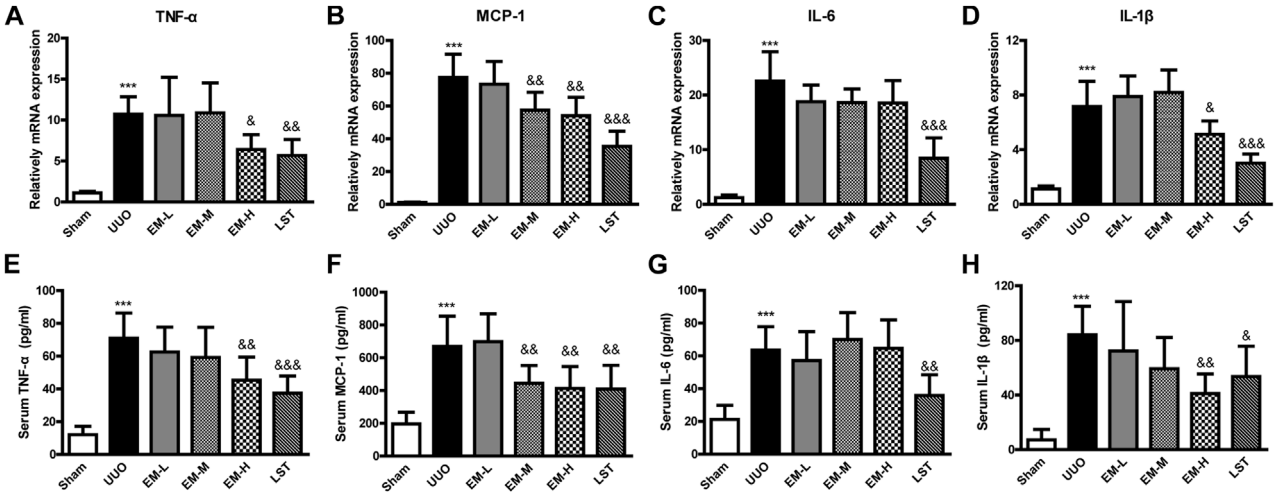


FIGURE 2
Emodin reduces inflammatory cytokines release in UUO mice. Mice were randomly divided into Sham, UUO, EM-L, EM-M, EM-H and LST groups. Mice were administrated with dosages of 10 mg/kg, 20 mg/kg, 40 mg/kg emodin, or 10 mg/kg Losartan started 2 h after UUO surgery, daily, orally, for 14 continuous days. Gene levels of **(A)** TNF-α, **(B)** MCP-1, **(C)** IL-6, and **(D)** IL-1β in renal tissues were determined by Real-time PCR. Serum levels of **(E)** TNF-α, **(F)** MCP-1, **(G)** IL-6, and **(H)** IL-1β were determined by ELISA. Data were shown as mean ± SD (n = 10 per group). *compared with Sham, $^{\&}$compared with UUO, $^{*}p < 0.05$, $^{**}p < 0.01$,$^{***}p < 0.001$ of each symbol, respectively. $^{\&}p < 0.05$, $^{\&\&}p < 0.01$, $^{\&\&\&}p < 0.001$ of each symbol, respectively. UUO, unilateral ureteral obstruction; EM-L, emodin low dosage; EM-M, emodin medium dosage, EM-H, emodin high dosage; LST, Losartan; TNF-α, tumor necrosis factor-α; MCP-1, monocyte chemoattractant protein-1; IL-6, interleukin-6; IL-1β, interleukin-1β.

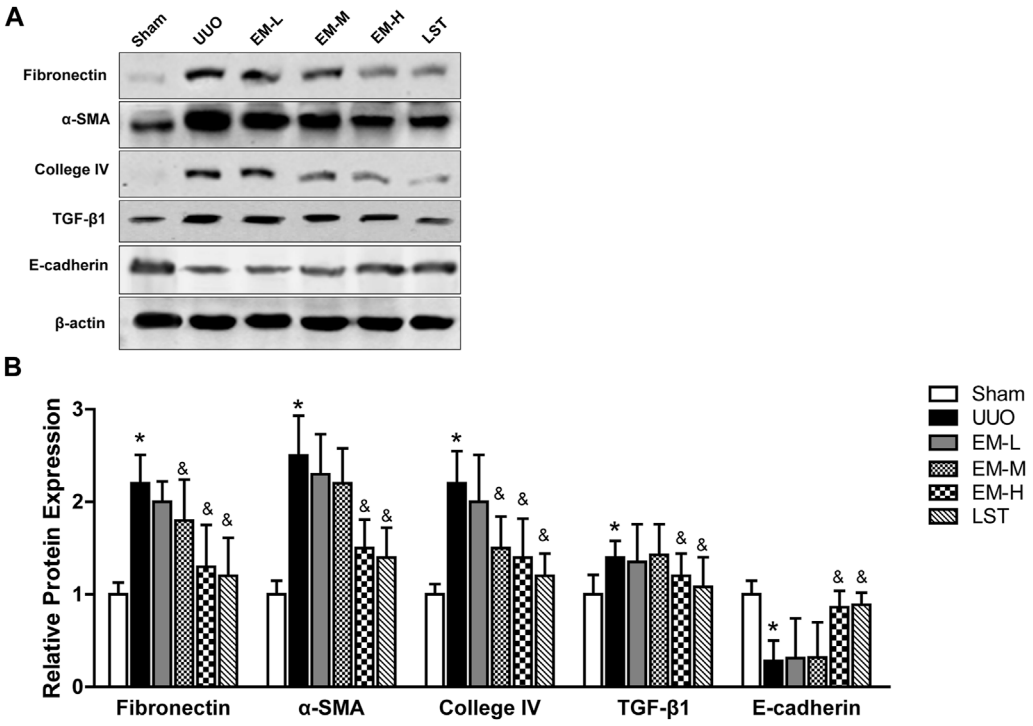


FIGURE 3
Emodin regulates fibrotic related protein expressions in UUO mice. Mice were randomly divided into Sham, UUO, EM-L, EM-M, EM-H and LST groups. Mice were administrated with dosages of 10 mg/kg, 20 mg/kg, 40 mg/kg emodin, or 10 mg/kg Losartan started 2 h after UUO surgery, daily, orally, for 14 continuous days. Representative blots of Fibronectin, α-SMA, Collagen IV,TGF-β1, E-cadherin and β-actin in the renal tissues, and **(B)** statistical analyses of relative protein expressions. Data were shown as mean ± SD (n = 10 per group). $^{*}p < 0.05$ vs. Sham, $^{\&}p < 0.05$ vs. UUO. UUO, unilateral ureteral obstruction; EM-L, emodin low dosage; EM-M, emodin medium dosage, EM-H, emodin high dosage; LST, Losartan. TGF-β1, transforming growth factor-β1; α-SMA, alpha-smooth muscle protein.

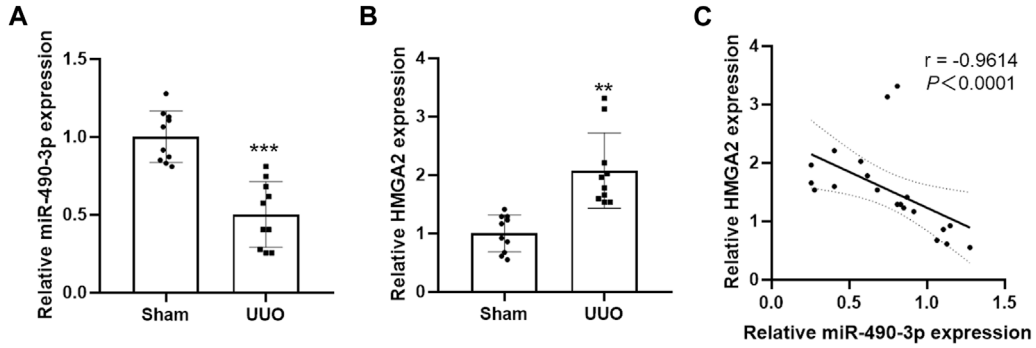


FIGURE 4
Decreased miR-490-3p expression and increased HMGA2 expression are negatively correlated in UUO mice. Gene Levels of **(A)** miR-490-3p, and **(B)** HMGA2 were detected by Real-Time PCR. **(C)** A negative correlation were found between miR-490-3p and HMGA2 mRNA expressins in the renal tissues of Sham and UUO mice (Spearman correlation analysis, r = −0.9614, $p < 0.0001$). Data were shown as mean ± SD (n = 10 per group). $^{**}p < 0.01$ vs. Sham, $^{***}p < 0.001$ vs. Sham. UUO, unilateral ureteral obstruction; HMGA2, high mobility protein A2.

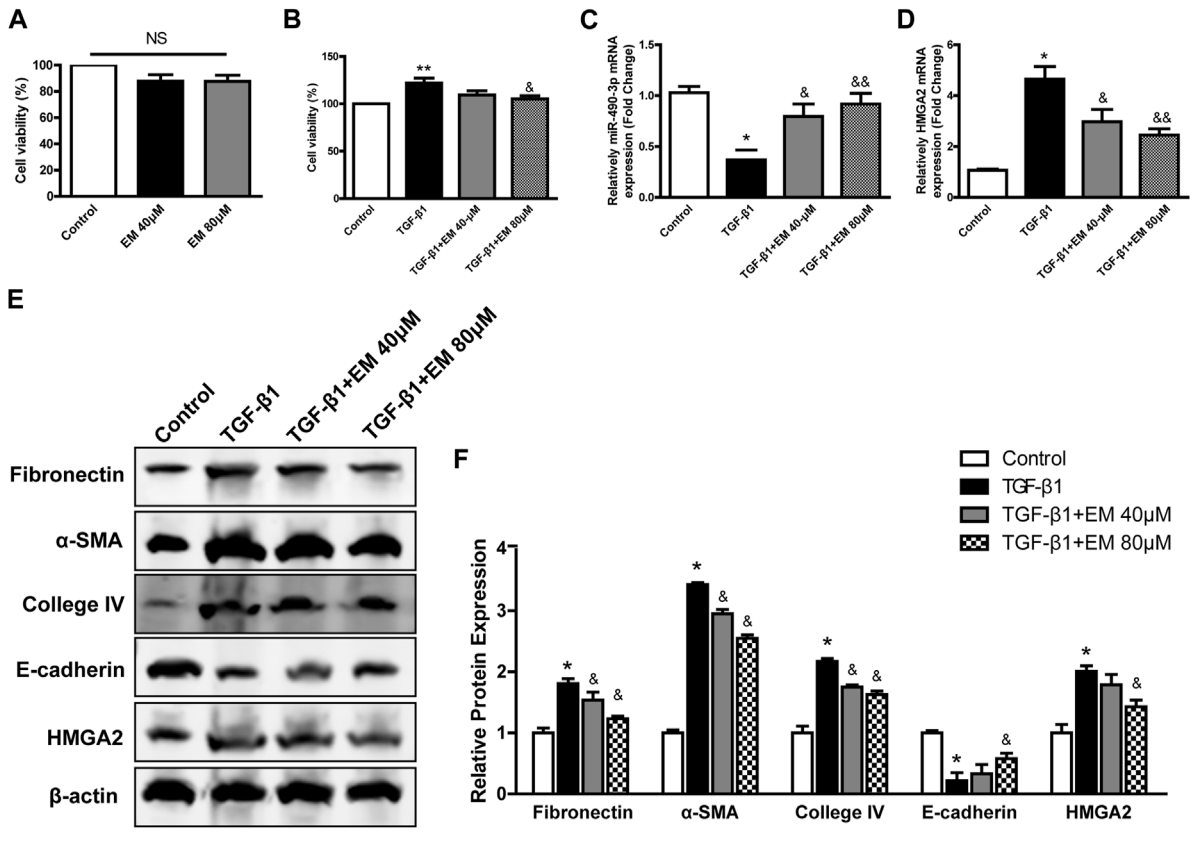


FIGURE 5
Emodin reversed the fibrosis in TGF-β1- induced NRK-52E cells. CCK-8 assay were performed in emodin-treated NRK-52E cells **(A)** without or **(B)** with TGF-β1 stimulation. The gene levels of **(C)** miR-490-3p and **(D)** HMGA2 were evaluated by Real-Time PCR. **(E)** Representative blots of Fibronectin, α-SMA, Collagen IV, E-cadherin, and HMGA2 in NRK-52E cells, and **(F)** statistical analyses of relative protein expressions. Data were shown as mean ± SD (n = 6). *compared with control, $^{\&}$compared with TGF-β1. $^{*}p < 0.05$, $^{**}p < 0.01$ of each symbol, respectively. $^{\&}p < 0.05$, $^{\&\&}p < 0.01$ of each symbol, respectively. TGF-β1, transforming growth factor-β1; HMGA2, high mobility protein A2; α-SMA, alpha-smooth muscle protein.

10.3389/fphar.2023.1042093

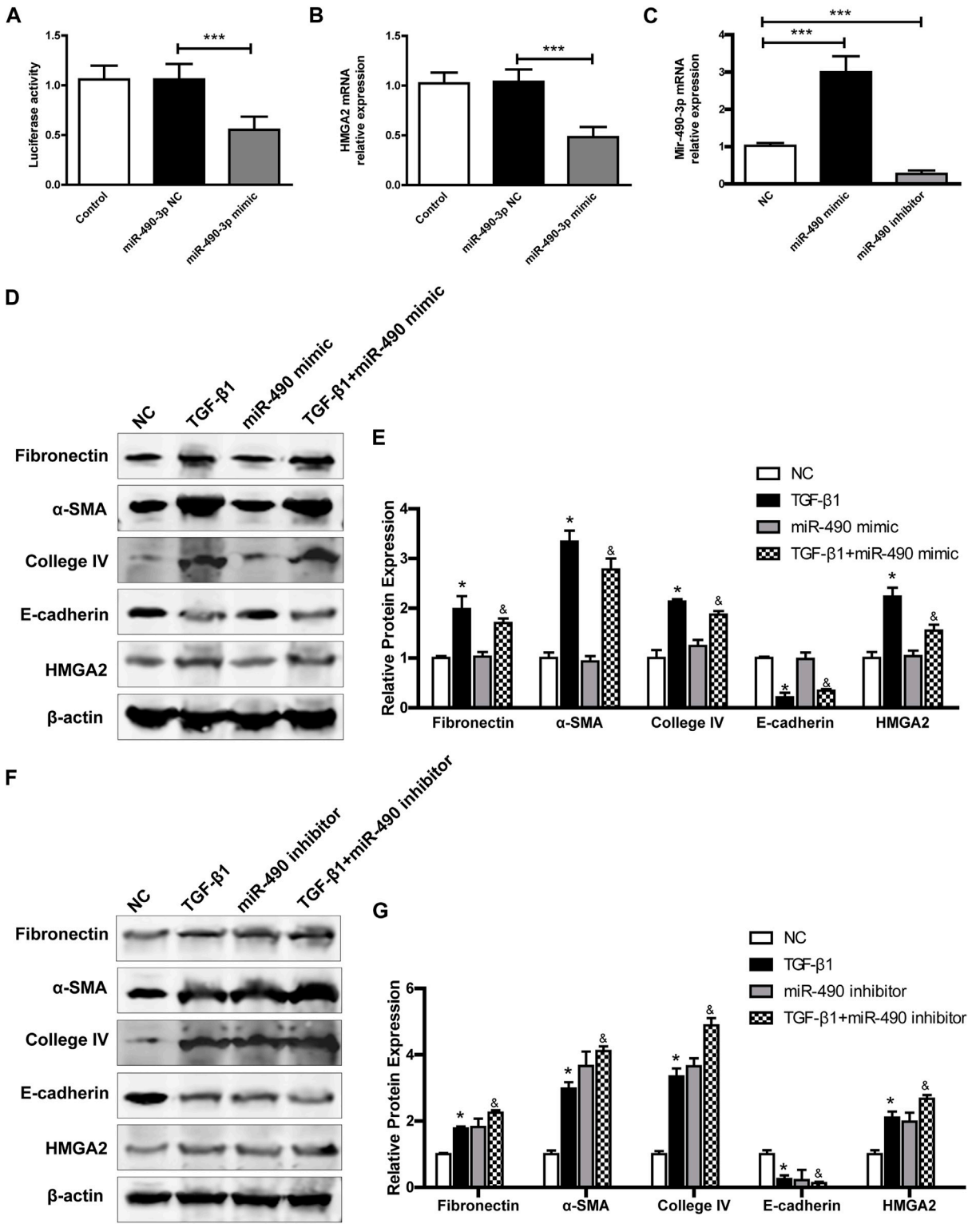


FIGURE 6
MiR-490-3p/HMGA2 axis are involved in TGF-β1-induced fibrotic effect in NRK-52E cells. HEK293 cells were co-transfected with a NC or miR-490-3p mimic. After 48 h, **(A)** dual luciferase reporter assay and **(B)** Real-time PCR were performed in control, miR-490-3p NC, and miR-490-3p mimic groups to evaluate the luciferase activities and gene level of HMGA2. NRK-52E cells were transfected with miR-490 mimic, NC, or inhibitor for 48 h, and then treated with or without TGF-β1 for 24 h. The gene levels of **(C)** miR-490-3p were evaluated by Real-Time PCR. **(D)** and **(F)**, the protein expressions of Fibronectin, α-SMA, Collagen IV, E-cadherin, and HMGA2 in miR-490-3p overexpression and inhibition experiment, respectively. **(E)** and **(G)**, statistical analyses of relative protein expression in each group. Data were shown as mean ± SD (n = 6). *compared with control, $^{\delta}$compared with TGF-β1. *$p < 0.05$, ***$p < 0.001$. $^{\delta}p < 0.05$. TGF-β1, transforming growth factor-β1; HMGA2, high mobility protein A2; α-SMA, alpha-smooth muscle protein.

using CCK-8. We found that different concentrations of emodin (40 and 80 μM) had no effect on cell viability (Figure 5A). As shown in Figure 5B, cell viability increased significantly in the TGF-β1 group, and decreased in the TGF-β1-induced NRK-52E cells in the emodin group (80 μM).

We next investigated the effects of emodin on renal fibrosis *in vitro* using western blot analysis to detect fibrosis-related protein levels. Compared to the TGF-β1 group, Fibronectin, α-SMA, Collagen IV decreased, while epithelial marker E-cadherin increased after emodin intervention (Figures 5E,F), consistent with the *in vivo* results, with the strongest effect observed in the high emodin dose group.

3.6 Emodin affects expression of miR-490-3p and HMGA2 in NRK-52E cells

The expression levels of miR-490-3p in NRK-52E cells treated with TGF-β1 and/or emodin were detected by Real-time PCR, and the protein and mRNA expression levels of HMGA2 were detected by western blot analysis and Real-time PCR. TGF-β1 treatment significantly down-regulated the expression of miR-490-3p mRNA in the NRK-52E cells (Figure 5C), but up-regulated HMGA2 protein and mRNA expression (Figures 5D–F). Compared with the TGF-β1 group, the expression level of miR-490-3p was significantly increased, while the expression level of HMGA2 was decreased in the NRK-52E cells after emodin intervention, with higher doses showing greater effects (Figures 5C–F). These results suggest that emodin can reverse the TGF-β1-induced decrease in miR-490-3p expression in NRK-52E cells.

3.7 MiR-490-3p/HMGA2 axis are involved in TGF-β1-induced fibrotic effect in NRK-52E cells

To verify whether HMGA2 is a potential target of miR-490-3p. We performed dual-luciferase reporter experiments. The HEK293 cells were transfected with miR-490-3p mimics and NCs. As shown in Figure 6A, the miR-490-3p mimic markedly inhibited luciferase activity of the HMGA2-5'UTR reporter, and Real-time PCR showed that, compared to the NC group, HMGA2 was down-regulated after miR-490-3p overexpression (Figure 6B). These results suggest that HMGA2 was targeted by miR-490-3p.

We further investigated the effects of miR-490-3p overexpression and inhibition on HMGA2 and TGF-β1-induced fibrosis in NRK-52E cells. Transfection efficiency was determined by Real-time PCR. As shown in Figure 6C, miR-490-3p expression was increased in the mimic group and decreased in the inhibitor group compared with the NC, indicating that the cells were successfully transfected with miR-490-3p mimic or inhibitor. Western blot analysis showed that TGF-β1 stimulation significantly up-regulated the expression levels of Fibronectin, α-SMA, and Collagen IV, but decreased the expression level of E-cadherin in the NRK-52E cells (Figures 6D–G). Compared with the TGF-β1 group, the miR-490-3p mimic group showed a decrease in the expression levels of Fibronectin, α-SMA, Collagen IV, and HMGA2 proteins but an increase in the expression level of E-cadherin protein (Figures 6D,E), while the miR-490-3p inhibitor group showed an increase in the expression levels of Fibronectin, α-SMA, Collagen IV, and HMGA2 proteins but a decrease in the expression of E-cadherin protein (Figures 6F,G). These data suggest that miR-490-3p is a potent regulator of HMGA2 involved in the regulation of fibrotic effects on NRK-52E cells.

3.8 Emodin reduces renal fibrosis by regulating miR-490-3p/HMGA2 axis

We further studied the regulatory role of miR-490-3p and HMGA2 in the anti-renal fibrotic effects of emodin. Results showed that TGF-β1 stimulation up-regulated Fibronectin, α-SMA, Collagen IV, and HMGA2 protein expression and decreased E-cadherin protein expression in the NRK-52E cells. Emodin treatment significantly alleviated the increase in Fibronectin, α-SMA, Collagen IV, and HMGA2 proteins and decline in E-cadherin protein. Compared with the TGF-β1 +EM + NC group, the TGF-β1 + EM + miR-490-3p mimic group showed a decrease in the Fibronectin, α-SMA, Collagen IV and HMGA2 protein levels and an increase in the E-cadherin protein level, while the TGF-β1 + EM + miR-490-3p inhibitor group showed an increase in the Fibronectin, α-SMA, Collagen IV, and HMGA2 protein levels and a decrease in the E-cadherin protein level (Figure 7). These results suggest that miR-490-3p mimics enhance the protective effects of emodin on TGF-β1-induced NRK-52E cells, while miR-490-3p inhibitors eliminate these protective effects. Thus, emodin may inhibit the HMGA2-dependent signaling pathway and reverse renal fibrosis by up-regulating miR-490-3p expression in NRK-52E cells.

4 Discussion

Renal fibrosis is known as the major pathological mechanism of CKD (Nogueira et al., 2017). Rhubarb, a traditional herbal medicine, is widely used in China to treat CKD (Wang et al., 2012). As the active ingredient in rhubarb, emodin exhibits anti-renal fibrosis activity through a variety of ways. Ma et al. reported that emodin ameliorates renal fibrosis by down-regulating TGF-β1 and Smurf two expression (Ma et al., 2018). Liu et al. reported that emodin alleviates epithelial-to-mesenchymal transition (EMT) by activating bone morphogenic protein (BMP)-7-mediated autophagy in renal fibrosis (Liu et al., 2021). Consistently, our research confirmed that emodin is an anti-renal fibrosis agent. Briefly, using a UUO mouse model, we found that emodin increased body weight, decreased blood creatinine, urea nitrogen, and uric acid levels, reduced renal pathological damage, and attenuated renal tissue inflammation and fibrosis in UUO mice. *In vitro*, using TGF-β1-induced NRK-52E cells, we found that miR-490-3p targeting HMGA2 was involved in renal fibrosis, and further showed that emodin *via* regulation of miR-490-3p/HMGA2 and ameliorates renal fibrosis.

The role of inflammation in the pathogenesis and progression of CKD has been recognized since the late 1990s. Recent studies have also confirmed that inflammation and the inflammatory response can alter or interfere with intrarenal microcirculatory regulation and perfusion distribution and can induce renal damage and promote disease progression. Persistent, low-grade inflammation is now considered a distinguishing feature of CKD and is associated

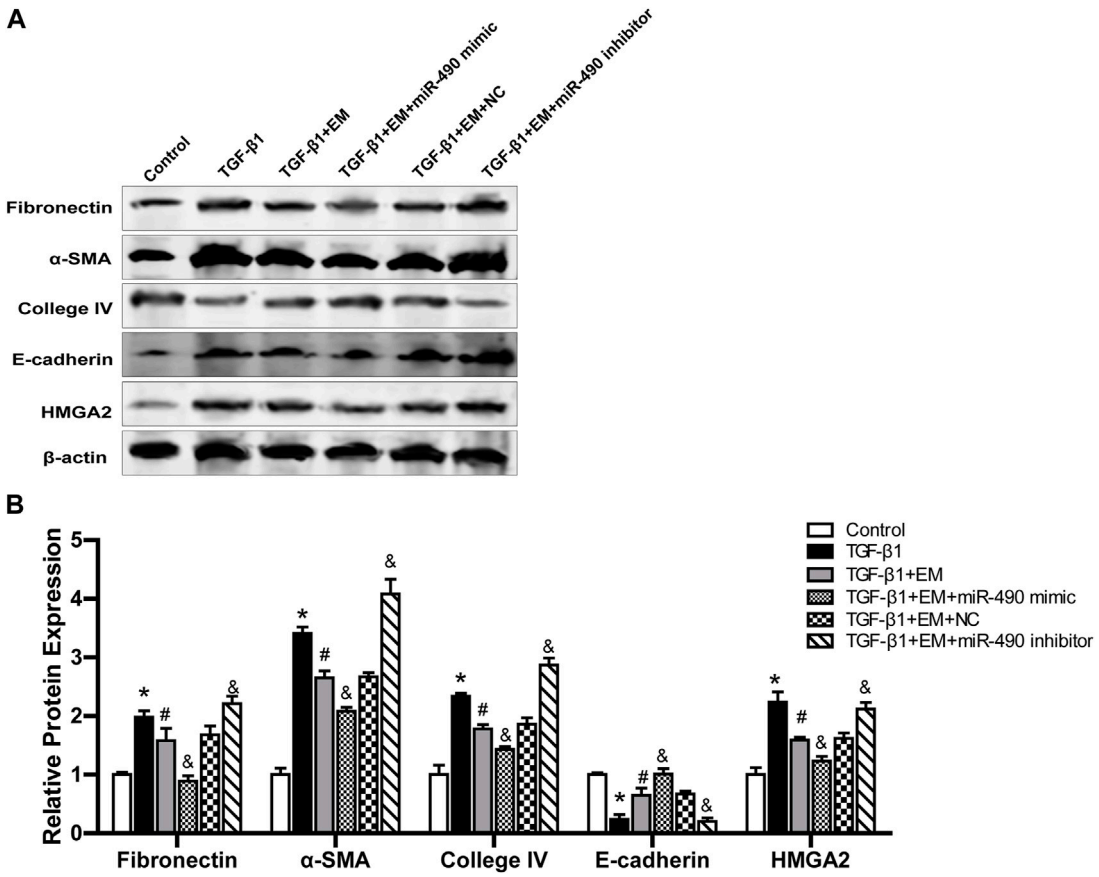


FIGURE 7
Emodin reduces renal fibrosis by regulating miR-490-3p/HMGA2 axis. MiR-490-3p mimic, miR-490-3p inhibitor, and NC groups of NRK-52E cells were transfected for 48 h, and then treated with or without emodin for 24 h, and finally exposed to TGF-β1 for 24 h. **(A)** Representative blots of Fibronectin, α-SMA, Collagen IV,TGF-β1, and E-cadherin in each group, and **(B)** statistical analyses of relative protein expression. Data were shown as mean ± SD (n = 6). *compared with control, #compared with TGF-β1, &compared with TGF-β1+EM + NC. *$p < 0.05$, &$p < 0.05$, #$p < 0.05$. TGF-β1, transforming growth factor-β1; EM, emodin; HMGA2, high mobility protein A2; α-SMA, alpha-smooth muscle protein.

with all-cause mortality in patients (Lv et al., 2018a; Mihai et al., 2018). Hirudin is reported to suppress fibrosis in renal tissues and renal tubular epithelial cells by inhibiting inflammation (Xie et al., 2020). Therefore, treating or preventing underlying inflammation may improve CKD prognosis. The anti-inflammatory effects of emodin have been confirmed in various disease studies. Notably, emodin has been shown to significantly down-regulate inflammatory factors, such as TNF-α, MCP-1, IL-1β, and IL-6, *via* regulation of the nuclear factor kappa-light-chain-enhancer of activated B cells (NF-κB) and p38 mitogen-activated protein kinase (MAPK) pathways (Zhu et al., 2013; Xia et al., 2019; Zang et al., 2020). In our study, emodin was selective for the regulation of inflammatory factors in the UUO model, down-regulating TNF-α, MCP-1, and IL-1β, but with no significant effect on IL-6. The result is different from previous results reported for IL-6 regulation by emodin used in other models, it may be due to the different pathophysiological processes of the models.

Fibrosis is a result of tissue repair and becomes dysregulated after many types of tissue damage (Rockey et al., 2015). The fact that changes in fibrosis are linked to various diseases in various organ systems, including heart, kidneys, liver, skin or any other body organ. A variety of cellular and molecular signaling mechanisms are involved in the pathogenesis of fibrosis (Alqudah et al., 2020). Overproduction of cytokines, chemokines, growth factors, extracellular matrix proteins, and loss of normal organ structure and function are common features of fibrosis in organs (Weiskirchen et al., 2019). The ability of fibrosis to resolve may depend on the organ involved, the nature of the injury stimulus, and host-specific factors. The liver stands out from all other tissues with its strong regenerative capacity. In metabolic liver disease, lifestyle changes and bariatric surgery can cause histological fibrosis to regress (Vilar-Gomez et al., 2015). The cardiac parenchymal cells are muscle cells (cardiomyocytes) displaying a very limited regenerative capacity (Zeisberg and Kalluri, 2013). Some researchs on diabetic cardiomyopathy that controlling autophagy and lowering cardiomyocyte apoptosis *via* a variety of routes can prevent cardiomyocyte fibrosis (Zhang et al., 2021; Xue et al., 2022). The kidney has a complex structure, and renal fibrosis is manifested by the presence of glomerulosclerosis, vascular sclerosis and tubulointerstitial fibrosis. Because existing knowledge about the progression of renal fibrosis is extremely complex, preventing or even eliminating renal fibrosis is difficult (Nogueira et al., 2017). TGF-β is considered as one of the common master

switches for the induction of the fibrotic program during chronic phases of inflammatory diseases in many organs and tissue. Many evidence suggests that miRNAs are both downstream effectors of TGF-β-dependent renal fibrosis and upstream regulators of TGF-β-dependent signaling pathways (Lv et al., 2018b). Therefore, the regulation of miRNA expression may be as a promising therapeutic strategy for the treatment of CKD.

Various studies have confirmed that HMGA2 is a key factor in the development of EMT. Notably, TGF-β1 is a potent fibrogenic factor that can mediate EMT through the regulatory effects of HMGA2 (Hills and Squires, 2010; Iwano, 2010; Wang et al., 2016)and mediate the development of renal fibrosis through different signaling pathways (Hills and Squires, 2010; Iwano, 2010). EMT is an important mechanism of renal fibrosis (Lovisa et al., 2016). Although the role of EMT in renal fibrosis has been questioned (Kriz et al., 2011), recent evidence suggests that EMT in renal tubular epithelial cells promotes renal fibrosis (Grande et al., 2015; Lovisa et al., 2015) and inhibition of EMT improves renal fibrosis (Sun et al., 2018; Wang et al., 2020; Nagavally et al., 2021). Accumulating evidence also suggests that specific miRNAs play important roles in CKD progression, and that miR-490-3p targeting HMGA2 is implicated in the metastasis and proliferation of multiple tumors (Liu W. et al., 2015; Zhang et al., 2019). Previous sequencing results showed that miR-490 was the most significant down-regulated miRNAs after UUO surgery (Chung et al., 2010; Qin et al., 2011). Our pre-experiment verified the regulatory effects of emodin on the top five miRNAs, including miR-490-3p, miR-137-3p, miR-208-3p, miR-429-3p, and miR-200a-3p, which reported to be significantly decreased in UUO mice (data not shown), and found that emodin had the best regulatory effects on elevating the expression of miR-490-3p. In this study, we found that miR-490-3p was negatively correlated with HMGA2 expression in UUO mice. Using dual luciferase reporter gene assay, we also verified that miR-490-3p exhibited a targeting relationship with HMGA2. Further experiments found that miR-490-3p mimic-inhibited fibrosis in NRK-52E cells was reversed by silencing the expression of HMGA2, and miR-490 inhibitor promoted fibrosis in NRK-52E cells by overexpressing HMGA2. These results suggest that miR-490-3p inhibits fibrosis in NRK-52E cells by down-regulating HMGA2-mediated expression. MiR-490 is also known to have tumor suppressive effects in many cancer types, preventing cancer cells from acquiring a mesenchymal phenotype by modulating EMT, thus inhibiting proliferation and metastasis (Vinchure and Kulshreshtha, 2021). MiR-490-3p is also involved in silicon-induced pulmonary fibrosis by targeting TGFBR1 modulators (Cheng et al., 2021). These findings support our results suggesting that miR-490-3p exerts a protective effect on renal fibrosis. Finally, to identify the underlying molecular mechanism, we detected the effects of emodin on the miR-490-3p/HMGA2 signaling pathway. Results indicated that the miR-490-3p mimic enhanced the protective effects, while the miR-490-3p inhibitor abrogated the protective effects of emodin on TGF-β1-induced NRK-52E cell fibrosis. These findings suggest that emodin alleviates renal fibrosis by up-regulating miR-490-3p. However, limitations of the present study should be considered, the downstream signaling pathways need to be further evaluated in future studies.

In conclusion, emodin increased miR-490-3p expression, inhibited HMGA2 expression, and blocked TGF-β1-induced fibrosis, thereby exerting significant nephroprotective effects and ameliorating UUO-induced renal injury in CKD mice. Therefore, miR-490-3p may be a new drug target for emodin to prevent HMGA2-dependent signaling pathway fibrosis, with potential implications in CKD pathology.

Data availability statement

The raw data supporting the conclusions of this article will be made available by the authors, without undue reservation.

Ethics statement

The animal study was reviewed and approved by Ethics Committee for Animal Experimentation of the Hubei Provincial Hospital of Traditional Chinese Medicine.

Author contributions

LW, XW, and YB conceived, designed the study, and wrote the manuscript, which as approved by all the authors. XW and LW carried out the UUO surgery, drug treatment, and the collection of samples. GL and RW histologic examination, physiological and biochemical parameters. LW, XW, SZ, MW, and HH carried out elisa evaluation, CCK-8 assay, transfection of miRNA mimics and inhibitors and real-time PCR. LW and QL performed data analysis.

Funding

Hubei Provincial Science and Technology Department 2020 Provincial Science and Technology Major Special Project (NO 2020ACA019). State Administration of Traditional Chinese Medicine (Project No.: National Chinese Medicine Human Education Letter [2022] No. 75).

Conflict of interest

The authors declare that the research was conducted in the absence of any commercial or financial relationships that could be construed as a potential conflict of interest.

Publisher's note

All claims expressed in this article are solely those of the authors and do not necessarily represent those of their affiliated organizations, or those of the publisher, the editors and the reviewers. Any product that may be evaluated in this article, or claim that may be made by its manufacturer, is not guaranteed or endorsed by the publisher.

Supplementary material

The Supplementary Material for this article can be found online at: https://www.frontiersin.org/articles/10.3389/fphar.2023.1042093/full#supplementary-material

References

Akchurin, O. M. (2019). Chronic kidney disease and dietary measures to improve outcomes. *Pediatr. Clin. North Am.* 66 (1), 247–267. doi:10.1016/j.pcl.2018.09.007

Alqudah, M., Hale, T. M., and Czubryt, M. P. (2020). Targeting the renin-angiotensin-aldosterone system in fibrosis. *Matrix Biol.* 91-92, 92–108. doi:10.1016/j.matbio.2020.04.005

Boor, P., Ostendorf, T., and Floege, J. (2010). Renal fibrosis: Novel insights into mechanisms and therapeutic targets. *Nat. Rev. Nephrol.* 6 (11), 643–656. doi:10.1038/nrneph.2010.120

Cao, M., Fang, Y., Jia, W., Wang, Y., Sun, J., and Tao, D. (2019). Emodin relieves hypoxia-triggered injury via elevation of microRNA-25 in PC-12 cells. *Artif. Cells Nanomed Biotechnol.* 47 (1), 2678–2687. doi:10.1080/21691401.2019.1633339

Cheng, D., Xu, Q., Liu, Y., Li, G., Sun, W., Ma, D., et al. (2021). Long noncoding RNA-SNHG20 promotes silica-induced pulmonary fibrosis by miR-490-3p/TGFBR1 axis. *Toxicology* 451, 152683. doi:10.1016/j.tox.2021.152683

Chung, A. C., Huang, X. R., Meng, X., and Lan, H. Y. (2010). MiR-192 mediates TGF-beta/Smad3-driven renal fibrosis. *J. Am. Soc. Nephrol.* 21 (8), 1317–1325. doi:10.1681/ASN.2010020134

Collaboration, G. C. K. D. (2020). Global, regional, and national burden of chronic kidney disease, 1990-2017: A systematic analysis for the global burden of disease study 2017. *Lancet* 395 (10225), 709–733. doi:10.1016/S0140-6736(20)30045-3

Curtis, S., and Komenda, P. (2020). Screening for chronic kidney disease: Moving toward more sustainable health care. *Curr. Opin. Nephrol. Hypertens.* 29 (3), 333–338. doi:10.1097/MNH.0000000000000597

Djudjaj, S., and Boor, P. (2019). Cellular and molecular mechanisms of kidney fibrosis. *Mol. Asp. Med.* 65, 16–36. doi:10.1016/j.mam.2018.06.002

Dong, X., Fu, J., Yin, X., Cao, S., Li, X., Lin, L., et al. (2016). Emodin: A review of its pharmacology, toxicity and pharmacokinetics. *Phytother. Res.* 30 (8), 1207–1218. doi:10.1002/ptr.5631

Fan, Y., Chen, H., Huang, Z., Zheng, H., and Zhou, J. (2020). Emerging role of miRNAs in renal fibrosis. *RNA Biol.* 17 (1), 1–12. doi:10.1080/15476286.2019.1667215

Gaitonde, D. Y., Cook, D. L., and Rivera, I. M. (2017). Chronic kidney disease: Detection and evaluation. *Am. Fam. Physician* 96 (12), 776–783.

Grande, M. T., Sanchez-Laorden, B., Lopez-Blau, C., De Frutos, C. A., Boutet, A., Arevalo, M., et al. (2015). Snail1-induced partial epithelial-to-mesenchymal transition drives renal fibrosis in mice and can be targeted to reverse established disease. *Nat. Med.* 21 (9), 989–997. doi:10.1038/nm.3901

Hills, C. E., and Squires, P. E. (2010). TGF-beta1-induced epithelial-to-mesenchymal transition and therapeutic intervention in diabetic nephropathy. *Am. J. Nephrol.* 31 (1), 68–74. doi:10.1159/000256659

Iwano, M. (2010). EMT and TGF-beta in renal fibrosis. *Front. Biosci. Sch. Ed.* 2 (1), 229–238. doi:10.2741/s60

Kalantar-Zadeh, K., Jafar, T. H., Nitsch, D., Neuen, B. L., and Perkovic, V. (2021). Chronic kidney disease. *Lancet* 398 (10302), 786–802. doi:10.1016/S0140-6736(21)00519-5

Klinkhammer, B. M., Goldschmeding, R., Floege, J., and Boor, P. (2017). Treatment of renal fibrosis-turning challenges into opportunities. *Adv. Chronic Kidney Dis.* 24 (2), 117–129. doi:10.1053/j.ackd.2016.11.002

Kriz, W., Kaissling, B., and Le Hir, M. (2011). Epithelial-mesenchymal transition (EMT) in kidney fibrosis: Fact or fantasy? *J. Clin. Invest.* 121 (2), 468–474. doi:10.1172/jci44595

Liu, H., Gu, L. B., Tu, Y., Hu, H., Huang, Y. R., and Sun, W. (2016). Emodin ameliorates cisplatin-induced apoptosis of rat renal tubular cells *in vitro* by activating autophagy. *Acta Pharmacol. Sin.* 37 (2), 235–245. doi:10.1038/aps.2015.114

Liu, N., Wang, L., Yang, T., Xiong, C., Xu, L., Shi, Y., et al. (2015). EGF receptor inhibition alleviates hyperuricemic nephropathy. *J. Am. Soc. Nephrol.* 26 (11), 2716–2729. doi:10.1681/ASN.2014080793

Liu, W., Gu, R., Lou, Y., He, C., Zhang, Q., and Li, D. (2021). Emodin-induced autophagic cell death hinders epithelial-mesenchymal transition via regulation of BMP-7/TGF-β1 in renal fibrosis. *J. Pharmacol. Sci.* 146 (4), 216–225. doi:10.1016/j.jphs.2021.03.009

Liu, W., Xu, G., Liu, H., and Li, T. (2015). MicroRNA-490-3p regulates cell proliferation and apoptosis by targeting HMGA2 in osteosarcoma. *FEBS Lett.* 589 (20), 3148–3153. doi:10.1016/j.febslet.2015.08.034

Lovisa, S., LeBleu, V. S., Tampe, B., Sugimoto, H., Vadnagara, K., Carstens, J. L., et al. (2015). Epithelial-to-mesenchymal transition induces cell cycle arrest and parenchymal damage in renal fibrosis. *Nat. Med.* 21 (9), 998–1009. doi:10.1038/nm.3902

Lovisa, S., Zeisberg, M., and Kalluri, R. (2016). Partial Epithelial-to-Mesenchymal transition and other new mechanisms of kidney fibrosis. *Trends Endocrinol. Metab.* 27 (10), 681–695. doi:10.1016/j.tem.2016.06.004

Lv, W., Booz, G. W., Wang, Y., Fan, F., and Roman, R. J. (2018a). Inflammation and renal fibrosis: Recent developments on key signaling molecules as potential therapeutic targets. *Eur. J. Pharmacol.* 820, 65–76. doi:10.1016/j.ejphar.2017.12.016

Lv, W., Fan, F., Wang, Y., Gonzalez-Fernandez, E., Wang, C., Yang, L., et al. (2018b). Therapeutic potential of microRNAs for the treatment of renal fibrosis and CKD. *Physiol. Genomics*. 50 (1), 20–34. doi:10.1152/physiolgenomics.00039.2017

Ma, L., Li, H., Zhang, S., Xiong, X., Chen, K., Jiang, P., et al. (2018). Emodin ameliorates renal fibrosis in rats via TGF-β1/Smad signaling pathway and function study of Smurf 2. *Int. Urol. Nephrol.* 50 (2), 373–382. doi:10.1007/s11255-017-1757-x

Ma, T. T., and Meng, X. M. (2019). TGF-β/Smad and renal fibrosis. *Adv. Exp. Med. Biol.* 1165, 347–364. doi:10.1007/978-981-13-8871-2_16

Mihai, S., Codrici, E., Popescu, I. D., Enciu, A. M., Albulescu, L., Necula, L. G., et al. (2018). Inflammation-Related mechanisms in chronic kidney disease prediction, progression, and outcome. *J. Immunol. Res.* 2018, 2180373. doi:10.1155/2018/2180373

Nagavally, R. R., Sunilkumar, S., Akhtar, M., Trombetta, L. D., and Ford, S. M. (2021). Chrysin ameliorates cyclosporine-A-induced renal fibrosis by inhibiting TGF-β_1-induced epithelial-mesenchymal transition. *Int. J. Mol. Sci.* 22 (19), 10252. doi:10.3390/ijms221910252

Nogueira, A., Pires, M. J., and Oliveira, P. A. (2017). Pathophysiological mechanisms of renal fibrosis: A review of animal models and therapeutic strategies. *Vivo* 31 (1), 1–22. doi:10.21873/invivo.11019

Qin, W., Chung, A. C., Huang, X. R., Meng, X. M., Hui, D. S., Yu, C. M., et al. (2011). TGF-β/Smad3 signaling promotes renal fibrosis by inhibiting miR-29. *J. Am. Soc. Nephrol.* 22 (8), 1462–1474. doi:10.1681/ASN.2010121308

Ren, Q., Wang, B., Guo, F., Huang, R., Tan, Z., Ma, L., et al. (2021). Natural flavonoid pectolinarigenin alleviated hyperuricemic nephropathy via suppressing tgfβ/SMAD3 and JAK2/STAT3 signaling pathways. *Front. Pharmacol.* 12, 792139. doi:10.3389/fphar.2021.792139

Rockey, D. C., Bell, P. D., and Hill, J. A. (2015). Fibrosis--A common pathway to organ injury and failure. *N. Engl. J. Med.* 373 (1), 95–96. doi:10.1056/NEJMc1504848

Sun, M., Zhou, W., Yao, F., Song, J., Xu, Y., Deng, Z., et al. (2021). MicroRNA-302b mitigates renal fibrosis via inhibiting TGF-β/Smad pathway activation. *Braz J. Med. Biol. Res.* 54 (3), e9206. doi:10.1590/1414-431X20209206

Sun, Z., Ma, Y., Chen, F., Wang, S., Chen, B., and Shi, J. (2018). miR-133b and miR-199b knockdown attenuate TGF-β1-induced epithelial to mesenchymal transition and renal fibrosis by targeting SIRT1 in diabetic nephropathy. *Eur. J. Pharmacol.* 837, 96–104. doi:10.1016/j.ejphar.2018.08.022

Van der Hauwaert, C., Savary, G., Hennino, M. F., Pottier, N., Glowacki, F., and Cauffiez, C. (2015). MicroRNAs in kidney fibrosis. *Nephrol. Ther.* 11 (6), 474–482. doi:10.1016/j.nephro.2015.03.007

Vilar-Gomez, E., Martinez-Perez, Y., Calzadilla-Bertot, L., Torres-Gonzalez, A., Gra-Oramas, B., Gonzalez-Fabian, L., et al. (2015). Weight loss through lifestyle modification significantly reduces features of nonalcoholic steatohepatitis. *Gastroenterology* 149 (2), 367–378. doi:10.1053/j.gastro.2015.04.005

Vinchure, O. S., and Kulshreshtha, R. (2021). MiR-490: A potential biomarker and therapeutic target in cancer and other diseases. *J. Cell Physiol.* 236 (5), 3178–3193. doi:10.1002/jcp.30119

Wang, H., Song, H., Yue, J., Li, J., Hou, Y. B., and Deng, J. L. (2012). Rheum officinale (a traditional Chinese medicine) for chronic kidney disease. *Cochrane Database Syst. Rev.* 7, CD008000. doi:10.1002/14651858.CD008000.pub2

Wang, R., Hu, B., Ye, C., Zhang, Z., Yin, M., Cao, Q., et al. (2022). Stewed rhubarb decoction ameliorates Adenine-Induced chronic renal failure in mice by regulating gut microbiota dysbiosis. *Front. Pharmacol.* 13, 842720. doi:10.3389/fphar.2022.842720

Wang, Y. C., Liu, J. S., Tang, H. K., Nie, J., Zhu, J. X., Wen, L. L., et al. (2016). miR-221 targets HMGA2 to inhibit bleomycin-induced pulmonary fibrosis by regulating TGF-β1/Smad3-induced EMT. *Int. J. Mol. Med.* 38 (4), 1208–1216. doi:10.3892/ijmm.2016.2705

Wang, Z., Chen, Z., Li, B., Zhang, B., Du, Y., Liu, Y., et al. (2020). Curcumin attenuates renal interstitial fibrosis of obstructive nephropathy by suppressing epithelial-mesenchymal transition through inhibition of the TLR4/NF-κB and PI3K/AKT signalling pathways. *Pharm. Biol.* 58 (1), 828–837. doi:10.1080/13880209.2020.1809462

Weiskirchen, R., Weiskirchen, S., and Tacke, F. (2019). Organ and tissue fibrosis: Molecular signals, cellular mechanisms and translational implications. *Mol. Asp. Med.* 65, 2–15. doi:10.1016/j.mam.2018.06.003

Xia, S., Ni, Y., Zhou, Q., Liu, H., Xiang, H., Sui, H., et al. (2019). Emodin attenuates severe acute pancreatitis via antioxidant and anti-inflammatory activity. *Inflammation* 42 (6), 2129–2138. doi:10.1007/s10753-019-01077-z

Xiang, H., Tao, X., Xia, S., Qu, J., Song, H., Liu, J., et al. (2017). Emodin alleviates sodium Taurocholate-Induced pancreatic acinar cell injury via MicroRNA-30a-5p-Mediated inhibition of High-Temperature requirement A/Transforming growth factor beta 1 inflammatory signaling. *Front. Immunol.* 8, 1488. doi:10.3389/fimmu.2017.01488

Xie, R., Liu, M., and Li, S. (2019). Emodin weakens liver inflammatory injury triggered by lipopolysaccharide through elevating microRNA-145 *in vitro* and *in vivo*. *Artif. Cells Nanomed Biotechnol.* 47 (1), 1877–1887. doi:10.1080/21691401.2019.1614015

Xie, Y., Bowe, B., Mokdad, A. H., Xian, H., Yan, Y., Li, T., et al. (2018). Analysis of the Global Burden of Disease study highlights the global, regional, and national trends of chronic kidney disease epidemiology from 1990 to 2016. *Kidney Int.* 94 (3), 567–581. doi:10.1016/j.kint.2018.04.011

Xie, Y., Lan, F., Zhao, J., and Shi, W. (2020). Hirudin improves renal interstitial fibrosis by reducing renal tubule injury and inflammation in unilateral ureteral obstruction (UUO) mice. *Int. Immunopharmacol.* 81, 106249. doi:10.1016/j.intimp.2020.106249

Xue, F., Cheng, J., Liu, Y., Cheng, C., Zhang, M., Sui, W., et al. (2022). Cardiomyocyte-specific knockout of ADAM17 ameliorates left ventricular remodeling and function in diabetic cardiomyopathy of mice. *Signal Transduct. Target Ther.* 7 (1), 259. doi:10.1038/s41392-022-01054-3

Yang, F., Deng, L., Li, J., Chen, M., Liu, Y., Hu, Y., et al. (2020). Emodin retarded renal fibrosis through regulating HGF and tgfβ-smad signaling pathway. *Drug Des. Devel Ther.* 14, 3567–3575. doi:10.2147/DDDT.S245847

Zang, L., Song, Y., Yu, F., and Liu, X. (2020). Emodin relieved lipopolysaccharide-evoked inflammatory damage in WI-38 cells by up-regulating taurine up-regulated gene 1. *Biofactors* 46 (5), 860–868. doi:10.1002/biof.1609

Zeisberg, M., and Kalluri, R. (2013). Cellular mechanisms of tissue fibrosis. 1. Common and organ-specific mechanisms associated with tissue fibrosis. *Am. J. Physiol. Cell Physiol.* 304 (3), C216–C225. doi:10.1152/ajpcell.00328.2012

Zhang, F., Wu, A., Wang, Y., and Liu, J. (2019). MiR-490-3p functions as a tumor suppressor in glioma by inhibiting high-mobility group AT-hook 2 expression. *Exp. Ther. Med.* 18 (1), 664–670. doi:10.3892/etm.2019.7606

Zhang, M., Sui, W., Xing, Y., Cheng, J., Cheng, C., Xue, F., et al. (2021). Angiotensin IV attenuates diabetic cardiomyopathy via suppressing FoxO1-induced excessive autophagy, apoptosis and fibrosis. *Theranostics* 11 (18), 8624–8639. doi:10.7150/thno.48561

Zhang, W., Zhang, C., Chen, H., Li, L., Tu, Y., Liu, C., et al. (2014). Evaluation of microRNAs miR-196a, miR-30a-5P, and miR-490 as biomarkers of disease activity among patients with FSGS. *Clin. J. Am. Soc. Nephrol.* 9 (9), 1545–1552. doi:10.2215/CJN.11561113

Zhong, X., Chung, A. C., Chen, H. Y., Dong, Y., Meng, X. M., Li, R., et al. (2013). MiR-21 is a key therapeutic target for renal injury in a mouse model of type 2 diabetes. *Diabetologia* 56 (3), 663–674. doi:10.1007/s00125-012-2804-x

Zhou, S., Ai, Z., Li, W., You, P., Wu, C., Li, L., et al. (2020). Deciphering the pharmacological mechanisms of Taohe-Chengqi decoction extract against renal fibrosis through integrating network pharmacology and experimental validation *in vitro* and *in vivo*. *Front. Pharmacol.* 11, 425. doi:10.3389/fphar.2020.00425

Zhu, X., Zeng, K., Qiu, Y., Yan, F., and Lin, C. (2013). Therapeutic effect of emodin on collagen-induced arthritis in mice. *Inflammation* 36 (6), 1253–1259. doi:10.1007/s10753-013-9663-6

frontiers | Frontiers in Pharmacology

TYPE Review
PUBLISHED 28 March 2023
DOI 10.3389/fphar.2023.1070973

Check for updates

OPEN ACCESS

EDITED BY
Zhe-Sheng Chen,
St. John's University, United States

REVIEWED BY
Camila Hochman-Mendez,
Texas Heart Institute, United States
Kshitiz Kz,
UCONN Health, United States
Hitoshi Kurose,
Kyushu University, Japan

*CORRESPONDENCE
Jiali Wang,
wangjiali_2000@126.com
Yuguo Chen,
chen919085@sdu.edu.cn

†These authors have contributed equally to this work and share first authorship

SPECIALTY SECTION
This article was submitted to Experimental Pharmacology and Drug Discovery, a section of the journal Frontiers in Pharmacology

RECEIVED 15 October 2022
ACCEPTED 13 March 2023
PUBLISHED 28 March 2023

CITATION
Yin X, Yin X, Pan X, Zhang J, Fan X, Li J, Zhai X, Jiang L, Hao P, Wang J and Chen Y (2023), Post-myocardial infarction fibrosis: Pathophysiology, examination, and intervention.
Front. Pharmacol. 14:1070973.
doi: 10.3389/fphar.2023.1070973

COPYRIGHT
© 2023 Yin, Yin, Pan, Zhang, Fan, Li, Zhai, Jiang, Hao, Wang and Chen. This is an open-access article distributed under the terms of the Creative Commons Attribution License (CC BY). The use, distribution or reproduction in other forums is permitted, provided the original author(s) and the copyright owner(s) are credited and that the original publication in this journal is cited, in accordance with accepted academic practice. No use, distribution or reproduction is permitted which does not comply with these terms.

Post-myocardial infarction fibrosis: Pathophysiology, examination, and intervention

Xiaoying Yin[1,2,3,4†], Xinxin Yin[1,2,3,4†], Xin Pan[1,2,3,4], Jingyu Zhang[1,2,3,4], Xinhui Fan[1,2,3,4], Jiaxin Li[1,2,3,4], Xiaoxuan Zhai[1,2,3,4], Lijun Jiang[1,2,3,4], Panpan Hao[4], Jiali Wang[1,2,3,4*] and Yuguo Chen[1,2,3,4*]

[1]Department of Emergency and Chest Pain Center, Qilu Hospital of Shandong University, Jinan, China, [2]Clinical Research Center for Emergency and Critical Care Medicine of Shandong Province, Institute of Emergency and Critical Care Medicine of Shandong University, Qilu Hospital of Shandong University, Jinan, China, [3]Key Laboratory of Emergency and Critical Care Medicine of Shandong Province, Qilu Hospital of Shandong University, Jinan, China, [4]Key Laboratory of Cardiovascular Remodeling and Function Research, Chinese Ministry of Education, Chinese Ministry of Health and Chinese Academy of Medical Sciences, The State and Shandong Province Joint Key Laboratory of Translational Cardiovascular Medicine, Qilu Hospital of Shandong University, Jinan, China

Cardiac fibrosis plays an indispensable role in cardiac tissue homeostasis and repair after myocardial infarction (MI). The cardiac fibroblast-to-myofibroblast differentiation and extracellular matrix collagen deposition are the hallmarks of cardiac fibrosis, which are modulated by multiple signaling pathways and various types of cells in time-dependent manners. Our understanding of the development of cardiac fibrosis after MI has evolved in basic and clinical researches, and the regulation of fibrotic remodeling may facilitate novel diagnostic and therapeutic strategies, and finally improve outcomes. Here, we aim to elaborate pathophysiology, examination and intervention of cardiac fibrosis after MI.

KEYWORDS

myocardial infarction, fibrosis, cardiac remodeling, antifibrotic therapy, extracellular matrix, fibroblast, myofibroblast

1 Introduction

Myocardial infarction (MI) is a leading cause of global morbidity and mortality and the primary contributor to heart failure (HF) (Groenewegen et al., 2020). The limited regenerative capacity leads to massive loss of cardiomyocytes (CMs) and excessive deposition of extracellular matrix (ECM) after MI (Prabhu and Frangogiannis, 2016; Dattagupta and Immaneni, 2018), which is called cardiac remodeling. Cardiac fibrosis is a pathological process of cardiac remodeling. Although timely and effective reperfusion can reverse this adverse effect, the incidence of cardiac fibrosis is increasing. During a life span of post-MI patients, fibrotic tissue accumulates in the process of left ventricular remodeling, and expands over time to remote non-infarcted region, which significantly alters cardiac structure and deteriorates cardiac function (Gil et al., 2022). Many patients survive with long-term adverse prognosis created strain on already overstretched healthcare systems and hampered medical management.

Abundant interstitial and perivascular fibroblasts in the adult heart play an essential role in maladaptive repair and fibrosis. Resident cardiac fibroblasts (CFs) are considered the primary cells that maintain ECM homeostasis by overseeing its quantity and quality, even if

they are activated by pathological signals. To prevent the catastrophic outcomes of MI, CFs and myofibroblasts (MFs) deposit ECM to replace necrotic CMs and maintain the structural integrity of the heart coming along with viable CMs hypertrophy, whereas excessive ECM accumulation forms a fibrotic scar that provokes cardiac dysfunction and lethal arrhythmias (Burke et al., 2021a). Moreover, cardiac systolic dysfunction can be induced *via* scar with low tensile strength after disordered healing, while diastolic dysfunction increases after excessively fibrogenic activation and collagen deposition (Venugopal et al., 2022). Unfortunately, interventions for post-MI fibrotic remodeling have been limited.

With the limitation of therapeutic effects of drugs and surgeries, cardiac fibrosis is normally in MI patients. Despite various studies now addressing myocardial fibrosis, the understanding of its pathogenesis, clinical implications, and managements remains limited.

2 Pathophysiology of post-MI cardiac fibrosis

Fibrosis is a crucial determinant of cardiac function, stiffness, and conduction, with cardiac elasticity and compliance decreasing as fibrosis increases, contributing to systolic and diastolic dysfunction and even lethal arrhythmia and impairment of oxygen utilization (Fan et al., 2012). Thereby, it is very important to note that the complex pathophysiology and multiple mechanisms have been implicated in the fibrotic process following AMI. Also, the related molecular signaling network is complex and sophisticated, which involves various inflammatory mediators, inflammatory cells, and activating stromal fibrogenic effector cells, such as fibroblasts (Rockey et al., 2015). Additionally, the cardiac stromal cells exert profibrotic action *via* secreting cardiokines, which can predict adverse fibrotic remodeling after MI. (Masurkar et al., 2023).

The post-MI remodeling has three phases: the inflammatory phase (the first 3 days), proliferative phase (3–14days), and maturation phase (2weeks–2months) accompanying the dilation of non-infarcted zone, hypertrophy of CMs, and phenotypic transformation of CFs (Venugopal et al., 2022). During cardiac remodeling, inflammation, oxidative stress, disordered ECM, and CFs collectively cause cardiac fibrosis. According to the features and location of ECM protein deposition, there are usually two species of post-MI fibrosis: reparative and reactive fibrosis, with the former directly replacing necrotic cardiac tissue after MI and the latter being the pathological consequence of over-activated CFs and including perivascular and interstitial fibrosis (de Boer et al., 2019). Since adverse events and mortality are regarded as being related to the severity of cardiac fibrosis (Benjamin et al., 2018), uncovering these mechanisms is critical to help source novel therapeutic targets, diagnostic or prognostic performance.

2.1 Fibroblasts and myofibroblasts

Noteworthily, there are relatively static CFs and no MFs in a healthy heart (Hall et al., 2021). Recent single-cell multi-omics studies have elevated our knowledge of CFs in cardiac fibrosis (Forte et al., 2021a). For example, new CFs have been found, presenting as early as 1 day after MI (Shi et al., 2021), which can promote inflammation and recruit leukocytes. Then, CFs transfer to a proliferative, reparative, and proangiogenic phenotype, with maximum proliferation within 2–4 days. Moreover, the DNA damage response-associated CFs are up-regulated from day 3 up to day 7, as well as some senescence-associated CFs at day 7, indicating that cardiac fibrosis can be limited *via* activating DNA damage response and senescence (Shibamoto et al., 2019). Finally, CFs downregulate angiogenesis and convert to MFs at week 1 (Mouton et al., 2019) under new baseline conditions that the ultimate profibrotic culprits MFs produce excessive ECM, consisting principally of collagen I and III accompanying proteoglycans and elastin fibers (Kruszewska et al., 2022). Interestingly, although collagen V is minimally expressed, its deficiency increases scar size and cardiac dysfunction in an MI mouse model (Yokota et al., 2020). Recent research also finds that CFs interact with platelet leading to the alteration of collagen composition and content, and platelets mediate the reduction of inflammation after 24 h and scar formation after 21 days post AMI (Reusswig et al., 2022).

In a fibroblast-ablated mice model, there is a pronounced downregulation of CFs and the network formed by the collagen VI, microfibrillar collagen and the basement membrane, without accompanying overtly alteration of fibrillar collagen and the ECM proteome. Surprisingly, cardiac function is better preserved after MI, which suggests that controlled fibroblast reduction may have cardioprotective and therapeutic value in heart disease (Kuwabara et al., 2022). Moreover, as the mainly producers of ECM, CFs also produce cytokines, together with macrophages (Blythe et al., 2019), while, inactivating transcription factor sex-determining region Y box nine in CFs reduces cardiac fibrosis and late inflammation (Scharf et al., 2019). Thus, it is very important to distinguish the various phenotypes and functions of CFs under different conditions through detecting the markers of CFs. For instance, a study has identified proangiogenic and fibroblast-specific protein 1 (FSP1)-positive CFs that were distinct from profibrotic MFs (Saraswati et al., 2019). Moreover, CFs with growth factor receptor platelet-derived growth factor receptor α (PDGFRα) deficiency are responsible for the 50% reduction in CFs quantity (Ivey et al., 2019), while CFs with smad3 deficiency produce a decreased level of collagen (Huang et al., 2020). Further, there are several other markers of CFs, such as vimentin, transcription factor Tcf21, and MEFSK4 (mouse embryonic fibroblasts) (Venugopal et al., 2022). However, except for Tcf21 and PDGFRα, these markers are insufficiently sensitive and due to a lack of specific features (Acharya et al., 2012; Alex et al., 2022).

MFs have the specific markers as well, such as periostin and α-smooth muscle actin (α-SMA) (Kanisicak et al., 2016; Venugopal et al., 2022). In addition, after 1 week of MI, MFs increase in number and express periostin, collagen triple helix repeat containing 1, and dimethylarginine dimethylaminohydrolase 1, while the last is also expressed in activated CFs (Zhuang et al., 2020). Further, MFs are heterogeneous, i.e., they have different phenotypes; for instance, some are proliferating cells, and others express different levels of transforming growth factor β1 (TGF-β1), thrombospondin 4, and periostin (Farbehi et al., 2019).

There is, therefore, a clear and pressing need to identify additional novel mediators of cardiac fibrosis presentation and progression in response to pathological stimuli to facilitate the development of alternative therapeutic strategies targeting cardiac fibrosis.

During the process of cardiac fibrosis, CFs and CF-to-MF transformation are pathologically activated by many damage stimuli, such as TGF-β, platelet-derived growth factor (PDGF), epidermal growth factor (EGF), fibroblast growth factor (FGF), tumor necrosis factor α (TNF-α), angiotensin II (Ang II), interleukin-1 (IL-1), IL-4, and aldosterone (Fan et al., 2012). Recent research finds G-protein-coupled receptor kinase (GRK)-5 regulates fibroblast activation *in vitro* and *in vivo*, which suggests the inhibitor of GRK5 may be a novel target (Eguchi et al., 2021).

2.2 Extracellular matrix

In the working hearts, the relative glide movement of CMs and blood flow generates shear forces, constituting mechanical force with stretch and strain constrains, which is an important regulator of cells activation in fibrosis. ECM provides the heart with a structural scaffold and interacts with cells *via* adhesion molecules, such as integrins and cadherins, and distributes mechanical force through the cardiac tissue to individual cell (Souders et al., 2009; Zheng et al., 2016). In brief, collagen binding is responsible for load transfer and unnormal stretching limitation (Weber et al., 1994), which suggests the amount, distribution, and organization of ECM components modulate cardiac morphology and function (Spinale, 2007; Chute et al., 2019). For example, a pure scar in a rat MI model has lower wall thickness reduction over time before and after the decellularization, indicating excess collagen deposition during scar maturation and overall stiffening (Brazile et al., 2021). Moreover, the CMs fusion significantly decreases along with massive CMs death producing space and unnormal mechanical forces, which alters activation patterns of the cells and promotes CF-to-MF transformation (Kachanova et al., 2022).

The production and degradation of ECM are commonly regulated by MFs, together with macrophages and other cell types (Yap et al., 2023), such as CFs produce matrix metalloproteinases (MMPs) degrading collagens and tissue inhibitors of MMPs (TIMPs) inducing collagen synthesis (Nikolov and Popovski, 2022). There are four major ECM-associated peptides: the N-terminal propeptide of collagen type III (PIIINP) (indicating collagen III synthesis), the C-terminal telopeptide of collagen type I (ICTP) (indicating collagen I degradation), N-terminal propeptide of collagen type I (PINP), and C-terminal propeptide of collagen type I (PICP) (both PINP and PICP indicate collagen I synthesis) (Nikolov and Popovski, 2022). A recent study finds that the single mutation of thioredoxin-interacting protein cysteine 247 reduces collagen I α1 chain in MI mice (Nakayama et al., 2021). During scar formation, optimal collagen crosslinks require disintegrin and metalloproteinases (Chute et al., 2022), whereas PXS-5153A, the lysyl oxidase-like 2/3 enzymatic inhibitor, reduces collagen crosslinking and fibrosis (Schilter et al., 2019). Additionally, anti-integrin α(v) therapy also diminishes cardiac fibrosis *via* suppressing integrin-ECM interactions and cell adhesin (Bouvet et al., 2020). Also, there are several other fibrosis-associated non-collagen components, such as osteopontin, periostin, and galectin-3 (Li et al., 2022b).

The imbalance of ECM production and degradation induces adverse cardiac remodeling and dysfunction, with the insufficient repair disrupting cardiac tissue integrity, and excessive scar diminishing therapeutic efficacy (Yap et al., 2023).

2.3 Neuroendocrine system

2.3.1 Renin-angiotensin-aldosterone system

The activation of renin-angiotensin-aldosterone system (RAAS) plays a crucial role in development and progression of MI (Shigemura et al., 2019), having independently association with a higher risk of adverse cardiovascular events and mortality (Ivanes et al., 2012). After MI, the cardiac overload causes chamber dilation and elevates cardiac wall stress, followed by activating RAAS and inflammation response, which promotes the formation of MFs and excessive fibrosis (Fan and Guan, 2016; Zhou et al., 2019).

The essential process of RAAS is activated as described below. As the initial and rate-limiting step of the classical RAAS, renin is an aspartyl protease mainly produced by the juxtaglomerular cells of the renal afferent arteriole (Shigemura et al., 2019). Its plasma activity is associated with greater burden of coronary artery disease (Unkart et al., 2020). The synthesis and release of renin are stimulated by three major mechanisms: the decrease of sodium chloride concentration in the macula dense and perfusion pressure as sensed by renal baroreceptors; and the activation of β-adrenergic receptors in juxtaglomerular cells by catecholamines (Gomez and Sequeira-Lopez, 2018).

The liver produces angiotensinogen in the circulation, which is then activated by renin in juxtaglomerular cells to generate inactive angiotensin I (Ang I) (AlQudah et al., 2020). Subsequently, angiotensin-converting enzyme (ACE) converts Ang I into biologically active octapeptide Ang II (AlQudah et al., 2020), which is degraded to angiotensin III and several other angiotensins (Boorsma et al., 2021). For example, Ang II can be converted to angiotensin (1–7) *via* ACE2 with subsequently activating Mas receptor to decrease myocardial fibrosis (Boorsma et al., 2021), alternatively converted to Ang III with binding type 1 receptor by aminopeptidase A (Boitard et al., 2019). Moreover, both Ang II and Ang (1–7) are cleaved enzymatically to Ang (3–7) and Ang (5–7) *via* fibroblast growth factor-23 (FGF-23) stimulating dipeptidyl peptidase 3, with countering the therapeutic benefits from angiotensin-converting enzyme inhibitors (ACEI) and angiotensin receptor blockers (ARB) binding Mas receptor, which can be suppressed *via* the specific dipeptidyl peptidase three antibody procizumab (Boorsma et al., 2021). Interestingly, Ang II stimulates osteopontin synthesis and increases the concentrations of FGF-23 to negatively regulate ACE2 concentrations (Boorsma et al., 2021). As the main RAAS effector peptide, Ang II usually has 2 G protein-coupled receptors (GPCRs): type 1 Ang II receptor (AT1R) and the type 2 receptor (AT2R) (Pugliese et al., 2020), with the activation of the former increasing proinflammatory response and aldosterone levels, and the later having anti-fibrotic and anti-inflammatory effects (Ziaja et al., 2021). At the meantime, Ang II causes CMs hypertrophy, CFs hyperplasia (Leancă et al., 2022), and the secretion of molecular mediators (e.g., norepinephrine and

endothelin) to promote cardiac remodeling (Williams, 2001; Gajarsa and Kloner, 2011). For example, endothelin 1 (ET-1), a potent vasoconstrictor peptide, promotes inflammatory and CMs hypertrophy to cause adverse remodeling (Zhang et al., 2019a; Haryono et al., 2022). Interestingly, alamandine, a substance with only one amino acid residue difference from Ang II, alleviates cardiac dysfunction and fibrosis *via* inhibiting oxidative stress *in vivo* and vitro models (Zhao et al., 2022a). In addition, the upregulation of left ventricle voltage-dependent anion channel one in MI patients is regulated *via* the RAAS activation, and inhibition of the anion channel reduces atrial fibrosis (Klapper-Goldstein et al., 2020).

The regulation of RAAS is relative with multiple signaling pathways (e.g., extracellular signal-regulated kinase (ERK) and janus kinase (JAK) pathways) (Chen et al., 2020b); for instance, RAAS promotes collagen secretion *via* TGF-β1/smad2/3 pathway (Li et al., 2022b). Moreover, microRNA (miRNA) can also regulate RAAS, such as miR-181/Adamts1/neutrophil gelatinase-associated lipocalin pathway (Garg et al., 2020). Further, Ang II promotes CFs viability, activation, and migration through the circCELF1/miR-636/dickkopf WNT signaling pathway inhibitor 2 pathway in AMI mice (Li et al., 2022g).

2.3.2 Sympathetic nervous system

After AMI, sympathetic nervous system (SNS) is activated immediately as a compensatory mechanism to increase cardiac output and maintain blood pressure. The norepinephrine is primarily synthesized and secreted from adrenal medulla and is modulated through β-adrenergic receptors (β-ARs) on the heart (Lymperopoulos et al., 2007).

The heart expresses various ARs belonging to GPCRs that the most predominant subtype belongs to β1-AR, 15% to β2-AR, and the remainder to β3-AR and α1-AR. Briefly, β-ARs regulate cardiac function *via* impacting myocardial contractility (Tanner et al., 2021), such as β1-AR and β2-AR with chronotropic and ionotropic effects, contrarily β3-AR with negative inotropic properties (Yoshikawa et al., 1996; Capote et al., 2015; Lymperopoulos, 2018). Noteworthily, the β2-AR, not the β1-AR, is the predominant subtype in the non-cardiocytes (e.g., fibroblasts, endothelial cells, immune cells) (Lymperopoulos et al., 2021). For example, CMs death, hypertrophy, and cardiac fibrosis are decreased in β2-AR knockout bone marrow transplantation mice following isoproterenol treatment, which suggests β2-AR expresses in the heart's immune cells (Atsuki et al., 2019; Tanner et al., 2021). As a GPCR, β2-AR couples to both Gs and Gi proteins, and the β2-AR-stimulated cardioprotective Gi signaling depends on the heterodimerization of β2-ARs and 5-hydroxytryptamine receptors 2B (Song et al., 2021c).

Recent years, β3-AR has become a therapeutic target for cardiac fibrosis. Mechanistically, the reduced reactive oxygen species (ROS) levels following β3-AR activation attenuate fibrosis through reduced release of paracrine profibrotic agents in β3-AR expressing myocytes. Moreover, β3-AR/protein kinase G (PKG) signaling emerged as a promising therapeutic target in heart failure with preserved ejection fraction (HFpEF). Diastolic dysfunction in patients with HFpEF mainly results from the combination of increased cardiomyocyte stiffness with left ventricle (LV) hypertrophic remodeling and interstitial fibrosis. Cardiomyocyte stiffness results from both increased myofilaments Ca^{2+} sensitivity and higher titin stiffness, related to reduced PKG activity in the myocardium of HFpEF patients and subsequent lower phosphorylation of these targets. Therefore, β3-AR stimulation, by improving nitric oxide synthase (NOS)/PKG signaling, should restore the phosphorylation of sarcomeric proteins but also improve the regulation of Ca^{2+} handling for cardiac myocytes relaxation (Michel et al., 2020). For example, treatment with β3-AR agonists can potentially address this because they stimulate cardiac myocyte Na^{+}/K^{+}-ATPase. This occurs *via* downstream activation of cyclic guanosine monophosphate-dependent signaling pathways which the β3-AR has in common with NO donors, GC-1 activators15 and the angiotensin receptor-neprilysin inhibitor (ARNI) (Bundgaard et al., 2022).

After MI, upregulated SNS activity induces hematopoietic stem and progenitor cells proliferation and release in the bone marrow. In the early stage, sympathetic overdrive activates apoptotic pathway and promotes neutrophil influx in the necrotic area and infarct expansion (Amin et al., 2011). Subsequently, the stimulation of β1-AR promotes CMs hypertrophy and renin release (Gajarsa and Kloner, 2011). In MI mice, exchange protein activated by cyclic-adenosine, which could be upregulated by β-AR activation, prevents left atrial fibrosis (Surinkaew et al., 2019), while β-AR mainly modulates collagen production by CFs and causes proliferation of human CFs and fibrotic remodeling (Turner et al., 2003; Humeres and Frangogiannis, 2019). Further, β2-AR upregulates CFs proliferation *via* the secretion of IL-6, depending on Gαs/ERK1/2 (Tanner et al., 2020). To sum up, the regulation of sympathetic neurohormone expression is a key therapeutic option in attenuating cardiac remodeling.

2.3.3 Natriuretic peptides

Natriuretic peptides (NPs), primarily as endocrine hormones, are secreted by atrial and ventricular CMs under upregulated wall stress and stretching in MI and regulate diuresis, natriuresis, and vasodilation, as well as inhibit SNS, RAAS, and ET-1 (Kuhn, 2016). NPs have three isoforms: A-type NP (ANP, which inhibits collagen synthesis and is a main fibrotic driver), B-type NP (BNP; a prognosis predictor after MI), and C-type NP (CNP) (Kangawa et al., 1984; Kuhn, 2016). NPs have anti-apoptotic, anti-inflammatory, and anti-fibrotic effects to prevent myocardial ischemic reperfusion injury (MIRI) and adverse remodeling, with their concentrations reflecting profibrotic environments and identifying patients at risk for remodeling, while ANP and BNP reduce vasoconstriction, CFs proliferation, CF-to-MF transformation, collagen synthesis, and MMP release by activating the cyclic guanosine monophosphate (cGMP) pathway (Goetze et al., 2020). The inhibition of phosphodiesterase-9 activity dose-dependently increases cGMP and the cGMP/NP ratio of plasma and urinary, which suggests that its inhibition may constitute a novel therapeutic approach in clinical HF. (Scott et al., 2019).

2.4 Immunity

The immune system plays an important role in maintaining homeostasis after MI, in which dying CMs release many damage-associated molecular patterns (DAMPs) and activate the cascade of

inflammatory mediators (e.g., inflammatory cytokines and chemokines) (Simões and Riley, 2022). Noteworthily, the severity of inflammatory responses dictates the degree of MI (Ong et al., 2018). Thus, it is important to strike an appropriate balance between inflammatory and anti-inflammatory response, and timely regulate inflammatory signals during cardiac remodeling (Yap et al., 2023). After MI, immune response is rapidly initiated *via* mobilizing distinct immune cell populations (Yap et al., 2023). The differentially altering immune cells infiltration affects cardiac fibrosis, for instance, allografts suppression of tumorigenicity 2 (ST-2) deficiency reduces infiltration of F4/80 (+) macrophages, CD3 (+) T cells and CD20 (+) B cells and thus alleviates vascular occlusion and fibrosis of allografts (Zhang et al., 2021e). In this section, we focus on different immune cell populations, cytokines, chemokines and growth factors to improve mechanistic understanding of immune responses. Then, later on in this article, we will focus in particular on preventing fibrosis with immune treatment. In what follows, we first describe the key features of different immune cells.

2.4.1 Neutrophils and macrophages

As the most abundant peripheral blood granulocytes, neutrophils constitute 50%–70% of the total amount of blood granulocytes in most mammals and 20%–30% in mice (Mestas and Hughes, 2004) in a physiologically circadian pattern (Aziz et al., 2021), exiting blood with night-time peaking (fresh neutrophils) and day-time peaking (aged neutrophils) (Adrover et al., 2019). Recent studies have shown that neutrophils modulate cardiac remodeling *via* the initiation and termination of an inflammatory response and largely infiltrate the infarct zone 1 day after MI and the peri-infarct zone 4 weeks after MI, with disturbed circadian rhythm, in mice (Zhong et al., 2022). However, neutrophil-mediated MIRI is limited by selectin-targeting glycosaminoglycan-peptide conjugate (Dehghani et al., 2022). Normally, massive leucocytes remain in the bone marrow, and only a low number of leucocytes stay in the circulation, whereas 2-arachidonoylglycerol induces massive cardiac infiltration by neutrophils and monocytes and increases cardiac dysfunction and fibrosis in a MIRI mouse model (Schloss et al., 2019). In MI patients, immature $CD10^{neg}$ neutrophils and $CD14+HLA\text{-}DR^{neg/low}$ monocytes increase in number (Fraccarollo et al., 2021), and there are still around 10-fold more leukocytes in the scar than in remote zone at 6 weeks after MI in mice (Scharf et al., 2019).

Recent evidence has associated monocytes/macrophages with the etiopathology of cardiac fibrosis, and the interventions targeting these cells have been challenging due to the heterogeneity and the antagonizing roles of different subtypes (Chen et al., 2022b). Remarkably, as the largest population of immune cells, macrophages can be classified into two general subtypes based on cell surface with or without C-C chemokine receptor 2 (CCR2): monocyte-derived CCR2+ macrophages, and yolk-sac-derived CCR2– macrophages. The former exerts pro-inflammatory effects and recruits monocytes, whereas the latter is considered to prevent excessive inflammation (Dick et al., 2019; Yap et al., 2023). At the meantime, macrophages also can be classified as classically activated (M1) or alternatively activated (M2) based on stimulatory environment. M1 macrophages degrade ECM and clear cell debris, and M2 macrophages promote angiogenesis and collagen deposition (Yang et al., 2021b). Further, M2b macrophages promote lymphangiogenesis to reduce myocardial fibrosis and cardiac dysfunction (Wang et al., 2022b). At the early stage following MI, macrophages and monocytes are almost exclusively derived from haematopoietic stem cells or extramedullary splenic reservoirs. They usually infiltrate the infarct area with pro-inflammatory phenotypes (Halade et al., 2018; Bajpai et al., 2019; Yap et al., 2023). Neonatally activated macrophages modulate angiogenesis, inflammation, and CMs proliferation, which is contrary to adult macrophages with different metabolites of oxygenation and nutrients (Lantz et al., 2021).

Herein, we describe the process of immune response after MI based on recent literature. At the beginning, these immune cells accumulate within hours, known as the inflammatory phase, and the peak recruitment of these immune cells occurs approximately 3 days after MI (Yap et al., 2023). Neutrophils are firstly recruited after MI and then phagocytized by proinflammatory CCR2+ $Ly6C^{high}$ monocyte-derived macrophages with the replacement of some CCR2(-) resident macrophages, which increase anti-inflammatory and profibrotic cytokines (e.g., IL-10 and TGF-β) and decrease proinflammatory cytokines (e.g., IL-1β and TNFα) (Simões and Riley, 2022). Concurrently, macrophages phagocytize dead cells, and anti-inflammatory T cells (e.g., regulatory T cells/Tregs) are recruited (Dobaczewski et al., 2010; Hofmann and Frantz, 2015). After 1–2 days of MI, the anti-inflammatory phase (also known as proliferative phase) ensues, in which the macrophages undergo rapid proliferation with anti-inflammatory or reparative properties (Dick et al., 2019). At this stage, cytokines also promote CF-to-MF transformation. Briefly, the resolution of inflammation and reparative tissue remodeling are initiated. Further, the recovery phase follows after 3–7 days of MI, MFs and CCR2+ macrophages mediate fibrosis and scar formation (Yap et al., 2023). Moreover, the macrophages subsequently transform into reparative CCR2+ $Ly6C^{low}$ macrophages *via* the transcriptional program dependent on a nuclear receptor subfamily four group A member 1, which promotes fibrotic scar formation *via* collagen deposition and MFs transformation (Simões and Riley, 2022). Additionally, histamine deficiency promotes monocyte/macrophage-to-MF transformation in MI-induced cardiac fibrosis (Zhu et al., 2022). In contrast, specifically marked Gata6(+) pericardial macrophages accumulate on the cardiac surface after MI and prevent fibrosis (Jin et al., 2022).

2.4.2 Other immune cells

Due to the regulative functions of immunity, it presents an intriguing direction for therapeutic intervention about cardiac fibrosis. Therefore, it is very important to comprehensively understand phenotypes and behaviours of different immune cells after MI.

Currently, there are also the up-to-date knowledge about other immune cells, such as B cells, T cells, and eosinophils. For example, B cells infiltrate into damaged myocardium within 1–7 days (Adamo et al., 2020), and B cells deficiency downregulates cytokines (e.g., TNF-α, IL-1β, IL-6, and TGF-1β) and collagen synthesis to alleviate fibrosis after MI (Mo et al., 2021). Additionally, MMP-2 increases the cytotoxicity of $CD8^+$ T cells in acute MI patients (Li et al., 2021g). Cross-priming dendritic cells activate cytotoxic $CD8^+$ T cells to exacerbate

inflammatory damage and fibrosis (Forte et al., 2021b). Moreover, OSU-ERb-012, an estrogen receptor-β agonist, inhibits $CD4^+$ T cells and improves cardiac remodeling in the MI-induced HF mouse model (Rosenzweig et al., 2022). Tregs promote $Ly6C^{high}$ monocyte conversion into M2 macrophages by secreting cytokines (e.g., IL-10, IL-13, and TGF-β) to initiate the anti-inflammatory or regenerative phase (Kino et al., 2020).

Furthermore, Tregs can directly regulate CFs (Kino et al., 2020). Eosinophils are increased in the blood and heart (mostly in the infarct area) in MI patients and mice, and eosinophil depletion promotes cardiac dysfunction and fibrosis (Liu et al., 2020a).

2.4.3 Cytokines

Massive researches have demonstrated the role of cytokines in MI that cytokines not only form a complex network to regulate inflammatory response, but also can form cytokine storm to worse myocardium injure following cardiac decompensation (He et al., 2022). Upon cardiac injury, the inflammatory signaling molecules immediately increased.

DAMPs bind toll-like receptors (TLRs), activate inflammasomes (e.g., nod-like receptor protein 3 (NLRP3)), and promote cytokines/chemokines synthesis to induce activation and recruitment of immune cells and engage immune defenses (Schroder and Tschopp, 2010). Most commonly, IL-1 family includes pro-inflammatory and anti-inflammatory members. For example, IL-1α reduces the remodeling in border zone CFs by upregulating steroidogenic acute regulatory protein (Razin et al., 2021). Moreover, IL-33 mediates the shift in the inflammatory phase toward its resolution through IL-1R4 (Fearon and Fearon, 2008). MFs with physiological stretching release IL-33 to bind the ST-2 receptor on the CMs membrane to promote cell survival and integrity (Vianello et al., 2019), whereas IL-33 worsens cardiac remodeling by recruiting eosinophils (Ghali et al., 2020). In a myeloid IL-4 receptor-α deficiency model, insufficient fibrotic remodeling is induced *via* downregulated TIMPs and collagen I deposition (Song et al., 2021a; Song et al., 2021b). IL-21 induces apoptosis of $Ly6C^{low}$ macrophages and prevents cardiac repair (Kubota et al., 2021). Furthermore, IL-38 influences dendritic cells to reduce inflammation and fibrosis (Wei et al., 2020).

2.4.4 Chemokines

Extensive evidence also implicates chemokines in the pathogenesis of cardiac fibrosis. Chemokines are key regulators controlling the migration and positioning of immune cells, and various cells proliferation to promote structural remodeling and functional recovery of the heart with inflammation quickly subsiding (Frangogiannis, 2014; Ma, 2021). However, persistent cytokines induce late cardiac contractility and adverse outcome (Wang et al., 2018). In the affected myocardium and heart-draining lymph nodes, MI induces complementary B-cell responses, while B cells infiltrate the infarct zone *via* the CXC-motif chemokine ligand 13 (CXCL13, the ligand of CXCR5-CXC-chemokine receptor type 5 (CXCR5)) axis and induce TGF-β1 expression (Heinrichs et al., 2021). CXCL8 induces neutrophil infiltration, whereas CC chemokines, such as chemokine CC-motif ligand 2 (CCL2), mediate the recruitment of mononuclear cells (Chen and Frangogiannis, 2021). In addition, CCL2, also known as monocyte chemoattractant protein-1 (MCP-1), has a higher serum level in ST-segment elevation myocardial infarction (STEMI) patients, but lower plasma levels in MI patients without collateral circulation (Kobusiak-Prokopowicz et al., 2007; Sahinarslan et al., 2010). Furthermore, CXCL10 and CXCL12 have leukocyte-independent mediatory effects, directly modulating CFs (Chen and Frangogiannis, 2021). Additionally, single-cell sequencing has found different immune cell abundance (resting and activated mast cells, activated CD4 memory T cells) and high expression of chemokines in MI patients (CCL3, CXCL3, CXCL8, and CXCL16 in CD1C-CD141-dendritic cells and CCL4 and CCL5 in natural killer cells) (Zhou et al., 2022).

2.4.5 Growth factors

To explore novel treatments targeting cardiac fibrosis, it is very important to identify and elucidate precise mechanisms of growth factors, such as PDGF, FGF, and TGF have been best studied.

The PDGF family is composed of cell division stimulators and has five subunits (PDGF-AA, PDGF-BB, PDGF-AB, PDGF-CC and PDGF-DD), as well as two receptors, PDGFRα and PDGFRβ. All PDGF members have been shown to play a role in cardiac fibrosis (Bertaud et al., 2023). For example, overexpression of PDGF-A modulates scar content, reduces scar size, and increases capillary and arteriolar density in the infarct border zone (Rashid et al., 2021), whereas PDGF-AB enhances angiogenesis and increases scar anisotropy (high fiber alignment) without affecting overall scar size or stiffness (Thavapalachandran et al., 2020).

The FGF family has 22 members and pleiotropic effects (Bertaud et al., 2023). For example, FGF21 inhibits inflammation and fibrosis by downregulating early growth response protein 1 (Li et al., 2021c; Li et al., 2021d). Additionally, FGF12 overexpression decreases collagen I and III and fibronectin in Ang II-induced CFs (Liu et al., 2022). FGF10 increases cardiomyocyte renewal and limits fibrosis to promote cardiac regeneration and repair, which suggests FGF10 may be a clinically relevant target for heart repair (Hubert et al., 2022). Conversely, FGF23 increases myocardial fibrosis and dysfunction *via* activating β-catenin and promoting the pro-fibrotic crosstalk between CMs and CFs in a paracrine manner (Hao et al., 2016; Leifheit-Nestler et al., 2018).

There are also other growth factors involved in cardiac fibrosis, such as neuregulin-1, a paracrine growth factor secreted by cardiac endothelial cells, modulates hypertrophic and fibrotic processes during early cardiac remodeling *via* the neuregulin-1/erythroblastic leukemia viral oncogene homolog (ERBB) four axis (Dugaucquier et al., 2020).

In this section, we mainly focus on the multifaceted contributions of diverse immune cells populations and mediators after MI. As immunity affecting the prognosis of MI patients has become an area of substantial therapeutic interest, we discuss novel interventions regarding immunity in a later section.

2.5 Molecular mechanisms

Many mechanisms (e.g., oxidative stress, inflammation, and mechanical stress) are known to affect cardiac fibrosis. Additionally, a large amount of antifibrotic therapy researches targeting underlying molecular mechanisms have been

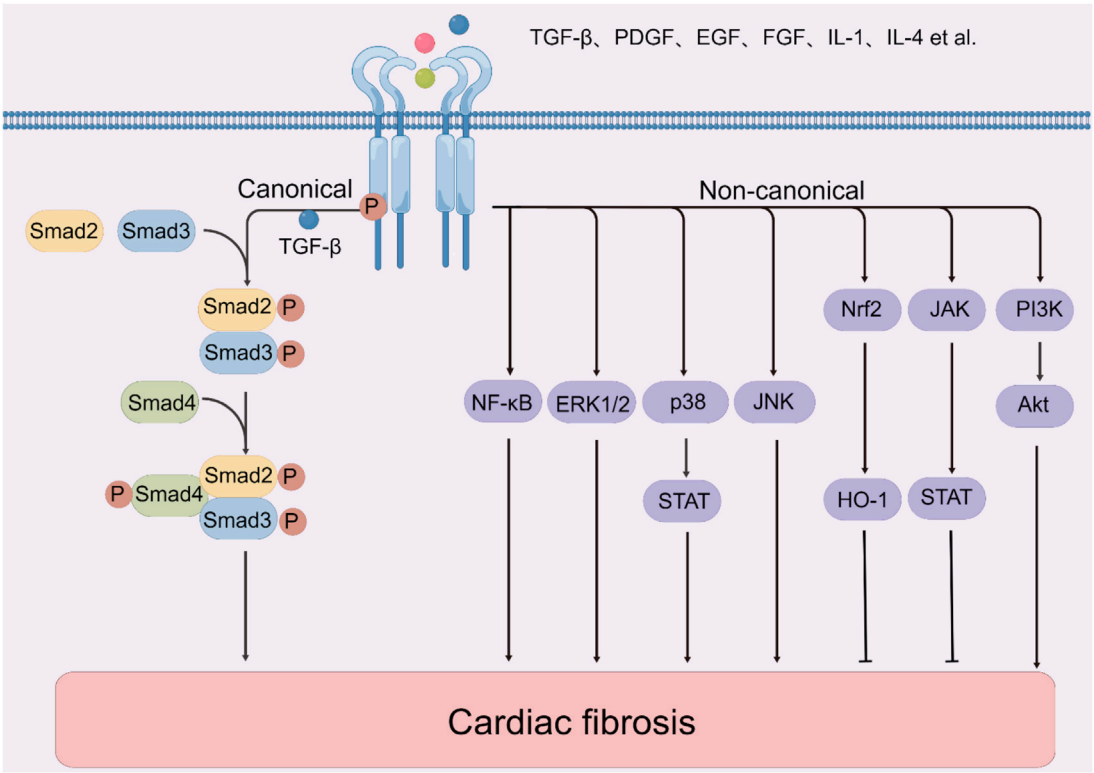


FIGURE 1
The molecular mechanisms of cardiac fibrosis. Note: Akt, protein kinase B; EGF, epidermal growth factor; ERK, extracellular signal-regulated kinase; FGF, fibroblast growth factor; HO-1, heme oxygenase-1; IL-1, interleukin-1; IL-4, interleukin-4; JAK, janus kinase; JNK, c-Jun N-terminal kinase; NF-κB, nuclear factor kappa-B; PDGF, platelet-derived growth factor; PI3K, phosphatidylinositol 3-kinase; STAT, signal transducer and activator of transcription 3; TGF-β, transforming growth factor β.

implemented with technological advancement (Figure 1) (The figure is drawn by figdraw). Due to the various signaling pathways involved in the process, an understanding of the precise mechanisms of cardiac fibrosis is still limited. From this viewpoint, it is essential to summarize and comprehend current evidence of cell signaling pathways associated with cardiac fibrosis. Hence, in the following sections, we summarize the recent data about the roles and crucial functions of several key signaling pathways in post-MI fibrosis: TGF-β, phosphatidylinositol 3-kinase (PI3K)/protein kinase B (Akt), nuclear factor erythroid 2-related factor 2 (Nrf2), mitogen-activated protein kinase (MAPK) and other molecular mechanisms. The molecularly targeted drugs may further decline the death rate of MI. Herein, it is indispensable and promising to target these aberrant signaling pathways and improve the pathological manifestations in post-MI fibrosis.

2.5.1 TGF-β signaling pathway

TGF-β is the most typical cytokine regulating fibrosis and inducing collagen synthesis, which is secreted by macrophages into the ECM in an inactive form (pro-TGF-β) and then activated by proteases (e.g., plasmin, MMP-2, MMP-9, and ROS) (Takawale et al., 2015; Hata and Chen, 2016). Firstly, it binds TGF-β receptor(TGFβR)II, and then TGFβRI is phosphorylated and forms a receptor heterocomplex to react with smads protein. Bruton's tyrosine kinase is up-regulated in MI, with directly binding and phosphorylating TGFβRI at tyrosine 182, and then activating the downstream to promote CF-to-MF transformation and the excessive ECM gene expression. And its second-generation inhibitor Acalabrutinib attenuates cardiac fibrosis (Wang et al., 2022a). Smads proteins have three types: receptor-regulated smad (smad1, smad2, smad3, smad5, and smad8), common smad (smad4), and inhibitory smad (smad6 and smad7). The TGF-β complex binds to R-smads (smad2 and smad3) and Co-smads (smad4), and then transfers into nucleus to regulate the transcription of target genes (Zhang et al., 2022c). The smad-dependent canonical pathway, coordinating with non-canonical pathways, transduces TGF-β signals (Zhang et al., 2022f).

TGF-β, as a critical molecule of MFs, promotes collagen synthesis, CF-to-MF transformation, and other fibrotic factors production, as well as activates multiple signaling pathways (Li et al., 2022b), while CFs and inflammatory cells express cystine knot protein gremlin-1 colocalizing with TGF-β and reduce collagen deposition (Müller et al., 2021). Further, TGF-β1 can activate CFs to increase collagen deposition, and sustained TGF-β1 expression subsequently leads to cardiac dysfunction (Xue et al., 2019). Moreover, TGF-β1 regulates ECM remodeling by promoting MMP/TIMP imbalance (Hodges et al., 2019). Additionally, a study has found that TGF-β3 expression gradually attained its peak in 1 month after MI with an opposite expression trend of TGF-β1 and

TGF-β2 in MI patients, while TGF-β3 downregulated proliferation, migration, and collagen synthesis and upregulated lysyl oxidase and osteopontin in Ang II-induced human CFs and MI patients by promoting smad7 expression (Xue et al., 2019). The recombinant osteopontin activates cell-cycle re-entry in CMs, stimulates multiple cardiac cells, and improves scar formation, LV remodeling, and regional and global function after MI (Rotem et al., 2022).

Even if TGF-β2 and TGF-β3 are involved in cardiac fibrosis, the fibrotic effects triggered by the TGF-β family have primarily been attributed to TGF-β1 (Dewald et al., 2004). For example, phosphoglycerate mutase one deficiency suppresses inflammation, apoptosis, and fibrosis in post-MI by targeting TGF-β1 (Wu et al., 2021c). High serum tissue non-specific alkaline phosphatase (TNAP) level in MI patients can serve as a fibrotic biomarker and is positively correlated with mortality risk (Cheng et al., 2021), while TNAP inhibition provokes an antifibrotic effect through adenosine monophosphate-activated protein kinase (AMPK)/TGF-β1/smads and p53 (Gao et al., 2020b). Two inhibitory smads (smad6 and smad7) can prevent R-smad phosphorylation (Bertaud et al., 2023). Further, smad7 also restrains MFs activation by suppressing profibrotic ERBB2 in a TGF-β-independent manner (Humeres et al., 2022) but does not restrain the anti-inflammatory function of TGF-β in macrophages (Li et al., 2022d). Another member of the TGF-β superfamily, lefty1 alleviates post-MI CFs proliferation, differentiation, and secretion by suppressing the p-smad2 and p-ERK1/2 axis (Li et al., 2021a). Moreover, SH2 domain-containing protein tyrosine phosphatase-2 inhibits fibrosis *via* the ERK/smad pathway (Lu et al., 2021). Chordin-like one inhibits extracellular bone morphogenetic protein 4 (BMP4) to inhibit smad1/5/8 activation and autophagy in CMs and suppresses TGF-β1-induced fibrosis and CF-to-MF transformation (Ruozi et al., 2022).

Noteworthily, many non-coding miRNAs have been reported to be involved in cardiac fibrosis *via* regulating TGF-β signaling pathway (Zhao et al., 2022b). In this section, we summarize recent studies focusing on this pathway. Briefly, post-MI repair requires tight regulation of the TGF-β signaling pathway in case of excessive fibrosis and adverse remodeling leading to heart failure.

2.5.2 PI3K/Akt signaling pathway

The PI3K/Akt/protein kinase B signaling pathway is one of the important intracellular signal transduction pathways. PI3K converts phosphatidylinositol 4,5-bisphosphate (PIP2) into phosphatidylinositol 3,4,5-trisphosphate (PIP3). Then PIP3 binds to the pleckstrin homology domain of Akt to alter its conformation and activate the downstream molecules, such as vascular endothelial growth factor (VEGF), endothelial nitric oxide synthase, while inhibiting mammalian target of rapamycin (mTOR) complex 1, glycogen synthase kinase 3β, forkhead box subfamily O, respectively (Zhang et al., 2022c). In recent years, basic research finds that targeting PI3K/Akt pathway is a beneficial signaling mechanism for anti-fibrotic treatments following AMI regulating cell proliferation, differentiation, migration and apoptosis. For example, Apelin-13 inhibits the PI3K/Akt axis to attenuate fibrosis in HF rats and AngII-induced CFs (Zhong et al., 2020). Further, visceral adipose tissue-derived serine protease inhibitor vaspin alleviates fibrotic remodeling and oxidative stress and decreases ANP, BNP, and collagen I and III by inhibiting the PI3K/Akt axis (Ji et al., 2022b). Additionally, inhibition of calcium and integrin binding protein one reduces cardiac fibrosis and levels of α-SMA, vimentin, and collagen I and III by inhibiting the PI3K/Akt pathway (Hu et al., 2022a). Since an essential requirement for the post-MI repair is recovering the capillary network in the injured area due to new vessel sprouting from existing ones (Gao et al., 2020a), transcription factor Yin-Yang one represses CMs apoptosis and fibrosis and promotes angiogenesis by enhancing Akt phosphorylation and increasing VEGF (Huang et al., 2021). The lysyl oxidase-like protein two increases MFs transformation, collagen fiber production and mechanical strength *via* the PI3K/Akt/mTOR pathway (Yang et al., 2016). By contrast, ivabradine prevents fibrosis and cardiac hypertrophy *via* suppressing PI3K/Akt/mTOR/p70S6K signaling (Yu et al., 2019; Dai et al., 2021). Klotho significantly reduces cardiac fibrosis and suppresses myocardial inflammation and apoptosis in MI-induced HF model *via* inducing autophagy through the inhibition of PI3k/Akt/mTOR signaling pathway (Wang et al., 2022d).

2.5.3 Nrf2 signaling pathway

As a transcription factor and the product of the nuclear factor erythroid-derived 2-like 2 gene, Nrf2 consists of seven functional domains and participates in regulating oxidative stress and antioxidant genes (Ray et al., 2012; Hayes and Dinkova-Kostova, 2014). It transfers signaling molecules to the nucleus and initiates antioxidant gene transcription (Kensler et al., 2007). And its downstream target, heme oxygenase-1 (HO-1), is a rate-limiting enzyme that catalyzes heme to biliverdin Ixα, carbon monoxide, and iron (Wu et al., 2021a). Nrf2 signaling pathway plays a crucial role in post-MI remodeling. For example, in the MI rat model and Ang II-treated CFs, ghrelin ameliorates cardiac fibrosis by activating Nrf2 to inhibit the nicotinamide adenine dinucleotide phosphate (NADPH)/ROS pathway (Wang et al., 2021c; Wang et al., 2021d). In addition, Pinocembrin ameliorates cardiac remodeling by ROS clearance and Nrf2/HO-1 pathway activation, which further suppresses collagen fibers deposition and apoptosis and promotes angiogenesis (Chen et al., 2021d). Moreover, corosolic acid regulates the AMPK-α/Nrf2/HO-1 axis to inhibit cardiac fibrosis, oxidative stress, inflammation, and apoptosis (Wang et al., 2020i). Furthermore, Nrf2 reduces innate immune response in MI mice (Bromage et al., 2022). Thus, the protective effect of Nrf2/HO-1 following AMI should not be ignored. And it constitutes an appealing target for anti-fibrotic treatments. Plantarum activates Nrf2 antioxidant defense pathway and ameliorates cardiac dysfunction and collagen expression (Aboulgheit et al., 2021).

2.5.4 MAPK signaling pathway

As a class of highly conserved serine/threonine protein kinases, MAPKs have four primary branches: ERK, c-jun N-terminal kinase (c-JNK), p38/MAPK and ERK5 (Gallo and Johnson, 2002; Cargnello and Roux, 2011). During variously physiological and pathological processes, these kinases can be sequentially activated and regulate proliferation, growth, and differentiation of cardiac cells, such as CMs, CFs, endothelial cells and macrophages (Muslin, 2008). In this section, we mainly introduce some recent studies of the MAPK pathway from the aspects of molecular regulation.

Calcium-activated chloride channels protein anoctamin-1 promotes CFs proliferation and secretion *via* the MAPK pathway

(Tian et al., 2020). The upregulation of OUT domain-containing 7B suppresses phosphorylated focal adhesion kinase and ERK/p38 activities and reduces the levels of α-SMA and collagen I (Zhang et al., 2022b), while nicotinamide riboside kinase-2 regulates the p38 pathway to alleviate post-MI scar size and fibrosis (Ahmad et al., 2020). Further, zinc finger protein ZBTB20 protects the heart by inhibiting the JNK pathway (Li et al., 2020a; Li et al., 2020b), while melatonin improves myocardial fibrosis in the infarct border zone and apoptosis *via* the JNK/p53 pathway after MI in a diabetic mouse model (Lu et al., 2020). In oxygen-glucose deprivation/reoxygenation (OGD/R)-induced H9c2 cells and myocardial fibrosis model of mice, protocatechualdehyde, a major component from Salvia miltiorrhiza, against ischemic injury by suppressing endoplasmic reticulum stress-associated protein kinase R-like endoplasmic reticulum kinase/transcription factor 6α/inositol-requiring enzyme1α pathways (Wan et al., 2021).

In short, comprehensive study and understanding the mechanism of the MAPK pathway, taking this signaling pathway as the anti-fibrotic target are the keys to address challenges of post-MI fibrosis.

2.5.5 Other molecular mechanisms

In addition to the above signaling pathways, other pathways have also been shown to be related to cardiac fibrosis. For example, ELABELA peptide increases angiogenesis and reduces cardiac interstitial fibrosis through activating ERK/hypoxia-inducible factor-1alpha/VEGF pathway in MIRI rat model (Rakhshan et al., 2022). A transcriptional complex (A-kinase anchoring protein 2, protein kinase A, and steroid receptor coactivator 3) modulates proangiogenic and antiapoptotic processes *via* protein kinase A-mediated phosphorylation and estrogen receptor α activation (Maric et al., 2021).

As a family of signal-dependent transcription factors, nuclear factor kappa B (NF-κB) is located in the cytoplasm in an inactive form, but it migrates to the nucleus following stimulation, and regulates its targets *via* binding to NF-κB response elements on the DNA (Li and Verma, 2002). As a typical pro-inflammatory signaling pathway, NF-κB regulates gene transcription and promotes inflammatory responses (He et al., 2022), for example, exendin-4 regulates the NF-κB axis to prevent inflammation and cardiac remodeling (Eid et al., 2020), and Nur77 improves cardiac fibrosis by inhibiting the NF-κB-dependent pathway (Chen et al., 2021a). Further, hippo pathways are vital mechanisms of cardiac repair. For example, hippo pathway kinases Lats1/2 inhibit yes associated protein (YAP)-induced injury response, while conditional deletion of Lats1/2 in adult resting CFs initiates CF-to-MF transformation (Xiao et al., 2019). Moreover, platelet-activating factor receptor and YAP1 are significantly increased in MI mice, accompanying with its positive feedback loop in cardiac fibrosis (Li et al., 2022f).

In addition to the common signaling pathways noted above, other recent studies of molecular mechanisms are summarized. For example, researchers have found that fibrosis is associated with calmodulin/p38/signal transducer and activator of transcription (STAT) 3, wnt/β-catenin, TLR4/calmodulin-dependent protein kinase II and B lymphoma Mo-MLV insertion region 1 homolog/p15/retinoblastoma pathways et al. (Li et al., 2020g; Han et al., 2020; Yang et al., 2021c; Fu et al., 2021; Bugg et al., 2022; Zhang et al., 2022e; Shi et al., 2022).

Crosstalk also exists in different signaling pathways; for instance, endogenous TGF-β1 repressor SKI activates the hippo pathway *via* LIM domain-containing protein one to inhibit CFs activation (Landry et al., 2021). There are some studies about ion channel; for instance, the mechanosensitive ion channel transient receptor potential vanilloid four deletion regulates CF-to-MF transformation to improve harmful remodeling after MI (Adapala et al., 2020; Adapala et al., 2021). Piezo1 activates CFs to induce MFs recruitment and excessive ECM deposit (Braidotti et al., 2022), while coronary vascular endothelial sodium channel activation promotes cardiac fibrosis and dysfunction (Hill et al., 2022). Further, embryonic CFs of mice with mitochondrial Ca^{2+} uniporter deletion are more sensitive to Ca^{2+} overload than normal CFs (Huo et al., 2020). Briefly, it is necessary to comprehensively understand the molecular mechanisms of cardiac fibrosis after MI before performing specific interventions.

To sum up, it is critical to develop and optimize therapeutic strategies according to fundamental mechanisms and pathophysiology of cardiac fibrosis. To date, research in basic science has disclosed a range of pathophysiological mechanisms of post-MI cardiac fibrosis, and many attractive inhibitors and antagonists have been developed based on the molecular mechanisms. However, a lot of them have not currently been launched in human clinical trials to advance toward clinical application, and investigations remain challenging and need to be studied further.

3 Evaluations of cardiac fibrosis

3.1 Cardiac magnetic resonance late gadolinium enhancement

Cardiac magnetic resonance (CMR) uses different sequences and modalities to assess the heart, such as extracellular volume, derived from T1-weighted imaging, examination of total interstitial space, T2 mapping and weighted imaging examination of edema, and late gadolinium enhancement (LGE) examination of scar and fibrosis (Kali et al., 2014; Gupta et al., 2021). Because extracellular space is enlarged by dead CMs and post-infarct fibrosis, CMR-LGE imaging with excessively retained gadolinium-based contrast agents represents a non-invasive standard for assessing myocardial viability and fibrosis (Holtackers et al., 2022); for instance, a subendocardial scar can be detected *via* dark-blood LGE-CMR (Holtackers et al., 2021). Feature tracking of CMR accurately quantifies cardiac strain, and a retrospective study has found that almost 75% of acute scars and 80% of subacute scars could be detected by CMR with a segmental circumferential strain of native cine sequences (Polacin et al., 2022). In the mouse MI models with monocyte populations deletion, elastin deposition, as an inflammatory response and a potential fibrotic biomarker, could be detected *via* CMR with an elastin/tropoelastin-specific contrast agent (Elkenhans et al., 2021). However, the use of CMR is limited by availability, time, cost, and severe renal insufficiency as an adverse effect of contrast administration, which can be solved by segmental peak circumferential strain calculation (Polacin et al., 2022).

Additionally, CMR screens post-MI patients at risk of ventricular tachycardia by identifying and quantifying a heterogeneous scar zone and substrate features (Merino-Caviedes et al., 2021). A case-control study has retrospectively reviewed LGE-CMR data of chronic post-MI and found that border zone channel mass was the strongest independent scar-derived variable and precision risk stratification relevant to sustained monomorphic ventricular tachycardia, while border zone channel mass was associated with the qualitative structure, heterogeneity, spatial distribution, and slow conducting channels within the scar (Jáuregui et al., 2022).

3.2 Echocardiography

Early detection of myocardial fibrosis can identify patients at risk of adverse events, which is independently associated with a measure of scar between echocardiography and defibrillator intervention (Gaibazzi et al., 2020). A large single-center clinical cohort study has found that diastolic dysfunction effectively identified mortality risk with relevance to higher incidence and extent of scar *via* echocardiography and LGE (Wang et al., 2020a; Wang et al., 2020b; Wang et al., 2020c; Wang et al., 2020d). Speckle tracking echocardiography (STE) can evaluate MI *via* end-systolic radial strain peak to reflect segmental scar with very high sensitivity and specificity, and when combined with blood pressure, non-invasive myocardial work parameters (e.g., myocardial work index, constructive work, and myocardial work efficiency) can be obtained and are significantly lower in the segment with the largest LGE than without LGE after contrasting with gadolinium (Mahdiui et al., 2021). These parameters are emerging potential markers of segmental myocardial viability, prognostic markers, and therapeutic targets in STEMI patients with primary percutaneous coronary intervention (PCI) (Mahdiui et al., 2021). Moreover, LV mechanical dispersion measured by CMR and STE is correlated with scar burden as a prognostic parameter (Holtackers et al., 2021).

3.3 Computed tomography

Cardiac computed tomography (CT) estimates the extracellular volume and macroscopic scar *via* CT delayed enhancement (CT-DE) with relatively low iodine contrast compared to CMR-LGE (Gupta et al., 2021). X-ray microCT implements quantitative 3D analysis and visualization of cardiac fibrosis in MI mice (Janbandhu et al., 2022).

3.4 Molecular imaging

CFs activation is promising for targeted therapy, which can be detected and tracked by fibroblast activation protein (FAP) imaging with novel radiotracer [68Ga]MHLL1 (Langer et al., 2021). FAP imaging has also detected activated CFs in the non-edematous and non-infarcted area in a prospective study of reperfused STEMI patients (Xie et al., 2022). Moreover, FAP-α deletion attenuates cardiac dilation in MI mice (Hoffmann et al., 2021). Additionally, a retrospective study has found a strong correlation between CFs activation volume with cardiac function and peak creatine kinase *via* 68Ga-FAP-α inhibitor positron-emission tomography (PET) (Kessler et al., 2021), while PET and single-photon emission computed tomography (SPECT) indirectly assessed cardiac fibrosis *via* myocardial perfusion imaging (Gupta et al., 2021). PET immunoimaging DOTATATE tracers can find high expression of somatostatin receptor two in M1 inflammatory macrophages (Toner et al., 2022). Multiparametric imaging characterizes the immune response transforming to tissue repair after MI (Hess et al., 2022).

3.5 Biomarkers

Rapidly advancing technologies favor post-MI fibrotic biomarkers identification, such as MMP, collagen peptides, galectin-3, and ST-2 (Bostan et al., 2020), which can be combined with MI biomarkers, such as creatine kinase-myocardial band (CK-MB), troponin, and N-terminal-pro type brain natriuretic peptides (NT-proBNP). A prospective study of 92 patients over 70 years old with MI finds that patients over 70 years old with MI and fragility have significantly higher levels of myocardial stress and fibrosis (Aidumova et al., 2022). Galectin-3, a β-galactoside-binding lectin mainly synthesized by macrophages, maintains cardiac structure and function in the early MI stage, and promotes tissue fibrosis and scar formation in the late stage (Leancă et al., 2022). The TNF-α, soluble tumour necrosis factor-α receptor-1 and 2 and oxidative stress could be considered as potential non-invasive diagnostic and therapeutic biomarkers for coronary chronic total occlusion in the oldest patients with coronary heart disease (Li et al., 2020e). Additionally, low miR-26a plasma level is highly correlated with certain markers (e.g., CK-MB and troponin I) in STEMI patients (Chiang et al., 2020), and immunoreactivity of Nε-(carboxymethyl)lysine is positively correlated with NT-proBNP and cardiac fibrosis (Nogami et al., 2020). Furthermore, abnormal myocardial collagen I and III release certain peptides in the circulation as fibrotic markers (Nikolov and Popovski, 2022), such as PICP and PIIINP, directly correlating with indexes of cardiac diastolic function (Osokina et al., 2020). Furthermore, serum PIIINP of ≥381.4 ng/ml on the 12th day increases the risk of cardiac fibrosis 1 year after the disease onset in STEMI patients with preserved ejection fraction (EF) of I–III degree (Osokina et al., 2021). Moreover, human epididymis factor-4 is an independent predictor of low EF as a diagnostic marker and therapeutic target in cardiac fibrosis (Kilci et al., 2021). ST-segment resolution (STR) is a marker for severe myocardial fibrosis and is associated with scar thickness and size, while STEMI patients with STR of <40.15% easily develop transmural scars (Dong et al., 2021b). The combination of the ICTP/PIIINP ratio and ST2 might aid in risk stratification and serve as prognosis biomarkers in HF patients (Dupuy et al., 2019).

In addition to the above, more and more new technologies have emerged, such as Bayesian cardiac strain imaging assessing murine cardiac fibrosis (Al Mukaddim et al., 2022), single-cell mRNA sequencing inspecting dynamic interstitial cell response in MI mice (Forte et al., 2020), stereological method quantifying CMs (Mühlfeld and Schipke, 2022), and high-throughput screening differential genes expression of monocytes-CFs communication (Wu et al., 2022b; Wu et al., 2022d).

TABLE 1 Recent progress in clinical trials for treating fibrosis and its complications.

	Interventions	NCT number	Status	Phases	Included patients (n)	Research topic
Renin inhibitor	Aliskiren	NCT00414609	Completed	Phase 3	820	Safety and efficacy of Aliskiren in patients with MI
ACEI and ARB	Ramipril, Candesartan Cilexetil, Allopurinol	NCT01052272	Completed	Phase 2| Phase 3	72	Impact of diabetes on left ventricular remodeling
	Ramipril, Irbesartan	NCT00517322	Unknown status	Phase 4	80	Left atrial remodeling in hypertension: effects of Ramipril or Irbesartan
	Lisinopril	NCT03422705	Not yet recruiting	Phase 2	75	Preventing adverse remodeling following pacemaker implantation
	Telmisartan, Amlodipine	NCT03956823	Unknown status	Not Applicable	300	Clinical efficacy of Telmisartan in reducing cardiac remodeling among obese patients with hypertension
	Candesartan, Diltiazem, Bisoprolol	NCT01162902	Unknown status	Phase 4	150	Comparison of vascular remodeling between different antianginal medication
	Losartan	NCT05607017	Not yet recruiting	Early Phase 1	10	Losartan in prevention of radiation-induced HF
	Valsartan	NCT00133328	Completed	Phase 4	3000	A morbidity-mortality and remodeling study with Valsartan
	Valsartan	NCT01340326	Completed	Phase 4	800	The impact of dose of Valsartan and genetic polymorphism on ventricular remodeling after MI
ARNI	Sacubitril/Valsartan	NCT02887183	Completed	Phase 4	794	Effects of Sacubitril/Valsartan therapy on biomarkers, myocardial remodeling and outcomes
	Sacubitril/Valsartan, Valsartan	NCT03552575	Completed	Phase 3	93	Effects of Sacubitril/Valsartan vs. Valsartan on left ventricular remodeling after MI
	Sacubitril/Valsartan, Amlodipine	NCT04929600	Recruiting	Phase 4	120	Sacubitril/Valsartan *versus* Amlodipine in hypertension and left ventricular hypertrophy
	Sacubitril/valsartan	NCT05089539	Not yet recruiting	Phase 2	60	The Effect of Sacubitril/Valsartan on cardiac fibrosis in patients with HFpEF
	Sacubitril/Valsartan, Enalapril, Valsartan	NCT04912167	Not yet recruiting	Phase 3	376	The Effects of Sacubitril-Valsartan vs. Enalapril on left ventricular remodeling in STEMI
Adrenergic receptor inhibitors	Seloken ZOK/Toprol-XL	NCT00038077	Completed	Phase 3	300	Reversal of ventricular remodeling with Toprol-XL
	Carvedilol, Metoprolol succinate, Metoprolol succinate + doxazosin	NCT01798992	Completed	Phase 4	56	Effect of Beta-blockers on structural remodeling and gene expression
MRA	Eplerenone	NCT00082589	Completed	Phase 4	250	Effect of Eplerenone in patients with mild to moderate HF
	Eplerenone	NCT00132093	Completed	Phase 4	100	Effects of Eplerenone on left ventricular remodeling following heart attack
	Spironolactone	NCT01069510	Completed	Phase 2	40	Spironolactone in adult congenital heart disease
Other diuretics	Torasemide, Furosemide	NCT00409942	Completed	Phase 4	142	Effect of a new formulation of Torasemide on myocardial fibrosis in patients with HF
	Furosemide	NCT04628325	Completed	Phase 3	136	Effects of Furosemide plus small HSS in subjects with HFrEF
Inflammation modulators	Colchicine	NCT03156816	Completed	Phase 2	194	Colchicine for left ventricular remodeling treatment in AMI
	Colchicine	NCT05709509	Recruiting	Phase 4	148	Effect of Colchicine on MMP-9, NOX2, and TGF-β1 in MI

(Continued on following page)

TABLE 1 (*Continued*) Recent progress in clinical trials for treating fibrosis and its complications.

	Interventions	NCT number	Status	Phases	Included patients (n)	Research topic
	Anakinra	NCT01175018	Completed	Phase 2	30	Anakinra to prevent adverse post-infarction remodeling
TGF-β inhibitor	Pirfenidone	NCT02932566	Completed	Phase 2	129	The Efficacy and safety of Pirfenidone in patients with HFpEF
Prostacyclin analogs	Beraprost	NCT05103813	Recruiting	Early Phase 1	100	Effect of Beraprost on reperfusion therapy for acute STEMI
	beprostaglandin	NCT05043558	Not yet recruiting	Phase 1| Phase 2	220	Effect of Prostaglandin on coronary microcirculation and ventricular remodeling after reperfusion therapy in acute STEMI
Platelet aggregation inhibitors	Ticagrelor, Clopidogrel	NCT02224534	Unknown status	Phase 4	326	Ticagrelor *versus* Clopidogrel in left ventricular remodeling after STEMI
MMPs	Doxycycline	NCT00469261	Completed	Phase 2	110	Doxycycline and post myocardial infarction remodeling
	Doxycycline	NCT03960411	Unknown status	Phase 3	80	Effect of Doxycycline on cardiac remodeling in STEMI patients
BNP	BNP	NCT04033861	Unknown status	Phase 4	352	Early rhBNP on myocardial remodeling and reperfusion in patients with STEMI
SGLT2i	Dapagliflozin	NCT02397421	Completed	Phase 4	56	Safety and effectiveness of SGLT2i in patients with HF and DM
	Dapagliflozin	NCT03782259	Completed	Phase 4	60	Effects of SGLT2i on myocardial fibrosis and inflammation in patients With DM2
	Dapagliflozin	NCT05606718	Recruiting	Phase 4	98	Effect of Dapagliflozin on functional mitral regurgitation and myocardial fibrosis
	Dapagliflozin	NCT04783870	Recruiting	Phase 4	60	Effect of Dapagliflozin on left ventricular remodeling after AMI
	Dapagliflozin	NCT05305911	Recruiting	Phase 2	80	SGLT2i and STEMI
	Empagliflozin	NCT04461041	Recruiting	Phase 4	164	Effect of Empagliflozin on cardiac remodeling in people without DM
	Ertugliflozin	NCT04490681	Unknown status	Phase 3	52	Validation of Ertugliflozin for inhibiting cardiac fibrosis in heart failure patients with non-ischemic cardiomyopathy
Antilipemic agents	Rosuvastatin	NCT00240292	Completed	Phase 3	160	Effect of Rosuvastatin on ventricular remodeling lipids and cytokines
	Rosuvastatin	NCT00505154	Completed	Phase 3	75	Effect of Rosuvastatin on left ventricular remodeling
	Rosuvastatin, Evolocumab	NCT05613426	Not yet recruiting	Phase 4	330	Effect of evolocumab on left ventricular remodeling in patients with anterior STEMI undergoing primary PCI
	Atorvastatin	NCT00795912	Completed	Phase 4	56	Effect of Statins in patients with HF
	Atorvastatin	NCT00286312	Completed	Phase 4	50	Effect of Atorvastatin on MI size
GRK2 Inhibitors	Paroxetine	NCT03274752	Completed	Phase 2	50	Paroxetine-mediated GRK2 inhibition to reduce cardiac remodeling after AMI
Others	Regadenoson	NCT02589977	Completed	Phase 4	55	Evaluation of myocardial blood flow, interstitial fibrosis and oxidative metabolism in HFpEF
	Epoetin alfa	NCT00378352	Completed	Phase 2	223	Effect of erythropoietin on ventricular remodeling in patients with AMI

(Continued on following page)

TABLE 1 (*Continued*) **Recent progress in clinical trials for treating fibrosis and its complications.**

	Interventions	NCT number	Status	Phases	Included patients (n)	Research topic
	Calcifediol	NCT02548364	Active, not recruiting	Phase 3	109	Effect of Vitamin D on ventricular remodeling in patients with AMI
	Ivabradine	NCT05348057	Recruiting	Phase 4	240	Effect of Ivabradine on the improvement of left ventricular remodeling in STEMI patients after primary PCI

Note: ACEI, angiotensin-converting enzyme inhibitors; ARB, angiotensin receptor blockers; BNP, brain natriuretic peptide; GRK, G-protein-coupled receptor kinase; HF, heart failure; HFpEF, heart failure with preserved ejection fraction; HFrEF, heart failure with reduced ejection fraction; HSS, hypertonic saline solutions; MI, myocardial infarction; MMPs, matrix metalloproteinases; MRA, mineralocorticoid receptor antagonists; NOX2, nicotinamide adenine dinucleotide phosphate oxidase 2; PCI, percutaneous coronary intervention; RAAS, Renin-Angiotensin-Aldosterone System; SGLT2i, sodium-glucose cotransporter 2 inhibitor; STEMI, ST-segment elevation myocardial infarction; TGF-β, transforming growth factor β.

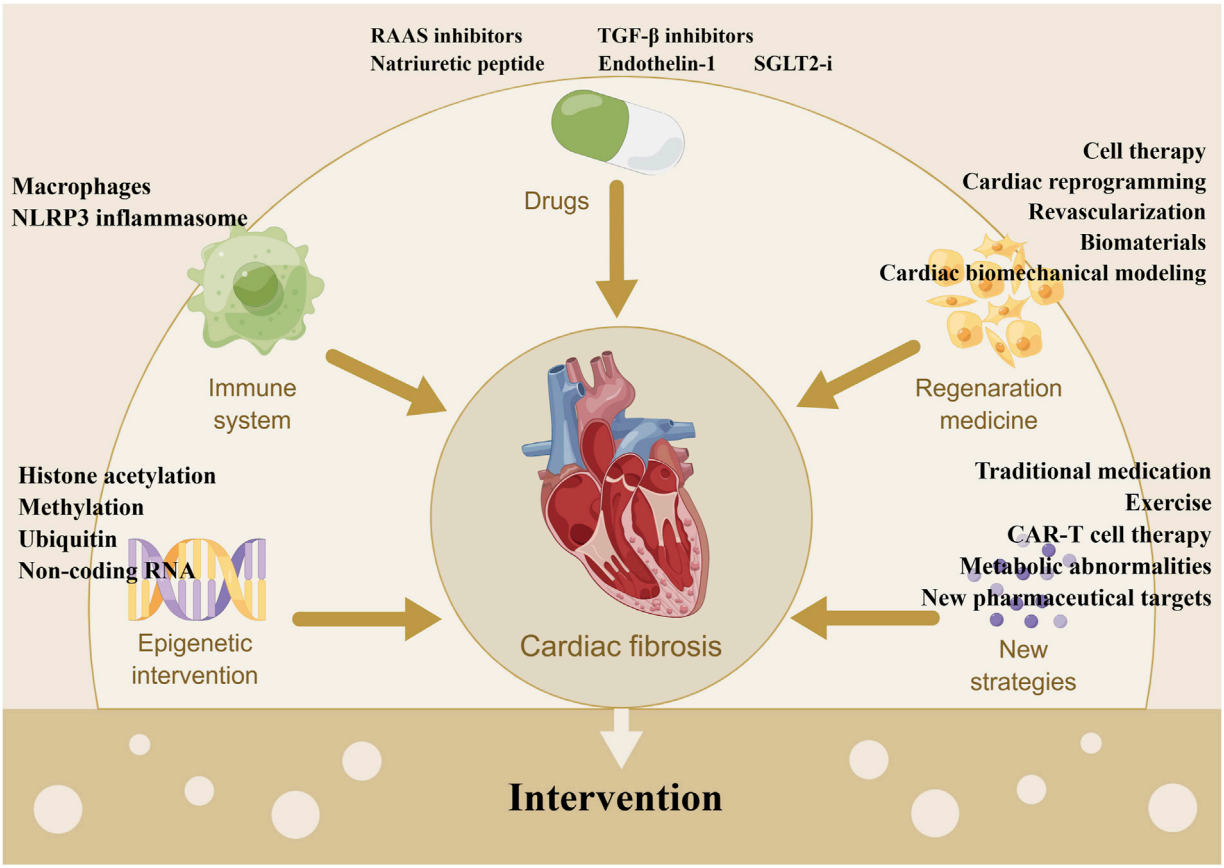


FIGURE 2
Summary of the interventions of cardiac fibrosis. Note: CAR, chimeric antigen receptor; NLRP3: nod-like receptor protein three; RAAS: renin-angiotensin-aldosterone system; SGLT2-i: sodium-glucose cotransporter-2 inhibitor; TGF-β: transforming growth factor β.

Therefore, developing new tools that allow both an early detection of cardiac fibrosis and the determination of its origin and characteristics will potentially lead to the rapid and efficient treatment of patients.

4 Interventions for cardiac fibrosis

The therapies against cardiac fibrosis are still a focus of clinical attention, and how to reverse fibrosis is always a hot topic. Unfortunately, the effective measures are still lacking and lead to the devastating clinical outcomes, despite the various encouraging results from experimental studies (Morfino et al., 2022). In the studies of clinical drugs, RAAS antagonists have been shown to attenuate cardiac fibrosis and dysfunction, with clinical applications limited by their hypotensive effects and inability to stop the fibrotic progression (AlQudah et al., 2020). Conversely, TGF-β inhibitors (e.g., pirfenidone) improve fibrosis, without affecting blood pressure, but with unexpected side effects (e.g., liver toxicity). At the meantime, some known drugs are going through different

phases of clinical trials (Table 1), such as RAAS inhibitors, sodium-glucose cotransporter-2 inhibitors (SGLT2is), BNP, and GRK2 inhibitors, in forms of monotherapy alone or combined with other drugs. Furthermore, fibrosis involves multiple molecules and processes (e.g., inflammatory cells recruitment, molecular mediators release, collagen synthesis, cells differention), which suggests small molecules targeting fibrosis would be the promising interventions. However, these novel therapies are still limited in preclinical studies without the validation of clinical efficacies against fibrosis. For the development of anti-fibrotic drugs, it is great important to apply novel molecular targets or drug repurposing *via* screening drugs tested and approved for other indications. In this section, we focus on the known drugs, novel compounds and other treatments with anti-fibrotic effects, which are shown in Figure 2 (The figure is drawn by figdraw).

4.1 Pharmaceutical interventions

4.1.1 RAAS inhibitors

Several clinical trials of RAAS inhibitors are currently progressing in different phases, which are presented in Table 1. Other non-clinical trials have been reported in the recent years. For example, sliskiren is not only the first Food and Drug Administration-approved and orally active renin inhibitor to treat hypertension, but also regulates collagen metabolism and cardiac fibrosis *in vivo* and *in vitro* (Kleinert, 1996; Zhi et al., 2013). Additionally, compound 21 is a non-peptide AT2R agonist with antifibrotic effect (Wang et al., 2017). Targeting RAAS represents a promising therapeutic approach to combat fibrosis, however, conventional RAAS inhibitors cannot completely hamper the fibrotic progression. Together with ACEI, ARNI sacubitril/valsartan suppresses cardiac dysfunction and fibrosis *via* the downregulation of TGF-β1, BNP, α-SMA, vimentin (Liu et al., 2021b). Furthermore, valsartan and sacubitril/valsartan prevent adverse remodeling in MI rats by reducing oxidative stress, inflammation, and fibrosis (Raj et al., 2021). In MI with hypertensive rats model, the mineralocorticoid receptor antagonist (MRA) spironolactone reduces CFs, MFs, and macrophages infiltration in the heart and kidney (Leader et al., 2021); however, it also binds other steroid receptors (e.g., progesterone and androgen receptors) causing side effects (e.g., gynecomastia and galactorrhea) (Weldon and Brown, 2019). Moreover, eplerenone, a well-tolerated selective MRA, decreases PIIINP with good efficacy when baseline PIIINP is ≥3.6 mmol/L after MI with HF or diabetes (Stienen et al., 2020). As a centrally acting aminopeptidase A inhibitor prodrug, QGC606 inhibits the overactivation of the brain renin-angiotensin system and fibrotic remodeling without lowering blood pressure (Boitard et al., 2022).

4.1.2 TGF-β inhibitors

Antifibrotic drug pirfenidone, a TGF-β1 inhibitor, has been identified from molecular information and transcriptomic data in a swine MI model (Aimo et al., 2022a), whereas evidence in humans has been limited to a phase 2 study evaluating extracellular volume changes with CMR (Aimo et al., 2022b). The clinical use of pirfenidone is limited by the high doses and various side effects. In an article, the total releasing duration of pirfenidone is prolonged by using acellular peritoneal matrix-loaded pirfenidone nanodroplets, which alleviates cardiac fibrosis (Fu et al., 2022b). Except pirfenidone, there are several interventions targeting TGF-β signaling pathway against cardiac fibrosis, such as dihydrolycorine, choline, indole alkaloids, and indole derivatives (Qin et al., 2022). Moreover, 2,5-dimethylcelecoxib inhibits the TGF-β axis and suppresses CF-to-MF transformation in a cryoinjury-induced MI model (Ikushima et al., 2022). The caffeic acid p-nitro phenethyl ester-pNO2 suppresses fibrosis, inflammation, and apoptosis *via* the TGF-β1/Gal-3 pathway (Wan et al., 2022b). Additionally, thymosin β4 decreases MFs growth and TGF-β1-induced activation to reduce fibrosis (Wang et al., 2022c). Salinomycin inhibits CFs activation and ECM secretion *via* the inhibition of TGF-β1-dependent p38/MAPK and Rho-kinase pathway in CFs Ang II-infused mice (Burke et al., 2021b). Nintedanib, another antifibrotic agent, was approved to improve pulmonary fibrosis. But the evidence for its role in the treatment of cardiac fibrosis is still lacking (Yvette, 2021).

4.1.3 Drugs targeting the natriuretic peptide family

Strong evidence shows that NPs treatment has beneficial effects on post-MI cardiac remodeling. For example, a previous study has demonstrated that intravenous administration of ANP inhibited RAAS, SNS activity, MIRI, and cardiac remodeling in MI patients (Kasama et al., 2008). Another study has found that continuous CNP infusion (0.1 mg/kg/min) by osmotic mini-pump for 2 weeks after permanent coronary artery occlusion prevents cardiac remodeling (Wang et al., 2007). Further, when BNP (15 mg/kg/day) is intravenously injected over 8 weeks in rats with permanent coronary occlusion, BNP treatment prevents cardiac hypertrophy and EF decline and decreases plasma Ang II level and collagen content in the myocardium (He et al., 2009). Furthermore, after the genetic knockout of *Npr1* gene encoding NPR-A in mice, blood pressure rises, and cardiac hypertrophy develops. Blood pressure becomes elevated by 41 mmHg in $Npr1^{-/-}$ mice, together with a 60% increased heart weight/body weight ratio and CM hypertrophy. These findings indicate that endogenous NPs can prevent the development of cardiac hypertrophy (Vellaichamy et al., 2014; Pandey, 2018). A fourth phase clinical trial is ongoing to evaluate early rhBNP intervention in myocardial remodeling and reperfusion in patients with STEMI (Table 1). However, the current evidence mainly exists at the level of animal experiments, and future clinical applications still need to be further explored.

4.1.4 Endothelin-1

ET-1 plays a major role in regulating myocardial fibrosis in several pathological conditions, and its receptor blocker might be beneficial in attenuating biventricular remodeling (Ramos et al., 2018). A few decades ago, studies found that ET-1 A and ET-1 A/B receptor antagonists substantially improved survival, cardiac function, and adverse cardiac remodeling (Sakai et al., 1996; Fraccarollo et al., 2002). Current evidence suggests that ET-1 is not only a molecular marker of cardiac fibrosis but also a novel therapeutic target (Hoffman et al., 2019). However, there is still no clinical evidence that drugs such as bosentan and enversentan have therapeutic effects on cardiac fibrosis.

4.1.5 Sodium-glucose cotransporter-2 inhibitors

In experimental studies and clinical trials, it has been demonstrated that SGLT2is are cardioprotective independently from controlling glucose, for instance, canagliflozin attenuates fibrosis *via* reducing JAK/STAT signaling, activating adenosine monophosphate-activated protein kinase, and antioxidant signaling (Sabe et al., 2023). In clinical practice, empagliflozin can significantly reduce mortality and hospitalization of HF patients (Kang et al., 2020). It reduces collagen deposit and fibrosis without improving cardiac function *via* the inhibition of the TGF-β1/smad3 pathway during the early post-MI period (Daud et al., 2021). However, another study reports that the short-term and low-dose empagliflozin increases cardiac systolic function by downregulating MMP-9 and sodium hydrogen exchanger one and upregulating sarco/endoplasmic reticulum Ca^{2+}-ATPase without changing arterial stiffness, blood pressure, fibrotic markers levels, and necroptosis (Goerg et al., 2021). Another selective SGLT1 inhibitor KGA-2727 improves fibrotic remodeling in MI mice (Sawa et al., 2020). Moreover, the DELIVER trial finds dapagliflozin reduces the combined risk of worsening heart failure or cardiovascular death among patients with mildly HFpEF (Solomon et al., 2022). In HFpEF pigs, it also decreases hypertension and reverses concentric remodeling of the heart, with the inhibition of inflammatory response and NO-cGMP-PKG pathway activation (Zhang et al., 2019b). Regrettably, SGLT2i cannot reduce extracellular volume expansion expanded by myocardial interstitial fibrosis (Bojer et al., 2022). Except SGLT2i, there are also other hypoglycemic agents associated with cardiac fibrosis. For example, metformin reduces collagen IIIA1, α-SMA, and CD68 levels after 2 weeks of reperfusion and improves fibrotic remodeling (Loi et al., 2021). Furthermore, metformin and cyclosporin A exert cardiac protection by regulating the balance between AMPK and apoptosis in the mitochondria of bile duct-ligated rats (Moheimani et al., 2021).

4.2 Targeting the immune system

The immune system is activated by MI, which can be a therapeutic target. Thus, immune-related interventions have been a study hotspot with the advance of precision medicine; for instance, the injection of human vascular cell adhesion molecule 1-expressing CFs restores cardiac function by promoting lymphangiogenesis (Iwamiya et al., 2020). Additionally, CD34 cells, isolated from mobilized human mononuclear peripheral blood cells, reduce cardiac scar and fibrosis in MI mice (Tripathi et al., 2020). A ligand-binding blocking anti-CD28 monoclonal antibody improves post-MI healing in mice (Gladow et al., 2020). Furthermore, the immune checkpoint programmed cell death protein one inhibits immune response to prevent damage, and its depletion increases T-cell infiltration in reperfused MI (Michel et al., 2022). In addition, high B cell counts are correlated with enhanced EF in MI patients with PCI, and empagliflozin can treat the MI-induced B cell developmental arrest (Xu et al., 2022b). Moreover, glucocorticoids released by the neuroendocrine system induce Na^+/H^+-exchanger 1-mediated autophagic death of bone marrow B cells and reduce B cell progenitor proliferation and differentiation (Xu et al., 2022b). Another study reports that adoptive transfer of atorvastatin-induced tolerogenic dendritic cells alleviates CMs apoptosis, fibrosis, inflammatory cells infiltration, and oxidative stress by suppressing TLR-4/NF-κB pathway in MI (Wang et al., 2023).

4.2.1 Targeting the macrophages

Recently, massive studies focus on the detrimental macrophages as the antifibrotic therapeutic targets. For example, cardiac rupture may be induced by macrophage-induced inflammation and downregulated activation of reparative MFs. In the macrophage protease-activated receptor two knockout mice, there are down-regulation of proinflammatory cytokines, recruitment of macrophages, fibrosis in a remote area, and macrophage-derived interferon-β expression, which stimulate the JAK/STAT3 pathway in CFs (Zuo et al., 2020). In addition, granulocyte colony-stimulating factor (G-CSF) improves cardiac remodeling by upregulating JAK2/STAT3 axis (Wang et al., 2020h). Further, N-Propargyl caffeate amide promotes pro-resolving macrophage polarization and prevents cardiac fibrosis by activating peroxisome proliferator-activated receptors-γ (PPAR-γ) pathway (Cheng et al., 2020). Interestingly, cortical bone stem cells can induce a novel macrophage phenotype to modify cardiac inflammation after MI (Hobby et al., 2021). Moreover, hypoxia-induced mitogenic factor deletion promotes M2 macrophages and inhibits M1 macrophages polarization to improve cardiac repair (Li et al., 2021f). M2b macrophages reduce the amount of collagen I and α-SMA, proliferation and migration of CFs, and differentiation of CFs into MFs, whereas M2a macrophages are profibrotic macrophages with opposite effects (Yue et al., 2020). The activation of M2-like macrophage-derived neuregulin-1/ERBB/PI3K/Akt signaling attenuates apoptosis and senescence of CFs in mice (Shiraishi et al., 2022). In infiltrated macrophages, a selective STING inhibitor H-151, alleviates cardiac fibrosis in the MI mouse model *via* the inhibition of cardiac dsDNA-triggered type I interferon response (Hu et al., 2022b). Furthermore, the knockdown of interferon-induced protein with tetratricopeptide repeats three in MI reduces the amount of $CD68^+$ macrophages, TNF-α, IL-1β and IL-6 levels, infarct size, fibrosis, and collagen content (Sun et al., 2021a; Sun et al., 2021b). 5-methoxytryptophan reduces fibrosis by downregulating macrophages and T-cells infiltration (Hsu et al., 2021). Additionally, 2-benzylidene-3-cyclohexylamino-2,3-dihydro-1H-inden-1-one, the dual-specificity phosphatase six inhibitor, improves cardiac dysfunction and fibrosis in MI rats by inhibiting macrophages formation and inflammation after MI (Zhang et al., 2023). Taken together, the future studies might focus on modulating different populations and phenotypes of macrophages to improve patient prognosis and cardiac remodeling.

4.2.2 Targeting the NLRP3 inflammasome

Several studies about NLRP3 inflammasome in the process of post-MI fibrosis have been reported. NLRP3 inflammasome is a proteolytic complex of the NLRP3 protein, procaspase-1, and apoptosis-associated speck-like protein (Zhang et al., 2022c), which regulates inflammatory response, pyroptosis and mitochondria and MF differentiation in cardiac fibrosis. Thus, it may represent a new therapeutical target, and its inhibitor oridonin decreases IL-1β and IL-18 levels and ameliorates myocardial fibrosis in MI mice (Gao et al., 2021). Moreover, calcium-sensing receptor

TABLE 2 The fibrotic modulatory effects of extracellular vesicles in myocardial infarction.

Extracellular vesicles	Model *in vitro*/vivo	Target gene/signaling pathway	The fibrotic modulatory effects	References
BMMSCs-derived-exosomal miR-29b-3p	MI rat model	ADAMTS16	cardiac fibrosis ↓	Zheng et al. (2022)
BMMSC-exosomes-miR-19a/19b	MI mouse model, hypoxic HL-1 cells	Bim and PTEN	cardiac fibrosis↓	Wang et al. (2020f)
BMMSCs-derived exosomes	MI rat model	EZH2/HMGA2/PI3K/Akt axis	cardiac fibrosis ↓	Jiao et al. (2022)
BMMSCs-derived EVs	AMI-induced HF rat model, hypoxic HUVECs	BMP2	cardiac fibrosis ↓	Xuan et al. (2022)
MSCs-EVs-miR-200b-3p	MI mouse model	BCL2L11/NLRP1	cardiac fibrosis↓	Wan et al. (2022a)
MSCs-derived EVs-miR-212-5p	clinical cardiac Samples, MI mouse model, CFs	NLRC5/VEGF/TGF-β1/smad	cardiac fibrosis ↓	Wu et al. (2022c)
telomerase/myocardin-coexpressing-MSCs	MI mouse model	miR-320a, miR-150-5p and miR-126-3p	myocardial revascularization ↑ tissue repair ↑cardiac fibrosis↓	Madonna et al. (2020)
EAT-secretory products	MI rat model, H9C2, CFs	EAT/miR-134-5p	cardiac fibrosis↑	Hao et al. (2021)
UMSC with β2 microglobulin deletion	MI rat model	Exosome/miR-24/Bim	cardiac fibrosis↓	Shao et al. (2020)
hAECs-derived exosomes	MI rat model	Exosomes	angiogenesis↑ apoptosis and fibrosis↓	Zhang et al. (2021c)
hPSCs–derived CPCs-EVs	MI mouse model; OGD-treated cardiomyocytes	LncRNA MALAT1/miR-497	cardiac fibrosis↓	Wu et al. (2020)
iPSC-derived CPC-EVs	MI mouse model	MiR-133-a1	expression of several pro-fibrotic genes↓ anti-fibrotic miR-133-a1↑	Lima Correa et al. (2021)
CBSC-derived exosomes	I/R mouse model, TGF-β1-treated CFs	small nucleolar RNA signaling	cardiac fibrosis↓	Schena et al. (2021)
Macrophages-EVs-circUbe3a	MI mouse model; CFs	miR-138-5p/RhoC	proliferation, migration, and phenotypic transformation of CFs↑ cardiac fibrosis↑	Wang et al. (2021f)
Macrophages-derived exosome-miR-21-5p	MI mouse model	Metalloproteinase 3	cardiac fibrosis↑	Dong et al. (2021a)
iCMs-exosomes-miR-181a	MI rat model; iPSC and iCMs	Sacubitril/Valsart inhibited exosomal miR-181a	cardiac fibrosis↓	Vaskova et al. (2020)
iCMs-exosomes	MI mouse model, hypoxic cardiomyocytes	the regulation of autophagy	cardiac fibrosis ↓	Santoso et al. (2020)

Note: ADSC, adipose-derived stem cells; ADAMTS16, a disintegrin and metalloproteinase with thrombospondin motifs 16; AT, adipose tissue; BCL2L11, Bcl-2–like protein 11; BMMSC, bone marrow mesenchymal stem cell; Bim, Bcl-2 interacting mediator of cell death; BMP2, bone morphogenetic protein 2; CBSC, cortical bone stem cell; CFs, cardiac fibroblasts; CPC, cardiovascular progenitor cells; CVPCs, cardiovascular progenitor cells; EAT, epicardial adipose tissue; EVs, extracellular vesicles; EZH2, enhancer of zeste 2 polycomb repressive complex 2 subunit; hAECs, human amniotic epithelial cells; HF, heart failure; HMGA2, high mobility group AT-hook 2; hPSCs, human pluripotent stem cells; HUVECs, human umbilical vein endothelial cells; iCMs, induced pluripotent stem cell-derived cardiomyocytes; I/R, ischemia/reperfusion; iPSC, induced pluripotent stem cell; MALAT1, metastasis-associated lung adenocarcinoma transcript 1; MI, myocardial infarction; MSC, mesenchymal stem cell; NLRP1, NLR family pyrin domain containing 1; NLRC5, nucleotidebinding and oligomerization domain-like receptor family Caspase recruitment domain–containing 5; OGD, oxygen-glucose deprivation; PI3K, phosphatidylinositol 3 kinase; PTEN, phosphatase and tensin homolog; TGF-β1, transforming growth factor β1; UMSC, umbilical mesenchymal stem cells; VEGF, vascular endothelial growth factor.

activates the NLRP3 inflammasome in neutrophils and promotes apoptosis and fibrosis after MI, which is inhibited by Calhex231 (Liu et al., 2020b). Further, the N-butylidenephthalide-pretreated aging MI rats improves human adipose-derived stem cell engraftment and attenuates NLRP3 inflammasome-mediated cardiac fibrosis (Lee et al., 2020). Additionally, glycogen synthase kinase-3 inhibition suppresses the activation of NLRP3 inflammasome in CFs but not in CMs (Wang et al., 2020g). Therapeutic hypothermia attenuates MIRI *via* regulating sirtuin 3/NLRP3 signalling pathway (Zhang et al., 2022a). Thereby, the NLRP3 inflammasome is a key anti-fibrotic mediator, and its inhibition has beneficial effects on cardiac remodeling. Furthermore, its non-specific inhibitor colchicine is going on some clinical trials (Table 1).

4.3 Interventions for epigenetic regulation

4.3.1 Histone acetylation and methylation

The challenge of epigenetic editing regarding specific cellular targets can provide promising therapeutic options in the coming years. Large preclinical studies have demonstrated the cardioprotective effects of histone deacetylase inhibitors *via*

various mechanisms, such as the suppression of cardiac fibrosis, enhancement of angiogenesis and mitochondrial biogenesis, and prevention of electrical remodeling (Chun, 2020). Moreover, polyunsaturated fatty acids, eicosapentaenoic acid, and docosahexaenoic acid prevent cardiac remodeling by inhibiting p300-histone acetyl-transferase activity in MI rats (Sunagawa et al., 2022a), with the same efficacy as the inhibition of jumonji domain-containing protein three histone demethylase (Long et al., 2020). The inhibition of the disruptor of telomeric silencing 1-like expression reduces methylation modification of histone H3 on spleen tyrosine kinase promoter, which can inhibit the TGF-β1/smad3 axis and prevent myocardial fibrosis and CFs proliferation (Li et al., 2022a). Moreover, silence of methyltransferase-like 3 decreases m6A modification on fibrotic genes and reduces CFs proliferation and TGF-β1-induced collagen production (Li et al., 2021e).

4.3.2 Intervention for ubiquitin

Conserved small molecular protein ubiquitin regulates protein turnover *via* the ubiquitin-proteasome system. Post-ischemic ubiquitin treatment attenuates cardiac dysfunction, myocardial fibrosis, apoptosis, hypertrophy, and serum cytokine/chemokine levels (Dalal et al., 2023), which suggests ubiquitin has a protective role in cardiac remodeling. Conversely, an endogenous E3 ubiquitin ligase ring-finger protein four knockdown induces extensive interstitial fibrosis after MI (Qiu et al., 2020). Additionally, ubiquitin C-terminal hydrolase L1 regulates cardiac fibrosis through glucose-regulated protein (Lei et al., 2020).

4.3.3 Non-coding RNAs

The protein-coding genes are rare, meanwhile the majority of the transcribed genome are non-coding RNAs that mainly including microRNA, circular RNA (circRNA), long non-coding RNA (lncRNA). Numerous studies suggest that non-coding RNAs participate in pathophysiological process of post-MI fibrosis as epigenetic regulators, with the specialization of tissues and cells, so it is necessary to study the role of non-coding RNAs in fibrotic regulation and molecular mechanisms (Supplemental Table S1). In addition, non-coding RNAs can be carried into target cells by extracellular vesicles (EVs) (e.g., exosomes) with capacity to escape from immunogen clearance, and emerging studies show that they regulate fibrosis as diagnostic markers and therapeutic targets in MI (Table 2). With technical advances, extrusion filters produce massive EVs from live cells with native effects (Wang et al., 2021e) and the modulation of exosome imprinting repairs damaged tissue without immune rejection (Hill et al., 2022). Based on the above information, future research might be focusing on their biodistribution and precise delivery to target cells against cardiac fibrosis.

4.4 Regenerative medicine

Regenerative medicine is a challenging and broad interesting topic with enormous potential to regenerate novel cells by injecting cells, growth factors, and biomaterials and reprogramming, considering fibrotic scar structure and mechanics, to facilitate novel cell differentiation, maintenance, and function in the extracellular microenvironment (French and Holmes, 2019).

4.4.1 Cell therapy

It's a novel direction for anti-fibrotic treatment based on cell therapy in recent years. Given revascularization after MI as a cornerstone of current treatment, cell therapy seems like an ideal therapy. Because of the paracrine effects promoting repair of mesenchymal stem cells (MSCs), preconditioned MSCs *in situ* may be promising for post-MI repair (Sim et al., 2021). The paracrine therapeutic anti-inflammatory and antifibrotic effects of human amniotic MSCs are increased by S100A8/A9 and calcium-binding proteins after MI (Chen et al., 2021c). Moreover, subcutaneous implantation of TheraCyte devices encapsulating human W8B2+ cardiac stem cells improves cardiac remodeling and function after MI (Kompa et al., 2021), and stem cells-derived CMs patches restore normal electrical propagation without the risk of arrhythmia (Fassina et al., 2022). Induced cardiosphere (iCS) can be produced by self-replicative RNA approach, differentiating into CMs, while intravenous and intramyocardial injection of C-X-C chemokine receptor four positive subpopulation of iCS-derived cells has similar therapeutic effects in the mice MI model (Xu et al., 2021a). Additionally, intracoronary injection of allogeneic cardiosphere-derived cells immediately prior to reperfusion in an AMI pig model impedes adverse remodeling (Sousonis et al., 2021). The human amniotic membrane MSCs-derived conditioned medium modulates autophagy *via* mTOR/ULK1 pathway to against MIRI. (Mokhtari et al., 2021). The skeletal muscle-derived Sca-1+/PW1+/Pax7− interstitial cells attenuate cardiac remodeling after transplanted into the infarcted myocardium (Ruchaya et al., 2022).

4.4.2 Cardiac reprogramming

Pluripotent stem cells generate functional CMs for post-MI regeneration, and cardiac reprogramming *in vivo* generates chamber-matched new CMs (Zhang et al., 2021d). Additionally, CFs can be reprogrammed into CMs and cardiovascular progenitor cells *via* lentiviral packaging techniques (Isomi et al., 2021) and CRISPR (Jiang et al., 2022), respectively. Moreover, microRNA-delivery platforms efficiently reprogram CFs into induced CMs (Yang et al., 2021a) or non-CMs into CMs-like cells (Kaur et al., 2021). Further, photo biomodulation therapy modulates gene transcription and miRNA expression to reverse the profibrotic signaling pathway (Feliciano et al., 2022), and fibroblast cilia regulates cardiac regeneration (Djenoune et al., 2022). A study has used miR-208b-3p mimic, ascorbic acid, and BMP4 to reprogram mouse tail-tip CFs into different cells (CMs, endothelial cells, and smooth muscle cells) and form cardiovascular tissue-like structure (Cho et al., 2021). Additionally, anti-BMP 1.3 monoclonal antibody inhibits the TGF-β pathway to reduce MFs activation and scar formation and exerts cardiac protection through BMP 5 (Vukicevic et al., 2022).

4.4.3 Revascularization

As the main goal of treatment in MI, revascularization restores myocardial perfusion and reduces the infarction size, and improves cardiac function (Solhpour and Yusuf, 2014). PCI is the standard therapy for patients presenting in the first 12h from symptom onset, however, early thrombolysis should be considered with the absence of PCI (Leancă et al., 2022). Despite the above therapies, cardiac

remodeling is still in one-third of MI patients (Solhpour and Yusuf, 2014). Macrophages and CFs also cause vascular disintegration and capillary rarefication (Wu et al., 2021b). Fortunately, the prevascularized cell sheets use reprogrammed cardiac cells to improve adverse remodeling (Song et al., 2020). High mobility group box one protein recruits bone marrow PDGFRα+-mesenchymal cells to induce angiogenesis and antifibrotic effect (Goto et al., 2020). However, these are basic studies without clinical applications. In a transmural scar distal to total coronary occlusion, up to 2 weeks after MI, large and medium coronary arteries maintain structural integrity, but are destroyed by subsequently progressive neointimal hyperplasia, intravascular fibrosis, and inward remodeling (Dedkov, 2021). Hence, the time frame for revascularization and optimizing cell-based regenerative therapies is the first 2 weeks in MI rats, but it is longer in humans (Dedkov, 2021).

4.4.4 Biomaterials

Biomaterials (e.g., hydrogels, nanocarriers, and cardiac patches) support self-renewal in the injured heart, with reliable biosafety and moderate promise, on-demand biodegradation, and multiple biofunctions to deliver the therapeutic drugs; for instance, a type of hydrogel injected in the peri-infarcted zone promotes fibrotic healing in the infarct zone and inhibits reactive fibrosis and hypertrophy in the remote zone (Wen et al., 2020). Another injectable thermosensitive hydrogel of chitosan/dextran/β-glycerophosphate delivers umbilical cord MSCs to repair the damaged heart (Ke et al., 2020), while injectable disulfide-cross-linked chitosan hydrogel loaded with basic FGF synergistically exerts antifibrotic, antiapoptotic, and proangiogenic effects (Fu et al., 2022a). Moreover, a conductive and MMP-degradable hydrogel stabilizes hypoxia-inducible factor 1-α to reduce the infarcted area and inflammation factors, promote vascularization and the expression of junctional protein connexin 43, and recover cardiac function (Wei et al., 2022). The miR-124-3p-loaded nanoparticles activate PTEN/P13K/Akt pathway to decrease oxidative stress and myocardial injury (Cheng et al., 2022). However, there are still many matters that have not been figured out, such as the analysis of dyskinesia of the infarct zone, the mechanical properties of myocardium, and the key mechanisms underlying the cardiac benefits of a hydrogel implantation. Thus, hydrogels are still difficult to translate from preclinical studies to humans.

4.4.5 Cardiac biomechanical modeling

Cardiac biomechanical modeling is a promising new tool for MI prognosis and therapy, such as a computational model predicting multiple time-dependent paracrine and intracellular drivers of CFs phenotype and post-MI fibrosis (Zeigler et al., 2020). Additionally, a library of scar tissue mechanical properties allows for the mechanics of cardiac modeling to assess the healing stage, rate, and collagen density, which can be potentially used as valuable biomarkers and therapies (Dempsey et al., 2020).

4.5 New strategies

4.5.1 Traditional medication

Traditional medication has developed for thousands of years as an ancient wisdom, with various herbal drugs and their isolated compounds. Recently, some studies have been performed to evaluate the anti-fibrotic efficacy of traditional medication and compounds as innovative antifibrotic therapies. For example, both fasudil and aconite ameliorate myocardial fibrosis (Xiang et al., 2022; Xing et al., 2022). Danqi soft capsule inhibits CFs proliferation and migration, collagen secretion, and CF-to-MF transformation in post-MI HF rats (Ma et al., 2022). Many studies have demonstrated the signaling pathways of traditional medication. Calycosin and taohong siwu decoction suppress TGF-β1-induced CFs proliferation and collagen deposition (Tan et al., 2021; Chen et al., 2022a). Moreover, zerumbone, ganxin V, nutmeg-5, ginsenoside Rg2, jatrorrhizine, cardiotonic pill, and huoxin pill all regulate the TGF-β1/smad pathway to attenuate fibrosis (Li et al., 2020d; Wang et al., 2021b; Yan et al., 2022a; Yan et al., 2022b; Li et al., 2022c; Hao and Jiao, 2022; Liang et al., 2022). Moreover, citri reticulatae pericarpium also reduces CMs apoptosis, CFs proliferation, and CF-to-MF transformation by upregulating PPAR-γ expression (Chen et al., 2022c), while auraptene improves cardiac hypertrophy and dysfunction *via* activating PPARα (Sunagawa et al., 2022b). Tanshinone IIA suppresses inflammation and fibrosis *via* the regulation of NADPH oxidase 4 (Chen et al., 2021b). Additionally, panaxatriol saponin inhibits CFs activation and proliferation and fibrosis by regulating oxidative stress and Nrf2 pathway (Yao et al., 2022). Astragaloside IV improves fibrosis by suppressing ROS/Caspase-1/GSDMD pathway (Zhang et al., 2022d), and liquiritin play the same role *via* the inhibition of CCL5 expression and NF-κB pathway (Han et al., 2022). Storax effectively protects cardiomyocytes against myocardial fibrosis and cardiac dysfunction by inhibiting the AT1R/ankyrin repeat domain 1/p53 signaling pathway (Xu et al., 2022c). In addition, nutraceuticals (e.g., curcumin, berberine, hibiscus roselle, flaxseed, and garlic alliin) are useful as antifibrotic substances acting *via* multiple signaling pathways (Zivarpour et al., 2022).

4.5.2 Exercise

In the modern era, unhealthy lifestyle (e.g., alcohol drinking, binge eating, smoking, physical inactivity) has been established as a risk factor for MI. Except for drug therapy, exercise-based cardiac rehabilitation should be taken into consideration to prevent the progression of adverse cardiac remodeling. For example, exercise significantly improves post-MI survival in the diet-induced obesity model (Peres Valgas Da Silva et al., 2022). Furthermore, moderate resistance exercise activates CMs proliferation through follistatin-like 1 (Hu et al., 2020). Moreover, exercise training increases FGF 21 and regulates the TGF-β1-smad2/3-MMP2/9 axis (Ma et al., 2021) and expression of lncRNAs H19, GAS5, and MIAT to decrease fibrosis in MI mice (Farsangi et al., 2021). Additionally, exercise inhibits tryptase release by mast cells and cardiac fibrosis (Bayat et al., 2021). The preconditioning with high-intensity interval training decreases heart injuries by increasing G-CSF and G-CSFR in the MI mouse model (Ghanimati et al., 2020). Noteworthily, the effect of combining the exercise with dietary intervention has been well validated. For example, aerobic-resistance training combined with vitamin D3 supplement suppresses the expression of TGF-β1, smad2/3, and collagen I and III to alleviate myocardial fibrosis and dysfunction (Mehdipoor et al., 2021).

4.5.3 CAR-T cell therapy

Anti-fibrotic T-cell therapy with chimeric antigen receptor (CAR) is engineered receptors with function to redirect lymphocytes to recognize and eliminate cells expressing a specific target antigen. This interaction occurs in a specific CAR domain called "antigen binding domain" and allows endogenous activation of T cells, with subsequent elimination of target cells (Morfino et al., 2022). Aghajanian and his colleagues firstly investigated that T-cell immunotherapy could specifically target pathologic cardiac fibrosis. The endogenous cardiac fibroblasts target FAP has been shown to benefit cardiac fibrosis. Adoptive transfer of T cells expressing a CAR against FAP, results in a significant reduction in cardiac fibrosis and restoration of function after injury in mice (Aghajanian et al., 2019). Moreover, a new approach is represented by the use of CAR-T cells engineered *in vivo* using lipid nanoparticles containing mRNA coding for a receptor directed against the FAP protein, expressed by MFs (Rurik et al., 2022). This strategy has proved to be safe and effective in reducing myocardial fibrosis and improving cardiac function in mice. However, there are still many limitations to this approach. For example, it may lead to antigen escape and the syndrome of release of pro-inflammatory cytokines (Asnani, 2018; Majzner and Mackall, 2018; Ghosh et al., 2020). Thus, potential toxicity associated with CAR-T cell therapy has stimulated the search for alternative approaches, such as the use of CAR-natural killer cells, and safer cell programming methods. To sum up, the anti-fibrotic management following MI is still a serious challenge, and current therapies involving protecting the remaining CMs and preventing fibrosis.

4.5.4 Intervention for metabolic abnormalities

Metabolism is an essential process for the maintenance of life, and metabolic homeostasis needs the coordination of anabolism and catabolism, which have been extensively studied. Recent studies involve metabolism of glucose, lipid, nucleotide, amino acid and so on. For example, glycolysis is not only related to TGF-β and Krüppel-like factor 5 signaling (Methatham et al., 2022), but also is inhibited by kallistatin/serpina3c to reduce post-MI fibrosis by activating Nr4a1 (Ji et al., 2022a). Protein kinase R regulates inflammation, insulin resistance, and glucose balance to improve cardiac fibrosis in isoproterenol-induced MI rats (Mangali et al., 2021). The high-density lipoproteins and stimulator of steroid receptor coactivators MCB-613 induce reverse remodeling *via* the reduction of cardiac dysfunction, hypertrophy, and fibrosis (De Geest and Mishra, 2021). Lysophosphatidic acid-lysophosphatidic acid receptor two signaling promotes angiogenesis and maintains vascular homeostasis to reduce scar formation and cardiac dysfunction (Pei et al., 2022). Furthermore, ketone ester reprograms gene expression of ketone body utilization and normalizes ATP production in post-infarct remodeling (Yurista et al., 2021). Sphingosine kinase one inhibitor PF543 reduces α-SMA, collagen, IL-1β, IL-6, and TNF-α levels to decrease myocardial injury, fibrosis, and inflammation (Wu et al., 2022a). Notably, deoxycholic acid-G protein-coupled bile acid receptor pathway activation also decreases inflammation and fibrosis (Wang et al., 2021a). Recombinant slit2, a secretive ECM protein, regulates the level of blood lipid decreasing total cholesterol, triglycerides, and low-density lipoprotein cholesterol, and increasing high-density lipoprotein cholesterol level in rats, which relieves the myocardial fibrosis, inflammation and oxidative stress in coronary heart disease (Liu et al., 2021a).

Following, we summarize the recent studies about amino acids and nucleotides. The inhibition of cardiac thyrotropin-releasing hormone reduces post-infarct hypertrophy and fibrosis (Schuman et al., 2021). Additionally, triiodothyronine pretreatment improves post-MI dysfunction and inhibits fibrosis by activating the insulin-like growth factor-1/PI3K/Akt signaling pathway (Zeng et al., 2021). In an MI sheep model, the upregulation of 5-hydroxytryptamine induces valve fibrosis, which could be improved by cyproheptadine (Marsit et al., 2022). Oral propionate, the important components of short-chain fatty acids, modulates macrophages polarization and pro-inflammatory cytokine *via* reducing JNK/p38/NF-κB phosphorylation to improve post-MI chronic cardiac remodeling (Zhou et al., 2023). The upregulated expression of ectonucleotide pyrophosphatase/phosphodiesterase 1 (ENPP1) after a cardiac injury can regulate cardiac repair, whereas uridine or ENPP1 inhibitor myricetin enhances cardiac repair by targeting the ENPP1/adenosine monophosphate (AMP) pathway (Li et al., 2022e).

Lastly, there are some other metabolic researches, for instance, chronic daily alcohol uptake enhances MI-induced cardiac dysfunction, fibrosis, and mitochondrial dysfunction (Liang et al., 2020). Urolithin A, a type of gut bacterial metabolite, inhibits myocardial fibrosis by activating the Nrf2 pathway (Chen et al., 2022d). Additionally, dimethyl fumarate promotes anti-inflammatory and preparative regulation by modulating oxidative metabolism in macrophages and CFs (Mouton et al., 2021). Furthermore, atypical chemokine receptor four deletion inhibits IL-6 expression and CFs proliferation to alleviate cardiac remodeling (Zhang et al., 2021a; Zhang et al., 2021b). Copper is reduced in myocardial ischemia-induced cardiac fibrosis, while it inhibits the CF-to-MF transformation as a pro-fibrinolytic switch and improves cardiac function (Xiao et al., 2023).

Post-MI cardiac fibrosis is related to unbalance of energy substrate metabolism (e.g., glucose, lipid, and amino acid). Furthermore, it is an energy-consuming process, which suggests that interventions of cardiac fibrosis combined with metabolic abnormalities are very important, with the positive efficacies against fibrosis.

4.5.5 New pharmaceutical targets

An increasing number of new pharmaceutical targets have been developed, such as a soluble epoxide hydrolase vaccine, which improves cardiac function, and boron, as well as a new ligand of the apelin peptide jejunum receptor apela, which reduce myocardial fibrosis and apoptosis (Bouchareb et al., 2020; Pan et al., 2020; Kitsuka et al., 2022). There are also interventions targeting inflammation response, for instance, the inhibition of coagulation protein tissue factor cytoplasmic domain improves cardiac remodeling by regulating inflammation and angiogenesis (Chong et al., 2021). Resveratrol supplementation also decreases proinflammatory cytokine levels, cardiac dysfunction, and atrial interstitial fibrosis in MI-induced rats (Jiang et al., 2021).

Moreover, There are many other drugs that can improve fibrosis, such as piperine, thymoquinone, an oleanolic acid Qi-Tai-Suan, spinal cord stimulation and exogenous hydrogen sulfide (Li et al., 2020f; Viswanadha et al., 2020; Farag et al.,

2021; Qian et al., 2022; He et al., 2023). Endostatin, alarin, L-carnitine, pentraxin 3 depletion, and mdivi-1 also can attenuate oxidative stress to inhibit myocardial fibrosis (Li et al., 2021b; Xu et al., 2021b; Emran et al., 2021; Xu et al., 2022a; Ding et al., 2022).

In experimental studies are useful to regulate cardiac fibrosis, even without clinical applications. For example, ephrinA1-Fc attenuates chronically non-reperfused post-MI remodeling (Whitehurst et al., 2020). Secreted frizzled protein three protects the heart *via* ischemic preconditioning in a pig model (Vatner et al., 2021). Upregulation of periostin regulates post-infarct fibrosis *via* cyclic AMP response element-binding protein 1 (Xue et al., 2020; Xue et al., 2022). Anti-proprotein convertase subtilisin/kexin type 9 intervention reduces infarct size and cardiac dysfunction (Guo et al., 2021). Epoxylipids improve cardiac fibrosis and dysfunction (Imig et al., 2022). Furthermore, menthol and HC-030031 reduces cardiac fibrosis *via* the regulation of cation channel (Li et al., 2020c; Wang et al., 2020e). As a pleiotropic hormone, serelaxin mitigates adverse remodeling and modulates bioactive sphingolipid signaling (Devarakonda et al., 2022). Additionally, nesfatin-1 suppresses necroptosis *via* regulating receptor-interacting protein kinase (RIPK) 1/RIPK3/mixed lineage kinase domain-like protein axis and RhoA/ Rho-associated coiled-coil-containing protein kinase/ RIP3pathway (Sharifi et al., 2021). Pulsed-field ablation exerts ablating ventricular scar, and eliminates viable myocardium separated from the catheter by collagen and fat (Younis et al., 2022). Calpain inhibition decreases collagen formation (Potz et al., 2022). The purified human tropoelastin significantly repairs the infarcted heart in a MI rodent model (Hume et al., 2023).

Together with, researches on cardiac fibrosis have evolved with the advancement of various genetics and proteomics approaches in recent years. However, a lot of novel targets with anti-fibrotic effects are limited in basic researches, without clinical application. Advances have been made in the therapeutic field, and timely coronary reperfusion in associations with novel therapies, such as ARNI and SGLT2i, along with MRAs and beta blockers, counteract adverse ventricular remodeling and promote reverse ventricular remodeling, decreasing progression to HF and mortality. Future therapeutic perspectives, such as microRNAs, bone marrow derived-cells, and molecules targeting inflammation are currently under research, with promising results.

5 Conclusion

In summary, regional fibrotic control in infarcted areas and suppression of collagen accumulation in non-infarcted areas are vital to improve adverse remodeling and clinical outcome after MI. Even being treated according to the guideline-recommended protocols, it is still adverse fibrotic remodeling in MI patients. In the future, the study should focus on the exploring the deeper pathophysiological mechanisms underlying the onset and progression of post-MI fibrosis, then further determining therapeutic targets, and optimizing intervention strategies. In the meantime, antifibrotic precision interventions still need a clinical translation. Although clinical trials associated with anti-fibrotic drugs already have been performed, the patients included in trials are rather small. Hence, it is urgent to explore integrated and personalized therapeutic strategies to inhibit progressively fibrotic remodeling after MI. Moreover, early identification, diagnosis, and management of cardiac fibrosis are significantly important in improving the survival and prognosis of MI patients.

Author contributions

XAY and XNY wrote the first draft of the review. XP, JZ, XF, JL, XZ, and LJ did literature search and date interpretation. JW, PH and YC designed the review and revised the report carefully.

Funding

This study was supported by the State Key Program of the National Natural Science Foundation of China (82030059), National Natural Science Foundation of China (81772036, 82072144,81873950, 82172178, 81873953), National Key R&D Program of China (2020YFC1512700, 2020YFC1512705, 2020YFC1512703), National S&T Fundamental Resources Investigation Project (2018FY100600, 2018FY100602), Key R&D Program of Shandong Province (2021ZLGX02, 2021SFGC0503), Taishan Pandeng Scholar Program of Shandong Province (tspd20181220), Taishan Young Scholar Program of Shandong Province (tsqn20161065, tsqn201812129), Youth Top-Talent Project of National Ten Thousand Talents Plan, Qilu Young Scholar Program and the Fundamental Research Funds of Shandong University (2018JC011).

Conflict of interest

The authors declare that the research was conducted in the absence of any commercial or financial relationships that could be construed as a potential conflict of interest.

Publisher's note

All claims expressed in this article are solely those of the authors and do not necessarily represent those of their affiliated organizations, or those of the publisher, the editors and the reviewers. Any product that may be evaluated in this article, or claim that may be made by its manufacturer, is not guaranteed or endorsed by the publisher.

Supplementary material

The Supplementary Material for this article can be found online at: https://www.frontiersin.org/articles/10.3389/fphar.2023.1070973/full#supplementary-material

References

Aboulgheit, A., Karbasiafshar, C., Zhang, Z., Sabra, M., Shi, G., Tucker, A., et al. (2021). Lactobacillus plantarum probiotic induces Nrf2-mediated antioxidant signaling and eNOS expression resulting in improvement of myocardial diastolic function. *Am. J. Physiol. Heart Circ. Physiol.* 321, H839–h849. doi:10.1152/ajpheart.00278.2021

Acharya, A., Baek, S. T., Huang, G., Eskiocak, B., Goetsch, S., Sung, C. Y., et al. (2012). The bHLH transcription factor Tcf21 is required for lineage-specific EMT of cardiac fibroblast progenitors. *Development* 139, 2139–2149. doi:10.1242/dev.079970

Adamo, L., Rocha-Resende, C., and Mann, D. L. (2020). The emerging role of B lymphocytes in cardiovascular disease. *Annu. Rev. Immunol.* 38, 99–121. doi:10.1146/annurev-immunol-042617-053104

Adapala, R. K., Kanugula, A. K., Paruchuri, S., Chilian, W. M., and Thodeti, C. K. (2020). TRPV4 deletion protects heart from myocardial infarction-induced adverse remodeling via modulation of cardiac fibroblast differentiation. *Basic Res. Cardiol.* 115, 14. doi:10.1007/s00395-020-0775-5

Adapala, R. K., Katari, V., Teegala, L. R., Thodeti, S., Paruchuri, S., and Thodeti, C. K. (2021). TRPV4 mechanotransduction in fibrosis. *Cells* 10.

Adrover, J. M., Del Fresno, C., Crainiciuc, G., Cuartero, M. I., Casanova-Acebes, M., Weiss, L. A., et al. (2019). A neutrophil timer coordinates immune defense and vascular protection. *Immunity* 50, 966–967. doi:10.1016/j.immuni.2019.11.001

Aghajanian, H., Kimura, T., Rurik, J. G., Hancock, A. S., Leibowitz, M. S., Li, L., et al. (2019). Targeting cardiac fibrosis with engineered T cells. *Nature* 573, 430–433. doi:10.1038/s41586-019-1546-z

Ahmad, F., Tomar, D., Aryal, A. C. S., Elmoselhi, A. B., Thomas, M., Elrod, J. W., et al. (2020). Nicotinamide riboside kinase-2 alleviates ischemia-induced heart failure through P38 signaling. *Biochim. Biophys. Acta Mol. Basis Dis.* 1866, 165609. doi:10.1016/j.bbadis.2019.165609

Aidumova, O. Y., Shchukin, Y. V., Limareva, L. V., and Piskunov, M. V. (2022). Geriatric status of patients over 70 years of age with myocardial infarction and the relationship with the severity of myocardial stress, fibrosis and angiogenesis. *Adv. Gerontol.* 35, 538–543.

Aimo, A., Iborra-Egea, O., Martini, N., Galvez-Monton, C., Burchielli, S., Panichella, G., et al. (2022a). Cardiac protection by pirfenidone after myocardial infarction: A bioinformatic analysis. *Sci. Rep.* 12, 4691. doi:10.1038/s41598-022-08523-3

Aimo, A., Spitaleri, G., Panichella, G., LupóN, J., Emdin, M., and Bayes-Genis, A. (2022b). Pirfenidone as a novel cardiac protective treatment. *Heart Fail Rev.* 27, 525–532. doi:10.1007/s10741-021-10175-w

AL Mukaddim, R., Weichmann, A. M., Taylor, R., Hacker, T. A., Pier, T., Hardin, J., et al. (2022). Murine cardiac fibrosis localization using adaptive Bayesian cardiac strain imaging *in vivo*. *Sci. Rep.* 12, 8522. doi:10.1038/s41598-022-12579-6

Alex, L., Tuleta, I., Harikrishnan, V., and Frangogiannis, N. G. (2022). Validation of specific and reliable genetic tools to identify, label, and target cardiac pericytes in mice. *J. Am. Heart Assoc.* 11, e023171. doi:10.1161/JAHA.121.023171

Alqudah, M., Hale, T. M., and Czubryt, M. P. (2020). Targeting the renin-angiotensin-aldosterone system in fibrosis. *Matrix Biol.* 91-92, 92–108. doi:10.1016/j.matbio.2020.04.005

Amin, P., Singh, M., and Singh, K. (2011). β-Adrenergic receptor-stimulated cardiac myocyte apoptosis: Role of β1 integrins. *J. Signal Transduct.* 2011, 179057. doi:10.1155/2011/179057

Asnani, A. (2018). Cardiotoxicity of immunotherapy: Incidence, diagnosis, and management. *Curr. Oncol. Rep.* 20, 44. doi:10.1007/s11912-018-0690-1

Atsuki, I., Shota, T., Kota, T., Shota, F., Masanori, O., Makiko, M., et al. (2019). Myofibroblast β2 adrenergic signaling amplifies cardiac hypertrophy in mice. *Biochem. Biophys. Res. Commun.* 510 (1), 149–155. doi:10.1016/j.bbrc.2019.01.070

Aziz, I. S., Mcmahon, A. M., Friedman, D., Rabinovich-Nikitin, I., Kirshenbaum, L. A., and Martino, T. A. (2021). Circadian influence on inflammatory response during cardiovascular disease. *Curr. Opin. Pharmacol.* 57, 60–70. doi:10.1016/j.coph.2020.11.007

Bajpai, G., Bredemeyer, A., Li, W., Zaitsev, K., Koenig, A. L., Lokshina, I., et al. (2019). Tissue resident CCR2-and CCR2+ cardiac macrophages differentially orchestrate monocyte recruitment and fate specification following myocardial injury. *Circ. Res.* 124, 263–278. doi:10.1161/CIRCRESAHA.118.314028

Bayat, M., Chien, S., and Chehelcheraghi, F. (2021). Aerobic exercise-assisted cardiac regeneration by inhibiting tryptase release in mast cells after myocardial infarction. *Biomed. Res. Int.* 2021, 5521564. doi:10.1155/2021/5521564

Benjamin, E. J., Virani, S. S., Callaway, C. W., Chamberlain, A. M., Chang, A. R., Cheng, S., et al. (2018). Heart disease and stroke statistics-2018 update: A report from the American heart association. *Circulation* 137, e67–e492. doi:10.1161/CIR.0000000000000558

Bertaud, A., Joshkon, A., Heim, X., Bachelier, R., Bardin, N., Leroyer, A. S., et al. (2023). Signaling pathways and potential therapeutic strategies in cardiac fibrosis. *Int. J. Mol. Sci.* 24, 1756. doi:10.3390/ijms24021756

Blythe, N. M., Muraki, K., Ludlow, M. J., Stylianidis, V., Gilbert, H. T. J., Evans, E. L., et al. (2019). Mechanically activated Piezo1 channels of cardiac fibroblasts stimulate p38 mitogen-activated protein kinase activity and interleukin-6 secretion. *J. Biol. Chem.* 294, 17395–17408. doi:10.1074/jbc.RA119.009167

Boitard, S. E., Keck, M., Deloux, R., Girault-Sotias, P. E., Marc, Y., DE Mota, N., et al. (2022). QGC606: A best-in-class orally active centrally acting aminopeptidase A inhibitor prodrug for treating heart failure following myocardial infarction. *Can. J. Cardiol.* 38, 815–827. doi:10.1016/j.cjca.2022.01.019

Boitard, S. E., Marc, Y., Keck, M., Mougenot, N., Agbulut, O., Balavoine, F., et al. (2019). Brain renin-angiotensin system blockade with orally active aminopeptidase A inhibitor prevents cardiac dysfunction after myocardial infarction in mice. *J. Mol. Cell Cardiol.* 127, 215–222. doi:10.1016/j.yjmcc.2018.12.008

Bojer, A. S., SøRENSEN, M. H., GæDE, P., and Madsen, P. L. (2022). Myocardial extracellular volume expansion in type 2 diabetes is associated with ischemic heart disease, autonomic neuropathy, and active smoking. *Diabetes Care* 45, 3032–3039. doi:10.2337/dc22-0942

Boorsma, E. M., Ter Maaten, J. M., Damman, K., VAN Veldhuisen, D. J., Dickstein, K., Anker, S. D., et al. (2021). Dipeptidyl peptidase 3, a marker of the antagonist pathway of the renin-angiotensin-aldosterone system in patients with heart failure. *Eur. J. Heart Fail* 23, 947–953. doi:10.1002/ejhf.2158

Bostan, M. M., Stătescu, C., Anghel, L., Şerban, I. L., Cojocaru, E., and Sascău, R. (2020). Post-myocardial infarction ventricular remodeling biomarkers-the key link between pathophysiology and clinic. *Biomolecules* 10, 1587. doi:10.3390/biom10111587

Bouchareb, R., Katz, M., Saadallah, N., Sassi, Y., Ali, S., and Lebeche, D. (2020). Boron improves cardiac contractility and fibrotic remodeling following myocardial infarction injury. *Sci. Rep.* 10, 17138. doi:10.1038/s41598-020-73864-w

Bouvet, M., Claude, O., Roux, M., Skelly, D., Masurkar, N., Mougenot, N., et al. (2020). Anti-integrin α(v) therapy improves cardiac fibrosis after myocardial infarction by blunting cardiac PW1(+) stromal cells. *Sci. Rep.* 10, 11404. doi:10.1038/s41598-020-68223-8

Braidotti, N., Chen, S. N., Long, C. S., Cojoc, D., and Sbaizero, O. (2022). Piezo1 channel as a potential target for hindering cardiac fibrotic remodeling. *Int. J. Mol. Sci.* 23, 8065. doi:10.3390/ijms23158065

Brazile, B. L., Butler, J. R., Patnaik, S. S., Claude, A., Prabhu, R., Williams, L. N., et al. (2021). Biomechanical properties of acellular scar ECM during the acute to chronic stages of myocardial infarction. *J. Mech. Behav. Biomed. Mater* 116, 104342. doi:10.1016/j.jmbbm.2021.104342

Bromage, D. I., Trevelin, S. C., Huntington, J., Yang, V. X., Muthukumar, A., Mackie, S. J., et al. (2022). Nrf2 attenuates the innate immune response after experimental myocardial infarction. *Biochem. Biophys. Res. Commun.* 606, 10–16. doi:10.1016/j.bbrc.2022.03.043

Bugg, D., Bailey, L. R. J., Bretherton, R. C., Beach, K. E., Reichardt, I. M., Robeson, K. Z., et al. (2022). MBNL1 drives dynamic transitions between fibroblasts and myofibroblasts in cardiac wound healing. *Cell Stem Cell* 29, 419–433. doi:10.1016/j.stem.2022.01.012

Bundgaard, H., Axelsson Raja, A., Iversen, K., Valeur, N., TøNDER, N., Schou, M., et al. (2022). Hemodynamic effects of cyclic guanosine monophosphate-dependent signaling through β3 adrenoceptor stimulation in patients with advanced heart failure: A randomized invasive clinical trial. *Circ. Heart Fail* 15, e009120. doi:10.1161/CIRCHEARTFAILURE.121.009120

Burke, R. M., Burgos Villar, K. N., and Small, E. M. (2021a). Fibroblast contributions to ischemic cardiac remodeling. *Cell Signal* 77, 109824. doi:10.1016/j.cellsig.2020.109824

Burke, R. M., Dirkx, R. A., JR., Quijada, P., Lighthouse, J. K., Mohan, A., O'Brien, M., et al. (2021b). Prevention of fibrosis and pathological cardiac remodeling by salinomycin. *Circ. Res.* 128, 1663–1678. doi:10.1161/CIRCRESAHA.120.317791

Capote, L. A., Mendez Perez, R., and Lymperopoulos, A. (2015). GPCR signaling and cardiac function. *Eur. J. Pharmacol.* 763, 143–148. doi:10.1016/j.ejphar.2015.05.019

Cargnello, M., and Roux, P. P. (2011). Activation and function of the MAPKs and their substrates, the MAPK-activated protein kinases. *Microbiol. Mol. Biol. Rev.* 75, 50–83. doi:10.1128/MMBR.00031-10

Chen, B., and Frangogiannis, N. G. (2021). Chemokines in myocardial infarction. *J. Cardiovasc Transl. Res.* 14, 35–52. doi:10.1007/s12265-020-10006-7

Chen, G., Huang, S., Song, F., Zhou, Y., and He, X. (2020a). Lnc-Ang362 is a pro-fibrotic long non-coding RNA promoting cardiac fibrosis after myocardial infarction by suppressing Smad7. *Arch. Biochem. Biophys.* 685, 108354. doi:10.1016/j.abb.2020.108354

Chen, G., Xu, H., Xu, T., Ding, W., Zhang, G., Hua, Y., et al. (2022a). Calycosin reduces myocardial fibrosis and improves cardiac function in post-myocardial infarction mice by suppressing TGFBR1 signaling pathways. *Phytomedicine* 104, 154277. doi:10.1016/j.phymed.2022.154277

Chen, H., Chew, G., Devapragash, N., Loh, J. Z., Huang, K. Y., Guo, J., et al. (2022b). The E3 ubiquitin ligase WWP2 regulates pro-fibrogenic monocyte infiltration and activity in heart fibrosis. *Nat. Commun.* 13, 7375. doi:10.1038/s41467-022-34971-6

Chen, H., Li, M., Liu, L., Zhu, D., and Tian, G. (2020b). Telmisartan improves myocardial remodeling by inhibiting leptin autocrine activity and activating PPARγ. *Exp. Biol. Med. (Maywood)* 245, 654–666. doi:10.1177/1535370220908215

Chen, J., Jia, J., Ma, L., Li, B., Qin, Q., Qian, J., et al. (2021a). Nur77 deficiency exacerbates cardiac fibrosis after myocardial infarction by promoting endothelial-to-mesenchymal transition. *J. Cell Physiol.* 236, 495–506. doi:10.1002/jcp.29877

Chen, M., Zhu, H., Zhu, Q., Wu, X., Zhou, Y., Gao, R., et al. (2022c). Citri Reticulatae Pericarpium alleviates postmyocardial infarction heart failure by upregulating PPARγ expression. *Clin. Exp. Pharmacol. Physiol.* 49, 661–673. doi:10.1111/1440-1681.13642

Chen, P., Pei, J., Wang, X., Tai, S., Tang, L., and Hu, X. (2022d). Gut bacterial metabolite Urolithin A inhibits myocardial fibrosis through activation of Nrf2 pathway *in vitro* and *in vivo*. *Mol. Med.* 28, 19. doi:10.1186/s10020-022-00444-1

Chen, R., Chen, W., Huang, X., and Rui, Q. (2021b). Tanshinone IIA attenuates heart failure via inhibiting oxidative stress in myocardial infarction rats. *Mol. Med. Rep.* 23, 404. doi:10.3892/mmr.2021.12043

Chen, T. J., Yeh, Y. T., Peng, F. S., Li, A. H., and Wu, S. C. (2021c). S100A8/A9 enhances immunomodulatory and tissue-repairing properties of human amniotic mesenchymal stem cells in myocardial ischemia-reperfusion injury. *Int. J. Mol. Sci.* 22, 11175. doi:10.3390/ijms222011175

Chen, X., Ding, Z., Li, T., Jiang, W., Zhang, J., and Deng, X. (2020c). MicroR-26b targets high mobility group, AT-hook 2 to ameliorate myocardial infarction-induced fibrosis by suppression of cardiac fibroblasts activation. *Curr. Neurovasc Res.* 17, 204–213. doi:10.2174/1567202617666200506101258

Chen, X., Wan, W., Guo, Y., Ye, T., Fo, Y., Sun, Y., et al. (2021d). Pinocembrin ameliorates post-infarct heart failure through activation of Nrf2/HO-1 signaling pathway. *Mol. Med.* 27, 100. doi:10.1186/s10020-021-00363-7

Cheng, X., Wang, L., Wen, X., Gao, L., Li, G., Chang, G., et al. (2021). TNAP is a novel regulator of cardiac fibrosis after myocardial infarction by mediating TGF-β/Smads and ERK1/2 signaling pathways. *EBioMedicine* 67, 103370. doi:10.1016/j.ebiom.2021.103370

Cheng, Y., He, Q., Li, N., and Luo, M. (2022). Activation of PTEN/P13K/AKT signaling pathway by miRNA-124-3p-loaded nanoparticles to regulate oxidative stress attenuates cardiomyocyte regulation and myocardial injury. *Oxid. Med. Cell Longev.* 2022, 8428596. doi:10.1155/2022/8428596

Cheng, Y., Luo, D., Zhao, Y., and Rong, J. (2020). N-Propargyl caffeate amide (PACA) prevents cardiac fibrosis in experimental myocardial infarction by promoting pro-resolving macrophage polarization. *Aging (Albany NY)* 12, 5384–5398. doi:10.18632/aging.102959

Chiang, M. H., Liang, C. J., Lin, L. C., Yang, Y. F., Huang, C. C., Chen, Y. H., et al. (2020). miR-26a attenuates cardiac apoptosis and fibrosis by targeting ataxia-telangiectasia mutated in myocardial infarction. *J. Cell Physiol.* 235, 6085–6102. doi:10.1002/jcp.29537

Cho, J., Kim, S., Lee, H., Rah, W., Cho, H. C., Kim, N. K., et al. (2021). Regeneration of infarcted mouse hearts by cardiovascular tissue formed via the direct reprogramming of mouse fibroblasts. *Nat. Biomed. Eng.* 5, 880–896. doi:10.1038/s41551-021-00783-0

Chong, S. Y., Zharkova, O., Yatim, S., Wang, X., Lim, X. C., Huang, C., et al. (2021). Tissue factor cytoplasmic domain exacerbates post-infarct left ventricular remodeling via orchestrating cardiac inflammation and angiogenesis. *Theranostics* 11, 9243–9261. doi:10.7150/thno.63354

Chun, P. (2020). Therapeutic effects of histone deacetylase inhibitors on heart disease. *Arch. Pharm. Res.* 43, 1276–1296. doi:10.1007/s12272-020-01297-0

Chute, M., Aujla, P., Jana, S., and Kassiri, Z. (2019). The non-fibrillar side of fibrosis: Contribution of the basement membrane, proteoglycans, and glycoproteins to myocardial fibrosis. *J. Cardiovasc Dev. Dis.* 6, 35. doi:10.3390/jcdd6040035

Chute, M., Aujla, P. K., Li, Y., Jana, S., Zhabyeyev, P., Rasmuson, J., et al. (2022). ADAM15 is required for optimal collagen cross-linking and scar formation following myocardial infarction. *Matrix Biol.* 105, 127–143. doi:10.1016/j.matbio.2021.12.002

Cui, S., Liu, Z., Tao, B., Fan, S., Pu, Y., Meng, X., et al. (2021). miR-145 attenuates cardiac fibrosis through the AKT/GSK-3β/β-catenin signaling pathway by directly targeting SOX9 in fibroblasts. *J. Cell Biochem.* 122, 209–221. doi:10.1002/jcb.29843

Dai, Y., Chen, Y., Wei, G., Zha, L., and Li, X. (2021). Ivabradine protects rats against myocardial infarction through reinforcing autophagy via inhibiting PI3K/AKT/mTOR/p70S6K pathway. *Bioengineered* 12, 1826–1837. doi:10.1080/21655979.2021.1925008

Dalal, S., Shook, P. L., Singh, M., and Singh, K. (2023). Post-ischemic cardioprotective potential of exogenous ubiquitin in myocardial remodeling late after ischemia/reperfusion injury. *Life Sci.* 312, 121216. doi:10.1016/j.lfs.2022.121216

Dattagupta, A., and Immaneni, S. (2018). ST2: Current status. *Indian Heart J.* 70 (1), S96–s101. doi:10.1016/j.ihj.2018.03.001

Daud, E., Ertracht, O., Bandel, N., Moady, G., Shehadeh, M., Reuveni, T., et al. (2021). The impact of empagliflozin on cardiac physiology and fibrosis early after myocardial infarction in non-diabetic rats. *Cardiovasc Diabetol.* 20, 132. doi:10.1186/s12933-021-01322-6

DE Boer, R. A., DE Keulenaer, G., Bauersachs, J., Brutsaert, D., Cleland, J. G., Diez, J., et al. (2019). Towards better definition, quantification and treatment of fibrosis in heart failure. A scientific roadmap by the Committee of Translational Research of the Heart Failure Association (HFA) of the European Society of Cardiology. *Eur. J. Heart Fail* 21, 272–285. doi:10.1002/ejhf.1406

DE Geest, B., and Mishra, M. (2021). Role of high-density lipoproteins in cardioprotection and in reverse remodeling: Therapeutic implications. *Biochim. Biophys. Acta Mol. Cell Biol. Lipids* 1866, 159022. doi:10.1016/j.bbalip.2021.159022

Dedkov, E. I. (2021). Large- and medium-sized arteries remaining in transmural scar distal to permanent coronary ligation undergo neointimal hyperplasia and inward remodeling. *J. Histochem Cytochem* 69, 321–338. doi:10.1369/00221554211004297

Dehghani, T., Thai, P. N., Sodhi, H., Ren, L., Sirish, P., Nader, C. E., et al. (2022). Selectin-targeting glycosaminoglycan-peptide conjugate limits neutrophil-mediated cardiac reperfusion injury. *Cardiovasc Res.* 118, 267–281. doi:10.1093/cvr/cvaa312

Dempsey, S., Jafari, P., So, A., and Samani, A. (2020). A composite material based neural network for tissue mechanical properties estimation toward stage assessment of infarction. *Annu. Int. Conf. IEEE Eng. Med. Biol. Soc.* 2020, 2800–2803. doi:10.1109/EMBC44109.2020.9176151

Devarakonda, T., Valle Raleigh, J., Mauro, A. G., Lambert, J. M., Cowart, L. A., and Salloum, F. N. (2022). Chronic treatment with serelaxin mitigates adverse remodeling in a murine model of ischemic heart failure and modulates bioactive sphingolipid signaling. *Sci. Rep.* 12, 8897. doi:10.1038/s41598-022-12930-x

Dewald, O., Ren, G., Duerr, G. D., Zoerlein, M., Klemm, C., Gersch, C., et al. (2004). Of mice and dogs: Species-specific differences in the inflammatory response following myocardial infarction. *Am. J. Pathol.* 164, 665–677. doi:10.1016/S0002-9440(10)63154-9

Dick, S. A., Macklin, J. A., Nejat, S., Momen, A., Clemente-Casares, X., Althagafi, M. G., et al. (2019). Self-renewing resident cardiac macrophages limit adverse remodeling following myocardial infarction. *Nat. Immunol.* 20, 29–39. doi:10.1038/s41590-018-0272-2

Ding, J., Zhang, Z., Li, S., Wang, W., DU, T., Fang, Q., et al. (2022). Mdivi-1 alleviates cardiac fibrosis post myocardial infarction at infarcted border zone, possibly via inhibition of Drp1-Activated mitochondrial fission and oxidative stress. *Arch. Biochem. Biophys.* 718, 109147. doi:10.1016/j.abb.2022.109147

Djenoune, L., Berg, K., Brueckner, M., and Yuan, S. (2022). A change of heart: New roles for cilia in cardiac development and disease. *Nat. Rev. Cardiol.* 19, 211–227. doi:10.1038/s41569-021-00635-z

Dobaczewski, M., Xia, Y., Bujak, M., Gonzalez-Quesada, C., and Frangogiannis, N. G. (2010). CCR5 signaling suppresses inflammation and reduces adverse remodeling of the infarcted heart, mediating recruitment of regulatory T cells. *Am. J. Pathol.* 176, 2177–2187. doi:10.2353/ajpath.2010.090759

Dong, J., Zhu, W., and Wan, D. (2021a). Downregulation of microRNA-21-5p from macrophages-derived exosomes represses ventricular remodeling after myocardial infarction via inhibiting tissue inhibitors of metalloproteinase 3. *Int. Immunopharmacol.* 96, 107611. doi:10.1016/j.intimp.2021.107611

Dong, Q., Wen, X., Chang, G., Xia, R., Wang, S., Yang, Y., et al. (2021b). ST-segment resolution as a marker for severe myocardial fibrosis in ST-segment elevation myocardial infarction. *BMC Cardiovasc Disord.* 21, 455. doi:10.1186/s12872-021-02269-y

Dufeys, C., Daskalopoulos, E. P., Castanares-Zapatero, D., Conway, S. J., Ginion, A., Bouzin, C., et al. (2021). AMPKα1 deletion in myofibroblasts exacerbates post-myocardial infarction fibrosis by a connexin 43 mechanism. *Basic Res. Cardiol.* 116, 10. doi:10.1007/s00395-021-00846-y

Dugaucquier, L., Feyen, E., Mateiu, L., Bruyns, T. A. M., DE Keulenaer, G. W., and Segers, V. F. M. (2020). The role of endothelial autocrine NRG1/ERBB4 signaling in cardiac remodeling. *Am. J. Physiol. Heart Circ. Physiol.* 319, H443–h455. doi:10.1152/ajpheart.00176.2020

Dupuy, A. M., Kuster, N., Curinier, C., Huet, F., Plawecki, M., Solecki, K., et al. (2019). Exploring collagen remodeling and regulation as prognosis biomarkers in stable heart failure. *Clin. Chim. Acta* 490, 167–171. doi:10.1016/j.cca.2018.08.042

Eguchi, A., Coleman, R., Gresham, K., Gao, E., Ibetti, J., Chuprun, J. K., et al. (2021). GRK5 is a regulator of fibroblast activation and cardiac fibrosis. *Proc. Natl. Acad. Sci. U. S. A.* 118, e2012854118. doi:10.1073/pnas.2012854118

Eid, R. A., Alharbi, S. A., EL-Kott, A. F., Eleawa, S. M., Zaki, M. S. A., EL-Sayed, F., et al. (2020). Exendin-4 ameliorates cardiac remodeling in experimentally induced myocardial infarction in rats by inhibiting PARP1/NF-κB Axis in A SIRT1-dependent mechanism. *Cardiovasc Toxicol.* 20, 401–418. doi:10.1007/s12012-020-09567-5

Elkenhans, B., Protti, A., Shah, A., Onthank, D., and Botnar, R. (2021). Visualization of elastin using cardiac magnetic resonance imaging after myocardial infarction as inflammatory response. *Sci. Rep.* 11, 11004. doi:10.1038/s41598-021-90092-y

Emran, T., Chowdhury, N. I., Sarker, M., Bepari, A. K., Hossain, M., Rahman, G. M. S., et al. (2021). L-carnitine protects cardiac damage by reducing oxidative stress and inflammatory response via inhibition of tumor necrosis factor-alpha and interleukin-1beta against isoproterenol-induced myocardial infarction. *Biomed. Pharmacother.* 143, 112139. doi:10.1016/j.biopha.2021.112139

Fan, D., Takawale, A., Lee, J., and Kassiri, Z. (2012). Cardiac fibroblasts, fibrosis and extracellular matrix remodeling in heart disease. *Fibrogenes. Tissue Repair* 5, 15. doi:10.1186/1755-1536-5-15

Fan, Z., and Guan, J. (2016). Antifibrotic therapies to control cardiac fibrosis. *Biomater. Res.* 20, 13. doi:10.1186/s40824-016-0060-8

Farag, M. M., Khalifa, A. A., Elhadidy, W. F., and Rashad, R. M. (2021). Thymoquinone dose-dependently attenuates myocardial injury induced by isoproterenol in rats via integrated modulations of oxidative stress, inflammation, apoptosis, autophagy, and fibrosis. *Naunyn Schmiedeb. Arch. Pharmacol.* 394, 1787–1801. doi:10.1007/s00210-021-02087-1

Farbehi, N., Patrick, R., Dorison, A., Xaymardan, M., Janbandhu, V., Wystub-Lis, K., et al. (2019). Single-cell expression profiling reveals dynamic flux of cardiac stromal, vascular and immune cells in health and injury. *Elife* 8, e43882. doi:10.7554/eLife.43882

Farsangi, S. J., Rostamzadeh, F., Sheikholeslami, M., Jafari, E., and Karimzadeh, M. (2021). Modulation of the expression of long non-coding RNAs H19, GAS5, and MIAT by endurance exercise in the hearts of rats with myocardial infarction. *Cardiovasc Toxicol.* 21, 162–168. doi:10.1007/s12012-020-09607-0

Fassina, D., Costa, C. M., Longobardi, S., Karabelas, E., Plank, G., Harding, S. E., et al. (2022). Modelling the interaction between stem cells derived cardiomyocytes patches and host myocardium to aid non-arrhythmic engineered heart tissue design. *PLoS Comput. Biol.* 18, e1010030. doi:10.1371/journal.pcbi.1010030

Fearon, W. F., and Fearon, D. T. (2008). Inflammation and cardiovascular disease: Role of the interleukin-1 receptor antagonist. *Circulation* 117, 2577–2579. doi:10.1161/CIRCULATIONAHA.108.772491

Feliciano, R. D. S., Manchini, M. T., Atum, A. L. B., Da Silva, G. A., AntôNIO, E. L., Serra, A. J., et al. (2022). Photobiomodulation therapy's effects on cardiac fibrosis activation after experimental myocardial infarction. *Lasers Surg. Med.* 54, 883–894. doi:10.1002/lsm.23544

Feng, Y., Bao, Y., Ding, J., Li, H., Liu, W., Wang, X., et al. (2022). MicroRNA-130a attenuates cardiac fibrosis after myocardial infarction through TGF-β/Smad signaling by directly targeting TGF-β receptor 1. *Bioengineered* 13, 5779–5791. doi:10.1080/21655979.2022.2033380

Forte, E., Mclellan, M. A., Skelly, D. A., and Rosenthal, N. A. (2021a). Ex uno, plures-from one tissue to many cells: A review of single-cell transcriptomics in cardiovascular biology. *Int. J. Mol. Sci.* 22, 2071. doi:10.3390/ijms22042071

Forte, E., Perkins, B., Sintou, A., Kalkat, H. S., Papanikolaou, A., Jenkins, C., et al. (2021b). Cross-priming dendritic cells exacerbate immunopathology after ischemic tissue damage in the heart. *Circulation* 143, 821–836. doi:10.1161/CIRCULATIONAHA.120.044581

Forte, E., Skelly, D. A., Chen, M., Daigle, S., Morelli, K. A., Hon, O., et al. (2020). Dynamic interstitial cell response during myocardial infarction predicts resilience to rupture in genetically diverse mice. *Cell Rep.* 30, 3149–3163.e6. doi:10.1016/j.celrep.2020.02.008

Fraccarollo, D., Bauersachs, J., Kellner, M., Galuppo, P., and Ertl, G. (2002). Cardioprotection by long-term ET(A) receptor blockade and ACE inhibition in rats with congestive heart failure: Mono-versus combination therapy. *Cardiovasc Res.* 54, 85–94. doi:10.1016/s0008-6363(01)00553-3

Fraccarollo, D., Neuser, J., MöLLER, J., Riehle, C., Galuppo, P., and Bauersachs, J. (2021). Expansion of CD10(neg) neutrophils and CD14(+)HLA-DR(neg/low) monocytes driving proinflammatory responses in patients with acute myocardial infarction. *Elife* 10, e66808. doi:10.7554/eLife.66808

Frangogiannis, N. G. (2014). The inflammatory response in myocardial injury, repair, and remodelling. *Nat. Rev. Cardiol.* 11, 255–265. doi:10.1038/nrcardio.2014.28

French, B. A., and Holmes, J. W. (2019). Implications of scar structure and mechanics for post-infarction cardiac repair and regeneration. *Exp. Cell Res.* 376, 98–103. doi:10.1016/j.yexcr.2019.01.001

Fu, B., Wang, X., Chen, Z., Jiang, N., Guo, Z., Zhang, Y., et al. (2022a). Improved myocardial performance in infarcted rat heart by injection of disulfide-cross-linked chitosan hydrogels loaded with basic fibroblast growth factor. *J. Mater Chem. B* 10, 656–665. doi:10.1039/d1tb01961a

Fu, H., Shuai, W., Kong, B., Jiang, X., and Huang, H. (2021). MD1 depletion predisposes to ventricular arrhythmias in the setting of myocardial infarction. *Heart Lung Circ.* 30, 869–881. doi:10.1016/j.hlc.2020.09.938

Fu, Y., Shi, J., Qian, H., Qin, C., Liu, L., Shen, J., et al. (2022b). Alleviation of cardiac fibrosis using acellular peritoneal matrix-loaded pirfenidone nanodroplets after myocardial infarction in rats. *Eur. J. Pharmacol.* 933, 175238. doi:10.1016/j.ejphar.2022.175238

Gaibazzi, N., Suma, S., Lorenzoni, V., Sartorio, D., Pressman, G., Siniscalchi, C., et al. (2020). Myocardial scar by pulse-cancellation echocardiography is independently associated with appropriate defibrillator intervention for primary prevention after myocardial infarction. *J. Am. Soc. Echocardiogr.* 33, 1123–1131. doi:10.1016/j.echo.2020.04.020

Gajarsa, J. J., and Kloner, R. A. (2011). Left ventricular remodeling in the post-infarction heart: A review of cellular, molecular mechanisms, and therapeutic modalities. *Heart Fail Rev.* 16, 13–21. doi:10.1007/s10741-010-9181-7

Gallo, K. A., and Johnson, G. L. (2002). Mixed-lineage kinase control of JNK and p38 MAPK pathways. *Nat. Rev. Mol. Cell Biol.* 3, 663–672. doi:10.1038/nrm906

Gao, L., Mei, S., Zhang, S., Qin, Q., Li, H., Liao, Y., et al. (2020a). Cardio-renal exosomes in myocardial infarction serum regulate proangiogenic paracrine signaling in adipose mesenchymal stem cells. *Theranostics* 10, 1060–1073. doi:10.7150/thno.37678

Gao, L., Wang, L. Y., Liu, Z. Q., Jiang, D., Wu, S. Y., Guo, Y. Q., et al. (2020b). TNAP inhibition attenuates cardiac fibrosis induced by myocardial infarction through deactivating TGF-β1/Smads and activating P53 signaling pathways. *Cell Death Dis.* 11, 44. doi:10.1038/s41419-020-2243-4

Gao, R. F., Li, X., Xiang, H. Y., Yang, H., Lv, C. Y., Sun, X. L., et al. (2021). The covalent NLRP3-inflammasome inhibitor Oridonin relieves myocardial infarction induced myocardial fibrosis and cardiac remodeling in mice. *Int. Immunopharmacol.* 90, 107133. doi:10.1016/j.intimp.2020.107133

Garg, A., Foinquinos, A., Jung, M., Janssen-Peters, H., Biss, S., Bauersachs, J., et al. (2020). MiRNA-181a is a novel regulator of aldosterone-mineralocorticoid receptor-mediated cardiac remodelling. *Eur. J. Heart Fail* 22, 1366–1377. doi:10.1002/ejhf.1813

Ghali, R., Habeichi, N. J., Kaplan, A., Tannous, C., Abidi, E., Bekdash, A., et al. (2020). IL-33 induces type-2-cytokine phenotype but exacerbates cardiac remodeling post-myocardial infarction with eosinophil recruitment, worsened systolic dysfunction, and ventricular wall rupture. *Clin. Sci. (Lond)* 134, 1191–1218. doi:10.1042/CS20200402

Ghanimati, R., Rajabi, H., Ramezani, F., Ramez, M., Bapiran, M., and Nasirinezhad, F. (2020). The effect of preconditioning with high-intensity training on tissue levels of G-CSF, its receptor and C-kit after an acute myocardial infarction in male rats. *BMC Cardiovasc Disord.* 20, 75. doi:10.1186/s12872-020-01380-w

Ghosh, A. K., Chen, D. H., Guha, A., Mackenzie, S., Walker, J. M., and Roddie, C. (2020). CAR T cell therapy-related cardiovascular outcomes and management: Systemic disease or direct cardiotoxicity? *JACC CardioOncol* 2, 97–109. doi:10.1016/j.jaccao.2020.02.011

Gil, H., Goldshtein, M., Etzion, S., Elyagon, S., Hadad, U., Etzion, Y., et al. (2022). Defining the timeline of periostin upregulation in cardiac fibrosis following acute myocardial infarction in mice. *Sci. Rep.* 12, 21863.

Gladow, N., Hollmann, C., Ramos, G., Frantz, S., Kerkau, T., Beyersdorf, N., et al. (2020). Treatment of mice with a ligand binding blocking anti-CD28 monoclonal antibody improves healing after myocardial infarction. *PLoS One* 15, e0227734. doi:10.1371/journal.pone.0227734

Goerg, J., Sommerfeld, M., Greiner, B., Lauer, D., Seckin, Y., Kulikov, A., et al. (2021). Low-dose empagliflozin improves systolic heart function after myocardial infarction in rats: Regulation of MMP9, NHE1, and SERCA2a. *Int. J. Mol. Sci.* 22, 5437. doi:10.3390/ijms22115437

Goetze, J. P., Bruneau, B. G., Ramos, H. R., Ogawa, T., DE Bold, M. K., and DE Bold, A. J. (2020). Cardiac natriuretic peptides. *Nat. Rev. Cardiol.* 17, 698–717. doi:10.1038/s41569-020-0381-0

Gomez, R. A., and Sequeira-Lopez, M. L. S. (2018). Renin cells in homeostasis, regeneration and immune defence mechanisms. *Nat. Rev. Nephrol.* 14, 231–245. doi:10.1038/nrneph.2017.186

Goto, T., Miyagawa, S., Tamai, K., Matsuura, R., Kido, T., Kuratani, T., et al. (2020). High-mobility group box 1 fragment suppresses adverse post-infarction remodeling by recruiting PDGFRα-positive bone marrow cells. *PLoS One* 15, e0230392. doi:10.1371/journal.pone.0230392

Groenewegen, A., Rutten, F. H., Mosterd, A., and Hoes, A. W. (2020). Epidemiology of heart failure. *Eur. J. Heart Fail* 22, 1342–1356. doi:10.1002/ejhf.1858

Guo, Y., Yan, B., Tai, S., Zhou, S., and Zheng, X. L. (2021). PCSK9: Associated with cardiac diseases and their risk factors? *Arch. Biochem. Biophys.* 704, 108717. doi:10.1016/j.abb.2020.108717

Gupta, S., Ge, Y., Singh, A., GräNI, C., and Kwong, R. Y. (2021). Multimodality imaging assessment of myocardial fibrosis. *JACC Cardiovasc Imaging* 14, 2457–2469. doi:10.1016/j.jcmg.2021.01.027

Halade, G. V., Norris, P. C., Kain, V., Serhan, C. N., and Ingle, K. A. (2018). Splenic leukocytes define the resolution of inflammation in heart failure. *Sci. Signal* 11, eaao1818. doi:10.1126/scisignal.aao1818

Hall, C., Gehmlich, K., Denning, C., and Pavlovic, D. (2021). Complex relationship between cardiac fibroblasts and cardiomyocytes in health and disease. *J. Am. Heart Assoc.* 10, e019338. doi:10.1161/JAHA.120.019338

Han, X., Yang, Y., Zhang, M., Li, L., Xue, Y., Jia, Q., et al. (2022). Liquiritin protects against cardiac fibrosis after myocardial infarction by inhibiting CCL5 expression and the NF-κB signaling pathway. *Drug Des. Devel Ther.* 16, 4111–4125. doi:10.2147/DDDT.S386805

Han, X., Zhao, Z. A., Yan, S., Lei, W., Wu, H., Lu, X. A., et al. (2020). CXADR-like membrane protein protects against heart injury by preventing excessive pyroptosis after myocardial infarction. *J. Cell Mol. Med.* 24, 13775–13788. doi:10.1111/jcmm.15955

Hao, H., Li, X., Li, Q., Lin, H., Chen, Z., Xie, J., et al. (2016). FGF23 promotes myocardial fibrosis in mice through activation of β-catenin. *Oncotarget* 7, 64649–64664. doi:10.18632/oncotarget.11623

Hao, M., and Jiao, K. (2022). Jatrorrhizine reduces myocardial infarction-induced apoptosis and fibrosis through inhibiting p53 and TGF-β1/Smad2/3 pathways in mice. *Acta Cir. Bras.* 37, e370705. doi:10.1590/acb370705

Hao, S., Sui, X., Wang, J., Zhang, J., Pei, Y., Guo, L., et al. (2021). Secretory products from epicardial adipose tissue induce adverse myocardial remodeling after myocardial infarction by promoting reactive oxygen species accumulation. *Cell Death Dis.* 12, 848. doi:10.1038/s41419-021-04111-x

Haryono, A., Ramadhiani, R., Ryanto, G. R. T., and Emoto, N. (2022). Endothelin and the cardiovascular system: The long journey and where we are going. *Biol. (Basel)* 11.

Hata, A., and Chen, Y. G. (2016). TGF-B signaling from receptors to smads. *Cold Spring Harb. Perspect. Biol.* 8, a022061. doi:10.1101/cshperspect.a022061

Hayes, J. D., and Dinkova-Kostova, A. T. (2014). The Nrf2 regulatory network provides an interface between redox and intermediary metabolism. *Trends Biochem. Sci.* 39, 199–218. doi:10.1016/j.tibs.2014.02.002

He, J., Chen, Y., Huang, Y., Yao, F., Wu, Z., Chen, S., et al. (2009). Effect of long-term B-type natriuretic peptide treatment on left ventricular remodeling and function after myocardial infarction in rats. *Eur. J. Pharmacol.* 602, 132–137. doi:10.1016/j.ejphar.2008.10.064

He, W., Chen, P., Chen, Q., Cai, Z., and Zhang, P. (2022). Cytokine storm: Behind the scenes of the collateral circulation after acute myocardial infarction. *Inflamm. Res.* 71, 1143–1158. doi:10.1007/s00011-022-01611-0

He, Y., Sun, Z., Jiang, J., Yin, X., Han, J., Zhang, Y., et al. (2023). Spinal cord stimulation attenuates neural remodeling, inflammation, and fibrosis after myocardial infarction. *Neuromodulation* 26, 57–67. doi:10.1016/j.neurom.2021.09.005

Heinrichs, M., Ashour, D., Siegel, J., BüCHNER, L., Wedekind, G., Heinze, K. G., et al. (2021). The healing myocardium mobilizes a distinct B-cell subset through a CXCL13-CXCR5-dependent mechanism. *Cardiovasc Res.* 117, 2664–2676. doi:10.1093/cvr/cvab181

Hess, A., Borchert, T., Ross, T. L., Bengel, F. M., and Thackeray, J. T. (2022). Characterizing the transition from immune response to tissue repair after myocardial infarction by multiparametric imaging. *Basic Res. Cardiol.* 117, 14. doi:10.1007/s00395-022-00922-x

Hill, M. A., Jaisser, F., and Sowers, J. R. (2022). Role of the vascular endothelial sodium channel activation in the Genesis of pathologically increased cardiovascular stiffness. *Cardiovasc Res.* 118, 130–140. doi:10.1093/cvr/cvaa326

Hobby, A. R. H., Berretta, R. M., Eaton, D. M., Kubo, H., Feldsott, E., Yang, Y., et al. (2021). Cortical bone stem cells modify cardiac inflammation after myocardial infarction by inducing a novel macrophage phenotype. *Am. J. Physiol. Heart Circ. Physiol.* 321, H684–h701. doi:10.1152/ajpheart.00304.2021

Hodges, M. M., Zgheib, C., Xu, J., Hu, J., Dewberry, L. C., Hilton, S. A., et al. (2019). Differential expression of transforming growth factor-β1 is associated with fetal regeneration after myocardial infarction. *Ann. Thorac. Surg.* 108, 59–66. doi:10.1016/j.athoracsur.2018.12.042

Hoffman, K. A., Reynolds, C., Bottazzi, M. E., Hotez, P., and Jones, K. (2019). Improved biomarker and imaging analysis for characterizing progressive cardiac fibrosis in a mouse model of chronic chagasic cardiomyopathy. *J. Am. Heart Assoc.* 8, e013365. doi:10.1161/JAHA.119.013365

Hoffmann, D. B., Fraccarollo, D., Galuppo, P., Frantz, S., Bauersachs, J., and Tillmanns, J. (2021). Genetic ablation of fibroblast activation protein alpha attenuates left ventricular dilation after myocardial infarction. *PLoS One* 16, e0248196. doi:10.1371/journal.pone.0248196

Hofmann, U., and Frantz, S. (2015). Role of lymphocytes in myocardial injury, healing, and remodeling after myocardial infarction. *Circ. Res.* 116, 354–367. doi:10.1161/CIRCRESAHA.116.304072

Holtackers, R. J., Emrich, T., Botnar, R. M., Kooi, M. E., Wildberger, J. E., and Kreitner, K. F. (2022). Late gadolinium enhancement cardiac magnetic resonance imaging: From basic concepts to emerging methods. *Rofo* 194, 491–504. doi:10.1055/a-1718-4355

Holtackers, R. J., VAN DE Heyning, C. M., Chiribiri, A., Wildberger, J. E., Botnar, R. M., and Kooi, M. E. (2021). Dark-blood late gadolinium enhancement cardiovascular magnetic resonance for improved detection of subendocardial scar: A review of current techniques. *J. Cardiovasc Magn. Reson* 23, 96. doi:10.1186/s12968-021-00777-6

Hsu, W. T., Tseng, Y. H., Jui, H. Y., Kuo, C. C., Wu, K. K., and Lee, C. M. (2021). 5-Methoxytryptophan attenuates postinfarct cardiac injury by controlling oxidative stress and immune activation. *J. Mol. Cell Cardiol.* 158, 101–114. doi:10.1016/j.yjmcc.2021.05.014

Hu, G., Ding, X., Gao, F., and Li, J. (2022a). Calcium and integrin binding protein 1 (CIB1) induces myocardial fibrosis in myocardial infarction via regulating the PI3K/Akt pathway. *Exp. Anim.* 71, 1–13. doi:10.1538/expanim.21-0063

Hu, S., Gao, Y., Gao, R., Wang, Y., Qu, Y., Yang, J., et al. (2022b). The selective STING inhibitor H-151 preserves myocardial function and ameliorates cardiac fibrosis in murine myocardial infarction. *Int. Immunopharmacol.* 107, 108658. doi:10.1016/j.intimp.2022.108658

Hu, S., Liu, H., Hu, Z., Li, L., and Yang, Y. (2020). Follistatin-like 1: A dual regulator that promotes cardiomyocyte proliferation and fibrosis. *J. Cell Physiol.* 235, 5893–5902. doi:10.1002/jcp.29588

Huang, S., Chen, B., Humeres, C., Alex, L., Hanna, A., and Frangogiannis, N. G. (2020). The role of Smad2 and Smad3 in regulating homeostatic functions of fibroblasts *in vitro* and in adult mice. *Biochim. Biophys. Acta Mol. Cell Res.* 1867, 118703. doi:10.1016/j.bbamcr.2020.118703

Huang, Y., Li, L., Chen, H., Liao, Q., Yang, X., Yang, D., et al. (2021). The protective role of yin-yang 1 in cardiac injury and remodeling after myocardial infarction. *J. Am. Heart Assoc.* 10, e021895. doi:10.1161/JAHA.121.021895

Hubert, F., Payan, S. M., Pelce, E., Bouchard, L., Sturny, R., Lenfant, N., et al. (2022). FGF10 promotes cardiac repair through a dual cellular mechanism increasing cardiomyocyte renewal and inhibiting fibrosis. *Cardiovasc Res.* 118, 2625–2637. doi:10.1093/cvr/cvab340

Hume, R. D., Kanagalingam, S., Deshmukh, T., Chen, S., Mithieux, S. M., Rashid, F. N., et al. (2023). Tropoelastin improves post-infarct cardiac function. *Circ. Res.* 132, 72–86. doi:10.1161/CIRCRESAHA.122.321123

Humeres, C., and Frangogiannis, N. G. (2019). Fibroblasts in the infarcted, remodeling, and failing heart. *JACC Basic Transl. Sci.* 4, 449–467. doi:10.1016/j.jacbts.2019.02.006

Humeres, C., Shinde, A. V., Hanna, A., Alex, L., HernáNDEZ, S. C., Li, R., et al. (2022). Smad7 effects on TGF-β and ErbB2 restrain myofibroblast activation and protect from postinfarction heart failure. *J. Clin. Invest* 132, e146926. doi:10.1172/JCI146926

Huo, J., Lu, S., Kwong, J. Q., Bround, M. J., Grimes, K. M., Sargent, M. A., et al. (2020). MCUb induction protects the heart from postischemic remodeling. *Circ. Res.* 127, 379–390. doi:10.1161/CIRCRESAHA.119.316369

Ikushima, E., Ishikane, S., Kishigami, T., Matsunaga, H., Igawa, K., Tomooka, K., et al. (2022). 2,5-Dimethylcelecoxib attenuates cardiac fibrosis caused by cryoinjury-induced myocardial infarction by suppressing the fibroblast-to-myofibroblast transformation via inhibition of the TGF-β signaling pathway. *Biochem. Pharmacol.* 197, 114950. doi:10.1016/j.bcp.2022.114950

Imig, J. D., Cervenka, L., and Neckar, J. (2022). Epoxylipids and soluble epoxide hydrolase in heart diseases. *Biochem. Pharmacol.* 195, 114866. doi:10.1016/j.bcp.2021.114866

Isomi, M., Sadahiro, T., Fujita, R., Abe, Y., Yamada, Y., Akiyama, T., et al. (2021). Direct reprogramming with Sendai virus vectors repaired infarct hearts at the chronic stage. *Biochem. Biophys. Res. Commun.* 560, 87–92. doi:10.1016/j.bbrc.2021.04.121

Ivanes, F., Susen, S., Mouquet, F., Pigny, P., Cuilleret, F., SautièRE, K., et al. (2012). Aldosterone, mortality, and acute ischaemic events in coronary artery disease patients outside the setting of acute myocardial infarction or heart failure. *Eur. Heart J.* 33, 191–202. doi:10.1093/eurheartj/ehr176

Ivey, M. J., Kuwabara, J. T., Riggsbee, K. L., and Tallquist, M. D. (2019). Platelet-derived growth factor receptor-α is essential for cardiac fibroblast survival. *Am. J. Physiol. Heart Circ. Physiol.* 317, H330–h344. doi:10.1152/ajpheart.00054.2019

Iwamiya, T., Segard, B. D., Matsuoka, Y., and Imamura, T. (2020). Human cardiac fibroblasts expressing VCAM1 improve heart function in postinfarct heart failure rat models by stimulating lymphangiogenesis. *PLoS One* 15, e0237810. doi:10.1371/journal.pone.0237810

Janbandhu, V., Martin, E., Chapman, G., Dunwoodie, S. L., and Harvey, R. P. (2022). Quantitative 3D analysis and visualization of cardiac fibrosis by microcomputed tomography. *Star. Protoc.* 3, 101055. doi:10.1016/j.xpro.2021.101055

JáUREGUI, B., Soto-Iglesias, D., Penela, D., Acosta, J., FernáNDEZ-Armenta, J., Linhart, M., et al. (2022). Cardiovascular magnetic resonance determinants of ventricular arrhythmic events after myocardial infarction. *Europace* 24, 938–947. doi:10.1093/europace/euab275

Ji, J. J., Qian, L. L., Zhu, Y., Jiang, Y., Guo, J. Q., Wu, Y., et al. (2022a). Kallistatin/Serpina3c inhibits cardiac fibrosis after myocardial infarction by regulating glycolysis via Nr4a1 activation. *Biochim. Biophys. Acta Mol. Basis Dis.* 1868, 166441. doi:10.1016/j.bbadis.2022.166441

Ji, M., Li, Y., Liu, Y., and Ma, G. (2022b). Vaspin ameliorates cardiac remodeling by suppressing phosphoinositide 3-kinase/protein kinase B pathway to improve oxidative stress in heart failure rats. *J. Cardiovasc Pharmacol.* 80, 442–452. doi:10.1097/FJC.0000000000001291

Jiang, J., Gu, X., Wang, H., and Ding, S. (2021). Resveratrol improves cardiac function and left ventricular fibrosis after myocardial infarction in rats by inhibiting NLRP3 inflammasome activity and the TGF-β1/SMAD2 signaling pathway. *PeerJ* 9, e11501. doi:10.7717/peerj.11501

Jiang, L., Liang, J., Huang, W., Ma, J., Park, K. H., Wu, Z., et al. (2022). CRISPR activation of endogenous genes reprograms fibroblasts into cardiovascular progenitor cells for myocardial infarction therapy. *Mol. Ther.* 30, 54–74. doi:10.1016/j.ymthe.2021.10.015

Jiao, W., Hao, J., Xie, Y., Meng, M., and Gao, W. (2022). EZH2 mitigates the cardioprotective effects of mesenchymal stem cell-secreted exosomes against infarction via HMGA2-mediated PI3K/AKT signaling. *BMC Cardiovasc Disord.* 22, 95. doi:10.1186/s12872-022-02533-9

Jin, H., Liu, K., Huang, X., Huo, H., Mou, J., Qiao, Z., et al. (2022). Genetic lineage tracing of pericardial cavity macrophages in the injured heart. *Circ. Res.* 130, 1682–1697. doi:10.1161/CIRCRESAHA.122.320567

Kachanova, O., Lobov, A., and Malashicheva, A. (2022). The role of the notch signaling pathway in recovery of cardiac function after myocardial infarction. *Int. J. Mol. Sci.* 23, 12509. doi:10.3390/ijms232012509

Kali, A., Cokic, I., Tang, R. L., Yang, H. J., Sharif, B., MarbáN, E., et al. (2014). Determination of location, size, and transmurality of chronic myocardial infarction without exogenous contrast media by using cardiac magnetic resonance imaging at 3 T. *Circ. Cardiovasc Imaging* 7, 471–481. doi:10.1161/CIRCIMAGING.113.001541

Kang, S., Verma, S., Hassanabad, A. F., Teng, G., Belke, D. D., Dundas, J. A., et al. (2020). Direct effects of empagliflozin on extracellular matrix remodelling in human cardiac myofibroblasts: Novel translational clues to explain EMPA-REG OUTCOME results. *Can. J. Cardiol.* 36, 543–553. doi:10.1016/j.cjca.2019.08.033

Kangawa, K., Fukuda, A., Kubota, I., Hayashi, Y., Minamitake, Y., and Matsuo, H. (1984). Human atrial natriuretic polypeptides (hANP): Purification, structure synthesis and biological activity. *J. Hypertens. Suppl.* 2 (2), S321–S323.

Kanisicak, O., Khalil, H., Ivey, M. J., Karch, J., Maliken, B. D., Correll, R. N., et al. (2016). Genetic lineage tracing defines myofibroblast origin and function in the injured heart. *Nat. Commun.* 7, 12260. doi:10.1038/ncomms12260

Kasama, S., Furuya, M., Toyama, T., Ichikawa, S., and Kurabayashi, M. (2008). Effect of atrial natriuretic peptide on left ventricular remodelling in patients with acute myocardial infarction. *Eur. Heart J.* 29, 1485–1494. doi:10.1093/eurheartj/ehn206

Kaur, K., Hadas, Y., Kurian, A. A., Żak, M. M., Yoo, J., Mahmood, A., et al. (2021). Direct reprogramming induces vascular regeneration post muscle ischemic injury. *Mol. Ther.* 29, 3042–3058. doi:10.1016/j.ymthe.2021.07.014

Ke, X., Li, M., Wang, X., Liang, J., Wang, X., Wu, S., et al. (2020). An injectable chitosan/dextran/β -glycerophosphate hydrogel as cell delivery carrier for therapy of myocardial infarction. *Carbohydr. Polym.* 229, 115516. doi:10.1016/j.carbpol.2019.115516

Kensler, T. W., Wakabayashi, N., and Biswal, S. (2007). Cell survival responses to environmental stresses via the Keap1-Nrf2-ARE pathway. *Annu. Rev. Pharmacol. Toxicol.* 47, 89–116. doi:10.1146/annurev.pharmtox.46.120604.141046

Kessler, L., Kupusovic, J., Ferdinandus, J., Hirmas, N., Umutlu, L., Zarrad, F., et al. (2021). Visualization of fibroblast activation after myocardial infarction using 68Ga-fapi PET. *Clin. Nucl. Med.* 46, 807–813. doi:10.1097/RLU.0000000000003745

Kilci, H., AltıNBILEK, E., Çetinkal, G., SıĞıRCı, S., KoçAŞ, B. B., YıLDıZ, S. S., et al. (2021). Relation of a novel fibrosis marker and post-myocardial infarction left ventricular ejection fraction in revascularized patients. *Biomark. Med.* 15, 1651–1658. doi:10.2217/bmm-2021-0003

Kino, T., Khan, M., and Mohsin, S. (2020). The regulatory role of T cell responses in cardiac remodeling following myocardial infarction. *Int. J. Mol. Sci.* 21, 5013. doi:10.3390/ijms21145013

Kitsuka, T., Shiraki, A., Oyama, J. I., Nakagami, H., Tanaka, A., and Node, K. (2022). A novel soluble epoxide hydrolase vaccine protects murine cardiac muscle against myocardial infarction. *Sci. Rep.* 12, 6923. doi:10.1038/s41598-022-10641-x

Klapper-Goldstein, H., Verma, A., Elyagon, S., Gillis, R., Murninkas, M., Pittala, S., et al. (2020). VDAC1 in the diseased myocardium and the effect of VDAC1-interacting compound on atrial fibrosis induced by hyperaldosteronism. *Sci. Rep.* 10, 22101. doi:10.1038/s41598-020-79056-w

Kleinert, H. D. (1996). Hemodynamic effects of renin inhibitors. *Am. J. Nephrol.* 16, 252–260. doi:10.1159/000169005

Kobusiak-Prokopowicz, M., Orzeszko, J., Mazur, G., Mysiak, A., Orda, A., Poreba, R., et al. (2007). Chemokines and left ventricular function in patients with acute myocardial infarction. *Eur. J. Intern Med.* 18, 288–294. doi:10.1016/j.ejim.2007.02.001

Kompa, A. R., Greening, D. W., Kong, A. M., Mcmillan, P. J., Fang, H., Saxena, R., et al. (2021). Sustained subcutaneous delivery of secretome of human cardiac stem cells promotes cardiac repair following myocardial infarction. *Cardiovasc Res.* 117, 918–929. doi:10.1093/cvr/cvaa088

Kruszewska, J., Cudnoch-Jedrzejewska, A., and Czarzasta, K. (2022). Remodeling and fibrosis of the cardiac muscle in the course of obesity-pathogenesis and involvement of the extracellular matrix. *Int. J. Mol. Sci.* 23, 4195. doi:10.3390/ijms23084195

Kubota, A., Suto, A., Suga, K., Iwata, A., Tanaka, S., Suzuki, K., et al. (2021). Inhibition of Interleukin-21 prolongs the survival through the promotion of wound healing after myocardial infarction. *J. Mol. Cell Cardiol.* 159, 48–61. doi:10.1016/j.yjmcc.2021.06.006

Kuhn, M. (2016). Molecular physiology of membrane guanylyl cyclase receptors. *Physiol. Rev.* 96, 751–804. doi:10.1152/physrev.00022.2015

Kuwabara, J. T., Hara, A., Bhutada, S., Gojanovich, G. S., Chen, J., Hokutan, K., et al. (2022). Consequences of PDGFRα(+) fibroblast reduction in adult murine hearts. *Elife* 11, e69854. doi:10.7554/eLife.69854

Landry, N. M., Rattan, S. G., Filomeno, K. L., Meier, T. W., Meier, S. C., Foran, S. J., et al. (2021). SKI activates the Hippo pathway via LIMD1 to inhibit cardiac fibroblast activation. *Basic Res. Cardiol.* 116, 25. doi:10.1007/s00395-021-00865-9

Lang, M., Ou, D., Liu, Z., Li, Y., Zhang, X., and Zhang, F. (2021). LncRNA MHRT promotes cardiac fibrosis via miR-3185 pathway following myocardial infarction. *Int. Heart J.* 62, 891–899. doi:10.1536/ihj.20-298

Langer, L. B. N., Hess, A., Korkmaz, Z., Tillmanns, J., Reffert, L. M., Bankstahl, J. P., et al. (2021). Molecular imaging of fibroblast activation protein after myocardial infarction using the novel radiotracer [(68)Ga]MHLL1. *Theranostics* 11, 7755–7766. doi:10.7150/thno.51419

Lantz, C., Becker, A., and Thorp, E. B. (2021). Can polarization of macrophage metabolism enhance cardiac regeneration? *J. Mol. Cell Cardiol.* 160, 87–96. doi:10.1016/j.yjmcc.2021.07.003

Leader, C. J., Wilkins, G. T., and Walker, R. J. (2021). The effect of spironolactone on cardiac and renal fibrosis following myocardial infarction in established hypertension in the transgenic Cyp1a1Ren2 rat. *PLoS One* 16, e0260554. doi:10.1371/journal.pone.0260554

Leancă, S. A., Crișu, D., Petriș, A. O., AfrăsâNIE, I., Genes, A., Costache, A. D., et al. (2022). Left ventricular remodeling after myocardial infarction: From physiopathology to treatment. *Life* 12.

Lee, T. L., Lai, T. C., Lin, S. R., Lin, S. W., Chen, Y. C., Pu, C. M., et al. (2021). Conditioned medium from adipose-derived stem cells attenuates ischemia/reperfusion-induced cardiac injury through the microRNA-221/222/PUMA/ETS-1 pathway. *Theranostics* 11, 3131–3149. doi:10.7150/thno.52677

Lee, T. M., Harn, H. J., Chiou, T. W., Chuang, M. H., Chen, C. H., Chuang, C. H., et al. (2020). Host pre-conditioning improves human adipose-derived stem cell transplantation in ageing rats after myocardial infarction: Role of NLRP3 inflammasome. *J. Cell Mol. Med.* 24, 12272–12284. doi:10.1111/jcmm.15403

Lei, Q., Yi, T., Li, H., Yan, Z., Lv, Z., Li, G., et al. (2020). Ubiquitin C-terminal hydrolase L1 (UCHL1) regulates post-myocardial infarction cardiac fibrosis through glucose-regulated protein of 78 kDa (GRP78). *Sci. Rep.* 10, 10604. doi:10.1038/s41598-020-67746-4

Leifheit-Nestler, M., Kirchhoff, F., Nespor, J., Richter, B., Soetje, B., Klintschar, M., et al. (2018). Fibroblast growth factor 23 is induced by an activated renin-angiotensin-aldosterone system in cardiac myocytes and promotes the pro-fibrotic crosstalk between cardiac myocytes and fibroblasts. *Nephrol. Dial. Transpl.* 33, 1722–1734. doi:10.1093/ndt/gfy006

Li, C. Y., Zhang, J. R., Li, X. X., Zhao, L., XI, H., Hu, W. N., et al. (2021a). Lefty1 ameliorates post-infarction fibrosis by suppressing p-smad2 and p-ERK1/2 signaling pathways. *J. Cardiovasc Transl. Res.* 14, 636–646. doi:10.1007/s12265-020-10089-2

Li, F., Li, L., Zhang, J., Yang, X., and Liu, Y. (2022a). Histone methyltransferase DOT1L mediates the TGF-β1/Smad3 signaling pathway through epigenetic modification of SYK in myocardial infarction. *Hum. Cell* 35, 98–110. doi:10.1007/s13577-021-00625-w

Li, F., Long, T. Y., Bi, S. S., Sheikh, S. A., and Zhang, C. L. (2020a). circPAN3 exerts a profibrotic role via sponging miR-221 through FoxO3/ATG7-activated autophagy in a rat model of myocardial infarction. *Life Sci.* 257, 118015. doi:10.1016/j.lfs.2020.118015

Li, F., Yang, Y., Xue, C., Tan, M., Xu, L., Gao, J., et al. (2020b). Zinc Finger Protein ZBTB20 protects against cardiac remodelling post-myocardial infarction via ROS-TNFα/ASK1/JNK pathway regulation. *J. Cell Mol. Med.* 24, 13383–13396. doi:10.1111/jcmm.15961

Li, G., Yang, J., Zhang, D., Wang, X., Han, J., and Guo, X. (2022b). Research progress of myocardial fibrosis and atrial fibrillation. *Front. Cardiovasc Med.* 9, 889706. doi:10.3389/fcvm.2022.889706

Li, J., Ding, H., Li, Y., Zhou, H., Wang, W., Mei, Y., et al. (2021b). Alarin alleviated cardiac fibrosis via attenuating oxidative stress in heart failure rats. *Amino Acids* 53, 1079–1089. doi:10.1007/s00726-021-03005-8

Li, J., Ge, F., Wuken, S., Jiao, S., Chen, P., Huang, M., et al. (2022c). Zerumbone, a humulane sesquiterpene from Syringa pinnatifolia, attenuates cardiac fibrosis by inhibiting of the TGF-β1/Smad signaling pathway after myocardial infarction in mice. *Phytomedicine* 100, 154078. doi:10.1016/j.phymed.2022.154078

Li, J., Gong, L., Zhang, R., Li, S., Yu, H., Liu, Y., et al. (2021c). Fibroblast growth factor 21 inhibited inflammation and fibrosis after myocardial infarction via EGR1. *Eur. J. Pharmacol.* 910, 174470. doi:10.1016/j.ejphar.2021.174470

Li, J., Li, R., Tuleta, I., Hernandez, S. C., Humeres, C., Hanna, A., et al. (2022d). The role of endogenous Smad7 in regulating macrophage phenotype following myocardial infarction. *Faseb J.* 36, e22400. doi:10.1096/fj.202101956RR

Li, J., Salvador, A. M., Li, G., Valkov, N., Ziegler, O., Yeri, A., et al. (2021d). Mir-30d regulates cardiac remodeling by intracellular and paracrine signaling. *Circ. Res.* 128, e1–e23. doi:10.1161/CIRCRESAHA.120.317244

Li, Q., and Verma, I. M. (2002). NF-kappaB regulation in the immune system. *Nat. Rev. Immunol.* 2, 725–734. doi:10.1038/nri910

Li, R., Liu, R., Yan, F., Zhuang, X., Shi, H., and Gao, X. (2020c). Inhibition of TRPA1 promotes cardiac repair in mice after myocardial infarction. *J. Cardiovasc Pharmacol.* 75, 240–249. doi:10.1097/FJC.0000000000000783

Li, S., Yokota, T., Wang, P., Ten Hoeve, J., Ma, F., LE, T. M., et al. (2022e). Cardiomyocytes disrupt pyrimidine biosynthesis in nonmyocytes to regulate heart repair. *J. Clin. Invest* 132, e149711. doi:10.1172/JCI149711

Li, T. Y., Su, W., Li, L. L., Zhao, X. G., Yang, N., Gai, J. X., et al. (2022f). Critical role of PAFR/YAP1 positive feedback loop in cardiac fibrosis. *Acta Pharmacol. Sin.* 43, 2862–2872. doi:10.1038/s41401-022-00903-9

Li, T., Zhuang, Y., Yang, W., Xie, Y., Shang, W., Su, S., et al. (2021e). Silencing of METTL3 attenuates cardiac fibrosis induced by myocardial infarction via

inhibiting the activation of cardiac fibroblasts. *Faseb J.* 35, e21162. doi:10.1096/fj.201903169R

Li, X., Xiang, N., and Wang, Z. (2020d). Ginsenoside Rg2 attenuates myocardial fibrosis and improves cardiac function after myocardial infarction via AKT signaling pathway. *Biosci. Biotechnol. Biochem.* 84, 2199–2206. doi:10.1080/09168451.2020.1793292

Li, X. X., Mu, B., Li, X., and Bie, Z. D. (2022g). circCELF1 inhibits myocardial fibrosis by regulating the expression of DKK2 through FTO/m(6)A and miR-636. *J. Cardiovasc Transl. Res.* 15, 998–1009. doi:10.1007/s12265-022-10209-0

Li, X., Zhang, F., Zhou, H., Hu, Y., Guo, D., Fang, X., et al. (2020e). Interplay of TNF-α, soluble TNF receptors and oxidative stress in coronary chronic total occlusion of the oldest patients with coronary heart disease. *Cytokine* 125, 154836. doi:10.1016/j.cyto.2019.154836

Li, Y., Dong, M., Wang, Q., Kumar, S., Zhang, R., Cheng, W., et al. (2021f). HIMF deletion ameliorates acute myocardial ischemic injury by promoting macrophage transformation to reparative subtype. *Basic Res. Cardiol.* 116, 30. doi:10.1007/s00395-021-00867-7

Li, Y., Liu, M., Yi, J., Song, X., Zheng, X., Liu, D., et al. (2020f). Exogenous hydrogen sulfide inhibits apoptosis by regulating endoplasmic reticulum stress-autophagy axis and improves myocardial reconstruction after acute myocardial infarction. *Acta Biochim. Biophys. Sin. (Shanghai)* 52, 1325–1336. doi:10.1093/abbs/gmaa133

Li, Y., Qi, Q., Yang, W. C., Zhang, T. L., Lu, C. C., Yao, Y. J., et al. (2020g). Sphingosylphosphorylcholine alleviates hypoxia-caused apoptosis in cardiac myofibroblasts via CaM/p38/STAT3 pathway. *Apoptosis* 25, 853–863. doi:10.1007/s10495-020-01639-9

Li, Y., Qin, L., Bai, Q., Zhang, J., Chen, R., and Song, K. (2021g). CD100 modulates cytotoxicity of CD8(+) T cells in patients with acute myocardial infarction. *BMC Immunol.* 22, 13. doi:10.1186/s12865-021-00406-y

Liang, B., Zhang, X. X., Li, R., Zhu, Y. C., Tian, X. J., and Gu, N. (2022). Guanxin V alleviates acute myocardial infarction by restraining oxidative stress damage, apoptosis, and fibrosis through the TGF-β1 signalling pathway. *Phytomedicine* 100, 154077. doi:10.1016/j.phymed.2022.154077

Liang, Y., Xu, X., Li, Q., Deng, Y., Xie, M., Zheng, Y., et al. (2020). Chronic alcohol intake exacerbates cardiac dysfunction after myocardial infarction. *Alcohol Alcohol* 55, 524–530. doi:10.1093/alcalc/agaa055

Lima Correa, B., EL Harane, N., Desgres, M., Perotto, M., Alayrac, P., Guillas, C., et al. (2021). Extracellular vesicles fail to trigger the generation of new cardiomyocytes in chronically infarcted hearts. *Theranostics* 11, 10114–10124. doi:10.7150/thno.62304

Liu, A., Zhang, Y., Xun, S., Zhou, G., Lin, L., and Mei, Y. (2022). Fibroblast growth factor 12 attenuated cardiac remodeling via suppressing oxidative stress. *Peptides* 153, 170786. doi:10.1016/j.peptides.2022.170786

Liu, J. W., Liu, H. T., and Chen, L. (2021a). The therapeutic role of Slit2 in anti-fibrosis, anti-inflammation and anti-oxidative stress in rats with coronary heart disease. *Cardiovasc Toxicol.* 21, 973–983. doi:10.1007/s12012-021-09688-5

Liu, J., Yang, C., Liu, T., Deng, Z., Fang, W., Zhang, X., et al. (2020a). Eosinophils improve cardiac function after myocardial infarction. *Nat. Commun.* 11, 6396. doi:10.1038/s41467-020-19297-5

Liu, W., Sun, J., Guo, Y., Liu, N., Ding, X., Zhang, X., et al. (2020b). Calhex231 ameliorates myocardial fibrosis post myocardial infarction in rats through the autophagy-NLRP3 inflammasome pathway in macrophages. *J. Cell Mol. Med.* 24, 13440–13453. doi:10.1111/jcmm.15969

Liu, Y., Fan, Y., Li, J., Chen, M., Chen, A., Yang, D., et al. (2021b). Combination of LCZ696 and ACEI further improves heart failure and myocardial fibrosis after acute myocardial infarction in mice. *Biomed. Pharmacother.* 133, 110824. doi:10.1016/j.biopha.2020.110824

Loi, H., Kramar, S., Laborde, C., Marsal, D., Pizzinat, N., Cussac, D., et al. (2021). Metformin attenuates postinfarction myocardial fibrosis and inflammation in mice. *Int. J. Mol. Sci.* 22, 9393. doi:10.3390/ijms22179393

Long, F., Wang, Q., Yang, D., Zhu, M., Wang, J., Zhu, Y., et al. (2020). Targeting JMJD3 histone demethylase mediates cardiac fibrosis and cardiac function following myocardial infarction. *Biochem. Biophys. Res. Commun.* 528, 671–677. doi:10.1016/j.bbrc.2020.05.115

Lu, L., Ma, J., Sun, M., Wang, X., Gao, E., Lu, L., et al. (2020). Melatonin ameliorates MI-induced cardiac remodeling and apoptosis through a JNK/p53-Dependent mechanism in diabetes mellitus. *Oxid. Med. Cell Longev.* 2020, 1535201. doi:10.1155/2020/1535201

Lu, Y. G., Tan, H., Ma, Q., Li, X. X., Cui, J., Zhang, X., et al. (2021). SH2 domain-containing protein tyrosine phosphatase-2 (SHP-2) prevents cardiac remodeling after myocardial infarction through ERK/SMAD signaling pathway. *Hum. Cell* 34, 325–334. doi:10.1007/s13577-020-00430-x

Luo, S., Zhang, M., Wu, H., Ding, X., Li, D., Dong, X., et al. (2021). Sail: A new conserved anti-fibrotic lncRNA in the heart. *Basic Res. Cardiol.* 116, 15. doi:10.1007/s00395-021-00854-y

Lymperopoulos, A. (2018). Arrestins in the cardiovascular system: An update. *Prog. Mol. Biol. Transl. Sci.* 159, 27–57. doi:10.1016/bs.pmbts.2018.07.003

Lymperopoulos, A., Cora, N., Maning, J., Brill, A. R., and Sizova, A. (2021). Signaling and function of cardiac autonomic nervous system receptors: Insights from the GPCR signalling universe. *Febs J.* 288, 2645–2659. doi:10.1111/febs.15771

Lymperopoulos, A., Rengo, G., and Koch, W. J. (2007). Adrenal adrenoceptors in heart failure: Fine-tuning cardiac stimulation. *Trends Mol. Med.* 13, 503–511. doi:10.1016/j.molmed.2007.10.005

Ma, J., Ren, M., Li, J., Zheng, C., Chen, Q., and Ma, S. (2022). Danqi soft caspule prevents atrial fibrillation by ameliorating left atrial remodeling through inhibiting cardiac fibroblasts differentiation and function. *Phytomedicine* 101, 154134. doi:10.1016/j.phymed.2022.154134

Ma, Y., Kuang, Y., Bo, W., Liang, Q., Zhu, W., Cai, M., et al. (2021). Exercise training alleviates cardiac fibrosis through increasing fibroblast growth factor 21 and regulating TGF-β1-smad2/3-MMP2/9 signaling in mice with myocardial infarction. *Int. J. Mol. Sci.* 22, 12341. doi:10.3390/ijms222212341

Ma, Y. (2021). Role of neutrophils in cardiac injury and repair following myocardial infarction. *Cells* 10, 1676. doi:10.3390/cells10071676

Madonna, R., Pieragostino, D., Rossi, C., Guarnieri, S., Nagy, C. T., Giricz, Z., et al. (2020). Transplantation of telomerase/myocardin-co-expressing mesenchymal cells in the mouse promotes myocardial revascularization and tissue repair. *Vasc. Pharmacol.* 135, 106807. doi:10.1016/j.vph.2020.106807

Mahdiui, M. E., VAN DER Bijl, P., Abou, R., DE Paula Lustosa, R., VAN DER Geest, R., Ajmone Marsan, N., et al. (2021). Myocardial work, an echocardiographic measure of post myocardial infarct scar on contrast-enhanced cardiac magnetic resonance. *Am. J. Cardiol.* 151, 1–9. doi:10.1016/j.amjcard.2021.04.009

Majzner, R. G., and Mackall, C. L. (2018). Tumor antigen escape from CAR T-cell therapy. *Cancer Discov.* 8, 1219–1226. doi:10.1158/2159-8290.CD-18-0442

Mangali, S., Bhat, A., Dasari, D., Sriram, D., and Dhar, A. (2021). Inhibition of double stranded RNA dependent protein kinase (PKR) abrogates isoproterenol induced myocardial ischemia *in vitro* in cultured cardiomyocytes and *in vivo* in wistar rats. *Eur. J. Pharmacol.* 906, 174223. doi:10.1016/j.ejphar.2021.174223

Maric, D., Paterek, A., Delaunay, M., LóPEZ, I. P., Arambasic, M., and Diviani, D. (2021). A-kinase anchoring protein 2 promotes protection against myocardial infarction. *Cells* 10, 2861. doi:10.3390/cells10112861

Marsit, O., Clavel, M. A., Paquin, A., DeschêNES, V., Hadjadj, S., SéNéCHAL-Dumais, I., et al. (2022). Effects of cyproheptadine on mitral valve remodeling and regurgitation after myocardial infarction. *J. Am. Coll. Cardiol.* 80, 500–510. doi:10.1016/j.jacc.2022.05.025

Masurkar, N., Bouvet, M., Logeart, D., Jouve, C., Dramé, F., Claude, O., et al. (2023). Novel cardiokine GDF3 predicts adverse fibrotic remodeling after myocardial infarction. *Circulation* 147, 498–511. doi:10.1161/CIRCULATIONAHA.121.056272

Mehdipoor, M., Damirchi, A., Razavi Tousi, S. M. T., and Babaei, P. (2021). Concurrent vitamin D supplementation and exercise training improve cardiac fibrosis via TGF-β/Smad signaling in myocardial infarction model of rats. *J. Physiol. Biochem.* 77, 75–84. doi:10.1007/s13105-020-00778-6

Merino-Caviedes, S., Gutierrez, L. K., Alfonso-AlmazáN, J. M., Sanz-EstéBANEZ, S., Cordero-Grande, L., Quintanilla, J. G., et al. (2021). Time-efficient three-dimensional transmural scar assessment provides relevant substrate characterization for ventricular tachycardia features and long-term recurrences in ischemic cardiomyopathy. *Sci. Rep.* 11, 18722. doi:10.1038/s41598-021-97399-w

Mestas, J., and Hughes, C. C. (2004). Of mice and not men: Differences between mouse and human immunology. *J. Immunol.* 172, 2731–2738. doi:10.4049/jimmunol.172.5.2731

Methatham, T., Nagai, R., and Aizawa, K. (2022). A new hypothetical concept in metabolic understanding of cardiac fibrosis: Glycolysis combined with TGF-β and KLF5 signaling. *Int. J. Mol. Sci.* 23, 4302. doi:10.3390/ijms23084302

Michel, L., Korste, S., Spomer, A., Hendgen-Cotta, U. B., Rassaf, T., and Totzeck, M. (2022). PD1 deficiency modifies cardiac immunity during baseline conditions and in reperfused acute myocardial infarction. *Int. J. Mol. Sci.* 23, 7533. doi:10.3390/ijms23147533

Michel, L. Y. M., Farah, C., and Balligand, J. L. (2020). The Beta3 adrenergic receptor in healthy and pathological cardiovascular tissues. *Cells* 9, 2584. doi:10.3390/cells9122584

Mo, F., Luo, Y., Yan, Y., Li, J., Lai, S., and Wu, W. (2021). Are activated B cells involved in the process of myocardial fibrosis after acute myocardial infarction? An *in vivo* experiment. *BMC Cardiovasc Disord.* 21, 5. doi:10.1186/s12872-020-01775-9

Moheimani, H. R., Amiriani, T., Alizadeh, A. M., Jand, Y., Shakiba, D., Ensan, P. S., et al. (2021). Preconditioning and anti-apoptotic effects of Metformin and Cyclosporine-A in an isolated bile duct-ligated rat heart. *Eur. J. Pharmacol.* 893, 173807. doi:10.1016/j.ejphar.2020.173807

Mokhtari, B., Badalzadeh, R., and Aboutaleb, N. (2021). Modulation of autophagy as the target of mesenchymal stem cells-derived conditioned medium in rat model of myocardial ischemia/reperfusion injury. *Mol. Biol. Rep.* 48, 3337–3348. doi:10.1007/s11033-021-06359-0

Morfino, P., Aimo, A., Castiglione, V., GáLVEZ-MontóN, C., Emdin, M., and Bayes-Genis, A. (2022). Treatment of cardiac fibrosis: From neuro-hormonal inhibitors to CAR-T cell therapy. *Heart Fail Rev.* 28, 555–569. doi:10.1007/s10741-022-10279-x

Mouton, A. J., Flynn, E. R., Moak, S. P., Aitken, N. M., Omoto, A. C. M., Li, X., et al. (2021). Dimethyl fumarate preserves left ventricular infarct integrity following myocardial infarction via modulation of cardiac macrophage and fibroblast oxidative metabolism. *J. Mol. Cell Cardiol.* 158, 38–48. doi:10.1016/j.yjmcc.2021.05.008

Mouton, A. J., Ma, Y., Rivera Gonzalez, O. J., Daseke, M. J., 2Nd, Flynn, E. R., Freeman, T. C., et al. (2019). Fibroblast polarization over the myocardial infarction time continuum shifts roles from inflammation to angiogenesis. *Basic Res. Cardiol.* 114, 6. doi:10.1007/s00395-019-0715-4

MüHLFELD, C., and Schipke, J. (2022)., 11. Cells.Methodological progress of stereology in cardiac research and its application to normal and pathological heart development

MüLLER, B., Schneider, M., MüLLER, K. A. L., Lunov, O., Borst, O., Simmet, T., et al. (2021). Protective role of Gremlin-1 in myocardial function. *Eur. J. Clin. Invest* 51, e13539. doi:10.1111/eci.13539

Muslin, A. J. (2008). MAPK signalling in cardiovascular health and disease: Molecular mechanisms and therapeutic targets. *Clin. Sci. (Lond)* 115, 203–218. doi:10.1042/CS20070430

Nakayama, Y., Mukai, N., Wang, B. F., Yang, K., Patwari, P., Kitsis, R. N., et al. (2021). Txnip C247S mutation protects the heart against acute myocardial infarction. *J. Mol. Cell Cardiol.* 155, 36–49. doi:10.1016/j.yjmcc.2021.02.013

Nikolov, A., and Popovski, N. (2022). Extracellular matrix in heart disease: Focus on circulating collagen type I and III derived peptides as biomarkers of myocardial fibrosis and their potential in the prognosis of heart failure: A concise review. *Metabolites* 12, 297. doi:10.3390/metabo12040297

Nogami, M., Hoshi, T., Toukairin, Y., Arai, T., and Nishio, T. (2020). Immunohistochemistry of advanced glycation end product N(ε)-(carboxymethyl) lysine in coronary arteries in relation to cardiac fibrosis and serum N-terminal-pro basic natriuretic peptide in forensic autopsy cases. *BMC Res. Notes* 13, 239. doi:10.1186/s13104-020-05082-6

Ong, S. B., HernáNDEZ-ReséNDIZ, S., Crespo-Avilan, G. E., Mukhametshina, R. T., Kwek, X. Y., Cabrera-Fuentes, H. A., et al. (2018). Inflammation following acute myocardial infarction: Multiple players, dynamic roles, and novel therapeutic opportunities. *Pharmacol. Ther.* 186, 73–87. doi:10.1016/j.pharmthera.2018.01.001

Osokina, A., Karetnikova, V., Polikutina, O., Ivanova, A., Gruzdeva, O., Dyleva, Y., et al. (2021). Prognostic potential of cardiac structural and functional parameters and N-terminal propeptide of type III procollagen in predicting cardiac fibrosis one year after myocardial infarction with preserved left ventricular ejection fraction. *Aging (Albany NY)* 13, 194–203. doi:10.18632/aging.202495

Osokina, A. V., Karetnikova, V. N., Polikutina, O. M., Ivanova, A. V., Artemova, T. P., Ryzhenkova, S. N., et al. (2020). Dynamics of parameters of transmitral blood flow and markers of myocardial fibrosis in patients with myocardial infarction. *Kardiologiia* 60, 84–91. doi:10.18087/cardio.2020.6.n994

Pan, Y., Li, Q., Yan, H., Huang, J., and Wang, Z. (2020). Apela improves cardiac and renal function in mice with acute myocardial infarction. *J. Cell Mol. Med.* 24, 10382–10390. doi:10.1111/jcmm.15651

Pandey, K. N. (2018). Molecular and genetic aspects of guanylyl cyclase natriuretic peptide receptor-A in regulation of blood pressure and renal function. *Physiol. Genomics* 50, 913–928. doi:10.1152/physiolgenomics.00083.2018

Pei, J., Cai, L., Wang, F., Xu, C., Pei, S., Guo, H., et al. (2022). LPA(2) contributes to vascular endothelium homeostasis and cardiac remodeling after myocardial infarction. *Circ. Res.* 131, 388–403. doi:10.1161/CIRCRESAHA.122.321036

Peres Valgas Da Silva, C., Shettigar, V. K., Baer, L. A., Abay, E., Pinckard, K. M., Vinales, J., et al. (2022). Exercise training after myocardial infarction increases survival but does not prevent adverse left ventricle remodeling and dysfunction in high-fat diet fed mice. *Life Sci.* 311, 121181. doi:10.1016/j.lfs.2022.121181

Polacin, M., Karolyi, M., Eberhard, M., Matziris, I., Alkadhi, H., Kozerke, S., et al. (2022). Segmental strain for scar detection in acute myocardial infarcts and in follow-up exams using non-contrast CMR cine sequences. *BMC Cardiovasc Disord.* 22, 226. doi:10.1186/s12872-022-02664-z

Potz, B. A., Sabe, A. A., Sabe, S. A., Lawandy, I. J., Abid, M. R., Clements, R. T., et al. (2022). Calpain inhibition decreases myocardial fibrosis in chronically ischemic hypercholesterolemic swine. *J. Thorac. Cardiovasc Surg.* 163, e11–e27. doi:10.1016/j.jtcvs.2019.11.150

Prabhu, S. D., and Frangogiannis, N. G. (2016). The biological basis for cardiac repair after myocardial infarction: From inflammation to fibrosis. *Circ. Res.* 119, 91–112. doi:10.1161/CIRCRESAHA.116.303577

Pugliese, N. R., Masi, S., and Taddei, S. (2020). The renin-angiotensin-aldosterone system: A crossroad from arterial hypertension to heart failure. *Heart Fail Rev.* 25, 31–42. doi:10.1007/s10741-019-09855-5

Qian, M., Feng, Z. Q., Zheng, R. N., Hu, K. W., Sun, J. Z., Sun, H. B., et al. (2022). Qi-Tai-Suan, an oleanolic acid derivative, ameliorates ischemic heart failure via suppression of cardiac apoptosis, inflammation and fibrosis. *Chin. J. Nat. Med.* 20, 432–442. doi:10.1016/S1875-5364(22)60156-0

Qin, R., Zhao, Q., Han, B., Zhu, H. P., Peng, C., Zhan, G., et al. (2022). Indole-based small molecules as potential therapeutic agents for the treatment of fibrosis. *Front. Pharmacol.* 13, 845892. doi:10.3389/fphar.2022.845892

Qiu, F., Han, Y., Shao, X., Paulo, P., Li, W., Zhu, M., et al. (2020). Knockdown of endogenous RNF4 exacerbates ischaemia-induced cardiomyocyte apoptosis in mice. *J. Cell Mol. Med.* 24, 9545–9559. doi:10.1111/jcmm.15363

Raj, P., Sayfee, K., Parikh, M., Yu, L., Wigle, J., Netticadan, T., et al. (2021). Comparative and combinatorial effects of resveratrol and sacubitril/valsartan alongside valsartan on cardiac remodeling and dysfunction in MI-induced rats. *Molecules* 26, 5006. doi:10.3390/molecules26165006

Rakhshan, K., Sharifi, M., Ramezani, F., Azizi, Y., and Aboutaleb, N. (2022). ERK/HIF-1α/VEGF pathway: A molecular target of ELABELA (ELA) peptide for attenuating cardiac ischemia-reperfusion injury in rats by promoting angiogenesis. *Mol. Biol. Rep.* 49, 10509–10519. doi:10.1007/s11033-022-07818-y

Ramos, S. R., Pieles, G., Sun, M., Slorach, C., Hui, W., and Friedberg, M. K. (2018). Early versus late cardiac remodeling during right ventricular pressure load and impact of preventive versus rescue therapy with endothelin-1 receptor blockers. *J. Appl. Physiol.* 124, 1349–1362. doi:10.1152/japplphysiol.00975.2017

Rashid, F. N., Clayton, Z. E., Ogawa, M., Perdomo, J., Hume, R. D., Kizana, E., et al. (2021). Platelet derived growth factor-A (Pdgf-a) gene transfer modulates scar composition and improves left ventricular function after myocardial infarction. *Int. J. Cardiol.* 341, 24–30. doi:10.1016/j.ijcard.2021.07.021

Ray, P. D., Huang, B. W., and Tsuji, Y. (2012). Reactive oxygen species (ROS) homeostasis and redox regulation in cellular signaling. *Cell Signal* 24, 981–990. doi:10.1016/j.cellsig.2012.01.008

Razin, T., Melamed-Book, N., Argaman, J., Galin, I., Lowy, Y., Anuka, E., et al. (2021). Interleukin-1α dependent survival of cardiac fibroblasts is associated with StAR/STARD1 expression and improved cardiac remodeling and function after myocardial infarction. *J. Mol. Cell Cardiol.* 155, 125–137. doi:10.1016/j.yjmcc.2020.10.013

Reusswig, F., Polzin, A., Klier, M., Dille, M. A., Ayhan, A., Benkhoff, M., et al. (2022)., 11. Cells.Only acute but not chronic thrombocytopenia protects mice against left ventricular dysfunction after acute myocardial infarction

Rockey, D. C., Bell, P. D., and Hill, J. A. (2015). Fibrosis-A common pathway to organ injury and failure. *N. Engl. J. Med.* 373, 96. doi:10.1056/NEJMc1504848

Rosenzweig, R., Kumar, V., Gupta, S., Bermeo-Blanco, O., Stratton, M. S., Gumina, R. J., et al. (2022). Estrogen receptor-β agonists modulate T-lymphocyte activation and ameliorate left ventricular remodeling during chronic heart failure. *Circ. Heart Fail* 15, e008997. doi:10.1161/CIRCHEARTFAILURE.121.008997

Rotem, I., Konfino, T., Caller, T., Schary, Y., Shaihov-Teper, O., Palevski, D., et al. (2022). Osteopontin promotes infarct repair. *Basic Res. Cardiol.* 117, 51. doi:10.1007/s00395-022-00957-0

Ruchaya, P. J., Lewis-Mcdougall, F. C., Sornkarn, N., Amin, S., Grimsdell, B., Shaalan, A., et al. (2022). Transplantation of skeletal muscle-derived sca-1(+)/PW1(+)/pax7(-) interstitial cells (PICs) improves cardiac function and attenuates remodeling in mice subjected to myocardial infarction. *Cells* 11, 4050. doi:10.3390/cells11244050

Ruozi, G., Bortolotti, F., Mura, A., Tomczyk, M., Falcione, A., Martinelli, V., et al. (2022). Cardioprotective factors against myocardial infarction selected *in vivo* from an AAV secretome library. *Sci. Transl. Med.* 14, eabo0699. doi:10.1126/scitranslmed.abo0699

Rurik, J. G., TombáCZ, I., Yadegari, A., MéNDEZ FernáNDEZ, P. O., Shewale, S. V., Li, L., et al. (2022). CAR T cells produced *in vivo* to treat cardiac injury. *Science* 375, 91–96. doi:10.1126/science.abm0594

Sim, W. S., Park, B. W., Ban, K., and Park, H. J. (2021). In Situ Preconditioning of Human Mesenchymal Stem Cells Elicits Comprehensive Cardiac Repair Following Myocardial Infarction. *Int. J. Mol. Sci.* 22.

Sabe, S. A., Xu, C. M., Sabra, M., Harris, D. D., Malhotra, A., Aboulgheit, A., et al. (2023). Canagliflozin improves myocardial perfusion, fibrosis, and function in a swine model of chronic myocardial ischemia. *J. Am. Heart Assoc.* 12, e028623. doi:10.1161/JAHA.122.028623

Sahinarslan, A., Kocaman, S. A., Topal, S., Ercin, U., Bukan, N., Yalcin, R., et al. (2010). Relation between serum monocyte chemoattractant protein-1 and coronary collateral development. *Coron. Artery Dis.* 21, 455–459. doi:10.1097/MCA.0b013e32833fd29b

Sakai, S., Miyauchi, T., Kobayashi, M., Yamaguchi, I., Goto, K., and Sugishita, Y. (1996). Inhibition of myocardial endothelin pathway improves long-term survival in heart failure. *Nature* 384, 353–355. doi:10.1038/384353a0

Santoso, M. R., Ikeda, G., Tada, Y., Jung, J. H., Vaskova, E., Sierra, R. G., et al. (2020). Exosomes from induced pluripotent stem cell-derived cardiomyocytes promote autophagy for myocardial repair. *J. Am. Heart Assoc.* 9, e014345. doi:10.1161/JAHA.119.014345

Saraswati, S., Marrow, S. M. W., Watch, L. A., and Young, P. P. (2019). Identification of a pro-angiogenic functional role for FSP1-positive fibroblast subtype in wound healing. *Nat. Commun.* 10, 3027. doi:10.1038/s41467-019-10965-9

Sawa, Y., Saito, M., Ishida, N., Ibi, M., Matsushita, N., Morino, Y., et al. (2020). Pretreatment with KGA-2727, a selective SGLT1 inhibitor, is protective against myocardial infarction-induced ventricular remodeling and heart failure in mice. *J. Pharmacol. Sci.* 142, 16–25. doi:10.1016/j.jphs.2019.11.001

Scharf, G. M., Kilian, K., Cordero, J., Wang, Y., Grund, A., Hofmann, M., et al. (2019). Inactivation of Sox9 in fibroblasts reduces cardiac fibrosis and inflammation. *JCI Insight* 5, e126721. doi:10.1172/jci.insight.126721

Schena, G. J., Murray, E. K., Hildebrand, A. N., Headrick, A. L., Yang, Y., Koch, K. A., et al. (2021). Cortical bone stem cell-derived exosomes' therapeutic effect on myocardial ischemia-reperfusion and cardiac remodeling. *Am. J. Physiol. Heart Circ. Physiol.* 321, H1014–h1029. doi:10.1152/ajpheart.00197.2021

Schilter, H., Findlay, A. D., Perryman, L., Yow, T. T., Moses, J., Zahoor, A., et al. (2019). The lysyl oxidase like 2/3 enzymatic inhibitor, PXS-5153A, reduces crosslinks and ameliorates fibrosis. *J. Cell Mol. Med.* 23, 1759–1770. doi:10.1111/jcmm.14074

Schloss, M. J., Horckmans, M., Guillamat-Prats, R., Hering, D., Lauer, E., Lenglet, S., et al. (2019). 2-Arachidonoylglycerol mobilizes myeloid cells and worsens heart function after acute myocardial infarction. *Cardiovasc Res.* 115, 602–613. doi:10.1093/cvr/cvy242

Schroder, K., and Tschopp, J. (2010). The inflammasomes. *Cell* 140, 821–832. doi:10.1016/j.cell.2010.01.040

Schuman, M. L., Peres Diaz, L. S., Aisicovich, M., Ingallina, F., Toblli, J. E., Landa, M. S., et al. (2021). Cardiac thyrotropin-releasing hormone inhibition improves ventricular function and reduces hypertrophy and fibrosis after myocardial infarction in rats. *J. Card. Fail* 27, 796–807. doi:10.1016/j.cardfail.2021.04.003

Scott, N. J. A., Rademaker, M. T., Charles, C. J., Espiner, E. A., and Richards, A. M. (2019). Hemodynamic, hormonal, and renal actions of phosphodiesterase-9 inhibition in experimental heart failure. *J. Am. Coll. Cardiol.* 74, 889–901. doi:10.1016/j.jacc.2019.05.067

Shao, L., Zhang, Y., Pan, X., Liu, B., Liang, C., Zhang, Y., et al. (2020). Knockout of beta-2 microglobulin enhances cardiac repair by modulating exosome imprinting and inhibiting stem cell-induced immune rejection. *Cell Mol. Life Sci.* 77, 937–952. doi:10.1007/s00018-019-03220-3

Sharifi, M., Nazarinia, D., Ramezani, F., Azizi, Y., Naderi, N., and Aboutaleb, N. (2021). Necroptosis and RhoA/ROCK pathways: Molecular targets of nesfatin-1 in cardioprotection against myocardial ischemia/reperfusion injury in a rat model. *Mol. Biol. Rep.* 48, 2507–2518. doi:10.1007/s11033-021-06289-x

Shi, J., Sun, J., Liu, L., Shan, T., Meng, H., Yang, T., et al. (2022). P16ink4a overexpression ameliorates cardiac remodeling of mouse following myocardial infarction via CDK4/pRb pathway. *Biochem. Biophys. Res. Commun.* 595, 62–68. doi:10.1016/j.bbrc.2022.01.077

Shi, S. Y., Luo, X., Yamawaki, T. M., Li, C. M., Ason, B., and Furtado, M. B. (2021). Recent advances in single-cell profiling and multispecific therapeutics: Paving the way for a new era of precision medicine targeting cardiac fibroblasts. *Curr. Cardiol. Rep.* 23, 82. doi:10.1007/s11886-021-01517-z

Shibamoto, M., Higo, T., Naito, A. T., Nakagawa, A., Sumida, T., Okada, K., et al. (2019). Activation of DNA damage response and cellular senescence in cardiac fibroblasts limit cardiac fibrosis after myocardial infarction. *Int. Heart J.* 60, 944–957. doi:10.1536/ihj.18-701

Shigemura, N., Takai, S., Hirose, F., Yoshida, R., Sanematsu, K., and Ninomiya, Y. (2019). Expression of renin-angiotensin system components in the taste organ of mice. *Nutrients* 11, 2251. doi:10.3390/nu11092251

Shiraishi, M., Yamaguchi, A., and Suzuki, K. (2022). Nrg1/ErbB signaling-mediated regulation of fibrosis after myocardial infarction. *Faseb J.* 36, e22150. doi:10.1096/fj.202101428RR

SimõES, F. C., and Riley, P. R. (2022). Immune cells in cardiac repair and regeneration. *Development* 149.

Solhpour, A., and Yusuf, S. W. (2014). Fibrinolytic therapy in patients with ST-elevation myocardial infarction. *Expert Rev. Cardiovasc Ther.* 12, 201–215. doi:10.1586/14779072.2014.867805

Solomon, S. D., Mcmurray, J. J. V., Claggett, B., DE Boer, R. A., Demets, D., Hernandez, A. F., et al. (2022). Dapagliflozin in heart failure with mildly reduced or preserved ejection fraction. *N. Engl. J. Med.* 387, 1089–1098. doi:10.1056/NEJMoa2206286

Song, J., Frieler, R. A., Whitesall, S. E., Chung, Y., Vigil, T. M., Muir, L. A., et al. (2021a). Myeloid interleukin-4 receptor α is essential in postmyocardial infarction healing by regulating inflammation and fibrotic remodeling. *Am. J. Physiol. Heart Circ. Physiol.* 320, H323–h337. doi:10.1152/ajpheart.00251.2020

Song, L., Duan, X., Zeng, X., Duan, X., and Li, L. (2021b). Regulatory mechanism of LINC00152 on aggravating heart failure through triggering fibrosis in an infarcted myocardium. *Dis. Markers* 2021, 2607358. doi:10.1155/2021/2607358

Song, S. Y., Kim, H., Yoo, J., Kwon, S. P., Park, B. W., Kim, J. J., et al. (2020). Prevascularized, multiple-layered cell sheets of direct cardiac reprogrammed cells for cardiac repair. *Biomater. Sci.* 8, 4508–4520. doi:10.1039/d0bm00701c

Song, Y., Xu, C., Liu, J., Li, Y., Wang, H., Shan, D., et al. (2021c). Heterodimerization with 5-HT(2B)R is indispensable for β(2)ar-mediated cardioprotection. *Circ. Res.* 128, 262–277. doi:10.1161/CIRCRESAHA.120.317011

Souders, C. A., Bowers, S. L., and Baudino, T. A. (2009). Cardiac fibroblast: The renaissance cell. *Circ. Res.* 105, 1164–1176. doi:10.1161/CIRCRESAHA.109.209809

Sousonis, V., Sfakianaki, T., Ntalianis, A., Nanas, I., Kontogiannis, C., Aravantinos, D., et al. (2021). Intracoronary administration of allogeneic cardiosphere-derived cells immediately prior to reperfusion in pigs with acute myocardial infarction reduces infarct size and attenuates adverse cardiac remodeling. *J. Cardiovasc Pharmacol. Ther.* 26, 88–99. doi:10.1177/1074248420941672

Spinale, F. G. (2007). Myocardial matrix remodeling and the matrix metalloproteinases: Influence on cardiac form and function. *Physiol. Rev.* 87, 1285–1342. doi:10.1152/physrev.00012.2007

Stienen, S., Rossignol, P., Barros, A., Girerd, N., Pitt, B., Zannad, F., et al. (2020). Determinants of anti-fibrotic response to mineralocorticoid receptor antagonist therapy: Insights from the eplerenone post-acute myocardial infarction heart failure efficacy and survival study (EPHESUS) and early eplerenone treatment in patients with acute ST-elevation myocardial infarction without heart failure (REMINDER) trials. *Clin. Res. Cardiol.* 109, 194–204. doi:10.1007/s00392-019-01500-3

Sun, B., Zhao, C., and Mao, Y. (2021a). MiR-218-5p mediates myocardial fibrosis after myocardial infarction by targeting CX43. *Curr. Pharm. Des.* 27, 4504–4512. doi:10.2174/1381612827666210929111622

Sun, J., Zhang, Q., Liu, X., and Shang, X. (2021b). Downregulation of interferon-induced protein with tetratricopeptide repeats 3 relieves the inflammatory response and myocardial fibrosis of mice with myocardial infarction and improves their cardiac function. *Exp. Anim.* 70, 522–531. doi:10.1538/expanim.21-0060

Sunagawa, Y., Katayama, A., Funamoto, M., Shimizu, K., Shimizu, S., Sari, N., et al. (2022a). The polyunsaturated fatty acids, EPA and DHA, ameliorate myocardial infarction-induced heart failure by inhibiting p300-HAT activity in rats. *J. Nutr. Biochem.* 106, 109031. doi:10.1016/j.jnutbio.2022.109031

Sunagawa, Y., Kawaguchi, S., Miyazaki, Y., Katanasaka, Y., Funamoto, M., Shimizu, K., et al. (2022b). Auraptene, a citrus peel-derived natural product, prevents myocardial infarction-induced heart failure by activating PPARα in rats. *Phytomedicine* 107, 154457. doi:10.1016/j.phymed.2022.154457

Surinkaew, S., Aflaki, M., Takawale, A., Chen, Y., Qi, X. Y., Gillis, M. A., et al. (2019). Exchange protein activated by cyclic-adenosine monophosphate (Epac) regulates atrial fibroblast function and controls cardiac remodelling. *Cardiovasc Res.* 115, 94–106. doi:10.1093/cvr/cvy173

Takawale, A., Sakamuri, S. S., and Kassiri, Z. (2015). Extracellular matrix communication and turnover in cardiac physiology and pathology. *Compr. Physiol.* 5, 687–719. doi:10.1002/cphy.c140045

Tan, Z., Jiang, X., Zhou, W., Deng, B., Cai, M., Deng, S., et al. (2021). Taohong siwu decoction attenuates myocardial fibrosis by inhibiting fibrosis proliferation and collagen deposition via TGFBR1 signaling pathway. *J. Ethnopharmacol.* 270, 113838. doi:10.1016/j.jep.2021.113838

Tanner, M. A., Maitz, C. A., and Grisanti, L. A. (2021). Immune cell β(2)-adrenergic receptors contribute to the development of heart failure. *Am. J. Physiol. Heart Circ. Physiol.* 321, H633–h649. doi:10.1152/ajpheart.00243.2021

Tanner, M. A., Thomas, T. P., Maitz, C. A., and Grisanti, L. A. (2020). β2-Adrenergic receptors increase cardiac fibroblast proliferation through the gαs/ERK1/2-dependent secretion of interleukin-6. *Int. J. Mol. Sci.* 21, 8507. doi:10.3390/ijms21228507

Thavapalachandran, S., Grieve, S. M., Hume, R. D., LE, T. Y. L., Raguram, K., Hudson, J. E., et al. (2020). Platelet-derived growth factor-AB improves scar mechanics and vascularity after myocardial infarction. *Sci. Transl. Med.* 12, eaay2140. doi:10.1126/scitranslmed.aay2140

Tian, X., Sun, C., Wang, X., Ma, K., Chang, Y., Guo, Z., et al. (2020). ANO1 regulates cardiac fibrosis via ATI-mediated MAPK pathway. *Cell Calcium* 92, 102306. doi:10.1016/j.ceca.2020.102306

Tian, Z., Zhang, Y., and Lyu, X. (2021). Promoting roles of KLF5 in myocardial infarction in mice involving microRNA-27a suppression and the following GFPT2/TGF-β/Smad2/3 axis activation. *Cell Cycle* 20, 874–893. doi:10.1080/15384101.2021.1907512

Toner, Y. C., Ghotbi, A. A., Naidu, S., Sakurai, K., VAN Leent, M. M. T., Jordan, S., et al. (2022). Systematically evaluating DOTATATE and FDG as PET immuno-imaging tracers of cardiovascular inflammation. *Sci. Rep.* 12, 6185. doi:10.1038/s41598-022-09590-2

Tripathi, H., Peng, H., Donahue, R., Chelvarajan, L., Gottipati, A., Levitan, B., et al. (2020). Isolation methods for human CD34 subsets using fluorescent and magnetic activated cell sorting: An *in vivo* comparative study. *Stem Cell Rev. Rep.* 16, 413–423. doi:10.1007/s12015-019-09939-7

Turner, N. A., Porter, K. E., Smith, W. H., White, H. L., Ball, S. G., and Balmforth, A. J. (2003). Chronic beta2-adrenergic receptor stimulation increases proliferation of human cardiac fibroblasts via an autocrine mechanism. *Cardiovasc Res.* 57, 784–792. doi:10.1016/s0008-6363(02)00729-0

Unkart, J. T., Allison, M. A., Abdelmalek, J. A., Jenny, N. S., Mcclelland, R. L., Budoff, M., et al. (2020). Relation of plasma renin activity to subclinical peripheral and coronary artery disease (from the multiethnic study of atherosclerosis). *Am. J. Cardiol.* 125, 1794–1800. doi:10.1016/j.amjcard.2020.03.022

Vaskova, E., Ikeda, G., Tada, Y., Wahlquist, C., Mercola, M., and Yang, P. C. (2020). Sacubitril/valsartan improves cardiac function and decreases myocardial fibrosis via downregulation of exosomal miR-181a in a rodent chronic myocardial infarction model. *J. Am. Heart Assoc.* 9, e015640. doi:10.1161/JAHA.119.015640

Vatner, D. E., Zhang, J., Zhao, X., Yan, L., Kudej, R., and Vatner, S. F. (2021). Secreted frizzled protein 3 is a novel cardioprotective mechanism unique to the clinically relevant fourth window of ischemic preconditioning. *Am. J. Physiol. Heart Circ. Physiol.* 320, H798–h804. doi:10.1152/ajpheart.00849.2020

Vellaichamy, E., Das, S., Subramanian, U., Maeda, N., and Pandey, K. N. (2014). Genetically altered mutant mouse models of guanylyl cyclase/natriuretic peptide receptor-A exhibit the cardiac expression of proinflammatory mediators in a gene-dose-dependent manner. *Endocrinology* 155, 1045–1056. doi:10.1210/en.2013-1416

Venugopal, H., Hanna, A., Humeres, C., and Frangogiannis, N. G. (2022)., 11. Cells, 1386. doi:10.3390/cells11091386Properties and functions of fibroblasts and myofibroblasts in myocardial infarction*Cells*

Vianello, E., Dozio, E., Tacchini, L., Frati, L., and Corsi Romanelli, M. M. (2019). ST2/IL-33 signaling in cardiac fibrosis. *Int. J. Biochem. Cell Biol.* 116, 105619. doi:10.1016/j.biocel.2019.105619

Viswanadha, V. P., Dhivya, V., Beeraka, N. M., Huang, C. Y., Gavryushova, L. V., Minyaeva, N. N., et al. (2020). The protective effect of piperine against isoproterenol-induced inflammation in experimental models of myocardial toxicity. *Eur. J. Pharmacol.* 885, 173524. doi:10.1016/j.ejphar.2020.173524

Vukicevic, S., Colliva, A., Kufner, V., Martinelli, V., Moimas, S., Vodret, S., et al. (2022). Bone morphogenetic protein 1.3 inhibition decreases scar formation and supports cardiomyocyte survival after myocardial infarction. *Nat. Commun.* 13, 81. doi:10.1038/s41467-021-27622-9

Wan, J., Lin, S., Yu, Z., Song, Z., Lin, X., Xu, R., et al. (2022a). Protective effects of MicroRNA-200b-3p encapsulated by mesenchymal stem cells-secreted extracellular vesicles in myocardial infarction via regulating BCL2L11. *J. Am. Heart Assoc.* 11, e024330. doi:10.1161/JAHA.121.024330

Wan, Q., Zhang, L., Zhou, Q., Han, Y., Li, Z., and Li, B. (2022b). Protection of CAPE-pNO(2) against chronic myocardial ischemia by the TGF-β1/galectin-3 pathway *in vivo* and *in vitro*. *Inflammation* 45, 1039–1058. doi:10.1007/s10753-021-01600-1

Wan, Y. J., Wang, Y. H., Guo, Q., Jiang, Y., Tu, P. F., and Zeng, K. W. (2021). Protocatechualdehyde protects oxygen-glucose deprivation/reoxygenation-induced myocardial injury via inhibiting PERK/ATF6α/IRE1α pathway. *Eur. J. Pharmacol.* 891, 173723. doi:10.1016/j.ejphar.2020.173723

Wang, B., Tan, Y., Zhou, W., Yang, J., Jiang, Y., Liu, X., et al. (2022a). Loss of BTK ameliorates the pathological cardiac fibrosis and dysfunction. *Matrix Biol.* 112, 171–189. doi:10.1016/j.matbio.2022.08.010

Wang, C., Yue, Y., Huang, S., Wang, K., Yang, X., Chen, J., et al. (2022b). M2b macrophages stimulate lymphangiogenesis to reduce myocardial fibrosis after myocardial ischaemia/reperfusion injury. *Pharm. Biol.* 60, 384–393. doi:10.1080/13880209.2022.2033798

Wang, D. M., Jin, J. J., Tian, L. M., and Zhang, Z. (2020a). MiR-195 promotes myocardial fibrosis in MI rats via targeting TGF-β1/Smad. *J. Biol. Regul. Homeost. Agents* 34, 1325–1332. doi:10.23812/20-201-A

Wang, F., He, Y., Yao, N., Ruan, L., and Tian, Z. (2022c). Thymosin β4 protects against cardiac damage and subsequent cardiac fibrosis in mice with myocardial infarction. *Cardiovasc Ther.* 2022, 1308651. doi:10.1155/2022/1308651

Wang, G., Wang, R., Ruan, Z., Liu, L., Li, Y., and Zhu, L. (2020b). MicroRNA-132 attenuated cardiac fibrosis in myocardial infarction-induced heart failure rats. *Biosci. Rep.* 40. doi:10.1042/BSR20201696

Wang, J., Zhang, J., Lin, X., Wang, Y., Wu, X., Yang, F., et al. (2021a). DCA-TGR5 signaling activation alleviates inflammatory response and improves cardiac function in myocardial infarction. *J. Mol. Cell Cardiol.* 151, 3–14. doi:10.1016/j.yjmcc.2020.10.014

Wang, J., Zhang, S., Li, X., and Gong, M. (2020c). LncRNA SNHG7 promotes cardiac remodeling by upregulating ROCK1 via sponging miR-34-5p. *Aging (Albany NY)* 12, 10441–10456. doi:10.18632/aging.103269

Wang, K., Li, Z., Li, Y., Liu, X., Sun, Y., Hong, J., et al. (2022d). Cardioprotection of Klotho against myocardial infarction-induced heart failure through inducing autophagy. *Mech. Ageing Dev.* 207, 111714. doi:10.1016/j.mad.2022.111714

Wang, L., Singh, H., Mulyala, R. R., Weber, J., Barasch, E., and Cao, J. J. (2020d). The association between left ventricular diastolic dysfunction and myocardial scar and their collective impact on all-cause mortality. *J. Am. Soc. Echocardiogr.* 33, 161–170. doi:10.1016/j.echo.2019.09.022

Wang, Q., Chen, Z., Guo, J., Peng, X., Zheng, Z., Chen, H., et al. (2023). Atorvastatin-induced tolerogenic dendritic cells improve cardiac remodeling by suppressing TLR-4/NF-κB activation after myocardial infarction. *Inflamm. Res.* 72, 13–25. doi:10.1007/s00011-022-01654-3

Wang, Q., Fu, W., Yu, X., Xu, H., Sui, D., and Wang, Y. (2021b). Ginsenoside Rg2 alleviates myocardial fibrosis by regulating TGF-β1/Smad signalling pathway. *Pharm. Biol.* 59, 106–113. doi:10.1080/13880209.2020.1867197

Wang, Q., Liu, A. D., Li, T. S., Tang, Q., Wang, X. C., and Chen, X. B. (2021c). Ghrelin ameliorates cardiac fibrosis after myocardial infarction by regulating the Nrf2/NADPH/ROS pathway. *Peptides* 144, 170613. doi:10.1016/j.peptides.2021.170613

Wang, Q., Yang, Y., Chen, K., Li, D., Tang, B., Peng, K., et al. (2020e). Dietary menthol attenuates inflammation and cardiac remodeling after myocardial infarction via the transient receptor potential melastatin 8. *Am. J. Hypertens.* 33, 223–233. doi:10.1093/ajh/hpz162

Wang, R., Peng, L., Lv, D., Shang, F., Yan, J., Li, G., et al. (2021d). Leonurine attenuates myocardial fibrosis through upregulation of miR-29a-3p in mice post-myocardial infarction. *J. Cardiovasc Pharmacol.* 77, 189–199. doi:10.1097/FJC.0000000000000957

Wang, S., Li, L., Liu, T., Jiang, W., and Hu, X. (2020f). miR-19a/19b-loaded exosomes in combination with mesenchymal stem cell transplantation in a preclinical model of myocardial infarction. *Regen. Med.* 15, 1749–1759. doi:10.2217/rme-2019-0136

Wang, S., Su, X., Xu, L., Chang, C., Yao, Y., Komal, S., et al. (2020g). Glycogen synthase kinase-3β inhibition alleviates activation of the NLRP3 inflammasome in myocardial infarction. *J. Mol. Cell Cardiol.* 149, 82–94. doi:10.1016/j.yjmcc.2020.09.009

Wang, W., Ye, S., Zhang, L., Jiang, Q., Chen, J., Chen, X., et al. (2020h). Granulocyte colony-stimulating factor attenuates myocardial remodeling and ventricular arrhythmia susceptibility via the JAK2-STAT3 pathway in a rabbit model of coronary microembolization. *BMC Cardiovasc Disord.* 20, 85. doi:10.1186/s12872-020-01385-5

Wang, X., Guo, Z., Ding, Z., and Mehta, J. L. (2018). Inflammation, autophagy, and apoptosis after myocardial infarction. *J. Am. Heart Assoc.* 7, e008024. doi:10.1161/JAHA.117.008024

Wang, X., Hu, S., Li, J., Zhu, D., Wang, Z., Cores, J., et al. (2021e). Extruded mesenchymal stem cell nanovesicles are equally potent to natural extracellular vesicles in cardiac repair. *ACS Appl. Mater Interfaces* 13, 55767–55779. doi:10.1021/acsami.1c08044

Wang, Y., DE Waard, M. C., Sterner-Kock, A., Stepan, H., Schultheiss, H. P., Duncker, D. J., et al. (2007). Cardiomyocyte-restricted over-expression of C-type natriuretic peptide prevents cardiac hypertrophy induced by myocardial infarction in mice. *Eur. J. Heart Fail* 9, 548–557. doi:10.1016/j.ejheart.2007.02.006

Wang, Y., Del Borgo, M., Lee, H. W., Baraldi, D., Hirmiz, B., Gaspari, T. A., et al. (2017). Anti-fibrotic potential of AT2 receptor agonists. *Front. Pharmacol.* 8, 564. doi:10.3389/fphar.2017.00564

Wang, Y., Li, C., Zhao, R., Qiu, Z., Shen, C., Wang, Z., et al. (2021f). CircUbe3a from M2 macrophage-derived small extracellular vesicles mediates myocardial fibrosis after acute myocardial infarction. *Theranostics* 11, 6315–6333. doi:10.7150/thno.52843

Wang, Z. P., Che, Y., Zhou, H., Meng, Y. Y., Wu, H. M., Jin, Y. G., et al. (2020i). Corosolic acid attenuates cardiac fibrosis following myocardial infarction in mice. *Int. J. Mol. Med.* 45, 1425–1435. doi:10.3892/ijmm.2020.4531

Weber, K. T., Sun, Y., Tyagi, S. C., and Cleutjens, J. P. (1994). Collagen network of the myocardium: Function, structural remodeling and regulatory mechanisms. *J. Mol. Cell Cardiol.* 26, 279–292. doi:10.1006/jmcc.1994.1036

Wei, X., Chen, S., Xie, T., Chen, H., Jin, X., Yang, J., et al. (2022). An MMP-degradable and conductive hydrogel to stabilize HIF-1α for recovering cardiac functions. *Theranostics* 12, 127–142. doi:10.7150/thno.63481

Wei, Y., Lan, Y., Zhong, Y., Yu, K., Xu, W., Zhu, R., et al. (2020). Interleukin-38 alleviates cardiac remodelling after myocardial infarction. *J. Cell Mol. Med.* 24, 371–384. doi:10.1111/jcmm.14741

Weldon, S. M., and Brown, N. F. (2019). Inhibitors of aldosterone synthase. *Vitam. Horm.* 109, 211–239. doi:10.1016/bs.vh.2018.10.002

Wen, Y., Li, X. Y., Li, Z. Y., Wang, M. L., Chen, P. P., Liu, Y., et al. (2020). Intra-myocardial delivery of a novel thermosensitive hydrogel inhibits post-infarct heart failure after degradation in rat. *J. Cardiovasc Transl. Res.* 13, 677–685. doi:10.1007/s12265-019-09941-x

Whitehurst, K. S., Chan, V. A., Estes, H. K., Valsaraj, S., Kent, S., Sharma, U. M., et al. (2020). EphrinA1-Fc attenuates ventricular remodeling and dysfunction in chronically nonreperfused WT but not EphA2-R-M mice. *Int. J. Mol. Sci.* 21, 5811. doi:10.3390/ijms21165811

Williams, B. (2001). Angiotensin II and the pathophysiology of cardiovascular remodeling. *Am. J. Cardiol.* 87, 10c–17c. doi:10.1016/s0002-9149(01)01507-7

Wu, J., Li, S., Li, C., Cui, L., Ma, J., and Hui, Y. (2021a). The non-canonical effects of heme oxygenase-1, a classical fighter against oxidative stress. *Redox Biol.* 47, 102170. doi:10.1016/j.redox.2021.102170

Wu, Q., Wang, J., Tan, W. L. W., Jiang, Y., Wang, S., Li, Q., et al. (2020). Extracellular vesicles from human embryonic stem cell-derived cardiovascular progenitor cells promote cardiac infarct healing through reducing cardiomyocyte death and promoting angiogenesis. *Cell Death Dis.* 11, 354. doi:10.1038/s41419-020-2508-y

Wu, X., Reboll, M. R., Korf-Klingebiel, M., and Wollert, K. C. (2021b). Angiogenesis after acute myocardial infarction. *Cardiovasc Res.* 117, 1257–1273. doi:10.1093/cvr/cvaa287

Wu, X., Xu, J., Li, X., Dai, J., and Wang, L. (2022a). Inhibition of SphK1/S1P signaling pathway alleviates fibrosis and inflammation of rat myocardium after myocardial infarction. *Comput. Math. Methods Med.* 2022, 5985375. doi:10.1155/2022/5985375

Wu, X., Zhao, X., Xiong, Y., Zheng, M., Zhong, C., and Zhou, Y. (2022b). Deciphering cell-type-specific gene expression signatures of cardiac diseases through reconstruction of bulk transcriptomes. *Front. Cell Dev. Biol.* 10, 792774. doi:10.3389/fcell.2022.792774

Wu, Y., Chen, S., Wen, P., Wu, M., Wu, Y., Mai, M., et al. (2021c). PGAM1 deficiency ameliorates myocardial infarction remodeling by targeting TGF-β via the suppression of inflammation, apoptosis and fibrosis. *Biochem. Biophys. Res. Commun.* 534, 933–940. doi:10.1016/j.bbrc.2020.10.070

Wu, Y., Peng, W., Fang, M., Wu, M., and Wu, M. (2022c). MSCs-derived extracellular vesicles carrying miR-212-5p alleviate myocardial infarction-induced cardiac fibrosis via NLRC5/VEGF/TGF-β1/SMAD Axis. *J. Cardiovasc Transl. Res.* 15, 302–316. doi:10.1007/s12265-021-10156-2

Wu, Y., Wang, T., Qiao, L., and Lin, H. (2022d). Upregulated microRNA-210-3p improves sevoflurane-induced protective effect on ventricular remodeling in rats with myocardial infarction by inhibiting ADCY9. *Funct. Integr. Genomics* 22, 279–289. doi:10.1007/s10142-021-00816-6

Xiang, C., Zhu, Y., Xu, M., and Zhang, D. (2022). Fasudil ameliorates osteoporosis following myocardial infarction by regulating cardiac calcitonin secretion. *J. Cardiovasc Transl. Res.* 15, 1352–1365. doi:10.1007/s12265-022-10271-8

Xiao, Y., Feng, Q., Huang, L., Meng, X., Han, P., Zhang, W., et al. (2023). Copper promotes cardiac functional recovery via suppressing the transformation of fibroblasts to myofibroblasts in ischemia-infarcted monkey hearts. *J. Nutr. Biochem.* 111, 109180. doi:10.1016/j.jnutbio.2022.109180

Xiao, Y., Hill, M. C., Li, L., Deshmukh, V., Martin, T. J., Wang, J., et al. (2019). Hippo pathway deletion in adult resting cardiac fibroblasts initiates a cell state transition with spontaneous and self-sustaining fibrosis. *Genes Dev.* 33, 1491–1505. doi:10.1101/gad.329763.119

Xie, B., Wang, J., XI, X. Y., Guo, X., Chen, B. X., Li, L., et al. (2022). Fibroblast activation protein imaging in reperfused ST-elevation myocardial infarction: Comparison with cardiac magnetic resonance imaging. *Eur. J. Nucl. Med. Mol. Imaging* 49, 2786–2797. doi:10.1007/s00259-021-05674-9

Xing, Z., Yang, C., He, J., Feng, Y., Li, X., Peng, C., et al. (2022). Cardioprotective effects of aconite in isoproterenol-induced myocardial infarction in rats. *Oxid. Med. Cell Longev.* 2022, 1090893. doi:10.1155/2022/1090893

Xiong, X., Liu, J., He, Q., Dai, R., Zhang, H., Cao, Z., et al. (2021). Long non-coding RNA NORAD aggravates acute myocardial infarction by promoting fibrosis and apoptosis via miR-577/COBLL1 axis. *Environ. Toxicol.* 36, 2256–2265. doi:10.1002/tox.23339

Xu, J., Wu, H., Mai, Z., Yi, J., Wang, X., Li, L., et al. (2021a). Therapeutic effects of CXCR4(+) subpopulation of transgene-free induced cardiosphere-derived cells on experimental myocardial infarction. *Cell Prolif.* 54, e13041. doi:10.1111/cpr.13041

Xu, X., Jiang, T., Li, Y., and Kong, L. (2021b). Endostatin attenuates heart failure via inhibiting reactive oxygen species in myocardial infarction rats. *Biosci. Rep.* 41. doi:10.1042/BSR20200787

Xu, Y., Hu, Y., Geng, Y., Zhao, N., Jia, C., Song, H., et al. (2022a). Pentraxin 3 depletion (PTX3 KD) inhibited myocardial fibrosis in heart failure after myocardial infarction. *Aging (Albany NY)* 14, 4036–4049. doi:10.18632/aging.204070

Xu, Y., Jiang, K., Chen, F., Qian, J., Wang, D., Wu, Y., et al. (2022b). Bone marrow-derived naïve B lymphocytes improve heart function after myocardial infarction: A novel cardioprotective mechanism for empagliflozin. *Basic Res. Cardiol.* 117, 47. doi:10.1007/s00395-022-00956-1

Xu, Z., Lu, D., Yuan, J., Wang, L., Wang, J., Lei, Z., et al. (2022c). Storax attenuates cardiac fibrosis following acute myocardial infarction in rats via suppression of at1r-ankrd1-P53 signaling pathway. *Int. J. Mol. Sci.* 23, 13161. doi:10.3390/ijms232113161

Xuan, L., Fu, D., Zhen, D., Wei, C., Bai, D., Yu, L., et al. (2022). Extracellular vesicles derived from human bone marrow mesenchymal stem cells protect rats against acute myocardial infarction-induced heart failure. *Cell Tissue Res.* 389, 23–40. doi:10.1007/s00441-022-03612-1

Xue, K., Chen, S., Chai, J., Yan, W., Zhu, X., Dai, H., et al. (2022). Upregulation of periostin through CREB participates in myocardial infarction-induced myocardial fibrosis. *J. Cardiovasc Pharmacol.* 79, 687–697. doi:10.1097/FJC.0000000000001244

Xue, K., Zhang, J., Li, C., Li, J., Wang, C., Zhang, Q., et al. (2019). The role and mechanism of transforming growth factor beta 3 in human myocardial infarction-induced myocardial fibrosis. *J. Cell Mol. Med.* 23, 4229–4243. doi:10.1111/jcmm.14313

Xue, Y., Fan, X., Yang, R., Jiao, Y., and Li, Y. (2020). miR-29b-3p inhibits post-infarct cardiac fibrosis by targeting FOS. *Biosci. Rep.* 40. doi:10.1042/BSR20201227

Yan, L. L., Wei, X. H., Shi, Q. P., Pan, C. S., Li, K. Y., Zhang, B., et al. (2022a). Cardiotonic Pills® protects from myocardial fibrosis caused by in stent restenosis in miniature pigs. *Phytomedicine* 106, 154405. doi:10.1016/j.phymed.2022.154405

Yan, M., Liu, Q., Jiang, Y., Wang, B., Ji, Y., Liu, H., et al. (2020). Long noncoding RNA LNC_000898 alleviates cardiomyocyte apoptosis and promotes cardiac repair after myocardial infarction through modulating the miR-375/PDK1 Axis. *J. Cardiovasc Pharmacol.* 76, 77–85. doi:10.1097/FJC.0000000000000845

Yan, T., Zhu, X., Zhang, X., Jia, X., Liu, J., Wang, X., et al. (2022b). The application of proteomics and metabolomics to reveal the molecular mechanism of Nutmeg-5 in ameliorating cardiac fibrosis following myocardial infarction. *Phytomedicine* 105, 154382. doi:10.1016/j.phymed.2022.154382

Yang, J., Savvatis, K., Kang, J. S., Fan, P., Zhong, H., Schwartz, K., et al. (2016). Targeting LOXL2 for cardiac interstitial fibrosis and heart failure treatment. *Nat. Commun.* 7, 13710. doi:10.1038/ncomms13710

Yang, L., Xue, S., DU, M., and Lian, F. (2021a). Highly efficient MicroRNA delivery using functionalized carbon dots for enhanced conversion of fibroblasts to cardiomyocytes. *Int. J. Nanomedicine* 16, 3741–3754. doi:10.2147/IJN.S304873

Yang, W., Lin, J., Zhou, J., Zheng, Y., Jiang, S., He, S., et al. (2021b). Innate lymphoid cells and myocardial infarction. *Front. Immunol.* 12, 758272. doi:10.3389/fimmu.2021.758272

Yang, W., Zhang, A., Han, Y., Su, X., Chen, Y., Zhao, W., et al. (2021c). Cyclin-dependent kinase inhibitor 2b controls fibrosis and functional changes in ischemia-induced heart failure via the BMI1-p15-Rb signalling pathway. *Can. J. Cardiol.* 37, 655–664. doi:10.1016/j.cjca.2020.05.016

Yao, H., He, Q., Huang, C., Wei, S., Gong, Y., Li, X., et al. (2022). Panaxatriol saponin ameliorates myocardial infarction-induced cardiac fibrosis by targeting Keap1/Nrf2 to regulate oxidative stress and inhibit cardiac-fibroblast activation and proliferation. *Free Radic. Biol. Med.* 190, 264–275. doi:10.1016/j.freeradbiomed.2022.08.016

Yap, J., Irei, J., Lozano-Gerona, J., Vanapruks, S., Bishop, T., and Boisvert, W. (2023). Macrophages in cardiac remodelling after myocardial infarction. *Nat. Rev. Cardiol.* 2023. doi:10.1038/s41569-022-00823-5

Yokota, T., Mccourt, J., Ma, F., Ren, S., Li, S., Kim, T. H., et al. (2020). Type V collagen in scar tissue regulates the size of scar after heart injury. *Cell* 182, 545–562.e23. doi:10.1016/j.cell.2020.06.030

Yoshikawa, T., Port, J. D., Asano, K., Chidiak, P., Bouvier, M., Dutcher, D., et al. (1996). Cardiac adrenergic receptor effects of carvedilol. *Eur. Heart J.* 17 (2), 8–16. doi:10.1093/eurheartj/17.suppl_b.8

Younis, A., Zilberman, I., Krywanczyk, A., Higuchi, K., Yavin, H. D., Sroubek, J., et al. (2022). Effect of pulsed-field and radiofrequency ablation on heterogeneous ventricular scar in a swine model of healed myocardial infarction. *Circ. Arrhythm. Electrophysiol.* 15, e011209. doi:10.1161/CIRCEP.122.011209

Yu, Y., Hu, Z., Li, B., Wang, Z., and Chen, S. (2019). Ivabradine improved left ventricular function and pressure overload-induced cardiomyocyte apoptosis in a transverse aortic constriction mouse model. *Mol. Cell Biochem.* 450, 25–34. doi:10.1007/s11010-018-3369-x

Yue, Y., Huang, S., Wang, L., Wu, Z., Liang, M., Li, H., et al. (2020). M2b macrophages regulate cardiac fibroblast activation and alleviate cardiac fibrosis after reperfusion injury. *Circ. J.* 84, 626–635. doi:10.1253/circj.CJ-19-0959

Yurista, S. R., Matsuura, T. R., Silljé, H. H. W., Nijholt, K. T., Mcdaid, K. S., Shewale, S. V., et al. (2021). Ketone ester treatment improves cardiac function and reduces pathologic remodeling in preclinical models of heart failure. *Circ. Heart Fail* 14, e007684. doi:10.1161/CIRCHEARTFAILURE.120.007684

Yvette, N. L. (2021). Nintedanib: A review in fibrotic interstitial lung diseases. *Drugs* 81 (5), 575–586. doi:10.1007/s40265-021-01487-0

Zeigler, A. C., Nelson, A. R., Chandrabhatla, A. S., Brazhkina, O., Holmes, J. W., and Saucerman, J. J. (2020). Computational model predicts paracrine and intracellular drivers of fibroblast phenotype after myocardial infarction. *Matrix Biol.* 91-92, 136–151. doi:10.1016/j.matbio.2020.03.007

Zeng, B., Liao, X., Liu, L., Zhang, C., Ruan, H., and Yang, B. (2021). Thyroid hormone mediates cardioprotection against postinfarction remodeling and dysfunction through the IGF-1/PI3K/AKT signaling pathway. *Life Sci.* 267, 118977. doi:10.1016/j.lfs.2020.118977

Zhang, J., Lu, Y., Yu, P., Li, Z., Liu, Y., Zhang, J., et al. (2022a). Therapeutic hypothermia alleviates myocardial ischaemia-reperfusion injury by inhibiting inflammation and fibrosis via the mediation of the SIRT3/NLRP3 signalling pathway. *J. Cell Mol. Med.* 26, 4995–5007. doi:10.1111/jcmm.17523

Zhang, J., Wang, Y. J., Wang, X., Xu, L., Yang, X. C., and Zhao, W. S. (2019a). PKC-mediated endothelin-1 expression in endothelial cell promotes macrophage activation in atherogenesis. *Am. J. Hypertens.* 32, 880–889. doi:10.1093/ajh/hpz069

Zhang, J., Zha, Y., Jiao, Y., Li, Y., Wang, J., and Zhang, S. (2022b). OTUD7B (Cezanne) ameliorates fibrosis after myocardial infarction via FAK-ERK/P38 MAPK signaling pathway. *Arch. Biochem. Biophys.* 724, 109266. doi:10.1016/j.abb.2022.109266

Zhang, M., Zhang, M., Zhou, T., Liu, M., Xia, N., Gu, M., et al. (2021a). Inhibition of fibroblast IL-6 production by ACKR4 deletion alleviates cardiac remodeling after myocardial infarction. *Biochem. Biophys. Res. Commun.* 547, 139–147. doi:10.1016/j.bbrc.2021.02.013

Zhang, N., Feng, B., Ma, X., Sun, K., Xu, G., and Zhou, Y. (2019b). Dapagliflozin improves left ventricular remodeling and aorta sympathetic tone in a pig model of heart failure with preserved ejection fraction. *Cardiovasc Diabetol.* 18, 107. doi:10.1186/s12933-019-0914-1

Zhang, Q., Wang, L., Wang, S., Cheng, H., Xu, L., Pei, G., et al. (2022c). Signaling pathways and targeted therapy for myocardial infarction. *Signal Transduct. Target Ther.* 7, 78. doi:10.1038/s41392-022-00925-z

Zhang, S., Wang, N., Ma, Q., Fan, F., and Ma, X. (2021b). LncRNA TUG1 acts as a competing endogenous RNA to mediate CTGF expression by sponging miR-133b in myocardial fibrosis after myocardial infarction. *Cell Biol. Int.* 45, 2534–2543. doi:10.1002/cbin.11707

Zhang, X., Qu, H., Yang, T., Liu, Q., and Zhou, H. (2022d). Astragaloside IV attenuate MI-induced myocardial fibrosis and cardiac remodeling by inhibiting ROS/caspase-1/

GSDMD signaling pathway. *Cell Cycle* 21, 2309–2322. doi:10.1080/15384101.2022.2093598

Zhang, Y., Fu, C., Zhao, S., Jiang, H., Li, W., and Liu, X. (2022e). PRELP promotes myocardial fibrosis and ventricular remodelling after acute myocardial infarction by the wnt/β-catenin signalling pathway. *Cardiovasc J. Afr.* 33, 228–233. doi:10.5830/CVJA-2022-001

Zhang, Y. Q., Hong, L., Jiang, Y. F., Hu, S. D., Zhang, N. N., Xu, L. B., et al. (2021c). hAECs and their exosomes improve cardiac function after acute myocardial infarction in rats. *Aging (Albany NY)* 13, 15032–15043. doi:10.18632/aging.203066

Zhang, Y., Zhang, H., Yang, Z., Zhang, X. H., Miao, Q., Li, M., et al. (2022f). miR-155 down-regulation protects the heart from hypoxic damage by activating fructose metabolism in cardiac fibroblasts. *J. Adv. Res.* 39, 103–117. doi:10.1016/j.jare.2021.10.007

Zhang, Z., Chen, Y., Zheng, L., DU, J., Wei, S., Zhu, X., et al. (2023). A DUSP6 inhibitor suppresses inflammatory cardiac remodeling and improves heart function after myocardial infarction. *Dis. Model Mech.* 16, dmm049662. doi:10.1242/dmm.049662

Zhang, Z., Villalpando, J., Zhang, W., and Nam, Y. J. (2021d). Chamber-specific protein expression during direct cardiac reprogramming. *Cells* 10, 1513. doi:10.3390/cells10061513

Zhang, Z., Zhang, N., Shi, J., Dai, C., Wu, S., Jiao, M., et al. (2021e). Allograft or recipient ST2 deficiency oppositely affected cardiac allograft vasculopathy via differentially altering immune cells infiltration. *Front. Immunol.* 12, 657803. doi:10.3389/fimmu.2021.657803

Zhao, K., Xu, T., Mao, Y., Wu, X., Hua, D., Sheng, Y., et al. (2022a). Alamandine alleviated heart failure and fibrosis in myocardial infarction mice. *Biol. Direct* 17, 25. doi:10.1186/s13062-022-00338-6

Zhao, Y., DU, D., Chen, S., Chen, Z., and Zhao, J. (2022b)., 13. Genes (Basel), 1390. doi:10.3390/genes13081390New insights into the functions of MicroRNAs in cardiac fibrosis: From mechanisms to therapeutic strategies*Genes*

Zheng, G., Zhang, J., Zhao, H., Wang, H., Pang, M., Qiao, X., et al. (2016). α3 integrin of cell-cell contact mediates kidney fibrosis by integrin-linked kinase in proximal tubular E-cadherin deficient mice. *Am. J. Pathol.* 186, 1847–1860. doi:10.1016/j.ajpath.2016.03.015

Zheng, J., Zhang, X., Cai, W., Yang, Y., Guo, T., Li, J., et al. (2022). Bone marrow mesenchymal stem cell-derived exosomal microRNA-29b-3p promotes angiogenesis and ventricular remodeling in rats with myocardial infarction by targeting ADAMTS16. *Cardiovasc Toxicol.* 22, 689–700. doi:10.1007/s12012-022-09745-7

Zhi, H., Luptak, I., Alreja, G., Shi, J., Guan, J., Metes-Kosik, N., et al. (2013). Effects of direct Renin inhibition on myocardial fibrosis and cardiac fibroblast function. *PLoS One* 8, e81612. doi:10.1371/journal.pone.0081612

Zhong, S., Guo, H., Wang, H., Xing, D., Lu, T., Yang, J., et al. (2020). Apelin-13 alleviated cardiac fibrosis via inhibiting the PI3K/Akt pathway to attenuate oxidative stress in rats with myocardial infarction-induced heart failure. *Biosci. Rep.* 40. doi:10.1042/BSR20200040

Zhong, Y., Yu, X., Li, X., Zhou, H., and Wang, Y. (2022). Augmented early aged neutrophil infiltration contributes to late remodeling post myocardial infarction. *Microvasc. Res.* 139, 104268. doi:10.1016/j.mvr.2021.104268

Zhou, J., Wen, T., Li, Q., Chen, Z., Peng, X., Wei, C., et al. (2022). Single-cell sequencing revealed pivotal genes related to prognosis of myocardial infarction patients. *Comput. Math. Methods Med.* 2022, 6534126. doi:10.1155/2022/6534126

Zhou, M. M., Li, D. W., Xu, L., Kong, B., Wang, X., Tang, Y. H., et al. (2023). Propionate alleviated post-infarction cardiac dysfunction by macrophage polarization in a rat model. *Int. Immunopharmacol.* 115, 109618. doi:10.1016/j.intimp.2022.109618

Zhou, X. L., Fang, Y. H., Wan, L., Xu, Q. R., Huang, H., Zhu, R. R., et al. (2019). Notch signaling inhibits cardiac fibroblast to myofibroblast transformation by antagonizing TGF-β1/Smad3 signaling. *J. Cell Physiol.* 234, 8834–8845. doi:10.1002/jcp.27543

Zhu, B., Zhu, X., Wang, X., Wu, J., Ding, S., Zhang, W., et al. (2022). Histamine deficiency promotes myofibroblasts transformation from HDC-expressing CD11b(+) myeloid cells in injured hearts post myocardial infarction. *J. Cardiovasc Transl. Res.* 15, 621–634. doi:10.1007/s12265-021-10172-2

Zhuang, L., Lu, L., Zhang, R., Chen, K., and Yan, X. (2020). Comprehensive integration of single-cell transcriptional profiling reveals the heterogeneities of non-cardiomyocytes in healthy and ischemic hearts. *Front. Cardiovasc Med.* 7, 615161. doi:10.3389/fcvm.2020.615161

Ziaja, M., Urbanek, K. A., Kowalska, K., and Piastowska-Ciesielska, A. W. (2021). Angiotensin II and angiotensin receptors 1 and 2-multifunctional system in cells biology, what do we know? *Cells* 10, 381. doi:10.3390/cells10020381

Zivarpour, P., Reiner, Ž., Hallajzadeh, J., Mirsafaei, L., and Asemi, Z. (2022). The effect of nutraceuticals on multiple signaling pathways in cardiac fibrosis injury and repair. *Heart Fail Rev.* 27, 321–336. doi:10.1007/s10741-020-09980-6

Zuo, P., Zhu, Y., Li, Y., Zuo, Z., Sheng, Z., Yan, G., et al. (2020). Protease-activated receptor 2 deficiency in hematopoietic lineage protects against myocardial infarction through attenuated inflammatory response and fibrosis. *Biochem. Biophys. Res. Commun.* 526, 253–260. doi:10.1016/j.bbrc.2020.03.077

Frontiers in Pharmacology

Explores the interactions between chemicals and living beings

The most cited journal in its field, which advances access to pharmacological discoveries to prevent and treat human disease.

Discover the latest Research Topics

See more →



Frontiers

Avenue du Tribunal-Fédéral 34
1005 Lausanne, Switzerland
frontiersin.org

Contact us

+41 (0)21 510 17 00
frontiersin.org/about/contact